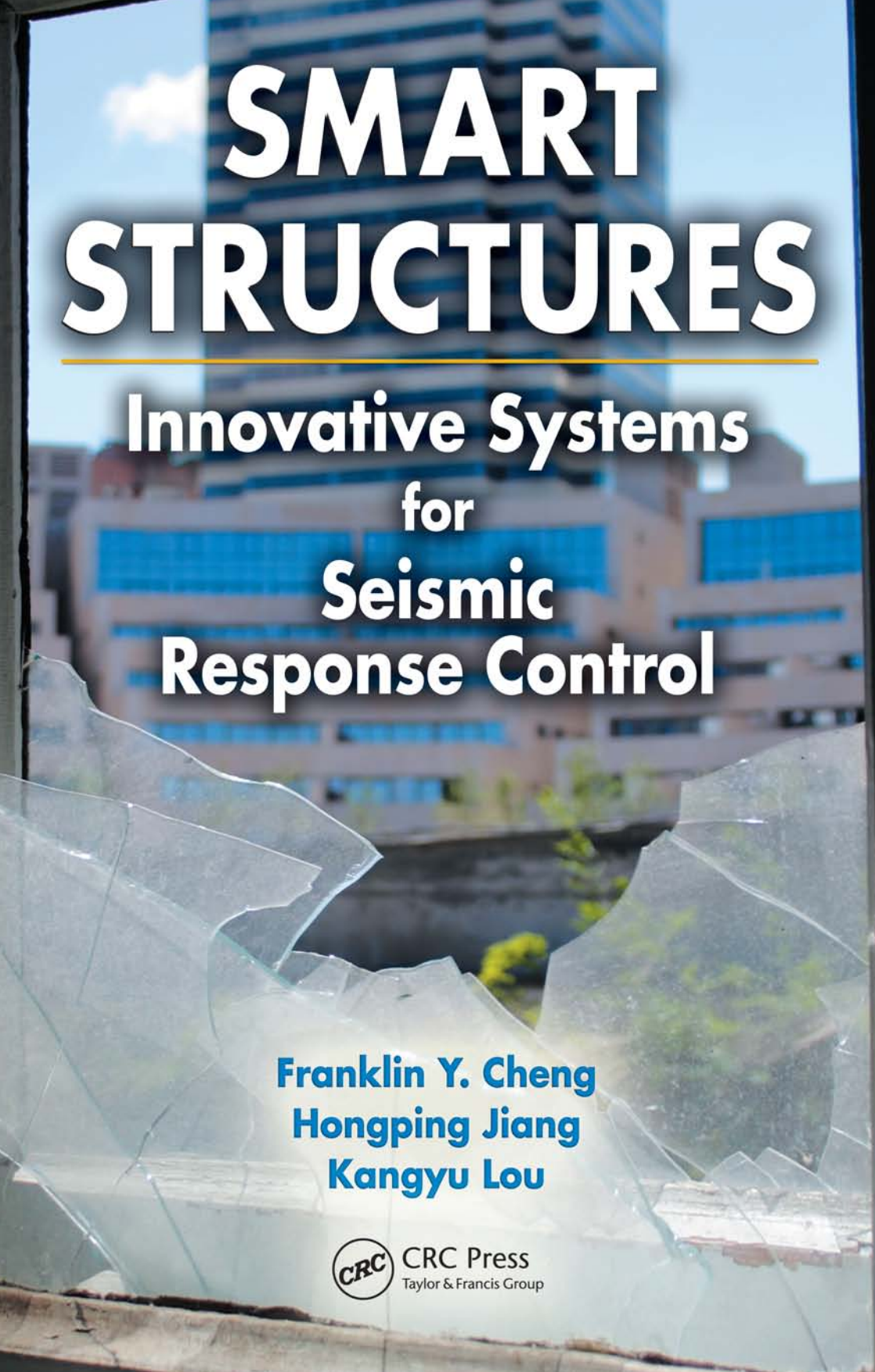
SMART
STRUCTURES
Innovative Systems
for
Seismic
Response Control
Franklin Y. Cheng
Hongping Jiang
Kangyu Lou
CRC
CRC Press
Taylor & Francis Group

SMART STRUCTURES

Innovative Systems for Seismic Response Control

SMART STRUCTURES

Innovative Systems for Seismic Response Control

Franklin Y. Cheng
Hongping Jiang
Kangyu Lou

CRC Press
Taylor & Francis Group
Boca Raton London New York

CRC Press is an imprint of the
Taylor & Francis Group, an **informa** business

CRC Press
Taylor & Francis Group
6000 Broken Sound Parkway NW, Suite 300
Boca Raton, FL 33487-2742

Printed in the United States of America on acid-free paper
10 9 8 7 6 5 4 3 2 1

International Standard Book Number-13: 978-0-8493-8532-2 (Hardcover)

Library of Congress Cataloging-in-Publication Data

Cheng, Franklin Y.
Smart structures : innovative systems for seismic response control / authors, Franklin Y. Cheng, Hongping Jiang, and Kangyu Lou.
p. cm.
Includes bibliographical references and index.
ISBN 978-0-8493-8532-2 (hardback : alk. paper)
1. Earthquake resistant design. 2. Smart structures. 3. Smart materials. I. Jiang, Hongping. II. Lou, Kangyu. III. Title.

TA658.44.C44 2008
624.1'762--dc22 2007035134

Visit the Taylor & Francis Web site at
http://www.taylorandfrancis.com

and the CRC Press Web site at
http://www.crcpress.com

Contents

Preface

The major challenge in today's structural engineering is to better design structures against the damaging effects of earthquakes and strong winds. Smart structural systems are an innovative concept that has been proven to be very effective in protecting structures. These systems absorb damaging energy and/or counteract damaging force on the structure, and thus reduce structural response and possible damage. Smart structure technology is being improved every day, and there is a great need for documented references in this field. This book is a useful reference for researchers and practicing engineers working in the field of structural engineering. It is also a key resource for senior undergraduates and all postgraduate students who need to find an organized collection of information of smart structure technology. Key features of the book include

1. Complete mathematical formulations and numerical procedures for the topics presented
2. New technologies
3. Design guidelines and examples based on current official codes
4. Detailed figures and illustrations
5. Extensive references

This book is prepared with the following emphases:

1. The book functions as a self-study unit. Essential information on structural formulations, mechanism of control systems, numerical algorithms, and so forth, is given in detail.
2. Step-by-step numerical examples are provided. These serve to illustrate mathematical formulations and to interpret physical representations, enabling the reader to understand the formulas vis-à-vis their applications.
3. Each chapter discusses a specific topic, and the topic areas are covered comprehensively and outlined as follows:
    - Chapter 1 introduces various smart structure systems currently in vogue so that the reader can have an overall view on the subject.
    - Chapters 2 and 3 present base isolation systems and their associated damping devices. Base isolation and damping systems have official design codes and are thus focused on herein with

extensive design examples that are believed to be beneficial to the practitioner to thoroughly comprehend the specifications.

- Chapter 4 focuses on active controlled systems, emphasizing mathematical derivation, control algorithm development, as well as system design and implementation.
- With the background of previous chapters, semiactive and hybrid control systems are developed and compared in Chapter 5.
- In today's engineering technology, information about real-world events is collected, stored, and analyzed by a computer using numerical data. Chapter 6 thus emphasizes sensing and data acquisition.
- To achieve optimal cost of a constructed facility, the number of control devices to be installed on a structure is of paramount importance. Chapter 7 develops optimal placement algorithms along with numerical examples of controlled systems.
- Controlled structures are traditionally assumed to be supported by a fixed base. However, a controlled system in reality is composed of three parts: structure, foundation, and soil base. Thus, Chapters 8 and 9 consider soil–structure interaction; the former deals with embedded foundations and the latter emphasizes shallow foundations. The soil properties, SSI formulations, and numerical procedures for response analysis are comprehensively presented for both conventional methodologies and MATLAB® applications.
- To achieve maximum protection of a controlled system from future earthquake destruction during the structure's lifetime, extensive details are given for generating future earthquakes on the basis of historic tectonic movements. Using the earthquake data resulting from simulation based on a probability approach, several case studies are provided to show response results of maximum floor displacements, the required control forces, and control effectiveness with various considerations with and without control, as well as with and without soil–structure interaction.

Acknowledgments

The book consolidates results from a number of research projects carried out at the University of Missouri-Rolla (UMR) that were awarded by several funding agencies including the National Science Foundation (NSF), the National Center for Earthquake Engineering Research (NCEER) (currently called the Multidisciplinary Center for Earthquake Engineering Research), Intelligent Systems Center at UMR, and the senior author's curators' professorship. The sustained support and encouragement of these agencies are gratefully acknowledged. Our deep gratitude also goes to our collaborators during the period of preparing the manuscripts, particularly to Dr. Zhang Xiaozhe, former PhD student and research assistant of civil engineering at UMR, for providing some numerical data. We extend special appreciation to Marsha Pronin, project coordinator, Joseph Clements, acquisition editor, and Rachael Panthier, project editor, CRC Press/Taylor & Francis, for their valuable assistance and guidance. Everlasting thanks go to our families for their care and encouragement throughout our careers. We dedicate this book to our spouses, Pi Yu (Beatrice) Cheng, PhD, Jinhong Lin Jiang, and Andong Hu Lou.

Franklin Y. Cheng
Hongping Jiang
Kangyu Lou

Authors

Franklin Y. Cheng, PE, honorary member of ASCE, joined the University of Missouri-Rolla, as assistant professor in 1966. In 1987, the Board of Curators of the University appointed him curators' professor, the highest professorial position in the system comprising four campuses, and curators' professor emeritus in 2000. He is a former senior investigator, Intelligent Systems Center, University of Missouri-Rolla. Dr. Cheng received 4 honorary professorships abroad and chaired 7 of his 24 National Science Foundation (NSF) delegations to various countries for research and development cooperation. He has also been the director of international earthquake engineering symposia and numerous state-of-the-art short courses. His work has warranted grants from several funding agencies including more than 30 from NSF. He has served as either chairman or member of 37 professional societies and committees, 12 of which are ASCE groups. He was the first chair of the Technical Administrative Committee on Analysis and Computation and initiated the Emerging Computing Technology Committee and Structural Control Committee. He also initiated and chaired the Stability Under Seismic Loading Task Group of the Structural Research Council (SSRC).

Dr. Cheng has served as a consultant for Martin Marietta Energy Systems Inc., Los Alamos National Laboratory, and Martin & Huang International, among others. The author, coauthor, or editor of 26 books and over 250 publications, Dr. Cheng's authorship includes two textbooks, *Matrix Analysis of Structural Dynamics: Applications and Earthquake Engineering*, and *Dynamic Structural Analysis*. Dr. Cheng is the recipient of numerous honors, including the MSM-UMR Alumni Merit, ASCE State-of-the-Art twice, the Faculty Excellence, and the Halliburtan Excellence awards. After receiving a BS degree (1960) from the National Cheng-Kung University, Taiwan, and a MS degree (1962) from the University of Illinois at Urbana-Champaign, he gained industrial experience with C.F. Murphy and Sargent & Lundy in Chicago, Illinois. Dr. Cheng received a PhD degree (1966) in civil engineering from the University of Wisconsin-Madison.

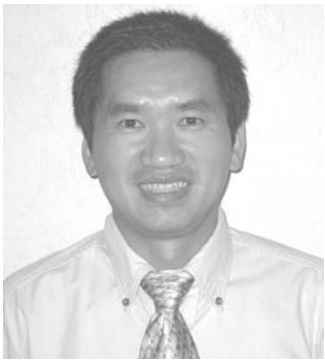

Hongping Jiang, PE, is a senior engineering systems specialist with the Technical Services Department of NCI Building Systems at Oklahoma City, Oklahoma. He received his PhD degree from the University of Missouri-Rolla in 1998, and MS and BS degrees from Tongji University of China in 1991 and Beijing University of Aeronautics and Astronautics in 1988, respectively. He taught in the Engineering Mechanics Department of Tongji University from 1992 to 1995. He has worked as a practicing engineer for several engineering companies and institutions, specializing in dynamic structural analysis, wind and seismic design, finite element applications, and development of engineering automation systems. He has performed considerable research and authored or coauthored more than 20 papers in the fields of smart seismic structures and wind effects of structures. Dr. Jiang is an active member of American Society of Civil Engineers (ASCE), Earthquake Engineering Research Institute (EERI), and American Institute of Steel Construction (AISC).

Kangyu Lou, senior structural engineer with the California Office of Statewide Health Planning and Development, is a registered structural engineer in California and a civil engineer in both California and Ohio. His professional practice covers design and nonlinear analysis of high-rise buildings and bridges as well as rehabilitation of existing structures.

Dr. Lou has designed health care facilities with energy-dissipated systems and performed evaluation and retrofit of health care facilities in California based on Senate Bill 1953 during his association with Taylor and Gaines Structural Engineers, Pasadena, California. After receiving his BS (1983) and MS degrees (1988) from Tongji University, Shanghai, China, he became an assistant professor at Shanghai Institute of Urban Construction, China. Dr. Lou completed his doctoral programs at the University of Missouri-Rolla in 1997. As a author and coauthor, he has published over 16 technical papers in professional journals and proceedings of national conferences. Dr. Lou is an active national and regional member of the American Concrete Institute (ACI) and the Structural Engineering Institute (SEI).

1 Basic Concept of Smart Structure Systems

1.1 Introduction

1.1.1 Structures and Smart Structures

A *structure* is a system that carries and/or transmits loads. It is engineered to perform such functions without experiencing irreparable damage during its designed service life. Engineering structures can serve as buildings, bridges, ships, airplanes, or space shuttles. The loads on a structure can be static, such as gravity, or dynamic, such as earthquakes. Structural components, such as columns, beams, plates, and shells, are load-bearing systems and are structures themselves. The behavior of a structure and its components, such as deformation under static loads and vibration under dynamic loads, is called *structural response*. Design of a structure simply refers to the determination of its profile and configuration in the three-dimensional space, the material and size of its components, and the connections between its components, so that the structural response can meet the established criteria. A typical structure design would ensure the *structural safety* (strength and stability) and *serviceability* (stiffness) of the structure and its components under expected loads. Multiple disciplines, such as material science, mathematics, and mechanics, are employed to obtain a structure design. Material science provides properties and limit states (failure modes) of the materials for the structure, mathematics calculates the structural response to loads, and mechanics ensures the equilibrium and stability of the structure.

The traditional approach is to design structures with sufficient strength to withstand loads and with the ability to deform in a ductile manner. Such designed structures have limited capacity owing to three factors. First, these structures rely on their inherently small material damping to dissipate dynamic energy. There are no guidelines for how to increase the damping of common structure materials, such as reinforced concrete or steel. Second, these structures have a fixed capacity of load resistance and energy dissipation. Thus, they cannot adapt to ever-changing environmental excitations, such as winds or earthquakes. Third, these structures totally depend on their stiffness to resist loads. Limitations in the traditional approach of structure design motivated researchers to explore alternatives. Advanced research has discovered natural and man-made materials with unusual properties, called *smart materials*, and systems that can automatically adjust themselves to environmental changes, called *adaptive systems*. These discoveries led to the innovative concept of *smart structures* [82]. With adaptive systems and/or smart materials and devices added to the structure, the structure

becomes "smart" because it can monitor itself and adapt to the environment. A *smart structure* system has the ability to sense any change in the environment or system, diagnose any problem at critical locations, store and process measured data, and command appropriate action to improve system performance and to preserve structural integrity, safety, and serviceability. The smart structure concept has been applied in aerospace and mechanical industries, such as aircraft structure crack monitoring systems and automobile vibration absorbers. Application of this concept for wind and seismic response reduction of large civil engineering structures is still a cutting-edge technology under research and development.

1.1.2 Significance of Smart Structure Technology for Civil Engineering Structures

Civil engineering structures, such as buildings, bridges, and towers, may vibrate severely or even collapse while subjected to strong wind or earthquake excitations. Designing structures to withstand seismic damage remains a challenge for civil engineers. Despite intensive effort toward wind- and earthquake-resistant designs in code development and construction, structures are still vulnerable to strong wind or earthquake excitations. This is because structures designed using the traditional approach have limited capacities of load resistance and energy dissipation. Such structures totally rely on their own stiffness to resist earthquake force and on their own small material damping to dissipate dynamic energy. These structures are *passive* in that they cannot adapt to ever-changing and uncertain wind and earthquake excitations. In order to withstand a stronger excitation, an increase in structure strength and ductility is required, but high-strength and ductile construction materials are usually expensive. Increasing strength by enlarging cross sections of partial constituent members of an indeterminate structure actually attracts more demand force on these members, subsequently requiring even greater strength. This can result in a fruitless spiral design. Moreover, there is no way to improve damping for common construction materials, such as reinforced concrete or steel.

The ineffectiveness of traditional wind- and seismic-resistant designs led to the application of innovative smart structure technology to civil engineering structures in the 1970s. It has steadily gained acceptance as research findings and practical implementation continue to show that this concept is a promising way to protect structures from wind and seismic excitations [7,17,25,26,40,46,49,76–78,80]. With smart structure technology, devices and/or systems are added to the structure to increase its seismic-resistant capacity. The structure then relies not only on its own strength to withstand earthquake force but also on these devices or systems to dissipate dynamic energy. Smart structure technology is becoming an attractive alternative to augment structural safety and serviceability as it can greatly improve seismic performance of structural systems.

When building a new structure or retrofitting an existing one for safety and serviceability requirements, using smart structure systems can save materials and

construction work, consequently reducing structural weight as well as construction cost. Today, such systems have been applied to the following civil engineering structures:

- Structures under unusual excitations, such as extreme winds or strong earthquakes.
- Structures with critical functions and high safety requirements, such as hospitals, fire stations, and power plants.
- Structures requiring serviceability considerations, such as towers, tall buildings, long-span roofs or bridges, and other flexible structures. Under large environmental excitation, excessive structural vibrations could affect occupant comfort or structural safety.

1.2 Basic Principles of Smart Structure Technology for Seismic Response Control

In this section, a simple single-degree-of-freedom (SDOF) structural model is used to illustrate the basic principles of smart structure technology for seismic response control. An SDOF structure subjected to earthquake excitation can be modeled as

$$m\ddot{x}(t) + c\dot{x}(t) + kx(t) = -m\ddot{x}_{\mathrm{g}}(t) \tag{1.1}$$

where m is the mass of the structure, c is the damping coefficient of the structure, and k is the linear elastic stiffness of the structure. While subjected to an earthquake ground motion $\ddot{x}_{\mathrm{g}}(t)$, this SDOF system responds with a lateral displacement $x(t)$ relative to the ground.

Equation 1.1 can be rewritten as

$$\ddot{x}(t) + 2\zeta\omega_{\mathrm{n}}\dot{x}(t) + \omega_{\mathrm{n}}^2 x(t) = -\ddot{x}_{\mathrm{g}}(t) \tag{1.2}$$

where ζ is the damping ratio and ω_{n} is the natural frequency in radians of the structure. The structure response can be solved easily using the theory of structural dynamics [13,61]

$$\begin{aligned} x(t) = {} & \mathrm{e}^{-\zeta\omega_{\mathrm{n}}t}(C_1\cos\bar{\omega}_{\mathrm{n}}t + C_2\sin\bar{\omega}_{\mathrm{n}}t) \\ & - \frac{1}{\bar{\omega}_{\mathrm{n}}}\int_0^{\mathrm{t}} \ddot{x}_{\mathrm{g}}(\tau)\mathrm{e}^{-\zeta\omega_{\mathrm{n}}(t-\tau)}\sin\bar{\omega}_{\mathrm{n}}(t-\tau)\,\mathrm{d}\tau \end{aligned} \tag{1.3}$$

where $\bar{\omega}_{\mathrm{n}} = \sqrt{1-\zeta^2}\omega_{\mathrm{n}}$ is the damped natural frequency, and C_1 and C_2 are constants to be determined by initial conditions. Since the earthquake ground motion can always be expanded into a Fourier series, the structural seismic response would be a summation of structural responses by a series of sinusoidal

excitations. The response of the SDOF system under sinusoidal excitation $P \sin \theta t$ is

$$x(t) = \mathrm{e}^{-\zeta \omega_\mathrm{n} t}(C_1 \cos \bar{\omega}_\mathrm{n} t + C_2 \sin \bar{\omega}_\mathrm{n} t) + \frac{P \sin(\theta t - \varphi)}{m\sqrt{(\omega_\mathrm{n}^2 - \theta^2)^2 + 4\zeta^2 \omega_\mathrm{n}^2 \theta^2}} \tag{1.4}$$

where $\varphi = \tan^{-1}\left[2\zeta\omega_\mathrm{n}\theta \big/ \left(\omega_\mathrm{n}^2 - \theta^2\right)\right]$.

Equations 1.3 and 1.4 show that, mathematically, there are three methods to reduce structural seismic response—reducing the magnitude of $\ddot{x}_\mathrm{g}(t)$, increasing the damping ratio ζ, and avoiding resonance by enlarging the difference of ω_n and θ. These mathematical concepts are realized by smart structures through the following mechanisms:

- Base-isolation systems that cut off the energy transmission of earthquake ground motions to the structure.
- Control devices or systems that apply a control force to serve as an extra damping mechanism by means of devices such as mass dampers/drivers, tendons, or bracings.
- Control devices or systems that utilize the energy absorption capability of materials by viscosity and/or nonlinear characteristics, such as yielding.
- Control devices or systems that distance the natural period of the structure from the predominant frequency of earthquake ground motions.

The above mechanism shows that a smart structure can use either a base-isolation system or a control system for seismic response reduction. Control systems add damping to the structure and/or alter the structure's dynamic properties. Adding damping increases the structural energy-dissipating capacity, and altering structural stiffness can avoid resonance to external excitation, thus reducing structural seismic response. Mathematically, an SDOF smart structure using a control system under seismic excitation can be expressed as

$$(m + m_\mathrm{c})\ddot{x}(t) + c\dot{x}(t) + kx(t) + F_\mathrm{c}(t) = -(m + m_\mathrm{c})\ddot{x}_\mathrm{g}(t) \tag{1.5}$$

where m_c is the mass of the control device/system, which is usually much smaller than structure mass m; $F_\mathrm{c}(t)$ is the control force generated by the control device/system. The force $F_\mathrm{c}(t)$ is highly dependent on the type of the control device or system. A typical linear model of $F_\mathrm{c}(t)$ can be expressed as

$$F_\mathrm{c}(t) = c_\mathrm{c}\dot{x}(t) + k_\mathrm{c}x(t) \tag{1.6}$$

Then Equation 1.5 can be rewritten as

$$(m + m_\mathrm{c})\ddot{x}(t) + (c + c_\mathrm{c})\dot{x}(t) + (k + k_\mathrm{c})x(t) = -(m + m_\mathrm{c})\ddot{x}_\mathrm{g}(t) \tag{1.7}$$

By comparing Equations 1.1 and 1.7, it is shown that the addition of the control system introduces control force $F_c(t)$, which modifies the structural properties so that it can respond more favorably to the designed or anticipated ground motion. Typically, the added devices/systems are designed to increase structure damping c and/or to avoid resonance by altering structure stiffness k or mass m so that the structure response can be reduced.

It is worth noting that for large civil engineering structures, adding damping to the system is more practical than altering system mass and stiffness. Thus, seismic response control systems are usually designed mainly to add damping to the system with only minor modifications to the system's stiffness or mass. This can be clarified with the SDOF system described by Equation 1.2 by studying its response amplitude of system forces. The displacement, velocity, and acceleration amplitudes of the steady-state response of the SDOF system described by Equation 1.2 to a resonant excitation $P\sin(\omega_n t)$ can be easily derived from Equation 1.4 as

$$x_m = \frac{P}{2\zeta m\omega_n^2}, \quad \dot{x}_m = \frac{P}{2\zeta m\omega_n}, \quad \ddot{x}_m = \frac{P}{2\zeta m} \tag{1.8}$$

Then, the amplitudes of the restoring force, R_m, the damping force, D_m, and the inertia force, I_m, are

$$R_m = \frac{P}{2\zeta}, \quad D_m = P, \quad I_m = \frac{P}{2\zeta} \tag{1.9}$$

Equation 1.9 shows that the amplitude of both the inertia and restoring forces is much larger (50 times for a 1% damping system) than that of the damping force for a lightly damped system. The same conclusion can be drawn by studying the system's root-mean-square (RMS) response to a white-noise excitation S_0. Its RMS displacement response, σ_x, and velocity response, $\sigma_{\dot{x}}$, are [53]

$$\sigma_x = \sqrt{\frac{\pi S_0}{2\zeta\omega_n^3}}, \quad \sigma_{\dot{x}} = \sqrt{\frac{\pi S_0}{2\zeta\omega_n}} \tag{1.10}$$

Then, the RMS values of the restoring force, σ_R, and the damping force, σ_D, are

$$\sigma_R = \omega_n^2\sqrt{\frac{\pi S_0}{2\zeta\omega_n^3}} = \sqrt{\frac{\pi S_0\omega_n}{2\zeta}}, \quad \sigma_D = 2\zeta\omega_n\sqrt{\frac{\pi S_0}{2\zeta\omega_n}} = 2\zeta\sqrt{\frac{\pi S_0\omega_n}{2\zeta}} \tag{1.11}$$

Thus, $\sigma_R = \sigma_D/2\zeta$, which shows that the RMS restoring force is much larger than the RMS damping force for lightly damped structures.

Civil engineering structures usually have very small damping, and the resonant component makes major contributions to the response of such lightly damped systems under wide-banded excitation [53]. If the control effort is to alter the

system's stiffness or mass, the control force must approximate the magnitude of the restoring force or inertia force; consequently, numerous sizeable force-generating devices would be required. If the control force mainly adds damping to the system, much less control effort is required. Thus, altering the system's mass or stiffness takes much more control effort and is less practical than adding damping to large civil engineering structures.

It is also important to note that a smart structure can use various types of control devices or systems. Thus, it is useful to distinguish the control devices/systems currently being used in practice. Sections 1.4 through 1.8 introduce the basic concepts of various systems developed for civil engineering structures. *Base-isolation systems* are introduced in Section 1.4. *Active control systems*, as described in Section 1.7, use external power to generate the control force. The control force is determined by a control algorithm with a measured structure response, and their c_c and k_c parameters expressed in Equation 1.6 can be adjusted by feedback gain within the actuator capacity. Thus, they are adaptive systems that make structures fully "smart" to environmental excitations. *Passive control systems*, on the other hand, use passive energy-dissipation devices, as described in Section 1.5. Structure motion drives these devices to produce the control force. Since their c_c and k_c are nonadjustable device properties, passive systems are less adaptable to excitations and thus are referred to as passive. The design specifications for base-isolation and passive damper systems have been officially established [6,33,34,42] in the engineering communities. Thus, base-isolation and passive damper systems are given more attention in later sections of this chapter. *Semiactive control systems*, as described in Section 1.6, add adaptive mechanisms to passive systems to adjust their force-generating behavior, thus often being viewed as controllable passive systems. Compared to active systems, a semiactive system is less adaptive because its force-generating capacity is limited by its passive device base. *Hybrid control systems* generally refer to a combined active control system and passive system or base-isolation system. Since a portion of the control objective is accomplished by the passive system, a less active control effort, implying a smaller active force-generating device and less power resource, is required. More discussion of hybrid systems can be found in Section 1.8. Hybrid control systems are more favorable than other systems in that they can utilize the advantages and avoid the disadvantages of both active and passive systems.

1.3 History of Smart Structure Technology for Seismic-Response Control

Adding devices to structures for vibration suppression has a long history. Passive dampers emerged in the early 1900s. An early application of damping devices to large civil engineering structures can be found in tower structures with elevated water tanks [72], as shown in Figure 1.1. Passive dampers have been commercially available since the 1970s and have been extensively applied for vibration

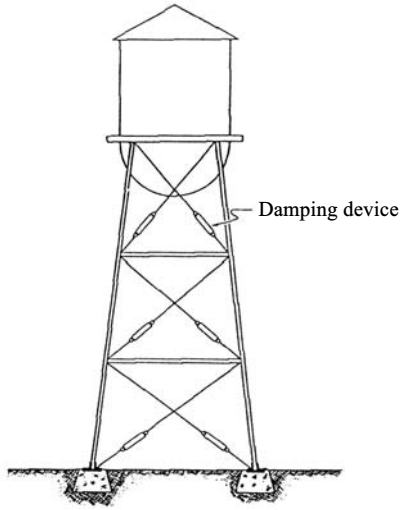

FIGURE 1.1 Water tower with damping devices.

suppression in automobiles, aircrafts, space structures, and civil engineering structures. Modern control technologies and adaptive systems are also mature in mechanical and electrical industries. However, smart structure technology for wind and seismic response control of civil engineering structures was not conceptualized until the 1950s [51] as it is a very challenging task to develop control devices and adaptive systems for large structures.

The concept of structural seismic response control originated in the 1950s with Japanese researchers Kobori and Minai [51]. They came to an important conclusion—as long as the precise characteristics of earthquake ground motion vis-à-vis a building cannot be predicted, seismic response must be controlled on the receiving end, the building structure. Yao's conceptual paper [95] marked a significant contribution to structural control research in the United States. He proposed an "error-activated structural system whose behavior varies automatically in accordance with unpredictable variations in the loading as well as environmental conditions and thereby produces desirable responses under all possible loading conditions." In such a structural system, earthquakes and winds are countered not only by structural members but also by a control force.

Remarkable progress has followed these initial concepts in structural seismic response control. Japan took the lead in the practical application of control systems to building structures. In 1985, full-scale control system tests were launched to progress toward further practical application. In 1989, an active mass driver (AMD) system was installed in a building for seismic response suppression. AMD efficiency was verified by real-time observation and numerical simulation [50]. In the United States, under the leadership of the National Science Foundation (NSF), following significant support of various control research projects in earthquake

engineering, the U.S. Panel on Structural Control Research was formally established, and a 5-year research program was initiated in 1992 for safety, performance, and hazard mitigation [54]. The Civil Infrastructure Systems (CIS) research program, closely related to structural control, was also initiated by the NSF [54]. Through these NSF programs, significant advances have been and continue to be made in the United States. As interest in structural control grows, international cooperation fosters research and development of seismic response control systems. Since the Ninth World Conference on Earthquake Engineering in 1988 recognized the importance of seismic response control, the United States and Japan have collaborated on research in this area. To promote global cooperation, the International Association for Structural Control (IASC) was established in 1992 at the Tenth World Conference on Earthquake Engineering. IASC sponsored the International Workshop on Structural Control in 1993, the First World Conference on Structural Control at Los Angeles in 1994, the Second World Conference on Structural Control at Kyoto, Japan in 1998, the Third World Conference on Structural Control at Como, Italy in 2002, and the Fourth World Conference on Structural Control at San Diego, California in 2006. In addition, numerous bilateral and trilateral workshops on smart structures were held in Asia, Europe, and the United States, such as the US–Korea Workshop on Smart Structural Systems [27,28]. Today, numerous full-scale control systems have been installed in actual structures and have performed well for seismic- and wind-response reduction [49,76,78,80]. Joint research projects are being conducted by researchers from the United States, Japan, China, South Korea, and elsewhere. These collaborative efforts contribute greatly to the development of seismic response control. Table 1.1 summarizes the history of smart structure technology for seismic response control [54,80].

With these research and development efforts, great achievements have been made in smart structure technology for seismic response control. These efforts can be grouped into the following categories:

- *Control system modeling and algorithm development*. This area focuses on improving the applicability of modern control theory to the seismic response of large civil structures characterized by severe uncertainty.
- *Control device development and experimental verification*. Dampers and actuators capable of generating the large force required for seismic response control are developed. Shaking table tests or field measurements are conducted to verify the effectiveness of control devices and proposed control algorithms.
- *Application of smart materials*. Electrorheological (ER) or magnetorheological (MR) materials, piezoelectric (PZT) layers, shape memory alloys, and optical fiber sensors are being studied for civil engineering applications. They are used to develop sensors, dampers, and structural members with embedded smart material layers for sensing and actuation. Structural components with smart materials, dampers, and sensors are applied to civil engineering structures such that these structures are

TABLE 1.1
History Summary of Smart Structure Technology for Seismic-Response Control

Year	Event
1988	Ninth WCEE recognized the importance of seismic response control
1989	U.S. Panel on Structural Control research
1990	Japan panel on structural response control
1991	5-year research initiative on structural control by NSF
1992	International Association for Structural Control (IASC) established at Tenth WCEE
1993	European association for control of structures
1993	Civil infrastructure systems research program initiated by NSF
1994	First world conference on structural control (Los Angeles, California, USA)
1996	First European conference on structural control (Barcelona, Spain)
1998	Chinese panel for structural control
1998	Korean panel for structural control
1998	Second world conference on structural control (Kyoto, Japan)
2000	Second European conference on structural control (Paris, France)
2002	Third world conference on structural control (Como, Italy)
2004	International Association for Structural Control and Monitoring (IASCM)
2006	Fourth world conference on structural control (San Diego, California, USA)

capable of responding spontaneously to seismic excitations in order to minimize undesired effects.

- *Applicability issues*. These studies have enhanced the applicability of control systems of full-scale structures. Issues here include system integration, robust control strategies for reliability, observer–controller techniques for a sensing system with acceleration measurements and insufficient state sensors, force-generating capacity of actuators and hybrid control strategies, maximizing control system effectiveness by optimally placing the control devices, and overall system safety, stability, and maintenance.
- *Full-scale implementation*. Here, control systems are installed on actual structures. While passive control systems were extensively applied to civil structures originally, full-scale active control systems made their debut with significant momentum [50,76].
- *Design standard development*. Seismic-design specifications are being updated with guidelines for smart structure design. Federal Emergency Management Agency (FEMA) takes the lead in developing guidelines for the design of seismic-isolated structures or structures with damper systems and has published four editions of the design guide in 1991 (FEMA 140), 1997 (FEMA 302), 2000 (FEMA 368), and 2003 (FEMA 450) [33,34]. These design guides have been adopted by model building

codes and ASCE-7 standards. In 1991, the Uniform Building Code (UBC), issued by the International Conference of Building Officials (ICBO), adopted design regulations for seismic-isolated structures in Appendix-Division III [41]. These provisions stem from Tentative Seismic-Isolation Design Requirements (September 1986), circulated by a base-isolation subcommittee on behalf of the Structural Engineers Association of Northern California (SEAONC). A later version of the UBC (UBC-97) specified design provisions for isolated structures in Division IV, Appendix-Chapter 16 [41]. Static and dynamic lateral response procedures are recommended for seismic design of base-isolated structures. Both response spectrum and time-history analysis are permitted in the dynamic procedure. The International Building Code, published by the International Code Council, adopted the FEMA guidelines for seismic-isolated structures in Section 1623 of both 2000 and 2003 editions [42]. ASCE-7 Standard Minimum Design Loads for Buildings and Other Structures, issued by the American Society of Civil Engineers, also adopted the FEMA provisions for seismic-isolated structures in its 1995, 1998, and 2002 editions [6]. The latest edition of ASCE-7, published in 2005, has adopted design guidelines for not only seismically isolated structures (Chapter 13) but also for structures with passive damper systems (Chapter 15) [6].

1.4 Base-Isolation Systems

1.4.1 Introduction

Base isolation is a well-established application of the passive control approach. A building mounted on a material with low lateral stiffness, such as rubber, achieves a flexible base. During the earthquake, the flexible base is able to filter out high frequencies from the ground motion and to prevent the building from being damaged or collapsing. Therefore, base isolation is an effective tool for providing seismic protection for low- and middle-rise building structures because these types of buildings are characterized as having high frequencies. The design specifications for base isolation have been officially established as indicated in the previous section. Thus, this book includes one chapter on this subject, focusing on the outline of code specifications, equations, and numerical illustrations of analysis and the design of sample buildings.

Applying base isolation to structural engineering began in the 1960s. Since the first base-isolated building, the Foothill Community Law and Justice Center located at Rancho Cucamonga, California [63], was constructed in the United States, base-isolation technology has been successfully utilized to isolate different types of building lateral-force-resisting systems, such as steel braced frames, concrete shear walls, reinforced or unreinforced masonry walls, and even wood frames [83]. A recent application of the base-isolation system combined with steel special moment resisting frames with reduced beam sections (RBSs) is the Sue &

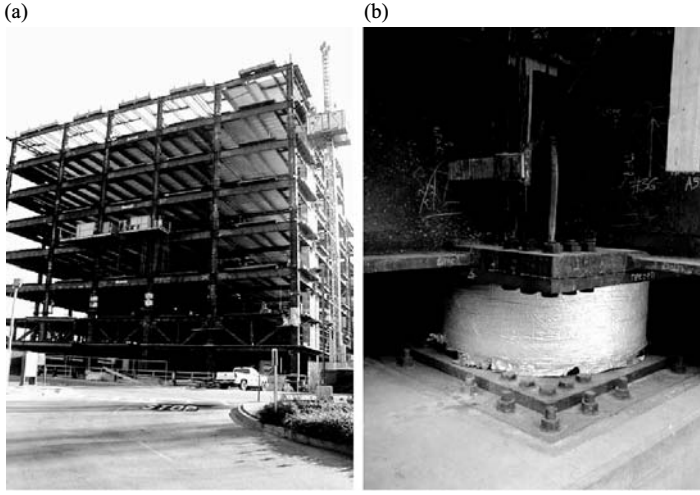

FIGURE 1.2 (a) Construction of Sue & Bill Gross Women's Pavilion at Hoag Memorial Hospital Presbyterian, Newport Beach, California and (b) installation of base-isolation system.

Bill Gross Women's Pavilion at Hoag Memorial Hospital Presbyterian, Newport Beach, California, as shown in Figure 1.2. This eight-story building structure, designed by Taylor & Gaines Structural Engineers in Pasadena, California, is isolated by 54-high-damping natural rubber bearings manufactured by BTR Andre in the United Kingdom.

Isolation components, usually called *isolators* or *bearings*, are generally classified as one of two major types: elastomeric- and sliding-type bearings. Elastomeric-type bearings are typically composed of rubber and steel plates, while sliding-type bearings rely upon friction between specially treated surfaces of an assembly unit. Some types of bearings combine characteristics of elastomeric and sliding bearings, but these two basic types are dominantly used in building structures. The following sections mainly focus on the introduction of elastomeric-type and sliding-type bearings.

1.4.2 Elastomeric Bearings

Elastomeric bearings were originally made from natural rubber; later on, their properties were improved by adding steel plates or shims. An elastomeric bearing with steel shims is schematically presented in Figure 1.3. The thickness of the steel shim is approximately 1 in., and the rubber layer between the steel shims varies from 3 to 7.5 in. Compared to the pure rubber bearing, using steel shims greatly reduces the bearing's vertical deformation and keeps the rubber layers from laterally bulging. Accordingly, the bearing's stiffness in the upward direction is much less than that in the downward direction. Since the steel shims do not prevent

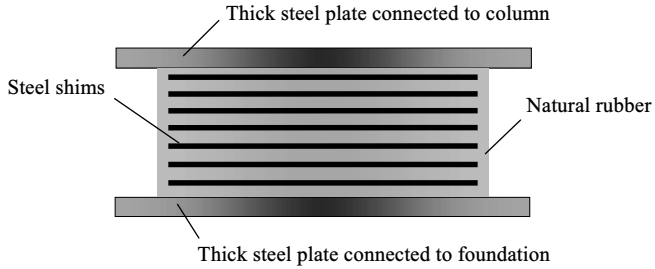

FIGURE 1.3 Elastomeric bearing with steel shims.

the rubber layers from lateral movement, the bearing's lateral stiffness is barely affected and is much less than the vertical stiffness.

Synthetic rubbers, such as neoprene, can be used as an alternative to natural rubber when manufacturing bearings. Both types of rubber properties are very stable and do not exhibit creep under long-term loading. Elastomeric bearings have been used successfully in buildings and other nonbuilding structures. They have functioned well for over 50 years of service.

Owing to the flexibility of rubber properties and the long range of elastic shear deformation, the critical damping of elastomeric bearings only varies from 2% to 3%. Therefore, elastomeric bearings are also called *low-damping bearings*.

Elastomeric bearings are easily manufactured, and the manufacturing cost is relatively low compared to other types of bearings. Also, their mechanical properties are independent of temperature and aging. However, owing to the low critical damping, elastomeric bearings have little resistance to service load, and additional damping devices are required in order to control higher lateral displacement.

1.4.3 Lead-Plug Bearings

The disadvantage of the elastomeric bearing's low-damping properties can be overcome by plugging a lead core into the bearing. A preformed hole, slightly smaller than the lead plug, is usually located in the center of the elastomeric bearing. Once the lead plug is tightly fitted into the preformed hole, both portions become a unit and form a *lead-plug bearing* as shown in Figure 1.4.

The performance of the lead-plug bearing depends on the imposed lateral force. If the lateral force is small, the movement of the steel shims is restrained by the lead core, and the bearing displays higher lateral stiffness. As the lateral force becomes larger, the steel shims force the lead core to deform or yield, and the hysteretic damping is developed with energy absorbed by the lead core. Consequently, the lateral stiffness of the bearing is reduced. The equivalent damping of the lead-plug bearing varies from 15% to 35%. A bilinear model is usually used to depict the mechanical properties of the lead-plug bearing.

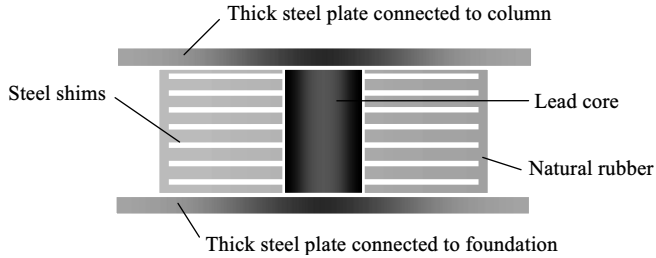

FIGURE 1.4 Lead-plug bearing.

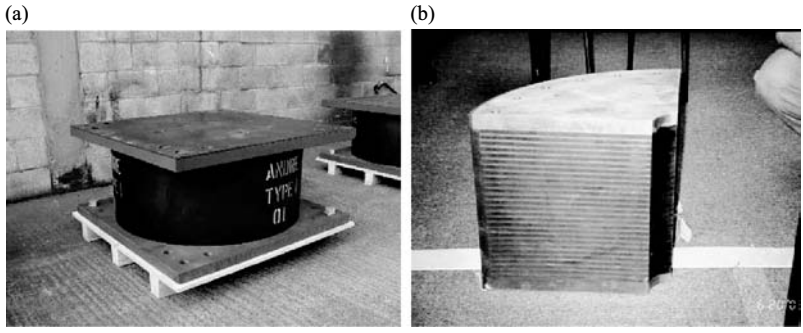

FIGURE 1.5 (a) High-damping natural rubber bearings manufactured by BTR Andre and (b) the section cut of tested bearing.

1.4.4 High-Damping Rubber Bearings

Another effective method to increase the damping of the electrometric bearing is to modify the rubber compounds no matter whether the rubber is natural or synthetic. For example, adding carbon black or other types of fillers to the natural rubber changes the rubber's properties and results in higher damping.

The *high-damping rubber bearing* is only composed of rubber and steel shims, but it possesses necessary flexibility as well as energy-dissipation capabilities. Figure 1.5 shows a high-damping rubber bearing 46 in. in diameter, which was manufactured by BTR Andre and installed in the Sue & Bill Gross Women's Pavilion (see Figure 1.2). During the prototype test, the bearing remained stable and did not fail even though it was vertically stretched by half an inch in order to simulate the applied overturning force and then sheared by 26 in. of horizontal movement.

A bilinear model can also be adopted to illustrate the effect of the applied lateral force on the bearing and the corresponding displacement. The effective damping of a high-damping rubber bearing is a function of the bearing's shear strains. For natural rubber, the effective damping changes from approximately 15% at low-shear strain to 10% at high-shear strain.

The mechanical properties of the high-damping rubber bearing are somehow affected by the effects of aging, temperature, and scragging. Also, the selection of the bearing's stiffness and damping is limited owing to the rubber compound itself [48].

1.4.5 Friction Pendulum Bearings

The original friction bearing features flat sliding surfaces. The imposed lateral force is resisted by the product of the friction coefficient and the vertical load applied on the bearing. The major disadvantage of the friction bearing with flat sliding surfaces is that the building structure is unable to return to its original position after an earthquake. This is because once the imposed lateral force is less than the resistance generated from the friction, the movement of the building structure stops and causes the structure stay some distance from the center of the bearing. Aftershocks may force the building to move from the stopping position and even further away from the original position. Accordingly, the building's movement might exceed the bearing's range and result in the failure of the bearings.

To reduce the distance to the center of the bearing after an earthquake, a friction bearing with a spherical or concave sliding surface was developed. This type of bearing is called a *friction pendulum bearing* and is shown in Figure 1.6. The spherical sliding surface is normally coated by Teflon with approximately 3% friction coefficient. The imposed lateral force pushes the bearing in both horizontal and vertical directions. Once the lateral force disappears, a restoring force is generated. A component of applied vertical load along the tangential direction to the spherical surface helps the bearing move back to the center. The movement stops when the friction is equal to or greater than the component of the applied vertical load.

One noticeable characteristic of the friction pendulum bearing, which is called static friction, is that the lateral force needed to initiate sliding is larger than that needed to maintain sliding. Once the imposed force overcomes the resistance from the friction, the articulated slider is activated and moves along the spherical surface. The friction coefficient is governed by the applied vertical load and velocity [48]. A higher applied vertical load results in a lower friction coefficient, while the friction coefficient greatly increases at high velocity. Detailed discussions of

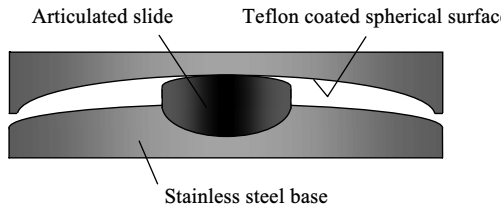

FIGURE 1.6 Friction pendulum bearing.

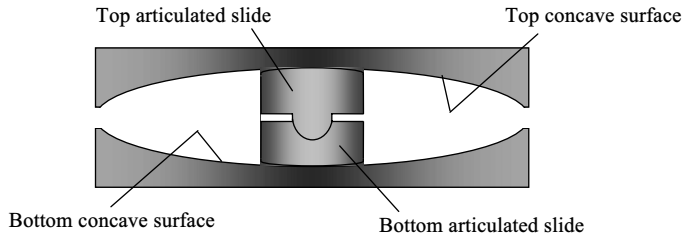

FIGURE 1.7 Friction pendulum bearing with double concave surface.

the mechanical properties of the friction pendulum bearing will be presented in Chapter 2.

The friction pendulum bearing has the advantage of low maintenance. The coated Teflon on the stainless steel effectively protects the sliding surface from corrosion. Since the bearing slides only during an earthquake, the coated Teflon can last for the entire design life. Also, the aging effects and temperature variations hardly affect the bearing's mechanical properties.

A friction pendulum bearing with double concave surfaces has recently been developed. Figure 1.7 schematically depicts this type of bearing. Compared to the friction pendulum bearing with a single concave surface, use of double concave surfaces can achieve the same horizontal movement with reduced bearing size because the horizontal movement of the bearing is contributed by the top and bottom concave surfaces.

1.4.6 Other Types of Base-Isolation Systems

Pot-type bearings, originally developed in Europe, are an example of the combination of elastomeric- and sliding-type bearings. The elastomer is confined by a pot-like piston coated by Teflon on its top surface. Figure 1.8 presents a schematic section of the pot bearing. Owing to the confinement of the piston, the elastomer is prevented from bulging under high pressure. Also, the pot bearing has rotational capacity so that the sliding face is subjected to more uniform loading under the earthquake's displacement. However, the eccentricity generated by lateral movement will result in an additional movement to the structure above the isolation system.

Another application of elastomeric bearings combined with Teflon-coated sliding bearings, such as the combined system tested by Earthquake Engineering Research Center (EERC) at Berkeley, California and the hybrid Taisei shake suspension system (TASS) system [63], is to install both systems in different locations of the building's foundation. Elastomeric bearings are used to resist lateral force and offer restoring force, while the sliding bearings are designed to support the vertical loads. The performance of the base-isolation system mainly relies on the layout of the bearings' locations. If not properly placed, the elastomeric bearing may experience high tensile force because it is not designed to carry any gravity loads.

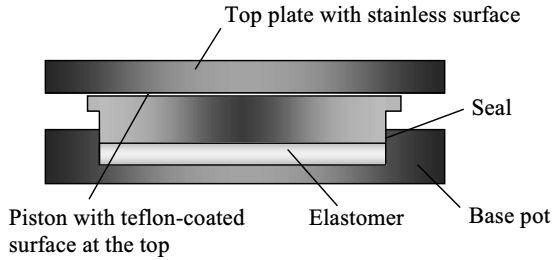

FIGURE 1.8 Pot bearing.

In addition to elastomeric bearings, sliding bearings, and combinations of both types of bearings, there are other types of base-isolation systems based on concepts of energy dissipated passively, such as *resilient-friction base-isolation systems*, *spring-type systems*, and *sleeved-pile isolation systems*. Some systems are only limited to certain building structures, and some are not yet commercially available. Owing to the space limitations herein, detailed discussions of these systems are referred to Reference 63.

1.5 PASSIVE ENERGY-DISSIPATION SYSTEMS

Passive energy-dissipating systems use mechanical devices to dissipate a portion of structural input energy, thus reducing structural response and possible structural damage. They have been used to mitigate structural vibration by wind and earthquake excitations. Typical passive systems are *tuned mass dampers* (TMDs), *tuned liquid dampers* (TLDs), *friction devices*, *metallic yield devices*, *viscous-elastic dampers*, and *viscous fluid dampers*. As described in the following subsections, these systems require no external power or measurements on structural response. Structures with such systems are smart because such systems can generate a larger damping force when the structural response gets higher. However, passive systems only have a limited control capacity. Some systems, such as TMDs and TLDs, are only effective within a narrow frequency band because they are tuned to the first-mode frequency of the structure. Such dampers can be applied to vibration suppression of structures under wind excitations in which the first mode dominates the response, but they lack the capacity to control seismic response in which multiple modes are significant. Smart structures using passive systems have limited intelligence as they are unable to adapt to the excitation and global structural response. Passive systems depend on the relative structure movement to drive the energy-dissipation mechanism, and dissipated energy can only be related to the local (where the passive device is located) structural response. As noted in Section 1.3, the design specifications for passive damper systems have been officially established. Thus, this book includes one chapter on this subject, focusing on the outline of code specifications, equations,

and numerical illustrations of analysis and design of sample buildings with passive dampers.

1.5.1 Tuned Mass Dampers

Tuned mass dampers, in their simplest form, consist of an auxiliary mass (m_d)-spring (k_d)-dashpot (c_d) system anchored or attached to the main structure, usually on the top of the structure, as shown in Figure 1.9. The basic mechanism of a TMD is a dynamic vibration absorber, as shown in Figure 1.10. The absorber comprises a small mass m_d and a spring with stiffness k_d, and it is attached to the main mass m with spring stiffness k. Under sinusoidal excitation $P_0 \sin \omega t$, the main mass remains stationary when the natural frequency of the attached absorber is equal to the excitation frequency, that is, $\omega_n = \omega_d = \sqrt{k_d/m_d}$ [32]. This external force

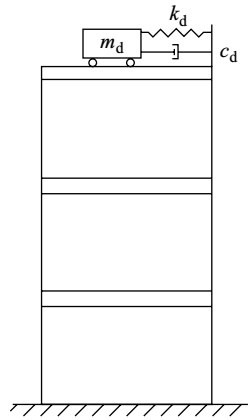

FIGURE 1.9 Tuned mass damper installed on structure.

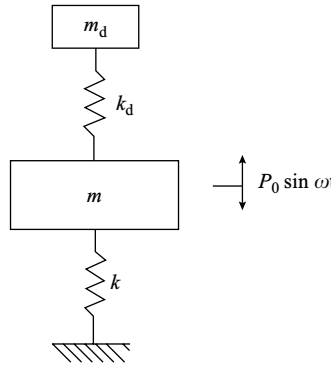

FIGURE 1.10 Undamped dynamic vibration absorber.

$P_0 \sin \omega t$ on the main mass m can be balanced by the restoring force of the small mass m_d.

Dynamic absorbers are widely used in mechanical systems. Application of a dynamic absorber or a TMD to a building structure is more complex as building structures are large and heavy. The TMD responds to structural vibrations, and part of the energy transfers to the vibration energy of the TMD. The TMD damping dissipates its vibration energy, and as a result, the vibration energy of the structure is absorbed by TMD damping. On the basis of the mechanism of the undamped vibration absorber, the energy-absorbing capacity of the TMD is related to the mass ratio of the TMD to the main structure, the stiffness ratio of the TMD to the structure (k_d/k), the frequency (tuning) ratio of the TMD to the structure, the natural frequencies of the TMD and the structure, and the damping ratios of the TMD and the structure. Details can be found in publications by Luft [57], Warburton [87], and Fujino and Abe [36].

A TMD's effect can be viewed as equivalent to changing the damping ratio of the structure itself to a larger value. For responses of lightly damped structures with a dominant mode, TMD can effectively reduce the peak response or resonant component. Given this characteristic, TMDs are increasingly used for wind-sensitive structures to curb excessive building motion and to ensure occupant comfort. Such structures include the CN Tower, Toronto, the John Hancock Tower, Boston, and Citicorp Center, New York City.

Figure 1.11 demonstrates some examples of the many types of TMDs available for practical implementation. The restoring force can be generated by the TMD gravity load (see types a, b, d, and e), by a spring (see types c, d, and f), or by a bearing (see types g and h). The damping force can be achieved by a dashpot (see types b, c, d, and f) or by high-damping materials such as rubber (see type h). For the one-mass pendulum type TMD (see types a and b in Figure 1.11), the vibration period T only depends on the pendulum arm length L ($T = 2\pi\sqrt{L/g}$). In order to tune the TMD frequency to the structural fundamental mode, the pendulum arm often requires too large space. To save the required space, this simple pendulum is modified in such a way that the pendulum period depends on both the pendulum arm length and the other properties. For example, the pendulum arm can be connected to a spring (see type c in Figure 1.11); a two-mass damper (see type d in Figure 1.11) can be used, with one mass sliding on the building floor and the other acting as a pendulum; or the multistage pendulum (see type e in Figure 1.11) can be employed, of which winded hangers reduce the vertical space requirement and keep the same horizontal occupied space. Citicorp Center's TMD system uses sliding mass with a spring and damper.

TMD applicability is still limited by three factors. First, TMDs are effective only for one mode, making them less suited for seismic response control. Second, they are sensitive to mistuning. Third, they occupy a relatively large space. As industrial technology progresses, TMD configurations are being enhanced to address these limitations. An interesting development is to add active capacity to the TMD so that it can be effective for multiple modes of seismic response.

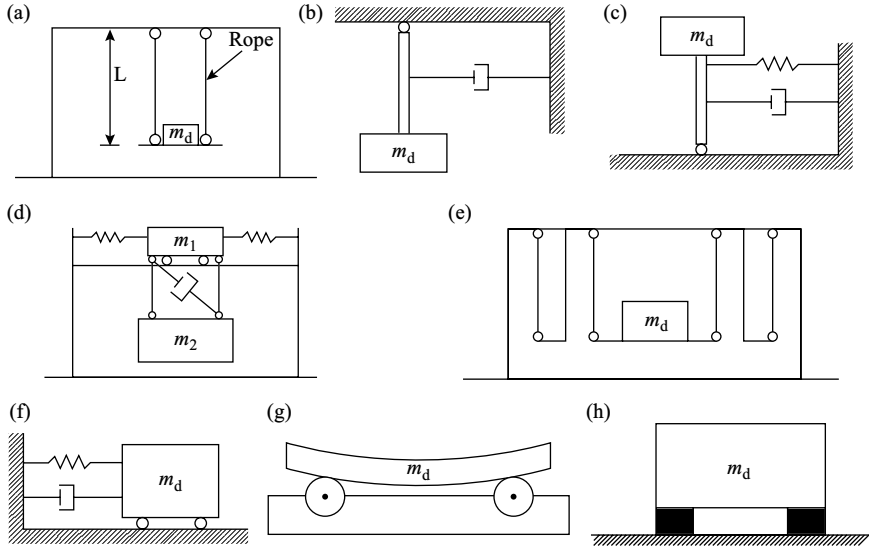

FIGURE 1.11 Typical types of TMDs: (a) simple pendulum, (b) pendulum with damper, (c) inverted pendulum with damper and spring, (d) two-mass damper, (e) multistage damper, (f) sliding mass with spring and damper, (g) swinging mass on rotational bearings, and (h) mass on rubber bearings.

Such devices are called *active mass dampers* (AMDs) and *hybrid mass dampers* (HMDs) described in Sections 1.7 and 1.8, respectively.

1.5.2 Tuned Liquid Dampers

Another type of dynamic absorber for structural vibration suppression is the TLD. In a TLD, water or some other liquid serves as the mass in motion, and the restoring force is generated by gravity. The structural vibration shakes the TLD and induces the liquid movement inside the container. The turbulence of the liquid flow and the friction between the liquid flow and the container convert the dynamic energy of the fluid flow to heat, thus absorbing structural vibration energy. Note that a TLD has the same basic principle as a TMD to absorb structural vibration energy, and neither one has complex mechanisms. The difference is that all characteristics of a TLD's auxiliary system—mass, damping, and restoring mechanisms—are provided by the liquid.

While TLDs were initially applied in ships, their application for vibration control of civil engineering structures began in the 1980s [9]. Figure 1.12 shows two typical types of TLDs. The *sloshing damper* places meshes or rods in the liquid to provide damping capacity, and its natural frequency is adjusted by the size of the container or depth of the liquid. The *column damper* generates high-flow turbulence through the orifice to provide damping capacity, and its

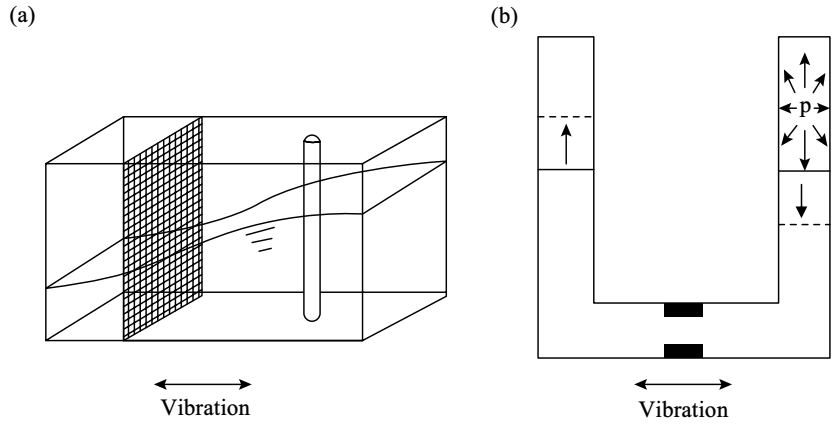

FIGURE 1.12 Tuned liquid dampers: (a) sloshing damper with meshes and rods and (b) column damper with orifice.

natural frequency is adjusted by column shape and air pressure. The column TLD can be adapted to crossed-tube containers for reducing structural vibration in any direction.

Similar to TMDs, TLDs have been used to suppress wind-excited vibrations of tall structures, such as airport towers and tall buildings [85]. Such structures include the Nagasaki airport tower, the Yokohama marine tower, and the Tokyo air traffic control towers at Haneda and Narita airports. TLDs have two advantages. A single TLD can be effective in any direction of lateral vibrations, and water used for TLD can serve a dual purpose as part of the building's fire protection supply. On the other hand, TLDs have two unfavorable properties. They require more space because liquids have less mass density than do the materials for TMD, such as concrete or steel. TLDs also exhibit a highly nonlinear response due to liquid sloshing and/or orificing. This inherent nonlinearity complicates the analysis and design process for TLD systems; thus, many research efforts have focused on their optimum parameters and nonlinearity.

1.5.3 Friction Devices

Friction is an effective, reliable, economical, and widely applied mechanism to dissipate kinetic energy by converting it to heat. This friction mechanism for energy dissipation has been utilized to develop dampers for structural vibration suppression. To achieve this essential friction, the damper must have two solid bodies that slide relative to each other.

In the early 1980s, Pall and Marsh [66] pioneered passive friction dampers on the basis of the model of friction brakes. Since then, considerable progress has been made in friction devices, and their behavior has been studied analytically and experimentally. Figure 1.13 illustrates several types of friction devices developed around the world. Pall and Marsh's *X-braced friction damper* [67] is shown in

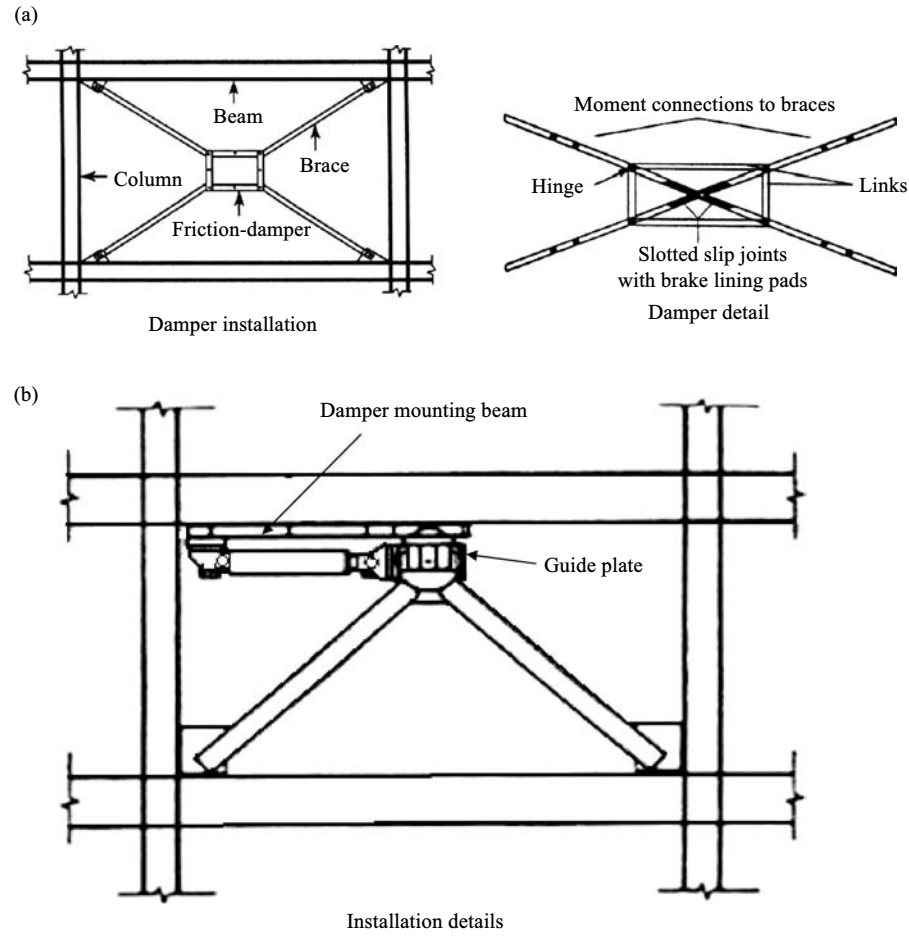

FIGURE 1.13 Typical types of friction dampers: (a) X-braced friction damper and (b) Sumitomo friction damper.

Figure 1.13a. *Slotted slip joints* provide consistent force resistance via friction by brake lining pads installed between the steel plates. When a seismic load is applied, the compression brace and tension brace induce slippage at the friction joint, and energy is thus dissipated. Figure 1.13b shows a Sumitomo friction damper [2,3] mounted on K-bracing. When the structure vibrates, relative movement between the structure and the brace drives the copper alloy friction pads as they slide along the inner surface of the cylinder's steel casing. Resistant force is then produced through the action of the spring against the inner and outer wedges. Nims et al. [64] developed a more sophisticated *energy-dissipating-restraint* (EDR) device dissipates energy on the interface between the bronze friction wedges and the steel cylinder wall. With an EDR, the structure vibrates and induces movement of the spherical rod. Then the combination of wedges, stops, and inner springs

produces friction proportional to the displacement of the device's edges. A friction device, proposed by Fitzgerald et al. [35], utilizes *slotted bolted connections* in concentrically braced frames. Sliding between structural steel components generates friction and dissipates energy. Extensive studies have been conducted on friction dampers, which has led to their practical application for structural seismic protection [2,78].

Friction dampers are simple to construct and effective for seismic protection. However, it is very difficult to maintain their mechanical properties over prolonged time intervals. In particular, corrosion, deformation due to temperature changes, and relaxation of the sliding metal interface jeopardize the friction-generating capacity of the damper. Moreover, friction dampers behave nonlinearly and are difficult to analyze and design. These two weaknesses limit the application of friction dampers.

1.5.4 Metallic Yield Devices

Inelastic deformation of metallic materials is another effective mechanism for energy dissipation. The traditional seismic-resistant design of structures depends on postyield ductility of structural members to dissipate earthquake input energy. This concept led to the idea of installing separate *metallic hysteretic devices* in a structure to absorb seismic energy. In the 1970s, conceptual and experimental work on metallic yield devices began [47,75]. Since then, development, testing, analytical modeling, and practical implementation of metallic yield dampers have progressed considerably [80,86,88]. Several kinds of metallic yield devices have been developed, of which two models are sketched in Figure 1.14. The device in Figure 1.14a dissipates energy by material hysteretic behavior in inelastic tensile deformation of the rectangular steel frame in the diagonal direction of the tension brace. Buckling of the bracings is not a concern as it rarely happens. This is because the compression brace disconnects and has a small effective length, and the buckling critical load is designed to be higher than the yielding load [86]. The other model is called *added damping and stiffness* (ADAS) as shown in Figure 1.14b, which consists of multiple X-steel plates, and yielding occurs over the entire length of the device. Rigid boundary members are used such that the X-plates are deformed in double curvature. Implementation of metallic yield dampers for full-scale structures began in New Zealand in the 1970s. Since then, various metallic yield devices have been used to improve the seismic-resistant design of new structures or to upgrade the seismic-resistant capacity of existing structures [2,47,60].

Metallic yield devices generally have stable hysteretic behavior, low-cycle fatigue, long-term reliability, and relative insensitivity to environmental temperature. However, they do not absorb much energy during their initial elastic behavior. Energy dissipation occurs after large inelastic deformation happens. Moreover, metallic yield dampers behave nonlinearly; they increase structural strength in addition to damping. This behavior complicates analysis and requires an iteration design process.

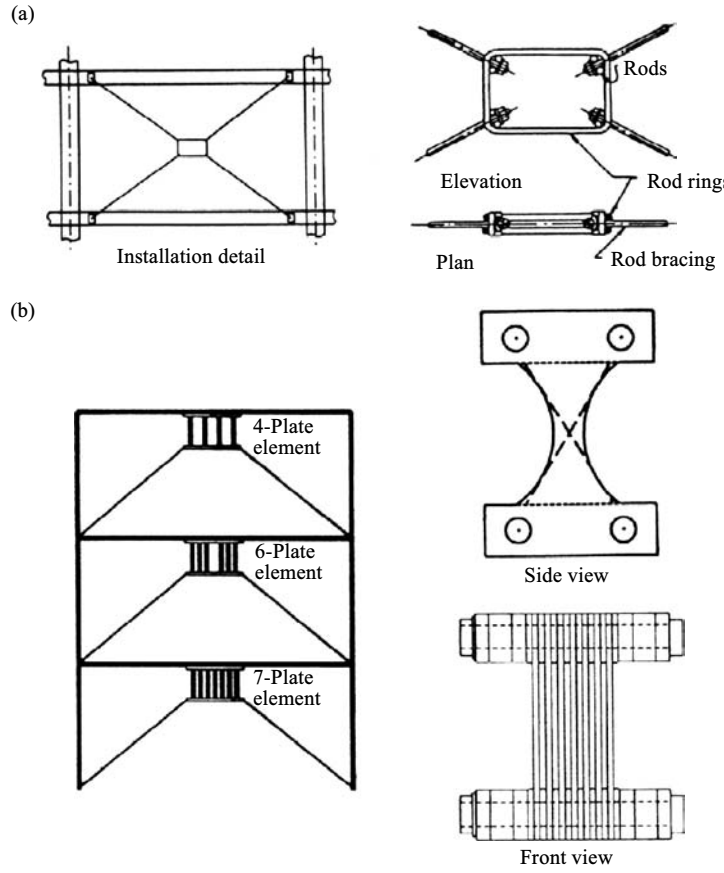

FIGURE 1.14 Typical types of metallic yield dampers: (a) Tyler's yielding steel bracing system and (b) added damping and stiffness (ADAS) device.

1.5.5 Viscoelastic Dampers

Viscoelastic (VE) dampers utilize high damping from VE materials to dissipate energy through shear deformation. Such materials include rubber, polymers, and glassy substances. A typical VE damper consists of VE layers bonded to steel plates as shown in Figure 1.15a. VE damper components are mounted on a structure as part of the chord (see Figure 1.15b) and the diagonal bracing system (see Figure 1.15c), respectively. Shear deformation occurs and energy is dissipated when the structural vibration induces relative motion between the outer steel flanges and the center plate. Applications of VE dampers can be found in References 31 and 78.

As noted, TLDs, friction dampers, and metallic yield dampers are all characterized by nonlinearity. VE dampers offer a distinct advantage in that they generally behave linearly as they use linear VE materials, which simplifies the analysis and design process. This linear behavior also enables VE dampers to absorb vibration

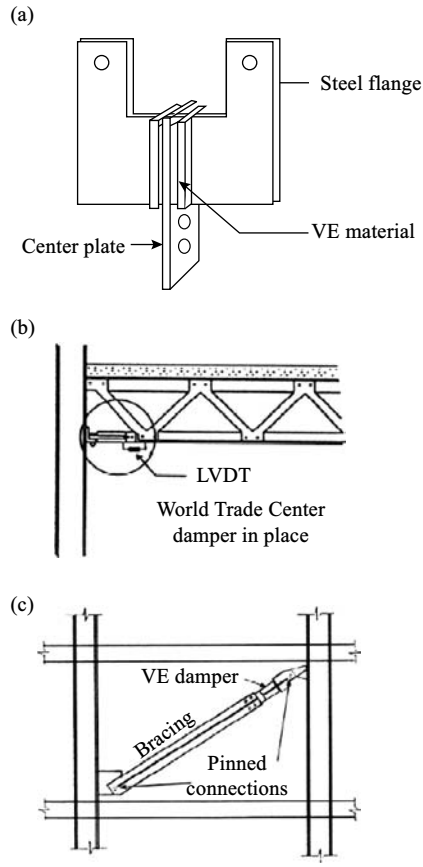

FIGURE 1.15 Viscoelastic (VE) damper: (a) damper detail, (b) installation as chord, and (c) installation as diagonal bracing.

energy caused by either severe earthquakes or small excitations such as wind, traffic, or mild earthquakes. However, VE dampers have the disadvantage of being frequency and temperature dependent. This can present a problem in the design process because the properties of VE materials can only be expressed by *shear storage modulus* (measure of the energy stored and recovered per cycle) and *shear loss modulus* (measure of the energy dissipated per cycle).

1.5.6 Viscous Fluid Dampers

Recall that metallic, friction, and VE dampers all utilize the action of solids to enhance the performance of structures subjected to environmental excitations. Use of viscous fluid for shock and vibration mitigation is familiar to heavy industry and the military. For example, automotive shock absorbers were invented in the

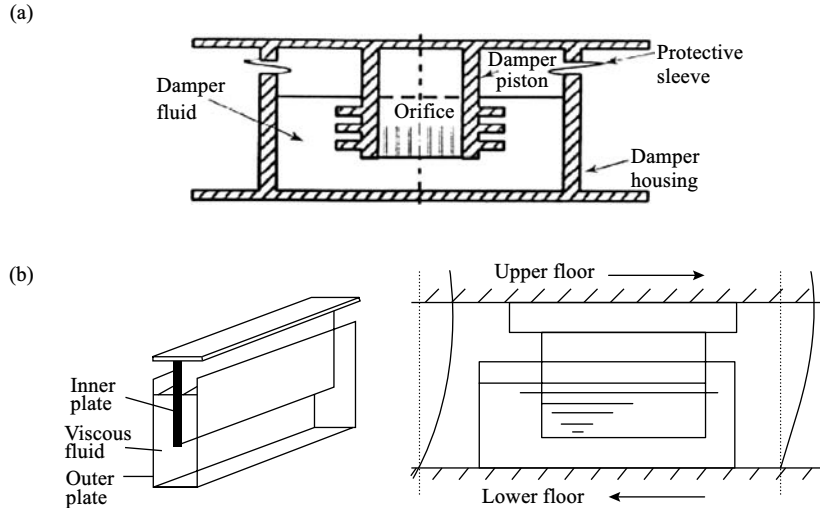

FIGURE 1.16 Typical types of viscous fluid dampers: (a) GERB viscous fluid damper and (b) viscous damping wall.

early 1900s. In the 1970s, the first full-scale implementation of viscous fluid dampers was done for bridges in Italy [78]. In the 1980s, significant efforts were made toward the conversion of this industrial technology for civil engineering structures. These efforts led to the development, analysis and modeling, and testing and full-scale implementation of viscous fluid dampers.

The most promising design of *viscous fluid dampers* is shown in Figure 1.16. A straightforward design is achieved with classical dashpot, and dissipation occurs by converting kinetic energy to heat as a piston moves and deforms a thick, highly viscous fluid. This viscous fluid damper (see Figure 1.16a) was first manufactured by GERB Vibration Control and used as a component of seismic base-isolation systems [39]. The relative movement of damper piston to damper housing drives the viscous damper fluid back and forth through the orifice. Energy is dissipated by the friction between the fluid and the orifice. This kind of damper configuration can provide motion and energy dissipation in all six degrees of freedom as vibration in any direction can shake the viscous fluid. An alternative design for superstructures (see Figure 1.16b), the viscous damping wall (VDW), was developed by the Sumitomo Construction Company in Japan [8]. The VDW's piston is a steel plate constrained to move in its plane within a narrow rectangular steel container filled with viscous fluid. To install a VDW, the piston is attached to the floor above, and the container is fixed to the floor below. Interstory motion deforms the fluid; thus, the friction between the inner plate and the viscous fluid dissipates energy. In order to be effective, these dampers must employ fluids with high viscosities. During the 1990s, modeling of viscous fluid dampers advanced. Macroscopic models were developed for structural application on the basis of the theory of fluid dynamics, the constitutive law of viscous fluid, and experimental investigation [25,30,55,59,70].

Similar to VE dampers, viscous fluid dampers behave linearly but are temperature and frequency dependent. High-strength seals are required to prevent viscous fluid from leaking. Cost remains relatively low while effectiveness is high. Thus, viscous fluid dampers hold promise for civil engineering structure applications.

1.6 Semiactive Damper Systems

Semiactive dampers are a natural evolution of passive energy-dissipating technology as they incorporate adaptive systems to improve effectiveness and intelligence. They are frequently referred to as controllable or intelligent dampers. Their adaptive system gathers information about the excitation and structural response and then adjusts the damper behavior on the basis of this information to enhance its performance. A semiactive damper system consists of sensors, a control computer, a control actuator, and a passive damping device. The sensors measure the excitation and/or structural response. The control computer processes the measurement and generates a control signal for the actuator. Then the actuator acts to adjust the behavior of the passive device. Note that the actuator is used to control the behavior of the passive device instead of applying a force directly onto the structure; thus, it only requires a small power supply such as batteries. This is a great advantage because the main power source to the building structure may fail during seismic events, and the actuator does not have any harmful potential such as destabilization of the structure. Although semiactive dampers are a bit more complex than passive dampers, they are still easy to manufacture, reliable to operate, and capable of performing better than passive dampers. The control capacity of semiactive dampers is still limited as they can only operate within the maximum capacity of corresponding passive devices.

Semiactive dampers were proposed earlier as automobile shock absorbers in the 1920s [44]. They were then the subject of extensive research in mechanical engineering, primarily for automotive applications. In the 1980s, their application to vibration control of civil engineering structures was considered. The research introduced the concept of semiactive dampers for wind-response control applications [38]. In the 1990s, this concept was introduced for seismic response control. Semiactive control systems are less advanced than passive control systems. However, because semiactive dampers combine the advantages of both passive and active control systems with small additional cost compared to passive dampers, they appear to be a promising approach for seismic response control of civil engineering structures.

1.6.1 Semiactive Tuned Mass Dampers

In 1983, Hrovat et al. [38] proposed a *semiactive TMD* for control of wind-induced vibrations in tall buildings (see Figure 1.17). This system consists of a TMD and an actuator installed on top of the main structure. The semiactive TMD has mass

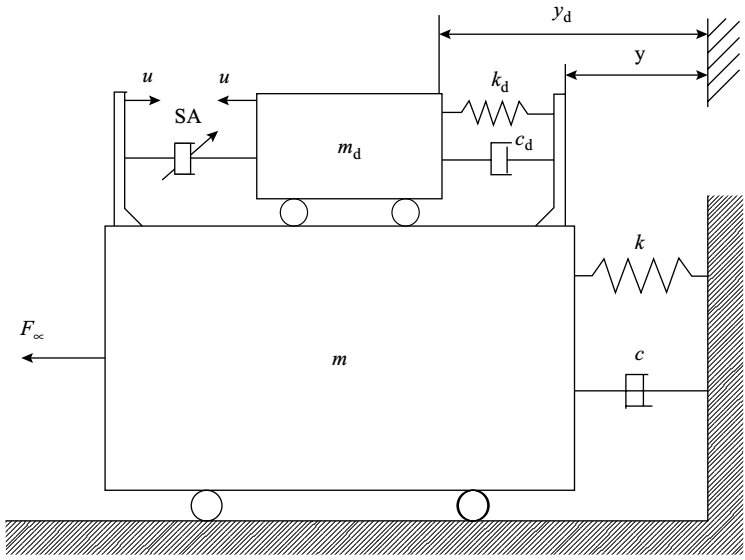

FIGURE 1.17 Semiactive TMD.

m_d, damping c_d, and stiffness k_d, while the main structure is represented by mass m, damping c, and stiffness k. The actuator, denoted by SA, generates the control force u. The control force u adjusts TMD damping such that it is always optimal to ever-changing excitation. Since the TMD mass m_d is much smaller than the structural mass m, and the active control force is used to change the damping force of the TMD (which is much less than the inertial force of the TMD), a small amount of external power is required to achieve this adjustment. Semiactive TMDs are still in the stage of research and development.

1.6.2 Semiactive Tuned Liquid Dampers

The *semiactive TLD* simply regulates the tuning of the liquid in operation. On the basis of the two major types of TLDs discussed in Section 1.5.2, researchers have developed the semiactive sloshing TLD and the column TLD. The semiactive sloshing TLD, as proposed by Lou et al. in 1994 [56], added a set of rotatable baffles in the liquid tank of a sloshing TLD. An actuator is used to adjust the orientation of these baffles on the basis of predefined algorithms. When the baffles are in the horizontal position, the liquid tank maintains its original length. When the baffles are in the vertical position, the liquid tank is divided into a number of shorter tanks. Since the natural frequency of the contained liquid changes with tank length, the tuning of the TLD can be controlled by rotating the baffles to a desired inclined position. With this mechanism, no powerful actuator is required as it is only used to rotate the light-weight baffles. TLD performance can thus be improved at low cost. The semiactive column TLD, as proposed by Yalla and Kareem in 2002 [89],

uses a variable orifice in a column TLD to maintain optimal damping conditions. An electropneumatic actuator is utilized to drive a ball valve to change the cross-section of a column TLD according to the control algorithm, thus adjusting the damper properties to achieve better performance. Similar to semiactive TMDs, semiactive TLDs remain a focus of research and device development.

1.6.3 Semiactive Friction Dampers

Akbay and Aktan developed a *semiactive friction damper* in 1991 [5] by using an electromechanical actuator. This device is based on a friction damper that consists of a preloaded friction shaft rigidly connected to the structural bracing. The brace applies a preloaded normal force to the friction interface of the device, and the energy is dissipated via friction. An electric motor is employed to drive the actuator piston that applies compression (normal force) to the friction interface. Since the friction force is proportional to the normal force, adjusting the movement of the actuator piston controls the friction force and damping capacity of the damper. By regulating the normal compression force through an optimal control algorithm, the friction is mechanically adjusted so as to achieve better performance.

Chen and Chen [12] have developed another type of semiactive friction damper by using *PZT actuators*. Owing to their strong electromechanical coupling property, smart PZT materials can generate a significant amount of stress when exposed to an electric field and subjected to a restraint in their motion. With this smart property, PZT materials have been widely used in mechanical and aerospace industries to suppress excessive structure vibration. However, the limited actuating capacity of PZT actuators makes them unable to directly control wind and seismic response of large civil engineering structures. Thus, the smart feature of PZT materials was employed to improve the effectiveness of passive friction dampers. This concept led to a *piezoelectric friction damper* (PFD). As shown in Figure 1.18, the PFD consists of four preloading units, four PZT stack actuators, a friction component, and a steel box housing other components. The friction component has a thin sheet of steel with friction material (brake linings) bonded to its top and bottom surfaces. When the PFD is installed on a structure, relative movement of the isolation plate and the bottom plate causes friction and thus dissipates energy. The PZT stack actuators are located directly above the isolation plate, and the actuation force serves as a normal force to the friction surface. By adjusting the electric field on the PZT actuators according to a predetermined algorithm, the normal force and thus the friction control force are regulated to enhance real-time effectiveness of the friction device. A semiactive control algorithm was developed for the PFD, and shaking table tests were conducted for a three-story steel structure model with PFD installed between a K-bracing support and the first floor [12]. Numerical simulations and experimental results both indicate that the PFD not only effectively suppresses structural vibration but also adapts to varying excitations from weak to strong earthquakes.

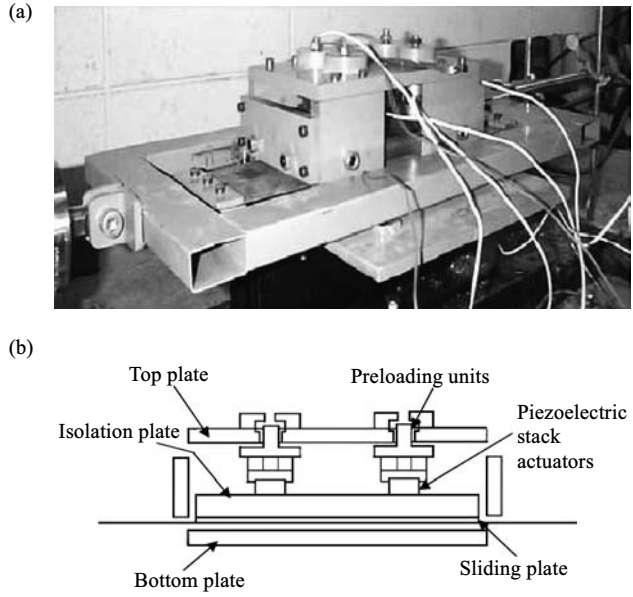

FIGURE 1.18 Piezoelectric friction damper: (a) view and (b) schematic.

Semiactive friction dampers have guaranteed energy dissipation by friction. The adaptive feature enhances the damper's behavior, and they operate with low energy and do not cause instability of the controlled structures. More research is needed for engineering application.

1.6.4 Semiactive Vibration Absorbers

One effective method to achieve a controllable damping device is to use a variable-orifice valve to adjust the flow of a hydraulic damper. This concept led to the emergence of *semiactive vibration absorbers* (SAVA), also called *semiactive hydraulic dampers* (SAHD). As shown schematically in Figure 1.19, such a device provides adjustment of both damping and stiffness. The damping capacity is generated from the viscous fluid, and the stiffness is adjusted by the opening of the flow valve. If the valve is closed, the SAVA works as a stiffness spring. If the valve is open, the fluid can easily flow through the tube and provides little stiffness to the structure. SAVA was applied to automobiles for improved ride and road-holding [43]. Applications of SAVA to buildings and bridges include experiments for seismic response control and implementation [68,69,80].

1.6.5 Semiactive Stiffness Control Devices

A *semiactive variable-stiffness* (SAVS) system, also called a *variable-stiffness device* (VSD) by the authors, has been studied and implemented in Japan [52]. As

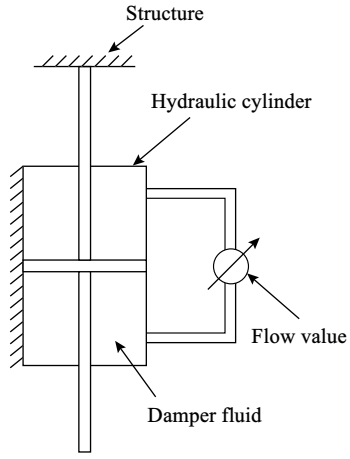

FIGURE 1.19 Schematic of semiactive vibration absorbers.

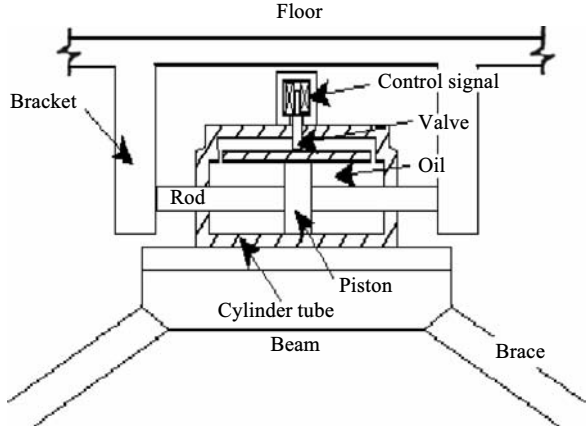

FIGURE 1.20 Semiactive variable-stiffness device.

shown schematically in Figure 1.20, this device is mounted on a bracing system of the structure. The VSD consists of a balanced hydraulic cylinder, a double-acting piston rod, a normally closed solenoid control valve, and a tube connecting the two cylinder chambers. The solenoid valve can be set open or closed. When the valve is open, fluid flows freely and disengages the beam–brace connection, thus decreasing structural stiffness. When the valve is closed, the fluid cannot flow and effectively locks the beam to the brace, thus increasing structural stiffness. With this mechanism, a VSD adjusts the stiffness of the structure's bracing system so as to minimize resonant-type structural responses during earthquake events.

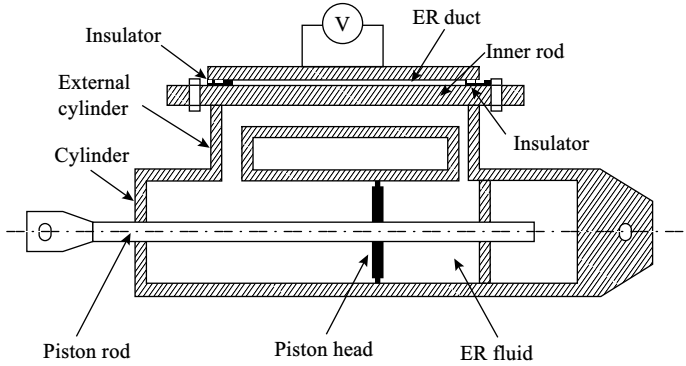

FIGURE 1.21 Schematic of ER damper.

1.6.6 Electrorheological Dampers

ER dampers use smart ER fluids that contain dielectric particles suspended within nonconducting viscous fluids (such as oil) absorbed onto the particles. When the ER fluid is subjected to an electric field, the dielectric particles polarize and become aligned, thus offering resistance to the flow. ER fluids are capable of undergoing dramatic reversible increases in resistance to flow; they can reversibly change from free-flowing linear viscous fluids to semisolids with controllable yield strength in milliseconds. Adjustment of the electric field can therefore easily regulate the behavior of ER fluids.

Researchers have proposed ER dampers that take advantage of the smart property of ER fluids to regulate the damping-force generation. The damping force generated by the ER damper is adjusted by varying the strength of the electric field according to a predefined control algorithm. A sample ER damper, which has a cylinder containing a balanced piston rod and a piston head, is shown in Figure 1.21. The head pushes the ER fluid through a stationary annular duct between the inner rod and the external cylinder. The voltage gradient, V, between the inner rod and the external cylinder generates an electric field applied to the ER fluid. Adjustment of the voltage V alters the electric field and thus controls the behavior of the ER fluid and regulates the damping capacity of the ER damper. Dynamic energy is dissipated owing to both the shearing of the fluid (ER effect) and the orificing of the viscous fluid (friction effect) [58].

ER dampers are still under research and development. Researchers have formulated a dynamic model on the basis of experimental results [10] and have developed a large-scale ER damper with a capacity of 445 kN [58]. Three factors limit the ER dampers for seismic response control of large civil engineering structures. First, the ER fluids have very limited yield stress (usually a maximum yield stress of 5–10 kPa). Second, common impurities that might be introduced during manufacturing may reduce the capacity of ER fluids significantly. Third, high-voltage

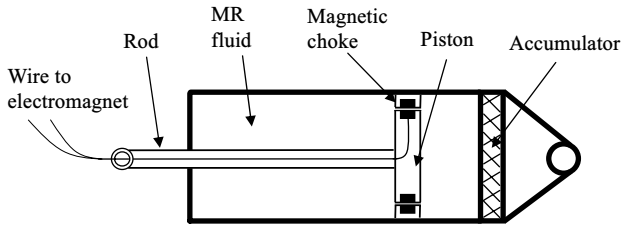

FIGURE 1.22 Schematic of MR damper.

(about 4000 V) power supplies required to control the ER fluid may result in safety, availability, and cost issues.

1.6.7 Magnetorheological Dampers

Magnetorheological dampers use smart MR fluid, which is a magnetic analog of ER fluid and typically consists of micron-size, magnetically polarizable particles dispersed in a viscous fluid, such as silicone oil. When the MR fluid is exposed to a magnetic field, the particles in the fluid polarize, and the fluid exhibits viscoplastic behavior, thus offering resistance to the fluid flow. MR fluid is also characterized by its ability to undergo reversible change from a free-flowing linear viscous fluid to a semisolid in milliseconds when subjected to a magnetic field. By varying the strength of the magnetic field according to a predefined algorithm, the control force generated by the MR damper can be adjusted accordingly. In comparison with ER fluids, MR fluids offer advantages of high-yielding strength (on the order of 50–100 kPa), insensitivity to contaminants, and stable behavior over a broad temperature range [81].

As illustrated schematically in Figure 1.22, the prototype of this MR damper is an orifice damper, and the energy is dissipated by orificing. However, this damper uses hydrocarbon oil randomly dispersed with micron-size, magnetically soft iron. The magnetic field is applied perpendicular to the direction of fluid flow, and an accumulator compensates the fluid volume change. Shaking table tests have been conducted for a three-story steel structure model with an MR damper installed in the first story. Test results show the damper behaves similar to a combination of a Coulomb damper and a viscous damper. A dynamic model of this MR damper was developed on the basis of test results and then implemented [91].

1.6.8 Semiactive Viscous Fluid Damper

A *semiactive viscous fluid damper* for structural seismic response control is illustrated schematically in Figure 1.23. Analytical and experimental studies have been conducted. This device uses a normally closed solenoid valve to control the intensity of the fluid through a bypass loop. Energy is dissipated through friction between the flow, the bypass loop, and orifices in the piston head. When the opening of the valve is large, the fluid can easily flow through the valve, and less damping

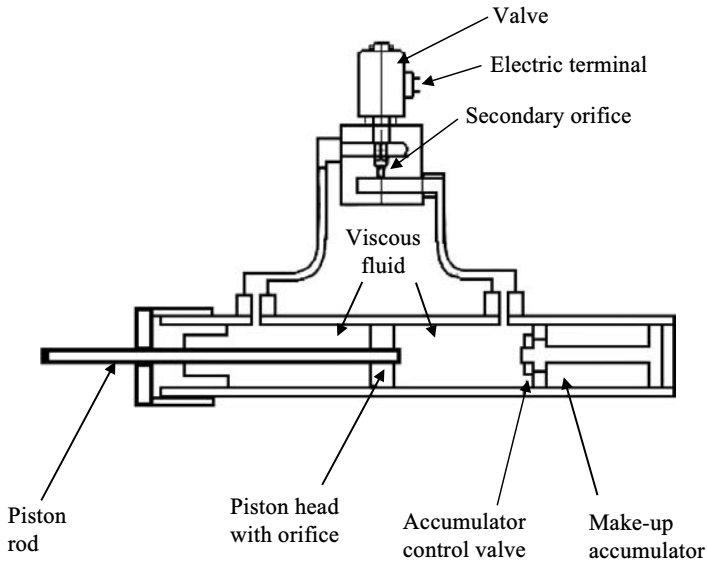

FIGURE 1.23 Construction of semiactive viscous fluid damper.

force develops. When the opening is small, the fluid cannot easily flow through the valve, and the damper provides greater control force. Damper behavior is controlled by adjusting the valve opening according to the control algorithm. Little external power supplied from the electric terminal is required [74,84]. The concept was utilized for a case study of bridge experiments [45].

1.7 ACTIVE CONTROL SYSTEMS

Sections 1.5 and 1.6 have discussed smart structures using passive and semiactive control systems. Both systems are cost-effective and reliable to operate, but their capacity and/or intelligence are limited for structural seismic response control. Passive systems have simple mechanisms and are easy to manufacture, but they are not sufficiently adaptive to ever-changing external excitation because they neither sense excitation and response nor use external power. Some of them, such as TMDs and TLDs, are only effective for the suppression of structural responses with one dominant mode, such as wind-induced structure vibrations. Semiactive dampers have an adaptive system incorporated, but they can only operate within the maximum capacity of the passive devices on which they are based. Thus, there is clearly a need for a more powerful adaptive system to protect structures from excessive vibrations and damages by strong earthquakes where multiple modes are significant in structural response. This has led to the emergence of smart structures with active seismic response control. This innovative technique uses special devices, such as electrohydraulic actuators, to generate the required

control force against earthquake loading by feeding back the measured structural response. This control force can serve as extra damping, thus reducing structural vibration under traffic, wind, and earthquake excitations.

Active control systems have been widely used to suppress noises and structural vibrations in mechanical and aerospace industries. Their application to large civil engineering structures is an innovative area under research and development [14,19,22,61,76]. Active seismic response control has received considerable attention in recent years owing to its following advantages:

- Enhanced control effectiveness. In theory, active systems can be as powerful as desired. In practice, the degree of control effectiveness is limited only by the actuator capacity. Modern industry can produce actuators capable of generating much larger control forces than passive or semiactive dampers.
- Adaptability to ground motion. An active control system can sense the ground motion and then adjust its control efforts.
- Selectivity of control objectives. The control system can be designed for various objectives, such as structural safety or human comfort.
- Applicability to different excitation mechanisms. Active control covers a wide frequency range, that is, all significant modes of the structure. An active control system can effectively reduce structural response under wind and/or earthquake excitations.

Although active structural control is a new area with less research and development than passive structural control, great advances have been made owing to its powerful capacity and adaptability. Advances continue to be made on active seismic response control as shown by a number of publications [26,40,80]. Active seismic response control has reached a stage of practical applications. Researchers have developed several active control devices, such as active tendon, AMD, active bracing, and pulse generation systems.

1.7.1 Basic Configuration of Active Control Systems

An *active control system* is fully adaptive. Smart structures using active control systems employ external power to generate the control force, which is directly applied to the structure to reduce its response. Since building structures are usually large, huge force-generating equipment and large external power supplies are required for active seismic response control. Thus, an active seismic response control system is usually designed mainly to increase structural damping with minor modifications of structural stiffness, as discussed in Section 1.2. Figure 1.24 schematically illustrates the basic configuration of such a system, which consists of three types of elements: sensor(s), actuator(s), and a controller with a predetermined control algorithm.

Sensors in a smart structure system are similar to sensing organs in the human body. The sensor(s) can be located at the structural base to measure external

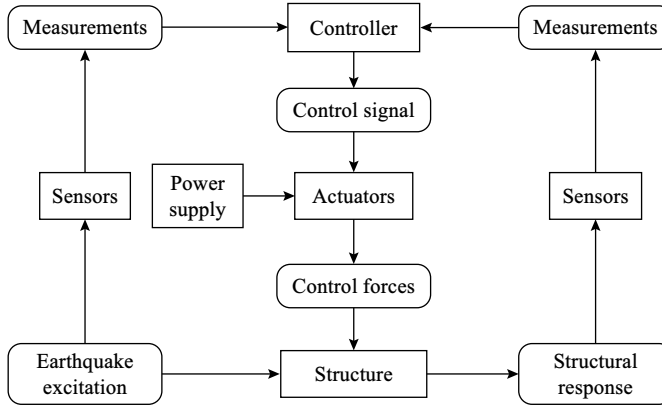

FIGURE 1.24 Schematic diagram of an active control system.

excitation or installed on the structure and/or the control device to measure system response variables, such as displacements, velocities, accelerations, and control forces. Control devices may also have built-in sensors to monitor their behavior. For example, a hydraulic actuator may have a built-in displacement sensor to measure the relative displacement of the actuator piston vis-à-vis the cylinder. *Linear variable differential transformers (LVDTs)*, *velocity transducers*, *accelerometers*, and *load cells*, which measure displacement, velocity, acceleration, and force, respectively, are common sensors for smart structure systems. These sensors can work as linear proportional devices in the frequency range of 0.1–100 Hz, which covers the frequency band of structural vibration under seismic or wind excitations. Sensor output is usually in the form of voltage signals that are sent to the controller for processing.

The *controller* in a smart structure system is similar to the human brain. It receives measurements from sensors, analyzes them, and generates necessary *control signals* (also called *control commands*) to drive the actuator on the basis of a predetermined *control algorithm*. Thus, the controller is an information processor that produces actuation signals by a feedback function of sensor measurements. In the design stage, the mathematical model of the controller is formulated by control theory, and the feedback control law is determined by control algorithms. For physical implementation, there are analogous and digital controllers. *Analogous controllers* are devices that implement a feedback control law formulated in a continuous-time domain; all physical components of such a controller work in a continuous way. *Digital controllers* have a control computer as the main component. Owing to advances in microelectronics, digital technology has surpassed that of the analogous controller. Figure 1.25 shows the configuration of a digital control computer, which may consist of analog/digital (A/D) and digital/analog (D/A) converters. A continuous-time-domain signal from sensors is sampled by an A/D converter. The signal is changed into a sequence of measured output values that represent each sampling instance. The digital controller then uses those values

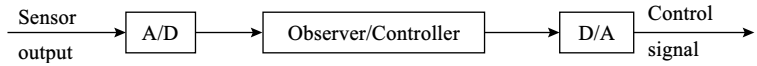

FIGURE 1.25 Configuration of digital control computers.

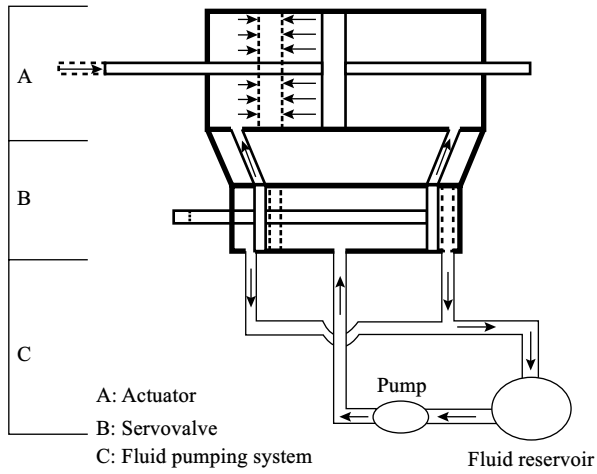

FIGURE 1.26 Servovalve-controlled hydraulic actuator.

to calculate a desired value for the control sequence. This sequence is converted into another continuous-time signal by a D/A converter to feed the actuators. If there are too few sensor measurements as feedback for the controller, an *observer* is used to estimate unmeasured system response.

When only the structural response variables are continually measured, the control configuration is referred to as *feedback control* because these measurements are used to make continual corrections to the applied control forces. When only earthquake inputs are measured, a *feed-forward control* can be achieved, and the control forces are regulated by the measured excitation.

Actuators are similar to the hands and feet of the human body. Actuators produce the required control forces according to the control signals from the brain—the controller. For seismic response control, the large size of civil engineering structures necessitates sizable actuators capable of generating a large control force. Electrohydraulic actuators and pulse generators are among the choices, and they both use external power sources. Figure 1.26 shows a schematic of the servovalve-controlled hydraulic actuator used by smart structure systems for seismic response control.

1.7.2 Active Mass Damper Systems

An AMD is also called an *active mass driver*. It evolved from TMDs with the introduction of an active control mechanism. As noted, TMDs are only effective

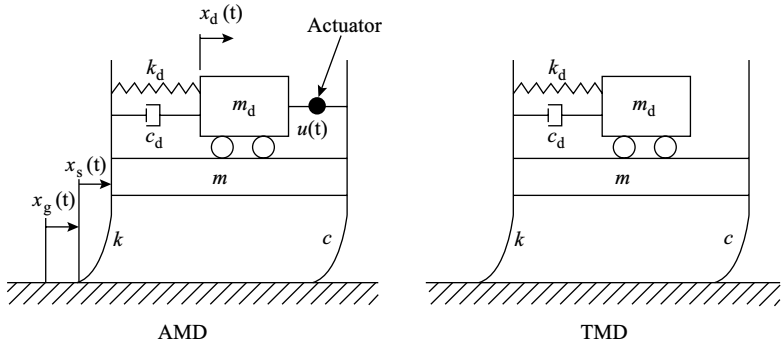

FIGURE 1.27 Schematic comparison of smart structures using active mass damper (AMD) and tuned mass damper (TMD).

for structural response control when the first mode is dominant, such as wind-induced structural vibration. Development of AMDs focuses on seeking control of structural seismic response with a wide frequency band. It is expected that structures with AMDs will demonstrate enhanced effectiveness over structures with TMDs. A conceptual model of an AMD-controlled structure is shown in Figure 1.27, with a schematic comparison of AMDs and TMDs. One actuator is installed between the primary (i.e., structure) and the auxiliary (i.e., TMD) systems. The motion of the auxiliary system can be controlled by the actuator to augment the control effectiveness.

AMDs were proposed in the early 1980s and have been studied analytically [11,65]. As shown in the conceptual model (see Figure 1.27), an actuator is installed on the AMD-controlled structure. This actuator is placed between the primary (i.e., structure) and the auxiliary (i.e., AMD) systems. The motion of the latter can be controlled by the actuator to augment the system's control effectiveness. Analytical study is aimed at how to operate the actuator to subdue response of the primary system most effectively with the *optimum control law* to find the appropriate feedback gain of the AMD in order to obtain optimal control input [11,18,19,21,65]. Researchers have also conducted numerous shaking table tests on AMD systems for seismic response control and full-scale AMD system implementation [4,29,76,80].

AMDs have an economic advantage in full-scale structures because far less control force and a much smaller actuator are required than for other active systems. The actuator in an AMD is used to drive the auxiliary mass, while the actuator in other active systems usually acts on the structure directly. However, the control effectiveness of an AMD is felt mainly at the fundamental frequency and less so at higher frequencies [93].

1.7.3 Active Tendon Systems

Active tendon control systems consist of a set of prestressed tendons whose tension is controlled by electrohydraulic servomechanisms. Figure 1.28 shows a typical

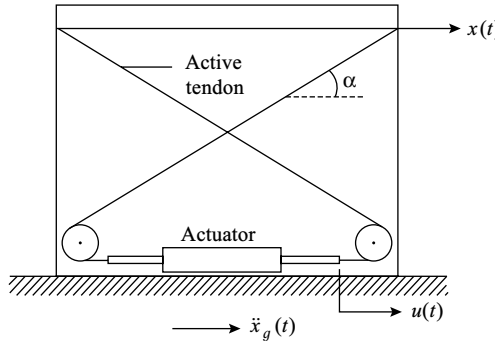

FIGURE 1.28 Schematic diagram of active tendon system.

configuration of an active control system using active tendons. Active tendons are installed between two stories of a building structure. The actuator cylinder is attached to the floor below. One end of the tendon is connected to the upper floor and the other end to the actuator piston. Under the earthquake excitation, the structural vibration induces interstory drift that drives the relative movement of the actuator piston to the actuator cylinder. This relative movement changes the tension of the prestressed tendons, thus applying dynamic control force to the structure to reduce its seismic response.

Active tendon control has been studied analytically [14,17,22,92] and experimentally [29]. Full-scale implementation of an active tendon system on a 6-story, 600-ton building has been tested in Tokyo, Japan [76]. Both experimental and simulation results show a significant reduction of seismic response of smart structures using active tendon systems.

Active tendons can operate in both the pulsed- and the continuous-time modes. Thus, active tendon control can accommodate both continuous-time and pulse control algorithms. Another advantage is that tendons of this system can use existing structural members, which minimizes the need for additions and modifications to the structure.

1.7.4 Active Brace Systems

An *active bracing system* uses existing structural braces to install an active control device (i.e., actuator) onto a structure. Three types of bracing systems—diagonal, K-braces, and X-braces—can be used, the same as those for passive dampers. Servovalve-controlled hydraulic actuators capable of generating a large control force are mounted on the bracing system between two adjacent floors. Figure 1.29 shows an active brace control system with a hydraulic actuator mounted on a K-brace. The actuator cylinder is bolted to the structural floor, and the actuator piston is connected to the brace. This system consists of a servovalve, a servovalve controller, a hydraulic actuator, a hydraulic power supply, sensors, and a control computer with a predetermined control algorithm. Sensors measure structure

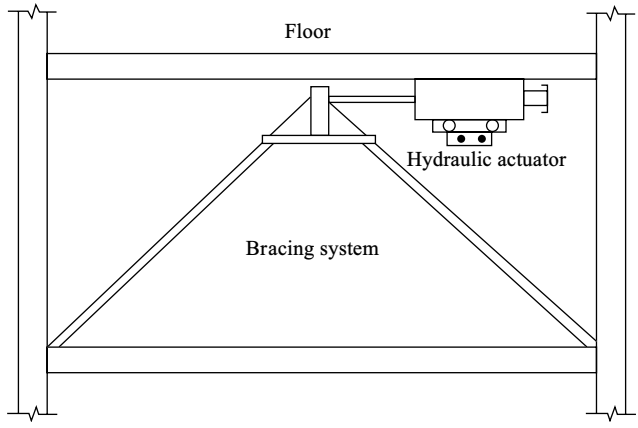

FIGURE 1.29 Active bracing system with hydraulic actuator.

motion due to the earthquake excitation. The control computer uses the control algorithm to process these measurements and to generate the control signal. The servovalve then uses the control signal to regulate flow direction and intensity, which yields a pressure difference in the two actuator chambers. The control force is thus generated by the pressure difference to resist seismic loads on the structure.

Active bracing systems have been studied analytically [23,76] and experimentally [79]. Active bracing systems offer the same advantage as active tendon systems: modifications of the structure are minimized because existing structural members can be used to install the actuator.

1.7.5 Pulse Generation Systems

A *pulse generation system* uses a pulse generator instead of a hydraulic actuator. Pulse generators use pneumatic mechanisms to produce an active control force. Such mechanisms utilize compressed air to generate a pulse-type actuation force, different from hydraulic actuators using high-pressure fluid. A smart structure system can be achieved by installing pulse generators at several locations within a structure. When a large relative velocity is detected at any of these locations, the pneumatic actuator at this location is triggered, and a control force opposite to the velocity is applied to the structure. Researchers have conducted shaking table tests on a six-story steel frame with a pulse generator at the top [62], and the test results have shown that pulse generators were a promising device for seismic response control.

Pulse generators use compressed gas energy and are not expensive. However, gas energy may not be powerful enough to drive full-scale building structures. Moreover, pulse-generation systems may have high nonlinearity as the force generated by pneumatic actuators may deviate from an ideal rectangular pulse shape.

1.8 Hybrid Control Systems

As noted, active control systems are introduced to address the limited capacity and intelligence of passive and semiactive dampers. However, active structural control still has two disadvantages. First, its operation depends totally on an external power supply and requires a complicated sensing and signal-processing system. This complexity limits its application and reduces control reliability. Second, to apply active control to civil engineering structures, large force-generating equipment, that is, big actuators, are required. Since seismic-resistant structures weigh hundreds or even thousands of tons, the required control force must exceed hundreds of kiloNewtons to augment the structural damping force sufficiently. Current industrial technology makes it feasible to design and manufacture such a large actuator, but its cost severely limits its application. Innovative hybrid control systems, which are achieved by combining passive and active control techniques, have become attractive. When these techniques work together, reliability is ensured by the former and the capacity is powered by the latter. A hybrid system gains the advantages of both techniques and alleviates limitations of either technique alone. As a result, it surpasses passive, semiactive, and active systems. Hybrid control systems have received significant attention since the 1990s [1,15,16,25,37,71,73,94,96]. Three typical hybrid control systems have been developed: HMD, *hybrid base-isolation systems*, and *damper–actuator systems*.

1.8.1 Hybrid Mass Dampers

Hybrid mass dampers combine a passive TMD and an active control actuator, or they add an AMD to a TMD, as shown in Figure 1.30 [37,73]. An AMD is attached to a TMD instead of to the structure so that the AMD can be small; its mass is 10–15% of that for the TMD. The vibration suppression capacity of HMDs mainly

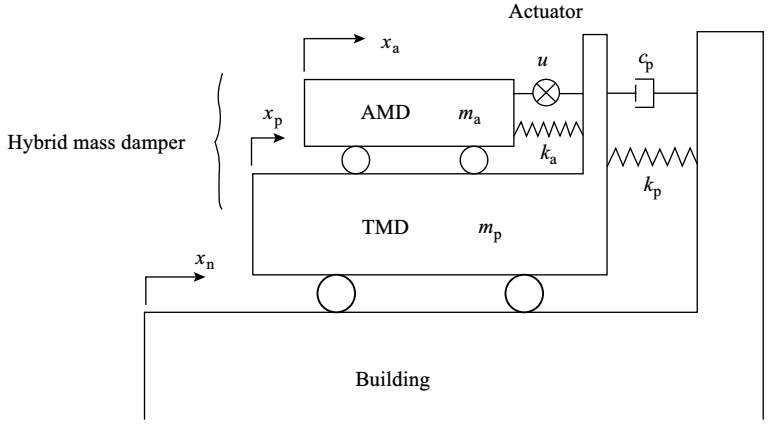

Figure 1.30 Schematic of hybrid mass damper.

relies on the natural motion of the TMD. The actuator generates a control force, which regulates the TMD and thus increases the device's efficiency and robustness to change the dynamic characteristics of the structure. In other words, the TMD is tuned to the fundamental mode of the structure, and the AMD is designed to improve control effectiveness for higher modes of the structure. Thus, the energy and forces required to operate an HMD are far less than those associated with a full AMD system with comparable performance. This feature makes HMDs relatively inexpensive to achieve improved control effectiveness, and they have been the most common control device employed in full-scale building structure applications [73,80,90]. On the other hand, design constraints, such as severe space limitations, can preclude the use of an HMD system.

1.8.2 Hybrid Base-Isolation System

A *hybrid base-isolation system* combining a base-isolation system and an active control system has also been proposed [94]. This system (see Figure 1.31) consists of an active tendon system on the superstructure and a base-isolation system between the foundation and the superstructure. Theoretical studies have been conducted for the base-isolation/actuator system, including system nonlinearity, direct output feedback, sliding mode control technique, and design of the sliding surface [1]. Researchers have also proposed another type of hybrid base-isolation system using MR fluid dampers on the superstructure [96]. This system, called a smart or intelligent base-isolation system by the authors, employs controllable MR fluid to adapt to ever-changing seismic excitations. Shaking table tests of a building

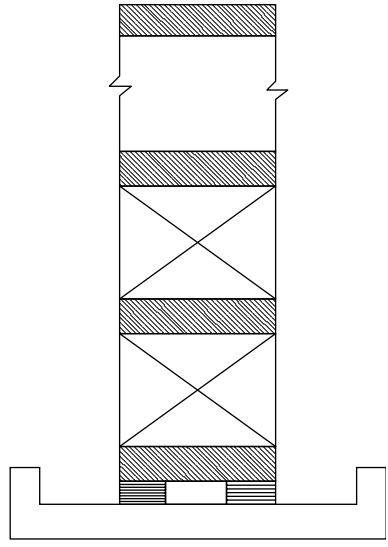

FIGURE 1.31 Hybrid system with base isolation and actuators.

structure model with such a smart base-isolation system have been conducted to verify its effectiveness.

1.8.3 Hybrid Damper-Actuator Bracing Control

In the early 1990s, Cheng and his associates began to develop a *hybrid damper-actuator bracing control* (also called a *hybrid bracing control system*) mounted by K-braces on the structure [15,25], as shown in Figure 1.32a. Owing to various control objectives and economic considerations, a hybrid device, an actuator, a damper, or no control device at all can be installed on one floor of the building structure. Liquid mass dampers, spring dampers, and viscous fluid dampers (see Figure 1.32b) are suggested as passive devices for the system. Hydraulic actuators are proposed as the active device for the system owing to their powerful force-generating capacity.

Extensive studies have been conducted for the hybrid damper-actuator system [15,16,24,25]. Theoretical studies focus on system modeling, optimal algorithm

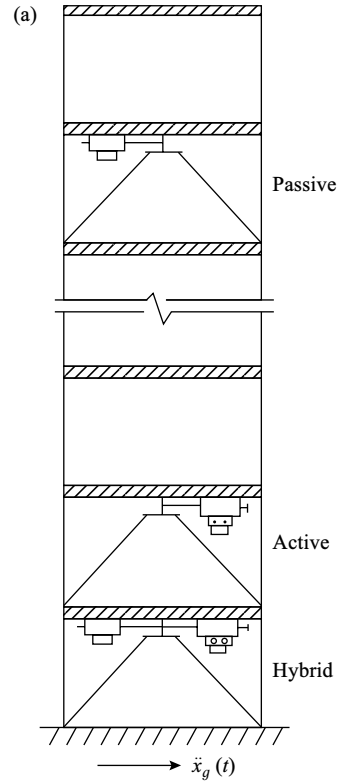

FIGURE 1.32 Hybrid bracing system and control devices: (a) configuration and (b) device installation.

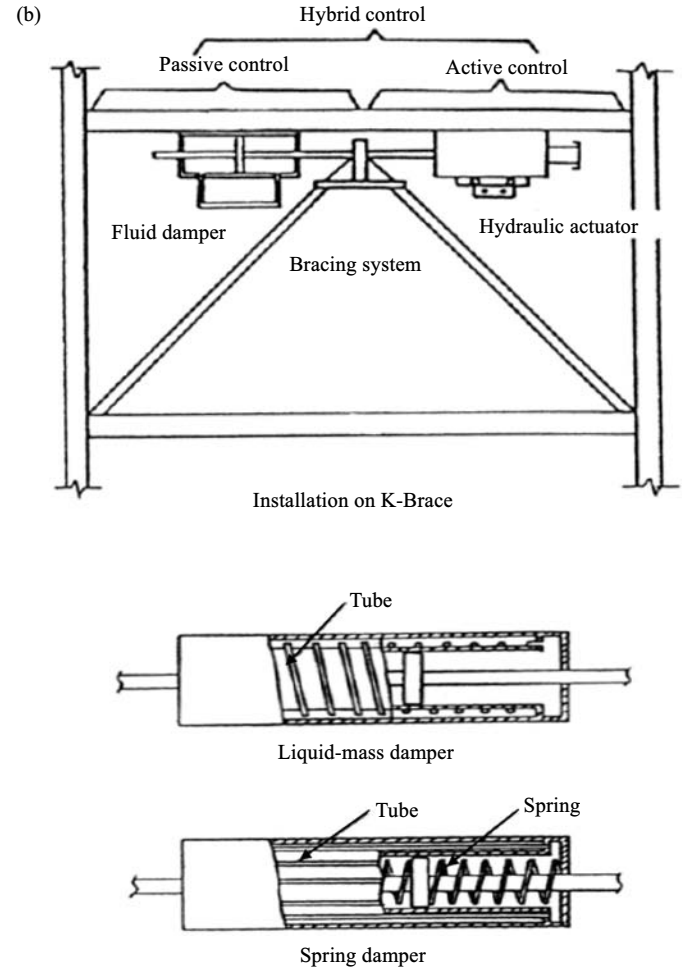

FIGURE 1.32 (Continued)

development, the damper mechanism (dynamics of the viscous fluid damper and parameter analysis of the liquid mass damper and the spring damper), and effectiveness evaluation. Experimental studies were conducted on the damper device (Figure 1.33a) and shaking table tests of a three-story structure model with a hybrid control device (see Figure 1.33b). The hybrid bracing control system consists of a hydraulic actuator and a viscous fluid damper mounted on a K-bracing at the first floor of the structure model. Modal tests, including impact and swept-sine techniques, are performed to find the natural frequencies and mode shapes of the structure. Closed-loop system identification is employed to identify the structure with hybrid control. An observer–controller identification (OCID) procedure determines the system's Markov parameters, and an eigensystem realization

(a)

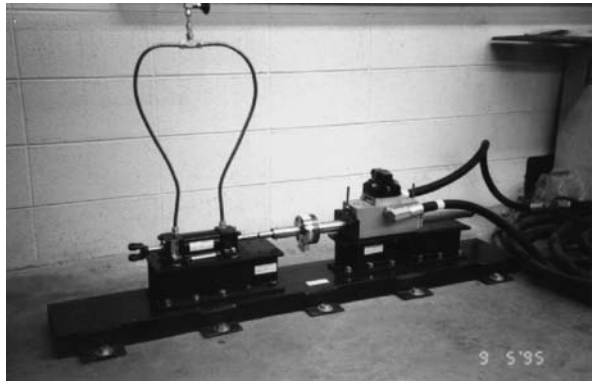

(b)

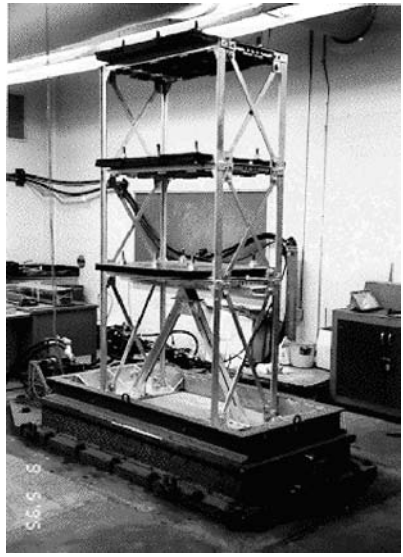

FIGURE 1.33 (a) Testing on damper device for hybrid damper-actuator bracing control (HDABC) and (b) three-story test building with HDABC.

algorithm (ERA) obtains the state-space model of the structure with hybrid control. These test results are used to verify the analytical modeling of the structure with hybrid control. Shaking table tests and computer simulation studies have shown that this system has greater capacity than a passive system in reducing seismic structural response, and it requires less active control force than an active control system to achieve a control objective [15,16,25,96].

A hybrid damper-actuator system is more attractive than other hybrid control systems owing to additional advantages. In this system, a damper and an actuator can either be combined or separated. Installation of control devices on a structure can utilize existing structural braces, and the active control force is

applied directly to the structure. Thus, a hybrid bracing system costs less than a base-isolation/actuator system and has more control capacity than an HMD.

Hybrid control, combining passive and active systems, is an attractive innovation and an effective protection system. Such systems overcome the disadvantages of passive, active, and semiactive control systems while gaining the reliability of passive systems and the capacity of active control systems. With two control techniques in operation together, limitations of either technique operating singly are alleviated. A hybrid system has a larger capacity and greater effectiveness than a passive system, and it costs less and requires smaller external power than an active control system. With these great features, hybrid control becomes very promising for seismic response reduction of civil engineering structures.

References

1. Agrawal, A.K. and Yang, J.N., Hybrid control of seismic response using nonlinear output feedback, in *Proceedings of the Twelfth ASCE Conference on Analysis and Computation*, Cheng, F.Y. (ed.), 1996, p. 339.
2. Aiken, I.D. and Kelly, J.M., Comparative study of four passive energy dissipation systems, *Bulletin of New Zealand National Society of Earthquake Engineering*, 25, 175, 1992.
3. Aiken, I.D. et al., Testing of passive energy dissipation systems, *EERI Earthquake Spectra*, 9, 335, 1993.
4. Aizawa, S. et al., An experimental study on the active mass damper, in *Proceedings of the Ninth World Conference on Earthquake Engineering*, International Association for Earthquake Engineering, Tokyo, 1988, V, p. 87l.
5. Akbay, A. and Aktan, H.M., Actively regulated friction slip braces, in *Proceedings of the Sixth Canadian Conference on Earthquake Engineering*, Toronto, Canada, 1991, p. 367.
6. American Society of Civil Engineers (ASCE), *Minimum Design Loads for Buildings and Other Structures (ASCE-7)*, 1995, 1998, 2002 and 2005 Editions, Reston, Virginia.
7. Applied Technology Council (ATC), *Proceedings of ATC-17-1 Seminar on Seismic Isolation: Passive Energy Dissipation and Active Control*, San Francisco, California, 1993.
8. Arima, F. et al., A study on buildings with large damping using viscous damping walls, in *Proceedings of the Ninth World Conference on Earthquake Engineering*, International Association for Earthquake Engineering, Tokyo, 1988, p. 821.
9. Bauer, H.F., Oscillations of invincible liquids in a rectangular container: a new damper for excitated structures, *Journal of Sound and Vibration*, 93, 117, 1984.
10. Burton, S.A. et al., Modeling the response of ER damper: phenomenology and emulation, *ASCE Journal of Engineering Mechanics*, 122, 897, 1996.
11. Chang, C.H. and Soong, T.T., Structural control using active tuned mass dampers, *ASCE Journal of Engineering Mechanics Division*, 106, 1091, 1980.
12. Chen, C. and Chen, G. Shaking table tests of a quarter-scale three-storey building model with piezoelectric friction dampers, *Structural Control and Health Monitoring*, 11, 239, 2004.

13. Cheng, F.Y., *Matrix Analysis of Structural Dynamics*, Marcel Dekker, Inc., New York, 2001.
14. Cheng, F.Y., Response control based on structural optimization and its combination with active protection, in *Proceedings of Ninth World Conference on Earthquake Engineering*, International Association for Earthquake Engineering, Tokyo, 1988, VIII: p. 471.
15. Cheng, F.Y. and Jiang, H., Optimum control of a hybrid system for seismic excitations with state observer technique, *Smart Materials and Structures*, 7, 654, 1998.
16. Cheng, F.Y. and Jiang, H., Hybrid control of seismic structures with optimal placement of control devices, *ASCE Journal of Aerospace Engineering*, 11, 52, 1998.
17. Cheng, F.Y. and Pantelides, C.P., Algorithm development for using optimal control in structural optimization subjected to seismic and wind forces, *NSF Report*, *NTIS No. PB90-133471/AS*, Fairfax, Virginia, 1988.
18. Cheng, F.Y. and Pantelides, C.P., Development in combining structural optimization and optimal control for seismic and wind structures, *Critical Engineering Systems*, Korea Advanced Institute of Science and Technology, Seoul, Korea, 1987, I: p. 80.
19. Cheng, F.Y. and Pantelides, C.P., Combining structural optimization and active mass damper controls and random process, in *Recent Developments in Structural Optimization*, ASCE, Reston, Virginia, 1986, p. 40.
20. Cheng, F.Y. and Pantelides, C.P., Optimal control of seismic structures, in *Proceedings of the Third Engineering Mechanics Conference*, ASCE, Reston, Virginia, 1986, p. 764.
21. Cheng, F.Y. and Pantelides, C.P., Deflection reduction and enhancement of human comfort for tall building optimum design with active controls, in *Stability of Tall Steel Buildings*, Council on Tall Buildings and Urban Habitat, Bethlehem, Pennsylvania, 1986, p. 93.
22. Cheng, F.Y. and Suthiwong, S., Active control of building structures on mat foundation embedded in unbounded soil, in *Proceedings of Fifth U.S. National Conference on Earthquake Engineering*, Earthquake Engineering Research Institute, Oakland, California, 1994, I, p. 45.
23. Cheng, F.Y. and Tian, P., Assessment of algorithms, material nonlinearity, and foundation effects on structural control of seismic structures, in *Proceedings of International Symposium on Public Infrastructure System Research*, Choi, C.K. and Penzien, J. (eds.), Korea Advanced Institute of Science and Technology, Seoul, Korea, 1995, p. 211.
24. Cheng, F.Y. and Tian, P., Design parameter analysis of hybrid optimal controlled structures, in *Proceedings of the Second International Conference on Intelligent Materials*, Willamsburg, Virginia, 1994, p. 340.
25. Cheng, F.Y. et al., Theoretical and experimental studies on hybrid control of seismic structures, in *Proceedings of the Twelfth ASCE Conference on Analysis and Computation*, Cheng, F.Y. (ed.), Chicago, ASCE, Reston, Virginia, 1996, p. 322.
26. Chu, S.Y., Soong, T.T., and Reinhorn, A.M., *Active, Hybrid, and Semi-Active Structural Control: A Design and Implementation Handbook*, John Wiley & Sons, Chichester, England, 2005.
27. Chun, B.Y. and Cheng, F.Y. (eds.), *Proceedings of US-Korea Workshop on Smart Structure Systems*, Techno-Press, Daejeon, Korea, 2002.

28. Chun, B.Y., Cheng, F.Y., and Choi, C.K. (eds.), *Smart Structure Systems, Special Issue of the International Journal of Structural Engineering and Mechanics*, Techno-Press, Daejeon, Korea, 2004.
29. Chung, L.L., Reinhom, A.M., and Soong, T.T., Experiments on active control of seismic structures, *ASCE Journal of Engineering Mechanics*, 114, 241, 1988.
30. Constantinou, M.C. and Symans, M.D., Experimental study of seismic response of tall buildings with supplemental fluid dampers, *Structural Design for Tall Buildings*, 2, 93, 1993.
31. Cosby, P., Kelly, J.M., and Singh, J., Utilizing viscoelastic dampers in the seismic retrofit of a thirteen story steel frame building, in *Proceedings of ASCE Structure Congress XII*, Atlanta, Georgia, American Society of Civil Engineers, 1994, p. 1286.
32. Den-Hartog, J.P., *Mechanical Vibrations*, 4th edn, McGraw-Hill, New York, 1956.
33. Federal Emergency Management Agency (FEMA), *Guide to Application of the 1991 Edition of the NEHRP Recommended Provisions in Earthquake Resistant Building Design, Revised Edition* (FEMA 140), Building Seismic Safety Council, Washington, DC, 1995.
34. Federal Emergency Management Agency (FEMA), *NEHRP Recommendations for New Buildings and Other Structures*, 1997 Edition (FEMA 302), 2000 Edition (FEMA 368), 2003 Edition (FEMA 450), Building Seismic Safety Council, Washington, D.C.
35. Fitzgerald, T.F. et al., Slotted bolted connections in aseismic design for concentrically braced connections, *Earthquake Spectra*, 5, 383, 1994.
36. Fujino, Y. and Abe, M., Design formulas for tuned mass dampers based on a perturbation technique, *Earthquake Engineering and Structural Dynamics*, 22, 833, 1993.
37. Fujita, T., Development of hybrid mass damper with convertible active and passive modes using AC-servomotor for vibration control of tall buildings, in *Proceedings of the First World Conference on Structural Control*, International Association for Structural Control, Los Angeles, California, 1994, p. 3, FA4:63.
38. Hrovat, D., Barak, P., and Rabins, M., Semi-active versus passive or active tuned mass dampers for structural control, *ASCE Journal of Engineering Mechanics*, 109, 691, 1983.
39. Huffmann, G.K., Full base isolation for earthquake protection by helical springs and viscodampers, *Nuclear Engineering Design*, 84, 331, 1985.
40. International Association of Structural Control (IASC), *Proceedings of the First, Second, and Third World Conferences on Structural Control*, 1994 (Los Angeles, California), 1998 (Kyoto, Japan), and 2002 (Como, Italy).
41. ICBO (International Conference of Building Officials), *Uniform Building Code*, Whittier, California, 1991, 1994, and 1997 Editions.
42. International Code Council (ICC), *International Building Code*, 2000, 2003, and 2006 Editions, Whittier, California.
43. Ivers, D.E. and Miller, L.R., Semi-active suspension technology: an evolutionary view, *ASME Advanced Automotive Technologies*, DE-40, WAM, Atlanta, Georgia, 1991, p. 327.
44. Karnopp, D., Crosby, M.J., and Harwood, R.A., Vibration control using semi-active force generators, *Journal of Engineering for Industry*, 96, 619, 1974.
45. Kawashima, K. et al., Effectiveness of the variable damper for reducing seismic response of highway bridges, in *Proceedings of Second US–Japan Workshop on*

Earthquake Protective Systems for Bridges, PWRI, Tsukuba Science City, Japan, 1992, p. 479.
46. Kelly, J.M., State-of-the-art and state-of-the-practice in base isolation, in *Proceedings, ATC-17-1 Seminar on Seismic Isolation, Passive Energy Dissipation, and Active Control*, San Francisco, California, 1993, p. 9.
47. Kelly, J.M., Skinner, R.I., and Heine, A.J., Mechanisms of energy absorption in special devices for use in earthquake resistant structures, *Bulletin of New Zealand National Society for Earthquake Engineering*, 5, 63, 1972.
48. Kelly, T.E., *Base Isolation of Structures, Design Guidelines*, Holmes Consulting Group Ltd., Wellington, New Zealand, 2001.
49. Kobori, T., Future direction on research and development of seismic-response controlled structure, in *Proceedings of the First World Conference on Structural Control*, Los Angeles, California, 1994, Panel:19.
50. Kobori, T., Seismic-response-controlled structure with active mass driver system, part 1 design and part 2 verification, *Earthquake Engineering and Structural Dynamics*, 20, 133, 1991.
51. Kobori, T. and Minai, R., Analytical study on active seismic response control, *Transactions, Architectural Institute of Japan*, 66, 257, 1960.
52. Kobori, T. et al., Seismic response controlled structure with active variable stiffness, *Earthquake Engineering and Structural Dynamics*, 122, 925, 1993.
53. Lin, Y.K. and Cai, G.Q., *Probabilistic Structural Dynamics*, McGraw-Hill, Professional, New York, 2004.
54. Liu, S.C., Tomizuka, M., and Ulsoy, A.G., Challenges and opportunities in the engineering of intelligent systems, *Smart Structures and Systems*, 1, 1, 2005.
55. Lohman, T., Experimental and modeling study of a viscous fluid damper with bingham plastic and effective mass for vibration reduction, M.S. Thesis, University of Missouri-Rolla, Missouri, 1996.
56. Lou, J.Y.K., Lutes, L.D., and Li, J., Active tuned liquid damper for structural control, in *Proceedings of the First World Conference on Structural Control*, Los Angeles, California, 1994, p. 2, TP1:70.
57. Luft, R.W., Optimal tuned mass dampers for buildings, *ASCE Journal of Structural Division*, 105, 2766, 1979.
58. Makris, N. et al., Electrorheological fluid damper for seismic protection of structures, *ASCE Journal of Engineering Mechanics*, 122, 1996.
59. Makris, N., Dargush, G.F., and Constantinou, M.C., Dynamic analysis of viscous fluid dampers, *ASCE Journal of Engineering Mechanics*, 121, 1114, 1995.
60. Martinez-Ramero, E., Experiences on the use of supplemental energy dissipaters on building structures, *Earthquake Spectra*, 9, 581, 1993.
61. MeiRovitch, L., *Dynamics and Control of Structures*, John Wiley & Sons, Inc., New York, 1990.
62. Miller, R.K. et al., Active vibration control of large civil structures, *ASCE Journal of Engineering Mechanics*, 114, 1542, 1988.
63. Naeim, F. and Kelly, J. M., *Design of Seismic Isolated Structures: From Theory to Practice*, John Wiley & Sons, Inc., New York, 1999.
64. Nims, D.K., Richter, P.J., and Bachman, R.E., The use of the energy dissipating restraint for seismic hazard mitigation, *Earthquake Spectra*, 9, 467, 1993.
65. Nishimura, I. et al., Active tuned mass damper, *Journal of Smart Materials and Structures*, 1, 306, 1992.

66. Pall, A.S. and Marsh, C., Response of friction damped braced frames, *ASCE Journal of Structural Division*, 108, 1313, 1982.
67. Pall, A. et al., Friction dampers for seismic control of Canadian Space Agency headquarters, *Earthquake Spectra*, 9, 547, 1993.
68. Patten, W.N. et al., Bridge vibration suppression using semi active vibration absorbers (SAVA), in *Proceedings of Development in Computer Aided Design and Modeling for Structural Engineering*, CJVIL-COMP Press, Edinburgh, 1995, p. 237.
69. Patten, W.N. et al., Seismic structural control via hydraulic semi-active vibration dampers (SAVD), in *Proceedings of the First World Conference on Structural Control*, International Association for Structural Control, Los Angeles, California, 1994, FA2:83.
70. Reinhorn, A.M. and Li, C., Experimental and analytical investigation of seismic retrofit of structures with supplemental damping, Part III: viscous damping walls, *Technical Report NCEER-95-0013*, National Center for Earthquake Engineering Research, Buffalo, New York, 1995.
71. Reinhorn, A.M. and Riley, M.A., Control of bridge vibrations with hybrid devices, in *Proceedings of the First World Conference on Structural Control*, International Association for Structural Control, Los Angeles, California, 1994, p. 2, TA2:50.
72. Ruge, A.C., Earthquake resistance of elevated water tanks, *Transactions, ASCE*, 103, 889, 1938.
73. Sakamoto, M. et al., Practical applications of active and hybrid response control systems and their verification by earthquake and strong wind observations, in *Proceedings of the First World Conference on Structural Control*, International Association for Structural Control, Los Angeles, California, 1994, p. 1, WP2:90.
74. Shinozuka, M., Constantinou, M.C., and Ghanem, R., Passive and active fluid dampers in structural applications, in *Proceedings of US–China–Japan Workshop on Structural Control*, Tongji University, Shanghai, 1992, p. 507.
75. Skinner, R.J., Kelly, J.M., and Heine, A.J., Hysteresis dampers for earthquake-resistant structures, *Earthquake Engineering and Structural Dynamics*, 43, 287, 1974.
76. Soong, T.T., *Active Structural Control: Theory and Practice*, 1st edn., Longman Scientific & Technical, UK and John Wiley & Sons, New York, 1990.
77. Soong, T.T. and Constantinou, M.C., *Passive and Active Structural Vibration Control in Civil Engineering*, 1st edn., Springer-Verlag Wien, New York, 1994.
78. Soong, T.T. and Dargush, G.F., *Passive Energy Dissipation System in Structural Engineering*, 1st ed., John Wiley & Sons, Chichester, England, 1997.
79. Soong, T.T. and Reinhorn, A.M., Case studies of active control and implementational issues, in *Proceedings of ATC-17-1 Seminar on Seismic Isolation, Passive Energy Dissipation, and Active Control*, Applied Technology Council, San Francisco, California, 1993, 2, p. 449.
80. Soong, T.T. and Spencer, B.F. Jr., Supplemental energy dissipation: state-of-the-art and state-of-the-practice, *Engineering Structures*, 24, 243, 2002.
81. Spencer, B.F. Jr. et al., Dynamic model of a magneto-rheological damper, in *Proceedings of the Twelfth ASCE Conference on Analysis and Computation*, Cheng, F.Y. (ed.), Chicago, ASCE, Reston, Virginia, 1996, p. 361.
82. Srinivasan, A.V. and McFarland, D.M., *Smart Structures: Analysis and Design*, Cambridge University Press, Cambridge, United Kingdom, 2001.

83. Symans, M.D., Cofer, W.F., and Fridley, K.J., Base isolation and supplemental damping systems for seismic protection of wood structures: literature review, *EERI Earthquake Spectra*, 18, 549, 2002.
84. Symans, M.D. and Constantinou, M.C., Development and experimental study of semi active fluid damping devices for seismic protection of structures, *Report No. NCEER-95-0011*, National Center for Earthquake Engineering Research, Buffalo, New York, 1995.
85. Tamura, Y. et al., Effectiveness of Tuned Liquid Dampers under Wind Excitation, *Engineering Structures*, 17, 609, 1995.
86. Tyler, R.G., Further notes on a steel energy-absorbing-element for braced frameworks, *Bulletin of New Zealand National Society for Earthquake Engineering*, 18, 270, 1985.
87. Warburton, G.B., Optimal absorber parameters for various combinations of response and excitation parameters, *Earthquake Engineering and Structural Dynamics*, 10, 381, 1982.
88. Whittaker, A.S. et al., Seismic testing of steel plate energy dissipation devices, *EERI Earthquake Spectra*, 7, 563, 1991.
89. Yalla, S.K and Kareem, A., Tuned liquid dampers for controlling earthquake responsed of structures by P. Banerji et al., *Earthquake Engineering and Structural Dynamics*, 31, 1037, 2002.
90. Yamamoto, M. and Aizawa, S., Control effects of active mass damper system installed on actual buildings, in *Proceedings of the First World Conference on Structural Control*, Los Angeles, California, 1994, p. 2, FP1:13.
91. Yang, G., Large-scale magnetorheological fluid damper for vibration mitigation: modeling, testing and control, Ph.D. Thesis, University of Notre Dame, Notre Dame, 2001.
92. Yang, J.N. and Giannopoulos, F., Active tendon control of structures, *ASCE Journal of Engineering Mechanics Division*, 104, 551, 1978.
93. Yang, J.N., Control of tall buildings under earthquake excitations, *ASCE Journal of Engineering Mechanics Division*, 108, 50, 1982.
94. Yang, J.N., Danielians, A., and Liu, S.C., Aseismic hybrid control systems for building structures, *ASCE Journal of Engineering Mechanics*, 117, 836, 1991.
95. Yao, J.T-P., Concept of structural control, *ASCE Journal of Structural Division*, 98, 1567, 1972.
96. Yoshioka, H., Ramallo, J.C., and Spencer, B.F. Jr., "Smart" base isolation strategies employing magnetorheological dampers, *ASCE Journal of Engineering Mechanic*s, 128, 540, 2002.

2 Base Isolation Systems

As introduced in Section 1.4, once a building is separated from its foundation with a base isolation system, the isolated structure is subjected to less seismic force from the ground motion and, as a result, the responses of the building itself are greatly reduced. This simple concept with feasible constructability has garnered extensive attention from researchers and structural engineers. Over the past five decades, numerous researches and investigations were focused on development of isolation systems' theories and experimental verifications of their stability and durability. Since then, more than 200 applications of base isolation systems to buildings and bridges in the United States have been completed, which demonstrates that this new technology is able to provide seismic protection for structures successfully. Now use of base isolation systems has been widely accepted as a useful strategy for the design of important facilities.

Studies and developments of isolation systems' theories and application technologies have been reported extensively in the literature. It is impossible and unnecessary to include all the concepts and application details in a single chapter. Therefore, only the basic but most important theories and applications are presented herein, which, as the authors intend, may guide interested readers to advanced topics in this field. The organization of this chapter is summarized as follows. In Section 2.1, basic concepts of seismically isolated structures are first introduced. Then, discussions of the mechanical properties of isolator units are presented in Section 2.2. Section 2.3 provides the important design requirements according to the American Society of Civil Engineers (ASCE) Standard ASCE 7-05 [2]. Design examples based on ASCE 7-05 are given in Section 2.4. Verifications and modifications of isolator's mechanical properties are presented in Section 2.5.

2.1 Basic Concepts of Seismically Isolated Building Structures

2.1.1 Single-Degree-of-Freedom Motion Equations

The motion of a seismically isolated building structure can be expressed by a single-degree-of-freedom (SDOF) motion equation assuming that the structure above the isolation interface is extremely rigid and the movement of the structural system mainly occurs at its base or at the isolation system. *Isolator units* usually refer to bearings, while an isolator system is defined as an assembly of isolator units, members structurally tying isolator units, such as steel beams with end fixities, and connections between isolator units and other structural members. In addition to the isolator unit and the isolator system, other terminologies of definitions, such

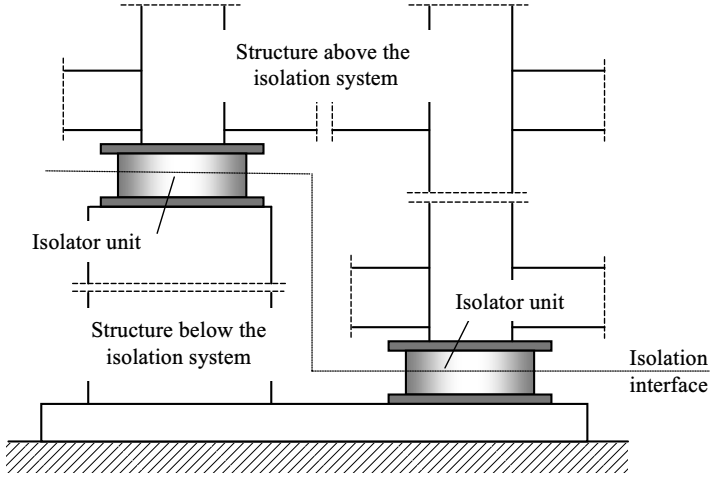

FIGURE 2.1 Terminology of seismically isolated structure.

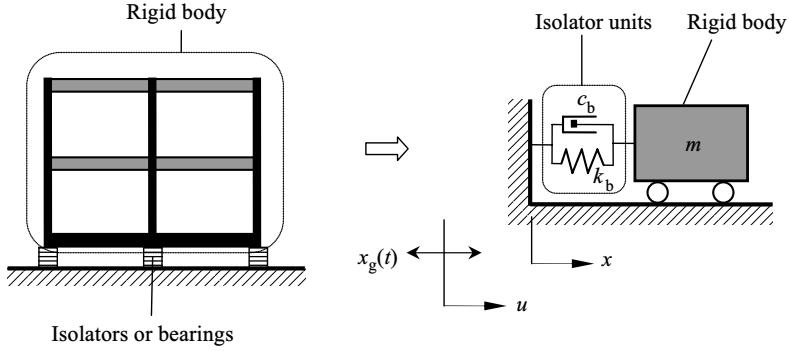

FIGURE 2.2 Sketch of SDOF seismically isolated structure.

as the structure above or below the isolation system, are graphically illustrated in Figure 2.1. A sketch of an SDOF seismically isolated structure is shown in Figure 2.2. A rigid body with a mass, m, represents the building structure above the isolation interface. The isolation system possesses lateral stiffness, k_b, and damping coefficient, c_b. The movement of the isolation system and the *ground motion* are expressed as $u(t)$ and $x_g(t)$, respectively. Utilizing simplified notations of u and x_g to represent $u(t)$ and $x_g(t)$, the motion equation, derived based on the equilibrium condition, is given as follows:

$$m\ddot{u} + c_b(\dot{u} - \dot{x}_g) + k_b(u - x_g) = 0 \tag{2.1}$$

Introducing the relative displacement, $x = u - x_g$, the angular frequency, $\omega_b = \sqrt{k_b/m}$, and the damping ratio, $\beta_b = c_b/2\omega_b m$, Equation 2.1 is rewritten as

$$m\ddot{x} + c_b\dot{x} + k_b x = -m\ddot{x}_g \quad \text{or} \quad \ddot{x} + 2\omega_b\beta_b\dot{x} + \omega_b^2 x = -\ddot{x}_g \tag{2.1a}$$

By applying the method of variation parameters, the general solution of Equation 2.1a can be expressed as below:

$$x(t) = C_1(t)e^{-\beta_b\omega_b t}\sin\overline{\omega}_b t + C_2(t)e^{-\beta_b\omega_b t}\cos\overline{\omega}_b t \tag{2.2}$$

where the *damped frequency is* $\overline{\omega}_b = \omega_b\sqrt{1-\beta_b^2}$. $C_1(t)$ and $C_2(t)$ are purposely selected to meet the following condition:

$$\dot{C}_1(t)e^{-\beta_b\omega_b t}\sin\overline{\omega}_b t + \dot{C}_2(t)e^{-\beta_b\omega_b t}\cos\overline{\omega}_b t = 0 \tag{2.3}$$

Successive derivatives of Equation 2.2 result in the following relation between $\dot{C}_1(t)$ and $\dot{C}_2(t)$:

$$\begin{aligned}&\dot{C}_1(t)e^{-\beta_b\omega_b t}(\overline{\omega}_b\cos\overline{\omega}_b t - \beta_b\omega_b\sin\overline{\omega}_b t)\\ &\quad - \dot{C}_2(t)e^{-\beta_b\omega_b t}(\overline{\omega}_b\sin\overline{\omega}_b t + \beta_b\omega_b\cos\overline{\omega}_b t) = -\ddot{x}_g(t)\end{aligned} \tag{2.3a}$$

Solving Equations 2.3 and a, coefficients $\dot{C}_1(t)$ and $\dot{C}_2(t)$ are obtained by

$$\dot{C}_1(t) = -\frac{1}{\overline{\omega}_b}\ddot{x}_g(t)e^{\beta_b\omega_b t}\cos\overline{\omega}_b t \tag{2.4}$$

$$\dot{C}_2(t) = \frac{1}{\overline{\omega}_b}\ddot{x}_g(t)e^{\beta_b\omega_b t}\sin\overline{\omega}_b t \tag{2.4a}$$

Taking the integration of Equations 2.4 and 2.4a, $C_1(t)$ and $C_2(t)$ are obtained as follows:

$$C_1(t) = -\frac{1}{\overline{\omega}_b}\int_0^t \ddot{x}_g(\tau)e^{\beta_b\omega_b\tau}\cos\overline{\omega}_b\tau\,\mathrm{d}\tau + C_1$$

$$C_2(t) = \frac{1}{\overline{\omega}_b}\int_0^t \ddot{x}_g(\tau)e^{\beta_b\omega_b\tau}\sin\overline{\omega}_b\tau\,\mathrm{d}\tau + C_2$$

where C_1 and C_2 are constants that are independent of time t.

Substituting $C_1(t)$ and $C_2(t)$ into Equation 2.2, the movement of the seismically isolated structure is therefore expressed by means of *Duhamel's integral*.

$$x(t) = e^{-\beta_b\omega_b t}(C_1\sin\overline{\omega}_b t + C_2\cos\overline{\omega}_b t) - \frac{1}{\overline{\omega}_b}\int_0^t \ddot{x}_g(\tau)e^{-\beta_b\omega_b t}\sin\overline{\omega}_b(t-\tau)\,\mathrm{d}\tau \tag{2.5}$$

Determinations of constants C_1 and C_2 are explicitly given by Cheng [3] on page 15. However, since there are no initial movement and velocity of the studied structure at the beginning of an earthquake, $C_1 = C_2 = 0$. Thus, Equation 2.5 is simplified as follows:

$$x(t) = -\frac{1}{\overline{\omega}_\mathrm{b}} \int_0^t \ddot{x}_\mathrm{g}(\tau) \mathrm{e}^{-\beta_\mathrm{b}\omega_\mathrm{b}(t-\tau)} \sin \overline{\omega}_\mathrm{b}(t-\tau)\, \mathrm{d}\tau \tag{2.5a}$$

As is the case with seismically isolated structures without damper devices, the damping ratio, β_b, usually does not exceed 20% of critical damping. Accordingly, the effects from the term $\sqrt{1-\beta_\mathrm{b}^2}$ are negligible and replacement of the damped frequency, $\overline{\omega}_\mathrm{b}$, by the angular frequency, ω_b, is appropriate. Equation 2.5a can be rewritten as

$$x(t) = -\frac{1}{\omega_\mathrm{b}} \int_0^t \ddot{x}_\mathrm{g}(\tau) \mathrm{e}^{-\beta_\mathrm{b}\omega_\mathrm{b}(t-\tau)} \sin \omega_\mathrm{b}(t-\tau)\, \mathrm{d}\tau \tag{2.5b}$$

The maximum absolute value of the integral portion in Equation 2.5b is defined as *pseudovelocity* [3] from pages 362 through 368, and is expressed as below:

$$S_\mathrm{V} = \left| \int_0^t \ddot{x}_\mathrm{g}(\tau) \mathrm{e}^{-\beta_\mathrm{b}\omega_\mathrm{b}(t-\tau)} \sin \omega_\mathrm{b}(t-\tau)\, \mathrm{d}\tau \right|_\mathrm{max} \tag{2.6}$$

The *spectral displacement*, S_D, has the following relation with the pseudovelocity:

$$S_\mathrm{V} = \omega_\mathrm{b} S_\mathrm{D} \tag{2.7}$$

For the damping ratio, β_b, less than 20% of the critical damping, the following relation between the *pseudoacceleration*, S_A, and the spectral displacement, S_D, can be further simplified with satisfactory accuracy:

$$S_\mathrm{A} = \omega_\mathrm{b}^2 S_\mathrm{D} \tag{2.8}$$

The ground motion, $\ddot{x}_\mathrm{g}(t)$, shown in Equation 2.6 is usually known. Thus, S_D, S_V, and S_A are functions of the angular frequency, ω_b, and the damping ratio, β_b of the seismically isolated structures. Equation 2.8 is the basis for establishing an *equivalent lateral force procedure* for the design of seismically isolated structures, which is explicitly discussed in Section 2.3.

2.1.2 Multiple-Degree-of-Freedom Motion Equations

Figure 2.3 shows a seismically isolated structure with multiple stories. By employing the equilibrium condition, the motion equation at the roof level, n,

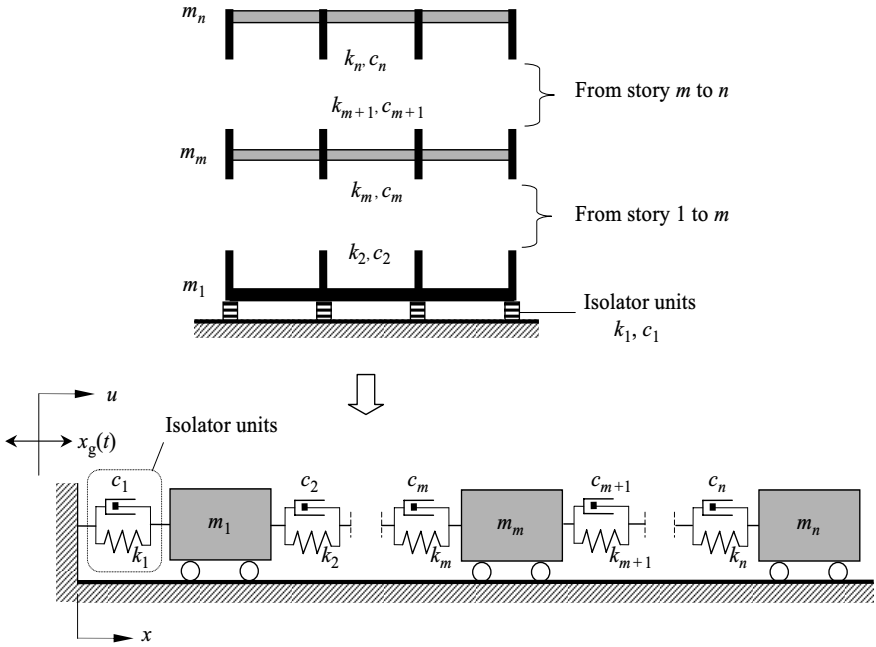

FIGURE 2.3 Sketch of MDOF seismically isolated structure.

is derived as

$$m_n\ddot{u}_n + c_n(\dot{u}_n - \dot{u}_{n-1}) + k_n(u_n - u_{n-1}) = 0 \tag{2.9}$$

where m_n is the roof mass; c_n and k_n denote the damping coefficient and the story stiffness between the roof and the story below the roof, respectively; u_n and u_{n-1}, simplified from $u_n(t)$ and $u_{n-1}(t)$, represent the movement at the roof and the story below the roof.

By applying the same methodology, the motion equation at story m is expressed as follows:

$$\begin{aligned} &m_m\ddot{u}_m + c_m(\dot{u}_m - \dot{u}_{m-1}) - c_{m+1}(\dot{u}_{m+1} - \dot{u}_m) + k_m(u_m - u_{m-1}) \\ &\quad - k_{m+1}(u_{m+1} - u_m) = 0 \end{aligned} \tag{2.10}$$

where m_m is the mass at story m; c_{m+1} and c_m are the damping coefficient between story $m+1$ and m, and between story m and $m-1$, respectively; k_{m+1} and k_m are denoted as the story stiffness between story $m+1$ and m, and between story m and $m-1$, respectively; u_{m+1}, u_m, and u_{m-1}, represent the movement at story $m+1$, m, and $m-1$.

At the level immediately above the isolation system denoted as story 1, considering the ground motion x_g, which is simplified from $x_g(t)$, the motion equation can be written as

$$m_1\ddot{u}_1 + c_1(\dot{u}_1 - \dot{x}_g) - c_2(\dot{u}_2 - \dot{u}_1) + k_1(u_1 - x_g) - k_2(u_2 - u_1) = 0 \tag{2.11}$$

where m_1 is the mass at story 1; c_2 and k_2 are the damping coefficient and the story stiffness between story 2 and 1, respectively; c_1 and k_1 are designated as the damping coefficient and stiffness of isolation system, respectively; u_2 and u_1 represent the movement at story 2 and 1.

Introducing the relative displacement between each story and the ground motion that is expressed in terms of $x_m = u_m - x_g$, Equations 2.9, 2.10, and 2.11 become

$$m_n\ddot{x}_n + c_n(\dot{x}_n - \dot{x}_{n-1}) + k_n(x_n - x_{n-1}) = -m_n\ddot{x}_g \tag{2.9a}$$

$$m_m\ddot{x}_m + c_m(\dot{x}_m - \dot{x}_{m-1}) - c_{m+1}(\dot{x}_{m+1} - \dot{x}_m) + k_m(x_m - x_{m-1}) - k_{m+1}(x_{m+1} - x_m) = -m_m\ddot{x}_g \tag{2.10a}$$

$$m_1\ddot{x}_1 + c_1\dot{x}_1 - c_2(\dot{x}_2 - \dot{x}_1) + k_1x_1 - k_2(x_2 - x_1) = -m_1\ddot{x}_g \tag{2.11a}$$

Equations 2.9a, 2.10a, and 2.11a form multiple-degree-of-freedom (MDOF) motion equations. These equations can be expressed in matrix notations and symbolically expressed as below:

$$[\mathrm{M}]\{\ddot{x}\} + [\mathrm{C}]\{\dot{x}\} + [\mathrm{K}]\{x\} = -\ddot{x}_g[\mathrm{M}]\{1\} \tag{2.12}$$

where the mass matrix, [M], the damping matrix, [C], and the structural stiffness, [K], are in the following forms:

$$[\mathrm{M}] = \begin{bmatrix} m_1 & 0 & 0 & 0 & 0 \\ & m_2 & 0 & 0 & 0 \\ & & \ddots & \vdots & \\ & & m_m & \cdots\ 0 & 0 \\ & & & \ddots & \\ & \text{sym.} & & m_{n-1} & \\ & & & & m_n \end{bmatrix} \tag{2.12a}$$

$$[\mathrm{C}] = \begin{bmatrix} c_1 + c_2 & -c_2 & & 0 & & 0 & 0 \\ & c_2 + c_3 & & 0 & & 0 & 0 \\ & & \ddots & \vdots & & & \\ & & & c_m + c_{m+1} & \cdots & 0 & 0 \\ & & & & \ddots & & \\ & \text{sym.} & & & & c_{n-1} + c_n & -c_n \\ & & & & & & c_n \end{bmatrix} \tag{2.12b}$$

$$[\mathrm{K}] = \begin{bmatrix} k_1 + k_2 & -k_2 & & 0 & & 0 & 0 \\ & k_2 + k_3 & & 0 & & 0 & 0 \\ & & \ddots & \vdots & & & \\ & & & k_m + k_{m+1} & \cdots & 0 & 0 \\ & & & & \ddots & & \\ & \text{sym.} & & & & k_{n-1} + k_n & -k_n \\ & & & & & & k_n \end{bmatrix} \tag{2.12c}$$

In Equation 2.12 $\{1\}$ is a $1 \times n$ unit vector, $\{x\}$, $\{\dot{x}\}$, and $\{\ddot{x}\}$ present the relative displacement vector, velocity vector, and acceleration vector of the seismically isolated structure:

$$\{x\}^{\mathrm{T}} = \{\, x_1 \quad x_2 \quad \ldots \quad x_m \quad \ldots \quad x_{n-1} \quad x_n \,\} \tag{2.13}$$

$$\{\dot{x}\}^{\mathrm{T}} = \{\, \dot{x}_1 \quad \dot{x}_2 \quad \ldots \quad \dot{x}_m \quad \ldots \quad \dot{x}_{n-1} \quad \dot{x}_n \,\} \tag{2.13a}$$

$$\{\ddot{x}\}^{\mathrm{T}} = \{\, \ddot{x}_1 \quad \ddot{x}_2 \quad \ldots \quad \ddot{x}_m \quad \ldots \quad \ddot{x}_{n-1} \quad \ddot{x}_n \,\} \tag{2.13b}$$

Let the relative displacement vector be expressed in terms of *generalized response vector*, $\{x'\}$. Equation 2.13 becomes

$$\{x\} = [\Phi]\{x'\} \tag{2.14}$$

where $[\Phi]$ is the modal matrix as shown below:

$$[\Phi] = \begin{bmatrix} \phi_{1,1} & \phi_{1,2} & \cdots & \phi_{1,m} & \cdots & \phi_{1,n-1} & \phi_{1,n} \\ \phi_{2,1} & \phi_{2,2} & \cdots & \phi_{2,m} & \cdots & \phi_{2,n-1} & \phi_{2,n} \\ \cdots & \cdots & \cdots & \cdots & \cdots & \cdots & \cdots \\ \phi_{m,1} & \phi_{m,2} & \cdots & \phi_{m,m} & \cdots & \phi_{m,n-1} & \phi_{m,n} \\ \cdots & \cdots & \cdots & \cdots & \cdots & \cdots & \cdots \\ \phi_{n-1,1} & \phi_{n-1,2} & \cdots & \phi_{n-1,m} & \cdots & \phi_{n-1,n-1} & \phi_{n-1,n} \\ \phi_{n,1} & \phi_{n,2} & \cdots & \phi_{n,m} & \cdots & \phi_{n,n-1} & \phi_{n,n} \end{bmatrix}$$

The successive derivatives of Equation 2.14 result in

$$[\mathrm{M}][\Phi]\{\ddot{x}'\} + [\mathrm{C}][\Phi]\{\dot{x}'\} + [\mathrm{K}][\Phi]\{x'\} = -\ddot{x}_{\mathrm{g}}[\mathrm{M}]\{1\} \tag{2.15}$$

Premultiplying and dividing both sides of Equation 2.15 by $[\Phi]^{\mathrm{T}}$ and $[\Phi]^{\mathrm{T}}[\mathrm{M}][\Phi]$, respectively, the motion equation becomes

$$\{\ddot{x}'\} + \frac{[\Phi]^{\mathrm{T}}[\mathrm{C}][\Phi]}{[\Phi]^{\mathrm{T}}[\mathrm{M}][\Phi]}\{\dot{x}'\} + \frac{[\Phi]^{\mathrm{T}}[\mathrm{K}][\Phi]}{[\Phi]^{\mathrm{T}}[\mathrm{M}][\Phi]}\{x'\} = -\frac{[\Phi]^{\mathrm{T}}[\mathrm{M}]\{1\}}{[\Phi]^{\mathrm{T}}[\mathrm{M}][\Phi]}\ddot{x}_{\mathrm{g}} \tag{2.15a}$$

Defining damping ratio at each mode, $\beta_m = c_m \big/ 2\omega_m m_m$, $m = 1, \ldots, n$, then

$$\frac{[\Phi]^{\mathrm{T}}[\mathrm{C}][\Phi]}{[\Phi]^{\mathrm{T}}[\mathrm{M}][\Phi]} = \begin{bmatrix} 2\beta_1\omega_1 & 0 & 0 & 0 & 0 \\ & 2\beta_2\omega_2 & 0 & 0 & 0 \\ & & \ddots & \vdots & \\ & & 2\beta_m\omega_m & \cdots & 0 & 0 \\ & & & \ddots & & \\ & \text{sym.} & & & 2\beta_{n-1}\omega_{n-1} & 0 \\ & & & & & 2\beta_n\omega_n \end{bmatrix} = [2\beta\omega]; \tag{2.16}$$

where $[2\beta\omega]$ is an $n \times n$ diagonal matrix. Note that for simplicity, β and ω are used to present β_m and ω_m, respectively. Theoretically, $[\Phi]^{\mathrm{T}}[\mathrm{C}][\Phi]$ $([\Phi]^{\mathrm{T}}[\mathrm{M}][\Phi])^{-1}$ cannot be decoupled into a diagonal matrix $[2\beta\omega]$ since the damping of the isolation system is larger than that of the structure above the isolation interface. However, the coupled damping effects, which exist at the off-diagonal components of the matrix, $[\Phi]^{\mathrm{T}}[\mathrm{C}][\Phi]([\Phi]^{\mathrm{T}}[M][\Phi])^{-1}$, are proved to be small and negligible for most structures [12]. Therefore, assuming that the damping ratios can be uncoupled, as shown in Equation 2.16, it will not lose the analytical accuracy of studying the entire system's behavior. If damping devices are added into the isolation system, the coupled damping effects cannot be neglected, and the complex modal analysis must be used to find the solutions [3,13]. A diagonal stiffness, $[\omega^2]$, is also achieved based on the properties of the structural system:

$$\frac{[\Phi]^{\mathrm{T}}[\mathrm{K}][\Phi]}{[\Phi]^{\mathrm{T}}[\mathrm{M}][\Phi]} = \begin{bmatrix} \omega_1^2 & 0 & 0 & 0 & 0 \\ & \omega_2^2 & 0 & 0 & 0 \\ & & \ddots & & \\ & & \omega_m^2 & \cdots & 0 & 0 \\ & & & \ddots & & \\ & \text{sym.} & & & \omega_{n-1}^2 & 0 \\ & & & & & \omega_n^2 \end{bmatrix} = [\omega^2] \tag{2.16a}$$

To the right side of Equation 2.15a, a *participation factor*, Γ, is defined as below:

$$\Gamma = \frac{[\Phi]^{\mathrm{T}}[\mathrm{M}]\{1\}}{[\Phi]^{\mathrm{T}}[\mathrm{M}][\Phi]} \tag{12.16b}$$

The participation factor can be written as $\Gamma = \{\Gamma_1 \quad \dots \quad \Gamma_m \quad \dots \quad \Gamma_n\}^{\mathrm{T}}$, where Γ_m represents the mth mode participation factor. Relying on the orthogonal conditions as presented in Equations 2.16, 2.16a, and 2.16b, Equation 2.15a becomes uncoupled and is expressed as

$$\{\ddot{x}'\} + [2\beta\omega]\{\dot{x}'\} + [\omega^2]\{x'\} = -\Gamma\ddot{x}_{\mathrm{g}} \tag{2.17}$$

Equation 2.17 is similar to Equation 2.1a for the SDOF motion equation, but it consists of n independent equations and can be solved separately for each mth mode of vibration:

$$\ddot{x}'_m + 2\beta_m\omega_m\dot{x}'_m + \omega_m^2 x'_m = -\Gamma_m\ddot{x}_{\mathrm{g}} = -\frac{\{\Phi\}_m^{\mathrm{T}}[\mathrm{M}]\{1\}}{\{\Phi\}_m^{\mathrm{T}}[\mathrm{M}]\{\Phi\}_m}\ddot{x}_{\mathrm{g}} \tag{2.17a}$$

where $\{\Phi\}_m^{\mathrm{T}} = \{\phi_{1,m} \quad \dots \quad \phi_{m,m} \quad \dots \quad \phi_{n,m}\}$. Applying *Duhamel's integral*, the solution of Equation 2.17a is obtained for each story of the seismically isolated structure.

$$x'_m(t) = -\frac{1}{\overline{\omega}_m}\Gamma_m \int_0^t \ddot{x}_{\mathrm{g}}(\tau)\mathrm{e}^{-\beta_m\omega_m(t-\tau)} \sin\overline{\omega}_m(t-\tau)\,\mathrm{d}\tau \quad m = 1, \dots, n \tag{2.18}$$

where $\overline{\omega}_m = \omega_m\sqrt{1-\beta_m^2}$ is the *damped frequency* at the mth mode. As discussed in Section 2.1.1, the expression of $\sqrt{1-\beta_m^2}$ is negligible for most seismically isolated structures without damping devices. Thus, $\overline{\omega}_m \approx \omega_m$, and Equation 2.18 is simplified as

$$x'_m(t) = -\frac{1}{\omega_m}\Gamma_m \int_0^t \ddot{x}_{\mathrm{g}}(\tau)\mathrm{e}^{-\beta_m\omega_m(t-\tau)} \sin\omega_m(t-\tau)\,\mathrm{d}\tau \quad m = 1, \dots, n \tag{2.18a}$$

Once the generalized response vector, $\{x'\}$, is computed from Equation 2.18a, the relative displacement vector, $\{x\}$, can be determined from Equation 2.14. The velocity vector, $\{\dot{x}\}$, and the acceleration vector, $\{\ddot{x}\}$, are also easily derived as follows:

$$\{\dot{x}\} = [\Phi]\{\dot{x}'\} \tag{2.19}$$

$$\{\ddot{x}\} = [\Phi]\{\ddot{x}'\} \tag{2.19a}$$

The procedure presented above, called *modal displacement superposition method*, is used for fixed-base structures, and has also demonstrated applicability to most MDOF seismically isolated structures, which have damping ratios of isolator units less than 20% of critical.

Example 2.1.1

A one-story seismically isolated structure has roof mass equal to 5 k-s^2/in. (876.4 $\times$ 10^3 kg). The mass of the floor, which is immediately above the isolation system, is approximately 4 k-s^2/in. (700.5 $\times$ 10^3 kg). The stiffness of the superstructure and the isolation system is 5000 k/in. (875.6 kN/mm) and 8 k/in. (1.4 kN/mm), respectively. Assume that the couple effects of damping between the superstructure and the isolation system are negligible. Critical damping of 2% is given for the superstructure and 15% of critical damping is experimentally determined for the isolation system. A sketch of the seismically isolated structure is shown in Figure 2.4. Customary units are used to resolve following items:

1. Find the periods of the system, $T_m = 2\pi/\omega_m$, $m = 1, 2$;
2. Determine the modal matrix, $[\Phi]$;
3. Derive the relative displacement, $\{x\}$, and the acceleration, $\{\ddot{x}\}$, of the system.

Solution

1. According to the given information, the mass matrix is expressed as

$$[\mathrm{M}] = \begin{bmatrix} m_1 & 0 \\ 0 & m_2 \end{bmatrix} = \begin{bmatrix} 4 & 0 \\ 0 & 5 \end{bmatrix} \quad \text{and} \quad \omega^2[\mathrm{M}] = \begin{bmatrix} 4\omega^2 & 0 \\ 0 & 5\omega^2 \end{bmatrix} \tag{a}$$

The stiffness matrix becomes

$$[\mathrm{K}] = \begin{bmatrix} k_1 + k_2 & -k_2 \\ -k_2 & k_2 \end{bmatrix} = \begin{bmatrix} 8 + 5000 & -5000 \\ -5000 & 5000 \end{bmatrix} = \begin{bmatrix} 5080 & -5000 \\ -5000 & 5000 \end{bmatrix} \tag{b}$$

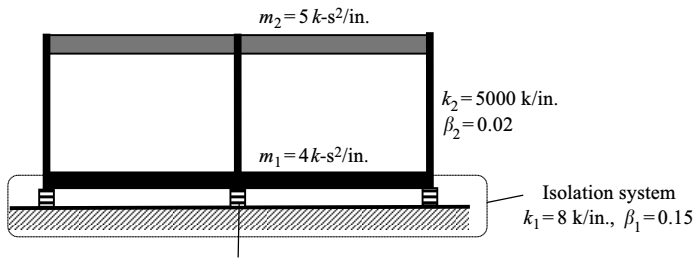

FIGURE 2.4 Example 2.1.1.

The angular frequencies can be determined using the following equation and assuming the determinant is zero for variables $\{x\}$:

$$([\mathrm{K}] - \omega^2[\mathrm{M}])\{x\} = \{0\}$$
$$\begin{vmatrix} 5080 - 4\omega^2 & -5000 \\ -5000 & 5000 - 5\omega^2 \end{vmatrix} = 0 \tag{c}$$

For $\omega_1^2 = 8.845$, $\omega_1 = 2.974$ rad/s.
The period related to the first mode is

$$T_1 = \frac{2\pi}{\omega_1} = \frac{2\pi}{2.974} = 2.113 \text{ s} \tag{d}$$

For $\omega_2^2 = 2261.155$, $\omega_2 = 47.552$ rad/s; the period related to the second mode is

$$T_2 = \frac{2\pi}{\omega_2} = \frac{2\pi}{47.552} = 0.132 \text{ s} \tag{e}$$

2. Assume that the natural modes corresponding to the first and second frequency are expressed as follows:

$$\{\Phi\}_1 = \begin{Bmatrix} \phi_{1,1} \\ \phi_{2,1} \end{Bmatrix}, \quad \{\Phi\}_2 = \begin{Bmatrix} \phi_{1,2} \\ \phi_{2,2} \end{Bmatrix} \tag{f}$$

For $\omega_1^2 = 8.845$,

$$\begin{bmatrix} 5080 - 4(8.845) & -5000 \\ -5000 & 5000 - 5(8.845) \end{bmatrix} \begin{Bmatrix} \phi_{1,1} \\ \phi_{2,1} \end{Bmatrix} = \begin{Bmatrix} 0 \\ 0 \end{Bmatrix} \tag{g}$$

$$\begin{Bmatrix} \phi_{1,1} \\ \phi_{2,1} \end{Bmatrix} = \begin{Bmatrix} 0.9912 \\ 1 \end{Bmatrix} \tag{h}$$

For $\omega_2^2 = 2261.155$,

$$\begin{bmatrix} 5080 - 4(2261.155) & -5000 \\ -5000 & 5000 - 5(2261.155) \end{bmatrix} \begin{Bmatrix} \phi_{1,2} \\ \phi_{2,2} \end{Bmatrix} = \begin{Bmatrix} 0 \\ 0 \end{Bmatrix} \tag{i}$$

$$\begin{Bmatrix} \phi_{1,2} \\ \phi_{2,2} \end{Bmatrix} = \begin{Bmatrix} 1 \\ -0.7929 \end{Bmatrix} \tag{j}$$

Therefore, the modal matrix is assembled as

$$[\Phi] = \begin{bmatrix} 0.9912 & 1.0000 \\ 1.0000 & -0.7929 \end{bmatrix} \tag{k}$$

3. On the basis of modal matrix determined from Equation k, then

$$\{\Phi\}_1^{\mathrm{T}}[\mathrm{M}]\{\Phi\}_1 = \{\phi_{1,1} \quad \phi_{2,1}\}\begin{bmatrix} m_1 & 0 \\ 0 & m_2 \end{bmatrix}\begin{Bmatrix} \phi_{1,1} \\ \phi_{2,1} \end{Bmatrix}$$

$$= \{0.9912 \quad 1\}\begin{bmatrix} 4 & 0 \\ 0 & 5 \end{bmatrix}\begin{Bmatrix} 0.9912 \\ 1 \end{Bmatrix} = 8.9299 \tag{l}$$

$$\{\Phi\}_2^{\mathrm{T}}[\mathrm{M}]\{\Phi\}_2 = \{\phi_{1,2} \quad \phi_{2,2}\}\begin{bmatrix} m_1 & 0 \\ 0 & m_2 \end{bmatrix}\begin{Bmatrix} \phi_{1,2} \\ \phi_{2,2} \end{Bmatrix}$$

$$= \{1 \quad -0.7929\}\begin{bmatrix} 4 & 0 \\ 0 & 5 \end{bmatrix}\begin{Bmatrix} 1 \\ -0.7929 \end{Bmatrix} = 7.1435 \tag{m}$$

$$[\Phi]^{\mathrm{T}}[\mathrm{M}][\Phi] = \begin{bmatrix} 8.9299 & 0 \\ 0 & 7.1435 \end{bmatrix} \tag{n}$$

$$([\Phi]^{\mathrm{T}}[\mathrm{M}][\Phi])^{-1} = \begin{bmatrix} \dfrac{1}{8.9299} & 0 \\ 0 & \dfrac{1}{7.1435} \end{bmatrix} \tag{o}$$

According to Equation 2.16a,

$$\frac{[\Phi]^{\mathrm{T}}[\mathrm{K}][\Phi]}{[\Phi]^{\mathrm{T}}[\mathrm{M}][\Phi]} = \begin{bmatrix} 0.9912 & 1.0000 \\ 1.0000 & -0.7929 \end{bmatrix}\begin{bmatrix} 5080 & -5000 \\ -5000 & 5000 \end{bmatrix}$$

$$\begin{bmatrix} 0.9912 & 1.0000 \\ 1.0000 & -0.7929 \end{bmatrix}\begin{bmatrix} \dfrac{1}{8.9299} & 0 \\ 0 & \dfrac{1}{7.1435} \end{bmatrix}$$

$$= \begin{bmatrix} 8.845 & 0 \\ 0 & 2261.155 \end{bmatrix} \tag{p}$$

Since the given condition assumes there are no damping coupled effects, Equation 2.16 is valid and is computed as follows:

$$\frac{[\Phi]^{\mathrm{T}}[\mathrm{C}][\Phi]}{[\Phi][\mathrm{M}][\Phi]} = \begin{bmatrix} 2(0.15)(2.974) & 0 \\ 0 & 2(0.02)(47.552) \end{bmatrix} = \begin{bmatrix} 0.8922 & 0 \\ 0 & 1.9021 \end{bmatrix} \tag{q}$$

The participation factor defined by Equation 2.16b for each degree of freedom is determined as

$$\Gamma_1 = \frac{\{\Phi\}_1^{\mathrm{T}}[\mathrm{M}]\{1\}}{\{\Phi\}_1^{\mathrm{T}}[\mathrm{M}]\{\Phi\}_1} = \{0.9912 \quad 1\}\begin{bmatrix} 4 & 0 \\ 0 & 5 \end{bmatrix}\begin{Bmatrix} 1 \\ 1 \end{Bmatrix}\frac{1}{8.9299} = 1.0039 \tag{r}$$

$$\Gamma_2 = \frac{\{\Phi\}_2^{\mathrm{T}}[\mathrm{M}]\{1\}}{\{\Phi\}_2^{\mathrm{T}}[\mathrm{M}]\{\Phi\}_2} = \{1 \quad -0.7929\}\begin{bmatrix} 4 & 0 \\ 0 & 5 \end{bmatrix}\begin{Bmatrix} 1 \\ 1 \end{Bmatrix}\frac{1}{7.1435} = 0.0050 \tag{s}$$

Substituting the above results into Equation 2.17a, the uncoupled motion equations are expressed as

$$\ddot{x}_1' + 0.8992\dot{x}_1' + 8.845x_1' = -1.0039\ddot{x}_g \tag{t}$$

$$\ddot{x}_2' + 1.9021\dot{x}_2' + 2261.155x_2' = -0.005\ddot{x}_g \tag{u}$$

On the basis of Duhamel's integral given in Equation 2.18a, $x_1'(t)$ and $x_2'(t)$ are shown as below:

$$x_1'(t) = -0.3375 \int_0^t \ddot{x}_g(\tau) e^{-0.4461(t-\tau)} \sin[2.974(t-\tau)]\, d\tau \tag{v}$$

$$x_2'(t) = -0.0001 \int_0^t \ddot{x}_g(\tau) e^{-0.951(t-\tau)} \sin[47.552(t-\tau)]\, d\tau \tag{w}$$

Substituting $x_1'(t)$ and $x_2'(t)$ into Equation 2.14, each component of $\{x\} = [\Phi]\{x'\}$ is written as

$$\phi_{1,1}x_1'(t) = -0.3346 \int_0^t \ddot{x}_g(\tau) e^{-0.4461(t-\tau)} \sin[2.974(t-\tau)]\, d\tau \tag{x}$$

$$\phi_{1,2}x_2'(t) = -0.0001 \int_0^t \ddot{x}_g(\tau) e^{-0.951(t-\tau)} \sin[47.552(t-\tau)]\, d\tau \tag{y}$$

$$\phi_{2,1}x_1'(t) = -0.3375 \int_0^t \ddot{x}_g(\tau) e^{-0.4461(t-\tau)} \sin[2.974(t-\tau)]\, d\tau \tag{z}$$

$$\phi_{2,2}x_2'(t) = 0.0001 \int_0^t \ddot{x}_g(\tau) e^{-0.951(t-\tau)} \sin[47.552(t-\tau)]\, d\tau \tag{aa}$$

Compared to $\phi_{1,1}x_1'(t)$ and $\phi_{2,1}x_1'(t)$, the contributions of $\phi_{1,2}x_2'(t)$ and $\phi_{2,2}x_2'(t)$ to the displacement at each level are very small and are negligible. It is well explained from this example that the lateral displacement is mainly generated by the isolation system and the structure above the isolation system barely displays movement or story drift. Therefore, the displacement at the floor immediately above the isolation system is expressed approximately as

$$\begin{aligned} x_1(t) &= \phi_{1,1}x_1'(t) + \phi_{1,2}x_2'(t) \\ &\approx -0.3346 \int_0^t \ddot{x}_g(\tau) e^{-0.4461(t-\tau)} \sin[2.974(t-\tau)]\, d\tau \end{aligned} \tag{bb}$$

The displacement at the roof is shown as follows:

$$\begin{aligned} x_2(t) &= \phi_{2,1}x_1'(t) + \phi_{2,2}x_2'(t) \\ &\approx -0.3375 \int_0^t \ddot{x}_g(\tau) e^{-0.4461(t-\tau)} \sin[2.974(t-\tau)]\, d\tau \end{aligned} \tag{cc}$$

Taking the second time derivative of $x_1(t)$ and $x_2(t)$, the acceleration at the floor immediately above the isolation system is determined as

$$\ddot{x}_1(t) = 2.8928 \int_0^t \ddot{x}_g(\tau) e^{-0.4461(t-\tau)} \sin[2.974(t-\tau)]\, d\tau + 0.8879 \int_0^t \ddot{x}_g(\tau) e^{-0.4461(t-\tau)} \cos[2.974(t-\tau)]\, d\tau \quad \text{(dd)}$$

The acceleration at the roof is expressed as

$$\ddot{x}_2(t) = 2.9178 \int_0^t \ddot{x}_g(\tau) e^{-0.4461(t-\tau)} \sin[2.974(t-\tau)]\, d\tau + 0.8956 \int_0^t \ddot{x}_g(\tau) e^{-0.4461(t-\tau)} \cos[2.974(t-\tau)]\, d\tau \quad \text{(ee)}$$

2.2 Base Isolator Mechanical Characteristics and Computer Modeling Techniques

2.2.1 Introduction

Motion equations derived in Section 2.1 for seismically isolated structures are established on the assumptions of the effective damping and the effective stiffness of the isolation system, as well as the linear stiffness of the structure's *seismic force-resisting system*. Consequently, the responses of the structure display a linear relation to the imposed seismic force on both the structure and the isolation system. However, with complicated building configurations, the impact of very soft soil condition on the structure above the isolation system, and the building's proximity to major active faults, a linear analysis is unable to capture accurately the building's performance, such as the actual pulse effects on both the building's seismic force-resisting system and the isolation system. The limited capabilities of the linear analysis have been eventually overcome by incorporating actual mechanical properties of isolator units or bearings into the analytical procedures, which results in a nonlinear analysis.

Theoretically, the nonlinearity of a seismically isolated structure comes from two sources: inelastic deformation of the building's seismic force-resisting system and the isolation system. However, since the seismic force-resisting system is much stiffer than the isolation system, the inelastic deformation mainly concentrates at the isolation system, and the building's seismic force-resisting system can be reasonably assumed to exhibit linear responses. Thus, for design practice, only consideration of nonlinear properties of bearings still conveys the actual performance of the seismically isolated structure and provides required accuracy.

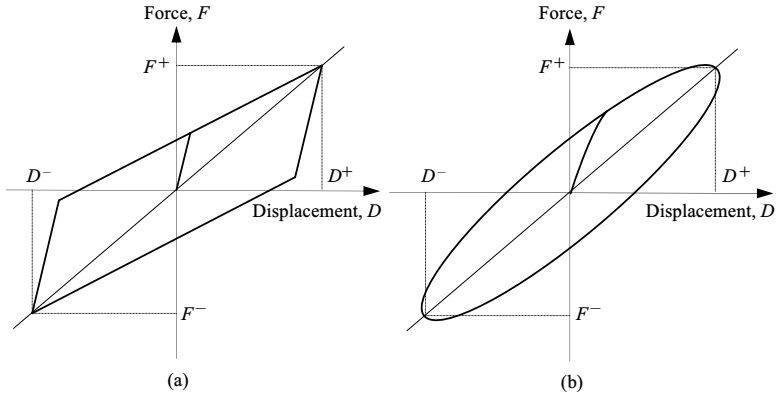

FIGURE 2.5 Idealized force–displacement relationships of isolation system: (a) hysteretic behavior and (b) viscoelastic behavior.

The mechanical properties of different types of bearings have been extensively investigated. Various mathematical models were developed to depict the hysteretic and viscoelastic behavior of bearings. Hysteretic behavior reflects velocity independence of the bearing properties, which exhibit the maximum and minimum displacement of the bearing occurring at the maximum and minimum shear force, respectively. However, viscoelastic behavior of the bearing possesses velocity-dependent properties, which show the maximum and minimum shear usually taking place before the maximum and minimum displacement, respectively. The idealized hysteretic and viscoelastic behavior of bearings is shown in Figure 2.5. Among all the proposed models, the bilinear model is mostly accepted for research and in design practice because its simplicity not only characterizes the mechanical properties of the bearings properly, but also fits both elastomeric-type and sliding-type bearings.

Development and application of a bilinear model to different types of bearings will be explicitly discussed in the following sections. The determination of a bilinear model is initiated by defining three basic parameters. Then, based on unique properties of each type of bearings, specific equations are presented to ascertain the three basic parameters. Other properties of bearings, such as effective damping and vertical stiffness, are also introduced for bearing model development. Application of the bilinear model to computer programs is discussed in the last section, along with an explanation of inputting a bearing's parameters into commercial software.

2.2.2 Bilinear Model and Model Parameters

The *bilinear model*, used to express the relation between the shear force and the lateral displacement, can be defined by three parameters: *elastic stiffness*, k_e, *postyield stiffness*, k_p, and *characteristic strength*, Q. The characteristic strength,

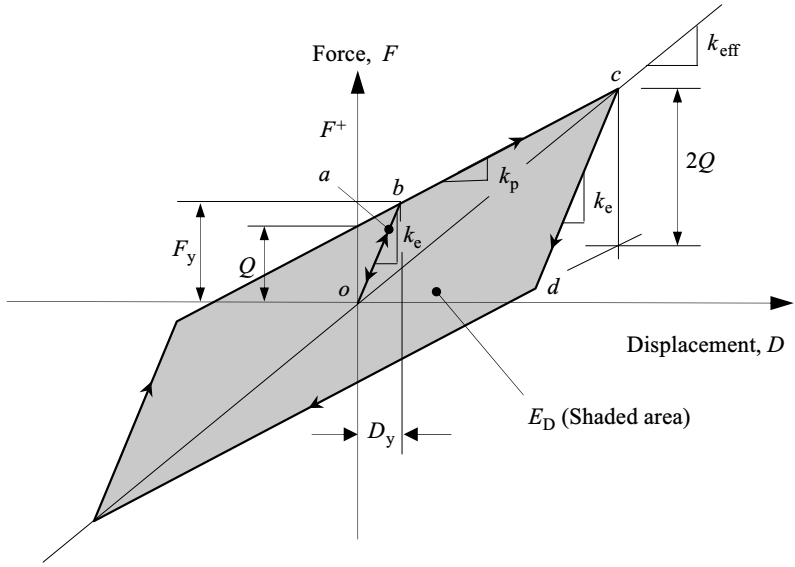

FIGURE 2.6 Bilinear model of isolator unit.

Q, is usually utilized to estimate the stability of hysteretic behavior when the bearing experiences many loading cycles. These three parameters properly reflect the mechanical properties of bearings and provide satisfactory estimations of a bearing's nonlinear behavior.

Figure 2.6 shows an idealized bilinear model based on test data. When a shear starts applying to a bearing, a linear relation, as expressed by line $\overline{oa}$, exists between the shear and the lateral displacement. If the applied shear is decreased from point a, the unloading path remains linearly along line, $\overline{ao}$. Once the shear increases to point b, the bearing yield occurs. Beyond point b, the bearing experiences larger displacement with a small increase in shear and its stiffness is defined postyield stiffness, k_p. If unloading starts at point c, the unloading path does not follow the previous path. Instead, it goes along path $\overline{cd}$ with the same initial stiffness of line $\overline{oa}$. The shear value of $\overline{cd}$ is equal to $2F_y$, where F_y is designated as the yield force. With the shear continues beyond point d, the unloading path is parallel to line $\overline{bc}$ with the same magnitude of k_p.

Effective stiffness of the bearing, k_{eff}, at the postyield region can be expressed in terms of the postyield stiffness, k_p, and the characteristic strength, Q, with corresponding lateral displacement, D.

$$k_{eff} = k_p + \frac{Q}{D} \tag{2.20}$$

The yield displacement, D_y, which is conveniently used in some computer programs to define the bilinear model, is also derived from k_e, k_p, and Q.

$$D_y = \frac{Q}{k_e - k_p} \tag{2.21}$$

The yield force, F_y, at the yield displacement, D_y is determined as

$$F_y = Q + k_p D_y \tag{2.22}$$

The *effective damping*, β_{eff}, is defined as follows:

$$\beta_{eff} = \frac{E_D}{2\pi k_{eff} D^2} \tag{2.23}$$

where E_D is the energy dissipated per cycle as shown in Figure 2.6. For the bilinear model, E_D is considered as the area of the hysteresis loop bounded by the lateral displacement $-D$ and $+D$ at each cycle. Thus, $E_D = 4Q(D - D_y)$, and the effective damping β_{eff}, becomes:

$$\beta_{eff} = \frac{4Q(D - D_y)}{2\pi k_{eff} D^2} = \frac{2Q(D - D_y)}{\pi k_{eff} D^2} \tag{2.23a}$$

In design practice, the effective stiffness and the effective damping are determined at the design displacement, D_D, and the maximum displacement, D_M. Explanations of the design displacement and the maximum displacement are given in Section 2.3.2.

2.2.3 Bilinear Model of Lead-Plug Bearing System

The characteristic strength, Q, of the *lead-plug bearing* is dominantly controlled by the shear strength of the lead core. Shear yield occurs at the lead core under a low level of shear stress. However, the hysteretic behavior of the bearing is quite stable even though the bearing is subjected to many loading cycles. Equation 2.24 exhibits the relation between the *characteristic strength*, Q, and the product of lead yield stress, f_{yl}, and the *lead-plug area*, A_l.

$$Q = A_l f_{yl} \tag{2.24}$$

The *postyield stiffness*, k_p, is shown as follows [6]:

$$k_p = \frac{A_b G f_L}{t} \tag{2.25}$$

where A_b is the bonded area of rubber; t is the total rubber thickness; and the coefficient, f_L, is typically 1.5. G represents the *tangent shear modulus* of rubber, which is determined from dynamic shear tests.

The *elastic stiffness*, k_e, is not easily determined, but it can be approximately estimated as shown below:

$$6.5k_p \le k_e \le 10k_p \tag{2.25a}$$

On the basis of on Equation 2.21, the yield displacement is determined as follows, assuming $k_e = \kappa k_p$ and the ratio of its elastic stiffness to postyield stiffness, κ, is between 6.5 and 10 [6]:

$$D_y = \frac{Q}{k_e - k_p} \approx \frac{Q}{\kappa k_p - k_p} = \frac{Q}{(\kappa - 1)k_p} \tag{2.26}$$

Substituting the yield displacement and the effective stiffness into Equation 2.23a, the *effective damping* becomes in terms of Q, k_p, and κ.

$$\beta_{eff} = \frac{2Q(D - D_y)}{\pi k_{eff} D^2} = \frac{2Q[(\kappa - 1)k_p D - Q]}{\pi(\kappa - 1)k_p(k_p D + Q)D} \tag{2.27}$$

After the determination of the characteristic strength, Q, and the postyield stiffness, k_p, from bearing's prototype tests, the bilinear model as present above is easily established and can be used to perform nonlinear analysis of a structure with lead-plug bearings.

2.2.4 Bilinear Model of High Damping Rubber System

The three parameters used to generate a bilinear model for a *high damping rubber bearing* are conventionally derived from the *tangent shear modulus*, G, and effective damping, β_{eff}. The tangent shear modulus is ascertained from dynamic shear tests. The *effective damping*, determined from bearing's prototype tests, varies between 10% and 20% of critical damping [13]. Then the *postyield stiffness* is calculated as:

$$k_p = \frac{GA_b}{t} \tag{2.28}$$

where A_b is the bonded area of rubber, and t is the total rubber thickness. The *characteristic strength*, Q, can be evaluated by the following equation:

$$Q = \frac{\pi \beta_{eff} k_p D_D^2}{(2 - \pi\beta_{eff})D_D - 2D_y} \tag{2.29}$$

where D_D is denoted as the design displacement. In Equation 2.29, the yield displacement, D_y, is unknown until the parameters, k_e, k_p, and Q are determined.

An approximate estimation of D_y, supported by test results, can be expressed in terms of the total rubber thickness, t: $D_y = \lambda t$, where coefficient, λ, varies between 0.05 and 0.1 [6].

Once k_p, D_y, and Q are known, the yield force of the bearing, F_y, is easily determined as follows:

$$F_y = Q + k_p D_y \tag{2.30}$$

Then the *elastic stiffness* of the high damping rubber bearing becomes

$$k_e = \frac{F_y}{D_y} = k_p + \frac{Q}{D_y} = k_p \left\{ 1 + \frac{\pi \beta_{eff} D_D^2}{\lambda t[(2 - \pi \beta_{eff}) D_D - 2\lambda t]} \right\} \tag{2.31}$$

By substituting $D_y = \lambda t$ into Equation 2.23a, the *effective stiffness* at the design displacement can be derived as follows:

$$k_{eff} = \frac{2Q(D_D - \lambda t)}{\pi \beta_{eff} D_D^2} \tag{2.32}$$

2.2.5 Bilinear Model of Friction Pendulum System

The characteristic strength of a *friction pendulum bearing*, Q, is expressed as

$$Q = \mu_s P_c \tag{2.33}$$

where P_c is the axial force applied at the bearing, which is composed of the gravity load, P_g, and the effects of vertical ground acceleration. If the effects of the vertical acceleration are not significant and can be neglected, then the axial force, P_c, is simplified as $P_c = P_g$. μ_s is the *coefficient of sliding friction* related to the *sliding velocity*, which is given as [5]

$$\mu_s = f_{max} - (f_{max} - f_{min}) e^{-\xi |\dot{D}|} \tag{2.34}$$

In Equation 2.34, f_{max} and f_{min} are friction coefficients at fast and slow velocity, respectively; $\dot{D}$ represents the velocity of the bearing movement; ξ is called the inverse of the *characteristic sliding velocity*, which controls the transition from f_{max} to f_{min} and is determined from experiments. A suggested value of ξ is approximately 2.54 s/in. [5].

The *postyield stiffness* is determined as shown below:

$$k_p = \frac{P_c}{R} \tag{2.35}$$

where R represents the radius of curvature of the sliding surface. Test results indicate that the elastic stiffness of the friction pendulum bearing, k_e, is normally over 100 times larger than the postyield stiffness, k_p. Accordingly, the yield displacement, D_y, becomes

$$D_y = \frac{Q}{k_e - k_p} \approx \frac{Q}{100k_p} = \frac{\mu_s P_c}{100\left(P_c/R\right)} = \frac{\mu_s R}{100} \tag{2.36}$$

Equation 2.36 implies that the yield displacement, D_y, is a very small value and is approximately 0.1 in.

From Equation 2.20, the *effective stiffness* of the friction pendulum bearing at the design displacement, D_D, can be written as

$$k_{eff} = k_p + \frac{Q}{D} = P_c\left(\frac{1}{R} + \frac{\mu_s}{D_D}\right) \tag{2.37}$$

Since the yield displacement, D_y, is much smaller than the design displacement, D_D, the *hysteresis loop area* of the friction pendulum bearing can be simplified and is approximately estimated as follows:

$$E_D = 4Q(D_D - D_y) \approx 4QD_D = 4\mu_s P_c D \tag{2.38}$$

By substituting Equations 2.37 and 2.38 into Equation 2.23a, the *effective damping* of the friction pendulum bearing is derived as follows:

$$\beta_{eff} = \frac{E_D}{2\pi k_{eff} D_D^2} = \frac{4\mu_s P_c D_D}{2\pi P_c\left(1/R + \mu_s/D_D\right) D_D^2} = \frac{2\mu_s}{\pi\left(D_D/R + \mu_s\right)} \tag{2.39}$$

2.2.6 Computer Modeling of Isolation System

Modeling of isolation systems by computers originally evolved from SDOF models that simply assumed the rigid structure above the isolation system and only accounted for the nonlinearity of the isolator units. However, with the improvement of computational technologies and the decrease in computer processing time, isolation systems have enabled to be incorporated into computer programs for two- or three-dimensional structural analyses. In the meantime, the invention of high-speed personal computers and price reduction of computer hardware have resulted in developing powerful computer programs to analyze and design complicated building structures with consideration of the nonlinear behavior of the isolator units and the structure above the isolation system.

Along with other popular computer programs, SAP2000 and ETABS [4] have been recognized as reliable programs to analyze and design seismically isolated structures. Both programs have capabilities to perform equivalent static analysis, response spectrum analysis, linear response history analysis, and nonlinear response history analysis, but each program also has its own unique

characteristics: SAP2000 has more sophisticated functions that can be tailored to study and investigate any types of seismically isolated structures, such as buildings and bridges, while ETABS mainly emphasizes the analysis and design of building structures with isolation systems. A user familiar with one program will not have problems operating the other. Since the assignment of isolator properties is basically the same for both programs, this section only introduces how to model isolator properties using ETABS.

There are two types of link elements that are built into ETABS: ISOLATOR1 is usually used to model elastomeric-type bearings and ISOLATOR2 is considered for friction pendulum bearings. For ISOLATOR1, *effective stiffness*, k_{eff}, and *effective damping*, β_{eff}, of a bearing along two principal directions of the superstructure shall be the input for response spectrum analysis and linear response history analysis. As discussed in Section 2.2.2, k_{eff} and β_{eff} are derived at the design displacement, D_{D}, or at the maximum displacement, D_{M}. However, D_{D} and D_{M} from ETABS results are usually not the same values as used to determine k_{eff} and β_{eff} initially. Iteration procedures are normally performed to adjust D_{D} and D_{M} until the ETABS results are satisfactorily close to the assumed values for determination of k_{eff} and β_{eff}. In addition, attention should be paid to the input of effective damping, β_{eff}. During linear analysis, such as response spectrum analysis, the total damping factor of the structural system consists of two portions: one is additionally specified to the structure above the isolation system, and the other is automatically converted by ETABS from the effective damping, β_{eff}, of each ISOOLATOR1 assigned in the structural model [4].

If ISOLATOR1 is used for nonlinear response history analysis, the following parameters of the bearing in both principal directions of the superstructure are required: *elastic stiffness*, k_{e}, yield displacement, D_{y}, and the ratio of postyield stiffness to elastic stiffness, $\eta = k_{\text{p}}/k_{\text{e}}$. On the basis of these parameters input into the program, ETABS automatically generates a biaxial hysteretic model of the bearing to consider the coupled shear–deformation relationship from the two assigned principal directions.

Elastomeric-type bearings have a higher vertical stiffness in compression than in tension. However, ISOLATOR1 only assumes the same magnitude of vertical stiffness in tension and compression. If the vertical stiffness in tension is modeled, the same as in compression, the overturning or uplift force in the bearing becomes abnormally higher and, in reality, the bearing does not have the capacity to resist such high tensile force. Consequently, the analytical results inaccurately reflect the actual performance of the seismically isolated structure. The modeling of different tensile and compressive stiffness in the vertical direction can be achieved by adding a gap element to ISOLATOR1. The gap element has only vertical stiffness in compression but does not resist tensile force. Therefore, use the tensile stiffness, k_{ten}, in ISOLATOR1 and assign the stiffness, $k_{\text{com}} - k_{\text{ten}}$, to the gap element in the vertical direction, where k_{com} is the bearing's compressive stiffness. Once the bearing is in compression and the vertical deformation is assumed to be u, the sum of the compressive force in ISOLATOR1 and the gap element is

$k_{en}u + (k_{com} - k_{en})u = k_{com}u$, which means that the compressive stiffness of the bearing is properly assigned by combining two elements at the same location.

ISOLATOR2, used to model the properties of a friction pendulum bearing, allows the bearing to move in the upward direction with no tensile stiffness. In the vertical direction, ISOLATOR2 behaves like a gap element and the user must define its compressive stiffness. The effective stiffness, k_{eff}, and the effective damping, β_{eff}, along two principal directions of the structure above the isolation system shall be input into ISOLATOR2. The elastic stiffness, k_e, must be assigned for nonlinear response history analysis. Unlike ISOLATOR1 for elastomeric-type bearings, ISOLATOR2 requires defining radius of curvature of the sliding surface, R. Also, the inverse of the characteristic sliding velocity, ξ, mainly related to the bearing pressure, and the coefficients of sliding friction at fast velocity, f_{max}, and at slow velocity, f_{min}, are needed in ISOLATOR2 in order to calculate the coefficient of sliding friction, μ_s, and the yield displacement, D_y. The postyield stiffness is automatically generated by ETABS from the applied axial force, P_c, and the radius of curvature of the sliding surface, R. A biaxial hysteretic model of the bearing showing the coupled shear–deformation relationship from the two assigned principal directions is also automatically developed by ETABS.

Both ISOLATOR1 and ISOLATOR2 require assigning the self-weight of the bearing, the translational mass, and the rotational mass moment of inertia because appropriate Ritz vectors need to be activated during nonlinear response history analysis.

2.3 Code Requirements for Design of Seismically Isolated Structures

2.3.1 Introduction

In the United States, the first design provisions for seismically isolated structures were developed by the Northern Section of the Structural Engineers Association of California (SEAOC) in 1986 [15]. The SEAOC Seismology Committee revised these design provisions and published the revisions as Appendix 1L to the 1990 SEAOC Blue Book [16]. Afterward, the International Conference of Building Officials (ICBO) made minor editorial changes to Appendix 1L and included it in the 1991 Uniform Building Code (UBC) as a nonmandatory appendix to Chapter 23 [10]. ICBO and the SEAOC Seismology Committee periodically reviewed and modified the design provisions for seismically isolated structures to update the UBC and the SEAOC Blue Book in each code development cycle [11,17]. Since 1991, the Federal Emergency Management Agency (FEMA) has developed guidelines for the design of new buildings and the rehabilitation of existing buildings with isolation systems in FEMA 273/274 [6], FEMA 356 [7], and FEMA 450 [8].

The most current version of design provisions for seismically isolated structures can be found in the ASCE Standard, ASCE 7-05 [2]. ASCE 7-05, Chapter 17

represents the state-of-the-art development of the design provisions for seismically isolated structures. In addition, these provisions have been entirely adopted in the seismic provisions of the 2006 International Building Code (IBC) [9]. It is expected that more and more state and local codes will reference ASCE 7-05, Chapter 17 for the design of seismically isolated structures. Therefore, the main focus of this section is to represent the ASCE 7-05 design provisions for seismically isolated structures. First, concepts of seismic ground motions are introduced. Then, the section of the analysis procedure for structural design, static or dynamic, is discussed. This section ends with summaries of the ASCE 7-05 special requirements for each analysis procedure.

2.3.2 Seismic Ground Motion

Two levels of earthquake forces are required by ASCE 7-05 for the design of seismically isolated structures: *maximum considered earthquake* (MCE) and *design earthquake*. The MCE, defined as the most severe earthquake effects, normally refers to 2% probability of exceedance in 50 years, which means that the average of the MCE return period is approximately 2500 years. The isolation system shall remain in stable condition under the MCE. The design earthquake, which is defined as the earthquake effects equal to two-thirds of the MCE effects, is used in design to ensure that life safety is guaranteed; structural and nonstructural damage are minimized or avoided; and facility functions are maintained.

The MCE spectral response acceleration is usually determined by performing a ground motion hazard analysis. However, ASCE 7-05 provides a convenient method to establish the MCE response spectrum relying upon two mapped acceleration parameters: the MCE spectral response acceleration parameter at short period, S_S, and the MCE spectral response acceleration parameter at a period of 1 s, S_1, which are given in ASCE 7-05, Figures 22-1 through 22-14 of the MCE ground motion maps. Note that the application of mapped acceleration parameters to the development of the MCE response spectrum is limited by soil profile and the region's seismicity, which will be discussed at the end of this section.

The development of the MCE ground motion maps is based on region seismicity of the United States, which is classified by the U.S. Geological Survey (USGS) into three regions:

1. Regions of negligible seismicity with a very low probability of structure collapse or damage are characterized as *body wave magnitude* not over 5.5 and recorded ground motions with *Modified Mercalli Intensity* V or less. Thus, the MCE ground motion maps specify 1% of acceleration on the mass as a minimum lateral force for structural design.
2. Regions with seismicity varying from low and moderate to high feature undefined earthquake sources and an MCE with long return periods, the acceleration parameters shown on the ASCE 7-05 MCE ground motion maps are determined from USGS probabilistic seismic hazard maps with a 2% probability of exceedance of 50 years.

3. For high seismicity regions that are close to known faults with short return periods, such as coastal California, the USGS deterministic hazard maps are used to determine the acceleration parameters of the ASCE 7-05 MCE ground motion maps. The establishment of the USGS deterministic hazard maps is in accordance with a 50% increase in the median estimate of *ground motion attenuation* functions.

Note that the ASCE 7-05 MCE ground motion maps are generated based on a 5% damped spectral response acceleration at Site Class B. Classifications of different Site Class that ranges from A through F mainly rely on parameters of average *shear wave velocity*, $\overline{v}_s$, standard *blow count*, $\overline{N}$, and *undrained shear strength*, $\overline{s}_u$. Detailed explanations of site clarifications can be found in Chapter 20 of ASCE 7-05 [2].

After selecting the spectral response acceleration parameters, S_S and S_1, from the MCE ground motion maps, the MCE spectral response acceleration at a short period, S_{MS}, and the MCE spectral response acceleration at 1 s, S_{M1}, can be computed as follows with consideration of the site class effects:

$$S_{MS} = F_a S_S \tag{2.40}$$

$$S_{M1} = F_v S_1 \tag{2.41}$$

where F_a and F_v are site coefficients and are specified in Tables 2.1 and 2.2.

Once S_{MS} and S_{M1} are determined, the design spectrum acceleration parameters at a short period, S_{DS}, and the design spectrum acceleration parameter at 1 s, S_{D1}, are expressed as

$$S_{DS} = \frac{2}{3} S_{MS} \tag{2.42}$$

$$S_{D1} = \frac{2}{3} S_{M1} \tag{2.42a}$$

TABLE 2.1
Site Coefficient, F_a

Site class	Mapped MCE spectral response acceleration parameters at short period				
	$S_S \leq 0.25$	$S_S = 0.5$	$S_S = 0.75$	$S_S = 1.0$	$S_S \geq 1.25$
A	0.8	0.8	0.8	0.8	0.8
B	1.0	1.0	1.0	1.0	1.0
C	1.2	1.2	1.1	1.0	1.0
D	1.6	1.4	1.2	1.1	1.0
E	2.5	1.7	1.2	0.9	0.9

TABLE 2.2
Site Coefficient, F_v

Site class	Mapped MCE spectral response acceleration parameters at 1 s period				
	$S_1 \leq 0.1$	$S_1 = 0.2$	$S_1 = 0.3$	$S_1 = 0.4$	$S_1 \geq 0.5$
A	0.8	0.8	0.8	0.8	0.8
B	1.0	1.0	1.0	1.0	1.0
C	1.7	1.6	1.5	1.4	1.3
D	2.4	2.0	1.8	1.6	1.5
E	3.5	3.2	2.8	2.4	2.4

If the period of the structural system, T, is less than $T_0 = 0.2S_{D1}/S_{DS}$, the *design spectral response acceleration*, S_a, displays a linear relation to T and is given as

$$S_a = S_{DS}\left(0.4 + 0.6\frac{T}{T_0}\right) \tag{2.43}$$

When the period of the structural system, T, is in the region of $T_0 < T < T_s = S_{D1}/S_{DS}$, S_a remains constant and is expressed as

$$S_a = S_{DS} \tag{2.44}$$

For $T_s < T < T_L$, where T_L is the long-period transition period and is given in Figures 22-15 through 22-20 of ASCE 7-05, S_a can be determined as

$$S_a = \frac{S_{D1}}{T} \tag{2.45}$$

Once T is longer than T_L, S_a has the following relation with T:

$$S_a = \frac{S_{D1}T_L}{T^2} \tag{2.46}$$

The MCE response spectrum is determined by simply increasing the design response spectrum by a factor of 1.5. Figure 2.7 shows the design response spectrum and the MCE response spectrum.

If the seismically isolated structure is located in Site Class F or on the site with S_1 over 0.6, spectral response acceleration parameters from the MCE ground motion maps are not applicable to the determination of the design response spectrum and the MCE response spectrum. Therefore, site-specific ground motions, as indicated in Chapter 21 of ASCE 7-05, have to be investigated in order to develop the design response spectrum and the MCE response spectrum.

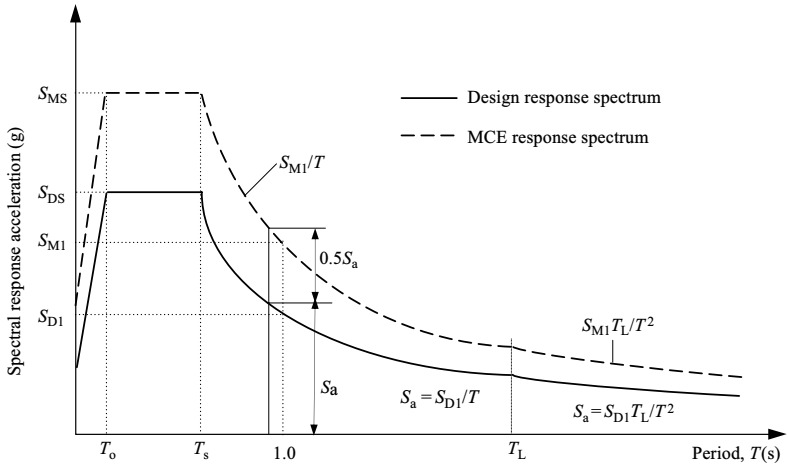

FIGURE 2.7 The design and the MCE response spectrum.

2.3.3 Analysis Procedure Selection

ASEC7-05 addresses three design procedures for seismically isolated structures: *equivalent lateral force analysis*, *response spectrum analysis*, and *response history analysis*. The response history procedure is the first choice for structural analysis because it is capable of taking the nonlinear behavior of both the seismic force-resisting system and the isolation system into account, and is able to capture the actual performance of the structure no matter how complicated the structural configuration is. Also, due to availability of powerful personal computers and the development of commercial software, the impact of unfavorable soil conditions and very near fields of active faults can be easily considered in computer models for structural design.

However, the equivalent lateral force procedure possesses its own advantages. For example, use of this static analysis can greatly simplify the design procedure for some particular structures. Moreover, the equivalent lateral force procedure can be utilized to quantify some crucial design parameters, such as the displacement and the lateral force, as lower-bound limits on response spectrum analysis or response history analysis. ASCE7-05 permits using the equivalent lateral force procedure if the following items are met:

Item 1: The MCE spectral response acceleration parameter at a period of 1 s, S_1, shall be less than 0.6 g at the structure's construction site.

Item 2: The location of the structure shall be limited to Site Class A, B, C, or D.

Item 3: The height of the structure above the isolation interface is less than or equal to four stories, also, the maximum height shall not be over 65 ft.

Item 4: The effective period of the isolated structure at the maximum displacement, T_M, shall not be over 3.0 s.

Item 5: The following relation between the effective period of the isolated structure at the design displacement, T_D, and the period of the *fixed-base structure* above the isolation interface may be computed from the approximate period, T_a, which shall satisfy

$$T_D > 3T_a = 3C_t h_n^x \tag{2.47}$$

where h_n is the height in ft (m) of the structure above the isolation system. Selected coefficients of C_t and x are provided in Table 2.3 according to different types of the structures' seismic force-resisting systems.

Alternatively, a simplified equation can be used to estimate the period of the fixed-base structure above the isolation interface for both steel and concrete moment frames, provided that the number of building stories, n, is less than or equal to 12 with the story height over 10 ft.

$$T_a = 0.1n \tag{2.48}$$

Item 6: The structure above the isolation system shall not have any horizontal or vertical structural irregularities.

Item 7: The effective stiffness of the isolation system at the design displacement shall be greater than one-third of the effective stiffness at 20% of the design displacement. Figure 2.8 illustrates the above relation.

Item 8: The isolation system has the capability to produce a restoring force. ASCE7-05 requires that the lateral force at the total design displacement be at least $0.025W$ greater than the lateral force at 50% of the total design displacement.

Item 9: The isolation system does not limit the MCE displacement to less than the total maximum displacement.

Use of the response spectrum procedure may be permitted provided that Items 2, 7, 8, and 9, as stated above for the equivalent lateral force procedure are satisfied.

TABLE 2.3
Parameters C_t and x

Structure type	C_t	x
Steel moment-resisting frames	0.028	0.8
Concrete moment-resisting frames	0.016	0.9
Eccentrically braced steel frames	0.03	0.75
All other structural systems	0.02	0.75

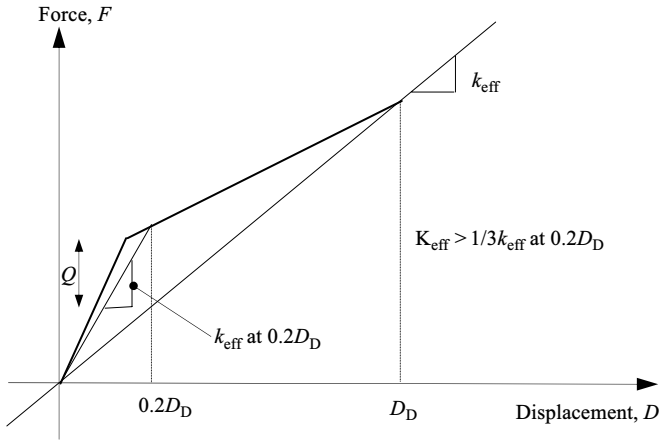

FIGURE 2.8 Requirement on k_{eff} for equivalent lateral force procedure.

2.3.4 Equivalent Lateral Force Procedure

2.3.4.1 Design displacement and corresponding effective stiffness

The equivalent lateral force procedure is developed based on a simple relationship between the spectral *displacement*, S_D, and the *pseudoacceleration*, S_A, as stated in Equation 2.8. Considering the design earthquake, S_D and S_A can be redenoted as the *design displacement*, D_D, in in. (mm), and the *design spectral response acceleration*, S_a, respectively. In addition, by introducing a numerical coefficient for effective damping, B_D, to reduce S_a, Equation 2.8 is rewritten as follows:

$$D_D = \frac{S_a}{\omega_b^2 B_D} \tag{2.49}$$

where the angular frequency is $\omega_b = 2\pi/T_D$; T_D represents the effective period of the seismically isolated structure, in *s*, at the design displacement. For most seismically isolated structures, T_D is normally between 2.0 and 4.0 s, and is given by

$$T_D = 2\pi\sqrt{\frac{W}{k_{D\,\min} g}}$$

where $k_{D\,\min}$ equals the minimum effective stiffness, in kips/in. (kN/mm), of the isolation system at the design displacement in the horizontal direction; W represents the effective seismic weight of the structure above the isolation interface. The units of W are in kips (kN).

Thus, substituting the design spectral response acceleration at T_D as given in Equation 2.45 into Equation 2.49, the design displacement, D_D, is derived as

$$D_D = \frac{S_a}{\omega_b^2 B_D} = \frac{1}{B_D}\left(\frac{T_D}{2\pi}\right)^2 \frac{S_{D1}}{T_D} g = \frac{g S_{D1} T_D}{4\pi^2 B_D} \tag{2.50}$$

where g is the acceleration of gravity. The unit for g is in./s^2 (mm/s^2).

The *numerical coefficient for effective damping*, B_D, is related to the effective damping of the isolation system at the design displacement, β_D, which is defined as follows:

$$\beta_D = \frac{\sum E_D}{2\pi k_{D\,max} D_D^2} \tag{2.51}$$

where $k_{D\,max}$ is the maximum effective stiffness, in kips/in. (kN/mm), of the isolation system at the design displacement in the horizontal direction; $\sum E_D$ represents the total energy dissipated per cycle of the design displacement response, which shall be taken as the sum of the energy dissipated at a complete cycle in all isolator units measured at the design displacement, D_D. After β_D is determined, the numerical coefficient for damping ratio, B_D, can be computed from the following equation [14] with limitation to 50% of critical damping:

$$B_D = \frac{2.31 - 0.41 \ln(5)}{2.31 - 0.41 \ln \beta_D} \tag{2.52}$$

Equation 2.52 is established on the basis of 5% of critical damping. Thus, β_D equal to 5% of critical damping results in a unit of numerical coefficient, B_D. ASCE 7-05 does minor adjustments to Equation 2.52 and the tabular values are given in Table 2.4.

β_M and B_M in Table 2.4 present the effective damping and the numerical coefficients at the MCE, respectively, and will be discussed in next section. Linear interpolation of β_D or β_M is permitted to calculate B_D or B_M.

TABLE 2.4
Damping Coefficient, B_D or B_M

β_D or β_M	≤2%	5%	10%	20%	30%	40%	≥50%
B_D or B_M	0.8	1.0	1.2	1.5	1.7	1.9	2.0

2.3.4.2 Maximum displacement and corresponding effective stiffness

If the seismically isolated structure is required considering the MCE, such as the design of the isolation system, the effective period at the maximum displacement, T_M, is calculated as

$$T_M = 2\pi\sqrt{\frac{W}{k_{M\,min}g}} \tag{2.53}$$

where $k_{M\,min}$ is the minimum effective stiffness, in kips/in. (kN/mm), of the isolation system at the maximum displacement in the horizontal direction.

Utilizing the same methodology as presented in Section 2.3.4.1, the maximum displacement, D_M, in (mm) can be expressed as follows:

$$D_M = \frac{gS_{M1}T_M}{4\pi^2 B_M} \tag{2.54}$$

where S_{M1} comes from Equation 2.41 and the numerical coefficient for effective damping, B_M, is determined from Table 2.4. The effective damping of the isolation system at the maximum displacement, β_M, used to determine B_M, is defined as follows:

$$\beta_M = \frac{\sum E_M}{2\pi k_{M\,max}D_M^2} \tag{2.55}$$

where $\sum E_M$ is the total energy dissipated per cycle of the maximum displacement response, which shall be taken as the sum of the energy dissipated at a complete cycle in all isolator units measured at the maximum displacement, D_M.

2.3.4.3 Total design displacement and total maximum displacement

The design displacement obtained from Equation 2.50 does not represent the maximum movement of the isolation system since it only accounts for the displacement at the isolation system's center of rigidity. In fact, an additional displacement exists owing to the eccentricity, e, in ft (mm) as shown in Figure 2.9. Thus, these two portions of displacements form the maximum movement of the isolation system that is normally called the *total design displacement*. The eccentricity, e, which results in the additional displacement, consists of the actual eccentricity measured from the mass of the structure above the isolation interface to the isolation system's center of rigidity, and the accidental eccentricity equal to 5% of the longest plan dimension of the structure perpendicular to the considered force direction. The additional displacement is determined assuming a rectangular plane of the isolation system with the longest plan dimension, d, and the shortest plan dimension, b.

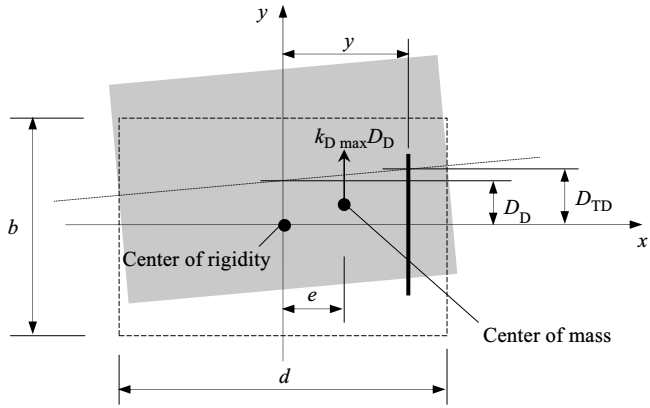

FIGURE 2.9 Determination of total design displacement, D_{TD}.

It is further assumed that the isolation system is uniformly distributed in this rectangular plane. Therefore, the *torsional stiffness of the isolation system*, $k_{torsion}$, can be expressed in terms of the maximum effective stiffness, $k_{D\,max}$:

$$k_{torsion} = \frac{b^2 + d^2}{12} k_{D\,max} \tag{2.56}$$

At the design displacement, the seismic force acting on the center of the rigidity of the isolation system is $k_{eff} D_D$. The *rotation of the isolation system*, γ, is derived as

$$\gamma = \frac{k_{D\,max} D_D e}{\left(b^2 + d^2/12\right) k_{D\,max}} = \frac{12 D_D e}{b^2 + d^2} \tag{2.57}$$

The additional displacement, D_a, at the distance, y, which is between the isolation system's center of rigidity and the designated structural element measured perpendicular to the force direction, can be determined as

$$D_a = \frac{12 D_D e}{b^2 + d^2} y \tag{2.57a}$$

By adding D_D to Equation 2.57a, the total design displacement, D_{TD}, in in. (mm), becomes

$$D_{TD} = D_D + D_a = D_D \left(1 + y \frac{12e}{b^2 + d^2}\right) \tag{2.58}$$

In the same way, the total maximum displacement, D_{TM}, can be determined as follows:

$$D_{TM} = D_M \left(1 + y\frac{12e}{b^2 + d^2}\right) \tag{2.58a}$$

2.3.4.4 Minimum lateral force

A *minimum lateral force*, V_b, in kips (kN), is specified by ASCE 7-05 to design the isolation system, the structural elements below the isolation system, and the foundation:

$$V_b = k_{D\,max} D_D \tag{2.59}$$

The *minimum shear force*, V_s, to design the structural elements above the isolation interface shall be evaluated based on the following equation:

$$V_s = \frac{k_{D\,max} D_D}{R_I} \tag{2.60}$$

where R_I is a numerical coefficient related to the type of the seismic force-resisting system above the isolation system. ASCE 7-05 requires that $1.0 \leq R_I = 3R/8 \leq 2.0$, where R represents the response modification factor that is given in Table 12.2-1 of ASCE 7-05. Selected values of R and R_I for commonly used seismic force-resisting systems are summarized in Table 2.5.

ASCE 7-05 indicates that the minimum shear force, V_s, computed from Equation 2.60 shall not be less than the seismic force determined by the following three conditions. If it is, then the largest seismic force controls the design of structural elements above the isolation system.

A fixed-base structure with the same effective period, T_D, is introduced to evaluate the minimum lateral force based on Section 12.8 of ASCE 7-05 [2]. This minimum lateral force is renoted as V, and the determination procedures are

TABLE 2.5
Selected Ω_0, R, R_I, and C_d

Seismic force resisting system	Ω_0	R	R_I	C_d
Bearing wall systems	Special reinforced concrete shear walls	2.5	5	1.875
	Special reinforced masonry shear walls	2.5	5	1.875
Building frame systems	Special steel concentrically braced frames	2	6	2
	Special reinforced concrete shear walls	2.5	6	2
Moment-resisting frame systems	Special steel moment frames	3	8	2
	Special reinforced concrete moment frames	3	8	2

TABLE 2.6
Importance Factor

Building occupancy category	*I*
Essential Facilities—IV	1.5
Substantial hazard to human life in the event of failure—III	1.25
Low hazard to human life in the event of failure—I	
Other buildings not specified in Occupancy Categories I, III, and IV—II	1.0

summarized as below:

$$V = C_S W \tag{2.61}$$

where C_S is the seismic response coefficient determined as follows:

$$C_S = \frac{S_{DS}}{(R/I)} \tag{2.62}$$

where I is the *occupancy importance factor*, which is given in Table 2.6.

The upper-bound value of C_S is specified in following Equations 2.63 and 2.63a:

$$C_S \leq \frac{S_{D1}}{T_D (R/I)} \quad \text{for } T_D \leq T_L \tag{2.63}$$

$$C_S \leq \frac{S_{D1} T_L}{T_D^2 (R/I)} \quad \text{for } T_D \geq T_L \tag{2.63a}$$

However, C_S determined from Equation 2.62 shall not be less than the value as given below:

$$C_S \geq 0.01 \tag{2.64}$$

If the seismically isolated structure is constructed at the site with the mapped MCE spectral response acceleration at a period of 1 s, S_1, equal to or greater than 0.6 g, the following equation has be used to check the lower-bound value of C_S:

$$C_S \geq \frac{0.5 S_1}{(R/I)} \tag{2.65}$$

Wind load effects must be considered to evaluate the minimum lateral force. In general, the wind load generates less lateral force than that of V_s and does

not control the design of most seismically isolated structures. In addition, due to substantial content concerning wind load determination provided in ASCE 7-05 and the limited space of this book, computations of wind load effects are not presented in this section. Detailed methods of determining the lateral force from the wind load can be found in ASCE 7-05, Chapter 6 [2].

A lateral force that fully activates the isolation system or the wind-restraint system shall be determined to evaluate the minimum lateral force V_s. For *sliding-type bearings*, such as a *friction pendulum system*, the minimum lateral force, as renoted as V_i, to activate the isolation system is expressed as follows:

$$V_i = 1.5\mu_b W \tag{2.66}$$

where μ_b is the breakaway friction coefficient of the friction pendulum system.

For *elastomeric-type bearings*, the minimum lateral force rewritten as V_i, which results in the yield of the isolation system, is determined as seen below.

$$V_i = 1.5k_e D_y \tag{2.67}$$

where k_e is the elastic stiffness of the isolation system and D_y represents the yield displacement of the isolation system.

2.3.4.5 Vertical distribution of lateral force and story drift limitation

The vertical distribution of the minimum lateral force, V_s, over the height of the structure above the isolation interface is provided by ASCE 7-05 and shown in Equation 2.68.

$$F_i = \frac{V_S w_i h_i}{\sum_{j=1}^{n} w_j h_j} \tag{2.68}$$

where w_i or w_j is portion of the effective seismic weight, W, at story i or j, and h_i or h_j at story i or j represents the height measured from the base level of the seismically isolated structure.

The story drift, δ_i, at each story level i from structural analysis is limited as

$$\frac{C_d \delta_i}{I} \leq 0.015 h_{si} \tag{2.69}$$

where I represents the important factor and C_d is a deflection amplification factor, which is given in Table 2.5. The story height is denoted as h_{si} at any level i.

2.3.5 Dynamic Analysis Procedure

2.3.5.1 General requirements for dynamic analysis

ASCE 7-05 specifies two dynamic analysis procedures to design seismically isolated structures: response spectrum analysis and response history analysis. Both procedures require that a structural model include the seismic force-resisting system above the isolation interface and the isolation system in order to capture sufficient design information.

A well-established structural model has the capability to reflect real system performance and provide convincing results for design. Therefore, the following criteria may be used to guide the development of the structural model:

1. The seismic force-resisting system shall be modeled. For concrete and masonry structures, the *effective cracked sections* of elements must be used to determine the stiffness of the seismic force-resisting system. For a steel moment frame system, the story drift shall count toward the *panel zone* deformation. If the assumption of *rigid diaphragm* is invalid, the diaphragm participation in the dynamic response shall be considered in the structural model. In addition, P–Δ effects shall be taken into account. Models of P–Δ effects, panel zones, and rigid diaphragms refer to pages 252, 463, and 615 of Reference 3.
2. For modeling the isolation system, the isolator units shall be assigned in the model based on the real locations as planned. The modeled isolation system is able to report the uplift force and vertical movement of each isolator, as well as to provide translational displacement and torsional movement of the structure above the isolation interface and the isolation system itself. The nonlinear behavior of the isolation system shall be incorporated into the structural model for nonlinear dynamic analysis.

A linear elastic model is permitted by ASCE 7-05 for dynamic analysis if the maximum effective stiffness of the isolation system is used to substitute the nonlinear properties of the isolation system and the seismic force-resisting system above the isolation system keeps its elasticity under the design earthquake.

2.3.5.2 Lower-bound lateral displacements and lateral forces

The total design displacement, D_{TD}, and the total maximum displacement, D_{TM}, are specified by ASCE 7-05 to provide limits on corresponding displacements obtained from dynamic analysis.

$$D_{\mathrm{TD}} = \frac{D_{\mathrm{D}}}{\sqrt{1 + \left(T/T_{\mathrm{D}}\right)^2}} \left[1 + y\left(\frac{12e}{b^2 + d^2}\right)\right] \tag{2.70}$$

$$D_{\mathrm{TM}} = \frac{D_{\mathrm{M}}}{\sqrt{1 + \left(T/T_{\mathrm{M}}\right)^2}} \left[1 + y\left(\frac{12e}{b^2 + d^2}\right)\right] \tag{2.71}$$

where T is the period of the fixed-base structure above the isolation system. For the meanings of other notations, refer to Equations 2.58 and 2.58a. The total displacement from the dynamic analysis shall not be less than 90% of D_{TD} as determined by Equation 2.70, and the total maximum displacement from the dynamic analysis shall not be less than 80% of D_{TM} as specified by Equation 2.71.

For the design of the isolation system, the structural elements below the isolation system, and the foundation, the forces determined from the dynamic analysis shall not be reduced and shall not be less than 90% of V_b as determined from Equation 2.59.

For the design of the structural elements above the isolation system, the forces obtained from the dynamic analysis may be reduced by a factor of R_I. If the superstructure is regular, the reduced force shall not be less than 80% of V_s for response spectrum analysis and 60% of V_s for response history analysis, where V_s is the minimum shear force determined from the equivalent lateral force procedure and its limits as given in Section 2.3.4.4. For the irregular superstructure, the reduced force must be the same as V_s for response spectrum analysis and shall not be less than 80% of V_s for response history analysis. The forces from dynamic analysis must be increased or scaled up in case they are below the lower bound as specified above.

The story drift is checked based on Equation 2.69. The story drift limitation is $0.015h_{sx}$ for response spectrum analysis and $0.020h_{sx}$ for response history analysis. P–Δ *effects* of the structure above the isolation system subjected to the MCE shall be considered if the story drift ratio is over $0.01/R_I$.

2.3.5.3 Response spectrum analysis

Response spectrum analysis is essentially a linear analytical procedure. As discussed in Section 2.2.1, minimization of nonlinear deformations of the structure above the isolation interface could be achieved on condition that a *seismic force-resisting system* is properly selected and its layout is well balanced. As a result, nonlinear deformations dominantly occur at the isolation system and the structure above the isolation interface can be assumed to deform within elastic ranges. Also, the conversion of the nonlinearity of the isolation system into a linear relation between the shear and its lateral displacement is accomplished by introducing an *effective stiffness* or secant stiffness, k_{eff}, at the design or maximum displacement. Figure 2.6 gives an example to determine the effective stiffness, k_{eff}, from a bilinear model of an isolator unit. On the basis of the above assumptions, use of linear properties for both the seismic force-resisting system and the isolation system makes the response spectrum procedure applicable to analyze seismically isolated structures.

Considering a structure with an isolation system under the design earthquake, the damping portion of the superstructure and the isolation system, $[2\beta\omega]\{\dot{x}'\}$, as given in Equation 2.17, can be eliminated [17] by employing a 5% damped pseudoacceleration, S_{am}, which is inclusively reduced by a numerical coefficient for effective damping, B_{mD}, at the mth mode of vibration. Thus, the motion

equation corresponding to the mth angular frequency, ω_m, is simplified as follows:

$$\ddot{x}'_m + \omega_m^2 x'_m = \Gamma_m S_{am}, \quad m = 1, 2, \ldots n \tag{2.72}$$

x'_m in Equation 2.72 represents the mth component of the generalized response vector and is used to define the structural displacements, $\{x\}_m = \{\Phi\}_m x'_m$, where $\{\Phi\}_m$ is the mth mode shape of the system and its component, $\phi_{n,m}$, at the isolation interface is designated as a unit. The angular frequency, ω_m, in Equation 2.72 is determined by the following equation:

$$\omega_m^2 = \frac{\{\Phi\}_m^{\mathrm{T}}[\mathrm{K}]\{\Phi\}_m}{\{\Phi\}_m^{\mathrm{T}}[\mathrm{M}]\{\Phi\}_m} \tag{2.73}$$

where [M] and [K] in Equation 2.73 are the matrices of mass and stiffness of the structure combined with the isolation system. The mth modal participation factor, Γ_m, in Equation 2.72 is defined as

$$\Gamma_m = \frac{\{\Phi\}_m^{\mathrm{T}}[\mathrm{M}]\{1\}}{\{\Phi\}_m^{\mathrm{T}}[\mathrm{M}]\{\Phi\}_m} = \frac{\sum_{i=1}^n m_i \phi_{i,m}}{\sum_{i=1}^n m_i \phi_{i,m}^2} \tag{2.74}$$

The application of Equation 2.72 to the analysis of a seismically isolated structure mainly depends on whether or not the input of the pseudoacceleration, S_{am}, reduced by the numerical coefficient, $B_{m\mathrm{D}}$, enables to capture the system performance and to provide satisfactory accuracy of structural responses. As required by ASCE 7-05, the damping of the base isolation system, normally related to the fundamental modes of the seismically isolated structure, must be the smaller value of the effective damping of the isolation system or 30% of critical damping. Damping of superstructure usually related to higher modes of vibration shall be selected based on the materials of the seismic force-resisting system. Determination of the pseudoacceleration with reduction by numerical coefficients, $B_{m\mathrm{D}}$, is schematically presented in Figure 2.10.

To determine the design displacement, the system displacement at the mth mode of vibration, $\{x\}_m = \{\Phi\}_m x'_m$, as given in Equation 2.72, shall be combined by means of the *square roof of the sum of the squares* (SRSS), *complete quadratic combination* (CQC), or other rational methods [3]. Note that the effective stiffness of an isolation unit, k_{eff}, is calculated from the assumed design displacement, D_{D}. However, the design displacement reported from the response spectrum analysis may not be the same as the assumed value. Thus, iteration procedures have to be employed to repeat response spectrum procedures by changing the effective stiffness of the isolator units with newly assumed design displacement until the computed and assumed design displacement are close to each other within the required accuracy. Once the displacement of the mth mode, $\{x\}_m = \{\Phi\}_m x'_m$, is obtained from Equation 2.72, the design lateral force that is vertically distributed at each level of the structure at the mth mode of vibration can be computed by

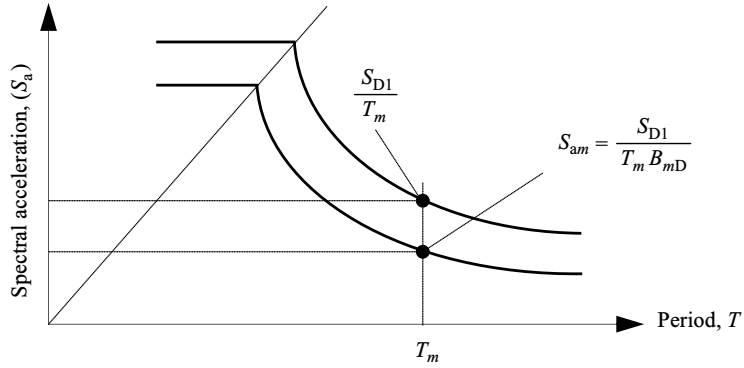

FIGURE 2.10 Response spectrum reduced by numerical coefficients, $B_{m\mathrm{D}}$.

applying Newton's law:

$$\{F\}_m = [\mathrm{M}]\{\ddot{x}\}_m = [\mathrm{M}]\{\Phi\}_m \ddot{x}'_m = [\mathrm{M}]\{\Phi\}_m \Gamma_m S_{\mathrm{a}m} \tag{2.75}$$

where $\{F\}_m$ is a $1 \times n$ vector that can be written as $\{F_{1,m} \quad \ldots \quad F_{i,m} \quad \ldots \quad F_{n,m}\}$. The design base shear of the mth mode is the sum of the design lateral force at each level and is given as follows:

$$V_m = \sum_{i=1}^{n} F_{i,m} = \left(\sum_{i=1}^{n} m_i \phi_{i,m}\right) \Gamma_m S_{\mathrm{a}m} = \frac{S_{\mathrm{a}m}}{g} \overline{W}_m \tag{2.76}$$

where $\overline{W}_m$ is the effective seismic weight of the mth mode and is defined as

$$\overline{W}_m = \left(\sum_{i=1}^{n} m_i \phi_{i,m}\right) \Gamma_m g = \frac{\left(\sum_{i=1}^{n} m_i \phi_{i,m}\right)^2}{\sum_{i=1}^{n} m_i \phi_{i,m}^2} g \tag{2.77}$$

For the structure above the isolation interface and the isolation system, the displacements, $\delta_{i,m\mathrm{D}}$ and $\delta_{i-1,m\mathrm{D}}$, at story i and $i-1$ of the mth mode are given as

$$\delta_{i,m\mathrm{D}} = D_{m\mathrm{D}} \phi_{i,m}; \quad \delta_{i-1,m\mathrm{D}} = D_{m\mathrm{D}} \phi_{i-1,m} \tag{2.78}$$

Accordingly, the story drift, $\Delta_{i,m\mathrm{D}}$, between story i and $i-1$ of the mth mode becomes

$$\Delta_{i,m\mathrm{D}} = D_{m\mathrm{D}}(\phi_{i,m} - \phi_{i-1,m}) \tag{2.78a}$$

The design values of the lateral force at each level of the structure and the isolation system, the base shear, and the story drift shall be determined by applying SRSS

or CQC method to combine Equations 2.75, 2.76, and 2.78a with sufficient modes included. The rule of selecting sufficient modes for computation of the design values is to ensure that the combined modal mass participation captures at least 90% of the actual mass in each principal direction.

The response spectrum procedure as presented above is also applicable to the structural analysis under the MCE. As indicated in ASCE 7-05, the total design displacement, D_{TD}, and the total maximum displacement, D_{TM}, shall be determined by combining 100% of the ground motion in the critical direction with 30% of the ground motion perpendicular to the critical direction. Accordingly, the maximum value of D_{TD} and D_{TM} shall be computed as a vector sum of the displacement in both principal axes of the structure. In addition, the design shear at any story from the response spectrum analysis shall not be less than the story shear determined by the equivalent lateral force procedure as given in Equation 2.68.

2.3.5.4 Special requirements for response history analysis

Response history analysis shall be performed with minimum of three properly selected horizontal ground motions. Each horizontal ground motion has two components, which are perpendicular to each other. Both components shall be applied simultaneously to the structural model to perform the response history analysis. At each time increment, the vector sum of the displacement in both principal axes of the structure is used to compute the maximum value of the total displacement, D_{TD}, and the total maximum displacement, D_{TM}. ASCE 7-05 permits using an average value of the analytical results for design if seven ground motion records are utilized. In case of less than seven ground motion records used to perform response history analysis, the maximum value of the analytical results shall be used for design. For examples of multiple seismic inputs, refer to Reference [3] from pages 397 through 410.

When selecting ground motion records, one must consider *earthquake magnitudes*, *fault distance*, *near source effects*, and *source mechanisms*. If there are no sufficient ground motion records available, ASCE 7-05 allows to use the appropriate simulated ground motion in order to provide the required number of ground motions. The ground motion records may be scaled according to the following method. First, for two components of each ground motion, a SRSS of 5% damped spectrum is constructed. Then a design response spectrum with 5% damping, as presented in Section 2.3.2, is determined. The next step is to apply the individual scaling factor to each SRSS spectrum and find the average value of SRSS spectra. At last, the selected scaling factors shall not cause the average value of SSRS spectra to fall below 1.3 times the design response spectrum by over 10% with period varying from $0.5T_D$ through $1.25T_M$. Figure 2.11 illustrates this method. Detailed computations for selecting scaling factors are given in Example 2.4.3.

Note that the input of ground motion into the structural model does not account for the accidental torsional effects. To simulate accidental torsion in the structural model, masses of the structure above the isolation system are usually moved

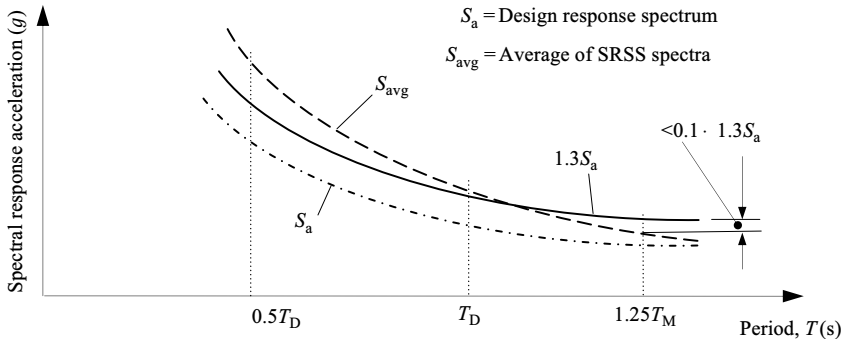

FIGURE 2.11 Determination of scaling factors for ground motions.

by 5% of the building dimension along each principal axis. Movement of masses could happen in any direction (positive or negative) along the principal axes, which results in tremendous computational efforts to determine the most disadvantageous case for the design of the seismically isolated structure. Unfortunately, there is no simple method to reduce the computational efforts. From the design practice viewpoint, reduction of running response history analysis may rely upon engineering judgment to identify the irregularities of the structural layout, the most disadvantageous mass eccentricity, and the critical ground motion records. It is because these major factors govern the maximum parameters of interest, such as the story drifts, the lateral displacement at the isolation system, and the uplift forces in isolator units.

2.4 Design Examples

Example 2.4.1

A four-story building designed, based on Occupancy Category IV, is 64 ft (19.52 m) high with equal story height of 16 ft (4.88 m). The longest and shortest plan dimensions for the building are measured as 240 ft (73.2 m) and 150 ft (45.75m), respectively. The effective seismic weight of the structure above the isolation system is approximately 24,000 kips (106.75 MN). There are no horizontal or vertical structural irregularities of the building structure above the isolation system. Special steel concentrically braced frames are selected as the seismic force-resisting system. The eccentricity between the mass center above the isolation system and the isolation system's center of the rigidity is approximately 2.0 ft in both principal directions. The isolation system consists of twenty 32-in. and thirty-four 38-in. bearings. The bearing properties are summarized in Table 2.7.

TABLE 2.7
Bearing Properties

Diameter in. (mm)	32 (813)	38 (965)
$K_{D\,min}$ in k/in. (kN/mm)	5.63 (0.986)	7.44 (1.303)
$D_{y,min}$ related to $K_{D\,min}$ in in. (mm)	2.00 (51)	2.00 (51)
$K_{e,min}$ in k/in. (kN/mm)	11.93 (2.089)	13.54 (2.371)
$K_{p,min}$ in k/in. (kN/mm)	4.40 (0.771)	6.25 (1.094)
$K_{D\,max}$ in k/in. (kN/mm)	6.75 (1.182)	8.19 (1.434)
$D_{y,D\,max}$ related to $K_{D\,max}$ in in. (mm)	2.00 (51)	2.00 (51)
$K_{e,max}$ in k/in. (mm)	14.32 (2.508)	16.23 (2.842)
$K_{p,max}$ in k/in. (mm)	5.28 (0.925)	7.49 (1.312)
$K_{M\,min}$ in k/in. (mm)	5.25 (0.919)	6.94 (1.215)
$K_{M\,max}$ in k/in. (mm)	6.42 (1.124)	8.48 (1.485)

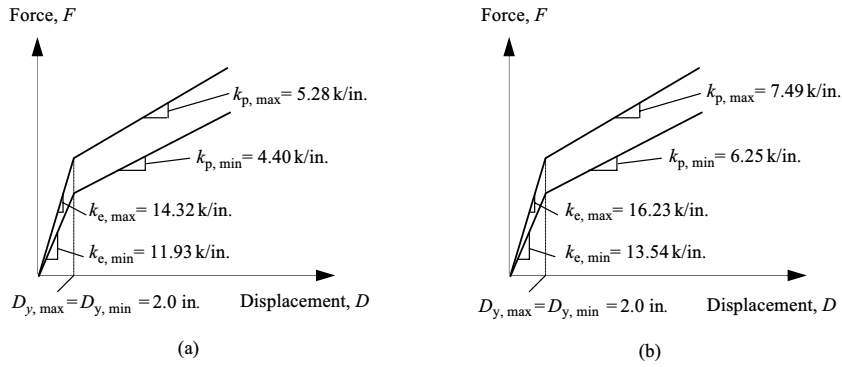

FIGURE 2.12 Bilinear model: (a) 32-in. bearing, (b) 38-in. bearing.

A bilinear relationship between the lateral force and the displacement properly reflects the mechanical properties of the bearings and is presented in Figure 2.12. At the preliminary design phase, 10% of the base isolation system's effective damping is tentatively used. Assume that the isolation system does not limit the MCE displacement to less than the total maximum displacement. The structure will be constructed at the site with S_1 and S_s equal to 0.58 and 1.25, respectively. Site soil is classified as Class D. On basis of the given information, design and check the following items using customary units:

1. Use the equivalent lateral force procedure to determine the total design displacement, D_{TD}, and the total maximum displacement, D_{TM}.

2. Find the minimum lateral force at the isolation system, above and below the isolation system. Assume that wind load is not the governing case.
3. Check if the assumptions of the equivalent lateral force procedure are valid or not.

Solution

1. To determine the total design displacement, D_{TD}, and the total maximum displacement, D_{TM}, the minimum or maximum stiffness of the isolation system and the effective period related to the design and maximum displacement shall be calculated.

The total design displacement is determined by the following steps.

$$k_{D\,min} = 20(5.63) + 34(7.44) = 365.56 \text{ k/in.} \tag{a}$$

$$T_D = 2\pi\sqrt{\frac{W}{k_{D\,min}g}} = 2\pi\sqrt{\frac{24{,}000}{(365.56)(386.1)}} = 2.59 \text{ s} \tag{b}$$

From Table 2.2, the site coefficient $F_v = 1.5$.
Accordingly, $S_{M1} = F_v S_1 = 1.5(0.58) = 0.87$, and $S_{D1} = (2/3)S_{M1} = (2/3)(0.87) = 0.58$. From Table 2.4, $B_D = B_M = 1.2$ for 10% of effective damping. Therefore, the design displacement is

$$D_D = \frac{gS_{D1}T_D}{4\pi^2 B_D} = \frac{(386.1)(0.58)(2.59)}{4\pi^2(1.2)} = 12.24 \text{ in.} \tag{c}$$

Some braced frames are usually located at the perimeters of the building structure in order to effectively resist the seismic force. In this example, $y = 240/2 = 120$ ft leads to the maximum eccentricity. The accident eccentricity is determined as $e_a = 0.05(240) = 12$ ft. The total eccentricity becomes $e = 2 + 12 = 14$ ft, which results in the total design displacement as follows:

$$\begin{aligned} D_{TD} &= D_D\left[1 + y\left(\frac{12e}{b^2 + d^2}\right)\right] \\ &= (12.24)\left[1 + \left(\frac{240}{2}\right)\left(\frac{(12)(14)}{150^2 + 240^2}\right)\right] = 15.32 \text{ in.} \end{aligned} \tag{d}$$

The total maximum displacement is calculated from the followings steps:

$$k_{M\,min} = 20(5.25) + 34(6.94) = 340.96 \text{ k/in.} \tag{e}$$

$$T_M = 2\pi\sqrt{\frac{W}{k_{M\,min}g}} = 2\pi\sqrt{\frac{24{,}000}{(340.96)(386.1)}} = 2.68 \text{ s} \tag{f}$$

From Table 2.1, the site coefficient $F_a = 1.0$. Therefore, $S_{MS} = F_a S_S = 1.0(1.25) = 1.25$, and $S_{DS} = 2S_{MS}/3 = 2(1.25)/3 = 0.83$. The maximum

displacement is

$$D_{\mathrm{M}} = \frac{gS_{\mathrm{M1}}T_{\mathrm{M}}}{4\pi^2 B_{\mathrm{M}}} = \frac{(386.1)(0.87)(2.68)}{4\pi^2(1.2)} = 19.00 \text{ in.} \tag{g}$$

The total maximum displacement is

$$D_{\mathrm{MD}} = D_{\mathrm{M}}\left(1 + y\left(\frac{12e}{b^2 + d^2}\right)\right)$$
$$= (19)\left(1 + \left(\frac{240}{2}\right)\left(\frac{(12)(14)}{150^2 + 240^2}\right)\right) = 23.78 \text{ in.} \tag{h}$$

2. The maximum effective stiffness of the isolation system at the design displacement is

$$k_{\mathrm{D\,max}} = 20(6.75) + 34(8.91) = 437.94 \text{ k/in.} \tag{i}$$

Thus, the minimum lateral force at the isolation system and for the design of structural elements below the isolation system is

$$V_{\mathrm{b}} = k_{\mathrm{D\,max}} D_{\mathrm{D}} = 437.94(12.24) = 5360.4 \text{ k} \tag{j}$$

The numerical coefficient, R_{I}, is equal to 2.0 from Table 2.5. Thus, the minimum lateral force used to design structural elements above the isolation system is

$$V_{\mathrm{s}} = \frac{k_{\mathrm{D\,max}} D_{\mathrm{D}}}{R_{\mathrm{I}}} = \frac{437.94(12.24)}{2} = 2680.2 \text{ k} \tag{k}$$

However, the minimum lateral force, V_{s}, shall be checked by two cases: the fixed-base structure with an effective period of T_{D}, and the yield of the isolation system multiplied by a factor of 1.5. Note that the given condition indicates that the wind load does not govern the lateral force, and this case does not need to be checked.

From Tables 2.5 and 2.6, $R = 6$ and $I = 1.5$. Accordingly, the seismic response coefficients based on Equations 2.62 through 2.64 are determined as below:

$$C_{\mathrm{S}} = \frac{S_{\mathrm{DS}}}{(R/I)} = \frac{0.83}{(6/1.5)} = 0.208 \tag{l}$$

$$C_{\mathrm{S}} = \frac{S_{\mathrm{D1}}}{T_{\mathrm{D}}(R/I)} = \frac{0.58}{2.59(6/1.5)} = 0.056 > 0.01 \tag{m}$$

Use V_{s1} to define the base shear for a fixed-base structure with the effective period, T_{D}. Then the base shear, V_{s1}, is calculated as shown below:

$$V_{\mathrm{s1}} = C_{\mathrm{S}} W = 0.056(24{,}000) = 1344 \text{ k} < V_{\mathrm{s}} = 2680.2 \text{ k} \tag{n}$$

At the yield level of the isolation system, the lateral force denoted as V_{s3} becomes

$$V_{s3} = 1.5k_{e,max}D_{Dy,max} = 1.5\,[(20)(28.64) + (34)(32.46)]$$
$$= 2514.7\text{ k} < V_s = 2680.2\text{ k} \quad \text{(o)}$$

Since V_{s1} and V_{s3} are less than V_s, the minimum lateral force is V_s = 2680.2k for the design of structural elements above the isolation system. Note that Equation 2.65 is not used here because S_1 is less than 0.6 g.

3. The design information given in this example has already met some requirements of the equivalent lateral force procedure. S_1 = 0.58 and the Site Class D meet Items 1 and 2 as required in Section 2.3.3. The building is four stories, and the height is less than 65 ft, thus also meeting Item 3. The effective period at the maximum displacement, T_M, is 2.68 s, which satisfies Item 4. Item 6 is met because the given condition specifies that the building does not have any irregularities. As specified in the given condition, the MCE displacement is not limited by the isolation system to the total maximum displacement. Therefore, Item 9 is automatically satisfied.

Only Items 5, 7, and 8 require further verification. These items are checked as follows:

For Item 5, the period of the fixed-base structure is $T_a = C_t h_n^x = 0.02(64)^{0.75} = 0.45$ s. $3T_a = 3(0.45) = 1.35$ s, which is much less than $T_D = 2.59$ s. Thus, Item 5 is met.

For Item 7, 20% of the design displacement is 0.2(12.24) = 2.45 in. The stiffness is accordingly calculated as follows:

$$\text{32-in. bearing: } \frac{1}{3}K_{32''} = \frac{2(14.32) + 5.28(2.45 - 2)}{3(2.45)}$$
$$= 4.22k\text{/in.} < K_{D\,max} = 6.75\text{ k/in.} \quad \text{(p)}$$
$$\text{38-in. bearing: } \frac{1}{3}K_{38''} = \frac{2(16.23) + 7.49(2.45 - 2)}{3(2.45)}$$
$$= 4.87k\text{/in.} < K_{D\,max} = 8.91\text{ k/in.} \quad \text{(q)}$$

Thus, the effective stiffness of both types of bearings at the design displacement is greater than one-third of the effective stiffness at 20% of the displacement. Note that the above demonstration is derived from the maximum stiffness at the design displacement. The same conclusion can be obtained for the minimum stiffness at the design displacement by applying the same methodology.

Item 8 is to check the capability of the isolation system to produce a restoring force. Fifty percent of the total design displacement is

$$50\%D_{TD} = 0.5(15.32) = 7.66\text{ in.} \quad \text{(r)}$$

For a 32-in. bearing, the lateral force at 50% D_{TD} is

$$V_{32"} = 2(14.32) + 5.28(7.66 - 2) = 58.52 \text{ k} \quad \text{(s)}$$

For a 38-in. bearing, the lateral force at 50% D_{TD} is

$$V_{38"} = 2(16.23) + 7.49(7.66 - 2) = 74.85 \text{ k} \quad \text{(t)}$$

Thus, the lateral force of the isolation system at 50% D_{TD} becomes

$$V_{50\%TD} = \frac{20(58.52) + 34(74.85)}{24{,}000} = 0.155 \text{ W} \quad \text{(u)}$$

The lateral force at the total design displacement can be written as follows:

$$V_{TD} = \frac{20[2(14.32) + 5.28(15.32 - 2)] + 34[2(16.23) + 7.49(15.32 - 2)]}{24{,}000}$$

$$= 0.270 \text{ W} \quad \text{(v)}$$

$$V_{TD} - V_{50\%TD} = 0.270 \text{ W} - 0.155 \text{ W} = 0.115 \text{ W} > 0.025 \text{ W} \quad \text{(w)}$$

Therefore, Item 8 is satisfied. On the basis of the above verifications, all the items are met, and use of the equivalent lateral force procedure is acceptable.

Example 2.4.2

Define lower-bound limits on response spectrum analysis for the seismically isolated structure as described in Example 2.4.1. All the given conditions remain the same except for the irregularities of the structure above the isolation system.

Solution

Using the response spectrum procedure, the following lower-bound limits as specified in Section 2.3.5.2 shall be established.

On the basis of the solutions from Example 2.4.1, the design displacement is D_D = 12.24 in. The approximate period of the fixed-base structure is used here. Then, T_a = 0.45 s, and the effective period at design displacement is T_D = 2.59 s. Thus, the design displacement to determine the total design displacement for response spectrum analysis is

$$D'_D = \frac{D_D}{\sqrt{1 + (T_a/T_D)^2}} = \frac{12.24}{\sqrt{1 + (0.45/2.59)^2}} = 12.06 \text{ in.} \quad \text{(a)}$$

The total design displacement becomes

$$D_{TD} = D'_D \left[1+y\left(\frac{12e}{b^2+d^2}\right)\right]$$
$$= (12.06)\left[1+\left(\frac{240}{2}\right)\left(\frac{(12)(14)}{150^2+240^2}\right)\right] = 15.10 \text{ in.} \quad \text{(b)}$$

The lower-bound limit on the total design displacement is $0.9D_{TD} = 0.9(15.1) = 13.59$ in.

The maximum displacement from Example 2.4.1 is $D_M = 19.0$ in., and the corresponding effective period is $T_M = 2.68$ s. The maximum displacement to define the total maximum displacement for response spectrum analysis is

$$D'_M = \frac{D_M}{\sqrt{1+\left(T_a/T_M\right)^2}} = \frac{19.0}{\sqrt{1+\left(0.45/2.68\right)^2}} = 18.74 \text{ in.} \quad \text{(c)}$$

The total maximum displacement is

$$D_{MD} = D'_M \left[1+y\left(\frac{12e}{b^2+d^2}\right)\right]$$
$$= (18.74)\left[1+\left(\frac{240}{2}\right)\left(\frac{(12)(14)}{150^2+240^2}\right)\right] = 23.46 \text{ in.} \quad \text{(d)}$$

The lower-bound limit on the total maximum displacement is $0.8D_{TM} = 0.8(23.46) = 18.78$ in.

The lower-bound limit on the design lateral force at and below the isolation system is

$$0.9V_b = 0.9(5360.4) = 4824.4 \text{ k} \quad \text{(e)}$$

The lower-bound limit on the design lateral force for the design of structural elements above the isolation system is $1.0V_s = 2680.2$ k, which is also greater than $V_{s1} = 1752$ k and $V_{s3} = 2514.7$ k.

The results from response spectrum analysis shall not be less than the lower-bound limits determined above.

Example 2.4.3

A seismically isolated building will be constructed on a Site Class D. The effective period at the design displacement is $T_D = 2.5$ s, and the effective period at the maximum displacement is $T_M = 2.6$ s. Response history analysis must be performed owing to structural irregularities. Three ground motion histories are selected for response history analysis and the maximum value of the response parameters shall be selected for the structure design. These three ground motion histories were recorded during the 1989 Loma Prieta

earthquake at Joshua Tree and the 1992 Landers earthquake at Gilroy Array and Hollister City Hall. Response spectra of three ground motion histories at 5% of damping are shown in Table 2.8. Response spectrums are identified as (1), (2), and (3). The MCE spectral acceleration parameters are $S_S = 2.0$ at the short period and $S_1 = 1.0$ at a period of 1 s, which will be used to determine the design response spectrum.

1. Find the design response spectrum based on the given information. The long-period transition period, T_L, is 6 s for this site.
2. Determine the scaling factor for each ground motion history.

Solution

1. From Tables 2.1 and 2.2, site coefficients F_a and F_v are 1.0 and 1.5, respectively, for Site Class D. Thus, $S_{MS} = F_a S_S = 1.0(2.0) = 2$ and $S_{M1} = F_v S_1 = 1.5(1.0) = 1.5$. The design spectral acceleration parameters are determined as follows:

$$S_{DS} = \frac{2}{3}S_{MS} = \frac{2}{3}(2) = \frac{4}{3} \quad \text{and} \quad S_{D1} = \frac{2}{3}S_{M1} = \frac{2}{3}(1.5) = 1.0 \tag{a}$$

$$T_0 = 0.2\left(\frac{S_{D1}}{S_{DS}}\right) = 0.2\left[\frac{1.0}{(4/3)}\right] = 0.15 \tag{b}$$

$$T_S = \frac{S_{D1}}{S_{DS}} = \frac{3}{4} = 0.75 \tag{c}$$

The design spectral response acceleration for a period less than T_0 is presented as shown below.

$$S_a = S_{DS}\left[0.4 + 0.6\left(\frac{T}{T_0}\right)\right] = \frac{4}{3}\left(0.4 + \frac{0.6T}{0.15}\right) = 0.533 + 5.333T \tag{d}$$

The design spectral response acceleration between T_0 and T_S is 1.333 in unit of g and the acceleration between T_s and T_L is given by

$$S_a = \frac{S_{D1}}{T} = \frac{1}{T} \tag{e}$$

On the basis of the above relationship between T and S_a, the design response spectrum can be developed and is shown in Figure 2.13. Since $1.25T_M$ is shorter than T_L, the portion of acceleration with period longer than T_L is not shown in Figure 2.13.

2. The scaling factor for each spectrum from the ground motion is determined between $0.5T_D$ and $1.25T_M$. $0.5T_D = 0.5(2.5) = 1.25$ s, and $1.25T_M = 1.25(2.6) = 3.25$ s. The design response spectrum is multiplied by a factor of 1.3 according to ASCE7-05. By trial and error to find a set of scaling factors that is able to meet the ASCE 7-05 requirements, scaling factors of

TABLE 2.8
Response Spectrums of Three Ground Motions

	(1) 1992 Landers Joshua Tree		(2) 1989 Loma Prieta Gilroy Array		(3) 1989 Loma Prieta Hollister City Hall	
T (s)	Component 1	Component 2	Component 1	Component 2	Component 1	Component 2
0.01	0.713	0.742	1.226	0.783	0.815	0.392
0.10	0.764	1.021	2.908	1.932	0.842	0.527
0.15	0.868	1.104	3.540	2.129	0.954	0.855
0.20	0.989	1.347	4.384	3.132	1.335	0.709
0.30	1.836	1.932	2.240	2.646	1.881	0.963
0.40	1.945	1.217	2.382	1.031	1.386	0.914
0.50	1.739	1.097	2.260	1.540	2.585	1.535
0.60	1.450	1.575	1.538	1.062	2.175	0.896
0.70	1.737	2.616	1.124	0.902	2.147	0.889
0.75	1.763	2.250	1.069	1.053	2.214	0.824
0.80	1.722	1.763	1.082	0.936	2.251	0.736
0.90	1.657	1.473	0.817	0.851	2.062	0.640
1.00	1.042	1.372	0.586	0.829	2.199	0.799
1.10	1.204	1.664	0.408	0.843	1.920	0.951
1.20	1.378	1.495	0.348	0.843	1.509	0.889
1.25	1.258	1.367	0.319	0.845	1.325	0.791
1.30	1.153	1.251	0.290	0.842	1.242	0.647
1.40	0.676	1.074	0.330	0.821	1.156	0.451
1.50	0.562	0.964	0.378	0.776	1.090	0.386
1.60	0.495	0.941	0.327	0.768	1.026	0.406
1.70	0.494	0.811	0.266	0.736	1.108	0.359
1.80	0.464	0.705	0.197	0.695	1.097	0.374
1.90	0.379	0.608	0.161	0.687	0.986	0.346
2.00	0.344	0.492	0.164	0.658	0.835	0.312
2.20	0.274	0.360	0.150	0.563	0.670	0.342
2.40	0.250	0.398	0.118	0.506	0.553	0.281
2.60	0.213	0.471	0.123	0.425	0.486	0.292
2.80	0.190	0.459	0.136	0.349	0.436	0.307
3.00	0.121	0.306	0.132	0.282	0.390	0.251
3.20	0.095	0.286	0.144	0.226	0.347	0.203
3.25	0.099	0.300	0.143	0.214	0.337	0.209
3.40	0.108	0.284	0.130	0.181	0.306	0.213
3.60	0.109	0.230	0.114	0.159	0.268	0.180
3.80	0.127	0.197	0.100	0.142	0.235	0.167
4.00	0.109	0.192	0.098	0.128	0.205	0.212

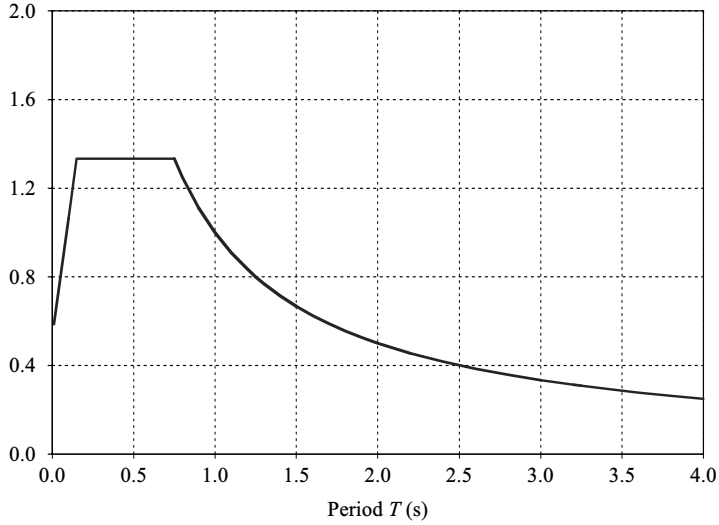

FIGURE 2.13 Design spectral acceleration.

1.07, 0.82, and 1.38 applied to ground motions (1), (2), and (3) are selected. Thus, the average of the SRSS spectra from three ground motions is not less than 10% of the design response spectrum increased by a factor of 1.3. Figure 2.14 shows that the average of the SRSS spectra is above 1.3 times the design response spectrum reduced by 10% between 1.25 s and 3.25 s. Scaling factors are selected using Microsoft Excel and are summarized in Table 2.9. Interpretations of results at a typical time interval are given step-by-step as follows.

At the time of 3.25s, the spectral acceleration from the design response spectrum is

$$S_a = \left(1/3.25\right) g = 0.308g, \quad 1.3S_a = 1.3(0.308) = 0.4g \tag{f}$$

For the spectrum (1) at the time of 3.25 s, two components of spectral acceleration are combined by SRSS. Thus $S_{a,(1)} = \sqrt{0.099^2 + 0.3^2} = 0.316g$. Do the same for the spectra (2) and (3),

$$S_{a,(2)} = \sqrt{0.143^2 + 0.214^2} = 0.257g \quad \text{and}$$
$$S_{a,(3)} = \sqrt{0.337^2 + 0.209^2} = 0.396g \tag{g}$$

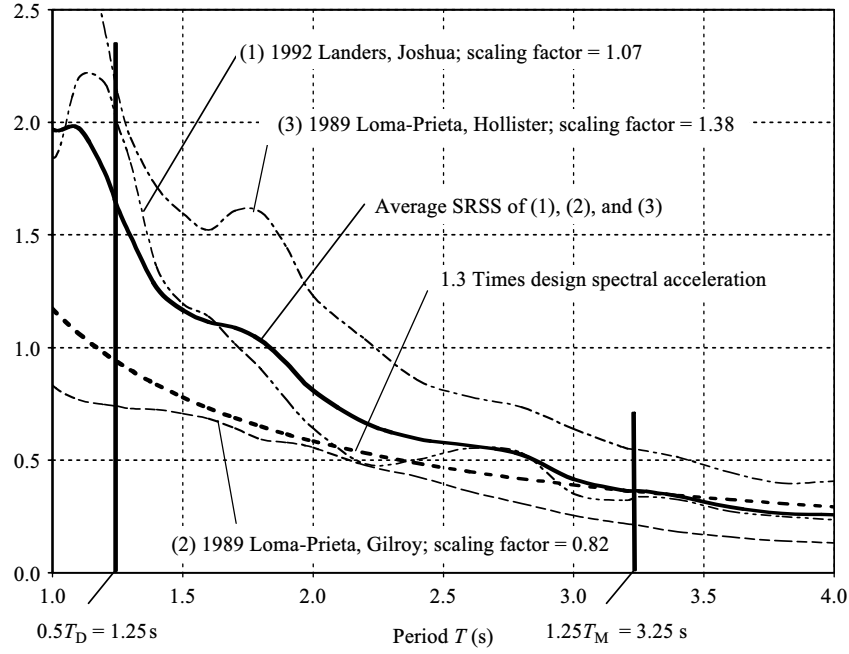

FIGURE 2.14 Scaling factor determination of ground motions.

Applying the selected scaling factors, the average of the SRSS spectra becomes

$$\overline{S}_a = \frac{1.07S_{a,(1)} + 0.82S_{a,(2)} + 1.38S_{a,(3)}}{3}$$

$$= \frac{1.07(0.316) + 0.82(0.257) + 1.38(0.396)}{3} = 0.365g \qquad \text{(h)}$$

Compared to the design response spectrum as represented in Figure 2.13, the following condition is satisfied:

$$0.9\,(1.3S_a) = 0.9(0.4) = 0.36\,g < \overline{S}_a = 0.365\,g \qquad \text{(i)}$$

Thus, the selected scaling factors meet ASCE7-05 requirements. As an exercise of applying the above methodology, demonstrations of the average of SRSS spectra not less than 10% of 1.3 times the design response spectrum are easily achieved at any time interval between 1.25 and 3.25 s.

TABLE 2.9
Determination of Scaling Factor for Three Ground Motions

	(1) 1992 Landers Joshua Tree			(2) 1989 Loma Prieta Gilroy Array			(3) 1989 Loma Prieta Hollister City Hall				
T (s)	Component 1	Component 2	SRSS	Component 1	Component 2	SRSS	Component 1	Componenet 2	SRSS	Average SRSS of (1), (2), (3)	1.3 S_a
0.01	0.763	0.794	1.101	1.005	0.642	1.193	1.125	0.542	1.249	1.181	0.686
0.10	0.818	1.092	1.364	2.385	1.584	2.863	1.161	0.728	1.370	1.866	1.248
0.15	0.928	1.182	1.503	2.903	1.746	3.387	1.317	1.179	1.768	2.219	1.560
0.20	1.058	1.441	1.788	3.595	2.568	4.418	1.842	0.979	2.086	2.764	1.560
0.30	1.964	2.068	2.852	1.837	2.170	2.843	2.595	1.329	2.916	2.870	1.560
0.40	2.081	1.302	2.455	1.953	0.845	2.128	1.912	1.261	2.291	2.291	1.560
0.50	1.861	1.174	2.200	1.853	1.263	2.243	3.567	2.119	4.148	2.864	1.560
0.60	1.552	1.685	2.291	1.261	0.871	1.533	3.002	1.236	3.246	2.357	1.560
0.70	1.858	2.799	3.360	0.921	0.739	1.181	2.962	1.226	3.206	2.582	1.560
0.75	1.886	2.408	3.058	0.877	0.863	1.230	3.055	1.137	3.259	2.516	1.560
0.80	1.843	1.886	2.637	0.888	0.767	1.173	3.106	1.016	3.268	2.359	1.463
0.90	1.773	1.576	2.372	0.670	0.698	0.968	2.845	0.883	2.979	2.106	1.300
1.00	1.115	1.468	1.843	0.480	0.680	0.833	3.035	1.103	3.229	1.968	1.170
1.10	1.288	1.780	2.197	0.335	0.692	0.768	2.649	1.313	2.956	1.974	1.064
1.20	1.475	1.599	2.175	0.285	0.691	0.748	2.083	1.226	2.417	1.780	0.975
1.25	1.346	1.463	1.988	0.261	0.693	0.740	1.829	1.091	2.130	1.619	0.936
1.30	1.234	1.338	1.820	0.237	0.690	0.730	1.714	0.892	1.932	1.494	0.900
1.40	0.723	1.149	1.358	0.271	0.673	0.725	1.596	0.622	1.713	1.265	0.836
1.50	0.602	1.031	1.194	0.310	0.636	0.708	1.504	0.533	1.595	1.166	0.780

Continued

TABLE 2.9
(Continued)

	(1) 1992 Landers Joshua Tree			(2) 1989 Loma Prieta Gilroy Array			(3) 1989 Loma Prieta Hollister City Hall			Average SRSS of (1),	
T (s)	Component 1	Component 2	SRSS	Component 1	Component 2	SRSS	Component 1	Componenet 2	SRSS	(2), (3)	1.3 S_a
1.60	0.530	1.007	1.138	0.268	0.630	0.684	1.415	0.560	1.522	1.115	0.731
1.70	0.529	0.867	1.016	0.218	0.604	0.642	1.529	0.495	1.607	1.088	0.688
1.80	0.496	0.754	0.903	0.161	0.570	0.592	1.513	0.517	1.599	1.031	0.650
1.90	0.406	0.650	0.766	0.132	0.563	0.578	1.361	0.477	1.442	0.929	0.616
2.00	0.368	0.527	0.642	0.135	0.539	0.556	1.152	0.430	1.229	0.809	0.585
2.20	0.293	0.385	0.484	0.123	0.462	0.478	0.925	0.472	1.038	0.667	0.532
2.40	0.267	0.426	0.503	0.097	0.415	0.426	0.763	0.388	0.856	0.595	0.488
2.60	0.228	0.503	0.553	0.101	0.348	0.363	0.671	0.403	0.782	0.566	0.450
2.80	0.203	0.491	0.532	0.111	0.286	0.307	0.602	0.424	0.736	0.525	0.418
3.00	0.129	0.327	0.352	0.108	0.231	0.255	0.538	0.346	0.640	0.416	0.390
3.20	0.102	0.306	0.323	0.118	0.185	0.219	0.479	0.280	0.555	0.366	0.366
3.25	0.106	0.321	0.338	0.117	0.175	0.211	0.465	0.289	0.547	0.365	0.360
3.40	0.116	0.304	0.325	0.107	0.148	0.183	0.423	0.294	0.515	0.341	0.344
3.60	0.116	0.246	0.272	0.093	0.130	0.160	0.370	0.248	0.446	0.293	0.325
3.80	0.135	0.211	0.251	0.082	0.116	0.142	0.324	0.231	0.398	0.264	0.308
4.00	0.116	0.205	0.236	0.081	0.105	0.132	0.283	0.292	0.407	0.258	0.293

2.5 Testing Verification and Determination of Isolator Properties

2.5.1 Testing Requirements of ASCE 7-05

Mechanical properties of isolation systems, used in the equivalent lateral force procedure and the dynamic analysis procedures, shall be verified by *prototype tests* in accordance with ASCE 7-05, Section 17.8 [2]. Two full-size bearings for each type and size are required for testing. The prototype tests shall include the following sequences:

1. An average of gravity load, P, which is equal to $D + 0.5L$, is preloaded on the bearing, where D and L are the dead load and live load, respectively. Under this sequence, 20 fully reversed cycles are performed under the lateral force equal to the design wind load.
2. The gravity load, P, remains applied on the bearing, which is forced to move three fully reversed cycles at each displacement increment of $0.25D_{\mathrm{D}}$, $0.5D_{\mathrm{D}}$, $1.0D_{\mathrm{D}}$, and $1.0D_{\mathrm{M}}$. If the tested bearing is used to resist the vertical seismic force transferred from the seismic force-resisting system, two additional vertical load cases shall be included in the testing sequences to perform the same cycle procedures as presented above.

$$(1.2 + 0.2S_{\mathrm{MS}})D + L + Q_{\mathrm{E}} \tag{2.79}$$

$$(0.9 - 0.2S_{\mathrm{MS}})D + Q_{\mathrm{E}} \tag{2.80}$$

   where Q_{E} is the seismic force determined from the MCE and S_{MS} represents the MCE spectral response acceleration at a short period.
3. Under the gravity load, P, three fully reversed cycles are performed with the total maximum displacement, D_{TM}.
4. Subjected to the same gravity load, P, the bearing is forced to move $\left(30S_{\mathrm{D1}}/S_{\mathrm{DS}}B_{\mathrm{D}}\right) \geq 10$ fully reversed cycles with the total design displacement, D_{TD}.

On the basis of the results from prototype tests, the minimum and maximum effective stiffness at the design displacement is determined as

$$k_{\mathrm{D\,min}} = \frac{\sum \left|F_{\mathrm{D}}^{+}\right|_{\mathrm{min}} + \sum \left|F_{\mathrm{D}}^{-}\right|_{\mathrm{min}}}{2D_{\mathrm{D}}} \tag{2.81}$$

$$k_{\mathrm{D\,max}} = \frac{\sum \left|F_{\mathrm{D}}^{+}\right|_{\mathrm{max}} + \sum \left|F_{\mathrm{D}}^{-}\right|_{\mathrm{max}}}{2D_{\mathrm{D}}} \tag{2.82}$$

where $\sum \left|F_{\mathrm{D}}^{+}\right|_{\mathrm{min}}$ and $\sum \left|F_{\mathrm{D}}^{-}\right|_{\mathrm{min}}$ are the sums of the minimum absolute lateral force at the positive and negative design displacement, D_{D}; $\sum \left|F_{\mathrm{D}}^{+}\right|_{\mathrm{max}}$ and

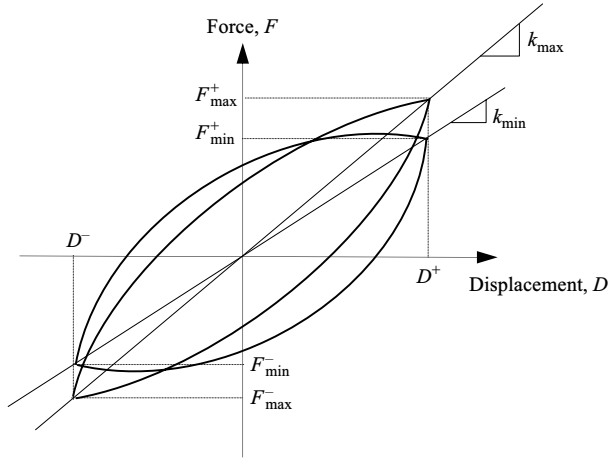

FIGURE 2.15 Definition of effective stiffness, k_{max} and k_{min}.

$\sum |F_D^-|_{max}$ present the sums of the maximum absolute lateral force at the positive and negative design displacement, D_D.

In the same way, the minimum and maximum effective stiffness at the maximum displacement are expressed as

$$k_{M\,min} = \frac{\sum |F_M^+|_{min} + \sum |F_M^-|_{min}}{2D_M} \tag{2.83}$$

$$k_{M\,max} = \frac{\sum |F_M^+|_{max} + \sum |F_M^-|_{max}}{2D_M} \tag{2.84}$$

where $\sum |F_M^+|_{min}$ and $\sum |F_M^-|_{min}$ are the sums of the minimum absolute lateral force at the positive and negative maximum displacement, D_M; $\sum |F_M^+|_{max}$ and $\sum |F_M^-|_{max}$ present the sums of the maximum absolute lateral force at the positive and negative maximum displacement, D_M. Figure 2.15 shows the relation of the effective stiffness with the corresponding absolute displacement.

After $k_{D\,max}$ and $k_{M\,max}$ are determined, and the total dissipated energy in the isolation system in a full cycle of the design displacement, $\sum E_D$, and in a full cycle of the maximum displacement $\sum E_M$ are calculated from prototype test results, the corresponding effective damping, β_D and β_M, are obtained based on Equations 2.51 and 2.55.

In addition to the prototype tests, *production tests* of all the bearings are required to ensure that testing results fall into the accepted ranges of the preselected design values. The production test usually includes bearing compression test to find its compressive stiffness, test of lateral stiffness at the design displacement, and determination of the effective damping at the design displacement.

Acceptance criteria of testing results for both prototype and production tests need to be reviewed and approved by the design review panel and the enforcement agency. This section only provides general requirements for the prototype and production test. Specific requirements are expected to test different types of bearings. Detailed explanations of prototype and production test requirements for different types of bearings can be found in Reference [13].

2.5.2 Modifications of Isolator Properties

The mechanical properties determined from tests have been proven to vary during years of service owing to environmental conditions, such as the effects of aging, contamination, travel, temperature, and *scragging*. Scragging is a unique characteristic of elastomeric-type bearings, which refers to the reduction of the bearing's shear stiffness at initial cycles of testing with large shear deformation. However, recovery time of the scragged bearing's original shear stiffness mainly depends on the bearing's rubber properties. All the effects as mentioned above shall be considered in the design stages. However, ASCE 7-05 [1] does not explicitly specify how to account for them. In the current design practice for seismically isolated structures, modifications of isolator properties are usually determined by a method of system property modification factors developed by Constantiou, et al. [5] based on their research work, which has been adopted by the 1999 AASHTO Guide Specifications for Seismic Isolation Design [1].

This method establishes upper- (maximum) and lower- (minimum) bound bearing properties by applying different modification factors to its nominal properties that are determined from tests. Assuming that the nominal properties of bearings are designated as P_n, the modified maximum and minimum properties of bearings become $P_{\max}$ and $P_{\min}$, respectively, and the relation of P to $P_{\max}$ and $P_{\min}$ is expressed as below:

$$P_{\max} = f(\lambda_{\max,1}, \ldots, \lambda_{\max,i})P_n \tag{2.85}$$

$$P_{\min} = f(\lambda_{\min,1}, \ldots, \lambda_{\min,i})P_n \tag{2.86}$$

where $f(\lambda_{\max,1}, \ldots, \lambda_{\max,i})$ and $f(\lambda_{\min,1}, \ldots, \lambda_{\min,i})$ are functions of modification factors or λ-factors owing to different effects and are defined in terms of $\prod \lambda_{\max,i}$ and $\prod \lambda_{\min,i}$. For sliding-type bearings, the modification factors include effects of aging, contamination, wear, and temperature, while the effects of aging, scragging, temperature, and heat are considered for elastomeric-type bearings. λ-factors can be determined from Tables 5-1 through 5-8 in the report by Constantiou, et al. [5]. Note that there is a slim probability of all the effects being applied during an earthquake event. Thus, a system property adjustment factor, χ, is proposed [5] to modify $\prod \lambda_{\max,i}$ and $\prod \lambda_{\min,i}$. By introducing $\lambda_{\max}$ and $\lambda_{\min}$ to express $f(\lambda_{\max,1}, \ldots, \lambda_{\max,i})$ and $f(\lambda_{\min,1}, \ldots, \lambda_{\min,i})$, respectively, the adjusted

modification factors become as follows:

$$\lambda_{\max} = 1 + \chi \left(\prod \lambda_{\max,i} - 1 \right) \tag{2.87}$$

$$\lambda_{\min} = 1 - \chi \left(\prod \lambda_{\min,i} - 1 \right) \tag{2.88}$$

where χ varies from 0.66 to 1.0 based on the importance of the structure. An application to the method of system property modification factors is depicted in the following example.

For a high damping rubber bearing with a diameter of 40 in., the nominal upper-bound properties are characterized as the elastic stiffness, $k_{\mathrm{e\,max}} = 27.6$ k/in., the postyield stiffness, $k_{\mathrm{p\,max}} = 10.08$ k/in.; and the yielding displacement, $D_{\mathrm{y\,max}} = 2.0$ in. Thus, the yielding force is $F_{\mathrm{y}} = 27.6(2) = 55.2$ k. By using Equation 2.21, the characteristic strength becomes $Q = (k_{\mathrm{e\,max}} - k_{\mathrm{p\,max}})D_{\mathrm{y}} = (27.6 - 10.08)(2) = 35.04$ k. The heat effect for high damping rubber bearing is negligible, and from Tables 5-5 and 5-6 of the report [5], a factor of 1.2 for both the effects of aging and scragging is obtained to modify the postyield stiffness, $k_{\mathrm{p\,max}}$, and the characteristic strength, Q. Assuming that this is not an essential structure, the system property adjustment factor, χ, is equal to 0.75, which leads Equation 2.87 to be $\lambda_{\max} = 1 + 0.75[1.2(1.2) - 1] = 1.33$. Thus, the adjusted $k_{\mathrm{p\,max}} = 1.33(10.08) = 13.41$ k/in., and adjusted $Q = 1.33(35.04) = 46.60$ k. Accordingly, $D_{\mathrm{y\,max}} = Q/(k_{\mathrm{e\,max}} - k_{\mathrm{p\,max}}) = 46.6/(27.6 - 13.41) = 3.28$ in., and $F_{\mathrm{y}} = 27.6 \times 3.28 = 90.53$ k.

The modified postyield stiffness, $k_{\mathrm{p\,max}}$, and yielding displacement, $D_{\mathrm{y\,max}}$, along with the elastic stiffness, $k_{\mathrm{e\,max}}$, will be used to perform equivalent lateral force analysis or be input into computer model for dynamic analysis of the building structure.

References

1. American Association of State Highway and Transportation Officials (AASHTO), *Guide Specifications for Seismic Isolation Design*, Washington, DC, 1999.
2. American Society of Civil Engineers (ASCE), *Minimum Design Loads for Building and Other Structures, ASCE/SEI 7-05*, 2005.
3. Cheng, F.Y., *Matrix Analysis of Structural Dynamics: Applications and Earthquake Engineering*, Marcel Dekker, Inc., New York, 2001.
4. Computer and Structures, Inc. (CSI), *CSI Analysis Reference Manual for SAP2000, ETABS, and SAFE*, Berkeley, California, 2005.
5. Constantinou, M.C., Tsopelas, P., Kasalanati, A., and Wolff, E., Property Modification Factors for Seismic Isolation Bearings, *Report No. NCEER-99-0012*, Multidisciplinary Center for Earthquake Engineering Research, Buffalo, New York, 1999.
6. Federal Emergency Management Agency (FEMA), *NEHRP Guidelines for the Seismic Rehabilitation of Buildings and NEHER Commentary on the Guidelines for the Seismic Rehabilitation of Buildings*, Reports No. FEMA-273 and FEMA 274, Building Seismic Safety Council, Washington, DC, 1997.

7. Federal Emergency Management Agency (FEMA), *Prestandard and Commentary for the Seismic Rehabilitation of Buildings*, Report No. FEMA-356, Building Seismic Safety Council, Washington, DC, 2000.
8. Federal Emergency Management Agency (FEMA), *NEHRP Recommended Provisions for Seismic Regulations for New Buildings and Other Structures*, Parts 1 and 2, Report No. FEMA-450, Building Seismic Safety Council, Washington, DC, 2003.
9. International Code Council, *International Building Code* (IBC), Falls Creek, VI, 2006.
10. International Conference of Building Code (ICBO), Division III—Earthquake Regulations for Seismic-Isolated Structures, Appendix to Chapter 23, *Uniform Building Code*, 1991 Edition, Whittier, CA, 1991.
11. International Conference of Building Code (ICBO), Earthquake Regulations for Seismic-Isolated Structures, Appendix to Chapter 16, *Uniform Building Code*, 1997 Edition, Whittier, CA, 1997.
12. Kelly, J.M., *Earthquake-Resistant Design with Rubber*, 2nd ed., Springer-Verlag, London, 1996.
13. Naeim, F. and Kelly, J.M., *Design of Seismic Isolated Structures: From Theory to Practice*, John Wiley & Sons Inc., New York, 1999.
14. Newark, N.M., and Hall, W.J., *Earthquake Spectra and Design*, Earthquake Engineering Research Institute (EERI), Oakland, CA, 1981.
15. Structural Engineers Association of California (SEAOC), *Tentative Seismic Isolation Design*, San Francisco, CA, 1986.
16. Structural Engineers Association of California (SEAOC), *Recommended Lateral Force Requirements and Commentary*, 5th ed., Sacramento, CA, 1990.
17. Structural Engineers Association of California (SEAOC), *Recommended Lateral Force Requirements and Commentary*, 7th ed., Sacramento, CA, 1999.

3 Damping Systems

The objective of utilizing dampers is to reduce structure responses and to mitigate damage or collapse of structures from severe earthquakes by participating energy dissipations. As a successful application, installation of dampers in an existing building structure, which does not possess sufficient lateral stiffness, enables control of the story drift within the required limitation and maintains its desired functions during an earthquake event. Since the first application of dampers in structural engineering took place in 1960s, abundant research work has been conducted to study the mechanisms of dampers and the behavior of damped structures. With the invention of different types of damping devices, improvement of modeling techniques, and development of new computational methodologies, use of dampers has become a mature technology in designing of new structures and retrofitting of existing facilities.

Study of damped structure performance mainly relies on types of dampers and configurations of their installations. The authors' intention being the same as mentioned in Chapter 2, this chapter only addresses commonly used types of dampers, and introduces corresponding basic theories and their important applications to damped building structures. In addition, this chapter could be considered as a stepping stone for reader's further studies. A brief summary of this chapter is presented as follows. In Section 3.1, basic concepts of damped structures with single or multiple degree-of-freedoms are introduced with consideration of nonlinear behavior of both building structures and dampers. Different analytical procedures with ASCE 7-05 [1] requirements are explained in detail in Section 3.2. Section 3.3 provides design examples according to ASCE 7-05 requirements. Testing requirements and properties verifications of dampers are summarized in Section 3.4.

3.1 Basic Concepts of Building Structures with Damping System

3.1.1 Single-Degree-of-Freedom Motion Equations

A building installed with dampers features two structural systems to resist seismic force: *seismic force-resisting system* and *damping system*. A seismic force-resisting system is characterized by selected structural materials and its configurations, such as steel braced frames, steel moment frames, and concrete shear walls. A damping system is usually defined as a collection of dampers, connections between dampers and structural members, and structural members transferring forces between *damping devices* and the seismic force-resisting system or the

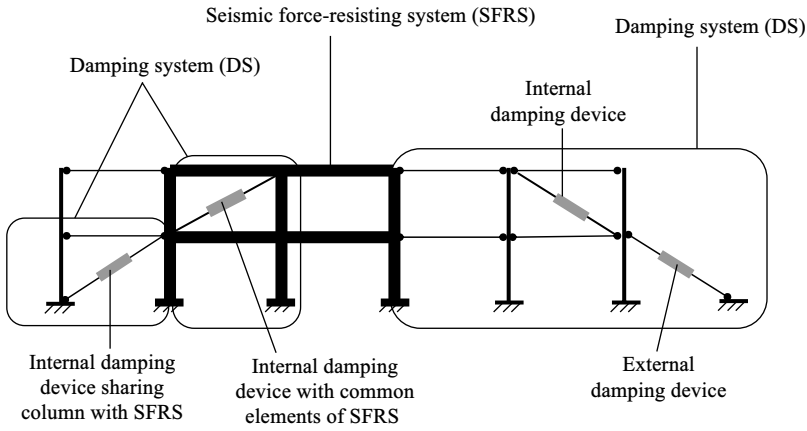

FIGURE 3.1 Definition of damping device and damping system.

foundation. Figure 3.1 illustrates both systems in a structural frame elevation. Note that the damping devices indicated earlier refer to a combination of dampers and their end connections, which could be in forms of pins, bolts, brace segments, or gusset plates.

On the basis of the location of the damping system, the damping device can be classified as internal or external [9]. As shown in Figure 3.1, if the damping system is combined with the seismic force-resisting system, some structural members are called shared elements or common elements.

Development of single-degree-of-freedom (SDOF) motion equations can be depicted from a single-story building structure installed with a damping system, which is schematically shown in Figure 3.2. The mass of this structure, assuming it is simply lumped at the roof level, is denoted as m. To consider the nonlinear behavior of the building structure, a general expression is utilized to define the structural force, Q, instead of $k_s x$, where k_s is linear lateral stiffness of the structure and x, simplified from $x(t)$, represents roof displacement or deflection of the structure at any time t. The structural damping coefficient is designated as c_s. Force, P, is defined along the movement of the damping device. Accordingly, its horizontal component becomes $D = P\cos\varphi$, where angle, φ, relies on assembly configurations of damping device and bracings. For the damping devices connected by *diagonal bracings* to the building structure, the angle, φ, represents the damping device's inclination to the horizontal movement of the structure. However, if the damping device is installed between *chevron bracings* and a horizontal structural member or a braced frame beam as shown in Figure 3.2, the movement of the damping device is parallel to the structure displacement and the angle, φ, becomes zero. Some sophisticated assemblies of damping devices and bracings structurally tied to the seismic force-resisting system have been developed in order to satisfy particular requirements of structural configurations and functions, such as damping device incorporated into *upper or lower toggle bracings*, or *scissor-jack bracings* [10]. Determination of their relations between the damping

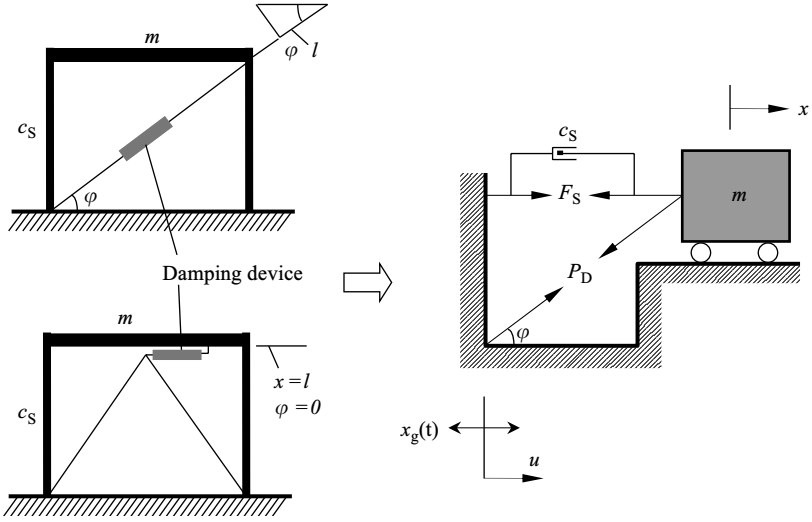

FIGURE 3.2 Sketch of SDOF structures with damping devices.

force in the direction of damping device movement and its horizontal component can be found in References 10 and 12.

For common configurations of damping devices assembled with diagonal or chevron bracings, the axial stiffness of bracings is usually much stronger than that of the damping device and the movement or deformation of the damping system is dominantly contributed by the damping device. Accordingly, the bracings can be reasonably assumed to be rigid components with infinite stiffness. On the basis of the assumption of infinite stiffness of the bracings and the well-known equilibrium condition, SDOF motion equation of the damped structure is easily expressed as follows:

$$m\ddot{x} + c_s\dot{x} + D + Q = -m\ddot{x}_g \quad \text{or} \quad m\ddot{x} + c_s\dot{x} + P\cos\varphi + Q = -m\ddot{x}_g \qquad (3.1)$$

where the structural acceleration, $\ddot{x}$, and the ground acceleration, $\ddot{x}_g$, are designated from simplified notations of $\ddot{x}(t)$ and $\ddot{x}_g(t)$, respectively.

As discussed in Section 1.5 and based on damper mechanical properties, damping devices can be classified as two major categories: *velocity dependent* and *displacement dependent*. Velocity-dependent damping devices include *fluid viscous damper*, *fluid viscoelastic damper*, and *solid viscoelastic damper*, whereas displacement-dependent damping devices consist of *friction damper* and *metallic yielding damper*. In addition, a combination of velocity- and displacement-dependent damping devices is somehow considered as a third category. Since each type of damping device possesses its own unique mechanical properties, development of a unified expression of the damping force, P, seems impossible.

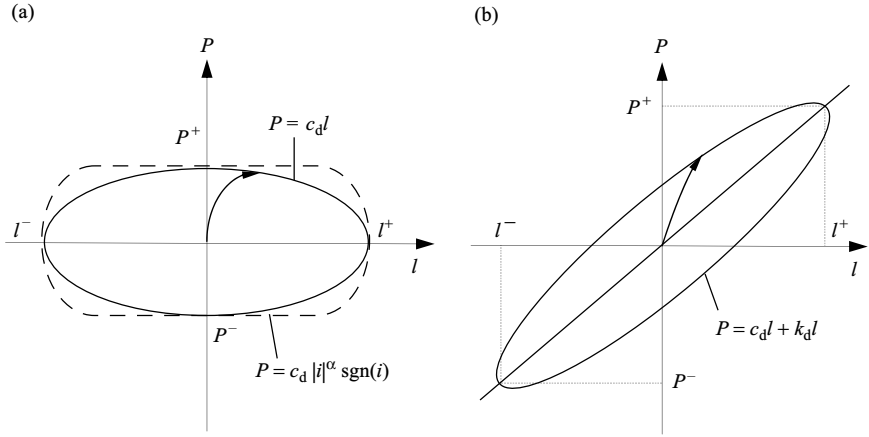

FIGURE 3.3 Force–displacement relations of velocity-dependent damping devices: (a) fluid viscous damper and (b) solid or fluid viscoelastic damper.

As a result, an individual expression of damping force, P, has to be developed based on its mechanical properties.

Figure 3.3 represents typical relations between the damping force and its displacement of linear or nonlinear viscous dampers, and solid or fluid viscoelastic dampers. Supported by test results for *linear fluid viscous damper*, the damping force, P, can be simply depicted as a linear relation to its velocity:

$$P = c_{\mathrm{d}}\dot{l} \tag{3.2}$$

where c_{d} is the *damping coefficient* of the fluid viscous damper, while $\dot{l}$ represents the relative velocity of the damper in the direction of P. As shown in Figure 3.2, l and x remain the following relation:

$$l = x\cos\varphi \quad \text{and} \quad \dot{l} = \dot{x}\cos\varphi.$$

Thus

$$P = c_{\mathrm{d}}\dot{x}\cos\varphi, \quad \text{or} \quad D = c_{\mathrm{d}}\dot{x}\cos^2\varphi \tag{3.2a}$$

If the fluid viscous damper exhibits nonlinear behavior to its relative velocity, then the force of a *nonlinear fluid viscous damper*, P, has the following relation to its movement:

$$P = c_{\mathrm{d}}|\dot{l}|^{\alpha}\mathrm{sgn}(\dot{l}) = c_{\mathrm{d}}|\dot{x}\cos\varphi|^{\alpha}\mathrm{sgn}(\dot{x}) \quad \text{or} \quad D = c_{\mathrm{d}}|\dot{x}|^{\alpha}\cos^{\alpha+1}\varphi\,\mathrm{sgn}(\dot{x}) \tag{3.3}$$

where α is the velocity exponent. According to mechanical properties of a *solid viscoelastic damper*, the damper force features a function of its relative velocity to

displacement, which can be simplified in terms of effective damping coefficient, c_d, and *effective stiffness*, k_d:

$$P = c_d\dot{l} + k_d l = c_d\dot{x}\cos\varphi + k_d x\cos\varphi, \quad \text{or} \quad D = c_d\dot{x}\cos^2\varphi + k_d x\cos^2\varphi \tag{3.4}$$

Unlike fluid viscous damper, the effective damping coefficient, c_d, and the effective stiffness, k_d, of a solid viscoelastic damper not only vary with frequency of oscillation, but also depend on ambient temperature and motion amplification [10]. As to fluid viscoelastic damper, similar properties as solid viscoelastic damper owns are observed from testing. Thus, its damper force can also be expressed by Equation 3.4 except that the fluid viscoelastic damper does not possess its effective stiffness during application of static load.

For displacement-dependent damping device, the damping force, P, is independent of the relative velocity and is mainly controlled by the relative displacement of the damping device. Figure 3.4 illustrates frequency-dependent hysteretic behavior from test results for friction damper and metallic yielding damper. On the basis of the different types of damping devices, their hysteretic behavior can be idealized as *elastoplastic model*, *bilinear model*, *polynomial model* [10], or other types of models, such as smoothed bilinear model [13,17]. The relation of the damping force, P, and the relative displacement, l, can be written in a general function $f(l)$:

$$P = f(l) \quad \text{or} \quad D = f(x\cos\varphi)\cos\varphi \tag{3.4a}$$

This general equation could be specifically expressed if the loading histories of the damping device are known. For example, as shown in Figures 3.5 and 3.6 for commonly adopted elastoplastic model or bilinear model, the damping force,

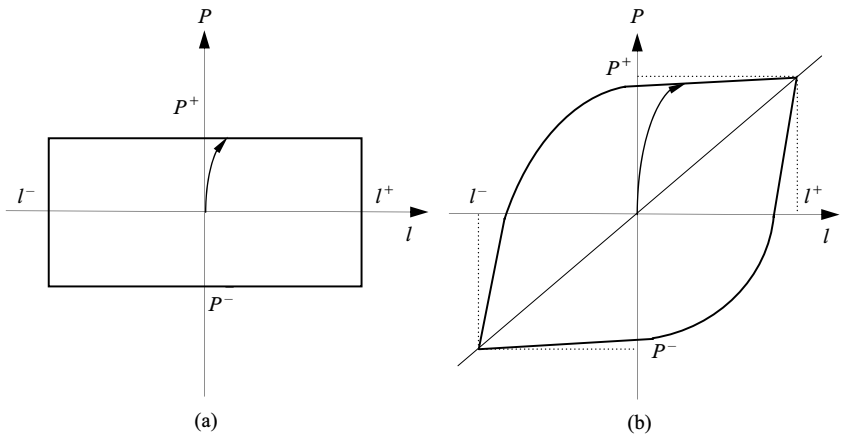

FIGURE 3.4 Force–displacement relations of displacement-dependent damping devices: (a) friction damper and (b) metallic yielding damper.

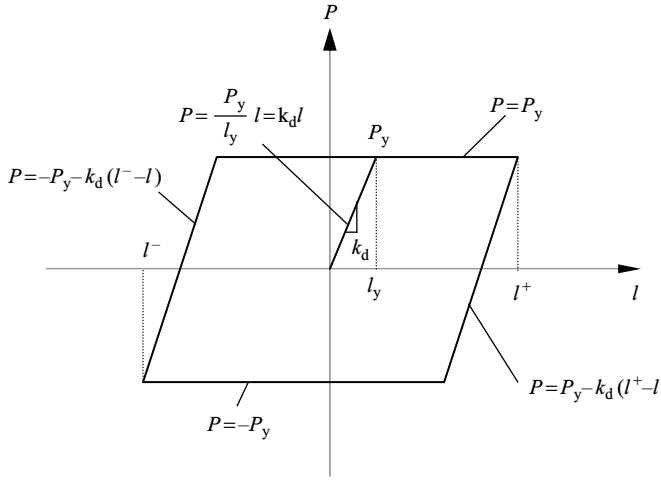

FIGURE 3.5 Elastoplastic model of displacement-dependent damping device.

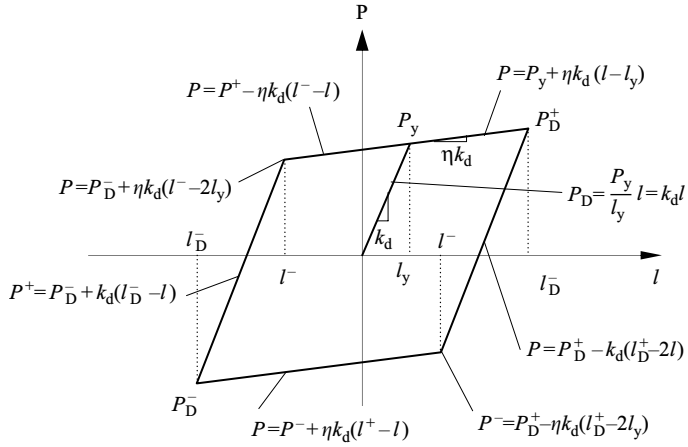

FIGURE 3.6 Bilinear model of displacement-dependent damping device.

P, can be determined by either loading or unloading case at any designated hysteretic loop. In the same way, Equation 3.4 is still applicable to models with more sophisticated expressions of loading and unloading paths [10].

The general expression of the structural force, Q, as given in Equation 3.1, can be used to capture the linear or nonlinear behavior of the structure subjected to seismic force. If the structure only exhibits linear behavior, then the term Q simply becomes $k_s x$. However, if the structure experiences nonlinear deformation or postyield behavior and the impact of imposed loading histories is not negligible, this general expression is still capable of taking the hysteretic behavior of the structure into account. Therefore, relying on the properties of structural materials, elastoplastic model, bilinear model, polynomial model, or other types

of models [2] can be selected to define the structural force, Q. Detailed expressions of the structural force for different types of models are given by Cheng [2].

3.1.2 Multiple-Degree-of-Freedom Motion Equations

A sketch of a multistory structure installed with damping system is shown in Figure 3.7. Applying the equilibrium conditions at the roof level n, and using relative displacement, x_n, which has been defined in Section 2.1.2, the motion equation due to the ground acceleration, $\ddot{x}_g$, is derived as

$$m_n\ddot{x}_n + c_{s,n}(\dot{x}_n - \dot{x}_{n-1}) + D_n + Q_n = -m_n\ddot{x}_g, \tag{3.5}$$

or

$$m_n\ddot{x}_n + c_{s,n}(\dot{x}_n - \dot{x}_{n-1}) + P_n\cos\varphi_n + Q_n = -m_n\ddot{x}_g \tag{3.5a}$$

where m_n is the roof mass and $c_{s,n}$ is denoted as the structural damping between the roof and the story below the roof. x_n, and x_{n-1} are utilized to identify the relative displacement at the roof and the story below. For the structural force between the roof level and the story below, a general expression of Q_n, is also

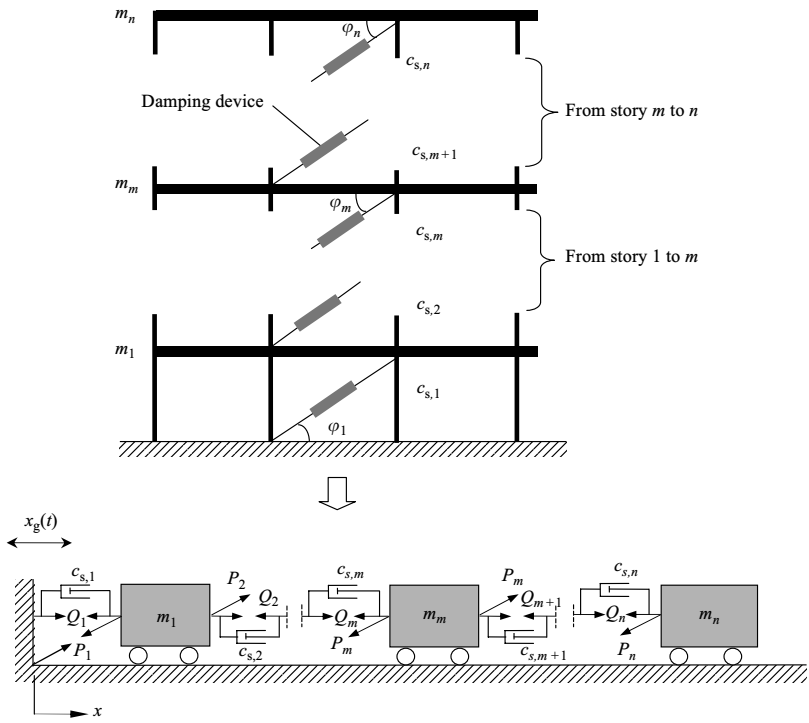

FIGURE 3.7 Sketch of MDOF structures with damping devices.

used to represent elastic or inelastic behavior of the seismic force-resisting system. According to material properties of the structure, Q_n can be idealized as a linear model, elastoplastic model, bilinear model, or other types of models, which have already been discussed in Section 3.1.1. In Equations 3.5 and 3.5a, P_n and D_n are used to define the axial force and its horizontal component of damping devices between the roof and the story below. The specific expression of the damping force and its relative velocity or relative displacement needs to be determined by selected damping devices as discussed in Section 3.1.1. φ_n presents the angle between the axial force and the horizontal component of the damping device.

By applying the same methodology used for Equation 3.5, the motion equation at story m is identified as below:

$$m_m\ddot{x}_m + c_{s,m}(\dot{x}_m - \dot{x}_{m-1}) - c_{s,m+1}(\dot{x}_{m+1} - \dot{x}_m) + D_m - D_{m+1} + Q_m - Q_{m+1} = -m_m\ddot{x}_g, \tag{3.6}$$

or

$$m_m\ddot{x}_m + c_{s,m}(\dot{x}_m - \dot{x}_{m-1}) - c_{s,m+1}(\dot{x}_{m+1} - \dot{x}_m) + P_m\cos\varphi_m - P_{m+1}\cos\varphi_{m+1} + Q_m - Q_{m+1} = -m_m\ddot{x}_g \tag{3.6a}$$

where m_m is the mass at the story m; $c_{s,m+1}$ and $c_{s,m}$ are the structural damping between story $m+1$ and m, and between story m and $m-1$, respectively. x_{m+1}, x_m, and x_{m-1}, are designated as the relative displacement at story $m+1$, m, and $m-1$. Q_{m+1} and Q_m are denoted as the structural force between story $m+1$ and m, and between story m and $m-1$, respectively. P_{m+1}, P_m, D_{m+1}, and D_m represent the axial force and the horizontal component of damping devices between story $m+1$ and m, and between story m and $m-1$. φ_{m+1} and φ_m are angles between the axial force, P_{m+1} or P_m, and the horizontal component D_{m+1} or D_m of the damping devices.

In the same way, the motion equation at the first level can be easily derived:

$$m_1\ddot{x}_1 + c_{s,1}\dot{x}_1 - c_{s,2}(\dot{x}_2 - \dot{x}_1) + D_1 - D_2 + Q_1 - Q_2 = -m_1\ddot{x}_g, \tag{3.7}$$

or

$$m_1\ddot{x}_1 + c_{s,1}\dot{x}_1 - c_{s,2}(\dot{x}_2 - \dot{x}_1) + P_1\cos\varphi_1 - P_2\cos\varphi_2 + Q_1 - Q_2 = -m_1\ddot{x}_g \tag{3.7a}$$

where m_1 is the mass at the first level. $c_{s,1}$ and $c_{s,2}$ are the structural damping between the second and the first story, and between the first story and the base, respectively. x_2 and x_1 represent the relative displacement at the second and the first story. Q_2 and Q_1 are denoted as the structural force between the second and the first story, and between the first story and the base, respectively. P_2, P_1, D_2, and D_1 are the axial force and the horizontal component of damping devices between the second and the first story, and between the first story and the base. φ_2 and φ_1

are angles between the axial force, P_2 or P_1, and the horizontal component D_2 or D_1 of the damping devices.

Equations 3.5, 3.6, and 3.7 form multiple-degree-of-freedom (MDOF) motion equations. These equations can be condensed in matrix notations and symbolically shown as below:

$$[M]\{\ddot{x}\} + [C]\{\dot{x}\} + [D]\{1\} + [Q]\{1\} = -\ddot{x}_g[M]\{1\} \tag{3.8}$$

where the mass matrix, $[M]$, the structural damping matrix, $[C]$, the damping force matrix $[D]$, and the structural force matrix, $[Q]$, are in following forms:

$$[M] = \begin{bmatrix} m_1 & 0 & 0 & 0 & 0 \\ & m_2 & 0 & 0 & 0 \\ & & \ddots & \vdots & \\ & & & m_m & \cdots & 0 & 0 \\ & & & & \ddots & & \\ & \text{sym.} & & & & m_{n-1} & 0 \\ & & & & & & m_n \end{bmatrix}$$

$$[C] = \begin{bmatrix} c_{s,1} + c_{s,2} & -c_{s,2} & & 0 & & 0 & 0 \\ & c_{s,2} + c_{s,3} & & 0 & & 0 & 0 \\ & & \ddots & \vdots & & & \\ & & & c_{s,m} + c_{s,m+1} & \cdots & 0 & 0 \\ & & & & \ddots & & \\ & \text{sym.} & & & & c_{s,n-1} + c_{s,n} & -c_{s,n} \\ & & & & & & c_{s,n} \end{bmatrix}$$

$$[D] = \begin{bmatrix} D_1 & -D_2 & 0 & 0 & 0 \\ & D_2 & 0 & 0 & 0 \\ & & \ddots & \vdots & \\ & & D_m & \cdots & 0 & 0 \\ & & & \ddots & & \\ & \text{sym.} & & & D_{n-1} & -D_n \\ & & & & & D_n \end{bmatrix}$$

$$= \begin{bmatrix} P_1 \cos\varphi_1 & -P_2 \cos\varphi_2 & & 0 & & 0 & 0 \\ & P_2 \cos\varphi_2 & & 0 & & 0 & 0 \\ & & \ddots & \vdots & & & \\ & & & P_m \cos\varphi_m & \cdots & 0 & 0 \\ & & & & \ddots & & \\ & \text{sym.} & & & & P_{n-1} \cos\varphi_{n-1} & -P_n \cos\varphi_n \\ & & & & & & P_n \cos\varphi_n \end{bmatrix}$$

$$[Q] = \begin{bmatrix} Q_1 & -Q_2 & & 0 & & 0 & 0 \\ & Q_2 & & 0 & & 0 & 0 \\ & & \ddots & \vdots & & & \\ & & & Q_m & \cdots & 0 & 0 \\ & & & & \ddots & & \\ & \text{sym.} & & & & Q_{n-1} & -Q_n \\ & & & & & & Q_n \end{bmatrix}$$

In Equation 3.8, $\{1\}$ is designated as a $1 \times n$ unit vector; $\{x\}$, $\{\dot{x}\}$, and $\{\ddot{x}\}$ represent the relative displacement vector, velocity vector, and acceleration vector of the structure with damping system:

$$\{x\}^{\mathrm{T}} = \{x_1 \quad x_2 \quad \ldots \quad x_m \quad \ldots \quad x_{n-1} \quad x_n\} \tag{3.9}$$

$$\{\dot{x}\}^{\mathrm{T}} = \{\dot{x}_1 \quad \dot{x}_2 \quad \ldots \quad \dot{x}_m \quad \ldots \quad \dot{x}_{n-1} \quad \dot{x}_n\} \tag{3.9a}$$

$$\{\ddot{x}\}^{\mathrm{T}} = \{\ddot{x}_1 \quad \ddot{x}_2 \quad \ldots \quad \ddot{x}_m \quad \ldots \quad \ddot{x}_{n-1} \quad \ddot{x}_n\} \tag{3.9b}$$

Equation 3.8 provides general motion equations of MDOF, which are applicable to building structures with either velocity-dependent devices or displacement-dependent devices considering the structure's linear or nonlinear characteristics. Once the damping devices are identified and the mechanical properties of the *seismic force-resisting system* are selected, the damping force matrix $[D]$ and the structural force matrix $[Q]$ can be explicitly determined from the relation between the damping force and the relative velocity or displacement, as well as from the relation between the structural force and its deformation, respectively. Consequently, the displacement, velocity, and acceleration of the seismic force-resisting system and the damping system are explicitly computed from Equation 3.8 in accordance with the input of the ground acceleration, $\ddot{x}_{\mathrm{g}}$.

3.2 Analysis Procedures and Code Requirements

3.2.1 Introduction

Analysis of a structure equipped with a damping system is a complicated procedure. It is because during an earthquake event, both the seismic force-resisting system and the damping system dissipate seismic-induced energy in the structure, which leads the seismic force-resisting system to experience *postyield hysteretic stage*. Thus, to obtain accurate solutions of the motion equations as given in Equation 3.8, the nonlinearity of the seismic force-resisting system has to be taken into account. Moreover, if the damping system also exhibits nonlinear behavior, the analytical process becomes much more complex.

Theoretically, nonlinear response history analysis is the only procedure to resolve Equation 3.8 on condition that the nonlinearity of the seismic force-resisting system and damping system has to be considered in a direct way. However,

because the mechanical properties of damping devices and the structural members are dependent upon time and history of the ground accelerations, iteration process has to be employed at each time interval in order to get results converged to a desired accuracy. In addition, from the design practice viewpoint, more than one-time history shall be utilized to envelop all possible seismic performances of the damped structure, and uncertainties of actual mass centers of the structure that result in accidental torsional effects shall be investigated in the response history analysis in order to capture the most unfavorable structural responses. Multiple inputs of time histories, shift of mass center locations, modeling techniques, and optimized layout of the seismic force resisting system combined with the damping system create tremendous computational efforts. Thus, this complicated analysis procedure became a major impediment to application of damping devices by means of energy dissipations to the design of building structures.

Before early 1990s, another impediment to the use of damping devices in building structures was the gap between the research achievements and the design practice: no codes or guidelines to regulate the design and test procedures of damping devices. But this gap was eventually bridged in 1992 by the Northern Section of the Structural Engineers Association of California (SEAOC), which published the first draft requirements in 1992 [18] to guide the design of structures with damping systems. Afterwards, the SEAOC Seismology Committee adopted these tentative guidelines for passive energy dissipation systems and published them as Appendix H to the 1999 Blue Book [16]. In addition, the Federal Emergency Management Agency (FEMA) developed guidelines for design of new buildings and rehabilitation of existing buildings with damping systems and published in FEMA 222A [9], FEMA 302 [5], FEMA 273/274 [6], and FEMA 356 [7].

Meanwhile, to remove the major impediment in design of damped structures, researchers [12,19] focused on development of an effective method that is able to simplify the design procedures and reduce computational efforts for some types of damped building structures. This method, normally called simplified method, assumes that a viscously damped structure with equivalent linear stiffness of the seismic force-resisting system is utilized to represent the damped structure characterized with nonlinear behavior of the seismic force-resisting system. In addition, a total effective damping is introduced to sum the structural inherent damping, viscous damping of damping system, and hysteretic damping owing to posty-ield hysteretic behavior of the structure. Consequently, the pseudoacceleration, reduced by a function of the total effective damping, is applied to compute the maximum responses, velocities, and accelerations of the damping system and the lateral force-resisting system. Use of this method has not only simplified the response spectrum procedure, but also resulted in the development of an *equivalent lateral force procedure*, a simplified method of response spectrum procedure with only two modes taken into account: the fundamental and residual modes. Comparisons of design examples based on the simplified method and nonlinear response history analysis were performed [15] to evaluate differences caused by

the influence of higher modes of vibration and force–displacement relation of the structural system. Analytical results revealed that the simplified method was able to provide satisfactory estimations of the peak displacement and acceleration. However, the peak velocity determined by this simplified method deviated from that obtained from the nonlinear response history analysis within a fairly reasonable range. FEMA 368/369 [8] adopted the simplified method and incorporated it into an appendix to Chapter 13. In FEMA 450 [9], this appendix became Chapter 15 with editorial revisions. ASCE 7-05 [1] adopted the entire Chapter 15 of FEMA 450 and formed Chapter 18 for the seismic design of structures with damping systems. Four design procedures for damped structures are presented in ASCE 7-05 [1] based on the seismic design category of the structure location, the selected seismic force-resisting system, the chosen damping system, and the structural configurations: response spectrum procedure, equivalent lateral force procedure, nonlinear static procedure or pushover analysis, and nonlinear response history procedure. Nonlinear procedures are generally recommended for the design of all types of damped structures. However, applications of the response spectrum procedure and the equivalent lateral force procedure, which are developed based on the simplified method, are only permitted on condition that limitations imposed by ASCE 7-05 are met. Detailed descriptions of each procedure with ASCE 7-05 specific requirements are presented in following sections.

3.2.2 Response Spectrum Analysis

3.2.2.1 Development of response spectrum procedure

As discussed in Section 2.3.5.3 for *response spectrum analysis*, the motion equation of a structure at the *m*th *angular frequency*, ω_m, can be rewritten in correspondence with the *pseudoacceleration*, S_{am} which is inclusively reduced by a *numerical coefficient for effective damping*, $B_{m\mathrm{D}}$, at the *m*th mode of vibration.

$$\ddot{x}'_m + \omega_m^2 x'_m = \Gamma_m S_{am}, \quad m = 1, 2, \ldots, n \tag{3.10}$$

where x'_m represents the *m*th component of the generalized response vector and is used to define the structural displacements: $\{x\} = \{\Phi\}_m x'_m$, where $\{\Phi\}_m$ is the *m*th mode shape of the structure and its component. $\phi_{n,m}$ at the roof level is designated as a unit. In Equation 3.10, the angular frequency, ω_m, is determined by the following equation:

$$\omega_m^2 = \frac{\{\Phi\}_m^{\mathrm{T}}[K]\{\Phi\}_m}{\{\Phi\}_m^{\mathrm{T}}[M]\{\Phi\}_m} \tag{3.11}$$

Matrixes $[M]$ and $[K]$ in Equation 3.11 represent the mass and stiffness of the damped structure. The *m*th modal *participation factor*, Γ_m, in Equation 3.10 is

defined as

$$\Gamma_m = \frac{\{\Phi\}_m^{\mathrm{T}}[M]\{1\}}{\{\Phi\}_m^{\mathrm{T}}[M]\{\Phi\}_m} = \frac{\sum_{i=1}^{n} m_i \phi_{i,m}}{\sum_{i=1}^{n} m_i \phi_{i,m}^2} \tag{3.12}$$

The application of Equation 3.10 to response spectrum analysis of a structure with damping system mainly depends on whether the input of pseudoacceleration, S_{am}, reduced by a numerical coefficient for effective damping, $B_{m\mathrm{D}}$, enables to reflect the structure performance with the damping system and to provide satisfactory accuracy of structural responses or not. In addition, compared to the structure with isolation system, the structure equipped with damping system is more likely to exhibit inelastic behavior under a strong earthquake event. To retain Equation 3.10 applicable without changing its format, an *effective ductility demand*, μ_{D}, is introduced by ASCE 7-05 [1] to take the inelastic deformation of the seismic force-resisting system into account, and the numerical coefficient for effective damping, $B_{m\mathrm{D}}$, is adopted to consider the effects of the structural damping, β or β_{I}, the effective damping of the damping devices, β_{V}, and the effective damping due to postyield hysteretic performance of the seismic force-resisting system combined with structural elements of the damping system, β_{H}. The development of response spectrum procedure for the structure with damping system is presented in detail subsequently.

For the mth angular frequency, ω_m, the period of the structure is expressed as $T_m = 2\pi/\omega_m$. Thus, the pseudoacceleration, S_{am}, at the effective yield point of the seismic force-resisting system can be determined from the corresponding T_m as shown in Figure 3.8. Divided by the numerical coefficient for effective damping, $B_{m\mathrm{D}}$, which is being discussed in detail in Section 3.2.2.2, and multiplied by a coefficient $R/(C_{\mathrm{d}}\Omega_{\mathrm{o}})$, which further adjusts the pseudoacceleration, S_{am}, to match the level of the structural performance with first yielding of a structural element, the modified pseudoacceleration is expressed in terms of *seismic response coefficient*, $C_{\mathrm{S}m}$:

$$S_{am} = \frac{S_{\mathrm{DS}}}{\Omega_{\mathrm{o}} B_{m\mathrm{D}}} \left(\frac{R}{C_{\mathrm{d}}}\right) g = C_{\mathrm{S}m} g, \quad T_m < T_{\mathrm{S}} \tag{3.13}$$

$$S_{am} = \frac{S_{\mathrm{D1}}}{T_m \Omega_{\mathrm{o}} B_{m\mathrm{D}}} \left(\frac{R}{C_{\mathrm{d}}}\right) g = C_{\mathrm{S}m} g, \quad T_m \geq T_{\mathrm{S}} \tag{3.13a}$$

where R is *response modification coefficient*, C_{d} is *deflection amplification factor*, and Ω_{o} is *overstrength factor*. Coefficients R, C_{d}, and Ω_{o} are defined in Table 12.2-1 of ASCE 7-05 [1] for all types of seismic force-resisting systems. Owing to space limitation, the coefficients only for commonly used seismic force-resisting systems are summarized here in Table 2.5. T_{S} is the period defined as the ratio of $S_{\mathrm{D1}}/S_{\mathrm{DS}}$. Definitions of S_{DS} and S_{D1} are given in Section 2.3.2.

Note that the effective yield point of the seismic force-resisting system and the first yielding of a structural element present different levels of the building's

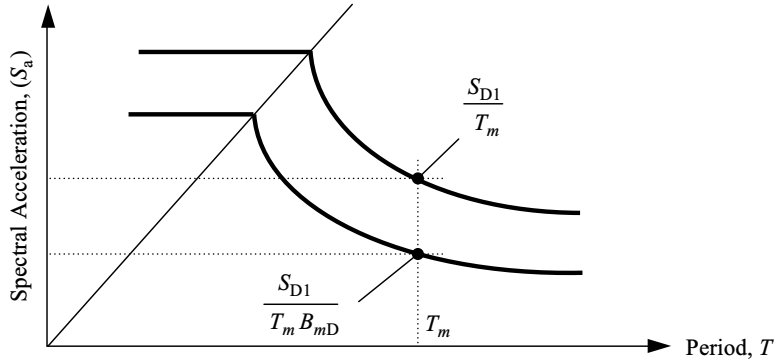

FIGURE 3.8 Reduction of spectral acceleration, S_a, by numerical coefficient, B_{mD}.

performance. For instance, the seismic force-resisting system of a damped structure is characterized with special steel moment frames. By performing nonlinear static analysis, a base shear versus roof displacement curve is developed as shown in Figure 3.9. After the first plastic hinge forms in a member of the steel moment frames, the relation between the base shear and the roof displacement still remains linear. However, with increase in applied seismic force, more plastic hinges occur in members of the steel moment frames. Consequently, a small increment of seismic force results in a large displacement and there is no linear relation between the applied force and the roof displacement. Actually, the base shear versus roof displacement curve as shown in Figure 3.9 reflects general characteristics of most seismic force-resisting systems and is usually simplified as an idealized elastoplastic model. The effective yield point is defined as the base shear at the effective yield displacement D_Y in in. (mm), of idealized model as shown in Figure 3.9. The determination of the effective yield point is based on the equivalent work done by both curves.

Since the stiffness, $[K]$, in Equation 3.8 is restricted to the linear behavior of the building structure, periods, T_m, used in Equations 3.13 and 3.13a only present the structure's performance at elastic stage. To account for the inelastic behavior of the structure, ASCE 7-05 introduces an effective period of the first mode or fundamental mode, T_{1D}, and replaces T_1 in Equation 3.13. Thus, Equations 3.13 and 3.13a become as follows:

$$S_{a1} = \frac{S_{DS}}{\Omega_o B_{1D}} \left(\frac{R}{C_d} \right) g = C_{S1} g, \quad T_{1D} < T_S \tag{3.13b}$$

$$S_{a1} = \frac{S_{D1}}{T_{1D} \Omega_o B_{1D}} \left(\frac{R}{C_d} \right) g = C_{S1} g, \quad T_{1D} \geq T_S \tag{3.13c}$$

Furthermore, based on Equation 2.8 for the relation between the pseudoacceleration, S_{a1}, and the design displacement, D_{1D} in in. (mm), as shown in Figure 3.9,

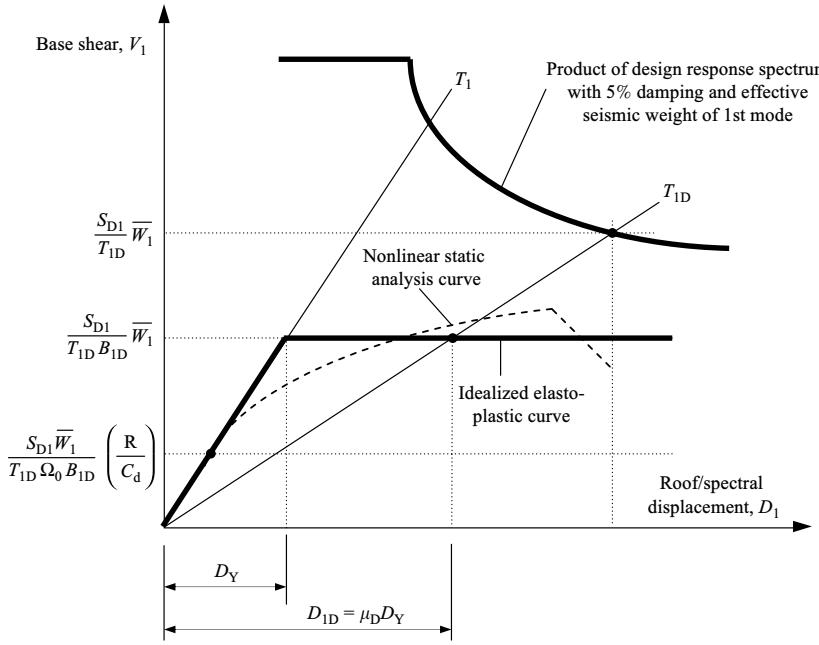

FIGURE 3.9 Relation between the base shear and the displacement of the first mode.

T_{1D} is defined as

$$T_{1D}^2 = \frac{4\pi^2 D_{1D}}{S_{a1}} \tag{3.14}$$

Relying on the relation of $D_{1D} = \mu_D D_Y$, where μ_D is designated as effective ductility demand and D_Y is denoted as displacement of the effective yield point, the effective period of the fundamental mode, T_{1D}, can be expressed in terms of the structural period of the fundamental mode, T_1.

$$T_{1D}^2 = \frac{4\pi^2(\mu_D D_Y)}{S_{a1}} = \mu_D T_1^2, \quad \text{or} \quad T_{1D} = T_1\sqrt{\mu_D} \tag{3.14a}$$

The maximum value of the effective ductility demand, μ_{max}, is set by ASCE 7-05 and given by the following expressions:

$$\mu_{max} = \frac{1}{2}\frac{T_S - T_1}{T_{1D} - T_1}\left(\frac{R}{\Omega_o I} - 1\right)^2 + \frac{R}{\Omega_o I}, \quad T_1 \le T_S \le T_{1D} \tag{3.15}$$

$$\mu_{max} = \frac{R}{\Omega_o I}, \quad T_S \le T_1 \tag{3.15a}$$

$$\mu_{\max} = \frac{1}{2}\left[\left(\frac{R}{\Omega_o I}\right)^2 + 1\right], \quad T_S \geq T_{1D} \tag{3.15b}$$

On the basis of Equation 3.14, the displacement of the structure at each model can be determined. From Equation 3.10, the maximum displacement is estimated as below:

$$x'_m = \frac{1}{\omega_m^2}\Gamma_m S_{am} \tag{3.16}$$

Substituting Equation 3.16 into $\{x\}_m = \{\Phi\}_m x'_m$, and multiplying it by $C_d\Omega_o/R$, the displacement related to the yield of the structure at each story level becomes

$$\{x\}_m = \{\Phi\}_m x'_m = \frac{g}{4\pi^2}\Gamma_m\left(\frac{C_d\Omega_o}{R}\right)C_{Sm}T_m^2\{\Phi\}_m \tag{3.17}$$

where $\{x\}_m$ is a $1 \times n$ vector and can be written as $\{x_{1,m} \cdots x_{m,m} \cdots x_{n,m}\}$. From Equation 3.17 for the fundamental mode ($m = 1$) and $\phi_{1.n} = 1$ at the roof level, the displacement at the effective yield point, D_Y, becomes

$$D_Y = \left(\frac{g}{4\pi^2}\right)\Gamma_1\left(\frac{C_d\Omega_o}{R}\right)C_{S1}T_1^2 \tag{3.18}$$

Substituting Equations 3.14a into the displacement at the effective yield point, D_Y and relying on the definition of the effective ductility demand, the design displacement at the roof level is derived as follows and its limitation of application is imposed by ASCE 7-05 [1]:

$$\begin{aligned} D_{1D} &= \left(\frac{g}{4\pi^2}\right)\Gamma_1\left(\frac{C_d\Omega_o}{R}\right)C_{S1}T_{1D}^2 \\ &= \left(\frac{g}{4\pi^2}\right)\Gamma_1\left(\frac{S_{DS}T_{1D}^2}{B_{1D}}\right) \geq \left(\frac{g}{4\pi^2}\right)\Gamma_1\left(\frac{S_{DS}T_1^2}{B_{1E}}\right), \quad T_{1D} < T_S \end{aligned} \tag{3.19}$$

$$\begin{aligned} D_{1D} &= \left(\frac{g}{4\pi^2}\right)\Gamma_1\left(\frac{C_d\Omega_o}{R}\right)C_{S1}T_{1D}^2 \\ &= \left(\frac{g}{4\pi^2}\right)\Gamma_1\left(\frac{S_{D1}T_{1D}}{B_{1D}}\right) \geq \left(\frac{g}{4\pi^2}\right)\Gamma_1\left(\frac{S_{D1}T_1}{B_{1E}}\right), \quad T_{1D} \geq T_S \end{aligned} \tag{3.19a}$$

For the mode other than 1 ($m > 1$), the design displacement, D_{mD}, in. (mm) at the roof level is

$$\begin{aligned} D_{mD} &= \left(\frac{g}{4\pi^2}\right)\Gamma_m\left(\frac{C_d\Omega_o}{R}\right)C_{Sm}T_{mD}^2 \\ &= \left(\frac{g}{4\pi^2}\right)\Gamma_m\left(\frac{S_{D1}T_m}{B_{mD}}\right) \leq \left(\frac{g}{4\pi^2}\right)\Gamma_m\left(\frac{S_{DS}T_m^2}{B_{mD}}\right) \end{aligned} \tag{3.19b}$$

The derivation of the seismic force at each story level is based on Equation 3.10. Thus, the maximum acceleration can be expressed as

$$\ddot{x}'_m = \Gamma_m S_{\mathrm{a}m} \tag{3.20}$$

Consequently, by applying Newton's law and using Equation 3.20, the design lateral force vertically distributed at each level of the structure at the mth mode becomes as below:

$$\{F\}_m = [M]\{\ddot{x}\}_m = [M]\{\Phi\}_m \ddot{x}'_m = [M]\{\Phi\}_m \Gamma_m S_{\mathrm{a}m} = [M]\{\Phi\}_m \Gamma_m C_{\mathrm{S}m} g \tag{3.21}$$

In Equation 3.21, $\{F\}_m$ is a $1 \times n$ vector and can be written as $\{F_{1,m} \ \cdots \ F_{m,m} \ \cdots \ F_{n,m}\}$. The design base shear of the mth mode is the sum of the design lateral force at each story level and is given as follows:

$$V_m = \sum_{i=1}^{n} F_{i,m} = \left(\sum_{i=1}^{n} m_i \phi_{i.m} \right) \Gamma_m C_{\mathrm{S}m} g = C_{\mathrm{S}m} \overline{W}_m \tag{3.22}$$

where $\overline{W}_m$ is the effective seismic weight of the mth mode in kip (kN), and is defined as

$$\overline{W}_m = \left(\sum_{i=1}^{n} m_m \phi_{i,m} \right) \Gamma_m g = \frac{\left(\sum_{i=1}^{n} m_m \phi_{i.m} \right)^2}{\sum_{i=1}^{n} m_m \phi_{i.m}^2} g \tag{3.23}$$

For a damped structure, the *design displacement*, $\delta_{i,m\mathrm{D}}$ and $\delta_{i-1,m\mathrm{D}}$, in. (mm) at story i and $i-1$ of the mth mode is given

$$\delta_{i,m\mathrm{D}} = D_{m\mathrm{D}} \phi_{i,m}; \quad \delta_{i-1,m\mathrm{D}} = D_{m\mathrm{D}} \phi_{i-1,m} \tag{3.24}$$

Thus, the story drift, $\Delta_{i,m\mathrm{D}}$, in (mm), becomes

$$\Delta_{i,m\mathrm{D}} = D_{m\mathrm{D}} (\phi_{i,m} - \phi_{i-1,m}) \tag{3.25}$$

On the basis of the Equation 2.7, the *design story velocity* of the fundamental mode ($m = 1$), $\nabla_{i,1\mathrm{D}}$, in in./s (mm/s), and higher modes ($m > 1$), $\nabla_{i,m\mathrm{D}}$, in in./s (mm/s), are expressed respectively, as follows:

$$\nabla_{i,1\mathrm{D}} = 2\pi \frac{\Delta_{i,1\mathrm{D}}}{T_{1\mathrm{D}}}, \quad m = 1 \ \text{ and } \ i = 1, 2, \ldots, n \tag{3.26}$$

$$\nabla_{i,m\mathrm{D}} = 2\pi \frac{\Delta_{i,m\mathrm{D}}}{T_m}, \quad m > 1 \ \text{ and } \ i = 1, 2, \ldots, n. \tag{3.26a}$$

Note that the response spectrum procedure itself is independent of the selected response spectrums. Even though the above procedure is depicted by utilizing the response spectrum developed from the *design earthquake*, it is still applicable to the input of response spectrums generated from the *maximum considered earthquake* (MCE). Thus the same analytical procedure can be used without any modification to determine the displacement at each story, the story velocity, and other items for design of damping devices under the MCE, except that the roof displacement, $D_{m\mathrm{M}}$, in (mm), $m = 1, \ldots, n$, is rewritten in terms of the MCE spectral response acceleration for short period, S_{MS}, and at 1s, S_{M1}, respectively.

$$D_{1\mathrm{M}} = \left(\frac{g}{4\pi^2}\right)\Gamma_1 \frac{S_{\mathrm{MS}} T_{1\mathrm{M}}^2}{B_{1\mathrm{M}}} \geq \left(\frac{g}{4\pi^2}\right)\Gamma_1 \frac{S_{\mathrm{MS}} T_1^2}{B_{1\mathrm{E}}}, \quad m = 1 \text{ and } T_{1\mathrm{M}} < T_{\mathrm{S}} \tag{3.27}$$

$$D_{1\mathrm{M}} = \left(\frac{g}{4\pi^2}\right)\Gamma_1 \frac{S_{\mathrm{M1}} T_{1\mathrm{M}}}{B_{1\mathrm{M}}} \geq \left(\frac{g}{4\pi^2}\right)\Gamma_1 \frac{S_{\mathrm{M1}} T_1}{B_{1\mathrm{E}}}, \quad m = 1 \text{ and } T_{1\mathrm{M}} \geq T_{\mathrm{S}} \tag{3.27a}$$

$$D_{m\mathrm{M}} = \left(\frac{g}{4\pi^2}\right)\Gamma_m \frac{S_{\mathrm{M1}} T_m}{B_{m\mathrm{M}}} \leq \left(\frac{g}{4\pi^2}\right)\Gamma_m \frac{S_{\mathrm{MS}} T_m^2}{B_{m\mathrm{M}}}, \quad m > 1 \tag{3.27b}$$

The limitations of using response spectrum procedure are specified by ASCE 7-05 [1]. Specifically, at least two damping devises shall be installed at each level of the building structure. The orientation of these damping devices shall be parallel to the imposed seismic force and they need to be installed at locations to resist the torsion generated by the seismic force. The effective damping of the fundamental mode, $\beta_{1\mathrm{D}}$, is not greater than 35% of critical damping. At last, the design spectral response acceleration parameter with 5% of critical at the period of 1 s, S_1, is not greater than 0.6. The above limitations ensure that analytical results of the response spectrum procedure are within acceptable accuracy.

3.2.2.2 Effective damping and damping coefficient

In general, the effective damping of a damped structure consists of three portions as described by ASCE 7-05: (1) *structural damping* due to inherent dissipation of energy by structural elements before the *effective yield displacement*, D_{Y}, of the seismic force-resisting system, which is also called inherent damping, β_{I}; (2) *viscous damping*, β_{V}, due to energy dissipation by the damping system before the effective yield displacement, D_{Y}, of the seismic force-resisting system; and (3) *hysteretic damping*, β_{H}, due to postyield hysteretic behavior of the seismic force-resisting system and elements of the damping system. Inherent damping, β_{I}, usually is within 2–5% of critical damping. Therefore, β_{I} is easily determined only on the basis of the properties of building materials. However, determination of viscous damping, β_{V}, depends on the selected type of damping devices: displacement dependent or velocity dependent. Extensive research has been reported [10] on how to evaluate viscous damping by means of analysis

and experiment. Owing to the space limitation, discussion of viscous damping in this section focuses only upon linear and nonlinear fluid viscous dampers. For the determination of viscous damping for other types of devices, refer to References 10 and 14.

For *linear fluid viscous damper* under the design earthquake, its velocity, $V_{i,j}$, and force $P_{i,j}$, are expressed in terms of the relative displacement, $l_{i,j}$ at mth mode based on Equation 3.26:

$$V_{i,j} = \frac{2\pi}{T_m} l_{i,j}; \quad P_{i,j} = c_{\mathrm{d}i,j} \frac{2\pi}{T_m} l_{i,j} \tag{3.28}$$

where $c_{\mathrm{d}i,j}$ is the damping coefficient of the fluid viscous damper. Subscripts i and j designated in Equation 3.28 present the jth damper at the ith story. Assuming there are k dampers at the ith story, damper j is within the region $j \leq k$.
According to the relation of the story drift and the relative movement of the damper as given in Equation 3.25, the damper force, $P_{i,j}$, can be written as

$$P_{i,j} = c_{\mathrm{d}i,j} \frac{2\pi}{T_m} D_{m\mathrm{D}} (\phi_{i,m} - \phi_{i-1,m}) \cos \varphi_{i,j} \tag{3.29}$$

where $\varphi_{i,j}$ is the angle of the damper axial direction to the story horizontal movement. The subscripts of i and j have the same meaning as defined in Equation 3.28. Accordingly, the work done by the jth damper at the ith story in one complete cycle of dynamic response at the mth mode is determined as follows:

$$W_{mi,j} = \pi P_{i,j} l_{i,j} = c_{\mathrm{d}i,j} \frac{2\pi^2}{T_m} D_{m\mathrm{D}}^2 (\phi_{i,m} - \phi_{i-1,m})^2 \cos^2 \varphi_{i,j} \tag{3.30}$$

Thus, the total work done by all the dampers at the mth mode becomes

$$W_{\mathrm{D}m} = \sum W_{mi,j} = \frac{2\pi^2}{T_m} D_{m\mathrm{D}}^2 \sum_{i=1}^{n} \sum_{j=1}^{k} c_{\mathrm{d}i,j} (\phi_{i,m} - \phi_{i-1,m})^2 \cos^2 \varphi_{i,j} \tag{3.31}$$

Since the *maximum strain energy* of the structure is equal to the *maximum kinetic energy*, the maximum strain energy of the mth mode, $W_{\mathrm{S}m}$, can be determined as below:

$$W_{\mathrm{S}m} = \frac{2\pi^2}{T_m^2} D_{m\mathrm{D}}^2 \sum_{i=1}^{n} m_i \phi_{i,m}^2 \tag{3.32}$$

On the basis of the definition of viscous damping specified by ASCE 7-05 [1], the *viscous damping* of the linear fluid viscous damping devices is expressed as

$$\beta_{\mathrm{V}m} = \frac{W_{\mathrm{D}m}}{4\pi W_{\mathrm{S}m}} = \frac{T_m}{4\pi} \frac{\sum_{i=1}^{n} \sum_{j=1}^{k} c_{\mathrm{d}i,j} (\phi_{i,m} - \phi_{i-1,m})^2 \cos^2 \varphi_{i,j}}{\sum_{i=1}^{n} m_i \phi_{i,m}^2} \tag{3.33}$$

For the first mode $m = 1$, taking the nonlinear deformation of the structure into account and substituting $T_{1\mathrm{D}} = T_1 \sqrt{\mu_{\mathrm{D}}}$ into Equation 3.33, the viscous damping at the first mode becomes $\beta_{\mathrm{V}1} \sqrt{\mu_{\mathrm{D}}}$.

For *nonlinear fluid viscous damper*, the work done by the *j*th damper at the *i*th story, determined by [10], is shown as below based on Equation 3.30:

$$W_{mi,j} = c_{\mathrm{d}i,j}\lambda_{i,j}\left(\frac{2\pi}{T_m}\right)^{\alpha_{i,j}}\left[D_{m\mathrm{D}}\left(\phi_{i,m}-\phi_{i-1,m}\right)\cos\varphi_{i,j}\right]^{(\alpha_{i,j}+1)} \tag{3.34}$$

where $\alpha_{i,j}$ is the velocity exponent. In Equation 3.34, $\lambda_{i,j}$is related to gamma functions, $\Gamma(\alpha_{i,j})$, and is expressed as

$$\lambda_{i,j} = 4\left(2^{\alpha_{i,j}}\right)\frac{\Gamma^2\left[\left(1+\alpha_{i,j}\right)/2\right]}{\Gamma\left(2+\alpha_{i,j}\right)} \tag{3.35}$$

Notations given in Equations 3.34 and 3.35 are defined the same as in Equation 3.31. Thus, the total work done by all the dampers is the sum of Equation 3.34.

$$\begin{aligned} W_{\mathrm{D}m} &= \sum_{i=1}^{n}\sum_{j=1}^{k} W_{i,j} \\ &= \sum_{i=1}^{n}\sum_{j=1}^{k} c_{\mathrm{d}i,j}\lambda_{i,j}\left(\frac{2\pi}{T_m}\right)^{\alpha_{i,j}}\left[D_{m\mathrm{D}}\left(\phi_{i,m}-\phi_{i-1,m}\right)\cos\varphi_{i,j}\right]^{(\alpha_{i,j}+1)} \end{aligned} \tag{3.36}$$

The maximum strain energy of the structure at *m*th mode is identical to that determined by Equation 3.32. Thus, the *viscous damping* of the nonlinear fluid viscous damping devices becomes

$$\begin{aligned} \beta_{\mathrm{V}m} &= \frac{W_{\mathrm{D}m}}{4\pi W_{\mathrm{S}m}} \\ &= \frac{\sum_{i=1}^{n}\sum_{j=1}^{k} c_{\mathrm{d}i,j}\lambda_{i,j}(2\pi/T_m)^{(\alpha_{i,j}-2)}D_{m\mathrm{D}}^{(\alpha_{i,j}-1)}[(\phi_{i,m}-\phi_{i-1,m})\cos\varphi_{i,j}]^{(\alpha_{i,j}+1)}}{2\pi\sum_{i=1}^{n} m_i\phi_{i,m}^2} \end{aligned} \tag{3.37}$$

For the first mode $m = 1$, considering the nonlinear deformation of the structure and substituting $T_{1\mathrm{D}} = T_1\sqrt{\mu_{\mathrm{D}}}$ and $D_{1\mathrm{D}} = \mu_{\mathrm{D}}D_{\mathrm{Y}}$ into Equation 3.37, the viscous damping at the first mode is simplified as $\beta_{\mathrm{V}1}\mu_{\mathrm{D}}^{1-\alpha/2}$ for $\alpha_{i,j} = \alpha$.

The determination of hysteretic damping relies on the mechanical properties of building materials. For example, the relation of the base shear and its roof displacement measured from a damped steel structure can be assumed as a bilinear model as shown in Figure 3.10. The *postyield stiffness* of the structure is denoted as ηk_{s} where k_{s} is the structural stiffness before the effective yield displacement, D_{Y}, and $0 \le \eta < 1$. Assuming at the design displacement, $D_{\mathrm{y}}\mu_{\mathrm{D}}$, the work done by the structure due to it postyield hysteretic behavior can be computed as follows:

$$W_{\mathrm{H}} = 4k_{\mathrm{s}}\mu_{\mathrm{D}}D_{\mathrm{Y}}^2(1-\eta)\left(1-\frac{1}{\mu_{\mathrm{D}}}\right) \tag{3.38}$$

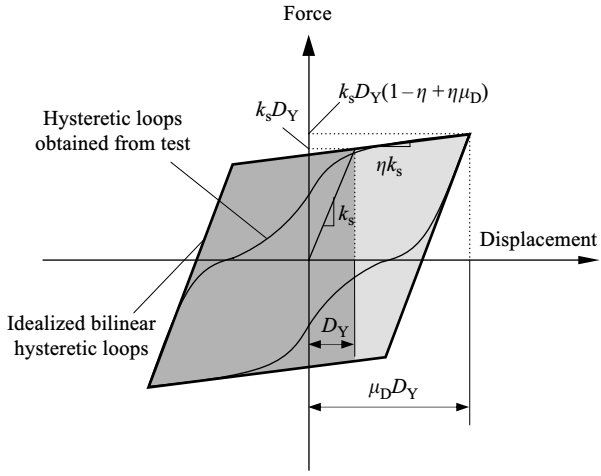

FIGURE 3.10 Determination of hysteretic damping.

The maximum strain energy of the structure is

$$W_s = \frac{1}{2}k_s\mu_D D_Y^2(1-\eta+\eta\mu_D) \tag{3.39}$$

Thus, the hysteretic damping of the structure is derived as below:

$$\beta_{HD} = \frac{2}{\pi}\frac{1-\eta}{1-\eta+\eta\mu_D}\left(1-\frac{1}{\mu_D}\right) \tag{3.40}$$

However, in reality the actual hysteretic loops of the structure do not perfectly match those as idealized by the bilinear model owing to pinching and other effects. Therefore, the actual area bounded by hysteretic loops is smaller than that assumed by the bilinear model. The reduction of hysteretic loop areas is considered in ASCE 7-05 [1] by introducing a *hysteretic loop adjustment factor*, q_H:

$$q_H = 0.67\frac{T_S}{T_1} \quad 0.5 \le q_H \le 1.0 \tag{3.41}$$

where $T_S = S_{D1}/S_{DS}$ and T_1 is fundamental period of the structure ($m = 1$). Also, ASCE 7-05 separates the inherent damping, β_I, from Equation 3.40 and utilizes the elastoplastic model with $\eta = 0$ to define the structural postyield behavior. Thus, Equation 3.40 becomes

$$\beta_{HD} = q_H\left(\frac{2}{\pi}-\beta_I\right)\left(1-\frac{1}{\mu_D}\right) = q_H(0.64-\beta_I)\left(1-\frac{1}{\mu_D}\right) \tag{3.42}$$

Note that Equation 3.42 is developed based on the design earthquake. The hysteretic damping under the MCE can be determined in the same way and is given as

$$\beta_{\mathrm{HM}} = q_{\mathrm{H}}(0.64 - \beta_{\mathrm{I}})\left(1 - \frac{1}{\mu_{\mathrm{M}}}\right) \tag{3.43}$$

where μ_{M} is the effective ductility demand on the seismic force-resisting system under the MCE and is defined as $\mu_{\mathrm{M}} = D_{1\mathrm{M}}/D_{\mathrm{Y}}$. Equations 3.15, 3.15a, and 3.15b are still applicable to the upper or lower bound of μ_{M}.

Once three portions of effective damping are computed from above equations, the total effective damping of the damped structure at the design earthquake or the MCE is easily determined and is summarized below, based on different modes of the structural vibration:

$$\beta_{1\mathrm{D}} = \beta_{\mathrm{I}} + \beta_{\mathrm{V}1}\sqrt{\mu_{\mathrm{D}}} + \beta_{\mathrm{HD}}, \quad m = 1 \tag{3.44}$$

$$\beta_{1\mathrm{M}} = \beta_{\mathrm{I}} + \beta_{\mathrm{V}1}\sqrt{\mu_{\mathrm{M}}} + \beta_{\mathrm{HM}}, \quad m = 1 \tag{3.44a}$$

$$\beta_{m\mathrm{D}} = \beta_{m\mathrm{M}} = \beta_{\mathrm{I}} + \beta_{\mathrm{V}m}, \quad m > 1 \tag{3.44b}$$

$$\beta_{\mathrm{V+I}} = \beta_{\mathrm{I}} + \beta_{\mathrm{V}1} \tag{3.44c}$$

The subscripts D and M as shown in Equations 3.44 through 3.44c indicate the effective damping at the design earthquake and the MCE, respectively. Accordingly, numerical coefficients for effective damping, $B_{1\mathrm{D}}$, $B_{1\mathrm{M}}$, $B_{m\mathrm{D}}$, $B_{m\mathrm{M}}$, and $B_{\mathrm{V+I}}$, can be determined from corresponding effective damping $\beta_{1\mathrm{D}}$, $\beta_{1\mathrm{M}}$, $\beta_{m\mathrm{D}}$, $\beta_{m\mathrm{M}}$, and $\beta_{\mathrm{V+I}}$ as given in Equations 3.44 through 3.44c.

As presented in Section 2.3.4.1, Equation 2.52, which describes the relation between the damping coefficient and the effective damping, is still applicable to the damped structure. However, the limitation of Equation 2.52 is extended to 100% of critical damping [11] and is shown in Figure 3.11.

3.2.2.3 Design requirements of seismic force-resisting system

Chapter 18 of ASCE 7-05 [1] requires that the *seismic force-resisting system* of the damped structure be designed under the design earthquake. Specifically, if a damped structure is analyzed by response spectrum procedure, then the design base shear, V_m, in kip (kN), corresponding to mode m is determined from Equation 3.22. A method of *the square root of the sum of the square* (SRSS) or *complete quadratic combination* (CQC) shall be utilized to combine the seismic base shear of mode m. For example, by applying the method of SRSS, the design base shear, V_{D}, in kip (kN), for design of the seismic force-resisting system is written as

$$V_{\mathrm{D}} = \left(\sum_{m=1}^{n} V_m^2\right)^{1/2} \tag{3.45}$$

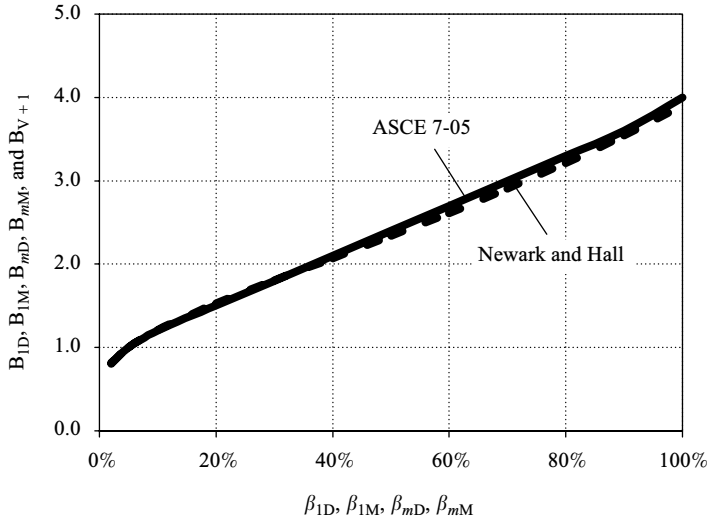

FIGURE 3.11 Damping coefficient, B_{1D}, B_{1M}, $B_{m\mathrm{D}}$, $B_{m\mathrm{M}}$, and $B_{\mathrm{V+I}}$.

TABLE 3.1
Coefficient of Upper Bound on Calculated Period, C_u

S_{D1}	≤ 0.1	0.15	0.2	≥ 0.3
C_u	1.7	1.6	1.5	1.4

The seismic base shear shall be satisfied with following limits:

$$V_D \geq V/B_{V+I}, \quad \text{and} \quad V_D \geq 0.75V \tag{3.46}$$

where V is the design base shear and can be determined based on Section 2.3.4.4 with additional requirements on the limitation of the fundamental period, T_1, $(m = 1)$.

$$T_1 \leq C_u T_a \tag{3.47}$$

where C_u as shown in Equation 3.47 is the coefficient as the upper bound to the calculated period, which is related to the design spectrum response acceleration at 1s, S_{D1}. Table 3.1 gives the value C_u corresponding to S_{D1}.

In Equation 3.47, T_a is called approximate fundamental period and is determined by the following equation:

$$T_a = C_t h_n^x \tag{3.48}$$

TABLE 3.2
Coefficient C_t and x

Structure type	Steel moment-resisting frames	Concrete moment-resisting frames	Eccentrically braced steel frames	All other structural system
C_t	0.028	0.016	0.03	0.02
x	0.8	0.9	0.75	0.75

where h_n is the height of the structure measured from the base to the top level. Coefficient C_t and x are related to types of the seismic force-resisting systems and are determined from Table 3.2.

In addition to the requirements on the design base shear as specified above, ASCE 7-05 also requires that the design lateral force, $F_{i,m}$, in kip (kN), in Equation 3.21, design story drift, $\Delta_{i,m\mathrm{D}}$, in. (mm), in Equation 3.25, as well as the design story velocity, $\nabla_{i,m\mathrm{D}}$, in in./s (mm/s), in Equations 3.26 and 3.26a, of all the modes be combined based on the method of SRSS or CQC for design of the seismic force-resisting system. The torsional effects of the structure shall be added to the design story drift and the design story drift shall be less than the product of R/C_d and the allowable story drift, Δ_a, in in. (mm). For most damped structures, the allowable story drift, Δ_a, is limited to $0.020h_{sx}$ for Occupancy Category I and II, $0.015h_{sx}$ for Occupancy Category III, and $0.010h_{sx}$ for Occupancy Category IV, where h_{sx} is denoted as the story height in (mm).

3.2.2.4 Design requirements of damping system

As required by ASCE 7-05 [1], damping devices and their connections shall be capable of resisting the peak displacement, velocity, and force under the MCE. Specifically, the design of the damping system shall consider three possible stages that would generate the maximum seismic force in the *damping system*: (1) maximum story drift or displacement, (2) maximum velocity, and (3) maximum acceleration.

At the stage of the maximum displacement, the design force, Q_E, in kip (kN), in an element of the damping system shall be determined by following Equation 3.49:

$$Q_E = \Omega_o \left(\sum_{m=1}^{n} Q_{m\mathrm{SFRS}}^2 \right)^{1/2} \pm Q_{\mathrm{DSD}} \tag{3.49}$$

where $Q_{m\mathrm{SFRS}}$ is the mth mode design force from the seismic force-resisting system. For use of displacement-dependent devices, the seismic force, Q_{DSD}, in kip (kN), considered in Equation 3.49 shall be determined at the maximum displacement in the positive or negative direction.

When the maximum velocity occurs, the design force, Q_E, in an element of the damping system shall be evaluated as follows:

$$Q_E = \left(\sum_{m=1}^{n} Q_{m\mathrm{DVS}}^2 \right)^{1/2} \tag{3.50}$$

$Q_{m\mathrm{DVS}}$ as given in Equation (3.50), in kip (kN), presents the mth mode design force of velocity-dependent damping devices.

At the stage of the maximum acceleration, the design force, Q_E, in an element of the damping system shall be computed based on following Equation 3.51:

$$Q_E = \left[\sum_{m=1}^{n} \left(C_{m\mathrm{FD}} \Omega_o Q_{m\mathrm{SFRS}} + C_{m\mathrm{FV}} Q_{m\mathrm{DSV}} \right)^2 \right]^{1/2} \pm Q_{\mathrm{DSD}} \tag{3.51}$$

Force coefficients, $C_{m\mathrm{FD}}$ and $C_{m\mathrm{FV}}$, as given in Equation 3.51, are determined as below [12]:

$$C_{m\mathrm{FD}} = \cos\delta, \quad D_{m\mathrm{D}} \quad \text{or} \quad D_{m\mathrm{M}} < D_Y \tag{3.52}$$

$$C_{m\mathrm{FD}} = \mu_D \cos\delta \le 1.0 \quad \text{or} \quad C_{m\mathrm{FD}} = \mu_M \cos\delta \le 1.0 \quad D_{m\mathrm{D}} \quad \text{or} \quad D_{m\mathrm{M}} > D_Y \tag{3.52a}$$

$$C_{m\mathrm{FV}} = \sin^{\alpha}\delta \tag{3.52b}$$

$$\delta = \left(\frac{2\pi\alpha\beta_{\mathrm{eff}}}{\lambda} \right)^{\frac{1}{2-\alpha}} \tag{3.52c}$$

$C_{m\mathrm{FD}}$ given in Equation 3.52a cannot exceed 1.0. In Equation 3.52c, λ is related to gamma function and is determined by Equation 3.35. α is the velocity exponent related to the velocity of the damping device. For the mth mode that is greater than 1, use $\alpha = 1$. Note that the exact value of δ is $\tan^{-1}(2\beta_{\mathrm{eff}})$ for linear viscous damping device.

The effective damping, β_{eff}, is evaluated by the mode of the structural vibration. For the fundamental mode ($m = 1$), the effective damping is $\beta_{\mathrm{eff}} = \beta_{1\mathrm{D}} - \beta_{\mathrm{HD}}$ for the design earthquake or $\beta_{\mathrm{eff}} = \beta_{1\mathrm{M}} - \beta_{\mathrm{HM}}$ for MCE. If the mth mode is greater than 1, the effective damping becomes $\beta_{\mathrm{eff}} = \beta_{m\mathrm{D}}$ for the design earthquake and $\beta_{\mathrm{eff}} = \beta_{m\mathrm{M}}$ for the MCE. Owing to the complexity of Equations 3.52 through 3.52c, ASCE 7-05 [1] provides force coefficients, $C_{m\mathrm{FD}}$ and $C_{m\mathrm{FV}}$ in tabular forms 18.7-1 and 18.7-2. Note that for viscoelastic damping devices, the force coefficients, $C_{m\mathrm{FD}}$ and $C_{m\mathrm{FV}}$ are equal to 1.0 unless the values are substantiated by analysis and test results.

3.2.3 Equivalent Lateral Force Analysis

Equivalent lateral force analysis is basically originated from response spectrum procedure. The philosophy of developing this procedure is to reduce modes of

a structural vibration with n degree-of-freedoms in the direction of interest into two: the fundamental mode ($m = 1$) and the residual mode, which can be imaged as a combination of all the higher modes ($m > 1$). Consequently, the displacement, velocity, and force in elements of a seismic force-resisting system and a damping system obtained from all higher modes of the structural vibration are condensed into the residual displacement, residual velocity, and residual force. Thus, the application of the equivalent lateral force procedure greatly simplifies the design process of a damped structure. Since the equivalent lateral force procedure is quite similar to the response spectrum procedure, all the notations used in the following equations, unless specifically specified, have the same physical meaning as given in the equations of the response spectrum procedure.

ASCE 7-05 [1] indicates that use of the equivalent lateral force procedure shall meet the following requirements:

1. At least two damping devises are installed at each level. These damping devices shall be parallel to the imposed seismic force and be located to resist the torsion generated by the seismic force.
2. The effective damping of the fundamental mode, β_{1D}, does not exceed 35% of critical damping.
3. Neither vertical irregularity nor horizontal irregularity exists in the selected seismic force-resisting system.
4. Floor at each level and the roof shall satisfy the assumption of rigid diaphragm.
5. The maximum height of the structure measured from the base is not over 100 ft (30 m).
6. The site for construction of the damped structure is characterized with the spectral response acceleration parameter with 5% of critical at the period of 1 s, S_1, not over 0.6 g.

3.2.3.1 Design base shear and design lateral force

The design base shear of the fundamental mode, V_1, in kip (kN), is given as below:

$$V_1 = C_{S1}\overline{W}_1 \tag{3.53}$$

where the fundamental mode seismic response coefficient is presented as

$$C_{S1} = \left(\frac{R}{C_d}\right)\frac{S_{DS}}{\Omega_o B_{1D}}, \quad T_{1D} < T_S \tag{3.54}$$

$$C_{S1} = \left(\frac{R}{C_d}\right)\frac{S_{D1}}{T_{1D}\Omega_o B_{1D}}, \quad T_{1D} \geq T_S \tag{3.54a}$$

All the notations used in Equations 3.54 and 3.54a have the same definitions as given in Equations 3.13 and 3.13a. The effective fundamental mode seismic

weight, $\overline{W}_1$, in kip (kN), as shown in Equation 3.53, may be computed by using the simplified fundamental mode shape

$$\phi_{i,1} = \frac{h_i}{h_r} \tag{3.55}$$

where subscripts 1 and i present the fundamental mode and the ith level of the structure, respectively. The height of the structure, h_r, is measured from the base to the roof level, while the height at level i from the based is designated as h_i. Note that the mode shape at the roof level, $\phi_{1,n}$, is always assumed to be 1.0. Thus fundamental mode participation factor, Γ_1, can be expressed in terms of $\overline{W}_1$

$$\Gamma_1 = \frac{\overline{W}_1}{\sum_{i=1}^{n} w_i \phi_{i,1}} \tag{3.56}$$

where w_i is seismic dead load in kip (kN) at the level i. The effective fundamental mode period, T_{1D}, as shown in Equations 3.54 and 3.54a has the following relation to the fundamental period, T_1:

$$T_{1D} = T_1 \sqrt{\mu_D} \tag{3.57}$$

The fundamental period, T_1, needs to be obtained from dynamic analysis with elastic behavior of the seismic force-resisting system. Alternately, T_1 can be determined from the following equation:

$$T_1 = 2\pi \left(\sum_{i=1}^{n} \frac{m_i \delta_i^2}{f_i \delta_i} \right)^{1/2} \tag{3.58}$$

where f_i is the lateral force applied at level i and δ_i presents the elastic deflection under the lateral force f_i. The period of the residual mode is defined as $T_R = 0.4T_1$.

In the same way, the residual mode base shear is expressed as below:

$$V_R = C_{SR} \overline{W}_R \tag{3.59}$$

where C_{SR} is the residual mode seismic response coefficient, which is given as

$$C_{SR} = \frac{S_{DS}}{\Omega_o B_R} \left(\frac{R}{C_d} \right) \tag{3.60}$$

Numerical coefficient for effective damping, B_R, in Equation 3.60 is obtained from Figure 3.11 corresponding to $\beta_R = \beta_I + \beta_{VR}$, where β_{VR} is the effective damping of the residual mode and is referred to in Section 3.2.2.2 for determination of β_{Vm}. The effective residual mode seismic weight, $\overline{W}_R$, in kip (kN), in

Equation 3.59 is defined as the difference of the effective seismic weight and the effective fundamental mode seismic weight:

$$\overline{W}_{\mathrm{R}} = W - \overline{W}_{1} \tag{3.61}$$

The design base shear is obtained from the combination of the fundamental mode base shear and the residual mode base shear, which is given as

$$V_{\mathrm{D}} = \sqrt{V_{1}^{2} + V_{\mathrm{R}}^{2}} > \max\left\{\frac{V}{B_{\mathrm{V+I}}}, \quad 0.75V\right\} \tag{3.62}$$

where the design base shear, V, in kip (kN), is determined from Section 3.2.2.3. On the basis of the Equation 3.21, the design lateral force at story level i in units of kip (kN), related to the fundamental and residual modes, respectively, is calculated from following equations:

$$F_{i,1} = \frac{w_i \phi_{i,1} \Gamma_1}{\overline{W}_1} V_1 \tag{3.63}$$

$$F_{i,\mathrm{R}} = \frac{w_i \phi_{i,\mathrm{R}} \Gamma_{\mathrm{R}}}{\overline{W}_{\mathrm{R}}} V_{\mathrm{R}} \tag{3.63a}$$

In Equation 3.63a, the residual mode shape, $\phi_{i,\mathrm{R}}$, and the residual mode participation factor, Γ_{R}, are given in terms of the fundamental mode shape, $\phi_{i,1}$, and the fundamental mode participation factor, Γ_1:

$$\phi_{i,\mathrm{R}} = \frac{1 - \Gamma_1 \phi_{i,1}}{\Gamma_{\mathrm{R}}} \tag{3.64}$$

$$\Gamma_{\mathrm{R}} = 1 - \Gamma_1 \tag{3.65}$$

The design lateral force at story level i in units of kip (kN), which is used to design the elements of seismic force-resisting system, shall be determined applying SRSS method:

$$F_i = \sqrt{F_{i,1}^{2} + F_{i,\mathrm{R}}^{2}} \tag{3.66}$$

3.2.3.2 Design story drift and story velocity

Determination of design roof displacement at the fundamental mode and the residual mode is essentially the same as the approach used in development of the response spectrum procedure. On the basis of Equations 3.19, 3.19a, and 3.19b, the roof displacement due to the fundamental mode and the residual mode, $D_{1\mathrm{D}}$, and, D_{RD}, in. s(mm) under the design earthquake is presented as follows:

$$D_{1\mathrm{D}} = \left(\frac{g}{4\pi^2}\right) \frac{\Gamma_1 S_{\mathrm{DS}} T_{1\mathrm{D}}^{2}}{B_{1\mathrm{D}}} \geq \left(\frac{g}{4\pi^2}\right) \frac{\Gamma_1 S_{\mathrm{DS}} T_{1}^{2}}{B_{1\mathrm{E}}} \quad T_{1\mathrm{D}} < T_{\mathrm{S}} \tag{3.67}$$

$$D_{1D} = \left(\frac{g}{4\pi^2}\right)\frac{\Gamma_1 S_{D1} T_{1D}}{B_{1D}} \geq \left(\frac{g}{4\pi^2}\right)\frac{\Gamma_1 S_{D1} T_1}{B_{1E}}, \quad T_{1D} > T_S \tag{3.67a}$$

$$D_{RD} = \left(\frac{g}{4\pi^2}\right)\frac{\Gamma_R S_{D1} T_R}{B_R} \leq \left(\frac{g}{4\pi^2}\right)\frac{\Gamma_R S_{DS} T_R^2}{B_R} \tag{3.67b}$$

The design floor deflections and the design story drifts due to the fundamental and residual modes are calculated as below, respectively, with $\phi_{n,1} = \phi_{n,R} = 1.0$:

$$\delta_{i,1D} = D_{1D}\phi_{i,1}, \quad \Delta_{i,1D} = \delta_{i,1D} - \delta_{i-1,1D} = D_{1D}(\phi_{i,1} - \phi_{i-1,1}) \tag{3.68}$$

$$\delta_{i,RD} = D_{RD}\phi_{i,R}, \quad \Delta_{i,RD} = \delta_{i,RD} - \delta_{i-1,RD} = D_{RD}(\phi_{i,R} - \phi_{i-1,R}) \tag{3.68a}$$

SRSS method is also used to combine the fundamental and residual mode design story drift into the total design drift at each level in units of in. (mm):

$$\Delta_{i,D} = \sqrt{\Delta_{i,1D}^2 + \Delta_{i,RD}^2} \tag{3.69}$$

The design fundamental and residual mode story velocity is given as below and SRSS method shall be used to combine two components as the design velocity in units of in./s (mm/s):

$$\nabla_{i,1D} = 2\pi\frac{\Delta_{i,1D}}{T_{1D}} \tag{3.70}$$

$$\nabla_{i,RD} = 2\pi\frac{\Delta_{i,RD}}{T_R} \tag{3.70a}$$

$$\nabla_{i,D} = \sqrt{\nabla_{i,1D}^2 + \nabla_{i,RD}^2} \tag{3.71}$$

For design of the damping system, determination of the floor deflection, story drift, and the story velocity under the MCE can follow the procedures as presented above. However, since the effective ductility demand, μ_M, and the spectral response acceleration parameters, S_{MS} and S_{M1}, are different from those under the design earthquake, the roof displacement under the MCE shall be computed by the following equations:

$$D_{1M} = \left(\frac{g}{4\pi^2}\right)\frac{\Gamma_1 S_{MS} T_{1M}^2}{B_{1M}} \geq \left(\frac{g}{4\pi^2}\right)\frac{\Gamma_1 S_{MS} T_1^2}{B_{1E}}, \quad T_{1M} < T_S \tag{3.72}$$

$$D_{1M} = \left(\frac{g}{4\pi^2}\right)\frac{\Gamma_1 S_{M1} T_{1M}}{B_{1M}} \geq \left(\frac{g}{4\pi^2}\right)\frac{\Gamma_1 S_{M1} T_1}{B_{1E}}, \quad T_{1M} > T_S \tag{3.72a}$$

$$D_{RM} = \left(\frac{g}{4\pi^2}\right)\frac{\Gamma_R S_{M1} T_R}{B_R} \leq \left(\frac{g}{4\pi^2}\right)\frac{\Gamma_R S_{MS} T_R^2}{B_R} \tag{3.72b}$$

where $T_{1M} = T_1\sqrt{\mu_M}$.

Requirements of the seismic force-resisting system and the damping system as given in Sections 3.2.2.3 and 3.2.2.4 are still applicable to the equivalent lateral force procedure. Application of the equivalent lateral force procedure to design of damped structures will be explicitly presented as an example in Section 3.3.

3.2.4 Nonlinear Static Procedure

Nonlinear static procedure or *pushover analysis* is essentially developed from the response spectrum analysis. Owing to availabilities of commercial computer programs, such as SAP 2000 and ETABS [3], there is no technical difficulty to perform nonlinear static analysis of any structures with damping systems. However, how to determine the design roof displacement, or target displacement, is the key to the procedure of the analysis. It is because the determination of the design roof displacement involves iteration process to identify mode shapes with effective stiffness of the seismic force-resisting system, effective fundamental period, and damping coefficients related to viscous damping plus hysteretic damping. Once the design roof displacement is obtained, the design displacement at other levels, velocity, and accelerations of the seismic force-resisting system and damping system can be easily calculated for design. Detailed steps of nonlinear static analysis are summarized as below [12]:

1. The construction of a mathematical model for the damped structure shall include modeling of the postyield hysteretic behavior of the seismic force-resisting system and the damping system. Specifically, the idealized force–deformation curves or moment–rotation relations with postyield portions shall be defined in the model for all the elements of the seismic force-resisting system. If damping devices are displacement-dependent, their stiffness shall be included into the model. To perform nonlinear static analysis, the vertical distribution of the base shear to each level needs to consider two patterns: uniform pattern and modal pattern. The uniform pattern refers to lateral force distribution proportional to the mass at each level, while the modal pattern is the lateral force distribution based on the first model shape of vibration. P–Δ effects induced by story drift and deformation of structural elements shall be captured during the analysis. Sufficient number of modes shall be utilized in the analysis to ensure combined modal mass participation is at least more than 90% of the total mass in the direction of interest.
2. Once the pushover analysis is completed, a base shear–roof displacement curve can be established as shown in Figure 3.12a. This curve is usually simplified based on a bilinear or *trilinear model*. To convert this curve into spectral acceleration–spectral displacement curve, which is conventionally called spectral capacity curve, a tentative design roof displacement, D_{1D}, has to be assumed. According to the assumed D_{1D}, the secant stiffness of the elements of the seismic force-resisting system is determined from the defined force–deformation curves, which are used to

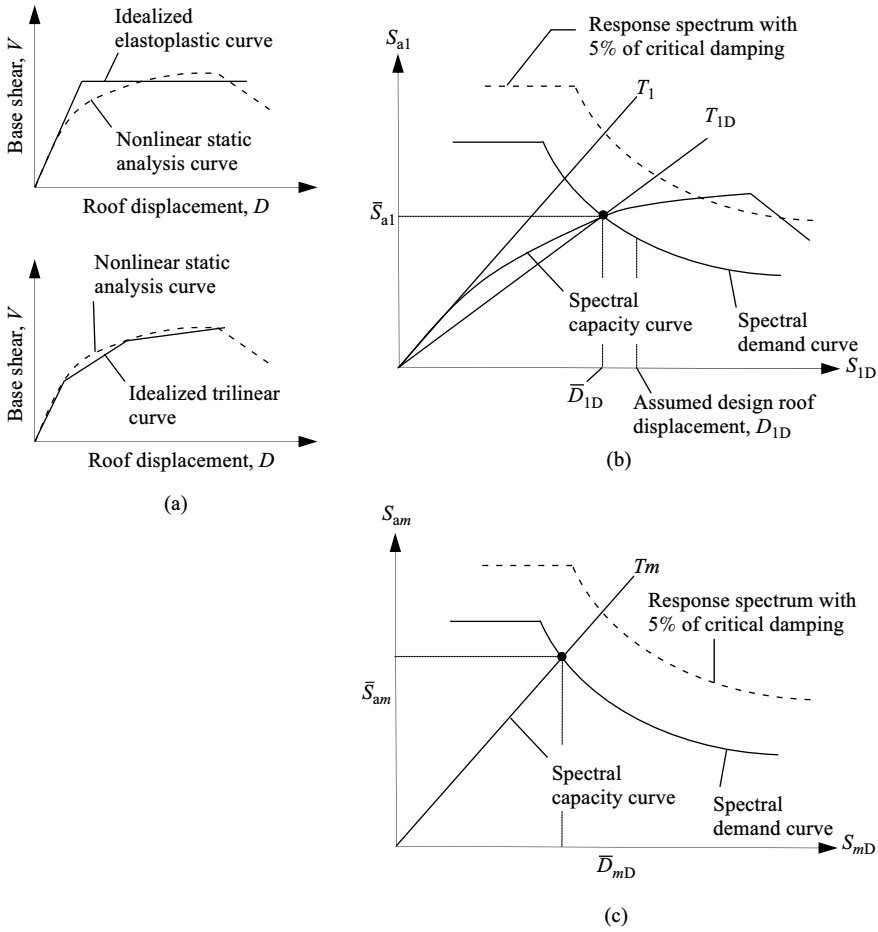

FIGURE 3.12 Nonlinear static analysis: (a) nonlinear static analysis curves with simplified mode, (b) spectral demand curve and spectral capacity curve of the fundamental mode, and (c) spectral demand curve and spectral capacity curve of higher mode.

perform eigenvalue analysis in order to obtain modal shapes, $\phi_{i,1}$, where subscripts 1 and i present the fundamental mode and level i, respectively. Substituting $\phi_{i,1}$ into Equations 3.12 and 3.23 and using $m = 1$, the participation factor of the fundamental mode, Γ_1, and the effective fundamental mode seismic weight, $\overline{W}_1$, are determined. Therefore, the relations between the base shear and the spectral acceleration, S_{a1}, as well as between the roof displacement and the spectral displacement, $S_{\mathrm{D}1}$, are calculated as follows:

$$S_{\mathrm{a}1} = \frac{Vg}{\overline{W}_1} \tag{3.73}$$

$$S_{\mathrm{D1}} = \frac{D}{\phi_{i,1}\Gamma_1} \tag{3.74}$$

where V and D are denoted as the base shear and the roof displacement as computed from pushover analysis, respectively. $\phi_{n,1}$ is the fundamental mode shape at the roof and equal to 1.

3. Meanwhile, the viscous damping, β_{V1}, and hysteretic damping, β_{HD}, can also be obtained from the assumed design roof displacement, $D_{1\mathrm{D}}$. The effective fundamental mode period, $T_{1\mathrm{D}}$, calculated from the eigenvalue analysis is used to determine β_{V1} and β_{HD}. Then, substituting β_{V1} and β_{HD} into Equation 3.44, the damping coefficient, $B_{1\mathrm{D}}$, is found from Figure 3.11. Note that the effective ductility demand, μ_{D}, is computed by the relation of the assumed design roof displacement, $D_{1\mathrm{D}}$, to the effective yield displacement, D_{Y}, identified from the base shear–roof displacement curve. The response spectrum with 5% of critical damping, which is selected for the design of the damped structure, is reduced by a numerical coefficient, $B_{1\mathrm{D}}$. The reduced response spectrum is usually called the design demand curve.
4. The spectral capacity curve and the design demand curve are plotted here in one diagram as shown in Figure 3.12b. The intersection of both curves gives the calculated design roof displacement, $\overline{D}_{1\mathrm{D}}$, and the design base shear of the fundamental mode, $V_1 = \overline{S}_{\mathrm{a1}}\overline{W}_1$, where V_1 shall not be less than that calculated from Equation 3.22 or (3.53) with $R/C_{\mathrm{d}} = 1.0$. In general $\overline{D}_{1\mathrm{D}}$ and $D_{1\mathrm{D}}$ are not the same. Therefore, iterations based on items 2 and 3 as discussed above are required until the difference between $\overline{D}_{1\mathrm{D}}$ and $D_{1\mathrm{D}}$ is within the acceptable accuracy.
5. Determination of the design roof displacements of higher modes is quite straightforward since the spectral capacity curve is linear and no iteration procedures are involved. In accordance with the modal shapes, $\phi_{i,m}(m = 2, 3, \ldots, n)$, determined from the eigenvalue analysis at the final iteration performed in Item 2, the participation factor of the mth mode, Γ_m, and the effective mth mode seismic weight, $\overline{W}_m$, are computed from Equations 3.12 and 3.23. Substituting $\phi_{i,m}$, Γ_m, and $\overline{W}_m$, into Equations 3.73 and 3.74, the spectral acceleration, $S_{\mathrm{a}m}$, and the spectral displacement, $S_{\mathrm{D}m}$, are computed. By using the same method as given in Item 3, the response spectrum is scaled down by the numerical coefficient, $B_{m\mathrm{D}}$, based on the total effective damping given in Equation 3.44b. Both the spectral capacity curve and the spectral demand curve of higher mode are plotted in one diagram as shown in Figure 3.12c. Thus the design roof displacement, $D_{m\mathrm{D}}$, is determined at the intersection of two curves. Also, the design base shear of high mode is $V_m = \bar{S}_{\mathrm{a}m}\overline{W}_m$, where V_m shall not be less than that calculated from Equation 3.22 or 3.59 with $R/C_{\mathrm{d}} = 1.0$.

6. Once the design roof displacement, $D_{m\mathrm{D}}$, and the design base shear, V_m, of all modes are determined from the above items, the design lateral force, story drift, and design story velocity can be identified. These values from all modes shall be combined by SRSS or CQC method for design of the damped structure. Note that the nonlinear static procedure explained above is for the design of the seismic force-resisting system under the design earthquake. The above procedures of nonlinear static analysis are also the same to design the damping system. However, the input of response spectrum shall be for MCE.

3.2.5 Special Requirements on Nonlinear Response History Procedure

Nonlinear response history analysis is a project-oriented procedure since the analysis directly relies on modeling of nonlinear behavior of the damping system and the seismic force-resisting system. Thus, there are no unified solutions to Equation 3.8. However, ASCE 7-05 provides guidelines to establish mathematical models for nonlinear response history procedure: The postyield hysteretic behavior of the seismic force-resisting system and nonlinear properties of damping devices, if any, shall be directly incorporated into the model. The properties of damping devices used in the model shall be verified from tests. Linear properties of elements in the seismic force-resisting system are permitted in the model when the demands of such elements are not over 150% of their nominal strength. In addition, maximum inherent damping used in the model shall not be greater than 5% of critical damping.

In addition, ASCE permits using average values of displacement, velocity, and acceleration in the seismic force-resisting system and damping system if nonlinear response history analyses are performed based on at least seven time histories. For time histories used in nonlinear response history analysis less than seven, the maximum values of displacement, velocity, and acceleration shall be selected to design the damped structure.

3.3 Design Examples

Example 3.3.1

A two-story building, which has16 ft (4.88 m) of story height at each level, is to be constructed with a linear viscous damping system. The building configuration is square with 145 ft (44.23 m) in each direction. Columns are equally spaced at 29 ft (8.85 m) as shown in Figure 3.13. Roof and floor framing systems consist of steel beams and lightweight concrete over steel metal deck, which ensure the validity of rigid diaphragm assumption. The seismic force-resisting system is located along frames at Line 1, 6, A, and G. The

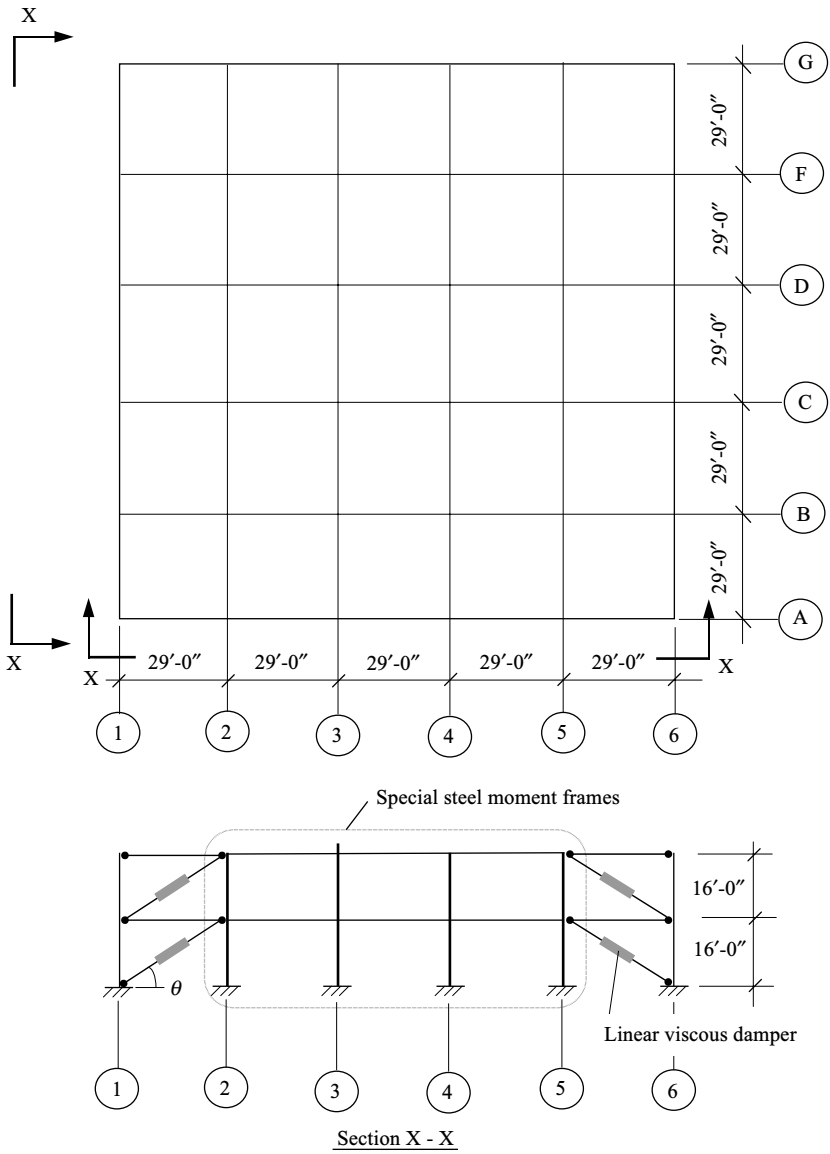

FIGURE 3.13 Example 3.3.1.

total seismic dead load at the floor, W_1, and at the roof, W_2, for each frame is approximately 1000 kips (4448 kN) and 1200 kips (5338 kN), respectively. Since Occupancy Category IV is required for the structural design, special steel moment frames are selected as the seismic force-resisting system with lateral stiffness of 374 k/in. (65.5 kN/mm) in each direction and at each level. It is further assumed that the building does not possess vertical

and horizontal structural irregularities. The effective damping of the structure owing to energy dissipation inherently is considered as $\beta_I = 0.05$. Each damping device has the same damping coefficient of 6.0 k·s/in. (1.05 kN·s/mm). Damping devices are located at the perimeters of the structure as shown in one typical frame elevation of Figure 3.13. The site of the building construction is characterized with S_1 and S_S equal to 0.58 and 1.25, respectively. Site soil is classified as Class D. This structure is intended to be designed applying the equivalent lateral force procedure and the following items shall be checked using customary units:

1. Determine the seismic base shear for each frame ignoring the building torsional effects.
2. Verify the validity of assumptions for the equivalent lateral force procedure.
3. Find the design lateral force, the story drift at each level, and the design story velocity.
4. Calculate the design lateral force for the damping system design.

Solution

1. According to the given information, masses at the floor level, m_1, and the roof, m_2, are determined as $m_1 = (W_1/g) = (1000/386.1) = 2.590\,\text{k} \cdot \text{s}^2/\text{in.}$ and $m_2 = (W_2/g) = (1200/386.1) = 3.108\,\text{k} \cdot \text{s}^2/\text{in.}$, respectively. Thus the mass matrix is expressed as follows:

$$[M] = \begin{bmatrix} m_1 & 0 \\ 0 & m_2 \end{bmatrix} = \begin{bmatrix} 2.590 & 0 \\ 0 & 3.108 \end{bmatrix}, \quad \text{and}$$

$$\omega^2[M] = \begin{bmatrix} 2.590\omega^2 & 0 \\ 0 & 3.108\omega^2 \end{bmatrix} \tag{a}$$

On the basis of the given stiffness, k_1 and k_2, the stiffness matrix becomes

$$[K] = \begin{bmatrix} k_1 + k_2 & -k_2 \\ -k_2 & k_2 \end{bmatrix} = \begin{bmatrix} 374 + 374 & -374 \\ -374 & 374 \end{bmatrix} = \begin{bmatrix} 748 & -374 \\ -374 & -374 \end{bmatrix} \tag{b}$$

The angular frequencies can be determined by following equation:

$$\begin{vmatrix} 748 - 2.590\omega^2 & -374 \\ -374 & 374 - 3.108\omega^2 \end{vmatrix} = 0 \tag{c}$$

One solution of Equation c is $\omega_1^2 = 48.134$, $\omega_1 = 6.938$ rad/s.

The period related to the first or fundamental mode is

$$T_1 = \left(\frac{2\pi}{\omega_1}\right) = \left(\frac{2\pi}{6.938}\right) = 0.906\,\text{s}$$

The other solution of Equation c is $\omega_2^2 = 361.005$, $\omega_2 = 19.0$ rad/s.
Accordingly, the period related to the second mode is

$$T_2 = \left(\frac{2\pi}{\omega_2}\right) = \left(\frac{2\pi}{19.0}\right) = 0.331\,\text{s}$$

For the first mode, the displacement amplitudes of the fundamental mode are calculated based on Equation 3.55 and are shown as follows:

$$\left\{ \begin{array}{c} \phi_{1,1} \\ \phi_{2,1} \end{array} \right\} = \left\{ \begin{array}{c} 16/32 \\ 32/32 \end{array} \right\} = \left\{ \begin{array}{c} 0.5 \\ 1.0 \end{array} \right\} \qquad \text{(d)}$$

Then the effective seismic weight of the first mode is determined as

$$\overline{W}_1 = \frac{\left(\sum_{i=1}^{2} w_i \phi_{i,1}\right)^2}{\sum_{i=1}^{2} w_i \phi_{i,1}^2} = \frac{[1000(0.5) + 1200(1.0)]^2}{1000(0.5^2) + 1200(1.0^2)} = 1993.1\,\text{k} \qquad \text{(e)}$$

The participation factor of the first mode becomes

$$\Gamma_1 = \frac{\overline{W}_1}{\sum_{i=1}^{2} w_i \phi_{i,1}} = \frac{1993.1}{1000(0.5) + 1200(1.0)} = 1.1724 \qquad \text{(f)}$$

From Table 2.2, the site coefficient $F_\text{v} = 1.5$.
Accordingly, $S_\text{M1} = F_\text{v} S_1 = 1.5(0.58) = 0.87$, and $S_\text{D1} = (2/3)S_\text{M1} = (2/3)(0.87) = 0.58$. The site coefficient $F_\text{a} = 1.0$ based on Table 2.1.
Therefore, $S_\text{MS} = F_\text{a} S_\text{S} = 1.0(1.25) = 1.25$, and $S_\text{DS} = (2/3)S_\text{MS} = (2/3)(1.25) = 0.83$.

$$T_\text{S} = \frac{S_\text{D1}}{S_\text{DS}} = \frac{0.58}{0.83} = 0.699\,\text{s} \qquad \text{(g)}$$

The hysteresis loop adjustment factor is $q_H = 0.67 T_\text{s}/T_1 = 0.67(0.699)/0.906 = 0.517$, which is between 0.5 and 1.0. Thus, use $q_\text{H} = 0.517$. Assuming the effective ductility demand on the seismic force-resisting system due to the design earthquake, μ_D, is approximately 1.3, which is less than the maximum value of 1.78 as computed from Equation 3.15a, the effective period of the first mode becomes

$$T_\text{1D} = T_1 \sqrt{\mu_\text{D}} = 0.906\sqrt{1.3} = 1.032\,\text{s} > T_\text{S} = 0.696\,\text{s} \qquad \text{(h)}$$

The effective hysteretic damping, β_{HD}, due to the postyield hysteretic behavior the seismic force-resisting system and the elements of the damping system at μ_D is determined as follows:

$$\beta_{HD} = q_H(0.64 - \beta_I)\left(1 - \frac{1}{\mu_D}\right) = 0.517(0.64 - 0.05)\left(1 - \frac{1}{1.3}\right) = 0.07 \tag{i}$$

The modal drift at the first mode is

$$\begin{Bmatrix} \phi_{1,1} \\ \phi_{2,1} - \phi_{1,1} \end{Bmatrix} = \begin{Bmatrix} 0.5 \\ 1.0 - 0.5 \end{Bmatrix} = \begin{Bmatrix} 0.5 \\ 0.5 \end{Bmatrix} \tag{j}$$

The angle between the viscous damper and the horizontal direction is $\varphi = \tan^{-1}(16/29) = 28.89°$. The effective viscous damping of the first mode, β_{V1}, based on Equation 3.33, becomes

$$\beta_{V1} = \frac{0.906}{4\pi} \cdot \frac{2(6)(\cos 28.89°)^2\left[(0.5)^2 + (0.5)^2\right]}{2.590(0.5)^2 + 3.108(1.0)^2} = 0.09 \tag{k}$$

The total effective damping at the fundamental mode is as follows:

$$\beta_{1D} = \beta_I + \beta_{V1}\sqrt{\mu_D} + \beta_{HD} = 0.05 + 0.09\sqrt{1.3} + 0.07 = 0.223 \tag{l}$$

Therefore, from Figure 3.11, the numerical coefficient is determined as $B_{1D} = 1.569$. Because of $T_{1D} > T_S$, the seismic coefficient of the first mode is calculated on the basis of the response modification factor, overstrength factor, and deflection amplification factor determined from Table 2.5 and ASCE 7-05, Table 12.2–1.

$$C_{S1} = \left(\frac{R}{C_d}\right)\frac{S_{D1}}{T_{1D}\Omega_o B_{1D}} = \frac{8}{5.5} \cdot \frac{0.58}{1.032(3)(1.569)} = 0.174 \tag{m}$$

The design value of the first mode is

$$V_1 = C_{S1}\overline{W}_1 = 0.174(1993.1) = 346.8\,\text{k} \tag{n}$$

For $\beta_{V1} + \beta_I = 0.09 + 0.05 = 0.14$, the damping coefficient, $B_{1E} = 1.32$ based on Figure 3.11. Since $T_{1D} > T_S$, the design displacement of the first mode at the roof level is

$$D_{1D} = \left(\frac{g}{4\pi^2}\right)\frac{\Gamma_1 S_{D1} T_{1D}}{B_{1D}} = \frac{386.1}{4\pi^2} \cdot \frac{1.1724(0.58)(1.032)}{1.569} = 4.37\,\text{in.} \tag{o}$$

$$\left(\frac{g}{4\pi^2}\right)\frac{\Gamma_1 S_{D1} T_1}{B_{1E}} = \frac{386.1}{4\pi^2} \cdot \frac{1.1724(0.58)(0.906)}{1.32}$$

$$= 4.56\,\text{in.} \quad > D_{1D} = 4.37\,\text{in.} \tag{p}$$

Thus, using $D_{1D} = 4.56$ in. the effective yield displacement of the seismic force-resisting system is

$$D_Y = \left(\frac{g}{4\pi^2}\right)\frac{\Omega_o C_d}{R}\Gamma_1 C_{s1} T_1^2 = \frac{386.1}{4\pi^2}\cdot\frac{3(5.5)(1.1724)(0.174)(0.906^2)}{8} = 3.38\,\text{in.} \quad \text{(q)}$$

$\mu_D = D_{1D}/D_Y = 4.56/3.38 = 1.349$. Compared to the assumed value of 1.3, the difference is less than 5%. Therefore, the assumed effective ductility demand is acceptable and no iterations are required to estimate μ_D.

For the residual mode, the effective seismic weight, $\overline{W}_R$, participation factor, Γ_R, and period, T_R, are determined as follows.

$$\overline{W}_R = W - \overline{W}_1 = 1000 + 1200 - 1993.1 = 206.9\,\text{k} \quad \text{(r)}$$

$$\Gamma_R = 1 - \Gamma_1 = 1 - 1.1724 = -0.1724 \quad \text{(s)}$$

$$T_R = 0.4T_1 = 0.4(0.906) = 0.362\,\text{s} \quad \text{(t)}$$

Consequently, the displacement amplitudes and modal drifts of the residual mode are computed as

$$\begin{Bmatrix}\phi_{1,R}\\ \phi_{2,R}\end{Bmatrix} = \frac{1}{(1-\Gamma_1)}\begin{Bmatrix}1-\Gamma_1\phi_{1,1}\\ 1-\Gamma\phi_{2,1}\end{Bmatrix} = \frac{1}{(1-1.1742)}\begin{Bmatrix}1-1.1742(0.5)\\ 1-1.1742(1.0)\end{Bmatrix} = \begin{Bmatrix}-2.4\\ 1.0\end{Bmatrix} \quad \text{(u)}$$

$$\begin{Bmatrix}\phi_{1,R}\\ \phi_{2,R}-\phi_{1,R}\end{Bmatrix} = \begin{Bmatrix}-2.4\\ 1.0-(-2.4)\end{Bmatrix} = \begin{Bmatrix}-2.4\\ 3.4\end{Bmatrix} \quad \text{(v)}$$

Thus, applying Equation 3.33, the effective viscous damping of the residual mode and the total effective mode in the residual mode are given below respectively.

$$\beta_{VR} = \frac{0.362}{4\pi}\cdot\frac{2(6)(\cos 28.89^\circ)^2[(-2.4)^2+(3.4)^2]}{2.590(-2.4)^2+3.108(1.0)^2} = 0.255 \quad \text{(w)}$$

$$\beta_R = \beta_I + \beta_{VR} = 0.05 + 0.255 = 0.305 \quad \text{(x)}$$

Determined from Figure 3.11, the numerical coefficient, B_R, is 1.815. The roof displacement and seismic response coefficient and the seismic base shear of the residual mode are as follows:

$$D_{RD} = \left(\frac{g}{4\pi^2}\right)\Gamma_R\frac{S_{D1}T_R}{B_R} = \left(\frac{386.1}{4\pi^2}\right)|-0.1724|\left(\frac{0.58(0.362)}{1.815}\right) = 0.20\,\text{in.} \quad \text{(y)}$$

$$\left(\frac{g}{4\pi^2}\right)\Gamma_{\mathrm{R}}\frac{S_{\mathrm{DS}}T_{\mathrm{R}}^2}{B_{\mathrm{R}}} = \left(\frac{386.1}{4\pi^2}\right)\left|-0.1724\right|\left(\frac{0.83(0.362^2)}{1.815}\right)$$
$$= 0.10\,\text{in.} < D_{\mathrm{RD}} = 0.20\,\text{in.}, \tag{z}$$

$$D_{\mathrm{RD}} = 0.10\,\text{in.} \tag{aa}$$

$$C_{\mathrm{SR}} = \left(\frac{R}{C_{\mathrm{d}}}\right)\frac{S_{\mathrm{DS}}}{\Omega_{\mathrm{o}}B_{\mathrm{R}}} = \frac{8}{5.5}\cdot\frac{0.83}{3(1.815)} = 0.222 \tag{bb}$$

$$V_{\mathrm{R}} = C_{\mathrm{SR}}\overline{W}_{\mathrm{R1}} = 0.222(206.9) = 45.9k \tag{cc}$$

On the basis of the Equation 3.62, the seismic base shear is

$$V_{\mathrm{D}} = \sqrt{V_{\mathrm{I}}^2 + V_{\mathrm{R}}^2} = \sqrt{346.8^2 + 45.9^2} = 349.8k \tag{dd}$$

The seismic base shear, V, as determined above shall not be less than $V_{\min}$ as given in Equation 3.62. The determination of $V_{\min}$ is based on the following procedures. First, the approximate fundamental period is determined by Equation 3.48 as $T_{\mathrm{a}} = C_{\mathrm{t}}h_n^x = 0.028(32)^{0.8} = 0.448\,\text{s}$. Since the coefficient for upper limit, C_{u}, is 1.4 as given by Table 3.1, and $C_{\mathrm{u}}T_{\mathrm{a}} = 1.4(0.448) = 0.627\,\text{s} < T_1 = 0.906\,\text{s}$, $T = 0.627\,\text{s}$ is used to find the value of C_{s}.

$$C_{\mathrm{S}} = \frac{S_{\mathrm{DS}}}{(R/I)} = \frac{0.83}{(8/1.5)} = 0.156 < \frac{S_{\mathrm{D1}}}{T(R/I)} = \frac{0.58}{0.627(8/1.5)} = 0.173 \tag{ee}$$

Since $C_{\mathrm{S}} > 0.01$, use $C_{\mathrm{s}} = 0.156$, which results in $V = C_{\mathrm{S}}W = 0.156(1000 + 1200) = 343.2k$. Thus, the minimum design base shear is

$$V_{\min} = 0.75V = 0.75(343.2) = 257.4k < V_{\mathrm{D}} = 349.8k \tag{ff}$$

Also, based on $\beta_{\mathrm{V1}} + \beta_{\mathrm{I}} = 0.14$, and $B_{\mathrm{V+I}} = 1.32$,

$$V_{\min} = \frac{V}{B_{\mathrm{V+I}}} = \frac{343.2}{1.32} = 260.0k < V_{\mathrm{D}} = 349.8k \tag{gg}$$

Therefore, the design base shear of the structure with the damping system shall be $V = 349.8\,k$.

2. Verifying the assumptions of using the equivalent lateral force procedure is summarized as follows:
   (a) In each principal direction, four damping devises are installed at each level. They are all in the frames of the seismic force-resisting system, and can effectively resist the imposed seismic force and resist the torsion generated by the seismic force.

(b) The effective damping of the fundamental mode, β_{1D}, is 22.3% of critical, which is less than 35% of critical.
(c) Neither vertical irregularity nor horizontal irregularity exists in the selected seismic force-resisting system.
(d) Floor at each level and the roof are given by the example as rigid diaphragms.
(e) The maximum height of the structure measured from the base is 32 ft.
(f) The site for construction of the damped structure is characterized with the spectral response acceleration parameter with 5% of critical at the period of 1 s, S_1, is 0.58, which is less than 0.6.

Investigation of the above conditions indicates that the equivalent lateral force procedure is applicable to the design of this damped structure.

3. The design lateral force due to the fundamental mode response and the residual mode response at each level are given as follows:

$$F_{1,1D} = W_1\phi_{1,1}\frac{\Gamma_1}{\overline{W}_1}V_1 = 1000(0.5)\frac{1.1724}{1993.1}\cdot 346.8 = 102.0k \qquad \text{(hh)}$$

$$F_{2,1D} = W_2\phi_{2,1}\frac{\Gamma_1}{\overline{W}_1}V_1 = 1200(1.0)\frac{1.1724}{1993.1}\cdot 346.8 = 244.8k \qquad \text{(hha)}$$

$$F_{1,R} = W_1\phi_{1,R}\frac{\Gamma_R}{\overline{W}_R}V_R = 1000(-2.4)\frac{|-0.1724|}{206.9}\cdot 45.9 = -91.8k \qquad \text{(ii)}$$

$$F_{2,R} = W_2\phi_{2,R}\frac{\Gamma_R}{\overline{W}_R}V_R = 1200(1.0)\frac{|-0.1724|}{206.9}\cdot 45.9 = 45.9k \qquad \text{(iia)}$$

The design lateral force at each level is obtained from SSRS method:

$$F_{1,D} = \sqrt{F_{1,1D}^2 + F_{1,RD}^2} = \sqrt{102.0^2 + (-91.8)^2} = 137.2k \qquad \text{(jj)}$$

$$F_{2,D} = \sqrt{F_{2,1D}^2 + F_{2,RD}^2} = \sqrt{244.8^2 + (45.9)^2} = 249.1k \qquad \text{(kk)}$$

The floor deflection and drift due to the fundamental mode response and the residual mode response at each level are determined as

$$\delta_{1,1D} = D_{1D}\phi_{1,1} = 4.56(0.5) = 2.28\,\text{in.}; \quad \Delta_{1,1D} = \delta_{1,1D} = 2.28\,\text{in.};$$

$$\delta_{2,1D} = D_{1D}\phi_{2,1} = 4.56(1.0) = 4.56\,\text{in.};$$

$$\Delta_{2,1D} = \delta_{2,1D} - \delta_{1,1D} = 4.56 - 2.28 = 2.28\,\text{in.};$$

$$\delta_{1,\mathrm{RD}} = D_{\mathrm{RD}}\phi_{1,\mathrm{R}} = 0.10(-2.4) = -0.24\,\text{in.};$$
$$\Delta_{1,\mathrm{RD}} = \delta_{1,\mathrm{RD}} = -0.24\,\text{in.};$$
$$\delta_{2,\mathrm{RD}} = D_{\mathrm{RD}}\phi_{2,\mathrm{R}} = 0.10(1.0) = 0.10\,\text{in.};$$
$$\Delta_{2,\mathrm{RD}} = \delta_{2,\mathrm{RD}} - \delta_{1,\mathrm{RD}} = 0.10 - (-0.24) = 0.34\,\text{in.}$$

The design story drift at each level is

$$\Delta_{1,\mathrm{D}} = \sqrt{\Delta_{1,1\mathrm{D}}^2 + \Delta_{1,\mathrm{RD}}^2} = \sqrt{2.28^2 + 0.24^2} = 2.29\,\text{in.} \quad \text{(ll)}$$

$$\Delta_{2,\mathrm{D}} = \sqrt{\Delta_{2,1\mathrm{D}}^2 + \Delta_{2,\mathrm{RD}}^2} = \sqrt{2.28^2 + 0.34^2} = 2.31\,\text{in.} \quad \text{(mm)}$$

The design story velocity owing to the fundamental mode response and the residual mode response, as well as their combinations based on SRSS, at each level are determined as below:

$$\nabla_{1,1\mathrm{D}} = 2\pi\frac{\Delta_{1,1\mathrm{D}}}{T_{1\mathrm{D}}} = 2\pi\cdot\frac{2.28}{1.032} = 13.881\,\text{in./s}$$
$$\nabla_{1,\mathrm{RD}} = 2\pi\frac{\Delta_{1,\mathrm{RD}}}{T_{\mathrm{R}}} = 2\pi\cdot\frac{(-0.24)}{0.362} = -4.166\,\text{in./s}$$
$$\nabla_{1,\mathrm{D}} = \sqrt{\nabla_{1,1\mathrm{D}}^2 + \nabla_{1,\mathrm{RD}}^2} = \sqrt{13.881^2 + (-4.166)^2}$$
$$= 14.493\,\text{in./s} \quad \text{(nn)}$$
$$\nabla_{2,1\mathrm{D}} = 2\pi\frac{\Delta_{2,1\mathrm{D}}}{T_{1\mathrm{D}}} = 2\pi\cdot\frac{2.28}{1.032} = 13.881\,\text{in./s}$$
$$\nabla_{2,\mathrm{RD}} = 2\pi\frac{\Delta_{2,\mathrm{RD}}}{T_{\mathrm{R}}} = 2\pi\cdot\frac{(0.34)}{0.362} = 5.901\,\text{in./s}$$
$$\nabla_{2,D} = \sqrt{\nabla_{2,1\mathrm{D}}^2 + \nabla_{2,\mathrm{RD}}^2} = \sqrt{13.881^2 + (5.901)^2}$$
$$= 15.083\,\text{in./s} \quad \text{(oo)}$$

4. To find the maximum design lateral force at each level for design of the damping system, three conditions as given in Section 3.2.2.4 shall be considered.

   (a.) The design lateral force at the stage of the maximum displacement is calculated from Equation 3.49. Thus, the design lateral force in elements of the seismic force-resisting system as given in Equations dd and kk are amplified by the over strength factor, Ω_{o}, to obtain the design lateral force for the damping system design.

$$Q_{1,\mathrm{E}} = \Omega_{\mathrm{o}}F_{1,\mathrm{D}} = 3(349.8) = 1049.4k \quad \text{(pp)}$$
$$Q_{2,\mathrm{E}} = \Omega_{\mathrm{o}}F_{2,\mathrm{D}} = 3(249.1) = 747.3k \quad \text{(qq)}$$

The damping system shall remain elastic under the design force. Accordingly, the design lateral force as given in Equations dd and kk is increased by a factor of $\Omega_o C_d/R$. ASCE 7-05 gives a more conservative method by multiplying the design lateral force by Ω_o instead of $\Omega_o C_d/R$.

(b.) At the stage of maximum velocity, the design lateral force at each level is equal to the total horizontal components of the axial forces of the damping devices. From Equations nn and oo, and 3.50, the design lateral force for the damping system design becomes

$$Q_{1,E} = \sum c_{di,j} \cos^2 \varphi \nabla_{1,D}$$

$$= 2(6)(\cos^2 28.89°)(14.493) = 133.3k \quad \text{(rr)}$$

$$Q_{2,E} = \sum c_{di,j} \cos^2 \varphi \nabla_{2,D}$$

$$= 2(6)(\cos^2 28.89°)(15.083) = 138.7k \quad \text{(ss)}$$

(c.) The design lateral force at the stage of maximum acceleration is determined from Equations 3.51 and 3.52. Since linear viscous damping devices are selected, the effective damping of the fundamental mode equals $\beta_{eff} = \beta_{1D} - \beta_{HD} = 0.153$. Thus, $\delta = \tan^{-1}(2\beta_{eff}) = 0.297$. The corresponding force coefficients, C_{mFD} and C_{mFV}, are computed on the basis of Equations 3.52a and 3.52b:

$$C_{mFD} = \mu_D \cos\delta = 1.3(\cos 0.297) = 1.24 > 1,$$

$$\text{use } C_{mFD} = 1.0. \quad \text{(tt)}$$

$$C_{mFV} = \sin\delta = \sin 0.297 = 0.29 \quad \text{(uu)}$$

For the residual mode, the effective damping is $\beta_{eff} = \beta_{1D} - \beta_{HD} = 0.305$, which results in $\delta = \tan^{-1}(2\beta_{eff}) = 0.548$. Accordingly, force coefficients, C_{mFD} and C_{mFV}, become

$$C_{mFD} = \mu_D \cos\delta = 1.3(\cos 0.548) = 1.11 > 1, \text{ use } C_{mFD} = 1.0. \quad \text{(vv)}$$

$$C_{mFV} = \sin\delta = \sin 0.548 = 0.52 \quad \text{(vva)}$$

The design lateral force at the floor and the roof is determined from Equation 3.51 as

$$Q_{1,\mathrm{E}} = \left\{ \sum_{1}^{2} (C_{m\mathrm{FD}} \Omega_o Q_{m\mathrm{SFRS}} + C_{m\mathrm{FV}} Q_{m\mathrm{DSV}})^2 \right\}_{1,\mathrm{E}}^{1/2}$$

$$= \{[1.0(3)(346.8) + 0.29(2)(6)(\cos^2 28.89°)(13.881)]^2$$

$$+ [(1.0(3)(45.9) + 0.52(2)(6)(\cos^2 28.29°)(4.166)]^2\}^{1/2} = 1088.9k \quad \text{(ww)}$$

$$Q_{2,E} = \left\{ \sum_{1}^{2} (C_{m\mathrm{FD}} \Omega_o Q_{m\mathrm{SFRS}} + C_{m\mathrm{FV}} Q_{m\mathrm{DSV}})^2 \right\}_{2,\mathrm{E}}^{1/2}$$

$$= \{[1.0(3)(244.8) + 0.29(2)(6)(\cos^2 28.89°)(13.881)]^2$$

$$+ [(1.0(3)(45.9) + 0.52(2)(6)(\cos^2 28.29°)(5.901)]^2\}^{1/2} = 789.1k \quad \text{(xx)}$$

From the results of three unfavorable conditions, the design lateral force for the damping system design is controlled at the stage of the maximum acceleration as shown in Equations xx and yy. Note that for design of damping devices, the design force shall be obtained from the maximum considered earthquake. Determination of the displacement, drift, and velocity at each level to calculate the force in the damping device is identical to the above procedures.

Example 3.3.2

An essential building will be designed for emergency responses. Accordingly, the base isolation system combined with damping devices is selected to satisfy this special requirement. Low-damping rubber bearings are utilized. The effective damping of bearings, β_{b}, is approximately 2.0%. Ten linear fluid viscous dampers are installed in each principal direction of the building structure at the isolation interface. The damping coefficient, c_{d}, is 4.2 k· s/in. (0.74 kN·s/mm) for each damper. Assume that the weight of the structure above the isolation system is $W = 12{,}000$ k (53.38 MN), and the design displacement under the design earthquake is D_{D} in units of in. (mm). Also, the effective period is $T_{\mathrm{D}} = 2.6$ s and the effective stiffness at the design displacement is designated as k_{D}, in kip/in. (kN/mm). The movement of the structure above the isolation system is assumed to be under harmonic vibration in the horizontal direction of interest.

Find the maximum lateral force at the isolation system and demonstrate that the maximum lateral force does not occur at the design displacement, D_D. Use customary units to resolve this example.

Solution

In designing of base isolation buildings, low-damping rubber bearings or friction pendulum bearings are usually utilized along with damping devices in order to control the lateral displacement of the isolation system. Unlike the isolation system without damping devices, the maximum lateral force at the isolation system with damping devices does not occur at the design displacement, D_D. This example illustrates how to find the maximum lateral force in the isolation system combined with damping devices.

On the basis of the given condition, the structure above the isolation system undergoes harmonic vibration and its movement, x, can be expressed in terms of time, t:

$$x = D_D \cos \omega_D t \tag{a}$$

where ω_D is the angular frequency and has the following the effective period:

$$\omega_D = \frac{2\pi}{T_D} = \left(\frac{m}{k_D}\right)^{1/2} \tag{b}$$

Taking derivative of Equation a with respect to x, the velocity of the structure, $\dot{x}$, is derived as

$$\dot{x} = -\omega_D \sin \omega_D t \tag{c}$$

The lateral force at the isolation damping system can be expressed based on the equilibrium condition:

$$\begin{aligned} V(t) &= k_D x + 2\omega_D m(\beta_b + \beta_d)\dot{x} \\ &= k_D D_D \cos \omega_D t - 2\omega_D^2 m(\beta_b + \beta_d) D_D \sin \omega_D t \end{aligned} \tag{d}$$

The building mass given in Equation d is $m = W/g = 12{,}000/386.1 = 31.08\,\text{k} \cdot \text{s}^2/\text{in}$.

To find the maximum lateral force, V_{max}, Equation d is differentiated as

$$V'(t) = -k_D D_D \omega_D \sin \omega_D t - 2\omega_D^3 m(\beta_b + \beta_d) D_D \cos \omega_D t \tag{e}$$

For $V'(t) = 0$, substituting $\omega_D^2 = k_D/m$ into Equation e, the corresponding t can be determined as

$$\omega_D t = -\tan^{-1}[2(\beta_b + \beta_d)] + k\pi, \quad k = 1, 2, \ldots \tag{f}$$

Therefore,

$$\cos\left\{-\tan^{-1}[2(\beta_b+\beta_d)]+k\pi\right\}=\frac{\cos(k\pi)}{\sqrt{1+4(\beta_b+\beta_d)^2}} \quad \text{(g)}$$

$$\sin\left\{-\tan^{-1}[2(\beta_b+\beta_d)]+k\pi\right\}=-\frac{2(\beta_b+\beta_d)}{\sqrt{1+4(\beta_b+\beta_d)^2}}\cos(k\pi) \quad \text{(h)}$$

Substituting Equations g and h into Equation d, the maximum lateral force, V_{max}, becomes

$$V_{max}=-k_D D_D\cos(k\pi)\sqrt{1+4(\beta_b+\beta_d)^2} \quad \text{(i)}$$

On the basis of the given damping coefficient of the damper, the effective damping, β_d, is calculated as

$$\beta_d=n\frac{T_D c_d}{4\pi m}=\frac{10(2.6)(4.2)}{4\pi(31.08)}=0.28$$

Then $\beta_b+\beta_d=0.02+0.28=0.3$. For $k=1$, the maximum lateral force

$$V_{max}=-k_D D_D\cos(\pi)\sqrt{1+4(0.3)^2}=1.166k_D D_D \quad \text{(j)}$$

at the displacement of

$$D_D\cos\left\{-\tan^{-1}[2(\beta_b+\beta_d)]+k\pi\right\}=\frac{\cos(\pi)D_D}{\sqrt{1+4(0.3)^2}}=0.857D_D \quad \text{(k)}$$

In the same way, $k=2$, the maximum lateral force in the reversed direction is

$$V_{max}=-k_D D_D\cos(2\pi)\sqrt{1+4(0.3)^2}=-1.166k_D D_D \quad \text{(l)}$$

at the displacement of $-0.857D_D$.

Compared to the lateral force at the displacement of D_D, the maximum value is increased by 16.6%.

Note that due to adding damping devices to the isolation system, the lateral force at the original position, or $x=0$, is

$$V|_{x=0}=\pm 2k_D(\beta_b+\beta_d)D_D=\pm 0.6k_D D_D \quad \text{(m)}$$

Figure 3.14 shows the lateral force contributed by low-damping rubber bearings, damping devises, and their combinations.

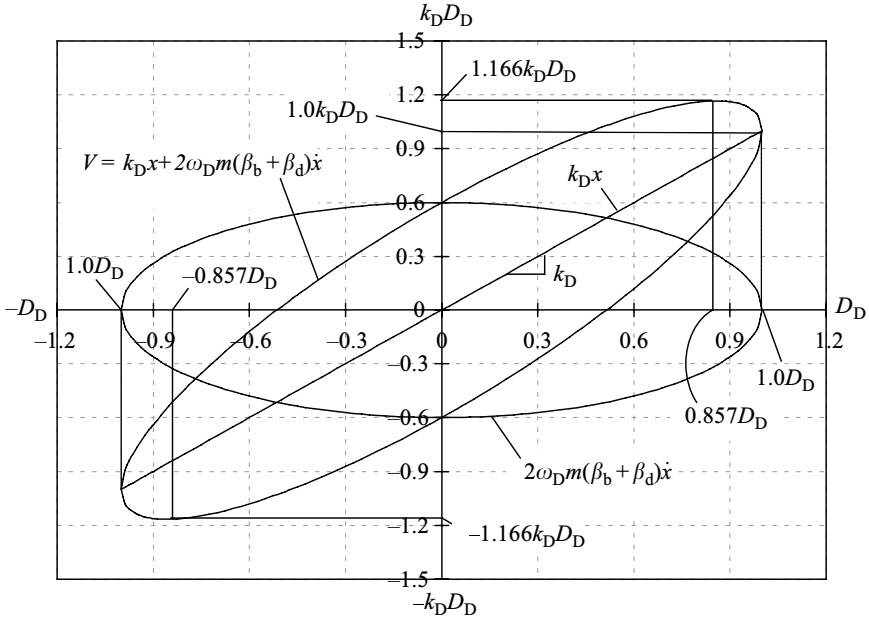

FIGURE 3.14 Relation of design base shear and lateral displacement.

3.4 Testing Verification and Determination of Damping Device Properties

3.4.1 Introduction

Mechanical properties of damping devices, no matter by which procedure they are selected as presented in Section 3.2, shall be verified by *prototype tests* based on ASCE 7-05 requirements. For each type and each size of damping devices, two full-size damping devices are required to perform prototype tests. If one type of damping devices is used with more than one size, ASCE 7-05 permits representative sizes for prototype test as long as the same quality control procedures and fabrication processes are assured and the professional engineer of record is responsible for the determined representative sizes.

During the tests, the force–velocity–displacement characteristics at each cycle shall be recorded for further review and analysis. For example, the stiffness of a solid viscoelastic damping device, k_d, can be determined from the recorded results in accordance with the following relation.

$$k_d = \frac{|P^+| + |P^-|}{|l^+| + |l^-|} \tag{3.75}$$

where P^+ and P^- are the positive and negative testing force at displacement of l^+ and l^- for each cycle, respectively. In general, specimens that have not failed in the prototype tests are not allowed for construction unless the professional engineer of record proves that the tested specimens meet the requirements of production tests.

The above requirements are indispensable for any size and type of prototype tests. Thus, testing procedures as specified by ASCE 7-05 are explicitly explained in Section 3.4.2. Acceptance criteria of prototype tests, which ensure validities of damper mechanical properties used in design, are summarized in Section 3.4.3 for velocity-dependent damping devices and in Section 3.4.4 for displacement-dependent damping devices, respectively. As to *production tests*, the testing procedures are similar to those for prototype tests. ASEC 7-05 only requires that the professional engineer of record be responsible for verification of design limitations on force–velocity–displacement characteristics.

3.4.2 Prototype Test Procedures

ASCE 7-05 [1] specified three testing sequences to perform prototype tests. The requirements of these testing sequences are summarized as follows:

Sequence 1: This testing sequence is to verify the quality and reliability of damping devices. It requires that at least 2000 continuous fully reversed cycles be undergone for each damping device to simulate the action of the design wind load. The displacement of the damping device used in the test is computed from the design wind load, while the applied frequency is determined based on the reverse of the fundamental period of the structure, T_1. This testing could be waived if the yield displacement or slip of the damping device is larger than the maximum displacement under the wind load.

Sequence 2: The variation of damping device properties with change of operating temperature is determined from this testing sequence. To each damping device five fully reversed sinusoidal cycles are applied at a frequency calculated from the reverse of the effective period of the fundamental mode, T_{1M}, at the maximum displacement, D_{1M}. This testing sequence shall be repeated at least at the maximum, ambient, and minimum temperature.

Sequence 3: The purpose of this testing sequence is to study whether the properties of the damping device are significantly affected by excitation frequencies. First, the test of Sequence 2 is repeated with a frequency of $2.5/T_1$. In the range of the maximum displacement, D_{1M}, if the force-deformation obtained based on the frequency of $1/T_{1M}$ is over 15% of that determined from the frequency of $2.5/T_1$, then another Sequence 2 shall be performed with the frequency of $1/T_1$.

Instead of the above three testing sequences, ASCE 7-05 permits using alternative testing sequences if the characteristics of damping devices affected by influence of operating temperature, excitation frequencies, and increase in temperature can be determined based on the equivalent requirements as presented above. In addition, the proposed alternative testing sequences shall be permitted by the professional engineer of record.

3.4.3 Acceptance Criteria for Velocity-Dependant Damping Devices

Once the prototype tests are completed, the performance of the damping device shall be evaluated. ASCE 7-05 [1] specifies the following acceptance criteria for velocity-dependent damping devices. If the tested damping device meets these criteria, then this prototype test is considered as acceptable:

1. After Sequence 1, the tested damping device shall be checked if it has any leakage, yielding, or breakage.
2. If the velocity-dependent damping device possesses its stiffness, similar to the solid viscoelastic damping device, the effective stiffness shall be determined from Equation 3.75. Under any designated frequency and operating temperature, the effective stiffness of a full cycle recorded from either Sequence 2 or 3 does not deviate by over 15% from the average effective stiffness obtained from the five full cycles.
3. Under any designated frequency and operating temperature, the maximum and minimum force at the original position of the damping device for any full cycle, which is obtained from Sequence 2 or 3, shall not be over 15% of the average values determined from five full cycles.
4. Under any designated frequency and operating temperature, the area of hysteretic loop for any full cycle, which is obtained from Sequence 2 or 3, shall not be over 15% of the average values determined from five full cycles.
5. No matter which sequence is selected, the effective stiffness determined from Item 2, the average maximum and minimum force obtained from Item 3, and the average area of hysteretic loops calculated from Item 4 shall not be over 15% from the target values used to design the damped structure.

3.4.4 Acceptance Criteria for Displacement-Dependant Damping Devices

ASCE 7-05 [1] specifies the following acceptance criteria for displacement-dependent damping devices. If the tested damping device meets these criteria, then this prototype test is considered as acceptable:

1. After Sequence 1, the tested damping device shall be checked if it has any yielding, or breakage.
2. Under any designated frequency and operating temperature, the maximum and minimum force at the original position of the damping device for any full cycle, which is obtained from Sequence 2 or 3, shall not be over 15% of the average values determined from five full cycles.
3. Under any designated frequency and operating temperature, the maximum and minimum force at the maximum displacement of the damping

device, D_{1M}, for any full cycle, which is obtained from Sequence 2 or 3, shall not be over 15% of the average values determined from five full cycles.

4. Under any designated frequency and operating temperature, the area of hysteretic loop for any full cycle, which is obtained from Sequence 2 or 3, shall not be over 15% of the average values determined from five full cycles.
5. No matter which sequence is selected, the average maximum and minimum force at the original position of the damping device obtained from Item 2, the average maximum and minimum force at the maximum displacement determined from Item 3, and the average area of hysteretic loops calculated from Item 4 shall not be over 15% from the target values used to design the damped structure.

References

1. ASCE/SEI 7-05, *Minimum Design Loads for Building and Other Structures*, American Society of Civil Engineers (ASCE), 2005.
2. Cheng, F.Y., *Matrix Analysis of Structural Dynamics: Applications and Earthquake Engineering*, Marcel Dekker, Inc., New York, 2001.
3. Computer and Structures, Inc. (CSI), CSI Analysis Reference Manual for SAP2000, ETABS, and SAFE, Berkeley, CA, 2005.
4. Federal Emergency Management Agency (FEMA), NEHRP Recommended Provisions for Seismic Regulations for New Buildings and Other Structures, *Report No. FEMA 222A*, Building Seismic Safety Council, Washington, DC, 1994.
5. Federal Emergency Management Agency, NEHRP Recommended Provisions for Seismic Regulations for New Buildings and Other Structures, *Report No. FEMA 302*, Building Seismic Safety Council, Washington, DC, 1997.
6. Federal Emergency Management Agency, NEHRP Guidelines for the Seismic Rehabilitation of Buildings and NEHER Commentary on the Guidelines for the Seismic Rehabilitation of Buildings, *Reports No. FEMA-273* and *FEMA 274*, Building Seismic Safety Council, Washington, DC, 1997.
7. Federal Emergency Management Agency, Prestandard and commentary for the Seismic Rehabilitation of Buildings, *Report No. FEMA-356*, Building Seismic Safety Council, Washington, DC, 2000.
8. Federal Emergency Management Agency, NEHRP Recommended Provisions for Seismic Regulations for New Buildings and Other Structures, Parts 1 and 2, *Report No. FEMA 368* and *FEMA 369*, Building Seismic Safety Council, Washington, DC, 2001.
9. Federal Emergency Management Agency, NEHRP Recommended Provisions for Seismic Regulations for New Buildings and Other Structures, Parts 1 and 2, *Report No. FEMA-450*, Building Seismic Safety Council, Washington, DC, 2003.
10. Hanson, R.D. and Soong, T.T., *Seismic Design with Supplemental Energy Dissipation Devices*, Earthquake Engineering Research Institute (EERI), MNO-8, Oakland, CA, 2001.

11. Newark, N.M. and Hall, W.J., *Earthquake Spectra and Design*, Earthquake Engineering Research Institute (EERI), Oakland, CA, 1981.
12. Ramirez, O.M. et al., Development and Evaluation of Simplified Procedures of Analysis and Design for Structures with Passive Energy Dissipation Systems, *Report No. NCEER-00-0010*, Revision 1, Multidisciplinary Center for Earthquake Engineering Research, Buffalo, New York, 2001.
13. Ramirez, O.M. et al., Evaluation of simplified methods of analysis of yielding structures with damping systems, *Earthquake Spectra*, 18, 501, 2002.
14. Ramirez, O.M. et al., Elastic and inelastic seismic response of buildings with damping systems, *Earthquake Spectra*, 18, 531, 2002.
15. Ramirez, O.M. et al., Validation of 2000 NEHRP provisions equivalent lateral forces and modal analysis procedures for buildings with damping systems, *Earthquake Spectra*, 19, 981, 2003.
16. Structural Engineers Association of California (SEAOC), *Recommended Lateral Force Requirements and Commentary*, 7th Edition, Sacramento, CA, 1999.
17. Wen, Y.K., Method of random vibration of hysteretic system, *ASCE Journal of Engineering Mechanics*, 102, 249, 1976.
18. Whittaker, A.S. et al., Code Requirements for the Design and Implementation of Passive Energy Dissipation System, Proceedings, ATC-17-1, Seminar on Seismic Isolation, Passive Energy Dissipation, and Active Control, Applied Technology Council, Redwood City, CA, 1993.
19. Whittaker, A.S. et al., Equivalent lateral forces and modal analysis procedures of the 2000 NEHRP provisions for buildings with damping systems, *Earthquake Spectra*, 19, 959, 2003.

4 Smart Seismic Structures Using Active Control Systems

Chapter 1 discussed the basic concepts and configurations of smart seismic structures using active control systems. Smart structures with active control are completely adaptive as they have fully functional sensing and actuation systems working together. The actuation device, called actuator, generates control force based on sensed external excitation and system response and applies the force directly to the structure to reduce its seismic response.

In this chapter, smart seismic structures using active control systems are studied in detail, emphasizing on mathematical modeling, control algorithm development, and system design and implementation. Section 4.1 develops a general mathematical model of active-controlled smart seismic structures. The mathematical model of the controller in an active control system, the feedback control law, is presented. Different implementation schemes of the active controller for smart seismic structures are discussed. The closed formula solutions of the system's seismic response are derived. In Section 4.2, the classical methods to determine the feedback law (Riccati and pole-placement control algorithms) are studied for their application to seismic response control of smart structures. In Section 4.3, innovative control algorithms for seismic response control (instantaneous and generalized optimal active closed-loop control algorithms) are presented. Section 4.4 provides the concluding remarks.

4.1 Analytical Model of Smart Seismic Structures with Active Control

In order to analyze and design a smart structure system using *active seismic response control*, an analytical model of the entire system needs to be formulated first. This system model should be based on the dynamic behavior or operating mechanism of all its components, the structure, actuators, sensors, and the controller. In theory, actuators, sensors, and the controller are dynamic systems. In seismic response control practice, they are usually assumed as linear systems with proportional relationship between input and output. Sensors used

in smart seismic structure systems, such as *linear variable displacement transducers* (LVDTs) and *accelerometers*, behave linearly in the frequency range of structural seismic response. Thus, they can be modeled by linear equations with a gain from input to output. More details on sensors can be found in Chapter 6. The controller can also be regarded as a linear device and its mathematical model is a linear matrix equation with a feedback gain from input to output. This linear equation is called *feedback control law* determined by *control algorithms*. Feedback law and control algorithms are discussed in detail in Sections 4.1.4, 4.2, and 4.3. Hydraulic actuators [1,31,36], capable of generating the large control force for smart seismic structures, are complicated mechanical dynamic systems themselves. Experimental studies [25,33,34] reveal that when hydraulic actuators are applied to a structure, their dynamics may adversely affect control action or even make the open-loop system unstable. Thus, the actuator interacts with the structure in smart seismic structure systems. However, studies have shown that [9,10,28,29,44,45], after the actuator stabilization, the actuator–structure interaction effects can be small and then the actuator behaves linearly. Thus, a linear stabilized actuator is assumed in this chapter. Details about actuator dynamics are discussed in Chapter 5.

In this section, a general analytical model of smart seismic structures with active control is formulated by considering dynamics of the structure and active control force applied to the structure. Deriving motion equations of the smart structures using theory of structural dynamics is the first step of the system modeling. Good references about this topic are References 6, 8, 11, 15, 17, and 18 for structures with active tendon control and References 12, 17, and 18 for structures with active mass damper (AMD). As shown in Figure 4.1, this section uses smart seismic structures with two types of active control systems, active tendon systems and an AMD, respectively, to demonstrate the modeling process. These models are condensed into matrix form with the consideration of arbitrary number and location of control devices. Finally, state-variable representations of the system model in both continuous and discrete time domains are developed.

4.1.1 Motion Equations of Smart Seismic Structures with Active Tendon Control

This section starts with an earthquake-excited n-story one-bay shear building structure equipped with active tendons at some floors, as shown in Figure 4.2. This active tendon system has multiple servovalve-controlled hydraulic actuators mounted on tendon systems on the structure. Each floor of the building structure can either have an actuator or no control device. Floors without a control device do not need the tendon system. When an n-story building structure is equipped with r actuators, $r \leq n$. The motion equations of such a smart structure system under seismic excitations can be

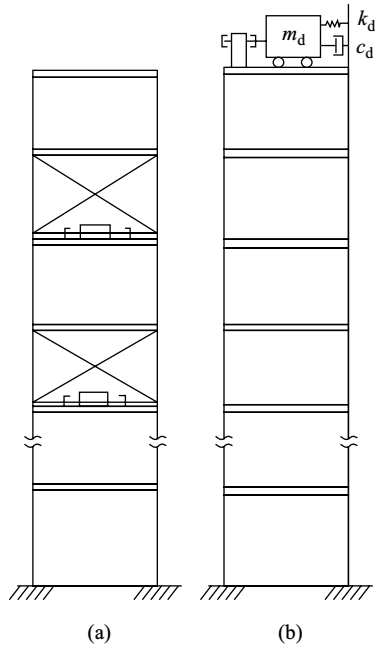

FIGURE 4.1 Smart building structures with active control: (a) active tendon and (b) active mass damper (AMD).

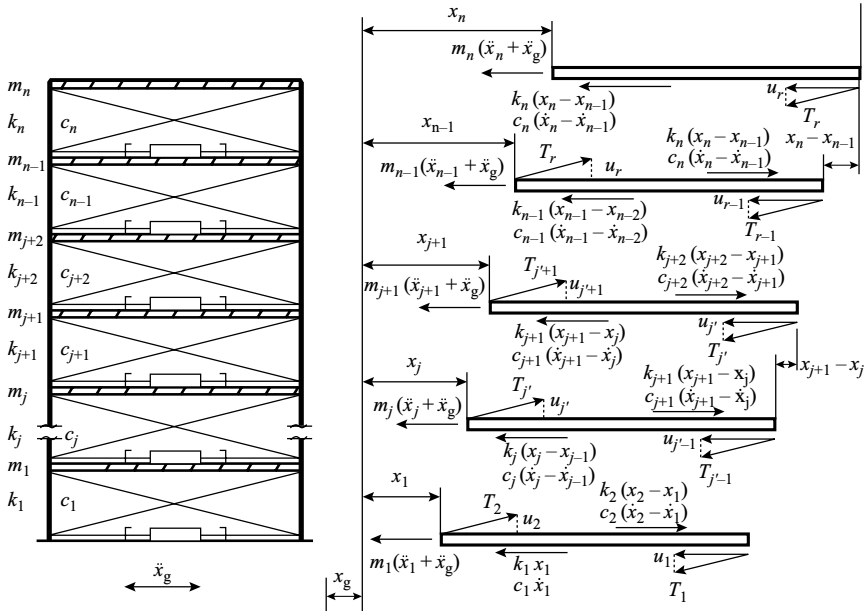

FIGURE 4.2 Model and free-body diagram for structures with active tendon control.

expressed as

$$\begin{cases} m_1(\ddot{x}_1+\ddot{x}_g)+c_1\dot{x}_1-c_2(\dot{x}_2-\dot{x}_1) \\ +k_1x_1-k_2(x_2-x_1)=-u_1+u_2 \\ \cdots \\ m_i(\ddot{x}_i+\ddot{x}_g)+c_i(\dot{x}_i-\dot{x}_{i-1})-c_{i+1}(\dot{x}_{i+1}-\dot{x}_i) \\ +k_i(x_i-x_{i-1})-k_{i+1}(x_{i+1}-x_i)=-u_j+u_{j+1} \\ m_{i+1}(\ddot{x}_{i+1}+\ddot{x}_g)+c_{i+1}(\dot{x}_{i+1}-\dot{x}_i)-c_{i+2}(\dot{x}_{i+2}-\dot{x}_{i+1}) \\ \quad +k_{i+1}(x_{i+1}-x_i)-k_{i+2}(x_{i+2}-x_{i+1})=-u_{j+1}+u_{j+2} \\ \cdots \\ m_{n-1}(\ddot{x}_{n-1}+\ddot{x}_g)+c_{n-1}(\dot{x}_{n-1}-\dot{x}_{n-2})-c_n(\dot{x}_n-\dot{x}_{n-1}) \\ \quad +k_{n-1}(x_{n-1}-x_{n-2})-k_n(x_n-x_{n-1})=-u_{r-1}+u_r \\ m_n(\ddot{x}_n+\ddot{x}_g)+c_n(\dot{x}_n-\dot{x}_{n-1})+k_n(x_n-x_{n-1})=-u_r \end{cases} \tag{4.1a}$$

where m_i, c_i, and k_i $(i=1,2,\ldots,n)$ denote, respectively, the mass, damping, and stiffness coefficients for the ith floor of the building structure; $u_j(j=1,2,\ldots,r)$ represents the horizontal component of the active tendon force generated by the jth actuator; $\ddot{x}_g$ is the absolute ground acceleration; x_i is the ith floor relative displacement defined by

$$x_i=\Delta_i-x_g \quad (i=1,2,\cdots,n) \tag{4.1b}$$

in which x_g and Δ_i are absolute displacements of the ground and the ith floor, respectively.

Equation 4.1 can be rewritten as

$$\begin{cases} m_1\ddot{x}_1+c_1\dot{x}_1-c_2(\dot{x}_2-\dot{x}_1) \\ +k_1x_1-k_2(x_2-x_1)=-u_1+u_2-m_1\ddot{x}_g \\ \cdots \\ m_i\ddot{x}_i+c_i(\dot{x}_i-\dot{x}_{i-1})-c_{i+1}(\dot{x}_{i+1}-\dot{x}_i) \\ +k_i(x_i-x_{i-1})-k_{i+1}(x_{i+1}-x_i)=-u_j+u_{j+1}-m_i\ddot{x}_g \\ m_{i+1}\ddot{x}_{i+1}+c_{i+1}(\dot{x}_{i+1}-\dot{x}_i)-c_{i+2}(\dot{x}_{i+2}-\dot{x}_{i+1}) \\ \quad +k_{i+1}(x_{i+1}-x_i)-k_{i+2}(x_{i+2}-x_{i+1})=-u_{j+1}+u_{j+2}-m_{i+1}\ddot{x}_g \\ \cdots \\ m_{n-1}\ddot{x}_{n-1}+c_{n-1}(\dot{x}_{n-1}-\dot{x}_{n-2})-c_n(\dot{x}_n-\dot{x}_{n-1}) \\ \quad +k_{n-1}(x_{n-1}-x_{n-2})-k_n(x_n-x_{n-1})=-u_{r-1}+u_r-m_{n-1}\ddot{x}_g \\ m_n\ddot{x}_n+c_n(\dot{x}_n-\dot{x}_{n-1})+k_n(x_n-x_{n-1})=-u_r-m_n\ddot{x}_g \end{cases} \tag{4.2}$$

which can be condensed into matrix form as

$$[M]\{\ddot{x}(t)\} + [C]\{\dot{x}(t)\} + [K]\{x(t)\} = [\gamma]\{u(t)\} + \{\delta\}\ddot{x}_{\mathrm{g}}(t) \tag{4.3}$$

where

$$[M] = \begin{bmatrix} m_1 & & & & & & \\ & m_2 & & & & & \\ & & \cdots & & & & \\ & & & m_i & & & \\ & & & & \cdots & & \\ & & & & & m_{n-1} & \\ & & & & & & m_n \end{bmatrix} \tag{4.4a}$$

$$[C] = \begin{bmatrix} (c_1 + c_2) & -c_2 & & & & & \\ -c_2 & (c_2 + c_3) & -c_3 & & & & \\ & & \cdots & & & & \\ & -c_i & (c_i + c_{i+1}) & -c_{i+1} & & & \\ & & & \cdots & & & \\ & & & -c_{n-1} & (c_{n-1} + c_n) & -c_n & \\ & & & & -c_n & c_n & \end{bmatrix} \tag{4.4b}$$

$$[K] = \begin{bmatrix} (k_1 + k_2) & -k_2 & & & & & \\ -k_2 & (k_2 + k_3) & -k_3 & & & & \\ & & \cdots & & & & \\ & & -k_i & (k_i + k_{i+1}) & -k_{i+1} & & \\ & & & & \cdots & & \\ & & & & -k_{n-1} & (k_{n-1} + k_n) & -k_n \\ & & & & & -k_n & k_n \end{bmatrix} \tag{4.4c}$$

$$\{\delta\} = [-m_1, -m_2, \ldots, -m_i, \ldots, -m_n]^{\mathrm{T}} \tag{4.4d}$$

$$\{x(t)\} = [x_1(t), x_2(t), \ldots, x_i(t), \ldots, x_n(t)]^{\mathrm{T}} \tag{4.4e}$$

$$\{u(t)\} = \left[u_1(t), u_2(t), \ldots, u_j(t), \ldots, u_{\mathrm{r}}(t)\right]^{\mathrm{T}} \tag{4.4f}$$

In Equation 4.4, $[M]$, $[C]$, and $[K]$ are $n \times n$ matrices of mass, damping, and stiffness of the building structure, respectively; $\{x(t)\}$ of $n \times 1$ and $\{u(t)\}$ of $r \times 1$ are vectors of floor displacements and control forces of active tendons, respectively; $[\gamma]$ of $n \times r$ is the location matrix of control forces of active tendons; and $\{\delta\}$ of $n \times 1$ is the coefficient vector for earthquake ground acceleration $\ddot{x}_{\mathrm{g}}(t)$. For a structure with active tendons installed at each floor, the controller location matrix $[\bar{\gamma}]$ of

$n \times n$ takes the following form:

$$[\bar{\gamma}] = \begin{bmatrix} -1 & 1 & & & & & \\ & -1 & 1 & & & & \\ & & -1 & 1 & & & \\ & & \cdots & \cdots & & & \\ & & & \cdots & \cdots & & \\ & & & & & -1 & 1 \\ & & & & & & -1 \end{bmatrix}_{n \times n} \tag{4.5}$$

and the control force $\{\bar{u}(t)\}$ is an $n \times 1$ vector, that is,

$$\{\bar{u}(t)\} = [u_1(t), u_2(t), \ldots, u_i(t), \ldots, u_n(t)]^{\mathrm{T}} \tag{4.6}$$

If there are only $r(r < n)$ active tendons located at some floors, the control force $\{u(t)\}$ will become an $r \times 1$ vector whose relationship to the control force vector $\{\bar{u}(t)\}$ of $n \times 1$ is

$$\begin{aligned} \{\bar{u}(t)\}_{n\times 1} &= \{u_1(t), u_2(t), \cdots, 0, \cdots, u_i(t), \cdots, 0, \cdots, u_{r-1}(t), u_r(t)\}^{\mathrm{T}} \\ &= \begin{bmatrix} 1 & 0 & 0 & \cdots & \cdots & \cdots & \cdots & \cdots & 0 \\ 0 & 1 & 0 & \cdots & \cdots & \cdots & \cdots & \cdots & 0 \\ \cdots & \cdots & \cdots & \cdots & \cdots & \cdots & \cdots & \cdots & \cdots \\ 0 & \cdots & \cdots & \cdots & \cdots & \cdots & \cdots & \cdots & 0 \\ 0 & \cdots & \cdots & 0 & 1 & 0 & \cdots & \cdots & 0 \\ \cdots & \cdots & \cdots & \cdots & \cdots & \cdots & \cdots & \cdots & \cdots \\ 0 & \cdots & \cdots & \cdots & \cdots & 0 & \cdots & \cdots & 0 \\ 0 & \cdots & \cdots & \cdots & \cdots & \cdots & 0 & 1 & 0 \\ 0 & \cdots & \cdots & \cdots & \cdots & \cdots & \cdots & 0 & 1 \end{bmatrix}_{n\times r} \begin{Bmatrix} u_1(t) \\ u_2(t) \\ \cdots \\ u_{r-1}(t) \\ u_r(t) \end{Bmatrix}_{r\times 1} \\ &= [\theta]_{n\times r}\{u(t)\}_{r\times 1} \end{aligned} \tag{4.7}$$

Therefore, the location matrix $[\gamma]$ for the r active tendons can be obtained as follows:

$$[\gamma]_{n\times r} = [\bar{\gamma}]_{n\times n}[\theta]_{n\times r} \tag{4.8}$$

When there is only one active tendon on the structure, $\{u(t)\}$ becomes a scalar and location matrix $[\gamma]$ will degrade to an $n \times 1$ location vector $\{\gamma\}$.

4.1.2 Motion Equations of Smart Seismic Structures with Active Mass Damper

Similar modeling processes can be used for an earthquake-excited n-story one-bay shear building structure equipped with an AMD at the top floor, as shown in Figure 4.3. The difference is that the AMD only has one hydraulic actuator on top of the structure. Thus, $\{u(t)\} = u_{\mathrm{d}}(t)$. Figure 4.3 also shows the free-body

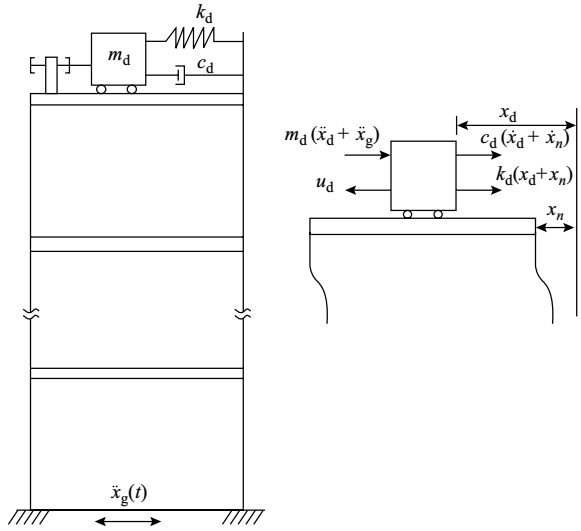

FIGURE 4.3 Model and free-body diagram for structures with AMD.

diagram of the structure with AMD. The mass of the AMD adds one more DOF to the system, and the relative displacement of the AMD with respect to the top floor displacement is

$$\Delta_d(t) = x_d(t) - x_n(t) \tag{4.9}$$

Then the system becomes a $(n + 1)$th order with the displacement vector defined as

$$\{x(t)\} = [x_1(t), x_2(t), \ldots, x_n(t), x_d(t)]^T \tag{4.10}$$

The motion equation of the structure is given by

$$\begin{cases} m_1\ddot{x}_1 + c_1\dot{x}_1 - c_2(\dot{x}_2 - \dot{x}_1) + k_1x_1 - k_2(x_2 - x_1) = -m_1\ddot{x}_g \\ \cdots \\ m_i\ddot{x}_i + c_i(\dot{x}_i - \dot{x}_{i-1}) - c_{i+1}(\dot{x}_{i+1} - \dot{x}_i) \\ + k_i(x_i - x_{i-1}) - k_{i+1}(x_{i+1} - x_i) = -m_i\ddot{x}_g \\ m_{i+1}\ddot{x}_{i+1} + c_{i+1}(\dot{x}_{i+1} - \dot{x}_i) - c_{i+2}(\dot{x}_{i+2} - \dot{x}_{i+1}) \\ \quad + k_{i+1}(x_{i+1} - x_i) - k_{i+2}(x_{i+2} - x_{i+1}) = -m_{i+1}\ddot{x}_g \\ \cdots \\ m_{n-1}\ddot{x}_{n-1} + c_{n-1}(\dot{x}_{n-1} - \dot{x}_{n-2}) - c_n(\dot{x}_n - \dot{x}_{n-1}) \\ \quad + k_{n-1}(x_{n-1} - x_{n-2}) - k_n(x_n - x_{n-1}) = -m_{n-1}\ddot{x}_g \\ m_n\ddot{x}_n + c_n(\dot{x}_n - \dot{x}_{n-1}) + k_n(x_n - k_{n-1}) = -u_d - m_n\ddot{x}_g \end{cases} \tag{4.11}$$

And the motion equation of the AMD is

$$m_{\mathrm{d}}\ddot{x}_{\mathrm{d}} + c_{\mathrm{d}}(\dot{x}_{\mathrm{d}} - \dot{x}_n) + k_{\mathrm{d}}(x_{\mathrm{d}} - x_n) = u_{\mathrm{d}} - m_{\mathrm{d}}\ddot{x}_{\mathrm{g}} \tag{4.12}$$

Equations 4.11 and 4.12 can be condensed into matrix form as

$$[M]\{\ddot{x}(t)\} + [C]\{\dot{x}(t)\} + [K]\{x(t)\} = \{\gamma\}u(t) + \{\delta\}\ddot{x}_{\mathrm{g}}(t) \tag{4.13}$$

where $[M]$, $[C]$ and $[K]$ are $(n+1) \times (n+1)$ matrices of mass, damping and stiffness of the system, respectively; $\{x(t)\}$ of $(n+1) \times 1$ is vector of floor and AMD displacements; $u(t)$ is AMD control force; $\{\gamma\}$ of $(n+1) \times 1$ is location matrix of AMD control forces; and $\{\delta\}$ of $(n+1) \times 1$ is coefficient vector for earthquake ground acceleration $\ddot{x}_{\mathrm{g}}(t)$.

$$[M] = \begin{bmatrix} m_1 & & & & & & \\ & m_2 & & & & & \\ & & \cdots & & & & \\ & & & m_i & & & \\ & & & & \cdots & & \\ & & & & & m_n & \\ & & & & & & m_{\mathrm{d}} \end{bmatrix} \tag{4.14a}$$

$$[C] = \begin{bmatrix} (c_1 + c_2) & -c_2 & & & & & \\ -c_2 & (c_2 + c_3) & -c_3 & & & & \\ & & \cdots & & & & \\ & & -c_i & (c_i + c_{i+1}) & -c_{i+1} & & \\ & & & & \cdots & & \\ & & & & -c_{n-1} & (c_{n-1} + c_n) & -c_n \\ & & & & & -c_n & c_n \\ & & & & & & -c_{\mathrm{d}}\ c_{\mathrm{d}} \end{bmatrix} \tag{4.14b}$$

$$[K] = \begin{bmatrix} (k_1 + k_2) & -k_2 & & & & & \\ -k_2 & (k_2 + k_3) & -k_3 & & & & \\ & & \cdots & & & & \\ & & -k_i & (k_i + k_{i+1}) & -k_{i+1} & & \\ & & & & \cdots\cdots & & \\ & & & & -k_{n-1} & (k_{n-1} + k_n) & -k_n \\ & & & & & -k_n & k_n \\ & & & & & & -k_{\mathrm{d}}\ k_{\mathrm{d}} \end{bmatrix} \tag{4.14c}$$

$$\{\gamma\} = [0, 0, ..., 0, -1, 1]^{\mathrm{T}} \tag{4.14d}$$

$$\{\delta\} = [-m_1, -m_2, ..., -m_{n-1}, -m_n, -m_{\mathrm{d}}]^{\mathrm{T}} \tag{4.14e}$$

It can be noted that Equations 4.3 and 4.13, the motion equations of smart structures with active tendons or an AMD, respectively, have the same format

except that the coefficient matrices have different elements. Typically, there would be one AMD on a structure, and an active tendon system can have actuators at multiple locations. This results in a scalar control force for an AMD system or a vector of control forces for active tendon systems. Thus, Equation 4.3 is used for further discussions in this chapter as Equation 4.13 can be treated as a special case of Equation 4.3.

4.1.3 State-Variable Representation of Smart Seismic Structures

Equation 4.3 can be rewritten as

$$\begin{aligned}\{\ddot{x}(t)\} = &- [M]^{-1}[C]\{\dot{x}(t)\} - [M]^{-1}[K]\{x(t)\} \\ &+ [M]^{-1}[\gamma]\{u(t)\} + [M]^{-1}\{\delta\}\ddot{x}_{\mathrm{g}}(t)\end{aligned} \tag{4.15}$$

and noticing that

$$\{\dot{x}(t)\} = [I]\{\dot{x}(t)\} \tag{4.16}$$

the following expression can be obtained as

$$\begin{aligned}\begin{Bmatrix}\{\dot{x}(t)\}\\ \{\ddot{x}(t)\}\end{Bmatrix} = &\left[\begin{array}{c|c}[0] & [I]\\ \hline -[M]^{-1}[K] & -[M]^{-1}[C]\end{array}\right]\begin{Bmatrix}\{x(t)\}\\ \{\dot{x}(t)\}\end{Bmatrix} + \begin{bmatrix}[0]\\ [M]^{-1}[\gamma]\end{bmatrix}\{u(t)\} \\ &+ \begin{Bmatrix}\{0\}\\ [M]^{-1}\{\delta\}\end{Bmatrix}\ddot{x}_{\mathrm{g}}(t)\end{aligned} \tag{4.17}$$

Linear optimal control theory has been developed for first-order dynamic systems. In order to apply this theory for seismic response control, the second-order motion equation 4.3 is cast into its first-order state-variable representation by defining the following state-vector [3,4,17,18]:

$$\{Z(t)\} = \begin{Bmatrix}\{x(t)\}\\ \{\dot{x}(t)\}\end{Bmatrix} \tag{4.18}$$

Then Equation 4.17 can be rewritten into state form as

$$\{\dot{Z}(t)\} = [A]\{Z(t)\} + [B_{\mathrm{u}}]\{u(t)\} + \{B_{\mathrm{r}}\}\ddot{x}_{\mathrm{g}}(t) \tag{4.19}$$

where

$$\{\dot{Z}(t)\} = \begin{Bmatrix}\{\dot{x}(t)\}\\ \{\ddot{x}(t)\}\end{Bmatrix}_{2n\times 1} \tag{4.20a}$$

$$[A] = \begin{bmatrix}[0] & [I]\\ -[M]^{-1}[K] & -[M]^{-1}[C]\end{bmatrix}_{2n\times 2n} \tag{4.20b}$$

$$[B_{\mathrm{u}}] = \begin{bmatrix} [0] \\ [M]^{-1}[\gamma] \end{bmatrix}_{2n\times r} \tag{4.20c}$$

$$\{B_{\mathrm{r}}\} = \begin{Bmatrix} \{0\} \\ [M]^{-1}\{\delta\} \end{Bmatrix}_{2n\times 1} \tag{4.20d}$$

Matrix $[A]$ is called *plant matrix* of the system. Equation 4.19, the state equation, is also suitable for smart structures with other types of control systems, such as *hybrid damper-actuator bracing control* (HDABC) systems to be discussed in Chapter 5.

Corresponding initials conditions for Equation 4.19 are

$$\{Z(0)\} = \{0\}, \quad \{u(0)\} = \{0\}, \quad \text{and} \quad \ddot{x}_{\mathrm{g}}(0) = 0 \tag{4.21}$$

It can be found that the motion equation, Equation 4.3, is an n-dimensional second-order differential equation, while the state equation, Equation 4.19, is a $2n$-dimensional first-order differential equation. Transformation from second-order motion equation to first-order state equation simplifies the solution procedure for the problem but doubles the number of equations or unknown variables.

From the structural dynamics point of view, a system described by motion equation 4.3 would be stable if all damping ratios are positive, but unstable if any of its damping ratios become negative. The system response would be smaller if its damping ratios of all significant modes are bigger. For a smart structure system described by Equation 4.19, the i-th eigenvalues of the plant matrix $[A], p_i (i = 1, 2, \ldots, n)$, are given by the following complex conjugage pairs [37,45]:

$$p_i = -\zeta_i \omega_i \pm j\omega_i \sqrt{1-\zeta_i^2},\ j = \sqrt{-1} \tag{4.22}$$

where ζ_i and ω_i are damping ratio and modal frequency, respectively, for the ith mode of the smart structure. For a system described by state equation 4.19, the eigenvalues of plant matrix $[A]$ are also referred as poles of the system in general control theory. As shown in Figure 4.4, pole locations in a complex plane determine the system stability. The real and imaginary components of the poles are the abscissa and ordinate, respectively, of the complex plane. If a pole were located in the left plane, its damping ratio would be positive. A stable system would have all its poles located in the left part of the complex plane. If a system has one or more poles in the right plane, the system is unstable. If the ith pair of the system poles moves left, bigger damping ratio and less system response for the ith mode would be achieved.

4.1.4 Feedback Law and Implementation Schemes

Note that Equation 4.19 cannot be solved directly. This is because there are only $2n$ equations but $(2n + r)$ unknown variables, that is, $\{Z(t)\}$ of $(2n \times 1)$ and $\{u(t)\}$ of

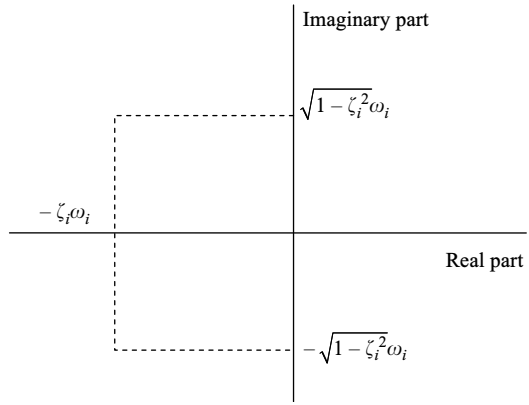

FIGURE 4.4 Plant matrix poles on the complex plane for smart seismic structures.

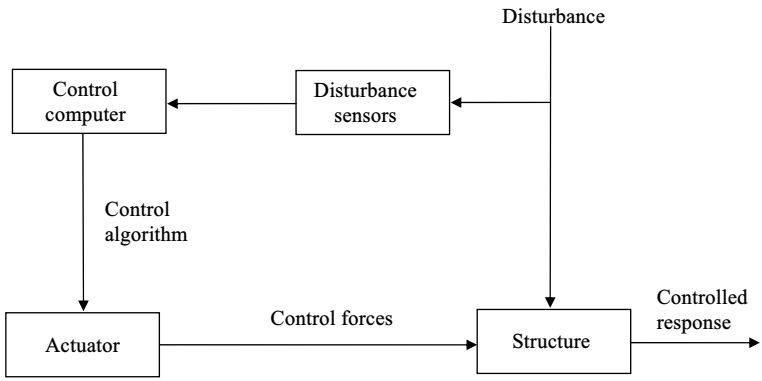

FIGURE 4.5 Schematic of open-loop control.

$(r \times 1)$. Therefore, r more equations are required in order to solve the active control problem in Equation 4.19. These r equations are referred as the *feedback control law* obtained from control algorithms. There are three active control schemes by which the feedback control law can be implemented to a smart seismic structure [3–5,18]

- Open-loop feedback control
- Closed-loop feedback control
- Open–closed-loop feedback control

In the open-loop structure control scheme shown in Figure 4.5, the control force is determined by a feedback of external excitation, such as earthquake ground motion. Thus, the control law only requires information about the earthquake excitation. The diagram for implementation of this scheme using an active tendon

is shown in Figure 4.6. An accelerometer placed at the base of the building structure measures the earthquake ground acceleration. This information is used to calculate the required control force based on the active control algorithm for open-loop control, and the force is then applied to the structure.

In the closed-loop control scheme shown in Figure 4.7, the control force is determined by a feedback of system response expressed by state variables. The state variables include structural displacements and velocities. Thus, in a closed-loop control system, the control law requires information of the system response such as the relative displacements and velocities of the structure. The diagram for this scheme is shown in Figure 4.8 with the active tendon system. The sensed information is used to calculate the required control force based on the closed-loop

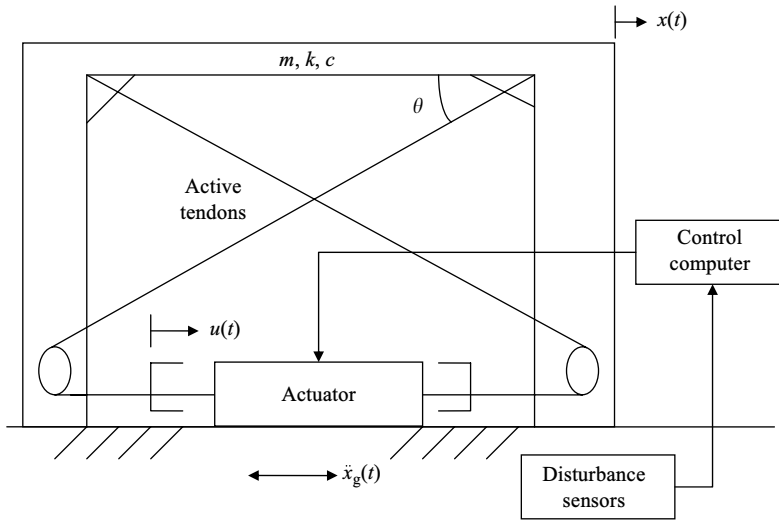

FIGURE 4.6 Open-loop control implementation.

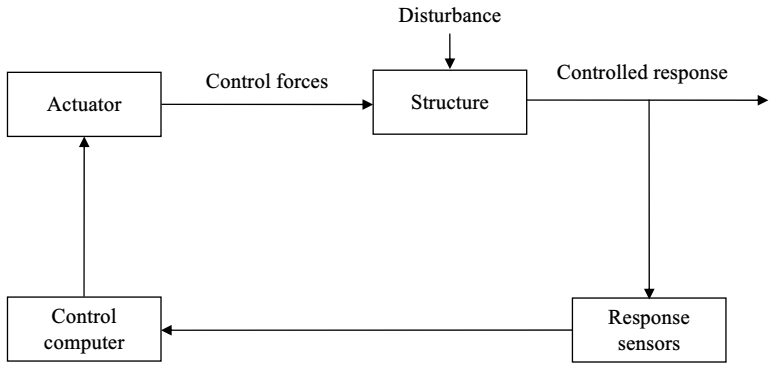

FIGURE 4.7 Schematic of closed-loop control.

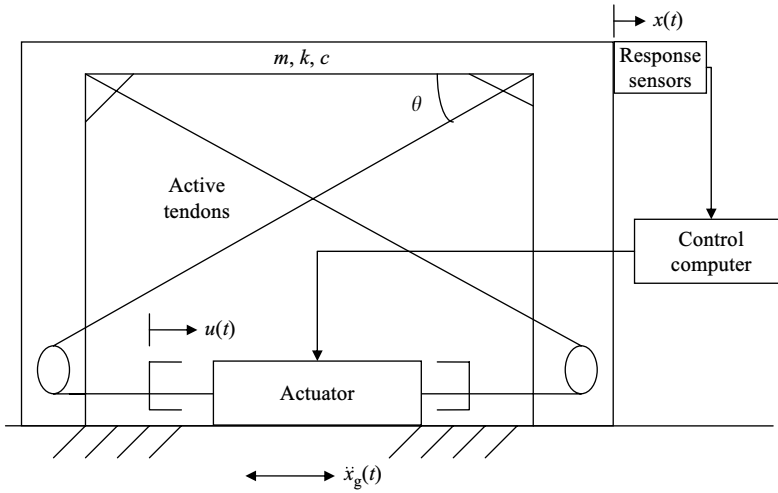

FIGURE 4.8 Closed-loop control implementation.

active control algorithm, and the force is then applied to the structure. It shall be emphasized that realization of a closed-loop feedback scheme for a $2n$th order system requires the measurements of the full-state vector, that is, $2n$ sensors are required to measure the response. However, when analog differentiators or state estimators (observers) are used, the number of sensors can be greatly reduced. Details on the sensor requirement will be discussed in Chapter 6.

The open-closed-loop scheme is a combination of the open-loop and closed-loop control schemes. As shown in Figure 4.9, this scheme required the information of both system response and external disturbance. The diagram for implementation of this scheme with an active tendon is shown in Figure 4.10. Both the earthquake ground acceleration and relative displacements and velocities are measured and then used to calculate the required control force based on the active control algorithm, and the force is then applied to the structure.

Open-loop seismic response control has the advantage of simple sensing system—only one accelerometer is required. However, its optimal feedback gain cannot be found unless the earthquake ground motion over the entire control duration is known a priori [17,18,45]. This is not possible for most smart seismic structures. Closed-loop control has the advantage of well-developed optimal control algorithms to determine the optimal feedback gain. Its weakness, requiring a complicated sensing system, recedes with the development of seismic observer technique (see Chapter 6) that greatly simplifies the sensing system. Closed-open-loop control combines the open-loop and closed-loop and is thus supposed to be superior to them. However, it has the same problem to determine the optimal feedback gain as open-loop scheme. Thus, closed-loop feedback is the most popular scheme while the other two are generally infeasible for seismic response control.

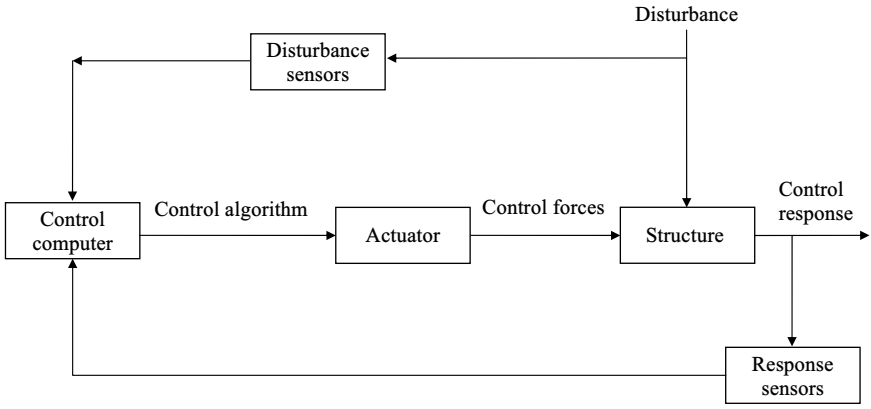

FIGURE 4.9 Open–closed-loop disturbance-compensated control.

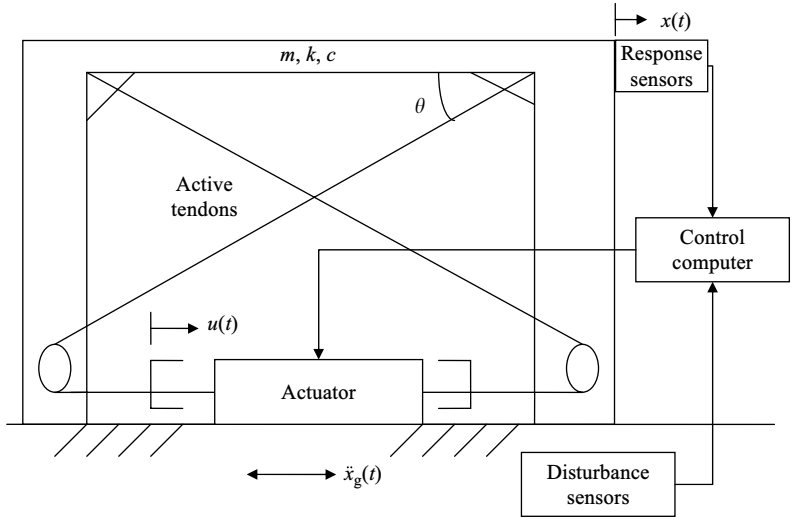

FIGURE 4.10 Open–closed-loop control implementation.

With one of these feedback control schemes, Equation 4.19 becomes mathematically solvable. Take the active control system with closed-loop feedback as an example, the control force vector is determined by feeding back the measurements of structural response. Thus, the feedback law can be expressed as

$$\{u(t)\}_{r\times 1} = -[G]_{r\times 2n}\{Z(t)\}_{2n\times 1} \tag{4.23}$$

where $[G]$ is $r \times 2n$ matrix of feedback gain. With these r extra equations, the control system response, $\{Z(t)\}$ in Equation 4.19, can be mathematically solved. Thus, the key point is to find gain matrix $[G]$. Once the $[G]$ matrix is determined,

the closed-loop system will take the form

$$\{\dot{Z}(t)\} = [A_c]\{Z(t)\} + \{B_r\}\ddot{x}_g(t) \tag{4.24a}$$

where

$$[A_c] = [A] - [B_u][G] \tag{4.24b}$$

is the closed-loop plant matrix obtained by substituting Equation 4.23 into Equation 4.19.

As observed, a closed-loop system can be a *full-state feedback* if all state variables are measured. For a seismic response control system, the state variables are displacements and velocities at all degrees of freedom (d.o.f.) of the seismic structure, and Equation 4.23 can be rewritten as

$$\{u(t)\}_{r\times 1} = -[G]\{Z(t)\} = -\begin{bmatrix}[G_d]_{r\times n} & [G_v]_{r\times n}\end{bmatrix}\begin{Bmatrix}\{x(t)\}_{n\times 1}\\ \{\dot{x}(t)\}_{n\times 1}\end{Bmatrix} \tag{4.25a}$$

where the $[G_d]$ and $[G_v]$ are gain matrices for displacements and velocities. With Equations 4.20 and 4.25a, the system's closed-loop plant matrix in Equation 4.24b can be rewritten as

$$\begin{aligned}[A_c] &= [A] - [B_u][G]\\ &= \begin{bmatrix}[0] & [I]\\ -[M]^{-1}[K] & -[M]^{-1}[C]\end{bmatrix} - \begin{bmatrix}[0]\\ [M]^{-1}[\gamma]\end{bmatrix}\begin{bmatrix}[G_d] & [G_v]\end{bmatrix}\\ &= \begin{bmatrix}[0] & [I]\\ -[M]^{-1}([K] + [\gamma][G_d]) & -[M]^{-1}([C] + [\gamma][G_v])\end{bmatrix}\end{aligned} \tag{4.25b}$$

There are chances that only part of the state variables is measured, full-state feedback cannot be achieved unless the observer technique is employed (see Chapter 6). A typical case is the *velocity feedback control* where only velocities are measured. For velocity feedback control, $[G_d]$ would be zero matrix and

$$\{u(t)\}_{r\times 1} = -[G_v]_{r\times n}\{\dot{x}(t)\}_{n\times 1} \tag{4.26}$$

Substituting Equation 4.26 into Equation 4.3 yields

$$[M]\{\ddot{x}(t)\} + ([C] + [\gamma][G_v])\{\dot{x}(t)\} + [K]\{x(t)\} = \{\delta\}\ddot{x}_g(t) \tag{4.27a}$$

which shows that velocity feedback control enhances system damping and thus mitigates system response. Note that the system stiffness is not modified by velocity

feedback control. Such closed-loop systems have the plant matrix as

$$[A_c] = \begin{bmatrix} [0] & [I] \\ -[M]^{-1}[K] & -[M]^{-1}([C] + [\gamma][G_v]) \end{bmatrix} \tag{4.27b}$$

It is worth noting that displacements and velocities are difficult to measure in a seismic response control system. Instead, accelerations are the most reliable measurements. Some researchers thus proposed direct acceleration feedback to address this issue [32–35,46]. This method would simplify the sensing system and thus make the control system more practical from the sensing system point of view. However, this method needs to be further enhanced to make the actuation system practical as it modifies system inertia force to avoid resonance. As discussed in Chapter 1, it would require huge and expensive actuators for smart seismic structures. More discussion on this issue can be found in Chapter 6.

4.1.5 Solution Procedure for State Equation

This section discusses how to solve Equation 4.19. Assuming optimal control force $\{u(t)\}$ has been obtained by feedback control law, and earthquake excitation $\ddot{x}_g(t)$ has been measured up to time instant t, structural response $\{Z(t)\}$ can then be found analytically by the following procedure.

Let the state vector be expressed in terms of modal transformation matrix $[T]$ of plant matrix $[A]$, that is,

$$\{Z(t)\} = [T]\{\psi(t)\} \tag{4.28}$$

where $[T]$ of $(2n \times 2n)$ is a matrix constructed from the eigenvectors of matrix $[A]$, that is,

$$[T] = \left[\{\alpha_1\}, \{\beta_1\}; \{\alpha_2\}, \{\beta_2\}; \ldots; \{\alpha_j\}, \{\beta_j\}; \ldots; \{\alpha_n\}, \{\beta_n\}\right] \tag{4.29}$$

in which $\{\alpha_j\}$ and $\{\beta_j\}$ are the real and imaginary parts of the jth eigenvector of matrix $[A]$.

Substituting Equation 4.28 into state Equation 4.19 yields

$$[T]\left\{\dot{\psi}(t)\right\} = [A][T]\{\psi(t)\} + [B_u]\{u(t)\} + \{B_r\}\ddot{x}_g(t) \tag{4.30}$$

Premultiplying Equation 4.30 by $[T]^{-1}$ results in the following modal state equation:

$$\{\dot{\psi}(t)\} = [\Phi]\{\psi(t)\} + \{\Gamma(t)\} \tag{4.31}$$

where $[\Phi]$ is the modal plant matrix defined as

$$[\Phi] = [T]^{-1}[A][T] \tag{4.32}$$

and vector $\{\Gamma(t)\}$ consists of control force and excitation terms as

$$\{\Gamma(t)\} = [T]^{-1}[B_{\mathrm{u}}]\{u(t)\} + [T]^{-1}\{B_{\mathrm{r}}\}\ddot{x}_{\mathrm{g}}(t) \tag{4.33}$$

The advantage of Equations 4.31 over Equation 4.19, the original state equation, is that the modal plant matrix is a decoupled matrix, that is,

$$[\Phi] = \begin{bmatrix} [\Phi]_1 & & & & & & & \\ & [\Phi]_2 & & & & & & \\ & & \cdot & & & & & \\ & & & \cdot & & & & \\ & & & & \cdot & & & \\ & & & & & [\Phi]_j & & \\ & & & & & & \cdot & \\ & & & & & & & \cdot \\ & & & & & & & & \cdot \\ & & & & & & & & & [\Phi]_n \end{bmatrix} \tag{4.34}$$

where each submatrix $[\Phi]_j$ is a (2×2) matrix given by

$$[\Phi]_j = \begin{bmatrix} \mu_j & \nu_j \\ -\nu_j & \mu_j \end{bmatrix}, \quad j = 1, 2, \ldots, n \tag{4.35}$$

in which μ_j and ν_j are the real and imaginary parts, respectively, of the jth eigenvalue of matrix $[A]$.

Initial conditions at time $t = 0$ are

$$\{\psi(0)\} = \{0\}, \quad \{u(0)\} = \{0\}, \quad \ddot{x}_{\mathrm{g}}(0) = 0 \tag{4.36}$$

The solution of Equation 4.31 can be obtained by solving the following integral:

$$\{\psi(t)\} = \int_0^{\mathrm{T}} \exp([\Phi](t-\tau))\{\Gamma(\tau)\}\,\mathrm{d}\tau \tag{4.37}$$

where τ is a dummy integration variable, and $\exp([\Phi](t-\tau))$ is a $(2n \times 2n)$ exponential matrix.

Using the initial conditions, the integration of Equation 4.37 can be solved numerically by employing the trapezoidal rule or numerical integration technique [7]. Let $t = m\Delta t$; then

$$\begin{aligned} \{\psi(t)\} = \frac{\Delta t}{2} \{ & \exp([\Phi](t - 0\cdot\Delta t))\Gamma(0\cdot\Delta t) + 2\exp([\Phi](t-\Delta t))\Gamma(\Delta t) \\ & + 2\exp([\Phi](t-2\Delta t))\Gamma(2\Delta t) + \cdots \\ & + 2\exp([\Phi][t-(m-1)\Delta t])\Gamma[(m-1)\Delta t] \\ & + \exp([\Phi][t-m\Delta t])\Gamma(m\Delta t)\} \end{aligned} \tag{4.38a}$$

From Equations 4.33 and 4.36, we have

$$\Gamma(0) = [T]^{-1}[B_{\mathrm{u}}]\{u(0)\} + [T]^{-1}\{B_{\mathrm{r}}\}\ddot{x}_{\mathrm{g}}(0) = 0 \tag{4.38b}$$

Thus, Equation 4.38a becomes (note that $t = m\Delta t$)

$$\begin{aligned}\{\psi(t)\} &= \frac{\Delta t}{2}\left\{0 + 2\sum_{l=1}^{m-1}\exp([\Phi][t - l\Delta t])\,\{\Gamma(l\Delta t)\}\right.\\ &\quad \left. + \exp([\Phi][t - m\Delta t])\,\{\Gamma(m\Delta t)\}\right\}\\ &= \sum_{l=1}^{m-1}\exp([\Phi][m\Delta t - l\Delta t])\,\{\Gamma(l\Delta t)\}\,\Delta t + \exp([\Phi]\cdot 0)\,\{\Gamma(t)\}\,\frac{\Delta t}{2}\\ &= \sum_{l=1}^{m-1}\exp([\Phi](m-l)\Delta t)\,\{\Gamma(l\Delta t)\}\,\Delta t + \{\Gamma(t)\}\left(\frac{\Delta t}{2}\right)\end{aligned} \tag{4.38c}$$

where Δt is the time increment. In order to simplify Equation 4.38, define the summation term as

$$\{\Lambda(t - \Delta t)\} = \sum_{l=1}^{m-1}\exp([\Phi](m-l)\Delta t)\,\{\Gamma(l\Delta t)\}\,\Delta t \tag{4.39}$$

so that Equation 4.38 can be rewritten as

$$\{\psi(t)\} = \{\Lambda(t - \Delta t)\} + \{\Gamma(t)\}\left(\frac{\Delta t}{2}\right) \tag{4.40}$$

The term $\{\Lambda(t - \Delta t)\}$ can be expressed in recurrent form as

$$\{\Lambda(t - \Delta t)\} = \exp([\Phi]\Delta t)\,(\{\Lambda(t - 2\Delta t)\} + \{\Gamma(t - \Delta t)\}\,\Delta t) \tag{4.41a}$$

This is because from Equation 4.39, we have (note $t = m\Delta t$)

$$\begin{aligned}\{\Lambda(t - \Delta t)\} &= \sum_{l=1}^{m-1}\exp([\Phi](m-l)\Delta t)\{\Gamma(l\Delta t)\}\Delta t\\ &= \sum_{l=1}^{m-2}\exp([\Phi](m-l)\Delta t)\{\Gamma(l\Delta t)\}\Delta t\\ &\quad + \exp([\Phi][m - (m-1)]\Delta t)\{\Gamma[(m-1)\Delta t]\}\Delta t\end{aligned}$$

$$= \sum_{l=1}^{m-2} \exp([\Phi](m-1-l)\Delta t)\exp([\Phi]\Delta t)\{\Gamma(l\Delta t)\} + \exp([\Phi]\Delta t)\{\Gamma[(m-1)\Delta t]\}\Delta t$$

$$= \exp([\Phi]\Delta t)\left[\sum_{l=1}^{m-2} \exp([\Phi](t-\Delta t-l\Delta t))\{\Gamma(l\Delta t)\}\Delta t + \{\Gamma[(m-1)\Delta t]\}\Delta t\right]$$

$$= \exp([\Phi]\Delta t)(\{\Lambda(t-2\Delta t)\} + \{\Gamma(t-\Delta t)\}\Delta t) \tag{4.41b}$$

Substituting Equation 4.40 into Equation 4.28, the state vector is returned to its physical coordinates as

$$\{Z(t)\} = [T]\left(\{\Lambda(t-\Delta t)\} + \{\Gamma(t)\}\left(\frac{\Delta t}{2}\right)\right) \tag{4.42}$$

Now the system response $\{Z(t)\}$ can be determined. In Equation 4.42, $\{\Gamma(t)\}$ is easily obtained using Equation 4.33 since $\{u(t)\}$ is assumed known and $\ddot{x}_g(t)$ is measured; then $\{\Lambda(t-\Delta t)\}$ can be derived from the result of $\{\Lambda(t-2\Delta t)\}$ as shown by Equation 4.41. Attention must be paid to the calculation of $\exp([\Phi]\Delta t)$ as follows. With Equation 4.34, we can prove that

$$\exp([\Phi]\Delta t) = \exp\left(\begin{bmatrix} [\Phi]_1 & & & \\ & [\Phi]_2 & & \\ & & \ddots & \\ & & & [\Phi]_n \end{bmatrix}\Delta t\right) \tag{4.43}$$

$$= \begin{bmatrix} \exp([\Phi]_1\Delta t) & & & \\ & \exp([\Phi]_2\Delta t) & & \\ & & \ddots & \\ & & & \exp([\Phi]_n\Delta t) \end{bmatrix}$$

and with Equation 4.35

$$\exp([\Phi]_j\Delta t) = \exp\left(\begin{bmatrix} \mu_j & \nu_j \\ -\nu_j & \mu_j \end{bmatrix}\Delta t\right) = e^{\mu_j\Delta t}\begin{bmatrix} \cos\nu_j\Delta t & \sin\nu_j\Delta t \\ -\sin\nu_j\Delta t & \cos\nu_j\Delta t \end{bmatrix} \tag{4.44}$$

where $j = 1, 2, \ldots, n$. Details of the proof procedure are shown in Equations 4.45 through 4.58. Using Taylor's series to expand $\exp([\Phi]\Delta t)$, we have

$$\exp([\Phi]\Delta t) = \sum_{k=0}^{\infty} \frac{([\Phi]\Delta t)^k}{k!} = [I]_{n\times n} + [\Phi]\Delta t + \frac{1}{2!}([\Phi]\Delta t)^2 + \ldots \quad (4.45)$$

where $[I]$ is unit matrix. Since,

$$\begin{aligned}([\Phi]\,\Delta t)^2 &= [\Phi][\Phi](\Delta t)^2 = \begin{bmatrix} [\Phi]_1 & & & \\ & [\Phi]_2 & & \\ & & \ddots & \\ & & & [\Phi]_n \end{bmatrix} \begin{bmatrix} [\Phi]_1 & & & \\ & [\Phi]_2 & & \\ & & \ddots & \\ & & & [\Phi]_n \end{bmatrix} (\Delta t)^2 \\ &= \begin{bmatrix} [\Phi]_1^2 & & & \\ & [\Phi]_2^2 & & \\ & & \ddots & \\ & & & [\Phi]_n^2 \end{bmatrix} (\Delta t)^2 \end{aligned} \quad (4.46)$$

and

$$\begin{aligned}([\Phi]\Delta t)^3 &= [\Phi][\Phi][\Phi](\Delta t)^3 \\ &= \begin{bmatrix} [\Phi]_1^2 & & & \\ & [\Phi]_2^2 & & \\ & & \ddots & \\ & & & [\Phi]_n^2 \end{bmatrix} \begin{bmatrix} [\Phi]_1 & & & \\ & [\Phi]_2 & & \\ & & \ddots & \\ & & & [\Phi]_n \end{bmatrix} (\Delta t)^3 \\ &= \begin{bmatrix} [\Phi]_1^3 & & & \\ & [\Phi]_2^3 & & \\ & & \ddots & \\ & & & [\Phi]_n^3 \end{bmatrix} (\Delta t)^3 \end{aligned} \quad (4.47)$$

we obtain

$$\begin{aligned}&\exp([\Phi]\Delta t) \\ &= \begin{bmatrix} [I]_{2\times 2} & & & \\ & [I]_{2\times 2} & & \\ & & \ddots & \\ & & & [I]_{2\times 2} \end{bmatrix} + (\Delta t) \begin{bmatrix} [\Phi]_1 & & & \\ & [\Phi]_2 & & \\ & & \ddots & \\ & & & [\Phi]_n \end{bmatrix} \\ &+ \tfrac{(\Delta t)^2}{2!} \begin{bmatrix} [\Phi]_1^2 & & & \\ & [\Phi]_2^2 & & \\ & & \ddots & \\ & & & [\Phi]_n^2 \end{bmatrix} + \tfrac{(\Delta t)^3}{3!} \begin{bmatrix} [\Phi]_1^3 & & & \\ & [\Phi]_2^3 & & \\ & & \ddots & \\ & & & [\Phi]_n^3 \end{bmatrix} + \cdots \end{aligned} \quad (4.48a)$$

Thus

$$
\begin{aligned}
&\exp\left([\Phi]\Delta t\right)\\
&= \begin{bmatrix}
[I]_{2\times 2} + (\Delta t)\,[\Phi]_1 & & & \\
+\frac{(\Delta t)^2}{2!}\,[\Phi]_1^2 & & & \\
+\frac{(\Delta t)^3}{3!}\,[\Phi]_1^3 + \cdots & & & \\
& [I]_{2\times 2} + (\Delta t)\,[\Phi]_2 & & \\
& +\frac{(\Delta t)^2}{2!}\,[\Phi]_2^2 & & \\
& +\frac{(\Delta t)^3}{3!}\,[\Phi]_2^3 + \cdots & & \\
& & \ddots & \\
& & & [I]_{2\times 2} + (\Delta t)\,[\Phi]_n \\
& & & +\frac{(\Delta t)^2}{2!}\,[\Phi]_n^2 \\
& & & +\frac{(\Delta t)^3}{3!}\,[\Phi]_n^3 + \cdots
\end{bmatrix}\\
&= \begin{bmatrix}
\exp([\Phi]_1\Delta t) & & & \\
& \exp([\Phi]_2\Delta t) & & \\
& & \ldots & \\
& & & \exp([\Phi]_n\Delta t)
\end{bmatrix}
\end{aligned}
\tag{4.48b}
$$

Equation 4.43 is thus proved. Note that Equation 4.44 shall be used to calculate each submatrix $\exp([\Phi]_j\Delta t), j = 1, 2, \ldots, n$ in Equation 4.48. Using the Taylor's series to expand the submatrix, the same way as Equation 4.45, yields

$$
\exp([\Phi]_j\Delta t) = \sum_{k=0}^{\infty} \frac{([\Phi]_j\Delta t)^k}{k!} = \sum_{k=0}^{\infty} \frac{(\Delta t)^k}{k!}([\Phi]_j)^k \tag{4.49}
$$

Equation 4.35 can be rewritten as

$$
[\Phi]_j = \begin{bmatrix} \mu_j & \nu_j \\ -\nu_j & \mu_j \end{bmatrix} = \mu_j[I] + \nu_j[J] \tag{4.50}
$$

where

$$
[I] = \begin{bmatrix} 1 & 0 \\ 0 & 1 \end{bmatrix}, \quad [J] = \begin{bmatrix} 0 & 1 \\ -1 & 0 \end{bmatrix} \tag{4.51}
$$

Substituting Equation 4.50 into Equation 4.49 yields

$$
\begin{aligned}
&\exp([\Phi]_j\Delta t)\\
&= \sum_{k=0}^{\infty} \frac{(\Delta t)^k}{k!}\left(\mu_j[I] + \nu_j[J]\right)^k
\end{aligned}
$$

$$= [I] + (\Delta t)\left(\mu_j[I] + \nu_j[J]\right) + \frac{(\Delta t)^2}{2!}\left(\mu_j[I] + \nu_j[J]\right)^2 + \frac{(\Delta t)^3}{3!}\left(\mu_j[I] + \nu_j[J]\right)^3 + \frac{(\Delta t)^4}{4!}(\mu_j[I] + \nu_j[J])^4 + \frac{(\Delta t)^5}{5!}(\mu_j[I] + \nu_j[J])^5 + \cdots \tag{4.52a}$$

which can be expanded as

$$\begin{aligned}
&\exp([\Phi]_j \Delta t) \\
&= [I] + \mu_j \Delta t[I] + \nu_j \Delta t[J] + \frac{(\Delta t)^2}{2!}\left(\mu_j^2[I]^2 + 2\mu_j\nu_j[I][J] + \nu_j^2[J]^2\right) \\
&\quad + \frac{(\Delta t)^3}{3!}\left(\mu_j^3[I]^3 + 3\mu_j^2\nu_j[I]^2[J] + 3\mu_j\nu_j^2[I][J]^2 + \nu_j^3[J]^3\right) \\
&\quad + \frac{(\Delta t)^4}{4!}\left(\mu_j^4[I] + 4\mu_j^3\nu_j[I]^3[J] + 6\mu_j^2\nu_j^2[I]^2[J]^2 + 4\mu_j\nu_j^3[I][J]^3 + \nu_j^4[J]^4\right) \\
&\quad + \frac{(\Delta t)^5}{5!}\left(\begin{array}{l}\mu_j^5[I]^5 + 5\mu_j^4\nu_j[I]^5[J] + 10\mu_j^3\nu_j^2[I]^3[J]^2 + 10\mu_j^2\nu_j^3[I]^2[J]^3 \\ +5\mu_j\nu_j^4[I][J]^4 + \nu_j^5[J]^5\end{array}\right) + \cdots
\end{aligned} \tag{4.52b}$$

Note that

$$[I]^k = [I],\ k = 1, 2, \cdots, \infty \tag{4.53}$$

$$\begin{cases}[I]^k[J]^l = [I][J]^l = [J]^l \\ [J]^l[I]^k = [J]^l[I] = [J]^l\end{cases} \quad k, l = 1, 2, \ldots, \infty \tag{4.54}$$

and

$$\begin{aligned}
[J]^2 &= \begin{bmatrix}0 & 1\\ -1 & 0\end{bmatrix}\begin{bmatrix}0 & 1\\ -1 & 0\end{bmatrix} = \begin{bmatrix}-1 & 0\\ 0 & -1\end{bmatrix} = -[I] \\
[J]^3 &= [J]^2[J] = -[I][J] = -[J] \\
[J]^4 &= [J]^2[J]^2 = -[I](-[I]) = [I]
\end{aligned} \tag{4.55}$$

which means

$$[J]^{4k} = [I], \quad [J]^{4k+1} = [J], \quad [J]^{4k+2} = -[I], \quad [J]^{4k+3} = -[J] \tag{4.56}$$

Substituting Equations 4.53, 4.54, and 4.56 into Equation 4.52b yields

$$\begin{aligned}
&\exp\left([\Phi]_j \Delta t\right) \\
&= [I] + \mu_j \Delta t[I] + \nu_j \Delta t[J] + \frac{(\Delta t)^2}{2!}\left(\mu_j^2[I] + 2\mu_j\nu_j[J] - \nu_j^2[I]\right)
\end{aligned}$$

$$
\begin{aligned}
&+\frac{(\Delta t)^3}{3!}\left(\mu_j^3[I]+3\mu_j^2\nu_j[J]-3\mu_j\nu_j^2[I]-\nu_j^3[J]\right)\\
&+\frac{(\Delta t)^4}{4!}\left(\mu_j^4[I]+4\mu_j^3\nu_j[J]-6\mu_j^2\nu_j^2[I]-4\mu_j\nu_j^3[J]+\nu_j^4[I]\right)\\
&+\frac{(\Delta t)^5}{5!}\Big(\mu_j^5[I]+5\mu_j^4\nu_j[J]-10\mu_j^3\nu_j^2[I]-10\mu_j^2\nu_j^3[J]+5\mu_j\nu_j^4[I]\\
&+\nu_j^5[J]\Big)+\cdots\\
=&\left[1+\mu_j\Delta t+\frac{1}{2!}(\mu_j\Delta t)^2-\frac{1}{2!}(\nu_j\Delta t)^2+\frac{1}{3!}(\mu_j\Delta t)^3-\frac{3}{3!}(\mu_j\Delta t)(\nu_j\Delta t)^2\right.\\
&+\frac{1}{4!}(\mu_j\Delta t)^4-\frac{6}{4!}(\mu_j\Delta t)^2(\nu_j\Delta t)^2+\frac{1}{4!}(\nu_j\Delta t)^4\\
&\left.+\frac{1}{5!}(\mu_j\Delta t)^5-\frac{10}{5!}(\mu_j\Delta t)^3(\nu_j\Delta t)^2+\frac{5}{5!}(\mu_j\Delta t)(\nu_j\Delta t)^4+\cdots\right][I]\\
&+\left[\nu_j\Delta t+\frac{2}{2!}(\mu_j\Delta t)(\nu_j\Delta t)+\frac{3}{3!}(\mu_j\Delta t)^2(\nu_j\Delta t)-\frac{1}{3!}\ (\nu_j\Delta t)^3\right.\\
&+\frac{4}{4!}(\mu_j\Delta t)^3(\nu_j\Delta t)-\frac{4}{4!}(\mu_j\Delta t)(\nu_j\Delta t)^3+\frac{5}{5!}(\mu_j\Delta t)^4(\nu_j\Delta t)\\
&\left.-\frac{10}{5!}(\mu_j\Delta t)^2(\nu_j\Delta t)^3+\frac{1}{5!}(\nu_j\Delta t)^5+\cdots\right][J] \qquad (4.57a)
\end{aligned}
$$

Thus

$$
\begin{aligned}
&\exp\big([\Phi]_j\Delta t\big)\\
&=\Bigg[\left(1+\mu_j\Delta t+\frac{1}{2!}(\mu_j\Delta t)^2+\frac{1}{3!}(\mu_j\Delta t)^3+\frac{1}{4!}(\mu_j\Delta t)^4+\frac{1}{5!}(\mu_j\Delta t)^5+\cdots\right)\cdot 1\\
&-\left(1+\mu_j\Delta t+\frac{1}{2!}(\mu_j\Delta t)^2+\frac{1}{3!}(\mu_j\Delta t)^3+\cdots\right)\frac{1}{2!}(\nu_j\Delta t)^2\\
&+\big(1+\mu_j\Delta t+\cdots\big)\frac{1}{4!}(\nu_j\Delta t)^4+\cdots\Bigg][I]\\
&+\Bigg[\left(1+\mu_j\Delta t+\frac{1}{2!}(\mu_j\Delta t)^2+\frac{1}{3!}(\mu_j\Delta t)^3+\frac{1}{4!}(\mu_j\Delta t)^4+\cdots\right)\nu_j\Delta t\\
&+\left(1+\mu_j\Delta t+\frac{1}{2!}(\mu_j\Delta t)^2+\cdots\right)\left(-\frac{1}{3!}(\nu_j\Delta t)^3\right)\\
&+(1+\cdots)\left(\frac{1}{5!}(\nu_j\Delta t)^5\right)+\cdots\Bigg][J]\\
&=\mathrm{e}^{\mu_j\Delta t}\left(1-\frac{1}{2!}(\nu_j\Delta t)^2+\frac{1}{4!}(\nu_j\Delta t)^4+\cdots\right)[I]
\end{aligned}
$$

$$
\begin{aligned}
&+e^{\mu_j \Delta t}\left[v_j \Delta t - \frac{1}{3!}\left(v_j \Delta t\right)^3 + \frac{1}{5!}(v_j \Delta t)^5 + \cdots\right][J] \\
&= e^{\mu_j \Delta t}\left[\cos v_j \Delta t[I] + \sin v_j \Delta t[J]\right] \\
&= e^{\mu_j \Delta t}\left(\begin{bmatrix} \cos v_j \Delta t & 0 \\ 0 & \cos v_j \Delta t \end{bmatrix} + \begin{bmatrix} 0 & \sin v_j \Delta t \\ -\sin v_j \Delta t & 0 \end{bmatrix}\right) \\
&= e^{\mu_j \Delta t}\begin{bmatrix} \cos v_j \Delta t & \sin v_j \Delta t \\ -\sin v_j \Delta t & \cos v_j \Delta t \end{bmatrix}
\end{aligned} \tag{4.57b}
$$

when $\Delta t = 0$, Equation 4.57 becomes

$$
\begin{aligned}
\exp([\Phi]_j \Delta t)|_{\Delta t=0} &= e^{\mu_j \Delta t}\begin{bmatrix} \cos v_j \Delta t & \sin v_j \Delta t \\ -\sin v_j \Delta t & \cos v_j \Delta t \end{bmatrix}\Bigg|_{\Delta t=0} \\
&= e^0 \begin{bmatrix} \cos 0 & \sin 0 \\ -\sin 0 & \cos 0 \end{bmatrix} = \begin{bmatrix} 1 & 0 \\ 0 & 1 \end{bmatrix} = [I]
\end{aligned} \tag{4.58}
$$

Now $\exp([\Phi]\Delta t)$ in Equation 4.41 has been determined by Equations 4.43, 4.44, and 4.58 and the system's response is then obtained.

The above procedure to solve system response has been implemented in commercial software packages such as MATLAB® function *LSIM*. Refer to Appendix A for details. Note that the above solution procedure for Equation 4.42 is based on the fact that the control force $\{u(t)\}$ is known. In an optimal closed-loop control system, optimal control force $\{u(t)\}$ is regulated by the feedback of the state vector $\{Z(t)\}$ alone; the measurements required are those of the response at time-instant t. This can be done by placing displacement and velocity sensors at each floor level. The determination of control force by feedback of state vector is called control algorithms, which are discussed in the following sections.

4.2 Classical Optimal Control Algorithms for Smart Seismic Structures

Active *control algorithms* are used to determine the control force from the measured structural response. They are implemented by means of software in the *digital controller*, the *control computer*. Control algorithms yield a *control law*, the mathematical model of the controller, for the active structural control system. Development and implementation of the control algorithm are also called *controller design*. This section reviews the concept of performance indexes and determination of feedback gain and control force by classical control algorithms, *Riccati optimal active control* (ROAC) and *pole placement*. Then application of these algorithms to seismic response control systems is discussed and numerical examples are employed to demonstrate these algorithms. Finally, advantages and weaknesses of these algorithms for seismic response control are studied.

4.2.1 Riccati Optimal Active Control Algorithm

Section 4.1 shows that optimal control force $\{u(t)\}$ was obtained by the control law expressed in Equation 4.23, in which the gain matrix $[G]$ is determined by control algorithms. This section discusses how the ROAC algorithm determines the gain matrix $[G]$.

4.2.1.1 Performance index

In order to design an optimal control system, the control law should achieve the control objective, such as maximizing the reduction of structural response with minimum control energy or control force. However, more reduction of structural response requires more control force. A performance index is used in this situation to find a compromise between the need to reduce structural response and the need to minimize control force. Different quantification of performance indices produces different types of algorithms. A *quadratic index* of n variables $x_1, x_2, \ldots, x_n$ is an expression in which each term contains either the square of a variable or the product of two different variables

$$\begin{aligned} J(x_k) = \sum_{i=1}^{n}\sum_{j=1}^{n} a_{ij}x_i x_j = {} & a_{11}x_1x_1 + a_{12}x_1x_2 + \cdots + a_{1n}x_1x_n \\ & + a_{21}x_2x_1 + a_{22}x_2x_2 + \cdots + a_{2n}x_2x_n \\ & + \cdots \\ & + a_{n1}x_nx_1 + a_{n2}x_nx_2 + \cdots + a_{nn}x_nx_n \end{aligned} \tag{4.59}$$

where $k = 1, 2, \ldots, n$. By denoting a vector

$$\{x\} = \{x_1, x_2, \ldots x_n\}^{\mathrm{T}} \tag{4.60}$$

Equation 4.59 can be put into the matrix form

$$J(\{x\}) = \sum_{i=1}^{n} x_i \sum_{j=1}^{n} a_{ij}x_j = \sum_{i=1}^{n} x_i([A]\{x\})_i = \{x\}^{\mathrm{T}}[A]\{x\} \tag{4.61}$$

in which a_{ij} is the (i, j) element of matrix $[A]$.

In the quadratic index $J = \{x\}^{\mathrm{T}}[A]\{x\}$, matrix $[A]$ is said to be *positive-definite* if the index is positive for all $\{x\}$ except $\{x\} = \{0\}$; matrix $[A]$ is said to be *positive semidefinite* if the index is nonnegative for all $\{x\}$ and there may be a nonzero vector $\{x\}$ for which $\{x\}^{\mathrm{T}}[A]\{x\} = 0$. From this definition, we have the following two theorems:

- *Theorem 1*. Matrix $[A]$ is positive-definite if and only if all eigenvalues of $[A]$ are positive, and matrix $[A]$ is positive semidefinite if and only

if all eigenvalues of $[A]$ are nonnegative and some of the eigenvalues may be zero.

- *Theorem 2*. Matrix $[A]$ is positive-definite if the naturally ordered principal minors of $[A]$ are all positive, that is,

$$a_{11} > 0, \quad \begin{vmatrix} a_{11} & a_{12} \\ a_{21} & a_{22} \end{vmatrix} > 0, \quad \begin{vmatrix} a_{11} & a_{12} & a_{13} \\ a_{21} & a_{22} & a_{23} \\ a_{31} & a_{32} & a_{33} \end{vmatrix} > 0, \ldots, |A| > 0 \quad (4.62a)$$

and matrix $[A]$ is positive semidefinite if the naturally ordered principal minors of $[A]$ are all nonpositive, that is,

$$a_{11} \geq 0, \quad \begin{vmatrix} a_{11} & a_{12} \\ a_{21} & a_{22} \end{vmatrix} \geq 0, \quad \begin{vmatrix} a_{11} & a_{12} & a_{13} \\ a_{21} & a_{22} & a_{23} \\ a_{31} & a_{32} & a_{33} \end{vmatrix} \geq 0, \ldots, |A| \geq 0 \quad (4.62b)$$

For example, matrix $\begin{bmatrix} 1 & 0 \\ 0 & 1 \end{bmatrix}$ is positive-definite because its principal minors $1 > 0$ and $\begin{vmatrix} 1 & 0 \\ 0 & 1 \end{vmatrix} = 1 > 0$; matrix $\begin{bmatrix} 1 & 0 \\ 0 & 0 \end{bmatrix}$ is positive semidefinite because its principal minors $1 > 0$ and $\begin{vmatrix} 1 & 0 \\ 0 & 0 \end{vmatrix} = 0$.

The Riccati optimal control algorithm determines control force $\{u(t)\}$ by minimizing a standard quadratic index, J, given by

$$J = \frac{1}{2} \int_{t_0}^{t_f} \left(\{Z(t)\}^T [Q] \{Z(t)\} + \{u(t)\}^T [R] \{u(t)\} \right) \, dt \quad (4.63)$$

and satisfying the state equation, Equation 4.19. t_0 and t_f in Equation 4.63 are, respectively, the initial and final time-instants under consideration. Matrix $[Q]$ is a $(2n \times 2n)$ positive semidefinite symmetrical matrix. If $[Q]$ is positive-definite, all d.o.f of the system are included in the index; if $[Q]$ is semidefinite matrix with some zero eigenvalues, some d.o.f of the system may not be included. For example, if we want to design a system with velocity feedback only, we may pick

$$[Q]_{2n \times 2n} = \begin{bmatrix} [0]_{n \times n} & [0]_{n \times n} \\ [0]_{n \times n} & [I]_{n \times n} \end{bmatrix} \quad (4.64)$$

where $[I]_{n\times n}$ is a unit matrix of nth order. Obviously, $[Q]$ in Equation 4.64 is positive semidefinite. Then

$$\begin{aligned}\{Z(t)\}^{\mathrm{T}}[Q]\{Z(t)\} &= \begin{Bmatrix}\{x(t)\}\\ \{\dot{x}(t)\}\end{Bmatrix}^{\mathrm{T}}\begin{bmatrix}[0] & [0]\\ [0] & [I]\end{bmatrix}\begin{Bmatrix}\{x(t)\}\\ \{\dot{x}(t)\}\end{Bmatrix}\\ &= \{\dot{x}(t)\}^{\mathrm{T}}[I]\{\dot{x}(t)\}\end{aligned} \tag{4.65}$$

which means the index J is only related to velocities $\{\dot{x}(t)\}$ instead of the full-state vector $\{Z(t)\} = \begin{Bmatrix}\{x(t)\}\\ \{\dot{x}(t)\}\end{Bmatrix}$. For active tendon systems, $[R]$ is an $(r \times r)$ positive-definite symmetrical matrix so that all control forces are effective. For an AMD, $[R]$ is reduced to a scalar number since there is only one control force. $[Q]$ and $[R]$ are weighting matrices for system response and control force, respectively. Performance index, J, represents a weighted balance between structural response and control energy. The performance shown by Equation 4.63 is chosen so as to minimize the structural response and control energy over the time period from t_0 to t_{f}. When the elements of $[Q]$ are large, system response is reduced at the expense of increased control force. When the elements of $[R]$ are large, control force is small but the system response may not be sufficiently reduced.

4.2.1.2 Determination of control force

Assume that the system is controllable, that is, available control force is sufficient to bring the system from any initial state to any desired final state. Assume also that the system is observable, that is, system response output yields sufficient information to determine the state vector at any time instant t. Then the solution to this optimization problem can be obtained by the following variational calculus approach.

Define the Hamiltonian $\mathcal{H}$ as

$$\begin{aligned}\mathrm{H} = &\frac{1}{2}\{Z(t)\}^{\mathrm{T}}[Q]\{Z(t)\} + \frac{1}{2}\{u(t)\}^{\mathrm{T}}[R]\{u(t)\}\\ &+ \{\lambda(t)\}^{\mathrm{T}}\left([A]\{Z(t)\} + [B_{\mathrm{u}}]\{u(t)\} - \{\dot{Z}(t)\}\right)\end{aligned} \tag{4.66}$$

where $\{\lambda(t)\}$ of $(2N \times 1)$ is the vector of *Langrange multipliers*.

From the theory of functionals, *Euler equations* (expressed as follows) are the necessary conditions for optimality:

$$\begin{cases}\dfrac{\partial H}{\partial\{Z(t)\}} - \dfrac{\mathrm{d}}{\mathrm{d}t}\left(\dfrac{\partial H}{\partial\{\dot{Z}(t)\}}\right) = \{0\}\\ \dfrac{\partial H}{\partial\{u(t)\}} - \dfrac{\mathrm{d}}{\mathrm{d}t}\left(\dfrac{\partial H}{\partial\{\dot{u}(t)\}}\right) = \{0\}\\ \dfrac{\partial H}{\partial\{\lambda(t)\}} - \dfrac{\mathrm{d}}{\mathrm{d}t}\left(\dfrac{\partial H}{\partial\{\dot{\lambda}(t)\}}\right) = \{0\}\end{cases} \tag{4.67}$$

Substituting Equation 4.66 into the first two relationships of Equation 4.67 yields (note that $\partial H/\partial\{\dot{u}(t)\} = 0$ as there is no term related to $\{\dot{u}(t)\}$)

$$\begin{cases} \frac{\partial}{\partial\{Z(t)\}}\left[\frac{1}{2}\{Z(t)\}^{\mathrm{T}}[Q]\{Z(t)\} + \{\lambda(t)\}^{\mathrm{T}}[A]\{Z(t)\}\right] - \frac{\mathrm{d}}{\mathrm{d}t}\left[\frac{\partial\left(-\{\lambda(t)\}^{\mathrm{T}}\{\dot{Z}(t)\}\right)}{\partial\{\dot{Z}(t)\}}\right] = \{0\} \\ \frac{\partial}{\partial\{u(t)\}}\left[\frac{1}{2}\{u(t)\}^{\mathrm{T}}[R]\{u(t)\} + \{\lambda(t)\}^{\mathrm{T}}[B_{\mathrm{u}}]\{u(t)\}\right] = \{0\} \end{cases} \tag{4.68}$$

For each term in Equation 4.68, we have

$$\begin{aligned} \frac{\partial}{\partial z_k}\left[\frac{1}{2}\{Z(t)\}^{\mathrm{T}}[Q]\{Z(t)\}\right] &= \frac{\partial}{\partial z_k}\left(\frac{1}{2}\sum_{i=1}^{2n}\sum_{j=1}^{2n} z_i q_{ij} z_j\right) \\ &= \frac{1}{2}\left(\sum_{i=1}^{2n} z_i q_{ik} + \sum_{j=1}^{2n} q_{kj} z_j\right) = \frac{1}{2}\left(\sum_{i=1}^{2n} z_i q_{ik} + \sum_{i=1}^{2n} q_{ki} z_i\right) \end{aligned} \tag{4.69}$$

Because $[Q]$ is a symmetrical matrix, $q_{ki} = q_{ik}, i, k = 1, 2, \ldots, 2n$. Equation 4.69 then becomes

$$\frac{\partial}{\partial z_k}\left[\frac{1}{2}\{Z(t)\}^{\mathrm{T}}[Q]\{Z(t)\}\right] = \frac{1}{2}\left(\sum_{i=1}^{2n} z_i q_{ki} + \sum_{i=1}^{2n} z_i q_{ki}\right) = \sum_{i=1}^{2n} q_{ki} z_i \tag{4.70}$$

thus

$$\frac{\partial}{\partial\{Z(t)\}}\left[\frac{1}{2}\{Z(t)\}^{\mathrm{T}}[Q]\{Z(t)\}\right] = [Q]\{Z(t)\} \tag{4.71}$$

Similarly,

$$\frac{\partial}{\partial z_k}\left(\{\lambda\}^{\mathrm{T}}[A]\{Z(t)\}\right) = \frac{\partial}{\partial z_k}\left(\sum_{i=1}^{2n}\sum_{j=1}^{2n}\lambda_i a_{ij} z_j\right) = \sum_{i=1}^{2n}\lambda_i a_{ik} = \sum_{i=1}^{2n} a_{ik}\lambda_i \tag{4.72}$$

thus

$$\frac{\partial}{\partial\{Z(t)\}}\left(\{\lambda\}^{\mathrm{T}}[A]\{Z(t)\}\right) = [A]^{\mathrm{T}}\{\lambda\} \tag{4.73}$$

And

$$\frac{\mathrm{d}}{\mathrm{d}t}\left[\frac{\partial}{\partial\dot{z}_k}(-\{\lambda(t)\}^{\mathrm{T}}\mathrm{T}\{\dot{Z}(t)\})\right] = \frac{\mathrm{d}}{\mathrm{d}t}\left[\frac{\partial}{\partial\dot{z}_k}\left(-\sum_{i=1}^{2n}\lambda_i\dot{z}_i\right)\right] = \frac{\mathrm{d}}{\mathrm{d}t}(-\lambda_k) = -\dot{\lambda}_k \tag{4.74}$$

thus

$$\frac{\mathrm{d}}{\mathrm{d}t}\left[\frac{\partial}{\partial\left\{\dot{Z}(t)\right\}}\left(-\{\lambda(t)\}^{\mathrm{T}}\{\dot{Z}(t)\}\right)\right]=-\{\dot{\lambda}(t)\} \tag{4.75}$$

Also

$$\begin{aligned}\frac{\partial}{\partial u_k}\left(\frac{1}{2}\{u(t)\}^{\mathrm{T}}[R]\{u(t)\}\right)&=\frac{\partial}{\partial u_k}\left(\frac{1}{2}\sum_{i=1}^{2n}\sum_{j=1}^{2n}u_i r_{ij}u_j\right)\\&=\frac{1}{2}\left(\sum_{i=1}^{2n}u_i r_{ik}+\sum_{j=1}^{2n}r_{kj}u_j\right)=\frac{1}{2}\left(\sum_{i=1}^{2n}u_i r_{ik}+\sum_{i=1}^{2n}r_{ki}u_i\right)\end{aligned} \tag{4.76}$$

Because $[R]$ is a symmetrical matrix, $r_{ik}=r_{ki}$, $i,\ k=1,2,\ldots,2n$. Equation 4.76 then becomes

$$\frac{\partial}{\partial u_k}\left(\frac{1}{2}\{u(t)\}^{\mathrm{T}}[R]\{u(t)\}\right)=\frac{1}{2}\left(\sum_{i=1}^{2n}r_{ki}u_i+\sum_{i=1}^{2n}r_{ki}u_i\right)=\sum_{i=1}^{2n}r_{ki}u_i \tag{4.77}$$

thus

$$\frac{\partial}{\partial}\{u(t)\}\left(\frac{1}{2}\{u(t)\}^{\mathrm{T}}[R]\{u(t)\}\right)=[R]\{u(t)\} \tag{4.78}$$

Similarly,

$$\frac{\partial}{\partial\{u(t)\}}\left(\{\lambda\}^{\mathrm{T}}[B_{\mathrm{u}}]\{u(t)\}\right)=\frac{\partial}{\partial u_k}\left(\sum_{i=1}^{2n}\sum_{j=1}^{2n}\lambda_i b_{ij}u_j\right)=\sum_{i=1}^{2n}\lambda_i b_{ik}=\sum_{i=1}^{2n}b_{ik}\lambda_i \tag{4.79}$$

thus

$$\frac{\partial}{\partial\{u(t)\}}(\{\lambda\}^{\mathrm{T}}[B_{\mathrm{u}}]\{u(t)\}=[B_{\mathrm{u}}]^{\mathrm{T}}\{\lambda(t)\} \tag{4.80}$$

Substituting Equations 4.71, 4.73, 4.75, 4.78, and 4.80 into Equation 4.68 yields

$$\begin{cases}[Q]\{Z(t)\}+[A]^{\mathrm{T}}\{\lambda(t)\}+\{\dot{\lambda}(t)\}=\{0\}\\[R]\{u(t)\}+[B_{\mathrm{u}}]^{\mathrm{T}}\{\lambda(t)\}=\{0\}\end{cases} \tag{4.81}$$

From the second equation in Equation 4.81, we obtain

$$\{u(t)\} = -[R]^{-1}[B_{\mathrm{u}}]^{\mathrm{T}}\{\lambda(t)\} \tag{4.82}$$

Since, there is no control at final time t_{f}, that is,

$$\{u(t_{\mathrm{f}})\} = \{0\} \tag{4.83}$$

From Equation 4.83 it can be seen that in order to apply Equation 4.82 to every arbitrarily selected positive-definite matrix $[R]^{-1}$, $\{\lambda(t_{\mathrm{f}})\}$ should also be $\{0\}$. This is referred to as the *transversality condition* that must be satisfied by the solution of Euler equation at the endpoint t_{f}.

$$\{\lambda(t_{\mathrm{f}})\} = \{0\} \tag{4.84}$$

The first equation in Equation 4.81 expresses the relationship between $\{\lambda(t)\}$ and $\{Z(t)\}$. Its solution can be assumed as

$$\{\lambda(t)\} = [P(t)]\{Z(t)\} \tag{4.85}$$

in which $[P(t)]$ is to be determined. Substituting Equation 4.85 into the first equation in Equation 4.81 gives

$$[Q]\{Z(t)\} + [A]^{\mathrm{T}}[P(t)]\{Z(t)\} + [\dot{P}(t)]\{Z(t)\} + [P(t)]\{\dot{Z}(t)\} = 0 \tag{4.86}$$

where $\{\dot{Z}(t)\}$ can be determined as follows. Because functional $\mathcal{H}$ has nothing to do with $\{\dot{\lambda}(t)\}$ and the first two terms in $\mathcal{H}$ are not related to $\{\lambda(t)\}$, substituting Equation 4.66 into the third relationship in Equation 4.67 yields

$$\frac{\partial}{\partial\{\lambda(t)\}}\left[\{\lambda(t)\}^{\mathrm{T}}\left([A]\{Z(t)\} + [B_{\mathrm{u}}]\{u(t)\} - \{\dot{Z}(t)\}\right)\right] = 0 \tag{4.87}$$

Assume

$$\{V(t)\} = [A]\{Z(t)\} + [B_{\mathrm{u}}]\{u(t)\} - \{\dot{Z}(t)\} \tag{4.88}$$

and $v_i(t)$ is the ith element of $\{V(t)\}$. Then we obtain

$$\begin{aligned}&\frac{\partial}{\partial\lambda_k}\left[\{\lambda(t)\}^{\mathrm{T}}\left([A]\{Z(t)\} + [B_{\mathrm{u}}]\{u(t) - \{\dot{Z}(t)\}\right)\right]\\ &\quad = \frac{\partial}{\partial\lambda_k}\left[\{\lambda(t)\}^{\mathrm{T}}\{V(t)\}\right] = \frac{\partial}{\partial\lambda_k}\sum_{i=1}^{2n}\lambda_i v_i = v_k(t)\end{aligned} \tag{4.89}$$

Thus

$$\frac{\partial}{\partial\{\lambda(t)\}}\left[\{\lambda(t)\}^{\mathrm{T}}\{V(t)\}\right] = \{V(t)\} \tag{4.90}$$

Combining Equations 4.87, 4.88, and 4.90 yields

$$[A]\{Z(t)\} + [B_{\mathrm{u}}]\{u(t)\} - \{\dot{Z}(t)\} = 0 \tag{4.91}$$

that is,

$$\left\{\dot{Z}(t)\right\} = [A]\{Z(t)\} + [B_{\mathrm{u}}]\{u(t)\} \tag{4.92}$$

A comparison of Equations 4.92 and 4.19 shows that in the Riccati optimal algorithm, the earthquake excitation $\ddot{x}_{\mathrm{g}}(t)$ is not considered in determining control force. This weakness is further discussed in Section 4.3.

Combining Equation 4.82 and Equation 4.85 gives

$$\{u(t)\} = -[R]^{-1}[B_{\mathrm{u}}]^{\mathrm{T}}[P(t)]\{Z(t)\} \tag{4.93}$$

Substituting Equation 4.93 into Equation 4.92 yields

$$\{\dot{Z}(t)\} = [A]\{Z(t)\} - [B_{\mathrm{u}}][R]^{-1}[B_{\mathrm{u}}]^{\mathrm{T}}[P(t)]\{Z(t)\} \tag{4.94}$$

and similarly substituting Equation 4.94 into Equation 4.86 yields

$$\left([Q] + [A]^{\mathrm{T}}[P(t)] + [\dot{P}(t)] + [P(t)][A] - [P(t)][B_{\mathrm{u}}][R]^{-1}[B_{\mathrm{u}}]^{\mathrm{T}}[P(t)]\right)\{Z(t)\} = \{0\} \tag{4.95}$$

The tranversality condition expressed by Equation 4.84 can be rewritten using Equation 4.85

$$[P(t_{\mathrm{f}})]\{Z(t_{\mathrm{f}})\} = \{\lambda(t_{\mathrm{f}})\} = \{0\} \tag{4.96}$$

Equations 4.95 and 4.96 are valid for any state $\{Z(t)\}$ that cannot always be zero at any time instant. Thus, the nontrivial solution is

$$[\dot{P}(t)] + [P(t)][A] + [A]^{\mathrm{T}}[P(t)] - [P(t)][B_{\mathrm{u}}][R]^{-1}[B_{\mathrm{u}}]^{\mathrm{T}}[P(t)] + [Q] = [0] \tag{4.97a}$$

$$[P(t_{\mathrm{f}})] = [0] \tag{4.97b}$$

Equation 4.97, the *matrix Riccati equation* (MRE), is a nonlinear equation about $[P(t)]$. The scalar form of MRE can be written as

$$\dot{p}(t) + 2ap(t) - \frac{b_u^2}{r}p^2(t) + q = 0 \tag{4.98}$$

After the solution of MRE is found, it is substituted into Equation 4.93 to obtain the optimal control force. MRE can be solved by using various numerical algorithms [30,47]. One method is to directly use numerical integration, such as the standard Runge-Kutta method [7].

Note that the solution of MRE is time-dependent. Consequently, the gain matrix $[P(t)]$ in Equation 4.93 is also time-dependent. When the final time t_f approaches infinity, that is, $t_f = \infty$, it can be shown that the time-dependent MRE becomes time-invariant. In fact, solution of MRE can quickly reach a steady state. For example, the first-order system expressed by Equation 4.98 has a step response as shown in Figure 4.11, which quickly reaches a time-invariant steady state.

For a stable building structure, the Ricatti matrix $[P(t)]$ remains constant over the entire duration of an earthquake and drops rapidly to zero near t_f. In other words, $[P(t)]$ establishes a stationary state, and MRE becomes time-invariant. Thus, we can approximate $[P(t)]$ by $[\dot{P}(t)] = [0]$ or $[P(t)] = [P]$; and Equation 4.97 becomes an *algebraic Riccati equation* (ARE)

$$[P][A] + [A]^T[P] - [P][B_u][R]^{-1}[B_u]^T[P] + [Q] = 0 \tag{4.99}$$

Note that ARE is a time-invariant equation, which can be much more easily solved than MRE [41,43]. Then the control law expressed by Equation 4.93 becomes

$$\{u(t)\} = -[R]^{-1}[B_u]^T[P]\{Z(t)\} = -[G]\{Z(t)\} \tag{4.100}$$

where the control gain matrix

$$[G] = [R]^{-1}[B_u]^T[P] \tag{4.101}$$

is also time-invariant. Owing to this property, it is easier to solve an ARE than an MRE, and the ARE yields a proportional control law, that is, the control forces

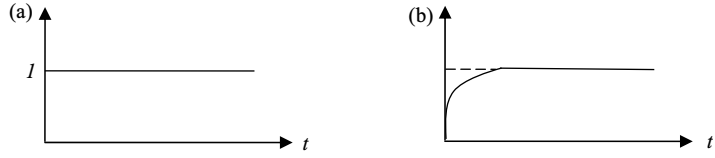

FIGURE 4.11 Step response of first-order system: (a) excitation and (b) response.

$\{u(t)\}$ is proportional to response $\{Z(t)\}$. Thus, the design of the controller can be simplified because the control law can be physically realized by an *amplifier*. A time-dependent control law using the MRE is difficult to implement from the standpoint of hardware realization.

When the ARE is lower-order, it can be solved by longhand calculation. However, special algorithms must be employed to solve the ARE when the system becomes higher-order due to the nonlinearity about $[P]$. An algorithm based on an iterative technique was presented by Kleinman [41]. Another algorithm developed by Laub [43] uses an eigenvector approach based on Schur vectors. Refer to these references for details.

It is worth noting that ROAC algorithm used here is a special case of *linear quadratic regulator* (LQR) in modern control theory [37,39]. The LQR quadratic cost function (performance index) is defined as

$$J = \frac{1}{2}\int_0^{\infty} \left(\{Z(t)\}^{\mathrm{T}}[Q]\{Z(t)\} + \{u(t)\}^{\mathrm{T}}[R]\{u(t)\} + 2\{Z(t)\}^{\mathrm{T}}[N]\{u(t)\}\right) \mathrm{d}t \tag{4.102}$$

If the seismic duration is $[t_0, t_{\mathrm{f}}]$, above index for seismic structures becomes

$$J = \frac{1}{2}\int_{t_0}^{t_{\mathrm{f}}} \left(\{Z(t)\}^{\mathrm{T}}[Q]\{Z(t)\} + \{u(t)\}^{\mathrm{T}}[R]\{u(t)\} + 2\{Z(t)\}^{\mathrm{T}}[N]\{u(t)\}\right) \mathrm{d}t \tag{4.103}$$

The associated ARE is

$$[P][A] + [A]^{\mathrm{T}}[P] - ([P][B_{\mathrm{u}}] + [N])\,[R]^{-1}\left([B_{\mathrm{u}}]^{\mathrm{T}}[P] + [N]^{\mathrm{T}}\right) + [Q] = 0 \tag{4.104}$$

And the control gain matrix is given by

$$[G] = [R]^{-1}\left([B_{\mathrm{u}}]^{\mathrm{T}}[P] + [N]^{\mathrm{T}}\right) \tag{4.105}$$

Note that Equation 4.104 degenerates into an ARE Equation 4.99 by setting $[N] = [0]$. Thus, LQR algorithm uses a more general ARE. Riccati and LQR algorithms have been implemented in commercial software packages such as MATLAB® functions *CARE* and *LQR*. Refer to Appendix A for details.

Example 4.2.1

Solve the algebraic Ricatti equation by longhand calculation. Matrices are given as

$$[A] = \begin{bmatrix} 0 & 1 \\ 0 & 0 \end{bmatrix}, \quad [B_u] = \begin{Bmatrix} 0 \\ 1 \end{Bmatrix}, \quad R = 1, \quad Q = \begin{bmatrix} 1 & 0 \\ 0 & 2 \end{bmatrix}$$

Solution

Substituting these matrices into the ARE equation 4.99 yields

$$\begin{bmatrix} p_{11} & p_{12} \\ p_{21} & p_{22} \end{bmatrix}\begin{bmatrix} 0 & 1 \\ 0 & 0 \end{bmatrix} + \begin{bmatrix} 0 & 0 \\ 1 & 0 \end{bmatrix}\begin{bmatrix} p_{11} & p_{12} \\ p_{21} & p_{22} \end{bmatrix} - \begin{bmatrix} p_{11} & p_{12} \\ p_{21} & p_{22} \end{bmatrix}\begin{bmatrix} 0 \\ 1 \end{bmatrix}[1]^{-1}\begin{bmatrix} 0 & 1 \end{bmatrix}\begin{bmatrix} p_{11} & p_{12} \\ p_{21} & p_{22} \end{bmatrix} + \begin{bmatrix} 1 & 0 \\ 0 & 2 \end{bmatrix} = \begin{bmatrix} 0 & 0 \\ 0 & 0 \end{bmatrix} \tag{a}$$

where $p_{ij}\,(i,j = 1,2)$ is the element of Ricatti matrix $[P]$ at ith row, jth column.

$$\begin{bmatrix} 0 & p_{11} \\ 0 & p_{21} \end{bmatrix} + \begin{bmatrix} 0 & 0 \\ p_{11} & p_{12} \end{bmatrix} - \begin{bmatrix} p_{12} \\ p_{22} \end{bmatrix}\begin{bmatrix} 0 & 1 \end{bmatrix}\begin{bmatrix} p_{11} & p_{12} \\ p_{21} & p_{22} \end{bmatrix} + \begin{bmatrix} 1 & 0 \\ 0 & 2 \end{bmatrix} = \begin{bmatrix} 0 & 0 \\ 0 & 0 \end{bmatrix} \tag{b}$$

$$\begin{bmatrix} 0 & p_{11} \\ p_{11} & p_{21}+p_{12} \end{bmatrix} - \begin{bmatrix} 0 & p_{12} \\ 0 & p_{22} \end{bmatrix}\begin{bmatrix} p_{11} & p_{12} \\ p_{21} & p_{22} \end{bmatrix} + \begin{bmatrix} 1 & 0 \\ 0 & 2 \end{bmatrix} = \begin{bmatrix} 0 & 0 \\ 0 & 0 \end{bmatrix} \tag{c}$$

$$\begin{bmatrix} -p_{12}p_{21}+1 & p_{11}-p_{12}p_{22} \\ p_{11}-p_{22}p_{21} & p_{21}+p_{12}-p_{22}^2+2 \end{bmatrix} = \begin{bmatrix} 0 & 0 \\ 0 & 0 \end{bmatrix} \tag{d}$$

$$\left\{ \begin{array}{l} \left.\begin{array}{c} p_{12}p_{21} = 1 \\ p_{11} = p_{12}p_{22} \\ p_{11} = p_{22}p_{21} \end{array}\right\} \Rightarrow p_{21} = p_{12} \Big\} \Rightarrow p_{21} = p_{12} = 1 \\ p_{22}^2 = p_{12} + p_{21} + 2 \end{array} \right\}$$

$$\Rightarrow p_{22}^2 = 4 \Rightarrow p_{22} = 2 \tag{e}$$

Thus

$$\left\{ \begin{array}{c} p_{11} = p_{12}p_{22} = 2 \\ p_{21} = p_{12} = 1 \\ p_{22} = 2 \end{array} \right. \Rightarrow [P] = \begin{bmatrix} 2 & 1 \\ 1 & 2 \end{bmatrix} \tag{f}$$

Example 4.2.2

A two-story shear building is installed with active tendons on each floor, as shown in Figure 4.12. Structural properties are mass $m_1 = 0.136$ k-s^2/in. (2.382×10^4 kg), $m_2 = 0.066$ k-s^2/in. (1.156×10^4 kg); stiffness $k_1 = 30.70$ k/in. (5.378×10^6 N/m), $k_2 = 44.30$ k/in. (7.760×10^6 N/m); and 1% damping ratios in both modes. Assume ground acceleration $\ddot{x}_g(t)$ has the shape shown in Figure 4.12c. Use ROAC algorithm to design the control system and find the response of the controlled structure.

Solution

(1) Mathematical model of the system: Motion equation of the controlled structure is

$$[M]\{\ddot{x}(t)\} + [C]\{\dot{x}(t)\} + [K]\{x(t)\} = [\gamma]\{u(t)\} + [\delta]\ddot{x}_g(t) \tag{a}$$

where

$$\{x(t)\} = \{x_1(t)\, x_2(t)\}^T \tag{b}$$

$$\{u(t)\} = \{u_1(t)\, u_2(t)\}^T \tag{c}$$

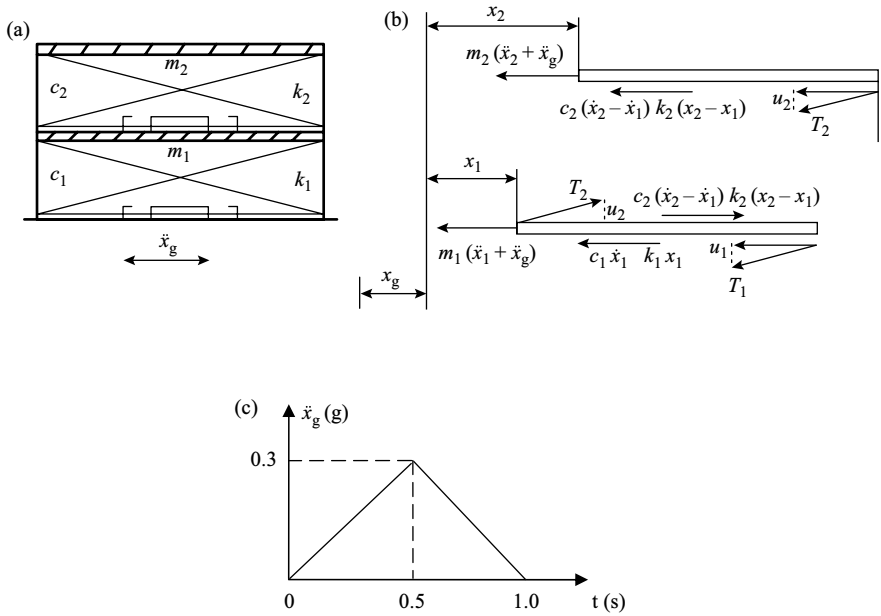

FIGURE 4.12 (a) Two-story structure with tendon control, (b) free-body diagram, and (c) excitation.

$$[M] = \begin{bmatrix} m_1 & 0 \\ 0 & m_2 \end{bmatrix} = \begin{bmatrix} 0.136 & \\ & 0.066 \end{bmatrix} \tag{d}$$

$$[K] = \begin{bmatrix} k_1 + k_2 & -k_2 \\ -k_2 & k_2 \end{bmatrix} = \begin{bmatrix} 75.00 & -44.30 \\ -44.30 & 44.30 \end{bmatrix} \tag{e}$$

$$[\gamma] = \begin{bmatrix} -1 & 1 \\ 0 & -1 \end{bmatrix} \tag{f}$$

$$\{\delta\} = -\begin{Bmatrix} m_1 \\ m_2 \end{Bmatrix} = -\begin{Bmatrix} 0.136 \\ 0.066 \end{Bmatrix} \tag{g}$$

and the damping matrix is given by [7]

$$[C] = \alpha[M] + \beta[K] \tag{h}$$

where

$$\alpha = 2\omega_1\omega_2\frac{\zeta_1\omega_2 - \zeta_2\omega_1}{\omega_2^2 - \omega_1^2}, \quad \beta = \frac{2(\zeta_2\omega_2 - \zeta_1\omega_1)}{\omega_2^2 - \omega_1^2} \tag{i}$$

In Equation i above, ω_1 and ω_2 are first and second natural frequencies; ζ_1 and ζ_2 are damping ratios of first and second modes that are given as

$$\zeta_1 = \zeta_2 = 1\% = 0.01 \tag{j}$$

ω_1 and ω_2 are roots of the characteristic equation

$$\left|-\omega^2[M] + [K]\right| = 0 \tag{k}$$

$$\begin{vmatrix} 75.00 - 0.136\omega^2 & -44.30 \\ -44.30 & 44.30 - 0.066\omega^2 \end{vmatrix} = 0 \tag{l}$$

$$\omega^4 - 1222.683\omega^2 + 151516.266 = 0 \tag{m}$$

$$\omega_1 = 11.829 \text{ rad/s}, \quad \omega_2 = 32.905 \text{ rad/s} \tag{n}$$

Substituting Equations j and n into Equation i yield

$$\begin{cases} \alpha = \dfrac{2(11.829)(32.905)(0.01)(32.095 - 11.829)}{32.905^2 - 11.829^2} = 0.174 \\ \beta = \dfrac{2(0.01)(32.905 - 11.829)}{32.905^2 - 11.829^2} = 4.471 \times 10^{-4} \end{cases} \tag{o}$$

Thus,

$$[C] = 0.174\begin{bmatrix} 0.136 & 0 \\ 0 & 0.066 \end{bmatrix} + 4.47 \times 10^{-4}\begin{bmatrix} 75.00 & -44.30 \\ -44.30 & 44.30 \end{bmatrix} = \begin{bmatrix} 0.0572 & -0.0198 \\ -0.0198 & 0.0313 \end{bmatrix} \quad \text{(p)}$$

By defining state vector

$$\{Z(t)\} = \{x_1(t) \quad x_2(t) \quad \dot{x}_1(t) \quad \dot{x}_2(t)\}^{\mathrm{T}} \quad \text{(q)}$$

Equation a can be rewritten as state equation

$$\{\dot{Z}(t)\} = [A]\{Z(t)\} + [B_{\mathrm{u}}]\{u(t)\} + \{B_{\mathrm{r}}\}\ddot{x}_{\mathrm{g}}(t) \quad \text{(r)}$$

where

$$[A] = \begin{bmatrix} [O] & [I] \\ -[M]^{-1}[K] & -[M]^{-1}[C] \end{bmatrix}, \quad [B_{\mathrm{u}}] = \begin{bmatrix} [0] \\ [M]^{-1}[\gamma] \end{bmatrix}, \quad \{B_{\mathrm{r}}\} = \begin{bmatrix} \{0\} \\ [M]^{-1}\{\delta\} \end{bmatrix} \quad \text{(s)}$$

Since

$$\begin{cases} [M]^{-1} = \begin{bmatrix} 0.136 & 0 \\ 0 & 0.066 \end{bmatrix}^{-1} = \begin{bmatrix} 7.353 & 0 \\ 0 & 15.152 \end{bmatrix} \\ [M]^{-1}[K] = \begin{bmatrix} 7.353 & 0 \\ 0 & 15.152 \end{bmatrix}\begin{bmatrix} 75.00 & -44.30 \\ -44.30 & 44.30 \end{bmatrix} = \begin{bmatrix} 551.475 & -325.738 \\ -671.234 & 671.234 \end{bmatrix} \\ [M]^{-1}[C] = \begin{bmatrix} 7.353 & 0 \\ 0 & 15.152 \end{bmatrix}\begin{bmatrix} 0.0572 & -0.0198 \\ -0.0198 & 0.0313 \end{bmatrix} = \begin{bmatrix} 0.421 & -0.146 \\ -0.300 & 0.474 \end{bmatrix} \\ [M]^{-1}[\gamma] = \begin{bmatrix} 7.353 & 0 \\ 0 & 15.152 \end{bmatrix}\begin{bmatrix} -1 & 1 \\ 0 & -1 \end{bmatrix} = \begin{bmatrix} -7.353 & 7.353 \\ 0 & -15.152 \end{bmatrix} \\ [M]^{-1}\{\delta\} = \begin{bmatrix} 7.353 & 0 \\ 0 & 15.152 \end{bmatrix}\begin{Bmatrix} -0.136 \\ -0.066 \end{Bmatrix} = \begin{Bmatrix} -1 \\ -1 \end{Bmatrix} \end{cases} \quad \text{(t)}$$

$$[A] = \left[\begin{array}{cc|cc} 0 & 0 & 1 & 0 \\ 0 & 0 & 0 & 1 \\ \hline -551.475 & 325.738 & -0.421 & 0.146 \\ 671.234 & -671.234 & 0.300 & -0.474 \end{array}\right]$$

$$[B_u] = \begin{bmatrix} 0 & 0 \\ 0 & 0 \\ -7.353 & 7.353 \\ 0 & -15.152 \end{bmatrix}, \quad \{B_r\} = \begin{Bmatrix} 0 \\ 0 \\ -1 \\ -1 \end{Bmatrix} \tag{u}$$

(2) Controller design: Let

$$[Q] = \begin{bmatrix} 1.0 & & & \\ & 1.0 & & \\ & & 1.0 & \\ & & & 1.0 \end{bmatrix}, \quad [R] = \begin{bmatrix} 0.01 & 0 \\ 0 & 0.01 \end{bmatrix} \tag{v}$$

The Riccati matrix $[P]$ satisfies Equation 4.99. With matrices $[A]$, $[B_u]$, $[Q]$, and $[R]$ given in Equations u and v, the Riccati matrix is obtained as

$$[P] = \begin{bmatrix} 5.068 & -2.176 & 1.368 \times 10^{-2} & 1.168 \times 10^{-2} \\ & 3.962 & -1.078 \times 10^{-2} & -4.958 \times 10^{-3} \\ & & 1.304 \times 10^{-2} & 4.241 \times 10^{-3} \\ symm & & & 8.271 \times 10^{-3} \end{bmatrix} \tag{w}$$

$$[R]^{-1}[B_u]^T = \begin{bmatrix} 0.01 & 0 \\ 0 & 0.01 \end{bmatrix}^{-1} \left[\begin{array}{cc} 0 & 0 \\ 0 & 0 \\ \hline -7.353 & 7.353 \\ 0 & -15.152 \end{array}\right]^T$$

$$= \left[\begin{array}{cc|cc} 100 & 0 & & \\ 0 & 100 & & \end{array}\right] \left[\begin{array}{cc|cc} 0 & 0 & -7.353 & 0 \\ 0 & 0 & 7.353 & -15.152 \end{array}\right]$$

$$= \begin{bmatrix} 0 & 0 & -735.3 & 0 \\ 0 & 0 & 735.3 & -1515.2 \end{bmatrix} \tag{x}$$

Thus, the control gain matrix can be obtained from Equation 4.101 as

$$[G] = [R]^{-1}[B_u]^T[P]$$

$$= \begin{bmatrix} 0 & 0 & -735.3 & 0 \\ 0 & 0 & 735.3 & -1515.2 \end{bmatrix}$$

$$\times \begin{bmatrix} 5.068 & -2.176 & 1.368 \times 10^{-2} & 1.168 \times 10^{-2} \\ & 3.962 & -1.078 \times 10^{-2} & -4.958 \times 10^{-3} \\ & & 1.304 \times 10^{2} & 4.241 \times 10^{-3} \\ symm & & & 8.271 \times 10^{-3} \end{bmatrix}$$

$$= \begin{bmatrix} -10.06 & 7.93 & -9.59 & -3.12 \\ -7.64 & -0.42 & 3.16 & -9.41 \end{bmatrix} \quad \text{(y)}$$

(3) Calculation of controlled-structure response: The transformation matrix $[T]$ is eigenvector of matrix $[A]$ that is calculated as

$$[T] = \begin{bmatrix} -6.653 \times 10^{-4} & -6.690 \times 10^{-2} & 1.861 \times 10^{-4} & 1.864 \times 10^{-2} \\ -8.417 \times 10^{-4} & -8.453 \times 10^{-2} & -3.035 \times 10^{-4} & -3.038 \times 10^{-2} \\ 0.7915 & 0 & -0.6132 & 0 \\ 1.000 & 0 & 1.000 & 0 \end{bmatrix} \quad \text{(z)}$$

$$[T]^{-1} = \begin{bmatrix} 4.208 \times 10^{-4} & 3.925 \times 10^{-4} & 0.7119 & 0.4365 \\ -8.421 & -5.165 & -7.084 \times 10^{-3} & -4.344 \times 10^{-3} \\ -4.209 \times 10^{-4} & -3.924 \times 10^{-4} & -0.7119 & 0.5635 \\ 23.430 & -18.540 & 7.097 \times 10^{-3} & -5.638 \times 10^{-3} \end{bmatrix} \quad \text{(aa)}$$

$$[T]^{-1}[B_u] = \begin{bmatrix} 4.208 \times 10^{-4} & 3.925 \times 10^{-4} & 0.7119 & 0.4365 \\ -8.421 & -5.165 & -7.084 \times 10^{-3} & -4.344 \times 10^{-3} \\ -4.209 \times 10^{-4} & -3.924 \times 10^{-4} & -0.7119 & 0.5635 \\ 23.430 & -18.540 & 7.09 \times 10^{-3} & -5.638 \times 10^{-3} \end{bmatrix}$$

$$\begin{bmatrix} 0 & 0 \\ 0 & 0 \\ -7.353 & 7.353 \\ 0 & -15.152 \end{bmatrix} = \begin{bmatrix} -5.235 & -1.379 \\ 0.052 & 0.014 \\ 5.235 & -13.770 \\ -0.052 & 0.138 \end{bmatrix} \quad \text{(bb)}$$

$$[T]^{-1}\{B_r\} = \begin{bmatrix} 4.208 \times 10^{-4} & 3.925 \times 10^{-4} & 0.7119 & 0.4365 \\ -8.421 & -5.165 & -7.084 \times 10^{-3} & -4.344 \times 10^{-3} \\ -4.209 \times 10^{-4} & -3.924 \times 10^{-4} & -0.7119 & 0.5635 \\ 23.430 & -18.540 & 7.097 \times 10^{-3} & -5.638 \times 10^{-3} \end{bmatrix}$$

$$\begin{Bmatrix} 0 \\ 0 \\ -1 \\ -1 \end{Bmatrix} = \begin{Bmatrix} -1.148 \\ 1.143 \times 10^{-2} \\ 0.1484 \\ -1.459 \times 10^{-3} \end{Bmatrix} \quad \text{(cc)}$$

From Equation 4.32 $[\Phi] = [T]^{-1}\,[A][T]$ we obtain

$$[\Phi] = \left[\begin{array}{cc|cc} -0.1183 & 11.829 & 0 & 0 \\ -11.829 & -0.1183 & 0 & 0 \\ \hline 0 & 0 & -0.3291 & 32.093 \\ 0 & 0 & -32.903 & -0.3291 \end{array}\right] \quad \text{(dd)}$$

Let the time increment be $\Delta t = 0.01$ s; then Equation 4.44 yields

$$\exp([\Phi]\Delta t) = \begin{bmatrix} \exp(-0.1183 \times 0.01) \begin{bmatrix} \cos(11.829 \times 0.01) & \sin(11.829 \times 0.01) \\ -\sin(11.829 \times 0.01) & \cos(11.829 \times 0.01) \end{bmatrix} & [0]_{2\times 2} \\ [0]_{2\times 2} & \exp(-0.3291 \times 0.01) \begin{bmatrix} \cos(32.903 \times 0.01) & \sin(32.903 \times 0.01) \\ -\sin(32.903 \times 0.01) & \cos(32.903 \times 0.01) \end{bmatrix} \end{bmatrix}$$

$$= \begin{bmatrix} 0.9988 \begin{bmatrix} 0.9930 & 0.1180 \\ -0.1180 & 0.9930 \end{bmatrix} & [0]_{2\times 2} \\ [0]_{2\times 2} & 0.9967 \begin{bmatrix} 0.9464 & 0.3231 \\ -0.3231 & 0.9464 \end{bmatrix} \end{bmatrix}$$

$$= \begin{bmatrix} 0.9918 & 0.1179 & 0 & 0 \\ -0.1179 & 0.9918 & 0 & 0 \\ 0 & 0 & 0.9432 & 0.3221 \\ 0 & 0 & -0.3221 & 0.9432 \end{bmatrix} \tag{ee}$$

At time $t_o = 0.00$ s, initial conditions are

$$\ddot{x}_g(0) = 0, \quad \{u(0)\} = \{0\}, \quad \{Z(0)\} = \{0\} \tag{ff}$$

From Equations 4.28, 4.33, and 4.39 we obtain

$$\begin{cases} \{\psi(0)\} = [T]^{-1}\{Z(0)\} = \{0\} \\ \{\Gamma(0)\} = [T]^{-1}\{B_u\}\{u(0)\} + [T]^{-1}\{B_r\}\ddot{x}_g(0) = \{0\} \\ \{\Lambda(0)\} = \exp([0])\{\Gamma(0)\} = \{0\} \end{cases} \tag{gg}$$

At time $t_1 = \Delta t = 0.01$ s.

$$\{\Gamma(t_1)\} = [T]^{-1}[B_u]\{u(t_1)\} + [T]^{-1}\{B_r\}\ddot{x}_g(t_1)$$

$$= \{0\} + \begin{Bmatrix} -1.148 \\ 1.143 \times 10^{-2} \\ 0.1484 \\ -1.459 \times 10^{-3} \end{Bmatrix} \left[\frac{0.01}{0.5}(0.3)(386.4)\right]$$

$$= \begin{Bmatrix} -2.662 \\ 2.649 \times 10^{-2} \\ 0.344 \\ -3.383 \times 10^{-3} \end{Bmatrix} \tag{hh}$$

where control force $\{u(t)\}$ is treated as zero between $t_0 = 0$ and $t_1 = \Delta t$. Rectangular rule is used for approximation of $\{u(t)\}$, which means between $k\Delta t$ and $(k+1)\Delta t$, $\{u(t)\} = \{u(k\Delta t)\}$, and Equation 4.33 becomes Equation hh.

From Equation 4.40, we have

$$\{\psi(t_1)\} = \{\Lambda(t_1 - \Delta t)\} + \{\Gamma(t_1)\}\frac{\Delta t}{2}$$

$$= \{\Lambda(0)\} + \begin{Bmatrix} -2.662 \\ 2.649 \times 10^{-2} \\ 0.344 \\ -3.383 \times 10^{-3} \end{Bmatrix} \frac{0.01}{2} = \begin{Bmatrix} -1.331 \times 10^{-2} \\ 1.325 \times 10^{-4} \\ 1.720 \times 10^{-3} \\ -1.692 \times 10^{-5} \end{Bmatrix} \quad \text{(ii)}$$

The state vector is then obtained from Equation 4.42

$$\{Z(t_1)\} = [T]\{\psi(t_1)\}$$

$$= \begin{bmatrix} -6.653 \times 10^{-4} & -6.690 \times 10^{-2} & 1.861 \times 10^{-4} & 1.864 \times 10^{-2} \\ -8.417 \times 10^{-4} & -8.453 \times 10^{-2} & -3.035 \times 10^{-4} & -3.038 \times 10^{-2} \\ 0.7915 & 0 & -0.6132 & 0 \\ 1.0 & 0 & 1.0 & 0 \end{bmatrix}$$

$$\times \begin{bmatrix} -1.331 \times 10^{-2} \\ 1.325 \times 10^{-4} \\ 1.720 \times 10^{-3} \\ -1.692 \times 10^{-5} \end{bmatrix}$$

$$= \begin{Bmatrix} -4.404 \times 10^{-9} \\ -5.188 \times 10^{-9} \\ -1.159 \times 10^{-2} \\ -1.159 \times 10^{-2} \end{Bmatrix} \quad \text{(jj)}$$

Using Equation 4.23 and numerical values in Equations y and jj, we obtain

$$\{u(t_1)\} = -[G]\{Z(t_1)\}$$

$$= -\begin{bmatrix} -10.06 & 7.93 & -9.59 & -3.12 \\ -7.64 & -0.42 & 3.16 & -9.41 \end{bmatrix} \begin{Bmatrix} -4.404 \times 10^{-9} \\ -5.188 \times 10^{-9} \\ -1.159 \times 10^{-2} \\ -1.159 \times 10^{-2} \end{Bmatrix}$$

$$= \begin{Bmatrix} -0.1473 \\ -0.0724 \end{Bmatrix} \text{kips} \quad \text{(kk)}$$

At $t_2 = 2$, $\Delta t = 0.02\,\text{s}$, $t_2 - \Delta t = t_1$, the above procedures are repeated

$$\{\Gamma(t_2)\} = [T]^{-1}[B_\text{u}]\{u(t_2)\} + [T]^{-1}\{B_\text{r}\}\ddot{x}_\text{g}(t_2)$$

$$= \begin{bmatrix} -5.235 & -1.379 \\ 0.052 & 0.014 \\ 5.235 & -13.770 \\ -0.052 & 0.138 \end{bmatrix} \begin{Bmatrix} -0.1473 \\ -0.0724 \end{Bmatrix}$$

$$+\begin{Bmatrix} -1.148 \\ 1.143\times10^{-2} \\ 0.1484 \\ -1.459\times10^{-3} \end{Bmatrix}\left[\frac{0.02}{0.5}(0.3)(386.4)\right]$$

$$=\begin{Bmatrix} 0.871 \\ -8.670\times10^{-3} \\ 0.227 \\ -2.280\times10^{-3} \end{Bmatrix}+\begin{Bmatrix} -5.325 \\ 0.053 \\ 0.688 \\ -0.007 \end{Bmatrix}=\begin{Bmatrix} -4.454 \\ 0.044 \\ 0.915 \\ -0.009 \end{Bmatrix} \tag{ll}$$

$$\{\psi(t_2)\}=\{\Lambda(t_2-\Delta t)\}+\{\Gamma(t_2)\}\frac{\Delta t}{2}=\{\Lambda(t_1)\}+\{\Gamma(t_2)\}\frac{\Delta t}{2}$$

$$=\begin{Bmatrix} -2.637\times10^{-2} \\ 3.401\times10^{-3} \\ 3.233\times10^{-3} \\ 1.140\times10^{-3} \end{Bmatrix}+\begin{Bmatrix} -4.454 \\ 0.044 \\ 0.915 \\ -0.009 \end{Bmatrix}\frac{0.01}{2}=\begin{Bmatrix} -4.864 \\ 0.362 \\ 0.781 \\ -0.118 \end{Bmatrix}\times10^{-2} \tag{mm}$$

where

$$\{\Lambda(t_1)\}=\exp([\Phi]\,\Delta t)\,\{\Gamma(t_1)\}\,\Delta t$$

$$=\begin{bmatrix} 0.9918 & 0.1179 & 0 & 0 \\ -0.1179 & 0.9918 & 0 & 0 \\ 0 & 0 & 0.9432 & 0.3221 \\ 0 & 0 & -0.3221 & 0.9432 \end{bmatrix}\begin{Bmatrix} -2.662 \\ 2.649\times10^{-2} \\ 0.344 \\ -3.383\times10^{-3} \end{Bmatrix}(0.01) \tag{nn}$$

$$=\begin{Bmatrix} -2.637\times10^{-2} \\ 3.401\times10^{-3} \\ 3.233\times10^{-3} \\ -1.140\times10^{-3} \end{Bmatrix}$$

$$\{Z(t_2)\}=[T]\{\psi(t_2)\}$$

$$=\begin{bmatrix} -6.653\times10^{-4} & -6.690\times10^{-2} & 1.861\times10^{-4} & 1.864\times10^{-2} \\ -8.417\times10^{-2} & -8.453\times10^{-2} & -3.035\times10^{-4} & -3.038\times10^{-2} \\ 0.7915 & 0 & -0.6132 & 0 \\ 1.0 & 0 & 1.0 & 0 \end{bmatrix}$$

$$\begin{Bmatrix} -4.864 \\ 0.362 \\ 0.781 \\ -0.118 \end{Bmatrix}\times10^{-2}=\begin{Bmatrix} -2.230\times10^{-4} \\ -2.232\times10^{-4} \\ -4.329\times10^{-2} \\ -4.080\times10^{-2} \end{Bmatrix} \tag{oo}$$

$$\{u(t_2)\}=-[G]\{Z(t_2)\}$$

$$=-\begin{bmatrix} -10.06 & 7.93 & -9.59 & -3.12 \\ -7.64 & -0.42 & 3.16 & -9.41 \end{bmatrix}\begin{Bmatrix} -2.230\times10^{-4} \\ -2.232\times10^{-4} \\ -4.329\times10^{-2} \\ -4.080\times10^{-2} \end{Bmatrix}=\begin{Bmatrix} -0.543 \\ -0.249 \end{Bmatrix}\text{ kips} \tag{pp}$$

4.2.2 Pole Placement Algorithm

Pole placement method, also referred to as *pole assignment method*, is another effective classical algorithm in modern control theory [37,39]. As discussed in Section 4.1.3, the plant matrix $[A]$ of open-loop system described by Equation 4.19 determines the system dynamics in that the eigenvalues of matrix $[A]$ provide the open-loop modal damping and stiffness characteristics. Similarly, the eigenvalues of plant matrix $[A_c]$ for the closed-loop system described by Equation 4.24 defines the closed-loop modal damping and natural frequencies. As shown by Equation (4.24b), the closed-loop plant matrix $[A_c] = [A] - [B_u][G]$ and its eigenvalues are generally different from those of open-loop plant matrix $[A]$. This is because the active control modified the system plant matrix by feedback gain $[G]$ and thus altered the modal damping ratios and frequencies. From the theory of structural dynamics, modal damping and frequencies determines a system's behavior and response to external excitations. Thus, the desired eigenvalues of the controlled system can be selected first based on the required response, and then the corresponding feedback control gain is determined by these preselected closed-loop system eigenvalues (poles). This control strategy led to the *pole placement algorithm*, which have been widely applied in electrical and mechanical fields [37,40]. Compared to Riccati/LQR algorithms that determine optimal feedback gain directly by solving Riccati equations, pole placement algorithm derives the feedback gain such that the closed-loop system has preselected poles. A system must be fully controllable in order to use pole placement method to design the feedback controller. Several pole placement algorithms have been developed [2,39,40] and readers can refer to these publications for details. Pole assignment algorithms are also implemented in commercial software packages such as MATLAB® *ACKER* and *PLACE* functions. Refer to Appendix A for details.

Application of pole placement algorithm to smart civil engineering structures is very promising and convenient. This is because structural wind response normally has only one dominant mode, and structural seismic response typically only has a few significant modes. The small number of significant modes makes the closed-loop eigenvalues be easily and clearly selected to achieve a control goal, as attentions only need to be paid to the significant modes.

Example 4.2.3

Consider the active-controlled structure in Example 4.2.2. Use pole placement method to design the active control system with velocity feedback so that the closed-loop system doubles the open-loop modal damping.

Solution

The state equation of the system has been derived in Example 4.2.2 as

$$\left\{\dot{Z}(t)\right\} = [A]\{Z(t)\} + [B_u]u(t) + \{B_r\}\ddot{x}_g(t) \qquad \text{(a)}$$

where the coefficient matrices and vector are

$$[A] = \begin{bmatrix} [0] & [I] \\ -[M]^{-1}[K] & -[M]^{-1}[C] \end{bmatrix}$$

$$= \left[\begin{array}{cc|cc} 0 & 0 & 1 & 0 \\ 0 & 0 & 0 & 1 \\ \hline -551.471 & 325.735 & -0.421 & 0.146 \\ 671.212 & -671.212 & 0.300 & -0.474 \end{array}\right] \quad \text{(b)}$$

$$[B_u] = \begin{bmatrix} 0 & 0 \\ 0 & 0 \\ \hline -7.353 & 7.353 \\ 0 & -15.152 \end{bmatrix}, \quad \{B_r\} = \begin{Bmatrix} 0 \\ 0 \\ -1 \\ -1 \end{Bmatrix} \quad \text{(c)}$$

As noted, the poles of this open-loop system are the eigenvalues of plant matrix $[A]$. They can be easily solved by MATLAB® function *eig*(A) as

$$\begin{cases} p_{1,2} = -0.1183 \pm 11.8289j \\ p_{3,4} = -0.3291 \pm 32.9035j \end{cases} \quad \text{(d)}$$

When the system damping ratios and natural frequencies are known, the system poles can also be calculated by Equation 4.22

$$\begin{cases} p_{1,2} = -\zeta_1\omega_1 \pm \sqrt{1-\zeta_1^2}\omega_1^2 j \\ p_{3,4} = -\zeta_2\omega_2 \pm \sqrt{1-\zeta_2^2}\omega_2^2 j \end{cases} \quad \text{(e)}$$

Thus, the poles in Equation d correspond to the following modal damping ratios and frequencies, respectively

$$\begin{cases} \zeta_1 = 0.01 \quad \omega_1 = 11.830 \text{ rad/s} \\ \zeta_1 = 0.01 \quad \omega_2 = 32.905 \text{ rad/s} \end{cases} \quad \text{(f)}$$

And mode shapes are

$$[\phi] = [\phi_1 \quad \phi_2] = \begin{bmatrix} 0.621 & -0.523 \\ 0.784 & 0.853 \end{bmatrix} \quad \text{(g)}$$

From the theory of structural dynamics [7] we have

$$\begin{cases} [\phi]^{-1}\left(-[M]^{-1}[K]\right)[\phi] = \begin{bmatrix} -\omega_1^2 & 0 \\ 0 & -\omega_2^2 \end{bmatrix} \\ [\phi]^{-1}\left(-[M]^{-1}[C]\right)[\phi] = \begin{bmatrix} -2\zeta_1\omega_1 & 0 \\ 0 & -2\zeta_2\omega_2 \end{bmatrix} \end{cases} \tag{h}$$

Augmenting the mode shapes into the following form

$$[\Phi] = \begin{bmatrix} [\phi] & [0] \\ [0] & [\phi] \end{bmatrix} \tag{i}$$

Then we have the modal decomposition for plant matrix of the state equation

$$\begin{aligned} [\Phi]^{-1}[A][\Phi] &= \begin{bmatrix} [\phi]^{-1} & [0] \\ [0] & [\phi]^{-1} \end{bmatrix} \begin{bmatrix} [0] & [I] \\ -[M]^{-1}[K] & -[M]^{-1}[C] \end{bmatrix} \begin{bmatrix} [\phi] & [0] \\ [0] & [\phi] \end{bmatrix} \\ &= \begin{bmatrix} [0] & [I] \\ [\phi]^{-1}\left(-[M]^{-1}[K]\right)[\phi] & [\phi]^{-1}\left(-[M]^{-1}[C]\right)[\phi] \end{bmatrix} \\ &= \begin{bmatrix} 0 & 0 & 1 & 0 \\ 0 & 0 & 0 & 1 \\ -\omega_1^2 & 0 & -2\zeta_1\omega_1 & 0 \\ 0 & -\omega_2^2 & 0 & -2\zeta_2\omega_2 \end{bmatrix} \end{aligned} \tag{j}$$

From the theory of Linear Algebra, it can be easily proved that matrix $[A]$ has the same eigenvalues as matrix $[\Phi]^{-1}[A][\Phi]$. As specified, modal damping ratios of the closed-loop system are double of those of the open-loop system. Thus, the closed-loop system will have the following modal damping ratios and frequencies

$$\begin{cases} \hat{\zeta}_1 = 0.02 \quad \hat{\omega}_1 = 11.830 \text{ rad/s} \\ \hat{\zeta}_2 = 0.02 \quad \hat{\omega}_2 = 32.905 \text{ rad/s} \end{cases} \tag{k}$$

Then substituting Equation k into Equation 4.22 yields the desired closed-loop poles

$$\begin{cases} \hat{p}_{1,2} = -0.2366 \pm 11.8271j \\ \hat{p}_{3,4} = -0.6581 \pm 32.8985j \end{cases} \tag{l}$$

According to Equation 4.26, the gain matrix of velocity feedback can be assumed as

$$[G] = \begin{bmatrix} 0 & 0 & g_1 & g_2 \\ 0 & 0 & g_3 & g_4 \end{bmatrix} \tag{m}$$

where $g_1 \sim g_4$ are four unknowns to be determined. Then substituting Equations b, c, and m into Equation 4.24b yields closed-loop plant matrix

$$
\begin{aligned}
[A_c] &= [A] - [B_u][G] \\
&= \begin{bmatrix} 0 & 0 & 1 & 0 \\ 0 & 0 & 0 & 1 \\ -551.471 & 325.735 & -0.421 & 0.146 \\ 671.212 & -671.212 & 0.300 & -0.474 \end{bmatrix} \\
&\quad - \begin{bmatrix} 0 & 0 \\ 0 & 0 \\ -7.353 & 7.353 \\ 0 & -15.152 \end{bmatrix} \begin{bmatrix} 0 & 0 & g_1 & g_2 \\ 0 & 0 & g_3 & g_4 \end{bmatrix} \\
&= \begin{bmatrix} 0 & 0 & 1 & 0 \\ 0 & 0 & 0 & 1 \\ -551.471 & 325.735 & -0.421 - 7.353g_1 + 7.353g_3 & 0.146 - 7.353g_2 + 7.353g_4 \\ 671.212 & -671.212 & 0.300 - 15.152g_3 & -0.474 - 15.152g_4 \end{bmatrix}
\end{aligned} \tag{n}
$$

Thus from Equation i

$$
\begin{aligned}
[\Phi]^{-1}[A_c][\Phi] &= \begin{bmatrix} 0 & 0 & 1 & 0 \\ 0 & 0 & 0 & 1 \\ -\hat{\omega}_1^2 & 0 & -2\hat{\zeta}_1\hat{\omega}_1 & 0 \\ 0 & -\hat{\omega}_2^2 & 0 & -2\hat{\zeta}_2\hat{\omega}_2 \end{bmatrix} \\
&= \begin{bmatrix} 0 & 0 & 1 & 0 \\ 0 & 0 & 0 & 1 \\ -139.937 & 0 & -0.473 & 0 \\ 0 & -1082.746 & 0 & -1.316 \end{bmatrix}
\end{aligned} \tag{o}
$$

With left multiplying $[\Phi]$ and right multiplying $[\Phi]^{-1}$, the above equation becomes

$$
[A_c] = \begin{bmatrix} 0 & 0 & 1 & 0 \\ 0 & 0 & 0 & 1 \\ -551.471 & 325.735 & -0.841 & 0.291 \\ 671.212 & -671.212 & 0.600 & -0.948 \end{bmatrix} \tag{p}
$$

Comparing Equations n and p yields the following four equations:

$$\begin{cases} -0.421 - 7.353g_1 + 7.353g_3 = 0.841 \\ 0.146 - 7.353g_2 + 7.353g_4 = 0.291 \\ 0.300 - 15.152g_3 = 0.600 \\ -0.474 - 15.152g_4 = -0.948 \end{cases} \quad \text{(q)}$$

that can solve the four unknown elements of the gain matrix as follows:

$$g_1 = 0.0374, \quad g_2 = 0.0115, \quad g_3 = -0.0198, \quad g_4 = 0.0313 \quad \text{(r)}$$

Then substituting Equation r into Equation m yields the velocity feedback control gain matrix

$$[G] = \begin{bmatrix} 0 & 0 & 0.0374 & 0.0115 \\ 0 & 0 & -0.0198 & 0.0313 \end{bmatrix} \quad \text{(s)}$$

With the feedback gain matrix determined, the closed-loop plant matrix can be calculated by Equation 4.24b, and then the seismic response of the controlled structure can be solved by the procedure described in Section 4.1.5, the same as Example 4.2.2.

4.3 Development of Active Control Algorithms for Seismic Smart Structures

As noted in Section 4.2, ROAC algorithm is based on performance integrated over the entire duration of the earthquake excitation. The control force is determined by minimizing this performance index J defined in Equation 4.63. This minimization is a *variational problem* with two fixed boundary values at $t = t_0$ and $t = t_f$. The solution of this variational problem means making a family of comparison functions and finding the extremal from them (see Figure 4.13). The extremal corresponds to the minimum value of performance index J. However, there is no guarantee that this extremal is optimum at any time-instant t_i or any time interval $[t_{i-1}, t_i]$. Furthermore, the earthquake excitation term is ignored in the derivation of the Riccati matrix $[P]$. Because of this neglect, the minimum value of the performance is always zero. In other words, the most optimum case without considering the external excitation is the system without response. Obviously, this is not the original objective of the active control design. The shortcomings of ROAC led to the development of *instantaneous optimal active control* (IOAC) *algorithm*, as discussed in the following section.

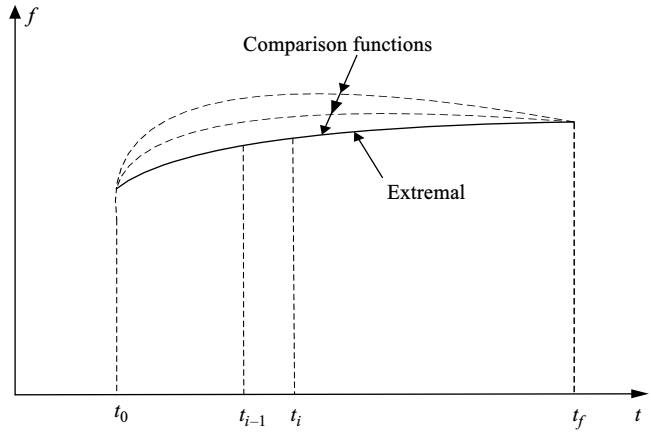

FIGURE 4.13 Solution of variational problems with fixed ends.

4.3.1 Instantaneous Optimal Active Closed-Loop Control Algorithm

Instead of minimizing the integral performance index in the Riccati algorithm, a sequence of single-stage processes was minimized to achieve optimality at each instant of time. This concept led to the advent of the IOAC and "per-interval" optimal controller [16,17,48]. Yang, Akbarpour, and Ghaemmaghami [48] adopted this idea for control of earthquake-excited structures. Cheng and Pantelides [13–15] extended the same concept to the optimum design of seismic structures equipped with AMD and active tendons. Cheng and Pantelides also applied this algorithm to optimal control of wind-excitated structures [16–18]. IOAC algorithm derives optimal control force $\{u(t)\}$ by minimizing an instantaneous time-dependent performance index $J_{\mathrm{p}}(t)$ rather than ROAC integral performance index J

$$J_{\mathrm{p}}(t) = \{Z(t)\}^{\mathrm{T}}[Q]\{Z(t)\} + \{u(t)\}^{\mathrm{T}}[R]\{u(t)\} \tag{4.106}$$

where $\{Z(t)\}$ and $\{u(t)\}$ are defined in Equations 4.20a and 4.4f, respectively. Performance index $J_{\mathrm{p}}(t)$ is minimized at every time-instant t in the interval of earthquake duration, $t_0 \leq t \leq t_{\mathrm{f}}$. Note that optimal control force $\{u(t)\}$ also satisfies the state equation, Equation 4.19, and its alternative form, Equation 4.42. Substituting Equation 4.42 into Equation 4.106 yields

$$\begin{aligned} J_{\mathrm{p}}(t) = &\left\{[T]\left(\{\Lambda(t-\Delta t)\} + \{\Gamma(t)\}\left(\frac{\Delta t}{2}\right)\right)\right\}^{\mathrm{T}}[Q] \\ &\times \left\{[T]\left(\{\Lambda(t-\Delta t)\} + \{\Gamma(t)\}\left(\frac{\Delta t}{2}\right)\right)\right\} + \{u(t)\}^{\mathrm{T}}[R]\{u(t)\} \end{aligned} \tag{4.107}$$

which can be simplified as

$$J_{\mathrm{p}}(t) = \left(\{\Lambda(t-\Delta t)\}^{\mathrm{T}} + \{\Gamma(t)\}^{\mathrm{T}}\left(\frac{\Delta t}{2}\right)\right)[T]^{\mathrm{T}}[Q][T] \times \left(\{\Lambda(t-\Delta t)\} + \{\Gamma(t)\}\left(\frac{\Delta t}{2}\right)\right) + \{u(t)\}^{\mathrm{T}}[R]\{u(t)\} \tag{4.108}$$

The Lagrangian function is given by

$$\mathrm{LF} = \{Z(t)\}^{\mathrm{T}}[Q]\{Z(t)\} + \{u(t)\}^{\mathrm{T}}[R]\{u(t)\} + \{\lambda(t)\}^{\mathrm{T}}\left(\{Z(t)\} - [T]\{\Lambda(t-\Delta t)\} - [T]\{\Gamma(t)\}(\Delta t/2)\right) \tag{4.109}$$

Substituting $\{\Gamma(t)\}$ of Equation 4.33 into above equation yields

$$\mathrm{LF} = \{Z(t)\}^{\mathrm{T}}[Q]\{Z(t)\} + \{u(t)\}^{\mathrm{T}}[R]\{u(t)\} + \{\lambda(t)\}^{\mathrm{T}}\left(\{Z(t)\} - [T]\{\Lambda(t-\Delta t)\} - \left([B_{\mathrm{u}}]\{u(t)\} + [B_{\mathrm{r}}]\ddot{x}_{\mathrm{g}}(t)\right)(\Delta t/2)\right) \tag{4.110}$$

The necessary conditions for optimality are

$$\begin{cases} \dfrac{\partial \mathrm{LF}}{\partial\{Z(t)\}} = \{0\} \Rightarrow 2[Q]\{Z(t)\} + \{\lambda(t)\} = \{0\} \\ \dfrac{\partial \mathrm{LF}}{\partial\{u(t)\}} = \{0\} \Rightarrow 2[R]\{u(t)\} - [B_{\mathrm{u}}]^{\mathrm{T}}\{\lambda(t)\}\left(\dfrac{\Delta t}{2}\right) = \{0\} \\ \dfrac{\partial \mathrm{LF}}{\partial\{\lambda(t)\}} = \{0\} \Rightarrow \{Z(t)\} - [T]\{\Lambda(t-\Delta t)\} - \left([B_{\mathrm{u}}]\{u(t)\} + [B_{\mathrm{r}}]\ddot{x}_{\mathrm{g}}(t)\right)\{\Gamma(t)\}\left(\dfrac{\Delta t}{2}\right) \end{cases} \tag{4.111}$$

Then optimal control force $\{u(t)\}$ can be solved from above equations as

$$\{u(t)\} = -\left(\frac{\Delta t}{2}\right)[R]^{-1}[B_{\mathrm{u}}]^{\mathrm{T}}[Q]\{Z(t)\} \tag{4.112}$$

Thus, the optimal control forces are proportional to the measured structural response.

Equation 4.112 shows that, the active control force is proportional to the time increment. This means the feedback gain matrix by IOAC is quite sensitive to incremental time intervals used in response analysis [21,22]. For a structure subjected to a certain earthquake loading, using different time intervals may yield various control forces and structural responses. Such nonuniform results are obviously irrational. The second shortcoming involves both Riccati and IOAC algorithms. A global optimum point cannot be discerned from the algorithms' integral performance index curves with the change of their control

design parameter, Q/R ratios. Actually, according to the definition of their performance indices, the minimum value of the integral performance index curves versus Q/R ratios for these two algorithms is always zero. This corresponds to the case without active control that is absolutely contrary to the original objective of the active control design. These shortcomings led to the development of a technique called *generalized optimal active control* (GOAC) *algorithm* for linear and nonlinear seismic structures [19–21,23,24] to be discussed in the subsequent sections.

4.3.2 Generalized Optimal Active Control Algorithm

In order to overcome the flaws in ROAC and IOAC algorithms, Cheng and Tian developed a technique called GOAC algorithm for seismic-resistant structures [19–21]. This section presents details of this GOAC algorithm.

4.3.2.1 Generalized performance index for GOAC algorithm

In order to obtain an optimal solution for state vector $\{Z(t)\}$ and control force vector $\{u(t)\}$, a performance index is defined and minimized. Equation 4.63 expresses standard quadratic performance index J. Clearly, the standard optimum controller is based on a fixed-end optimization problem for integrand J. However, this optimization may not be the physical case in discrete time domain for digital controllers. By dividing duration $[t_0, t_f]$ into n segments, Equation 4.63 can be written as

$$J = \sum_{i=1}^{n} \frac{1}{2} \int_{t_{i-1}}^{t_i} \left(\{Z(t)\}^{\mathrm{T}} [Q] \{Z(t)\} + \{u(t)\}^{\mathrm{T}} [R] \{u(t)\} \right) \mathrm{d}t \tag{4.113}$$

In Equation 4.63, integrand J has the following boundary values:

$$\begin{cases} \{Z(t_0)\} = \{Z(t_f)\} = \{0\} \\ \{u(t_0)\} = \{u(t_f)\} = \{0\} \end{cases} \tag{4.114}$$

The performance index J in Equation 4.113 will be integrated step by step in discrete time domain. At each step "i", the initial value of the state vector, $\{Z(t_{i-1})\}$, is specified from the earlier step, but the final value, $\{Z(t_i)\}$, is unknown. For each integration from t_{i-1} to t_i $(i = 1, 2, \ldots, n)$, at least one of the two boundary values is then unspecified. The minimization of integrand J in Equation 4.113 is related to a free-end boundary value problem [26] as shown in Figure 4.14. There are many families of comparison functions corresponding to the different endpoint values. In Figure 4.14, the value at $t = t_{i-1}$ is specified, and the value at $t = t_i$ is unspecified and this end is movable, as points 1, 2, 3, and 4 shown in Figure 4.14. By employing the Euler's equation to this free-end problem, a series of extremals can be found, each refers to the optima of one end point at $t = t_i$.

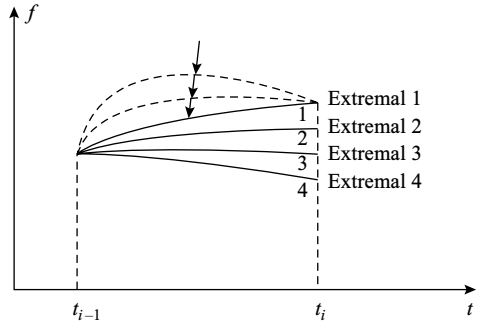

FIGURE 4.14 Solution of variational problems with one fixed end and one movable end.

In order to find the optimal function among these extremals, *transversality conditions* at $t = t_f$ must be employed. $\{Z(t_i)\}$ is unknown and should also be minimized, the performance index should include a function of $\{Z(t_i)\}$. Thus, a new performance index is defined at time interval $[t_{i-1}, t_i]$ as [19–21]

$$J_i = g(\{Z(t_i)\}) + \frac{1}{2}\int_{t_{t-1}}^{t_i} \left(\{Z(t)\}^{\mathrm{T}}[Q]\{Z(t)\} + \{u(t)\}^{\mathrm{T}}[R]\{u(t)\}\right) \mathrm{d}t$$

$$= g(\{Z(t_i)\}) + \frac{1}{2}\int_{t_{i-1}}^{t_i} \bar{f}(t)\, \mathrm{d}t \tag{4.115}$$

where $g(\{Z(t_i)\})$ can be chosen in the form of

$$g(\{Z(t_i)\}) = \frac{1}{2}\{Z(t_i)\}^{\mathrm{T}}[S][Z(t_i)\} \tag{4.116}$$

that is a function for optimizing the end conditions at each end point t_i; $[S]$ and $[Q]$ of $2n \times 2n$ are positive semidefinite matrix; $[R]$ or $r \times r$ is a positive-definite matrix and

$$\bar{f}(t) = \{Z(t)\}^{\mathrm{T}}[Q]\{Z(t)\} + \{u(t)\}^{\mathrm{T}}[R]\{u(t)\} \tag{4.117}$$

Recall that the problem involved is a free-end boundary value problem. Therefore, the minimization of generalized performance index J that determines the control force, should meet not only the Euler equations but also the transversality conditions at endpoint t_i. These requirements are further discussed in the following section.

4.3.2.2 Determination of feedback gain matrix and control force

By introducing vector of multipliers $\{\lambda(t)\}$ of $2n \times 1$ and considering earthquake excitation, an augmented function is formed as

$$\begin{aligned} F(t) &= \bar{f}(t) + \{\lambda(t)\}^{\mathrm{T}} \{f(t)\} \\ &= \{Z(t)\}^{\mathrm{T}}[Q]\{Z(t)\} + \{u(t)\}^{\mathrm{T}}[R]\{u(t)\} \\ &\quad + \{\lambda(t)\}^{\mathrm{T}} \left([A]\{Z(t)\} + [B_{\mathrm{u}}]\{u(t)\} + \{B_{\mathrm{r}}\}\ddot{x}_{\mathrm{g}}(t) - \{\dot{Z}(t)\}\right) \end{aligned} \tag{4.118}$$

where $f(t)$ is defined by the system's state-variable representation, Equation 4.19, as

$$f(t) = [A]\{Z(t)\} + [B_{\mathrm{u}}]\{u(t)\} + \{B_{\mathrm{r}}\}\ddot{x}_{\mathrm{g}}(t) - \{\dot{Z}(t)\} \tag{4.119}$$

Euler equations can be expressed as

$$\begin{cases} \dfrac{\partial F(t)}{\partial \{Z(t)\}} - \dfrac{\mathrm{d}}{\mathrm{d}t}\left(\dfrac{\partial F(t)}{\partial \{\dot{Z}(t)}\right) = \{0\} \\ \dfrac{\partial F(t)}{\partial \{u(t)\}} - \dfrac{\mathrm{d}}{\mathrm{d}t}\left(\dfrac{\partial F(t)}{\partial \{\dot{u}(t)}\right) = \{0\} \end{cases} \tag{4.120}$$

Substitute Equation 4.118 into Equation 4.120 and note in Section 4.2.1.2 that we proved

$$\begin{cases} \dfrac{\partial}{\partial \{Z(t)\}}\left[\dfrac{1}{2}\{Z(t)\}^{\mathrm{T}}[Q]\{Z(t)\}\right] = [Q]\{Z(t)\} \\ \dfrac{\partial}{\partial \{Z(t)\}}\left[\{\lambda(t)\}^{\mathrm{T}}[A]\{Z(t)\}\right] = [A]^{\mathrm{T}}\{\lambda(t)\} \\ \dfrac{\mathrm{d}}{\mathrm{d}t}\left[\dfrac{\partial}{\partial \{\dot{Z}(t)\}}(-\{\lambda(t)\}^{\mathrm{T}}\{\dot{Z}(t)\})\right] = -\{\dot{\lambda}(t)\} \\ \dfrac{\partial}{\partial \{u(t)\}}(\{u(t)\}^{\mathrm{T}}[R]\{u(t)\}) = [R]\{u(t)\} \\ \dfrac{\partial}{\partial \{u(t)\}}(\{\lambda(t)\}^{\mathrm{T}}[B_{\mathrm{u}}]\{u(t)\}) = [B_{\mathrm{u}}]^{\mathrm{T}}\{\lambda(t)\} \end{cases} \tag{4.121}$$

as shown in Equations 4.71, 4.73, 4.75, 4.78, and 4.80. Then we obtain

$$\begin{aligned} \{0\} &= \frac{\partial F(t)}{\partial \{Z(t)\}} - \frac{\mathrm{d}}{\mathrm{d}t}\left(\frac{\partial F(t)}{\partial \{\dot{Z}(t)\}}\right) \\ &= \frac{\partial\left(\{Z(t)\}^{\mathrm{T}}[Q]\{Z(t)\} + \{\lambda(t)\}^{\mathrm{T}}[A]\{Z(t)\}\right)}{\partial \{Z(t)\}} - \frac{\mathrm{d}}{\mathrm{d}t}\left(-\frac{\partial\left(\{\lambda(t)\}^{\mathrm{T}}\left\{\dot{Z}(t)\right\}\right)}{\partial\left\{\dot{Z}(t)\right\}}\right) \\ &= [Q]\{Z(t)\} + [A]^{\mathrm{T}}\{\lambda(t)\} + \{\dot{\lambda}(t)\} \end{aligned} \tag{4.122}$$

$$\begin{aligned}\{0\} &= \frac{\partial F(t)}{\partial\{u(t)\}} - \frac{\mathrm{d}}{\mathrm{d}t}\left(\frac{\partial F(t)}{\partial\{\dot{u}(t)\}}\right) \\ &= \frac{\partial}{\partial\{u(t)\}}\left(\frac{1}{2}\{u(t)\}^{\mathrm{T}}[R]\{u(t)\} + \{\lambda(t)\}^{\mathrm{T}}[B_{\mathrm{u}}]\{u(t)\}\right) - 0 \\ &= [R]\{u(t)\} + [B_{\mathrm{u}}]^{\mathrm{T}}\{\lambda(t)\}\end{aligned} \tag{4.123}$$

End conditions of the system governed by Equation 4.19 are

$$\begin{cases} t_{i-1} = t_0 + \sum_{k=1}^{i-1} \Delta t_k \\ \{Z(t_{i-1})\} = \{Z_{i-1}\} \\ t_i = t_{i-1} + \Delta t_i = t_0 + \sum_{k=1}^{i-1} \Delta t_k + \Delta t_i = t_0 + \sum_{k=1}^{i} \Delta t_k \end{cases} \tag{4.124}$$

where $\Delta t_k (k = 1, 2, \ldots, n)$ is the time increment for the kth segment of time duration $[t_0, t_{\mathrm{f}}]$, that is, $\sum_{k=1}^{n} \Delta t_k = t_{\mathrm{f}} - t_0$. Time segments may have time increments of different values.

Equation 4.124 can be rewritten as

$$\{\Omega\} = \begin{Bmatrix} \Omega_1 \\ \Omega_2 \\ \Omega_3 \end{Bmatrix} = \begin{Bmatrix} (t_{i-1} - t_0) - \sum_{k=1}^{i-1} \Delta t_k \\ \{Z(t_{i-1})\} \; -\{Z_{i-1}\} \\ (t_i - t_0) \; - \sum_{k=1}^{i} \Delta t_k \end{Bmatrix} = \{0\} \tag{4.125}$$

By introducing multiplier $\{\mu\}$ and forming an augmented function

$$G = g\left(\{Z(t_i)\}\right) + \{\mu\}^{\mathrm{T}}\{\Omega\} \tag{4.126}$$

the tranversality condition is expressed as

$$\mathrm{d}G - \left[\left\{\frac{\partial F(t)}{\partial\{\dot{Z}(t)\}}\right\}^{\mathrm{T}}\left\{\dot{Z}(t)\right\} - F(t)\right]\mathrm{d}t\Big|_{t_{i-1}}^{t_i} + \left\{\frac{\partial F(t)}{\partial\left\{\dot{Z}(t)\right\}}\right\}^{\mathrm{T}}\mathrm{d}\left\{Z(t)\right\}\Big|_{t_{i-1}}^{t_i} = 0 \tag{4.127}$$

Since function G is related to $t_{i-1}, t_i, \{Z(t_i)\}$, and $\{Z(t_{i-1})\}$, we have

$$\mathrm{d}G = \frac{\partial G}{\partial t_{i-1}}\mathrm{d}t_{i-1} + \frac{\partial G}{\partial t_i}\mathrm{d}t_i + \frac{\partial G}{\partial\{Z(t_{i-1})\}}\mathrm{d}\{Z(t_{i-1})\} + \frac{\partial G}{\partial\{Z(t_i)\}}\mathrm{d}\{Z(t_i)\} \tag{4.128}$$

and

$$\left[\left\{\frac{\partial F(t)}{\partial\{\dot{Z}(t)\}}\right\}^{\mathrm{T}}\{\dot{Z}(t)\}-F(t)\right]\mathrm{d}t\Bigg|_{t_{i-1}}^{t_i}=\left[\left\{\frac{\partial F(t_i)}{\partial\{\dot{Z}(t_i)\}}\right\}^{\mathrm{T}}\{\dot{Z}(t_i)\}-F(t_i)\right]\mathrm{d}t_i$$
$$-\left[\left\{\frac{\partial F(t_{i-1})}{\partial\{\dot{Z}(t_{i-1})\}}\right\}^{\mathrm{T}}\{\dot{Z}(t_{i-1})\}-F(t_{i-1})\right]\mathrm{d}t_{i-1} \tag{4.129}$$

$$\left\{\frac{\partial F(t)}{\partial\{\dot{Z}(t_i)\}}\right\}^{\mathrm{T}}\mathrm{d}\{Z(t)\}\Bigg|_{t_{i-1}}^{t_i}=\left\{\frac{\partial F(t_i)}{\partial\{\dot{Z}(t_i)\}}\right\}\mathrm{d}\{Z(t_i)\}-\left\{\frac{\partial F(t_{i-1})}{\partial\{\dot{Z}(t_{i-1})\}}\right\}\mathrm{d}\{Z(t_{i-1})\} \tag{4.130}$$

Substituting Equations 4.128, 4.129, and 4.130 into Equation 4.127 yields

$$\left[\frac{\partial G}{\partial t_{i-1}}+\left\{\frac{\partial F}{\partial\{\dot{Z}(t_i)\}}\right\}^{\mathrm{T}}\{\dot{Z}(t)\}-F(t)\right]_{t=t_{i-1}}\mathrm{d}t_{i-1}$$
$$+\left[\frac{\partial G}{\partial t_i}-\left\{\frac{\partial F}{\partial\{\dot{Z}(t)\}}\right\}^{\mathrm{T}}\{\dot{Z}(t)\}+F(t)\right]_{t=t_i}\mathrm{d}t_i$$
$$+\left[\frac{\partial G}{\partial\{Z(t_{i-1})\}}-\left\{\frac{\partial F(t_{i-1})}{\partial\{\dot{Z}(t_{i-1})\}}\right\}\right]\mathrm{d}\{Z(t_{i-1})\}$$
$$+\left[\frac{\partial G}{\partial\{Z(t_i)\}}+\frac{\partial F(t_i)}{\partial\{\dot{Z}(t_i)\}}\right]\mathrm{d}\{Z(t_i)\}=0 \tag{4.131}$$

Thus

$$\begin{cases}\dfrac{\partial G}{\partial t_{i-1}}+\left\{\dfrac{\partial F(t)}{\partial\{\dot{Z}(t)\}}\right\}^{\mathrm{T}}\{Z(t)\}-F(t)\Big|_{t=t_{i-1}}=0\\ \dfrac{\partial G}{\partial t_i}-\left\{\dfrac{\partial F(t)}{\partial\{\dot{Z}(t)\}}\right\}^{\mathrm{T}}\{\dot{Z}(t)\}+F(t)\Big|_{t=t_i}=0\\ \dfrac{\partial G}{\partial\{Z(t_{i-1})\}}-\left\{\dfrac{\partial F(t)}{\partial\{\dot{Z}(t)\}}\right\}\Big|_{t=t_{i-1}}=\{0\}\\ \dfrac{\partial G}{\partial\{Z(t_i)\}}+\left\{\dfrac{\partial F(t)}{\partial\{\dot{Z}(t)\}}\right\}\Big|_{t=t_i}=\{0\}\end{cases} \tag{4.132}$$

Substituting Equations 4.116 and 4.125 into Equation 4.126 yields

$$G = \frac{1}{2}\{Z(t_i)\}^{\mathrm{T}}[S]\{Z(t_i)\} + \mu_1\left[(t_{i-1} - t_0) - \sum_{k=1}^{i-1}\Delta t_k\right] + \{\mu_2\}^{\mathrm{T}}\left[\{Z(t_{i-1})\} - \{Z_{i-1}\}\right] + \mu_3\left[(t_i - t_0) - \sum_{k=1}^{i}\Delta t_k\right] \tag{4.133}$$

where the multiplier $\{\mu\}^{\mathrm{T}} = [\mu_1, \{\mu_2\}^{\mathrm{T}}, \mu_3]$. Thus

$$\begin{cases} \dfrac{\partial G}{\partial t_{i-1}} = \mu_1 \\ \dfrac{\partial G}{\partial t_i} = \mu_3 \\ \dfrac{\partial G}{\partial\{Z(t_{i-1})\}} = \{\mu_2\} \\ \left\{\dfrac{\partial G}{\partial\{Z(t_i)\}}\right\} = [S]\{Z(t_i)\} \end{cases} \tag{4.134}$$

From Equation 4.118 we obtain

$$\frac{\partial F(t)}{\partial\{\dot{Z}(t)\}} = \frac{\partial\left(-\{\lambda(t)\}^{\mathrm{T}}\{\dot{Z}(t)\}\right)}{\partial\{\dot{Z}(t)\}} = -\{\lambda(t)\} \tag{4.135}$$

Because

$$\frac{\partial(-\{\lambda(t)\}^{\mathrm{T}}\{\dot{Z}(t)\})}{\partial\dot{Z}_k(t)} = \frac{\partial}{\partial\dot{Z}_k}\left[-\frac{\sum_{i=1}^{2n}\lambda_i(t)\dot{Z}_i(t)}{\partial\dot{Z}_k(t)}\right] = -\lambda_k(t) \tag{4.136}$$

Substituting Equation 4.135 and the fourth equation in Equation 4.134 into the fourth equation in Equation 4.132 yields

$$[S]\{Z(t_i)\} - \{\lambda(t_i)\} = \{0\} \tag{4.137}$$

which is the transversality condition of the free-end minimization problem. Since Equation 4.137 holds true at every end point $t = t_i$ $(i = 1, 2, \ldots, n)$ and t_i can be any point between t_0 and t_{f}, the transversality condition can be generalized as

$$\{\lambda(t)\} = [S]\{Z(t)\} \tag{4.138}$$

Equation 4.123, obtained from Euler equation, leads to

$$\{u(t)\} = -[R]^{-1}[B_u]^T\{\lambda(t)\} \tag{4.139}$$

Substituting Equation 4.138 into Equation 4.139 yields the feedback control force

$$\{u(t)\} = -[R]^{-1}[B_u]^T[S]\{Z(t)\} = -[G]\{Z(t)\} \tag{4.140}$$

where the feedback gain matrix

$$[G] = [R]^{-1}[B_u]^T[S] \tag{4.141}$$

which is invariant with t and valid at every end point t_i. Since the gain matrix is neither a function of t_i nor a function of time increment Δt_i, Δt_i can be arbitrarily changed in accord with the range of precision during the computation process. This change will not affect control effectiveness.

In Equation 4.141, if $[S]$ is chosen to be algebraic Riccati matrix $[P]$ (i.e., let $[S] = [P]$), the feedback gain matrix is identical to Equation 4.101, the gain matrix of the Ricatti closed-loop algorithm. Thus, the Ricatti closed-loop control algorithm is included in this generalized algorithm. This is why the method is named GOAC algorithm. After the feedback gain matrix $[G]$ is obtained, Equation 4.19, the state equation, can be solved by using the flow chart shown in Figure 4.15.

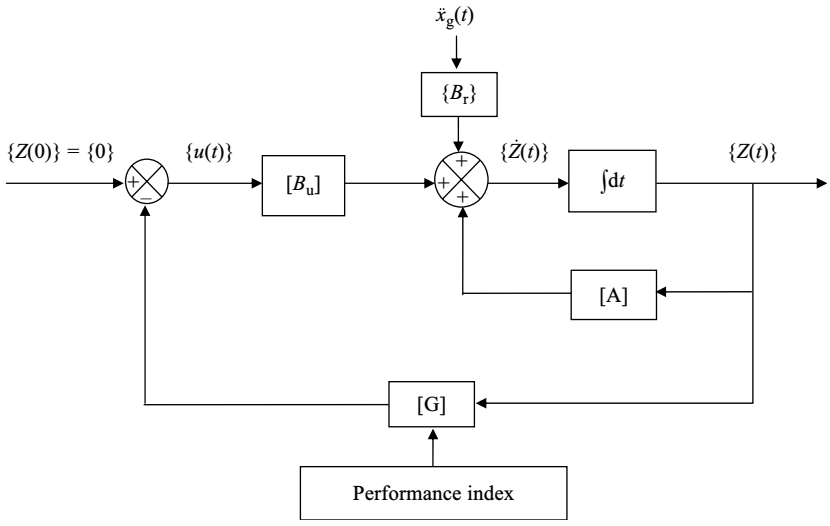

FIGURE 4.15 Flow chart for solving state equation with active control.

4.3.2.3 Solution technique

Once the feedback gain matrix $[G]$ is determined, the closed-loop system (i.e. the controlled structure) can be modeled by substituting Equation 4.140 into Equation 4.19, which yields Equation 4.24. The closed-loop plant matrix is

$$\begin{aligned}[A_c] &= [A] - [B_u]\,[G] \\ &= [A] - [B_u][R]^{-1}[B_u]^T[S] \end{aligned} \tag{4.142}$$

Thus all coefficient matrices in Equation 4.24 have been determined. Then the closed-loop response, that is, the response of the controlled structure, can be solved in a manner similar to that described in Section 4.1.5. There are two differences in the solution for the closed-loop response. One is that the modal transformation matrix $[T]$ is for the closed-loop plant matrix $[A_c]$ instead of $[A]$; the other is that vector $\{\Gamma(t)\}$ is only related to $\ddot{x}_g(t)$, that is,

$$\{\Gamma(t)\} = [T]^{-1}\{B_r\}\ddot{x}_g(t) \tag{4.143}$$

which differs from Equation 4.33. The solution technique can be described as follows.

Let $\{Z(t)\}$ be expressed in terms of the modal transformation matrix, $[T]$, of the closed-loop plant matrix $[A_c]$, that is,

$$\{Z(t)\} = [T]\{\psi(t)\} \tag{4.144}$$

in which $[T]$ has the following property

$$[T]^{-1}[A_c][T] = [\Phi] \tag{4.145}$$

where elements of $[\Phi]$ are eigenvalues of the plant matrix $[A_c]$. Substituting Equation 4.144 into Equation 4.24a and premultiplying by $[T]^{-1}$ yields

$$\{\dot{\psi}(t)\} = [\Phi]\{\psi(t)\} + \{\Gamma(t)\} \tag{4.146}$$

Corresponding initial conditions are

$$\{Z(0)\} = \{0\}, \ddot{x}_g(0) = 0, \text{ thus } \{\psi(0)\} = \{0\} \tag{4.147}$$

Equation 4.146's solution is

$$\{\psi(t)\} = \int_0^t \exp([\Phi](t-\tau))\,\{\Gamma(\tau)\}\,\mathrm{d}\tau \tag{4.148}$$

which can be determined by numerical integration as discussed in Section 4.1.5. After $\{\psi(t)\}$ is determined, $\{Z(t)\}$ and $\{u(t)\}$ can be derived from Equations 4.144 and 4.140, respectively.

4.3.2.4 Sensitivity of time increment to instantaneous optimal active control

Instantaneous optimal active control algorithms define a performance index without integration and minimize the index at each time-instant. However, its control effectives is sensitive to the incremental time intervals used in response analysis [24]. For the GOAC algorithm, the control force is not related to the time increment thus solving the shortcoming of IOAC. This advantage of the GOAC algorithm is demonstrated by following numerical example.

A six-story shear building with active tendon control is used to illustrate the advantages of this generalized active control algorithm. Assume only one active tendon installed on the first floor. Its structural properties are as follows: (1) mass coefficients $m_1 = 109.78$, $m_2 = 109.62$, $m_3 = 109.24$, $m_4 = 108.86$, $m_5 = 108.48$, $m_6 = 107.03$ (tons); (2) stiffness coefficients $k_1 = 351284$, $k_2 = 225{,}167$, $k_3 = 169{,}665$, $k_4 = 124{,}242$, $k_5 = 87{,}872$, $k_6 = 59{,}532$ (kN/m); (3) undamped natural frequencies $\omega_1 = 9.79$, $\omega_2 = 24.05$, $\omega_3 = 37.40$, $\omega_4 = 49.56$, $\omega_5 = 63.44$, $\omega_6 = 83.76$ (rad/s); (4) 2% structural damping ratio. For dynamic time-history analysis, N-S component of El-Centro earthquake (1940), as shown in Figure 4.16, is employed.

The influence of time increment Δt on the IOAC and GOAC algorithms is compared. Weighting matrices $[Q]$ and $[S]$ are formed with only the first row of $[Q_{21}]$, $[Q_{22}]$, $[S_{21}]$ and $[S_{22}]$as nonzero elements: $(Q_{21})_{ij}/R = (Q_{22})_{ij}/R = 1.2 \times 10^8$ for IOAC and $(S_{21})_{ij}/R = (S_{22})_{ij}/R = 6.0 \times 10^5$for GOAC ($j = 1, 2, \ldots, 6$). Figures 4.17 and 4.18 show the influence of Δt on top-floor displacement of the structure and control force, respectively. For IOAC algorithm, when two different time increments, $\Delta t = 0.0025$ and 0.01 s are used, both the displacement and

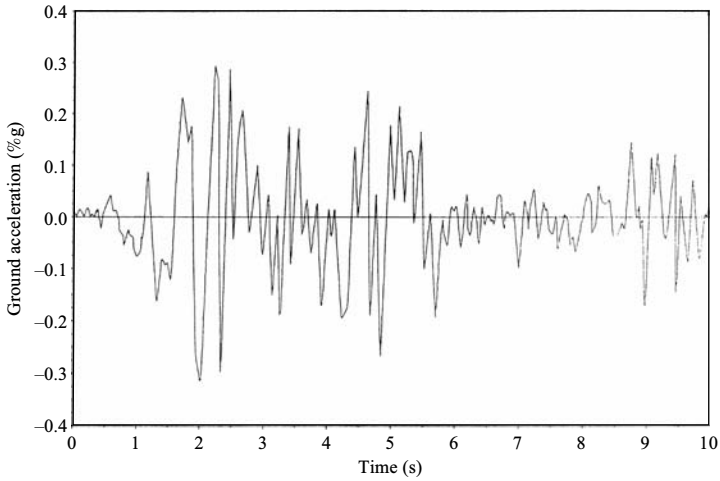

FIGURE 4.16 N-S component of May 18, 1940 El-Centro earthquake.

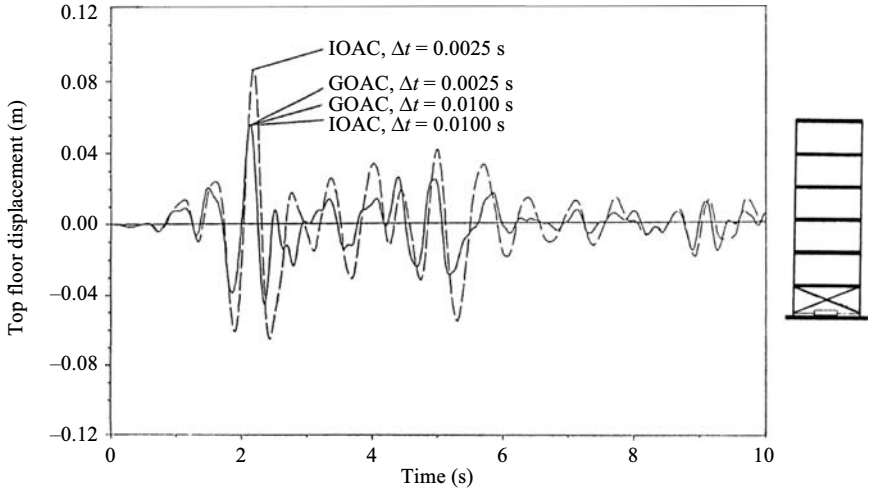

FIGURE 4.17 Influence of time increment Δt on top-floor displacement.

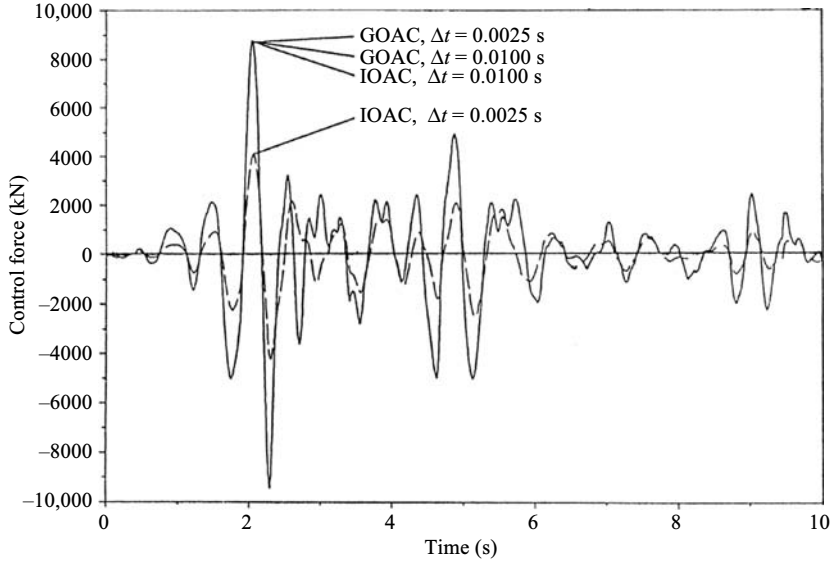

FIGURE 4.18 Influence of time increment Δt on control force.

control force associated with these time increments differ significantly. However, a change in Δt does not influence the response obtained by using GOAC algorithm. Apparently, IOAC is sensitive to time increment while GOAC is independent of it. In actual engineering practice, both structural response and control force should be free from the selection of Δt.

Example 4.3.1

A single-story building has active tendon control. Structural properties are mass $m = 345.6$ tons, damping $c = 734.3$ kN-s/m, and stiffness $k = 3.404 \times 10^5$ kN/m. Assume the structure is subject to excitation of ground acceleration $\ddot{x}_g(t) = 0.25\,g \sin[(20\pi/3)\,t]$. Use GOAC algorithm to design the control system and find the response of the controlled structure.

Solution

The motion equation for the structure is

$$m\ddot{x}(t) + c\dot{x}(t) + kx(t) = -m\ddot{x}_g(t) - u(t) \tag{a}$$

By defining state vector

$$\{Z(t)\} = \{x(t) \quad \dot{x}(t)\}^T \tag{b}$$

Equation a can be rewritten as state equation

$$\{\dot{Z}(t)\} = [A]\{Z(t)\} + \{B_u\}\,u(t) + \{B_r\}\ddot{x}_g(t) \tag{c}$$

where the plant matrix is

$$[A] = \begin{bmatrix} 0 & 1 \\ -\dfrac{k}{m} & -\dfrac{c}{m} \end{bmatrix} = \begin{bmatrix} 0 & 1 \\ -\dfrac{3.404 \times 10^5}{345.6} & -\dfrac{734.3}{345.6} \end{bmatrix} \tag{d}$$

$$= \begin{bmatrix} 0 & 1 \\ -984.954 & -2.125 \end{bmatrix}$$

$$\{B_u\} = \begin{Bmatrix} 0 \\ -\dfrac{1}{m} \end{Bmatrix} = \begin{Bmatrix} 0 \\ -2.894 \times 10^{-3} \end{Bmatrix} \tag{e}$$

$$\{B_r\} = \begin{Bmatrix} 0 \\ -\dfrac{m}{m} \end{Bmatrix} = \begin{Bmatrix} 0 \\ -1 \end{Bmatrix} \tag{f}$$

and weighting matrices are assumed as

$$[Q] = \begin{bmatrix} 10^6 & 0 \\ 0 & 10^6 \end{bmatrix}, \quad R = 0.001, \quad \alpha = 0.007,$$

$$[S] = \alpha[Q] = \begin{bmatrix} 7{,}000 & 0 \\ 0 & 7{,}000 \end{bmatrix} \tag{g}$$

where weighting matrix $[S]$ is assumed to be proportional to matrix $[Q]$ and α is the coefficient.

Plant matrix for the controlled structure is

$$\begin{aligned}[A_c] &= [A] - [B_u][R]^{-1}[B_u]^T[S] \\ &= \begin{bmatrix} 0 & 1 \\ -984.954 & -2.125 \end{bmatrix} - \begin{Bmatrix} 0 \\ -2.894 \times 10^{-3} \end{Bmatrix} (0.001)^{-1} \\ &\quad \begin{bmatrix} 0 & -2.894 \times 10^{-3} \end{bmatrix} \begin{bmatrix} 7{,}000 & 0 \\ 0 & 7{,}000 \end{bmatrix} \\ &= \begin{bmatrix} 0 & 1 \\ -984.954 & -2.125 - (2.894 \times 10^{-3})(7{,}000)/0.001 \end{bmatrix} \\ &= \begin{bmatrix} 0 & 1 \\ -984.954 & -60.752 \end{bmatrix} \end{aligned} \tag{h}$$

The eigenvalue of $[A_c]$ is $\mu \pm \nu j$ and

$$\begin{aligned}\mu &= -\frac{1}{2m^2}\left(mc + \alpha\frac{q_{22}}{r}\right) \\ &= -\frac{1}{2(345.6^2)}\left(345.6 \times 734.3 + 0.007\frac{10^6}{0.001}\right) \\ &= -30.366 \end{aligned} \tag{i}$$

$$\begin{aligned}\nu &= \sqrt{\frac{k}{m} - \frac{1}{4m^4}\left(mc + \alpha\frac{q_{22}}{r}\right)^2} \\ &= \sqrt{\frac{3.404 \times 10^5}{345.6} - \frac{1}{4(345.6^4)}\left(345.6 \times 734.3 + 0.007\frac{10^6}{0.001}\right)^2} \\ &= 7.929 \end{aligned} \tag{j}$$

in which q_{22} is the (2,2) element of weighting matrix $[Q]$ and r is the value of scalar weighting coefficient R.

$$[\Phi] = \begin{bmatrix} \mu & \nu \\ -\nu & \mu \end{bmatrix} = \begin{bmatrix} -30.366 & 7.929 \\ -7.929 & -30.366 \end{bmatrix} \tag{k}$$

$$\begin{aligned}[T] &= \begin{bmatrix} \mu/(\mu^2 + \nu^2) & -\nu/(\mu^2 + \nu^2) \\ 1 & 0 \end{bmatrix} \\ &= \begin{bmatrix} \dfrac{30.366}{7.929^2 + 30.366^2} & -\dfrac{7.929}{7.929^2 + 30.366^2} \\ 1 & 0 \end{bmatrix} \end{aligned} \tag{l}$$

$$= \begin{bmatrix} -3.083 \times 10^{-2} & -8.050 \times 10^{-3} \\ 1 & 0 \end{bmatrix}$$

$$[T]^{-1} = \begin{bmatrix} 0 & 1 \\ -\dfrac{\mu^2 + \nu^2}{\nu} & \dfrac{\mu}{\nu} \end{bmatrix} = \begin{bmatrix} 0 & 1 \\ -\dfrac{7.929^2 + 30.366^2}{7.929} & \dfrac{-30.366}{7.929} \end{bmatrix}$$

$$= \begin{bmatrix} 0 & 1 \\ -124.223 & -3.830 \end{bmatrix} \tag{m}$$

The gain matrix is

$$[G] = -[R]^{-1}[B_{\mathrm{u}}]^{\mathrm{T}}[S]$$

$$= -(0.001)^{-1} \begin{Bmatrix} 0 \\ -2.894 \times 10^{-3} \end{Bmatrix}^{\mathrm{T}} \begin{bmatrix} 7{,}000 & 0 \\ 0 & 7{,}000 \end{bmatrix}$$

$$= \begin{bmatrix} 0 & \dfrac{2.894 \times 10^{-3} \times 7{,}000}{0.001} \end{bmatrix} = [0 \quad 20{,}258] \tag{n}$$

Let $\Delta t = 0.01$ s; then

$$\exp([\Phi]\Delta t) = \exp(\mu \Delta t) \begin{bmatrix} \cos(\nu \Delta t) & \sin(\nu \Delta t) \\ -\sin(\nu \Delta t) & \cos(\nu \Delta t) \end{bmatrix}$$

$$= \mathrm{e}^{(-30.366 \times 0.01)} \begin{bmatrix} \cos(7.929 \times 0.001) & \sin(7.929 \times 0.01) \\ -\sin(7.929 \times 0.01) & \cos(7.929 \times 0.01) \end{bmatrix}$$

$$= 0.7381 \begin{bmatrix} 0.9969 & 0.0792 \\ -0.0792 & 0.9969 \end{bmatrix}$$

$$= \begin{bmatrix} 0.736 & 0.0585 \\ -0.0585 & 0.736 \end{bmatrix} \tag{o}$$

At $t_0 = 0$ s, the initial conditions are

$$\{Z(0)\} = \{0\}, \quad u(0) = 0, \quad \ddot{x}_{\mathrm{g}}(0) = 0 \tag{p}$$

Thus,

$$\begin{cases} \{\psi(0)\} = [T]^{-1}\{Z(0)\} = \{0\} \\ \{\Gamma(0)\} = [T]^{-1}\{B_{\mathrm{r}}\}\ddot{x}_{\mathrm{g}}(0) = \{0\} \\ \{\Lambda(0)\} = \exp([0])\{\Gamma(0)\} = \{0\} \end{cases} \tag{q}$$

at $t_1 = \Delta t = 0.01$ s,

$$\{\Lambda(t_1 - \Delta t)\} = \{\Lambda(0)\} = \{0\} \tag{r}$$

$$\begin{aligned}\{\Gamma(t_1)\} &= [T]^{-1}\{B_\mathrm{r}\}\ddot{x}_\mathrm{g}(t_1)\\ &= \begin{bmatrix} 0 & 1 \\ -124.223 & -3.830 \end{bmatrix} \begin{Bmatrix} 0 \\ -1 \end{Bmatrix} 0.25(9.81) \sin\left[\frac{20\pi}{3}(0.01)\right]\\ &= \begin{Bmatrix} -0.510 & 1.953 \end{Bmatrix}^\mathrm{T}\end{aligned} \tag{s}$$

$$\begin{aligned}\{\psi(t_1)\} &= \{\Lambda(t_1 - \Delta t)\} + \{\Gamma(t_1)\}\frac{\Delta t}{2}\\ &= \{0\} + \begin{Bmatrix} -0.510 \\ 1.953 \end{Bmatrix} \frac{0.01}{2} = \begin{Bmatrix} -2.550 \times 10^{-3} \\ 9.765 \times 10^{-3} \end{Bmatrix}\end{aligned} \tag{t}$$

$$\begin{aligned}\{Z(t_1)\} &= [T]\{\psi(t_1)\}\\ &= \begin{bmatrix} -3.083 \times 10^{-2} & -8.050 \times 10^{-3} \\ 1 & 0 \end{bmatrix} \begin{Bmatrix} -2.550 \times 10^{-3} \\ 9.765 \times 10^{-3} \end{Bmatrix}\\ &= \begin{Bmatrix} 8.25 \times 10^{-9} \\ -2.55 \times 10^{-3} \end{Bmatrix}\end{aligned} \tag{u}$$

$$u(t_1) = [G]\{Z(t_1)\} = \begin{bmatrix} 0 & 20{,}258 \end{bmatrix} \begin{Bmatrix} 8.25 \times 10^{-9} \\ -2.55 \times 10^{-3} \end{Bmatrix} = 51.658\,\mathrm{kN} \tag{v}$$

At $t_2 = 2\Delta t = 0.02$ s.

$$\begin{aligned}\{\Lambda(t_2 - \Delta t)\} &= \exp([\Phi]\,\Delta t)\,(\{\Lambda(t_2 - 2\Delta t)\} + \{\Gamma(t_2 - \Delta t)\}\,\Delta t)\\ &= \exp([\Phi]\,\Delta t)(\{\Lambda(0)\} + \{\Gamma(t_1)\}\,\Delta t)\\ &= \begin{bmatrix} 0.736 & 0.0585 \\ -0.0585 & 0.736 \end{bmatrix} \left(\begin{Bmatrix} 0 \\ 0 \end{Bmatrix} + \begin{Bmatrix} -0.510 \\ 1.953 \end{Bmatrix} (0.01) \right)\\ &= \begin{Bmatrix} -2.611 \times 10^{-3} \\ 1.467 \times 10^{-2} \end{Bmatrix}\end{aligned} \tag{w}$$

$$\begin{aligned}\{\Gamma(t_2)\} &= [T]^{-1}\{B_\mathrm{r}\}\ddot{x}_\mathrm{g}(t_2)\\ &= \begin{bmatrix} 0 & 1 \\ -124.223 & -3.830 \end{bmatrix} \begin{Bmatrix} 0 \\ -1 \end{Bmatrix} 0.25(9.81) \sin\left[\frac{20\pi}{3}(0.02)\right]\\ &= \begin{Bmatrix} -0.998 \\ 3.822 \end{Bmatrix}\end{aligned} \tag{x}$$

$$\{\psi(t_2)\} = \{\Lambda(t_2 - \Delta t)\} + \{\Gamma(t_2)\}\frac{\Delta t}{2}$$

$$= \begin{Bmatrix} -2.611 \times 10^{-3} \\ 1.467 \times 10^{-2} \end{Bmatrix} + \begin{Bmatrix} -0.998 \\ 3.822 \end{Bmatrix} \frac{0.01}{2}$$

$$= \begin{Bmatrix} -7.601 \times 10^{-3} \\ 3.378 \times 10^{-2} \end{Bmatrix} \quad \text{(y)}$$

$$\{Z(t_2)\} = [T]\{\psi(t_2)\}$$

$$= \begin{bmatrix} -3.830 \times 10^{-2} & -8.050 \times 10^{-3} \\ 1 & 0 \end{bmatrix} \begin{Bmatrix} -7.601 \times 10^{-3} \\ 3.378 \times 10^{-2} \end{Bmatrix}$$

$$= \begin{Bmatrix} -3.761 \times 10^{-5} \\ -7.601 \times 10^{-3} \end{Bmatrix} \quad \text{(z)}$$

$$u(t_2) = [G]\{Z(t_2)\}$$

$$= \begin{bmatrix} 0 & 20{,}258 \end{bmatrix} \begin{Bmatrix} -3.761 \times 10^{-5} \\ -7.601 \times 10^{-3} \end{Bmatrix} = 153.98\,\text{kN} \quad \text{(aa)}$$

At $t = 3\ \Delta t = 0.03$ s.

$$\{\Lambda(t_3 - \Delta t)\} = \exp([\Phi]\Delta t)\ (\{\Lambda(t_1)\} + \{\Gamma(t_2)\}\ \Delta t)$$

$$= \begin{bmatrix} 0.736 & 0.0585 \\ -0.0585 & 0.736 \end{bmatrix} \left(\begin{Bmatrix} -2.611 \times 10^{-3} \\ 1.467 \times 10^{-2} \end{Bmatrix} + \begin{Bmatrix} -0.998 \\ 3.822 \end{Bmatrix} \times 0.01 \right)$$

$$= \begin{bmatrix} 0.736 & 0.0585 \\ -0.0585 & 0.736 \end{bmatrix} \begin{Bmatrix} -1.259 \times 10^{-2} \\ 5.289 \times 10^{-2} \end{Bmatrix}$$

$$= \begin{Bmatrix} -0.6172 \\ 3.965 \end{Bmatrix} \times 10^{-2} \quad \text{(bb)}$$

$$\{\Gamma(t_3)\} = [T]^{-1}\{B_r\}\ddot{x}_g(t_3)$$

$$= \begin{bmatrix} 0 & 1 \\ -124.223 & -3.830 \end{bmatrix} \begin{Bmatrix} 0 \\ -1 \end{Bmatrix} 0.25(9.81) \sin\left[\frac{20\pi}{3}(0.03)\right]$$

$$= \begin{Bmatrix} -1.442 \\ 5.523 \end{Bmatrix} \quad \text{(cc)}$$

$$\{\psi(t_3)\} = \{\Lambda(t_3 - \Delta t)\} + \{\Gamma(t_3)\} \frac{\Delta t}{2}$$

$$= \begin{Bmatrix} -0.6172 \\ 3.965 \end{Bmatrix} \times 10^{-2} + \begin{Bmatrix} -1.442 \\ 5.523 \end{Bmatrix} \frac{0.01}{2}$$

$$= \begin{Bmatrix} -1.338 \\ 6.727 \end{Bmatrix} \times 10^{-2} \quad \text{(dd)}$$

$$\{Z(t_3)\} = [T]\{\psi(t_3)\}$$
$$= \begin{bmatrix} -3.083 \times 10^{-2} & -8.050 \times 10^{-3} \\ 1 & 0 \end{bmatrix} \begin{Bmatrix} -1.338 \\ 6.727 \end{Bmatrix} \times 10^{-2}$$
$$= \begin{Bmatrix} -1.289 \times 10^{-4} \\ -1.338 \times 10^{-2} \end{Bmatrix} \quad \text{(ee)}$$

$$u(t_3) = [G]\{Z(t_3)\} = \begin{bmatrix} 0 & 20{,}258 \end{bmatrix} \begin{Bmatrix} -1.289 \times 10^{-4} \\ -1.338 \times 10^{-2} \end{Bmatrix}$$
$$= 271.05\,\text{kN} \quad \text{(ff)}$$

4.3.3 GOAC Algorithm for Nonlinear Smart Seismic Structures

Building structures behave nonlinearly under strong seismic excitations. Thus, it is very important to develop a control algorithm for nonlinear smart structures. Cheng and Tian [20,23] successfully applied GOAC algorithm for such purposes, as discussed in this section. On the basis of unknown state variables the end point of a time interval should be minimized, and a generalized performance index is selected. Corresponding transversality conditions for nonlinear seismic structures are then derived, and a time-independent optimal feedback gain matrix is achieved. The state equation of motion is solved in the real-time domain by using Wilson-θ method and the concept of unbalanced force correction. Numerical comparisons between GOAC and ROAC algorithms are performed, which indicates that the GOAC method is the most superior algorithm for nonlinear smart structures.

4.3.3.1 Motion equation for nonlinear seismic structures with active tendon control

The motion equation for an n-story nonlinear seismic structure equipped with active tendons at some floors (see Figure 4.2) can be expressed as

$$[M]\{\ddot{x}(t)\} + \{F_D(t)\} + \{F_K(t)\} = [\gamma]\{u(t)\} + \{\delta\}\ddot{x}_g(t) \tag{4.149}$$

where $[M]$ is $n \times n$ mass matrix, $\{x(t)\}$ of $n \times 1$ and $u(t)$ of $r \times 1$ are vectors of relative displacements and control forces, respectively, in which r is the number of active tendons; and $[\gamma]$ of $n \times r$ and $\{\delta\}$ of $n \times 1$ are location matrix for control force and coefficient vector for the earthquake ground acceleration $\ddot{x}_g(t)$. $\{F_D(t)\}$ and $\{F_K(t)\}$ of $n \times 1$ are damping and restoring force vectors, respectively, which

can be approximated by the following expression:

$$\begin{cases} \{F_{\mathrm{D}}(t)\} = \{F_{\mathrm{D}}(t-\Delta t)\} + [C(t-\Delta t)]\left(\{\dot{x}(t)\} - \{\dot{x}(t-\Delta t)\}\right) \\ \{F_{\mathrm{K}}(t)\} = \{F_{\mathrm{K}}(t-\Delta t)\} + [K(t-\Delta t)]\left(\{x(t)\} - \{x(t-\Delta t)\}\right) \end{cases} \tag{4.150}$$

where $[C(t-\Delta t)]$ and $[K(t-\Delta t)]$ of $n \times n$ are damping and stiffness matrices at time instant $t-\Delta t$, respectively, whose coefficients are defined by

$$\begin{cases} C_{ij}(t-\Delta t) = \dfrac{F_{\mathrm{D}i}(t-\Delta t) - F_{\mathrm{D}i}(t-2\Delta t)}{\dot{x}_j(t-\Delta t) - \dot{x}_j(t-2\Delta t)} \\ K_{ij}(t-\Delta t) = \dfrac{F_{\mathrm{K}i}(t-\Delta t) - F_{\mathrm{K}i}(t-2\Delta t)}{x_j(t-\Delta t) - x_j(t-2\Delta t)} \end{cases} \tag{4.151}$$

Substitution of Equation 4.150 into Equation 4.149 yields

$$\begin{aligned} &[M]\{\ddot{x}(t)\} + [C(t-\Delta t)]\{\dot{x}(t)\} + [K(t-\Delta t)]\{x(t)\} \\ &\quad = \{F(t-\Delta t)\} + [\gamma]\{u(t)\} + \{\delta\}\ddot{x}_{\mathrm{g}}(t) \end{aligned} \tag{4.152}$$

where

$$\begin{aligned} \{F(t-\Delta t)\} = {} & [C(t-\Delta t)]\{\dot{x}(t-\Delta t)\} + [K(t-\Delta t)]\{x(t-\Delta t)\} \\ & - \{F_{\mathrm{D}}(t-\Delta t)\} - \{F_{\mathrm{K}}(t-\Delta t)\} \end{aligned} \tag{4.153}$$

By defining the state vector

$$\{Z(t)\} = \begin{Bmatrix} \{x(t)\} \\ \{\dot{x}(t)\} \end{Bmatrix} \tag{4.154}$$

Equations 4.149 and 4.150 can be combined as

$$\begin{aligned} \begin{Bmatrix} \{\dot{x}(t)\} \\ \{\ddot{x}(t)\} \end{Bmatrix} = {} & \begin{bmatrix} [0] \\ \hline -[M]^{-1}[K] \end{bmatrix} \begin{bmatrix} [I] \\ \hline -[M]^{-1}[C] \end{bmatrix} \begin{Bmatrix} \{x(t)\} \\ \{\dot{x}(t)\} \end{Bmatrix} + \begin{bmatrix} [0] \\ \hline [M]^{-1}[\gamma] \end{bmatrix} \{u(t)\} \\ & + \begin{bmatrix} [0] \\ \hline [M]^{-1}[\delta] \end{bmatrix} \ddot{x}_{\mathrm{g}}(t) + \begin{Bmatrix} [0] \\ \hline [M]^{-1}\{F\} \end{Bmatrix} \end{aligned} \tag{4.155}$$

in which $[K] = [K(t-\Delta t)]$, $[C] = [C(t-\Delta t)]$, and $\{F\} = \{F(t-\Delta t)\}$. The compact form of Equation 4.155 is

$$\left\{\dot{Z}(t)\right\} = [A]\{Z(t)\} + [B]\{u(t)\} + [C]\ddot{x}_{\mathrm{g}}(t) + \{F\} \tag{4.156}$$

4.3.3.2 Performance index, transversality condition, and feedback gain

Suppose that the performance index is to be minimized in the time interval $[t_{i-1}, t_i]$. Since the value of the state vector at the right end point t_i, $\{Z(t_i)\}$, is unknown,

the problem involved has a free endpoint boundary whose value, $\{Z(t_i)\}$, should be minimized. Accordingly, a functional of $\{Z(t_i)\}$ should be included in the expression of the proposed performance index as follows:

$$J_i = g\left(\{Z\left(t_i\right)\}\right) + \frac{1}{2}\int_{t_{i-1}}^{t_i}\left(\{Z\left(t\right)\}^{\mathrm{T}}\left[Q\right]\{Z\left(t\right)\} + \{u\left(t\right)\}^{\mathrm{T}}\left[R\right]\{u\left(t\right)\}\right)]\,\mathrm{d}t$$
$$= g\left(\{Z\left(t_i\right)\}\right) + \int_{t_{i-1}}^{t_i}\bar{f}\left(t\right)\,\mathrm{d}t \tag{4.157}$$

where $[Q]$ is a $2n \times 2n$ positive semidefinite matrix, $[R]$ is a $r \times r$ positive-definite matrix, and $g\left(\{Z\left(t_i\right)\}\right)$ can be put in the form of

$$g\left(\{Z\left(t_i\right)\}\right) = \{Z\left(t_i\right)\}^{\mathrm{T}}\left[S\right]\{Z\left(t_i\right)\} \tag{4.158}$$

in which $[S]$ is a $2n \times 2n$ positive semidefinite matrix.

Since the problem is a free endpoint boundary value problem, in order to minimize the generalized performance index, J_i not only Euler equations but also transversality conditions should be met at the end point t_i. Suppose that the end conditions relating the endpoint variables are given by

$$\begin{cases} t_{i-1} = t_0 + \sum_{k=1}^{i-1}\Delta t_k \\ \{Z\left(t_{i-1}\right)\} = \{Z_{i-1}\} \\ t_i = t_0 + \sum_{k=1}^{i}\Delta t_k \end{cases} \tag{4.159}$$

where Δt is the time increment. Equation 4.159 can also be written as

$$\{\Omega\} = \begin{Bmatrix} \Omega_1 \\ \Omega_2 \\ \Omega_3 \end{Bmatrix} = \begin{Bmatrix} \left(t_{i-1} - t_0\right) - \sum_{k=1}^{i-1}\Delta t_k \\ \{Z\left(t_{i-1}\right)\} - \{Z_{i-1}\} \\ \left(t_{\mathrm{i}} - t_0\right) - \sum_{k=1}^{i}\Delta t_k \end{Bmatrix} = 0 \tag{4.160}$$

By introducing multipliers $\{\mu\}$ and $\{\lambda\}$ and forming the following augmented functions:

$$G = g + \{\mu\}^{\mathrm{T}}\{\Omega\} \tag{4.161}$$
$$F = \bar{f} + \{\lambda(t)\}^{\mathrm{T}}\left([A]\{Z\left(t\right)\} + [B]\{u\left(t\right)\} + \{C\}\ddot{x}_{\mathrm{g}}\left(t\right) + \left\{\bar{F}\right\} - \left\{\dot{Z}\left(t\right)\right\}\right)$$
$$= \bar{f} + \{\lambda\left(t\right)\}^{\mathrm{T}}\{f\left(t\right)\} \tag{4.162}$$

The transversality condition can be expressed as

$$\mathrm{d}G - \left(\left\{ \frac{\partial F}{\partial \left\{ \dot{Z}(t) \right\}} \right\}^{\mathrm{T}} \left\{ \dot{Z}(t) \right\} - F \right) \mathrm{d}t \Big|_{t_{i-1}}^{t_i} + \left\{ \frac{\partial F}{\partial \left\{ \dot{Z}(t) \right\}} \right\} \cdot \mathrm{d}\left\{ Z(t) \right\} \Big|_{t_{i-1}}^{t_i} = 0 \tag{4.163}$$

Substitution of Equations 4.161 and 4.162 into Equation 4.163 yields

$$[S]\{Z(t_i)\} - \{\lambda(t_i)\} = \{0\} \tag{4.164}$$

Equations 4.157 through 4.164 for nonlinear systems look similar to equations in Section 4.3.2.2 for linear systems. However, since the format of their motion equations and solution procedures are different, the derivation process for their transversality conditions is quite different. By applying Euler equation in Equation 4.157, the following characteristic equations can be obtained:

$$[Q]\{Z(t)\} + [A]^{\mathrm{T}}\{\lambda(t)\} + \{\lambda(t)\} = \{0\} \tag{4.165}$$

$$[R]\{u(t)\} + [B]^{\mathrm{T}}\{\lambda(t)\} = \{0\} \tag{4.166}$$

Equation 4.166 can be rewritten as

$$\{u(t)\} = -[R]^{-1}[B]^{\mathrm{T}}\{\lambda(t)\} \tag{4.167}$$

For a closed-loop control system, the relation between the state vector $\{Z(t)\}$ and the control force vector can be expressed as

$$\{u(t)\} = -[G]\{Z(t)\} \tag{4.168}$$

where $[G]$ is called feedback gain matrix. By combining Equations 4.167, 4.168, and transversality condition 4.164, the expression of feedback gain matrix at each endpoint t_i is obtained as follows:

$$[G(t_i)] = [R]^{-1}[B]^{\mathrm{T}}[S] \tag{4.169}$$

Note that the feedback gain matrix $[G(t_i)]$ is actually a constant matrix, it is neither a function of time t_i nor a function of time increment Δt. Therefore, during the computation process, Δt can be arbitrarily changed within the range of precision.

4.3.3.3 Solution technique

By substituting Equations 4.168 and 4.169 into Equation 4.152 and employing Wilson-θ method, the solution of the state equation of motion can be derived as [7]:

$$\{Z(t)\} = \left([I] + [A_2][R]^{-1}[B][S]\right)^{-1} (\{D(t-\Delta t)\}) + [A_1]\ddot{x}_g(t) \tag{4.170}$$

where

$$\begin{aligned}\{D(t-\Delta t)\} = {} & [A_3]\{Z(t-\Delta t)\} + [A_4](\{F_D(T-\Delta T)\} + \{F_S(t-\Delta t)\}) \\ & + [A_5]\{u(t-\Delta t)\} + \{A_6\}\ddot{x}_g(t-\Delta t)\end{aligned} \tag{4.171}$$

in which matrices $[A_i]\,(i = 1, 2, \ldots, 6)$ are functions of $t - \Delta t$ as follows:

$$\begin{cases} [A_1] = \theta^{-2}\left\{\dfrac{\{T_1\}}{3/\Delta t\,\{T_2\}}\right\}, [A_2] = \theta^{-2}\left[\dfrac{[T_3]}{3/\Delta t\,[T_4]}\right] \\ [A_3] = \theta^{-2}\left[\dfrac{[I]}{[0]}\middle|\dfrac{\theta^{-2}[E][T_3]}{[I]+\theta^{-2}[E][T_4]}\right], [A_4] = \theta^{-2}\left[\dfrac{[E][T_5]}{[E][T_6]}\right] \\ [A_5] = -\theta^{-2}\left[\dfrac{[E][T_7]}{[E][T_8]}\right][M]\{C\}, [A_6] = \theta^{-2}\left[\dfrac{[E][T_7]}{[E][T_8]}\right][B] \end{cases} \tag{4.172}$$

in which

$$\left.\begin{aligned} & \theta = \text{constant greater than } 1.37 \\ & [I] = (n \times n) \text{ identity matrix} \\ & [T_1] = -[E][M]\{C\} \\ & [T_2] = [E][B] \\ & [T_3] = \frac{6}{\Delta t}[M] + 3\theta[C] + \Delta t\left(\theta^2 - 1\right)[K] \\ & [T_4] = -3[K] \\ & [T_5] = -(3[I] + [S_1]) \\ & [T_6] = -\frac{6}{\Delta t}[I] - [S_2] \\ & [T_7] = 2[I] + [S_1] \\ & [T_8] = \frac{3}{\Delta t}[I] + [S_2] \\ & [E] = \left(\frac{6}{(8\Delta t)^2}[M] + \frac{3}{\Delta t}[C] + [K]\right)^{-1} \\ & [S_1] = \left(\Delta t\,(1.5\theta - 1)[C] + 0.5\,(\Delta t)^2\left(\theta^2 - \theta\right)[K]\right)[M]^{-1} \\ & [S_2] = (3(\theta - 1)[C] + \Delta t\theta\,(\theta - 1.5)[K])[M]^{-1} \end{aligned}\right\} \tag{4.173}$$

4.3.3.4 Concept of unbalanced force correction

In order to improve the precision of the numerical solution for the analysis of nonlinear structural systems, the concept of unbalanced force correction is introduced for simplicity. Consider only a single degree-of-freedom active control system, mechanical characteristics of the structural members follow a bilinear model as shown in Figure 4.19. On the basis of this bilinear model, the following equilibrium equations can be obtained:

$$\begin{cases} m\ddot{x}(t_1) + c\dot{x}(t_1) + k_1 x(t_1) = p(t_1) \\ m\ddot{x}\left(t_{\xi^-}\right) + c\dot{x}\left(t_{\xi^-}\right) + k_1 x\left(t_{\xi^-}\right) = p\left(t_\xi\right) \\ m\ddot{x}\left(t_{\xi^+}\right) + c\dot{x}\left(t_{\xi^+}\right) + k_1 x\left(t_\xi^+\right) = p\left(t_\xi\right) \\ m\ddot{x}(t_2) + c\dot{x}(t_2) + k_2 x(t_2) = p(t_2) \\ m\ddot{x}(t_3) + c\dot{x}(t_3) + k_2 x(t_3) = p(t_3) \end{cases} \tag{4.174}$$

where m and c are mass and damping coefficient, and k_1 and k_2 denote stiffness coefficients before and after the structural member yields, respectively, p represents external excitation. Assume that deformation $x\left(t_\xi\right)$ equals x_y at time instant $t = t_\xi$, in which x_y is the yield deformation of the structural member and t_ξ is located inside the time interval (t_1, t_2).

In theory, the above equation group can be solved in the following way:

1. At $t = t_\xi$,

$$\begin{cases} m\left(\ddot{x}\left(t_{\xi^-}\right) - \ddot{x}(t_1)\right) + c\left(\dot{x}\left(t_{\xi^-}\right) - \dot{x}(t_1)\right) \\ \quad + k_1\left(x\left(t_{\xi^-}\right) - x(t_1)\right) = p\left(t_\xi\right) - p(t_1) \text{ or} \\ m\ddot{\hat{x}}\left(t_{\xi^-}\right) + c\dot{\hat{x}}\left(t_{\xi^-}\right) + k_1\hat{x}\left(t_{\xi^-}\right) = \hat{p}\left(t_\xi\right) \end{cases} \tag{4.175}$$

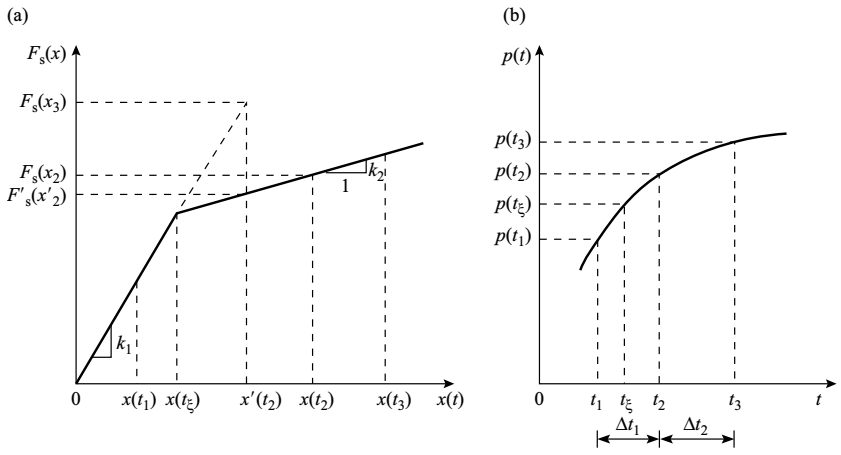

FIGURE 4.19 Bilinear model and concept of unbalanced force.

where $\hat{x}\left(t_{\xi^-}\right) = x\left(t_{\xi^-}\right) - x\left(t_1\right)$ and $\hat{p}\left(t_\xi\right) = p\left(t_\xi\right) - p\left(t_1\right)$. By solving Equation 4.175 $\hat{x}\left(t_{\xi^-}\right)$ can be found and $x\left(t_\xi\right)$ can be obtained by

$$x\left(t_\xi\right) = x\left(t_1\right) + \hat{x}\left(t_{\xi^-}\right) = x_{\mathrm{y}} \tag{4.176}$$

2. In the same way, at $t = t_2$ and $t = t_3$

$$\begin{cases} m\ddot{\hat{x}}\left(t_2\right) + c\dot{\hat{x}}\left(t_2\right) + k_2\hat{x}\left(t_2\right) = \hat{p}\left(t_2\right) \\ m\ddot{\hat{x}}\left(t_3\right) + c\dot{\hat{x}}\left(t_3\right) + k_2\hat{x}\left(t_3\right) = \hat{p}\left(t_3\right) \end{cases} \tag{4.177}$$

where $\hat{x}\left(t_2\right) = x\left(t_2\right) - x\left(t_{\xi^-}\right)$, $\hat{x}\left(t_3\right) = x\left(t_3\right) - x\left(t_2\right)$ and $\hat{p}\left(t_2\right) = p\left(t_2\right) - p\left(t_\xi\right)$, $\hat{p}\left(t_3\right) = p\left(t_3\right) - p\left(t_2\right)$. After solving Equation 4.177, $x\left(t_2\right)$ and $x\left(t_3\right)$ can be obtained by

$$\begin{cases} x\left(t_2\right) = x\left(t_{\xi^-}\right) + \hat{x}\left(t_2\right) \\ x\left(t_3\right) = x\left(t_2\right) + \hat{x}\left(t_3\right) \end{cases} \tag{4.178}$$

However, the problem now is that t_ξ unknown, which implies the second and third equations of the group in Equation 4.174 are difficult to establish. In order to find t_ξ, many trial and error steps are needed. This is quite time-consuming [7]. Instead of trying to find t_ξ, simply use k_1 in time interval $[t_1, t_2]$ that yields

$$m\ddot{\hat{x}}'(t_2) + c\dot{\hat{x}}'(t_2) + k_1\hat{x}\left(t_2\right) = \hat{p}'\left(t_2\right) \tag{4.179}$$

where $\hat{x}'(t_2) = x\left(t_2\right) - x\left(t_1\right)$ and $\hat{p}'\left(t_2\right) = p\left(t_2\right) - p\left(t_1\right)$. By solving Equation 4.179, displacement increment $\hat{x}'(t_2)$ can be obtained; then the displacement at $t = t_2$ is

$$x'(t_2) = x\left(t_1\right) + \hat{x}'(t_2) \tag{4.180}$$

Note that (1) $x'(t_2)$ is not the actual displacement at $t = t_2$; (2) $x'(t_2)$ is smaller than $x\left(t_2\right)$, the actual displacement at $t = t_2$; (3) the internal force given in Equation 4.179 is $F_k\left(x'\left(t_2\right)\right) = k_1x'\left(t_2\right)$, which is greater than the actual value $F_k\left(x\left(t_2\right)\right) = k_1x_y + k_2\left(x\left(t_2\right) - x_y\right)$. This means that there is an overshooting on the loop of the internal force if Equation 4.180 is used. The overshooting of the internal force produced by Equation 4.180 can be detected as

$$U = \left(k_1 - k_2\right)\left(x'(t_2) - x_{\mathrm{y}}\right) \tag{4.181}$$

where U is the unbalanced force. Subtracting unbalanced force U on both sides of Equation 4.179 yields

$$m\ddot{\hat{x}}'(t_2) + c\dot{\hat{x}}\left(t_2\right) + k_2\hat{x}\left(t_2\right) - U = \hat{P}'\left(t_2\right) - U \tag{4.182}$$

in which the overshooting on the internal force loop is eliminated.

It needs to be pointed out that this does not mean $x'(t_2)$ in the solution of Equation 4.182 is correct. As indicated earlier, $x'(t_2)$ is smaller than actual displacement $x(t_2)$. Using the incremental external force for the next interval $[t_2, t_3]$ expressed as

$$\hat{p}'(t_3) = p(t_3) - p(t_2) + U \tag{4.183}$$

In addition, using small time increment, the structural response at $t = t_3$, is expected to be the correct value [7].

4.3.3.5 Numerical illustrations

The same tendon-controlled six-story structure employed in Section 4.3.2.4 is used to study the fundamental behavior of various active control algorithms for nonlinear seismic structures. N-S component of May 18, 1940 El-Ceatro earthquake is again used as ground acceleration input. In order to investigate the structural nonlinear behavior, the earthquake-excitation magnitude is increased by a factor of 2.0. The nonlinear structure is modeled with bilinear model as shown in Figure 4.19. Yielding deformation for each of the columns is 1.0 cm. Assume the second stiffness $(k_i)_2$ is 1/10 of the linear stiffness coefficient $(k_i)_1$. The structure is equipped with active tendon at the first floor. GOAC and ROAC algorithms for nonlinear seismic structures are employed. In the GOAC algorithm, the configuration of [S] matrix is generated by using one row of identical element scheme as mentioned in Section 4.3.2.4.

Figure 4.20a and b plot the maximum top-floor displacement, maximum active force, and integral performance index for the six-story nonlinear seismic structure, obtained by using from ROAC and GOAC algorithms, respectively, with the change of control design parameter. These figures show that the integral performance index for ROAC algorithm keeps growing, but the performance index for GOAC algorithm shows a minimum point at S_0/R equal to 8×10^5. Recall that in an optimization problem, an objective function or performance index must be minimized to find the optimal solution. If the performance index cannot be minimized, then its solution is not a global optimal solution. It can also be found that this scant difference in the optimum S_0/R ratio does not make the performance of the active control system change a lot since performances of the system is quite stable in the neighborhood of the optimum S_0/R ratio. Hence, active control design for a linear seismic structure can be directly used for the corresponding nonlinear seismic structure.

Figure 4.21 shows hysteretic loops of the third-floor columns for the nonlinear structure with and without active control subjected to two times the earthquake acceleration, respectively. It indicates that the active control effectiveness is very significant: when the active control system is used, displacement is reduced from 1.41 to 0.67 cm.

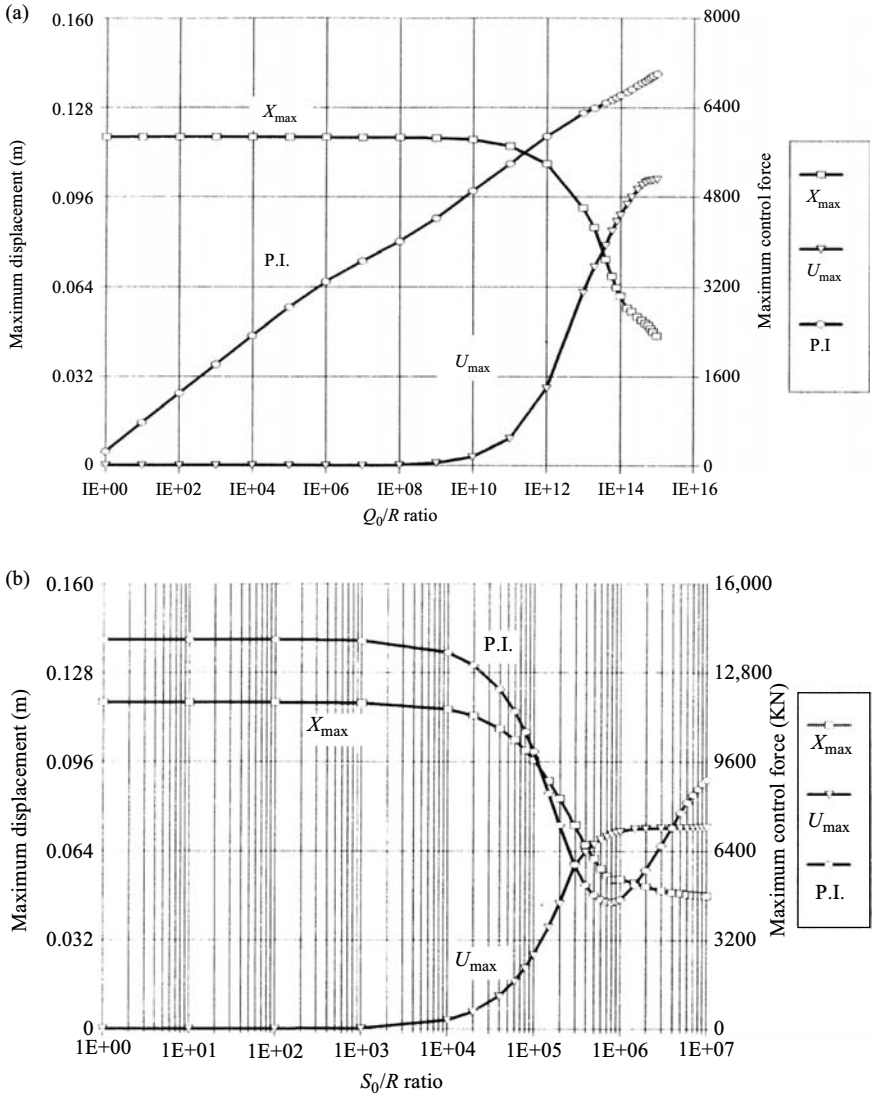

FIGURE 4.20 Influence of Q_0/R ratio on X_{max}, U_{max} and P.I. for nonlinear system: (a) Influence in ROAC and (b) influence in GOAC.

Earthquake responses of the linear and nonlinear seismic structure with active tendon control at the first floor are compared in Figure 4.22. Note that the same structural properties are used as those for the earlier cases shown in Section 4.3.2.4. This figure shows the relative top-floor displacement of a linear and nonlinear structure less than 2.0 times of the earthquake acceleration, respectively. In comparison, it can be seen that for linear and nonlinear structures with active control, their top-floor responses are quite different.

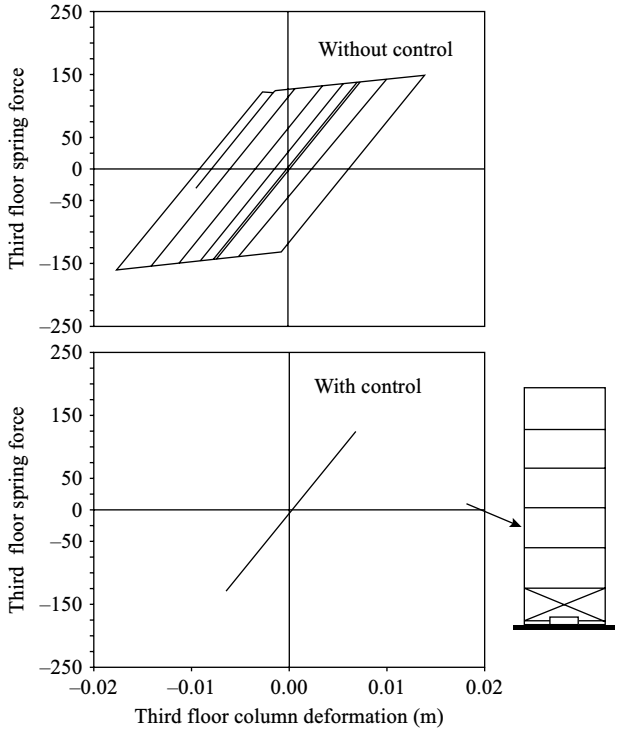

FIGURE 4.21 Effectiveness of active control on third floor column deformation.

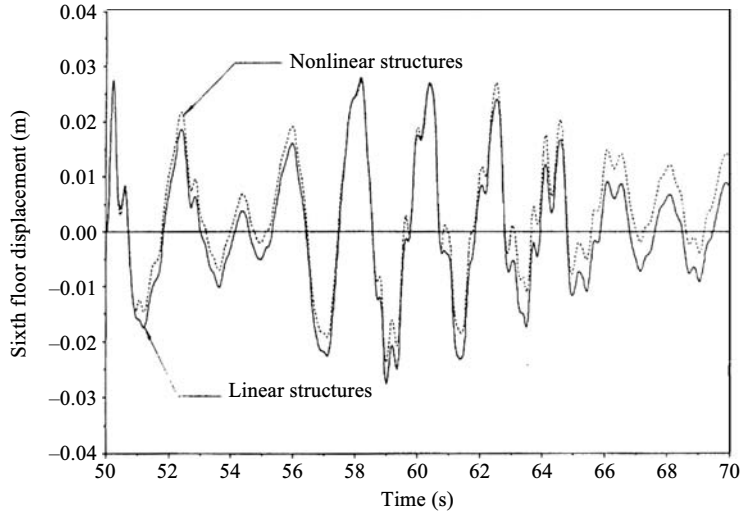

FIGURE 4.22 Top-floor displacement of linear and nonlinear seismic structures.

4.4 Concluding Remarks

This chapter presents the analytical study of smart seismic structures with active control. A general model is formulated first. Then two major numerical algorithms, ROAC algorithm and GOAC algorithm, are encompassed. By introducing a generalized performance index and employing transversality conditions, a generalized feedback gain matrix is derived in GOAC. The derivation has significant importance over the IOAC, because the generalized feedback gain matrix is not dependent on incremental time intervals as IOAC does. Therefore, with the generalized algorithm, the control force and structural response are identical even if time increments are different. Furthermore, during the computation process, the time increment can be arbitrarily changed within a range of precision and not lead to discontinuous results. This chapter also includes inelastic response of active-controlled structures for which the technique of unbalanced force correction is introduced. The technique can save significant computation time because nonlinear materials can change properties within the time interval used in the control algorithm. Numerical examples show the effectiveness of GOAC on nonlinear structures. By using active control, the inelastic deformation of structures can be significantly reduced. Numerical analysis also shows that the active control design for a linear seismic structure can still be used even when a larger earthquake causes it to enter its inelastic range since the performance index is very stable in the neighborhood of the optimum S_0/R ratio.

In recent years, numerous shaking table tests have been conducted to study the feasibility of active seismic response control, to evaluate the effectiveness and stability of the system, as well as to verify the developed optimal control algorithms on structural models. Full-scale active control systems have also been tested in the laboratory or installed on real building structures, and test results and real-time measurements show such systems are very adaptive to the seismic excitations and effective for seismic response reduction. Readers are encouraged to read pertinent reference materials [28,29,32–35,38,42,44,45] for details, especially the full-scale implementation and real-time measurements.

References

1. Babcock, D.A., Simulated dynamic response of a servo valve controlled hydraulic actuator, *NASA Technical Memorandum 101644*, 1990.
2. Brogan, W.L., Applications of a determinant identity to pole assignment and observer problems, *IEEE Transactions on Automatic Control*, AC-19, 612, 1974.
3. Cheng, F.Y., Response control based on structural optimization and its combination with active protection, in *Proceedings of the Ninth World Conference on Earthquake Engineering*, International Association for Earthquake Engineering, VIII, Tokyo, 1988, p. 471.
4. Cheng, F.Y., Application and assessment of structural optimization and active control for seismic structures, in *Proceedings of Recent Advances in Multidisciplinary Analysis and Optimization, Third Air Force and NASA Symposium*, National Aeronautics and Space Administration, Washington, DC, 1990, p. 171.

5. Cheng, F.Y., Optimum design and control of tall buildings, in *Proceedings of the Fourth World Congress: 2000 and Beyond*, Council on Tall Buildings and Urban Habitat, Bethlehem, Pennsylvania, 1990.
6. Cheng, F.Y., Generalized optimal active control algorithm for seismic-resistant structures with active and hybrid control, *International Journal of Computer Applications in Technology*, 13, 2000.
7. Cheng, F.Y., *Matrix Analysis of Structural Dynamics*, Marcel Dekker, Inc., New York, 2001.
8. Cheng, F.Y., Choi, C.K., and Juang, D.S., Developments of optimum design and control of seismic structures, in *Intelligent Structures*, Elsevier Science Ltd., London, 1990, p. 264.
9. Cheng, F.Y. and Jiang, H., Optimum control of a hybrid system for seismic excitations with state observer technique, *Smart Materials and Structures*, 7, 654, 1998.
10. Cheng, F.Y. and Jiang, H., Hybrid control of seismic structures with optimal placement of control devices, *ASCE Journal of Aerospace Engineering*, 11, 52, 1998.
11. Cheng, F.Y. and Pantelides, C.P., Deflection reduction and enhancement of human comfort for tall building optimum design with active controls, in *Stability of Tall Steel Buildings*, Council on Tall Buildings and Urban Habitat, Bethlehem, Pennsylvania, 1986, p. 93.
12. Cheng, F.Y. and Pantelides, C.P., Combining structural optimization and active mass damper controls and random process, in *Recent Developments in Structural Optimization*, American Society of Civil Engineers, Reston, Virginia, 1986, p. 40.
13. Cheng, F.Y. and Pantelides, C.P., Optimal control of seismic structures, in *Proceedings of the Third ASCE Engineering Mechanics Conference*, 1986, American Society of Civil Engineers, Reston, Virginia, p. 764.
14. Cheng, F.Y. and Pantelides, C.P., Optimization of structures and controls under seismic loading, in *Proceedings of International Conference on Computational Mechanics*, Springer-Verlag, Tokyo, 1986, p. X-135.
15. Cheng, F.Y. and Pantelides, C.P., Optimum seismic structural design with tendon control, American Society of Civil Engineers, Reston, Virginia, 1987, p. 592.
16. Cheng, F.Y. and Pantelides, C.P., Optimal active control of wind structures using instantaneous algorithm, *ASME Journal of Vibration Control and Active Vibration Suppression*, 21, 21, 1987.
17. Cheng, F.Y. and Pantelides, C.P., Development in combining structural optimization and optimal control for seismic and wind structures, in *Critical Engineering Systems*, Korea Advanced Institute of Science and Technology, I, 80, Seoul, Korea, 1987.
18. Cheng, F.Y. and Pantelides, C.P., Algorithm development for using optimal control in structural optimization subjected to seismic and wind forces, *NSF Report*, *NTIS No. PB90-133471/AS*, U.S. Department of Commerce, National Technical Information Service, VA, 1988.
19. Cheng, F.Y., Suthiwong, S., and Tian, P., Generalized optimal active control with embedded and half-space soil-structure interaction, in *Proceedings of the Eleventh ASCE Analysis & Computation Conference*, 1994, p. 337.
20. Cheng, F.Y. and Tian, P., Generalized optimal active control algorithm for nonlinear seismic structures, in *Proceedings of the Tenth World Conference on Earthquake*

Engineering, International Association for Earthquake Engineering, A.A. Balkema Publisher, 7, 3677, 1992.
21. Cheng, F.Y. and Tian, P., Generalized optimal active control algorithm with weighting matrix configuration, stability and time-delay, *International Journal of Structural Engineering and Mechanics*, 1, 119, 1993.
22. Cheng, F.Y. and Tian, P., Integrated optimal control and structural optimization, in *Proceedings of US–China–Japan Trilateral Workshop on Structural Control*, Tongji University, Shanghai, China, 1993, p. 61.
23. Cheng, F.Y. and Tian, P., Generalized optimal active control for linear and nonlinear seismic structures, in *Proceedings of the First World Conference on Structural Control*, International Association for Structural Control, TP1:21, 1994.
24. Cheng, F.Y., Tian, P., and Suthiwong, S., Generalized optimal active control algorithm of seismic structures and related soil-structure formulations, in *Computational Mechanics in Structural Engineering, Recent Developments and Future Trends*, Cheng, F.Y. and Fu, Zizhi (eds.), Elsevier Science Ltd., London and New York, 1991, p. 49.
25. Cheng, F.Y. et al., Theoretical and experimental studies on hybrid control of seismic structures, in *Proceedings of the Twelfth ASCE Conference on analysis and Computation*, Cheng, F.Y., (ed.), Chicago, 1996.
26. Citron, S.J., *Elements of Optimal Control*, Holt, Rinehart & Winston, Inc., Austin, Texas, 1969.
27. Chung, L.L., Reinhorn, A.M., and Soong, T.T., Experiments on active control of seismic structures, *ASCE Journal of Engineering Mechanics*, 114, 241, 1988.
28. Chung, L.L. et al., Experimental study of active control MDOF structures under seismic excitations, *NCEER Technical Report 88-0025*, National Center for Earthquake Engineering, Buffalo, New York, 1988.
29. Chung, L.L. et al., Experimental study of active control for MDOF seismic structures, *ASCE Journal of Engineering Mechanics*, 115, 1609, 1989.
30. Davison, E.J. and Maki, M.C., Numerical solution of the matrix Riccati equation, *IEEE Transactions on Automatic Control*, AC-18, 71, 1973.
31. DeSilva, C.W. *Control Sensors and Actuators*, Prentice-Hall, Englewood Cliffs, New Jersey, 1989.
32. Dyke, S.J. et al., Absolute acceleration feedback control strategies for the active mass driver, in *Proceedings of the First World Conference on Structural Control*, Los Angeles, California, 2, TP1:51 1994.
33. Dyke, S.J. et al., Experimental verification of acceleration feedback control strategies for an active tendon system, *NCEER Technical Report 94-0024*, National Center for Earthquake Engineering Research, Buffalo, New York, 1994.
34. Dyke, S.J. et al., Acceleration feedback control of MDOF structures, *ASCE Journal of Engineering Mechanics*, 122, 907, 1996.
35. Dyke, S.J. et al., Implementation of an active mass driver using acceleration feedback control, *Microcomputers in Civil Engineering*, 11, 305, 1996.
36. Funakubo, H., *Actuators for Control*, Gordon and Breach Science Publishers, New York, 1991.
37. Grantham, W.J. and Vincent, T.L., *Modern Control Systems: Analysis and Design*, John Wiley & Sons, New York, 1993.
38. International Association of Structural Control (IASC), *Proceedings of the First, Second, and Third World Conferences on Structural Control*, 1994 (Los Angeles,

California), 1998 (Kyoto, Japan), 2002 (Como, Italy), and 2006 (San Diego, California).

39. Kailath, T., *Linear Systems*, Prentice-Hall, Englewood Cliffs, New Jersey, 1980.
40. Kautsky, J. and Nichols, N.K., Robust pole assignment in linear state feedback, *International Journal of Control*, 41, 1129, 1985.
41. Kleinman, D.L., On an iteration technique for Ricatti equation computations, *IEEE Transactions on Automatic Control*, AC-13, 114, 1968.
42. Kobori T., Kanayama H., and Kamagata S, A proposal of new anti-seismic structure with active seismic response control system—dynamic intelligent building, in *Proceedings of the ninth World Conference on Earthquake Engineering*, VIII, Tokyo/Kyoto, Japan, 465, 1988.
43. Laub, A.J., A Schur method for solving algebraic Ricatti equations, *IEEE Transactions on Automatic Control*, AC-24, 913, 1979.
44. Rodellar, J. et al., Experimental digital predictive control of structures, *ASCE Journal of Engineering Mechanics*, 115, 1245, 1989.
45. Soong, T.T., *Active Structural Control: Theory and Practice*, 1st edn, Longman Scientific & Technical, UK and John Wiley & Sons, New York, 1990.
46. Spencer, B.F. Jr. et al., Acceleration feedback control strategies for aseismic protection, in *Proceedings of the American Control Conference*, San Francisco, California, 1993, p. 1317.
47. Vaugan, D.R., A negative exponential solution for the matrix Riccati equation, *IEEE Transactions on Automatic Control*, AC-14, 72, 1969.
48. Yang, J.N., Akbarpur, A. and Ghaemmaghami, P., Instantaneous optimal control laws for tall buildings under seismic excitations, *NCEER Technical Report 87-0007*, National Center for Earthquake Engineering, Buffalo, New York, 1987.

5 Smart Seismic Structures Using Semiactive and Hybrid Control Systems

In Chapters 2, 3, and 4, smart seismic structures using base-isolation systems, passive dampers, and active control systems have been discussed in detail. Recall that two more types of control systems were introduced earlier: semiactive and hybrid. They both combine active and passive control mechanisms and thus are both "hybrid" systems in some sense. They both gain the *reliability* of passive devices and *adaptability* of active control systems. The difference is the function of the active device of the two systems. The one in hybrid systems applies control force directly to the structure, while the one in semiactive systems adjusts the behavior of the passive device. In other words, a semiactive system has adjustable properties in real time but cannot directly apply energy to the smart structure to control its seismic response. Thus, the capacity of a semiactive system is somewhat limited by its base, a passive device. A hybrid system such as the *hybrid damper-actuator bracing control* (HDABC) system can gain the *capacity* of its active control device in addition to its reliability and adaptability.

A brief introduction of semiactive and hybrid control systems for smart seismic structures has been provided in Chapter 1. This chapter presents detailed discussion of semiactive and hybrid control systems for seismic response control of building structures. In particular, the electrorheological (ER) and magnetorheological (MR) dampers serve as examples for semiactive systems, and HDABC systems serve as the example for hybrid systems. Section 5.1 formulates the dynamic model of semiactive dampers and hybrid control devices on the basis of their mechanism. Section 5.2 develops a general analytical model of smart seismic structures using semiactive dampers or hybrid control system, with dynamic interaction between the structure and control devices considered. Section 5.3 discusses the stability and control strategy of the hybrid system. Section 5.4 uses numerical studies to demonstrate the effectiveness of the hybrid system, and to compare the effectiveness of the MR damper and the HDABC system for seismic response control. Section 5.5 presents experimental studies of semiactive and hybrid systems, with the shaking table tests of a three-story model structure with an HDABC system as example.

5.1 Dynamic Model of Control Devices for Semiactive and Hybrid Systems

To design control devices for a smart seismic structure, their analytical model must be developed first with their dynamic behavior captured. Many studies on smart seismic structures made the assumption that control devices be linear proportional. Sizable control devices such as hydraulic actuators, MR dampers, and viscous fluid dampers are usually employed for seismic response control as they can generate required control force for large civil engineering structures. Studies show that hydraulic actuators [1,13,17], MR dampers [16,27], and viscous fluid dampers [11,20] are mechanical dynamic systems themselves and have no proportional relation between input and output. Subsequent experiments [10,14,15] reveal that when hydraulic actuators are applied to a structure, their dynamics interact with the structure, thus adversely affecting control action or even making the open-loop system unstable. Therefore, an accurate analytical study of smart seismic structures shall consider the dynamic behavior of control devices. The challenge is that these devices are complicated mechanical systems with intrinsic nonlinear dynamics.

Control devices can be installed on a smart structure in many different ways. Figure 5.1a shows one typical way that installs the control device on a K-brace between two floors of the structure. Its cylinder is bolted to the upper floor of the structure, and its piston is connected to the K-brace supported by the lower floor of the structure. Figure 5.1b provides more details on a damper, an actuator, or a hybrid device of HDABC system installed on the first floor of a structure and supported by a K-brace. The hybrid device consists of a viscous fluid damper and a servovalve-controlled hydraulic actuator. Under the excitation of earthquake ground motion $\ddot{x}_g(t)$, the structure floor and the brace will vibrate. Relative displacement between the brace and the upper floor of the structure drives pistons moving with respect to their cylinders, thus generating the control force. By denoting displacements of the upper floor and the K-brace as $x_i(t)$ and $x_{bj}(t)$, respectively, the piston displacement of the control device is

$$\Delta(t) = x_{bj}(t) - x_i(t) \tag{5.1}$$

In the following sections for system modeling and analysis, it is assumed that the control devices are installed on K-braces. The modeling and analysis process is the same for any other ways of device installation except that the relative displacement between the piston and the cylinder of the control device may be different.

5.1.1 Modeling of Servovalve-Controlled Hydraulic Actuators

This section derives the model of the hydraulic actuator, which can generate large force for seismic response control. Since the actuator is a mechanical dynamic

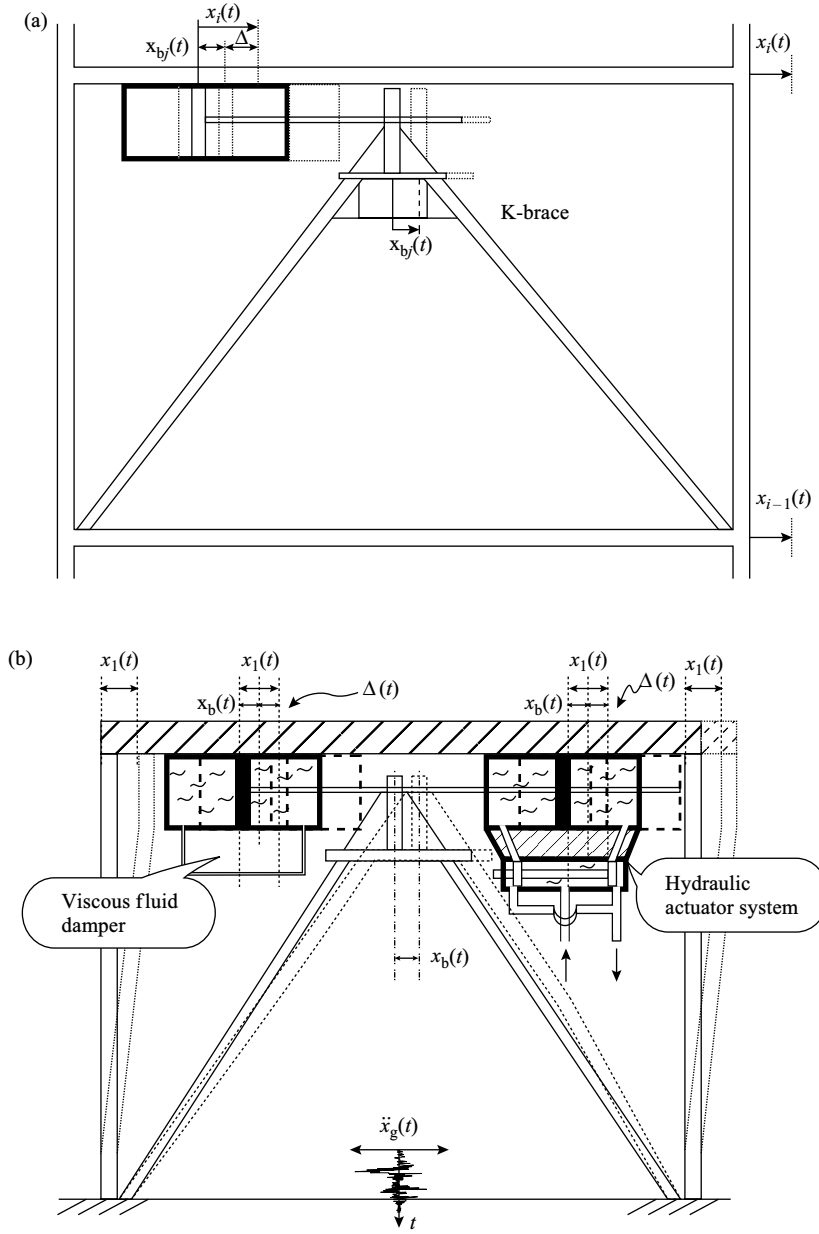

FIGURE 5.1 (a) Smart seismic structure with control device mounted on K-brace and (b) one-story structure with HDABC.

system, its model must be formulated on the basis of its dynamic behavior. Pulse generators have also been proposed for seismic response control but they are less common. Readers are encouraged to read references [22,25] for more details.

As shown in Figure 5.2, the *hydraulic actuator* system consists of an actuator, a *servovalve*, and a *fluid pumping system* [1,13,17]. The servovalve regulates flow direction and density between fluid supply and *actuator chambers* according to *valve-piston* displacement $c(t)$, thus changing fluid pressure in both actuator chambers. Given the high pressure of the fluid supply, the pressure difference between the two chambers can generate a large active control force $f_a(t)$.

Continuity of mass flow into left chamber gives

$$\frac{dm_1(t)}{dt} = \rho_1(t)Q_1(t) \tag{5.2}$$

where $m_1(t)$ and $\rho_1(t)$ are mass and mass density of the fluid in the left chamber, respectively; $Q_1(t)$ is volumetric flow to the left chamber. If the fluid volume in the left chamber is denoted as $V_1(t)$,

$$m_1(t) = \rho_1(t)V_1(t) \tag{5.3}$$

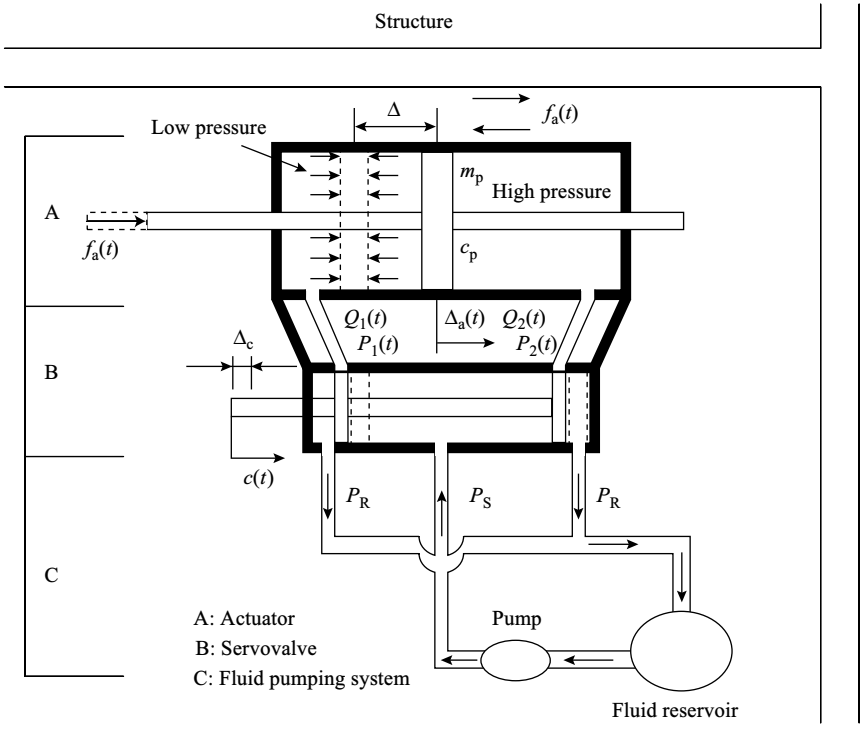

FIGURE 5.2 Servovalve-controlled hydraulic actuator system.

Substituting Equation 5.3 into Equation 5.2 yields

$$\rho_1(t)Q_1(t) = \frac{\mathrm{d}\rho_1(t)}{\mathrm{d}t}V_1(t) + \rho_1(t)\frac{\mathrm{d}V_1(t)}{\mathrm{d}t} \tag{5.4}$$

Since fluid bulk modulus β is defined as

$$\beta = \frac{\mathrm{d}P}{\mathrm{d}\rho/\rho} \tag{5.5}$$

and noting that

$$\frac{\mathrm{d}V_1(t)}{\mathrm{d}t} = A\frac{\mathrm{d}\Delta_\mathrm{a}(t)}{\mathrm{d}t} \tag{5.6}$$

then Equation 5.4 can be written as

$$Q_1(t) = \frac{V_1(t)}{\mathrm{d}P_1(t)/\left[\mathrm{d}\rho_1(t)/\rho_1(t)\right]}\frac{\mathrm{d}P_1(t)}{\mathrm{d}t} + A\frac{\mathrm{d}\Delta_\mathrm{a}(t)}{\mathrm{d}t} = \frac{V_1(t)}{\beta}\frac{\mathrm{d}P_1(t)}{\mathrm{d}t} + A\frac{\mathrm{d}\Delta_\mathrm{a}(t)}{\mathrm{d}t} \tag{5.7}$$

where A is cross-section area of the actuator cylinder, $P_1(t)$ is fluid pressure in the left chamber, and $\Delta_a(t)$ is displacement of the actuator piston. Thus,

$$\frac{\mathrm{d}P_1(t)}{\mathrm{d}t} = \beta\frac{Q_1(t)}{V_1(t)} - \frac{\beta A}{V_1(t)}\frac{\mathrm{d}\Delta_\mathrm{a}(t)}{\mathrm{d}t} \tag{5.8}$$

Similarly, for the right chamber,

$$Q_2(t) = \frac{V_2(t)}{\beta}\frac{\mathrm{d}P_2(t)}{\mathrm{d}t} - A\frac{\mathrm{d}\Delta_\mathrm{a}(t)}{\mathrm{d}t} \tag{5.9}$$

and

$$\frac{\mathrm{d}P_2(t)}{\mathrm{d}t} = \beta\frac{Q_2(t)}{V_2(t)} + \frac{\beta A}{V_2(t)}\frac{\mathrm{d}\Delta_\mathrm{a}(t)}{\mathrm{d}t} \tag{5.10}$$

where $Q_2(t)$, $P_2(t)$, and $V_2(t)$ are volumetric flow, fluid pressure, and fluid volume of the right chamber, respectively.

Force balance on the piston yields

$$f_\mathrm{a}(t) = A\left[P_2(t) - P_1(t)\right] + c_\mathrm{p}\dot{\Delta}_\mathrm{a}(t) + m_\mathrm{p}\ddot{x}_\mathrm{b}(t) \tag{5.11}$$

where c_p and m_p are damping and mass coefficients, respectively, of the piston and its rods.

The servovalve itself is a controller made up of an amplifier and an actuator, and its behavior can be described as a first-order dynamic system [1,23]

$$\tau \dot{c}(t) + c(t) = u(t) \tag{5.12a}$$

where $u(t)$ is control command, $c(t)$ is servovalve-piston displacement, and τ is defined as (f_b is servovalve bandwidth)

$$\tau = \frac{1}{2\pi f_{\mathrm{b}}} \tag{5.12b}$$

Parameters τ and f_{b} are usually specified by the manufacturer or can be easily identified from frequency response tests on the servovalve.

Flow of the viscous fluid across the servovalve gives [1]

$$Q_1(t) = K_{\mathrm{V}}\sqrt{P_{\mathrm{S}} - P_1(t)},\ Q_2(t) = K_{\mathrm{V}}\sqrt{P_2(t) - P_{\mathrm{R}}} \tag{5.13a}$$

where K_{V} is pressure-loss coefficient of the servovalve. K_{v} can be computed from manufacturer ratings of flow at a given differential pressure. For example, if a servovalve is rated for 40 gpm at 1000 psi pressure loss,

$$K_{\mathrm{V}} = \frac{3.85(40)}{\sqrt{1000}} = 4.87\,\mathrm{in}^4/(\mathrm{sec} - \sqrt{lb}) \tag{5.13b}$$

Model of the hydraulic actuator can be linearized with the following assumptions:

- Supply pressure $\mathrm{P_S}$ is constant.
- Discharge pressure $\mathrm{P_R}$ is much smaller than $\mathrm{P_S}$ and can be neglected.
- Actuator-piston displacement $\Delta_{\mathrm{a}}(t)$ and valve-piston displacement $c(t)$ are small.
- Initial conditions are

at $t = 0^-$	at $t = 0^+$
$\Delta_{\mathrm{a}}(0) = c(0) = 0, u(0) = 0$	Same
$V_1(0) = V_2(0) = V$	Same
$Q_1(0) = Q_2(0) = 0$	$Q_1(0) = Q_2(0) = Q_0$
$P_1(0) = P_2(0) = 0$	$P_1(0) = P_2(0) = P_0$

Then at initial time $t = 0^+$, Equation 5.13a becomes

$$K_{\mathrm{V}}\sqrt{P_S - P_0} = Q_0 = K_{\mathrm{V}}\sqrt{P_0 - 0} \Rightarrow P_0 = 0.5P_{\mathrm{S}}, Q_0 = K_{\mathrm{V}}\sqrt{0.5P_{\mathrm{S}}} \tag{5.13c}$$

Thus,

$$\begin{cases} P_1(t) = P_0 + \delta P_1(t) = 0.5P_S + \delta P_1(t) \\ P_2(t) = P_0 + \delta P_2(t) = 0.5P_S + \delta P_2(t) \end{cases} \tag{5.14}$$

$$\begin{cases} Q_1(t) = Q_0 + \delta Q_1(t) = K_V\sqrt{0.5P_S} + \delta Q_1(t) \\ Q_2(t) = Q_0 + \delta Q_2(t) = K_V\sqrt{0.5P_S} + \delta Q_2(t) \end{cases} \tag{5.15}$$

$$\begin{cases} V_1(t) = V + \delta V_1(t) = V + A\Delta_a(t) \\ V_2(t) = V + \delta V_2(t) = V - A\Delta_a(t) \end{cases} \tag{5.16}$$

Under normal working conditions, piston displacements of the servovalve and actuator are small, and the following assumptions can be made

$$\frac{\delta V_1}{V} \ll 1, \quad \frac{\delta V_2}{V} \ll 1; \quad \frac{\delta P_1}{P_S/2} \ll 1, \quad \frac{\delta P_2}{P_S/2} \ll 1 \tag{5.17}$$

Take the hydraulic actuator system at University of Missouri-Rolla as an example. In this system, $P_S = 3000$ psi, $A = 1.1$ in.^{2}, and $\beta = 10^6$ psi. The fluid volume change equals the fluid pressure divided by the fluid bulk modulus. Since the maximum fluid pressure is P_S, maximum volume change of the fluid is

$$\left(\frac{\delta V}{V}\right)_{\max} = \frac{P_S}{\beta} = 0.3\% \ll 1 \tag{5.18}$$

For the shaking table test, numerical simulation shows that the maximum required active control force is 170 lb for scaled El-Centro earthquake excitation (scale factors for amplitude and frequency are 0.3 and 2, respectively). Assume $\delta P = -\delta P_1 = \delta P_2$; then, force balance on the actuator piston yields $[P_2(t) - P_1(t)]A = [0.5P_S + \delta P_2(t) - 0.5P_S - \delta P_1(t)]A = 2(\delta P)A = 170$, that is, $\delta P = 170/(2 \times 1.1) = 77.3$ psi, and

$$\frac{\delta P}{P_S/2} = \frac{77.3}{3000/2} = 5.15\% \ll 1 \tag{5.19}$$

It is clear that numerical results in Equations 5.18 and 5.19 perfectly confirm the assumption expressed by Equation 5.17.

Substituting Equation 5.14 into Equation 5.13a yields

$$\begin{cases} Q_1(t) = K_V\sqrt{P_S - 0.5P_S - \delta P_1(t)} = K_V\sqrt{0.5P_S}\sqrt{1 - 2x_1(t)} \\ Q_2(t) = K_V\sqrt{P_S + 0.5P_S + \delta P_2(t)} = K_V\sqrt{0.5P_S}\sqrt{1 + 2x_2(t)} \end{cases} \tag{5.20}$$

where $x_1 = \delta P_1/P_S$ and $x_2 = \delta P_2/P_S$. Equation 5.19 shows x_1 and x_2 are much smaller than 1; thus, the first-order approximation by Taylor Series for

Equation 5.20 becomes

$$\begin{cases} Q_1(t) = K_V\sqrt{0.5P_S}\,[1 - x_1(t)] = Q_0\,[1 - x_1(t)] \\ Q_2(t) = K_V\sqrt{0.5P_S}\,[1 + x_2(t)] = Q_0\,[1 + x_2(t)] \end{cases} \tag{5.21}$$

By neglecting the elastic deformation of the fluid, the continuity of volumetric flow gives

$$Q_0 - Q_1(t) = Q_2(t) - Q_0 = \delta Q(t) \tag{5.22}$$

and with small valve displacement, it can be assumed that

$$Q(t) = kc(t) \tag{5.23}$$

Let $k = Q_0$; then

$$x_1(t) = x_2(t) = c(t) \tag{5.24}$$

Since

$$\int_0^t \frac{\mathrm{d}P_i\,(t)}{\mathrm{d}t}\mathrm{d}t = P_i\,(t) - P_i\,(0) = P_i\,(t) - 0.5P_s; \quad i = 1, 2 \tag{5.25}$$

then the integration of Equations 5.8 and 5.10 yields

$$\begin{cases} P_1(t) - 0.5P_S = \beta\displaystyle\int_0^t \frac{Q_1(t)}{V_1(t)}\,\mathrm{d}t - \beta A\int_0^t \frac{\dot{\Delta}_a(t)}{V_1(t)}\,\mathrm{d}t \\ P_2(t) - 0.5P_S = \beta\displaystyle\int_0^t \frac{Q_2(t)}{V_2(t)}\,\mathrm{d}t + \beta A\int_0^t \frac{\dot{\Delta}_a(t)}{V_2(t)}\,\mathrm{d}t \end{cases} \tag{5.26}$$

For the first term on the right side of Equation 5.26, $V_1(t)$ and $V_2(t)$ can be regarded as constant. This is because $V_i(t)$ changes much less than $Q_i(t), i = 1, 2$. For example, from Equations 5.18, 5.19 and 5.21, it is clear that the hydraulic actuator system at the University of Missouri-Rolla has

$$\begin{aligned} \left|\frac{\delta Q_i}{Q_0}\right| = \left|\frac{Q_i - Q_0}{Q_0}\right| = \left|\frac{Q_0(1 \pm x_i) - Q_0}{Q_0}\right| = |x_i| = \left|\frac{\delta P_i}{P_S}\right| \\ = 0.5 \times 5.15\% = 2.58\% \gg 0.3\% = \left(\frac{\delta V_i}{V}\right)_{\max} \end{aligned} \tag{5.27}$$

For the second term on the right side of Equation 5.26, $V_1(t)$ and $V_2(t)$ are expressed by Equation 5.16. Then this term becomes

$$\int_0^t \frac{\dot{\Delta}_a(t)}{V_1(t)}dt \approx \int_0^{\Delta_a} \frac{d\Delta_a(t)}{V_1(t)+A\Delta_a(t)} = \frac{1}{A}\ln\left(1+\frac{A\Delta_a(t)}{V_1(t)}\right)$$
$$= \frac{1}{A}\left(\frac{A\Delta_a(t)}{V_1(t)} - \frac{A^2\Delta_a^2(t)}{V_1^2(t)} + \cdots\right) \approx \frac{\Delta_a(t)}{V_1(t)} \tag{5.28}$$

Note that the first-order approximation of the Taylor series is used in the above equation because $A\Delta_a/V = \delta V/V \ll 1$ as Equation 5.18 shows. Similarly,

$$\int_0^t \frac{\dot{\Delta}_a(t)}{V_2(t)}dt \approx \int_0^{\Delta_a} \frac{d\Delta_a(t)}{V_2(t)-A\Delta_a(t)} = -\frac{1}{A}\ln\left(1-\frac{A\Delta_a(t)}{V_2(t)}\right) \tag{5.29}$$
$$= -\frac{1}{A}\left(\frac{-A\Delta_a(t)}{V_2(t)} + \frac{A^2\Delta_a^2(t)}{V_2^2(t)} + \cdots\right) \approx \frac{\Delta_a(t)}{V_2(t)}$$

Then, Equation 5.26 becomes

$$\begin{cases} P_1(t) - 0.5P_S \approx \dfrac{\beta}{V}\int_0^t Q_1(t)dt - \dfrac{\beta A}{V}\Delta_a(t) \\ P_2(t) - 0.5P_S \approx \dfrac{\beta}{V}\int_0^t Q_2(t)dt + \dfrac{\beta A}{V}\Delta_a(t) \end{cases} \tag{5.30}$$

and

$$A\left[P_2(t) - P_1(t)\right] = \frac{2\beta A^2}{V}\Delta_a(t) + \frac{\beta A}{V}\int_0^t \left[Q_2(t) - Q_1(t)\right]dt \tag{5.31}$$

Combining Equations 5.13c, 5.21, 5.24, and 5.31 leads to

$$A\left[P_2(t) - P_1(t)\right] = \frac{2\beta A^2}{V}\Delta_a(t) + \frac{\beta A}{V}\int_0^t \left[Q_0 + Q_0\, c(t) - Q_0 + Q_0\, c(t)\right]dt$$
$$= \frac{2\beta A^2}{V}\Delta_a(t) + \frac{2\beta A K_V}{V}\sqrt{\frac{P_S}{2}}\int_0^t c(t)\,dt \tag{5.32}$$

and substituting Equation 5.32 into Equation 5.11 yields the linearized model for the actuator

$$f_a(t) = \left[\frac{2\beta A^2}{V}\Delta_a(t) + c_p\dot{\Delta}_a(t) + m_p\ddot{x}_b(t)\right] + \frac{\beta A K_V}{V}\sqrt{2P_S}\int_0^t c(t)\,dt \tag{5.33}$$

In structural seismic response control, earthquake ground motion results in additional inertia force for the valve-piston, that is,

$$f_{\mathrm{a}}(t) = \left[\frac{2\beta A^2}{V}\Delta_{\mathrm{a}}(t) + c_{\mathrm{p}}\dot{\Delta}_{\mathrm{a}}(t) + m_{\mathrm{p}}\left(\ddot{x}_{\mathrm{b}}(t) + \ddot{x}_{\mathrm{g}}(t)\right)\right] + \frac{\beta A K_{\mathrm{V}}}{V}\sqrt{2P_{\mathrm{S}}}\int_0^t c(t)\,\mathrm{d}t \tag{5.34}$$

Since f_{a} is much larger than $c_{\mathrm{p}}\dot{\Delta}_{\mathrm{a}}(t)$ and $m_{\mathrm{p}}[\ddot{x}_{\mathrm{b}}(t) + \ddot{x}_{\mathrm{g}}(t)]$ for a structural control system, Equation 5.34 can be simplified as

$$f_{\mathrm{a}}(t) = \frac{2\beta A^2}{V}\Delta_{\mathrm{a}}(t) + \frac{\beta A K_{\mathrm{V}}}{V}\sqrt{2P_{\mathrm{S}}}\int_0^t c(t)\,\mathrm{d}t \tag{5.35a}$$

or

$$\dot{f}_{\mathrm{a}}(t) = \frac{2\beta A^2}{V}\dot{\Delta}_{\mathrm{a}}(t) + \frac{\beta A K_{\mathrm{V}}}{V}\sqrt{2P_{\mathrm{S}}}c(t) \tag{5.35b}$$

Equations 5.12 and 5.35 form the mathematical model of the hydraulic actuator for structural control. Because there is no $f_{\mathrm{a}}(t)$ term in the right side of Equation 5.35b, this actuator model indicates that the system has a zero eigenvalue (i.e., a pole at origin). This means that the servovalve-controlled hydraulic actuator is a marginally stable system, and small deviations due to initial imperfections may cause the system to be unstable. This theoretical result matches well with experiments [10,14,15]. This actuator model also indicates that actuator force and actuator-piston displacement interact as shown by the first term of the right side of Equations 5.35a or 5.35b. Because actuator-piston displacement is equal to the relative displacement between the K-brace and the structure (see Equation 5.1), the actuator model indicates that the structure and the actuator have dynamic interaction in a smart structure system. More details on the interaction issue is discussed in Sections 5.3.3 and 5.3.4.

When two or more hydraulic actuators are applied to the system, say the kth hydraulic actuator ($k = 1, 2, \ldots, r$) is attached to the ith floor ($i = 1, 2, \ldots, n$) and supported by the jth bracing system ($j = 1, 2, \ldots, m$), actuator-piston displacement $\Delta_{\mathrm{a}k}(t) = x_{\mathrm{b}j}(t) - x_i(t)$. Then, from Equations 5.12a and 5.35b

$$\begin{cases} \dot{f}_{\mathrm{a}k}(t) = \left(\dfrac{2\beta A^2}{V}\right)_k \left[\dot{x}_{\mathrm{b}j}(t) - \dot{x}_i(t)\right] + \left(\dfrac{\beta A K_{\mathrm{V}}}{V}\sqrt{2P_{\mathrm{S}}}\right)_k c_k(t) \\ \dot{c}_k(t) = -\dfrac{1}{\tau_k}c_k(t) + \dfrac{1}{\tau_k}u_k(t) \end{cases} \tag{5.36}$$

5.1.2 Modeling of Passive Dampers

Application of passive dampers for seismic response control has been discussed in Chapter 3 in detail. This section presents dynamic models of passive dampers used

in hybrid systems, particularly these viscous fluid dampers, liquid mass dampers, and spring dampers.

5.1.2.1 Model of viscous fluid dampers

As shown in Figure 5.3, the viscous fluid damper consists of a hydraulic piston–cylinder filled with viscous fluid and a tube connecting the two chambers separated by the piston head. The cylinder can be attached to a structural floor and the

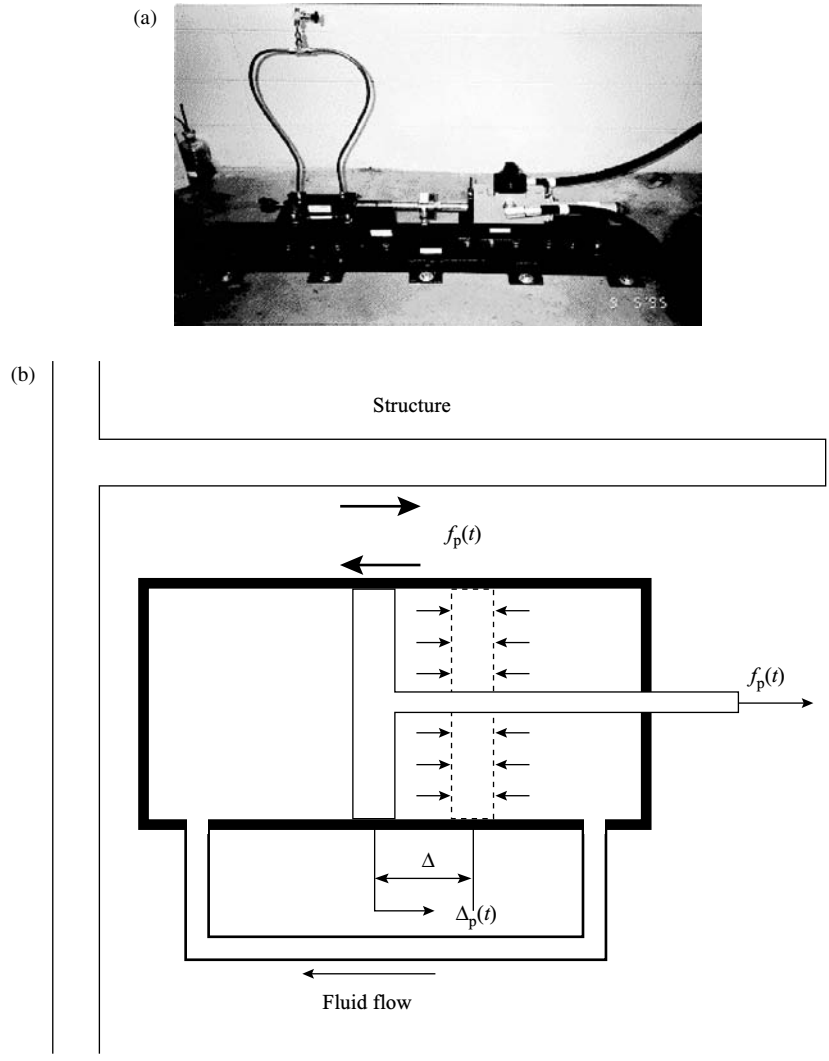

FIGURE 5.3 Viscous fluid damper: (a) view and (b) schematic.

piston's rod connected to a bracing system. Structural and bracing vibration drives movement of the piston relative to the cylinder. This allows the viscous fluid in both chambers to flow back and forth through the tube. Friction force between the fluid flow and the tube and cylinder absorbs energy and thus reduces structural vibration.

As well known, the linear elastic and viscous behavior of materials are respectively governed by the following two equations

$$\begin{cases} \tau_{yx} = -G\dfrac{\mathrm{d}u_x}{\mathrm{d}y} = -G\gamma_{yx} \\ \tau_{yx} = -\mu\dfrac{\mathrm{d}v_x}{\mathrm{d}y} = -\mu\dfrac{\mathrm{d}}{\mathrm{d}y}\left(\dfrac{\mathrm{d}\mu_x}{\mathrm{d}t}\right) = -\mu\dot{\gamma}_{yx} \end{cases} \tag{5.37a}$$

where τ_{yx} is the shear stress; G is the shear modulus of the elastic materials, such as *Hookean solids*; μ is viscosity of the linear viscous materials, such as *Newtonian liquids*; v_x is the fluid velocity; u_x is the displacement in the x-direction; the qualities γ_{yx} and $\dot{\gamma}_{yx}$ are components of the strain tensor and the rate of strain (or rate of deformation), respectively. Equation 5.37a can be rewritten as

$$\begin{cases} \dfrac{1}{G}\dfrac{\partial\tau_{yx}}{\partial t} = -\dot{\gamma}_{yx} \\ \dfrac{1}{\mu}\tau_{yx} = -\dot{\gamma}_{yx} \end{cases} \tag{5.37b}$$

Viscous fluid dampers use a fluid type of viscoelastic materials. Viscoelastic materials have combined elastic and viscous properties. The mechanical behavior of such a material, called viscoelasticity, exhibits viscous and elastic behaviors simultaneously. Such behaviors can be mathematically expressed as [12]

$$\tau = f(\gamma, \dot{\gamma}, t) \tag{5.37c}$$

where τ and γ are the shear stress and shear strain, respectively, t is the time instant. Equation 5.37c shows that the shear stress is a function of shear strain, rate of the strain and time. A linear viscoelastic material would have a linearized relationship to reveal combined viscous and elastic behavior. Thus, a direct thought will be superposition of linear elastic and linear viscous models of Equation 5.37b as

$$\tau_{yx} + \frac{\mu}{G}\frac{\partial\tau_{yx}}{\partial t} = -\mu\dot{\gamma}_{yx} \tag{5.37d}$$

The above equation is called *Maxwell model*. By introducing new notations for the constants and replacing μ with C_0 and μ/G with λ_0, the Maxwell model becomes

$$\tau + \lambda_0\frac{\partial\tau}{\partial t} = -C_0\dot{\gamma} \tag{5.37e}$$

C_0 and λ_0 are the *relaxation modulus* and material *viscosity*, respectively. The Maxwell model shows that the shear stress at any time instant, t, depends on the

rate of strain at the present time, t, and also the rate of strain at all past time t', with the weighting factor (the relaxation modulus) that decays exponentially as one goes backwards in time, and displays the material characteristics of memory.

The above governing equations of elastic, viscous, and viscoelastic materials are stress–strain relationships. Their integration along the shear area leads to force–displacement relationship, which is the base of the following mechanical analogies:

- The stress–strain relationship of a Hookean solid has the same form as the force–displacement relationship for a linear spring with stiffness constant of k, which is shown in Figure 5.4a. This linear spring model is expressed as

$$f_{\mathrm{p}}(t) = k\Delta_1(t) \tag{5.38a}$$

  where f_{p} is the force applied on the spring and Δ_1 is the force-caused displacement as shown in Figure 5.4a. Equation 5.38a can be rewritten as

$$\frac{\mathrm{d}}{\mathrm{d}t} f_{\mathrm{p}}(t) = k\frac{\mathrm{d}}{\mathrm{d}t}\Delta_1(t) \tag{5.38b}$$

  Multiplying above equation by constant C_0/k yields

$$\frac{C_0}{k}\dot{f}_{\mathrm{p}}(t) = C_0\dot{\Delta}_1(t) \tag{5.38c}$$

- The relationship of stress and rate of strain for a Newtonian fluid has the same form as the relationship of force and rate of displacement for a dashpot, where the dashpot consists of a loose-fitting position that moves in a cylinder containing a Newtonian fluid, as in Figure 5.4b. The dashpot is modeled by

$$f_{\mathrm{p}}(t) = C_0\frac{\mathrm{d}}{\mathrm{d}t}\Delta_2(t) = C_0\dot{\Delta}_2(t) \tag{5.38d}$$

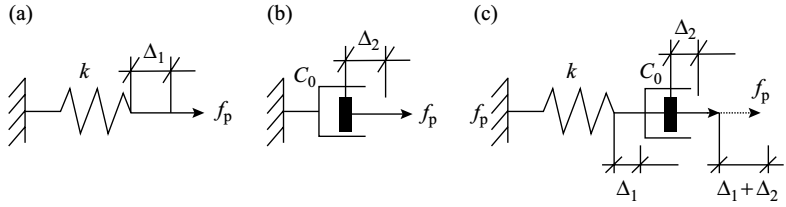

FIGURE 5.4 Mechanical analogies of various material behaviors: (a) elastic material, (b) viscous material, and (c) viscoelastic material.

- The Maxwell model for a viscoelastic material has a stress–strain relationship of the same form as for the force–displacement relationship of a spring and dashpot in series, as shown in Figure 5.4c. With superposition law for linear systems, the model for viscoelastic materials can be obtained by adding Equations 5.38c and 5.38d together

$$f_{\mathrm{p}}(t) + \frac{C_0}{k}\frac{\mathrm{d}}{\mathrm{d}t}f_{\mathrm{p}}(t) = C_0\frac{\mathrm{d}}{\mathrm{d}t}\Delta_1(t) + C_0\frac{\mathrm{d}}{\mathrm{d}t}\Delta_2(t) \tag{5.38e}$$

The summation of displacements in the spring and in the dashpot is the total displacement at the point where the force is applied, as shown in Figure 5.4c. Thus, by introducing a new constant $\lambda_0 = C_0/k$, Equation 5.38e can be rewritten as

$$\lambda_0\dot{f}_{\mathrm{p}}(t) + f_{\mathrm{p}}(t) = C_0\dot{\Delta}_{\mathrm{p}}(t) \tag{5.39a}$$

The viscous fluid damper is composed of a moving piston in a cylinder filled with viscoelastic material. Thus, its dynamic behavior follows the Maxwell model in force–displacement format [10–12,20] as expressed by Equation 5.39a. Then, $f_{\mathrm{p}}(t)$ and $\Delta_{\mathrm{p}}(t)$ are force applied to the fluid damper and resulting piston displacement, respectively; damper parameters, namely, λ_0 is relaxation time factor and C_0 is damping coefficient at zero frequency. Parameters λ_0 and C_0 can be determined through parameter identification tests [10,20].

If two or more dampers are employed, say the kth damper ($k = 1, 2, \ldots, s$) is mounted on the jth bracing ($j = 1, 2, \ldots, m$) and attached to ith floor ($i = 1, 2, \ldots, n$), then piston displacement $\Delta_{\mathrm{p}k}(t) = x_{\mathrm{b}j}(t) - x_i(t)$, and Equation 5.39a becomes

$$\lambda_{0k}\dot{f}_{\mathrm{p}k}(t) + f_{\mathrm{p}k}(t) = C_{0k}\left[\dot{x}_{\mathrm{b}j}(t) - \dot{x}_i(t)\right] \tag{5.39b}$$

5.1.2.2 Linear model of liquid mass dampers

As shown in Figure 5.5a, the *liquid mass damper* is composed of a viscous damper and a tube that connects both ends of the damper's cylinder. The damper generates passive inertia force and damping force, which are respectively proportional to the piston's acceleration and velocity. If such a damper is installed on jth K-brace at ith floor, its linear model can be expressed as

$$\begin{aligned} f_{\mathrm{p}k} &= m_{ek}(\ddot{x}_i - \ddot{x}_{\mathrm{b}j}) + c_{\mathrm{p}k}(\dot{x}_i - \dot{x}_{\mathrm{b}j}), \quad i = 1, 2, \ldots, n; \\ & j = 1, 2, \ldots, m; \quad k = 1, 2, \ldots, s \end{aligned} \tag{5.40}$$

where x_i and $x_{\mathrm{b}j}$ are displacements of the ith floor and the jth K-brace, respectively; n, m, and s are numbers of stories, K-braces and dampers, respectively; $c_{\mathrm{p}k}$ is damping coefficient of the kth damper; and $m_{e\mathrm{k}}$ is effective liquid mass caused by

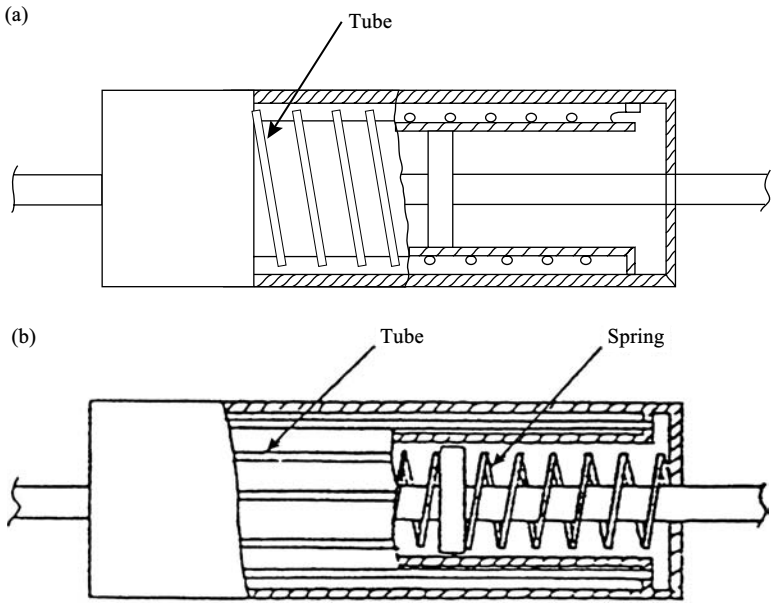

FIGURE 5.5 Two types of damper for hybrid control: (a) liquid mass damper and (b) spring damper.

the motion of the liquid in the tube of the kth damper, which can be calculated by the following formula

$$m_{\mathrm{e}} = \rho L_{\mathrm{t}} A_{\mathrm{t}} \left(\frac{A_{\mathrm{p}}}{A_{\mathrm{t}}} \right)^2 \tag{5.41}$$

where ρ is mass density of liquid used in the viscous damper, L_{t} is length of the tube, and A_{p} and A_{t} are cross-sectional areas of the cylinder and tube, respectively.

5.1.2.3 Linear model of spring dampers

The *spring damper*, as shown in Figure 5.5b, consists of a viscous damper and a parallel spring, which provide passive damping and spring forces, respectively. If such a damper is installed on jth K-brace at ith floor, its linear model can be expressed as

$$\begin{aligned} f_{\mathrm{p}k} &= c_{\mathrm{p}k}(\dot{x}_i - \dot{x}_{\mathrm{b}j}) + k_{\mathrm{p}k}(x_i - x_{\mathrm{b}j}), \quad i = 1, 2, \ldots, n; \\ & j = 1, 2, \ldots, m; \quad k = 1, 2, \ldots, s \end{aligned} \tag{5.42}$$

where $c_{\mathrm{p}k}$ and $k_{\mathrm{p}k}$ are damping and spring coefficients, respectively, of the kth spring damper.

5.1.3 Modeling of Semiactive Dampers

Chapter 1 has presented a brief introduction of semiactive dampers. Various semiactive dampers have been proposed by adding performance-adjustment functions to passive energy-dissipating devices using friction, yielding, or viscous fluid mechanisms, and so forth. To analyze and design a smart seismic structure with semiactive systems, the model of the semiactive device must first be formulated on the basis of its dynamic behavior. This task is usually challenging as most semiactive devices are complicated and behave in a highly nonlinear manner. One class of semiactive dampers uses controllable fluids, the electrorheological (ER) or magnetorheological (MR) fluids. This kind of semiactive dampers is currently in vogue and thus serves as example for analysis of semiactive dampers in this chapter.

5.1.3.1 Model of electrorheological dampers

The stress–strain behavior of ER fluids is often described by the *Bingham viscoplastic model* [24], which defines the plastic viscosity as the slope of shear stress versus shear strain rate. Thus, the total shear stress τ is given by

$$\tau = \tau_{\mathrm{u}} + \eta\dot{\gamma} \tag{5.43}$$

where τ_{u} is the yield stress induced by the electric field, η is the viscosity of the fluid, and $\dot{\gamma}$ is the shear rate. On the basis of this model for the rheological behavior of ER fluids, Stanway et al. [28] proposed an idealized mechanical model, called the Bingham model, for the behavior of an ER damper. As shown in Figure 5.6, this model consists of a *Coulomb friction element* placed in parallel with a linear viscous damper. The force generated by the linear viscous damper is proportional to the relative velocity $\dot{\Delta}(t)$ of the piston to the cylinder of the ER damper. If the relative velocity is zero, the damper force is generated by the Coulomb friction element only. Thus, the force $f_{\mathrm{sa}}(t)$ generated by the device is given by

$$f_{\mathrm{sa}}(t) = f_{\mathrm{c}}\mathrm{sign}\left(\dot{\Delta}(t)\right) + c_0\dot{\Delta}(t) + f_0 \tag{5.44}$$

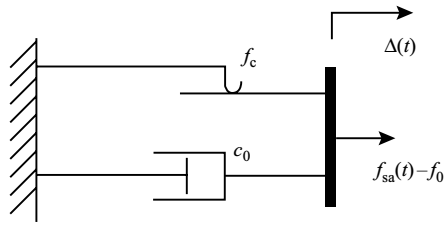

FIGURE 5.6 Bingham model of ER damper.

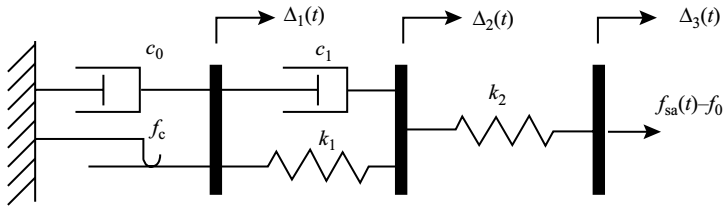

FIGURE 5.7 Extended Bingham model of ER damper.

where c_0 is damping coefficient, f_c is friction force related to the fluid yield stress, and f_0 is offset force that accounts for the nonzero mean value of the measured force owing to the presence of the accumulator.

The Bingham model is based on the assumption that the ER damper behaves in viscoplastic way. Gamota and Filisko [18] discovered that the ER fluid has mixed viscoelastic and viscoplastic behavior, and thus proposed an extension of the Bingham model. As described schematically by the viscoelastic–plastic model in Figure 5.7, two linear spring elements and a dashpot, which describe the viscoelastic behavior of the ER damper, are added to the Bingham model. While $\Delta_3(t)$ is the relative displacement of the piston and the cylinder of the ER damper, two more internal states (degrees of freedom), $\Delta_1(t)$ and $\Delta_2(t)$, are added to the system. The damper model is then expressed as

$$\begin{cases} \left.\begin{aligned} f_{sa}(t) &= f_c \text{sign}\left(\dot{\Delta}_1(t)\right) + c_0\dot{\Delta}_1(t) + f_0 \\ &= c_1\left[\dot{\Delta}_2(t) - \dot{\Delta}_1(t)\right] + k_1\left[\Delta_2(t) - \Delta_1(t)\right] + f_0 \\ &= k_2\left[\Delta_3(t) - \Delta_2(t)\right] + f_0 \end{aligned}\right\} & |f_{sa}| > f_c \\ \left.\begin{aligned} f_{sa}(t) &= c_1\dot{\Delta}_2(t) + k_1\left[\Delta_2(t) - \Delta_1(t)\right] + f_0 \\ &= k_2\left[\Delta_3(t) - \Delta_2(t)\right] + f_0 \\ \dot{\Delta}_1(t) &= 0 \end{aligned}\right\} & |f_{sa}| \le f_c \end{cases} \tag{5.45}$$

Again, c_0, f_c, and f_0 are coefficients associated with the Bingham model; k_1, k_2, and c_1 are spring and damping coefficients for the viscoelastic part of the model.

5.1.3.2 Model of magnetorheological dampers

As discussed in Chapter 1, MR dampers use the *MR fluid* and are very promising alternatives for seismic response control [16,27]. MR fluid and dampers have the following advantages that make them highly potential for seismic response control:

- Transition of MR fluid to rheological equilibrium can be achieved in a few milliseconds, allowing construction of MR dampers with high bandwidth.
- MR fluid can achieve much higher yield stress than ER fluid.

- MR damper can operate at temperatures from −40° C to 150° C with only slight variations in yield stress.
- MR fluids are not sensitive to impurities caused during manufacturing and usage.
- MR fluid has little separation between magnetic particle and carrier fluid under common flow conditions.
- MR fluid can be readily controlled with low voltage (e.g., 12–24 V) and low energy requirement (1–2 Å).

Because the MR fluid and ER fluid behave similarly, Spencer et al. [27] evaluated the above Bingham models for their application to MR dampers. An MR damper manufactured by Lord Corporation of Cary, North Carolina was tested and the measured data was used to fit the above model to identify the model parameters. Then, the response predicted by the model using these parameters was compared to test response. It was shown that the Bingham model predicted the force–displacement behavior of the damper well, but it did not capture the force–velocity behavior very well, especially for the region with small velocities. It was also shown that the extended Bingham model could predict the response better but had a major numerical weakness that this model was extremely stiff and required a time step in the order of 10^{-6} s.

To improve these models, Spencer et al. proposed a model that is numerically tractable and predicts response well. As shown in Figure 5.8 schematically, this model combines the *Bouc-Wen model* [29] and a *spring-dashpot model*, which are for the hysteretic behavior and the linear viscoelastic behavior of the MR damper, respectively. The Bouc-Wen model is extremely versatile and can exhibit a wide variety of hysteretic behavior. This model expresses the force generated by the

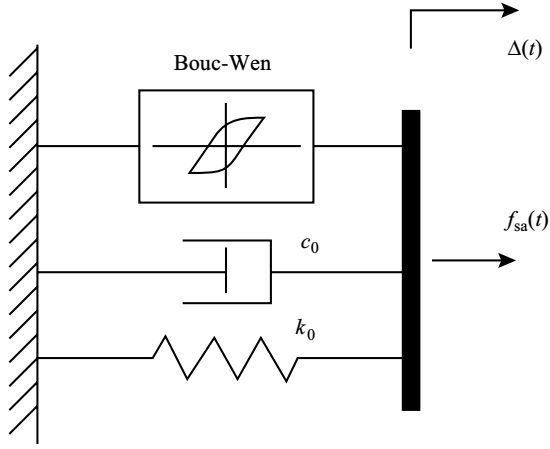

FIGURE 5.8 Bouc-Wen model of MR damper.

damper $f_{sa}(t)$ as

$$f_{sa}(t) = c_0\dot{\Delta}(t) + k_0\left[\Delta(t) - \Delta_0\right] + \alpha\Delta_1(t) \tag{5.46}$$

Again, k_0 and c_0 are spring and damping coefficients for the viscoelastic part of the model, the force f_0 due to the accumulator is modeled by an initial deflection of the linear spring Δ_0, and α is the constant in Bouc-Wen model. Besides the relative displacement $\Delta(t)$ between the damper piston and cylinder, this model introduces an internal state (degree-of-freedom), the evolutionary variable $\Delta_1(t)$, which is governed by

$$\dot{\Delta}_1(t) = -\gamma\left|\dot{\Delta}(t)\right|\Delta_1(t)\left|\Delta_1(t)\right|^{n-1} - \beta\dot{\Delta}(t)\left|\Delta_1(t)\right|^n + A\dot{\Delta}(t) \tag{5.47}$$

where γ, n, β, and A are the parameters. By adjusting them, the above model can well match the hysteretic behavior of the MR damper. Again, for the same test, data were used to determine these parameters by best fitting the Bouc-Wen model response to the test. A comparison between the model predicted response and experimental data shows that this model predicts the force–displacement behavior well, but not very well for the force–velocity relationship in the small velocity region, which is similar to the Bingham model though it more closely resembles the experimental data. Thus, Spencer et al. [27] proposed an improved model by adding one more set of spring-dashpot (k_1 and c_1) to the model. As shown schematically by Figure 5.9, this model introduced another internal state $\Delta_2(t)$, the displacement of the new dashpot. The new spring k_1 represents the accumulator stiffness, and the new dashpot c_1 produces the round-off observed in the region with low velocities. The existing spring and dashpot would then control the stiffness and viscous damping at large velocities, and Δ_0 becomes the initial displacement of the accumulator associated with its own spring k_1.

Force balance of the new dashpot yields

$$c_1\dot{\Delta}_2(t) = \alpha\Delta_1(t) + c_0\left[\dot{\Delta}(t) - \dot{\Delta}_2(t)\right] + k_0\left[\Delta(t) - \Delta_2(t)\right] \tag{5.48}$$

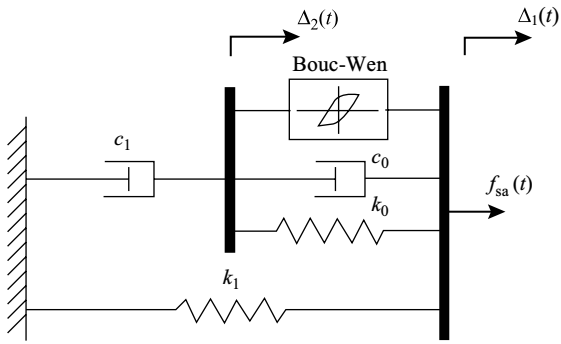

FIGURE 5.9 Improved Bouc-Wen model of MR damper.

This can be rewritten as

$$\dot{\Delta}_2(t) = \frac{1}{c_0 + c_1}\left[-k_0\Delta_2(t) + \alpha\Delta_1(t) + c_0\dot{\Delta}(t) + k_0\Delta(t)\right] \tag{5.49}$$

The internal displacement for the Bouc-Wen model is $[\Delta(t) - \Delta_2(t)]$ now. Thus, the evolutionary variable $\Delta_1(t)$ is governed by

$$\begin{aligned}\dot{\Delta}_1(t) = &-\gamma\left|\dot{\Delta}(t) - \dot{\Delta}_2(t)\right|\Delta_1(t)\left|\Delta_1(t)\right|^{n-1} \\ &- \beta\left[\dot{\Delta}(t) - \dot{\Delta}_2(t)\right]\left|\Delta_1(t)\right|^n + A\left[\dot{\Delta}(t) - \dot{\Delta}_2(t)\right]\end{aligned} \tag{5.50}$$

and the force generated by the damper $f_{sa}(t)$ is then given by

$$f_{sa}(t) = \alpha\Delta_1(t) + c_0\left[\dot{\Delta}(t) - \dot{\Delta}_2(t)\right] + k_0\left[\Delta(t) - \Delta_2(t)\right] + k_1\left[\Delta(t) - \Delta_0\right] \tag{5.51}$$

By substituting Equation 5.48 into the above equation yields

$$f_{sa}(t) = c_1\dot{\Delta}_2(t) + k_1\left[\Delta(t) - \Delta_0\right] \tag{5.52}$$

As shown by Equations 5.49, 5.50, and 5.52, this model describes the MR damper as first-order nonlinear dynamic system with two internal states, $\Delta_1(t)$ and $\Delta_2(t)$. By fitting the model with the same test data, it is shown that the proposed model predicts the damper behavior very well in all regions.

Note that the above model is based on a constant magnetic field. However, optimal seismic response control would expect an ever-changing magnetic field on the basis of the feedback of measured structural seismic response. Thus, the model must be enhanced to predict the damper behavior under a fluctuating magnetic field for seismic response control. It has been found that parameters α, c_0, and c_1 would have functional dependence with the magnetic field and a linear relationship has been assumed [27]

$$\begin{cases}\alpha = \alpha(u) = \alpha_0 + \alpha_1 u(t) \\ c_0 = c_0(u) = c_{00} + c_{01}u(t) \\ c_1 = c_1(u) = c_{10} + c_{11}u(t)\end{cases} \tag{5.53}$$

where the magnetic field measure $u(t)$ would have first-order dynamics with the applied voltage $v(t)$ due to the setting time for the MR fluid to reach rheological equilibrium

$$\dot{u}(t) = -\eta\left[u(t) - v(t)\right] \tag{5.54}$$

Equations 5.49, 5.50, and 5.52–5.54 fully define the dynamic behavior of an MR damper. It introduces first-order device dynamics to a smart seismic structure system using an MR damper with five device states, $\Delta(t), \Delta_2(t), u(t)$, and $v(t)$. There are 14 parameters involved and must be identified for the prototype MR

TABLE 5.1
Identified Model Parameters for an MR Damper

Parameter	A	c_{00} N-s/cm	c_{01} N-s/(cm-V)	c_{10} N-s/cm	c_{11} N-s/(cm-V)	k_0 N/cm	k_1 N/cm
Value	301	21.0	3.50	283	2.95	46.9	5.0
Parameter	x_0 cm	N	α_0 N/cm	α_1 N/cm	β cm^{-2}	γ cm^{-2}	η s^{-1}
Value	14.3	2	140	695	363	363	190

damper. Table 5.1 shows the parameters identified for the aforementioned MR damper [27].

5.2 Dynamic Model of Smart Seismic Structures with Semiactive or Hybrid Control

To analyze and design a semiactive or hybrid control system for a full-scale seismic-resistant structure, an analytical model of the entire system needs to be formulated first. Its accurate model shall be based on the dynamic behavior and/or operating mechanism of all the system's components: the structure, braces, and control devices (dampers and actuators). Moreover, it is desirable to have a general model that addresses arbitrary number and location of control devices. This is because a system model with fixed number and location of control devices has two weaknesses. First, owing to the dynamic interaction between the structure and control devices, this model does not work for the same structure with different number and/or the location of control devices. In other words, the model has to be reformulated. Thus, this approach is not practical for computer analysis because not only the input data but also the program must be changed. Second, fixed number and location of control devices have no meaning for optimal design of a control system because the location and number of control devices are not known at the design stage. Thus, researchers have taken efforts to develop a general and accurate model to address these weaknesses [6–8,19,22,25], as discussed in this section. In detail, this section formulates such a model for the analysis of smart seismic structures. The HDABC system, which consists of servovalve-controlled hydraulic actuators and passive dampers mounted on K-braces between two stories of a structure, serves as the example for the process. Three types of passive dampers—viscous fluid damper, liquid mass damper, and spring damper—are considered for HDABC system. Analytical models for each component of the HDABC system are formulated on the basis of the dynamic behavior of the structure with braces and the dynamic model of control devices. Thus, the integrated system model considers dynamics of the structure, braces, and control devices as well as their dynamic interaction. The model is then condensed into matrix form by considering arbitrary number and location of control devices. Finally, a state-variable representation of the system model in both continuous and discrete time domain is developed.

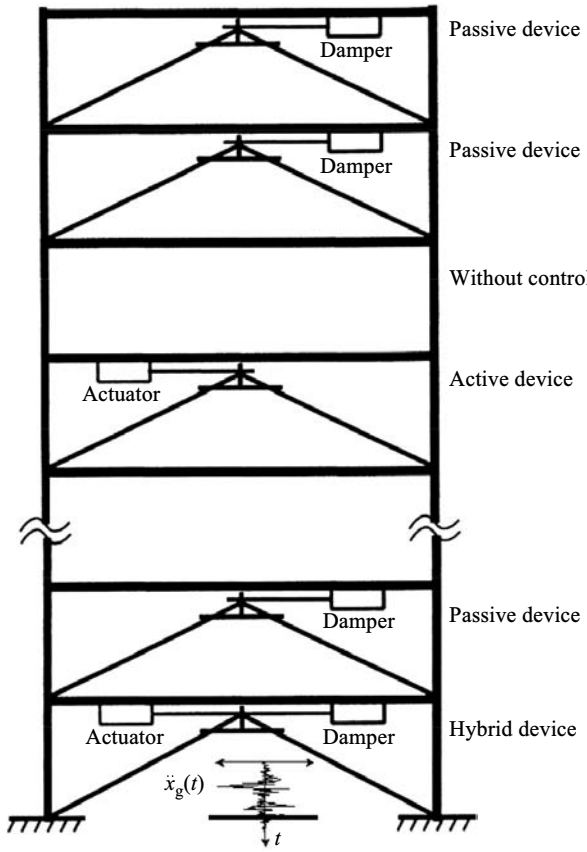

FIGURE 5.10 Shear building with HDABC system.

5.2.1 System Description

Figure 5.10 shows a typical n-story seismic-resistant structure equipped with a HDABC system. This system has multiple servovalve-controlled hydraulic actuators, viscous fluid dampers, and hybrid devices supported by K-braces on the structure. The hybrid device is a combination of a damper and an actuator. Installed at each floor of the building structure can be a hybrid device, a damper only, an actuator only, or no control device at all. Floors without a control device do not need the bracing system. When an n-story building structure is equipped with r actuators, s passive dampers, and m bracing systems, the following relationship exists because a bracing system may support a damper, an actuator, or their combination (i.e., a hybrid device).

$$r \leq m, \quad s \leq m, \quad m \leq (r+s), \quad m \leq n \tag{5.55}$$

5.2.2 Shear Building Structures with Hybrid Devices on All Floors

To simplify the problem, an n-story shear building structure equipped with a hybrid control device on each floor (see Figure 5.11) is studied. In this case, the control system has n braces, n actuators, and n passive dampers. m_i, c_i, and $k_i (i = 1, 2, \ldots, n)$ are coefficients of mass, damping, and stiffness of the ith floor of the structure, respectively; m_{bi}, c_{bi}, and k_{bi} are coefficients of mass, damping, and stiffness of the ith bracing, respectively; f_{ai} and f_{pi} are active and passive control forces generated by ith actuator and ith damper, respectively; x_i is ith floor displacement relative to the ground; x_{bi} is displacement of ith bracing relative to the ground; and $\ddot{x}_g$ is earthquake ground acceleration. Obviously, the absolute displacement of the ith floor and ith bracing are $(x_i + x_g)$ and $(x_{bi} + x_g)$, respectively.

From the free-body diagram in Figure 5.11, motion equations for the controlled structure under earthquake excitation can be expressed as

$$\begin{cases} m_1(\ddot{x}_1 + \ddot{x}_g) + c_1\dot{x}_1 - c_2(\dot{x}_2 - \dot{x}_1) - c_{b2}(\dot{x}_{b2} - \dot{x}_1) \\ \quad + k_1x_1 - k_2(x_2 - x_1) - k_{b2}(x_{b2} - x_1) = f_{a1} + f_{p1} \\ m_2(\ddot{x}_2 + \ddot{x}_g) + c_2(\dot{x}_2 - \dot{x}_1) - c_3(\dot{x}_3 - \dot{x}_2) - c_{b3}(\dot{x}_{b3} - \dot{x}_2) \\ \quad + k_2(x_2 - x_1) - k_3(x_3 - x_2) - k_{b3}(x_{b3} - x_2) = f_{a2} + f_{p2} \\ \cdots\cdots \\ m_i(\ddot{x}_i + \ddot{x}_g) + c_i(\dot{x}_i - \dot{x}_{i-1}) - c_{i+1}(\dot{x}_{i+1} - \dot{x}_i) - c_{bi+1}(\dot{x}_{bi+1} - \dot{x}_i) \\ \quad + k_i(x_i - x_{i-1}) - k_{i+1}(x_{i+1} - x_i) - k_{bi+1}(x_{bi+1} - x_i) = f_{ai} + f_{pi} \\ \cdots\cdots \\ m_{n-1}(\ddot{x}_{n-1} + \ddot{x}_g) + c_{n-1}(\dot{x}_{n-1} - \dot{x}_{n-2}) - c_n(\dot{x}_n - \dot{x}_{n-1}) - c_{bn}(\dot{x}_{bn} - \dot{x}_{n-1}) \\ \quad + k_{n-1}(x_{n-1} - x_{n-2}) - k_n(x_n - x_{n-1}) - k_{bn}(x_{bn} - x_{n-1}) = f_{an-1} + f_{pn-1} \\ m_n(\ddot{x}_n + \ddot{x}_g) + c_n(\dot{x}_n - \dot{x}_{n-1}) + k_n(x_n - x_{n-1}) = f_{an} + f_{pn} \end{cases} \tag{5.56}$$

Note that k_i represents the stiffness of all columns at ith floor, and c_i signifies the damping coefficient on that floor. Each bracing is modeled as a single d.o.f. system.

Motion equations for the bracing systems are

$$\begin{cases} m_{b1}(\ddot{x}_{b1} + \ddot{x}_g) + c_{b1}\dot{x}_{b1} + k_{b1}x_{b1} = -f_{a1} - f_{p1} \\ m_{b2}(\ddot{x}_{b2} + \ddot{x}_g) + c_{b2}(\dot{x}_{b2} - \dot{x}_1) + k_{b2}(x_{b2} - x_1) = -f_{a2} - f_{p2} \\ \cdots\cdots \\ m_{bi}(\ddot{x}_{bi} + \ddot{x}_g) + c_{bi}(\dot{x}_{bi} - \dot{x}_{i-1}) + k_{bi}(x_{bi} - x_{i-1}) = -f_{ai} - f_{pi} \\ \cdots\cdots \\ m_{bn-1}(\ddot{x}_{bn-1} + \ddot{x}_g) + c_{bn-1}(\dot{x}_{bn-1} - \dot{x}_{n-2}) + k_{bn-1}(x_{bn-1} - x_{n-2}) \\ \qquad = -f_{an-1} - f_{pn-1} \\ m_{bn}(\ddot{x}_{bn} + \ddot{x}_g) + c_{bn}(\dot{x}_{bn} - \dot{x}_{n-1}) + k_{bn}(x_{bn} - x_{n-1}) = -f_{an} - f_{pn} \end{cases} \tag{5.57}$$

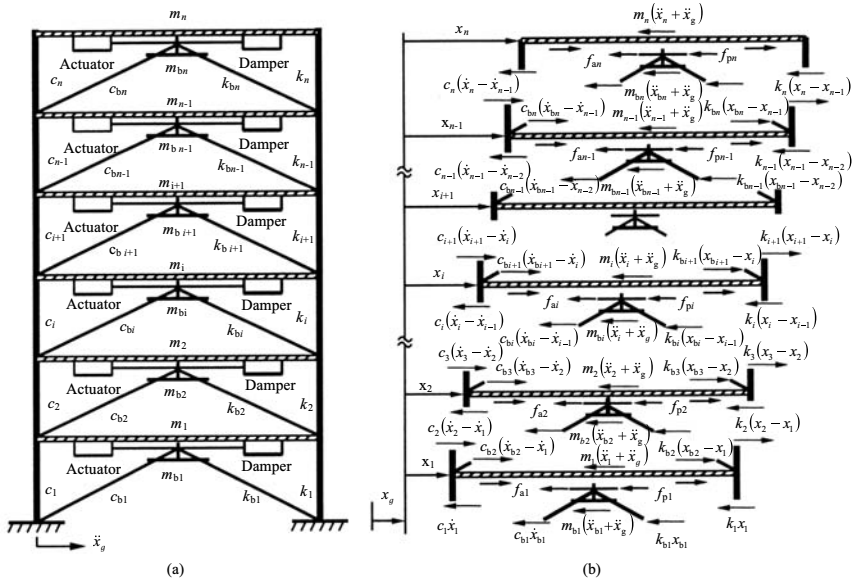

FIGURE 5.11 Shear building with HDABC on every floor: (a) schematic and (b) free-body diagram.

Equations 5.56 and 5.57 can be condensed in matrix form as

$$[M]\{\ddot{x}(t)\} + [C]\{\dot{x}(t)\} + [K]\{x(t)\} = [\gamma_a]\{f_a(t)\} + [\gamma_p]\{f_p(t)\} + \{\delta\}\ddot{x}_g(t) \quad (5.58)$$

which forms the analytical model of a smart structure with HDABC system. In Equation 5.58, $\{x(t)\}$ of $2n \times 1$ is vector of structural and bracing displacements; $\{f_a(t)\}$ of $n \times 1$ and $\{f_p(t)\}$ of $n \times 1$ are vectors of active and passive control forces, respectively; $[M]$, $[C]$, and $[K]$ are $2n \times 2n$ matrices of mass, damping, and stiffness of the structure with bracing systems, respectively; $[\gamma_a]$ and $[\gamma_p]$ of $2n \times n$ are location matrices for actuators and dampers, respectively; and $\{\delta\}$ of $2n \times 1$ is the coefficient vector for earthquake ground acceleration, $\ddot{x}_g(t)$. These vectors and matrices can be expressed as

$$\{x(t)\} = [x_1(t), x_2(t), \cdots, x_n(t); x_{b1}(t), x_{b2}(t), \cdots, x_{bn}(t)]^T \quad (5.59)$$

$$\{f_a(t)\} = [f_{a1}(t), f_{a1}(t), \cdots, f_{an}(t)]^T \quad (5.60)$$

$$\{f_p(t)\} = [f_{p1}(t), f_{p1}(t), \cdots, f_{pn}(t)]^T \quad (5.61)$$

$$[M] = \begin{bmatrix} [M_s] & \\ & [M_b] \end{bmatrix}, \quad [C] = \begin{bmatrix} [C_s] + [C_{bsb}] & [C_{sb}] \\ [C_{bs}] & [C_b] \end{bmatrix},$$

$$[K] = \begin{bmatrix} [K_{\mathrm{s}}] + [K_{\mathrm{bsb}}] & [K_{\mathrm{sb}}] \\ [K_{\mathrm{bs}}] & [K_{\mathrm{b}}] \end{bmatrix} \tag{5.62}$$

$$[\gamma_{\mathrm{a}}]_{2n\times n} = [\gamma_{\mathrm{p}}]_{2n\times n} = \begin{bmatrix} [\gamma_{\mathrm{s}}] \\ [\gamma_{\mathrm{b}}] \end{bmatrix}_{2n\times n} \tag{5.63}$$

$$[\gamma_{\mathrm{s}}] = -[\gamma_{\mathrm{b}}] = [I]_{n\times n} = \begin{bmatrix} 1 & & & & & & \\ & 1 & & & & & \\ & & \cdots & & & & \\ & & & 1 & & & \\ & & & & \cdots & & \\ & & & & & 1 & \\ & & & & & & 1 \end{bmatrix}_{n\times n} \tag{5.64}$$

$$\{\delta\} = -[m_1, m_2, \cdots, m_i, \cdots, m_{n-1}, m_n; m_{\mathrm{b}1}, m_{\mathrm{b}2}, \cdots, m_{\mathrm{b}i}, \cdots, m_{\mathrm{b}n-1}, m_{\mathrm{b}n}]^{\mathrm{T}} \tag{5.65}$$

And the submatrices of $[M]$ and $[C]$ in Equation 5.62 are defined as

$$[M_{\mathrm{s}}] = \begin{bmatrix} m_1 & & & & & \\ & m_2 & & & & \\ & & \cdots & & & \\ & & & m_{n-1} & & \\ & & & & m_n & \end{bmatrix}_{n\times n} \tag{5.66}$$

$$[M_{\mathrm{b}}] = \begin{bmatrix} m_{\mathrm{b}1} & & & & & \\ & m_{\mathrm{b}2} & & & & \\ & & \cdots & & & \\ & & & m_{\mathrm{b}n-1} & & \\ & & & & m_{\mathrm{b}n} & \end{bmatrix}_{n\times n} \tag{5.67}$$

$$[C_{\mathrm{s}}] = \begin{bmatrix} c_1 + c_2 & -c_2 & & & & & & & \\ -c_2 & c_2 + c_3 & -c_3 & & & & & & \\ & \cdots & \cdots & \cdots & & & & & \\ & & -c_i & c_i + c_{i+1} & -c_{i+1} & & & & \\ & & & \cdots & \cdots & & & \cdots & \\ & & & & -c_{n-1} & c_{n-1} & +c_n & -c_n & \\ & & & & & & -c_n & c_n & \end{bmatrix}_{n\times n} \tag{5.68}$$

$$[C_{\mathrm{b}}] = \begin{bmatrix} c_{\mathrm{b}1} & & & & & & \\ & c_{\mathrm{b}2} & & & & & \\ & & \cdots & & & & \\ & & & c_{\mathrm{b}i} & & & \\ & & & & \cdots & & \\ & & & & & c_{\mathrm{b}n-1} & \\ & & & & & & c_{\mathrm{b}n} \end{bmatrix}_{n\times n} \tag{5.69}$$

$$[C_{sb}] = [C_{bs}]^T = [\Upsilon]^T [C_b] = \begin{bmatrix} 0 & -c_{b2} & & & & & & \\ & 0 & -c_{b3} & & & & & \\ & & \cdots & \cdots & & & & \\ & & & 0 & -c_{bi} & & & \\ & & & & \cdots & \cdots & & \\ & & & & & 0 & -c_{bn} & \\ & & & & & & 0 & \end{bmatrix}_{n \times n} \tag{5.70}$$

$$[C_{bsb}] = [\Upsilon]^T [C_b][\Upsilon] = \begin{bmatrix} c_{b2} & & & & & & \\ & c_{b3} & & & & & \\ & & \cdots & & & & \\ & & & c_{bi+1} & & & \\ & & & & \cdots & & \\ & & & & & c_{bn} & \\ & & & & & & 0 \end{bmatrix}_{n \times n} \tag{5.71}$$

where

$$[\Upsilon] = \begin{bmatrix} 0 & & & & & & \\ -1 & 0 & & & & & \\ & \cdots & \cdots & & & & \\ & & -1 & 0 & & & \\ & & & \cdots & \cdots & & \\ & & & & -1 & 0 & \\ & & & & & -1 & 0 \end{bmatrix}_{n \times n} \tag{5.72}$$

Similarly, the submatrices of $[K]$ in Equation 5.62 are defined as

$$[K_s] = \begin{bmatrix} k_1 + k_2 & -k_2 & & & & & & \\ -k_2 & k_2 + k_3 & -k_3 & & & & & \\ & \cdots & \cdots & \cdots & & & & \\ & & -k_i & k_i + k_{i+1} & -k_{i+1} & & & \\ & & & \cdots & \cdots & \cdots & & \\ & & & & -k_{n-1} & k_{n-1} + k_n & -k_n & \\ & & & & & -k_n & k_n & \end{bmatrix}_{n \times n} \tag{5.73}$$

$$[K_b] = \begin{bmatrix} k_{b1} & & & & & & \\ & k_{b2} & & & & & \\ & & \cdots & & & & \\ & & & k_{bi} & & & \\ & & & & \cdots & & \\ & & & & & k_{bn-1} & \\ & & & & & & k_{bn} \end{bmatrix}_{n \times n} \tag{5.74}$$

$$[K_{\mathrm{sb}}] = [K_{\mathrm{bs}}]^{\mathrm{T}} = [\Upsilon]^{\mathrm{T}}[K_{\mathrm{b}}] = \begin{bmatrix} 0 & -k_{\mathrm{b}2} & & & & & & \\ & 0 & -k_{\mathrm{b}3} & & & & & \\ & & \cdots & \cdots & & & & \\ & & & 0 & -k_{\mathrm{b}i} & & & \\ & & & & \cdots & \cdots & & \\ & & & & & 0 & -k_{\mathrm{b}n} & \\ & & & & & & 0 & \end{bmatrix}_{n\times n} \tag{5.75}$$

$$[K_{\mathrm{bsb}}] = [\Upsilon]^{\mathrm{T}}[K_{\mathrm{b}}][\Upsilon] = \begin{bmatrix} k_{\mathrm{b}2} & & & & & & \\ & k_{\mathrm{b}3} & & & & & \\ & & \cdots & & & & \\ & & & k_{\mathrm{b}i+1} & & & \\ & & & & \cdots & & \\ & & & & & k_{\mathrm{b}n} & \\ & & & & & & 0 \end{bmatrix}_{n\times n} \tag{5.76}$$

5.2.3 Structures with Control Devices on Some Floors

Consider a general case where a structure cannot be modeled as shear building and only some floors of the structure are installed with control devices. If the structure is equipped with r actuators, s passive dampers, and m bracing systems (as defined in Section 5.2.1), there are r active control forces $f_{\mathrm{a}i}$ $(i = 1, 2, \ldots, r)$, s passive control forces $f_{\mathrm{p}i}$ $(i = 1, 2, \ldots, s)$, and m d.o.f. $x_{\mathrm{b}i}$ $(i = 1, 2, \ldots, m)$ for bracing systems. Equations 5.59 (the vector of structural and bracing displacements), 5.60 (the vector of active control force), and 5.61 (the vector of passive control force) then become

$$\{x(t)\}_{(n+m)\times 1} = [x_1(t), x_2(t), \cdots, x_n(t); x_{\mathrm{b}1}(t), x_{\mathrm{b}2}(t), \cdots, x_{\mathrm{b}m}(t)]^{\mathrm{T}} \tag{5.77}$$

$$\{f_{\mathrm{a}}(t)\}_{r\times 1} = [f_{\mathrm{a}1}(t), f_{\mathrm{a}2}(t), \cdots, f_{\mathrm{ar}}(t)]^{\mathrm{T}} \tag{5.78}$$

$$\{f_{\mathrm{p}}(t)\}_{\mathrm{s}\times 1} = \left[f_{\mathrm{p}1}(t), f_{\mathrm{p}2}(t), \cdots, f_{\mathrm{ps}}(t)\right]^{\mathrm{T}} \tag{5.79}$$

Although Equations 5.58, 5.62, 5.63, and 5.75 are still applicable, orders of matrices and vectors in these equations are different. Since there are only m bracings, Equations 5.57 and 5.58 become in the orders of m and $(n + m)$, respectively, and $[M]$, $[C]$, and $[K]$ are of the $(n + m) \times (n + m)$ matrices now. For shear building structures, $[M_{\mathrm{s}}]$, $[C_{\mathrm{s}}]$, and $[K_{\mathrm{s}}]$ are the same as defined in Equations 5.66, 5.68, and 5.73, respectively. If the structure cannot be modeled as a shear building, matrices $[C]$ and $[K]$ are no longer tridiagonal. For the current

case of a shear building, $[M_\mathrm{b}]$, $[C_\mathrm{b}]$, and $[K_\mathrm{b}]$ are of $m \times m$ and

$$[M_\mathrm{b}] = \begin{bmatrix} m_{\mathrm{b}1} & & & \\ & m_{\mathrm{b}2} & & \\ & & \cdots & \\ & & & m_{\mathrm{b}m} \end{bmatrix} \tag{5.80a}$$

$$[C_\mathrm{b}] = \begin{bmatrix} c_{\mathrm{b}1} & & & \\ & c_{\mathrm{b}2} & & \\ & & \cdots & \\ & & & c_{\mathrm{b}m} \end{bmatrix} \tag{5.80b}$$

$$[K_\mathrm{b}] = \begin{bmatrix} k_{\mathrm{b}1} & & & \\ & k_{\mathrm{b}2} & & \\ & & \cdots & \\ & & & k_{\mathrm{b}m} \end{bmatrix} \tag{5.80c}$$

Let $[\theta_\mathrm{b}]_{n\times m}$ denote the location matrix of bracing systems on the structure; elements of this matrix are zero except that $\theta_\mathrm{b}(i,j) = 1$ when the jth bracing is supported by the ith floor. Then

$$\begin{cases} [C_\mathrm{bs}]^\mathrm{T}_{m\times n} = [C_\mathrm{sb}]_{m\times n} = [\Upsilon]^\mathrm{T}_{n\times n}\,[\theta_\mathrm{b}]_{n\times m}\,[C_\mathrm{b}]_{m\times m} \\ [K_\mathrm{bs}]^\mathrm{T}_{m\times n} = [K_\mathrm{sb}]_{m\times n} = [\Upsilon]^\mathrm{T}_{n\times n}\,[\theta_\mathrm{b}]_{n\times m}\,[K_\mathrm{b}]_{m\times m} \end{cases} \tag{5.81}$$

and

$$\begin{cases} [C_\mathrm{bsb}]_{n\times n} = [\Upsilon]^\mathrm{T}_{n\times n}\,[\theta_\mathrm{b}]_{n\times m}\,[C_\mathrm{b}]_{m\times m}\,[\theta_\mathrm{b}]^\mathrm{T}_{m\times n}\,[\Upsilon]_{n\times n} = [C_\mathrm{sb}]_{n\times m}\,[\theta_\mathrm{b}]^\mathrm{T}_{m\times n}\,[\Upsilon]_{n\times n} \\ [K_\mathrm{bsb}]_{n\times n} = [\Upsilon]^\mathrm{T}_{n\times n}\,[\theta_\mathrm{b}]_{n\times m}\,[K_\mathrm{b}]_{m\times m}\,[\theta_\mathrm{b}]^\mathrm{T}_{m\times n}\,[\Upsilon]_{n\times n} = [K_\mathrm{sb}]_{n\times m}\,[\theta_\mathrm{b}]^\mathrm{T}_{m\times n}\,[\Upsilon]_{n\times n} \end{cases} \tag{5.82}$$

The relationship between Equations 5.78 and 5.62 can be expressed as

$$\{f_\mathrm{a}(t)\}_{n\times 1} = \begin{Bmatrix} f_{\mathrm{a}1}(t) \\ f_{\mathrm{a}2}(t) \\ \cdots \\ 0 \\ \cdots \\ f_{\mathrm{a}i}(t) \\ \cdots \\ 0 \\ \cdots \\ f_{\mathrm{a}r-1}(t) \\ f_{\mathrm{a}r}(t) \end{Bmatrix} = \begin{bmatrix} 1 & 0 & 0 & \cdots & \cdots & \cdots & \cdots & \cdots & 0 \\ 0 & 1 & 0 & \cdots & \cdots & \cdots & \cdots & \cdots & 0 \\ \cdots & \cdots & \cdots & \cdots & \cdots & \cdots & \cdots & \cdots & \cdots \\ 0 & \cdots & \cdots & 0 & \cdots & \cdots & \cdots & \cdots & 0 \\ \cdots & \cdots & \cdots & \cdots & \cdots & \cdots & \cdots & \cdots & \cdots \\ 0 & \cdots & \cdots & 0 & 1 & 0 & \cdots & \cdots & 0 \\ \cdots & \cdots & \cdots & \cdots & \cdots & \cdots & \cdots & \cdots & \cdots \\ 0 & \cdots & \cdots & \cdots & \cdots & 0 & \cdots & \cdots & 0 \\ \cdots & \cdots & \cdots & \cdots & \cdots & \cdots & \cdots & \cdots & \cdots \\ 0 & \cdots & \cdots & \cdots & \cdots & \cdots & 0 & 1 & 0 \\ 0 & \cdots & \cdots & \cdots & \cdots & \cdots & 0 & 0 & 1 \end{bmatrix}$$

$$\times \begin{Bmatrix} f_{\mathrm{a}1}(t) \\ f_{\mathrm{a}2}(t) \\ \cdots \\ f_{\mathrm{a}r-1}(t) \\ f_{\mathrm{a}r}(t) \end{Bmatrix} = [\theta_\mathrm{a}]_{n\times r}\,\{f_\mathrm{a}(t)\}_{r\times 1} \tag{5.83}$$

which means that zero elements are filled to $\{f_a(t)\}_{n\times 1}$ for those floors without an actuator. In Equation 5.83, $[\theta_a]_{n\times r}$ is matrix of actuator location on the structure, and its elements are zero except that $\theta_a(i,j) = 1$ when the jth actuator is attached on the ith floor.

Similarly, for passive control forces

$$\{f_p(t)\}_{n\times 1} = \begin{Bmatrix} f_{p1}(t) \\ f_{p2}(t) \\ \cdots \\ 0 \\ \cdots \\ f_{pi}(t) \\ \cdots \\ 0 \\ \cdots \\ f_{ps-1}(t) \\ f_{ps}(t) \end{Bmatrix} = \begin{bmatrix} 1 & 0 & 0 & \cdots & \cdots & \cdots & \cdots & \cdots & 0 \\ 0 & 1 & 0 & \cdots & \cdots & \cdots & \cdots & \cdots & 0 \\ \cdots & \cdots & \cdots & \cdots & \cdots & \cdots & \cdots & \cdots & \cdots \\ 0 & \cdots & \cdots & 0 & \cdots & \cdots & \cdots & \cdots & 0 \\ \cdots & \cdots & \cdots & \cdots & \cdots & \cdots & \cdots & \cdots & \cdots \\ 0 & \cdots & \cdots & 0 & 1 & 0 & \cdots & \cdots & 0 \\ \cdots & \cdots & \cdots & \cdots & \cdots & \cdots & \cdots & \cdots & \cdots \\ 0 & \cdots & \cdots & \cdots & \cdots & 0 & \cdots & \cdots & 0 \\ \cdots & \cdots & \cdots & \cdots & \cdots & \cdots & \cdots & \cdots & \cdots \\ 0 & \cdots & \cdots & \cdots & \cdots & \cdots & 0 & 1 & 0 \\ 0 & \cdots & \cdots & \cdots & \cdots & \cdots & 0 & 0 & 1 \end{bmatrix}$$

$$\times \begin{Bmatrix} f_{p1}(t) \\ f_{p2}(t) \\ \cdots \\ f_{ps-1}(t) \\ f_{ps}(t) \end{Bmatrix} = [\theta_p]_{n\times s} \{f_p(t)\}_{s\times 1} \tag{5.84}$$

where $[\theta_p]_{n\times s}$ is matrix of damper location on the structure. If the jth damper is attached on the ith floor, $\theta_a(i,j) = 1$, otherwise, $\theta_a(i,j) = 0$. Actuator and damper location matrices $[\gamma_a]$ and $[\gamma_p]$ can be further expressed as

$$[\gamma_a]_{(n+m)\times r} = \begin{bmatrix} [\gamma_s]_{n\times n}[\theta_a]_{n\times r} \\ [\theta_b]^T_{m\times n}[\gamma_b]_{n\times n}[\theta_a]_{n\times r} \end{bmatrix}$$

$$[\gamma_p]_{(n+m)\times s} = \begin{bmatrix} [\gamma_s]_{n\times n}[\theta_p]_{n\times r} \\ [\theta_b]^T_{m\times n}[\gamma_b]_{n\times n}[\theta_p]_{n\times r} \end{bmatrix} \tag{5.85}$$

where $[\gamma_s]$ and $[\gamma_b]$ are defined in Equation 5.75.

Coefficient vector for earthquake excitation, $\{\delta\}$, now of $(n + m) \times 1$, is expressed as

$$\{\delta\} = -[m_1, m_2, \cdots, m_i, \cdots, m_{n-1}, m_n; m_{b1}, m_{b2}, \cdots, m_{bi}, \cdots, m_{b\,m-1}, m_{bm}]^T \tag{5.86}$$

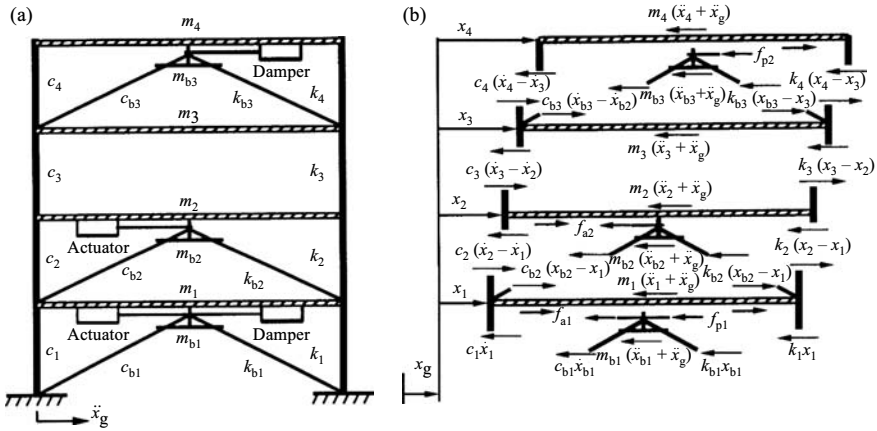

FIGURE 5.12 Four-story shear building with HDABC system: (a) schematic and (b) free-body diagram.

5.2.4 Verification of the General Model for HDABC-Controlled Structures

A four-story shear building with an HDABC system (see Figure 5.12) serves as an example to verify the general model. This control system consists of a hybrid control device at the first floor, an actuator at the second floor, and a damper at the fourth floor. Analytical models are developed in two ways. One uses equations from the general model while the other is obtained directly from the free-body diagram. The validity of the general model is verified if both methods yield the same results for this four-story building with control.

Since there are two actuators, two dampers, and three bracings on the four-story building, $n = 4$, $m = 3$, and $r = s = 2$. From Equations 5.77 through 5.79, vectors of displacements, active control forces, and passive control forces are expressed respectively as

$$\{x(t)\}_{7\times 1} = [x_1(t), x_2(t), x_3(t), x_4(t); x_{b1}(t), x_{b2}(t), x_{b3}(t)]^{\mathrm{T}} \tag{5.87}$$

$$\{f_a(t)\}_{2\times 1} = [f_{a1}(t), f_{a2}(t)]^{\mathrm{T}} \tag{5.88}$$

$$\{f_p(t)\}_{2\times 1} = [f_{p1}(t), f_{p2}(t)]^{\mathrm{T}} \tag{5.89}$$

and

$$[M_s] = \begin{bmatrix} m_1 & & & \\ & m_2 & & \\ & & m_3 & \\ & & & m_4 \end{bmatrix} \tag{5.90}$$

$$[C_s] = \begin{bmatrix} c_1 + c_2 & -c_2 & & \\ -c_2 & c_2 + c_3 & -c_3 & \\ & -c_3 & c_3 + c_4 & -c_4 \\ & & -c_4 & c_4 \end{bmatrix} \tag{5.91}$$

$$[K_s] = \begin{bmatrix} k_1 + k_2 & -k_2 & & \\ -k_2 & k_2 + k_3 & -k_3 & \\ & -k_3 & k_3 + k_4 & -k_4 \\ & & -k_4 & k_4 \end{bmatrix} \tag{5.92}$$

$$[\Upsilon] = \begin{bmatrix} 0 & & & \\ -1 & 0 & & \\ & -1 & 0 & \\ & & -1 & 0 \end{bmatrix} \tag{5.93}$$

$$[M_b] = \begin{bmatrix} m_{b1} & & \\ & m_{b2} & \\ & & m_{b3} \end{bmatrix}$$

$$[C_b] = \begin{bmatrix} c_{b1} & & \\ & c_{b2} & \\ & & c_{b3} \end{bmatrix}$$

$$[K_b] = \begin{bmatrix} k_{b1} & & \\ & k_{b2} & \\ & & k_{b3} \end{bmatrix} \tag{5.94}$$

Since there are three bracings, two actuators, and two dampers on the four-story structure, location matrices for bracings $[\theta_b]$, for actuators $[\theta_a]$, and for dampers $[\theta_p]$ are of 4×3, 4×2, and 4×2, respectively. $\theta_b(1,1) = \theta_b(2,2) = \theta_b(4,3) = 1$ for the three bracings installed on the first, second, and fourth floors, respectively; $\theta_a(1,1) = \theta_a(2,2) = 1$ for the two actuators equipped on the first and second floors, respectively; and $\theta_p(1,1) = \theta_p(4,2) = 1$ for the two dampers equipped on the first and fourth floors, respectively. Other elements in these three matrices are zero. Thus,

$$[\theta_b] = \begin{bmatrix} 1 & 0 & 0 \\ 0 & 1 & 0 \\ 0 & 0 & 0 \\ 0 & 0 & 1 \end{bmatrix}, \quad [\theta_a] = \begin{bmatrix} 1 & 0 \\ 0 & 1 \\ 0 & 0 \\ 0 & 0 \end{bmatrix}, \quad [\theta_p] = \begin{bmatrix} 1 & 0 \\ 0 & 0 \\ 0 & 0 \\ 0 & 1 \end{bmatrix} \tag{5.95}$$

From Equations 5.81, 5.82, 5.85, and 5.86

$$\begin{cases} [C_{sb}]_{4\times3} = \begin{bmatrix} 0 & -1 & 0 & 0 \\ 0 & 0 & -1 & 0 \\ 0 & 0 & 0 & -1 \\ 0 & 0 & 0 & 0 \end{bmatrix} \begin{bmatrix} 1 & 0 & 0 \\ 0 & 1 & 0 \\ 0 & 0 & 0 \\ 0 & 0 & 1 \end{bmatrix} \begin{bmatrix} c_{b1} & 0 & 0 \\ 0 & c_{b2} & 0 \\ 0 & 0 & c_{b3} \end{bmatrix} \\ \quad = \begin{bmatrix} 0 & -c_{b2} & 0 \\ 0 & 0 & 0 \\ 0 & 0 & -c_{b3} \\ 0 & 0 & 0 \end{bmatrix} \\ [K_{sb}]_{4\times3} = \begin{bmatrix} 0 & -1 & 0 & 0 \\ 0 & 0 & -1 & 0 \\ 0 & 0 & 0 & -1 \\ 0 & 0 & 0 & 0 \end{bmatrix} \begin{bmatrix} 1 & 0 & 0 \\ 0 & 1 & 0 \\ 0 & 0 & 0 \\ 0 & 0 & 1 \end{bmatrix} \begin{bmatrix} k_{b1} & 0 & 0 \\ 0 & k_{b2} & 0 \\ 0 & 0 & k_{b3} \end{bmatrix} \\ \quad = \begin{bmatrix} 0 & -k_{b2} & 0 \\ 0 & 0 & 0 \\ 0 & 0 & -k_{b3} \\ 0 & 0 & 0 \end{bmatrix} \end{cases} \tag{5.96}$$

$$\begin{cases} [C_{bsb}]_{4\times4} = \begin{bmatrix} 0 & -c_{b2} & 0 \\ 0 & 0 & 0 \\ 0 & 0 & -c_{b3} \\ 0 & 0 & 0 \end{bmatrix} \begin{bmatrix} 1 & 0 & 0 & 0 \\ 0 & 1 & 0 & 0 \\ 0 & 0 & 0 & 1 \end{bmatrix} \\ \begin{bmatrix} 0 & 0 & 0 & 0 \\ -1 & 0 & 0 & 0 \\ 0 & -1 & 0 & 0 \\ 0 & 0 & -1 & 0 \end{bmatrix} = \begin{bmatrix} c_{b2} & 0 & 0 & 0 \\ 0 & 0 & 0 & 0 \\ 0 & c_{b3} & 0 & 0 \\ 0 & 0 & 0 & 0 \end{bmatrix} \\ [K_{bsb}]_{4\times4} = \begin{bmatrix} 0 & -k_{b2} & 0 \\ 0 & 0 & 0 \\ 0 & 0 & -k_{b3} \\ 0 & 0 & 0 \end{bmatrix} \begin{bmatrix} 1 & 0 & 0 & 0 \\ 0 & 1 & 0 & 0 \\ 0 & 0 & 0 & 1 \end{bmatrix} \\ \begin{bmatrix} 0 & 0 & 0 & 0 \\ -1 & 0 & 0 & 0 \\ 0 & -1 & 0 & 0 \\ 0 & 0 & -1 & 0 \end{bmatrix} = \begin{bmatrix} k_{b2} & 0 & 0 & 0 \\ 0 & 0 & 0 & 0 \\ 0 & k_{b3} & 0 & 0 \\ 0 & 0 & 0 & 0 \end{bmatrix} \end{cases} \tag{5.97}$$

$$[\gamma_{\mathrm{a}}]_{7\times 2} = \begin{bmatrix} & \begin{bmatrix} 1 & 0 & 0 & 0 \\ 0 & 1 & 0 & 0 \\ 0 & 0 & 1 & 0 \\ 0 & 0 & 0 & 1 \end{bmatrix} \begin{bmatrix} 1 & 0 \\ 0 & 1 \\ 0 & 0 \\ 0 & 0 \end{bmatrix} \\ \begin{bmatrix} 1 & 0 & 0 & 0 \\ 0 & 1 & 0 & 0 \\ 0 & 0 & 0 & 1 \end{bmatrix} \begin{bmatrix} -1 & 0 & 0 & 0 \\ 0 & -1 & 0 & 0 \\ 0 & 0 & -1 & 0 \\ 0 & 0 & 0 & -1 \end{bmatrix} \begin{bmatrix} 1 & 0 \\ 0 & 1 \\ 0 & 0 \\ 0 & 0 \end{bmatrix} & \end{bmatrix}$$

$$= \begin{bmatrix} 1 & 0 \\ 0 & 1 \\ 0 & 0 \\ 0 & 0 \\ -1 & 0 \\ 0 & -1 \\ 0 & 0 \end{bmatrix} \tag{5.98}$$

$$[\gamma_{\mathrm{p}}]_{7\times 2} = \begin{bmatrix} & \begin{bmatrix} 1 & 0 & 0 & 0 \\ 0 & 1 & 0 & 0 \\ 0 & 0 & 1 & 0 \\ 0 & 0 & 0 & 1 \end{bmatrix} \begin{bmatrix} 1 & 0 \\ 0 & 0 \\ 0 & 0 \\ 0 & 1 \end{bmatrix} \\ \begin{bmatrix} 1 & 0 & 0 & 0 \\ 0 & 1 & 0 & 0 \\ 0 & 0 & 0 & 1 \end{bmatrix} \begin{bmatrix} -1 & 0 & 0 & 0 \\ 0 & -1 & 0 & 0 \\ 0 & 0 & -1 & 0 \\ 0 & 0 & 0 & -1 \end{bmatrix} \begin{bmatrix} 1 & 0 \\ 0 & 0 \\ 0 & 0 \\ 0 & 1 \end{bmatrix} & \end{bmatrix}$$

$$= \begin{bmatrix} 1 & 0 \\ 0 & 0 \\ 0 & 0 \\ 0 & 1 \\ -1 & 0 \\ 0 & 0 \\ 0 & -1 \end{bmatrix} \tag{5.99}$$

and

$$\{\delta\} = -[m_1, m_2, m_3, m_4; m_{\mathrm{b}1}, m_{\mathrm{b}2}, m_{\mathrm{b}3}]^{\mathrm{T}} \tag{5.100}$$

Modeling the system directly from the free-body diagram (see Figure 5.12) leads to

$$\begin{cases} m_1(\ddot{x}_1+\ddot{x}_g)+c_1\dot{x}_1-c_2(\dot{x}_2-\dot{x}_1)-c_{b2}(\dot{x}_{b2}-\dot{x}_1) \\ \qquad +k_1x_1-k_2(x_2-x_1)-k_{b2}(x_{b2}-x_1)=f_{a1}+f_{p1} \\ m_2(\ddot{x}_2+\ddot{x}_g)+c_2(\dot{x}_2-\dot{x}_1)-c_3(\dot{x}_3-\dot{x}_2) \\ \qquad +k_2(x_2-x_1)-k_3(x_3-x_2)=f_{a2} \\ m_3(\ddot{x}_3+\ddot{x}_g)+c_3(\dot{x}_3-\dot{x}_2)-c_4(\dot{x}_4-\dot{x}_3)-c_{b3}(\dot{x}_{b3}-\dot{x}_3) \\ \qquad +k_3(x_3-x_2)-k_4(x_4-x_3)-k_{b3}(x_{b3}-x_3)=0 \\ m_4(\ddot{x}_4+\ddot{x}_g)+c_4(\dot{x}_4-\dot{x}_3)+k_4(x_4-x_3)=f_{p2} \end{cases} \tag{5.101a}$$

$$\begin{cases} m_{b1}(\ddot{x}_{b1}+\ddot{x}_g)+c_{b1}\dot{x}_{b1}+k_{b1}x_{b1}=-f_{a1}-f_{p1} \\ m_{b2}(\ddot{x}_{b2}+\ddot{x}_g)+c_{b2}(\dot{x}_{b2}-\dot{x}_1)+k_{b2}(x_{b2}-x_1)=-f_{a2} \\ m_{b3}(\ddot{x}_{b3}+\ddot{x}_g)+c_{b3}(\dot{x}_{b3}-\dot{x}_3)+k_{b3}(x_{b3}-x_3)=-f_{p2} \end{cases} \tag{5.101b}$$

By condensing Equations 5.101a and 5.101b into matrix form as shown in Equation 5.58, the following coefficient matrices are obtained

$$[C_s]=\begin{bmatrix} c_1+c_2+c_{b2} & -c_2 & 0 & 0 & 0 & -c_{b2} & 0 \\ -c_2 & c_2+c_3 & -c_3 & 0 & 0 & 0 & 0 \\ 0 & -c_3 & c_3+c_4+c_{b3} & -c_4 & 0 & 0 & -c_{b3} \\ 0 & 0 & -c_4 & c_4 & 0 & 0 & 0 \\ 0 & 0 & 0 & 0 & c_{b1} & 0 & 0 \\ -c_{b2} & 0 & 0 & 0 & 0 & c_{b2} & 0 \\ 0 & 0 & -c_{b3} & 0 & 0 & 0 & c_{b3} \end{bmatrix} \tag{5.102}$$

$$=\begin{bmatrix} [C_s]_{4\times4}+[C_{bsb}]_{4\times4} & [C_{sb}]_{4\times3} \\ [C_{bs}]_{3\times4} & [C_b]_{3\times3} \end{bmatrix}$$

$$[K_s]=\begin{bmatrix} k_1+k_2+k_{b2} & -k_2 & 0 & 0 & 0 & -k_{b2} & 0 \\ -k_2 & k_2+k_3 & -k_3 & 0 & 0 & 0 & 0 \\ 0 & -k_3 & k_3+k_4+k_{b3} & -k_4 & 0 & 0 & -k_{b3} \\ 0 & 0 & -k_4 & k_4 & 0 & 0 & 0 \\ 0 & 0 & 0 & 0 & k_{b1} & 0 & 0 \\ -k_{b2} & 0 & 0 & 0 & 0 & k_{b2} & 0 \\ 0 & 0 & -k_{b3} & 0 & 0 & 0 & k_{b3} \end{bmatrix} \tag{5.103}$$

$$=\begin{bmatrix} [K_s]_{4\times4}+[K_{bsb}]_{4\times4} & [K_{sb}]_{4\times3} \\ [K_{bs}]_{3\times4} & [K_b]_{3\times3} \end{bmatrix}$$

$$[\gamma_a]_{7\times2}=\begin{bmatrix} 1 & 0 & 0 & 0 & -1 & 0 & 0 \\ 0 & 1 & 0 & 0 & 0 & -1 & 0 \end{bmatrix}^T,$$

$$[\gamma_p]_{7\times2}=\begin{bmatrix} 1 & 0 & 0 & 0 & -1 & 0 & 0 \\ 0 & 0 & 0 & 1 & 0 & 0 & -1 \end{bmatrix}^T \tag{5.104}$$

These results are exactly the same as those from the general model. Clearly, mass matrix $[M]$ and coefficient vector for earthquake excitation $\{\delta\}$ are also the same as general modeling.

5.2.5 State-Variable Representation of the HDABC System

As noted in Chapter 4, the linear system in modern control theory is expressed by the first-order state equations. This section shows how motion equations of an HDABC system are consolidated into state equations, with the HDABC system using viscous fluid damper as the example.

With the definition of displacement vector $\{x(t)\}$ for the structure and braces by Equation 5.77, the actuator models expressed by Equation 5.36 can be condensed into matrix form as

$$\begin{aligned} \{\dot{f}_{\mathrm{a}}(t)\} &= [B_{\mathrm{x}}]\{\dot{x}(t)\} + [B_{\mathrm{c}}]\{c(t)\} \\ \{\dot{c}(t)\} &= [C_{\mathrm{c}}]\{c(t)\} + [C_{\mathrm{u}}]\{u(t)\} \end{aligned} \tag{5.105}$$

where $\{f_{\mathrm{a}}(t)\}$ is defined by Equation (5.78); $\{c(t)\}$ and $\{u(t)\}$ are vectors of valve-piston displacements and active control commands, respectively; parameter matrices $[B_{\mathrm{x}}]$ of $r \times (n+m)$, $[B_{\mathrm{c}}]$ of $r \times r$, $[C_{\mathrm{c}}]$ of $r \times r$, and $[C_{\mathrm{u}}]$ of $r \times r$ are determined by coefficients in Equation 5.36. Elements in $[B_{\mathrm{x}}]$ are zero except $B_{\mathrm{x}}(k,i) = -2(\beta \mathrm{A}^2/V)_k$ and $B_{\mathrm{x}}(k, i+n) = 2(\beta \mathrm{A}^2/V)_k$; $[B_{\mathrm{c}}]$, $[C_{\mathrm{c}}]$, and $[C_{\mathrm{u}}]$ are diagonal with elements $B_{\mathrm{c}}(k,\ k) = \left(\beta A K_{\mathrm{v}} \sqrt{2P_{\mathrm{S}}/V}\right)_k$, $C_{\mathrm{c}}(k,k) = -1/\tau_k$, and $C_{\mathrm{u}}(k,k) = 1/\tau_k$; τ_k is a parameter of the kth actuator defined in Equation 5.12b.

Similarly, the damper models expressed by Equation 5.39b can be condensed into matrix form as

$$\left\{\dot{f}_{\mathrm{p}}(t)\right\} = [P_1]\,\{\dot{x}(t)\} + [P_2]\left\{f_{\mathrm{p}}(t)\right\} \tag{5.106}$$

where $\{x(t)\}$ and $\{f_{\mathrm{p}}(t)\}$ are defined by Equations 5.77 and 5.79, respectively; parameter matrices $[P_1]$ of $s \times (n+m)$ and $[P_2]$ of $s \times s$ can be easily obtained from Equation 5.39b. Elements in $[P_1]$ are zero except that $P_1(k,i) = -C_{0\mathrm{k}}/\lambda_{0\mathrm{k}}$ and $P_1(k, j+n) = C_{0\mathrm{k}}/\lambda_{0\mathrm{k}}$; $[P_2]$ is a diagonal matrix with elements $P_2(k,k) = -1/\lambda_{0\mathrm{k}}$.

Owing to the existence of actuator and damper dynamics, state variables must include d.o.f. for actuator dynamics, $\{f_{\mathrm{a}}(t)\}$ and $\{c(t)\}$, and damper dynamics, $\{f_p(t)\}$,in addition to d.o.f. for dynamics of the structure and K-braces. Thus, the state vector is defined as

$$\{Z(t)\}_{N\times 1} = \begin{Bmatrix} \{x(t)\} \\ \{\dot{x}(t)\} \\ \left\{f_{\mathrm{a}}(t)\right\} \\ \left\{f_{\mathrm{p}}(t)\right\} \\ \{c(t)\} \end{Bmatrix} \tag{5.107}$$

If r actuators and s dampers are supported by m bracings on a building structure with n d.o.f., there are $(n+m)$ elements in either $\{x(t)\}$ or $\{\dot{x}(t)\}$, r elements in either $\{f_a(t)\}$ or $\{c(t)\}$, and s elements in $\{f_p(t)\}$. Thus, the order of $\{Z(t)\}$—vector of state variables—is

$$N = 2n + 2m + 2r + s \tag{5.108}$$

Combining Equations 5.58, 5.105, and 5.106 yields the following state-variable representation of the hybrid structural control system

$$\left\{\dot{Z}(t)\right\} = [A]\{Z(t)\} + [B_u]\{u(t)\} + \{B_r\}\ddot{x}_g(t) \tag{5.109a}$$

where $[A]$ of $N \times N$ is plant matrix; $[B_u]$ of $N \times r$ is coefficient matrix for control commands; and $\{B_r\}$ of $N \times 1$ is coefficient vector for earthquake excitation. These matrices can be further expressed as

$$[A] = \begin{bmatrix} [0] & [I] & [0] & [0] & [0] \\ -[M]^{-1}[K] & -[M]^{-1}[C] & -[M]^{-1}[\gamma_a] & -[M]^{-1}[\gamma_p] & [0] \\ [0] & [B_x] & [0] & [0] & [B_c] \\ [0] & [P_1] & [0] & [P_2] & [0] \\ [0] & [0] & [0] & [0] & [C_c] \end{bmatrix} \tag{5.109b}$$

$$[B_u] = \begin{bmatrix} [0] \\ [0] \\ [0] \\ [0] \\ [C_u] \end{bmatrix} \quad [B_r] = \begin{bmatrix} \{0\} \\ \{-1\} \\ \{0\} \\ \{0\} \\ \{0\} \end{bmatrix} \tag{5.109c}$$

For a digital control system with zero-order hold and sampling period T, the values of $\{Z(t)\}$, $\{u(t)\}$, and $\ddot{x}_g(t)$ at kth sampling time (i.e., at $t = kT$, $k = 0, 1, 2, \ldots, +\infty$) are $z(k)$, $u(k)$, and $r(k)$, respectively; the relationship during time interval $kT \le t < (k+1)T$ $(k = 0, 1, 2, \ldots, +\infty)$ becomes

$$\begin{aligned} \{Z(t)\} &= \{Z(kT)\} = z(k) \\ \{u(t)\} &= \{u(kT)\} = u(k) \\ \ddot{x}_g(t) &= \ddot{x}_g(kT) \ = r(k) \end{aligned} \tag{5.110}$$

The solution to Equation 5.109 is

$$\{Z(t)\} = \Pi(t - t_0)\{Z(t_0)\} + \int_{t_0}^{t} \Pi(t - \tau)\left([B_u]\{u(\tau)\} + \{B_r\}\ddot{x}_g(\tau)\right) d\tau \tag{5.111}$$

where *state transition matrix* $\Pi(t)$ is in the same order as plant matrix $[A]$ and is given by

$$\Pi(t) = \exp([\Phi]\,\Delta t) = \sum_{k=0}^{\infty} \frac{([\Phi]\Delta t)^k}{k!}$$
$$= [I]_{N\times N} + [\Phi]\Delta t + \frac{1}{2!}([\Phi]\Delta t)^2 + \frac{1}{3!}([\Phi]\Delta t)^3 \ldots \tag{5.112}$$

In Equation 5.112, $[\Phi]$ is modal plant matrix defined by Equation 4.31, and $[I]$ is unit matrix.

Let $t_0 = kT$ and $t = (k+1)T$; then, with the zero-order hold expressed by Equation 5.110, Equation 5.111 can be rewritten as

$$z(k+1) = \Pi(T)z(k) + \int_{kT}^{(k+1)T} \Pi(kT + T - \tau)[B_{\mathrm{u}}]\,\mathrm{d}\tau u(k) + \int_{kT}^{(k+1)T} \Pi(kT + T - \tau)\{B_{\mathrm{r}}\}\,\mathrm{d}\tau r(k) \tag{5.113}$$

By denoting

$$A = \Pi(T)$$
$$B_{\mathrm{u}} = \int_{kT}^{(k+1)\mathrm{T}} \Pi(kT + T - \tau)[B_{\mathrm{u}}]\,\mathrm{d}\tau \tag{5.114}$$
$$B_{\mathrm{r}} = \int_{kT}^{(k+1)\mathrm{T}} \Pi(kT + T - \tau)\{B_{\mathrm{r}}\}\,\mathrm{d}\tau$$

the state-variable representation of the system in *discrete time domain* is obtained as

$$z(k+1) = Az(k) + B_{\mathrm{u}}u(k) + B_{\mathrm{r}}r(k) \tag{5.115}$$

For HDABC systems using liquid mass damper or spring damper, the damping force $\{f_{\mathrm{p}}(t)\}$, as expressed by Equations 5.40 or 5.42, is not an independent state but rather directly related to the states of the structure and braces $\{x(t)\}, \{\dot{x}(t)\}$, and $\{\ddot{x}(t)\}$. The state vector of such system shall be defined as

$$\{Z(t)\}_{N\times 1} = \begin{Bmatrix} \{x(t)\} \\ \{\dot{x}(t)\} \\ \{f_{\mathrm{a}}(t)\} \\ \{c(t)\} \end{Bmatrix} \tag{5.116}$$

and

$$N = 2(n + m + r) \tag{5.117}$$

The state equation will be in the same format as Equation 5.109. The plant matrix is different, and it shall be derived by substituting the damper model, Equation 5.40 or Equation 5.42, into motion equations of structure and braces, Equations 5.56 and 5.57. Such process is further demonstrated by numerical examples in Sections 5.3 and 5.4.

EXAMPLE 5.2.1

Derive the analytical model of the one-story seismic structure with HDABC system as shown in Figure 5.1b. This model shall be in state-variable representation as Equation 5.109a shows. Structural properties are mass $m_1 = 1000$ lb (454 kg), damping ratio $\zeta_1 = 1\%$, and natural frequency $f_1 = 2.0$ Hz. K-brace properties are $m_b = 27.778$ lb (12.6 kg), $\zeta_b = 0.1\%$, and $k_b = 3.416 \times 10^6$ lb/s^2 (1549.3 kN/m). The HDABC system uses a servovalve-controlled hydraulic actuator and a viscous fluid damper. The servovalve is rated for 5 gpm (3.1542×10^{-4} m^3/s) at 1000 psi (6.895 MPa) pressure loss and has a bandwidth $f_b = 35.63$ Hz. The actuator chamber has volume $V = 3.3$ in.^{3} and cross-sectional area $A = 1.1$ in.^{2}. The hydraulic supply pressure $P_s = 3000$ psi (20.684 MPa) and hydraulic fluid bulk modulus $\beta = 10^5$ psi (689.48 MPa). The damper is analyzed by a Maxwell model with damping coefficient $C_0 = 120$ lb/s (533.6688 Ns/m) and relaxation time $\lambda_0 = 0.025$ s. Also, find their open-loop system poles on the basis of the derived state equations.

Solution

The natural frequency of the structure in radians is

$$\omega_1 = 2\pi f_1 = 2(\pi)(2.0) = 12.566 \text{ rad/s} \tag{a}$$

From the structural dynamics, the damping and stiffness coefficients of the structure are given by

$$c_1 = 2\zeta_1\omega_1 m_1 = 2(0.01)(12.566)(1000) = 251.327 \text{ lb/s} \tag{b}$$

$$k_1 = m_1\omega_1^2 = (1000)(12.566^2) = 1.579 \times 10^5 \text{ lb/s}^2 \tag{c}$$

and the natural frequency and damping ratio of the K-brace are

$$\omega_b = \sqrt{\frac{k_b}{m_b}} = \sqrt{\frac{3.416 \times 10^6}{27.778}} = 350.657 \text{ rad/s} \tag{d}$$

$$c_b = 2\zeta_b \omega_b m_b = 2(0.001)(350.657)(27.778) = 19.481 \text{ lb/s} \tag{e}$$

The motion equations of the structure and the K-brace can be obtained on the basis of the force balance of the free bodies shown in Figure 5.13. For the structure floor

$$m_1 \left(\ddot{x}_1 + \ddot{x}_g\right) + c_1 \dot{x}_1 + k_1 x_1 = f_a + f_p \tag{f}$$

And for the brace

$$m_b \left(\ddot{x}_b + \ddot{x}_g\right) + c_b \dot{x}_b + k_b x_b = -f_a - f_p \tag{g}$$

The motion Equations f and g of the system can be condensed in a matrix form as

$$[M]\{\ddot{x}(t)\} + [C]\{\dot{x}(t)\} + [K]\{x(t)\} = \{\gamma_a\} f_a(t) + \{\gamma_p\} f_p(t) + \{\delta\}\ddot{x}_g(t) \tag{h}$$

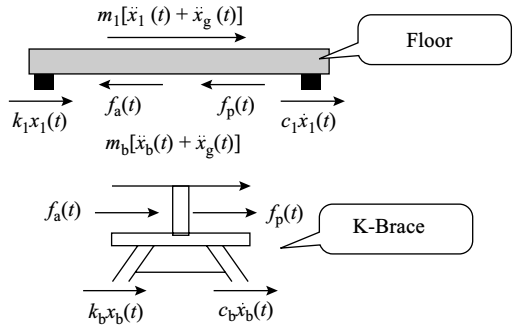

FIGURE 5.13 Example 5.2.1: free-body diagram of one-story building with HDABC system.

where

$$\begin{cases} [M] = \begin{bmatrix} m_1 & 0 \\ 0 & m_b \end{bmatrix} = \begin{bmatrix} 1000.0 & 0 \\ 0 & 27.778 \end{bmatrix} \\ [C] = \begin{bmatrix} c_1 & 0 \\ 0 & c_b \end{bmatrix} = \begin{bmatrix} 251.327 & 0 \\ 0 & 19.481 \end{bmatrix} \\ [K] = \begin{bmatrix} k_1 & 0 \\ 0 & k_b \end{bmatrix} = \begin{bmatrix} 1.579 \times 10^5 & 0 \\ 0 & 3.416 \times 10^6 \end{bmatrix} \\ \{\gamma_a\} = \{\gamma_p\} = \begin{Bmatrix} 1 \\ -1 \end{Bmatrix} \\ \{\delta\} = \begin{Bmatrix} -m_1 \\ -m_b \end{Bmatrix} = \begin{Bmatrix} -1000.0 \\ -27.778 \end{Bmatrix} \end{cases} \tag{i}$$

Equations h and i, motion equations of the structure and the K-brace, can also be formulated using Equation 5.58 directly. Equation h can be rewritten as

$$\begin{aligned} \{\ddot{x}(t)\} = &-[M]^{-1}[C]\{\dot{x}(t)\} - [M]^{-1}[K]\{x(t)\} \\ &+ [M]^{-1}\{\gamma_a\}f_a(t) + [M]^{-1}\{\gamma_p\}f_p(t) + [M]^{-1}\{\delta\}\ddot{x}_g(t) \end{aligned} \tag{j}$$

where

$$\begin{cases} [M]^{-1}[C] = \begin{bmatrix} 0.2513 & 0 \\ 0 & 0.7013 \end{bmatrix} \\ [M]^{-1}[K] = \begin{bmatrix} 157.914 & 0 \\ 0 & 1.230 \times 10^5 \end{bmatrix} \\ [M]^{-1}\{\gamma_a\} = [M]^{-1}\{\gamma_p\} = \begin{Bmatrix} 0.001 \\ -0.036 \end{Bmatrix} \\ [M]^{-1}\{\delta\} = \begin{Bmatrix} -1 \\ -1 \end{Bmatrix} \end{cases} \tag{k}$$

The dynamic model of the hydraulic actuator is given by Equations 5.12 and 5.35b with Equation 5.1 as

$$\begin{cases} \dot{f}_a(t) = \frac{2\beta A^2}{V}(\dot{x}_b(t) - \dot{x}_1(t)) + \frac{\beta A K_V}{V}\sqrt{2P_S}c(t) \\ \dot{c}(t) = (-1/\tau)c(t) + (1/\tau)u(t) \end{cases} \tag{l}$$

and the passive damper model is given by Equation 5.39a as

$$\dot{f}_{\mathrm{p}}(t) = -\left(\frac{1}{\lambda_0}\right) f_{\mathrm{p}}(t) + \left(\frac{C_0}{\lambda_0}\right)\left(\dot{x}_{\mathrm{b}}(t) - \dot{x}_1(t)\right) \tag{m}$$

With given data, coefficients in Equations l and m can be calculated as

$$\begin{aligned}
&\frac{2\beta A^2}{V} = \frac{2(10^5)(1.1^2)}{3.3} = 7.333 \times 10^5 \text{ pli} \\
&K_{\mathrm{V}} = \frac{3.85(5)}{\sqrt{1000}} = 0.6087 \text{ in}^4 \Big/ (\sec - \sqrt{\text{lb}}) \\
&\frac{\beta A K_{\mathrm{V}}}{V}\sqrt{2P_{\mathrm{S}}} = \left(\frac{(10^5)(1.1)(0.6087)}{3.3}\right)\sqrt{2(3000)} = 1.572 \times 10^6 \text{ lb/s} \\
&\frac{1}{\tau} = 2\pi f_{\mathrm{b}} = 2\pi(35.63) = 223.870
\end{aligned} \tag{n}$$

where Kv is calculated by Equation 5.13b; and

$$\begin{cases} 1/\lambda_0 = 1/0.025 = 40.0 \\ C_0/\lambda_0 = 120.0/0.025 = 4800.0 \end{cases} \tag{o}$$

Thus, Equations l and m become

$$\begin{cases} \dot{f}_{\mathrm{a}}(t) = -7.333 \times 10^5 \dot{x}_1(t) + 7.333 \times 10^5 \dot{x}_{\mathrm{b}}(t) + 1.572 \times 10^6 c(t) \\ \dot{c}(t) = -223.870 c(t) + 223.870 u(t) \end{cases} \tag{p}$$

$$\dot{f}_{\mathrm{p}}(t) = -40.0 f_{\mathrm{p}}(t) - 4800.0 \dot{x}_1(t) + 4800.0 \dot{x}_{\mathrm{b}}(t) \tag{q}$$

By defining the state vector

$$\{Z(t)\} = \left[x_1(t), x_{\mathrm{b}}(t); \dot{x}_1(t), \dot{x}_{\mathrm{b}}(t); f_{\mathrm{a}}(t), f_{\mathrm{p}}(t), c(t)\right]^{\mathrm{T}} \tag{r}$$

Equations j, l, and m can be condensed into matrix form as

$$\left\{\dot{Z}(t)\right\} = [A]\{Z(t)\} + \{B_{\mathrm{u}}\}u(t) + \{B_{\mathrm{r}}\}\ddot{x}_{\mathrm{g}} \tag{s}$$

which is the state-space representation of the single-story building with HDABC system. In Equation s, $[A]$ is the system plant matrix and $\{B_{\mathrm{u}}\}$

and $\{B_r\}$ are coefficient vectors for control command and earthquake input, respectively. Their element values are determined by Equations k, p, and q

$$[A] = \begin{bmatrix} 0 & 0 & 1 & 0 & 0 & 0 & 0 \\ 0 & 0 & 0 & 1 & 0 & 0 & 0 \\ -159.714 & 0 & -0.2513 & 0 & 0.001 & 0.001 & 0 \\ 0 & -1.230 \times 10^5 & 0 & -0.7013 & -0.036 & -0.036 & 0 \\ 0 & 0 & -733333.3 & 733333.3 & 0 & 0 & 1.572 \times 10^6 \\ 0 & 0 & -4800.0 & 4800.0 & 0 & -40.0 & 0 \\ 0 & 0 & 0 & 0 & 0 & 0 & -223.870 \end{bmatrix}$$

$$\{B_u\} = \begin{bmatrix} 0 & 0 & 0 & 0 & 0 & 0 & 223.870 \end{bmatrix}^T, \{B_r\} = \begin{bmatrix} 0 & 0 & -1 & -1 & 0 & 0 & 0 \end{bmatrix}^T \quad \text{(t)}$$

The system poles, as defined by Equation 4.22, are given by the eigenvalues of matrix $[A]$. Using MATLAB® eigensolution function *EIG* [21], the poles are solved as

$$\begin{cases} p_1 = 0 \\ p_2 = -39.844 \\ p_3 = -223.870 \\ p_{4,5} = -0.176 \pm 15.174j \\ p_{6,7} = -0.378 \pm 354.640j \end{cases} \quad \text{(u)}$$

The first pole at origin confirms that the actuator is marginally stable. The two conjugate complex pairs represent the mode of the structure and the K-brace, respectively. Note that they are altered owing to the dynamic interaction between the structure/brace and the control devices. From Equation 4.22 we have

$$\left.\begin{aligned} \zeta_1\omega_1 &= 0.176 \\ \sqrt{1-\zeta_1^2}\omega_1 &= 15.174 \end{aligned}\right\} \Rightarrow \begin{cases} \zeta_1 = 0.0116 \\ \omega_1 = 15.174\,\text{rad/s} \end{cases}$$
$$\left.\begin{aligned} \zeta_b\omega_b &= 0.378 \\ \sqrt{1-\zeta_b^2}\omega_b &= 354.640 \end{aligned}\right\} \Rightarrow \begin{cases} \zeta_b = 1.065 \times 10^{-3} \\ \omega_b = 354.640\,\text{rad/s} \end{cases} \quad \text{(v)}$$

Without the control devices, the system poles can be calculated by directly substituting the damping ratio and natural frequency of the structure and

TABLE 5.2
Comparison of Damping Ratios and Natural Frequencies

Control devices	Structure			K-brace		
Exist?	ζ_1	ω_1	$p_{4,5}$	ζ_b	ω_b	$p_{6,7}$
No	0.01	12.	$-0.126 \pm 12.566j$	0.001	350.657	$-0.351 \pm 350.657j$
Yes	0.0116	15.175	$-0.176 \pm 15.174j$	0.00165	354.640	$-0.378 \pm 354.640j$

K-brace into Equation 4.22

$$\begin{cases} p_{4,5} = -\zeta_1\omega_1 \pm \sqrt{1-\zeta_1^2}\omega_1 j \\ \quad\quad = -(0.01)(12.566) \pm \sqrt{1-(0.01)^2}(12.566)j \\ \quad\quad = -0.126 \pm 12.566j \\ p_{6,7} = -\zeta_b\omega_b \pm \sqrt{1-\zeta_b^2}\omega_b \\ \quad\quad = -(0.001)(350.657) \pm \sqrt{1-(0.001)^2}(350.657)j \\ \quad\quad = -0.351 \pm 350.657j \end{cases} \tag{w}$$

Table 5.2 is a comparison of the eigenvalues of the structure and K-brace with and without considering dynamics of control devices. It shows that their damping ratios and natural frequencies are increased owing to the viscous behavior of the passive damper and stiffness of the actuator and damper systems.

5.2.6 Summary

This section has presented analytical modeling of smart seismic structures using semiactive and hybrid control systems. The control devices are mounted on the K-bracing system of a structure. On the basis of the dynamic models of control devices formulated in Section 5.1, a general model of the smart structure system is formulated with consideration of dynamics and arbitrary number and location of control devices. State-variable representation of the system with analog and digital controllers is developed. A four-story building structure equipped with actuators and dampers on K-bracing serves as an example to verify the general modeling of the system. Although the general model seems tedious for hand formulation, it is convenient for computer programming; this convenience is the rationale for the general model.

5.3 Control Strategy and System Stability

This section addresses the control algorithms, intelligent scheme, and actuator stability issues for semiactive and hybrid systems, with HDABC systems serving as the example in some particular areas.

5.3.1 Control Algorithms

Note that the analytical model of smart seismic structures using semiactive and hybrid systems (Equation 5.109) is in exactly the same format as the one for smart structures with active control (Equation 4.19). Thus, the classical algorithms (such as Riccati and pole placement) and generalized algorithms discussed in Chapter 4 should also be applicable to semiactive and hybrid control systems [2,3]. Note that they are full-state feedback algorithms and have the following feedback law

$$\{u(t)\} = -[G]\{Z(t)\} \tag{5.118}$$

The feedback gain matrix $[G]$, determined by control algorithms, is constant here. Take the Riccati algorithm as an example. On the basis of the Riccati performance index

$$J = \frac{1}{2}\int_{t_0}^{t_f} (\{z(t)\}^T[Q]\{z(t)\} + \{u(t)\}^T[R]\{u(t)\})\, dt \tag{5.119}$$

The feedback gain is given by

$$[G] = [R]^{-1}[B_u]^T[P] \tag{5.120}$$

Equation 5.118 shows that the control force is proportional to the state variables, such as velocities and displacements of the structures. Thus, a system with such control algorithms is usually referred as *state control*. As noted in Section 4.2, state feedback—feedback of structural velocities and displacements—changes the damping and stiffness coefficients of the structure. Thus, an active system with state control behaves in the same way as a spring damper. A hybrid system using spring damper usually employs state control algorithms to synchronize actuator and damper behavior, as its actuator provides active damping and spring forces to withstand earthquake loads.

For a hybrid system using liquid mass dampers, the damper changes the mass and damping coefficients of the structure. An active system behaves in the same way if the active control force changes the inertia and damping forces of the system, which corresponds to the feedback of structural accelerations and velocities, that is, the derivative of the state vector $\{Z(t)\}$. This led to the concept of *state-slope control*, whose performance index is defined in terms of the derivative of the state

vector $\{Z(t)\}$

$$J = \frac{1}{2}\int_{t_0}^{t_f} (\{\dot{Z}(t)\}^{\mathrm{T}}[Q]\{\dot{Z}(t)\} + \{u(t)\}^{\mathrm{T}}[R]\{u(t)\})\,\mathrm{d}t \tag{5.121}$$

And the feedback law as

$$\{u(t)\} = -[G]\left\{\dot{Z}(t)\right\} = -[R]^{-1}[B_{\mathrm{u}}]^{\mathrm{T}}[Q]\left\{\dot{Z}(t)\right\} \tag{5.122}$$

A hybrid system using liquid mass dampers usually employs state-slope control algorithms to synchronize actuator and damper behavior, as its active part provides active inertia and damping forces to withstand earthquake loads.

Both state control and state-slope control feed back structural velocities and thus improve the system damping and seismic resistance. The difference is that state control feeds back displacements while state-slope control feeds back accelerations. Thus, state control is more effective in reducing structure displacements, while state-slope control is more effective in controlling structural acceleration. Because classical control algorithms can be used for semiactive and hybrid control systems, the controlled structural behavior can also be simulated in MATLAB® control toolbox functions [21] such as LQR in the same way to adjust the weighting matrices $[Q]$ and $[R]$. Take an Nth order hybrid system with one hydraulic actuator as an example. The weighting matrix $[Q]$ is in order of N, and R becomes a scalar value. By setting $[Q]$ as unit matrix and adjusting the value of R, an increasing and decreasing magnitude for the active control force can be obtained. As noted in Chapter 4, when the $Q(i,i)/R$ value decreases, the active control force increases (and so does the total hybrid control force), and then the structural response is further reduced.

5.3.2 Intelligent Hybrid Control Systems

As noted, passive systems are effective for seismic response control of structures under small earthquakes. Active control systems have powerful capacity for strong earthquakes but are quite expensive. Hybrid systems combine passive and active systems; however, its expensive active part is not necessary for small earthquakes. This led to the concept of *intelligent hybrid control systems* [8–10] whose active part is not in operation unless it is required. The intelligent system can activate its active part at any time during the dynamic history of the earthquake-excited structure. A threshold response, TR, is defined so that the active part begins to operate once maximum structural response exceeds this threshold value. The working principle is described by the flowchart in Figure 5.14. Note that when $TR = 0$, the intelligent system becomes a full hybrid control system as both passive and active part are in operation at any time. When a large TR is selected, the system degenerates into a passive control system whenever the system response is less than TR. With this control strategy, small earthquakes are handled by the passive

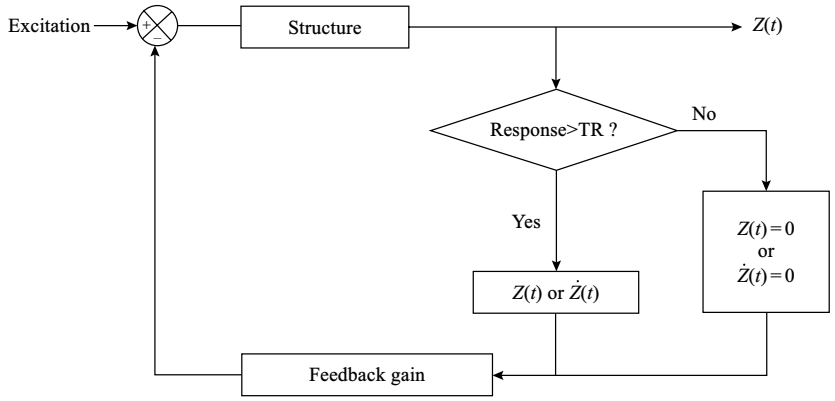

FIGURE 5.14 Working mechanism of the intelligent hybrid system.

control system, and the expensive active control part operates only when strong earthquakes occur.

Though the intelligent control strategy is developed for the HDABC system, it can be applied to any hybrid systems. Its goal is to maximize the passive damping power and to minimize the use of control energy. The two-stage intelligent system shown by Figure 5.14 can be further extended to a three-stage system [9,31,32], on the basis of the uncontrolled structural response and capacity of passive dampers. These stages are based on two threshold values selected to utilize optimally the hydraulic actuator's capacity. The threshold values can be set for the most important response, such as floor acceleration or story drift, which is monitored in real-time. At stage 1, the passive damper operates alone during small earthquake excitations, as long as it can restrain structural seismic response within the first threshold value with its designed capacity. For stronger earthquakes where the passive damper cannot adequately control the structural response (i.e., response is higher than the first threshold value), the hydraulic actuator will be activated and the system then functions in stage 2 or 3. The system becomes hybrid and combines the passive force with the active force generated by the actuator to keep the response within the second threshold value. If the response exceeds the second threshold limit, the HDABC system automatically adjusts the feedback gain for the actuator to generate larger control force so that the system response meets the safety and serviceability requirements. In detail, when the observed response is larger than the first threshold value, the control system moves from stage 1 into stage 2, and the active actuator(s) starts with small feedback gain so that the passive damper continues operating with its maximum capacity. If the structural response is restrained below the second threshold value, the system keeps working in stage 2. Otherwise, the hybrid system moves into stage 3; its active part plays the dominant role as the weighting matrix and the feedback gain are adjusted to yield higher active control force. This three-stage intelligent control strategy is illustrated by the flowchart in Figure 5.15, and its working mechanism

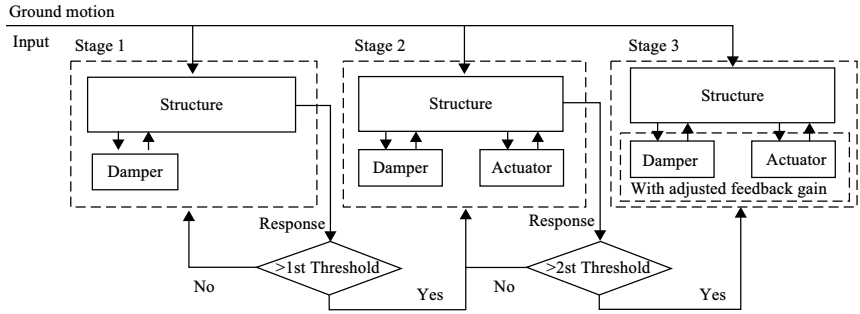

FIGURE 5.15 Flowchart of the three-stage intelligent hybrid system.

is summarized as follows:

1. The most critical structural response is determined and two threshold values are set for it.
2. The system works within stage 1 for small earthquake excitations that yield structural response lower than the first threshold.
3. The actuator starts working and the system moves into stage 2 whenever the response exceeds the first threshold value.
4. When the response exceeds the second threshold value, the feedback gain is adjusted to generate larger control force. The system functions in stage 3.

5.3.3 Stabilization of Servovalve-Controlled Hydraulic Actuators

As noted in Section 5.1.1, the servovalve-controlled hydraulic actuator is a marginally stable system. Small derivations such as initial imperfections may cause the actuator system to be unstable. When the actuator is applied to a structural control system, the actuator must be stabilized such that the control system can be identified and control algorithm implemented. Thus, it is important to develop a technique for actuator stabilization and to study the stability behavior of structural control systems using servovalve-controlled hydraulic actuator(s) [3,4].

5.3.3.1 One-story building with active bracing control

To simplify the problem without loss of generality, a one-story building with the hydraulic actuator mounted on a rigid K-brace system (see Figure 5.16) is employed to demonstrate the actuator's application to a structural control system, to study the actuator's stability behavior, and to develop a stabilization method for the system.

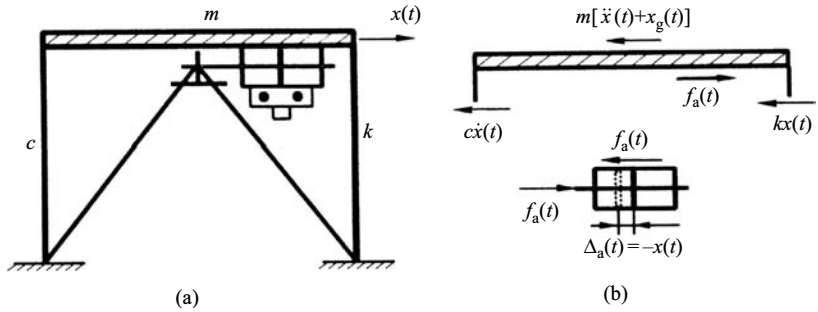

FIGURE 5.16 One-story building with hydraulic actuator mounted on K-brace: (a) schematic and (b) free-body diagram.

The free-body diagram of the structure yields

$$m\ddot{x}(t) + c\dot{x}(t) + kx(t) - f_{\mathrm{a}}(t) = 0 \tag{5.123}$$

Applying *Laplace transform* to Equation 5.123 gives

$$ms^2X(s) + csX(s) + kX(s) - F_{\mathrm{a}}(s) = 0 \tag{5.124}$$

Thus, the transfer function from structural displacement $x(t)$ to control force $f_{\mathrm{a}}(t)$ is

$$T_{\mathrm{fx}}(s) = \frac{F_{\mathrm{a}}(s)}{X(s)} = ms^2 + cs + k \tag{5.125}$$

Substituting Equation 5.35 into Equation 5.123 yields

$$m\ddot{x}(t) + c\dot{x}(t) + kx(t) - \frac{2\beta A^2}{V}\Delta_{\mathrm{a}}(t) - \frac{\beta AK_{\mathrm{v}}}{V}\sqrt{2P_{\mathrm{s}}}\int_0^t c(t)\,\mathrm{d}t = 0 \tag{5.126}$$

Assume that the bracing is rigid without elastic deformation; then, actuator-piston displacement $\Delta_a(t) = -x(t)$, and Equation 5.126 becomes

$$m\ddot{x}(t) + c\dot{x}(t) + kx(t) + \frac{2\beta A^2}{V}x(t) - \frac{\beta AK_{\mathrm{v}}}{V}\sqrt{2P_{\mathrm{s}}}\int_0^t c(t)\,\mathrm{d}t = 0 \tag{5.127}$$

Applying Laplace transform to Equation 5.127 gives the *transfer function* from valve-piston displacement $c(t)$ to structural displacement $x(t)$ as

$$T_{\mathrm{xc}}(s) = \frac{X(s)}{C(s)} = \frac{\beta AK_{\mathrm{v}}\sqrt{2P_{\mathrm{s}}}/V}{s(ms^2 + cs + k + 2\beta A^2/V)} = \frac{\beta AK_{\mathrm{v}}\sqrt{2P_{\mathrm{s}}}/(Vm)}{s(s^2 + 2\,\zeta_n\,\omega_n s + \omega_n^2)} \tag{5.128}$$

where natural frequency ω_n and damping ratio ζ_n are

$$\omega_n = \sqrt{\frac{2\beta A^2 + kV}{Vm}} = \sqrt{\frac{k + 2\beta A^2/V}{m}}, \zeta_n = \frac{c}{2m\omega_n} \tag{5.129}$$

The relationship between control command $u(t)$ and valve-piston displacement $c(t)$ is expressed by Equation 5.12a. Applying *Laplace transform* to that equation yields the corresponding transfer function of the servovalve as

$$T_{\mathrm{cu}}(s) = \frac{C(s)}{U(s)} = \frac{1}{\tau s + 1} = \frac{1/\tau}{s + 1/\tau} \tag{5.130}$$

Combining Equations 5.128 and 5.130 gives the transfer function from $u(t)$ to $x(t)$

$$\begin{aligned} T_{\mathrm{xu}}(s) &= \frac{X(s)}{U(s)} = \frac{X(s)}{C(s)}\frac{C(s)}{U(s)} = T_{\mathrm{xc}}(s) \cdot T_{\mathrm{cu}}(s) \\ &= \frac{\beta A K_{\mathrm{v}} \sqrt{2P_{\mathrm{s}}}/(Vm\tau)}{s(s + 1/\tau)(s^2 + 2\,\zeta_n\,\omega_n s + \omega_n^2)} = \frac{\gamma}{s(s + 1/\tau)(s^2 + 2\,\zeta_n\,\omega_n s + \omega_n^2)} \end{aligned} \tag{5.131}$$

where $\gamma = \frac{\beta A K_{\mathrm{v}} \sqrt{2P_{\mathrm{s}}}}{Vm\tau}$. Equation 5.131 shows that this control system is of the fourth order with a pole at the origin, a pole far from the imaginary axis, and a pair of conjugate complex poles with natural frequency ω_{n} and damping ratio ζ_{n}. The two conjugate complex poles come from the structure, and actuator dynamics is the source of the two additional real poles.

Having a first-order pole at the origin makes this control system marginally stable in open loop. Although the structure is stable, the actuator-structure system becomes marginally stable owing to actuator dynamics. In theory, a marginally stable system has bounded nonzero steady-state response. In practice, such a system tends to be unstable. This is because the pole at the origin easily becomes positive owing to initial imperfections. An actuator-structure system must therefore be stabilized before it can be identified and the control algorithm implemented.

Setting up a closed loop with feedback mechanism is a common way to stabilize a system. A sensing system and a controller are required for the closed loop. From the standpoint of hardware realization, the most reliable sensing method is to install a load cell to measure active control force $f_{\mathrm{a}}(t)$. In addition, the actuator has a built-in *linear variable displacement transducer* (LVDT) to measure actuator-piston displacement $\Delta_{\mathrm{a}}(t)$. Three choices are thus available to set up a closed loop: displacement feedback only, force feedback only, and a combination of displacement and force feedback. Figure 5.17 is a schematic of the open-loop and three closed-loop systems.

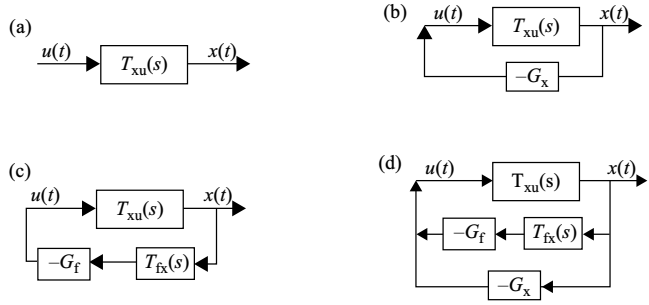

FIGURE 5.17 Schematic of open- and closed-loop systems for actuator stabilization: (a) open-loop system, (b) displacement feedback, (c) force feedback, and (d) displacement and force feedback.

The closed-loop transfer function of a displacement feedback system shown in Figure 5.17b is given by linear control theory as

$$T_{c1}(s) = \frac{T_{xu}(s)}{1 + G_x T_{xu}(s)} = \frac{\gamma}{s(s + 1/\tau)(s^2 + 2\,\zeta_n\,\omega_n s + \omega_n^2) + G_x\,\gamma} \tag{5.132}$$

where G_x is displacement feedback gain. Similarly, for a force feedback system (see Figure 5.17c)

$$\begin{aligned} T_{c2}(s) &= \frac{T_{xu}(s)}{1 + G_f T_{fu}(s)} \\ &= \frac{T_{xu}(s)}{1 + G_f[-(ms^2 + cs + k)T_{xu}(s)]} \\ &= \frac{\gamma}{s(s + 1/\tau)(s^2 + 2\,\zeta_n\,\omega_n s + \omega_n^2) + G_f\,\gamma\,(ms^2 + cs + k)} \end{aligned} \tag{5.133}$$

and for the system with combination of force and displacement feedback (see Figure 5.17d)

$$\begin{aligned} T_{c3}(s) &= \frac{T_{xu}(s)}{1 + G_f T_{fu}(s) + G_x T_{xu}(s)} \\ &= \frac{\gamma}{s(s + 1/\tau)(s^2 + 2\,\zeta_n\,\omega_n s + \omega_n^2) + G_f\,\gamma\,(ms^2 + cs + k) + G_x\gamma} \end{aligned} \tag{5.134}$$

where G_f is the gain for force feedback. $T_{fu}(s)$ in the above equations is obtained by

$$\begin{aligned} T_{fu}(s) &= \frac{F_a(s)}{U(s)} = \frac{F_a(s)}{X(s)}\frac{X(s)}{U(s)} = T_{fx}(s)T_{xu}(s) \\ &= (ms^2 + cs + k)T_{xu}(s) \end{aligned} \tag{5.135}$$

and $T_{fx}(s)$ is given by Equation 5.125.

Effectiveness of the three closed-loop systems for actuator stabilization can be investigated by *root-locus plot*s based on closed-loop transfer functions from $u(t)$ to $x(t)$. These plots demonstrate the locus of closed-loop system poles (eigenvalues of the transfer function) in a complex plane as the feedback gain (G_f and/or G_x) varies from 0 to $+\infty$. The abscissa and ordinate of a root-locus plot are real and imaginary parts of these poles, respectively. As noted in Section 4.1.3, a system is stable if all its poles stay in the left half-plane. Thus, root-locus plots are useful tools for analyzing the closed-loop system stability. The root-locus method has been implemented in commercial software packages such as MATLAB® control toolbox function *rlocus* [21].

The system shown in Figure 5.16 is used as an example to study actuator stabilization. Structural properties are mass $M = 454$ kg, damping ratio $\zeta_N = 2\%$, and natural frequency $f = 2.0$ Hz. The active system uses a Moog 760-102A servovalve-controlled hydraulic actuator. Figures 5.18 through 5.20 are root-locus plots of the three closed-loop feedback systems expressed by Equations 5.132 through 5.134, respectively. With these plots we can conclude

- A closed loop by displacement feedback cannot stabilize the actuator. This is because, as Figure 5.18 shows, while the pole at the origin moves to the left half-plane, two conjugate complex poles move to the right half-plane and destabilize the system at the same time.
- A closed loop with force feedback stabilizes the actuator by any feedback gain. This is because all poles are always in the left half-plane as shown by Figure 5.19.

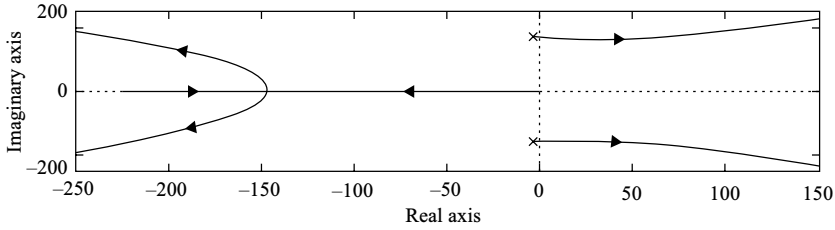

FIGURE 5.18 Root-locus plot of one-story building with displacement feedback.

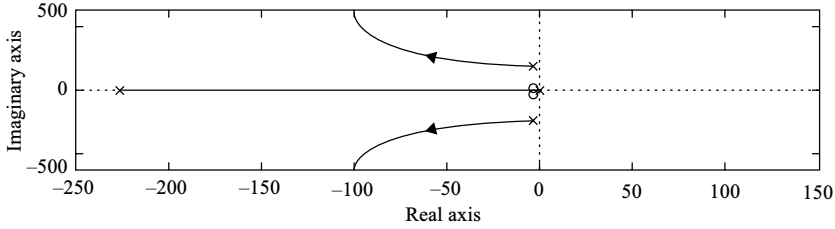

FIGURE 5.19 Root-locus plot of one-story building with force feedback.

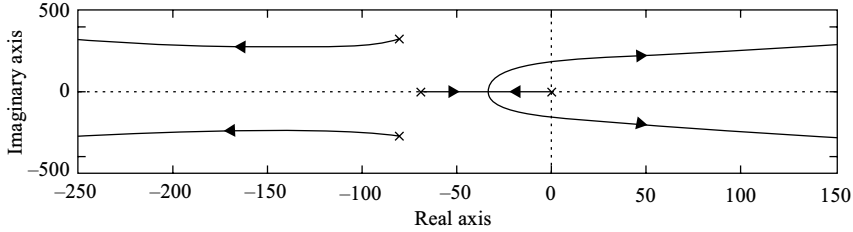

FIGURE 5.20 Root-locus plot of one-story building with displacement and force feedback.

- A closed loop with both displacement and force feedback stabilizes the actuator sometimes. As Figure 5.20 shows, the system poles are all in left side if feedback gains are properly selected. If the gains are too large, the actuator becomes unstable again because the two real poles move to the right half-plane. Furthermore, two sensors and two-channel hardware are required to implement this feedback system.

With above comparison, a closed loop with force feedback is the best way for the actuator stabilization in that it only requires one sensor and works with any feedback gain.

5.3.3.2 Three-story building with HDABC system

Actuator stability is evaluated through numerical study of a one-fourth scale model of a three-story building with HDABC at the first floor (see Figure 5.21) tested on a shaking table. The hybrid control device consists of a Moog 760-102A servovalve-controlled hydraulic actuator and a viscous fluid damper. The actuator has a built-in LVDT to measure its piston displacement. A load cell is installed between actuator piston and K-brace to measure the active control force. The damper is analyzed by a Maxwell model with damping coefficient $C_0 = 21.04$ kN-s/m and relaxation time $\lambda_0 = 0.05$ s. Structural properties are (1) mass coefficients $m_1 = 593.8$, $m_2 = 590.2$, $m_3 = 576.6$ (kg); (2) natural frequencies $f_1 = 2.622$, $f_2 = 9.008$, $f_3 = 17.457$ (Hz); and (3) damping ratios $\zeta_1 = 0.364\%$, $\zeta_2 = 0.354\%$, $\zeta_3 = 0.267\%$. K-brace properties are $m_b = 12.6$ kg, $\zeta_b = 0.1\%$, and $k_b = 1549.3$ kN/m.

According to the formulation in Section 5.2, the mathematical model of the structure and the K-brace is

$$[M]\{\ddot{x}(t)\} + [C]\{\dot{x}(t)\} + [K]\{x(t)\} = [\gamma_a]\{f_a(t)\} + [\gamma_p]\{f_p(t)\} + \{\delta\}\ddot{x}_g(t) \tag{5.136}$$

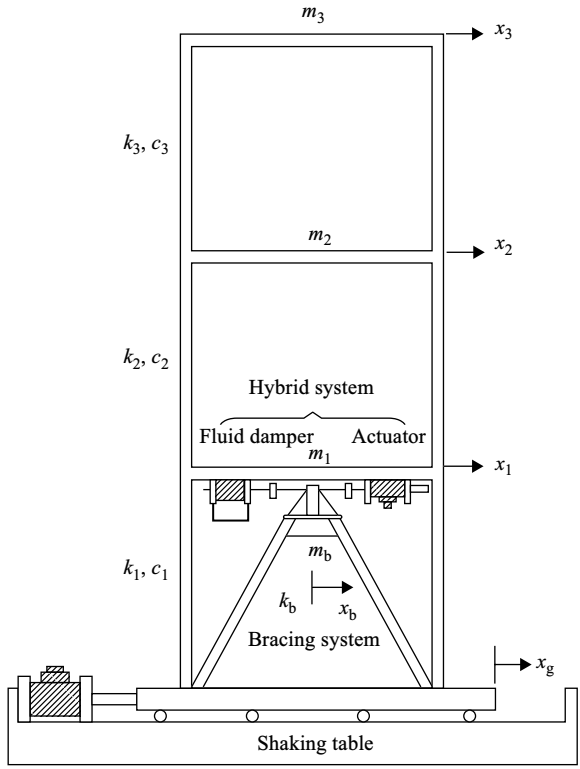

FIGURE 5.21 Three-story building model with HDABC.

where

$$\{x(t)\} = [x_1(t), x_2(t), x_3(t), x_b(t)]^T \tag{5.137}$$

$$[M] = \begin{bmatrix} [M_s]_{3\times3} & \{0\}_{3\times1} \\ [0]_{1\times3} & M_b \end{bmatrix}, [C] = \begin{bmatrix} [C_s]_{3\times3} & \{0\}_{3\times1} \\ [0]_{1\times3} & C_b \end{bmatrix}, [K] = \begin{bmatrix} [K_s]_{3\times3} & \{0\}_{3\times1} \\ [0]_{1\times3} & K_b \end{bmatrix} \tag{5.138}$$

$$\{\delta\} = -[m_1, m_2, m_3; m_b]^T \tag{5.139}$$

and $[M_s]$, $[C_s]$, and $[K_s]$ are matrices of mass, damping, and stiffness, respectively, of the three-story structure.

Damper-piston displacement $\Delta_p(t) = x_b(t) - x_1(t)$. Substituting it into Equation 5.39a yields the mathematical model of the viscous fluid damper

$$\lambda_0 \dot{f}_p(t) + f_p(t) = C_0 [\dot{x}_b(t) - \dot{x}_1(t)] \tag{5.140}$$

Equations 5.12 and 5.35 are the dynamic models of the actuator. Note that actuator-piston displacement $\Delta_a(t) = \Delta_p(t) = x_b(t) - x_1(t)$, with the piston

deformation neglected. Thus, the mathematical model of the hydraulic actuator is

$$\begin{aligned} &\tau\dot{c}(t) + c(t) = u(t) \\ &\dot{f}_{\mathrm{a}}(t) = \frac{2\beta A^2}{V}\left[\dot{x}_{\mathrm{b}}(t) - \dot{x}_1(t)\right] + \frac{\beta A K_{\mathrm{v}}}{V}\sqrt{2P_{\mathrm{s}}}c(t) \end{aligned} \tag{5.141}$$

Equations 5.136, 5.140, and 5.141 form the mathematical model of the hybrid structural control system and can be condensed into matrix form using state-variable representation. State variables of the system comprise three displacements and three velocities of the structure, displacement and velocity of the brace, active control force, servovalve displacement, and passive control force. Thus, the hybrid structural control system is of the 11th order. This system's state-variable representation is expressed by Equation 5.109 while the state vector and plant matrix are

$$\{Z(t)\} = \left[x_1(t), x_2(t), x_3(t), x_{\mathrm{b}}(t); \dot{x}_1(t), \dot{x}_2(t), \dot{x}_3(t), \dot{x}_{\mathrm{b}}(t); f_{\mathrm{a}}(t), f_{\mathrm{p}}(t), c(t)\right]^{\mathrm{T}} \tag{5.142}$$

$$[A] = \begin{bmatrix} [0]_{4\times4} & & & & [I]_{4\times4} & & & & [0]_{4\times3} & & \\ mk_{11} & mk_{12} & mk_{13} & 0 & mc_{11} & mc_{11} & mc_{11} & 0 & \frac{1}{m_1} & \frac{1}{m_1} & 0 \\ mk_{21} & mk_{22} & mk_{23} & 0 & mc_{11} & mc_{11} & mc_{11} & 0 & 0 & 0 & 0 \\ mk_{31} & mk_{23} & mk_{33} & 0 & mc_{11} & mc_{11} & mc_{11} & 0 & 0 & 0 & 0 \\ 0 & 0 & 0 & -\frac{k_{\mathrm{b}}}{m_{\mathrm{b}}} & 0 & 0 & 0 & -\frac{c_{\mathrm{b}}}{m_{\mathrm{b}}} & -\frac{1}{m_{\mathrm{b}}} & -\frac{1}{m_{\mathrm{b}}} & 0 \\ 0 & 0 & 0 & 0 & -\alpha_1 & 0 & 0 & \alpha_1 & 0 & 0 & \alpha_2 \\ 0 & 0 & 0 & 0 & -\frac{C_0}{\lambda_0} & 0 & 0 & \frac{C_0}{\lambda_0} & 0 & -\frac{1}{\lambda_0} & 0 \\ 0 & 0 & 0 & 0 & 0 & 0 & 0 & 0 & 0 & 0 & 1/\tau \end{bmatrix} \tag{5.143}$$

where mk_{ij} and mc_{ij} are elements at jth column and ith row of $-[M_{\mathrm{s}}]^{-1}[K_{\mathrm{s}}]$ and $-[M_{\mathrm{s}}]^{-1}[C_{\mathrm{s}}]$, respectively; matrices $[M_{\mathrm{s}}]$, $[C_{\mathrm{s}}]$, and $[K_{\mathrm{s}}]$ are defined in Equations 5.66, 5.68, and 5.73, respectively; $\alpha_1 = 2\beta A^2/V, \alpha_2 = \left(\beta A K_{\mathrm{v}}/V\right)\sqrt{2P_{\mathrm{s}}}$; and

$$\begin{cases} \{B_{\mathrm{u}}\} = \left[\begin{array}{cccccccccccc} 0 & 0 & 0 & 0 & 0 & 0 & 0 & 0 & 0 & 0 & -1/\tau \end{array}\right]^{\mathrm{T}} \\ \{B_{\mathrm{r}}\} = \left[\begin{array}{cccccccccccc} 0 & 0 & 0 & 0 & -1 & -1 & -1 & -1 & 0 & 0 & 0 \end{array}\right]^{\mathrm{T}} \end{cases} \tag{5.144}$$

Many commercial software packages have eigensolution functions that can easily solve eigenvalues of plant matrix $[A]$ (poles of the system), such as MATLAB® function *EIG*. Table 5.3 lists these open-loop poles of the structure with hybrid control. The first three modes come from the structure and the fourth mode comes from the K-brace. Real poles 1 and 3 are induced by actuator dynamics, while real pole 2 is induced by damper dynamics. The same as that of the one-story building with active bracing control (see Figure 5.16), this hybrid system with hydraulic

TABLE 5.3
Open-Loop Poles of Structure with HDABC System

Conjugate complex poles				Real poles		
First mode	**Second mode**	**Third mode**	**Fourth mode**	**1**	**2**	**3**
−0.070± 23.29*j*	−0.207± 66.61*j*	−0.295± 112.85*j*	−0.633± 1,094.40*j*	0	−19.40	−223.87

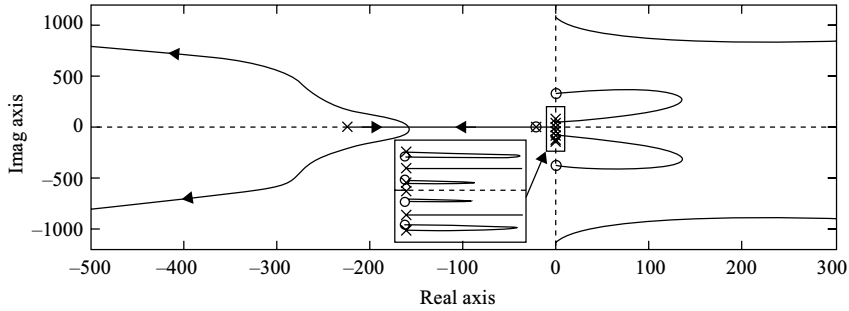

FIGURE 5.22 Root-locus plot of hybrid system with displacement feedback.

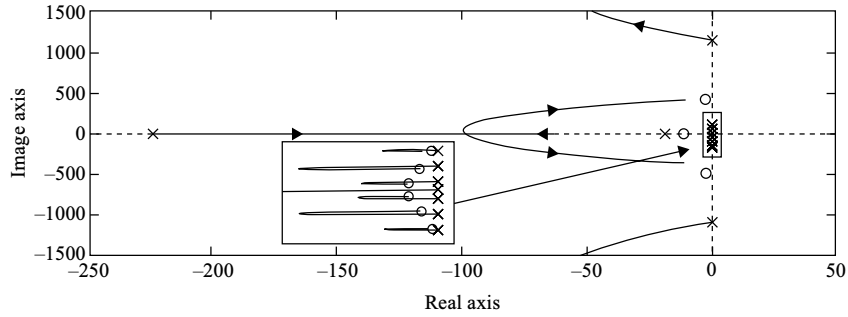

FIGURE 5.23 Root-locus plot of hybrid system with force feedback.

actuator is a marginally stable system owing to the existence of a pole at the origin (real pole 1). A closed loop must be formed to stabilize this system. Note that $j = \sqrt{-1}$ in Table 5.3.

Figures 5.22 and 5.23 show root-locus plots for the hybrid system with displacement feedback and force feedback, respectively. They match well with results for the system shown in Figure 5.16. While displacement feedback stabilizes the pole at the origin, two other poles become unstable; the system is not stabilized. With force feedback, all poles of the system stay in the left half-plane, so the system is stabilized.

5.3.4 Effect of Actuator Dynamics on System Response

Equation 5.35 shows that a structural control system with hydraulic actuators is *marginally stable* in open loop due to *actuator dynamics*. It also shows an interaction effect between structural displacement and active control force. To study the effect of actuator dynamics on system response, the seismic response in time history is simulated numerically for the hybrid-controlled structure (see Figure 5.21). Scaled E-W component of the New Mexico earthquake (time increment $\Delta t = 0.02$ s) and scaled N-S component of the El-Centro earthquake ($\Delta t = 0.01$ s) are adopted as excitations; amplitude and frequency scale factors are 0.3 and 2, respectively. This system is modeled by Equations 5.109 and 5.142 through 5.144. Rectangular rule is used to calculate the time history of structural response.

Figure 5.24 shows that, since the hybrid structural control system in open loop is marginally stable; its maximum displacement response at the third floor is 1.013 cm, 30% larger than that of the structure without control, despite the presence of a damper. Note that the response cannot dampen out and will eventually damage the system. If the actuator is stabilized by force feedback with gain $G_f = 1$ (see Equation 5.133) but generates little control force, the stable system has a smaller response than that of a structure without control; structural vibration is quickly dissipated because of the passive control by the viscous fluid damper.

As noted, the hydraulic actuator adds two real poles to the system: one at origin and the other far from the imaginary axis (see real poles 1 and 3 in the Table 5.3). Since this structural control system possesses more dynamics than systems with a linear proportional actuator, its closed-loop response may be affected by the actuator dynamics. As shown in Figures 5.19 and 5.23, the stabilized closed-loop system places the poles as two negative poles or a pair of conjugate complex poles with a negative real part. If the two poles are not far from the imaginary axis, they have a significant effect on system response. The effect of actuator dynamics on closed-loop response is demonstrated by comparing system response with and without considering actuator dynamics. The hybrid structural control system shown in Figure 5.21 is employed here for such purposes. When actuator dynamics is not considered, the actuator is modeled as a linear device with proportional relation from input $u(t)$ to output $f_a(t)$. Pole assignment algorithm, as described

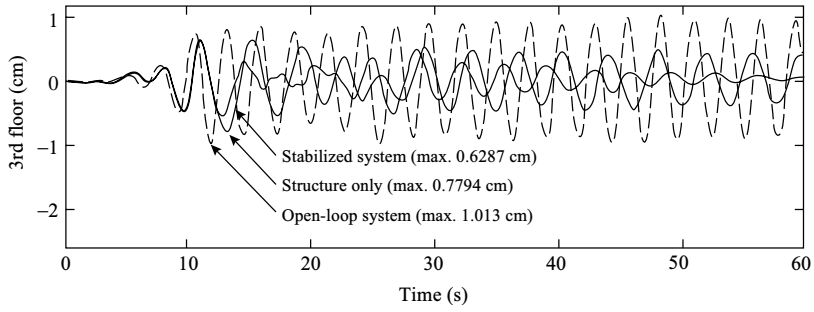

FIGURE 5.24 Structural response to scaled El-Centro earthquake.

TABLE 5.4
Closed-Loop Poles of Structure with HDABC

Conjugate complex poles					
First mode	**Second mode**	**Third mode**	**Fourth mode**	**Fifth mode**	**Real pole**
$-2.019\pm$ $18.59j$	$-2.071\pm$ $59.48j$	$-0.682\pm$ $110.51j$	$-42.41\pm$ $397.67j$	$-27{,}983\pm$ $28{,}001j$	-10.64

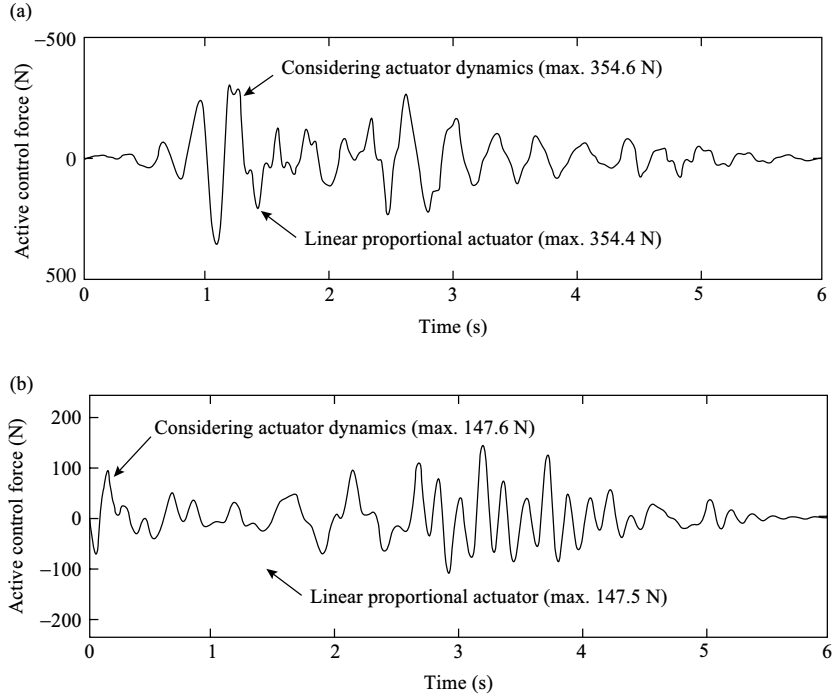

FIGURE 5.25 Effect of actuator dynamics on closed-loop response: (a) required active control force for N-S El-Centro earthquake and (b) required active control force for E-W New Mexico earthquake.

in Section 4.2.2, is used to design the feedback controller. For the hybrid system with actuator dynamics, desired closed-loop poles are listed in Table 5.4; for the hybrid system with linear proportional actuator, closed-loop poles are also given in Table 5.4 but excluding the two poles of the fifth mode.

Since the two poles for actuator dynamics is placed far from the imaginary axis in closed loop, that is, $-27{,}983 \pm 28{,}001j$ ($j = \sqrt{-1}$) in Table 5.4, actuator dynamics is expected to have little effect on closed-loop response. This expectation is verified by numerical results shown in Figure 5.25 that compares

required active control forces of the hybrid system with and without considering actuator dynamics. Figure 5.25a illustrates time-history response of the hybrid-controlled structure to scaled N-S component of the El-Centro earthquake. By setting maximum top-floor displacements the same at 0.5805 cm, the system considering actuator dynamics demands 354.6 N active control force while the system using linear proportional actuator demands 354.4 N. Very little difference ($<0.1\%$) is found for the required active control force. A similar result can be found for system responses to scaled E-W component of the New Mexico earthquake, as shown in Figure 5.25b. By setting maximum displacement at 0.2785 cm, the system considering actuator dynamics demands 147.6 N active control force while the system using linear proportional actuator demands 147.5 N. Again, less than 0.1% difference is found in the required active control force.

If the two poles for actuator dynamics are not placed far from the imaginary axis, a sizeable difference is expected in system response with or without considering actuator dynamics. This expectation is verified by numerical results for the closed-loop hybrid control system that places the two poles at –10.0 and –192.19 (see Table 5.5). Pole assignment control algorithm is also used here. The closed-loop poles for the hybrid system with actuator dynamics are listed in Table 5.5. For the hybrid system with linear proportional actuator, the closed-loop poles are also given in Table 5.5 but excluding real poles 1 and 3. Numerical results are shown in Figure 5.26 that compares required active control forces in time history for closed-loop hybrid systems with and without considering actuator dynamics. Figure 5.26a illustrates this comparison for the excitation of scaled N-S component of the El-Centro earthquake. By setting maximum top-floor displacement the same at 0.45 cm, 2,076 Newtons active control force is demanded if the actuator is modeled as a linear proportional device, while 1,822 Newtons active control force is demanded if actuator dynamics is considered. Here the error is 13.94%. For the excitation of scaled E-W component of the New Mexico earthquake, maximum top-floor displacement is set the same at 0.21 cm. As shown in Figure 5.26b, the system without considering actuator dynamics demands 490.8 Newtons active control force while 469.5 Newtons active control force is demanded for the system considering actuator dynamics. Here the error is 4.54%.

A suggestion emerges from these findings. Actuator dynamics should be considered in the analysis and design of a control system with a hydraulic actuator,

TABLE 5.5
Closed-Loop Poles of Hybrid-Controlled Structure

Conjugate complex poles				Real poles		
First mode	**Second mode**	**Third mode**	**Fourth mode**	**1**	**2**	**3**
$-3.880\pm 22.54j$	$-2.395\pm 66.73j$	$-0.769\pm 113.00j$	$-3.655\pm 1{,}109.20j$	−10.0	−24.45	−192.19

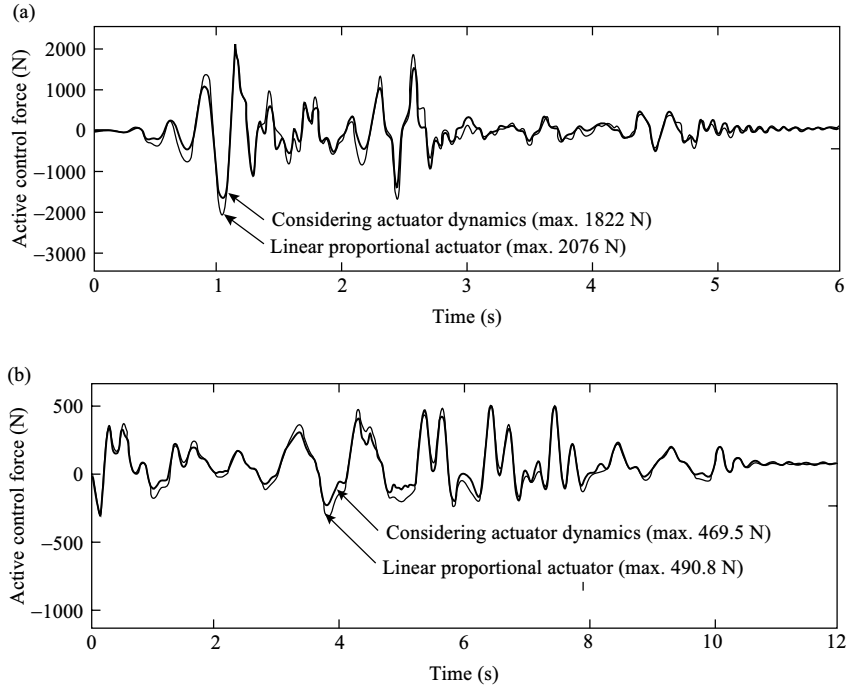

FIGURE 5.26 Effect of actuator dynamics on system response: (a) required active control force under El-Centro earthquake and (b) required active control force under New Mexico earthquake.

and the two poles by actuator dynamics be placed far from the imaginary axis to minimize their effect on closed-loop response. If so, the actuator dynamics can be ignored for further study of a smart seismic structure system.

5.3.5 Summary

This section has studied control strategy and stability of the HDABC system using servovalve-controlled hydraulic actuators mounted on a K-brace system. State and state-slope control techniques are proposed for hybrid systems using spring dampers and liquid mass dampers, respectively. The effect of actuator dynamics on open-loop system stability is investigated and a method to stabilize the actuator is developed. A one-story building structure with active control and a three-story structure with hybrid control serve as numerical examples to reveal the stability behavior and demonstrate the effectiveness of the proposed method for actuator stabilization. Then effects of actuator dynamics on closed-loop response are discussed for structural control systems using hydraulic actuators. Results show that a structure with a hydraulic actuator is marginally stable in open-loop owing to

actuator dynamics. Force feedback is the best method for actuator stabilization. Actuator dynamics must be considered to analyze and design a control system, and the two poles induced by actuator dynamics must be placed far from the imaginary axis such that they have little effect on closed-loop response.

5.4 Effectiveness of HDABC System for Seismic Response Control

In this section, numerical simulations of smart seismic structures using HDABC system are conducted to demonstrate the system effectiveness. Seismic responses of a controlled structure in time history is simulated numerically to demonstrate the capacity and effectiveness of the active and hybrid bracing systems using hydraulic actuators [4–7,19]. The effectiveness of the HDABC system is also compared with an MR damper system installed on a K-brace [30].

5.4.1 One-Story Smart Seismic Structure with HDABC System

A single-story model structure is used first to demonstrate the effectiveness of HDABC system for seismic response control. The structure properties are $m_1 = 1.48$ lb-s^2/in., $c_1 = 0.74$ lb-s/in., $k_1 = 233.09$ lb/in. The K-brace properties are $m_b = 0.01$, $m_1 = 0.0148$ lb-s^2/in., $c_b = 0.0$, $k_b = 100$, $k_1 = 23{,}309.0$ lb/in. The actuator is stabilized and the closed-loop poles are designed far away from imaginary axis. Thus, the actuator is assumed to be linear proportional. The hybrid control system employs either active state-slope control with a liquid mass damper whose $m_e = 0.2\,m_1 = 0.296$ lb-s^2/in., or active state control with spring damper whose $k_p = 0.2\,k_1 = 46.62$ lb/in. Both dampers have damping coefficient $c_p = 5\,c_1 = 3.70$ lb-s/in. The N-S component of El-Centro (1940) earthquake data with scale factor 0.2 is employed.

5.4.1.1 Analytical model

Assume $x_1(t)$ and $x_b(t)$ denote the displacements of the structure floor and K-brace, respectively. Then the motion equations of the structure and K-brace are

$$\begin{cases} m_1\left(\ddot{x}_1(t)+\ddot{x}_g(t)\right)+c_1\dot{x}_1(t)+k_1x_1(t)=f_a(t)+f_p(t) \\ m_b\left(\ddot{x}_b(t)+\ddot{x}_g(t)\right)+c_b\dot{x}_b(t)+k_bx_b(t)=-f_a(t)-f_p(t) \end{cases} \tag{5.145}$$

With the liquid mass damper whose model is expressed as

$$f_p(t)=m_e\left(\ddot{x}_1(t)-\ddot{x}_b(t)\right)+c_p\left(\dot{x}_1(t)-\dot{x}_b(t)\right) \tag{5.146}$$

Substituting Equation 5.146 into Equation 5.145 yields

$$\begin{cases} (m_1 - m_e)\ddot{x}_1(t) + m_e\ddot{x}_b(t) + (c_1 - c_p)\dot{x}_1(t) + c_p\dot{x}_b(t) + k_1x_1(t) = f_a(t) - m_1\ddot{x}_g(t) \\ m_e\ddot{x}_1(t) + (m_b + m_e)\ddot{x}_b(t) + c_p\dot{x}_1(t) + (c_b + c_p)\dot{x}_b(t) + k_bx_b(t) = -f_a(t) - m_b\ddot{x}_g(t) \end{cases} \tag{5.147}$$

And Equation 5.147 can be condensed into matrix format

$$[M]\{\ddot{x}(t)\} + [C]\{\dot{x}(t)\} + [K]\{x(t)\} = \{\gamma_a\}f_a(t) + \{\delta\}\ddot{x}_g(t) \tag{5.148}$$

where

$$[M] = \begin{bmatrix} m_1 - m_e & m_e \\ m_e & m_b + m_e \end{bmatrix},\ [C] = \begin{bmatrix} c_1 - c_p & c_p \\ c_p & c_b + c_p \end{bmatrix},\ [K] = \begin{bmatrix} k_1 & 0 \\ 0 & k_b \end{bmatrix}$$
$$\{x(t)\} = \begin{Bmatrix} x_1(t) \\ x_b(t) \end{Bmatrix},\ \{\gamma_a\} = \begin{Bmatrix} 1 \\ -1 \end{Bmatrix},\ \{\delta\} = \begin{Bmatrix} -m_1 \\ -m_b \end{Bmatrix} \tag{5.149}$$

By defining the state-variable as

$$\{Z(t)\} = \begin{Bmatrix} \{x(t)\} \\ \{\dot{x}(t)\} \end{Bmatrix} = \begin{bmatrix} x_1(t) & x_b(t) & \dot{x}_1(t) & \dot{x}_b(t) \end{bmatrix}^T \tag{5.150}$$

Equation 5.150 can be rewritten in state equation format as

$$\begin{aligned} \{\dot{Z}(t)\} &= [A]\{Z(t)\} + \{B_u\}f_a(t) + \{B_r\}\ddot{x}_g(t) \\ &= \begin{bmatrix} [0] & [I] \\ -[M]^{-1}[K] & -[M]^{-1}[C] \end{bmatrix}\{Z(t)\} + \begin{Bmatrix} \{0\} \\ -[M]^{-1}\{\gamma_a\} \end{Bmatrix} f_a(t) \\ &\quad + \begin{Bmatrix} \{0\} \\ -[M]^{-1}\{\delta\} \end{Bmatrix}\ddot{x}_g(t) \end{aligned} \tag{5.151}$$

Similarly, for the HDABC system with spring damper

$$\begin{bmatrix} m_1 & 0 \\ 0 & m_b \end{bmatrix}\begin{Bmatrix} \ddot{x}_1(t) \\ \ddot{x}_b(t) \end{Bmatrix} + \begin{bmatrix} c_1 - c_p & c_p \\ c_p & c_b + c_p \end{bmatrix}\begin{Bmatrix} \dot{x}_1(t) \\ \dot{x}_b(t) \end{Bmatrix}$$
$$+ \begin{bmatrix} k_1 - k_p & k_p \\ k_p & k_b + k_p \end{bmatrix}\begin{Bmatrix} x_1(t) \\ x_b(t) \end{Bmatrix} = \begin{Bmatrix} 1 \\ -1 \end{Bmatrix} f_a(t) + \begin{Bmatrix} -m_1 \\ -m_b \end{Bmatrix}\ddot{x}_g(t) \tag{5.152}$$

Thus Equations 5.150 and 5.151 can still be used except the coefficient matrices $[M]$, $[C]$, and $[K]$ are different

$$[M] = \begin{bmatrix} m_1 & 0 \\ 0 & m_b \end{bmatrix},\ [C] = \begin{bmatrix} c_1 - c_p & c_p \\ c_p & c_b + c_p \end{bmatrix},\ [K] = \begin{bmatrix} k_1 - k_p & 0 \\ 0 & k_b - k_p \end{bmatrix} \tag{5.153}$$

5.4.1.2 Effectiveness of hybrid-state control

To show the effectiveness of the hybrid-state control system, earthquake response and required control forces are evaluated for three cases: passive spring damper only, active state control, and hybrid-state control. Figure 5.27a shows the displacement time history of the three cases. Note that the passive control is less effective than active or hybrid control in that the passive-only case can only reduce the maximum floor displacement to 0.322 in, while the other two can reduce it to 0.200 in. Figure 5.27b shows the comparison of active and hybrid control. It compares the maximum required active control force with the controlled response—the maximum floor displacement set same at 0.2 in. It shows the maximum active force by hybrid-state control is 14.85 lb, only 53.1% of that for active state control. This means that the hybrid system requires a much smaller actuator that can significantly reduce the cost of the system.

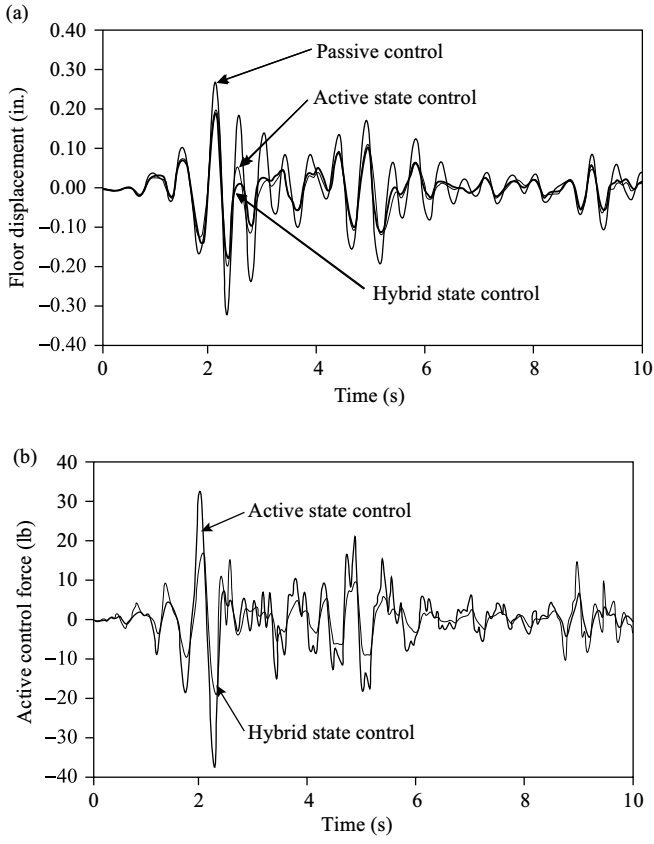

FIGURE 5.27 Effectiveness of hybrid-state control: (a) floor displacement and (b) active control force.

5.4.1.3 Effectiveness of hybrid state-slope control

Similarly, to show the effectiveness of the hybrid state-slope control system, earthquake response and required control forces are evaluated for three cases: passive liquid mass damper only, active state-slope control, and hybrid state-slope control. Figure 5.28a shows the displacement time history of the three cases. Again, it shows that the passive control is less effective than active or hybrid control in that the maximum floor displacement of the passive-only case is much larger than the other two. Figure 5.28b also compares the required active control force by active and hybrid control with the maximum floor displacement set to 0.200 in. It also shows that the maximum active force by hybrid state-slope control is much less than that for active state-slope control.

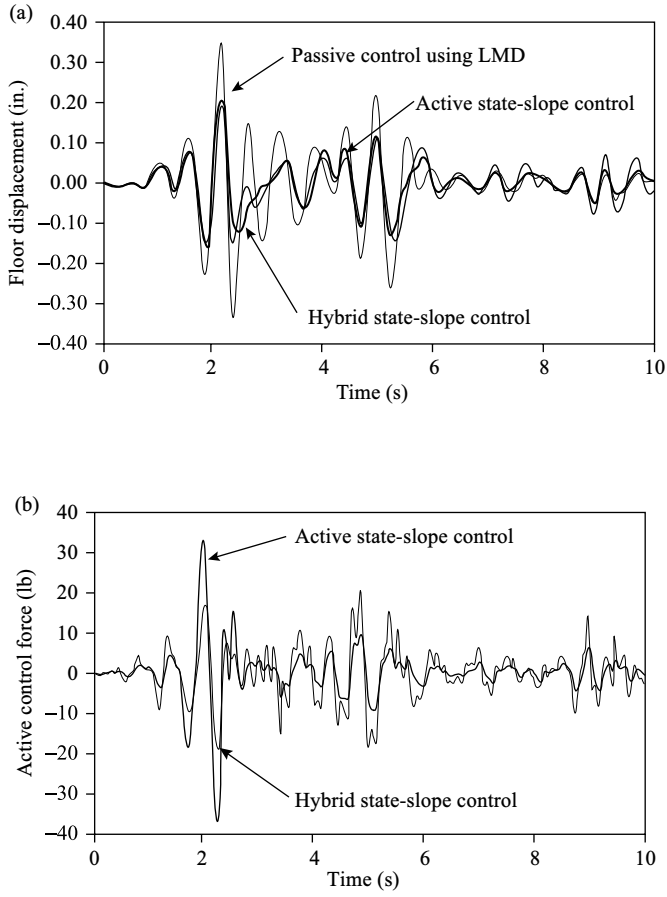

FIGURE 5.28 Effectiveness of hybrid state-slope control: (a) floor displacement and (b) active control force.

5.4.1.4 Comparison of state and state-slope control strategies

Note that a comparison of Figures 5.27b and 5.28b shows that the maximum required control force by active state-slope control is larger than that by active state control (31.56 lb vs. 27.97 lb). A further comparison is shown by Figure 5.29 with the maximum floor displacement of both cases set to the same 0.2 in. Figure 5.29a shows that both state and state-slope control strategies are effective in reducing structural displacement response. Figure 5.29b compares the acceleration response and it shows that more acceleration can be reduced by state-slope control (to 25.99 in./s^2) than state control (to 55.75 in./s^2). Thus, active state control is more effective in reducing structural displacement while active state-slope control is more effective in controlling structural acceleration. State-slope control is preferred if acceleration is a concern though it requires little bit larger control efforts.

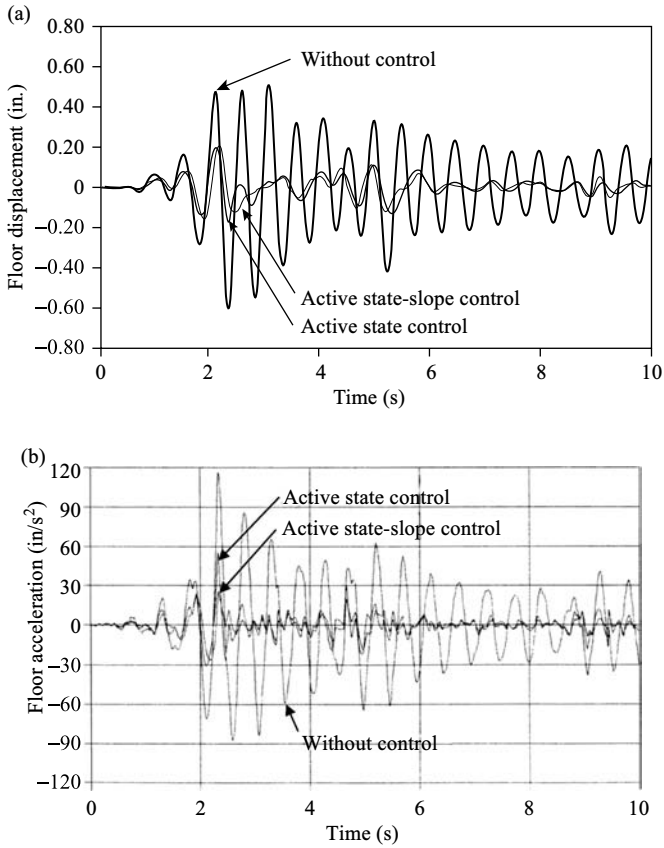

FIGURE 5.29 Comparison of active state control and active state-slope control: (a) floor displacement and (b) floor acceleration.

5.4.1.5 Illustration of intelligent hybrid-state control

Dynamic response and active control force are compared with three different threshold values, TR = 0, 0.2, and 0.4. TR = 0 means that the active control is always effective, thus resulting in hybrid control. Recall that the maximum floor displacement by passive only is 0.322 in. Thus TR = 0.4 means the active control is never effective and leads to passive control only. TR = 0.2 means the active control will be effective when the controlled response exceeds 0.2 in., thus yielding an intelligent hybrid control. Figure 5.30a,b compare the floor displacement and active control force, respectively, for the three different TR values. It can be seen that the active control is switched on at t = 2.02 s. when the response exceeds the threshold value. The only weakness of this intelligent setup is that, during the first

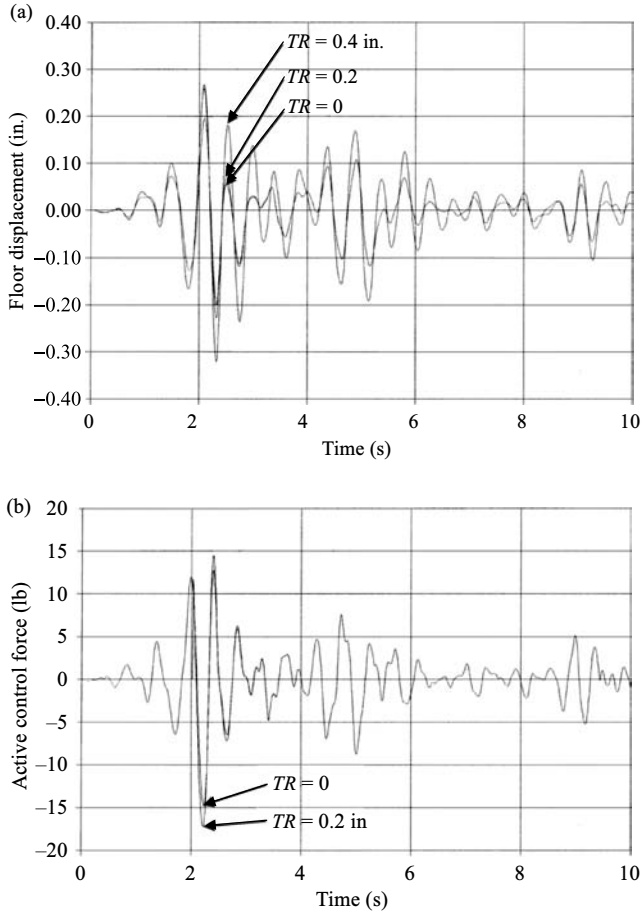

FIGURE 5.30 Demonstration of intelligent hybrid control system: (a) floor displacement and (b) active control force.

couple of cycles right after the active control is activated, larger floor displacement is produced and larger active control force is required than the hybrid control ($TR = 0$). However, observations reveal that sudden involvement of active control during structural response requires more control force to reduce floor displacement but does not disturb the stability of the structural system. For small earthquakes, only passive system is needed to control the structural response.

5.4.2 Three-Story Smart Seismic Structure with HDABC System

The system shown in Figure 5.21 is again employed to demonstrate the powerful capacity of hydraulic actuators and the effectiveness of HDABC system. Properties of the structure with brace, the damper, and the actuator are given in Section 5.3.3.2. Recall that this system is of 11th order. LQR and pole assignment control algorithms are used for controller design. The controller design and system seismic response are analyzed with MATLAB® control toolbox. Refer to Appendix A for details of MATLAB® control toolbox and *.m* program.

5.4.2.1 Capacity of control systems with hydraulic actuator

A hydraulic actuator can be used in an active control system and a hybrid control system. To demonstrate the control capacity of active and hybrid systems with a hydraulic actuator, seismic response in time history is evaluated for the following four cases: (1) structure only; (2) structure with passive control using viscous fluid damper mounted on K-brace at the first floor; (3) structure with active control using an actuator mounted on K-brace at the first floor; (4) structure with hybrid device mounted on K-brace at the first floor. The hybrid device in case 4 consists of a damper and an actuator that are same as those in cases 2 and 3, respectively.

Figure 5.31 compares the displacement response of cases 1, 2, and 3 under the excitation of scaled N-S component of the El-Centro earthquake. The dashed line, solid line, and darkened solid line refer to responses for case 1, 2, and 3, that is, structure without control, structure with passive control, and structure with active control, respectively. Results show that the maximum displacement at the third floor is 0.7794 cm for the structure without control. By applying passive control, maximum displacement can only be reduced to 80.7%, that is, 0.6287 cm. With active control, it can be further reduced to 58.5%, that is, 0.4561 cm, which is 72.5% of that for the passive control system. This result shows that active control systems have a greater capacity to mitigate structural seismic response.

Similarly, Figure 5.32 compares the displacement response of cases 1, 2, and 4 to scaled N-S component of the El-Centro earthquake. The dashed line, solid line, and darkened solid line refer to responses for case 1, 2, and 4, that is, structure without control, structure with passive control, and structure with hybrid control, respectively. Results show that the maximum displacement at the third floor can be reduced to 0.4042 cm by hybrid control, which is 51.9% of that for structure without control and 64.3% of that for the passive system. This result shows that

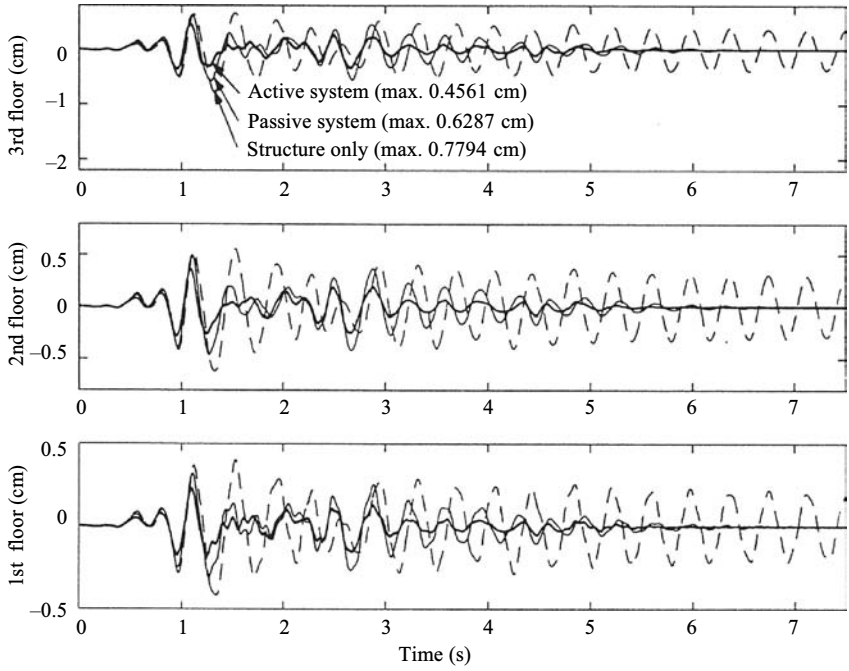

FIGURE 5.31 Demonstration of capacity of active bracing control.

hybrid control systems have a powerful capacity to mitigate structural seismic response.

5.4.2.2 Effectiveness of the HDABC system

To show the effectiveness of hybrid control structural seismic responses, and required control forces are evaluated for three cases: (1) structure with hybrid control, (2) structure with active control, and (3) structure with passive control. The same hydraulic actuators are used in cases 1 and 2, and the same viscous fluid dampers are used for cases 1 and 3.

As observed, the force-generating capacity of the hydraulic actuator is a major concern for full-scale implementation of structural control. Therefore, the required active control force for active and hybrid control systems is compared using the same control objective. Pole assignment control algorithm is used to design the feedback controller. Desired closed-loop poles for the hybrid system and closed-loop poles for the active control system are the same as listed in Equation 5.154 but excluding the real pole –21.269. Figure 5.33 compares the required active control force in the active and hybrid systems. Assume that the control objective is the maximum closed-loop displacement at the third floor of the structure. Under the excitation of the scaled N-S component of the El-Centro earthquake, the control objective of both systems are set the same at 0.5 cm. Results show that for the hybrid control system, maximum required active control force is 785.9 N, which

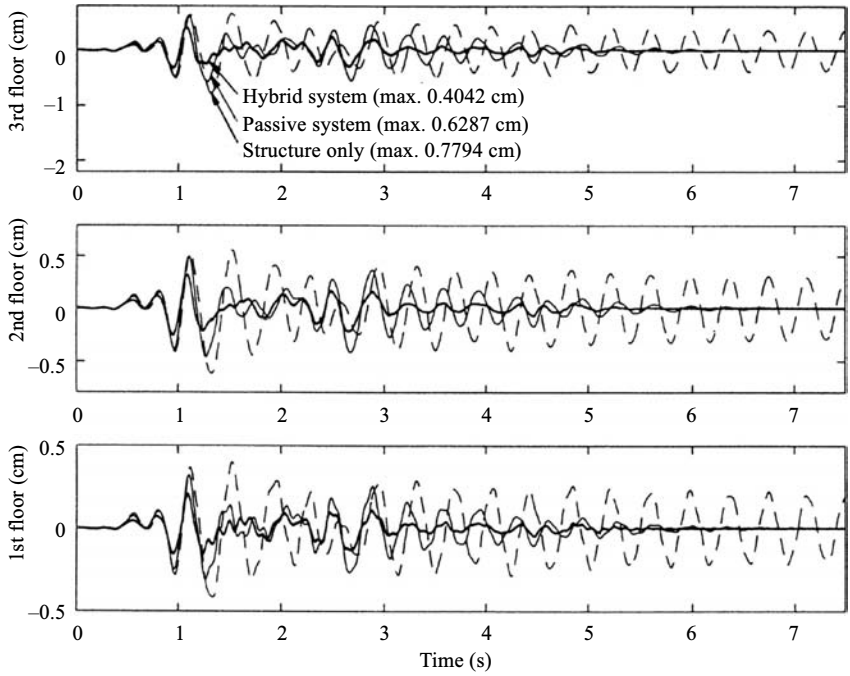

FIGURE 5.32 Demonstration of capacity of HDABC system.

is only 68.3% of that for the active control system (see Figure 5.33a). If the control objective of both systems is set the same at 0.54 cm, the required active control force for the hybrid system is 609.4 N, which is 56.1% of that for the active control system (see Figure 5.33b). This is because the passive damper uses structural vibration to generate the passive control force. When the structural response is larger, the passive damper generates more control force and thus takes a more important role in the hybrid system.

$$\{p\} = \begin{Bmatrix} -2.453 \pm 18.589j \\ -2.071 \pm 59.477j \\ -0.682 \pm 110.51j \\ -42.409 \pm 397.67j \\ -2.798 \times 10^4 \pm 2.800 \times 10^4 j \\ -21.269 \end{Bmatrix}, \; j = \sqrt{-1} \tag{5.154}$$

5.4.3 Effectiveness Comparison of HDABC System and MR Damper

This section uses numerical studies to compare the effectiveness of hybrid and semiactive systems for seismic response control, with the HDABC system and the MR damper as the examples, respectively. For this comparison, it is assumed that

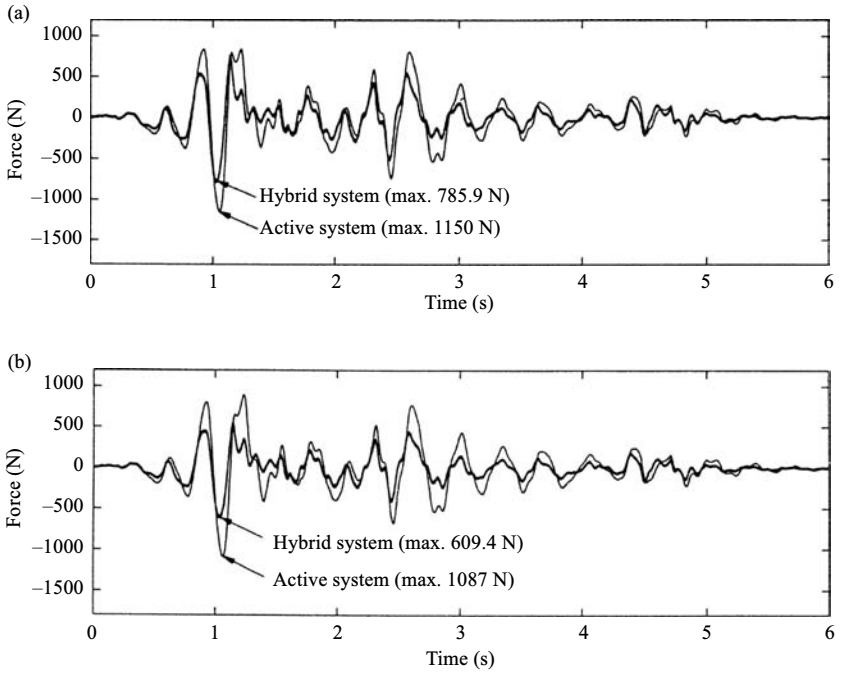

FIGURE 5.33 Comparison of required active control force for El-Centro earthquake: (a) smaller structural response and (b) larger structural response.

both systems are installed on the same brace-structure system subjected to three different earthquake excitations [30]. The same three-story structure and K-brace as Section 5.3.3.2 are used here. Two control systems are installed at the same three-story building and brace system was introduced in the intelligent control example. Then three ground motions recorded, El-Centro earthquake in 1940, Northridge earthquake in 1994, and Kobe earthquake in 1995, were adopted as input. As noted, the natural frequencies of the structure model are two times of its prototype thus all the three earthquake records are scaled with 1:2 time factors for the numerical simulation. To compare the control effectiveness of two control systems, the controlled top-floor displacement for two control systems is set to be the same and other responses are evaluated.

By setting controlled top-floor displacement the same, the structural response of acceleration, displacement, and column shear is compared and evaluated. The HDABC system model and MR damper model have been developed in Section 5.1. LQR optimal algorithm is used by the HDABC system. For the semiactive control, the clipped-optimal control [16] is utilized here and the command signal (voltage applied on MR damper) is given by

$$v = v_{\max} H\{(f_c - f)f\} \tag{5.155}$$

where v_{max} is the voltage associated with the saturation of the magnetic field in the MR damper. H (•) is the *Heaviside step function*; f_c is optimal active control force.

5.4.3.1 El-Centro earthquake

In this case, the magnitude of the earthquake input is scaled to 50% of its original and the reduction of maximum top-floor displacement is set as 29%. Figure 5.34 shows the top-floor displacement response (MR-controlled) and MR control force and voltage applied on MR fluid. Figure 5.35a plots the top-floor displacements by two control systems and shows that the maximum displacements of the two systems are set approximately the same. For further clarification, Figure 5.36 illustrates the peak values of displacement, acceleration, and shear force at the three floors for three cases, uncontrolled structure, the HDABC system, and the MR damper. Figure 5.36b shows that the controlled displacements are almost the same for two control systems except that the MR system provides a little bit more reduction. Figure 5.36a compares the maximum acceleration response of the three cases. It shows that the HDABC system reduces the acceleration response significantly at all three floors, while the MR system does not provide much reduction at the second and third floor but even results in larger peak acceleration at the first floor than the uncontrolled system. Note that this symptom only happens to the peak acceleration. In other words, the MR system can provide acceleration reduction during the time history (see Figure 5.35b) except for some time instants with impulse-like increase, such as the 1.3 s shown in Figure 5.35b. This phenomenon is directly related to the MR control force (Figure 5.34b) by the clipped-optimal control. The voltage

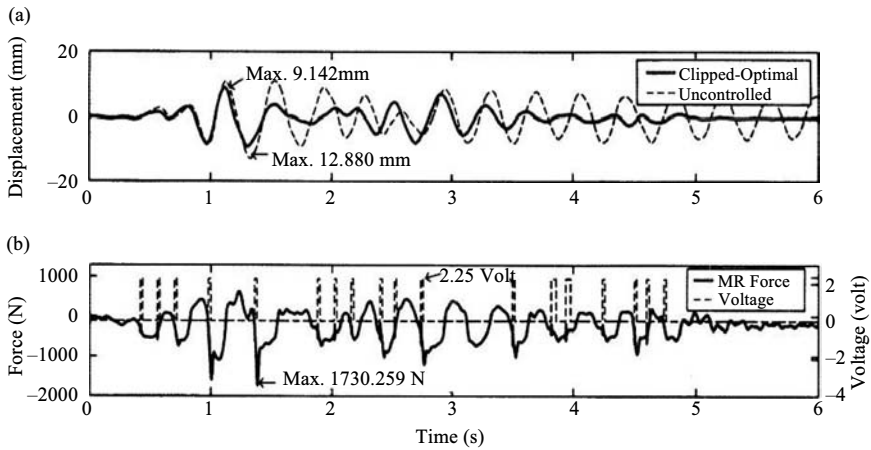

FIGURE 5.34 Demonstration of MR damper control: (a) applied voltage and generated force and (b) top-floor displacement response.

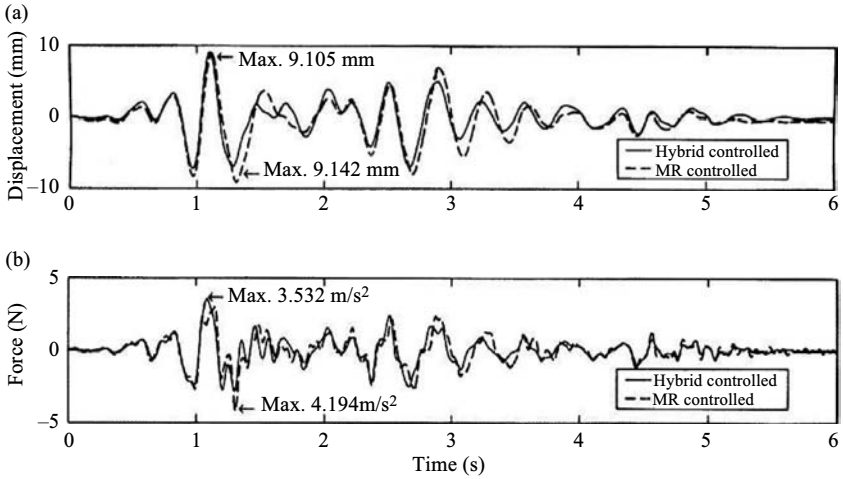

FIGURE 5.35 Comparison of MR damper and HDABC system-controlled structure response at top-floor: (a) displacement and (b) acceleration.

modification always causes a sudden increase of MR force, consequently resulting in impulse-like acceleration. Figure 5.36c shows both systems are effective for the peak shear force reduction, and the HDABC system reduced more column shear force at each story.

5.4.3.2 Northridge and Kobe earthquakes

For *Northridge Earthquake* input, magnitude is scaled to 30% of the original, and 25% for the *Kobe Earthquake* input. In comparison, the reduction of top-floor peak displacement is set as 44% and 47% for Northridge and Kobe earthquake inputs, respectively.

The peak displacement, acceleration, column shear of the structure under the two earthquake inputs for the three cases, uncontrolled, hybrid control, and MR control, are compared in Table 5.6. Similar results are observed, that is, the two controlled systems yield similar peak responses of floor displacement, while the MR control system provides less peak acceleration reduction than the hybrid control system at the first floor, where the control devices are installed. Again, this symptom of the MR control is due to the force thrust caused by voltage modification.

5.4.4 Summary

This section has studied the capacity and effectiveness of active and hybrid control systems with servovalve-controlled hydraulic actuator mounted on K-brace.

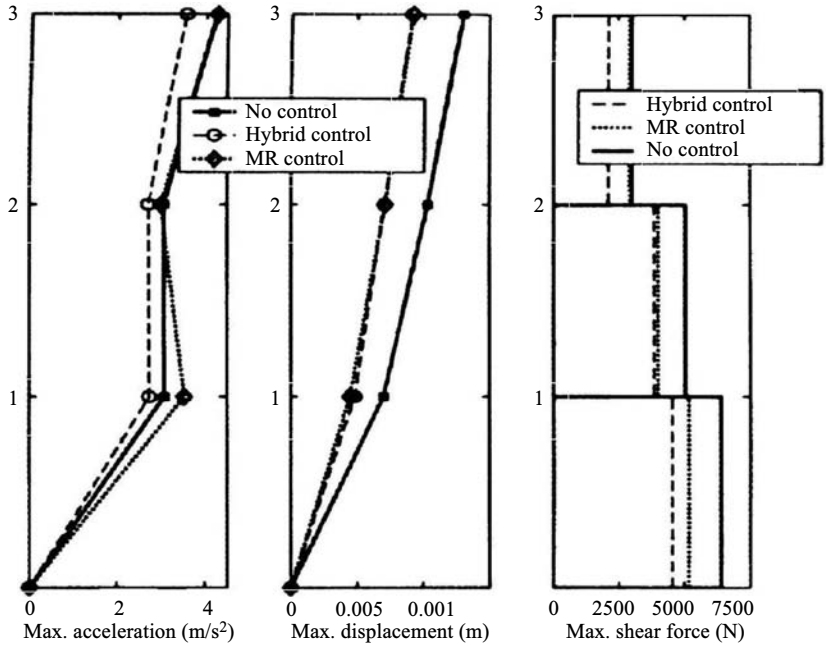

FIGURE 5.36 Peak response comparisons of MR damper and HDABC system-controlled structure.

The effectiveness of HDABC system and MR damper system is compared. A HDABC-controlled one-story building is employed to demonstrate the effectiveness of state and state-slope control of the system with spring and liquid mass dampers, respectively, as well as the intelligent hybrid control strategy. Numerical comparisons of seismic response for a three-story structure with passive, active, and hybrid control are used to demonstrate the effectiveness and capacity of hybrid control systems using hydraulic actuator and viscous fluid damper. Active and hybrid control systems have greater control capacity than passive control systems, while hybrid control technique is more efficient than active control in that smaller actuators are required in hybrid control systems.

In the effectiveness comparison of HDABC and MR damper systems, one phenomenon was found that the MR-controlled floor acceleration response exhibits some impulse-like increase when such active force appears at the instance associated with MR voltage modification, especially for the floor directly connected with the MR damper. This needs to be taken into account for the building designed with high restrictions on floor acceleration. The MR-controlled floor acceleration has exhibited some impulse-like increase caused by thrust-like MR force at the instance of the MR voltage modification that may affect the performance of the acceleration-sensitive equipment on the floor.

TABLE 5.6
Effectiveness Comparison for the Two Control Systems

Earthquake inputs	Cases ↓ Floors ↓	Peak accelerations (m/s^2)			Peak displacements (cm)			Peak shear forces (N)		
		First	Second	Third	First	Second	Third	First	Second	Third
El-Centro	No control	3.047	3.037	4.181	0.69	1.02	1.29	6,340	4,968	2,974
	Hybrid system	2.730	2.701	3.532	0.48	0.71	0.91	4,598	3,546	2,582
	MR damper	3.472	2.984	4.194	0.44	0.71	0.91	5,172	4,007	2,899
Kobe	No control	4.641	6.457	8.011	1.57	2.30	2.83	10,961	8,303	4,549
	Hybrid system	2.452	3.904	5.240	0.79	1.18	1.50	6,319	5,981	2,978
	MR damper	3.489	3.995	4.995	0.79	1.20	1.50	8,110	5,686	2,966
Northridge	No control	7.361	8.544	11.98	2.07	3.00	3.67	14,514	11,268	7,000
	Hybrid system	4.493	6.541	7.543	1.31	1.95	2.42	7,690	8,619	4,410
	MR damper	6.693	6.246	7.923	1.28	1.94	2.46	10,680	7,853	4,974

5.5 Implementation of Hybrid Control for Smart Seismic Structures

Hybrid seismic response control systems have been implemented in various ways. For instance, full-scale hybrid mass dampers were installed on physical buildings in Japan for evaluating their effectiveness by real-time measurements [26]. Shaking table tests are conducted at the University of Missouri-Rolla (UMR) to study the feasibility of hybrid seismic response control, evaluate the effectiveness and stability of the system, as well as to verify the developed optimal control algorithms [10, 20]. This section provides a brief introduction of the experimental studies of HDABC systems at UMR.

5.5.1 Test Setup

5.5.1.1 Structure and K-braces

Figure 5.21 shows the quarter-scale, three-story steel building model. Its dimensions are 4 ft long, 2 ft wide and 8 ft 4 in. tall. The floor heights are 3 ft 4 in. for the first floor and 2 ft 6 in. for the second and third floors. All structural beam and column members use AISC standard A36 steel (36 ksi yielding stress) and ST 1.5×3.75 shape. Floor weights are $m_1 = m_2 = m_3 = 1250$ lb so that the structural fundamental frequency is close to 2.0 Hz by analysis. The K-brace at the first story consists of double angles $2L2 \times 2 \times 1/4$ with cross-sectional area 1.88 in.^{2}. Nominal length of each arm is 37 in., and the angle of both arms to the ground is 56.8°. The K-brace is designed to be much stiffer (with horizontal stiffness 8.84 kips/in.) than the first floor (with horizontal stiffness 2.90 kips/in.) so that it can provide sound support to the control devices and produce reasonable relative displacement between device pistons and cylinders.

5.5.1.2 Control devices

The HDABC control system consists of a viscous fluid damper for passive control and a Moog 760-102A servovalve-controlled hydraulic actuator for active control. The cylinders of the damper and actuator are bolted to the first floor and their pistons are connected to the K-brace. As shown in Figure 5.3, this damper consists of a hydraulic cylinder, a piston, and a tube. The piston separates the cylinder into two chambers, which is filled with viscous fluid and connected by the tube. The relative movement between the damper cylinder and the piston drives the viscous fluid to flow back and forth in the tube and thus dissipates energy. Damper properties can vary through changing the size and length of the tube. The hydraulic actuator, as shown in Figure 5.2, comprises a hydraulic cylinder with a piston, a servovalue with a piston, and a valve control system. It also has a built-in LVDT to monitor the relative displacement between the piston and the cylinder. The actuator is powered by the same hydraulic power supply for the shaking table described below. The hydraulic power supply pumps the hydraulic fluid into the servovalue

first. When the servovalue piston moves to one side, the hydraulic fluid can be pumped into this side of the actuator cylinder and sucked from the other side of the cylinder. The pressure difference in the two sides generates the active control force. The piston movement can be controlled by the servocontrol system with a predetermined control algorithm. Maximum stoke for both the damper and the actuator is ± 1.5 in. The structure and K-brace are sitting on the shaking table. The cylinders of the damper and the actuator are bolted to the bottom of the second floor and their pistons are connected to ground through the K-brace.

Sensing system includes three LVDTs to measure the displacement response of each structural floor and four accelerometers to measure acceleration at each floor and the shaking table. Measurement range is 5 g for accelerometers and ± 3 in for LVDTs. The sensors send signals of the system response to a control computer, which analyzes the signals and sends a feedback signal to the active control system.

5.5.1.3 Earthquake simulator system

The earthquake simulator system includes a shaking table, a hydraulic power supply, and a random vibration controller system. The shaking table is 3 ft 6 in. wide and 7 ft 0 in. long. It can provide a horizontal vibration along its longitudinal direction. It is driven by a hydraulic actuator that can provide a visible vibration up to 10 Hz and can move ± 1 in. at 1 Hz or ± 0.75 in. at 2 Hz. The hydraulic actuator, which uses a hydraulic power supply with 3000 psi working pressure at 22 gpm flow rate, can generate maximum control force 22 kips. The vibration controller system is to control the shaking table to produce different types of vibrations such as sine function, triangular function, and random vibration with specified power spectrum. Scaled N-S component of El-Centro earthquake (1940) is simulated by the shaking table as ground acceleration excitation.

5.5.2 Parameter Identification of Control Devices

The governing equation for viscous fluid damper is expressed by Equation 5.39a. Parameters appearing in this equation, C_0 and λ_0, can be determined through parameter identification tests. In such a test, the damper is driven by a speed-adjustable motor to produce a sinusoidal motion. Driving force, $f_{\mathrm{p}}(t)$, damper displacement and velocity, $x_{\mathrm{p}}(t)$, and $\dot{x}_{\mathrm{p}}(t)$, are monitored and recorded. This test is repeated with motions in different frequencies, $\omega_1, \omega_2, \ldots, \omega_{\mathrm{N}}$. The damper characteristic equation at frequency ω_{i} can be expressed as

$$f_{\mathrm{p}}^{(i)}(t) = K(\omega_i) x_{\mathrm{p}}^{(i)}(t) + C(\omega_i) \dot{x}_{\mathrm{p}}^{(i)}(t) \tag{5.155}$$

where $K(\omega_i)$ and $C(\omega_i)$ are constant, and $x_{\mathrm{p}}^{(i)}(t), \dot{x}_{\mathrm{p}}^{(i)}(t)$ and $f_{\mathrm{p}}^{(i)}(t)$ are sine functions.

TABLE 5.7
Test Results for Identifying Parameters of the Viscous Fluid Damper

Test No. i	f_i (Hz)	ω_i (rad)	$C(\omega_i)$	$K(\omega_i)$	$\lambda_0^i = \frac{1}{n}\sum_{i=1}^{n}\frac{1}{\omega^2}\frac{K(\omega_i)}{C(\omega_i)}$	$C_0 = \frac{1}{n}\sum_{i=1}^{n} C(\omega_i)\cdot\left[1+(\lambda_0\omega_i)^2\right]$
1	1.5	9.425	105.13	306.03	0.0328	111.53
2	2.0	12.566	102.99	434.80	0.0267	114.14
3	2.5	15.708	98.31	572.91	0.0236	114.94
4	3.0	18.850	89.75	777.50	0.0244	111.61
5	3.5	21.991	82.37	991.26	0.0249	109.68
6	4.0	25.132	79.44	1239.85	0.0247	113.84
$\sum$ Total					0.1571	674.74
Average					0.0262	112.64

If $x_p^{(i)}(t_1) = 0$ at $t = t_1$, $C(\omega_i)$ is found by

$$C(\omega_i) = \frac{f_p^{(i)}(t_1)}{\dot{x}_p^{(i)}(t_1)} \tag{5.156}$$

And if $\dot{x}_p^{(i)}(t_2) = 0$ at $t = t_2$, $K(\omega_i)$ is found by

$$K(\omega_i) = \frac{f_p^{(i)}(t_2)}{x_p^{(i)}(t_2)} \tag{5.157}$$

When all $K(\omega_i)$ and $C(\omega_i)$ $(i = 1, 2, \ldots, N)$ are found, parameters of the viscous fluid damper, C_0 and λ_0, are obtained by

$$\lambda_0 = \frac{1}{n}\sum_{i=1}^{n}\frac{1}{\omega^2}\frac{K(\omega_i)}{C(\omega_i)},\ C_0 = \frac{1}{n}\sum_{i=1}^{n} C(\omega_i)\left[1+(\lambda_0\omega_i)^2\right] \tag{5.158}$$

Table 5.7 provides a group of experiment results for identifying parameters of the viscous fluid damper [8,10,20]. Similar tests can be conducted to verify parameters (such as K_v and τ) of the hydraulic actuator specified by the manufacturer.

REFERENCES

1. Babcock, D.A., Simulated dynamic response of a servovalve controlled hydraulic actuator, *NASA Technical Memorandum* 101644, 1990.

2. Cheng, F.Y., Generalized optimal active control algorithm for seismic-resistant structures with active and hybrid control, *International Journal of Computer Applications in Technology*, 13, 42, 2000.
3. Cheng, F.Y. and Jiang, H.P., Optimal control of a hybrid system for seismic excitations, in *Proceedings of US–Japan Workshop on Smart Structures Technology: Application to Large Civil Structures*, College Park, Maryland, 1996.
4. Cheng, F.Y. and Jiang, H.P., Stability and effectiveness of hybrid control for seismic-resistant structures, in *Seismic Design and Mitigation for the Third Millennium: Proceedings of Sixth National Conference on Earthquake Engineering,* Seattle, Washington, 1998.
5. Cheng, F.Y. and Jiang, H.P., Optimum control of a hybrid system for seismic excitations with state observer technique, *Smart Materials and Structures*, 7, 654, 1998.
6. Cheng, F.Y. and Jiang, H.P., Hybrid control of seismic structures with optimal placement of control devices, *ASCE Journal of Aerospace Engineering,* 11, 52, 1998.
7. Cheng, F.Y., Jiang, H.P., and Zhang, X.Z., Optimal placement of damper and actuators based on stochastic approach, *Journal of Earthquake Engineering and Engineering Vibration,* 1, 237, 2002.
8. Cheng, F.Y. and Tian, P., Design parameter analysis of hybrid optimal controlled structures, in *Proceedings of 2nd International Conference on Intelligent Materials,* Willamsburg, Virginia, 340, 1994.
9. Cheng, F.Y., Lou, M.L. and Zhang, X.Z., Intelligent controlled structures with soil-structure interactions, *Journal of Engineering Mechanics and Structure-International Journal*, 12, 573, 2004.
10. Cheng, F.Y. et al., Theoretical and experimental studies on hybrid control of seismic structures, in *Proceedings of the 12th ASCE Conference on analysis and Computation*, Cheng, F.Y., (ed.), Chicago, 1996.
11. Constantinou, M.C., Symans, M.D., and Taylor, D.P., Fluid viscous damper for improving the earthquake resistance of buildings, in *Proceedings of ASCE Symposium on Structural Engineering in Natural Hazards Mitigation*, New York, 1993.
12. Darby, R., *Viscoelastic Fluids: An Introduction to their Properties and Behavior*, Marcel Dekker, New York, 1976.
13. DeSilva, C.W., *Control Sensors and Actuators*, Prentice-Hall, Englewood Cliffs, New Jersey, 1989.
14. Dyke, S.J. et al., Acceleration feedback control of MDOF structures, *ASCE Journal of Engineering Mechanics*, 122, 907, 1996.
15. Dyke, S.J. et al., Implementation of an active mass driver using acceleration feedback control, *Microcomputers in Civil Engineering*, 11, 305, 1996.
16. Dyke, S.J. et al., An experimental study of MR damper for seismic protection, *Smart Materials and Structures*, 7, 693, 1998.
17. Funakubo, H., *Actuators for Control*, Gordon and Breach Science Publishers, New York, 1991.
18. Gamota, D.R. and Filisko, F.E., Dynamic mechanical studies of electro-rheological materials: moderate frequencies, *Journal of Rheology*, 35, 399, 1991.
19. Jiang, H.P., Cheng, F.Y., and Wang, Z.Q., State-of-the-art in hybrid control and issues on optimum seismic observer and device placement, in *Proceedings of the*

12th World Conference on Earthquake Engineering, International Association for Earthquake Engineering, Auckland, New Zealand, 2000.
20. Lohman, T., Experimental and modeling study of a viscous fluid damper with bingham plastic and effective mass for vibration reduction, M.S. Thesis, University of Missouri-Rolla, 1996.
21. MATLAB. The Mathworks Inc., Natick, Massachusetts, 1993.
22. Miller, R.K. et al., Active vibration control of large civil structures, *ASCE Journal of Engineering Mechanics*, 114, 1542, 1988.
23. Nikzard, K., Ghaboussi, J., and Paul, S.L., Actuator dynamics and delay compensation using neurocontrollers, *ASCE Journal of Engineering Mechanics*, 122, 966, 1996.
24. Shames, I.H. and Cozzarelli, F.A., *Elastic and Inelastic Stress Analysis*, Prentice-Hall, Englewood Cliffs, New Jersey, 120, 1992.
25. Soong, T.T., *Active Structural Control: Theory and Practice*, 1st ed., Longman Scientific & Technical, UK and John Wiley & Sons, New York, 1990.
26. Soong, T.T. and Spencer, B.F. Jr., Supplemental energy dissipation: state-of-the-art and state-of-the-practice, *Engineering Structures*, 24, 243, 2002.
27. Spencer, B.F. Jr. et al., Phenomenological model of a magneto rheological damper, ASCE *Journal of Engineering Mechanics*, 123, 230, 1997.
28. Stanway, R., Sproston, J.L., and Stevens, N.G., Nonlinear modeling of an electro-rheological vibration damper, *Journal of Electrostatics*, 20, 167, 1987.
29. Wen, Y.K., Method of random vibration of hysteretic systems, *ASCE Journal of Engineering Mechanics*, 102, 249, 1976.
30. Zhang, X.Z. et al., Hybrid control realization in building structures and effectiveness comparison with MR control, in *CD-ROM Proceedings of the 15th ASCE Engineering Mechanics Conference*, Smyth, A.W., (ed.), Columbia University, New York, 2002.
31. Zhang, X.Z., Cheng, F.Y., and Lou, M.L., Intelligent hybrid controlled structures with soil-structure interaction, *Structural Engineering and Mechanics: An International Journal*, 17, 573, 2004.
32. Zhang, X.Z., Cheng, F.Y., and Jiang, H.P., Hybrid actuator-damper bracing control (HDABC) system with intelligent strategy and soil–structure interaction, *Journal of Engineering Structures*, 28, 2010, 2006.

6 Sensing and Data Acquisition Systems for Smart Seismic Structures

Similar to many other automation systems, information of excitations and system response are essential for smart seismic structures [3,4,19,25]. *Sensing and data acquisition* is the process of collecting information from the real world. For smart seismic structure applications, such information can be ground motion, control forces, as well as displacements, velocities, and accelerations of the structure. The information is first converted to electrical signals using *sensors*. Real-world seismic events and system response are analogs, and the sensor output signals, called *measurements*, are also analogs with continuous range of values. Because the sensor output signals have noises and may be weak, the signal is amplified and/or filtered by electrical instrumentation called *signal conditioners*. Figure 6.1a shows analog sensing and data acquisition in the smart structure system.

In today's digital world, information of real-world events are usually collected, stored, and analyzed with a computer by numerical data [1,12,18]. The computer can automate the data acquisition process, enabling fewer errors in data collection. It can easily record measurements with very small time intervals (i.e., much less than a millisecond), minimizing the difference between the analog signal and its digital representation. Moreover, the information can be easily displayed graphically, analyzed, and/or processed by the computer. Owing to the decreasing cost and increasing functionality of computers in both hardware and software, digital data acquisition and control have superseded the analog technology in both laboratories and the industry. As computers are common in today's world, implementing a digital data acquisition system is often just a moderate expense of add-in boards and support software. Figure 6.1b shows a schematic of digital sensing and data acquisition system. As noted, the real-word signals are analogs, not in a form of binary numbers that can be directly stored by a computer. Thus, *analog-to-digital* (A/D) boards are added to convert the analog signal to digital data before the data feed the digital controller in the computer.

This chapter focuses on how smart seismic structures obtain and process these measurements by *sensors* and the *data acquisition system*. Conventional sensors and digital data acquisition systems are first discussed in Sections 6.1 and 6.2, respectively, for their application to smart seismic structures. Then the latest research advances are introduced to address the weaknesses of conventional

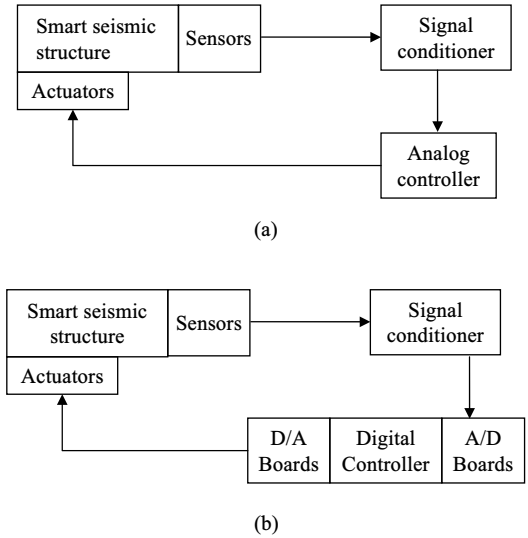

FIGURE 6.1 Schematic of sensing and data acquisition for smart seismic structures: (a) analog and (b) digital.

sensing technology. Section 6.3 presents the new sensing technology, namely, *smart sensors*, and Section 6.4 develops the *seismic observer technique*.

6.1 COMMON SENSORS FOR SMART SEISMIC STRUCTURES

A *sensor* is an electrical, electronic, and/or mechanical device that responds to external excitation or stimulus with an electrical signal [5,8,29]. The external excitation or stimulus is referred to as *measurand* and the electrical signal is called *measurement*. Sensors can be regarded as a translator with measurand and measurement as input and output, respectively. Sensors are usually classified by its input/measurand (i.e., what it measures). For example, sensors that measure accelerations are called *accelerometers*. Sensor input can be of many types such as temperature, pressure, forces, accelerations, velocities, and displacements, and so forth. Sensor output can be in the form of current, charge, or voltage. The output signal can be expressed in time domain (amplitude and phase) or frequency domain (spectrum). A sensor sometimes is referred to as a transducer, but the difference is that the transducer output can be in any form of energy other than the input while sensor output must be an electrical signal. Sensors can be passive and active. Passive sensors use input energy by external excitation/stimulus to generate the output signal, such as piezoelectric sensors. Active sensors require external power (excitation signal) and modify this signal to produce sensor output. Sensors in smart structures are designed to acquire information to feed the controller. They do not function alone but rather as a part of *sensing and data acquisition system* discussed in Section 6.2.

This section discusses the basic mechanisms and specifications of several sensors and transducers that are commonly used for smart seismic structures. These sensors are usually analog devices that generate analog output signals. They measure system responses of the control devices and controlled structures, such as displacements, velocities, accelerations, strain, or forces. These sensors are listed below and discussed later in detail:

- *Position transducers*. Linear variable differential transformer (LVDT) and rotary variable differential transformer (RVDT).
- *Velocity transducers*. Electromagnetic linear velocity transducers and tachometers.
- *Accelerometers*. Capacitive, piezoelectric, and thermal accelerometers.
- *Force transducers*. Strain gauge–based, piezoelectric, or spring-displacement load cells.

All these sensors are commercially available. Common sensor vendors include Omega Engineering (http://www.omega.com/prodinfo), Honeywell Sensing and Control (http://www.sensotec.com), PCB Piezotronics, Inc. (http://www.pcb.com), Analog Devices (http://www.analog.com), and GlobalSpec (http://www.globalspec.com), and so forth. Some of them are also suppliers of data acquisition devices (such as signal conditioners) and digital control systems (such as *digital-to-analog* (D/A) and A/D converters).

In a smart structure system, the control algorithm requires certain measurements and thus dictates what sensors shall be used. Many factors and specifications (see Table 6.1 for examples) such as the following shall be considered in the selection of any particular sensor for smart seismic structures:

- Frequency bandwidth shall cover the range of seismic excitations and structural response.
- Format and strength of the output signal.
- Linear range and dynamic accuracy.
- Sensitivity and resolution.

TABLE 6.1
Examples of Sensor Specifications

Types	Frequency bandwidth	Resolution	Accuracy	Sensitivity
LVDT	DC → 2500 Hz	0.001 mm	0.3%	50 mV/mm
Piezoelectric accelerometer	1 Hz → 25 kHz	1 mm/s^2	1%	0.5 mV/mm/s^2

Source: Chu, S.Y., et al., *Active, Hybrid, and Semi-Active Structural Control: A Design and Implementation Handbook*, John Wiley & Sons, Chichester, England, 2005.

- Environmental factors such as temperature, pressure, humidity, chemicals, and electric or magnetic fields, and so forth.
- Reliability and cost.

6.1.1 Linear or Rotary Variable Differential Transducer

An LVDT (or an RVDT) measures linear (or angular) displacement by the method of electromagnetic induction. As shown in Figure 6.2, the LVDT consists of a core and two coils called the primary winding and the secondary winding. The two coils work as a transformer in that the primary winding carries an AC excitation, V_i, which induces a steady AC output voltage, V_o, in the secondary winding. The level of the induced voltage depends on the flux coupling between the two coils. By associating the measurand motion with the magnetic flux coupling between two coils, the output voltage in the secondary winding can represent the measurement of the motion. There are two methods to change the flux coupling. One is to move physically one coil with respect to the other. The other way, which is more common, is to use a nonmagnetized ferromagnetic medium to alter the reluctance (magnetic resistance) of the flux path, which, in turn, changes the coupling between the two coils. Thus, motion sensors that employ the principle of electromagnetic induction, such as LVDTs and RVDTs, are also referred to as variable-reluctance transducer. LVDTs and RVDTs are active sensors, as they require excitation voltage.

As shown in Figure 6.2, the LVDT core attaches to the smart structure to measure its movement. The core, made of a ferromagnetic material, is inserted coaxially into the cylindrical opening without physically touching the coils. The two subcoils in secondary winding are connected in the opposed phase. When the core is positioned in the center, the induced voltage in the two subcoils cancels and there is no output signal (called neutral calibration). The core movement from the neutral position unbalances the flux linkage of the two subcoils in the secondary winding to the primary winding, developing an output signal. Thus, the

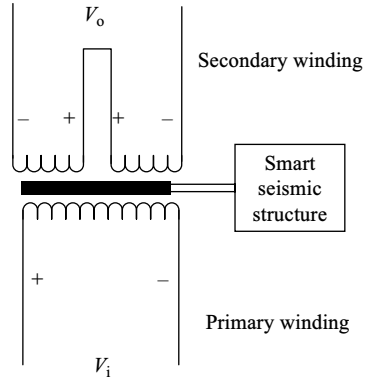

FIGURE 6.2 Schematic of induction displacement sensors (LVDTs).

movement of the smart structure, which determines the axial position of the core, is associated to the flux coupling and the output signal. It changes the reluctance of the flux path, with an associated change of the flux linkage in the secondary coil. Thus, the degree of flux linkage depends on the axial position of the core, and the amplitude of the induced voltage is proportional to the core displacement. Consequently, this voltage can be used as a measure of the displacement, which is the operating principle of an LVDT. The RVDT operates on the same mechanism as the LVDT, except that a rotary ferromagnetic core is used, as its primary use is to measure angular displacement.

For smart structure applications, the selected LVDT or RVDT must be able to measure transient motions accurately. This requires that the frequency of the excitation voltage have to be at least ten times larger than the largest significant frequency in the measured structural response. Usually structural seismic response has significant modal frequencies less than 5 Hz, and thus a standard AC supply (at 60 Hz line frequency) would work.

There are many advantages of the LVDT (RVDT) for smart structure applications, such as little friction resistance; small resistive forces due to near-ideal electromechanical energy conversion and light weight core; no signal amplification needed with low output impedance, low susceptibility to noises; directional (positive/negative) measurements; fine resolutions; low cost and durability due to a simple and robust construction; and availability in small sizes. However, as you may notice, external fixed support is required for the LVDT to measure the structural absolute displacement. This can be done in a laboratory but is impossible for full-scale physical structures. However, LVDTs are useful to measure relative displacements inside a physical smart seismic structure. One example is the built-in LVDT in some hydraulic actuators to monitor the relative displacement between actuator piston and cylinder.

6.1.2 Velocity Sensors

In theory, the velocity can be derived from displacement measurements, as velocity is a first derivative of displacement. However, taking derivatives may result in high noises in the signal, even with sophisticated conditioning devices. Thus, velocity sensors are essential for some smart structure applications.

Velocity sensors, such as *linear velocity transducers* and *tachometers*, take advantage of the mechanism of magnetic induction. According to Faraday's law, moving a magnet through a coil of wire will induce a voltage in the coil and the voltage is proportional to the magnet's velocity and the field strength. This principle of electromagnetic induction between a permanent magnet and a conducting coil is used in speed measurement by permanent magnet transducers. A distinctive feature of permanent magnet transducers is that they generate a uniform and steady magnetic field. The relative motion between the magnetic field and an electrical conductor induces a voltage that is proportional to the speed at which the conductor crosses the magnetic field. Thus, such a sensor is usually enclosed in a steel casing to isolate it from ambient magnetic fields. Depending on the configuration, either

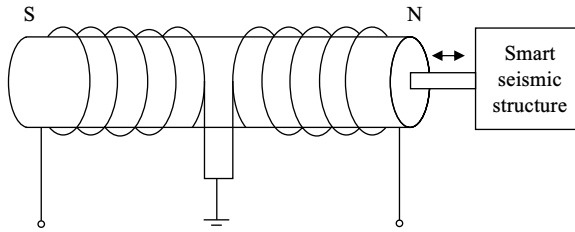

FIGURE 6.3 Mechanism of linear electromagnetic velocity sensors.

translational velocities or angular speeds can be measured. Tachometers use the same principle and the only difference is that they have rotary core. Unlike LVDTs, velocity sensors are passive devices in that they do not need external excitation but generate current/voltage signals with a moving permanent magnet. Thus, velocity sensors are passive.

Figure 6.3 shows the mechanism of a linear velocity sensor for application to smart seismic structures. It uses a permanent magnet and a fixed geometry coil so that the output voltage signal is directly proportional to the relative velocity of the magnet or the structure over its working range. In this velocity sensor, both ends of the magnet are inside the coil. With one coil, this would give a zero output because the voltage generated by one end of the magnet would cancel the voltage generated by the other end. The coil is divided into two sections to address this issue. The north pole of the magnet induces a current in one coil, while the south pole induces a current in the other coil. The two coils are connected in a series-opposite direction to obtain an output proportional to the magnet's velocity. Maximum detectable velocity depends primarily on the input stages of the interface electronic circuit. Minimum detectable velocity depends on the noise level in current and nearby equipment. Specifications of velocity sensors also need to be evaluated for a particular application. Table 6.2 lists the range of typical specifications of electromagnetic velocity sensors.

6.1.3 Accelerometers

As their name implies, *accelerometers* are devices that measure accelerations of the motion or vibration of a structure. An accelerometer is a useful instrument for detecting and measuring vibrations or for measuring accelerations such as gravity. It can be configured into a single-, dual-, and triple-axis model to measure accelerations in single or multiple directions simultaneously. Accelerometers have been widely used in modern industry and scientific/engineering systems to measure seismic activities and structural vibration of buildings, automobiles, airplanes, and so forth. A typical example is the accelerometer in automobile's airbag deployment systems. It measures the acceleration of the automobile to detect collisions and their severity so as to determine if triggering off the airbag is needed. The wide use of accelerometers has cut their cost down drastically.

TABLE 6.2
Specification Ranges of Electromagnetic Velocity Sensors

Property	Range
Magnet core displacement (inches)	0.5–24
Sensitivity (mV/in/s)	35–500
Coil resistance (kΩ)	2–45
Coil inductance (Henry)	0.06–7.5
Frequency response (Hz)	500–1500
Weight (g)	20–1500

Source: Fraden, J., *Handbook of Modern Sensors: Physics, Designs and Applications*, American Institute of Physics Press, Woodbury, New York, 1997.

Direct sensing of accelerations is more difficult than measuring forces. However, the Newton's second law interprets that a force F causes a mass M to accelerate. If the acceleration of the mass is a, the product Ma is called inertia force and equal to external force F. Thus by sensing the inertia force of a mass, the acceleration of the mass can then be measured. This is the mechanism of common accelerometers that have a built-in seismic mass. Take the piezoelectric accelerometer as an example. The inertia force induced by the acceleration causes the mass to squeeze the piezoelectric material, and an electrical signal is then generated. With the linear piezoelectric materials (meaning the electric signal is proportional to the applied force) and the constant seismic mass, the signal would be proportional to the acceleration. Note this acceleration is the one for the accelerometer mass, not the one of the external excitation (the measurand). However, if we can correlate the acceleration of the accelerometer mass to the measurand acceleration linearly, the measurement of external acceleration can be obtained. To achieve this goal, an accelerometer usually consists of an SDOF mass-spring system, and a frame structure with damping device properties. Under external excitation $a_e = \ddot{x}_e(t)$, the motion equation of the accelerometer system can be described by

$$m_a\ddot{x}_a(t) + c_a\dot{x}_a(t) + k_a x_a(t) = -m_a\ddot{x}_e(t) \tag{6.1}$$

As noted above, the measurand is $\ddot{x}_e(t)$ but the directly sensed value by the accelerometer is $\ddot{x}_a(t)$. The frequency response from $x_e(t)$ to $x_a(t)$ of this SDOF system is given by [10]

$$G(j\omega) = \frac{1}{\omega_n^2 - \omega^2 + 2\zeta\omega_n j\omega}, \quad j = \sqrt{-1} \tag{6.2}$$

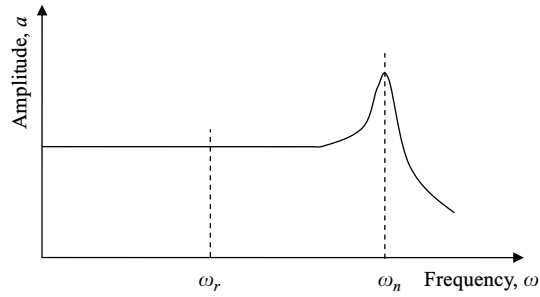

FIGURE 6.4 Frequency response of accelerometers.

which is illustrated by Figure 6.4. A correctly designed, installed, and calibrated accelerometer should have one obvious resonant frequency ω_{n} and a frequency range with flat response, where the accelerometer is linear and thus accurate measurements can be made. This useful flat region is created by having much bigger natural frequency ω_{n} than the reference frequency ω_{r}, and improved by using viscous damping to limit the resonant effects. If the measurand frequency range is inside the flat region, the accelerations of accelerometer mass and the measurand have linear relationship.

Accelerometers can be classified by their force-sensing mechanism. These using piezoelectric materials are called *piezoelectric accelerometers* and their detailed discussion is in Section 6.1.3.1. The second type takes advantage of electromagnetic induction. Such accelerometers convert the inertia force into a proportional displacement using a spring element, and this displacement is measured by an electromagnetic sensor, such as an LVDT. Examples are *differential transformer* and *capacitive accelerometers*. The third type is *strain-gage accelerometers*. It determines the acceleration by measuring the strain at certain locations of a structural member deflected by inertia force. Other types include *thermal*, *acoustic*, and *laser accelerometers*, which correlate the acceleration to temperature change, surface acoustic wave, and optimal signal, respectively.

6.1.3.1 Piezoelectric accelerometers

Piezoelectricity (PZT) is a natural phenomenon that certain materials can generate an electrical charge and voltage when subjected to mechanical stress or strain. Such materials can be certain ceramic materials (barium titanate, lead zirconite titanate, lead metaniobite, and so forth) and quartz crystals. The *piezoelectric effect* is reversible in that piezoelectric crystals, when subjected to an externally applied voltage, can change shape in a small amount. PZT was discovered by Pierre Curie and the word is derived from the Greek piezein, which means to squeeze or press. The piezoelectric effect finds useful applications in many fields and is utilized to sense forces and acceleration accordingly. A piezoelectric accelerometer usually

consists of a crystal sandwiched between the case and the mass so that the force is proportional to the acceleration. In miniature accelerometers, a thin film of PZT material is deposited on a micromachined silicon layer.

Piezoelectric accelerometers can be low- or high-impedance output accelerometers. The high-impedance one produces an electrical charge signal. It is directly connected to the signal conditioning devices but requires external charge-to-voltage converter/amplifier. It is most commonly found in research facilities and high-temperature ($>120°C$) environments. The low-impedance output accelerometer has a charge accelerometer and a built-in charge-to-voltage converter to produce a low impedance voltage. They are commonly found in industry applications as they can easily interface with standard data acquisition instrumentation. Piezoelectric accelerometers have the advantages of being light in weight, little noises, high linearity, and a wide operating temperature range. They operate from a frequency as low as 1 Hz and up to about 5 kHz and have good high-frequency response. However, piezoelectric materials can only generate small voltage signals (in the order of 1 mV). Thus, some piezoelectric accelerometers are built into a charge-to-voltage converter that can also amplify the piezoelectric crystal signal. The other approach is to use a large mass so that the inertia force on the crystal is large for a given acceleration, thus generating a relatively large output signal. However, the large accelerometer mass may distort the measurand acceleration due to the mechanical loading effect.

6.1.3.2 Accelerometer specifications

To select an appropriate accelerometer for practical applications to smart seismic structures, the accelerometer specifications provided by its vendor shall be consulted. These specifications are

- *Frequency response*. The accelerometer's resonance frequency ω_n and reference frequency ω_{r} are usually given in its manufacturer specification. A good accelerometer shall have a ω_r much smaller than ω_{n}. In addition, the low cutoff frequency (where the output starts to fall off below the stated accuracy) and high frequency limit (where the output exceeds the stated output deviation) are usually specified. The high limit shall be much lower than the resonance frequency of the accelerometer to ensure accuracy. All significant natural frequencies of the smart seismic structure under consideration (usually in 0.1–10 Hz) shall be in the range between low cutoff and high limit.
- *Amplitude range*. It is the range between plus/minus maximum acceleration amplitude that the accelerometer can accurately measure. It is typically specified in gs, where g is the acceleration due to the earth's gravity (i.e., 9.8 m/s^2). Beyond this range, the accelerometer output signal may be distorted or clipped.
- *Linearity and accuracy*. The maximum error in amplitude of the output signal of the accelerometer is typically specified by a deviation, such as

±5%. The frequency of the output signal usually matches the vibration frequency of the measurand very well. Obviously the more accurate the better. In addition, the accelerometer mass shall be much smaller than the measurand mass to ensure the accuracy. It is not an issue for smart seismic structures as the structural mass is huge compared to the accelerometer mass.

- *Sensitivity*. It is the voltage (measured in mV) of the accelerometer output signal produced by a certain force (measured in g). It is measured by the ratio of the electrical output to the acceleration input at reference frequency ω_r and in unit of mV/g. Because accelerometers are linear devices and their output signal is proportional to the measurand vibration, the sensitivity is a constant number. There are two typical values of accelerometer sensitivity 10 mV/g or 100 mV/g. Accelerometers with small sensitivity can work for applications with strong vibrations/motions while accelerometers with big sensitivity are used to measure low vibrations.
- *Signal grounding*. Accelerometers can be ground-isolated or case-grounded. The former is much less susceptible to ground-induced noise while care must be given to the latter to avoid ground noise.
- *Noise level*. Electronic noise may be generated by the built-in circuit in the accelerometer. Noise levels can be specified in gs at a specific frequency, that is, 0.0025 g at 10 Hz. Such noise at low frequencies (in order of 1 Hz) is more of an issue for smart seismic structures.
- *Temperature range and sensitivity*. Typically, accelerometer temperature range is -50 to 120°C. The accelerometer can be inaccurate and very sensitive to temperature if outside this range.
- *Environment factors*. These factors can be available space, moisture, presence of electric noises, corrosive chemicals, and magnetic and electric fields.

Motion sensors discussed above may have different preferences in applications. As a rule of thumb, displacement measurements generally provide good accuracy in low-frequency (in the order of 1 Hz) applications. Velocity measurements are usually favored in intermediate-frequency ($<$1 kHz) applications. Acceleration measurements are preferred for high-frequency motions with reasonable noise levels.

6.1.4 Strain Gauges

A *strain gauge* is a resistive elastic device used to measure deformation (strain) of an object. It was invented by Edward E. Simmons in 1938 [8,29]. Strain gauges use materials whose electrical resistance changes linearly by applied strain. When a strain gauge is attached to an object, it deforms as the object is deformed, causing its resistance to change. This linear relationship of the gauge between the strain

and the resistance change is expressed through a constant gauge factor (GF), which is defined as

$$GF = \Delta R \big/ (R \cdot \varepsilon) \tag{6.3}$$

where R is the resistance of the undeformed gauge, ΔR is the resistance change caused by strain, and ε is strain. ΔR can be easily measured by the variation of the electrical current through the gauge. Then with the specified GF and resistance R, the strain ε is determined. Strain gauges are passive sensors as external power supply is needed to measure the resistance change.

There are two common types of strain gauges: metal foil and *semiconductor* ones. They are usually small in size; for example, the active area of foil gauges is typically 2–10 mm. Their resistance R can vary from a hundred to several thousand ohms. Foil strain gauges have a GF usually around 2 (except about 6 for these using platinum alloys). They can measure wide range of strains (up to at least 10%). Metal foil strain gauges can be fabricated with many metal materials, such as alloys of constantan, nichrome, and karma. The semiconductor gauge, also called *piezoresistors*, usually has a larger GF (as high as 150) than a foil gauge. Thus, semiconductor gauges are often used to measure small strain. However, piezoresistors are more expensive, more sensitive to temperature, and more fragile than foil gauges. Strain gauges normally have stable performance over a period of years, which is essential for smart seismic structure applications.

The following issues are worth noting for applying strain gauges to smart structures:

- The gauge shall be attached to the object by strong adhesives so that there is no relative deformation between the gauge and the object.
- The direction is important for installing metal foil gauges, as they are more sensitive to vertical strain than horizontal. In order to measure strains in different axes, multiple gauges can be used either separately or in a bridge circuit.

Thermal expansion exists in many materials, especially for the temperature-sensitive materials (metals or semiconductors) used by strain gauges. Thus, temperature variations can induce extra strain in the gauge, resulting in significant measurement error. A common way to address this issue is to build a temperature-compensating network or to setup a gauge bridge with multiple gauges compensating each other for strains by temperature change. The *Wheatstone bridge* arrangement, as shown in Figure 6.5, is a popular way for temperature compensation. It connects two parallel branches, containing four resistors (gauges). Two gauges are attached to the object and two are unattached. The two unattached gauges produce signal because of temperature change and cancel the thermal strain in the two attached ones.

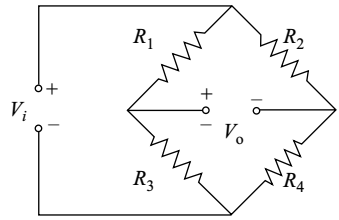

FIGURE 6.5 Schematic of Wheatstone bridge.

6.1.5 Force Transducers

The measurement of force is commonly required in a smart structure system. A typical example is to monitor the control force. Sensors used for such measurements are called *force transducers*. Force transducers in smart structures are quantitative sensors that respond to the force with an electrical signal. Examples of these sensors are strain gauges and load cells fabricated in a stainless steel cylinder. Capacity and frequency ranges are two major factors to select a particular force transducer for smart structure applications. They must be designed to have an axial load capacity at least exceeding the limit of the measurand (e.g., control force). Commercially available force transducers have capacity ranging from one-thousandth of a Newton to very large forces (e.g., 10 tons) of heavy-duty load cells. They can monitor impulsive, slowly varying, and high-frequency forces.

A force is proportional to the acceleration according to Newton's second law. Thus, force transducers can also employ the sensing mechanism of accelerometers. For example, force transducers also commonly employ piezoelectric crystals with built-in microelectronics. The common methods to sense force are

- By measuring the acceleration of a known mass to which the force is applied
- By balancing the force against an electromagnetically developed force
- By converting the force to a fluid pressure and measuring that pressure and
- By measuring the strain produced in an elastic member by the unknown force

Most of force sensors do not directly convert the force into an electric signal, but rather require some intermediate steps. Such mechanism details are described in the following sections for typical force sensors.

6.1.5.1 Strain gauge–based load cells

They are the most common force transducers, which use the theory that forces cause strain or deformation when applied to any object. These sensors convert a force to an electrical signal with two steps. The first step is to deform a strain gauge and the

second step is to convert the deformation (strain) to electrical signals by the strain gauge. A load cell can use any strain-gauge bridge configuration. Its output signal is typically in the order of a few millivolts and thus signal amplification is usually required. Strain gauge–based load cells have the advantage that they are applicable to cases with bending moments. The load cell can be constructed with resistive foil strain gages arrayed in a full Wheatstone bridge. Each arm of the bridge has two gauges connected in series and physically placed such that any strains due to bending moments would cancel and only the axial force would be measured. As noted in Section 6.1.4, strain gauges can remain stable over a period of years. Thus, strain gauge–based load cells are durable sensors for smart structures.

6.1.5.2 Electromagnetic force sensors

Such a force sensor consists of a force-to-displacement converter such as a linear spring and an electromagnetic induction-based displacement sensor such as an LVDT. Within its linear range, the spring converts the axial tension/compression force P to a displacement δ. This relationship can be defined through the spring coefficient k

$$\delta = P/k \tag{6.4}$$

Then the displacement sensor converts the δ into a voltage signal V. Figure 6.6a shows a schematic of such a sensor. Because the spring and the LVDT are both linear, the sensor output voltage V is proportional to the applied force P.

Electromagnetic force sensors have two weaknesses for smart structure applications. The first is that such a load cell has mass-spring behavior, exhibiting vibrations at its natural frequency when subjected to dynamic excitations and abrupt load changes. This oscillating data pattern is commonly referred as

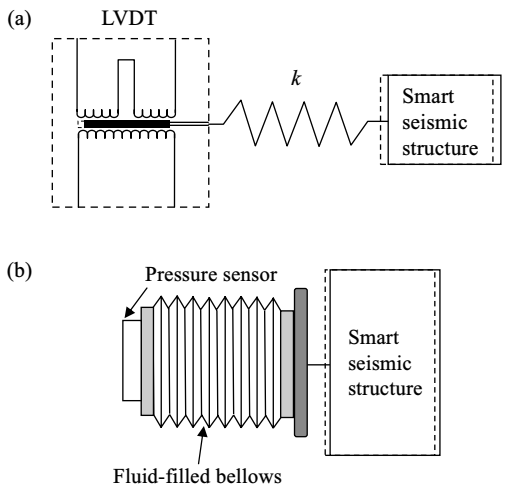

FIGURE 6.6 Force sensors: (a) using a spring and an LVDT and (b) using a pressure transducer.

"ringing," which can result in noises in the output signal. Ringing can be suppressed by passive techniques or by conditioning the signal if the noises are outside of the measurand frequency. The second is that such sensors may require an LVDT component allowing very large deflection in order to measure large forces in smart seismic structures.

6.1.5.3 Hydraulic (or hydrostatic) load cells

When the force is distributed over an area or applied to fluids (i.e., liquids or gases), it is easier to measure the pressure; and the force can be obtained by integrating the pressure over the area or surface. Force sensors with such mechanism are called *hydraulic load cells*, which use pressure sensors. Figure 6.6b shows a schematic of hydraulic force sensor. They have fluid-filled bellows that responds to applied force with hydraulic pressure. The pressure is applied to the sensing membrane of the pressure sensor and the output signal is then generated. With such a mechanism, the voltage signal is proportioned to the force. Compared to induction force sensors and strain gauge load cells, a hydraulic load cell is immune to ambient electric or magnetic fields thus it can be a more effective device in outdoor environments. Hydraulic load cells can measure large force and thus they are commonly used in industrial applications.

6.1.5.4 Piezoelectric force sensors

These force sensors have the same mechanism as the piezoelectric accelerometers discussed in Section 6.1.3.1. The only difference is that the accelerometer sensitivity shall be multiplied by the seismic mass to obtain the sensitivity of the force sensor.

6.2 Sensing, Data Acquisition, and Digital Control Systems

As discussed above, a smart structure system contains sensors that convert system responses to electrical signals—typically voltages. The sensor output signal is normally analog signal. In today's digital world, a control computer is usually used for smart structure systems. Thus, the analog signal is converted to digital before feeding into the digital controller in the computer. The digital control signal generated by the controller is then converted back to analog to feed the actuator. In addition, the electrical signals from sensor output need conditioning before the controller can process them and take appropriate action. For example, some sensors may have weak output signal thus requiring amplification; the nature of the wiring and the analog sensor circuit can surely add some high-frequency noise to the signal, which needs signal filtering or it may seriously affect the effectiveness of a digital control system. This is because such noise, along with high-frequency response in the electrical or mechanical devices and high-mode structural response

in the system, may become low-frequency response when the analog signal is converted to digital, and thus altering the control signal. This effect is usually referred as "aliasing" and shall be filtered out. The required signal processing is done by the *data acquisition system* (or called *signal interface system* sometimes) as discussed in this section.

6.2.1 Elements of Data Acquisition and Digital Control Systems

Figure 6.7 shows a traditional data acquisition system for smart seismic structures with a digital controller. It collects sensor outputs, conditions (filters the noise in the signal and/or amplifies the signal) them, and feeds the brain of the smart structure (i.e., the control computer). The data acquisition system usually consists of sensors, a signal conditioner (a filter and/or an amplifier), a control computer (signal processors, memory devices, data recorders, and a monitor), and A/D and D/A converters. The control computer also comprises of a digital controller and an observer (a state estimator) if the measurements are insufficient for the controller. Figure 6.7 also indicates the data flow in the whole system as follows:

1. Acquire measurand information by sensor(s) with their output (analog electrical signal).
2. Amplify the signal as necessary and filter out the noises in the signal by the signal conditioner.
3. Convert the conditioned analog signal to digital for the control computer by the A/D converter.
4. Estimate the unmeasured state variables by the observer in the control computer.
5. Generate a digital control signal by the controller in the control computer.
6. Convert the digital control signal to analog by the D/A converter. The analog control signal feeds the actuator to generate the control force.

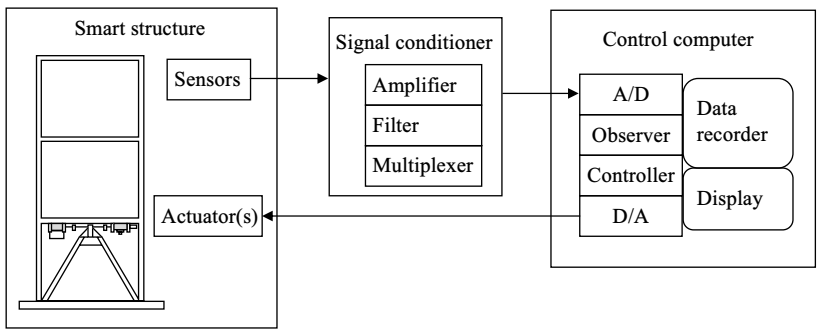

FIGURE 6.7 Data acquisition and digital control system for smart seismic structures.

The important specifications for selecting the system are sampling speed, accuracy, resolution, amount of data, multitasking capacities, and required data processing and display. Software selection is more complex than hardware selection but has the same level of importance. Well-written software can maximize computer hardware performance. It can also improve the data analysis and presentation with the computer capacities. The software may include the controller ability, which analyzes system response, makes decisions based on those measurements, and varies the computer outputs accordingly. The software may also have observer function to estimate unmeasured system states. Today, such software packages are commercially available, which can collect, analyze, and graphically display data with few programming efforts.

This data acquisition and digital control system may have some extra devices such as the wiring for signal communications and false-safe circuit that detects and limits large signal to avoid the structure damage by excess of actuator force and displacement. Devices in the system may also have additional built-in functions, such as recording the measurements and monitoring the system performance as necessary by the control computer. The mechanism of some complex devices in the system is discussed in the following subsections.

6.2.1.1 Signal amplifiers

The basic mechanism of voltage signal amplifiers can be illustrated by the circuit shown in Figure 6.8. By using Kirchhoff's current law [16]

$$\frac{V_{\mathrm{i}}(t) - V_{\mathrm{o}}(t)}{R_2} + \frac{V_{\mathrm{i}}(t)}{R_1} = 0 \tag{6.5}$$

where $V_{\mathrm{i}}(t)$ and $V_{\mathrm{o}}(t)$ are voltages of input and output signals; R_1 and R_2 are resistors in the amplifiers. Rewriting Equation 6.5 yields the amplified output voltage $V_{\mathrm{o}}(t)$

$$V_{\mathrm{o}}(t) = \left(1 + \frac{R_2}{R_1}\right) V_{\mathrm{i}}(t) \tag{6.6}$$

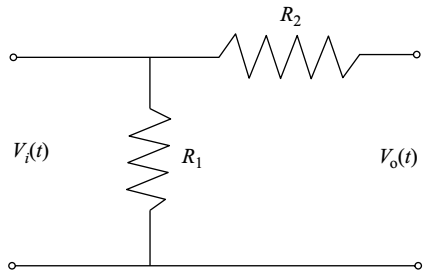

FIGURE 6.8 Mechanism of voltage signal amplifiers.

6.2.1.2 Signal filters

As mentioned, sensor output signals in a smart structure system may have high-frequency noises. Thus, an analog low-pass filter is usually used to weaken the noise. Mechanism of such a filter can be illustrated by the frequency response in Figure 6.9. The filter's transfer function is in the form of damped SDOF system as

$$G(s) = \frac{1}{s^2 + 2\zeta\omega_{\mathrm{n}} + \omega_{\mathrm{n}}^2} \tag{6.7}$$

where ζ and ω_{n} are the filter's damping ratio and natural frequency, respectively. The filter's frequency response is similar to the accelerometer shown in Figure 6.3. Because the filter's amplitude drops sharply in high frequency range, the high-frequency component of the signal is weakened by passing the filter. Note the signal could be amplified around the filter's natural frequency. This issue can be relieved by using a filter with higher damping. It is also desired that when a filter is selected, the expected noise shall have much higher frequency than the filter's natural frequency, ω_{n}.

6.2.1.3 A/D and D/A converters

The process of converting an analog voltage or current signal into a series of binary numbers is called A/D conversion, and the electronic device that does this conversion is called A/D converter. As shown in Figure 6.10, an A/D converter digitalizes an analog signal to a stepped one with specified time interval between values. Three steps are involved in the conversion, sampling and hold, quantization, and encoding. The resulting digital signal is usually an array of numerical values usually separated by fixed time intervals. Each step has constant value and thus can be represented by binary numbers in a computer. When the time interval becomes small enough, the digital signal can be a good approximation to the analog one. The reverse process of decoding a series of binary data into an analog voltage or current signal is called D/A conversion, and the device that does this conversion is called a D/A converter. A/D and D/A converters are commercially

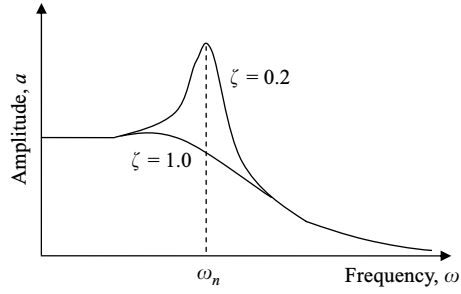

FIGURE 6.9 Frequency response of low-pass filters.

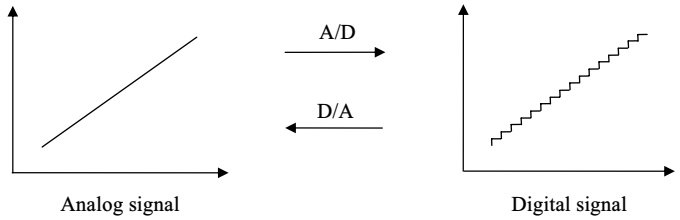

FIGURE 6.10 Example of analog-to-digital (A/D) and digital-to-analog (D/A) conversions.

available. Important specifications of an A/D or a D/A converter, such as resolution, range of analog input or output, linearity error, and conversion time, need be evaluated for the use in a particular smart structure system.

6.2.1.4 Control computer

The control computer has a digital controller, which is the software implementation of the control algorithm. Details of the controller and control algorithm have been discussed in Chapter 4. The computer may also have a state observer if the sensor output does not have enough measurements of system states. Details of the state observer will be discussed in Section 6.3. The control computer also analyzes, records, and displays the information received from data acquisition system.

6.2.2 Challenges in Sensing System of Smart Structures

Researchers have made great advances in smart seismic structures in proving concept, system analysis, device development, and laboratory tests. Optimal control algorithms with full-state feedback are generally used for such systems [3,25] as they have been widely applied in modern control systems [10,12]. This is because the full-state feedback technique can improve damping at each degree of freedom (d.o.f.) of the structure and thus effectively reduces structural vibration. However, these algorithms require measurements of all state variables because the control force is generated by feedback of all state variables. Many studies on smart seismic structures implicitly assumed that all state variables were measured for the full-state feedback controller. In reality, measuring all state variables is a big challenge for practical design and construction of large smart seismic structures because of the complexity and reliability of the sensing system. Detailed reasons are as follows:

- Direct measurement of state variables is difficult to achieve in the real world. State variables of a smart structure system include displacements and velocities at each structural d.o.f. as well as variables for the dynamics of control devices. As noted, a velocity or displacement sensor requires an extra support. The structural displacements must be

measured with respect to an external reference structure that has no elastic deformation. Such an additional structure can be constructed for laboratory tests, but it is not practical for a physical smart structure system. During seismic activity, this situation is exacerbated because the structural foundation is moving with the ground and cannot provide an inertial reference to measure absolute displacement or velocity of the smart structure.

- Too many sensors may be required for a large smart seismic structure. The full-state feedback algorithm requires that the displacements and velocities at each d.o.f. be measured. Seismic structures are usually large and have many d.o.f. and state variables. Numerous sensors are required to measure the full-state vector of full-scale smart seismic structure systems, that is, the control system presents complications if sensors are installed to measure all state variables. Such complexity seriously affects the system reliability, cost, and maintenance.
- Conventional control algorithms assume that all data are centrally collected and processed. Complex wiring is required to link wired sensors to signal conditioning and data acquisition hardware. With a dense array of sensors installed on a smart seismic structure, the wiring can be very complex and unreliable. Moreover, they are easily affected by environment excitations, which may result in significant noises in the signal.
- Sensors for smart seismic structures need to be effective over decades (i.e., during the structure's life). It is very difficult to ensure conventional sensors to work for such a long periods, and even if it is possible, the maintenance of sensors, their installation, and the complex wiring would be very expensive.

6.2.3 Solutions for the Sensing System of Smart Seismic Structures

Several techniques [2,6,7,9,11,13–15,17,20–24,26–28], as discussed in this section, have been proposed to address above issues in sensing system. Such advance of sensing technology for smart structures not only makes the technology more implementable, but also enhances the ability to monitor continuously the structural performance in real time and to detect damage at an early stage. This is essential for public safety and repair cost reduction with respect to the aging seismic structures in today's world.

6.2.3.1 Using accelerometers

Accelerometers do not need any reference structure, thus this approach addresses the unpractical requirement of supporting structures by displacement and velocity sensors. However, the conventional state feedback controller does not work for a system using accelerometers, as it requires state variables (velocities and

displacements). A new feedback controller has to be designed for acceleration measurements. Moreover, it is unrealistic to measure accelerations at all structural degrees of freedom. Installing accelerometers at strategic points of the structure is the most reliable and least expensive measurement method for a smart seismic structure system. Thus, for practical implementation of a structural control system with full-state feedback technique, insufficient sensors and acceleration measurements have to be addressed. Three approaches have been suggested: direct acceleration feedback [6,7,11,27], feedback of pseudovelocities calculated from acceleration measurements [9,24], and seismic observer technique [2,13–15].

The first method, direct acceleration feedback, has been studied analytically and experimentally. Analytical studies extend the H_∞ control algorithm for acceleration feedback [11]. Experimental studies include implementation of H_2/LQG control strategies with acceleration feedback for an active mass driver, an active bracing system, and an active tendon system [6,7]. The experimental studies have verified the proposed acceleration feedback control strategy. Test results have indicated that effective and robust controllers can be developed using acceleration feedback control strategies, and that acceleration feedback can achieve comparable effectiveness to full-state feedback for seismic response reduction. The second method is psuedovelocity feedback [9,24]. In this method, psuedovelocities are obtained by online computing (integration) from acceleration measurements. The first two approaches have proven that a smart structure system can be realized with a sensing system using accelerometers, thus they have improved the implementability of the sensing system for smart seismic structures.

The third method, seismic observer technique, further enhances the implementability of the whole control system in addition to allowing the usage of accelerometers. It addresses two other common practical implementation issues, numerous sensors, and expensive sizeable actuators for large civil engineering structures. These issues not only complicate the system, but also lead to expensive and hard-to-maintain smart seismic structures. Thus the seismic observer technique, which is able to solve the two issues, is very significant for practical application of smart seismic structure technology. While two other methods require accelerometers installed at each structural degree-of-freedom, the seismic observer technique allows the accelerometers installed only at strategic points on the structure. Moreover, the control force by acceleration feedback alters system inertia force to avoid resonance and thus reducing seismic response. This means the control force needs to be in the same magnitude order as the structural seismic inertia force in order to significantly reduce its seismic response. The seismic observer technique enables the full-state feedback control be implemented with accelerometers, and the control force mainly improves system damping. Thus it only requires a control force, which approximates the magnitude of structural damping force. As noted in Chapter 1, damping force of a smart structure system is significantly lower than its inertia and restoring forces. Therefore, the seismic observer technique can also reduce the system cost and complexity by cutting the number of required sizeable actuators.

6.2.3.2 Using integrated sensors and smart sensors

As mentioned, sensor output signals need to be conditioned by filtering and amplification before feeding the controller. For large smart seismic structure applications, lots of wiring is required to link the sensors with signal conditioning hardware. This can increase system complexity and signal noise level. Integrated sensor is one approach to partially address this issue. As shown in Figure 6.11a, signal conditioning and processing devices are directly built into the sensor [17,26] and thus its output signal can directly feed the controller.

Smart sensors [17,19–21,23,26,28], as illustrated in Figure 6.11b, further simplify the complex wiring by adopting wireless sensing technology and embedding with an onboard microprocessor. A smart sensor is an enhanced integrated sensor with wireless and intelligence capabilities. The microprocessor is able to handle signal processing and A/D conversion. Thus, the signal from smart sensors can be directly sent to a digital controller without any wiring. As the industry technology advances, the size and cost of smart sensors have been decreasing. This makes smart sensors easier to install, as they have less effects on the system and are more applicable to smart seismic structures. With such great properties of smart sensors, researchers have been extensively exploring their application to smart seismic structures for both response control and health monitoring [20,21,28]. These studies have shown that smart wireless sensors are very promising emerging technologies that can greatly improve the way that smart seismic structure

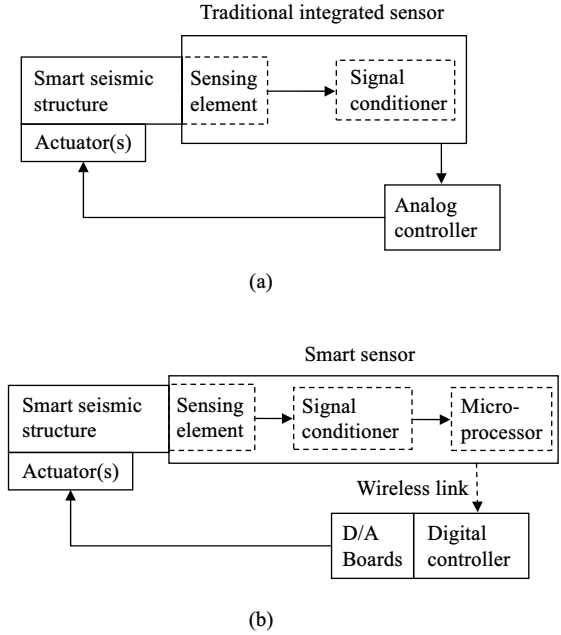

FIGURE 6.11 Innovation sensing system: (a) integrated sensors and (b) smart sensors.

systems are monitored, controlled, and maintained. There are still some challenges for smart sensors, such as low-resolution data acquisition and small memory of the microprocessor inside the sensor.

6.3 Seismic Observer Technique

In this section, an observer technique is established for smart seismic structures. This newly developed seismic observer is able to simplify greatly the sensing system and to estimate the full-state vector from acceleration measurements. With an *observer-controller system*, an optimum full-state feedback algorithm can be implemented for active or hybrid control of seismic-resistant structures. Determination of the required number of sensors and simplification of the sensing system in seismic response control are studied. Numerical simulation of building structures with an observer-controller system is used to demonstrate the effectiveness of the proposed seismic observer technique.

6.3.1 Analytical Modeling of Smart Seismic Structures with Accelerometers

6.3.1.1 Plant equation

In Chapters 4 and 5, the plant equation of a smart structure system for seismic response control has been developed as

$$\{\dot{Z}(t)\} = [A]\{Z(t)\} + [B_{\mathrm{u}}]\{u(t)\} + \{B_{\mathrm{r}}\}\ddot{x}_{\mathrm{g}}(t) \tag{6.8}$$

where $\{Z(t)\}$ is state vector, $[A]$ is the plant matrix, $[B_{\mathrm{u}}]$ is coefficient matrix of the control command vector $\{u(t)\}$ and $\{B_{\mathrm{r}}\}$ is coefficient vector of reference input (i.e., earthquake excitation) $\ddot{x}_{\mathrm{g}}(t)$. Chapters 4 and 5 show these vectors and matrices can have different elements in different systems.

For a digital seismic response control system, the plant equation becomes

$$z(k+1) = Az(k) + B_{\mathrm{u}}u(k) + B_{\mathrm{r}}r(k) \tag{6.9}$$

where $z(k)$, $u(k)$, and $r(k)$ are sampled values of $\{Z(t)\}, \{u(t)\}$, and $\ddot{x}_{\mathrm{g}}(t)$ at kth sampling time (i.e., at $t = kT, k = 0, 1, 2, \ldots, +\infty$), respectively, and T is sampling period; matrices A, B_{u}, and B_{r} are defined in Equation 5.114 and rectangular rule is used for the integration.

6.3.1.2 Equation for sensor output

For seismic response control, the signals are in the frequency range of 0.1–100 Hz. Sensors can work as linear proportional devices in this range [5,8,29], that is, the sensor output (usually voltage signal) is proportional to the measurand. Assume

that there are s_1 accelerometers and s_2 state sensors; then the sensor output $\{y(t)\}$ can be modeled as

$$\{y(t)\} = \begin{bmatrix} [C_1]\{\ddot{x}(t)\} \\ [C_2]\{Z(t)\} \end{bmatrix} \tag{6.10}$$

where $[C_1]$ of $s_1 \times n$ and $[C_2]$ of $s_2 \times N$ are location matrices of accelerometers and other kinds of sensors (such as load cells), respectively; $C_1(i,j) = 1$ if the ith accelerometer is mounted on the jth floor and $C_2(i,j) = 1$ if the ith sensor is used to measure the jth state variables; n is number of d.o.f. The order of $\{y(t)\}$ is equal to the total number of sensors, $S = (s_1 + s_2)$. S is usually smaller than the order of the system (i.e., the order of plant matrix $[A]$), N.

The motion equation of smart seismic structures, Equation 5.58, can be rewritten as

$$\begin{aligned} \{\ddot{x}(t)\} = -[M]^{-1}\big([C]\{\dot{x}(t)\} + [K]\{x(t)\}\big) + [M]^{-1}\big([\gamma_a]\{f_a(t)\} \\ + [\gamma_p]\{f_p(t)\} + \{\delta\}\ddot{x}_g(t)\big) \end{aligned} \tag{6.11}$$

Substituting it into Equation 6.10 yields

$$\{y(t)\} = [C_z]\{Z(t)\} + [D_u]\{u(t)\} + \{D_r\}\ddot{x}_g(t) \tag{6.12a}$$

where

$$[C_z] = \begin{bmatrix} [C_{z1}] \\ [C_{z2}] \end{bmatrix}, \quad [D_u] = \begin{bmatrix} [0] \\ [0] \end{bmatrix}, \quad [D_r] = \begin{bmatrix} -[C_1][M]^{-1}\{\delta\} \\ \{0\} \end{bmatrix} \tag{6.12b}$$

and

$$[C_{z1}] = [C_1][M]^{-1}\begin{bmatrix} -[K] & -[C] & [\gamma_a] & [\gamma_p] & [0] \end{bmatrix}, \quad [C_{z2}] = [C_2] \tag{6.12c}$$

In discrete time domain, the sensor equation can be expressed as

$$y(k) = Cz(k) + D_u u(k) + D_r r(k) \tag{6.13}$$

Then the entire system is described by Equations 6.9 and 6.13. Since the sensor equation (Equation 6.12) is in algebraic proportion relation, matrices C, D_u, and vector D_r in Equation 6.13 are the same as $[C_z]$, $[D_u]$, and $[D_r]$ in Equation 6.12a, respectively.

Equation 6.13 shows that the sensor output $y(k)$ is not state variable $z(k)$, but rather linear transformation of state variables and related to control command $u(k)$ and reference input $r(k)$. If an optimal control algorithm by full-state feedback is to be implemented, a technique must be employed to estimate all state variables from the sensor output, $y(k)$.

6.3.2 Conventional Observer Technique

An Nth order linear control system using state sensors can be modeled as

$$z(k+1) = Az(k) + Bu(k) \tag{6.14a}$$

$$y(k) = Cz(k) \tag{6.14b}$$

Since state sensors are used and each sensor output is equal to a state variable, the sensor equation here (Equation 6.14b is different from Equation 6.13. Elements in matrix C are zero except that $C(i,j) = 1$ if the ith sensor measures the jth state variable.

This system described by Equation 6.14 is observable if the initial state, $z(0)$, can be calculated from N measurements, $y(0)$, $y(1)$, $y(2), \ldots, y(N-1)$, with N finite. This definition comes with the following theorem: the Nth order system described by Equation 6.14 is observable if and only if its observability matrix M_o, defined by the following equation, is of rank N [10,12,18]:

$$M_o = \begin{bmatrix} C \\ CA \\ CA^2 \\ \vdots \\ CA^{N-1} \end{bmatrix} \tag{6.15}$$

If a system is observable, available measurements are sufficient to estimate all state variables by means of the observer technique. The controller then uses these estimated states to generate control action, $u(k)$, according to the full-state feedback algorithm. Figure 6.12 illustrates the observer configuration and its application in a control system.

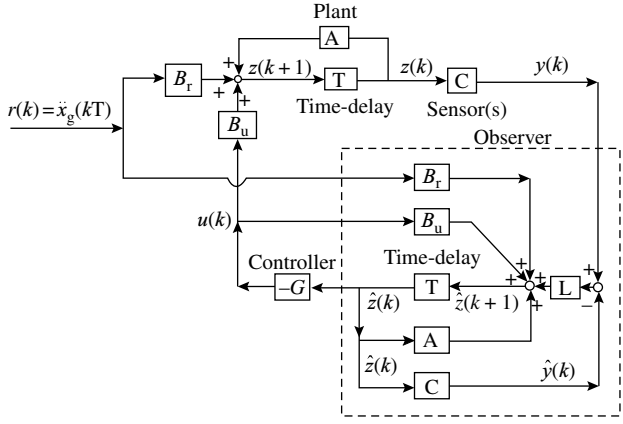

FIGURE 6.12 Closed-loop system with observer and controller.

The optimum control algorithm yields the following full-state feedback law:

$$u(k) = -Gz(k) \tag{6.16}$$

where G is control gain matrix determined by the control algorithm. For the observer-controller system shown in Figure 6.12, Equation 6.16 becomes

$$u(k) = -G\hat{z}(k) \tag{6.17}$$

and the observer is described by

$$\hat{z}(k+1) = A\hat{z}(k) + B_{\mathrm{u}}u(k) + B_{\mathrm{r}}r(k) + L[y(k) - \hat{y}(k)] \tag{6.18a}$$

$$\hat{y}(k) = C\hat{z}(k) \tag{6.18b}$$

Modern control theory [10,12] has shown that the system (Equation 6.14) with observer (Equation 6.18) and control law (Equation 6.17) has exactly the same transfer function from $r(k)$ to $y(k)$ as the full-state feedback system described by Equations 6.14 and 6.16. This means, in theory, an observer-controller technique is as effective as full-state sensing and feedback.

When configuring the observer, measurements of reference input $r(k)$ and control input $u(k)$ are assumed to be available in addition to $y(k)$, and the open-loop dynamics of the observer is selected the same as the plant. Note that only matrix L is unknown in the observer model (see Equation 6.18). The determination of matrix L is called *observer design*. The criterion for picking L should be that $\hat{z}(k)$ tends to $z(k)$ as soon as possible. Let error function be

$$\tilde{z}(k) = z(k) - \hat{z}(k) \tag{6.19a}$$

Then from Equations 6.14, 6.18, and 6.19a

$$\tilde{z}(k+1) = (A - LC)\tilde{z}(k) = A_{\mathrm{L}}\tilde{z}(k) \tag{6.19b}$$

where

$$A_{\mathrm{L}} = A - LC \quad \text{and} \quad A_{\mathrm{L}}^{\mathrm{T}} = A^{\mathrm{T}} - C^{\mathrm{T}}L^{\mathrm{T}} \tag{6.19c}$$

Recall that a closed-loop control system with gain matrix G is modeled as

$$z(k+1) = (A - B_{\mathrm{u}}G)z(k) = A_{\mathrm{c}}z(k) \tag{6.20a}$$

where

$$A_{\mathrm{c}} = A - B_{\mathrm{u}}G \tag{6.20b}$$

The comparison of Equations 6.19c and 6.20b shows that the observer design (to determine L) is similar to the controller design (to determine G) except that the dynamics of A^{T} is improved by C^{T} instead of A by B_{u}. Thus, L^{T} can be

determined by optimal control algorithms. Kalman filter is an example of optimal observer [12,18].

Note that this conventional observer theory implicitly assumes that sensors are used to measure state variables. This is because the observer is based on a system in which sensor output is proportional to state variables, as shown in Equation 6.14b. Enough state sensors must be employed to meet the observability requirement expressed by Equation 6.15. A seismic response control system may have no state sensor but accelerometers; state measurements required by this observer theory may not be available. Therefore, this observer technique cannot be directly applied to seismic response control.

Example 6.3.1

The two-story smart structure in Example 4.2.2 serves as an example here. Assume there is only one displacement sensor installed at the top of the structure. Check the system observability and design the observer.

Solution

As the Equation q in Example 4.2.2 shows, state variables of this system include the displacements and velocities at each story of the structure. Thus,

$$\{Z(t)\} = \{x_1(t) \quad x_2(t) \quad \dot{x}_1(t) \quad \dot{x}_2(t)\}^{\mathrm{T}} \tag{a}$$

The sensor output can be expressed as

$$y(t) = x_2(t) = [C]\{Z(t)\} \tag{b}$$

where

$$[C] = [0 \quad 1 \quad 0 \quad 0] \tag{c}$$

The system plant matrix has been calculated in Example 4.2.2 as

$$[A] = \left[\begin{array}{cc|cc} 0 & 0 & 1 & 0 \\ 0 & 0 & 0 & 1 \\ \hline -551.475 & 325.738 & -0.421 & 0.146 \\ 671.234 & -671.234 & 0.300 & -0.474 \end{array}\right] \tag{d}$$

Then

$$[C][A] = [\,0 \quad 0 \quad 0 \quad 1] \tag{e}$$

$$[C][A]^2 = [\,671.234 \quad -671.234 \quad 0.300 \quad -0.474] \tag{f}$$

$$[C][A]^3 = [\,-483.607 \quad 415.886 \quad 670.965 \quad -670.965] \tag{g}$$

Substituting Equations c and e–g into Equation 6.15 yields the observability matrix of this system

$$[M_o] = \begin{bmatrix} 0 & 1 & 0 & 0 \\ 0 & 0 & 0 & 1 \\ 671.234 & -671.234 & 0.300 & -0.474 \\ -483.607 & 415.886 & 670.965 & -670.965 \end{bmatrix} \quad \text{(h)}$$

The rank of above observability matrix can be directly checked by MATLAB® function $RANK(M_o)$ [22], which gives in 4, that is, it is full rank. It can also be checked by calculating its eigenvalues with MATLAB® function $EIG(M_o)$ that yields the four eigenvalues

$$p_1 = 672.11; \quad p_{2,3} = 0.223 \pm 25.913j; \quad p_4 = 0.998 \quad \text{(i)}$$

where $j = \sqrt{-1}$. Equation i shows that the observability matrix is full rank for it has no zero eigenvalue. Thus, this system is observable with one displacement sensor at top.

The governing equation for observer design is Equation 6.19c in which matrices A and C are given and observer gain matrix L is to be determined. As noted, a comparison of Equations 6.19c and 6.20b shows that the observer design is similar to controller design except that the transposed form in Equation 6.19c shall be used. Thus, the Riccati optimal control algorithm is used here to determine the observer gain matrix $[L]$. The transpose of matrices $[A]$ and $[C]$ are

$$[A]^T = \begin{bmatrix} 0 & 0 & -551.475 & 671.234 \\ 0 & 0 & 325.738 & -671.234 \\ 1 & 0 & -0.421 & 0.300 \\ 0 & 1 & 0.146 & -0.474 \end{bmatrix}; \quad [C]^T = \begin{Bmatrix} 0 \\ 1 \\ 0 \\ 0 \end{Bmatrix} \quad \text{(j)}$$

Let the weighting matrices in the algebraic Riccati equation (see Equation 4.99) be

$$[Q] = \begin{bmatrix} 1 & 0 & 0 & 0 \\ 0 & 1 & 0 & 0 \\ 0 & 0 & 1 & 0 \\ 0 & 0 & 0 & 1 \end{bmatrix}; \quad R = 0.01 \quad \text{(k)}$$

Use the MATLAB® function $LQR(\ldots)$ to solve the algebraic Riccati equation with the syntax

$$\gg \text{LT} = \text{LQR(AT, CT, Q, R)} \quad \text{(l)}$$

then the observer gain matrix $[L]$ is obtained as

$$[L]^T = \begin{bmatrix} 1.540 & 15.949 & -67.172 & 77.182 \end{bmatrix} \quad \text{(m)}$$

or

$$[L] = \begin{bmatrix} 1.540 & 15.949 & -67.172 & 77.182 \end{bmatrix}^{\mathrm{T}} \tag{n}$$

Thus the closed-loop observer plant matrix

$$\begin{aligned} [A]_{\mathrm{L}} &= [A] - [L][C] \\ &= \begin{bmatrix} 0 & 0 & 1 & 0 \\ 0 & 0 & 0 & 1 \\ -551.475 & 325.738 & -0.421 & 0.146 \\ 671.234 & -671.234 & 0.300 & -0.474 \end{bmatrix} \\ &\quad - \begin{Bmatrix} 1.540 \\ 15.949 \\ -67.172 \\ 77.182 \end{Bmatrix} \begin{bmatrix} 0 & 0 & 1 & 0 \end{bmatrix} \\ &= \begin{bmatrix} 0 & -1.540 & 1 & 0 \\ 0 & -15.949 & 0 & 1 \\ -551.48 & 392.910 & -0.421 & 0.146 \\ 671.234 & -748.420 & 0.300 & -0.474 \end{bmatrix} \end{aligned} \tag{o}$$

and its eigenvalues can be calculated by MATLAB® function *EIG*(*AL*) as

$$p_{1,2} = -0.329 \pm 32.904j; \quad p_{3,4} = -0.118 \pm 11.829j \tag{p}$$

Since all its poles are in left side of the complex plane, the observer is stable. Details on how this example uses MATLAB® functions are listed in Section A.2 of Appendix A.

6.3.3 Development of Observer Technique for Smart Seismic Structures

As discussed in Section 6.3.1, a seismic response control system can be modeled by Equations 6.8 and 6.12a in the continuous time domain, or by Equations 6.9 and 6.13 in discrete time domain. Since digital control is getting more common with the advance of microcomputers, the seismic observer technique is developed in discrete time domain. A similar procedure can be used to develop a seismic observer for an analog system.

6.3.3.1 Formulation of the seismic observer

Equation 6.18 is the proposed mathematical model of the conventional observer for the control system expressed by Equation 6.14. Since the model of a smart seismic structure system has two extra terms $D_{\mathrm{u}}u(k)$ and $D_{\mathrm{r}}r(k)$ in the sensor

equation (see Equation 6.13), the seismic observer may be configured by adding these two terms to Equation 6.18b. Then Equation 6.18 becomes

$$\hat{z}(k+1) = A\hat{z}(k) + B_u u(k) + B_r r(k) + L[\,y(k) - \hat{y}(k)] \tag{6.21a}$$

$$\hat{y}(k) = C\hat{z}(k) + D_u u(k) + D_r r(k) \tag{6.21b}$$

Equation 6.21 is the mathematical model of the seismic observer. A seismic response control system with this observer, called seismic observer-controller system, is then described by a combination of Equations 6.9, 6.13, 6.17, and 6.21. Simulation diagram of this system is shown by Figure 6.13. A comparison of the seismic observer (see Figure 6.13) and the conventional observer (see Figure 6.12) shows that the seismic observer does not require any extra measurements but $u(k)$, $r(k)$, and $y(k)$. Moreover, this observer can be realized totally by similar computer software for controller implementation. No additional device is needed.

6.3.3.2 Closed-form verification

To ensure the validity of this observer configuration, it must be verified that the observer-controller system functions the same as the corresponding full-state sensing and feedback system. This can be done by proving that the observer-controller system has the same transfer function between input $r(k)$ and output $y(k)$ as the full-state sensing and feedback system.

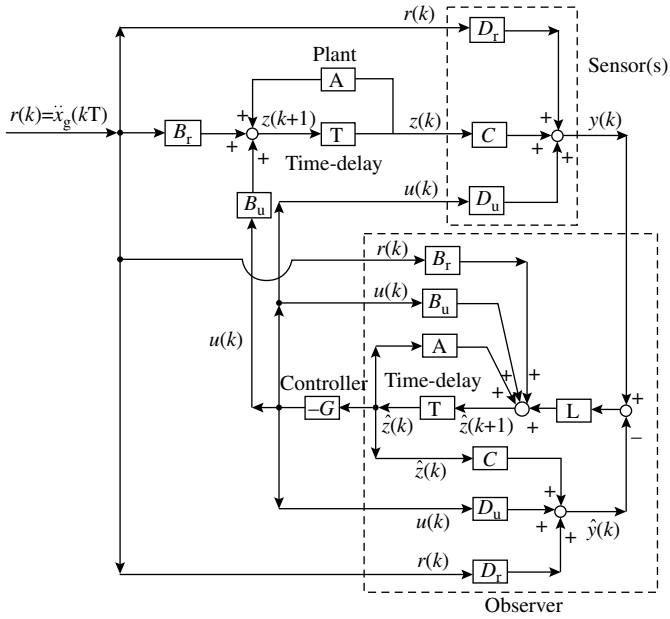

FIGURE 6.13 Simulation diagram of seismic response control system with observer.

A seismic response control system with full-state sensing and feedback can be described by Equations 6.9, 6.13, and 6.16. Substituting Equation 6.16 into Equations 6.9 and 6.13 yields the system model in closed-loop as

$$z(k+1) = (A - B_{\mathrm{u}}G)\, z(k) + B_{\mathrm{r}} r(k) \tag{6.22a}$$

$$y(k) = (C - D_{\mathrm{u}}G)\, z(k) + D_{\mathrm{r}} r(k) \tag{6.22b}$$

For digital systems, a transfer function is usually expressed in z-domain. Applying z-transform to Equation 6.22 leads to

$$(zI - A + B_{\mathrm{u}}G)\, Z(z) = B_{\mathrm{r}} R(z) \tag{6.23a}$$

$$Y(z) = (C - D_{\mathrm{u}}G)\, Z(z) + D_{\mathrm{r}} R(z) \tag{6.23b}$$

where I is unit matrix. Equation 6.23a can be rewritten as

$$Z(z) = (zI - A + B_{\mathrm{u}}G)^{-1} B_{\mathrm{r}} R(z) \tag{6.24}$$

Substituting Equation 6.24 into Equation 6.23b yields the transfer function from $r(k)$ to $y(k)$ of the full-state sensing and feedback system as

$$T_1(z) = \frac{Y(z)}{R(z)} = (C - D_{\mathrm{u}}G)\,(zI - A + B_{\mathrm{u}}G)^{-1} B_{\mathrm{r}} + D_{\mathrm{r}} \tag{6.25}$$

A seismic response control system with the observer-controller can be described by Equations 6.9, 6.13, 6.17, and 6.21; $y(k)$ and $\hat{y}(k)$ are defined by Equations 6.13 and 6.21b, respectively. Substituting them into the observer plant equation, that is, Equation 6.21a, yields

$$\begin{aligned}
&\hat{z}(k+1) \\
&\quad = A\hat{z}(k) + B_{\mathrm{u}}u(k) + B_{\mathrm{r}}r(k) + L[Cz(k) + D_{\mathrm{u}}u(k) + D_{\mathrm{r}}r(k) - C\hat{z}(k) \\
&\qquad - D_{\mathrm{u}}u(k) - D_r r(k)] \\
&\quad = LCz(k) + (A - LC)\,\hat{z}(k) + B_{\mathrm{u}}u(k) + B_{\mathrm{r}}r(k)
\end{aligned} \tag{6.26}$$

Substituting Equations 6.17–6.26 yields the observer model in closed loop as

$$\begin{aligned}
\hat{z}(k+1) &= LCz(k) + (A - LC)\hat{z}(k) - B_{\mathrm{u}}G\hat{z}(k) + B_{\mathrm{r}}r(k) \\
&= LCz(k) + (A - B_{\mathrm{u}}G - LC)\hat{z}(k) + B_{\mathrm{r}}r(k)
\end{aligned} \tag{6.27a}$$

and substituting Equation 6.17 into Equation 6.9 yields the plant equation of the control system in closed-loop as

$$z(k+1) = Az(k) - B_{\mathrm{u}}G\hat{z}(k) + B_{\mathrm{r}}r(k) \tag{6.27b}$$

Equations 6.27a and b can be condensed in matrix form as

$$\begin{Bmatrix} z(k+1) \\ \hat{z}(k+1) \end{Bmatrix} = \begin{bmatrix} A & -B_u G \\ LC & A - B_u G - LC \end{bmatrix} \begin{Bmatrix} z(k) \\ \hat{z}(k) \end{Bmatrix} + \begin{Bmatrix} B_r \\ B_r \end{Bmatrix} r(k) \tag{6.27c}$$

Equation 6.27c is the mathematical model of the observer-controller system in closed-loop. It shows that this system is of the $2N$th order, where N is the order of plant matrix A. This means that the observer-controller system here has more mode shapes than a full-state sensing and feedback system. Thus, it is important to verify the function of the observer-controller system. A closed-form formulation, described as follows, is used for this verification.

Applying z-transform to Equation 6.27c gives

$$B_u G\hat{Z}(z) + (zI - A)Z(z) = B_r R(z) \tag{6.28a}$$

$$(zI - A + B_u G + LC)\,\hat{Z}(z) - LCZ(z) = B_r R(z) \tag{6.28b}$$

Eliminating $\hat{Z}(z)$ in Equation 6.28 leads to

$$\begin{aligned} &\left[zI - A + B_u G\,(zI - A + B_u G + LC)^{-1} LC\right] Z(z) \\ &\quad = \left[I - B_u G\,(zI - A + B_u G + LC)^{-1}\right] B_r R(z) \end{aligned} \tag{6.29}$$

The Lemma for frame matrix inversion is expressed as

$$\left[I + \varphi(zI - \alpha)^{-1}\beta\right]^{-1} = I - \varphi(zI - \alpha + \beta\varphi)^{-1}\beta \tag{6.30}$$

Let

$$\varphi = B_u G, \quad \alpha = A - B_u G - LC, \quad \beta = -I \tag{6.31}$$

Then the following two equations are obtained by applying the Lemma in Equation 6.30

$$\begin{aligned} &\left[I - B_u G(zI - A + B_u G + LC)^{-1}\right]^{-1} \\ &\quad = I + B_u G(zI - A + B_u G + LC - B_u G)^{-1} \\ &\quad = I + B_u G(zI - A + LC)^{-1} \\ &zI - A + B_u G(zI - A + B_u G + LC)^{-1} LC \\ &\quad = zI - A + LC - LC + B_u G(zI - A + B_u G + LC)^{-1} LC \\ &\quad = (zI - A + LC) - \left[I - B_u G(zI - A + B_u G + LC)^{-1}\right] LC \end{aligned} \tag{6.32}$$

$$= (zI - A + LC) - \left[I + B_u G(zI - A + LC)^{-1}\right]^{-1} LC$$
$$= (zI - A + LC) - \left[(zI - A + LC + B_u G)(zI - A + LC)^{-1}\right]^{-1} LC$$
$$= (zI - A + LC) - (zI - A + LC)(zI - A + LC + B_u G)^{-1} LC$$
$$= (zI - A + LC)\left[I - (zI - A + LC + B_u G)^{-1} LC\right] \tag{6.33}$$

Substituting Equations 6.32 and 6.33 into Equation 6.29 yields

$$\begin{aligned} B_r R(z) &= \left[I - B_u G\,(zI - A + B_u G + LC)^{-1}\right]^{-1} [zI - A \\ &\quad + B_u G(zI - A + B_u G + LC)^{-1} LC] Z(z) \\ &= \left[I + B_u G\,(zI - A + LC)^{-1}\right] \left\{(zI - A + LC)\left[I - (zI - A + B_u G \right.\right. \\ &\quad \left.\left. + LC)^{-1} LC\right]\right\} Z(z) \\ &= (zI - A + LC + B_u G)\left[I - (zI - A + LC + B_u G)^{-1} LC\right] Z(z) \\ &= [(zI - A + LC + B_u G) - LC]\, Z(z) \\ &= (zI - A + B_u G)\, Z(z) \end{aligned} \tag{6.34a}$$

which can be rewritten as

$$Z(z) = (zI - A + B_u G)^{-1} B_r R(z) \tag{6.34b}$$

Substituting Equation 6.34a into Equation 6.28a yields

$$B_u G\hat{Z}(z) + (zI - A)Z(z) = (zI - A + B_u G)Z(z) \tag{6.35a}$$

Thus,

$$\hat{Z}(z) = Z(z) \tag{6.35b}$$

Equation 6.35b shows that, in theory, the observer output is exactly the same as the full-state vector in z-domain. This result verifies the function of the seismic observer. In practice, errors in $\hat{Z}(z)$ exist due to system nonlinearity, noises, and nonzero initial conditions.

Substituting Equation 6.17 into Equation 6.13 yields

$$y(k) = Cz(k) - D_u G\hat{z}(k) + D_r r(k) \tag{6.36a}$$

Applying z-transform to Equation 6.36a gives

$$Y(z) = CZ(z) - D_u G\hat{Z}(z) + D_r R(z) \tag{6.36b}$$

and with Equation 6.35b

$$Y(z) = (C - D_u G)Z(z) + D_r R(z) \tag{6.36c}$$

Substituting Equations 6.34b into 6.36c yields the corresponding transfer function

$$T_2(z) = \frac{Y(z)}{R(z)} = (C - D_u G)\,(zI - A + B_u G)^{-1} B_r + D_r \tag{6.37}$$

which is exactly same as Equation 6.25. This means that the response of the observer-controller system is identical to that of the full-state sensing and feedback system. Thus, with the seismic observer shown in Figure 6.13, any full-state feedback control algorithm can be implemented if the number of sensors, including accelerometers, meets the observability requirement. If a system is observable, measurements are sufficient for the observer to estimate the full-state vector. Consequently, the minimum required number of sensors can be determined by the observability requirement, as discussed in the following section.

6.3.4 Simplified Sensing System for Smart Seismic Structures

The seismic observer is able not only to estimate state variables from acceleration measurements, but also to simplify the sensing system. This section will determine the minimum required sensors for a smart structure system using the seismic observer, which would demonstrate the great potential of sensing system simplification by the seismic observer.

6.3.4.1 Analytical studies

As in Section 6.3.2, the observability requirement (see Equation 6.15) determines if the available number of sensors is sufficient to estimate the full-state vector by observer technique. Since the rank of observability matrix M_o cannot be calculated unless the number and location of sensors are known, the minimum required number of sensors cannot be explicitly determined by closed-form formulation. To make this determination, a trial-and-error procedure described below can be used.

An n-story shear building with r active tendons (see Figure 6.14) serves as an example to determine the minimum required number of sensors. All actuators in the active tendon control system are considered as linear proportional devices. It is first assumed that there is only one sensor at the top floor. Then system observability

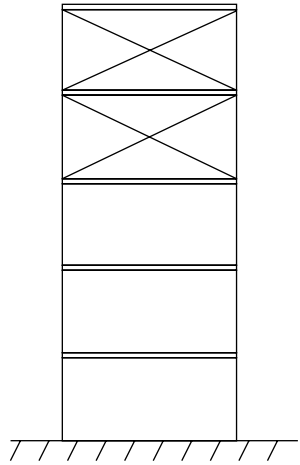

FIGURE 6.14 Shear building with active tendon control.

is checked by determining if the observability matrix is of full rank. If not, add one more sensor to the structure and check the rank of the observability matrix again. Repeat this trial-and-error procedure until the observability requirement is met. If the observability requirement can be met with a small number of sensors, there is great potential for the observer technique to simplify the sensing and data acquisition system.

The plant equation in the state-variable representation of the structure with active tendon control has been derived in Chapter 4 as

$$\left\{\dot{Z}(t)\right\} = [A]\{Z(t)\} + [B_{\mathrm{u}}]\{u(t)\} + \{B_{\mathrm{r}}\}\ddot{x}_{\mathrm{g}}(t) \tag{6.38}$$

where $\{Z(t)\}$ and $\{u(t)\}$ are state vector and vector of control commands, respectively, and can be expressed as

$$\{Z(t)\} = [x_1(t), x_2(t), \ldots, x_n(t); \dot{x}_1(t), \dot{x}_2(t), \ldots, \dot{x}_n(t)]^{\mathrm{T}} \tag{6.39}$$

$$\{u(t)\} = [u_1(t), u_2(t), \ldots, u_{\mathrm{r}}(t)]^{\mathrm{T}} \tag{6.40}$$

and coefficient matrices $[A]$, $[B_{\mathrm{u}}]$, and $\{B_{\mathrm{r}}\}$ are expressed as

$$[A] = \begin{bmatrix} [0] & [I] \\ -[M]^{-1}[K] & -[M]^{-1}[C] \end{bmatrix}_{2n\times 2n} \tag{6.41a}$$

$$[B_{\mathrm{u}}] = \begin{bmatrix} [0] \\ [M]^{-1}[\gamma] \end{bmatrix}_{2n\times r} \tag{6.41b}$$

$$\{B_r\} = \begin{Bmatrix} \{0\} \\ [M]^{-1}\{\delta\} \end{Bmatrix}_{2n\times 1} \tag{6.41c}$$

In Equation 6.41, matrices of mass, stiffness, and damping, $[M]$, $[K]$, and $[C]$, respectively, of shear buildings are defined by Equation 4.14; $[\gamma]$ is location matrix of active tendons; its elements are zero except that $\gamma(i,j) = 1$ if jth active tendon is attached on ith floor; $\{\delta\}$ is vector of coefficients for earthquake excitation $\ddot{x}_g(t)$ defined as

$$\{\delta\} = [-m_1 \ -m_2 \ \cdots \ -m_n]^T \tag{6.42}$$

Equations 6.38 and 6.39 show that this is a $2n$th order system. Full-state sensing and feedback technique requires $2n$ sensors (n displacement sensors and n velocity sensors). This complicates the control hardware and the sensing and data acquisition system when a building has many stories. Thus, it is significant to study the possibility of simplifying the system with the seismic observer technique.

First, the case of only an LVDT (displacement sensor) at the top floor is considered. The sensor equation can be expressed as

$$y(t) = [C]\{Z(t)\} \tag{6.43}$$

where

$$\begin{array}{rcccccccc} [C] = [0 & 0 & \ldots & 0 & 1; & 0 & 0 & \ldots & 0\ ] \\ 1 & 2 & \ldots & n-1 & n & n+1 & n+2 & \ldots & 2n \end{array} \tag{6.44}$$

To determine if this system is observable, that is, to check if the observability matrix is of full rank, four theorems are introduced as follows.

Theorem 1. $[A]_{2n\times 2n}$ is a full-rank matrix.

Proof If $[A]$ is not a full-rank matrix, it should have one or more zero eigenvalues. In fact, eigenvalues of matrix $[A]$ are

$$-\zeta_i\omega_i \pm \sqrt{1-\zeta_i^2}\omega_i j, \quad i = 1, 2, \ldots, n \tag{6.45}$$

where ζ_i and ω_i are ith damping ratio and natural frequency, $j = \sqrt{-1}$. If any eigenvalue of $[A]$ is zero, the corresponding ζ_i and ω_i are both zero. This cannot be true for civil engineering structures that are stable and statically indeterminate. Thus, $[A]$ must be a full-rank matrix.

Theorem 2. Matrix M_{oa}, defined as follows, is of rank n.

$$M_{oa} = \begin{bmatrix} [C] \\ [C][A] \\ [C][A]^2 \\ \cdots \\ [C][A]^{n-1} \end{bmatrix} \tag{6.46}$$

This is because

$$\begin{array}{rcccccc}
 & 1\ \ldots n-1 & n-2 & n & n+1\ldots 2n-2 & 2n-1 & 2n \\
[C] = & [0\ldots 0 & 0 & 1 & 0\quad\ldots 0 & 0 & 0] \\
[C][A] = & [0\ldots 0 & 0 & 0 & 0\quad\ldots 0 & 0 & 1] \\
[C][A]^2 = & [0\ldots 0 & k_n/m_n & -k_n/m_n & 0\quad\ldots 0 & c_n/m_n & -c_n/m_n] \\
[C][A]^3 = & [0\ldots s(3,n-2) & s(3,n-1) & s(3,n) & 0\quad\ldots s(3,2n-2) & s(3,2n-1) & s(3,2n)]
\end{array} \tag{6.47}$$

and so on; where

$$\begin{cases}
s(3,n-2) = \dfrac{c_n k_{n-1}}{m_n m_{n-1}} & s(3,2n-2) = \dfrac{c_n c_{n-1}}{m_n m_{n-1}} \\
s(3,n-1) = -\dfrac{c_n k_{n-1}}{m_n^2} - \dfrac{c_n(k_n + k_{n-1})}{m_n m_{n-1}} & s(3,2n-1) = -\dfrac{k_n}{m_n} + \dfrac{c_n^2}{m_n^2} - \dfrac{c_n(c_n + c_{n-1})}{m_n m_{n-1}} \\
s(3,n) = \dfrac{c_n k_n}{m_n m_{n-1}} + \dfrac{c_n k_n}{m_n^2} & s(3,2n) = \dfrac{k_n}{m_n} + \dfrac{m_n^2}{m_n m_{n-1}} - \dfrac{c_n^2}{m_n^2}
\end{cases} \tag{6.48}$$

Thus,

$$M_{\text{oa}} = \begin{bmatrix}
0 & 0 & 0 & \cdots & 0 & 0 & 1 & 0 & 0 & 0 & \cdots & 0 & 0 & 0 \\
0 & 0 & 0 & \cdots & 0 & 0 & 0 & 0 & 0 & 0 & \cdots & 0 & 0 & 1 \\
0 & 0 & 0 & \cdots & 0 & * & * & 0 & 0 & 0 & \cdots & 0 & * & * \\
\cdots & \cdots & \cdots & \cdots & \cdots & \cdots & \cdots & \cdots & \cdots & \cdots & \cdots & \cdots & \cdots & \cdots \\
0 & 0 & * & \cdots & * & * & * & 0 & 0 & * & \cdots & * & * & * \\
0 & * & * & \cdots & * & * & * & 0 & * & * & \cdots & * & * & *
\end{bmatrix}_{n\times 2n} \tag{6.49}$$

where the symbol $*$ refers to a nonzero element. After full Gauss elimination, each row still has at least one nonzero element. Thus, matrix M_{oa} has n linearly unrelated rows, that is, it is of rank n.

Theorem 3. Matrix M_{ob}, defined as follows, is of rank n.

$$M_{\text{ob}} = \begin{bmatrix} [C][A]^n \\ [C][A]^{n+1} \\ \cdots \\ [C][A]^{2n-1} \end{bmatrix} = \begin{bmatrix} [C] \\ [C][A] \\ \cdots \\ [C][A]^{n-1} \end{bmatrix} [A]^n = M_{\text{oa}}[A]^n \tag{6.50}$$

Proof Two Lemmas in linear algebra theory are introduced to prove this theorem.

Lemma 1. If matrix $A_{m\times n}$ is of rank r and matrix $B_{n\times n}$ is of full rank, then matrix $C_{m\times n} = A_{m\times n}B_{n\times n}$ is of rank r, where $r \le \min(m,n)$.

Lemma 2. The product of two full-rank matrices is of full rank.

From Lemma 2, A^n is of full rank $2n$ because A is of full rank $2n$. From Lemma 1, M_{ob} is of rank n because M_{oa} is of rank n and A^n is of full rank $2n$.

Theorem 4. Matrix M_{oc}, defined as follows, is of rank $(n+1)$.

$$M_{oc} = \begin{bmatrix} [C] \\ [C][A] \\ \cdots \\ [C][A]^{n-1} \\ [C][A]^{i} \end{bmatrix} = \begin{bmatrix} M_{oa} \\ [C][A]^{i} \end{bmatrix}, \quad i = n, n+1, \ldots, 2n-1 \tag{6.51}$$

This is because $[C][A]^i = [*, *, \cdots, *, *, \cdots, *]$, that is, all elements are nonzero. Thus $[C][A]^i$ is linearly unrelated to any row of M_{oa}, which means M_{oa} is of rank $(n+1)$.

Theorem 4 shows that any row of full-rank matrix M_{ob} is not linearly related to full rank matrix M_{oa}; thus, the observability matrix, $M_{o1} = \begin{bmatrix} M_{oa} \\ M_{ob} \end{bmatrix}$, is of full-rank $2n$. This means that only one LVDT is enough for the observer to estimate the full-state vector.

Second, the case that only an accelerometer is installed at the top floor is considered. The sensor equation can be expressed as

$$y(t) = [C']\{z(t)\} + [D_u]\{u(t)\} + \{D_r\}\ddot{x}_g(t) \tag{6.52}$$

where

$$\begin{aligned} [C'] &= \Big[0 \;\; 0 \;\; \cdots \;\; \tfrac{k_{n-1}}{m_n} \;\; -\tfrac{k_n}{m_n};\; 0 \;\; 0 \;\; \cdots \;\; \tfrac{c_{n-1}}{m_n} \;\; -\tfrac{c_n}{m_n}\Big] \\ &\quad\; 1 \;\; 2 \;\; \cdots \;\; n-1 \;\; n; \qquad n+1 \;\; n+2 \;\; \cdots \;\; 2n-1 \;\; 2n \\ &= [\; 0 \;\; 0 \;\; \cdots \;\; 0 \;\; 1;\; 0 \;\; 0 \;\; \cdots \;\; 0 \;\; 0 \;\;][A]^2 \\ &= [C][A]^2 \end{aligned} \tag{6.53}$$

The sensor equation in discrete time domain is the same as Equation 6.52 because it is in proportional relation. Then the observability matrix is

$$M_{o2} = \begin{bmatrix} [C'] \\ [C'][A] \\ [C'][A]^2 \\ \cdots \\ [C'][A]^{2n-1} \end{bmatrix} = -\begin{bmatrix} [C][A]^2 \\ [C][A]^3 \\ [C][A]^4 \\ \cdots \\ [C][A]^{2n+1} \end{bmatrix} = -\begin{bmatrix} [C] \\ [C][A] \\ [C][A]^2 \\ \cdots \\ [C][A]^{2n-1} \end{bmatrix} [A]^2 = -M_{o1}[A]^2 \tag{6.54}$$

Since both M_{o1} and A^2 are of full rank, M_{o2} is of full rank, and the system is observable. This result shows that the required number of sensors can be reduced from $2n$ to 1 if a seismic observer is employed by the smart structure system.

Thus, the observer technique can greatly simplify the sensing and data acquisition system for seismic response control.

6.3.4.2 Numerical illustrations

In order to verify the analytical formulation and demonstrate the effectiveness of the proposed seismic observer technique, two numerical examples are employed as follows. The advantages of a seismic observer are illustrated by comparing the required number of sensors and closed-loop response of the observer-controller system to those of the full-state sensing and feedback system. For time-history analysis, scaled N–S component of the El-Centro earthquake is adopted (scale factors for amplitude and frequency are 0.3 and 2, respectively).

6.3.4.2.1 Three-story smart seismic structure with HDABC system

This system, as shown in Figure 5.21, installs a hybrid control device on a K-brace at the first floor. An accelerometer is used to measure acceleration response at the top floor, and a load cell is employed to measure active control force. The structural properties and parameters of control devices are given in Section 5.3.3.2.

From the formulation in Section 5.3.3.2 and Equation 5.142, it is shown that state variables for this smart structure with the HDABC system comprise three displacements and three velocities for the three-story building, one displacement and one velocity for the K-brace, active control force and servo-valve displacement for the hydraulic actuator, and passive control force for the viscous fluid damper. Thus, this hybrid control system is of the 11th order, and 11 sensors must be used to implement an optimal control algorithm by full-state sensing and feedback.

To evaluate the potential system simplification and the effectiveness of the observer-controller technique, computer simulation with MATLAB®. *m* code is used to analyze the hybrid-controlled smart structure system. Linear quadratic and pole assignment control algorithms are used for controller and observer design.

With an accelerometer at the top floor and a load cell for active control force, numerical results indicate that observability matrix M_0 is of rank 11, so the system is observable. Figure 6.15 shows that, consistent with the theory, closed-loop displacement response of the observer-controller system is exactly the same as that of the full-state feedback system. These results fully reveal the advantage of the observer-controller system: the system is as effective as a full-state feedback system yet it uses a simple sensing system because far fewer sensors are required.

When the load cell is absent and only the accelerometer is installed at the top floor, observability matrix M_0 is of rank 10; thus, the system is unobservable. This result shows that a sensor must be employed to observe the actuator dynamics.

Note that there is an alternative method. Since the actuator usually has a built-in LVDT to measure relative displacement of an actuator piston with respect to its cylinder, this LVDT may be employed for the observer instead of an extra load cell so the sensing system can be further simplified. In this case, sensor output is

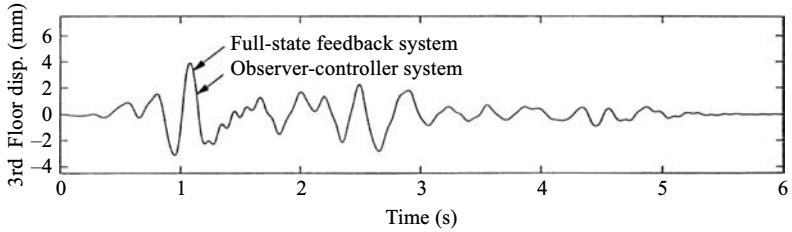

FIGURE 6.15 Comparison of closed-loop displacement responses of a three-story building.

expressed as

$$\{y(t)\} = \begin{Bmatrix} \ddot{x}_3(t) \\ x_a(t) \end{Bmatrix} = \begin{Bmatrix} \ddot{x}_3(t) \\ x_b(t) - x_1(t) \end{Bmatrix} = [C]\{Z(t)\} + [D_u]u(t) + \{D_r\}\ddot{x}_g(t) \tag{6.55}$$

where

$$[C] = \begin{bmatrix} -\dfrac{k_{31}}{m_3} & -\dfrac{k_{32}}{m_3} & -\dfrac{k_{33}}{m_3} & 0 & -\dfrac{c_{31}}{m_3} & -\dfrac{c_{32}}{m_3} & -\dfrac{c_{33}}{m_3} & 0 & 0 & 0 \\ -1 & 0 & 0 & 1 & 0 & 0 & 0 & 0 & 0 & 0 \end{bmatrix} \tag{6.56}$$

$$[D_u] = 0, \quad \{D_r\} = \begin{Bmatrix} -1 \\ 0 \end{Bmatrix}$$

and k_{ij} and c_{ij} are elements at ith row jth column of the stiffness and damping matrices, respectively. Numerical result shows that the corresponding observability matrix is of rank 11; thus, the system is observable.

From this example, it can be seen that the observer-controller system requires only four sensors: an accelerometer at the top floor, a load cell or an LVDT for the actuator, and two sensors for reference input (earthquake excitation $\ddot{x}_g$) and control command $u(t)$. To implement a full-state feedback algorithm without a state observer, 11 sensors and control hardware with 11 channels must be used. Thus, a seismic response control system can be simplified with the seismic observer technique.

In Figure 6.16, direct output feedback is compared to the observer-controller system. For the former, the control command $u(t)$ is a feedback of the sensor output $\ddot{x}(t)$ and $f_a(t)$, and control command $u(t) = g_a\ddot{x}_3(t) + g_f f_a(t)$; for the latter, the control command $u(t)$ is a feedback of all 11 state variables (see Equation 5.142) estimated by the observer from the sensor output $\ddot{x}(t)$ and $f_a(t)$. With identical settings for maximum active control force at 1,330.8 N, the direct output feedback system exhibits 5.24 mm maximum displacement at the top floor, which is 34% larger than full-state feedback achieved by the seismic observer

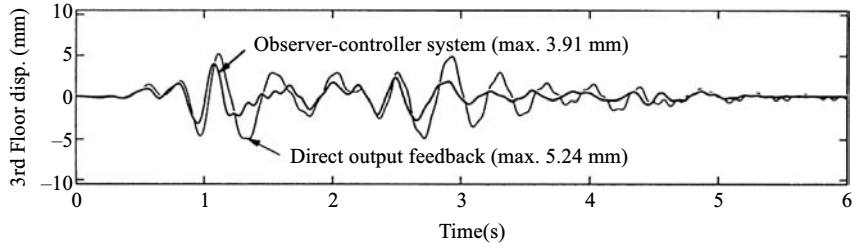

FIGURE 6.16 Response comparison of observer-controller and direct output feedback systems.

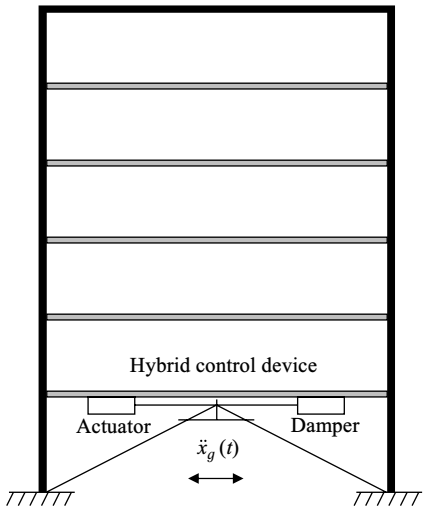

FIGURE 6.17 Six-story shear building with hybrid damper-actuator bracing control (HDABC).

technique. Therefore, the observer-controller system is more effective than direct output feedback in reducing seismic structural response.

6.3.4.2.2 Six-story shear building with HDABC system

This system installs a hybrid control system on a K-brace system at the first floor, as shown in Figure 6.17. Structural properties are: (1) mass coefficients $m_1 = 109.78$, $m_2 = 109.62$, $m_3 = 109.24$, $m_4 = 108.86$, $m_5 = 108.48$, $m_6 = 107.03$ (tons); (2) stiffness coefficients $k_1 = 351{,}284$, $k_2 = 225{,}167$, $k_3 = 169{,}665$, $k_4 = 124{,}242$, $k_5 = 87{,}872$, $k_6 = 59{,}532$ (kN/m); (3) undamped natural frequencies $\omega_1 = 9.79$, $\omega_2 = 24.05$, $\omega_3 = 37.40$, $\omega_4 = 49.56$, $\omega_5 = 63.44$, $\omega_6 = 83.76$ (rad/s); and (4) 2% structural damping ratio. K-brace properties are $m_b = 2.0$ tons; $k_b = 2.0 \times 10^5$ kN/m; and 0.1% damping. State variables include six displacements and six velocities for the six-story building, one displacement and one velocity for

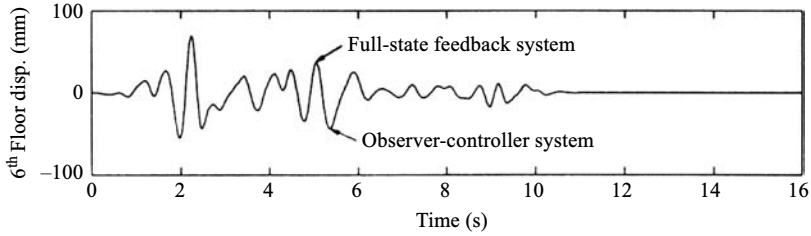

FIGURE 6.18 Comparison of closed-loop displacement responses of a six-story building.

the K-brace, active control force and servo-valve displacement for the hydraulic actuator, and passive control force for the viscous fluid damper. Thus, this smart structure with HDABC system is of the 17th order.

To set up a full-state sensing and feedback system, 17 sensors (eight displacement sensors [LVDTs], seven velocity sensors, and two load cells) are required and a data-acquisition system with 17 or more channels must be employed. If the observer-controller is applied to the system, numerical simulation results show that two sensors can meet the observability requirement. These two sensors are an accelerometer at the top floor and a load cell to measure active control force. With two additional sensors to measure the reference input (earthquake ground motion) and the control command for the observer, only four sensors are required for the observer-controller system. Compared to the full-state sensing and feedback system that requires 17 sensors, the observer technique can greatly simplify the sensing and data acquisition system. Furthermore, since the actuator has a built-in LVDT to measure its piston displacement, this LVDT may be employed for the observer instead of an extra load cell. Numerical simulation results also show that the system with the LVDT in the actuator and an accelerometer at the top floor is observable. This further simplifies the setup of the sensing system. Similar to the system in Section 6.3.4.2.1, closed-loop displacement response of the observer-controller system is exactly the same as that of the full-state feedback system, as shown in Figure 6.18. Details on how to use MATLAB® functions for this example is discussed in Section A.3 of Appendix A.

6.3.5 Summary

A seismic observer is developed to estimate the full-state vector from acceleration measurements for the optimum controller. Such an observer does not require extra devices but is implemented with software in control computer. Studies show that a smart seismic structure system with the proposed observer-controller technique works as effectively as a full-state sensing and feedback system, yet is able to handle acceleration sensors and needs far fewer sensors. With the seismic observer, the full-state feedback control system and algorithms discussed in other chapters of this book can be implemented with accelerometers at strategic points. Therefore, this observer-controller technique offers a promising alternative to process

insufficient sensors and acceleration measurements. With this technique, a smart seismic structure system becomes more practical because it is easier to implement and maintain.

References

1. Austerlitz, H., *Data Acquisition Techniques Using PCs*, 2nd edn., Academic Press, San Diego, California, 2002.
2. Cheng, F.Y. and Jiang, H., Optimum control of a hybrid system for seismic excitations with state observer technique, *Smart Materials and Structures*, 7, 654, 1998.
3. Cheng, F.Y. et al., Theoretical and experimental studies on hybrid control of seismic structures, in *Proceedings of the Twelfth ASCE Conference on Analysis and Computation*, Cheng, F.Y. (ed.), Chicago, American Society of Civil Engineers, Reston, Virginia, 1996.
4. Chu, S.Y., Soong, T.T., and Reinhorn, A.M., *Active, Hybrid, and Semi-Active Structural Control: A Design and Implementation Handbook*, John Wiley & Sons, Chichester, England, 2005.
5. DeSilva, C.W., *Control Sensors and Actuators*, Prentice-Hall, Englewood Cliffs, New Jersey, 1989.
6. Dyke, S.J. et al., Acceleration feedback control of MDOF structures, *ASCE Journal of Engineering Mechanics*, 122, 907, 1996.
7. Dyke, S.J. et al., Implementation of an active mass driver using acceleration feedback control, *Microcomputers in Civil Engineering*, 11, 305, 1996.
8. Fraden, J., *Handbook of Modern Sensors: Physics, Designs and Applications*, American Institute of Physics Press, Woodbury, New York, 1997.
9. Fujita, T. et al., Development of hybrid mass damper with convertible active and passive modes using AC-servomotor for vibration control of tall buildings, in *Proceedings of the First World Conference on Structural Control*, Los Angles, California, 1994, 3, FA4:63.
10. Grantham, W.J. and Vincent, T.L., *Modern Control Systems: Analysis and Design*, John Wiley & Sons, New York, 1993.
11. Jabbari, F., Schmitendorf, W.E., and Yang, J.N., H_∞ control for seismic-excited buildings with acceleration feedback, *ASCE Journal of Engineering Mechanics*, 121, 994, 1995.
12. Jacquot, R.G., *Modern Digital Control Systems*, Marcel Dekker, New York, 1995.
13. Jiang, H.P., Cheng, F.Y., and Wang, Z.Q., Damper-actuator system with observer technique and optimal placement, in *Proceedings of International Symposium/Workshop on Seismic Isolation, Energy Dissipation and Control of Structures*, Zhou, F.L. and Spencer, B.F. Jr., (eds.), Seismological Press, China, 1999, p. 362.
14. Jiang, H.P., Cheng, F.Y., and Wang, Z.Q., Observer technique for seismic response control, in *Proceedings of US-Korea Workshop on New Frontiers in Infrastructural and Seismic Problems*, Seoul, Korea, 1999.
15. Jiang, H.P., Cheng, F.Y., and Wang, Z.Q., State-of-the-art in hybrid control and issues on optimum seismic observer and device placement, in *Proceedings of the Twelfth World Conference on Earthquake Engineering*, International Association for Earthquake Engineering, Auckland, New Zealand, 2000.
16. Jones, M.H., *A Practical Introduction to Electronic Circuits*, Cambridge University Press, New York, 1995.

17. Kirianaki, N.V. et al., *Data Acquisition and Signal Processing for Smart Sensors*, 1st edn., John Wiley & Sons, Ltd., Chichester, England, 2002.
18. Kuo, B.C., *Digital Control Systems*, Saunders College Publishing, Orlando, Florida, 1992.
19. Liu, S.C., Tomizuka, M., and Ulsoy, A.G., Challenges and opportunities in the engineering of intelligent systems, *Smart Structures and Systems*, 1, 1, 2005.
20. Liu, R.C. et al., Wireless sensors for structural monitoring, in *Strong Motion Instrumentation for Civil Engineering Structures*, Erdik, M.O. (ed.), Kluwer Academic Publishers, The Netherlands, 2001, p. 253.
21. Lynch, J.P. et al., The design of a wireless sensing unit for structural health monitoring, in *Proceedings of the Third International Workshop on Structural Health Monitoring*, Stanford, California, 2001, p. 1041.
22. MATLAB (http://www.mathworks.com/products/matlab/), *The Mathworks Inc.*, Natick, Massachusetts, 2002.
23. Nagayama, T. et al., Wireless strain sensor development for civil infrastructure, in *Proceedings of First International Workshop on Networked Sensing Systems*, Tokyo, Japan, 2004, p. 97.
24. Sakamoto, M. et al., Practical applications of active and hybrid response control systems and their verification by earthquake and strong wind observations, in *Proceedings of the First World Conference on Structural Control*, Los Angeles, California, 1994, 1, WP2:90.
25. Soong, T.T., *Active Structural Control: Theory and Practice*, 1st edn., Longman Scientific & Technical, UK and John Wiley & Sons, New York, 1990.
26. Spencer Jr., B.F., Ruiz-Sandoval M., and N. Kurata, Smart sensing technology: opportunities and challenges, *Journal of Structural Control and Health Monitoring*, 11, 349, 2004.
27. Spencer, B.F. Jr. et al., Acceleration feedback control strategies for seismic protection, in *Proceedings of the American Control Conference*, San Francisco, California, 1993, p. 1317.
28. Straser, E.G. et al., A modular, wireless network platform for monitoring structures, *SPIE Proceedings International Society for Optical Engineering*, 3243:1, 450, 1998.
29. Wilson, J.S., *Sensor Technology Handbook*, Elsevier, Burlington, Maryland, 2005.

7 Optimal Device Placement for Smart Seismic Structures

This chapter carries out a theoretical study on optimal placement of control devices (dampers and actuators) for a smart seismic structure system. Section 7.1 reviews the study background and numerically demonstrates the significance of *optimal device placement* for smart seismic structures. Section 7.2 presents three methods based on controllability and performance indices for optimal actuator placement. Numerical simulations of structural seismic response to various earthquake records are carried out to evaluate these methods. Section 7.3 develops a statistical method for optimal placement of hybrid control devices. A *stochastic theory* is established first for seismic response of controlled structures that have first-order dynamics and nonorthogonal damping and stiffness. Then a statistical criterion is developed based on this theory for optimal placement of a viscous fluid damper, a servovalve controlled hydraulic actuator, and their combination (i.e., a hybrid device) on a seismic-resistant structure. A general optimization problem for optimal device placement is formulated, and a solution procedure is established. Numerical analysis of the seismic response of a hybrid-controlled smart structure is used to verify the proposed method for optimal device placement and to demonstrate the effectiveness of a control system with optimal location.

7.1 Introduction

7.1.1 Basic Concepts of Engineering Optimization

Accomplishing the best possible design is vital in engineering practice because of economy and performance. For this reason, *optimization theory* has emerged to seek the best solution for engineering design. This theory formulates an *optimization problem* whose solution corresponds to the best design. In such a problem, maximization or minimization of a function serves as the *optimization criterion*. This function, called *cost function* or *objective function*, represents a quantitative measure of the "goodness" of the engineering system. The objective function depends on a detailed configuration of the system, and variables of the objective function are called *design variables* of the optimization problem. Optimization problems are classified into two categories: those with continuous variables and those with discrete variables [6,9,30]. The former seeks a set of real numbers or even a function from a continuous design space as the optimal solution,

while the latter, also called *combinatorial optimization*, finds an optimum object from a finite or countably infinite set, such as an integer set.

To solve an optimization problem, a special technique called *optimization algorithm* is employed. In theory, the optimization algorithm is a simple search procedure composed of the following five steps: (1) Selection of initial design in the design space, (2) Evaluation of objective function for the design, (3) Assessment of design feasibility with constraints, (4) Comparison of current design with preceding designs, (5) Rational way to select a new design and repeat the process. In practice, too much calculation is involved in evaluation of the objective function, comparison of different designs, and search procedure, especially when the objective function has many independent variables. This computational complexity remains a challenge in engineering optimization.

There are three types of optimization algorithms: *calculus-based*, *enumerative*, and *random* [15]. *Calculus-based algorithms* seek local extrema by setting the gradient of the objective function equal to zero. These algorithms are not suitable for combinatorial optimization and are not effective for optimization problems with a high degree of nonlinearity and discontinuity. Moreover, there is no guarantee that these algorithms can find global optimal solutions. *Enumerative schemes* are fairly straightforward. Within a finite search space, or a discretized infinite search space, the search algorithm starts looking at values of the objective function at every point in the space, one at a time. Enumerative algorithms are attractive because of their simple principle and perfect applicability for combinatorial optimization. It is guaranteed that an enumerative scheme can find the global extrema within a finite search space because all designs have been evaluated and compared. The weakness is that such schemes lack efficiency with a large optimization problem. *Random search algorithms* have achieved popularity because of their efficiency with large problems. They use random choices as a tool to guide a highly exploitative search through the design space. *Genetic algorithms* [15] and *simulated annealing* [22] are typical random search techniques. Although these randomized searches are not directionless, they can be easily trapped in local extrema. This is because these algorithms only search part of the design space and the global optima may not be in this part. In the long run, random algorithms are not expected to do better than enumerative schemes. This is because enumerative schemes are more accurate than random algorithms, and the efficiency of such schemes improves everyday with the rapid advance of digital computing technologies.

The optimal placement of dampers and actuators on smart building structures is a typical combinatorial optimization problem as its design space—the building stories and bays, are discrete. The discrete nature of available locations of control devices makes it impossible to use calculus-based algorithms; and as noted above, enumerative schemes will be realistic for large design space with improved efficiency by evolving digital computing technologies, and do better than a random search procedure for their accuracy. Thus, enumerative schemes are used throughout this chapter to accurately determine the optimal locations of the control devices, while the computing cost is greatly reduced by simplified optimization objective function.

7.1.2 Significance of Optimal Device Placement for Smart Seismic Structures

Structural control offers a promising alternative to protect structures from seismic damage. However, the force-generating capacity of control devices (dampers and actuators) limits the application of control systems for full-scale seismic-resistant structures. Since seismic-resistant structures can weigh hundreds or thousands of tons, under strong earthquake excitations, their inertia and restoring forces may be thousands of kilo-Newtons, and their damping force may be hundreds of kilo-Newtons. Because the inertia or restoring force is much larger than the damping force, the control mechanism is to add damping force to a structure with a minor modification of inertia or restoring force; the required control force should have same magnitude order as the damping force to reduce seismic response significantly. Current industrial technology makes such a big actuator or damper feasible, but the cost would limit its application. This cost issue can be partially addressed by placing these devices optimally to maximize their efficiency, as demonstrated by the following numerical example.

To show how significant the optimal placement of control devices is, the three-story building model with hybrid control device shown in Figure 5.21 serves as an example here. Time-history response of the controlled structure for scaled N-S component of the El-Centro earthquake (with amplitude and frequency scale factors at 0.3 and 2, respectively) is evaluated for three possible locations of the hybrid device: first, second, or third floor. Required active control force is compared for the three locations with an identical control objective, say, reducing the maximum displacement at the third floor from 0.7794 cm (structure without control) to 0.508 cm. Figure 7.1 compares the time histories of required control forces for scaled El-Centro earthquake. Required active force is 752.7, 3610.2, and 1908.9 (N) for the hybrid device at the first, second, and third floor, respectively. Apparently, the first floor is the optimal device location because the least active control force is required to reduce the maximum displacement at the third floor to 0.508 cm. If the hybrid device is installed at nonoptimal locations, that is, second and third floors, 2.54 and 4.80 times larger active control forces are respectively required to achieve the same control objective. Thus, effectiveness of control devices is strongly dependent on their locations on the structure, and such device locations greatly influence the efficiency of a control system. Therefore, it is very significant to study optimal device placement for smart seismic structures as such studies make the concept of smart structures more practical for vibration reduction of structures under earthquake excitations.

7.1.3 Review of Former Studies on Optimal Device Placement

Because it is vital to install control devices at optimal locations on a structure, optimal device placement has been a very important issue in smart structure

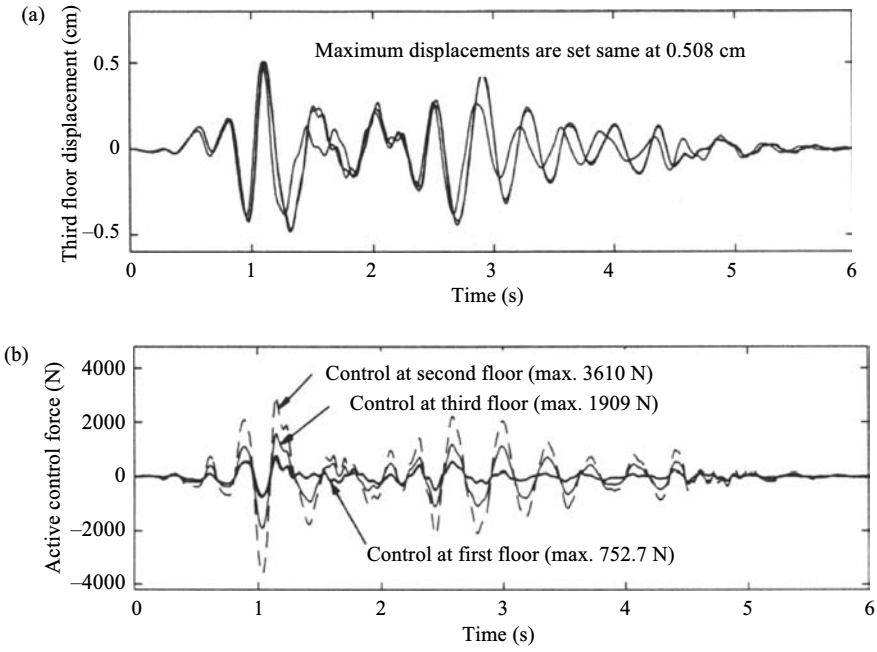

FIGURE 7.1 Response of HDABC system to scaled El-Centro earthquake: (a) displacement at third floor and (b) required active control force.

technology for seismic response control. Researchers have made some progress on optimal placement of control devices [1–3,7,8,10–12,18–20,24,26,29,31]. A preferred approach for control device placement is formulation of an optimization problem in which the objective function is the criterion for optimal placement. Optimal device placement is a combinatorial optimization problem because the design space—different locations on the structure—is discrete. No efficient algorithm can solve the general problem of optimal device placement [24]. There are two reasons for this. First, a combinatorial problem cannot be solved with calculus-based techniques because no gradient is defined in discrete space. Second, random search techniques have limited applicability for combinatorial optimization because of the danger of falling into local optima. Fortunately, control devices for seismic-resistant structures has limited location choices. If an actuator is installed between stories of a one-bay building, the number of choices equals the number of stories. The finite design space of the optimum placement problem makes it possible to search the optimal location by enumerative techniques.

Recall that calculation complexity is of major concern in engineering optimization. Two kinds of calculation complexity may exist for optimal device placement in seismic response control. First is enormous design space. When the number of structural members or the number of control devices is large, a structural control system has a huge number of possible configurations. For example, if

r control devices (dampers or actuators) are to be placed in a one-bay n-story building ($r \leq n$), the total combinations for the selection of r device locations out of n possible story units, which are feasible locations of control devices, is $n!/[r!(n-r)!]$. This number can be very large for complex structures, that is, the control devices have too many possible locations. Second is complex objective function. An objective function may require that seismic response of controlled structures in time history be calculated. Even worse, multiple earthquake records may have to be employed owing to the uncertainty of earthquake excitations. Since objective function must be evaluated for each design, a complex objective function would greatly increase computation time. Consequently, two approaches have been proposed to reduce the computation cost for optimal placement of control devices: development of efficient algorithms with reduced design space and simplification of the objective function.

The first approach, development of efficient algorithms, cuts the computing cost by reducing design space. This approach is usually employed when the design space is large. To search the global optimum device locations in a large design space, the huge number of possible configurations may lead to high computation cost. Alternatively, a practical and efficient way is to place control devices at near-optimal locations in part of the design space (such as substructure) so that the amount of calculation is reasonable. This idea led to the development of random search algorithms, such as genetic algorithms and simulated annealing proposed in the 1990s [2,4,17,26,27,31]. Instead of searching all possible configurations, random algorithms only search part of the design space guided by random choice. Computation cost is reduced as less searching is required. However, this method has a major challenge of accuracy for combinational optimization. Random techniques do not guarantee how close the near-optimal solution is to the global extrema; instead, they are easily trapped in local optimal solutions. It is the same situation for substructure approach, and there is no guide as to how to split the structure in order to be accurate enough. Moreover, a limitation on the total number of control devices applies if a genetic algorithm is used to formulate the placement problem as zero–one optimization. This limitation seriously affects crossover and mutation operations in the genetic algorithm.

The other approach focuses on development and simplification of optimal criteria; calculation complexity is reduced by simplifying the objective function. For optimal device placement in seismic response control, evaluation of the objective function may be complex because civil engineering structures are usually large and earthquake excitation has severe uncertainty. If the objective function is simplified, calculation time in its evaluation for each design is decreased, and total computation cost is greatly reduced for the optimization problem. Thus, this approach researchers have been concentrating on it and have developed various criteria for optimal placement of control devices, as described in the subsequent paragraphs.

In the research by Milman and Chu [26], damping in selected modes and an H_2 norm (a *quadratic integral*) of selected transfer functions are chosen as the criteria for optimal damper placement. This method is effective when structural

response has one dominant mode, such as wind response control. However, the criterion has less applicability for optimal damper placement on seismic-resistant structures. Seismic structural response usually has multiple significant modes, and one damper location is unlikely to yield the largest damping for all significant modes. Moreover, the participation of each mode in seismic response must be calculated to select significant modes for each damper location. This seriously increases the computation complexity for the evaluation of objective functions.

Agrawal and Yang [1] defined five objective functions for optimal placement of energy dissipative devices. These objective functions are

1. Average dissipated energy

$$J_1 = E\left[\int_0^\infty \Delta^{\mathrm{T}} C_{\mathrm{d}} \Delta \mathrm{d}t\right] \tag{7.1}$$

where $\Delta = [\delta_1, \delta_2, \ldots, \delta_n]^{\mathrm{T}}$ is an nth order vector for interstory drifts for an n-story building; C_{d} is a $(n \times n)$ diagonal matrix with $C_{\mathrm{d}}(i,i)$ being coefficient of the damper installed at the ith story.

2. Weighted sum of damping ratios for dominant modes

$$J_2 = \sum_{i=1}^{q} \psi_i \zeta_i \tag{7.2}$$

where q is number significant modes, ψ_i is scalar weighting factor and ζ_i is damping ratio for ith mode.

3. H_2 cost of interstory drift J_3

$$J_3 = \left\| H_{\delta\gamma} \right\|_2 = \sqrt{\mathrm{trace}\left([C]\,[G_{\mathrm{C}}]\,[C]^{\mathrm{T}}\right)} \tag{7.3}$$

in which $H_{\delta\gamma}$ is the transfer function from reference input r (i.e., earthquake excitation $\ddot{x}_{\mathrm{g}}$) to interstory drift $\delta(t)$. For a seismic response control system described by Equations 4.19 and 5.109, the interstory drift can be expressed as

$$\delta(t) = [C]\,\{Z(t)\} \tag{7.4}$$

In Equation 7.3, the Lyapunov matrix $[G_{\mathrm{C}}]$ is obtained from

$$[A_{\mathrm{C}}]\,[G_{\mathrm{C}}] + [G_{\mathrm{C}}]\,[A_{\mathrm{C}}]^{\mathrm{T}} + \{B_{\mathrm{r}}\}\,\{B_{\mathrm{r}}\}^{\mathrm{T}} = 0 \tag{7.5}$$

and the operator trace() is defined as

$$\mathrm{trace}([C]\,[G_{\mathrm{C}}]\,[C]^{\mathrm{T}}) = \sum_{i,j=1}^{N} C(i) G_{\mathrm{C}}(i,j) C(j) \tag{7.6}$$

where N is order of plant matrix $[A_C]$ or Lyapunov matrix $[G_C]$.
4. Maximum of peak interstory drift

$$J_4 = \max\{\delta_i\}, \quad i = 1, 2, \ldots, n \tag{7.7}$$

where δ_i is interstory drift at ith story.

5. Maximum *root-mean-square* (RMS) interstory drift

$$J_5 = \max\{\sigma_{\delta i}\}, \quad i = 1, 2, \ldots, n \tag{7.8}$$

where $\sigma_{\delta i}$ is RMS value for interstory drift at ith story.

The optimal locations for the energy dissipative systems are determined such that a particular objective function is optimized, that is, either maximizing J_1, J_2 or minimizing J_3, J_4, J_5. These objective functions are suitable for seismic response control because they can consider multiple significant modes for structural response. However, J_1 and J_4 require the interstory drift of structure be calculated that it may increase calculation complexity. The study shows optimal locations obtained by minimizing J_4 depending on the specific design earthquake. For J_2, there is no guideline on how to select the weighting factor ψ_i.

Shukla and Datta defined a criterion called *controllability index* for optimal damper placement [11]. The controllability index is expressed as

$$x = \max\left[\frac{\sigma_{xi}}{h_i}\right], \quad i = 1, 2, \ldots, n \tag{7.9}$$

where x and σ_{xi} are the value of the index and RMS value of interstory drift at ith story, respectively; h_i is the ith story height. Thus, the ith story is the optimal damper location when x is maximum. The basic idea behind the controllability index is that a passive damper is optimally located if it is placed where the displacement response of the uncontrolled structure is the largest. This idea may be inaccurate because the passive control force generated by the damper is usually related to velocity response, and the largest displacement response of a complex seismic-resistant structure may not occur at same location where the largest velocity happens.

As noted above, many research studies have been done for the optimal placement of dampers. In the following sections, we will focus on detail discussion of optimal placement of actuators and hybrid devices on a smart structure for seismic response control.

7.2 Optimal Actuator Placement for Smart Seismic Structures with Active Control

Active control systems use actuators powered by external energy to generate control force. The cost of actuators and the power required to operate them are

significant factors for the design of an active control system. Optimal actuator placement is very important because it can greatly improve the actuator's effectiveness. Studies on optimal actuator placement started in early 1980s and again these studies are concentrated on simplification of the optimization criteria. Since then, various optimal criteria for actuator placement on structures have been developed, as discussed throughout this section.

7.2.1 Measure of Modal Controllability

7.2.1.1 System controllability

Chapters 4 and 5 show that a smart structure system with active, semiactive, or hybrid control can be expressed by the same state variable representation, Equations 4.19 and 5.109. Such a system is controllable if and only if its *controllability matrix* $[M_c]$, defined by the following equation, and is of full rank N [14].

$$[M_c] = [B_u, AB_u, A^2B_u, \ldots, A^{N-1}B_u] \tag{7.10}$$

where N is the order of plant matrix $[A]$.

7.2.1.2 Modal controllability

This definition of system controllability reveals that a system is either controllable or uncontrollable. It is desirable to consider how controllable a system is. This leads to the definition of *measure of modal controllability* [16, 24], which are the modal coefficients of the active control force. Application of this concept for active seismic response control is discussed in detail as follows.

Smart seismic structures with an active control system using a linear proportional actuator can be modeled as

$$[M]\{\ddot{x}(t)\} + [C]\{\dot{x}(t)\} + [K]\{x(t)\} = \{\gamma\}u(t) + \{\delta\}\ddot{x}_g(t) \tag{7.11a}$$

or using the state variable representation by Equation 4.19. Using modal analysis for the system described by Equation 7.11a

$$\{x(t)\} = [\Phi]\{q(t)\} \tag{7.11b}$$

Then

$$\left[M^*\right]\{\ddot{q}(t)\} + \left[C^*\right]\{\dot{q}(t)\} + \left[K^*\right]\{q(t)\} = [\Phi]^T\{\gamma\}u(t) + [\Phi]^T\{\delta\}\ddot{x}_g(t) \tag{7.11c}$$

where $[M^*]$, $[C^*]$, and $[K^*]$ are diagonal matrices of mass, damping, and stiffness coefficients in modal space, respectively; $[\Phi]$ and $\{q(t)\}$ are matrix of mode

shapes and vector of modal coordinates, respectively. The ith modal equation from Equation 7.11c becomes

$$\ddot{q}_i(t) + 2\zeta_i\omega_i\dot{q}(t) + \omega_i^2 q_i(t) = \gamma_i u(t) + \delta_i\ddot{x}_g(t) \tag{7.12}$$

and $\gamma_i = \{\phi_i\}^T\{\gamma\}/M_i$, $\delta_i = \{\phi_i\}^T\{\delta\}/M_i$, and $M_i = \{\phi_i\}^T[M]\{\phi_i\}$ $(i = 1, 2, \ldots, n)$, n is the number of d.o.f for the system. State variable representation of the ith modal equation is

$$\begin{Bmatrix} \dot{q}_i(t) \\ \ddot{q}_i(t) \end{Bmatrix} = \begin{pmatrix} 0 & 1 \\ -\omega_i^2 & -2\zeta_i\omega_i \end{pmatrix} \begin{Bmatrix} q_i(t) \\ \dot{q}_i(t) \end{Bmatrix} + \begin{Bmatrix} 0 \\ \gamma_i \end{Bmatrix} u(t) + \begin{Bmatrix} 0 \\ \delta_i \end{Bmatrix} \ddot{x}_g(t) \tag{7.13}$$

Obviously, the value of γ_i shows how sensitive the effect of active control force $u(t)$ is to the response in the mode i. If the magnitude (absolute value) of γ_i is large, it is easy for the active force to control the ith modal response; if γ_i is small, the active control force has little effect on the ith modal response. If $\gamma_i = 0$, the control force has no effect on this mode, which means that mode i is uncontrollable. Thus, the effectiveness of the control force and the control system on the ith mode is proportional to the magnitude of γ_i. This is the reason why $\gamma_i (i = 1, 2, \ldots, n)$ in Equation 7.12 is the *measure of modal controllability* of the ith mode. This concept can serve as a criterion for optimal actuator placement in that the optimum corresponds to the largest value of the measure of controllability [11,24]. The optimal actuator location for mode i should correspond to largest absolute value of γ_i. If a system has only one critical mode, the optimum actuator location should have the largest magnitude of γ_i for this critical mode. If there are multiple significant modes, a more general criterion is needed for the optimal device placement in seismic response control.

EXAMPLE 7.2.1

The two-story shear building in Example 4.2.2 serves as the example here. Assume there is only one active tendon installed on the structure. Find the optimal tendon location.

Solution

The motion equation of the system has been developed in Example 4.2.2 as

$$[M]\{\ddot{x}(t)\} + [C]\{\dot{x}(t)\} + [K]\{x(t)\} = \{\gamma\}u(t) + \{\delta\}\ddot{x}_g(t) \tag{a}$$

where

$$[M] = \begin{pmatrix} 0.136 & \\ & 0.066 \end{pmatrix} \text{ k-s}^2/\text{in.}, \quad [C] = \begin{pmatrix} 0.0572 & -0.0198 \\ -0.0198 & 0.0313 \end{pmatrix} \text{ k-s/in.}$$

$$[K] = \begin{pmatrix} 75.00 & -44.30 \\ -44.30 & 44.30 \end{pmatrix} \text{ k/in.}, \quad \{\delta\} = \begin{Bmatrix} -0.136 \\ -0.066 \end{Bmatrix} \text{ k-s}^2/\text{in.} \tag{b}$$

If the active tendon is installed at the first floor

$$\{\gamma\}_1 = \begin{Bmatrix} -1 \\ 0 \end{Bmatrix} \tag{c}$$

or the second floor

$$\{\gamma\}_2 = \begin{Bmatrix} 1 \\ -1 \end{Bmatrix} \tag{d}$$

Natural frequencies of this system have been calculated as

$$\omega_1 = 11.829 \text{ rad/s}, \quad \omega_2 = 32.905 \text{ rad/s} \tag{e}$$

and mode shapes $\{x\}$ satisfies

$$\left[-\omega^2 [M] + [K]\right] \{x\} = \{0\} \tag{f}$$

For the first mode,

$$\left[-11.829^2 \begin{pmatrix} 0.136 & \\ & 0.066 \end{pmatrix} + \begin{pmatrix} 75.00 & -44.30 \\ -44.30 & 44.30 \end{pmatrix}\right] \begin{Bmatrix} x_1 \\ x_2 \end{Bmatrix}_1 = \begin{Bmatrix} 0 \\ 0 \end{Bmatrix} \tag{g}$$

$$\begin{pmatrix} 55.97 & -44.30 \\ -44.30 & 35.06 \end{pmatrix} \begin{Bmatrix} x_1 \\ x_2 \end{Bmatrix}_1 = \begin{Bmatrix} 0 \\ 0 \end{Bmatrix} \tag{h}$$

$$\{\phi\}_1 = \begin{Bmatrix} x_1 \\ x_2 \end{Bmatrix} = \begin{Bmatrix} 0.7915 \\ 1.0 \end{Bmatrix} \tag{i}$$

For the second mode,

$$\left[-32.905^2 \begin{pmatrix} 0.136 & 0 \\ 0 & 0.066 \end{pmatrix} + \begin{pmatrix} 75.00 & -44.30 \\ -44.30 & 44.30 \end{pmatrix}\right] \begin{Bmatrix} x_1 \\ x_2 \end{Bmatrix}_2 = \begin{Bmatrix} 0 \\ 0 \end{Bmatrix} \tag{j}$$

$$\begin{pmatrix} -72.253 & -44.30 \\ -44.30 & -27.161 \end{pmatrix} \begin{Bmatrix} x_1 \\ x_2 \end{Bmatrix}_2 = \begin{Bmatrix} 0 \\ 0 \end{Bmatrix} \tag{k}$$

$$\{\phi_2\} = \begin{Bmatrix} x_1 \\ x_2 \end{Bmatrix}_2 = \begin{Bmatrix} -0.6131 \\ 1.0 \end{Bmatrix} \tag{l}$$

The measure of modal controllability for the first and second modes is illustrated as follows:

For the first mode

When actuator at first floor

$$\gamma_1^1 = \{\phi_1\}^{\mathrm{T}} \{\gamma\}_1 = \begin{bmatrix} 0.7915 & 1.0 \end{bmatrix} \begin{Bmatrix} -1 \\ 0 \end{Bmatrix} = -0.7915 \tag{m}$$

and when actuator at second floor

$$\gamma_1^2 = \{\phi_1\}^{\mathrm{T}} \{\gamma\}_2 = \begin{bmatrix} 0.7915 & 1.0 \end{bmatrix} \begin{Bmatrix} 1 \\ -1 \end{Bmatrix} = -0.2085 \tag{n}$$

Since $|\gamma_1^1| > |\gamma_1^2|$, the first floor is the optimal actuator location for the first mode.

Similarly, for the second mode

When the actuator is at the first floor

$$\gamma_2^1 = \{\phi_2\}^{\mathrm{T}} \{\gamma\}_1 = [-0.6131 \;\; 1.0] \begin{Bmatrix} -1 \\ 0 \end{Bmatrix} = 0.6131 \tag{o}$$

and when the actuator is at the second floor

$$\gamma_2^2 = \{\phi_2\}^{\mathrm{T}} \{\gamma\}_2 = \begin{bmatrix} -0.6131 & 1.0 \end{bmatrix} \begin{Bmatrix} 1 \\ -1 \end{Bmatrix} = -1.6131 \tag{p}$$

Since $|\gamma_2^2| > |\gamma_2^1|$, the second floor is the optimal actuator location for the second mode.

As expected, this example has shown that optimal actuator location is different in different modes by the measure of modal controllability. Thus, the measure of modal controllability can find the optimal device location only when one mode dominates the system response, for example, the first floor is the optimal actuator location if the first mode dominates the response.

The method of modal controllability is simple and straightforward as the optimal actuator locations can be determined in open loop (i.e., no active control force). This criterion is effective for structural response with one dominant mode, but less applicable for structural seismic response control systems. This is because structural seismic response usually has multiple significant modes while one actuator location may not have the biggest modal coefficients for all significant modes as shown by above example. Moreover, this method does not work for a smart structure system with significant dynamics of control devices in that its open-loop dynamics can be very different from its closed-loop behavior.

7.2.2 Performance Index

Owing to the weakness of modal controllability method, better approaches are needed for optimal device placement of smart seismic structures with multiple significant modes in system response. *Performance index* is such an approach as discussed below.

7.2.2.1 Basic concepts

The method of performance indices employs a scalar measure that is defined by the integration of control energy or seismic structural response in time history. Optimal actuator location corresponds to the minimization of the scalar measure. One of such indices, *control energy index* J_E, is defined as [3]

$$J_{\mathrm{E}} = \int_{t_0}^{t_{\mathrm{f}}} \{u(t)\}^{\mathrm{T}} \{u(t)\} \, \mathrm{d}t \tag{7.14}$$

where $\{u(t)\}$ is vector of active control forces, t_0 and t_f are initial and final time, respectively. This concept is based on that if the actuator is optimally placed, the work performed by the control system reflected by Equation 7.14 shall be the minimum. However, minimization of control energy by Equation 7.14 alone may not lead to the optimal solution since the reduction of control energy may result in an increase of structural response. Thus a new performance index, the *response index* J_{R}, was proposed [11,29]. This index is defined as

$$J_{\mathrm{R}} = \int_{0}^{\mathrm{T}_0} \{Z(t)\}^{\mathrm{T}} \{Z(t)\} \, \mathrm{d}t \tag{7.15}$$

where $\{Z(t)\}$ is state variables, which includes structural displacements and velocities. This index reflects upon the measure of the reduction of the structural response. The optimal actuator location corresponds to the minimization of performance index J_R, that is, the smallest structural response.

Compared to modal controllability, performance indices do not require a dominant mode but consider the response by all modes. However, they require much more calculation in solving and integrating system response.

7.2.2.2 Numerical illustrations

The performance index methods are applied to an eight-story shear building with two active tendons [11]. The two tendons can be located on any of the eight possible locations. The structural properties are (1) stiffness coefficients $k_1 = 1026.3$ k/in., $k_2 = 937.4$ k/in., $k_3 = 790.6$ k/in., $k_4 = 684.1$ k/in., $k_5 = 538.5$ k/in., $k_6 = k_7 = k_8 = 1026.3$ k/in.; (2) mass coefficients $m_j = 2$ k-s^2/in., $j = 1, 2, \ldots, 8$; (3) 1% critical damping for all modes. An artificial earthquake excitation is used that is

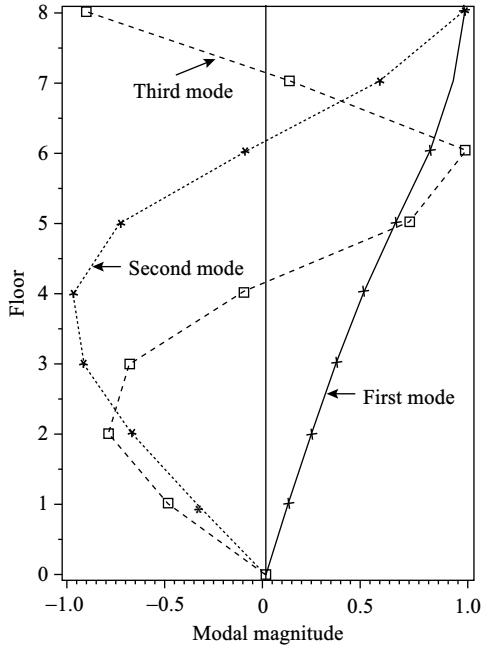

FIGURE 7.2 First three mode shapes of an eight-story building.

expressed as

$$\ddot{x}_g(t) = 0.05g\,(0.2\sin 3.5t + \sin 9t + 3\sin 15t) \tag{7.16}$$

Riccati optimal active control algorithm is used to design the control system, and the weighting matrices $[Q]$ and $[R]$ are assumed to be diagonal with the values $Q(i,i) = 1500$, $i = 1, 2, \ldots, 16$; and $R(1,1) = R(2,2) = 0.15$.

As an initial selection of the optimal actuator location, the eighth and the fourth floors can be suggested as the suitable choice. This is because the modal coordinates are maxima at eighth floor for the first mode, and at fourth floor for the second mode, as Figure 7.2 shows. Using performance indices expressed by Equations 7.14 and 7.15, several trials were made and part of the results is shown in Tables 7.1 and 7.2. Table 7.1 shows that, if the response index by Equation 7.15 is used as the criterion for optimal actuator placement, the best locations would be fifth and sixth floors. Obviously, this choice (fifth and sixth floors) has least maximum displacement and acceleration response. However, the maxima of the control forces for the fifth and sixth floor choice is slightly greater. In order to carry out a better comparison, the maxima of control forces are set to be equal at about 150 kips by allowing the elements of weighting matrix $[R]$ to be different for each choice of actuator location as Table 7.2 shows. Since the required control forces are approximately equal, the choice that has least structural response maximizes the

TABLE 7.1
Optimal Actuator Locations—Fixed $R(i,i) = 0.15$ and Excitation by Equation 7.16

Actuator location	4 and 8	5 and 6	1 and 2	6 and 7	7 and 8
Control energy	74,829	74,132	78,514	61,429	60,075
Response index	368	266	346	294	386
Maximum displacement (in.)					
Floor 1	1.94	1.72	1.87	1.77	2.00
Floor 2	3.27	2.95	3.21	3.03	3.44
Floor 3	3.43	3.21	3.50	3.33	3.72
Floor 4	3.40	2.45	3.20	2.56	2.88
Floor 5	5.95	4.74	5.83	4.95	5.58
Floor 6	6.67	5.78	6.66	6.18	7.46
Floor 7	5.61	4.16	5.15	4.21	5.37
Floor 8	8.64	6.89	8.33	7.13	8.60
Maximum acceleration (g%)					
Floor 1	90	80	83	84	93
Floor 2	146	127	131	134	150
Floor 3	134	109	116	117	135
Floor 4	55	40	47	39	46
Floor 5	148	140	150	146	151
Floor 6	189	173	183	188	212
Floor 7	59	47	57	42	51
Floor 8	179	152	167	158	185
Maximum control force (kips)	4th . . . 8th	5th . . . 6th	1st . . . 2nd	6th . . . 7th	7th . . . 8th
	92 . . . 164	95 . . . 179	158 . . . 149	142 . . . 137	163 . . . 99
R(1,1)	0.15	0.15	0.15	0.15	0.15
R(2,2)	0.15	0.15	0.15	0.15	0.15

actuator effectiveness and thus is optimal actuator location. The response index, maximum displacements, and accelerations are least for the fifth and sixth floor choice, thus this choice is optimal actuator location. Both Tables 7.1 and 7.2 shows that the control energy index is the least for the choice of seventh and eighth floor. However, this choice is not optimal actuator location because its structural response is much higher than that of the choice of fifth and sixth floors. This means that the control energy index may not be a good criterion for optimal actuator placement.

To verify this optimal actuator location, time-history responses of the eighth floor displacement to the excitation expressed by Equation 7.16 are compared for the choice of fifth and sixth floors and the choice of fourth and eighth floors. Figures 7.3, 7.4, and 7.5 shows the total response, first mode response and second mode response, respectively. Since the maximum active control forces are set approximately to 150 kips, the choice of fifth and sixth floor is better because

TABLE 7.2
Optimal Actuator Locations—Equal Control Force and Excitation by Equation 7.16

Actuator locations	4 and 8	5 and 6	1 and 2	6 and 7	7 and 8
Control energy	93,283	83,716	75,333	70,955	70,856
Response index	331	249	349	280	390
Maximum displacement (in.)					
Floor 1	1.96	1.71	1.86	1.79	2.11
Floor 2	3.31	2.93	3.21	3.02	3.61
Floor 3	3.44	3.17	3.50	3.31	3.87
Floor 4	3.20	2.38	3.73	2.49	2.88
Floor 5	5.70	4.64	5.87	4.90	5.61
Floor 6	6.29	5.59	6.68	6.09	7.62
Floor 7	5.09	4.03	5.20	3.99	5.35
Floor 8	8.06	6.64	8.38	6.88	8.67
Maximum acceleration (g%)					
Floor 1	92	80	84	86	98
Floor 2	149	127	132	136	158
Floor 3	138	110	117	119	142
Floor 4	55	41	48	39	46
Floor 5	149	138	150	148	156
Floor 6	189	172	183	192	222
Floor 7	57	47	57	42	54
Floor 8	180	152	167	159	195
Maximum control forces (kips)	4th . . . 8th	5th . . . 6th	1st . . . 2nd	6th . . . 7th	7th . . . 8th
	150 . . . 154	149 . . . 151	148 . . . 151	152 . . . 152	149 . . . 147
R(1, 1)	0.085	0.095	0.16	0.13	0.155
R(2, 2)	0.160	0.180	0.15	0.125	0.095

more reduction of structural response is achieved by this choice. To test if this optimal actuator location is still optimal for a different earthquake excitation, the following artificial earthquake ground motion is employed.

$$\ddot{x}_g(t) = 0.02\,(0.2\sin 3.5t + 7.0\sin 9t + 3.3\sin 15t) \tag{7.17}$$

Compared to the excitation by Equation 7.16, this ground motion excites the second modes more than other modes. The elements of the weighting matrix $[Q]$ are fixed at $Q(i, i) = 1500$, and the elements of the weighting matrix $[R]$ are different such that the maximum active control forces are approximately equal at 150 kips. Two choices, fourth and eighth floor and fifth and sixth floor are evaluated. The results are shown in Table 7.3. The fifth and sixth floor choice is still better than the choice of fourth and eighth floor since the former has less response index. Again, the control energy index is higher at the optimal actuator location, the fifth and

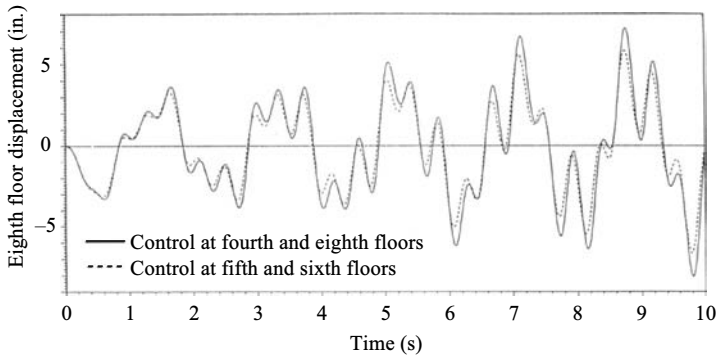

FIGURE 7.3 Response comparisons for two actuator locations on the eight-story building.

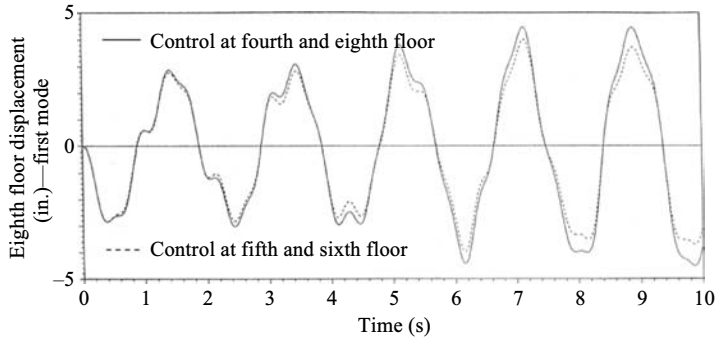

FIGURE 7.4 Comparison of first mode response for two actuator locations on the eight-story building.

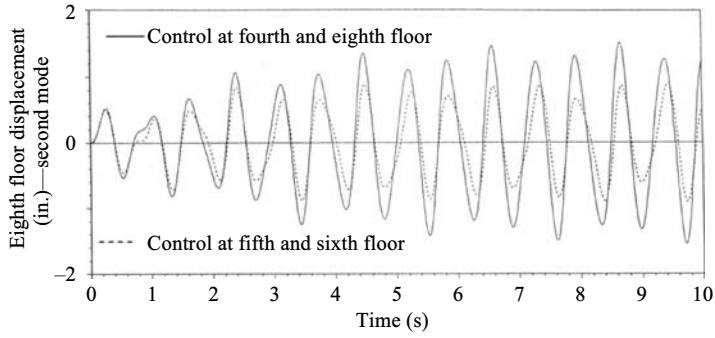

FIGURE 7.5 Comparison of second mode response for two actuator locations on the eight-story building.

TABLE 7.3
Optimal Actuator Locations—Equal Control Forces and Excitation by Equation 7.17

Actuator locations	4 and 8	5 and 6
Control energy	124,966	130,195
Response index	604	480
Maximum displacement (in.)		
Floor 1	2.77	2.39
Floor 2	5.07	4.37
Floor 3	6.39	5.46
Floor 4	6.39	5.39
Floor 5	6.05	5.25
Floor 6	3.65	4.05
Floor 7	6.49	6.05
Floor 8	8.75	8.18
Maximum acceleration (%g)		
Floor 1	298	80
Floor 2	149	127
Floor 3	138	110
Floor 4	55	41
Floor 5	149	138
Floor 6	189	172
Floor 7	57	47
Floor 8	180	152
Maximum control forces (kips)	4th . . . 8th	5th . . . 6th
	150 . . . 152	153 . . . 152
R(1, 1)	0.075	0.30
R(2, 2)	0.620	0.720

sixth floor choice. Thus, the response index can be a better measurement than the control energy index.

7.2.3 Controllability Index

The earlier two methods for optimal actuator placement have their weaknesses: the measure of modal controllability may not be suitable for these systems with multiple significant modes; the performance indices require that the integration of the seismic structural response in time history be calculated, which is a complicated procedure. To further reduce the calculation complexity, researchers have developed the *controllability index* for optimal actuator placement [10,11,29]. This method is discussed in detail through this section.

7.2.3.1 Basic concepts

As discussed in Section 7.2.1.1, Laskin [23] first defined a controllability index, which is linked with initial disturbance problem. A system is controllable if it is possible to find certain control action to dampen any initial system state $\{Z(t_0)\}$ to the origin (the neutral state) in finite time $T^* = (t_f - t_0)$. This definition only reveals that a system is either controllable or uncontrollable. It is desirable to consider how controllable a system is. This motivation leads to the definition of the degree of controllability (DOC).

The state equation of a second-order system subjected to an initial disturbance $\{Z(t_0)\}$ can be written as

$$\left\{\dot{Z}(t)\right\} = [A]\{Z(t)\} + [B]\{u(t)\} \tag{7.18}$$

with

$$\{Z(t)\}\big|_{t=t_0} = \{Z(t_0)\} \tag{7.19}$$

where $\{Z(t)\}$ is state vector of structural displacement and velocities, $[A]$ is plant matrix, $[B]$ is actuator location matrix, and $\{u(t)\}$ is vector of active control forces. Since all actuators have limitation on their force-generating capacity, the active control forces are accompanied by the constraint

$$|u_i(t)| \leq u_{i,\max}, \quad i = 1, 2 \ldots, r \tag{7.20}$$

where $u_{i,\max}$ is saturation limit of the ith control force; r is number of actuators.

The control objective is to drive the initial disturbed state $\{Z(t_0)\}$ to the origin. Assume this control objective is achieved with the control energy E^* and in the possible time T^*. Laskin [23] defines a recovery region for the special $E^*$and T^* as the volume in which every initial condition $\{Z(t_0)\}$ can be driven to the origin at time T^*, with a set of control forces $|u_i(t)| \leq u_{i,\max}$, and for which the total energy required for all r actuators during period t_0 to $t_f = T^* + t_0$ is less than or equal to E^*. The DOC is thus equal to the lower limit of the recovery region. In other words, the DOC is a scalar measure of the recovery region, which determines the region's smallest dimension.

7.2.3.2 Controllability index for seismic-resistant structures

With the definition of DOC, the optimal actuator location corresponds to where the DOC is to be maximized, that is, the location of actuators is optimized in the sense that it maximizes the smallest dimension of the recovery region. Following the Lashin's definition of DOC, the controllability index has been proposed [11] as the criterion for optimal actuator placement on seismic-resistant structures. This criterion is discussed as follows.

The motion equations of structures with active control have been derived in Chapter 4 as

$$[M]\{\ddot{x}(t)\} + [C]\{\dot{x}(t)\} + [K]\{x(t)\} = [\gamma]\{u(t)\} + \{\delta\}\ddot{x}_g(t) \tag{7.21}$$

Its modal equations can be written as

$$\ddot{q}_i(t) + 2\zeta_i\omega_i\dot{q}_i(t) + \omega_i^2 q_i(t) = \frac{\{\phi_i\}^T[\gamma]\{u(t)\} + \{\phi_i\}^T\{\delta\}\ddot{x}_g(t)}{\{\phi_i\}^T[M]\{\phi_i\}} \tag{7.22}$$

To develop the criterion for optimal actuator placement on seismic-resistant structures, the following facts must be taken into consideration:

(a) Lower modes are dominant in structural seismic response.
(b) The control objective is to reduce the structural seismic response and improve the stability of the seismic-resistant structure.
(c) The control effort in terms of control power is limited.
(d) The structural response should not exceed certain thresholds for the safety and serviceability of the structure.

On the basis of these facts, the following assumptions are used to develop a meaningful criterion for actuator placement:

(a) Use the modal shapes of the uncontrolled structure to evaluate the influence of each mode.
(b) Use the response spectra of the actual earthquake when evaluating the response of the uncontrolled structure.
(c) Active tendons are used to implement the active control system in which the actuator is linear proportional device.

Subject to the above assumptions and facts, a controllability index is defined as the criterion for optimal actuator placement on seismic-resistant structures. This criterion assumes that the optimal actuator location is where the displacement of an uncontrolled structure is largest. For an active tendon control system, the controllability index $\rho(X)$ is defined as [11]

$$\rho(X) = \max \sqrt{\sum_{j=1}^{n} \left\{ \frac{\Delta[\phi_j(X)]}{\Delta X} Y_j(t) \right\}^2} \tag{7.23}$$

where X is a percentage of total structure height at the actuator location ($0 \le X \le 1$); n is number of significant modes; $\phi_j(X)$ is jth mode shape; $Y_j(t)$ is maximum response spectrum value for jth mode; $\Delta[\ ]$ refers to spatial difference of the quantity from position X_1 to position X_2; X_1 is height where the actuator cylinder is attached and X_2 is height where the tendon is anchored; and ΔX is height difference

between X_1 and X_2. The algebraic difference of the mode shapes is taken because the relative displacement between floors is a critical parameter for active tendons. The effect of earthquake excitations is taken care by the maximum spectrum value. The different modes are weighted in a RMS fashion since the modal maxima do not occur at the same time. With the stipulations outlined above, the optimal actuator location is defined to be the value of X for which $\rho(X)$ is maximum. The next best actuator location is one for which $\rho(X)$ has the second largest value, and so on.

Advantages of this criterion by controllability index are the simple objective function and the ability to handle multiple significant modes. However, it is based on response spectra and mode shapes of an uncontrolled structure. This approximation affects the accuracy and limits the applicability of the criterion. The reason is as follows. Mode shapes of controlled structures are different from these of uncontrolled structures due to actuator dynamics, interaction between structure and actuator, and nonorthogonal damping and stiffness of a controlled structure. Moreover, response spectra are based on *effective peak accelerations* (EPA) and *effective peak velocities* (EPV) of uncontrolled structures with assumed damping such as 5% used here.

EXAMPLE 7.2.2

The two-story shear building with one active tendon system in Example 7.2.2 serves as an example here. Using the controllability index find the optimal actuator location.

Solution

The natural frequencies and mode shapes of this system have been calculated in Example 7.2.1 as

$$\omega_1 = 11.829 \text{ rad/s}, \quad \{\phi_1\} = \begin{Bmatrix} 0.7915 \\ 1.0 \end{Bmatrix} \tag{a}$$

$$\omega_2 = 32.905 \text{ rad/s}, \quad \{\phi_2\} = \begin{Bmatrix} -0.6131 \\ 1.0 \end{Bmatrix} \tag{b}$$

Thus the natural frequencies in cps are

$$f_1 = \frac{\omega_1}{2\pi} = \frac{11.829}{[2(3.1415926)]} = 1.883 \text{ cps} \tag{c}$$

$$f_2 = \frac{\omega_2}{2\pi} = \frac{32.905}{[2(3.1415926)]} = 5.237 \text{ cps} \tag{d}$$

Using the response spectra for the 1940 N-S El-Centro earthquake record [5] as shown in Figure 7.6, the two maximum modal response values in

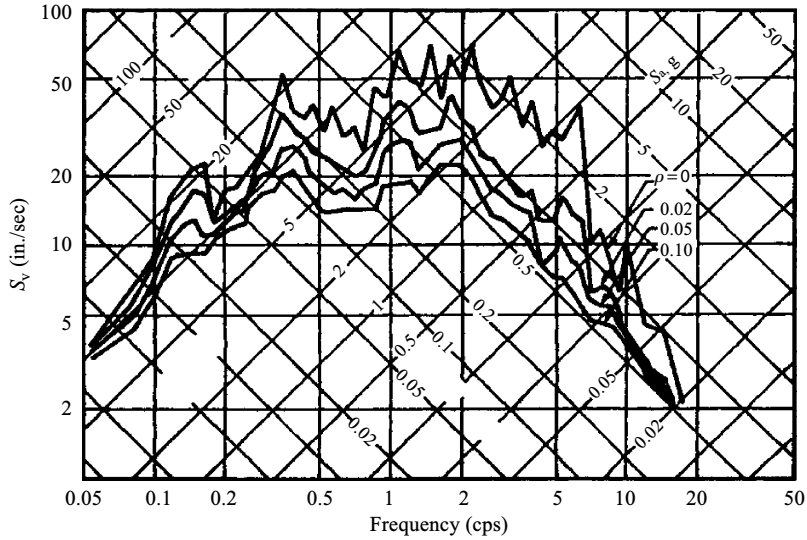

FIGURE 7.6 Response spectra for N-S component of El-Centro earthquake, May 18, 1940.

inches are

$$\begin{cases} Y_1 = 3.29 \\ Y_2 = 0.49 \end{cases} \tag{e}$$

Let the active tendon be at the first floor, and assume that the first and the second floors have same story heights. Then

$$\begin{cases} x_2 = 0.5, x_1 = 0 \\ \Delta x = x_2 - x_1 = 0.5 \\ \Delta\left[\phi_1(x)\right] = \phi_1(x_2) - \phi_1(x_1) = 0.7915 - 0 = 0.7915 \\ \Delta\left[\phi_2(x)\right] = \phi_2(x_2) - \phi_2(x_1) = -0.6131 - 0 = -0.6131 \end{cases} \tag{f}$$

Then from Equation 7.23 the controllability index for active tendon at first floor is

$$\begin{aligned} \rho_1 &= \sqrt{\sum_{j=1}^{2} \left\{ \frac{\Delta\left[\phi_j(x)\right]}{\Delta x} Y_j \right\}^2} \\ &= \sqrt{\left[\frac{0.7915}{0.5}(3.29)\right]^2 + \left[\frac{-0.6131}{0.5}(0.49)\right]^2} \\ &= 5.24 \end{aligned} \tag{g}$$

If the active tendon is installed on the second floor,

$$\begin{cases} x_2 = 1.0,\ x_1 = 0.5 \\ \Delta x = 1.0 - 0.5 = 0.5 \\ \Delta\left[\phi_1(x)\right] = 1.0 - 0.7915 = 0.2085 \\ \Delta\left[\phi_2(x)\right] = 1.0 - (-0.6131) = 1.6131 \end{cases} \tag{h}$$

$$\rho_2 = \sqrt{\sum_{j=1}^{j=2} \left\{ \frac{\Delta\left[\phi_j(x)\right]}{\Delta x} Y_j \right\}^2} = \sqrt{\left[\frac{0.2085}{0.5}(3.29)\right]^2 + \left[\frac{1.6131}{0.5}(0.49)\right]^2}$$

$$= 2.09 \tag{i}$$

Since $\rho_1 > \rho_2$, the largest value of controllability index occurs when tendon is located at the first floor. Thus, according to the controllability index criterion, the first floor is the optimal actuator location for the active tendon system.

7.2.3.3 Numerical studies

A 15-story shear building, as shown in Figure 7.7, is studied for the optimal location of two active tendons on two of its floors. Structural properties are floor stiffness $k_i = 3000$ k/in. and floor mass $m_i = 2$ k-s^2/in ($i = 1, 2, \ldots, 15$), and

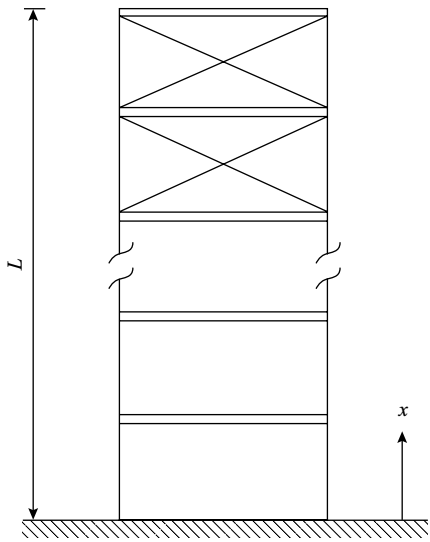

FIGURE 7.7 Fifteen-story shear building with two active tendon systems.

TABLE 7.4
Determination of Controllability Index

Floor	x	1st mode $\phi_1(x)$	2nd mode $\phi_2(x)$	$\Delta\phi_1/\Delta x$	$\Delta\phi_2/\Delta x$	$\rho(x)$
1	0.067	0.026	−0.076	0.390	1.140	10.60
2	0.133	0.051	−0.145	0.375	1.035	9.76
3	0.200	0.076	−0.201	0.375	0.840	8.45
4	0.267	0.100	−0.238	0.360	0.555	6.59
5	0.333	0.123	−0.254	0.345	0.240	5.01
6	0.400	0.145	−0.246	0.330	0.120	4.52
7	0.467	0.165	−0.216	0.300	0.450	5.42
8	0.533	0.184	−0.165	0.285	0.765	7.27
9	0.600	0.201	−0.100	0.255	0.975	8.60
10	0.667	0.216	−0.026	0.225	1.110	9.47
11	0.733	0.228	0.051	0.180	1.155	9.65
12	0.800	0.238	0.123	0.150	1.080	8.97
13	0.867	0.246	0.184	0.120	0.915	7.57
14	0.933	0.251	0.228	0.075	0.660	5.43
15	1.000	0.254	0.251	0.045	0.345	2.86

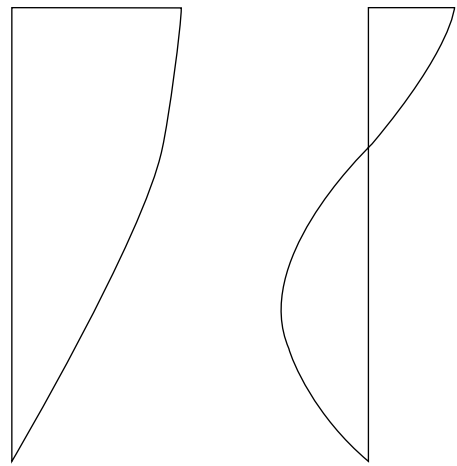

FIGURE 7.8 First two mode shapes of the 15-story building.

damping 3% critical. The first two natural frequencies of the structure with control are $\omega_{n1} = 3.923$ rad/s and $\omega_{n2} = 11.730$ rad/s, which correspond to periods $T_1 = 1.60$ s and $T_2 = 0.54$ s. The mode shapes of the first two modes are given in Table 7.4 and shown in Figure 7.8.

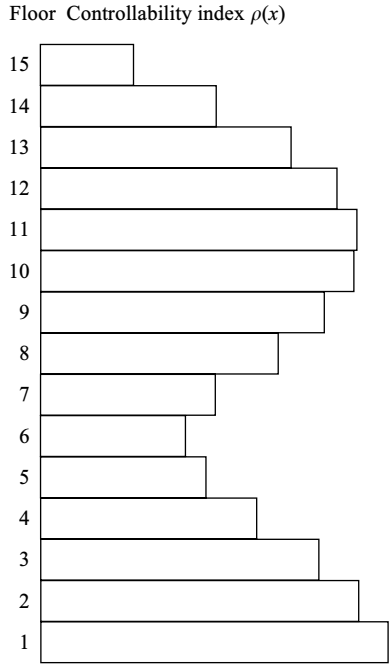

FIGURE 7.9 Controllability index values for optimal actuator locations on the 15-story building.

7.2.3.3.1 Determination of optimal placement of active tendons

The controllability index of Equation 7.23 is used to establish optimal locations of the two active tendons. Using response spectra for the 1940 N-S El-Centro earthquake record (see Figure 7.6), the first two maximum modal response values are

$$\begin{cases} Y_1 = 0.439 \text{ ft} \\ Y_2 = 0.265 \text{ ft} \end{cases} \tag{7.24}$$

The first two modes are considered in evaluating the value of the controllability index. Values of the index $\rho(x)$ for each tendon location is given in Table 7.4 and a plot of $\rho(x)$ is shown in Figure 7.9. It is seen that the two largest values of $\rho(x)$ occur at the first and second floors, which are optimal locations for the active tendons according to the controllability index criterion.

7.2.3.3.2 Comparison of controllability index and control energy index

To show the consistency of two optimal actuator placement criteria, $\rho(x)$ and J_E, numerical analysis of two cases of locating active tendons is made to compare the

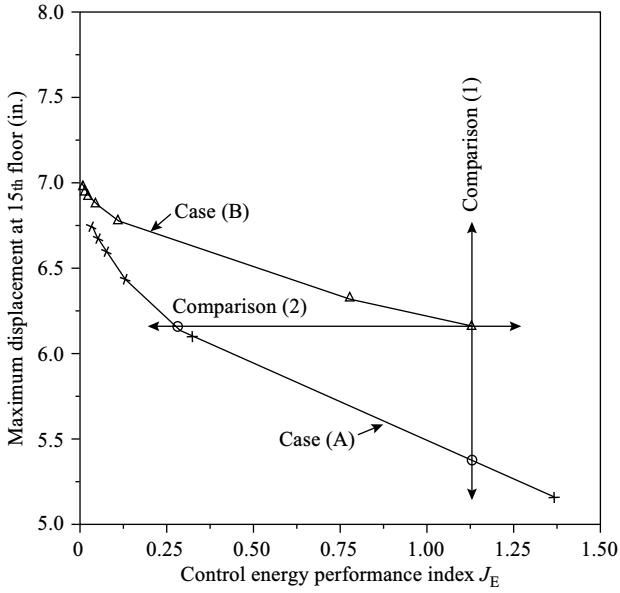

FIGURE 7.10 Response comparisons for two actuator locations on the 15-story building.

two criteria. In case (A), floors one and two are equipped with active tendons. In case (B), the two active tendons are installed at floors six and fifteen. Recall that using the controllability index criterion, the case (A) is optimal and thus is superior to the case (B). Figure 7.10 is a plot of two cases. The horizontal axis of the figure is the control energy index of Equation 7.14 and the vertical axis is the maximum displacement response at the 15th floor. As shown in Figure 7.10, case (A) produces less response with same amount of control energy, and requires less control energy to reduce the maximum displacement response at the 15th floor. Similar results are true for other tendon locations and all the other response quantities [11]. Thus, the criterion of control energy index J_E is automatically satisfied by the criterion controllability index $\rho(x)$.

7.2.3.3.3 Demonstration of significance of optimal actuator placement

In order to show the effectiveness of optimal actuator placement, two comparisons are made for the two cases (A) and (B), as shown in Figure 7.10. In the first comparison (1), the two cases have the same control energy index fixed at a level of 1.1×10^6. Figures 7.11 and 7.12 shows the displacement response of the 1st and the 15th stories for the fixed control energy level. It is observed that the optimal tendon location can maximize the control effectiveness, thus has smaller displacement response. Adversely, less control force or less control energy are required for an optimally placed active tendon system to reduce the structural response to a certain level. This is demonstrated in the second comparison (2) where the 15th

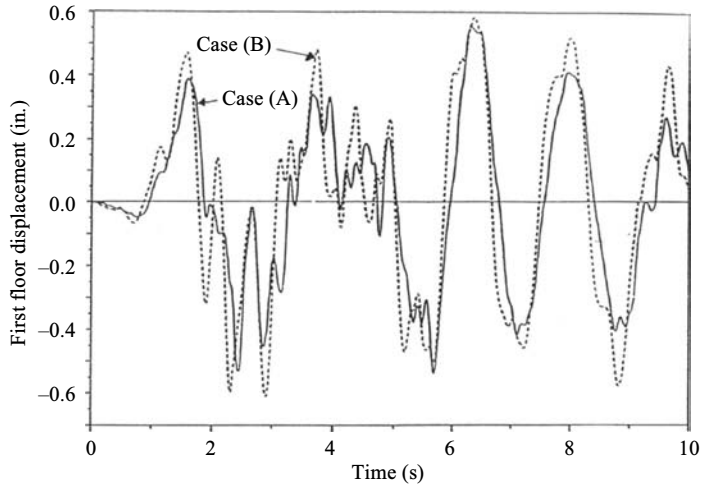

FIGURE 7.11 Comparison of first floor response for two actuator locations on the 15-story building with fixed control energy.

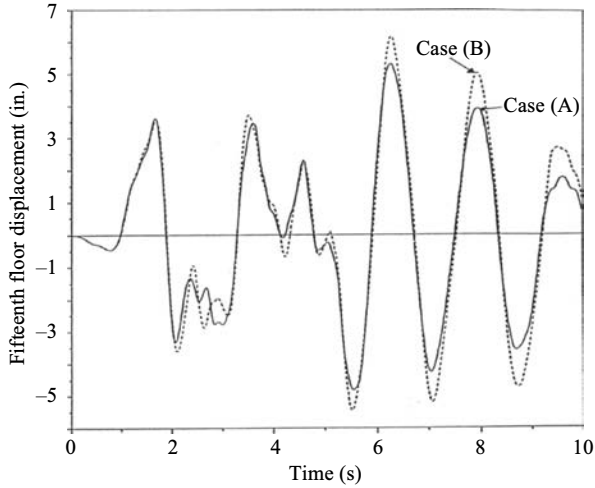

FIGURE 7.12 Comparison of top-floor response for two actuator locations on the 15-story building with fixed control energy.

story maximum displacement was made equal for both cases (A) and (B) at 6.16 in. as shown in Figures 7.10 and 7.13. Then the two sets of the pairs of control forces required were studied for cases (A) and (B). Figure 7.14 compares the first-story control force of case (A) and the sixth-story control force of case (B). Figure 7.15 compares the second-story control force of case (A) with the 15th story control force of case (B). Again, it can be seen that case (A) requires less control force.

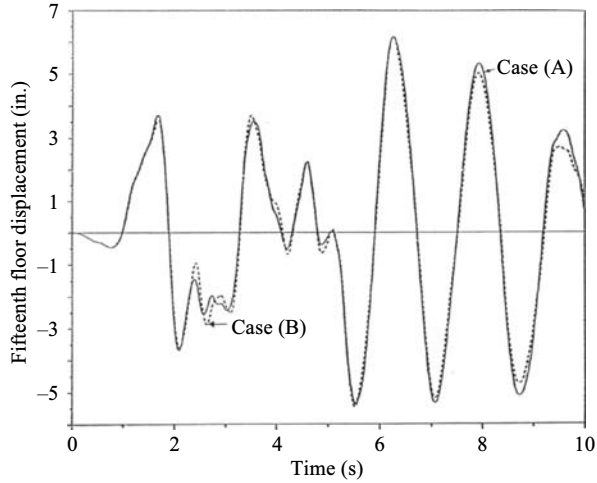

FIGURE 7.13 Top-floor displacement responses for two actuator locations with maximum set same.

The control energy index for case (A) is 0.28×10^6, as compared to 1.1×10^6 for case (B). Hence, case (A) is optimal from both the response and control energy points of view.

7.2.3.3.4 Effect of controlled mode shapes on optimal locations

Recall that the controllability index by Equation 7.23 is based on the mode shape of uncontrolled structure. With control force applied to the structure, the structural damping and stiffness are changed, and thus mode shapes of controlled structure are no longer the same as those of the uncontrolled structure. Thus, it is desirable to investigate whether this difference is significant enough to alter the optimal locations found by the criterion of controllability index.

The closed-loop mode shapes can be found by solving eigenvectors of the closed-loop plant matrix $[A_C]$ by Equation 4.99. Riccati optimal active control algorithm determines the feedback gain matrix $[G]$ in Equation 4.99. The weighting matrix $[Q]$ is assumed to be diagonal with $q_{ii} = 15{,}000$ and $[R]$ matrix is varied to achieve different levels of control forces. The controllability index $\rho(x)$ is recalculated using the mode shapes of the controlled structure, and the result is shown in Table 7.5 and Figure 7.16. It can be observed that the first and second stories are still optimal. Thus, the criterion of controllability index is not sensitive to the mode shapes of controlled or uncontrolled structures.

7.2.3.3.5 Effect of different earthquakes on optimal locations

Recall that the optimal tendon locations for the 15-story building were found using response spectra of the N-S horizontal component of the El-Centro 1940 earthquake. It is desirable to determine whether this location would still be optimal for another earthquake. For this purpose, the response spectra of the 1985 Mexico

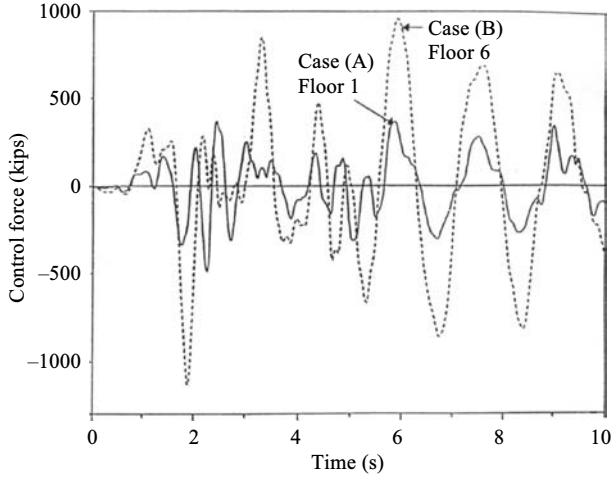

FIGURE 7.14 Comparison of required control forces by tendons at first floor of Case (A) and sixth floor of Case (B).

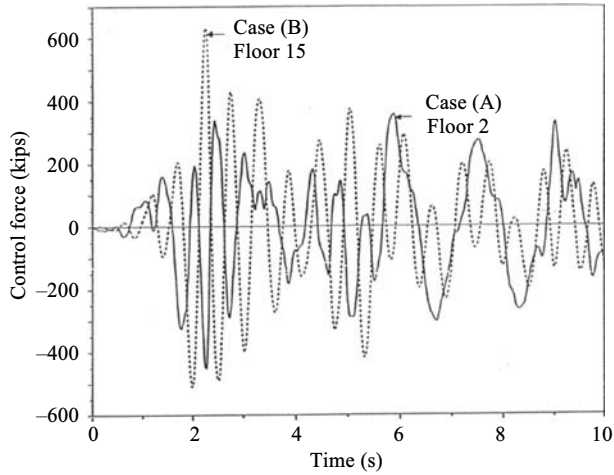

FIGURE 7.15 Comparison of required control forces by tendons at second floor of Case (A) and 15th floor of Case (B).

City earthquake (see Figure 7.17) is used. Judgment of whether the optimal locations will remain the same is made by observing the response spectra for the displacement of the two records, since this will be the only parameter that will change in the controllability index by Equation 7.23. Figure 7.17 shows that the two curves though not identical are parallel for the range of periods of interest. Note that in calculating the optimal locations the relative (not the absolute) magnitude of displacement response spectra is of importance. The fact that the

TABLE 7.5
Optimal Locations Using Mode Shapes of Controlled Structures

Floor	x	1st mode $\phi_1(x)$	2nd mode $\phi_2(x)$	$\Delta\phi_1/\Delta x$	$\Delta\phi_2/\Delta x$	$\rho(x)$
1	0.067	−0.001834	−0.003151	0.390	0.375	6.04
		$-0.025766j$	$-0.024536j$			
2	0.133	−0.003617	−0.005974	0.375	0.330	5.69
		$-0.051317j$	$-0.046907j$			
3	0.200	−0.004338	−0.005457	0.375	0.270	5.48
		$-0.076337j$	$-0.065211j$			
4	0.267	−0.004998	−0.004615	0.375	0.195	5.26
		$-0.100578j$	$-0.077544j$			
5	0.333	−0.005639	−0.003596	0.345	0.075	4.66
		$-0.123802j$	$-0.082845j$			
6	0.400	−0.006209	−0.002401	0.330	0.045	4.43
		$-0.145723j$	$-0.080325j$			
7	0.467	−0.006738	−0.001225	0.300	0.135	4.16
		$-0.166170j$	$-0.070538j$			
8	0.533	−0.007216	−0.000119	0.285	0.255	4.34
		$-0.184904j$	$-0.054262j$			
9	0.600	−0.007645	0.000852	0.255	0.315	4.26
		$-0.201744j$	$-0.032982j$			
10	0.667	−0.008018	0.001665	0.225	0.360	4.19
		$-0.216518j$	$-0.008683j$			
11	0.733	−0.008335	0.002288	0.180	0.390	3.97
		$-0.229068j$	$+0.016392j$			
12	0.800	−0.008590	0.002749	0.150	0.345	3.44
		$-0.239264j$	$+0.039978j$			
13	0.867	−0.008780	0.003071	0.120	0.300	2.91
		$-0.247005j$	$+0.059882j$			
14	0.933	−0.008910	0.003252	0.075	0.210	1.97
		$-0.252214j$	$+0.074234j$			
15	1.000	−0.008969	0.003347	0.045	0.120	1.14
		$-0.254830j$	$+0.081778j$			

response spectra are parallel will produce the same optimal locations. Thus, it can be predicted that the locations found for El-Centro will still be optimal for the Mexico earthquake. Calculation of the controllability index $\rho(x)$ for the Mexico earthquake shows that the case of floors 1 and 2 is still optimal.

7.2.3.3.6 Variability of optimal locations with structural properties

The structural properties of the 15-story building are modified to observe whether or not the optimal locations will be different from those found earlier. Recall that the optimal locations were the first and second floor for the choice of two active

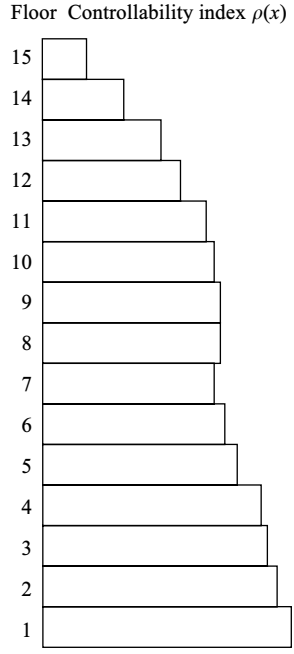

FIGURE 7.16 Controllability index for the 15-story building using mode shapes of controlled structure.

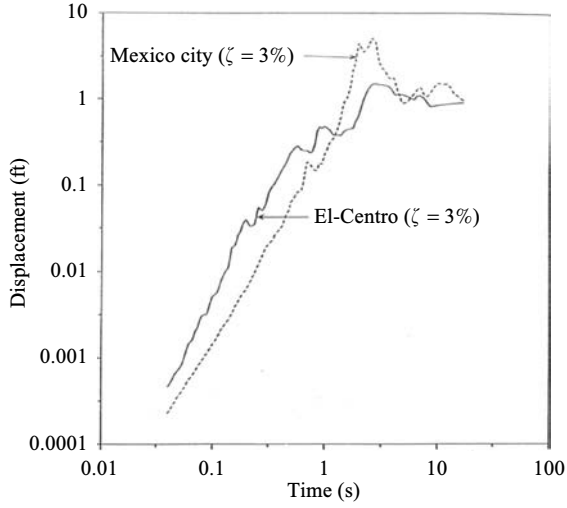

FIGURE 7.17 Comparison of displacement response spectra for 1940 El-Centro and 1985 Mexico City earthquakes.

TABLE 7.6
Controllability Index for the 15-Story Building

Floor	1st mode (ϕ_1)	2nd mode (ϕ_2)	$\Delta\phi_1/\Delta x$	$\Delta\phi_2/\Delta x$	$\rho(x)$
1	0.013	−0.042	0.195	0.630	0.647
2	0.027	−0.086	0.210	0.660	0.687
3	0.042	−0.130	0.225	0.660	0.711
4	0.059	−0.173	0.255	0.645	0.754
5	0.077	−0.211	0.270	0.570	0.747
6	0.097	−0.240	0.300	0.435	0.755
7	0.120	−0.255	0.345	0.225	0.801
8	0.145	−0.250	0.375	0.075	0.853
9	0.174	−0.214	0.435	0.540	1.067
10	0.207	−0.138	0.495	1.140	1.412
11	0.235	−0.042	0.420	1.440	1.441
12	0.259	0.060	0.360	1.530	1.409
13	0.277	0.154	0.270	1.410	1.222
14	0.289	0.225	0.180	1.065	0.897
15	0.295	0.263	0.190	0.570	0.474

tendons. The structural parameters used here are $k_1 = 3{,}000$ k/in., $k_2 = 2{,}750$ k/in., $k_3 = 2{,}500$ k/in., $k_4 = 2{,}250$ k/in., $k_5 = 2{,}000$ k/in., $k_6 = 1{,}750$ k/in., $k_7 = 1{,}500$ k/in., $k_8 = 1{,}250$ k/in., $k_9 = 1{,}000$ k/in., $k_{10} = k_{11} = k_{12} = k_{13} = k_{14} = k_{15} = 800$ k/in.; $m_i = 2$ k-s^2/in., $i = 1, 2, \ldots, 15$; damping = 3% critical. The weighting matrix is diagonal with $Q_{i,i} = 15{,}000$ as before. The first two natural frequencies of structure without control are $\omega_1 = 2.896$ rad/s and $\omega_2 = 7.635$ rad/s, which correspond to periods of $T_1 = 2.17$ s and $T_2 = 0.82$ s, respectively. Using the response spectra values for the El-Centro 1940, N-S component, the following maximum response values are obtained: $Y_1 = 0.894$ ft, $Y_2 = 0.294$ ft. The first two modes are considered in evaluating the controllability index and the procedure is shown in Table 7.6. A plot of the controllability index of Table 7.6 is shown on Figure 7.18. It can be seen that the first and second floor locations are no longer optimal; instead, the optimal locations are the 10th and 11th floor. Thus, different structures have different optimal actuator location; even their number of stories and geometrical shapes are same.

7.2.3.3.7 Effect of number of modes considered in optimal locations selection

In these numerical studies above, it is assumed that two modes are enough to evaluate the optimal tendon locations. In order to find the truly optimal locations of active tendons, it is important to investigate if this assumption is accurate enough, or if not, how many modes are required.

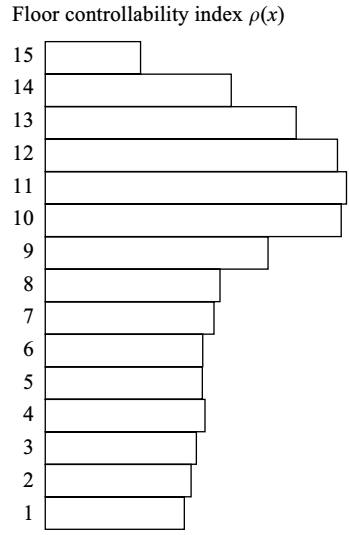

FIGURE 7.18 Controllability index for the modified 15-story structure.

In this study, the structural properties for the 15-story building in this example are as follows: $k_i = 300$ k/in.; $m_i = 6$ k-s^2/in., $i = 1, 2, \ldots, 7$ and $k_j = 200$ k/in.; $m_j = 5$ k-s^2/in., $j = 8, 9, \ldots, 15$; damping = 3% critical. Two active tendons are to be located optimally and, we consider only two modes at the start. The first natural frequency is $\omega_1 = 0.732$ rad/s and the second frequency and $\omega_2 = 1.954$ rad/s, with corresponding periods of $T_1 = 8.58$ s and $T_2 = 3.22$ s, respectively. Using response spectra of the 1985 Mexico City earthquake (shown in Figure 7.17), the following maximum response values are obtained: $Y_1 = 1.143$ ft, $Y_2 = 2.238$ ft. The first two modes are then used to calculate the controllability index of Equation 7.23 and the results are shown in Table 7.7. A plot of the controllability index is given in Figure 7.19. It is seen that the 10th and 11th floors are the optimal locations. Next, three modes are considered in calculating the controllability index of Equation 7.23, the first, second, and third. The third mode natural frequency is $\omega_3 = 3.350$ rad/s with corresponding period $T_3 = 1.88$ s. The maximum response value is $Y_3 = 2.684$ ft. The optimal locations are calculated using Equation 7.23 and the results are shown on Table 7.8. A plot of $\rho\,(x)$ for three modes is given in Figure 7.20. It can be seen that the optimal locations are no longer at the 10th and 11th floors but are at the 8th and 12th floors. The same result is obtained if one considers four modes, or five modes, as shown on Table 7.8 and Figure 7.9. Hence, the 8th and 12th floor locations are optimal.

From this study, we know that three modes are sufficient to use the controllability index by Equation 7.23 for optimal tendon placement on the 15-story structure. In other situations, more modes may need to be considered. The procedure can be terminated when an increase of the number of modes considered does not change the optimal locations.

TABLE 7.7
Controllability Index Using Two Modes

Floor	First mode (ϕ_1)	Second mode (ϕ_2)	$\Delta\phi_1/\Delta x$	$\Delta\phi_2/\Delta x$	$\rho(x)$
1	0.014	−0.041	0.21(0.88*)	0.62(0.84*)	5.42
2	0.024	−0.078	0.23(0.96)	0.56(0.76)	5.14
3	0.043	−0.110	0.21(0.88)	0.48(0.65)	4.49
4	0.056	−0.133	0.20(0.83)	0.35(0.47)	3.60
5	0.069	−0.146	0.20(0.83)	0.20(0.27)	2.86
6	0.081	−0.148	0.18(0.75)	0.03(0.04)	2.19
7	0.092	−0.138	0.17(0.71)	0.15(0.20)	2.35
8	0.108	−0.108	0.24(1.0)	0.45(0.61)	4.52
9	0.122	−0.068	0.21(0.88)	0.600.(0.81)	5.27
10	0.134	−0.021	0.18(0.75)	0.71(0.96)	5.88
11	0.145	0.028	0.17(0.71)	0.740.(10.0)	6.05
12	0.153	0.074	0.12(0.50)	0.69(0.93)	5.49
13	0.160	0.113	0.11(0.46)	0.59(0.80)	4.74
14	0.164	0.141	0.06(0.25)	0.42(0.57)	3.23
15	0.166	0.156	0.03(0.13)	0.23(0.31)	1.80

*Normalized.

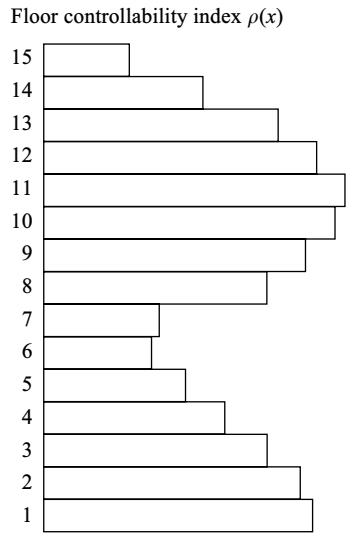

FIGURE 7.19 Controllability index using the first two modes.

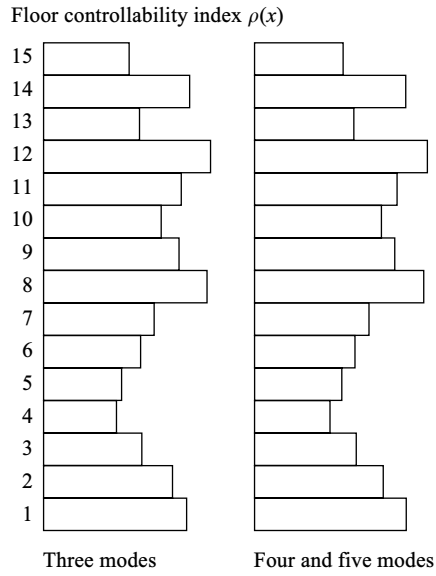

FIGURE 7.20 Controllability index with higher modes considered.

TABLE 7.8
Controllability Index—Higher Modes

	$\rho(x)$		
Floor	**Three modes**	**Four modes**	**Five modes**
1	7.27	7.36	7.361
2	6.41	6.44	6.443
3	4.88	4.88	4.884
4	3.65	3.75	3.752
5	3.95	4.13	4.136
6	4.88	5.00	5.004
7	5.57	5.59	5.590
8	8.18	8.20	8.197
9	6.80	6.91	6.908
10	5.90	6.05	6.052
11	6.88	6.93	6.927
12	8.39	8.39	8.392
13	4.84	4.96	4.962
14	7.28	7.41	7.414
15	4.22	4.33	4.335

TABLE 7.9
Frequencies and Mode Shapes when First Floor Stiffness Changes

	Frequency (Hz)	First mode	Second mode	Third mode
Original	2.863, 9.502, 15.06	[0.678 0.889 1.0]	[1.0 0.194 −0.850]	[−0.602 1.0 −0.480]
Case 1	3.318, 9.958, 15.18	[0.573 0.850 1.0]	[1.0 0.284 −0.815]	[−0.666 1.0 −0.469]
Case 2	3.871, 10.79, 15.50	[0.430 0.796 1.0]	[1.0 0.470 −0.805]	[−0.825 1.0 −0.441]
Case 3	4.192, 11.49, 15.91	[0.340 0.761 1.0]	[1.0 0.682 −0.859]	[−1.0 0.967 −0.396]

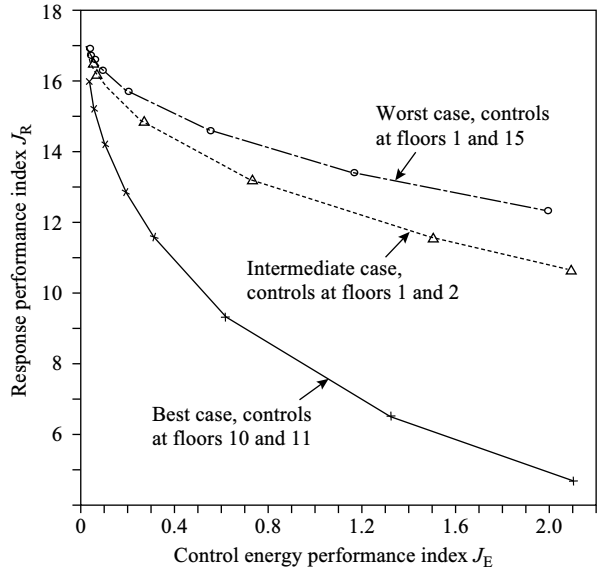

FIGURE 7.21 Relationship between control energy and response indices.

7.2.3.3.8 Validation of controllability index as optimal placement criterion

In order to verify the controllability index, a comparison is made between different optimal placement criterion and time-history response of the controlled structure is simulated. The 15-story building with structural properties same as those in Section 7.2.3.3.6 serves as an example here. The controllability index of Equation 7.23 using two modes is shown in Table 7.6 and Figure 7.18. According to the criterion of the controllability index, locations of the two active tendons are best at floors 10 and 11, intermediate at floors 1 and 2, and worst at floors 1 and 15. Figure 7.21 plots the control energy and response performance indices for these three cases. Consistent with the result by the controllability index, the case of floors 10 and 11 is the best because of giving the least response and the case of floors 1 and 15 gives the largest response thus is the worst, for all levels of control energy.

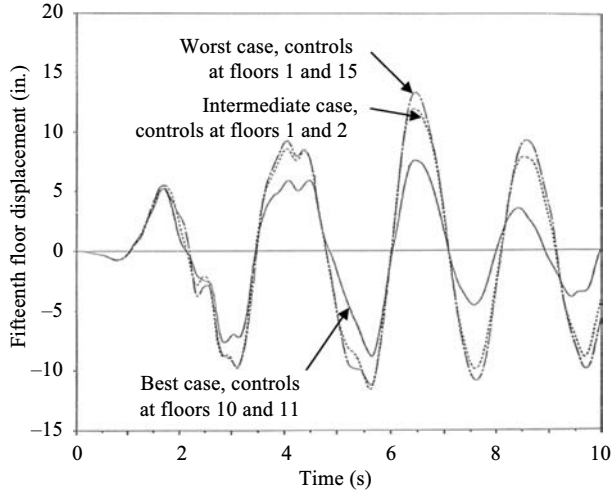

FIGURE 7.22 Response comparisons for three actuator placement options.

Actual time-history responses of the three cases to the El-Centro 1940 earthquake are compared, as shown in Figure 7.22. This figure confirms the validity of the controllability index as the optimum placement criterion for active control devices.

7.2.4 Discussions on Performance Indices

Performance indices have the advantage of applicability to seismic response control where multiple modes are significant. However, they have two weaknesses for optimal device placement of seismic response control systems. First, a trial and error procedure must be employed [11]. Second, seismic structural response in time history has to be solved and integrated, which means the performance index approach still requires large computing cost. Third, specific earthquake records have to be employed to determine the optimal device location. With great uncertainty in the nature of earthquake excitation, using different earthquake records can yield different optimal location. In the following section, a statistical method is developed for optimal placement of control devices. This method can overcome weaknesses of above approaches in that it is applicable to smart seismic structures with any control system, considers multiple significant modes of the structure, uses analytical model of controlled structures, and requires no complex calculation of seismic structural response in time history.

7.3 Statistical Method for Optimal Device Placement of Smart Seismic Structures

As noted, it is important to place dampers and actuators optimally so as to maximize the control efficiency of a control system. This section develops a general, accurate, and statistical method for optimal device placement of smart seismic structures

[7,8,18,20]. It is general as it is applicable to smart structures using dampers, actuators, and their combination (i.e., hybrid devices). It is accurate as it starts with a mathematical models that considers dynamics of actuators and dampers and nonorthogonal damping and stiffness of controlled structures. The statistical nature of this method gives a further advantage that the optimal device locations do not depend on the earthquake records. This section uses hybrid systems as the example to demonstrate the method. A hybrid control system can be complicated as it may consist of multiple actuators and dampers, as shown in Figure 1.34a. Pure passive (or active) systems are simplified cases of hybrid systems in that they are a "hybrid" system without active devices (or passive dampers).

7.3.1 System Description

7.3.1.1 Dynamic model of hybrid-controlled seismic-resistant structures

A structure with hybrid bracing control system, as shown in Figure 1.34a, uses K-brace mounted viscous fluid dampers and servovalve controlled actuators. The analytical model of this controlled structure under earthquake excitation $\ddot{x}_g(t)$ has been derived as

$$\{\dot{Z}(t)\} = [A]\{Z(t)\} + [B_u]\{u(t)\} + \{B_r\}\ddot{x}_g(t) \tag{7.25}$$

where $\{Z(t)\}$ is state vector, $[A]$ is plant matrix, $[B_u]$ is coefficient matrix of the control command vector $\{u(t)\}$, and $\{B_r\}$ is coefficient vector of the reference input (i.e., earthquake excitation) $\ddot{x}_g(t)$. Different systems have different elements for these vectors and matrices. Since dynamics of control devices (dampers and actuators) is considered here, the state vector should include variables for control devices in addition to those for structural responses, as discussed in Chapter 4.

Optimal algorithms by full-state feedback lead to the following control law:

$$\{u(t)\} = -[G]\{Z(t)\} \tag{7.26}$$

Substituting Equation 7.26 into Equation 7.25 yields the state variable representation of the closed-loop system (i.e., the controlled structure) as

$$\left\{\dot{Z}(t)\right\} = [A_C]\{Z(t)\} + \{B_r\}\ddot{x}_g(t) \tag{7.27}$$

and the plant matrix of the controlled structure system as

$$[A_c] = [A] - [B_u][G] \tag{7.28}$$

7.3.1.2 Stochastic model of earthquake ground motions

As proposed by Kanai and Tajimi [21,33], earthquake horizontal ground acceleration $\ddot{x}_g(t)$ can be modeled as a stationary *Gaussian random process* with a zero

mean and characterized by its power spectral density $G(\omega)$

$$G(\omega) = \frac{(1 + 4\zeta_g^2\omega^2/\omega_g^2)G_0}{(1 - \omega^2/\omega_g^2)^2 + 4\zeta_g^2\omega^2/\omega_g^2}; \quad \omega \geq 0 \tag{7.29}$$

where G_0 is spectral intensity of the ground acceleration, ζ_g and ω_g are damping ratio and prevailing circular frequency, respectively, which describe soil deposit characteristics. ω_g is called prevailing frequency because it corresponds the largest *power spectral density*. Parameters in the spectrum model are proposed by the authors [28] as

$$\begin{cases} \text{Firm soil:} & \omega_g = 31.4 \text{ rad/s}; \ \zeta_g = 0.55 \\ \text{Medium soil:} & \omega_g = 15.6 \text{ rad/s}; \ \zeta_g = 0.60 \\ \text{Soft soil:} & \omega_g = 10.5 \text{ rad/s}; \ \zeta_g = 0.65 \end{cases} \tag{7.30}$$

In shaking table tests on structural control, Spencer et al. [32] suggested that

$$\begin{cases} 20 \leq \omega_g \leq 120 \text{ rad/s}, 0.3 \leq \zeta_g \leq 0.75, \\ \sigma_{\ddot{x}_g} = 0.12 \text{ g}, G_0 = \dfrac{0.03\zeta_g}{\pi\omega_g(4\zeta_g^2 + 1)} \ g^2 \cdot \text{s} \end{cases} \tag{7.31}$$

for a three-story structure model with active mass driver system, and

$$\begin{cases} 8 \leq \omega_g \leq 50 \text{ rad/s}, 0.3 \leq \zeta_g \leq 0.75 \\ \sigma_{\ddot{x}_g} = 0.034 \text{ g}, G_0 = \dfrac{2.35 \times 10^{-3}\zeta_g}{\pi\omega_g(4\zeta_g^2 + 1)} \ g^2 \cdot \text{s} \end{cases} \tag{7.32}$$

for a three-story structure model with active tendon system. These values match Palazzo and Petti's parameters with consideration of the similarity of structure models.

The Kanai-Tajimi spectrum can be modified [13] by applying a low-band frequency filter, and the formulation is

$$G(\omega) = H_{CP}^2(\omega)H_{KT}^2(\omega)G_0 \tag{7.33}$$

where $H_{CP}(\omega)$ is the Clough and Penzien low-band frequency filter given by

$$H_{CP}(\omega) = \frac{\omega^2/\omega_1^2}{(1 - \omega^2/\omega_1^2) + 2j\zeta_1\omega/\omega_1}, \ j = \sqrt{-1} \tag{7.34}$$

and $H_{KT}(\omega)$ is the Kanai and Tajimi filter given by

$$H_{KT}(\omega) = \frac{1 + 2j\zeta_g\omega/\omega_g}{(1 - \omega^2/\omega_g^2) + 2j\zeta_g\omega/\omega_g} \tag{7.35}$$

The ith moment of $G(\omega)$ is defined as

$$\lambda_i = \int_0^\infty \omega^i G(\omega)\, \mathrm{d}\omega \tag{7.36}$$

that can be used to express statistical properties of ground motion. λ_0 is the mean square value or variance of the ground acceleration.

7.3.2 Review of Stochastic Theory of Structural Seismic Response

A structure with n dynamic d.o.f. under seismic excitation can be modeled as

$$[M]\{\ddot{x}(t)\} + [C]\{\ddot{x}(t)\} + [K]\{\ddot{x}(t)\} = \{\delta\}\ddot{x}_g(t) \tag{7.37}$$

where $\{\delta\}$ is vector of coefficients for earthquake ground acceleration. In general, it is assumed that this system has orthogonal damping and stiffness matrices. Then with modal transformation, the response at kth d.o.f. is

$$x_k(t) = \sum_{i=1}^{n} \phi_{ki} q_i(t); \quad k = 1, 2, \ldots, n \tag{7.38}$$

and Equation 7.37 becomes

$$\ddot{q}_i(t) + 2\zeta_i \omega_i \dot{q}_i(t) + \omega_i^2 q_i(t) = r_i \ddot{x}_{\mathrm{g}}(t) = F_i(t) \tag{7.39}$$

where ζ_i and ω_i are damping ratio and natural frequency of the ith mode; $r_i = \{\phi_i\}^{\mathrm{T}}\{\delta\}/M_i$ and $M_i = \{\phi_i\}^{\mathrm{T}}[M]\{\phi_i\}$; $i = 1, 2, \ldots, n$.

The power spectrum density of the response at the lth d.o.f. will be

$$S_{x_l}(\omega) = \sum_{i=1}^{n}\sum_{k=1}^{n} \phi_{li}\phi_{lk} H_i(-j\omega) H_k(j\omega) S_{\mathrm{F}_i\mathrm{F}_k}(\omega) \approx \sum_{i=1}^{n} \phi_{li}^2 |H_i(j\omega)|^2 S_{\mathrm{F}_i}(\omega) \tag{7.40}$$

where ω is excitation frequency and

$$S_{\mathrm{F}_i}(\omega) = r_i^2 S_{\ddot{x}_{\mathrm{g}}}(\omega) = r_i^2 G(\omega); \quad \omega \geq 0 \tag{7.41}$$

$$H_i(j\omega) = \frac{1}{\omega_i^2 - \omega^2 + 2j\zeta_i\omega_i\omega}; \quad j = \sqrt{-1} \tag{7.42}$$

The RMS value of the response of the lth d.o.f. is

$$\sigma_{x_l} = \sqrt{\int_{-\infty}^{+\infty} S_{x_l}(\omega)\,\mathrm{d}\omega} = \sqrt{\sum_{i=1}^{n} \phi_{li}^2 r_i^2 \int_0^{\infty} |H_i(j\omega)|^2 G(\omega)\,\mathrm{d}\omega} \tag{7.43}$$

Integration in the above equation can be found by the theorem of residue [25]. Since Equation 7.37 describes a linear system, its responses are a Gaussian random process with zero mean values, the same as the excitation.

Design value of response of the lth d.o.f. is

$$x_l = \mu\sigma_{x_l} \tag{7.44}$$

where the factor μ is determined by the required probability of structural safety. Therefore, if the control objective is to reduce the response at freedom l of the structure, optimal placement of the control device will yield the smallest values of σ_{x_l}.

7.3.3 Modal Analysis of Smart Structures with Hybrid System

As noted, control devices are a first-order dynamic system in a structural control system. This characteristic results in real eigenvalues (poles) of the system plant matrix. In addition, control force will change damping and stiffness coefficients of the structure, which leads to nonorthogonal damping and stiffness matrices. Thus, the classical modal analysis cannot be applied to controlled structures. A new approach needs to be developed.

7.3.3.1 Eigenvalues and eigenvectors of plant matrix for controlled structures

The analytical model of controlled structures is expressed by Equations 7.27 and 7.28. Since actuator and damper dynamics is considered, both $[A]$ and $[A_c]$ have first-order real poles. In addition, each structural mode corresponds to a pair of conjugate complex poles. Eigenvalues of matrix $[A_c]$ (i.e., poles of the system) are

- n pairs of conjugate complex number

$$\mu_i \pm \nu_i j = -\zeta_i\omega_i \pm \sqrt{1-\zeta_i^2}\,\omega_i j \tag{7.45}$$

and each pair refers to one mode of the system; ζ_i and ω_i are damping ratio and natural frequency of ith mode, respectively; $j = \sqrt{-1}$.

- m negative real numbers $-p_i$, which come from dynamics of control devices.

Thus, the corresponding eigenvectors can be expressed as

$$[T] = [T_1, T_2, \ldots, T_n; T_{n+1}, T_{n+2}, \ldots, T_{n+m}] \tag{7.46}$$

where T_{n+i} $(i = 1, 2, \ldots, m)$ are real vectors expressed as

$$[T_{n+i}] = [\alpha_{1,n+i} \;\; \alpha_{2,n+i} \ldots \alpha_{n,n+i} \;\; \alpha_{n+1,n+i} \ldots \alpha_{n+m,n+i}]^{\mathrm{T}} \tag{7.47}$$

and $T_i (i = 1, 2, \ldots, n)$ is a pair of conjugate complex vectors expressed as

$$[T_i] = \begin{bmatrix} \alpha_{1i} + \beta_{1i}j & \alpha_{1i} - \beta_{1i}j \\ \alpha_{2i} + \beta_{2i}j & \alpha_{2i} - \beta_{2i}j \\ \vdots & \vdots \\ \alpha_{ni} + \beta_{ni}j & \alpha_{ni} - \beta_{ni}j \\ \alpha_{n+1,i} + \beta_{n+1,i}j & \alpha_{n+1,i} - \beta_{n+1,i}j \\ \vdots & \vdots \\ \alpha_{n+m,i} + \beta_{n+m,i}j & \alpha_{n+m,i} - \beta_{n+m,i}j \end{bmatrix}_{2\times(n+m)} \tag{7.48}$$

7.3.3.2 Modal decomposition

Let

$$\{Z(t)\} = [T]\{\psi(t)\} \tag{7.49}$$

Then Equation 7.27 can be rewritten as

$$[T]\{\dot{\psi}(t)\} = [A_{\mathrm{C}}][T]\{\psi(t)\} + \{B_{\mathrm{r}}\}\ddot{x}_{\mathrm{g}}(t) \tag{7.50}$$

Thus

$$\{\dot{\psi}(t)\} = [T]^{-1}[A_{\mathrm{C}}][T]\{\psi(T)\} + [T]^{-1}\{B_{\mathrm{r}}\}\ddot{x}_{\mathrm{g}}(t) = [\Lambda]\{\psi(t)\} + \{\Gamma\}\ddot{x}_{\mathrm{g}}(t) \tag{7.51}$$

where

$$\{\psi(t)\} = [\psi_1(t), \bar{\psi}_1(t); \psi_2(t), \bar{\psi}_2(t); \ldots; \psi_n(t), \bar{\psi}_n(t); \psi_{n+1}(t), \ldots, \psi_{n+m}(t)]^{\mathrm{T}} \tag{7.52}$$

and $\{\psi_i(t), \bar{\psi}_i(t)\}$ is ith pair of conjugate complex modal coordinates; $[\Lambda]$ is a diagonal matrix expressed as

$$[\Lambda] = [T]^{-1}[A_C][T] = \begin{bmatrix} \mu_1 + \nu_1 j & & & & & & & \\ & \mu_1 - \nu_1 j & & & & & & \\ & & \cdots & & & & & \\ & & & \mu_n + \nu_n j & & & & \\ & & & & \mu_n - \nu_n j & & & \\ & & & & & -p_1 & & \\ & & & & & & \cdots & \\ & & & & & & & -p_m \end{bmatrix} \tag{7.53}$$

and

$$[\Gamma] = [T]^{-1}\{B_r\} = [x_1 + y_1 j, x_1 - y_1 j; x_2 + y_2 j, x_2 - y_2 j; \ldots; x_n + y_n j, x_n - y_n j; x_{n+1}, \ldots, x_{n+m}]^T \tag{7.54}$$

Thus, Equation 7.51 can be rewritten as

$$\begin{cases} \dot{\psi}_i(t) = (\mu_i + \nu_i j)\psi_i(t) + (x_i + y_i j)\ddot{x}_g(t) \\ \dot{\bar{\psi}}_i(t) = (\mu_i - \nu_i j)\bar{\psi}_i(t) + (x_i - y_i j)\ddot{x}_g(t) \end{cases} \qquad i = 1, 2, \ldots, n \tag{7.55a}$$

$$\dot{\psi}_{n+k}(t) = -p_k \psi_{n+k}(t) + x_{n+k}\ddot{x}_g(t) \qquad k = 1, 2, \ldots, m \tag{7.55b}$$

and the response of kth d.o.f. is given by Equation 7.49 as

$$z_k(t) = \sum_{i=1}^{n} \left[(\alpha_{ki} + \beta_{ki} j)\psi_i(t) + (\alpha_{ki} - \beta_{ki} j)\bar{\psi}_i(t)\right] + \sum_{i=1}^{m} \alpha_{k,n+i}\psi_{n+i}(t) \tag{7.56}$$

7.3.4 Stochastic Seismic Response of Hybrid-Controlled Smart Structures

7.3.4.1 Transformation of pair of complex equations to second-order real equation

Equations 7.55a and b are not convenient for stochastic response analysis because they are complex equations, as it is difficult to define the power spectrum of complex variables. However, there is a way to simplify the process. Since each complex pair of the summation in Equation 7.56 refers to a modal contribution,

the ith pair of the first-order complex equations in Equation 7.55a may be transformed into an equivalent second-order equation as Equation 7.39 shows. Rewrite Equation 7.39 as

$$\begin{Bmatrix} \dot{q}_i(t) \\ \ddot{q}_i(t) \end{Bmatrix} = \begin{bmatrix} 0 & 1 \\ -\omega_i^2 & -2\zeta_i\omega_i \end{bmatrix} \begin{Bmatrix} q_i(t) \\ \dot{q}_i(t) \end{Bmatrix} + \begin{Bmatrix} 0 \\ r_i \end{Bmatrix} \ddot{x}_g(t) \tag{7.57}$$

The ith pair of conjugate complex equations in Equation 7.55a can be rewritten as

$$\frac{d}{dt} \begin{Bmatrix} \psi_i(t) \\ \bar{\psi}_i(t) \end{Bmatrix} = \begin{bmatrix} \mu_i + \nu_i j & 0 \\ 0 & \mu_i - \nu_i j \end{bmatrix} \begin{Bmatrix} \psi_i(t) \\ \bar{\psi}_i(t) \end{Bmatrix} + \begin{Bmatrix} x_i + y_i j \\ x_i - y_i j \end{Bmatrix} \ddot{x}_g(t) \tag{7.58}$$

Comparing Equations 7.57 and 7.58, a linear transform relationship may be assumed between $\begin{Bmatrix} \psi(t) \\ \bar{\psi}(t) \end{Bmatrix}$ and $\begin{Bmatrix} q(t) \\ \dot{q}(t) \end{Bmatrix}$ as follows:

$$\begin{Bmatrix} q_i(t) \\ \dot{q}_i(t) \end{Bmatrix} = [\Theta] \begin{Bmatrix} \psi_i(t) \\ \bar{\psi}_i(t) \end{Bmatrix} = \begin{bmatrix} a & b \\ c & d \end{bmatrix} \begin{Bmatrix} \psi_i(t) \\ \bar{\psi}_i(t) \end{Bmatrix} \tag{7.59}$$

Substituting Equation 7.59 into Equation 7.57 yields

$$\begin{bmatrix} a & b \\ c & d \end{bmatrix} \begin{Bmatrix} \dot{\psi}_i(t) \\ \dot{\bar{\psi}}_i(t) \end{Bmatrix} = \begin{bmatrix} 0 & 1 \\ -\omega_i^2 & -2\zeta_i\omega_i \end{bmatrix} \begin{bmatrix} a & b \\ c & d \end{bmatrix} \begin{Bmatrix} \psi_i(t) \\ \bar{\psi}_i(t) \end{Bmatrix} + \begin{Bmatrix} 0 \\ r_i \end{Bmatrix} \ddot{x}_g(t) \tag{7.60}$$

and it can be rewritten as

$$\begin{Bmatrix} \dot{\psi}_i(t) \\ \dot{\bar{\psi}}_i(t) \end{Bmatrix} = \begin{bmatrix} a & b \\ c & d \end{bmatrix}^{-1} \begin{bmatrix} 0 & 1 \\ -\omega_i^2 & -2\zeta_i\omega_i \end{bmatrix} \begin{bmatrix} a & b \\ c & d \end{bmatrix} \begin{Bmatrix} \psi_i(t) \\ \bar{\psi}_i(t) \end{Bmatrix} + \begin{bmatrix} a & b \\ c & d \end{bmatrix}^{-1} \begin{Bmatrix} 0 \\ r_i \end{Bmatrix} \ddot{x}_g(t) \tag{7.61}$$

By comparing Equations 7.61 and 7.58, we obtain the equations for determining the transformation matrix $[\Phi]$ as

$$\begin{bmatrix} a & b \\ c & d \end{bmatrix}^{-1} \begin{bmatrix} 0 & 1 \\ -\omega_i^2 & -2\zeta_i\omega_i \end{bmatrix} \begin{bmatrix} a & b \\ c & d \end{bmatrix} = \begin{bmatrix} \mu_i + \nu_i j & 0 \\ 0 & \mu_i - \nu_i j \end{bmatrix} \tag{7.62a}$$

$$\begin{bmatrix} a & b \\ c & d \end{bmatrix}^{-1} \begin{Bmatrix} 0 \\ r_i \end{Bmatrix} = \begin{Bmatrix} x_i + y_i j \\ x_i - y_i j \end{Bmatrix} \tag{7.62b}$$

Since

$$\begin{bmatrix} a & b \\ c & d \end{bmatrix}^{-1} = \frac{1}{ad - bc} \begin{bmatrix} d & -b \\ -c & a \end{bmatrix} \tag{7.63}$$

Equation 7.62 can be rewritten as

$$\frac{1}{ad-bc}\begin{bmatrix} ab\omega_i^2+2bc\zeta_i\omega_i+cd & b^2\omega_i^2+d^2+2bd\zeta_i\omega_i \\ -a^2\omega_i^2-c^2-2ac\zeta_i\omega_i & -ab\omega_i^2-cd-2ad\zeta_i\omega_i \end{bmatrix} = \begin{bmatrix} \mu_i+\nu_i j & 0 \\ 0 & \mu_i-\nu_i j \end{bmatrix} \tag{7.64a}$$

$$\frac{1}{ad-bc}\begin{Bmatrix} -br_i \\ ar_i \end{Bmatrix} = \begin{Bmatrix} x_i+y_i j \\ x_i-y_i j \end{Bmatrix} \tag{7.64b}$$

The equivalence of elements (1, 2) and (2, 1) in Equation 7.64a leads to

$$\begin{cases} b^2\omega_i^2+d^2+bd\cdot 2\zeta_i\omega_i=0 \\ a^2\omega_i^2+c^2+ac\cdot 2\zeta_i\omega_i=0 \end{cases} \tag{7.65}$$

Since $\mu_i=-\zeta_i\omega_i$ and $\mu_i^2+\nu_i^2=\omega_i^2$, the above equations yield

$$\begin{cases} b^2(\mu_i^2+\nu_i^2)+d^2-2bd\mu_i=0 \\ a^2(\mu_i^2+\nu_i^2)+c^2-2ac\mu_i=0 \end{cases} \tag{7.66}$$

that is,

$$\begin{cases} (b\mu_i-d)^2+b^2\nu_i^2=0 \\ (a\mu_i-c)^2+a^2\nu_i^2=0 \end{cases} \tag{7.67}$$

Thus,

$$\begin{cases} b\mu_i-d=\pm b\nu_i j \\ a\mu_i-c=\pm a\nu_i j \end{cases} \tag{7.68}$$

that is,

$$c=a(\mu_i\pm\nu_i j), d=b(\mu_i\pm\nu_i j) \tag{7.69}$$

Let's pick

$$c=a(\mu_i+\nu_i j), d=b(\mu_i-\nu_i j) \tag{7.70}$$

Then for element (1, 1) in Equation 7.64a

$$\begin{aligned} \frac{ab\omega_i^2+cd+2\zeta_i\omega_i bc}{ad-bc} &= \frac{ab(\mu_i^2+\nu_i^2)+cd-2\mu_i bc}{ad-bc} \\ &= \frac{ad/(\mu_i-\nu_i j)(\mu_i^2+\nu_i^2)+cb(\mu_i-\nu_i j)-2\mu_i bc}{ad-bc} \\ &= \mu_i+\nu_i j \end{aligned} \tag{7.71}$$

and for element (2, 2)

$$\begin{aligned}\frac{-ab\omega_i^2 - cd - 2\zeta_i\omega_i bc}{ad - bc} &= \frac{-ab(\mu_i^2 + \nu_i^2) - cd + 2\mu_i bc}{ad - bc} \\ &= \frac{-ad/(\mu_i - \nu_i j)(\mu_i^2 + \nu_i^2) - cb(\mu_i - \nu_i j) + 2\mu_i bc}{ad - bc} \\ &= \mu_i - \nu_i j \end{aligned} \tag{7.72}$$

Equations 7.71 and 7.72 show that, whatever the values of a and b are, Equation 7.64a is always valid if Equation 7.70 is valid.

With Equation 7.70 we have

$$\begin{aligned}[\Theta]^{-1} = \begin{bmatrix} a & b \\ c & d \end{bmatrix}^{-1} &= \begin{bmatrix} a & b \\ (\mu_i + \nu_i j)a & (\mu_i - \nu_i j)b \end{bmatrix}^{-1} \\ &= \frac{j}{2ab\nu_i} \begin{bmatrix} b(\mu_i - \nu_i j) & -b \\ -a(\mu_i + \nu_i j) & a \end{bmatrix} \end{aligned} \tag{7.73}$$

Thus Equation 7.62b becomes

$$\begin{aligned}\begin{bmatrix} a & b \\ c & d \end{bmatrix}^{-1} \begin{Bmatrix} 0 \\ r_i \end{Bmatrix} &= \frac{j}{2ab\nu_i} \begin{bmatrix} b(\mu_i - \nu_i j) & -b \\ -a(\mu_i + \nu_i j) & a \end{bmatrix} \begin{Bmatrix} 0 \\ r_i \end{Bmatrix} \\ &= \frac{jr_i}{2ab\nu_i} \begin{Bmatrix} -b \\ a \end{Bmatrix} = \begin{Bmatrix} x_i - y_i j \\ x_i + y_i j \end{Bmatrix} \end{aligned} \tag{7.74}$$

Then we obtain

$$\begin{aligned} -\frac{jr_i}{2a\nu_i} &= x_i + y_i j, \text{ i.e., } a = \frac{-y_i + x_i j}{2\nu_i(x_i^2 + y_i^2)} r_i \\ \frac{jr_i}{2b\nu_i} &= x_i - y_i j, \text{ i.e., } b = \frac{-y_i + x_i j}{2\nu_i(x_i^2 + y_i^2)} r_i \end{aligned} \tag{7.75}$$

Thus, the elements of the transformation matrix $[\Theta]$ in Equation 7.59 are

$$\begin{cases} a = \dfrac{-y_i - x_i j}{2\nu_i(x_i^2 + y_i^2)} r_i \\ b = \dfrac{-y_i - x_i j}{2\nu_i(x_i^2 + y_i^2)} r_i \\ c = a(\mu_i + \nu_i j) \\ d = b(\mu_i - \nu_i j) \end{cases} \tag{7.76}$$

This solution shows that, no matter what the value (except zero) of r_i is, the transform expressed by Equation 7.59 is always valid if the elements of transformation

matrix $[\Theta]$ are given by Equation 7.76. To simplify the problem, let $r_i = 1$. The ith pair of summations in Equation 7.56 becomes

$$\begin{aligned}
&[\alpha_{ki} + \beta_{ki}j \quad \alpha_{ki} - \beta_{ki}j] \begin{Bmatrix} \psi_i(t) \\ \overline{\psi}_i(t) \end{Bmatrix} \\
&= \left[\alpha_{ki} + \beta_{ki}j \quad \alpha_{ki} - \beta_{ki}j\right][\Theta]^{-1} \begin{Bmatrix} q_i(t) \\ \dot{q}_i(t) \end{Bmatrix} \\
&= \frac{j[\alpha_{ki} + \beta_{ki}j \quad \alpha_{ki} - \beta_{ki}j]}{2ab\nu_i} \begin{bmatrix} b(\mu_i - \nu_i j) & -b \\ -a(\mu_i + \nu_i j) & a \end{bmatrix} \begin{Bmatrix} q_i(t) \\ \dot{q}_i(t) \end{Bmatrix} \\
&= \frac{2}{r_i}[(\beta_{ki}\mu_i - \alpha_{ki}\nu_i)y_i - (\alpha_{ki}\mu_i + \beta_{ki}\nu_i)x_i \quad (\alpha_{ki}x_i - \beta_{ki}y_i)] \\
&= f_{ki}q_i(t) + g_{ki}\dot{q}_i(t)
\end{aligned} \tag{7.77}$$

where

$$f_{ki} = \frac{2}{r_i}[(\beta_{ki}\mu_i - \alpha_{ki}\nu_i)y_i - (\alpha_{ki}\mu_i + \beta_{ki}\nu_i)x_i], \quad g_{ki} = \frac{2}{r_i}(\alpha_{ki}x_i - \beta_{ki}y_i) \tag{7.78}$$

and f_{ki} and g_{ki} are known because they relate only to coefficients given by Equations 7.47, 7.48, 7.53, and 7.54. Substituting Equation 7.77 into Equation 7.56 yields the seismic response of the controlled structure ($k = 1, 2, \ldots, n + m$)

$$z_k(t) = \sum_{i=1}^{n} f_{ki}q_i(t) + \sum_{i=1}^{n} g_{ki}\dot{q}_i(t) + \sum_{i=1}^{m} \alpha_{k,n+i}\psi_{n+i}(t) \tag{7.79}$$

A comparison of the above equation and Equation 7.38 shows that the modal superposition for a system with first-order dynamics and nonorthogonal damping and stiffness is different in that it includes the contribution of real poles and modal velocities. This further shows that classical theory of stochastic seismic response cannot be applied to controlled structures. In order to obtain statistics of system response, variances of modal coordinates and modal velocities for each pair of complex poles as well as stochastic seismic response of the first-order system must be examined first. Since the system is linear, $q(t)$, $\dot{q}(t)$ and $\psi(t)$ are Gaussian stochastic process with zero mean values, the same as that of the excitation. Thus if their variances or RMS values are found, the stochastic seismic response is determined.

7.3.4.2 Stochastic response of first-order dynamic system under seismic excitation

The contribution of the real poles to the total response can be readily shown by the following simple equation because each seismic excitation can be expanded to a

Fourier series

$$\dot{y}(t) + py(t) = \sin \omega t \tag{7.80}$$

The response is given by

$$y(t) = Ce^{-pt} + \frac{p}{p^2 + \omega^2} \sin \omega t - \frac{\omega}{p^2 + \omega^2} \cos \omega t \tag{7.81}$$

Equation 7.81 shows that $y(t)$ may be significant if p is small. Thus, the effect of real poles on system response must be considered unless they are far from the origin.

In Equation 7.79, $\psi_{n+i}(t)$ is found by solving the first-order real equations in Equation 7.55b which can be rewritten as

$$\dot{\psi}_{n+k}(t) + p_k \psi_{n+k}(t) = x_{n+k} \ddot{x}_g(t) \tag{7.82}$$

Response power spectrum density is obtained by

$$S_{\psi_{n+k}}(\omega) = |H_{n+k}(\omega)|^2 G(\omega) = \left| \frac{x_{n+k}}{j\omega + p_k} \right|^2 G(\omega) \tag{7.83}$$

and the variance is

$$\begin{aligned}
\sigma_{n+k}^2 &= \int_0^\infty S_{\psi_{n+k}}(\omega)\, \mathrm{d}\omega \\
&= \int_0^\infty \frac{x_{n+k}^2}{p_k^2 + \omega^2} \frac{(1 + 4\zeta_g^2 \omega^2/\omega_g^2) G_0}{(1 - \omega^2/\omega_g^2)^2 + 4\zeta_g^2 \omega^2/\omega_g^2}\, \mathrm{d}\omega \\
&= \int_0^\infty \frac{x_{n+k}^2/\omega_g^2}{p_k^2/\omega_g^2 + \omega^2/\omega_g^2} \frac{(1 + 4\zeta_g^2 \omega^2/\omega_g^2) G_0 \omega_g}{(1 - \omega^2/\omega_g^2)^2 + 4\zeta_g^2 \omega^2/\omega_g^2}\, \mathrm{d}(\omega/\omega_g) \\
&= \frac{x_{n+k}^2 G_0}{\omega_g} \int_0^\infty \frac{(1 + 4\zeta_g^2 x^2)\, \mathrm{d}x}{(x^2 + q^2)[(1 - x^2)^2 + 4\zeta_g^2 x^2]}
\end{aligned} \tag{7.84}$$

where $x = \omega/\omega_g$, $q = p_k/\omega_g$. This integration can be found by applying the theorem of residue described as follows.

Lemma 7.1 If $F(z)$ is an even function, the integration

$$\int_0^\infty F(z)\mathrm{d}z = \pi j \sum_{i=1}^{N} (z - z_i) F(z)|_{z=z_i} \tag{7.85}$$

where z_i are poles of $F(z)$ and N is number of these poles in the upper half-plane.

The integrand in Equation 7.84 has three poles in upper half-plane, qj and $\pm\sqrt{1-\zeta_g^2}+\zeta_g j$. Their residues are

$$R_1=\lim_{x\to qj}(x-qj)\cdot\frac{1+4\zeta_g^2x^2}{(x^2+q^2)\left[(1-x^2)^2+4\zeta_g^2x^2\right]}$$
$$=\frac{1}{2qj}\frac{1-4\zeta_g^2q^2}{(1+q^2)^2-4\zeta_g^2q^2} \tag{7.86}$$

$$R_2=\lim_{x\to\left(-\sqrt{1-\zeta_g^2}+\zeta_g j\right)}\left(x+\sqrt{1-\zeta_g^2}-\zeta_g j\right)\cdot\frac{1+4\zeta_g^2x^2}{(x^2+q^2)[(1-x^2)^2+4\zeta_g^2x^2]}$$
$$=\frac{\left[1+4\zeta_g^2\left(-\sqrt{1-\zeta_g^2}+\zeta_g j\right)^2\right]\left[-\sqrt{1-\zeta_g^2}+\zeta_g j-\sqrt{1-\zeta_g^2}-\zeta_g j\right]^{-1}}{\left[\left(-\sqrt{1-\zeta_g^2}+\zeta_g j\right)^2+2\zeta_g j\left(-\sqrt{1-\zeta_g^2}+\zeta_g j\right)-1\right]\left[\left(-\sqrt{1-\zeta_g^2}+\zeta_g j\right)^2+q^2\right]}$$
$$=\frac{\zeta_g\left(3+q^2-4\zeta_g^2q^2\right)-\sqrt{1-\zeta_g^2}\left(1+q^2+4\zeta_g^2q^2\right)j}{8\zeta_g\sqrt{1-\zeta_g^2}\left[\left(q^2+1\right)^2-4\zeta_g^2q^2\right]} \tag{7.87}$$

$$R_3=\lim_{x\to\left(\sqrt{1-\zeta_g^2}+\zeta_g j\right)}\left(x-\sqrt{1-\zeta_g^2}-\zeta_g j\right)\cdot\frac{1+4\zeta_g^2x^2}{(x^2+q^2)[(1-x^2)^2+4\zeta_g^2x^2]}$$
$$=\frac{\left[1+4\zeta_g^2\left(\sqrt{1-\zeta_g^2}+\zeta_g j\right)^2\right]\left[\left(\sqrt{1-\zeta_g^2}+\zeta_g j\right)^2+q^2\right]^{-1}}{\left[\left(\sqrt{1-\zeta_g^2}+\zeta_g j\right)^2+2\zeta_g j\left(\sqrt{1-\zeta_g^2}+\zeta_g j\right)-1\right]\left[\sqrt{1-\zeta_g^2}+\zeta_g j+\sqrt{1-\zeta_g^2}-\zeta_g j\right]}$$
$$=\frac{\zeta_g\left(-3-q^2+4\zeta_g^2q^2\right)-\sqrt{1-\zeta_g^2}\left(1+q^2+4\zeta_g^2q^2\right)j}{8\zeta_g\sqrt{1-\zeta_g^2}\left[\left(q^2+1\right)^2-4\zeta_g^2q^2\right]} \tag{7.88}$$

Therefore,

$$\sigma_{n+k}^2=\frac{x_{n+k}^2G_0}{\omega_g}\left[\pi j(R_1+R_2+R_3)\right]$$
$$=\frac{\pi x_{n+k}^2G_0}{\omega_g}\left[\frac{1-4\zeta_g^2q_k^2}{2q_k\left[(q_k^2+1)^2-4\zeta_g^2q_k^2\right]}+\frac{1+q_k^2+4\zeta_g^2q_k^2}{4\zeta_g\left[(q_k^2+1)^2-4\zeta_g^2q_k^2\right]}\right]$$

$$= \frac{\pi x_{n+k}^2 G_0}{4q_k\zeta_g\omega_g} \frac{q_k + q_k^3 + 2\zeta_g - 8\zeta_g^3 q_k^2 + 4\zeta_g^2 q_k^3}{\left[\left(q_k^2+1\right)^2 - 4\zeta_g^2 q_k^2\right]}$$
$$= \frac{\pi x_{n+k}^2 G_0\omega_g}{4p_k\zeta_g} \frac{p_k + 4\zeta_g^2 p_k + 2\zeta_g\omega_g}{\omega_g^2 + 2\zeta_g\omega_g p_k + p_k^2} \tag{7.89}$$

7.3.4.3 Stochastic response of second-order dynamic system under seismic excitation

The second-order dynamic system in modal space is expressed by Equation 7.39. Power spectrum density of the modal displacement response $q_i(t)$ is

$$S_{q_i}(\omega) = |H_i(\omega)|^2 G(\omega) = \left|\frac{r_i}{-\omega^2 + 2\zeta_i\omega_i\omega j + \omega_i^2}\right| G(\omega) \tag{7.90}$$

and the variance can be obtained by

$$\begin{aligned}\sigma_{q_i}^2 &= \int_0^\infty S_{q_i}(\omega)\,\mathrm{d}\omega \\ &= \int_0^\infty \frac{r_i^2/\omega_i^4}{\left(1-\frac{\omega^2}{\omega_i^2}\right)^2 + 4\zeta_i^2\frac{\omega^2}{\omega_i^2}} \cdot \frac{\left(1+4\zeta_g^2\omega^2/\omega_g^2\right)G_0}{\left(1-\frac{\omega^2}{\omega_g^2}\right)^2 + 4\zeta_g^2\frac{\omega^2}{\omega_g^2}}\,\mathrm{d}\omega \\ &= \frac{r_i^2 G_0\omega_g}{2\omega_i^4}\int_{-\infty}^{+\infty} \frac{(1+4\zeta_g^2x^2)\mathrm{d}x}{\left[(s^2x^2-1)^2 + 4\zeta_i^2 s^2 x^2\right]\left[(x^2-1)^2 + 4\zeta_g^2 x^2\right]}\end{aligned} \tag{7.91}$$

where $x = \omega/\omega_g$, $s = \omega_g/\omega_i$. The above integration can also be found by the theorem of residue, but the procedure is too complicated. So the following Lemma [34] is introduced to find the above integration.

Lemma 7.2

$$I_k = \int_{-\infty}^{+\infty} \frac{G_k(j\omega)}{H_k(j\omega)H_k(-j\omega)}\,\mathrm{d}\omega = (-1)^{k+1}\frac{\pi}{a_0}\frac{N_k}{D_k} \tag{7.92}$$

where

$$\begin{aligned}G_k(j\omega) &= b_0(j\omega)^{2k-2} + b_1(j\omega)^{2k-4} + \cdots + b_{k-1} \\ H_k(j\omega) &= a_0(j\omega)^k + a_1(j\omega)^{k-1} + \cdots + a_k\end{aligned} \tag{7.93}$$

$$D_{\mathrm{k}} = \begin{vmatrix} d_{11} & d_{12} & \cdots & d_{1k} \\ d_{21} & d_{22} & \cdots & d_{2k} \\ \cdots & \cdots & \cdots & \cdots \\ d_{k1} & d_{k2} & \cdots & d_{kk} \end{vmatrix}, \quad N_{\mathrm{k}} = \begin{vmatrix} b_0 & d_{12} & \cdots & d_{1k} \\ b_1 & d_{22} & \cdots & d_{2k} \\ \cdots & \cdots & \cdots & \cdots \\ b_{k1} & d_{k2} & \cdots & d_{kk} \end{vmatrix} \tag{7.94}$$

and $d_{mn} = a_{2m-n}$ ($a_{\mathrm{s}} = 0$ if $s < 0$ or $s > k$). All roots of $H_k(j\omega)$ are in upper half-plane.

From this lemma, the integrand in Equation 7.91 contains

$$G_4(jx) = 4\zeta_{\mathrm{g}}^2 x^2 + 1 \tag{7.95}$$

and

$$\begin{aligned} H_4(jx) &= (x^2 - 2\zeta_{\mathrm{g}} jx - 1)(s^2 x^2 - 2\zeta_k\, s jx - 1) \\ &= s^2 x^4 - 2s(\zeta_{\mathrm{g}} s + \zeta_k) jx^3 - (1 + 4\zeta_{\mathrm{g}}\zeta_i s + s^2)x^2 \\ &\quad + 2(\zeta_i s + \zeta_{\mathrm{g}}) jx + 1 \end{aligned} \tag{7.96}$$

The comparison of Equation 7.96 and Equation 7.93 yields

$$b_0 = 0, \quad b_1 = 0, \quad b_2 = -4\zeta_{\mathrm{g}}^2, \quad b_3 = 1 \tag{7.97}$$

and

$$a_0 = s^2, \quad a_1 = 2s(\zeta_{\mathrm{g}} s + \zeta_j), \quad a_2 = 1 + 4\zeta_{\mathrm{g}}\zeta_j s + s^2, \quad a_3 = 2(\zeta_j + \zeta_{\mathrm{g}}), \quad a_4 = 1 \tag{7.98}$$

Then

$$\begin{aligned} D_4 &= \begin{vmatrix} d_{11} & d_{12} & d_{13} & d_{14} \\ d_{21} & d_{22} & d_{23} & d_{24} \\ d_{31} & d_{32} & d_{33} & d_{34} \\ d_{41} & d_{42} & d_{43} & d_{44} \end{vmatrix} = \begin{vmatrix} a_1 & a_0 & 0 & 0 \\ a_3 & a_2 & a_1 & a_0 \\ 0 & a_4 & a_3 & a_2 \\ 0 & 0 & 0 & a_4 \end{vmatrix} = a_4 \begin{vmatrix} a_1 & a_0 & 0 \\ a_3 & a_2 & a_1 \\ 0 & a_4 & a_3 \end{vmatrix} \\ &= a_4(a_1 a_2 a_3 - a_0 a_3^2 - a_1^2 a_4) \\ &= 4s[\zeta_{\mathrm{g}}\zeta_i + 4\zeta_i^2\zeta_{\mathrm{g}}^2 s + 2\zeta_{\mathrm{g}}\zeta_i(2\zeta_{\mathrm{g}}^2 + 2\zeta_i^2 - 1)s^2 + 4\zeta_{\mathrm{g}}^2\zeta_i^2 s^3 + \zeta_{\mathrm{g}}\zeta_i s^4] \end{aligned} \tag{7.99}$$

$$\begin{aligned} N_4 &= \begin{vmatrix} b_0 & d_{12} & d_{13} & d_{14} \\ b_1 & d_{22} & d_{23} & d_{24} \\ b_2 & d_{32} & d_{33} & d_{34} \\ b_3 & d_{42} & d_{43} & d_{44} \end{vmatrix} = \begin{vmatrix} b_0 & a_0 & 0 & 0 \\ b_1 & a_2 & a_1 & a_0 \\ b_2 & a_4 & a_3 & a_2 \\ b_3 & 0 & 0 & a_4 \end{vmatrix} = -a_0 \begin{vmatrix} 0 & a_1 & a_0 \\ b_2 & a_3 & a_2 \\ b_3 & 0 & a_4 \end{vmatrix} \\ &= -a_0(a_1 a_2 b_3 - a_0 a_3 b_3 - a_1 a_4 b_2) \\ &= -2s^3\left[\left(1 + 4\zeta_{\mathrm{g}}^2\right)\zeta_i + 4\zeta_{\mathrm{g}}\left(\zeta_i^2 + \zeta_{\mathrm{g}}^2\right)s + 4\zeta_{\mathrm{g}}^2\zeta_i s^2 + \zeta_{\mathrm{g}} s^3\right] \end{aligned} \tag{7.100}$$

Thus the variance of modal displacement $q_i(t)$ in Equation 7.39 is

$$\sigma_{q_i}^2 = \frac{\pi r_i^2 G_0 \omega_g}{4\omega_i^4} \frac{\left(1+4\zeta_g^2\right)\zeta_i + 4\zeta_g\left(\zeta_i^2+\zeta_g^2\right)s + 4\zeta_g^2\zeta_i^2 s^2 + \zeta_g^3 s^3}{\zeta_g\zeta_i + 4\zeta_i^2\zeta_g^2 s + 2\zeta_g\zeta_i\left(2\zeta_g^2+2\zeta_i^2-1\right)s^2 + 4\zeta_g^2\zeta_i^2 s^3 + \zeta_g\zeta_i s^4}$$

$$= \frac{\pi r_i^2 G_0}{4}\frac{\omega_g}{\omega_i^4}\frac{N_{q_i}}{D_{q_i}} \tag{7.101a}$$

where

$$N_{q_i} = \left(1+4\zeta_g^2\right)\zeta_i + 4\zeta_g\left(\zeta_i^2+\zeta_g^2\right)s + 4\zeta_g^2\zeta_i s^2 + \zeta_g s^3 \tag{7.101b}$$

$$D_{q_i} = \zeta_g\zeta_i + 4\zeta_i^2\zeta_g^2 s + 2\zeta_g\zeta_i\left(2\zeta_g^2+2\zeta_i^2-1\right)s^2 + 4\zeta_g^2\zeta_i^2 s^3 + \zeta_g\zeta_i s^4 \tag{7.101c}$$

Similarly, the square variance of modal velocity $\dot{q}_i(t)$ in Equation 7.39 is given by

$$\sigma_{\dot{q}_i}^2 = \int_0^\infty S_{\dot{q}_i}(\omega)\,\mathrm{d}\omega$$

$$= \int_0^\infty \frac{r_i^2\omega^2}{\left(\omega^2-\omega_i^2\right)^2 + 4\zeta_i^2\omega_i^2\omega^2} \cdot \frac{\left(1+4\zeta_g^2\omega^2/\omega_g^2\right)G_0}{\left(1-\omega^2/\omega_g^2\right)^2 + 4\zeta_g^2\omega^2/\omega_g^2}\,\mathrm{d}\omega$$

$$= \frac{r_i^2 G_0}{2}\frac{\omega_g^3}{\omega_i^4}\int_{-\infty}^{+\infty} \frac{(x^2+4\zeta_g^2x^4)\mathrm{d}x}{\left[\left(s^2x^2-1\right)^2 + 4\zeta_i^2 s^2 x^2\right]\left[(x^2-1)^2 + 4\zeta_g^2 x^2\right]} \tag{7.102}$$

where $x = \omega/\omega_g$, $s = \omega_g/\omega_k$. Comparing the above integrand to that in Equation 7.91, it is known that only the numerator of the integrand is different. D_4 for Equation 7.102 is then given by Equation 7.100 but N_4 is different. Note that for Equation 7.102

$$G_4(ix) = 4\zeta_g^2 x^4 + x^2 \tag{7.103}$$

In this case

$$b_0 = 0, \quad b_1 = 4\zeta_g^2, \quad b_2 = -1, \quad b_3 = 0 \tag{7.104}$$

and

$$
\begin{aligned}
N_4 &= \begin{vmatrix} b_0 & d_{12} & d_{13} & d_{14} \\ b_1 & d_{22} & d_{23} & d_{24} \\ b_2 & d_{32} & d_{33} & d_{34} \\ b_3 & d_{42} & d_{43} & d_{44} \end{vmatrix} = \begin{vmatrix} b_0 & a_0 & 0 & 0 \\ b_1 & a_2 & a_1 & a_0 \\ b_2 & a_4 & a_3 & a_2 \\ b_3 & 0 & 0 & a_4 \end{vmatrix} \\
&= -a_0 \begin{vmatrix} b_1 & a_1 & a_0 \\ b_2 & a_3 & a_2 \\ 0 & 0 & a_4 \end{vmatrix} = -a_0 a_4 \begin{vmatrix} b_1 & a_1 \\ b_2 & a_3 \end{vmatrix} = -a_0 a_4 (a_3 b_1 - a_1 b_2) \\
&= -2s^2 \left[4\zeta_g^3 + \zeta_k \left(1 + 4\zeta_g^2 \right) s + 2\zeta_g s^2 \right]
\end{aligned}
\tag{7.105}
$$

where $s = \omega_g / \omega_k$. Thus the square variance of $\dot{q}_i(t)$ is

$$
\begin{aligned}
\sigma_{\dot{q}_i}^2 &= \frac{\pi r_i^2 G_0 \omega_g^3}{4\omega_i^4} \frac{4\zeta_g^3 + \zeta_i \left(1 + 4\zeta_g^2 \right) s + 2\zeta_g s^2}{s\zeta_g \left[\zeta_i + 4\zeta_i^2 \zeta_g s + 2\zeta_i (2\zeta_g^2 + 2\zeta_i^2 - 1) s^2 + 4\zeta_g \zeta_i^2 s^3 + \zeta_i s^4 \right]} \\
&= \frac{\pi r_i^2 G_0}{4} \frac{\omega_g^3}{\omega_i^4} \frac{N_{\dot{q}_i}}{D_{\dot{q}_i}}
\end{aligned}
\tag{7.106a}
$$

where

$$
N_{\dot{q}_i} = 4\zeta_g^3 + \zeta_i \left(1 + 4\zeta_g^2 \right) s + \zeta_g s^2 \tag{7.106b}
$$

$$
D_{\dot{q}_i} = s\zeta_g \left[\zeta_i + 4\zeta_i^2 \zeta_g s + 2\zeta_i \left(2\zeta_g^2 + 2\zeta_i^2 - 1 \right) s^2 + 4\zeta_g \zeta_i^2 s^3 + \zeta_i s^4 \right] \tag{7.106c}
$$

7.3.4.4 Stochastic response of controlled structure under seismic excitation

For linear systems, $\sigma_{q\dot{q}} = 0$ under stationary random excitation and the interaction effect between different modes is small if the modes are well-spaced. The variance of the system's closed-loop response, which is defined by Equation 7.79, can be found by the *square-root-of-the-sum-of-the-squares* (SRSS) method as

$$
\sigma_{z_k}^2 = \sum_{i=1}^{n} \left(f_{ki}^2 \sigma_{q_i}^2 + g_{ki}^2 \sigma_{\dot{q}_i}^2 \right) + \sum_{i=1}^{m} \alpha_{k,n+i}^2 \sigma_{n+i}^2 \tag{7.107}
$$

Equation 7.107 shows that there are two additional terms in the stochastic seismic response of controlled structures compared to that of uncontrolled structures with orthogonal damping and stiffness matrices. First is $\sum_{i=1}^{m} \alpha_{k,n+i}^2 \sigma_{n+i}^2$, which expresses the effect of first-order dynamics of control devices; second is $\sum_{i=1}^{n} g_{ki}^2 \sigma_{\dot{q}_i}^2$, which means that the stochastic response of a controlled structure is

related not only to modal coordinate $q_i(t)$, but also to the first derivative of the modal coordinate, that is, $\dot{q}_i(t)$.

7.3.5 Determination of Optimal Placement of Control Devices

7.3.5.1 Optimization problem definition

The goal of optimal placement of control devices is to maximize control system effectiveness, that is, to reduce structural responses to a given level with the least control force. Thus, the general optimization problem for control device placement can be expressed as

$$\begin{aligned} &\text{Minimize } \{f(x)\} \\ &\text{Subject to } \begin{cases} g(x) = g_0 \\ 1 \le x \le N \end{cases} \end{aligned} \tag{7.108}$$

where $f(x)$ is objective function that expresses the optimization goal, for the optimization of control device placement, $f(x)$ can be active control force, passive control force, or their weighted summation; $g(x)$ is control objective that can be structural displacement, velocity or drift, and g_0 is desired structural response level with control; x is design variable; for the hybrid bracing control system presented in Figure 5.21, x is story number where a control device is placed, and N is the total number of stories in the building. If there are more than two control devices used in the hybrid bracing control system, x will be a vector and each element of x refers to the location of one control device.

Equation 7.44 shows that the design values of both control force and structural response are proportional to their RMS values determined by Equation 7.107. Thus, if the control objective is to reduce the response at freedom l of the structure, optimal placement of the control device will yield the smallest values of σ_{x_l} with RMS value of control force set same, or the optimal location of control devices is where the smallest RMS value of control force is required to achieve a control objective. Thus, the optimization problem expressed by Equation 7.108 can be rewritten as

$$\begin{aligned} &\text{Minimize } \{\sigma_{\mathrm{f}}(x)\} \\ &\text{Subject to } \begin{cases} \sigma_{\mathrm{g}}(x) = \sigma_0 \\ 1 \le x \le N \end{cases} \end{aligned} \tag{7.109}$$

7.3.5.2 Solution procedure

As noted, there is no efficient algorithm for the optimization problem of control device placement. Since the number of locations for control devices in seismic-resistant structures is limited by the number of bays and stories, an enumerative technique (a sequential search procedure) is implemented by MATLAB®. *m* code to solve this optimization problem. It is expressed by the following step-by-step

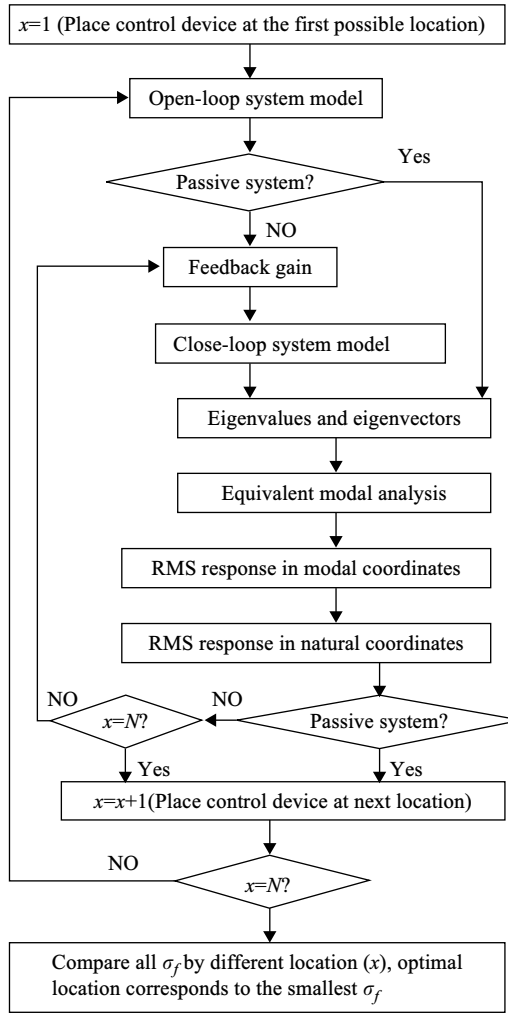

FIGURE 7.23 Flowchart of solution procedure for optimal placement problem.

procedure and the flowchart in Figure 7.23. This procedure works for any structure with multiple bays and stories.

Step 1. Let $x = 1$, that is, place the control device at the first floor. Establish its model according to Equation 7.25.
Step 2. Find gain matrix $[G]$ by certain control algorithms and closed-loop plant matrix $[A_c]$ according to Equations 7.26 and 7.28.
Step 3. Calculate and sort the eigenvalues and the eigenvectors of matrix $[A_c]$.
Step 4. Solve coefficients x_i, y_i and f_{ki}, g_{ki} for each mode, and x_{n+i} for each real pole.

Step 5. Use Equations 7.89, 7.101, and 7.106 to find RMS values of the system response in the modal space.
Step 6. Solve RMS values of structural response σ_g using Equation 7.107.
Step 7. Check the RMS value of structural response σ_g. It should equal required level σ_0. If not, change feedback gain $[G]$ and repeat steps 2–7 till $\sigma_g = \sigma_0$.
Step 8. Find the RMS value of required control force σ_f solved by Equation 7.107.
Step 9. Increase x by 1 and repeat steps 1–7 until $x = N$.
Step 10. Compare σ_f obtained for each x; the optimum location x_0 is the one with the smallest σ_f.

EXAMPLE 7.3.1

The two-story building in Example 7.2.1 serves as an example here. Assume the building is constructed on medium soil. Find its stochastic seismic displacement response of the structure with active control at the first floor.

Solution
The motion equation of the system has been given in Example 7.2.1. By defining the state vector

$$\{Z(t)\} = \begin{Bmatrix} \{x(t)\} \\ \{\dot{x}(t)\} \end{Bmatrix} = \{x_1(t), x_2(t), \dot{x}_1(t), \dot{x}_2(t)\}^{\mathrm{T}} \tag{a}$$

we obtain the state variable representation of the system as

$$\{\dot{Z}(t)\} = [A]\{Z(t)\} + \{B_u\}\, u(t) + \{B_r\}\, \ddot{x}_g(t) \tag{b}$$

where

$$\begin{aligned} [A] &= \begin{pmatrix} [O]_{2\times 2} & [I]_{2\times 2} \\ -[M]^{-1}[K] & -[M]^{-1}[C] \end{pmatrix} \\ &= \begin{pmatrix} [O]_{2\times 2} & \\ -\begin{bmatrix} 0.136 & \\ & 0.066 \end{bmatrix}^{-1} \begin{bmatrix} 75.00 & -44.30 \\ -44.30 & 44.30 \end{bmatrix} & \\ & [I]_{2\times 2} \\ & -\begin{bmatrix} 0.136 & \\ & 0.066 \end{bmatrix}^{-1} \begin{bmatrix} 0.0572 & -0.0198 \\ -0.0198 & 0.0313 \end{bmatrix} \end{pmatrix} \\ &= \begin{bmatrix} 0 & 0 & 1.0 & 0 \\ 0 & 0 & 0 & 1.0 \\ -551.471 & 325.735 & -0.421 & 0.146 \\ 671.212 & -671.212 & 0.300 & -0.474 \end{bmatrix} \end{aligned} \tag{c}$$

$$\{B_u\} = \begin{Bmatrix} \{0\} \\ [M]^{-1}\{\gamma\} \end{Bmatrix} \tag{d}$$

when the control is at the first floor,

$$\{B_{\mathrm{u}}\} = \left\{ \begin{array}{c} 0 \\ 0 \\ \left[\begin{array}{cc} 0.136 & \\ & 0.066 \end{array} \right]^{-1} \left\{ \begin{array}{c} -1 \\ 0 \end{array} \right\} \end{array} \right\} = \left\{ \begin{array}{c} 0 \\ 0 \\ -7.353 \\ 0 \end{array} \right\} \tag{e}$$

and when the control is at the second floor,

$$\{B_{\mathrm{u}}\} = \left\{ \begin{array}{c} 0 \\ 0 \\ \left[\begin{array}{cc} 0.136 & \\ & 0.066 \end{array} \right]^{-1} \left\{ \begin{array}{c} 1 \\ -1 \end{array} \right\} \end{array} \right\} = \left\{ \begin{array}{c} 0 \\ 0 \\ 7.353 \\ -15.152 \end{array} \right\} \tag{f}$$

$$\{B_{\mathrm{r}}\} = \left\{ \begin{array}{c} \{0\} \\ [M]^{-1}\{\delta\} \end{array} \right\} = \left\{ \begin{array}{c} 0 \\ 0 \\ \left[\begin{array}{cc} 0.136 & \\ & 0.066 \end{array} \right]^{-1} \left\{ \begin{array}{c} -0.136 \\ -0.066 \end{array} \right\} \end{array} \right\} = \left\{ \begin{array}{c} 0 \\ 0 \\ -1 \\ -1 \end{array} \right\} \tag{g}$$

Assume the control is at the first-story; Linear quadratic control algorithm is used to design the controller. Let the weighting matrices

$$[Q] = [I]_{4\times 4} = \left[\begin{array}{cccc} 1 & & & \\ & 1 & & \\ & & 1 & \\ & & & 1 \end{array} \right] \tag{h}$$

$$[R] = 50 \tag{i}$$

Use MATLAB® built–in function lqr for the controller design as

$$\gg G = lqr(A, B_{\mathrm{u}}, Q, R) \tag{j}$$

then we obtain the gain matrix

$$[G] = [-0.0821 \quad 0.0814 \quad -0.159 \quad -0.0153] \tag{k}$$

and the closed-loop plant matrix

$$[A_{\mathrm{c}}] = [A] - \{B_{\mathrm{u}}\}[G] = [A] - \left\{ \begin{array}{c} 0 \\ 0 \\ -7.353 \\ 0 \end{array} \right\} [-0.0821 \;\; 0.0814 \;\; -0.159 \;\; 0.0153]$$

$$= \begin{bmatrix} 0 & 0 & 1.0 & 0 \\ 0 & 0 & 0 & 1.0 \\ -551.471 & 325.735 & -0.421 & 0.146 \\ 671.212 & -671.212 & 0.300 & -0.474 \end{bmatrix}$$

$$- \begin{bmatrix} 0 & 0 & 0 & 0 \\ 0 & 0 & 0 & 0 \\ 0.603 & -0.599 & 1.171 & 0.112 \\ 0 & 0 & 0 & 0 \end{bmatrix}$$

$$= \begin{bmatrix} 0 & 0 & 1.0 & 0 \\ 0 & 0 & 0 & 10. \\ -552.074 & 326.334 & -1.591 & 0.033 \\ 671.212 & -671.212 & 0.300 & -0.474 \end{bmatrix} \quad \text{(l)}$$

The eigenvalues and eigenvectors of $[A_c]$ are solved as

$$[\Lambda] = \begin{bmatrix} -0.488 + 11.818j & & & \\ & -0.488 - 11.818j & & \\ & & -0.545 + 32.906j & \\ & & & -0.545 - 32.906j \end{bmatrix} \quad \text{(m)}$$

$$[T] = \begin{bmatrix} 0.0463 + 0.0243j & 0.0463 - 0.0243j & 0.0159 + 0.0004j & 0.0159 - 0.0004j \\ 0.0579 + 0.0317j & 0.0579 - 0.0317j & -0.0259 + 0.0003j & -0.0259 - 0.0003j \\ -0.310 + 0.535j & -0.310 - 0.535j & -0.0203 + 0.523j & -0.0203 - 0.523j \\ -0.421 + 0.669j & -0.421 - 0.669j & 0.0037 - 0.852j & 0.0037 + 0.852j \end{bmatrix} \quad \text{(n)}$$

Thus there are two modes for this system, and

$$\mu_1 = -0.488, \quad \nu_1 = 11.818 \quad \text{(o)}$$

$$\mu_2 = -0.545, \quad \nu_2 = 32.906 \quad \text{(p)}$$

$$\begin{cases} \alpha_{11} = 0.0463, \beta_{11} = 0.0243 \\ \alpha_{21} = 0.0579, \beta_{21} = 0.0317 \\ \alpha_{31} = -0.310, \beta_{31} = 0.535 \\ \alpha_{41} = -0.421, \beta_{41} = 0.669 \end{cases} \quad \text{(q)}$$

$$\begin{cases} \alpha_{12} = 0.0159, \beta_{12} = 0.0004 \\ \alpha_{22} = -0.0259, \beta_{22} = 0.0003 \\ \alpha_{32} = -0.0203, \beta_{32} = 0.523 \\ \alpha_{42} = 0.0037, \beta_{42} = -0.852 \end{cases} \quad \text{(r)}$$

$$\{\Gamma\} = [T]^{-1}\{B_r\}$$

$$= \begin{bmatrix} 4.537-2.934j & 2.936-1.522j & -0.217-0.401j & -0.130-0.248j \\ 4.537+2.934j & 2.936+1.522j & -0.217+0.401j & -0.130+0.248j \\ 13.751-0.220j & -10.885+0.239j & 0.010-0.418j & 0.008+0.331j \\ 13.751+0.220j & -10.885-0.239j & 0.010+0.418j & 0.008-0.331j \end{bmatrix} \begin{Bmatrix} 0 \\ 0 \\ -1 \\ -1 \end{Bmatrix}$$

$$= \begin{Bmatrix} 0.3473+0.6486j \\ 0.3473-0.6486j \\ -0.0171+0.0869j \\ -0.0171-0.0869j \end{Bmatrix} \quad \text{(s)}$$

Thus

$$x_1 = 0.3473, \quad y_1 = 0.6486 \quad \text{(t)}$$

$$x_2 = -0.0171, \quad y_2 = 0.0869 \quad \text{(u)}$$

From Equation 7.78 and recall that we can let $\gamma_1 = 1$, then

$$f_{11} = \frac{2}{r_1}\left[(\beta_{11}\mu_1 - \alpha_{11}\nu_1)\, y_1 - (\alpha_{11}\mu_1 + \beta_{11}\nu_1)\, x_1\right]$$

$$= \frac{2}{1}\left\{\begin{array}{l}[0.0243 \times (-0.488) - 0.0463 \times 11.818] \times 0.6486 \\ -[0.0463 \times (-0.488) + 0.0243 \times 11.818] \times 0.3473\end{array}\right\}$$

$$= -0.909 \quad \text{(v)}$$

$$g_{11} = \frac{2}{r_1}(\alpha_{11}x_1 - \beta_{11}y_1)$$

$$= \frac{2}{1}(0.0463 \times 0.3473 - 0.0243 \times 0.6486)$$

$$= 6.380 \times 10^{-4} \quad \text{(w)}$$

$$f_{21} = \frac{2}{r_1}\left[(\beta_{21}\mu_1 - \alpha_{21}\nu_1)\, y_1 - (\alpha_{21}\mu_1 + \beta_{21}\nu_1)\, x_1\right]$$

$$= \frac{2}{1}\left\{\begin{array}{l}[0.0317\,(-0.488) - 0.0579\,(11.818)]\,(0.6486) \\ -[0.0579\,(-0.488) + 0.0317\,(11.818)]\,(0.3473)\end{array}\right\}$$

$$= -1.148 \quad \text{(x)}$$

$$g_{21} = \frac{2}{r_1}(\alpha_{21}x_1 - \beta_{21}y_1)$$

$$= \frac{2}{1}[0.0579\,(0.3473) - 0.0317\,(0.6486)]$$

$$= -9.039 \times 10^{-4} \quad \text{(y)}$$

$$f_{12} = \frac{2}{r_2}\left[\left(\beta_{12}\mu_2 - \alpha_{12}\nu_2\right) y_2 - \left(\alpha_{12}\mu_2 + \beta_{12}\nu_2\right) x_2\right]$$
$$= \frac{2}{1}\left\{\begin{array}{l}\left[0.004 \times (-0.545) - 0.0159\,(32.906)\right](0.0869) \\ -\left[0.0159\,(-0.545) + 0.0004\,(32.906)\right](-0.0171)\end{array}\right\}$$
$$= -0.091 \tag{z}$$

$$g_{12} = \frac{2}{r_2}\left(\alpha_{12}x_2 - \beta_{12}y_2\right)$$
$$= \frac{2}{1}\left[0.0159\,(-0.0171) - 0.0004\,(0.0869)\right]$$
$$= -6.133 \times 10^{-4} \tag{aa}$$

$$f_{22} = \frac{2}{r_2}\left[\left(\beta_{22}\mu_2 - \alpha_{22}\nu_2\right) y_2 - \left(\alpha_{22}\mu_2 + \beta_{22}\nu_2\right) x_2\right]$$
$$= \frac{2}{1}\left\{\begin{array}{l}\left[0.0003\,(-0.545) - (-0.0259)\,(32.906)\right](0.0869) \\ -\left[-0.0259\,(-0.545) + 0.0003\,(32.906)\right](-0.0171)\end{array}\right\}$$
$$= 0.149 \tag{bb}$$

$$g_{22} = \frac{2}{r_2}\left(\alpha_{22}x_2 - \beta_{22}y_2\right)$$
$$= \frac{2}{1}\left[-0.0259\,(-0.0171) - 0.0003\,(0.0869)\right]$$
$$= 3.644 \times 10^{-4} \tag{cc}$$

The properties of medium soil is given by Equation 7.30 as

$$\omega_g = 15.6 \text{ rad/s} \quad \text{and} \quad \zeta_g = 0.60 \tag{dd}$$

The natural frequencies and damping ratios can be found from Equations o and p using Equation 7.45, that is,

$$\left\{\begin{array}{l} -\zeta_1\omega_1 = \mu_1 = -0.488 \\ \sqrt{1-\zeta_1^2}\,\omega_1 = \nu_1 = 11.818 \end{array}\right. \tag{ee}$$

$$\omega_1^2 = \mu_1^2 + \nu_1^2 = (-0.488)^2 + 11.818^2 = 139.9 \tag{ff}$$

$$\omega_1 = 11.828 \text{ rad/s} \tag{gg}$$

$$\zeta_1 = \frac{-0.488}{-11.828} = 0.0413 \tag{hh}$$

Similarly,

$$\begin{cases} -\zeta_2\omega_2 = \mu_2 = -0.545 \\ \sqrt{1-\zeta_2^2}\omega_2 = \nu_2 = 32.906 \end{cases} \tag{ii}$$

$$\omega_2^2 = \mu_2^2 + \nu_2^2 = (-0.545)^2 + 32.906^2 = 1083.10 \tag{jj}$$

$$\omega_2 = 32.911 \text{ rad/s} \tag{kk}$$

$$\zeta_2 = \frac{-0.545}{32.911} = 0.0166 \tag{ll}$$

From Equation 7.101

$$\begin{aligned} N_{q1} &= \left(1+4\zeta_g^2\right)\zeta_1 + 4\zeta_g\left(\zeta_1^2+\zeta_g^2\right)s + 4\zeta_g^2\zeta_1 s^3 + \zeta_g s \\ &= \left[1+4\left(0.6^2\right)\right]0.0413 + 4\,(0.6)\left(0.0413^2+0.6^2\right)(1.319) \\ &\quad + 4\left(0.6^2\right)(0.0413)\left(1.319^2\right) + 0.6\left(1.319^3\right) \\ &= 2.726 \end{aligned} \tag{mm}$$

$$\begin{aligned} D_{q1} &= \zeta_g\zeta_1 + 4\zeta_1^2\zeta_g^2 s + 2\zeta_g\zeta_1\left(2\zeta_g^2+2\zeta_1^2-1\right)s^2 + 4\zeta_g^2\zeta_1^2 s^3 + \zeta_g\zeta_1 s^4 \\ &= 0.6\,(0.0413) + 4\left(0.0413^2\right)\left(0.6^2\right)(1.319) \\ &\quad + 2\,(0.6)\,(0.0413)\left(2\times 0.6^2 + 2\times 0.0413^2 - 1\right)\left(1.319^2\right) \\ &\quad + 4\left(0.6^2\right)\left(0.0413^2\right)\left(1.319^3\right) + 0.6\,(0.0413)\left(1.319^4\right) \\ &= 0.0848 \end{aligned} \tag{nn}$$

in which

$$s = \frac{\omega_g}{\omega_1} = \frac{15.6}{11.828} = 1.319 \tag{oo}$$

Thus,

$$\sigma_{q1}^2 = \frac{\pi r_1^2 G_0}{4}\frac{\omega_g}{\omega_1^4}\frac{N_{q1}}{D_{q1}} = \frac{\pi\left(1^2\right)G_0}{4}\frac{15.6}{11.828^4}\frac{2.726}{0.0848} = 0.0201G_0 \tag{pp}$$

From Equation 7.106,

$$N_{\dot{q}1} = 4\zeta_g^3 + \zeta_1\left(1+4\zeta_g^2\right)s + \zeta_g s^2$$

$$= 4(0.6^3) + 0.0413\left[1 + 4(0.6^2)\right](1.319) + 0.6(1.319^2)$$

$$= 2.041 \tag{qq}$$

$$D_{\dot{q}1} = s\left[\zeta_g\zeta_1 + 4\zeta_1^2\zeta_g^2 s + 2\zeta_g\zeta_1\left(2\zeta_g^2 + 2\zeta_1^2 - 1\right)s^2 + 4\zeta_g^2\zeta_1^2 s^3 + \zeta_g\zeta_1 s^4\right]$$

$$= sD_{q1} = 1.319\,(0.0848) = 0.112 \tag{rr}$$

Thus,

$$\sigma_{\dot{q}1}^2 = \frac{\pi r_1^2 G_0}{4}\frac{\omega_g^3}{\omega_1^4}\frac{N_{\dot{q}1}}{D_{\dot{q}1}}$$

$$= \frac{\pi 1^2 G_0}{4}\frac{15.6^3}{11.828^4}\frac{2.041}{0.112}$$

$$= 2.776G_0 \tag{ss}$$

Then for the second mode,

$$s = \frac{\omega_g}{\omega_2} = \frac{15.6}{32.911} = 0.474 \tag{tt}$$

$$N_{q2} = \left(1 + 4\zeta_g^2\right)\zeta_2 + 4\zeta_g^2\left(\zeta_2^2 + \zeta_g^2\right)s + 4\zeta_g^2\zeta_2 s^2 + \zeta_g s^3$$

$$= \left(1 + 4 \times 0.6^2\right)(0.0166) + 4 \times 0.6^2\left(0.0166^2 + 0.6^2\right)(0.474)$$

$$+ 4\left(0.6^2\right)(0.0166)\left(0.474^2\right) + 0.6\left(0.474^3\right)$$

$$= 0.356 \tag{uu}$$

$$D_{q2} = \zeta_g\zeta_2 + 4\zeta_2^2\zeta_g^2 s + 2\zeta_g\zeta_2\left(2\zeta_g^2 + 2\zeta_2^2 - 1\right)s^2 + 4\zeta_g^2\zeta_2^2 s^3 + \zeta_g\zeta_2 s^4$$

$$= 0.6\,(0.0166) + 4\left(0.0166^2\right)\left(0.6^2\right)(0.474)$$

$$+ 2\,(0.6)\,(0.0166)\left(2 \times 0.6^2 + 2 \times 0.0166^2 - 1\right)\left(0.474^2\right)$$

$$+ 4\left(0.6^2\right)\left(0.0166^2\right)\left(0.474^3\right) + 0.6\,(0.0166)\left(0.474^4\right)$$

$$= 9.442 \times 10^{-3} \tag{vv}$$

$$N_{\dot{q}2} = 4\zeta_g^3 + \zeta_2\left(1 + 4\zeta_g^2\right)s + \zeta_g s^2$$

$$= 4 \times 0.6^3 + 0.0166\left(1 + 4 \times 0.6^2\right)(0.474) + 0.6\left(0.474^2\right)$$

$$= 1.018 \tag{ww}$$

$$
\begin{aligned}
D_{\dot{q}2} &= s\left[\zeta_g\zeta_2 + 4\zeta_2^2\zeta_g^2 s + 2\zeta_g\zeta_2\left(2\zeta_g^2 + 2\zeta_2^2 - 1\right)s^2 + 4\zeta_g^2\zeta_2^2 s^3 + \zeta_g\zeta_2 s^4\right] \\
&= sD_{q2} = 0.474\left(9.442 \times 10^{-3}\right) \\
&= 4.476 \times 10^{-3} \qquad \text{(xx)}
\end{aligned}
$$

$$
\begin{aligned}
\sigma_q^2 &= \frac{\pi r_2^2 G_0}{4}\frac{\omega_g}{\omega_2^4}\frac{N_{q2}}{D_{q2}} \\
&= \frac{\pi \cdot 1^2 G_0}{4}\frac{15.6}{32.911^4}\frac{0.356}{9.442 \times 10^{-3}} \\
&= 3.938 \times 10^{-4} G_0 \qquad \text{(yy)}
\end{aligned}
$$

$$
\begin{aligned}
\sigma_{\dot{q}2}^2 &= \frac{\pi r_2^2 G_0}{4}\frac{\omega_g^3}{\omega_2^4}\frac{N_{\dot{q}2}}{D_{\dot{q}2}} \\
&= \frac{\pi \cdot 1^2 G_0}{4}\frac{15.6^3}{32.911^4}\frac{1.018}{4.476 \times 10^{-3}} \\
&= 0.578 G_0 \qquad \text{(zz)}
\end{aligned}
$$

Then from Equation 7.107, we obtain the variance of closed-loop displacements as

$$
\begin{aligned}
\sigma_{z1}^2 &= f_{11}^2\sigma_{q1}^2 + g_{11}^2\sigma_{\dot{q}1}^2 + f_{12}^2\sigma_{q2}^2 + g_{12}^2\sigma_{\dot{q}2}^2 \\
&= (-0.909)^2\,(0.0201G_0) + \left(6.380 \times 10^{-4}\right)^2\,(2.776G_0) \\
&\quad + (-0.091)^2\left(3.938 \times 10^{-4}G_0\right) + \left(-6.133 \times 10^{-4}\right)^2\,(0.578G_0) \\
&= 0.0166G_0 \qquad \text{(aaa)}
\end{aligned}
$$

thus the RMS value of first floor displacement

$$
\sigma_{x1} = \sigma_{z1} = \sqrt{0.0166G_0} = 0.129\sqrt{G_0} \qquad \text{(bbb)}
$$

Similarly,

$$
\begin{aligned}
\sigma_{z2}^2 &= f_{21}^2\sigma_{q1}^2 + g_{21}^2\sigma_{\dot{q}1}^2 + f_{22}^2\sigma_{q2}^2 + g_{22}^2\sigma_{\dot{q}2}^2 \\
&= (-0.148)^2\,(0.0201G_0) + \left(9.039 \times 10^{-4}\right)^2\,(2.776G_0) \\
&\quad + 0.149^2\left(3.938 \times 10^{-4}G_0\right) + \left(3.644 \times 10^{-4}\right)(0.578G_0) \\
&= 0.0265G_0 \qquad \text{(ccc)}
\end{aligned}
$$

thus the RMS value of second floor displacement

$$\sigma_{x2} = \sigma_{z2} = \sqrt{0.0265 G_0} = 0.162\sqrt{G_0} \tag{ddd}$$

This example demonstrates that the statistical method only requires some algebraic calculation besides eigenanalysis in order to evaluate optimization objective function. It is based on the earthquake spectrum and works for any seismic excitations statistically. Thus, the statistical method is more simple and more general than the method of performance or controllability index that requires time-history analysis of specific earthquake excitation and numerical integration of seismic response.

7.3.6 Numerical Studies

A structure with hybrid damper-actuator bracing control system in Figure 5.21 serves as an example to demonstrate the method and to illustrate the effectiveness of optimal placement of control devices. Specifications and analytical modeling of the HDABC system are given in Section 5.3.3.2. As shown by the 11-element state vector in Equation 5.142, there are 11 state variables for the HDABC system, which are 3 displacements and 3 velocities of the structure, 1 displacement and 1 velocity of the K-bracing, 1 active control force, 1 servovalve displacement, and 1 passive control force. Thus, the smart structure with HDABC system is of the 11th order.

7.3.6.1 Optimal placement of hybrid control device

Assume the structure is built on medium soil with $\omega_g = 15.6$ rad/s and $\zeta_g = 0.60$. Owing to time scaling, ω_g in the Kanai–Tajimi spectrum used here is twice that of the prototype. To determine optimal controller placement, G_0 can be any value because RMS values of control force and structural response are proportional to $\sqrt{G_0}$. To simplify the problem, let $G_0 = 1$. If displacement at the third floor is the control goal and its required RMS value is 0.04, and if the active control force is the optimization objective for control device placement, the optimization problem becomes

$$\begin{aligned} &\text{Minimize } \{\sigma_{f_a}(x)\} \\ &\text{Subject to } \begin{cases} \sigma_{x_3}(x) = 0.04 \\ 1 \le x \le N \end{cases} \end{aligned} \tag{7.110}$$

Using the proposed solution procedure, the normalized RMS values of active control forces σ_{f_a} determined by Equation 7.107 are found to be 41.7, 283.4, and 143.5 for the hybrid control device at the first, second, and third floor, respectively.

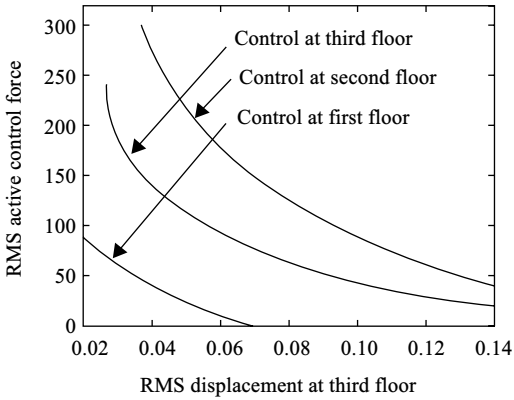

FIGURE 7.24 Comparison of RMS active control forces for three hybrid device locations.

Thus the objective function σ_{f_a} in Equation 7.110 is minimum when $x = 1$. This means that the first floor is the optimal location for the hybrid control device.

Figure 7.24 illustrates the relationship between RMS active control force and RMS displacement at the third floor for the hybrid device at three floors. As shown in the figure, the curve for the control device at the first floor is always lowest. At this location, the controller has maximum effectiveness since it uses the least control force to achieve the control goal. Figure 7.24 also shows that the first floor is the best location, the third floor is less desirable, and the second floor is the worst.

7.3.6.2 Optimal actuator placement for active control systems

If the damper does not exist, the system becomes active control in the tenth order. If the third floor displacement is the control goal and its required RMS value is 0.05, and if the active force is the optimization objective for device placement, the optimization problem becomes

$$\begin{aligned} &\text{Minimize } \{\sigma_{f_a}(x)\} \\ &\text{Subject to } \begin{cases} \sigma_{x_3}(x) = 0.05 \\ 1 \le x \le N \end{cases} \end{aligned} \tag{7.111}$$

Similarly, by using the proposed solution procedure, the normalized RMS values of active control forces σ_{f_a} are found as 41.3, 189.1, and 101.3 for the actuator at the first, second, and third floor, respectively. The objective function σ_{fa} in Equation 7.111 is minimum when $x = 1$. This means that the first floor is the optimal location for the actuator. Figure 7.25 illustrates the relationship between RMS active control force and RMS displacement at the third floor for the actuator at three floors. As in Figure 7.24, the curve for the control device at the first floor is always lowest, which means that the actuator has maximum effectiveness at this

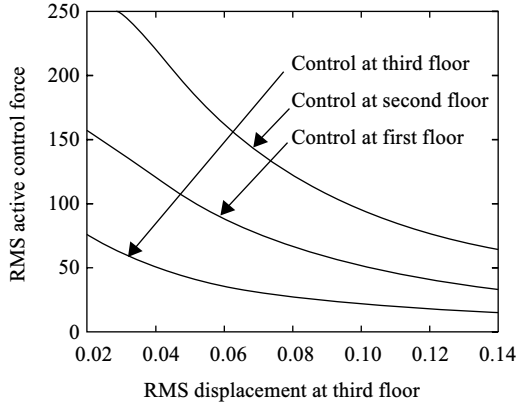

FIGURE 7.25 Comparison of RMS active control forces for three actuator locations.

location. Figure 7.25 also shows that the first floor is the best location, the third floor is less desirable, and the second floor is the worst.

7.3.6.3 Demonstration of effectiveness of optimal placement

As noted, this optimization criterion for control device placement is based on a statistical method. To verify this method and show the effectiveness of the hybrid bracing system with optimum placement, a procedure is taken as follows. Dynamic responses in time history of the structure with hybrid bracing system for scaled E-W component of New Mexico and N-S component of El-Centro earthquakes (with amplitude and frequency scale factors at 0.3 and 2, respectively) are evaluated for three control device locations: first, second, and third floor. Maximum displacement at the third floor is the control goal, and active control force is the optimization objective.

Time-history response of the system for scaled El-Centro earthquake is shown in Figure 7.1. Recall that the maximum displacement at the third floor of the uncontrolled structure is 0.7794 cm. Control objective is to reduce maximum displacement at the third floor of the structure to 0.508 cm. This Figure shows that the first floor is optimum because the least active control force is required to achieve the control objective. Here the result conforms to that in Section 7.3.6.1 that was obtained by the proposed statistical optimization criterion; the statistical method has the advantage of not requiring complex calculation of time-history responses. Note that the location of control devices greatly affects the control system. For example, if the hybrid device is at the second floor instead of the first, 4.8 times larger active control force is required to achieve same control objective.

Figure 7.26 compares the time histories of required active control force for scaled New Mexico earthquake. As expected, the first floor is the optimum location because the least maximum active control force (161.8 N) is required to reduce structural displacement at the third floor from 0.509 cm (structure without control)

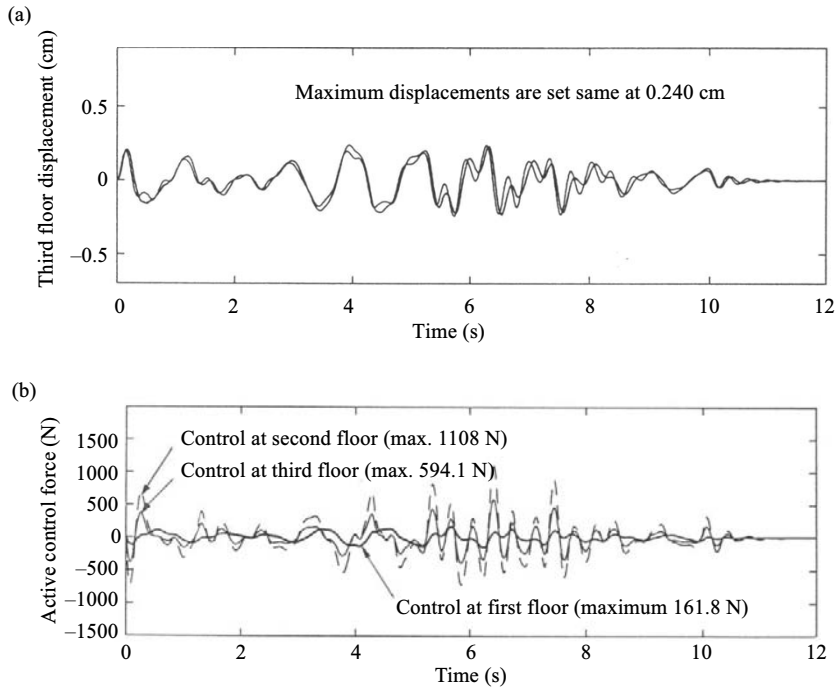

FIGURE 7.26 Response of HDABC system to scaled New Mexico earthquake: (a) displacement at the third floor and (b) required active control force.

to 0.24 cm. This figure also shows that a hybrid bracing control system with optimum device location is the most effective because it requires less active control force than a hybrid bracing control system with nonoptimal device location. Here the effectiveness of optimum device placement is more significant than that for scaled El-Centro earthquake. Maximum active control force for the hybrid device at the first floor is 14.6% and 27.2% of that for the hybrid device at second and third floor, respectively.

7.3.6.4 Influence of structural property on optimal device location

As the optimal location criteria implies, optimal device location highly depends on the structural properties. To demonstrate how the structural properties influence the optimal control location, a similar three-story building equipped with the same hybrid control device is used and one story's stiffness is changed gradually while the rest of structural properties are kept same. The three-story steel structure is treated as a shear building with column stiffness $EI = 1732.81\ \text{N} \cdot \text{m}^2$, lumped mass 635.6 kg at all three floors and story height 1.016, 0.762, and 0.762 (m) for first though third floor, respectively. Damping ratios are chosen as 0.35% for all

TABLE 7.10
Frequencies and Mode Shapes when First Floor Stiffness Changes Third Mode

	Frequency (Hz)	First mode	Second mode	Third mode
Original	2.863, 9.502, 15.06	[0.678 0.889 1.0]	[1.0 0.194 −0.850]	[−0.602 1.0 −0.480]
Case 1	3.318, 9.958, 15.18	[0.573 0.850 1.0]	[1.0 0.284 −0.815]	[−0.666 1.0 −0.469]
Case 2	3.871, 10.79, 15.50	[0.430 0.796 1.0]	[1.0 0.470 −0.805]	[−0.825 1.0 −0.441]
Case 3	4.192, 11.49, 15.91	[0.340 0.761 1.0]	[1.0 0.682 −0.859]	[−1.0 0.967 −0.396]

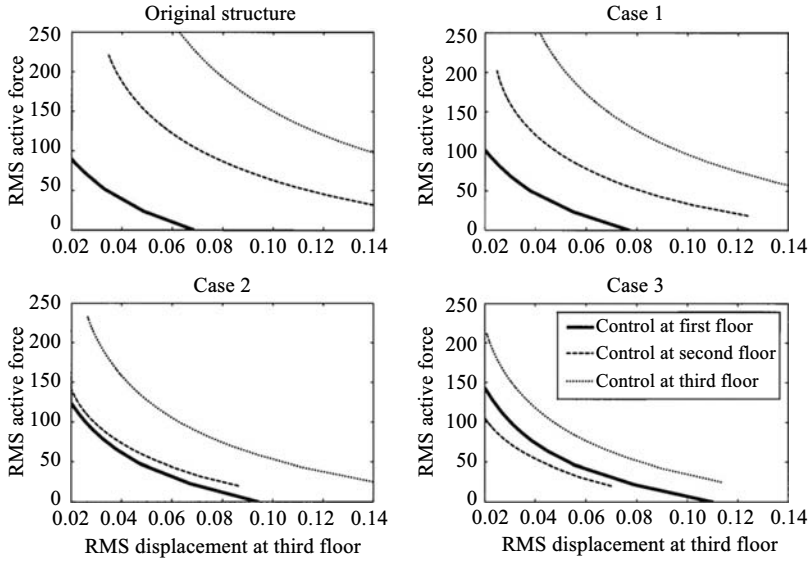

FIGURE 7.27 Optimal control location when first floor stiffness changes.

modes. The K-braces and Kanai–Tajimi spectrum parameters are the same as in earlier example.

Table 7.10 lists the frequencies and mode shapes of three additional cases where the first floor stiffness is chosen as 1.5, 2.5, and 3.5 times the original case. Figure 7.27 demonstrates the RMS active forces versus third floor RMS displacements for each case with the three different control locations. It is shown that the curve for the control at the first floor is going up as the first floor stiffness increases. Finally, for Case 3, the second floor becomes the optimal control location. Similarly, the second floor stiffness is chosen as 1.5 times, 1.8 times, and 2.5 times the original one for Case 1 through Case 3, respectively. The frequencies and mode shapes of each case are listed in Table 7.11. For each case, the RMS active forces verse third floor RMS displacements are presented in Figure 7.28 with three different control locations. It is found that the curve for control at the second floor

TABLE 7.11
Frequencies and Mode Shapes when Second Floor Stiffness Changes

	Frequency	First mode	Second mode	Third mode
Original	2.863, 9.502, 15.06	[0.678 0.889 1.0]	[1.0 0.194 −0.850]	[−0.602 1.0 −0.480]
Case 1	2.949, 9.980, 17.04	[0.733 0.882 1.0]	[0.937 0.355 −1.0]	[−0.740 1.0 −0.339]
Case 2	2.979, 10.13, 18.20	[0.753 0.879 1.0]	[0.865 0.397 −1.0]	[−0.789 1.0 −0.285]
Case 3	3.022, 10.33, 20.73	[0.783 0.876 1.0]	[0.771 0.453 −1.0]	[−0.855 1.0 −0.206]

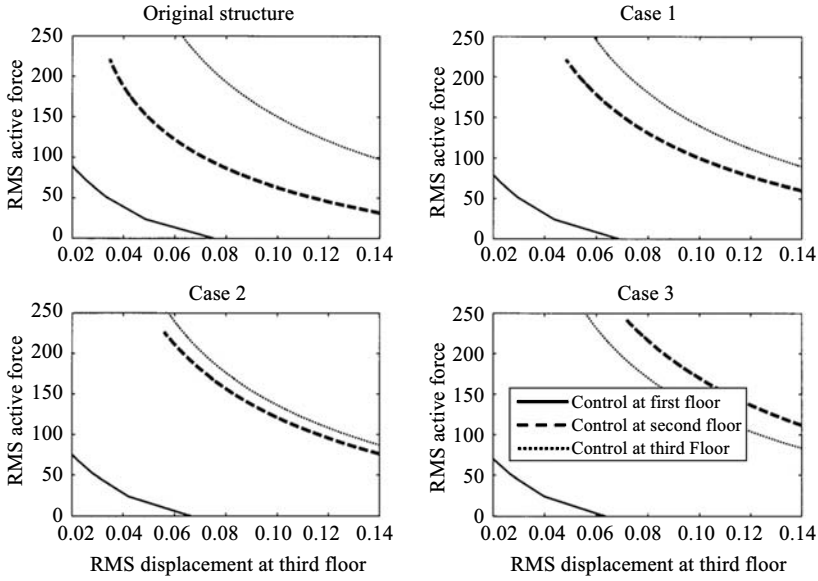

FIGURE 7.28 Optimal control location when second floor stiffness changes.

is going up as the second floor stiffness increases. Finally, in Case 3, control at the second floor becomes the worst. Results for changing the third floor stiffness are presented in Table 7.12 and Figure 7.29. In Case 1, the third floor stiffness is increased to 1.5 times the original value and the curve with third floor control goes up. When the stiffness is reduced to 60% and 40% of the original in Case 2 and Case 3, the curve goes down and is located below the curve with second floor control in Case 3.

Please note that to expedite the illustration of the proposed method, above numerical examples are simple one-bay two or three-story structures with one control device. As the flowchart in Figure 7.23 shows, the method also works for multiple-bay tall buildings. The only difference is that the design variable N, possible locations of the control device, would be a larger number. For structures with multiple control devices, the whole process in the flowchart just needs to

TABLE 7.12
Frequency and Mode Shapes when Third Floor Stiffness Changes

	Frequency	First mode	Second mode	Third mode
Original	2.863, 9.502, 15.06	[0.678 0.889 1.0]	[1.0 0.194 −0.850]	[−0.602 1.0 −0.480]
Case 1	2.886, 10.31, 16.85	[0.706 0.924 1.0]	[1.0 −0.024 −0.684]	[−0.410 1.0 −0.635]
Case 2	2.814, 8.126, 13.87	[0.624 0.820 1.0]	[0.949 0.497 −1.0]	[−0.837 1.0 −0.298]
Case 3	2.752, 7.011, 13.42	[0.563 0.742 1.0]	[0.891 0.671 −1.0]	[−0.972 1.0 −0.195]

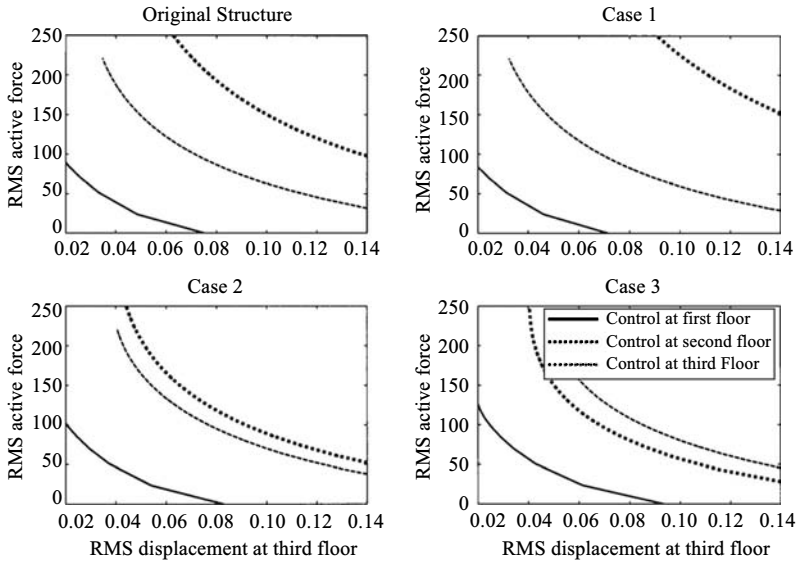

FIGURE 7.29 Optimal control location when third floor stiffness changes.

be repeated to determine optimal location of each control device. Of course, the occupied location would be deleted from the design space of optimal placement of following control devices.

7.4 Summary

This chapter carrier out a theoretical study on optimal device placements of a seismic response control system. First, basic concepts, the significance, and an overview of current study of optimal device placement in seismic response control are discussed. Second, three methods for optimal actuator placement for an active control system are presented and compared. These methods include the measure of modal controllability, control energy and response performance indices, and the controllability index. Third, a statistical method is developed for optimal device placement of dampers and actuators, with HDABC systems serving as

the example. This statistical method is based on the establishment of stochastic seismic response of the controlled structure with dynamics of control devices considered. To account for actuator and damper dynamics as well as nonorthogonal damping and stiffness matrices of the controlled structure, an equivalent modal analysis procedure is developed to study the stochastic seismic response of the controlled structure. On the basis of the study, a general definition for optimal device placement is established in a statistical manner, and a solution procedure for this optimization problem is developed. A numerical example, time-history response of a building structure for El-Centro and New Mexico earthquakes, is used to verify the proposed method and to demonstrate the effectiveness of the optimally located hybrid control system. The influence of structural properties on optimal control locations are analyzed numerically.

The following conclusions can be reached for optimal actuator placement studied in this chapter. The measure of modal controllability is effective for device placement on structures with one dominant mode in its seismic response. The method of controllability index is in agreement with the methods of control energy and response performance indices. The latter methods, however, needs a lot of computation time because seismic response in time history must be computed. Investigations of the mode shapes of a structure (not equipped with control) show that they are sufficient for evaluating the scalar index and that considering the mode shapes of the controlled structure does not affect the results. The optimal locations of active tendons were found to remain optimal for two different earthquakes. The optimal locations index depends on the structural parameters of the building. A building of the same height with different structural properties has different optimal locations for active tendons. Studies of how many modes are sufficient in using the method, showed that the procedure can be terminated when an increase in the number of modes considered does not alter the optimal locations.

The statistical method for optimal placement of hybrid control device is simple because it does not require complex computation of seismic structural response in time history and response integration. This method is also general because it does not require a specific earthquake record, and it can handle the combination of actuators and dampers and dynamics of control device. It is also worth noting that this method is based on a general analytical model of smart seismic structures, and thus it works for any configuration of structures and control systems. Numerical studies show that the effectiveness of control devices is greatly influenced by their location, thus the efficiency of control devices can be much improved by placing them on optimal location. It is also shown that the optimal control location is sensitive to structural properties of a smart seismic structure system.

References

1. Agrawal, A.K. and Yang, J.N., Optimal placement of energy dissipative systems using combinatorial optimization, in *Proceedings of the Thirteenth ASCE Conference on Analysis and Computation*, American Society of Civil Engineers, Reston, Virginia, 1998, p. 339.

2. Beak, K.H. and Elliott, S.J., Natural algorithms for choosing source locations in active control systems, *Journal of Sound and Vibration*, 186, 245, 1995.
3. Chang, M.L.J. and Soong, T.T., Optimal controller placement in modal control of complex systems, *Journal of Mathematical Analysis and Applications*, 75, 340, 1980.
4. Chen, G., Bruno, R.J., and Salama, M., Optimal placement of active/passive members in truss structures using simulated annealing, *AIAA Journal*, 29, 1327, 1991.
5. Cheng, F.Y., *Matrix Analysis of Structural Dynamics*, Marcel Dekker, Inc., New York, 2001.
6. Cheng, F.Y. and Botkin, M.E., Nonlinear optimum design of dynamic damped frames, *ASCE Journal of Structural Engineering*, 102, 609, 1976.
7. Cheng, F.Y. and Jiang, H.P., Hybrid control of seismic structures with optimal placement of control devices, *ASCE Journal of Aerospace Engineering*, 11, 52, 1998.
8. Cheng, F.Y., Jiang, H.P., and Zhang, X.Z., Optimal placement of dampers and actuators based on stochastic approach, *Journal of Earthquake Engineering and Engineering Vibration*, 1, 237, 2002.
9. Cheng, F.Y. and Li, D., Multiobjective optimization design with Pareto genetic algorithm, *ASCE Journal of Structural Engineering*, 123, 1252, 1997.
10. Cheng, F.Y. and Pantelides, C.P., Optimal control of seismic structures, in *Proceedings of the Third ASCE Engineering Mechanics Conference*, American Society of Civil Engineers, Reston, Virginia, 1986, p. 764.
11. Cheng, F.Y. and Pantelides, C.P., Optimal placement of actuators for structural control, *NCEER Technical Report 88-0037*, National Center for Earthquake Engineering, Buffalo, New York, 1988.
12. Cheng, F.Y. and Pantelides, C.P., Combining structural optimization and structural control, *NCEER Technical Report 88-0006*, National Center for Earthquake Engineering, Buffalo, New York, 1988.
13. Clough, R.W. and Penzien, J., *Dynamics of Structures*, McGraw Hill, New York, 1975.
14. Grantham, W.J. and Vincent, T.L., *Modern Control Systems: Analysis and Design*, John Wiley & Sons, New York, 1993.
15. Goldberg, D.E., *Genetic Algorithms in Search, Optimization, and Machine Learning, Reading*, Addison-Wesley Publishing Company, Inc., Massachusetts, 1989.
16. Hamdan, A.M.A and Nayfeh, A.H., Measures of modal controllability and observability for first- and second-order linear systems, *Journal of Guidance, Control, and Dynamics*, 12, 421, 1989.
17. Hamernik, T.A., Garcia, E., and Stech, D., Optimal placement of damped struts using simulated annealing, *Journal of Spacecraft and Rockets*, 32, 653, 1995.
18. Jiang, H.P., Cheng, F.Y., and Wang, Z.Q., Damper-actuator system with observer technique and optimal placement, in *Proceedings of International Symposium/Workshop on Seismic Isolation, Energy Dissipation and Control of Structures*, Zhou, F.L. and Spencer, B.F. Jr., (eds), Seismological Press, China, 1999, p. 362.
19. Jiang, H.P., Cheng, F.Y., and Wang, Z.Q., Observer technique for seismic response control, in *Proceedings of US-Korea Workshop on New Frontiers in Infrastructural and Seismic Problems*, Techno Press, Taejon, Korea, 1999, p. 209.

20. Jiang, H.P., Cheng, F.Y., and Wang, Z.Q., State-of-the-art in hybrid control and issues on optimum seismic observer and device placement, in *Proceedings of the Twelfth World Conference on Earthquake Engineering*, International Association for Earthquake Engineering, Auckland, New Zealand, 2000, p. 1622:1–8.
21. Kanai, K., Semi-empirical formula for the seismic characteristics of the ground, in *Bulletin of Earthquake Research Institute, University of Tokyo*, 35, 309, 1957.
22. Kirkpatrick, S., Gelatt, C.D. Jr, and Vecchi, M.P., Optimization by simulated annealing, *Science*, 220, 671, 1983.
23. Laskin, R.A., Aspects of the dynamics and controllability of large flexible structures, Ph.D. Dissertation, Columbia University, New York, 1982.
24. Lu, J., et al., Optimal tendon configuration of a tendon control system for a flexible structure, *Journal of Guidance, Control, and Dynamics*, 17, 161, 1994.
25. Mathews, M.H. and Howell, H., *Complex Analysis for Mathematics and Engineering*, William C. Brown Publishing, Dubuque, Iowa, 1996.
26. Milman, M.H. and Chu, C.H., Optimization methods for passive damper placement and tuning, *Journal of Guidance, Control, and Dynamics*, 17, 848, 1994.
27. Onoda, J, and Hanama, Y., Actuator placement optimization by genetic and improved simulated annealing algorithms, *AIAA Journal*, 31, 1167, 1992.
28. Palazzo, B. and Petti, L., Stochatic response comparison between base isolated and fixed-base structure, *Earthquake Spectra*, 13, 77, 1997.
29. Pantelides, C.P. and Cheng, F.Y., Optimum placement of actuators for seismic structures, *International Journal of Engineering Structures*, 12, 254, 1990.
30. Papadimitrion, C.H. and Steiglitz, K., *Combinatorial Optimization: Algorithms and Complexity*, Prentice-Hall, Inc., Englewood Cliffs, New Jersey, 1982.
31. Rao, S.S., Pan, T., and Venkayya, V.B., Optimal placement of actuators in actively controlled structures using genetic algorithms, *AIAA Journal*, 29, 942, 1991.
32. Spencer, B,F., Dyke, S.J., and Deoskar, H.S., A benchmark problem in structural control, in *Proceedings of the 1997 ASCE Structure Congress*, Portland, Oregon, American Society of Civil Engineers, Reston, Virginia, 1997, p. 1.
33. Tajimi, H., A statistical method of determining the maximum response of a building structure during an earthquake, in *Proceedings of the Second World Conference on Earthquake Engineering*, International Association for Earthquake Engineering, 1960, p. 781.
34. Yu, Z. and Cao, G., *Theory of Random Vibration*, Tongji University Press, Shanghai, China, 1989.

8 Active Control on Embedded Foundation

In Chapter 4, the study of active structural control was based on the fixed-base model in which the structure is assumed to be fixed at its base. This model may be well founded where the structure is built on rock. If the structure is constructed on soil, both the control algorithm and the structural system shall include the soil–structure interaction (SSI) that covers the flexibility of the soil and the displacement of the foundation. This leads to an increase in the number of the system's degrees of freedom (d.o.f.) that changes the structural response behavior and accordingly controls action and effectiveness.

In this chapter, analytical model considering SSI is developed for seismic-resistant structures with active control. Generalized optimal control algorithm is extended for the soil-structure system. Numerical examples are employed to demonstrate the analytical procedures.

8.1 Motion Equation of Actively Controlled Structure with Soil–Structure Interaction

8.1.1 System Definition

Figure 8.1 shows a multistory building with active tendon control constructed on a mat foundation embedded in unbounded soil. The soil consists of horizontal layers that rest on an elastic half-space subjected to seismic P- and S-waves generated from epicenter [2,11]. The soil is considered as isotropic viscoelastic material with *hysteretic damping*. Its properties may vary with depth but remain constant within individual layers.

Substructure method is used to model the system. The whole system is divided into two subsystems, that is, superstructure system and ground system, through an artificial interface. The superstructure consists of the structure and its foundation, including the active controllers installed on the structure. The ground system includes the soil layers and the underneath elastic half-space. It is assumed that the interfaces between the superstructure and the ground system are always in complete contact with each other.

To model the superstructure, building masses m_i are lumped on each floor i, where $i = 1, 2, \ldots, N$ and N is the number of building floors. To simplify the problem, shear-building structure is selected as shown in Figure 8.2. Floor translational spring stiffness is represented by two columns on each floor, each column having a stiffness of $k_i/2$. Proportional damping ratios of two translational modes are

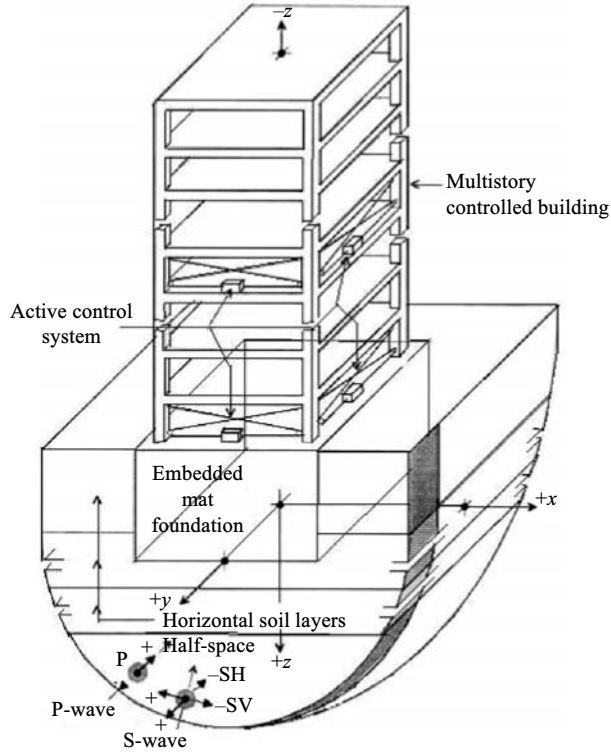

FIGURE 8.1 Multistory controlled building embedded in unbounded soil.

used to determine the viscous damping of the structure. The mat foundation is assumed to be rigid. Foundation mass and mass moment of inertia are denoted by m_0 and I_0, respectively. It is assumed that the foundation depth h_0 is not very deep so that the ground acceleration can be considered to be applied on the mass center of the foundation. With this consideration, the superstructure would have $(N+2)$ d.o.f. that are N horizontal translations of the structure x_i $(i = 1, 2, \ldots, N)$, the horizontal translation of the foundation x_0 and the rotation of the foundation θ_0. Included in the model of the controlled structure are m active tendons. Since the parameters of the superstructure system are frequency-independent, it can be analyzed in time-domain.

The ground system is modeled as an unbounded continuous domain represented by $(s-1)$ unbounded horizontal layers resting on a half-space, as shown in Figure 8.3. Each layer i $(i = 1, 2, \ldots, s-1)$ has constant properties: soil density ρ_i, modulus of elasticity E_i, Poisson's ratio ν_i, hysteretic damping ratio β_{gi}, and layer depth d_i. The half-space has the following properties: density ρ_R, modulus of elasticity E_R, Poisson's ratio ν_R, and hysteretic damping ratio β_R. Since the *mat foundation* is modeled as a rigid block; the interface is rigid represented by the d.o.f. at point O, a horizontal translational x_0^g and rotation θ_0^g, where superscript

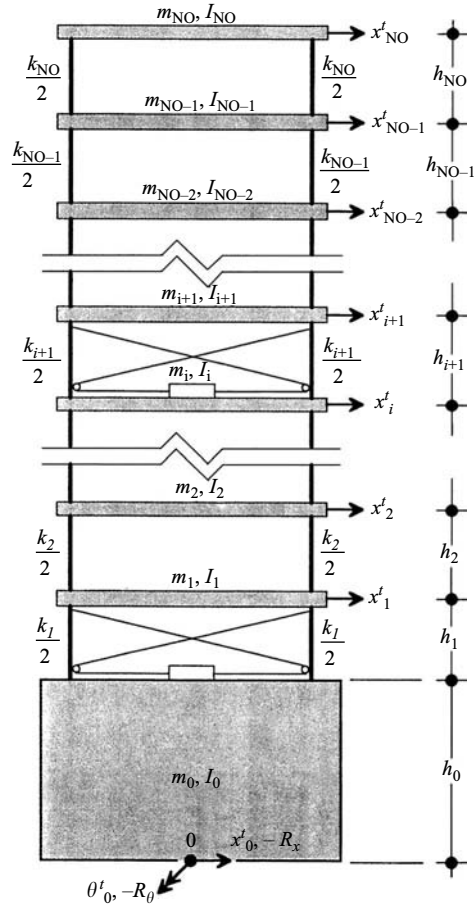

FIGURE 8.2 Structure system modeling.

g denotes the ground system. Since we assume the superstructure and the ground system are in perfect contact, then $x_0^g = x_0$ and $\theta_0^g = \theta_0$. Length $2B$ and height D of the interface are equal to those of the foundation, respectively. Since the unbounded soil has infinite length in x-direction, and the properties of the unbounded soil are frequency dependent, the indirect boundary element method in frequency domain is appropriately applied to analyze the system.

8.1.2 Single-Story Building

In order to simplify the problem, let us formulate the SSI model for the single-story building with control (see Figure 8.4) first. For a SSI model subjected to a vertically incident shear wave, rotational seismic input may be omitted. From the

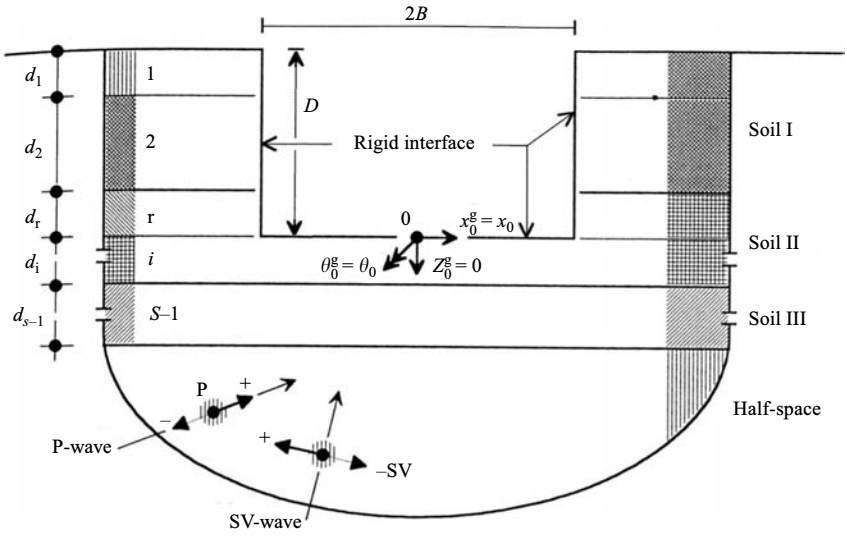

FIGURE 8.3 Ground system with rigid interface.

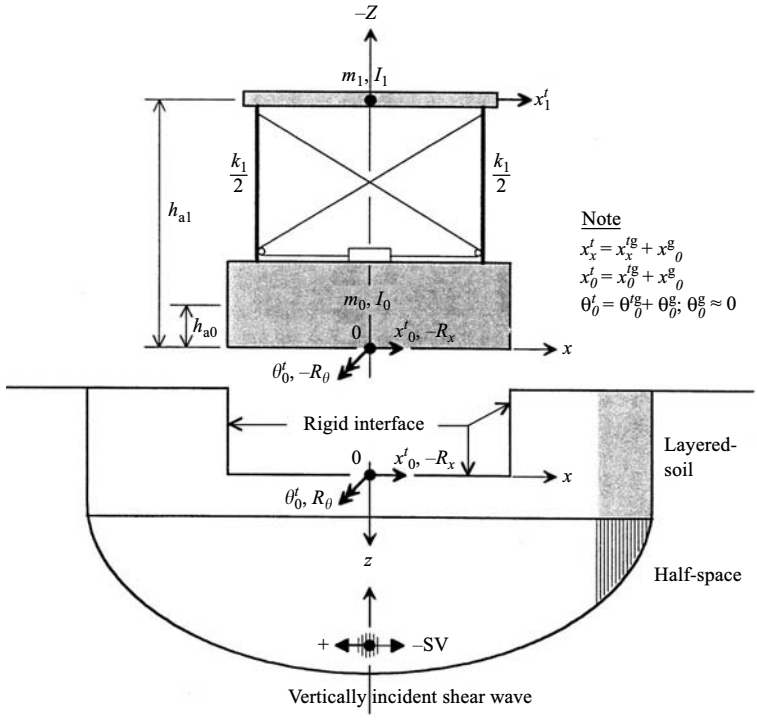

FIGURE 8.4 Single-story SSI model.

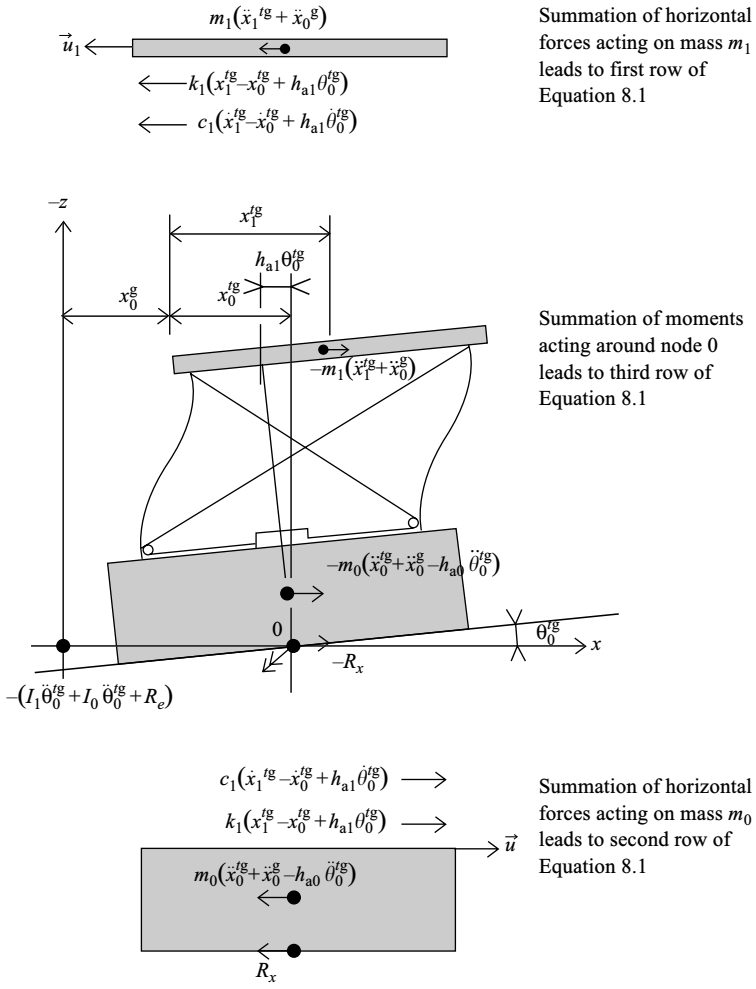

FIGURE 8.5 Free-body diagram of single-story SSI model.

free-body diagram as shown in Figure 8.5, the motion equation of the single-story shear building equipped with an active tendon system can be obtained as

$$\begin{cases} m_1(\ddot{x}_1^{tg} + \ddot{x}_0^{g}) + c_1(\dot{x}_1^{tg} - \dot{x}_0^{tg} + h_{a1}\dot{\theta}_0^{tg}) + k_1(x_1^{tg} - x_0^{tg} + h_{a1}\theta_0^{tg}) + \vec{u}_1 = 0 \\ m_0(\ddot{x}_1^{tg} + \ddot{x}_1^{g} - h_{a0}\ddot{\theta}_0^{tg}) - c_1(\dot{x}_1^{tg} - \dot{x}_1^{tg} + h_{a1}\dot{\theta}_0^{tg}) \\ -k_1(x_1^{tg} - x_0^{tg} + h_{a1}\theta_0^{tg}) - \vec{u}_1 + R_x = 0 \\ (I_1 + I_0)\ddot{\theta}_1^{tg} - m_0(\ddot{x}_0^{tg} + \ddot{x}_0^{tg} - h_{a0}\ddot{\theta}_0^{tg})h_{a0} - m_1(\ddot{x}_1^{tg} + \ddot{x}_0^{g})h_{a1} + R_\theta = 0 \end{cases} \tag{8.1}$$

At any nth time interval, the above motion equation can be considered in matrix form as

$$\begin{bmatrix} m_1 & 0 & 0 \\ 0 & m_0 & -h_{a0}m_0 \\ -h_{a1}m_1 & -h_{a0}m_0 & I_1 + I_0 + h_{a0}^2 m_0 \end{bmatrix} \begin{Bmatrix} \ddot{x}_1^{tg}(n) \\ \ddot{x}_0^{tg}(n) \\ \ddot{\theta}_0^{tg}(n) \end{Bmatrix} + \begin{bmatrix} c_1 & -c_1 & h_{a1}c_1 \\ -c_1 & c_1 & -h_{a1}c_1 \\ 0 & 0 & 0 \end{bmatrix} \begin{Bmatrix} \dot{x}_1^{tg}(n) \\ \dot{x}_0^{tg}(n) \\ \dot{\theta}_0^{tg}(n) \end{Bmatrix} + \begin{bmatrix} k_1 & -k_1 & h_{a1}k_1 \\ -k_1 & k_1 & -h_{a1}k_1 \\ 0 & 0 & 0 \end{bmatrix} \begin{Bmatrix} x_1^{tg}(n) \\ x_0^{tg}(n) \\ \theta_0^{tg}(n) \end{Bmatrix} = \begin{Bmatrix} -m_1 \\ -m_0 \\ h_{a1}m_1 + h_{a0}m_0 \end{Bmatrix} \ddot{x}_0^{g}(n) + \begin{Bmatrix} -1 \\ 1 \\ 0 \end{Bmatrix} \vec{u}_1(n) + \begin{Bmatrix} 0 \\ -R_x(n) \\ -R_\theta(n) \end{Bmatrix} \tag{8.2}$$

where m_1 and m_0 are floor lumped mass and foundation lumped mass, respectively. I_1 and I_0 are floor and foundation mass moments of inertia around point 0. h_{a1} and h_{a0} are heights from rotational point 0 to the centroid of floor lumped mass and foundation lumped mass, respectively. k_1 is translational spring–stiffness coefficient. c_1 is translational damping coefficient approximated by $2\beta_1\sqrt{k_1 m_1}$. β_1 is damping ratio of the translational mode. It should be noted that external translation and rotation damping of the structural system are neglected. x_1^{tg}, x_0^{tg}, and θ_0^{tg} are floor translation, foundation translation, and foundation rotation, respectively. Superscript tg indicates all responses are of the total dynamic system and relative to those of the ground system. $\ddot{x}_0^{g}$ is the horizontal acceleration, at point 0, of the ground system with rigid interface. A dot and a double dot over a symbol denote the first derivative and second derivative in relation to time, respectively. $\vec{u}_1$ is a horizontal control force. R_x and R_θ are horizontal interaction force and interaction moment between the structural system and ground system at point 0, respectively.

8.1.3 Multiple-Story Building

Analogous to a derivation of Equation 8.2, motion equation of a multiple-story seismic shear structure (see Figure 8.6) can written in general form as

$$\begin{bmatrix} [M_{SS}] & [M_{S0}] \\ [M_{0S}] & [M_{00}] \end{bmatrix} \begin{Bmatrix} \{\ddot{X}_S^{tg}(n)\} \\ \ddot{X}_0^{tg}(n) \end{Bmatrix} + \begin{bmatrix} [C_{SS}] & [C_{S0}] \\ [C_{0S}] & [C_{00}] \end{bmatrix} \begin{Bmatrix} \{\dot{X}_S^{tg}(n)\} \\ \dot{X}_0^{tg}(n) \end{Bmatrix} + \begin{bmatrix} [K_{SS}] & [K_{S0}] \\ [K_{0S}] & [K_{00}] \end{bmatrix} \times \begin{Bmatrix} \{X_S^{tg}(n)\} \\ X_0^{tg}(n) \end{Bmatrix} = \begin{Bmatrix} \{\delta_s\} \\ \{\delta_0\} \end{Bmatrix} \ddot{x}_0^{g}(n) + \begin{bmatrix} [\gamma_S] \\ [\gamma_0] \end{bmatrix} \{\vec{U}(n)\} + \begin{Bmatrix} \{0\} \\ -\{R_0(n)\} \end{Bmatrix} \tag{8.3}$$

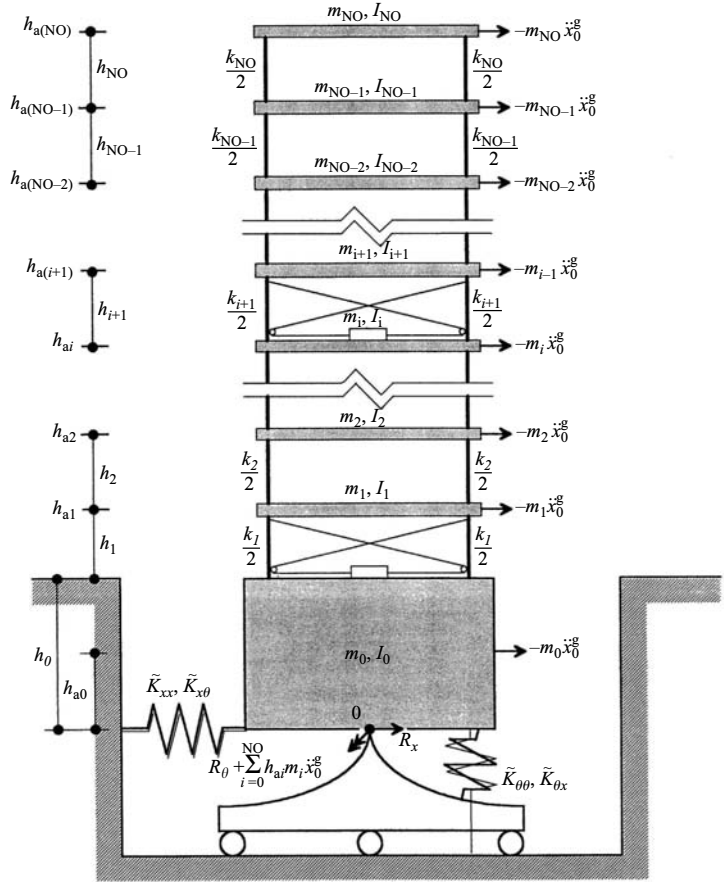

FIGURE 8.6 Structure system with fictitious springs subjected to equivalent forces.

$$[M_{SS}] = \begin{bmatrix} m_{NO} & \vdots & 0 & \vdots & 0 \\ \cdots & \ddots & \vdots & \vdots & \vdots \\ 0 & \cdots & m_i & \vdots & 0 \\ \cdots & \cdots & \cdots & \ddots & \vdots \\ 0 & \cdots & 0 & \cdots & m_1 \end{bmatrix} \tag{8.4}$$

$$[M_{S0}] = [0]; \quad [M_{0S}] = \begin{bmatrix} 0 & \cdots & 0 & \cdots & 0 \\ -h_{aNO}m_{NO} & \cdots & -h_{ai}m_i & \cdots & -h_{a1}m_1 \end{bmatrix} \tag{8.5}$$

$$[M_{00}] = \begin{bmatrix} m_0 & -h_{a0}m_0 \\ -h_{a0}m_0 & \sum_{i=0}^{NO} I_i + h_{a0}^2 m_0 \end{bmatrix} \tag{8.6}$$

$$[K_{SS}] = \begin{bmatrix} k_{NO} & -k_{NO} & 0 & \vdots & 0 & \vdots & 0 & 0 \\ -k_{NO} & k_{NO}+k_{NO-1} & -k_{NO-1} & \vdots & 0 & \vdots & 0 & 0 \\ 0 & -k_{NO-1} & k_{NO-1}+k_{NO-2} & \vdots & 0 & \vdots & 0 & 0 \\ \dots & \dots\dots\dots & \dots\dots\dots\dots & \ddots & \vdots & \vdots & \vdots & \vdots \\ 0 & 0 & 0 & \dots & k_i+k_{i-1} & \vdots & 0 & 0 \\ \dots & \dots\dots\dots & \dots\dots\dots\dots & \dots & \dots\dots & \ddots & \vdots & \vdots \\ 0 & 0 & 0 & \dots & 0 & \dots & k_3+k_2 & -k_2 \\ 0 & 0 & 0 & \dots & 0 & \dots & -k_2 & k_2+k_1 \end{bmatrix} \tag{8.7}$$

$$[K_{S0}] = \begin{bmatrix} 0 & h_{NO}k_{NO} \\ 0 & h_{NO-1}k_{NO-1} - h_{NO}k_{NO} \\ 0 & h_{NO-2}k_{NO-2} - h_{NO-1}k_{NO-1} \\ \vdots & \vdots \\ 0 & h_ik_i - h_{i+1}k_{i+1} \\ \vdots & \vdots \\ 0 & h_2k_2 - h_3k_3 \\ -k_1 & h_{a1}k_1 - h_2k_2 \end{bmatrix} \tag{8.8}$$

$$[K_{0S}] = \begin{bmatrix} 0 & 0 & 0 & \dots & 0 & \dots & 0 & -k_1 \\ 0 & 0 & 0 & \dots & 0 & \dots & 0 & 0 \end{bmatrix} \tag{8.9}$$

$$[K_{00}] = \begin{bmatrix} k_1 & -h_{a1}k_1 \\ 0 & 0 \end{bmatrix} \tag{8.10}$$

$$[C_{SS}] = \alpha_m[M_{SS}] + \Omega_k\,[K_{SS}] \tag{8.11}$$

$$[C_{S0}] = \begin{bmatrix} 0 & \Omega_k(h_{NO}k_{NO}) \\ 0 & \Omega_k(h_{NO-1}k_{NO-1} - h_{NO}k_{NO}) \\ 0 & \Omega_k(h_{NO-2}k_{NO-2} - h_{NO-1}k_{NO-1}) \\ \vdots & \vdots \\ 0 & \Omega_k(h_ik_i - h_{i+1}k_{i+1}) \\ \vdots & \vdots \\ 0 & \Omega_k(h_2k_2 - h_3k_3) \\ -\Omega_k k_1 & \Omega_k(h_{a1}k_1 - h_2k_2) \end{bmatrix} \tag{8.12}$$

$$[C_{0S}] = \begin{bmatrix} 0 & 0 & 0 & \dots & 0 & \dots & 0 & -\Omega_k k_1 \\ 0 & 0 & 0 & \dots & 0 & \dots & 0 & 0 \end{bmatrix} \tag{8.13}$$

$$[C_{00}] = \begin{bmatrix} \alpha_m m_1 + \Omega_k k_1 & -\Omega_k h_{a1} k_1 \\ 0 & 0 \end{bmatrix} \tag{8.14}$$

$$\{\delta_S\} = \begin{Bmatrix} -m_{NO} \\ \vdots \\ -m_i \\ \vdots \\ -m_1 \end{Bmatrix} \tag{8.15}$$

$$\{\delta_0\} = \begin{Bmatrix} -m_0 \\ \sum_{i=0}^{NO} h_{ai} m_i \end{Bmatrix} \tag{8.16}$$

where $[M_{SS}], [K_{SS}]$, and $[C_{SS}]$ of dimension NO by NO are diagonal lumped mass, symmetrical spring stiffness, and *proportional damping* matrices related to the superstructure, respectively. $[M_{S0}], [K_{S0}], [C_{S0}]$ of dimension NO by 2 and $[M_{0S}], [K_{0S}], [C_{0S}]$ of dimension 2 by NO are mass, stiffness, and damping matrices related to superstructure and rigid foundation. $[M_{00}]$, $[K_{00}]$, and $[C_{00}]$ of dimension 2 by 2 are mass, stiffness, and damping matrices related to rigid foundation, respectively. Subscripts S and 0 indicate that elements in the denoted vector or matrix correspond to the d.o.f. of superstructure and foundation, respectively. α_m and Ω_k can be determined by solving $\alpha_m \Omega_k \omega_i^2 = 2\omega_i \beta_i$ for $i = 1, 2$ where β_i are damping ratios of translational mode of frequency ω_i. $\{\delta_S\}$ of dimension NO by 1 and $\{\delta_0\}$ of dimension 2 by 1 are horizontal ground-acceleration coefficient vectors for superstructure and foundation, respectively. $h_{ai}, i = 0, 1, \dots, NO$, are accumulated heights from rotational point 0 to the centroid of mass m_i. $h_i = 1, \dots, NO$, are the ith floor height.

Vector $\{X_S^{tg}\}$ of dimension NO by 1 is the floor translation vector, $[x_{NO}^{tg} x_{NO-1}^{tg} \dots x_i^{tg} \dots x_2^{tg} x_1^{tg}]^T$. $\{X_0^{tg}\}$ of dimension 2 by 1 is a vector consisting of foundation translation and rotation at point 0, $\begin{bmatrix} x_0^{tg} & \theta_0^{tg} \end{bmatrix}^T$. $\{R_0\}$ of dimension 2 by 1 is a vector consisting of horizontal interaction force and interaction moment at point 0. Other notations are given in Section 8.1.2.

Matrices $[\gamma_S]$ of dimension NO by NCR and $[\gamma_0]$ of dimension 2 by NCR are controller-location matrices for superstructure and foundation, respectively. NCR is the number of active controllers. $\{\vec{U}\}$ of dimension NCR by 1 is the vector of horizontal control forces, $[\vec{u}_{NCR} \dots \vec{u}_i \dots \vec{u}_1]^T$. An example of matrices $[\gamma_S]$ and $[\gamma_0]$ for a two-controller system, having controller no. 1 attached between rigid foundation and first floor (node no. 1) and controller no. 2 attached between second

floor (node no. 2) and third floor (node no. 3), is shown as

$$[\gamma_S] = \begin{bmatrix} 0 & 0 \\ \vdots & \vdots \\ 0 & 0 \\ -1 & 0 \\ 1 & 0 \\ 0 & -1 \end{bmatrix} \tag{8.17}$$

and

$$[\gamma_0] = \begin{bmatrix} 0 & 1 \\ 0 & 0 \end{bmatrix} \tag{8.18}$$

In the model used in this study, an active tendon system provides only horizontal control forces. Thus the bottom row of $[\gamma_0]$, corresponding to rotational d.o.f. is always equal to zero despite the controller's location.

Apply the general model for the one-story building shown in Figure 8.4 using Equations 8.4 through 8.18, we have

$$\begin{cases} [M_{SS}] = m_1, \ [M_{S0}] = \begin{bmatrix} 0 & 0 \end{bmatrix}, \ [M_{0S}] = \begin{Bmatrix} 0 \\ -h_{a1}m_1 \end{Bmatrix} \\ [M_{00}] = \begin{bmatrix} m_0 & -h_{a0}m_0 \\ -h_{a0}m_0 & I_0 + I_1 + h_{a0}^2 m_0 \end{bmatrix} \end{cases}$$

$$\begin{cases} [K_{SS}] = k_1, \quad [K_{S0}] = \begin{bmatrix} -k_1 & h_{a1}k_1 \end{bmatrix}, \ [K_{0S}] = \begin{Bmatrix} 0 \\ -k \end{Bmatrix} \\ [K_{00}] = \begin{bmatrix} k_1 & -h_{a1}k_1 \\ 0 & 0 \end{bmatrix} \end{cases}$$

$$\begin{cases} [C_{SS}] = c_1, \ [C_S] = \begin{bmatrix} -c_1 & h_{ai}c_1 \end{bmatrix} \\ [C_{0S}] = \begin{Bmatrix} -c_1 \\ 0 \end{Bmatrix}, \ [C_{00}] = \begin{bmatrix} c_1 & -h_{a1}c_1 \\ 0 & 0 \end{bmatrix} \end{cases}$$

$$\begin{cases} \{\delta_S\} = -m_1, \ \{\delta_0\} = \begin{Bmatrix} -m_0 \\ h_{a0}m_0 + h_{a1}m_1 \end{Bmatrix} \\ [\gamma_S] = -1, \ [\gamma_0] = \begin{Bmatrix} 1 \\ 0 \end{Bmatrix} \end{cases}$$

8.1.4 Determination of Interaction Force at Foundation-Soil Interface

Earthquake excitation imposed on the ground system with rigid interface (see Figure 8.3) causes point 0 of the system to move at velocities $\dot{x}_0^g$, $\dot{z}_0^g$, and $\dot{\theta}_0^g$

in x-, z-direction and around y-direction, respectively. Interaction between this system and the structure system leads to velocities $\dot{x}_0^{\mathrm{t}}$, $\dot{z}_0^{\mathrm{t}}$, and $\dot{\theta}_0^{\mathrm{t}}$ at the same point. Changes in velocities, $\dot{x}_0^{\mathrm{tg}}$, $\dot{z}_0^{\mathrm{tg}}$, and $\dot{\theta}_0^{\mathrm{tg}}$ that is $\dot{x}_0^{\mathrm{t}} - \dot{x}_0^{\mathrm{g}}$, $\dot{z}_0^{\mathrm{t}} - \dot{z}_0^{\mathrm{g}}$, and $\dot{\theta}_0^{\mathrm{t}} - \dot{\theta}_0^{\mathrm{g}}$, respectively, induce interaction forces R_x, R_z, and R_θ. The interaction forces are related to the ground system's impulse velocity matrix that can be obtained by convolution integral, taking causality conditions into account (amplitude of impulse velocity function equal zero for time $t < 0$). Since vertical (z-direction) translation is omitted, the convolution integral corresponding to the other two d.o.f. can be expressed as

$$\left\{\dot{X}_0^{\mathrm{tg}}(t)\right\} = \int_0^t \left[\dot{\chi}_{00}^{\mathrm{g}}(\tau)\right]\{R_0(t-\tau)\}\,\mathrm{d}\tau \tag{8.19}$$

with

$$\left[\dot{\chi}_{00}^{\mathrm{g}}(\tau)\right] = \begin{bmatrix} \dot{\chi}_{xx}^{\mathrm{g}} & \dot{\chi}_{x\theta}^{\mathrm{g}} \\ \dot{\chi}_{\theta x}^{\mathrm{g}} & \dot{\chi}_{\theta\theta}^{\mathrm{g}} \end{bmatrix} \tag{8.20}$$

where t and τ are time variables. $\left[\dot{\chi}_{00}^{\mathrm{g}}\right]$ is the ground system's impulse velocity matrix with rigid interface. Coefficients $\dot{\chi}_{xx}^{\mathrm{g}}$, $\dot{\chi}_{x\theta}^{\mathrm{g}}$, $\dot{\chi}_{\theta x}^{\mathrm{g}}$, and $\dot{\chi}_{\theta\theta}^{\mathrm{g}}$ are velocities, at time equals τ, corresponding to the first subscript's d.o.f. due to a unit impulse force, at time equals zero, corresponding to the second subscript's d.o.f. (see Section 8.6.4.3 for detailed derivations). On the basis of causality conditions, interaction forces and velocities under a unit impulse force, before time equal to zero, must be zero. Thus τ varies from 0 to t. Since the solution procedure of a state equation is carried on in the discrete time-domain, the convolution integral can be replaced by summation as

$$\left\{\dot{X}_0^{\mathrm{tg}}(n)\right\} = \Delta t \sum_{m=0}^{n} \left[\dot{\chi}_{00}^{\mathrm{g}}(m)\right]\{R_0(n-m)\} \tag{8.21}$$

where Δt and n are time increment and time-instant number, respectively. m varies from zero to n. To reduce the number of operations in Equation 8.21, one may take advantage of the fact that a ground system with half-space has radiation damping. Then the amplitude of velocity under a unit impulse load (impulse velocity function) attenuates as time proceeds. At time-instant number equals l, for instance, all elements in the impulse velocity matrix approximately equal zero, and nl is the minimum of n and l. Then Equation 8.21 can be written as

$$\left\{\dot{X}_0^{\mathrm{tg}}(n)\right\} = \Delta t \sum_{m=0}^{nl} \left[\dot{\chi}_{00}^{\mathrm{g}}(m)\right]\{R_0(n-m)\} \tag{8.22}$$

Assuming velocities at midpoint of nth time step equal average velocities between nth point and $(n-1)$th point leads to

$$\left\{\dot{X}_0^{\mathrm{tg}}(n)\right\} = \frac{2}{\Delta t}\left(\left\{X_0^{\mathrm{tg}}(n)\right\} - \left\{X_0^{\mathrm{tg}}(n-1)\right\}\right) - \left\{\dot{X}_0^{\mathrm{tg}}(n-1)\right\} \tag{8.23}$$

By separating the first term of Equation 8.22 and then combining the separated equation and Equation 8.23, interaction forces can be formulated as follows:

$$\begin{aligned}&\Delta t\left[\dot{\chi}_{00}^{\mathrm{g}}(0)\right]\{R_0(n)\} + \Delta t\sum_{m=1}^{nl}\left[\dot{\chi}_{00}^{\mathrm{g}}(m)\right]\{R_0(n-m)\}\\ &\quad = \frac{2}{\Delta t}\left(\left\{X_0^{\mathrm{tg}}(n)\right\} - \left\{X_0^{\mathrm{tg}}(n-1)\right\}\right) - \left\{\dot{X}_0^{\mathrm{tg}}(n-1)\right\}\end{aligned}$$

which results

$$\begin{aligned}\{R_0(n)\} = \frac{2}{\Delta t^2}\left[\dot{\chi}_{00}^{\mathrm{g}}(0)\right]^{-1}\left\{X_0^{\mathrm{tg}}(n)\right\} - \frac{2}{\Delta t^2}\left[\dot{\chi}_{00}^{\mathrm{g}}(0)\right]^{-1}\Bigg[\left\{X_0^{\mathrm{tg}}(n-1)\right\}\\ + \frac{\Delta t}{2}\left(\left\{\dot{X}_0^{\mathrm{tg}}(n-1)\right\} + \Delta t\sum_{m=1}^{nl}\left[\dot{\chi}_{00}^{\mathrm{g}}(m)\right]\{R_0(n-m)\}\right)\Bigg]\end{aligned} \tag{8.24}$$

Grouping terms in Equation 8.24, the compact form of interaction force expression can be written as

$$\{R_0(n)\} = \left[\tilde{K}_{00}\right]\left\{X_0^{\mathrm{tg}}(n)\right\} - \left\{\tilde{R}_0(n-1)\right\} \tag{8.25}$$

with

$$\left[\tilde{K}_{00}\right] = \frac{2}{\Delta t^2}\left[\dot{\chi}_{00}^{\mathrm{g}}(0)\right]^{-1} \tag{8.26}$$

$$\begin{aligned}\left\{\tilde{R}_0(n-1)\right\} = \left[\tilde{K}_{00}\right]\Bigg[\left\{X_0^{\mathrm{tg}}(n-1)\right\} + \frac{\Delta t}{2}\Bigg(\left\{\dot{X}_0^{\mathrm{tg}}(n-1)\right\}\\ + \Delta t\sum_{m=1}^{nl}\left[\dot{\chi}_{00}^{\mathrm{g}}(m)\right]\{R_0(n-m)\}\Bigg)\Bigg]\end{aligned} \tag{8.27}$$

where the time-independent matrix $[\tilde{K}_{00}]$ of dimension 2 by 2 is a pseudostatic stiffness matrix of ground system. Vector $\{\tilde{R}_0\}$ of dimension 2 by 1 is a dynamic-equivalent-force vector making up for the ground system's dynamic effect. This vector depends only on the events before nth time-instant.

8.2 State Equation of SSI—Model and Solution Technique

8.2.1 Formulation of State Equation of SSI-Model

Substituting interaction force vector (Equation 8.25) in the multiple-story equation of motion (Equation 8.3) results in

$$\begin{bmatrix} [M_{SS}] & [M_{S0}] \\ [M_{0S}] & [M_{00}] \end{bmatrix} \begin{Bmatrix} \{\ddot{X}_S^{tg}(n)\} \\ \{\ddot{X}_S^{tg}(n)\} \end{Bmatrix} + \begin{bmatrix} [C_{SS}] & [C_{S0}] \\ [C_{0S}] & [C_{00}] \end{bmatrix} \begin{Bmatrix} \{\dot{X}_S^{tg}(n)\} \\ \{\dot{X}_0^{tg}(n)\} \end{Bmatrix}$$
$$+ \begin{bmatrix} [K_{SS}] & [K_{S0}] \\ [K_{0S}] & [K_{00}] + \left[\tilde{K}_{00}\right] \end{bmatrix} \begin{Bmatrix} \{X_S^{tg}(n)\} \\ \{X_0^{tg}(n)\} \end{Bmatrix}$$
$$= \begin{Bmatrix} \{\delta_S\} \\ \{\delta_0\} \end{Bmatrix} \ddot{x}_0^g(n) + \begin{bmatrix} [\gamma_S] \\ [\gamma_0] \end{bmatrix} \left\{\vec{U}(n)\right\} + \begin{Bmatrix} \{0\} \\ \left\{\tilde{R}_0(n-1)\right\} \end{Bmatrix} \tag{8.28}$$

Taking $\left[\tilde{K}_{00}\right]$ in the total system's stiffness matrix could be physically interpreted as attaching a set of fictious springs, having coefficients of $\tilde{K}_{xx}$, $\tilde{K}_{x\theta}$, $\tilde{K}_{\theta x}$, and $\tilde{K}_{\theta\theta}$ $\left(\text{elements of } \left[\tilde{K}_{00}\right]\right)$, to a structure system's rigid foundation as shown in Figure 8.6. Meanwhile the total system is subjected to the equivalent forces of amplitude $-m_i\ddot{x}_0^g$ at the centroid of each mass i, where $i = 0, 1, \ldots, \text{NO}$, and is subjected to an equivalent moment of amplitude $\sum_{i=0}^{\text{NO}} h_{ai} m_i \ddot{x}_0^g$ around point 0 (contribution of $\{\delta_S\}\ddot{x}_0^g$ and $\{\delta_0\}\ddot{x}_0^g$). Furthermore, at point 0, dynamic-equivalent force $\tilde{R}_x$ and moment $\tilde{R}_\theta$ $\left(\left\{\tilde{R}_0\right\} = \begin{bmatrix} \tilde{R}_x & \tilde{R}_\theta \end{bmatrix}^T\right)$ are added to compensate for the ground system's dynamic effect.

Rearranging Equation 8.28, acceleration vector can be expressed as

$$\begin{Bmatrix} \{\ddot{X}_S^{tg}(n)\} \\ \{\ddot{X}_0^{tg}(n)\} \end{Bmatrix} = -\begin{bmatrix} [M_{SS}] & [M_{S0}] \\ [M_{0S}] & [M_{00}] \end{bmatrix}^{-1} \begin{bmatrix} [C_{SS}] & [C_{S0}] \\ [C_{0S}] & [C_{00}] \end{bmatrix} \begin{Bmatrix} \{\dot{X}_S^{tg}(n)\} \\ \{\dot{X}_0^{tg}(n)\} \end{Bmatrix}$$
$$- \begin{bmatrix} [M_{SS}] & [M_{S0}] \\ [M_{0S}] & [M_{00}] \end{bmatrix}^{-1} \begin{bmatrix} [K_{SS}] & [K_{S0}] \\ [K_{0S}] & [K_{00}] + \left[\tilde{K}_{00}\right] \end{bmatrix} \begin{Bmatrix} \{X_S^{tg}(n)\} \\ \{X_0^{tg}(n)\} \end{Bmatrix}$$
$$+ \begin{bmatrix} [M_{SS}] & [M_{S0}] \\ [M_{0S}] & [M_{00}] \end{bmatrix}^{-1} \begin{Bmatrix} \{\delta_S\} \\ \{\delta_0\} \end{Bmatrix} \ddot{x}_0^g(n) + \begin{bmatrix} [M_{SS}] & [M_{S0}] \\ [M_{0S}] & [M_{00}] \end{bmatrix}^{-1} \begin{bmatrix} [\gamma_S] \\ [\gamma_0] \end{bmatrix} \left\{\vec{U}(n)\right\}$$
$$+ \begin{bmatrix} [M_{SS}] & [M_{S0}] \\ [M_{0S}] & [M_{00}] \end{bmatrix}^{-1} \begin{Bmatrix} \{0\} \\ \left\{\tilde{R}_0\,(n-1)\right\} \end{Bmatrix} \tag{8.29}$$

State vector of dimension 2(NO + 2) by 1 is introduced as

$$\left\{Z^{\mathrm{tg}}(n)\right\} = \left\{\begin{array}{c} \left\{X_{\mathrm{S}}^{\mathrm{tg}}(n)\right\} \\ \left\{X_{0}^{\mathrm{tg}}(n)\right\} \\ \left\{\dot{X}_{\mathrm{S}}^{\mathrm{tg}}(n)\right\} \\ \left\{\dot{X}_{0}^{\mathrm{tg}}(n)\right\} \end{array}\right\} \tag{8.30a}$$

and noting that

$$\left\{\begin{array}{c} \left\{\dot{X}_{\mathrm{S}}^{\mathrm{tg}}(n)\right\} \\ \left\{\dot{X}_{0}^{\mathrm{tg}}(n)\right\} \end{array}\right\} = [I] \left\{\begin{array}{c} \left\{\dot{X}_{\mathrm{S}}^{\mathrm{tg}}(n)\right\} \\ \left\{\dot{X}_{0}^{\mathrm{tg}}(n)\right\} \end{array}\right\} \tag{8.30b}$$

Combining Equations 8.29 and 8.30, state equation of the SSI model can be expressed as

$$\left\{\dot{Z}^{\mathrm{tg}}(n)\right\} = [A]\left\{Z^{\mathrm{tg}}(n)\right\} + [B]\left\{\vec{U}(n)\right\} + \{C\}\,\ddot{x}_{0}^{\mathrm{g}}(n) + \left\{\check{R}_{0}(n-1)\right\} \tag{8.31}$$

with

$$[A] = \begin{bmatrix} [0] & (I) \\ -[A_{\mathrm{K}}] & -[A_{\mathrm{C}}] \end{bmatrix} \tag{8.32}$$

$$[A_{\mathrm{K}}] = \begin{bmatrix} [M_{\mathrm{SS}}] & [M_{\mathrm{S0}}] \\ [M_{0\mathrm{S}}] & [M_{00}] \end{bmatrix}^{-1} \begin{bmatrix} [K_{\mathrm{SS}}] & [K_{\mathrm{S0}}] \\ [K_{0\mathrm{S}}] & [K_{00}] + \left[\tilde{K}_{00}\right] \end{bmatrix} \tag{8.33}$$

$$[A_{\mathrm{C}}] = \begin{bmatrix} [M_{\mathrm{SS}}] & [M_{\mathrm{S0}}] \\ [M_{0\mathrm{S}}] & [M_{00}] \end{bmatrix}^{-1} \begin{bmatrix} [C_{\mathrm{SS}}] & [C_{\mathrm{S0}}] \\ [C_{0\mathrm{S}}] & [C_{00}] \end{bmatrix} \tag{8.34}$$

$$[B] = \begin{bmatrix} [0] \\ \begin{bmatrix} [M_{\mathrm{SS}}] & [M_{\mathrm{S0}}] \\ [M_{0\mathrm{S}}] & [M_{00}] \end{bmatrix}^{-1} \begin{bmatrix} [\gamma_{\mathrm{S}}] \\ [\gamma_{0}] \end{bmatrix} \end{bmatrix} \tag{8.35}$$

$$\{C\} = \left\{\begin{array}{c} \{0\} \\ \begin{bmatrix} [M_{\mathrm{SS}}] & [M_{\mathrm{S0}}] \\ [M_{0\mathrm{S}}] & [M_{00}] \end{bmatrix}^{-1} \left\{\begin{array}{c} \{\delta_{\mathrm{S}}\} \\ \{\delta_{0}\} \end{array}\right\} \end{array}\right\} \tag{8.36}$$

$$\left\{\check{R}_{0}(n-1)\right\} = \left\{\begin{array}{c} \{0\} \\ \begin{bmatrix} [M_{\mathrm{SS}}] & [M_{\mathrm{S0}}] \\ [M_{0\mathrm{S}}] & [M_{00}] \end{bmatrix}^{-1} \left\{\begin{array}{c} \{0\} \\ \left\{\tilde{R}_{0}(n-1)\right\} \end{array}\right\} \end{array}\right\} \tag{8.37}$$

where the characteristic matrix $[A]$ of dimension $2(\mathrm{NO}+2)$ by $2(\mathrm{NO}+2)$ is a time-independent matrix as are matrix $[B]$ of dimension $2(\mathrm{NO}+2)$ by NCR and vector $\{C\}$ of dimension $2(\mathrm{NO}+2)$ by 1. Acceleration vector $\{\breve{R}_0\}$ of dimension $2(\mathrm{NO}+2)$ by 1 is associated with dynamic–equivalent forces, depending only on the outcomes before nth time instant.

8.2.2 Solution Technique

As discussed in Chapter 4, for a closed-loop control, control forces and structural responses are related to an optimal control law as

$$\left\{\vec{U}(n)\right\} = \left[G^{\mathrm{SSI}}\right]\left\{Z^{\mathrm{tg}}(n)\right\} \tag{8.38}$$

where $\left[G^{\mathrm{SSI}}\right]$ of dimension NCR by $2(\mathrm{NO}+2)$ is time-independent feedback gain matrices. Therefore, the state equation of Equation 8.31 can be written in a similar form as

$$\left\{\dot{Z}^{\mathrm{tg}}(n)\right\} = [D]\left\{Z^{\mathrm{tg}}(n)\right\} + \{E(n)\} \tag{8.39}$$

with

$$[D] = [A] + [B]\left[G^{\mathrm{SSI}}\right] \tag{8.40}$$

$$\{E(n)\} = \{C\}\,\ddot{x}_0^{\mathrm{g}}(n) + \{\breve{R}_0(n-1)\} \tag{8.41}$$

where $[D]$ of dimension $2(\mathrm{NO}+2)$ by $2(\mathrm{NO}+2)$ is time-independent plant matrix; $\{E\}$ of dimension $2(\mathrm{NO}+2)$ by 1 is external disturbance vector. In the system without control, term associated with gain matrix in Equation 8.40 is omitted. For simplicity, let Equation 8.39 be written as

$$\left\{\dot{Z}(n)\right\} = [D]\,\{Z(n)\} + \{E(n)\} \tag{8.42}$$

The natural frequencies and corresponding damping ratios evaluated from the plant matrix $[D]$ that yields $\mathrm{NO}+2$ *complex conjugate pairs* of *eigenvalues* $\mu_i \pm \iota\nu_i$ and their corresponding *eigenvectors* $\{a_i\} \pm \iota\{b_i\}$, where $\iota = \sqrt{-1}$; μ_i, ν_i are real scalars; $\{a_i\}$, $\{b_i\}$ are real vectors of dimension $2(\mathrm{NO}+2)$ by 1; and $i = 1, 2, \ldots, 2(\mathrm{NO}+2)$.

Transformation matrix $[T]$ is needed to transform the state equation into canonical form. $[T]$ is a real matrix of dimension $2(\mathrm{NO}+2)$ by $2(\mathrm{NO}+2)$, considering of real parts $\{a_i\}$ and imaginary parts $\{b_i\}$ of the plant matrix's eigenvectors, and can be expressed as

$$[T] = [\{a_1\}\{b_1\}\ldots\{a_i\}\{b_i\}\ldots\{a_{\mathrm{NO}+2}\}\{b_{\mathrm{NO}+2}\}] \tag{8.43}$$

Transformation matrix $[T]$ and plant matrix $[D]$ are related to matrix$[\Lambda]$, consisting of real parts μ_i and imaginary parts ν_i of the plant matrix's eigenvalues, as

$$[T]^{-1}[D][T] = [\Lambda] \tag{8.44}$$

where $[\Lambda]$ of dimension $2(\mathrm{NO}+2)$ by $2(\mathrm{NO}+2)$ is a real matrix of the following form:

$$[\Lambda] = \begin{bmatrix} [\Lambda_1] & \dots & [0] & \dots & [0] \\ \vdots & \ddots & \dots & \dots & \dots \\ [0] & \vdots & [\Lambda_i] & \dots & [0] \\ \vdots & \vdots & \vdots & \ddots & \dots \\ [0] & \vdots & [0] & \vdots & [\Lambda_{\mathrm{NO}+2}] \end{bmatrix} \tag{8.45}$$

$$[\Lambda_i] = \begin{bmatrix} \mu_i & \nu_i \\ -\nu_i & \mu_i \end{bmatrix} \tag{8.46}$$

Let solution of the state equation of Equation 8.42 be expressed as

$$\{Z(n)\} = [T]\{\Phi(n)\} \tag{8.47}$$

Using Equations 8.44 and 8.47, the state Equation 8.42 is transformed into

$$\left\{\dot{\Phi}(n)\right\} = [\Lambda]\{\Phi(n)\} + \{\Gamma(n)\} \tag{8.48}$$

with

$$\{\Gamma(n)\} = [T]^{-1}\{E(n)\} \tag{8.49}$$

where $\{\Phi\}$ and $\{\Gamma\}$ are vectors of dimension $2(\mathrm{NO}+2)$ by 1. A dot over a symbol denotes the derivative in relation to time.

Since at time equals zero ($n = 0$), total dynamic system is at rest, initial conditions can be formulated as

$$\{Z(0)\} = \{0\} \Rightarrow \{\Phi(0)\} = \{0\} \tag{8.50}$$

in which $\ddot{x}_0^{\mathrm{g}}(0) = 0, \{R_0(0)\} = \{0\}$. Thus

$$\{\Gamma(0)\} = \{0\} \tag{8.51}$$

Equation 8.48, the canonical form of state Equation 8.42, is a first-order differential equation whose time-continuous form can be expressed as

$$\left\{\dot{\Phi}(t)\right\} - [\Lambda]\{\Phi(t)\} = \{\Gamma(t)\} \tag{8.52}$$

where the solution of differential equation of Equation 8.52 becomes

$$\{\Phi(t)\} = [\exp([\Lambda]t)]\{\Phi(0)\} + [\exp([\Lambda]t)]\int_0^t [\exp(-[\Lambda]\tau)]\{\Gamma(\tau)\}\,\mathrm{d}\tau$$
$$= [\exp([\Lambda]t)]\{\Phi(0)\} + \int_0^t [\exp([\Lambda](t-\tau))]\{\Gamma(\tau)\}\mathrm{d}\tau \quad (8.53)$$

As derived in Equation 4.58 $[\exp([0])]$ is equal to an identity matrix $[I]$ and

$$[\exp([\Lambda]t)] = \begin{bmatrix} [\exp([\Lambda_1]t)] & \cdots & [0] & \cdots & [0] \\ \vdots & \ddots & \cdots & \cdots & \cdots \\ [0] & \vdots & [\exp([\Lambda_i]t)] & \cdots & [0] \\ \vdots & \vdots & \vdots & \ddots & \cdots \\ [0] & \vdots & [0] & \vdots & [\exp([\Lambda_{NO+2}]t)] \end{bmatrix} \quad (8.54)$$

with

$$[\exp([\Lambda_i]t)] = \exp(\mu_i t)\begin{bmatrix} \cos(\nu_i t) & \sin(\nu_i t) \\ -\sin(\nu_i t) & \cos(\nu_i t) \end{bmatrix} \quad (8.55)$$

Applying the initial conditions in Equations 8.50 and 8.51 and utilizing *trapezoidal rule* with time increment Δt, the solution of Equation 8.53 at nth time-instant can be written as (see derivation in Equations 4.38a through 4.38c)

$$\{\Phi(n\Delta t)\} = [\exp([\Lambda]n\Delta t)]\{\Phi(0)\} + \frac{\Delta t}{2}[\exp([\Lambda]n\Delta t)]\{\Gamma(0)\}$$
$$+ \Delta t\sum_{m=1}^{n-1}[\exp([\Lambda](n-m)\Delta t)]\{\Gamma(m\Delta t)\} + \frac{\Delta t}{2}\{\Gamma(n\Delta t)\}$$
$$= \Delta t\sum_{m=1}^{n-1}[\exp([\Lambda](n-m)\Delta t)]\{\Gamma(m\Delta t)\} + \frac{\Delta t}{2}\{\Gamma(n\Delta t)\} \quad (8.56)$$

In compact form, the solution of Equation 8.56 can be derived as

$$\{\Phi(n)\} = \{\Pi(n-1)\} + \frac{\Delta t}{2}\{\Gamma(n)\} \quad (8.57)$$

with

$$\{\Pi\,(n-1)\} = \Delta t \sum_{m=1}^{n-1} [\exp(\,[\Lambda]\;\;(n-m)\,\Delta t)]\,\{\Gamma\,(m)\} \tag{8.58}$$

where vector $\{\Pi\,(n-1)\}$ can be written in a recursive form as

$$\{\Pi\,(n-1)\} = [\exp([\Lambda]\,\Delta t)]\;[\,\{\Pi\,(n-2)\} + \Delta t\,\{\Gamma\,(n-1)\}] \tag{8.59}$$

By using Equations 8.57 and 8.58, the state vector at nth time-instant of Equation 8.42 can be determined in a discrete real-time fashion.

8.3 Generalized Optimal Active Control Algorithm for the SSI System

Generalized optimal active control (GOAC) algorithm was introduced in Chapter 4 (see Section 4.3.2). Since this chapter is for SSI system with various notations different from previous presentations, essential equations for the algorithm are thus systematically and briefly derived herein for clarity purposes.

8.3.1 System Model

The time-continuous version of state equation expressed in Equation 8.31 for SSI model can be written as

$$\left\{\dot{Z}^{\mathrm{tg}}\,(t)\right\} = [A]\left\{Z^{\mathrm{tg}}\,(t)\right\} + [B]\left\{\vec{U}\,(t)\right\} + \{E(t)\} \tag{8.60}$$

with

$$\{E(t)\} = \{C\}\,\ddot{x}_0^{\mathrm{g}}\,(t) + \left\{\check{R}_0\,(t-\Delta t)\right\} \tag{8.61}$$

where $\{E\}$ of dimension $2(\mathrm{NO}+2)$ by 1 is external disturbance vector. The other notations are defined in Equations 8.31 through 8.37. Let the notation of tg be omitted in Equation 8.60, which is simplified as

$$\left\{\dot{Z}(t)\right\} = [A]\,\{Z\,(t)\} + [B]\left\{\vec{U}(t)\right\} + \{E(t)\} \tag{8.62}$$

8.3.2 Generalized Performance Index

To obtain an optimal solution for state vector $\{Z(t)\}$ and control force vector $\{\vec{U}(t)\}$ in Equation 8.62, a *performance index* or an objective functional needs to be defined and minimized. An integral *quadratic performance index* J, which may

describe a system's energy during a given time duration, can be expressed as

$$J\left(\{Z(t)\},\left\{\vec{U}(t)\right\}\right) = \frac{1}{2}\int_{t_0}^{t_f}\left(\{Z(t)\}^{\mathrm{T}}[Q]\{Z(t)\} + \left\{\vec{U}(t)\right\}^{\mathrm{T}}[R]\left\{\vec{U}(t)\right\}\right)\mathrm{d}t \tag{8.63}$$

where the state-weighting matrix $[Q]$ of dimension $2(\mathrm{NO}+2)$ by $2(\mathrm{NO}+2)$ is a positive semidefinite. The control-weighting matrix $[R]$ of dimension NCR by NCR is a positive definite. These conditions are imposed to guarantee a nonzero positive value for the integrand. Then the performance index's function of time t increases in the interval $[t_0, t_f]$. t_0 and t_f are an initial and a final time instant, respectively.

By splitting up the time duration $[t_0, t_f]$ into NT intervals, the performance index in Equation 8.63 can be written as

$$J\left(\{Z(t)\},\left\{\vec{U}(t)\right\}\right) = \sum_{n=1}^{\mathrm{NT}} J_n\left(\{Z(t)\},\left\{\vec{U}(t)\right\}\right) \tag{8.64}$$

with

$$J_n\left(\{Z(t)\},\left\{\vec{U}(t)\right\}\right) = \frac{1}{2}\int_{t_{n-1}}^{t_n}\left(\{Z(t)\}^{\mathrm{T}}[Q]\{Z(t)\} + \left\{\vec{U}(t)\right\}^{\mathrm{T}}[R]\left\{\vec{U}(t)\right\}\right)\mathrm{d}t \tag{8.65}$$

For each time interval n, the amplitude of state variables $z_i(t)$ for $i = 1, 2, \ldots, 2(\mathrm{NO}+2)$ and control forces $\vec{u}_i(t)$ at time t_{n-1}, are specified from the previous time interval; those at time t_n are not. This leads to the problem of minimizing a variable-end-point functional for which the unknown amplitude of state vector $\{Z(t)\}$ at time t_n should also be minimized. Therefore, the function of this state vector needs to be included in the expression of performance index. A new objective functional or *generalized performance index*, at time interval $[t_{n-1}, t_n]$ can be defined as

$$J_n\left(\{Z(t_n)\},\{Z(t)\},\left\{\vec{U}(t)\right\}\right) = g\left(\{Z(t_n)\}\right) + \int_{t_{n-1}}^{t_n} f\left(t,\{Z(t)\},\left\{\vec{U}(t)\right\}\right)\mathrm{d}t \tag{8.66}$$

with

$$g(\{Z(t_n)\}) = \frac{1}{2}\{Z(t_n)\}^{\mathrm{T}}[S]\{Z(t)\} \tag{8.67}$$

$$f\left(t, \{Z(t)\}, \left\{\vec{U}(t)\right\}\right) = \frac{1}{2}\left(\{Z(t)\}^{\mathrm{T}}[Q]\{Z(t)\} + \left\{\vec{U}(t)\right\}^{\mathrm{T}}[R]\left\{\vec{U}(t_n)\right\}\right) \tag{8.68}$$

To ensure the positive value for Equation 8.67, the weighting matrix [S] of dimension $2(\mathrm{NO}+2)$ by $2(\mathrm{NO}+2)$ is a positive semidefinite.

8.3.3 Feedback Gain Matrix and Active Control Force

8.3.3.1 Transversality condition

To minimize the generalized performance index J_n in Equation 8.66 with a free end point condition and consequently the performance index J in Equation 8.64, not only *Euler's equation* but also *transversality condition* must be satisfied. Assume that the boundary condition at endpoints is given by

$$\left\{\Theta_g\left(t_{n-1}, \{Z(t_{n-1})\}, t_n\right)\right\} = \left\{\begin{array}{c} t_{n-1} - t_0 - (n-1)\,\Delta t \\ \{Z(t_{n-1})\} - \{Z_{n-1}\} \\ t_n - t_0 - n\Delta t \end{array}\right\} = \{0\} \tag{8.69}$$

where $\left\{\Theta_{\mathrm{g}}\right\}$ is a $\{2(\mathrm{NO}+2)+2\} \times 1$ vector. Δt is a time increment that equals $(t_{\mathrm{f}} - t_0)/\mathrm{NT}$. t_0, t_{f}, and NT are initial time instant, final time instant, and a number of divided time intervals, respectively. Vector $\{Z_{n-1}\}$ of dimension $2(\mathrm{NO}+2)$ by 1 comprises the amplitude of $\{Z(t)\}$ at time t_{n-1}.

State equation of Equation 8.62 can serve as a constraint of the quadratic energy Equation 8.68 and can be rewritten into a vector $\{\Xi_{\mathrm{f}}\}$ of dimension $2(\mathrm{NO}+2)\times 1$ as

$$\begin{aligned}&\left\{\Xi_{\mathrm{f}}\left(\left\{\dot{Z}(t)\right\}, \{Z(t)\}, \left\{\vec{U}(t)\right\}\right)\right\} \\ &\quad = \left\{\dot{Z}(t)\right\} - [A]\{Z(t)\} - [B]\left\{\vec{U}(t)\right\} - \{E(t)\} = \{0\}\end{aligned} \tag{8.70}$$

By introducing multiplier vectors $\left\{\lambda_{\mathrm{g}}\right\}$ of dimension $2(\mathrm{NO}+2)+2$ by 1 and $\{\lambda_{\mathrm{f}}\}$ of dimension $2(\mathrm{NO}+2)$ by 1, and combining vector $\left\{\Theta_{\mathrm{g}}\right\}$ in Equation 8.69 and vector $\{\Xi_{\mathrm{f}}\}$ in Equation 8.70 with the former, the augmented function and functional of the generalized performance index in Equation 8.66 becomes

$$\begin{aligned}J_n &= G\left(t_{n-1}, \{Z(t_{n-1})\}, \{Z(t_n)\}, t_n\right) \\ &\quad + \int_{t_{n-1}}^{t_n} F\left(t, \left\{\dot{Z}(t)\right\}, \{Z(t)\}, \left\{\vec{U}(t)\right\}\right) \mathrm{d}t\end{aligned} \tag{8.71}$$

with

$$G = \frac{1}{2}\{Z(t_n)\}^{\mathrm{T}}[S]\{Z(t_n)\} + \left\{\lambda_{\mathrm{g}}\right\}^{\mathrm{T}}\begin{Bmatrix} t_{n-1} - t_0 - (n-1)\,\Delta t \\ \{Z(t_{n-1})\} - \{Z_{n-1}\} \\ t_n - t_0 - n\Delta t \end{Bmatrix} \tag{8.72}$$

$$F = \frac{1}{2}\left(\{Z(t)\}^{\mathrm{T}}[Q]\{Z(t)\} + \left\{\vec{U}(t)\right\}^{\mathrm{T}}[R]\left\{\vec{U}(t)\right\}\right) + \left\{\lambda_{\mathrm{f}}(t)^{\mathrm{T}}\right\}\left(\left\{\dot{Z}(t)\right\} - [A]\{Z(t)\} - [B]\left\{\vec{U}(t)\right\} - \{E(t)\}\right) \tag{8.73}$$

Applying the fundamental necessary condition (variable of $J_n = 0$) to Equation 8.71 with unknown end points leads to the transversality condition as

$$\mathrm{d}G + \left[\left(F - \left\{F_{,\{\dot{Z}(t)\}}\right\}^{\mathrm{T}}\left\{\dot{Z}(t)\right\}\right)\mathrm{d}t\right]_{t_{n-1}}^{t_n} + \left[\left\{F_{,\{\dot{Z}(t)\}}\right\}^{\mathrm{T}}\{\mathrm{d}\{Z(t)\}\}\right]_{t_{n-1}}^{t_n} = 0 \tag{8.74}$$

where the letter d represents differential of function or variable following it. A comma denotes a partial derivative with respect to the subscript following it. Since t_{n-1}, $\{Z(t_{n-1})\}$, and t_n are known and fixed, their differentials $\mathrm{d}t_{n-1}$, $\mathrm{d}\{Z(t_{n-1})\}$, and $\mathrm{d}t_n$ equal zero. Therefore, the transversality condition in Equation 8.74 can be reduced as

$$\left\{\left\{G_{,\{Z(t_n)\}}\right\} + \left\{F_{,\{\dot{Z}(t)\}}\right\}_{t_n}\right\}^{\mathrm{T}}\{\mathrm{d}\{Z(t_n)\}\} = 0 \tag{8.75}$$

Substituting Equations 8.72 and 8.73 in Equation 8.75 and knowing that $\{\mathrm{d}\{Z(t_n)\}\} \neq \{0\}$, leads to

$$[S]\{Z(t_n)\} + \{\lambda_{\mathrm{f}}(t_n)\} = \{0\} \tag{8.76}$$

8.3.3.2 Euler's equation

This equation is a necessary condition for an extremum in a fixed-endpoint problem. Since the solution of a variable-end-problem is a subset of the extremals of various fixed-endpoint problems, the former also requires the *Euler equation* as a necessary condition. By applying the fundamental necessary condition (variation of functional = 0) to the second term of Equation 8.71 with fixed endpoints, the Euler equation can be expressed as

$$\left\{F_{,\{Z(t)\}}\right\} - \left\{\frac{\mathrm{d}}{\mathrm{d}t}\left\{F_{,\{\dot{Z}(t)\}}\right\}\right\} = \{0\} \tag{8.77a}$$

$$\left\{F_{,\left\{\vec{U}(t)\right\}}\right\} - \left\{\frac{\mathrm{d}}{\mathrm{d}t}\left\{F_{,\left\{\dot{\vec{U}}(t)\right\}}\right\}\right\} = \{0\} \tag{8.77b}$$

Equation 8.77a is satisfied in the process of deriving the *transversality condition*. By substituting Equation 8.73 in Equation 8.77b, the latter can be formulated as

$$[R]\left\{\vec{U}\{t\}\right\} - [B]^{\mathrm{T}}\{\lambda_{\mathrm{f}}\{t\}\} = \{0\} \tag{8.78}$$

8.3.3.3 Control force and gain matrix

In a closed-loop control algorithm, a relation between force vector $\left\{\vec{U}(t)\right\}$ and state vector $\{Z(t)\}$ can be given by

$$\left\{\vec{U}(t)\right\} = [G]\{Z(t)\} \tag{8.79}$$

where $[G]$ of dimension NCR by 2(NO + 2) is an *optimal control law*, known as a *feedback gain* matrix. This matrix is a result of an attempt to minimize the generalized performance index that can be done by satisfying the Euler equations and the transversality condition earlier described.

At each end point n ($t = t_n$) for $n = 1, 2, \ldots, NT$, the Euler Equation 8.78 can be written as

$$\left\{\vec{U}(t_n)\right\} = [R]^{-1}[B]^{\mathrm{T}}\{\lambda_{\mathrm{f}}(t_n)\} \tag{8.80}$$

Substituting transversality condition from Equation 8.76 in Equation 8.80 leads to

$$\left\{\vec{U}(t_n)\right\} = -[R]^{-1}[B]^{\mathrm{T}}[S]\{Z(t_n)\} \tag{8.81}$$

By comparing Equations 8.81 to 8.79, the feedback gain matrix at each end point n can be expressed as

$$[G(t_n)] = -[R]^{-1}[B]^{\mathrm{T}}[S] \tag{8.82}$$

Gain matrix $[G(t_n)]$ is constant and neither a function of time t nor time increment Δt. Therefore, it is valid at every end point n. Note Equation 8.82 is similarly expressed shown in Equation 4.169 for fixed-base structures. Apparently, the individual matrices must include SSI effects. In order to signify SSI, Equation 8.82 is rewritten as

$$\left[G^{\mathrm{SSI}}\right] = -[R]^{-1}[B]^{\mathrm{T}}[S] \tag{8.83}$$

8.3.4 Weighting Matrix Configuration

As discussed in Chapter 4, state-weighting matrices $[Q]$ and $[S]$ are arbitrary positive semidefinite. Control-weighting matrix $[R]$ is an arbitrary positive definite. From a practical point of view, the integral performance index may be treated as

system energy during a given time duration [5,6]. For the case of SSI, the performance index is also chosen to provide an approximate measure of strain, kinetic, and potential energies of the total dynamic system. However, the dimensions of $[Q]$ and $[R]$ are $2(\mathrm{NO}+2)$ by $2(\mathrm{NO}+2)$ and NCR by NCR, respectively as

$$[Q] = \begin{bmatrix} [K_{\mathrm{SS}}] & [K_{\mathrm{S0}}] & [0] & [0] \\ [K_{\mathrm{S0}}]^{\mathrm{T}} & \left[\check{K}_{00}\right] & [0] & [0] \\ [0] & [0] & [M_{\mathrm{SS}}] & [0] \\ [0] & [0] & [0] & [M_{00}] \end{bmatrix} \tag{8.84}$$

and

$$[R] = \begin{bmatrix} [\gamma_{\mathrm{S}}] \\ [\gamma_0] \end{bmatrix}^{\mathrm{T}} \begin{bmatrix} [K_{\mathrm{SS}}] & [K_{\mathrm{S0}}] \\ [K_{\mathrm{S0}}]^{\mathrm{T}} & \left[\check{K}_{00}\right] \end{bmatrix}^{-1} \begin{bmatrix} [\gamma_{\mathrm{S}}] \\ [\gamma_0] \end{bmatrix} \tag{8.85}$$

with

$$\left[\check{K}_{00}\right] = \begin{bmatrix} k_1 + \tilde{K}_{xx} & -h_{\mathrm{a1}}k_1 + \tilde{K}_{x\theta} \\ -h_{\mathrm{a1}}k_1 + \tilde{K}_{\theta x} & h_{\mathrm{a1}}^2 k_1 + \tilde{K}_{\theta\theta} \end{bmatrix}^{-1} \tag{8.85a}$$

where $[K_{\mathrm{SS}}], [K_{\mathrm{S0}}], [M_{\mathrm{SS}}], [M_{00}], [\gamma_{\mathrm{S}}]$, and $[\gamma_0]$ are given in Equations 8.7, 8.8, 8.4, 8.6, 8.17, and 8.18, respectively. A weighting matrix $[S]$ of dimension $2(\mathrm{NO}+2)$ by $2(\mathrm{NO}+2)$ is selected as an arbitrary row matrix as

$$[S] = \begin{bmatrix} [0] & [0] \\ [S_{\mathrm{D}}] & [S_{\mathrm{V}}] \end{bmatrix} \tag{8.86}$$

where elements on the Rth row of submatrices $[S_{\mathrm{D}}]$ and $[S_{\mathrm{V}}]$ of dimension $(\mathrm{NO}+2)$ by $(\mathrm{NO}+2)$ equal the arbitrary constants s_{D} and s_{V}, respectively, which satisfy a positive semidefinite assumption. For each controller, R equals $N - \mathrm{ONC} + 1$, where ONC is one of the controller's node numbers that does not allow any two consecutive rows of the matrix to be filled. To assure a positive semidefinite condition of matrix $[S]$, alternately, a symmetrical matrix can be chosen as

$$[S] = \gamma_{\mathrm{D}} \begin{bmatrix} \Omega_{\mathrm{V}}^{-1}\left[\check{K}\right] & \left[\check{K}\right] \\ \left[\check{K}\right] & \Omega_{\mathrm{V}}\left[\check{K}\right] \end{bmatrix} \tag{8.87}$$

with

$$\left[\check{K}\right] = \begin{bmatrix} [K_{\mathrm{SS}}] & [K_{\mathrm{S0}}] \\ [K_{\mathrm{S0}}]^{\mathrm{T}} & \left[\check{K}_{00}\right] \end{bmatrix} \tag{8.88}$$

where γ_D and Ω_V are a stiffness scaling factor and a damping scaling factor, respectively. The influence of S_D, S_V, and γ_D, Ω_V on the total system can be studied by substituting the gain matrix equation of Equation 8.83 in the plant matrix of Equation 8.40 as

$$[D] = [A] - \frac{1}{R}\{B\}\{B\}^T[S] \tag{8.89}$$

For simplicity, let us use fixed-base single-story shear building shown in Figure 8.4 for demonstration for which

$$[A] = [M_{SS}]^{-1}[K_{SS}] = \begin{bmatrix} 0 & 1 \\ -(k_1/m_1) & -(c_1/m_1) \end{bmatrix} \tag{8.90}$$

$$[B] = [M_{SS}]^{-1}\{\gamma_S\} = \begin{Bmatrix} 0 \\ -(1/m_1) \end{Bmatrix} \tag{8.91}$$

$$R = \{\gamma_S\}^T[K_{SS}]^{-1}\{\gamma_S\} = \frac{1}{k_1} \tag{8.92}$$

Inserting the row matrix $[S]$ of Equation 8.86 into Equation 8.89 leads to

$$[D] = \begin{bmatrix} 0 & 1 \\ -(k_1/m_1)(1 + S_D/m_1) & -(c_1/m_1)(1 + S_V k_1/c_1 m_1) \end{bmatrix} \tag{8.93}$$

Similarly, inserting the symmetric weighting matrix of $[S]$ in Equation 8.87 into Equation 8.89 we have

$$[D] = \begin{bmatrix} 0 & 1 \\ -(k_1/m_1)(1 + \gamma_D k_1/m_1) & -(c_1/m_1)(1 + \Omega_V \gamma_D k_1^2/c_1 m_1) \end{bmatrix} \tag{8.94}$$

By comparing the characteristic matrix $[A]$ of the structure system in Equation 8.90 to the plant matrices $[D]$ of the structure system with control (Equations 8.93 and 8.94), the constants s_D, γ_D, and s_V, γ_V increase the stiffness and damping coefficient of the new system, respectively. As the stiffness and damping coefficients correspond to displacement and velocity vectors, s_D, γ_D and s_V, γ_V can also be described as displacement control and velocity control factors, respectively. The complex conjugate pairs of eigenvalues of the plant matrices in Equations 8.93 and 8.94 can be expressed as $\alpha \pm \iota\Omega$, where

$$\alpha = -\frac{c_1(1 + s_V k_1/c_1 m_1)}{2m_1} \quad \text{for Equation 8.93} \tag{8.95}$$

$$\alpha = -\frac{c_1(1 + \Omega_V \gamma_D k_1^2/c_1 m_1)}{2m_1} \quad \text{for Equation 8.94} \tag{8.96}$$

and

$$\Omega = \sqrt{\frac{k_1\left(1+s_{\mathrm{D}}/m_1\right)}{m_1} - \left(\frac{c_1\left(1+s_{\mathrm{V}}k_1/c_1m_1\right)}{2m_1}\right)^2} \quad \text{for Equation 8.93} \tag{8.97}$$

$$\Omega = \sqrt{\frac{k_1\left(1+\gamma_{\mathrm{D}}k_1/m_1\right)}{m_1} - \left(\frac{c_1\left(1+\Omega_{\mathrm{V}}\gamma_{\mathrm{D}}k_1^2/c_1m_1\right)}{2m_1}\right)^2} \quad \text{for Equation 8.94} \tag{8.98}$$

For a *subcritical damping* system, an imaginary part of the root, Ω, can be interpreted as a damped free vibration frequency ω and $-\alpha/\Omega$ as a damping ratio. In order to maintain the system in the subcritical range (Ω is a real number $\neq 0$), $s_{D,}s_{\mathrm{V}}$ or γ_D, Ω_{V} must be selected according to the following inequality condition:

$$s_{\mathrm{V}} < \frac{2m_1}{k_1}\sqrt{m_1k_1\left(1+\frac{s_{\mathrm{D}}}{m_1}\right)} - c_1 \tag{8.99}$$

$$\Omega_{\mathrm{V}} < \frac{2m_1}{\gamma_{\mathrm{D}}k_1^2}\sqrt{m_1k_1\left(1+\frac{\gamma_{\mathrm{D}}k_1}{m_1}\right)} - \frac{c_1}{\gamma_{\mathrm{D}}k_1} \tag{8.100}$$

8.4 Soil Properties and Wave Equations

8.4.1 Dynamic-Equilibrium Equation

The fundamental equations of elastodynamics relevant to the formulations of soil system are crucial and are summarized in this section [1,11]. The infinitesimal cube, shown in Figure 8.7 is assumed to be an isotropic homogeneous elastic medium with hysteretic damping. For harmonic excitation with frequency ω, the dynamic-equilibrium equations without body forces can be expressed as

$$\sigma_{x,x}(x,y,z) + \tau_{xy,y}(x,y,z) + \tau_{xz,z}(x,y,z) = -\rho\omega^2 u(x,y,z) \tag{8.101}$$

$$\tau_{yx,x}(x,y,z) + \sigma_{y,y}(x,y,z) + \tau_{yz,z}(x,y,z) = -\rho\omega^2 v(x,y,z) \tag{8.102}$$

$$\tau_{zx,x}(x,y,z) + \tau_{zy,y}(x,y,z) + \sigma_{z,z}(x,y,z) = -\rho\omega^2 w(x,y,z) \tag{8.103}$$

Normal stress and shear stress amplitudes are denoted as σ and τ, respectively. The first subscript denotes the direction of the stress component. The second one denotes the direction of the infinitesimal area's normal on which the stress component acts. A comma denotes a partial derivative with respect to the subscript following it. The letter ρ represents the mass density. Displacements u, v, and w are in x-, y-, and z-direction, respectively. All amplitudes are a function of x, y,

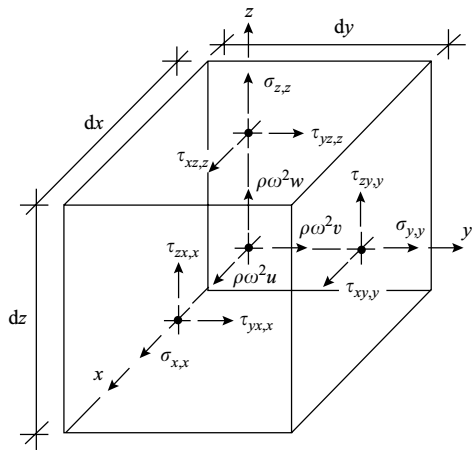

FIGURE 8.7 Infinitesimal cubes in harmonic motion.

and z. Hook's law, the constitutive equation, is specified as

$$\varepsilon_x = \frac{1}{E}(\sigma_x - \upsilon\sigma_y - \upsilon\sigma_z) \tag{8.104}$$

$$\varepsilon_y = \frac{1}{E}(-\upsilon\sigma_x + \sigma_y - \upsilon\sigma_z) \tag{8.105}$$

$$\varepsilon_z = \frac{1}{E}(-\upsilon\sigma_x - \upsilon\sigma_y + \sigma_z) \tag{8.106}$$

$$\gamma_{xy} = \gamma_{yx} = \frac{\tau_{xy}}{\wp} = \frac{\tau_{yx}}{\wp} \tag{8.107}$$

$$\gamma_{xz} = \gamma_{zx} = \frac{\tau_{xz}}{\wp} = \frac{\tau_{zx}}{\wp} \tag{8.108}$$

$$\gamma_{yz} = \gamma_{zy} = \frac{\tau_{yz}}{\wp} = \frac{\tau_{zy}}{\wp} \tag{8.109}$$

where the normal strain and shear strain amplitudes are denoted by ε and γ, respectively. Shear modulus $\wp$ can be expressed as a function of Young's modulus of elasticity E and Poisson's ratio υ as

$$\wp = \frac{E}{2\,(1+\upsilon)} \tag{8.110}$$

Stress amplitudes in Equations 8.104 through 8.109 can be written in terms of strain amplitudes as

$$\sigma_x = (2\wp + \lambda)\varepsilon_x + \lambda(\varepsilon_y + \varepsilon_z) \tag{8.111}$$

$$\sigma_y = (2\wp + \lambda)\varepsilon_y + \lambda(\varepsilon_x + \varepsilon_z) \tag{8.112}$$

$$\sigma_z = (2\wp + \lambda)\varepsilon_z + \lambda(\varepsilon_x + \varepsilon_y) \tag{8.113}$$

$$\tau_{xy} = \tau_{yx} = \wp\gamma_{xy} = \wp\gamma_{yx} \tag{8.114}$$

$$\tau_{xz} = \tau_{zx} = \wp\gamma_{xz} = \wp\gamma_{zx} \tag{8.115}$$

$$\tau_{yz} = \tau_{zy} = \wp\gamma_{yz} = \wp\gamma_{zy} \tag{8.116}$$

where the Lame constant λ is expressed as

$$\lambda = \frac{\upsilon E}{(1+\upsilon)(1-2\upsilon)} \tag{8.117}$$

Strain–displacement equations are formulated as

$$\varepsilon_x = u_{,x}\,(x,y,z) \tag{8.118}$$

$$\varepsilon_y = v_{,y}\,(x,y,z) \tag{8.119}$$

$$\varepsilon_z = w_{,z}\,(x,y,z) \tag{8.120}$$

$$\gamma_{xy} = \gamma_{yx} = u_{,y}\,(x,y,z) + v_{,x}\,(x,y,z) \tag{8.121}$$

$$\gamma_{xz} = \gamma_{zx} = u_{,z}\,(x,y,z) + w_{,x}\,(x,y,z) \tag{8.122}$$

$$\gamma_{yz} = \gamma_{zy} = v_{,z}\,(x,y,z) + w_{,y}\,(x,y,z) \tag{8.123}$$

Substituting the stress–strain relationship in Equations 8.111 through 8.116 and the strain–displacement relationship in Equations 8.118 through 8.123 into the equilibrium equations 8.101 through 8.103 leads to

$$(2\wp + \lambda)\,u_{,xx} + \lambda\left(v_{,yx} + w_{,zx}\right) + \wp\left(u_{,yy} + v_{,xy} + u_{,zz} + w_{,xz}\right) = -\rho\omega^2 u \tag{8.124}$$

$$(2\wp + \lambda)\,v_{,yy} + \lambda\left(u_{,xy} + w_{,zy}\right) + \wp\left(v_{,xx} + u_{,yx} + v_{,zz} + w_{,yz}\right) = -\rho\omega^2 v \tag{8.125}$$

$$(2\wp + \lambda)\,w_{,zz} + \lambda\left(u_{,xz} + v_{,yz}\right) + \wp\left(w_{,xx} + u_{,zx} + w_{,yy} + v_{,zy}\right) = -\rho\omega^2 w \tag{8.126}$$

In order to uncouple the displacements in Equations 8.124, 8.125, and 8.126 and to identify the different types of waves the volumetric strain with amplitude e and the rotational-strain vector $\{\Omega\}$ with amplitudes Ω_x, Ω_y, and Ω_z, are introduced as

$$e\,(x,y,z) = u_{,x} + v_{,y} + w_{,z} \tag{8.127}$$

$$\{\Omega\,(x,y,z)\} = \begin{Bmatrix} \Omega_x \\ \Omega_y \\ \Omega_z \end{Bmatrix} = \frac{1}{2}\begin{Bmatrix} w_{,y} - v_{,z} \\ u_{,z} - w_{,x} \\ v_{,x} - u_{,y} \end{Bmatrix} \tag{8.128}$$

Note that

$$\Omega_{x,x} + \Omega_{y,y} + \Omega_{z,z} = \frac{\left(w_{,yx} - v_{,zx} + u_{,zy} - w_{,xy} + v_{,xz} - u_{,yz}\right)}{2} = 0 \quad (8.129)$$

By using Equations 8.127 through 8.129 dynamic-equilibrium formulation of Equations 8.124 through 8.126 can be written as

$$(2\wp + \lambda)\, e_{,x} + 2\wp \left(\Omega_{y,z} - \Omega_{z,y}\right) = -\rho\omega^2 u \quad (8.130)$$

$$(2\wp + \lambda)\, e_{,y} + 2\wp \left(\Omega_{z,x} - \Omega_{x,z}\right) = -\rho\omega^2 v \quad (8.131)$$

$$(2\wp + \lambda)\, e_{,z} + 2\wp \left(\Omega_{x,y} - \Omega_{y,x}\right) = -\rho\omega^2 w \quad (8.132)$$

The material damping occurring in a soil system involves frictional loss of energy or linear hysteretic damping. The effect of material damping, which may differ for various types of waves, is assumed to be the same. This frequency-independent property can be incorporated by replacing the elastic material constants with the corresponding complex ones. Complex shear modulus $\wp^*$ and Lame constant λ^* can be expressed as

$$\wp^* = (1 + 2\iota\zeta)\,\wp \quad \text{and} \quad \lambda^* = (1 + 2\iota\zeta)\,\lambda \quad (8.133)$$

where symbols ζ and ι represent the ratio of linear hysteretic damping and $\sqrt{-1}$, respectively. Replacing the elastic material constants in Equations 8.130 through 8.132 with the complex ones leads to

$$\left(2\wp^* + \lambda^*\right) e_{,x} + 2\wp^* \left(\Omega_{y,z} - \Omega_{z,y}\right) = -\rho\omega^2 u \quad (8.134)$$

$$\left(2\wp^* + \lambda^*\right) e_{,y} + 2\wp^* \left(\Omega_{z,x} - \Omega_{x,z}\right) = -\rho\omega^2 v \quad (8.135)$$

$$\left(2\wp^* + \lambda^*\right) e_{,z} + 2\wp^* \left(\Omega_{x,y} - \Omega_{y,x}\right) = -\rho\omega^2 w \quad (8.136)$$

Eliminating rotational strains Ω_x, Ω_y, and Ω_z by differentiating Equations 8.134 through 8.136 with respect to x, y, and z, respectively, and then adding these three relationship lead to

$$\left(2\wp^* + \lambda^*\right)\left(e_{,xx} + e_{,yy} + e_{,zz}\right) = -\rho\omega^2 e$$

$$e_{,xx} + e_{,yy} + e_{,zz} = -\frac{\omega^2}{C_P^2} e \quad (8.137)$$

where the dilatational wave velocity is specified as

$$C_P = \sqrt{\frac{(2\wp^* + \lambda^*)}{\rho}} \quad (8.138)$$

Use the following procedures to eliminate volumetric strain e by differentiating Equation 8.135 with respect to y, subtracting these two expressions, and noting that the derivative of Equation 8.129 with respect to x also vanishes. The final result is

$$\wp^* \left(\Omega_{x,xx} + \Omega_{x,yy} + \Omega_{x,zz}\right) = -\rho\omega^2 \Omega_x$$

$$\Omega_{x,xx} + \Omega_{x,yy} + \Omega_{x,zz} = -\frac{\omega^2}{C_S^2}\Omega_x \tag{8.139}$$

The detailed derivation of Equation 8.139 is as follows:

$$\left(2\wp^* + \lambda^*\right) e_{,yz} + 2\wp^* \left(\Omega_{z,xz} - \Omega_{x,zz}\right) = -\rho\omega^2 v_{,z} \tag{8.139a}$$

$$\left(2\wp^* + \lambda^*\right) e_{,zy} + 2\wp^* \left(\Omega_{x,yy} - \Omega_{y,xy}\right) = -\rho\omega^2 w_{,y} \tag{8.139b}$$

Subtracting the above equations yields

$$\left(2\wp^* + \lambda^*\right)\left(e_{,zy} - e_{,yz}\right) + 2\wp^* \left(\Omega_{x,yy} - \Omega_{y,xy} - \Omega_{z,xz} + \Omega_{x,zz}\right) = -\rho\omega^2 \left(w_{,y} - v_{,z}\right) \tag{8.139c}$$

Since

$$\Omega_x = \frac{\left(w_{,y} - v_{,z}\right)}{2}; \quad \Omega_{x,x} + \Omega_{y,y} + \Omega_{z,z} = 0 \tag{8.139d}$$

we have

$$2\wp^* \left(\Omega_{x,xx} + \Omega_{y,yy} + \Omega_{z,zx}\right) + 2\wp^* \left(\Omega_{x,yy} - \Omega_{y,xy} - \Omega_{z,xz} + \Omega_{x,zz}\right) = -2\rho\omega^2 \Omega_x \tag{8.139e}$$

In Equation 8.139, the shear wave velocity is defined as

$$C_S = \sqrt{\frac{\wp*}{\rho}} \tag{8.140}$$

Analogously, two other expressions can result as

$$\Omega_{y,xx} + \Omega_{y,yy} + \Omega_{y,zz} = -\frac{\omega^2}{C_S^2}\Omega_y \tag{8.141}$$

$$\Omega_{z,xx} + \Omega_{z,yy} + \Omega_{z,zz} = -\frac{\omega^2}{C_S^2}\Omega_z \tag{8.142}$$

Putting Equations 8.139, 8.141, and 8.142 together becomes

$$\{\Omega\}_{,xx} + \{\Omega\}_{,yy} + \{\Omega\}_{,zz} = -\frac{\omega^2}{C_S^2}\{\Omega\} \tag{8.143}$$

Therefore, for harmonic excitation, the equations of motion are specified in Equations 8.137 and 8.143 with the unknown amplitudes of the volumetric strain e and the rotational-strain vector $\{\Omega\}$, respectively. These wave equations are linear partial differential equations of second order.

8.4.2 Earthquake Propagation Waves

Earthquake propagation waves consist of primary wave and secondary wave so-called P- and S-waves, respectively. The equations associated with these two waves are derived in the following sections.

8.4.2.1 Primary-wave equation

The displacement associated with body waves owing to earthquakes are sketched in Figure 8.8a,b; and the primary wave is shown in Figure 8.8c. As the *P-wave* (*primary wave* or dilatational wave) travels, it alternately compresses and dilates the medium. The *volumetric strain e* defined in Equation 8.127 can be used to describe this behavior. To find the unknown amplitude of the volumetric strain for Equation 8.137, the following trial function is assumed:

$$e(x,y,z) = \frac{\iota\omega}{C_p} A_p \exp\left[-\frac{\iota\omega}{C_p}(l_x x + l_y y + l_z z)\right] \tag{8.144}$$

The trial function in Equation 8.144 satisfies the wave equation of Equation 8.137 only if $l_x^2 + l_y^2 + l_z^2 = 1$. These three scalars l_x, l_y, and l_z may be considered as the direction cosines of the wave propagation's direction. $l_x^2 + l_y^2 + l_z^2 = 1$ can be proved as follows: to prove the trial function let us substitute the function and its derivative into Equation 8.137 as

$$e_{,xx} = \frac{\iota\omega^3 l_x^2}{C_p^3} A_p \exp\left[\frac{\iota\omega}{C_p}(-l_x x - l_y y - l_z z)\right]$$

$$e_{,yy} = \frac{\iota\omega^3 l_y^2}{C_p^3} A_p \exp\left[\frac{\iota\omega}{C_p}(-l_x x - l_y y - l_z z)\right]$$

$$e_{,zz} = \frac{\iota\omega^3 l_z^2}{C_p^3} A_p \exp\left[\frac{\iota\omega}{C_p}(-l_x x - l_y y - l_z z)\right]$$

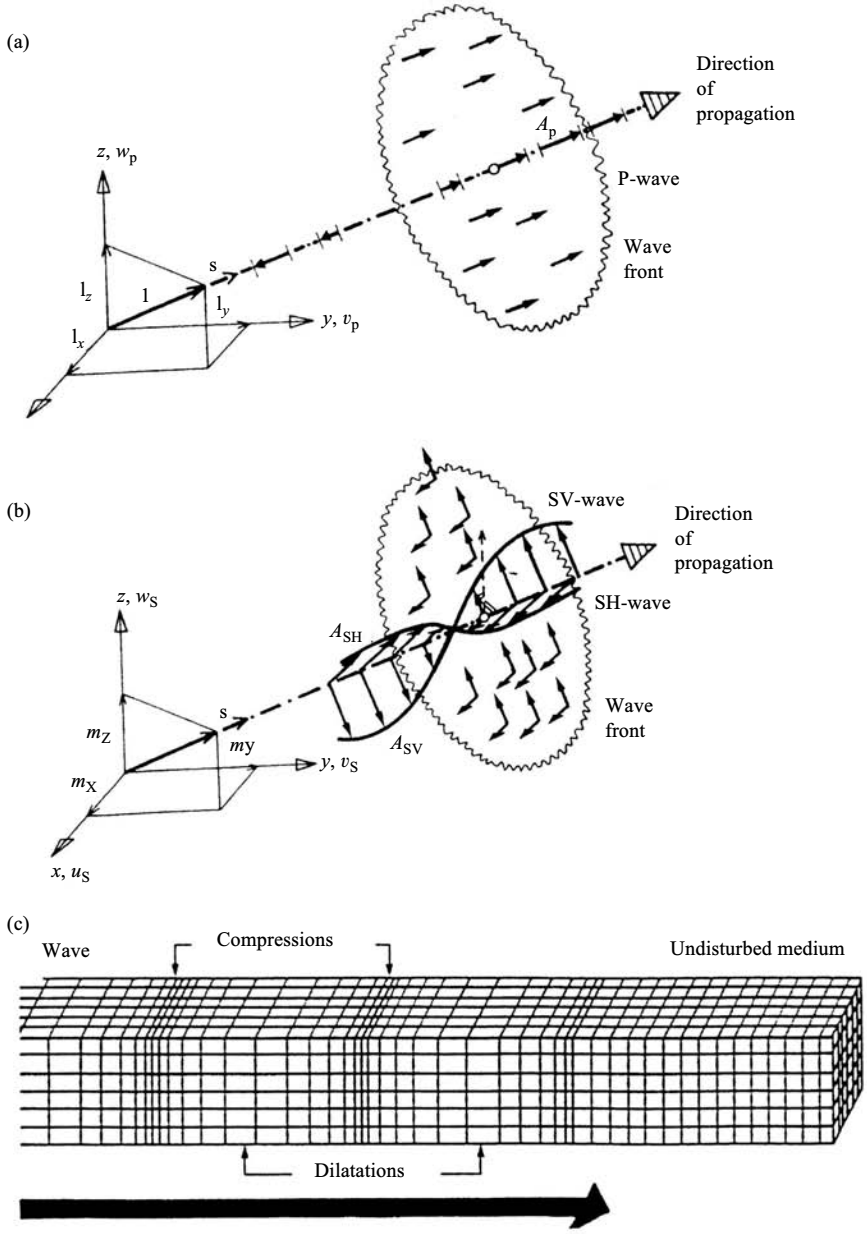

FIGURE 8.8 Displacement associated with body waves: (a) P-wave, (b) S-wave, and (c) cross section of incident P-wave.

Then substituting the above and Equation 8.144 into Equation 8.137 yields

$$\frac{\iota\omega^3}{C_\mathrm{p}^3}(l_x^2+l_y^2+l_z^2)A_\mathrm{p}\exp\left[\frac{\iota\omega}{C_\mathrm{p}}(-l_x x-l_y y-l_z z)\right] = \frac{-\omega^2}{C_\mathrm{p}^2}\left[\frac{-\iota\omega}{C_\mathrm{p}}A_\mathrm{p}\exp\left(\frac{\iota\omega}{C_\mathrm{p}}\left[-l_x x-l_y y-l_z z\right]\right)\right]$$

The proof is thus obtained as

$$\frac{\iota\omega^3}{C_\mathrm{p}^3}A_\mathrm{p}\exp\left[\frac{\iota\omega}{C_\mathrm{p}}(-l_x x-l_y y-l_z z)\right] \equiv \frac{\iota\omega^3}{C_\mathrm{p}^3}A_\mathrm{p}\exp\left[\frac{\iota\omega}{C_\mathrm{p}}(-l_x x-l_y y-l_z z)\right]$$

Substituting Equation 8.144 into Equation 8.127 and using $l_x^2+l_y^2+l_z^2=1$ yield

$$e=u_{,x}+v_{,y}+w_{,z}=-\frac{\iota\omega}{C_\mathrm{p}}(l_x^2+l_y^2+l_z^2)A_\mathrm{p}\exp\left[-\frac{\iota\omega}{C_\mathrm{p}}(l_x x+l_y y+l_z z)\right]$$

Collecting the terms corresponding to $u_{,x}$, $v_{,y}$, and $w_{,z}$, respectively yields

$$u_{,x}=-\frac{\iota\omega}{C_\mathrm{p}}l_x^2A_\mathrm{p}\exp\left[-\frac{\iota\omega}{C_\mathrm{p}}(l_x x+l_y y+l_z z)\right]$$
$$v_{,y}=-\frac{\iota\omega}{C_\mathrm{p}}l_y^2A_\mathrm{p}\exp\left[-\frac{\iota\omega}{C_\mathrm{p}}(l_x x+l_y y+l_z z)\right]$$
$$w_{,z}=-\frac{\iota\omega}{C_\mathrm{p}}l_z^2A_\mathrm{p}\exp\left[-\frac{\iota\omega}{C_\mathrm{p}}(l_x x+l_y y+l_z z)\right]$$

Integrating the above equations leads to the following displacements u_P, v_P, and w_P corresponding to x-, y-, and z-direction (see Figure 8.9), respectively.

$$u_\mathrm{P}=l_x A_\mathrm{p}\exp\left[-\frac{\iota\omega}{C_\mathrm{p}}(l_x x+l_y y+l_z z)\right] \tag{8.145}$$

$$v_\mathrm{P}=l_y A_\mathrm{p}\exp\left[-\frac{\iota\omega}{C_\mathrm{p}}(l_x x+l_y y+l_z z)\right] \tag{8.146}$$

$$w_\mathrm{P}=l_z A_\mathrm{p}\exp\left[-\frac{\iota\omega}{C_\mathrm{p}}(l_x x+l_y y+l_z z)\right] \tag{8.147}$$

At $x=y=z=0$, the amplitude of P-wave equal to A_P is defined an initial condition. Therefore, in x-, y-, and z-direction, amplitudes of the wave at the same location are equal to $l_x A_\mathrm{P}$, $l_y A_\mathrm{P}$, and $l_z A_\mathrm{P}$, respectively. By enforcing these

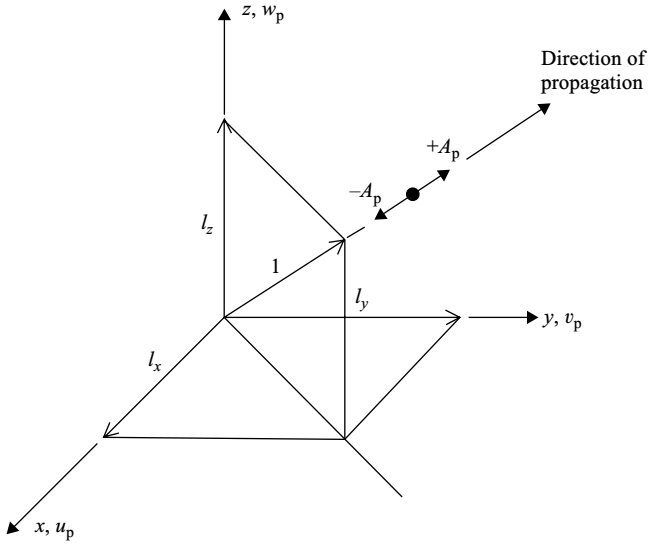

FIGURE 8.9 Displacement associated with incident P-wave.

conditions, the integration constants in Equations 8.145 through 8.147 are equal to zero. Subscript P indicates that the corresponding displacements are associated with P-wave. Equations 8.145 through 8.147 also show that the P-wave amplitude is constant over a plane perpendicular to the direction of propagation. The velocity of propagation C_P is constant and depends on material properties only.

8.4.2.2 Secondary-wave equation

As the S-wave (secondary wave or distortional wave) propagates, it shears the medium sideways at right angles to the direction of propagation (see Figure 8.10). The rotational strain vector $\{\Omega\}$ defined in Equation 8.128 can be used to interpret this behavior. To find the unknown amplitudes of the rotational-strain vector for Equation 8.143, the trial vector is assumed as

$$\{\Omega\,(x,y,z)\} = -\frac{\iota\omega}{2C_S}\{C\}\exp\left[-\frac{\iota\omega}{C_S}\left(m_x x + m_y y + m_z z\right)\right] \tag{8.148}$$

The trial vector in Equation 8.148 satisfies equilibrium Equation 8.143, only if $m_x^2 + m_y^2 + m_z^2 = 1$ and $m_x C_x + m_y C_y + m_z C_z = 0$ where C_x, C_y, and C_z are components of vector $\{C\}$. Direction cosines m_x, m_y, and m_z in the former specify the direction of propagation. The proof of the trial function can be similarly done for Equation 8.144. First, differentiate trial function $\{\Omega\}$ with respect to x, y, z twice which and Equation 8.148 are then substituted into Equation 8.143. After

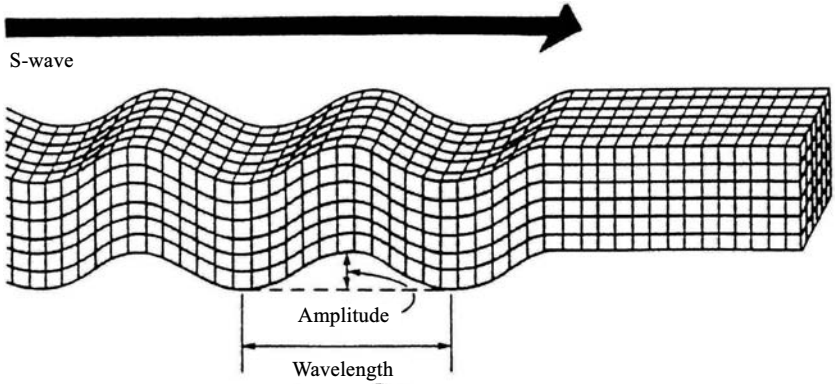

FIGURE 8.10 Cross section of incident S-wave.

substitution, the first row of the matrix may be written as

$$\frac{\iota\omega^3}{C_S^3}(m_x^2+m_y^2+m_z^2)C_x \exp\left[\frac{\iota\omega}{C_S}(-m_x x - m_y y - m_z z)\right]$$
$$= \frac{-\omega^2}{C_S^2}\left[\frac{-\iota\omega}{2C_S}C_x \exp\left(\frac{\iota\omega}{C_S}\left[-m_x x - m_y y - m_z z\right]\right)\right]$$

that yields the following proof:

$$\frac{\iota\omega^3}{C_S^3}C_x \exp\left[\frac{\iota\omega}{C_S}(-m_x x - m_y y - m_z z)\right] \equiv \frac{\iota\omega^3}{C_S^3}C_x \exp\left[\frac{\iota\omega}{C_S}(-m_x x - m_y y - m_z z)\right]$$

The above proof is identical for second and third row.

Since the scalar product in the latter vanishes, vector {C} and thus {Ω} are perpendicular to the direction of propagation. Applying $m_x^2 + m_y^2 + m_z^2 = 1$, $m_x C_x + m_y C_y + m_z C_z = 0$ and Equation 8.128 to the trial vector (Equation 8.148), each row of the trail vector is expanded and separated into groups corresponding to $u_{,y}$, $u_{,z}$, $v_{,x}$, $v_{,z}$, and $w_{,x}$, $w_{,y}$. Then, integrating each group and setting its integration constant to zero result in displacements u_S, v_S, and w_S corresponding to x-, y-, and z- direction, respectively, as

$$u_S = \left(m_z C_y - m_y C_z\right)\exp\left[-\frac{\iota\omega}{C_S}\left(m_x x + m_y y + m_z z\right)\right] \tag{8.149}$$

$$v_S = \left(m_x C_z - m_z C_x\right)\exp\left[-\frac{\iota\omega}{C_S}\left(m_x x + m_y y + m_z z\right)\right] \tag{8.150}$$

$$w_S = \left(m_y C_x - m_x C_y\right)\exp\left[-\frac{\iota\omega}{C_S}\left(m_x x + m_y y + m_z z\right)\right] \tag{8.151}$$

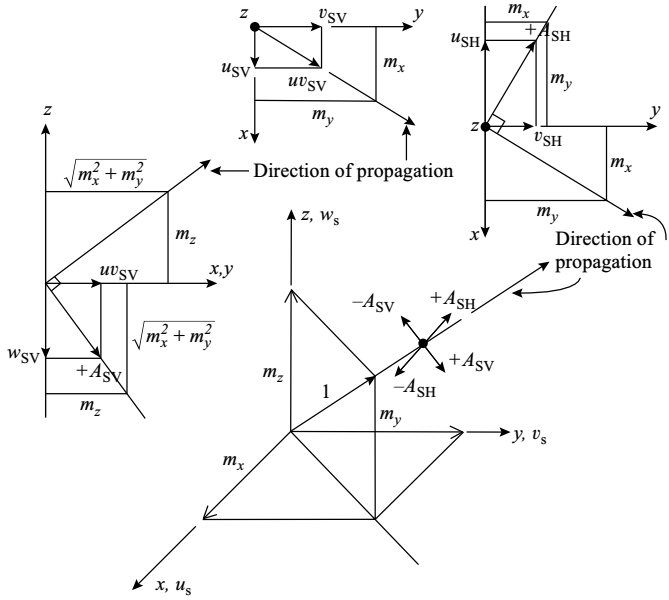

FIGURE 8.11 Displacement associated with incident S-wave.

Subscript S indicates that the corresponding displacements are associated with S-wave. Equations 8.149 through 8.151 show that the displacement amplitudes are proportional to the components of the vector product of {C} and the direction of propagation. It follows that the particle motion of S-wave lies in the plane perpendicular to the direction of propagation and is constant over this plane. The material dependent velocity of propagation C_s is constant.

Since the original equation of Equation 8.139 is based on the rotational strain, the displacements in Equations 8.149 through 8.151 represent the S-wave. The displacement vector can be further decomposed by using geometric consideration in Figure 8.11, into a horizontal component with amplitude A_{SH}, lying in the plane parallel to x–y plane, and into a component with amplitude A_{SV}, lying in the plane, which contains the vertical z-axis and direction of propagation as follows:

$$A_{SH} = \frac{C_z}{\sqrt{m_x^2 + m_y^2}} \tag{8.152}$$

$$A_{SV} = \frac{m_x C_y - m_y C_x}{\sqrt{m_x^2 + m_y^2}} \tag{8.153}$$

where A_{SH} and A_{SV} are the amplitudes of SH- and SV-wave at the point at $x = y = z = 0$, respectively. The displacements (see Figure 8.11) can be reformulated

in terms of these amplitudes as

$$u_S = u_{SH} + u_{SV} = \frac{-m_y A_{SH} + m_x m_z A_{SV}}{\sqrt{m_x^2 + m_y^2}} \exp\left[-\frac{\iota\omega}{C_S}\left(m_x x + m_y y + m_z z\right)\right] \tag{8.154}$$

$$v_S = v_{SH} + v_{SV} = \frac{m_x A_{SH} + m_y m_z A_{SV}}{\sqrt{m_x^2 + m_y^2}} \exp\left[-\frac{\iota\omega}{C_S}\left(m_x x + m_y y + m_z z\right)\right] \tag{8.155}$$

$$w_S = w_{SV} = -\sqrt{m_x^2 + m_y^2} A_{SV} \exp\left[-\frac{\iota\omega}{C_S}\left(m_x x + m_y y + m_z z\right)\right] \tag{8.156}$$

As described in Equations 8.138 and 8.140, P- and S-wave velocities are equal to $\sqrt{(2\wp^* + \lambda^*)/\rho}$ and $\sqrt{\wp^*/\rho}$, respectively. The always-larger numerator of the former leads to P-wave velocity being faster than S-wave velocity. Therefore, at an observation point on the surface, amplitude of P-wave is first recorded and then that of S-wave as shown in Figure 8.12.

8.4.2.3 In-plane displacement equation for horizontal layer

A. *For incident wave when* $k \neq 0$

The origin of the local coordinate with the z-axis pointing downward is located at the top of the horizontal layer as shown in Figure 8.13. Assuming the directions of propagation of the P- and S-wave lie in the same vertical plane , say the x–z plane, leads to the condition of $l_y = m_y = 0$. Adding the displacement caused by P-wave Equations 8.145 and 8.147 and S-wave in Equations 8.154 and 8.156 with

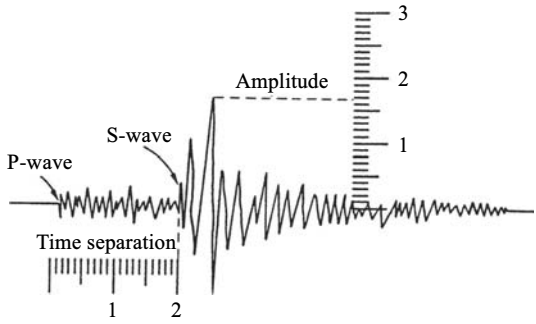

FIGURE 8.12 Typical earthquake record.

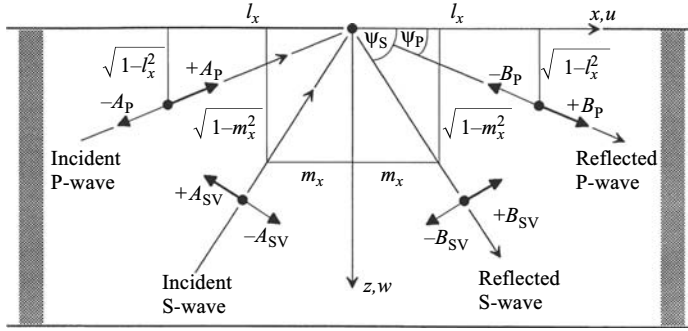

FIGURE 8.13 In-plane displacements for horizontal layer.

the above condition, the total motion in x- and z-direction can be expressed as

$$u(x,z) = l_x A_P \exp\left[-\frac{\iota\omega}{C_P}(l_x x + l_z z)\right] + m_z A_{SV} \exp\left[-\frac{\iota\omega}{C_S}(m_x x + m_z z)\right] \tag{8.157}$$

$$w(x,z) = l_z A_P \exp\left[-\frac{\iota\omega}{C_P}(l_x x + l_z z)\right] - m_x A_{SV} \exp\left[-\frac{\iota\omega}{C_S}(m_x x + m_z z)\right] \tag{8.158}$$

Note that in- plane displacements with amplitudes u and w depend only on the P- and SV-wave. The out-of-plane displacement with amplitude v (perpendicular to x–z plane), caused by the SH-wave, is independent of u, w and not mentioned here. The form of Equations 8.157 and 8.158 compels the boundary conditions at the top and bottom of the layer to vary as $\exp(-\iota\omega\, l_x x/C_p)$ and as $\exp(-\iota\omega\, m_x x/C_s)$. To achieve the same variation with x, the following condition needs to be imposed.

$$\frac{l_x}{C_P} = \frac{m_x}{C_S} \tag{8.159}$$

As a total of four boundary conditions has to be satisfied (displacements with amplitudes u and w at top and bottom of layer), a second P- and SV-wave with the same variation in x is introduced (see Figure 8.13). Since $l_y = 0$, for any value of l_x, l_z can be selected as $\pm\sqrt{1-l_x^2}$. The value of l_x equals $\cos\psi_P$, whereby ψ_P is the angle of incidence of the P-wave measured from x-axis. This interpretation holds only for a real value that is smaller than or equal to 1. Analogously, m_z can be chosen as $\pm\sqrt{1-m_x^2}$ with $m_x = \cos\psi_S$ whereby ψ_S is the angle of incidence of the S-wave measured from x-axis. Substituting l_z and m_z into Equations 8.157

and 8.158 leads to

$$u(x,z) = l_x \left[A_{\mathrm{P}} \exp\left(\iota\omega \frac{\sqrt{1-l_x^2}}{C_{\mathrm{P}}} z \right) + B_{\mathrm{P}} \exp\left(-\iota\omega \frac{\sqrt{1-l_x^2}}{C_{\mathrm{P}}} z \right) \right] \times \exp\left(-\iota\omega \frac{l_x}{C_{\mathrm{P}}} x \right) - \sqrt{1-m_x^2} \tag{8.160}$$

$$w(x,z) = -\sqrt{1-l_x^2} \left[A_{\mathrm{P}} \exp\left(\iota\omega \frac{\sqrt{1-l_x^2}}{C_{\mathrm{P}}} z \right) - B_{\mathrm{P}} \exp\left(-\iota\omega \frac{\sqrt{1-l_x^2}}{C_{\mathrm{P}}} z \right) \right] \times \exp\left(-\iota\omega \frac{l_x}{C_{\mathrm{P}}} x \right) - m_x \left[A_{\mathrm{SV}} \exp\left(\iota\omega \frac{\sqrt{1-m_x^2}}{C_S} z \right) + B_{\mathrm{SV}} \exp\left(-\iota\omega \frac{\sqrt{1-m_x^2}}{C_S} z \right) \right] \exp\left(-\iota\omega \frac{m_x}{C_S} x \right) \tag{8.161}$$

where A_{P}, A_{SV} and B_{P}, B_{SV} are amplitudes of waves traveling in the negative and positive z-direction, respectively (see Figure 8.13). Definitions of A_{P} and A_{SV} here differ from Equations 8.157 and 8.158 where they are defined as the amplitudes of general waves. For convenience, the following notation is introduced:

$$\text{Phase velocity:} \quad C = \frac{C_{\mathrm{P}}}{l_x} = \frac{C_{\mathrm{S}}}{m_x} \tag{8.162}$$

$$\text{Wave number:} \quad k = \frac{\omega}{C} \tag{8.163}$$

$$\text{Scalar } f\text{:} \quad f = \sqrt{\frac{1}{l_x^2} - 1} \tag{8.164}$$

$$\text{Scalar } s\text{:} \quad s = \sqrt{\frac{1}{m_x^2} - 1} \tag{8.165}$$

Using Equations 8.162 through 8.165, the in-plane displacements in Equations 8.160 and 8.161 can be rewritten as

$$u(x,z) = u(k,z) \exp(-\iota k x) \tag{8.166}$$

$$w(x,z) = w(k,z) \exp(-\iota k x) \tag{8.167}$$

with

$$u(k,z) = l_x\left[A_{\mathrm{P}}\exp(\iota kfz) + B_{\mathrm{P}}\exp(-\iota kfz)\right] - m_x s\left[A_{\mathrm{SV}}\exp(\iota ksz) - B_{\mathrm{SV}}\exp(-\iota ksz)\right] \quad (8.168)$$

$$w(k,z) = l_x f\left[A_{\mathrm{P}}\exp(\iota kfz) - B_{\mathrm{P}}\exp(-\iota kfz)\right] - m_x\left[A_{\mathrm{SV}}\exp(\iota ksz) + B_{\mathrm{SV}}\exp(-\iota ksz)\right] \quad (8.169)$$

where $l_x/C_{\mathrm{P}} = m_x/C_{\mathrm{S}}$ needs to be enforced. Displacements $u(k,z)$ and $w(k,z)$ in Equations 8.166 and 8.167 can be interpreted as the amplitudes of waves propagating in the positive x-direction (for a positive wave number k) with phase velocity C.

B. *For incident wave when* $k = 0$

For the *vertically incident wave*, the angle of incident $\psi_{\mathrm{P}} = \psi_{\mathrm{S}} = 90^\circ$ ($l_x = m_x = 0$). Therefore, the phase velocity C equals infinity and $k = 0$. Since $l_x = m_x = 0$, the in-plane displacements in Equations 8.160 and 8.161 can be reformulated as

$$u(x,z)^{k=0} = -A_{\mathrm{SV}}\exp\left(\frac{\iota\omega}{C_{\mathrm{S}}}z\right) + B_{\mathrm{SV}}\exp\left(-\frac{\iota\omega}{C_{\mathrm{S}}}z\right) \quad (8.170)$$

$$w(x,z)^{k=0} = -A_{\mathrm{P}}\exp\left(\frac{\iota\omega}{C_{\mathrm{P}}}z\right) + B_{\mathrm{P}}\exp\left(-\frac{\iota\omega}{C_{\mathrm{P}}}z\right) \quad (8.171)$$

In this special case, it should be noted that the displacements have no variation in x-direction.

8.4.2.4 In-plane displacement equation for half plane

A half plane can be regarded as a horizontal layer with depth approaching infinity. Applying an external load at the free surface of a half plane, only waves travel in the positive z-direction (outgoing waves); the radiation condition states that no energy can propagate from infinity toward the free surface. Therefore, the incoming waves with amplitudes A_{P} and A_{SV} in Equations 8.168 and 8.169 are excluded.

8.5 Stiffness Coefficients of Horizontal Layer and Half Plane

8.5.1 Dynamic-Stiffness Coefficients of Horizontal Layer

8.5.1.1 For incident wave when $k \neq 0$

The soil properties and wave equations are presented in Sections of 8.4.1 and 8.4.2, respectively. Following the relationship between soil properties and wave equations, we can now derive the stiffness coefficient expressed in force–displacement relationship in k-domain for harmonic excitation.

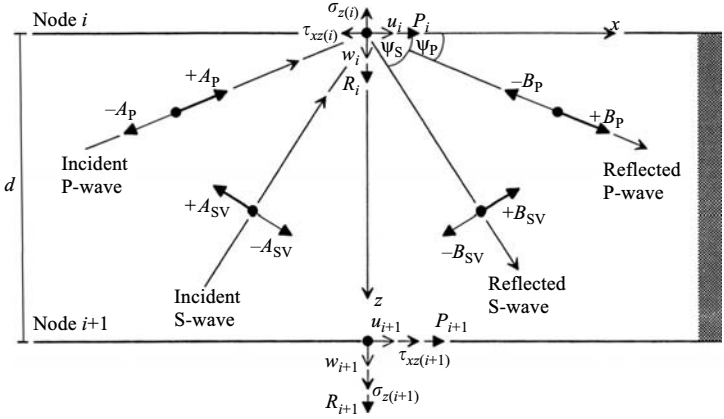

FIGURE 8.14 Displacements, stresses, and external forces on layer i

In Figure 8.14, the horizontal layer i of depth d, extending to infinity in both x-directions, has constant materiel properties. Origin of the local coordinate system with the z-axis pointing downwards is located at the top of the layer. The in-plane displacement equations of layer are given in Equations 8.166 through 8.169. By using the stress–strain relationship (Hook's law) and strain–displacement relationship, normal stress and shear stress amplitudes on the horizontal interface can be obtained as follows:

$$\sigma_z(x,z) = \left[2\wp^* + \lambda^*\right] w_{,z}(x,z) + \lambda^* u_{,x}(x,z) \tag{8.172}$$

$$\tau_{xz}(x,z) = \wp^* \left[u_{,z}(x,z) + w_{,x}(x,z)\right] \tag{8.173}$$

Substituting the displacements in Equations 8.166 through 8.169 into Equations 8.172 and 8.173 and omitting term $\exp(-\imath kx)$, normal stress and shear stress amplitudes in k-domain can be expressed as

$$\begin{aligned}
\sigma_z(k,z) &= \left[2\wp^* + \lambda^*\right] w_{,z}(k,z) - \imath k\lambda^* u(k,z) \\
&= -\imath k\left[2\wp^* + \lambda^*\right]\Big\{l_x f^2 \left[A_{\mathrm{P}} \exp(\imath kfz) + B_{\mathrm{P}} \exp(-\imath kfz)\right] \\
&\quad + m_x s \left[A_{\mathrm{SV}} \exp(\imath ksz) - B_{\mathrm{SV}} \exp(-\imath ksz)\right]\Big\} \\
&\quad - \imath k\lambda^* \{l_x \left[A_{\mathrm{P}} \exp(\imath kfz) + B_{\mathrm{P}} \exp(-\imath kfz)\right] \\
&\quad - m_x s \left[A_{\mathrm{SV}} \exp(\imath ksz) - B_{\mathrm{SV}} \exp(-\imath ksz)\right]\} \\
&= \imath k\wp^* \Big\{l_x \left(1 - s^2\right) \left[A_{\mathrm{P}} \exp(\imath kfz) + B_{\mathrm{P}} \exp(-\imath kfz)\right] \\
&\quad - 2m_x s \left[A_{\mathrm{SV}} \exp(\imath ksz) - B_{\mathrm{SV}} \exp(-\imath ksz)\right]\Big\}
\end{aligned} \tag{8.174}$$

$$\begin{aligned}\tau_{xz}(k,z) &= \wp^*\left[u_{,z}(x,z) - \iota k w\ (k,z)\right] \\ &= \iota k \wp^* \{l_x f\left[A_{\mathrm{P}} \exp(\iota k f z) - B_{\mathrm{P}} \exp(-\iota k f z)\right] \\ &\quad - m_x s^2 \left[A_{\mathrm{SV}} \exp(\iota k s z) + B_{\mathrm{SV}} \exp(-\iota k s z)\right] \\ &\quad + l_x f\left[A_{\mathrm{P}} \exp(\iota k f z) - B_{\mathrm{P}} \exp(-\iota k f z)\right] \\ &\quad + m_x \left[A_{\mathrm{SV}} \exp(\iota k s z) + B_{\mathrm{SV}} \exp(-\iota k s z)\right]\} \\ &= \iota k \wp^* \{2 l_x f\left[A_{\mathrm{P}} \exp(\iota k f z) - B_{\mathrm{P}} \exp(-\iota k f z)\right] \\ &\quad + m_x (1 - s^2)\left[A_{\mathrm{SV}} \exp(\iota k s z) + B_{\mathrm{SV}} \exp(-\iota k s z)\right]\}\end{aligned} \tag{8.175}$$

By using Equations 8.168, 8.169, 8.174, and 8.175, displacements and stresses at the top (node i, $z = 0$) of layer i can be expressed in matrix form in terms of wave amplitude A_{P}, B_{P}, A_{SV}, and B_{SV} as

$$\begin{Bmatrix} u_i(k) \\ w_i(k) \\ \tau_{xz\,(i)}(k) \\ \sigma_{z\,(i)}(k) \end{Bmatrix} = \left[uw\tau\sigma AB_i(k)\right]^{k\neq 0} \begin{Bmatrix} A_{\mathrm{P}} \\ B_{\mathrm{P}} \\ A_{\mathrm{SV}} \\ B_{\mathrm{SV}} \end{Bmatrix} \tag{8.176}$$

with

$$\left[uw\tau\sigma AB_i(k)\right]^{k\neq 0} = \begin{bmatrix} \left[uw\tau\sigma AB_i^{(1,1)}\right] & \left[uw\tau\sigma AB_i^{(1,2)}\right] \\ \left[uw\tau\sigma AB_i^{(2,1)}\right] & \left[uw\tau\sigma AB_i^{(2,2)}\right] \end{bmatrix} \tag{8.177}$$

where

$$\left[uw\tau\sigma AB_i^{(1,1)}\right] = l_x \begin{bmatrix} 1 & 1 \\ -f & f \end{bmatrix} \tag{8.178}$$

$$\left[uw\tau\sigma AB_i^{(1,2)}\right] = m_x \begin{bmatrix} -s & s \\ -1 & -1 \end{bmatrix} \tag{8.179}$$

$$\left[uw\tau\sigma AB_i^{(2,1)}\right] = \iota k l_x \wp^* \begin{bmatrix} 2f & -2f \\ 1 - s^2 & 1 - s^2 \end{bmatrix} \tag{8.180}$$

$$\left[uw\tau\sigma AB_i^{(2,2)}\right] = \iota k m_x \wp^* \begin{bmatrix} 1 - s^2 & 1 - s^2 \\ -2s & 2s \end{bmatrix} \tag{8.181}$$

At the bottom (node $i+1, z=d$) of layer i, displacements and stresses can be expressed in terms of the wave amplitudes A_{P}, B_{P}, A_{SV}, and B_{SV} as

$$\begin{Bmatrix} u_{i+1}(k) \\ w_{i+1}(k) \\ \tau_{xz(i+1)}(k) \\ \sigma_{z(i+1)}(k) \end{Bmatrix} = [uw\tau\sigma AB_{i+1}(k)]^{k\neq 0} \begin{Bmatrix} A_{\mathrm{P}} \\ B_{\mathrm{P}} \\ A_{\mathrm{SV}} \\ B_{\mathrm{SV}} \end{Bmatrix} \tag{8.182}$$

with

$$[uw\tau\sigma AB_{i+1}(k)]^{k\neq 0} = \begin{bmatrix} \left[uw\tau\sigma AB_{i+1}^{(1,1)}\right] & \left[uw\tau\sigma AB_{i+1}^{(1,2)}\right] \\ \left[uw\tau\sigma AB_{i+1}^{(2,1)}\right] & \left[uw\tau\sigma AB_{i+1}^{(2,2)}\right] \end{bmatrix} \tag{8.183}$$

where

$$\left[uw\tau\sigma AB_{i+1}^{(1,1)}\right] = l_x \begin{bmatrix} \exp(\iota kfd) & \exp(-\iota kfd) \\ -f\exp(\iota kfd) & f\exp(-\iota kfd) \end{bmatrix} \tag{8.184}$$

$$\left[uw\tau\sigma AB_{i+1}^{(1,2)}\right] = m_x \begin{bmatrix} -s\exp(\iota ksd) & s\exp(-\iota ksd) \\ -\exp(\iota ksd) & -\exp(-\iota ksd) \end{bmatrix} \tag{8.185}$$

$$\left[uw\tau\sigma AB_{i+1}^{(2,1)}\right] = \iota kl_x\wp^* \begin{bmatrix} 2f\exp(\iota kfd) & -2f\exp(-\iota kfd) \\ \left(1-s^2\right)\exp(\iota kfd) & \left(1-s^2\right)\exp(-\iota kfd) \end{bmatrix} \tag{8.186}$$

$$\left[uw\tau\sigma AB_{i+1}^{(2,2)}\right] = \iota km_x\wp^* \begin{bmatrix} \left(1-s^2\right)\exp(\iota ksd) & \left(1-s^2\right)\exp(-\iota ksd) \\ -2s\exp(\iota ksd) & 2s\exp(-\iota ksd) \end{bmatrix} \tag{8.187}$$

Using Equations 8.176 and 8.182, displacement and stress amplitude at node $i+1$ are expressed as a function of those at node i by the transfer matrix as

$$\begin{Bmatrix} u_{i+1}(k) \\ w_{i+1}(k) \\ \tau_{xz(i+1)}(k) \\ \sigma_{z(i+1)}(k) \end{Bmatrix} = \left[uw\tau\sigma_i^{i+1}(k)\right]^{k\neq 0} \begin{Bmatrix} u_i(k) \\ w_i(k) \\ \tau_{xz(i)}(k) \\ \sigma_{z(i)}(k) \end{Bmatrix} \tag{8.188}$$

with

$$\left[uw\tau\sigma_i^{i+1}(k)\right]^{k\neq 0} = [uw\tau\sigma AB_{i+1}(k)]^{k\neq 0}\left[[uw\tau\sigma AB_i(k)]^{k\neq 0}\right]^{-1} \tag{8.189}$$

When assembling the stiffness matrix, applied loads are defined in the global-coordinate system. The local system used to define the stresses is opposite to it on the negative side of a layer. Therefore, as shown in Figure 8.14, introducing external load amplitudes $P_i = -\tau_{xz(i)}$, $R_i = -\sigma_{z(i)}$, $P_{i+1} = \tau_{xz(i+1)}$, and

$R_{i+1} = \sigma_{z(i+1)}$, into Equation 8.189 and performing a partial inversion leads to the dynamic-stiffness matrix of a horizontal layer as

$$\begin{Bmatrix} P_i(k) \\ R_i(k) \\ P_{i+1}(k) \\ R_{i+1}(k) \end{Bmatrix} = \left[S^{\mathrm{L}}_{\mathrm{P-SV}}(k)\right]_i^{k\neq 0} \begin{Bmatrix} u_i(k) \\ w_i(k) \\ u_{i+1}(k) \\ w_{i+1}(k) \end{Bmatrix} \tag{8.190}$$

with

$$\left[S^{\mathrm{L}}_{\mathrm{P-SV}}(k)\right]_i^{k\neq 0} = Cof \begin{bmatrix} S_{11} & S_{12} & S_{13} & S_{14} \\ S_{21} & S_{22} & S_{23} & S_{24} \\ S_{31} & S_{32} & S_{33} & S_{34} \\ S_{41} & S_{42} & S_{43} & S_{44} \end{bmatrix} \tag{8.191}$$

where

$$Cof = \frac{(1+s^2)k_{\wp}^*}{2\left[1-\cos(kfd)\cos(ksd)\right] + (fs+1/fs)\sin(kfd)\sin(ksd)} \tag{8.192}$$

$$S_{11} = S_{33} = \frac{1}{s}\cos(kfd)\sin(ksd) + f\sin(kfd)\cos(ksd) \tag{8.193}$$

$$S_{12} = -S_{21} = -S_{34} = S_{43} = \frac{(3-s^2)\,\iota}{(1+s^2)}\left[1-\cos(kfd)\cos(ksd)\right] + \frac{(1+2f^2s^2-s^2)\iota}{fs(1+s^2)}\sin(kfd)\sin(ksd) \tag{8.194}$$

$$S_{13} = S_{31} = -f\sin(kfd) - \frac{1}{s}\sin(ksd) \tag{8.195}$$

$$S_{14} = -S_{41} = S_{23} = -S_{32} = \iota[\cos(kfd) - \cos(ksd)] \tag{8.196}$$

$$S_{22} = S_{44} = \frac{1}{f}\sin(kfd)\cos(ksd) + s\left[\cos(kfd)\sin(ksd)\right] \tag{8.197}$$

$$S_{24} = S_{42} = \frac{-1}{f}\sin(kfd) - s\left[\sin(ksd)\right] \tag{8.198}$$

Note that superscript L stands for horizontal layer i and subscript P-SV indicates the corresponding stiffness matrix associated with P- and SV-wave.

8.5.1.2 For vertically incident waves when $k = 0$

This special case corresponds to a zero wave number k. The derivation is analogous to that presented in Section 8.5.1.1, except the in-plane displacement equations of a layer are based on Equations 8.170 and 8.171. Using the displacement in

Equations 8.170 and 8.171 and the stresses in Equations 8.172 and 8.173 , normal stress and shear stress amplitudes can be expressed as

$$\begin{aligned}\sigma_z(z) &= \left[2\wp^* + \lambda^*\right] w_{,z}(x,z) \\ &= -\frac{\iota\omega C_\mathrm{p}}{C_\mathrm{S}^2}\wp^*\left[A_\mathrm{p}\exp\left(\frac{\iota\omega}{C_\mathrm{p}}z\right) + B_\mathrm{p}\exp\left(-\frac{\iota\omega}{C_\mathrm{p}}z\right)\right] \qquad (8.199)\\ \tau_{xz}(z) &= \wp^* u_{,z}(x,z) \\ &= -\frac{\iota\omega}{C_\mathrm{S}}\wp^*\left[A_\mathrm{SV}\exp\left(\frac{\iota\omega}{C_\mathrm{S}}z\right) + B_\mathrm{SV}\exp\left(-\frac{\iota\omega}{C_\mathrm{S}}\right)z\right] \qquad (8.200)\end{aligned}$$

Using Equations 8.170 through 8.200, the displacements and the stresses at node $i(z=0)$ can be expressed as

$$\begin{Bmatrix} u_i \\ w_i \\ \tau_{xz(i)} \\ \sigma_{z(i)} \end{Bmatrix} = [uw\tau\sigma AB_i]^{k=0} \begin{Bmatrix} A_\mathrm{P} \\ B_\mathrm{P} \\ A_\mathrm{SV} \\ B_\mathrm{SV} \end{Bmatrix} \qquad (8.201)$$

with

$$[uw\tau\sigma AB_i]^{k=0} = \begin{bmatrix} \left[uw\tau\sigma AB_i^{(1,1)}\right] & \left[uw\tau\sigma AB_i^{(1,2)}\right] \\ \left[uw\tau\sigma AB_i^{(2,1)}\right] & \left[uw\tau\sigma AB_i^{(2,2)}\right] \end{bmatrix} \qquad (8.202)$$

where

$$\left[uw\tau\sigma AB_i^{(1,1)}\right] = \begin{bmatrix} 0 & 0 \\ -1 & 1 \end{bmatrix} \qquad (8.203)$$

$$\left[uw\tau\sigma AB_i^{(1,2)}\right] = \begin{bmatrix} -1 & 1 \\ 0 & 0 \end{bmatrix} \qquad (8.204)$$

$$\left[uw\tau\sigma AB_i^{(2,1)}\right] = -\frac{\iota\omega C_\mathrm{P}}{C_\mathrm{S}^2}\wp^*\begin{bmatrix} 0 & 0 \\ 1 & 1 \end{bmatrix} \qquad (8.205)$$

$$\left[uw\tau\sigma AB_i^{(2,2)}\right] = -\frac{\iota\omega}{C_\mathrm{S}}\wp^*\begin{bmatrix} 1 & 1 \\ 0 & 0 \end{bmatrix} \qquad (8.206)$$

At node $i+1(z=d)$ the displacements and the stresses can be expressed as

$$\begin{Bmatrix} u_{i+1} \\ w_{i+1} \\ \tau_{xz(i+1)} \\ \sigma_{z(i+1)} \end{Bmatrix} = [uw\tau\sigma AB_{i+1}]^{k=0} \begin{Bmatrix} A_\mathrm{P} \\ B_\mathrm{P} \\ A_\mathrm{SV} \\ B_\mathrm{SV} \end{Bmatrix} \qquad (8.207)$$

with

$$[uw\tau\sigma\, AB_{i+1}]^{k=0} = \begin{bmatrix} \left[uw\tau\sigma\, AB_{i+1}^{(1,1)}\right] & \left[uw\tau\sigma\, AB_{i+1}^{(1,2)}\right] \\ \left[uw\tau\sigma\, AB_{i+1}^{(2,1)}\right] & \left[uw\tau\sigma\, AB_{i+1}^{(2,2)}\right] \end{bmatrix} \tag{8.208}$$

where

$$\left[uw\tau\sigma\, AB_{i+1}^{(1,1)}\right] = \begin{bmatrix} 0 & 0 \\ -\exp(\iota\omega d/C_{\mathrm{P}}) & \exp(-\iota\omega d/C_{\mathrm{P}}) \end{bmatrix} \tag{8.209}$$

$$\left[uw\tau\sigma\, AB_{i+1}^{(1,2)}\right] = \begin{bmatrix} -\exp(\iota\omega d/C_{\mathrm{S}}) & \exp(-\iota\omega d/C_{\mathrm{S}}) \\ 0 & 0 \end{bmatrix} \tag{8.210}$$

$$\left[uw\tau\sigma\, AB_{i+1}^{(2,1)}\right] = -\frac{\iota\omega C_{\mathrm{p}}}{C_{\mathrm{S}}^2}\wp^* \begin{bmatrix} 0 & 0 \\ \exp(\iota\omega d/C_{\mathrm{P}}) & \exp(-\iota\omega d/C_{\mathrm{P}}) \end{bmatrix} \tag{8.211}$$

$$\left[uw\tau\sigma\, AB_{i+1}^{(2,1)}\right] = -\frac{\iota\omega}{C_{\mathrm{S}}}\wp^* \begin{bmatrix} \exp(\iota\omega d/C_{\mathrm{S}}) & \exp(-\iota\omega d/C_{\mathrm{S}}) \\ 0 & 0 \end{bmatrix} \tag{8.212}$$

Using Equations 8.201 and 8.207, the displacement and stress amplitudes at node i+1 are expressed as a function of those at node i by the transfer matrix as

$$\begin{Bmatrix} u_{i+1} \\ w_{i+1} \\ \tau_{xz(i+1)} \\ \sigma_{z(i+1)} \end{Bmatrix} = \left[uw\tau\sigma\,{}_{i}^{i+1}\right]^{k=0} \begin{Bmatrix} u_i \\ w_i \\ \tau_{xz(i)} \\ \sigma_{z(i)} \end{Bmatrix} \tag{8.213}$$

with

$$\left[uw\tau\sigma_{i}^{i+1}\right]^{k=0} = [uw\tau\sigma\, AB_{i+1}]^{k=0}\left[[uw\tau\sigma\, AB_i]^{k=0}\right]^{-1} \tag{8.214}$$

Introducing external load amplitudes $P_i = -\tau_{xz(i)}$, $R_i = -\sigma_{z(i)}$, $P_{i+1} = \tau_{xz(i+1)}$, and $R_{i+1} = \sigma_{z(i+1)}$ into Equation 8.213 and performing a partial inversion leads to the dynamic-stiffness matrix of a layer ($k = 0$) as

$$\begin{Bmatrix} P_i \\ R_i \\ P_{i+1} \\ R_{i+1} \end{Bmatrix} = \left[S_{\mathrm{P-SV}}^{\mathrm{L}}\right]_{i}^{k=0} \begin{Bmatrix} u_i \\ w_i \\ u_{i+1} \\ w_{i+1} \end{Bmatrix} \tag{8.215}$$

with

$$\left[S^{\mathrm{L}}_{\mathrm{P-SV}}\right]_i^{k=0} = Cof \begin{bmatrix} S_{11} & 0 & S_{13} & 0 \\ 0 & S_{22} & 0 & S_{24} \\ S_{31} & 0 & S_{33} & 0 \\ 0 & S_{42} & 0 & S_{44} \end{bmatrix} \tag{8.216}$$

where

$$Cof = \frac{\omega}{C_{\mathrm{S}}} \wp^* \tag{8.217}$$

$$S_{11} = S_{33} = \cot\left(\frac{\omega d}{C_{\mathrm{S}}}\right) \tag{8.218}$$

$$S_{13} = S_{31} = \frac{-1}{\sin(\omega d / C_{\mathrm{S}})} \tag{8.219}$$

$$S_{22} = S_{44} = \left(\frac{C_{\mathrm{P}}}{C_{\mathrm{S}}}\right) \cot\left(\frac{\omega d}{C_{\mathrm{P}}}\right) \tag{8.220}$$

$$S_{24} = S_{42} = \left(\frac{C_{\mathrm{P}}}{C_{\mathrm{S}}}\right) \frac{-1}{\sin(\omega d / C_{\mathrm{P}})} \tag{8.221}$$

8.5.2 Dynamic-Stiffness Coefficients of Half Plane

A *half plane* can be regarded as a horizontal layer with depth approaching infinity. Applying an external load at the free surface of a half plane, only wave traveling in the positive z-direction (outgoing waves) is developed as shown in Figure 8.15. The radiation condition states that no energy can propagate from infinity toward the free surface. Therefore, the incoming waves with amplitudes A_{P} and A_{SV} in Equations 8.168 and 8.169 are excluded. The wave number k can be positive, negative, and zero for which three cases presented in Sections 8.5.2.1 through 8.5.2.3, respectively.

8.5.2.1 Positive wave number *k*

The in-place displacement equations for a positive wave number k can be expressed as

$$u(k,z) = l_x B_{\mathrm{P}} \exp(-\iota k f z) + m_x s B_{\mathrm{SV}} \exp(-\iota k s z) \tag{8.222}$$

$$w(k,z) = l_x f B_{\mathrm{P}} \exp(-\iota k f z) - m_x B_{\mathrm{SV}} \exp(-\iota k s z) \tag{8.223}$$

Substituting displacement Equations 8.166, 8.167, 8.222, and 8.223 into stress Equations 8.172 and 8.173, and omitting term $\exp(-\iota k x)$, the stress amplitudes in

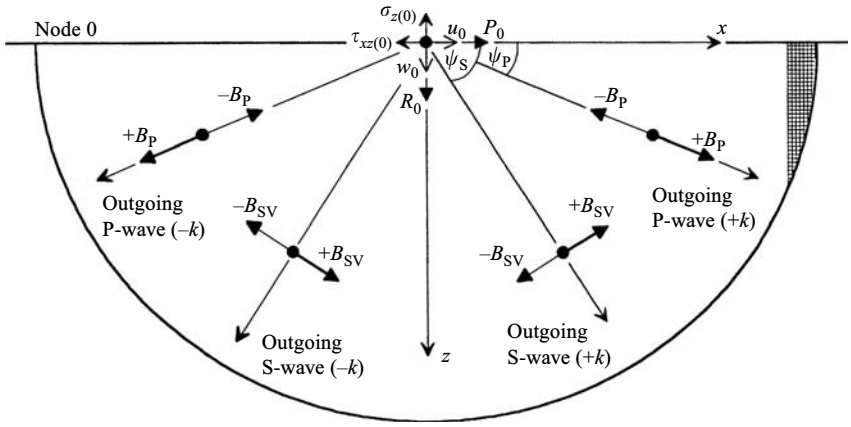

FIGURE 8.15 Displacements, stresses, and external forces on half plane.

k-domain can be expressed as

$$\begin{aligned}\sigma_z(k,z) &= [2\wp^* + \lambda^*]w_{,z}(k,z) - \iota k\lambda^* u(k,z)\\ &= \iota k\wp^*[l_x(1-s^2)B_P \exp(-\iota kfz) + 2sm_xB_{SV}\exp(-\iota ksz)] \qquad (8.224)\\ \tau_{xz}(k,z) &= \wp^*[u_{,z}(k,z) - \iota kw(k,z)]\\ &= \iota k\wp^*[-2l_xfB_P \exp(-\iota kfz) + m_x(1-s^2)B_{SV}\exp(-\iota ksz)] \qquad (8.225)\end{aligned}$$

At node 0 ($z = 0$) on the surface of a half plane, displacements and external forces ($P_0 = -\tau_{xz(0)},$) $R_0 = -\sigma_{z(0)}$ in Figure 8.15 can be expressed in terms of wave amplitudes B_P and B_{SV} as

$$\begin{Bmatrix} u_0(k) \\ w_0(k) \end{Bmatrix} = \begin{bmatrix} l_x & m_xs \\ l_xf & -m_x \end{bmatrix} \begin{Bmatrix} B_P \\ B_{SV} \end{Bmatrix} \qquad (8.226)$$

$$\begin{Bmatrix} P_0(k) \\ R_0(k) \end{Bmatrix} = \iota k\wp^* \begin{bmatrix} 2l_xf & -m_x(1-s^2) \\ -l_x(1-s^2) & -2m_xs \end{bmatrix} \begin{Bmatrix} B_P \\ B_{SV} \end{Bmatrix} \qquad (8.227)$$

Eliminating B_P, B_{SV} in Equations 8.226 and 8.227, the dynamic-stiffness matrix of a half plane, for a positive nonzero k, can be expressed as

$$\begin{Bmatrix} P_0(k) \\ R_0(k) \end{Bmatrix} = \left[S^R_{P-SV}(k)\right]^{k>0} \begin{Bmatrix} u_0(k) \\ w_0(k) \end{Bmatrix} \qquad (8.228)$$

with

$$\left[S^{\mathrm{R}}_{\mathrm{P-SV}}(k)\right]^{k>0} = \iota k \wp^* \begin{bmatrix} 2l_x f & -m_x(1-s^2) \\ -l_x(1-s^2) & -2m_x s \end{bmatrix} \begin{bmatrix} l_x & m_x s \\ l_x f & -m_x \end{bmatrix}^{-1}$$

$$= \iota k \wp^* \begin{bmatrix} f(1+s^2)/(1+fs) & 2-[(1+s^2)/(1+fs)] \\ -2+[(1+s^2)/(1+fs)] & s(1+s^2)/(1+fs) \end{bmatrix} \tag{8.229}$$

As the half plane is used mainly to represent rock bed, a superscript R is introduced. Subscript P-SV indicates that the corresponding stiffness matrix is associated with P- and SV-wave.

8.5.2.2 Negative wave number *k*

The displacement equations having the outgoing waves (propagating in the positive z-direction and the negative x-direction as shown in Figure 8.15) with amplitudes B_{P} and B_{SV} can be expressed as

$$u(k,z) = l_x B_{\mathrm{P}} \exp(\iota k f z) - m_x s B_{\mathrm{SV}} \exp(\iota k s z) \tag{8.230}$$

$$w(k,z) = -l_x f B_{\mathrm{P}} \exp(\iota k f z) - m_x B_{\mathrm{SV}} \exp(\iota k s z) \tag{8.231}$$

Substituting displacement Equations 8.166, 8.127, 8.230, and 8.231 into stress Equations 8.172 and 8.173, and omitting term $\exp(-\iota k x)$, normal stress and shear stress amplitudes can be expressed as

$$\sigma_z(k,z) = \iota k \wp^* [l_x(1-s^2) B_{\mathrm{P}} \exp(\iota k f z) - 2s m_x B_{\mathrm{SV}} \exp(\iota k s z)] \tag{8.232}$$

$$\tau_{xz}(k,z) = \iota k \wp^* [2 l_x f B_{\mathrm{P}} \exp(\iota k f z) + m_x(1-s^2) B_{\mathrm{SV}} \exp(\iota k s z)] \tag{8.233}$$

At node $0(z = 0)$ on the surface of a half plane, the displacements and external forces ($P_0 = -\tau_{xz(0)}$, $R_0 = -\sigma_{z(0)}$) shown in Figure 8.15 can be expressed as

$$\begin{Bmatrix} u_0(k) \\ w_0(k) \end{Bmatrix} = \begin{bmatrix} l_x & -m_x s \\ -l_x f & -m_x \end{bmatrix} \begin{Bmatrix} B_{\mathrm{P}} \\ B_{\mathrm{SV}} \end{Bmatrix} \tag{8.234}$$

$$\begin{Bmatrix} P_0(k) \\ R_0(k) \end{Bmatrix} = \iota k \wp^* \begin{bmatrix} -2l_x f & -m_x(1-s^2) \\ -l_x(1-s^2) & 2m_x s \end{bmatrix} \begin{Bmatrix} B_{\mathrm{P}} \\ B_{\mathrm{SV}} \end{Bmatrix} \tag{8.235}$$

Eliminating B_P, B_{SV} in Equations 8.234 and 8.235, the dynamic-stiffness matrix of half plane, for a negative k, can be expressed as

$$\begin{Bmatrix} P_0(k) \\ R_0(k) \end{Bmatrix} = \left[S^R_{P-SV}(k)\right]^{k<0} \begin{Bmatrix} u_0(k) \\ w_0(k) \end{Bmatrix} \tag{8.236}$$

with

$$\begin{aligned} \left[S^R_{P-SV}(k)\right]^{k<0} &= \iota k \wp^* \begin{bmatrix} -2l_x f & -m_x(1-s^2) \\ -l_x(1-s^2) & 2m_x s \end{bmatrix} \begin{bmatrix} l_x & -m_x s \\ -l_x f & -m_x \end{bmatrix}^{-1} \\ &= \iota k \wp^* \begin{bmatrix} -f(1+s^2)/(1+fs) & 2-[(1+s^2)/(1+fs)] \\ -2+[(1+s^2)/(1+fs)] & -s(1+s^2)/(1+fs) \end{bmatrix} \end{aligned} \tag{8.237}$$

8.5.2.3 Wave associated with $k = 0$

As presented earlier, only the outgoing waves with amplitudes B_P and B_{SV} are developed. Therefore, the displacements in Equations 8.170 and 8.171 are reduced to

$$u(x,z)^{k=0} = B_{SV} \exp\left(-\frac{\iota\omega}{C_S} z\right) \tag{8.238}$$

$$w(x,z)^{k=0} = B_P \exp\left(-\frac{\iota\omega}{C_P} z\right) \tag{8.239}$$

Using the displacements in Equations 8.238 and 8.239 and the stresses in Equations 8.172 and 8.173, the normal stress and shear stress amplitudes can be expressed as

$$\sigma_z(z) = -\frac{\iota\omega C_P}{C_S^2} \wp^* B_P \exp\left(-\frac{\iota\omega}{C_P} z\right) \tag{8.240}$$

$$\tau_{xz}(z) = -\frac{\iota\omega}{C_S} \wp^* B_{SV} \exp\left(-\frac{\iota\omega}{C_S} z\right) \tag{8.241}$$

At node 0 ($z = 0$) on the surface of a half plane, the displacements and external forces $\left(P_0 = -\tau_{xz(0)},\ R_0 = -\sigma_{z(0)}\right)$ can be expressed as

$$\begin{Bmatrix} u_0 \\ w_0 \end{Bmatrix} = \begin{bmatrix} 0 & 1 \\ 1 & 0 \end{bmatrix} \begin{Bmatrix} B_P \\ B_{SV} \end{Bmatrix} \tag{8.242}$$

$$\begin{Bmatrix} P_0 \\ R_0 \end{Bmatrix} = \frac{\iota\omega}{C_S} \wp^* \begin{bmatrix} 0 & 1 \\ C_P/C_S & 0 \end{bmatrix} \begin{Bmatrix} B_P \\ B_{SV} \end{Bmatrix} \tag{8.243}$$

Using Equations 8.242 and 8.234, the dynamic-stiffness, matrix of a half plane, for $k = 0$, can be expressed as

$$\begin{Bmatrix} P_0 \\ R_0 \end{Bmatrix} = \left[S^{\mathrm{R}}_{\mathrm{P-SV}}\right]^{k=0} \begin{Bmatrix} u_0 \\ w_0 \end{Bmatrix} \tag{8.244}$$

with

$$\left[S^{\mathrm{R}}_{\mathrm{P-SV}}\right]^{k=0} = \frac{\iota\omega}{C_{\mathrm{S}}} \wp^* \begin{bmatrix} 1 & 0 \\ 0 & C_{\mathrm{P}}/C_{\mathrm{S}} \end{bmatrix} \tag{8.245}$$

8.6 Dynamic-Stiffness Matrices of Ground System

8.6.1 Definition and Concept

The ground system with embeded foundation is constructed by excavating a part of the soil from free-field soil as shown in Figure 8.16. Free-field system is the site before excavation and construction. Excavated part is the soil to be removed and then replaced by embedded foundation. Thus, all three parts have the same soil properties for which the mathematical model must be consistent. For instance, they have common rigid interface and three d.o.f. at point 0, x_0, z_0, and θ_0, in x-, z-direction and around y-direction, represent the d.o.f. along the rigid interface. Superscripts g, f, and e, only identify ground, free field, and excavated part of the whole system. Because free-field is an unbounded continuous domain and excavated part is a bounded medium; the stiffness matrices of these two systems must be first derived independently according to the characteristics of soils and wave equations presented in Sections 8.4 and 8.5, ground system's stiffness matrix is then obtained.

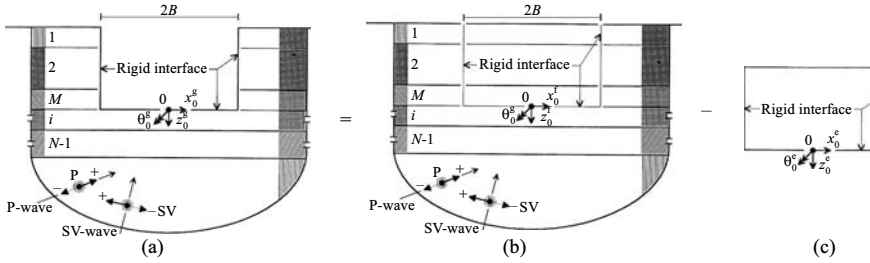

Figure 8.16 Ground system with rigid interface: (a) ground system, (b) free-field system, and (c) excavated part.

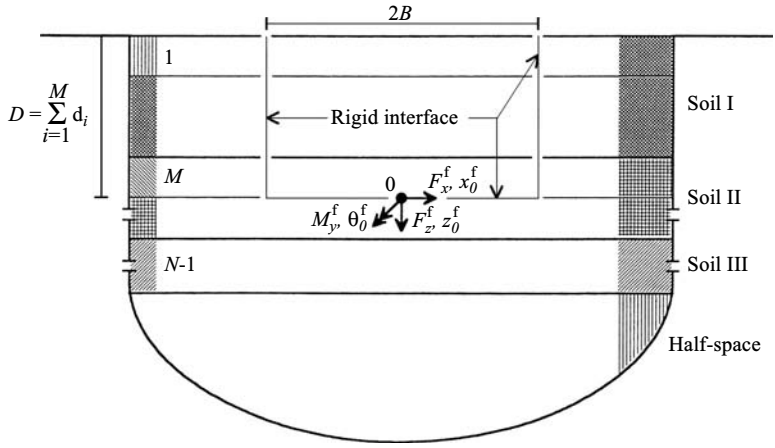

FIGURE 8.17 Forces and displacements of free-field system with rigid interface.

8.6.2 Free-Field System's Stiffness Matrix

8.6.2.1 Force–displacement relationship in frequency domain

The dynamic stiffness matrix $\left[S_{00}^{f}(\omega)\right]$ of the continuous free-field system with rigid interface is represented in Figure 8.17. It specifies the amplitude of forces F_x^f, M_y^f, F_z^f due to unit amplitude of displacement x_0^f, θ_0^f, z_0^f applied at node 0 of the rigid interface for harmonic motion with excitation frequency ω as

$$\begin{Bmatrix} F_x^f \\ M_y^f \\ F_z^f \end{Bmatrix} = \left[S_{00}^{f}(\omega)\right] \begin{Bmatrix} x_0^f \\ \theta_0^f \\ z_0^f \end{Bmatrix} \tag{8.246}$$

The concept of the *indirect boundar-element method*, a special case of *weighted-residual technique* [9,10,12], can be applied to the free-field system even though the rigid interface is not a boundary. Assume that loading patterns acting along the rigid interface do exist and that these loads result along the same interface, in the prescribed displacement of unit nodal values x_0^f, θ_0^f, z_0^f. This can be achieved by adjusting load intensities to satisfy this condition. Integrating loading patterns with prescribed displacement will lead to the dynamic-stiffness matrix. Since only a finite number of load intensities can be chosen, an approximate solution results.

In Figure 8.18, the rigid interface consists of two vertical interfaces for length D and a horizontal interface for length $2B$. As additional horizontal interfaces are introduced into the system, the former is divided into elements of length d_i, for $i = 1, 2, \ldots, M$, on each of the vertical interface. The latter is equally divided into $2L$ elements, each of length b. The elements are numbered from 1 to $2(M + L)$. Element 1 is started from the top element of the left vertical interface to the bottom one, element M. Elements $M + 1, \ldots, M + 2L$ define the element of the horizontal

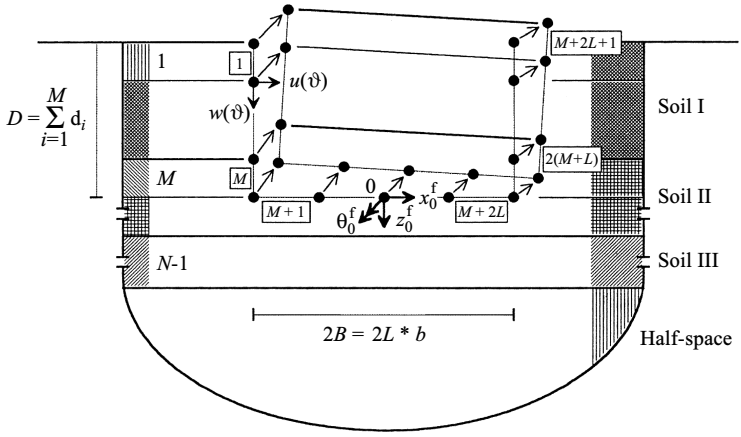

FIGURE 8.18 Prescribed displacements along rigid interface.

interface from the left element to the right one. On the right vertical interface, elements $M + 2L + 1, \ldots, 2(M + L)$ are used to describe the element from top to bottom.

Rigid body kinematics relate the prescribed displacement amplitudes $u(\vartheta)$, $w(\vartheta)$ along the rigid interface (see Figure 8.18) to the rigid body d.o.f. associated with the dynamic-stiffness's definition as

$$\begin{Bmatrix} u(\vartheta) \\ w(\vartheta) \end{Bmatrix} = [\mathrm{N}(\vartheta)] \begin{Bmatrix} x_0^{\mathrm{f}} \\ \theta_0^{\mathrm{f}} \\ z_0^{\mathrm{f}} \end{Bmatrix} \tag{8.247}$$

where ϑ denotes symbolically a point on the assumed line that subsequently forms the rigid interface. A bold letter in the matrix used herein indicates the corresponding matrix in the space domain of frequency.

On the continuous system in Figure 8.19, load amplitudes $p(\vartheta)$, $r(\vartheta)$ along the assumed line are related to the initially unknown intensities p_i, r_i on node i as

$$\begin{Bmatrix} p(\vartheta) \\ r(\vartheta) \end{Bmatrix} = [\mathrm{L}(\vartheta)] \begin{bmatrix} p_1 & r_1 & \ldots & p_i & r_i & \ldots & p_{\mathrm{NN}} & r_{\mathrm{NN}} \end{bmatrix}^{\mathrm{T}} \tag{8.248}$$

$[\mathrm{L}(\vartheta)]$ represents a selected interpolation function (e.g., a linearly distributed function). Nodes are numbered from 1 to NN, where NN is a number of notes along the assumed line and equals $2(M+L)+3$ as the discontinuities of load patterns are introduced at the corners of the assumed line. Node 1 goes from the top node of the left vertical interface to the bottom one, note $M+1$. Nodes $M+2, \ldots, M+2L+2$ define the nodes of the horizontal interface from the left note to the right one. On the right vertical interface, nodes $M + 2L + 3, \ldots, 2(M + L) + 3$ are used to describe the nodes from top to bottom.

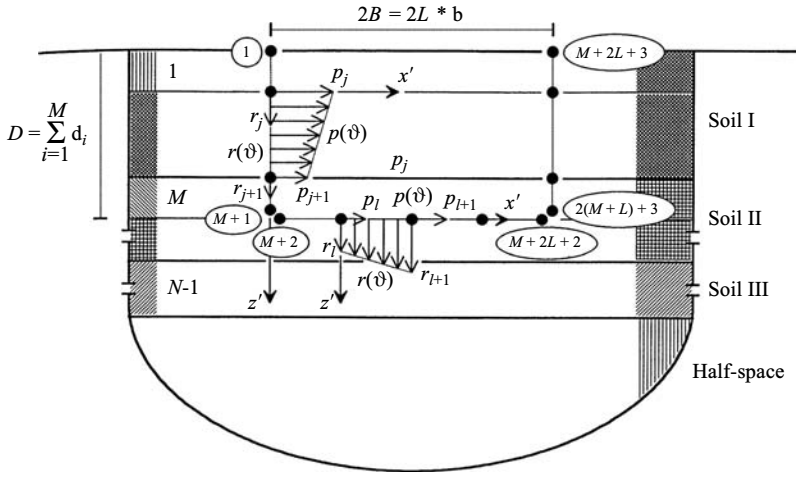

FIGURE 8.19 Linearly distributed loads along assumed line.

Green's influence functions (see Appendix B) relate the amplitudes of displacement $u_{\mathrm{pr}}(\vartheta)$, $w_{\mathrm{pr}}(\vartheta)$ along the assumed line to initially unknown intensities p_i, r_i on node i as

$$\begin{Bmatrix} u_{\mathrm{pr}}(\vartheta) \\ w_{\mathrm{pr}}(\vartheta) \end{Bmatrix} = \left[uw_{\mathrm{pr}}(\vartheta) \right] \begin{bmatrix} p_1 & r_1 & \dots & p_i & r_i & \dots & p_{\mathrm{NN}} & r_{\mathrm{NN}} \end{bmatrix}^{\mathrm{T}} \tag{8.249}$$

Since only a finite number of load intensities p_i, r_i can be introduced, the displacement-boundary condition on the interface cannot be satisfied exactly but is expressed in an average sense as

$$\int_{\vartheta} [\mathrm{W}(\vartheta)]^{\mathrm{T}} \left(\begin{Bmatrix} u_{\mathrm{pr}}(\vartheta) \\ w_{\mathrm{pr}}(\vartheta) \end{Bmatrix} - \begin{Bmatrix} u(\vartheta) \\ w(\vartheta) \end{Bmatrix} \right) \mathrm{d}\vartheta = \{0\} \tag{8.250}$$

In order to guarantee the symmetry of the dynamic-stiffness matrix, for indirect boundary-element method, the weighting matrix $[\mathrm{W}(\vartheta)]$ is chosen to be equal to $[\mathrm{L}(\vartheta)]$ [6].

Substituting Equations 8.247 and 8.124 in Equation 8.250, the total load intensities p_i, r_i that satisfy the condition in Equation 8.250 can be determined as

$$\begin{bmatrix} p_1 & r_1 & \dots & p_i & r_i & \dots & p_{\mathrm{NN}} & r_{\mathrm{NN}} \end{bmatrix}^{\mathrm{T}} = [\mathrm{F}]^{-1} [\mathrm{T}] \begin{Bmatrix} x_0^{\mathrm{f}} \\ \theta_0^{\mathrm{f}} \\ z_0^{\mathrm{f}} \end{Bmatrix} \tag{8.251}$$

where

$$[\mathrm{F}] = \int_{\vartheta} [\mathrm{L}(\vartheta)]^{\mathrm{T}} \left[uw_{\mathrm{pr}}(\vartheta) \right] \mathrm{d}\vartheta \tag{8.252}$$

$$[\mathrm{T}] = \int_{\vartheta} [\mathrm{L}(\vartheta)]^{\mathrm{T}} [\mathrm{N}(\vartheta)] \mathrm{d}\vartheta \tag{8.253}$$

The flexibility matrix [F] of a dimension 2(NN) by 2(NN), where $\mathrm{NN} = 2(M + L) + 3$, is symmetric. The generalized strain–displacement matrix [T] has a dimension of 2(NN) by 3.

As is well known from *virtual work* consideration, amplitudes of the concentrated loads F_x^{f}, M_y^{f}, F_z^{f} can be obtained by integrating loading patterns with prescribed displacement as

$$\begin{Bmatrix} F_x^{\mathrm{f}} \\ M_y^{\mathrm{f}} \\ F_z^{\mathrm{f}} \end{Bmatrix} = \int_{\vartheta} [\mathrm{N}(\vartheta)]^{\mathrm{T}} \begin{Bmatrix} p(\vartheta) \\ r(\vartheta) \end{Bmatrix} \mathrm{d}\vartheta \tag{8.254}$$

Using Equations 8.248 and 8.251 in Equation 8.254 leads to the dynamic-stiffness matrix of free-field system with rigid interface as

$$\begin{Bmatrix} F_x^{\mathrm{f}} \\ M_y^{\mathrm{f}} \\ F_z^{\mathrm{f}} \end{Bmatrix} = \left[S_{00}^{\mathrm{f}}(\omega) \right] \begin{Bmatrix} x_0^{\mathrm{f}} \\ \theta_0^{\mathrm{f}} \\ z_0^{\mathrm{f}} \end{Bmatrix} \tag{8.255}$$

where

$$\left[S_{00}^{\mathrm{f}}(\omega) \right] = [\mathrm{T}]^{\mathrm{T}} [\mathrm{F}]^{-1} [\mathrm{T}] \tag{8.256}$$

8.6.2.2 Strain–displacement relationship in frequency domain

Integration of Equation 8.253 is performed, along the rigid interface, on each element based on its local coordinates. Origin of the local coordinates is located at the top node for the vertical element and at the left node for the horizontal element. By using the geometric configuration shown in Figure 8.18, the rigid body kinematics in Equation 8.247 can be broken down into one of each

element as

$$\left[\overline{\mathrm{N}}\,(z)\right]_i = \begin{bmatrix} 1 & -\left(\sum_{n=i}^{M} \mathrm{d}_n\right) + z & 0 \\ 0 & B & 1 \end{bmatrix} \quad \text{for element } i, i = 1, \ldots, M \tag{8.257}$$

$$\left[\overline{\mathrm{N}}\,(x)\right]_i = \begin{bmatrix} 1 & 0 & 0 \\ 0 & \left(\sum_{n=i}^{M+L} b\right) - x & 1 \end{bmatrix} \quad \text{for element } i, i = M+1, \ldots, M+L \tag{8.258}$$

$$\left[\overline{\mathrm{N}}\,(x)\right]_i = \begin{bmatrix} 1 & 0 & 0 \\ 0 & -\left(\sum_{n=M+L+1}^{i} b\right) + b - x & 1 \end{bmatrix}$$

$$\text{for element } i, i = M+L+1, \ldots, M+2L \tag{8.259}$$

$$\left[\overline{\mathrm{N}}\,(z)\right]_i = \begin{bmatrix} 1 & -\left(\sum_{n=i-M-2L}^{M} \mathrm{d}_n\right) + z & 0 \\ 0 & -B & 1 \end{bmatrix}$$

$$\text{for element } i, i = M+2L+1, \ldots, 2(M+L) \tag{8.260}$$

where a horizontal bar on top of a letter denotes that the given matrix is element matrix. As an example, the determination of the terms on the first row and the second column of the matrix in Equation 8.257 are described as follows. The term $\sum_{n=i}^{M} \mathrm{d}_n$ represents the distance from the top node of ith element to the level of point 0. Subtracting z (distance from the top node of ith element to a considering point) from $\sum_{n=i}^{M} \mathrm{d}_n$ results in $\sum_{n=i}^{M} \mathrm{d}_n - z$, which represents the distance from a considering point to the level of point 0. Multiplying $\sum_{n=i}^{M} \mathrm{d}_n - z$ by θ_0^{f} (rotation point of 0) leads to a negative horizontal displacement at a considering point. The expression on the first row and second column of this matrix relates to the horizontal displacement at a considering point, $u\,(z)$, to the rotation at point 0, θ_0^{f}, therefore it equals $-\sum_{n=i}^{M} \mathrm{d}_n + z$.

For linearly distributed loads in Figure 8.19, a two-node element is employed. Since only the nodal values on these two corresponding nodes dictates loading patterns on the element, the interpolation matrix in Equation 8.248 can be written as

$$\left[\overline{L}(z)\right]_i = \begin{bmatrix} 1 - z/\mathrm{d_i} & 0 & z/\mathrm{d_i} & 0 \\ 0 & 1 - z/\mathrm{d_i} & 0 & z/\mathrm{d_i} \end{bmatrix} \quad \text{for element } i \text{ on vertical interface} \tag{8.261}$$

$$\left[\overline{L}(x)\right]_i = \begin{bmatrix} 1 - x/b & 0 & x/b & 0 \\ 0 & 1 - x/b & 0 & x/b \end{bmatrix} \quad \text{for element } i \text{ on horizontal interface} \tag{8.262}$$

Using Equations 8.257 through 8.262, the element strain–displacement matrix $[\overline{T}]$, can be obtained as

$$[\overline{T}] = \int_0^{d_i} [\overline{L}(z)]_i^{\mathrm{T}} [\overline{N}(z)]_i \, \mathrm{d}z \quad \text{for element } i \text{ on vertical interface} \tag{8.263}$$

$$[\overline{T}] = \int_0^{b} [\overline{L}(x)]_i^{\mathrm{T}} [\overline{N}(x)]_i \, \mathrm{d}x \quad \text{for element } i \text{ on horizontal interface} \tag{8.264}$$

Completing the integration in Equations 8.263 and 8.264 results, for element i, in

$$[\overline{\mathrm{T}}]_i = \begin{bmatrix} \mathrm{d}_i/2 & -\left(\sum_{n=i}^{M} \mathrm{d}_n\right)\mathrm{d}_i/2 + \mathrm{d}_i^2/6 & 0 \\ 0 & B\mathrm{d}_i/2 & \mathrm{d}_i/2 \\ \mathrm{d}_i/2 & -\left(\sum_{n=i}^{M} \mathrm{d}_n\right)\mathrm{d}_i/2 + \mathrm{d}_i^2/3 & 0 \\ 0 & B\mathrm{d}_i/2 & \mathrm{d}_i/2 \end{bmatrix} \quad i = 1, \ldots, M \tag{8.265}$$

$$[\overline{\mathrm{T}}]_i = \begin{bmatrix} b/2 & 0 & 0 \\ 0 & \left(\sum_{n=i}^{M+L} b\right) b/2 - b^2/6 & b/2 \\ b/2 & 0 & 0 \\ 0 & \left(\sum_{n=i}^{M+L} b\right) b/2 - b^2/3 & b/2 \end{bmatrix} \quad i = M+1, \ldots, M+L \tag{8.266}$$

$$[\overline{\mathrm{T}}]_i = \begin{bmatrix} b/2 & 0 & 0 \\ 0 & -\left(\sum_{n=M+L+1}^{i} b\right) b/2 + b^2/3 & b/2 \\ b/2 & 0 & 0 \\ 0 & -\left(\sum_{n=M+L+1}^{i} b\right) b/2 + b^2/6 & b/2 \end{bmatrix} \quad i = M+L+1, \ldots, M+2L \tag{8.267}$$

$$[\overline{\mathrm{T}}]_i = \begin{bmatrix} \mathrm{d}_i/2 & -\left(\sum_{n=i-M-2L}^{M} \mathrm{d}_n\right)\mathrm{d}_i/2 + \mathrm{d}_i^2/6 & 0 \\ 0 & -B\mathrm{d}_i/2 & \mathrm{d}_i/2 \\ \mathrm{d}_i/2 & -\left(\sum_{n=i-M-2L}^{M} \mathrm{d}_n\right)\mathrm{d}_i/2 + \mathrm{d}_i^2/3 & 0 \\ 0 & -B\mathrm{d}_i/2 & \mathrm{d}_i/2 \end{bmatrix} \quad i = M+2L+1, \ldots, 2(M+L) \tag{8.268}$$

Therefore, the generalized strain–displacement matrix [T] of a dimension of 2(NN) by 3 can be obtained by assembling the element strain–displacement matrices. In the assembling process, the element matrices of two adjacent elements are overlapped on the rows corresponding to the same node. This overlapping does not apply to the nodes corresponding to the corners of the assumed line since discontinuities in loading patterns were introduced. Note that the integration of

Equation 8.252 is performed in the same manner as that of Equation 8.253 for generalized strain–displacement matrix.

8.6.3 Excavated Part's Stiffness Matrix in Frequency Domain

For harmonic motion with excitation frequency ω, the dynamic stiffness matrix $\left[S_{00}^{\mathrm{e}}(\omega)\right]$ of the bounded excavated part of the system with rigid interface is demonstrated in Figure 8.20. It defines amplitude of forces $F_x^{\mathrm{e}}, M_y^{\mathrm{e}}, F_z^{\mathrm{e}}$ due to unit amplitude displacements $x_0^{\mathrm{e}}, \theta_0^{\mathrm{e}}, z_0^{\mathrm{e}}$ applied at node 0 of the rigid interface as

$$\begin{Bmatrix} F_x^{\mathrm{e}} \\ M_y^{\mathrm{e}} \\ F_z^{\mathrm{e}} \end{Bmatrix} = \left[S_{00}^{\mathrm{e}}(\omega)\right] \begin{Bmatrix} x_0^{\mathrm{e}} \\ \theta_0^{\mathrm{e}} \\ z_0^{\mathrm{e}} \end{Bmatrix} \tag{8.269}$$

with

$$\left[S_{00}^{\mathrm{e}}(\omega)\right] = [K^{\mathrm{e}}](1 + 2\zeta\iota) - \omega^2[M^{\mathrm{e}}] \tag{8.270}$$

where $[K^{\mathrm{e}}]$ and $[M^{\mathrm{e}}]$ are the stiffness matrix and the mass matrix of the excavated part of the system respectively. Symbols ζ and ι represent the linear hysteretic damping ratio and $\sqrt{-1}$, respectively.

As the excavated part of the system represents a bounded domain, the concept of the *finite element method* can be applied. First, the domain is discretized into elements connected to each other at nodal points. Determining and assuming the element dynamic stiffness matrix leads to dynamic stiffness matrix corresponding to d.o.f. of all nodal points. Then the condensation process is needed to eliminate the d.o.f. of the nodes not lying on the rigid interface. Finally, relating the d.o.f. of the nodes along the interface to the rigid body d.o.f. at point 0 yields the desired dynamic stiffness matrix.

As shown in Figure 8.21, depth D of the excavated domain is equally divided into M^{e} portions each of length d_{e}. In addition, the domain's width at length

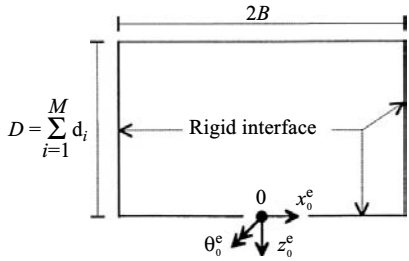

FIGURE 8.20 Excavated part of system with rigid interface.

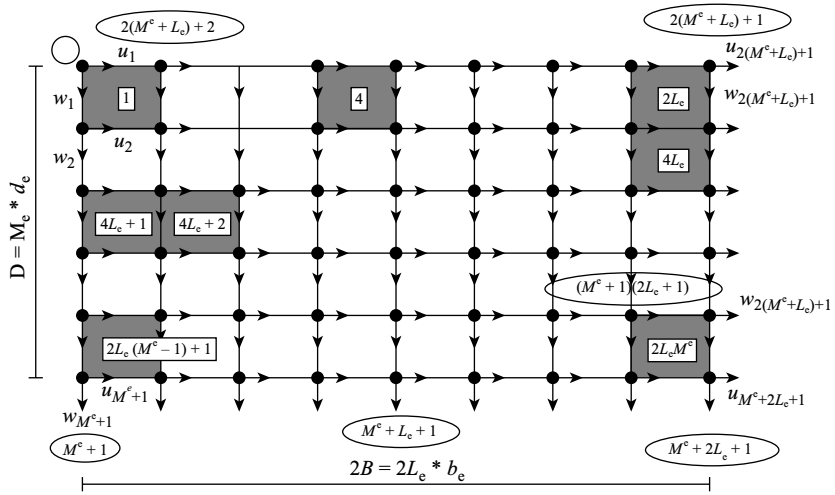

FIGURE 8.21 Discretization of excavated part of system.

$2B$ is evenly divided into $2L_e$ portions, each of length b_e. This results in $2L_eM^e$ rectangular elements of dimensions d_e by b_e, each having four nodal points.

Also shown in the same figure, rectangular elements are numbered from 1 to $2L_eM_e$ starting from left to right and top to bottom. The nodes are categorized into two groups: nodes along the interfaces (subscript B) and nodes in the domains interior, including those along the top boundary (subscript I). The former are numbered from 1 to $M^e + 1$, going from top to bottom of the vertical left interface, from $M^e + 1$ to $M^e + 2L_e + 1$ going from left to right of the horizontal interface, and from $M^e + 2L_e + 1$ to $2(M^e + L_e) + 1$ going from bottom to top of the vertical right interface. The latter are numbered from $2(M^e + L_e) + 2$ to $(M^e + 1)(2L_e + 1)$ going from top to bottom and left to right for the interior.

The 8×8 dynamic stiffness $\left[\overline{S}^e(\omega)\right]_j$ of element j, where $j = 1, \ldots, 2L_eM^e$, can be obtained as

$$\left[\overline{S}^e(\omega)\right]_j = \left[\overline{K}^e\right]_j (1 + 2\zeta_j \iota) - \omega^2 \left[\overline{M}^e\right]_j \tag{8.271}$$

where $\left[\overline{K}^e\right]$ and $\left[\overline{M}^e\right]$ are stiffness matrix and mass matrix of element j. They are discussed in Appendix C.

In the standard assembling process, the element dynamic stiffness matrices $\left[\overline{S}^e(\omega)\right]$ of adjacent discretizing elements are overlapped on the matrix's elements corresponding to the same nodes. The resulting matrix can be expressed as

$$\begin{Bmatrix} \{PR_B\} \\ \{PR_I\} \end{Bmatrix} = \left[S^e(\omega)\right] \begin{Bmatrix} \{uw_B\} \\ \{uw_I\} \end{Bmatrix} \tag{8.272}$$

with

$$\begin{cases} \{PR_{\mathrm{B}}\} = \left[P_1 \quad R_1 \quad \ldots \quad P_i \quad R_i \quad \ldots \quad P_{2(M^{\mathrm{e}}+L_{\mathrm{e}})+1} \quad R_{2(M^{\mathrm{e}}+L_{\mathrm{e}})+1}\right]^{\mathrm{T}} \\ \{PR_{\mathrm{I}}\} = \left[P_{2(M^{\mathrm{e}}+L_{\mathrm{e}})+2} \; R_{2(M^{\mathrm{e}}+L_{\mathrm{e}})+2} \; \ldots \; P_i \; R_i \; \ldots \; P_{(M^{\mathrm{e}}+L_{\mathrm{e}})(2L_{\mathrm{e}}+1)} \right. \\ \qquad\qquad \left. R_{(M^{\mathrm{e}}+L_{\mathrm{e}})(2L_{\mathrm{e}}+1)}\right]^{\mathrm{T}} \end{cases} \tag{8.273}$$

$$\left[S^{\mathrm{e}}(\omega)\right] = \begin{bmatrix} \left[\tilde{S}_{\mathrm{BB}}\right] & \left[\tilde{S}_{\mathrm{BI}}\right] \\ \left[\tilde{S}_{\mathrm{IB}}\right] & \left[\tilde{S}_{\mathrm{II}}\right] \end{bmatrix} \tag{8.274}$$

$$\begin{cases} \{uw_{\mathrm{B}}\} = \left[u_1 \; w_1 \; \ldots \; u_i \; w_i \; \ldots \; u_{2(M^{\mathrm{e}}+L_{\mathrm{e}})+1} \; w_{2(M^{\mathrm{e}}+L_{\mathrm{e}})+1}\right]^{\mathrm{T}} \\ \{uw_{\mathrm{I}}\} = [u_{2(M^{\mathrm{e}}+L_{\mathrm{e}})+2} \; w_{2(M^{\mathrm{e}}+L_{\mathrm{e}})+2} \; \ldots \; u_i \; w_i \; \ldots \; u_{(M^{\mathrm{e}}+L_{\mathrm{e}})(2L_{\mathrm{e}}+1)} \\ \qquad\qquad w_{(M^{\mathrm{e}}+L_{\mathrm{e}})(2L_{\mathrm{e}}+1)}\right]^{\mathrm{T}} \end{cases} \tag{8.275}$$

where P_i and R_i are the horizontal and vertical forces at node i, respectively. u_i and w_i are the horizontal and vertical displacement at node i, respectively. The dynamic stiffness matrix $[S^{\mathrm{e}}(\omega)]$ of dimension $2(M^{\mathrm{e}}+1)(2L_{\mathrm{e}}+1)$ by $2(M^{\mathrm{e}}+1)(2L_{\mathrm{e}}+1)$ consists of four submatrices, each corresponding to the d.o.f. of subscripts' nodes. Subscript B indicated indicates the nodes along the interfaces. Subscript I stand for the interior nodes, including those along the top boundary. Subscripts e denotes the excavated part system.

Since no external forces act on the nodes in the interior ($\{PR_I\} = 0$), Equation 8.272 can be condensed and expressed as

$$\{PR_{\mathrm{B}}\} = \left[S^{\mathrm{e}}_{\mathrm{BB}}(\omega)\right]\{uw_{\mathrm{B}}\} \tag{8.276}$$

with

$$\left[S^{\mathrm{e}}_{\mathrm{BB}}(\omega)\right] = \left[\tilde{S}_{\mathrm{BB}}\right] - \left[\tilde{S}_{\mathrm{BI}}\right]\left[\tilde{S}_{\mathrm{II}}\right]^{-1}\left[\tilde{S}_{\mathrm{IB}}\right] \tag{8.277}$$

where $\left[S^{\mathrm{e}}_{\mathrm{BB}}(\omega)\right]$ has a dimension of $4(M^{\mathrm{e}}+L_{\mathrm{e}})+2$ by $4(M^{\mathrm{e}}+L_{\mathrm{e}})+2$. Since the interface is rigid, as shown in Figure 8.22, the d.o.f. of the nodes along the interface relate to the rigid body d.o.f., at point 0 as

$$\{uw_{\mathrm{B}}\} = [A]\begin{Bmatrix} x_0^{\mathrm{e}} \\ \theta_0^{\mathrm{e}} \\ z_0^{\mathrm{e}} \end{Bmatrix} \tag{8.278}$$

with

$$[A] = \begin{bmatrix} [A_1] \\ [A_2] \\ [A_3] \\ [A_4] \end{bmatrix} \tag{8.279}$$

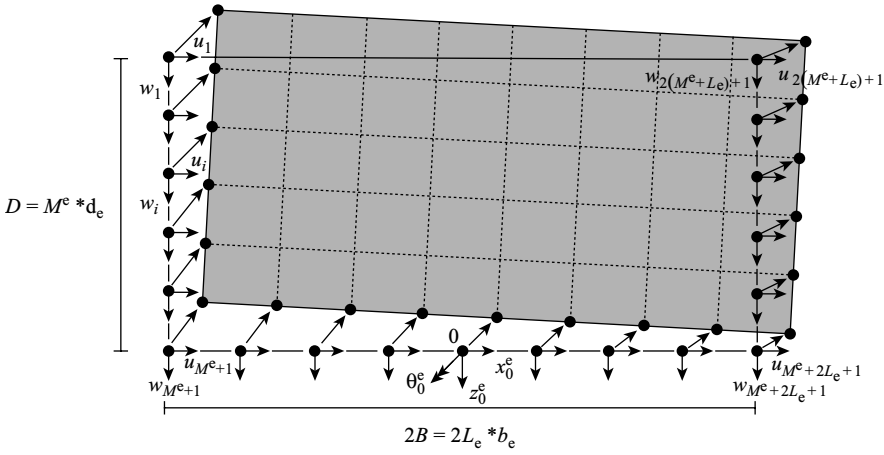

FIGURE 8.22 Rigid body d.o.f. of excavated part of system.

where

$$[A_1] = \begin{bmatrix} \vdots & \vdots & \vdots \\ 1 & -\left(\sum_{n=i}^{M^e} d_e\right) & 0 \\ 0 & B & 1 \\ \vdots & \vdots & \vdots \end{bmatrix} \quad \text{for node } i, i = 1, \ldots, M, \tag{8.280}$$

$$[A_2] = \begin{bmatrix} \vdots & \vdots & \vdots \\ 1 & 0 & 0 \\ 0 & \sum_{n=i}^{M^e+L_e} b_e & 1 \\ \vdots & \vdots & \vdots \end{bmatrix} \quad \text{for node } i, i = M^e + 1, \ldots, M^e + L_e \tag{8.281}$$

$$[A_3] = \begin{bmatrix} \vdots & \vdots & \vdots \\ 1 & 0 & 0 \\ 0 & -\left(\sum_{n=M^e+L_e+1}^{i} b_e\right) + b_e & 1 \\ \vdots & \vdots & \vdots \end{bmatrix}$$

$$\text{for node } i, i = M^e + L_e + 1, \ldots, M^e + 2L_e + 1 \tag{8.282}$$

$$[A_4] = \begin{bmatrix} \vdots & \vdots & \vdots \\ 1 & -\left(\sum_{M^e+2L_e+2}^{i} d_e\right) & 0 \\ 0 & -B & 1 \\ \vdots & \vdots & \vdots \end{bmatrix}$$

$$\text{for node } i,\ i = M^e + 2L_e + 2, \ldots, 2(M^e + L_e) + 1 \tag{8.283}$$

Matrix $[A]$ of dimension $4(M^e + L_e) + 2$ by 3 consists of four submatrices, $[A_1]$, $[A_2]$, $[A_3]$, and $[A_4]$. Matrix $[A_1]$, having a dimension of $2M^e$ by 3, corresponds to the d.o.f. along the vertical left interface. Matrix $[A_2]$, having a dimension of $2L_e$ by 3, corresponds to the d.o.f. along the left portion of the horizontal interface. Matrix $[A_3]$, having a dimension of $2L_e+2$ by 3, corresponds to the d.o.f. along the right portion of the horizontal interface. Matrix $[A_4]$ having a dimension of $2M^e$ by 3, corresponds to the d.o.f. along the vertical right interface. These submatrices can be determined by using consideration in Figure 8.22. For example, the term $-\sum_{M^e+2L_e+2}^{i} d_e$ in Equation 8.283 relates a horizontal displacement at node i of the vertical right interface, u_i, to the rotation at point 0, θ_0^e. This term represents the negative distance from node i to the level of point 0 as positive rotation results in the negative horizontal displacement at node i. The summation of d_e from $M^e + 2L_e + 2$ to i leads to the distance from the level of point 0 to the node i.

Using matrix [A] in Equation 8.278 and its transposed form in Equation 8.276 the dynamic stiffness matrix of the excavated part of the system with rigid interface can be expressed as

$$\begin{Bmatrix} F_x^e \\ M_y^e \\ F_z^e \end{Bmatrix} = \left[S_{00}^e(\omega)\right] \begin{Bmatrix} x_0^e \\ \theta_0^e \\ z_0^e \end{Bmatrix} \tag{8.284}$$

where

$$\left[S_{00}^e(\omega)\right] = [A]^T \left[S_{BB}^e(\omega)\right] [A] \tag{8.285}$$

and

$$\begin{Bmatrix} F_x^e \\ M_y^e \\ F_z^e \end{Bmatrix} = [A]^T \{PR_B\} \tag{8.286}$$

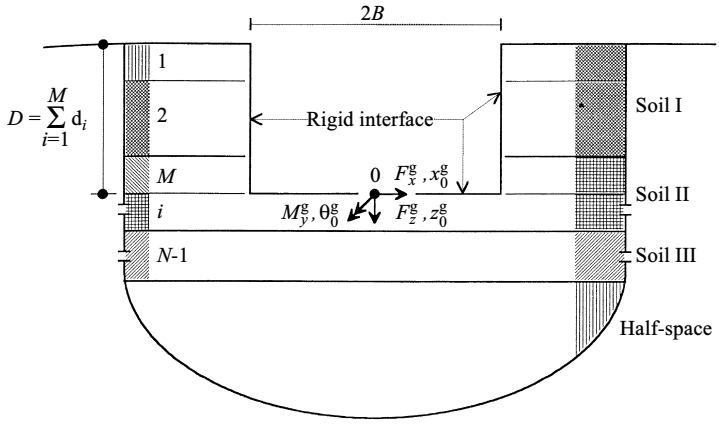

FIGURE 8.23 Forces and displacements of ground system with rigid interface.

8.6.4 Ground System's Stiffness and Flexibility Matrix

8.6.4.1 Transformation of stiffness matrix to flexibility matrix in frequency domain

In Figure 8.23, the dynamic stiffness matrix $\left[S_{00}^{g}(\omega)\right]$of the unbounded ground system with rigid interface is depicted. It specifies the amplitude of forces F_x^g, M_y^g, F_z^g due to unit amplitude displacements x_0^g, θ_0^g, z_0^g applied at the node 0. These forces, for harmonic motion with excitation frequency ω, are expressed as

$$\begin{Bmatrix} F_x^g \\ M_y^g \\ F_z^g \end{Bmatrix} = \left[S_{00}^{g}(\omega)\right] \begin{Bmatrix} x_0^g \\ \theta_0^g \\ z_0^g \end{Bmatrix} \tag{8.287}$$

with

$$\left[S_{00}^{g}(\omega)\right] = \begin{bmatrix} S_{xx}^g & S_{x\theta}^g & 0 \\ S_{\theta x}^g & S_{\theta\theta}^g & 0 \\ 0 & 0 & S_{zz}^g \end{bmatrix} \tag{8.288}$$

where ground system coefficients S_{xx}^g, $S_{x\theta}^g$, $S_{\theta x}^g$, $S_{\theta\theta}^g$ and S_{zz}^g are forces corresponding to the first subscript's d.o.f. due to a unit displacement excitation corresponding to the second subscripts d.o.f. Since we assume the soil domain to be a linear system the law of superposition is valid. Thus the dynamic stiffness matrix of the ground system can be obtained by subtracting that of the excavate part

of the system, Equation 8.285, from that of the free-field system Equation 8.256 as

$$\left[S_{00}^{\mathrm{g}}(\omega)\right] = \left[S_{00}^{\mathrm{f}}(\omega)\right] - \left[S_{00}^{\mathrm{e}}(\omega)\right] \tag{8.289}$$

Near the natural frequency of the system's excavated part, that system's dynamic stiffness coefficients as well as the free-field system's will be large. Since the dynamic stiffness coefficients of the ground system involve two large numbers obtained from two different methods, a number of discretzing elements must be chosen carefully in this vicinity.

Since harmonic motion is represented as $\exp(\iota\omega t)$, the ground system's force–displacement relationship in Equation 8.287 can also be written as

$$\exp(\iota\omega t)\begin{Bmatrix} F_x^{\mathrm{g}} \\ M_y^{\mathrm{g}} \\ F_z^{\mathrm{g}} \end{Bmatrix} = \exp(\iota\omega t)\left[S_{00}^{\mathrm{g}}(\omega)\right]\begin{Bmatrix} x_0^{\mathrm{g}} \\ \theta_0^{\mathrm{g}} \\ z_0^{\mathrm{g}} \end{Bmatrix} \tag{8.290}$$

where ι and t represent $\sqrt{-1}$ and time variable, respectively. Dynamic flexibility matrix is the inverse form of dynamic stiffness matrix. In the case of a ground system with rigid interface (see Figure 8.23), the dynamic flexibility matrix specifies amplitude of displacement $x_0^{\mathrm{g}}, \theta_0^{\mathrm{g}}, z_0^{\mathrm{g}}$ due to unit amplitude of forces $F_x^{\mathrm{g}}, M_y^{\mathrm{g}}, F_z^{\mathrm{g}}$ applied at node 0 of the rigid interface for harmonic motion with excitation frequency ω. This relationship can be expressed as

$$\exp(\iota\omega t)\begin{Bmatrix} x_0^{\mathrm{g}} \\ \theta_0^{\mathrm{g}} \\ z_0^{\mathrm{g}} \end{Bmatrix} = \exp(\iota\omega t)\left[F_{00}^{\mathrm{g}}(\omega)\right]\begin{Bmatrix} F_x^{\mathrm{g}} \\ M_y^{\mathrm{g}} \\ F_z^{\mathrm{g}} \end{Bmatrix} \tag{8.291}$$

with

$$\left[F_{00}^{\mathrm{g}}(\omega)\right] = \left[S_{00}^{\mathrm{g}}(\omega)\right]^{-1} \tag{8.292}$$

where $\left[F_{00}^{\mathrm{g}}(\omega)\right]$ of dimension 3 by 3 is *dynamic flexibility matrix* of ground system with rigid interface for the harmonic motion with excitation frequency ω.

8.6.4.2 Time derivative of flexibility matrix

Differentiating the displacement–force Equation 8.291 with respect to time, and omitting term $\exp(\iota\omega t)$, results in a velocity–force relationship of ground system in harmonic motion as

$$\begin{Bmatrix} \dot{x}_0^{\mathrm{g}} \\ \dot{\theta}_0^{\mathrm{g}} \\ \dot{z}_0^{\mathrm{g}} \end{Bmatrix} = \left[\dot{F}_{00}^{\mathrm{g}}(\omega)\right]\begin{Bmatrix} F_x^{\mathrm{g}} \\ M_y^{\mathrm{g}} \\ F_z^{\mathrm{g}} \end{Bmatrix} \tag{8.293}$$

where $\left[\dot{F}^{\mathrm{g}}_{00}(\omega)\right]$ is a symbolic form, not a derivative, representing the so-called *time–derivative dynamic flexibility matrix* of ground system as shown later in Equation 8.295:

$$\begin{Bmatrix} \dot{x}^{\mathrm{g}}_0 \\ \dot{\theta}^{\mathrm{g}}_0 \\ \dot{z}^{\mathrm{g}}_0 \end{Bmatrix} = \iota\omega \begin{Bmatrix} x^{\mathrm{g}}_0 \\ \theta^{\mathrm{g}}_0 \\ z^{\mathrm{g}}_0 \end{Bmatrix} \tag{8.294}$$

$$\begin{aligned} \left[\dot{F}^{\mathrm{g}}_{00}(\omega)\right] &= \iota\omega \left[F^{\mathrm{g}}_{00}(\omega)\right] = \iota\omega \left[S^{\mathrm{g}}_{00}(\omega)\right]^{-1} \\ &= \begin{bmatrix} \dot{F}^{\mathrm{g}}_{xx} & \dot{F}^{\mathrm{g}}_{x\theta} & 0 \\ \dot{F}^{\mathrm{g}}_{\theta x} & \dot{F}^{\mathrm{g}}_{\theta\theta} & 0 \\ 0 & 0 & \dot{F}^{\mathrm{g}}_{zz} \end{bmatrix} \end{aligned} \tag{8.295}$$

where $\left[\dot{F}^{\mathrm{g}}_{00}(\omega)\right]$ of dimension 3 by 3 specifies *amplitude of velocities* $\dot{x}^{\mathrm{g}}_0$, $\dot{\theta}^{\mathrm{g}}_0$, $\dot{z}^{\mathrm{g}}_0$ due to unit amplitude of forces F^{g}_x, M^{g}_y, F^{g}_z applied at node 0 of the rigid interface for harmonic motion with excitation frequency ω.

8.6.4.3 Flexibility matrix in time domain

Observe Equation 8.27, $\left[\dot{\chi}^{\mathrm{g}}_{00}(m)\right]$ is in time domain because the online control must respond to seismic excitation according to earthquake time–history record. Thus $\left[\dot{F}^{\mathrm{g}}_{00}(\omega)\right]$ in Equation 8.295 needs to be converted to time-domain. Note that Equation 8.294 is a velocity expression of $\dot{x}^{\mathrm{g}}_0$, $\dot{\theta}^{\mathrm{g}}_0$, $\dot{z}^{\mathrm{g}}_0$ at time t for which the velocity amplitude is a series of amplitudes of impulse forces F^{g}_x, M^{g}_y, F^{g}_z. Thus, the velocity can be related to the impulse forces by the following:

$$\begin{Bmatrix} \dot{x}^{\mathrm{g}}_0(t) \\ \dot{\theta}^{\mathrm{g}}_0(t) \\ \dot{z}^{\mathrm{g}}_0(t) \end{Bmatrix} = \int_{-\infty}^{\infty} \left[\dot{\chi}^{\mathrm{g}}_{00}(\tau)\right] \begin{Bmatrix} F^{\mathrm{g}}_x(1-\tau) \\ M^{\mathrm{g}}_y(1-\tau) \\ F^{\mathrm{g}}_z(1-\tau) \end{Bmatrix} \mathrm{d}\tau \tag{8.296}$$

with

$$\left[\dot{\chi}^{\mathrm{g}}_{00}(\tau)\right] = \begin{bmatrix} \dot{\chi}^{\mathrm{g}}_{xx} & \dot{\chi}^{\mathrm{g}}_{x\theta} & 0 \\ \dot{\chi}^{\mathrm{g}}_{\theta x} & \dot{\chi}^{\mathrm{g}}_{\theta\theta} & 0 \\ 0 & 0 & \dot{\chi}^{\mathrm{g}}_{zz} \end{bmatrix} \tag{8.297}$$

where $\left[\dot{\chi}^{\mathrm{g}}_{00}\right]$ is impulse velocity matrix of ground system with rigid interface. Coefficients $\dot{\chi}^{\mathrm{g}}_{xx}$ $\dot{\chi}^{\mathrm{g}}_{x\theta}$ $\dot{\chi}^{\mathrm{g}}_{\theta x}$ $\dot{\chi}^{\mathrm{g}}_{\theta\theta}$ and $\dot{\chi}^{\mathrm{g}}_{zz}$ are velocities at time τ, corresponding to the first subcript's d.o.f. due to a unit impulse force, at time equal to zero, corresponding to the second subscript's d.o.f. Clearly, these coefficients are time-dependent *causal functions*.

This *impulse velocity matrix* $\left[\dot{\chi}_{00}^{\mathrm{g}}(t)\right]$ can be obtained by the *inverse Fourier transformation* of the ground system's time-derivative dynamic flexibility matrix $\left[\dot{F}_{00}^{\mathrm{g}}(\omega)\right]$ in Equation 8.295 as

$$\left[\dot{\chi}_{00}^{\mathrm{g}}(t)\right] = \frac{1}{2\pi}\int_{-\infty}^{\infty}\left[\dot{F}_{00}^{\mathrm{g}}(\tau)\right]\exp(\iota\omega t)\ \mathrm{d}\omega \tag{8.298}$$

Since the soil system's dynamic-stiffness matrices and the time-derivative dynamic-flexibility matrix used in Equation 8.298 are obtained in discrete-frequency domain, the discrete version of inverse Fourier transform applies as

$$\left[\dot{\chi}_{00}^{\mathrm{g}}(n\Delta t)\right] = \frac{\Delta\omega}{2\pi}\sum_{m=1-\mathrm{NS}}^{\mathrm{NS}}\left[\dot{F}_{00}^{\mathrm{g}}(m\Delta\omega)\right]\exp(\iota m\Delta\omega\Delta t) \tag{8.299}$$

where Δt and n are time increments and time-instant number, respectively. $\Delta\omega$ and m are frequency increment and frequency number, respectively. NS is a number of sampling steps where (NS) $\Delta\omega$ and (NS) Δt equal a *truncated frequency* Ω_{T} and time range $T_{\dot{\chi}}$ of impulse velocity function, respectively [1,8].

In the discrete version, the time-derivative dynamic flexibility functions $\dot{F}_{xx}^{\mathrm{g}}(\omega)$, $\dot{F}_{x\theta}^{\mathrm{g}}(\omega)$, $\dot{F}_{\theta x}^{\mathrm{g}}(\omega)$, $\dot{F}_{\theta\theta}^{\mathrm{g}}(\omega)$, $\dot{F}_{zz}^{\mathrm{g}}(\omega)$ in Equation 8.295, non-periodic ones, are truncated at an arbitrary frequency. This truncated frequency Ω_{T} must include all predominant frequencies of total dynamic system, ground system, and incident waves. As a result of the truncation, band-limited functions having frequency range from $-\Omega_{\mathrm{T}}$ to Ω_{T} are formed. Then periodic extensions of these band-limited functions, required by the form of Equation 8.299 are used in the transformation. Therefore, only within time range $\left[-T_{\dot{\chi}}, T_{\dot{\chi}}\right]$ is the discrete version in Equation 8.299 similar to the continuous version in Equation 8.298.

Truncated frequency Ω_{T} dictates a size of time increment Δt. Size of frequency increment $\Delta\omega$ depends on a number of sampling steps, NS. Their relationship can be expressed as

$$\Delta t = \frac{\pi}{\Omega_{\mathrm{T}}} = \frac{\pi}{(\mathrm{NS})\ \Delta\omega} \tag{8.300}$$

and

$$\Delta\omega = \frac{\Omega_{\mathrm{T}}}{\mathrm{NS}} = \frac{\pi}{(\mathrm{NS})\ \Delta t} = \frac{\pi}{T_{\dot{\chi}}} \tag{8.301}$$

According to Equation 8.300, if truncated frequency Ω_{T} is too small (not including all predominant frequencies), time increment Δt will be too large for discrete representation of the continuous functions of the entire dynamic system's response, impulse velocity, and earthquake excitation. Since impulse velocity functions attenuate as time goes on and the discrete version's precision is only within a time range $\left[-T_{\dot{\chi}}, T_{\dot{\chi}}\right]$ where $T_{\dot{\chi}} = (\mathrm{NS})\Delta t$, this time range must cover all significant ranges of impulse velocity functions and beyond. (From a practical point of

view, $T_{\dot{\chi}}$ should double the significant limit of impulse velocity functions to guarantee causality condition.) Therefore, the number of sampling steps, NS, needs to be large enough to cover these ranges. According to Equation 8.301, NS must also be large enough to make frequency increment $\Delta\omega$ small enough for discrete representation of the continuous band-limited functions of time-derivative flexibility functions $\dot{F}^{\mathrm{g}}_{xx}(\omega)$, $\dot{F}^{\mathrm{g}}_{x\theta}(\omega)$, $\dot{F}^{\mathrm{g}}_{\theta x}(\omega)$, $\dot{F}^{\mathrm{g}}_{\theta\theta}(\omega)$, $\dot{F}^{\mathrm{g}}_{zz}(\omega)$.

Band-limited sequence of the time derivative flexibility matrix $\left[\dot{F}^{\mathrm{g}}_{00}(m\Delta\omega)\right]$, from frequency $-(\mathrm{NS}-1)\,\Delta\omega$ to $(\mathrm{NS}-1)\,\Delta\omega$, is used for the transformation in Equation 8.299. Knowing that the time-derivative flexibility pair corresponds to a positive–negative frequency pair is complex conjugate, the band-limited sequence can be constructed from a given sequence along the positive half of the frequency range. This complex conjugate relationship can be proved by substituting a positive–negative frequency pair in the discrete Fourier transform formula for a causal function. This formula describes time-derivative flexibility matrix as

$$\left[\dot{F}^{\mathrm{g}}_{00}(m\Delta\omega)\right] = \Delta t \sum_{n=0}^{\mathrm{NS}} \left[\dot{\chi}^{\mathrm{g}}_{00}(n\Delta t)\right] \exp(-\iota m\Delta\omega n\Delta t) \tag{8.302}$$

Substituting $m = l$

$$\begin{aligned}
&\left[\dot{F}^{\mathrm{g}}_{00}(l\Delta\omega)\right] \\
&\quad = \Delta t \sum_{n=0}^{\mathrm{NS}} \left[\dot{\chi}^{\mathrm{g}}_{00}(n\Delta t)\right] \exp(-\iota l\Delta\omega n\Delta t) \\
&\quad = \cos(l\Delta\omega n\Delta t)\,\Delta t \sum_{n=0}^{\mathrm{NS}} \left[\dot{\chi}^{\mathrm{g}}_{00}(n\Delta t)\right] - \iota \sin(l\Delta\omega n\Delta t)\,\Delta t \sum_{n=0}^{\mathrm{NS}} \left[\dot{\chi}^{\mathrm{g}}_{00}(n\Delta t)\right]
\end{aligned} \tag{8.303}$$

Substituting $m = -l$

$$\begin{aligned}
&\left[\dot{F}^{\mathrm{g}}_{00}(-l\Delta\omega)\right] \\
&\quad = \Delta t \sum_{n=0}^{\mathrm{NS}} \left[\dot{\chi}^{\mathrm{g}}_{00}(n\Delta t)\right] \exp(\iota l\Delta\omega n\Delta t) \\
&\quad = \cos(l\Delta\omega n\Delta t)\,\Delta t \sum_{n=0}^{\mathrm{NS}} \left[\dot{\chi}^{\mathrm{g}}_{00}(n\Delta t)\right] + \iota \sin(l\Delta\omega n\Delta t)\,\Delta t \sum_{n=0}^{\mathrm{NS}} \left[\dot{\chi}^{\mathrm{g}}_{00}(n\Delta t)\right]
\end{aligned} \tag{8.304}$$

Equations 8.303 and 8.304 always form a complex conjugate pair because signs of their imaginary part are opposite for any integer l.

Phase angle of impulse velocity response is assumed to be either 0° or 180°. Impulse velocity functions $\dot{\chi}^{g}_{xx}(t)$, $\dot{\chi}^{g}_{x\theta}(t)$, $\dot{\chi}^{g}_{\theta x}(t)$, $\dot{\chi}^{g}_{\theta\theta}(t)$, $\dot{\chi}^{g}_{zz}(t)$ are then assumed to be real number. Therefore the following properties are applied.

1. Impulse velocity function $\dot{\chi}(t)$ can be expressed as the sum of an even part $\dot{\chi}_{e}(t)$ and an odd part $\dot{\chi}_{o}(t)$

$$\dot{\chi}(t) = \dot{\chi}_{e}(t) + \dot{\chi}_{o}(t) \tag{8.305}$$

2. The even part $\dot{\chi}_{e}(t)$ or conjugate-symmetric one, can be obtained by inverse Fourier transform of the real part of time-derivative flexibility $\dot{F}(\omega)$. If the even part is defined as

$$\dot{\chi}_{e}(t) = \dot{\chi}_{e}(-t) \quad \text{and} \quad \dot{\chi}_{e}(0) = \dot{\chi}(0) \tag{8.306}$$

then

$$\dot{\chi}_{e}(t) = \frac{1}{2\pi}\int_{-\infty}^{\infty} \text{Real}\left(\dot{F}(\omega)\right)\exp(\iota\omega t)\ \mathrm{d}\omega \tag{8.307}$$

3. The odd part $\dot{\chi}_{o}(t)$or conjugate-antisymmetric one, can be obtained by inverse Fourier transform of the imaginary part of time derivative flexibility $\dot{F}(\omega)$. If the odd part is defined as

$$\dot{\chi}_{o}(t) = \dot{\chi}_{o}(-t) \quad \text{and} \quad \dot{\chi}_{o}(0) = 0 \tag{8.308}$$

then

$$\dot{\chi}_{o}(t) = \frac{1}{2\pi}\int_{-\infty}^{\infty} \text{Imag}\left(\dot{F}(\omega)\right)\exp(\iota\omega t)\ \mathrm{d}\omega \tag{8.309}$$

Impulse velocity function $\dot{\chi}(t)$ is casual (amplitude of functions equals zero for time $t < 0$). Therefore, for $t < 0$, the summation of even and odd parts must be zero. Their relationship can be expressed as

$$\dot{\chi}_{e}(t) = -\dot{\chi}_{o}(t) \quad \text{for time } t < 0 \tag{8.310}$$

Using Equations 8.305, 8.306, and 8.308 and the *causality condition* in Equation 8.310, impulse velocity function can be expressed in terms of either an even part or an odd part as

$$\dot{\chi}(t) = 2\dot{\chi}_{e}(t)\,U(t) - \dot{\chi}_{e}(0)\,\delta t \tag{8.311}$$

and

$$\dot{\chi}\,(t) = 2\dot{\chi}_{\mathrm{o}}\,(t)\,U\,(t) + \dot{\chi}\,(0)\,\delta t \tag{8.312}$$

where $U(t)$ is a unit step function in the interval of time t greater than or equal to zero. $\delta\,(t)$ is the Dirac-delta function equal to 1 at time t equal to zero. It should be noted that impulse velocity function $\dot{\chi}(t)$, for $t = 0$, cannot be determined by using the odd part alone (see Equation 8.312).

Therefore, by using Equations 8.307 and 8.311, impulse velocity function $\dot{\chi}\,(t)$ can be determined by using only the real part of $\dot{F}(\omega)$as

$$\dot{\chi}\,(0) = \frac{1}{2\pi}\int_{-\infty}^{\infty} \mathrm{Real}\left(\dot{F}(\omega)\right)\mathrm{d}\omega \quad \text{for time } t = 0 \tag{8.313}$$

and

$$\dot{\chi}\,(t) = \frac{1}{\pi}\int_{-\infty}^{\infty} \mathrm{Real}\left(\dot{F}(\omega)\right)\exp(\iota\omega t)\,\mathrm{d}\omega \quad \text{for time } t > 0 \tag{8.314}$$

For a ground system with rigid interface, discrete impulse velocity matrix can be obtained by applying the discrete version of transformation (Equation 8.299) and its complex conjugate property (demonstrated in Equations 8.303 and 8.304) to Equations 8.313 and 8.314 as

$$\begin{aligned}\left[\dot{\chi}^{\mathrm{g}}_{00}\,(0)\right] &= \frac{\Delta\omega}{2\pi}\sum_{m=1-\mathrm{NS}}^{\mathrm{NS}} \mathrm{Real}\left(\left[\dot{F}^{\mathrm{g}}_{00}\,(m\Delta\omega)\right]\right)\\ &= \frac{\Delta\omega}{\pi}\sum_{m=1}^{\mathrm{NS}-1} \mathrm{Real}\left(\left[\dot{F}^{\mathrm{g}}_{00}\,(m\Delta\omega)\right]\right) + \frac{\Delta\omega}{2\pi}\mathrm{Real}\left(\left[\dot{F}^{\mathrm{g}}_{00}\,(\Omega_{\mathrm{T}})\right]\right)\end{aligned} \tag{8.315}$$

and

$$\begin{aligned}\left[\dot{\chi}^{\mathrm{g}}_{00}\,(n\Delta t)\right] &= \frac{\Delta\omega}{\pi}\sum_{m=1-\mathrm{NS}}^{\mathrm{NS}} \mathrm{Real}\left(\left[\dot{F}^{\mathrm{g}}_{00}\,(m\Delta\omega)\right]\right)\exp(\iota m\Delta\omega n\Delta t)\\ &\qquad \text{for } n = 1, 2, \ldots, \mathrm{NS}\end{aligned} \tag{8.316}$$

Note that the static components of the ground system's time-derivative flexibility matrix $\left[\dot{F}^{\mathrm{g}}_{00}(\omega) = 0\right]$ always equal zero (see Equation 8.295). Therefore, those of ground system's stiffness matrix need not to be determined. Only the dynamic-stiffness matrices on the positive half of frequency range are needed due to their complex conjugate property. To minimize computing time, *Fast Fourier Transform* (FTT), an efficient technique of calculating discrete Fourier transform, is employed [1,8].

8.7 Numerical Illustrations

The mathematical formulations and concepts presented in earlier sections of this chapter are now illustrated with numerical examples in this section. Since the equations were derived according to the fundamental concepts of various disciples of soils, earthquake waves, SSI, and control. The number of equation is numerous and the sequential order of the equation number is based on the theoretical developments. For numerical illustrations, only portions of the equations are needed and they are not in the order of equation derivations. For reader's convenience, the equations used in the numerical examples are rewritten along with the original equation number.

8.7.1 Solution Procedure of SSI System without Control

EXAMPLE 8.7.1

A single-story shear building shown in Figure 8.4 is constructed on a rectangular mat foundation embedded in half-space. Their properties are described as

Structure floor: mass (m_1)	0.54 kton
Moment of inertia with respect to point 0 (I_1)	148.14 kton-m^2
Height (h_1)	15.0 m
Width(w_s)	5.0 m
EI	9368.4141 MN-m^2
β_1	2%
Foundation: Mass(m_0)	0.108 kton
Moment of inertia w/respect to point 0 (I_0)	0.405 kton-m^2
Depth ($2h_0$)	1.5 m
Width (w_f)	6.0 m
Half-space: Mass density	2.0 gram/cm^3
Poisson's ratio	0.33
Shear modulus	320 MN/m^2
Shear wave velocity	400 m/s
Hysteretic damping ratio	0.05

Assume the structure is subjected to 1940 N-S EI Centro earthquake; find the structural response without control.

Solution

Since the building configuration is given in Figure 8.4, the motion of equation of the structure already established in Equation 8.2 is rewritten as

$$[M]\left\{\ddot{X}\right\} + [K]\{X\} + [C]\left\{\dot{X}\right\} = \{\delta\}\,\ddot{x}_0^{\mathrm{g}} + \{\gamma\}\,\vec{U} + \{R\} \tag{a}$$

in which

$$[M] = \begin{bmatrix} 0.54 & 0 & 0 \\ 0 & 0.108 & -0.75(0.108) \\ -16.5(0.54) & -0.75(0.108) & 148.14 + 0.405 + (0.75)^2 0.108 \end{bmatrix}$$
$$= \begin{bmatrix} 0.54 & 0 & 0 \\ 0 & 0.108 & -0.081 \\ -8.91 & -0.081 & 148.60575 \end{bmatrix} \quad \text{(b)}$$

The structural stiffness is $k_1 = 12EI/L^3 = (12)9368.4141/15^3 = 33.3099$ MN/m, and the structural damping coefficient is $C_1 = 2\beta_1\sqrt{k_1 m_1} = 2(0.02)\sqrt{33.3099(0.54)} = 0.169$ MN s/m^2. Thus the damping matrix is

$$[C] = \begin{bmatrix} 0.169 & -0.169 & 16.5(0.169) \\ -0.169 & 0.169 & -16.5(0.169) \\ 0 & 0 & 0 \end{bmatrix}$$
$$= \begin{bmatrix} 0.169 & -0.169 & 2.789 \\ -0.169 & 0.169 & -2.789 \\ 0 & 0 & 0 \end{bmatrix} \quad \text{(c)}$$

and the stiffness matrix is

$$[K] = \begin{bmatrix} 33.3099 & -33.3099 & 16.5(33.3099) \\ -33.3099 & 33.3099 & -16.5(33.3099) \\ 0 & 0 & 0 \end{bmatrix}$$
$$= \begin{bmatrix} 33.3099 & -33.3099 & 549.6134 \\ -33.3099 & 33.3099 & -549.6134 \\ 0 & 0 & 0 \end{bmatrix} \quad \text{(d)}$$

The acceleration coefficient vector is

$$\{\delta\} = \begin{bmatrix} -0.54 \\ -0.108 \\ 16.5(0.54) + 0.75(0.108) \end{bmatrix}^{\mathrm{T}} = \begin{bmatrix} -0.54 \\ -0.108 \\ 8.991 \end{bmatrix} \quad \text{(e)}$$

At point 0 of foundation–soil interface, the interaction force and displacement vector can be expressed as

$$\{R_0\} = \begin{bmatrix} R_x \\ R_\theta \end{bmatrix} \quad \text{and} \quad \left\{X_0^{\mathrm{tg}}\right\} = \begin{bmatrix} x_0^{\mathrm{tg}} \\ \theta_0^{\mathrm{tg}} \end{bmatrix} \quad \text{(f)}$$

The interaction force vector relates to the displacement vector can be found using Equations 8.25 through 8.27 for $\{R_0(n)\}$, $[\tilde{K}_{00}]$, $\{\tilde{R}_0(n-1)\}$. The time

derivative dynamic flexibility matrix of ground syatem at $t = 0$ is obtained by using Equations 8.297 with numerical procedures in Equations 8.315 and 8.136 as

$$\left[\dot{F}_{00}^{g}(0)\right] = \begin{bmatrix} 14.7321 & 0.8429 \\ 0.8429 & 1.9208 \end{bmatrix} \tag{g}$$

for which $\Delta\omega = 0.1571$ rad/s and NS = 3200. Therefore, $\left[\tilde{K}_{00}\right]$ in Equation 8.26 can be determined for $\Delta t = 0.00625$sec associated with $n = 1$ as

$$\left[\tilde{K}_{00}\right] = \frac{2}{(0.00625)^2}\begin{bmatrix} 14.7321 & 0.8429 \\ 0.8429 & 1.9208 \end{bmatrix}^{-1} = \begin{bmatrix} 3564.91 & -1564.38 \\ -1564.38 & 27342.1 \end{bmatrix} \tag{h}$$

Thus, $\left[\dot{F}_{00}^{g}(n\Delta t)\right]$ for n = 1,…, 160 are obtained, as

$$\left[\dot{F}_{00}^{g}(n)\right] = \begin{bmatrix} A & B \\ B & C \end{bmatrix} \tag{i}$$

where A, B, C are calculated by computer for $n = 1$ through 60 of which typical results corresponding to $n = 1, 2, 59$, and 60 are given in the following (using $\Delta\omega = 0.1571$ rad/s and NS = 3200):

n	t	A	B	C
1	0.006	−0.557462E + 01	−0.801356E + 00	−0.139152E + 01
2	0.013	−0.271077E + 01	−0.271282E + 00	−0.473180E + 00
⋮				
59	0.369	−0.734280E − 02	0.133634E − 03	−0.297111E − 04
60	0.375	−0.473949E − 02	−0.141021E − 03	−0.501287E − 04

Note that Equation 8.2 or Equation a can be rewritten in submatrix form corresponding to structure and foundation d.o.f. as shown in Equation 8.3 for which the state equation force is shown in Equation 8.31 as $\left\{\dot{Z}^{tg}(n)\right\}$ with submatrices in Equations 8.32 through 8.37 representing $\{Z^{tg}(n)\}$, $[A]$, $[A_K]$, $[A_C]$, $[B]$, $[C]$, and $\{\tilde{R}_0(n-1)\}$, respectively. $\{Z^{tg}(n)\}$ is signified by

Equation 8.30a. Thus,

$$[A_K] = \begin{bmatrix} 0.54 & 0 & 0 \\ 0 & 0.108 & -0.081 \\ -8.91 & -0.081 & 148.60575 \end{bmatrix}^{-1} \times \begin{bmatrix} 33.3099 & -33.3099 & 549.6134 \\ -33.3099 & 33.3099 + 3564.91 & -549.6134 - 1564.38 \\ 0 & -1564.38 & 27342.1 \end{bmatrix} = \begin{bmatrix} 61.685 & -61.685 & 1017.8 \\ -305.776 & 33319.8 & -19398.4 \\ 3.5318 & 3.9359 & 234.442 \end{bmatrix} \quad \text{(j)}$$

$$[A_C] = \begin{bmatrix} 0.54 & 0 & 0 \\ 0 & 0.108 & -0.081 \\ -8.91 & -0.081 & 148.60575 \end{bmatrix}^{-1} \begin{bmatrix} 0.169 & -0.169 & 2.789 \\ -0.169 & 0.169 & -2.789 \\ 0 & 0 & 0 \end{bmatrix} = \begin{bmatrix} 0.312963 & -0.312963 & 5.16481 \\ -1.55138 & 1.55138 & -25.6023 \\ 0.0179 & -0.0179 & 0.2957 \end{bmatrix} \quad \text{(k)}$$

$$[A] = \begin{bmatrix} 0 & 0 & 0 & 1 & 0 & 0 \\ 0 & 0 & 0 & 0 & 1 & 0 \\ 0 & 0 & 0 & 0 & 0 & 1 \\ -61.685 & 61.685 & -1017.8 & -0.312963 & 0.312963 & -5.16481 \\ 305.776 & -33319.8 & 19398.4 & 1.55138 & -1.55138 & 25.6023 \\ -3.5318 & -3.9359 & -234.442 & -0.0179 & 0.0179 & -0.2957 \end{bmatrix} \quad \text{(l)}$$

$$[B] = \begin{bmatrix} 0 \\ 0 \\ 0 \\ \begin{bmatrix} 0.54 & 0 & 0 \\ 0 & 0.108 & -0.081 \\ -8.91 & -0.081 & 148.60575 \end{bmatrix}^{-1} \begin{bmatrix} -1 \\ 1 \\ 0 \end{bmatrix} \end{bmatrix} = \begin{bmatrix} 0 \\ 0 \\ 0 \\ -1.85185 \\ -9.17974 \\ -0.106028 \end{bmatrix} \quad \text{(m)}$$

$$[C] = \begin{bmatrix} 0 \\ 0 \\ 0 \\ \begin{bmatrix} 0.54 & 0 & 0 \\ 0 & 0.108 & -0.081 \\ -8.91 & -0.081 & 148.60575 \end{bmatrix}^{-1} \begin{bmatrix} -0.54 \\ -0.108 \\ 8.991 \end{bmatrix} \end{bmatrix} = \begin{bmatrix} 0 \\ 0 \\ 0 \\ -1 \\ -1 \\ 0 \end{bmatrix} \quad \text{(n)}$$

For a closed-loop control, the control force is related to the displacement by a gain matrix for which we have formulas given in Equations 8.38 through 8.41 representing $\left\{\vec{U}(n)\right\}$, $\left\{\dot{Z}^{\text{tg}}(n)\right\}$, $[D]$, and $\{E(n)\}$, respectively. For the given structure without control, $\left[G^{\text{SSI}}\right]$ is not applicable and the second term of Equation 8.40 should be omitted. Therefore,

$$[D] = [A] = \text{Equation (l)} \tag{o}$$

Ground acceleration at point 0 is subjected to be 1940 N-S EI Centro earthquake of which a few sample data are given as follows:

t (s)	$\ddot{x}_0^{\text{g}}$ (m/s^2)	t (s)	$\ddot{x}_0^{\text{g}}$ (m/s^2)	t (s)	$\ddot{x}_0^{\text{g}}$ (m/s^2)
0.00625	0.0268941	0.11875	0.0209321	0.23125	0.1193730
0.01250	0.0537882	0.12500	0.0151565	0.23750	0.1259408
⋮					
7.21875	0.8469194	7.35625	0.16155535	7.49375	−0.6268811
7.22500	0.8736786	7.36250	0.1072675	7.50000	−0.5913664

Solution of the differential equation of Equation 8.39 $\left\{\dot{Z}^{\text{tg}}(n)\right\}$ is given in Equation 8.47 as $\{Z(n)\}$ for which the relevant matrices of $[T]$, $\{\Gamma(n)\}$, $[\exp([\Lambda]\,t)]$, $[\exp([\Lambda_i]\,t)]$, $\{\Phi(n)\}$, $\{\Pi(n-1)\}$ are given in Equations 8.43, 8.49, 8.54, 8.55, 8.57, and 8.59, respectively.

For Equation 8.43, the plant matrix $[D]$ (see Equation o) yields eigenvalues shown in Equation p and eigenvectors in Equation q (only with ith value shown here), respectively.

$$\mu_i \pm \nu_i \iota\text{:}$$
$$\begin{cases} -0.06989 \pm 6.56059\iota, & i = 1 \\ -0.228733 \pm 15.9561\,\iota, & i = 2 \\ -0.784867 \pm 182.528\,\iota, & i = 3 \end{cases} \tag{p}$$

In Equation p, the imaginary part ν_i of eigenvalues can be interpreted as a damped free vibration frequency ω and $-\mu/\nu$ as a damping ratio as

$$\begin{cases} \omega_1 = 6.56 \text{ rad/s} = 1.044 \text{ Hz}; & \omega_2 = 15.96 \text{ rad/s} = 2.539 \text{ Hz}; \\ \omega_3 = 82.53 \text{ rad/s} = 29.05 \text{ Hz}; & \beta_1 = 0.06989/6.56059 = 0.0107; \\ \beta_2 = 0.228733/15.9561 = 0.0143; & \beta_3 = 0.784867/182.528 = 0.0043; \end{cases} \tag{q}$$

$\{a_i\} \pm \{b_i\}\, \iota$:

$$\left\{ \begin{bmatrix} -1.62361 \times 10^{-3} \\ -1.07401 \times 10^{-5} \\ -4.87957 \times 10^{-5} \\ 1.0 \\ -1.54656 \times 10^{-3} \\ -1.84182 \times 10^{-2} \end{bmatrix} \pm \begin{bmatrix} 0.1524078 \\ -2.35964 \times 10^{-4} \\ -2.80792 \times 10^{-3} \\ 0 \\ 8.62127 \times 10^{-5} \\ 5.16379 \times 10^{-4} \end{bmatrix} \iota, \quad i = 1 \right.$$

$$\left\{ \begin{bmatrix} -8.97797 \times 10^{-4} \\ -4.08421 \times 10^{-4} \\ -1.01518 \times 10^{-3} \\ 1.0 \\ 0.1245738 \\ 0.1963721 \end{bmatrix} \pm \begin{bmatrix} 6.26453 \times 10^{-2} \\ 7.79954 \times 10^{-3} \\ 1.22898 \times 10^{-2} \\ 1.49012 \times 10^{-8} \\ 4.73768 \times 10^{-3} \\ 1.33908 \times 10^{-2} \end{bmatrix} \iota, \quad i = 2 \right. \tag{r}$$

$$\left\{ \begin{bmatrix} -9.32613 \times 10^{-6} \\ -2.35579 \times 10^{-5} \\ -5.52762 \times 10^{-7} \\ -1.85285 \times 10^{-3} \\ 0.9999999 \\ 1.18674 \times 10^{-4} \end{bmatrix} \pm \begin{bmatrix} -1.01928 \times 10^{-5} \\ 5.47851 \times 10^{-3} \\ 6.47687 \times 10^{-7} \\ 1.71029 \times 10^{-3} \\ 0 \\ 1.00388 \times 10^{-4} \end{bmatrix} \iota, \quad i = 3 \right.$$

The transformation matrix in $[T]$ in Equation 8.43 can be written a

$$[T] = \begin{bmatrix} -1.62361 & 152.4078 & -.897797 & 62.6453 & -.00932613 & -.0101928 \\ -.0107401 & -.235964 & -.408421 & 7.79954 & -.0235579 & 5.47851 \\ -.0487957 & -2.80792 & -1.01518 & 12.2898 & -.000552762 & .000647687 \\ 1000 & 0 & 1000 & .0000149012 & -1.85285 & 1.71029 \\ -1.54656 & .0862127 & 124.5738 & 4.73768 & 999.9999 & 0 \\ -18.4182 & .516379 & 196.3721 & 13.3908 & .118674 & .100388 \end{bmatrix} \times 10^{-3} \tag{s}$$

of which the inversion is

$$[T]^{-1} = \begin{bmatrix} -101.2986 & -201.044 & 4662.54 & 914.9927 & 2.24439 & -4636.76 \\ -6001.28 & 15.9689 & -30429.5 & 5.36387 & .06812 & -157.10 \\ -98.3985 & 111.139 & -4478.99 & 85.0049 & -.398673 & 4635.9 \\ 1363.51 & -15.95 & 74070.22 & 11.8802 & .0362996 & 328.50 \\ -5.43729 & 13.6082 & 216.8785 & -9.23106 & 1000.05 & -586.23 \\ -1689.81 & 182546.1 & -107085 & -8.59120 & 4.22621 & -140.6 \end{bmatrix} \times 10^{-3} \tag{t}$$

Verify the transformation matrix $[T]$ by Equation 8.44, $[T]^{-1}[D][T] = [\Lambda]$, in which detailed matrices are given in Equations 8.45 and 8.46. Thus,

$$[T]^{-1}[D][T] = \begin{bmatrix} -.0699 & -6.56059 & 0 & 0 & 0 & 0 \\ 6.5606 & -.0699 & 0 & 0 & 0 & 0 \\ 0 & 0 & -0.228732 & -15.9596 & 0 & 0 \\ 0 & 0 & 15.9596 & -0.228736 & 0 & 0 \\ 0 & 0 & 0 & 0 & -0.784868 & -182.528 \\ 0 & 0 & 0 & 0 & -182.5279 & -0.78488 \end{bmatrix} \quad \text{(u)}$$

which confirms $[T]^{-1}[D][T] \cong [\Lambda]$ as Equations p and u are approximately identical.

For $[\exp([\Lambda]\,\Delta t)]$ in Equation 8.54, the numerical results are given in Equation v for $\Delta t = 0.00625$

$$[\exp([\Lambda]\,\Delta t)] = \begin{bmatrix} 0.99872 & -0.04097 & 0 & 0 & 0 & 0 \\ 0.04097 & 0.99872 & 0 & 0 & 0 & 0 \\ 0 & 0 & 0.99361 & -0.09944 & 0 & 0 \\ 0 & 0 & 0.09944 & 0.99361 & 0 & 0 \\ 0 & 0 & 0 & 0 & 0.41483 & -0.90453 \\ 0 & 0 & 0 & 0 & 0.90453 & 0.41483 \end{bmatrix} \quad \text{(v)}$$

where the numerical values of first row is calculated from Equation 8.55 as follows:

$$\begin{aligned} \exp(\mu_i \Delta t)\cos(\nu_i \Delta t) &= \exp[0.00625\,(-0.06989)]\cos[0.00625\,(-6.56059)] \\ &= 0.99956(0.99916) = 0.99872;\ i = 1 \\ \exp(\mu_i \Delta t)\sin(\nu_i \Delta t) &= \exp[0.00625\,(-0.06989)]\sin[0.00625\,(-6.56059)] \\ &= 0.99956(-0.04099) = -0.04097;\ \ i = 1 \end{aligned}$$

The response analysis includes using Equations 8.41, $\{E(n)\}$, 8.49, $\{\Gamma(n)\}$, and 8.59, $\{\Pi(n-1)\}$, which respectively yield the results in Equations w, x, and y for $t = 0$ $(n = 0)$, as well as Equations z, aa, and bb at $\Delta t = 0.00625$ $(n = 1)$.

At $t = 0$ $(n = 0)$

$$\{E(0)\} = \{C\}\ddot{x}_0^{\mathrm{g}}(0) + \{\check{R}_0(0-1)\} = \{0\} \tag{w}$$

$$\{\Gamma(0)\} = [T]^{-1}\{E(0)\} = \{0\} \tag{x}$$

$$\{\Pi(0)\} = [\exp([\Lambda]\Delta t)][\{\Pi(-1) + 0.00625\}\{\Gamma(0)\}] = \{0\} \tag{y}$$

At $t = 0.00625$ $(n = 1)$

$$\begin{aligned}\{E(1)\} &= \begin{bmatrix}0 & 0 & 0 & -1 & -1 & 0\end{bmatrix}^{\mathrm{T}} 0.0268941 + \{\check{R}_0(0)\} \\ &= \begin{bmatrix}0 & 0 & 0 & -0.0268941 & -0.0268941 & 0\end{bmatrix}^{\mathrm{T}}\end{aligned} \tag{z}$$

where $\{\check{R}_0(0)\} = 0$. From Equation 8.49

$$\begin{aligned}&\{\Gamma(1)\} \\ &= [T]^{-1}\{E(1)\} \\ &= \begin{bmatrix}-24.6683 & -0.146088 & -2.27541 & -0.320484 & -26.6472 & 0.117392\end{bmatrix}^{\mathrm{T}} \times 10^{-3}\end{aligned} \tag{aa}$$

$$\begin{aligned}&\{\Pi(1)\} \\ &= [\exp([\Lambda]\Delta t)][\{\Pi(0)\} + 0.00625\ \{\Gamma(1)\}] \\ &= \begin{bmatrix}-0.15394 & -0.00723 & -0.01393 & -0.00034 & -0.06975 & -0.15034\end{bmatrix}^{\mathrm{T}} \times 10^{-3}\end{aligned} \tag{bb}$$

Using Equation 8.57 yields

$$\begin{aligned}&\{\Phi(1)\} \\ &= \{\Pi(0)\} + \frac{0.00625}{2}\{\Gamma(1)\} \\ &= \begin{bmatrix}-0.07709 & -0.00046 & -0.00711 & -0.001 & -0.08327 & 0.000037\end{bmatrix}^{\mathrm{T}} \times 10^{-3}\end{aligned} \tag{cc}$$

For Equation 8.47, we have

$$\{Z(1)\} = [T]\{\Phi(1)\} = \begin{bmatrix}0 & 0 & 0 & -0.00008408 & -0.00008408 & 0\end{bmatrix}^{\mathrm{T}} \tag{dd}$$

Similarly for Equation 8.47, we have

$$\begin{aligned}\left\{\dot{Z}(1)\right\} &= [D]\{Z(1)\} + \{E(1)\} \\ &= [-0.00008408 \quad -0.00008408 \quad 0 \quad -0.0268941 \quad -0.0268941]^{\mathrm{T}}\end{aligned} \tag{ee}$$

Using Equations 8.27 and 8.25 yields Equations ff and gg, respectively

$$\left\{\tilde{R}_0(0)\right\} = \left[\tilde{K}_{00}\right] \times \left[\left\{X_0^{\mathrm{tg}}(0)\right\} + \frac{\Delta t}{2}\left(\left\{\dot{X}_0^{\mathrm{tg}}(0)\right\} + \Delta t \sum_{m=1}^{160}\left[\dot{\chi}_{00}^{\mathrm{g}}(m)\right]\{R_0(1-m)\}\right)\right] = \{0\} \tag{ff}$$

$$\{R_0(1)\} = \left[\tilde{K}_{00}\right]\left\{X_0^{\mathrm{tg}}(1)\right\} - \left\{\tilde{R}_0(0)\right\} = \{0\} \tag{gg}$$

in which $\left\{X_0^{\mathrm{tg}}(0)\right\}$, $\left\{\dot{X}_0^{\mathrm{tg}}(0)\right\}$, $\{R_0(1-m)\}$, and $\left\{\dot{X}_0^{\mathrm{tg}}(1)\right\}$ are all zero. Note that $\{R_0\}$ represent R_x and R_θ as explained in Equation ff, which can also be obtained by using structure's free-body diagram shown in Figure 8.5, the interacting forces at the footing base $(R_x, R_\theta)$and the shear at the column end $\left(S_{\mathrm{base}}^{\mathrm{SSI}}, M_{\mathrm{base}}^{\mathrm{SSI}}\right)$ are expressed in Equations hh through kk

$$R_x = -\sum_{i=1}^{\mathrm{NO}} m_i(\ddot{x}_i^{\mathrm{tg}} + \ddot{x}_0^{\mathrm{g}}) - m_0(\ddot{x}_0^{\mathrm{tg}} + \ddot{x}_0^{\mathrm{g}} - h_{\mathrm{a}0}\ddot{\theta}_0^{\mathrm{tg}}) \tag{hh}$$

$$R_\theta = -\sum_{i=1}^{\mathrm{NO}} I_i\ddot{\theta}_0^{\mathrm{tg}} - I_0\ddot{\theta}_0^{\mathrm{tg}} + \sum_{i=1}^{\mathrm{NO}} m_i h_{\mathrm{a}i}(\ddot{x}_i^{\mathrm{tg}} + \ddot{x}_0^{\mathrm{g}}) + m_0 h_0(\ddot{x}_0^{\mathrm{tg}} + \ddot{x}_0^{\mathrm{g}} - h_{\mathrm{a}0}\ddot{\theta}_0^{\mathrm{tg}}) \tag{ii}$$

$$S_{\mathrm{base}}^{\mathrm{SSI}} = -\sum_{i=1}^{\mathrm{NO}} m_i(\ddot{x}_i^{\mathrm{tg}} + \ddot{x}_0^{\mathrm{g}}) \tag{jj}$$

$$M_{\mathrm{base}}^{\mathrm{SSI}} = -\sum_{i=1}^{\mathrm{NO}} I_i\ddot{\theta}_0^{\mathrm{tg}} + \sum_{i=1}^{\mathrm{NO}} m_i(h_{\mathrm{a}i} - 2h_0)(\ddot{x}_i^{\mathrm{tg}} + \ddot{x}_0^{\mathrm{g}}) \tag{kk}$$

Substituting appropriate data into Equations hh through kk yields the following results:

$$R_x = -0.54(-0.0268941 + 0.0268941) - 0.108(-0.0268941 + 0.0268941 - 0.75(0)) = 0 \tag{ll}$$

$$R_\theta = -148.14(0) - 0.405(0) + 0.54(16.5)(-0.0268941 + 0.0268941) + 0.108(0.75)(-0.0268941 + 0.0268941 - 0.75(0)) = 0 \tag{mm}$$

$$S_{\mathrm{base}}^{\mathrm{SSI}} = -0.54(-0.0268941 + 0.0268941) = 0 \tag{nn}$$

$$M_{\mathrm{base}}^{\mathrm{SSI}} = -148.14(0) + 0.54(15.0)(-0.0268941 + 0.0268941) = 0 \tag{oo}$$

The results in Equations ll and mm confirm that in Equation gg.

At $t = 0.00125$ $(n = 2)$

From Equation 8.41 along with Equations 8.36 and 8.37, we have

$$\{E(2)\} = \begin{bmatrix} 0 \\ 0 \\ 0 \\ -1 \\ -1 \\ 0 \end{bmatrix} 0.0537882 + \left[\begin{bmatrix} & & 0 \\ & & 0 \\ & & 0 \\ \begin{bmatrix} 0.54 & 0 & 0 \\ 0 & 0.108 & -0.081 \\ -8.91 & -0.081 & 148.60575 \end{bmatrix}^{-1} & & \begin{bmatrix} 0 \\ -0.00093668 \\ 0.00041104 \end{bmatrix} \end{bmatrix} \right]$$

$$= \begin{bmatrix} 0 & 0 & 0 & -0.0537882 & -0.0624626 & -0.0000020 \end{bmatrix}^{\mathrm{T}} \quad \text{(pp)}$$

for which $\left\{\tilde{R}_0(1)\right\}$ is from Equation 8.27 as

$$\left\{\tilde{R}_0(1)\right\} = \left[\tilde{K}_{00}\right] \left[\left\{X_0^{\mathrm{tg}}(1)\right\} + \frac{0.00625}{2} \times \left(\begin{bmatrix} -0.00008408 & 0 \end{bmatrix}^{\mathrm{T}} + \Delta t \sum_{m=1}^{160} \left[\dot{F}_{00}^{\mathrm{g}}(m)\right] \{R_0(2-m)\} \right) \right]^{\mathrm{T}}$$

$$= \begin{bmatrix} -0.00093668 & 0.00041104 \end{bmatrix}^{\mathrm{T}} \quad \text{(qq)}$$

where $\left\{X_0^{\mathrm{tg}}(0)\right\}$, and $\{R_0(2-m)\}$ are zero for which $\left[\dot{F}_{00}^{\mathrm{g}}(m)\right]$ is not yet employed here but should always be evaluated as shown in Equation i.

From Equation 8.49

$$\{\Gamma(2)\} = [T]^{-1} \{E(2)\}$$

$$= \begin{bmatrix} -49.34672 & -0.29245 & -4.55664 & -0.64194 & -61.96822 & 0.1984 \end{bmatrix}^{\mathrm{T}} \times 10^{-3} \quad \text{(rr)}$$

$$\{\Phi(2)\} = \{\Pi(1)\} + \frac{\Delta t}{2} \{\Gamma(1)\}$$

$$= \begin{bmatrix} -0.3081485 & -0.008143 & -0.0281695 & -0.005406 & -0.263400 & -0.14972 \end{bmatrix}^{\mathrm{T}} \times 10^{-3} \quad \text{(ss)}$$

in which $\{\Pi(1)\}$ and $\{\Gamma(2)\}$ are from Equations bb and rr, respectively. Using Equation 8.47 yields

$$\{Z(2)\} = [T]\{\Phi(2)\}$$

$$= \begin{bmatrix} -0.00105 & -0.00084 & 0 & -0.33609 & -0.26646 & 0.00002 \end{bmatrix}^{\mathrm{T}} \times 10^{-3} \quad \text{(tt)}$$

in which the floor displacement is -1.05×10^{-6} m. For Equation 8.39, we have

$$\begin{aligned}\left\{\dot{Z}(2)\right\} &= [D]\{Z(2)\} + \{E(2)\} \\ &= \left[0.33609 \;\; -0.26646 \;\; 0.00002 \;\; -53.75363 \;\; -34.91826 \;\; 0.00623\right]^{\mathrm{T}} \times 10^{-3}\end{aligned} \tag{uu}$$

Following Equation 8.25 gives

$$\{R_0(2)\} = \left[\tilde{K}_{00}\right]\left\{X_0^{\mathrm{tg}}(2)\right\} - \left\{\tilde{R}_0(1)\right\} = \left[-0.00205784 \quad 0.00090384\right]^{\mathrm{T}} \tag{vv}$$

that is calculated as shown for $\{R_0(1)\}$. $[\tilde{K}_{00}]$ and $\{\tilde{R}_0(1)\}$ are from Equations hh and qq, respectively. $\{X_0^{\mathrm{tg}}(2)\} = \{X_0^{\mathrm{t}}(2)\} - \{X_0^{\mathrm{g}}(2)\}$ (see Figure 8.4 and Equation t) is calculated as $[-0.0000084 \quad 0]^{\mathrm{T}}$. Again R_x and R_θ in (vv) can be checked with Equations hh and ii as

$$\begin{aligned} R_x &= -0.54(-0.05375363 + 0.0537882) \\ &\quad - 0.108(-0.03491826 + 0.0537882 - 0.75(0.00000623)) \\ &= -0.002056116 \backsimeq -0.00205784 \end{aligned} \tag{ww}$$

$$\begin{aligned} R_\theta &= -148.14(0.00000623) - 0.405(0.00000623) \\ &\quad + 0.54(16.5)(-0.05375363 + 0.0537882) \\ &\quad + 0.108(0.75)(-0.03491826 + 0.0537882 - 0.75(0.00000623)) \\ &= 0.00091067 \cong 0.00090384 \end{aligned} \tag{xx}$$

The intersection at base is

$$S_{\mathrm{base}}^{\mathrm{SSI}} = -0.54(-0.05375363 + 0.0537882) = -0.0000186678 \tag{yy}$$

$$\begin{aligned} M_{\mathrm{base}}^{\mathrm{SSI}} &= -148.14(0.00000623) + 0.54(15.0)(-0.05375363 + 0.0537882) \\ &= -0.0006428952 \end{aligned} \tag{zz}$$

The subsequent responses can be similarly calculated as shown above. Note that the numerical values listed are with several unnecessary decimal numbers from engineering practice point of view; it is for the purpose of demonstrating a solution correctness.

8.7.2 Solution Procedure of SSI System with Control

EXAMPLE 8.7.2

The single-story shear building of Example 8.7.1 is now studied with an active tendon system of closed-loop control. The structure is constructed on the same foundation with rectangular mat foundation embedded in half-space subjected to the same earthquake as given in that example. Find the SSI response of the controlled system.

Solution

For a closed-loop control, the gain matrix is needed along with other equations as shown below in Equations 8.83, 8.85, 8.85a, and 8.86, which respectively represent $[G^{\mathrm{SSI}}]$, $[R]$, $[\check{K}_{00}]$, and $[S]$. Let us calculate Equation 8.85a for which $[\check{K}_{00}]$ is given in Equation d of Example 8.7.1 and $k_1 = 33.309$ MN/m, therefore,

$$\left[\check{K}_{00}\right] = \begin{bmatrix} 33.309 + 3564.91 & -(16.5)33.309 - 1564.38 \\ -(16.5)33.309 - 1564.38 & (16.5)^2 33.309 + 27342.1 \end{bmatrix}^{-1} = \begin{bmatrix} 3598.2199 & -2113.99335 \\ -2113.99335 & 36410.7203 \end{bmatrix} \tag{a}$$

For Equation 8.85

$$[R] = \begin{bmatrix} [\gamma_S] \\ [\gamma_0] \end{bmatrix}^{\mathrm{T}} \begin{bmatrix} [K_{SS}] & [K_{S0}] \\ [K_{S0}]^{\mathrm{T}} & \left[\check{K}_{00}\right] \end{bmatrix}^{-1} \begin{bmatrix} [\gamma_S] \\ [\gamma_0] \end{bmatrix}$$

$$= \begin{bmatrix} -1 & 1 & 0 \end{bmatrix} \begin{bmatrix} 33.3099 & -33.3099 & 549.6134 \\ -33.3099 & 3598.2199 & -2113.9934 \\ 549.6134 & -2113.9934 & 36410.7203 \end{bmatrix}^{-1} \begin{bmatrix} -1 \\ 1 \\ 0 \end{bmatrix}$$

$$= 0.0402347 \tag{b}$$

For Equation 8.86, one needs a computer to evaluate optimal performance, which yields $S_d = S_v = 0.17685$ and $R = 0.0402$ as

$$[S] = \begin{bmatrix} 0 & 0 & 0 & 0 & 0 & 0 \\ 0 & 0 & 0 & 0 & 0 & 0 \\ 0 & 0 & 0 & 0 & 0 & 0 \\ 0.17685 & 0.17685 & 0.17685 & 0.17685 & 0.17685 & 0.17685 \\ 0 & 0 & 0 & 0 & 0 & 0 \\ 0 & 0 & 0 & 0 & 0 & 0 \end{bmatrix} \quad \text{(c)}$$

Thus, Equation 8.83 results

$$\left[G^{SSI}\right] = \frac{1}{R}[B]^T[S] = \begin{bmatrix} 8.139732 & 8.139732 & 8.139732 & 8.139732 & 8.139732 & 8.139732 \end{bmatrix} \quad \text{(d)}$$

in which

$$[B]^T[S] = \begin{bmatrix} -0.3275 & -0.3275 & -0.3275 & -0.3275 & -0.3275 & -0.3275 \end{bmatrix} \quad \text{(e)}$$

$[B]$ is given by Equation m of Example 8.7.1. The plant matrix given in Equation 8.40 that can now be evaluated as

$$[D] = [A] + [\mathrm{B}]\left[G^{SSI}\right] = \begin{bmatrix} 0 & 0 & 0 & 1 & 0 & 0 \\ 0 & 0 & 0 & 0 & 1 & 0 \\ 0 & 0 & 0 & 0 & 0 & 1 \\ -76.7585 & 46.6114 & -1032.8735 & -15.3865 & -14.76059 & -20.2383 \\ 380.4966 & -33245.079 & 19473.1206 & 76.2720 & 73.1692 & 100.3229 \\ -4.3948 & -4.7989 & -235.3050 & -0.88093 & -0.8451 & -1.15874 \end{bmatrix} \quad \text{(f)}$$

in which $[A]$ is in Equation l of Example 8.7.1.

The eigenvalues and eigenvectors of [D] are

$$\mu_i \pm v_i\iota: \begin{cases} -6.306 \pm 5.42986\iota; \ i = 1 \\ -1.94979 \pm 13.6656\iota; \ i = 2 \\ 36.56449 \pm 181.9853\iota; \ i = 3 \end{cases} \quad \text{(g)}$$

$\{a\}_i \pm \{b\}_i\, \iota$:

$$\begin{bmatrix}-91.0626 & -3.06433\times10^{-2} & 2.25055 & 1000.0 & 2.59304 & 9.53035\end{bmatrix}^{\mathrm{T}}\times10^{-3} \pm \begin{bmatrix}78.4108 & 0.441987 & -0.858508 & 0 & -2.62076 & 17.6339\end{bmatrix}^{\mathrm{T}}\times10^{-3}\iota;\quad i=1 \tag{h}$$

$$\begin{bmatrix}-10.2323 & -6.15607 & -14.7678 & 1000 & 58.9209 & 71.3070\end{bmatrix}^{\mathrm{T}}\times10^{-3} \pm \begin{bmatrix}71.7163 & 3.43333 & 3.11093 & 0 & 77.4324 & 0.1957457\end{bmatrix}^{\mathrm{T}}\times10^{-3}\iota;\quad i=2 \tag{i}$$

$$\begin{bmatrix}3.68106 & 10.6121 & 0.218122 & -232.108 & 10000.0 & -11.4302\end{bmatrix}^{\mathrm{T}}\times10^{-4} \pm \begin{bmatrix}-2.01504 & 52.8173 & -0.106634 & -743.578 & 0 & -43.594\end{bmatrix}^{\mathrm{T}}\times10^{-4}\iota;\ i=3 \tag{j}$$

As discussed in Equation r of the earlier example, the natural frequencies

$$\begin{cases}\omega_1=\nu_1=5.42986\ \text{rad/s}=0.864\ \text{Hz};\\ \omega_2=\nu_2=13.6656\ \text{rad/s}=2.175\ \text{Hz};\\ \omega_3=\nu_3=181.9853\ \text{rad/s}=28.964\ \text{Hz};\end{cases} \tag{k}$$

and the damping ratios are from Equation h

$$\begin{aligned}\beta_1&=\frac{\mu_1}{\nu_1}=\frac{6.306}{5.42986}=1.161\\ \beta_2&=\frac{\mu_2}{\nu_2}=\frac{1.94979}{13.6656}=0.143\\ \beta_3&=\frac{\mu_3}{\nu_3}=\frac{36.56449}{181.9853}=0.201\end{aligned} \tag{l}$$

Following Equation 8.43, the transformation matrix $[T]$ is obtained from Equations i through k as

$$[T]=\left[\{a_1\}\{b_1\}\ldots\{a_i\}\{b_i\}\ldots\left\{a_{\mathrm{NO}+2}\right\}\left\{b_{\mathrm{NO}+2}\right\}\right]$$

$$=\begin{bmatrix}-91.0626 & 78.4108 & -10.2323 & 71.7163 & 0.368106 & -0.2011504\\ -0.306433 & 0.441987 & -6.15607 & 3.43333 & 1.06121 & 5.28173\\ -2.25055 & -0.858508 & -14.7678 & 3.11093 & 0.0218122 & -0.0106634\\ 1000.0 & -0.00003 & 1000 & 0 & -23.2108 & -74.3578\\ 2.59304 & -2.62076 & 58.9209 & 77.324 & 1000.0 & 0\\ 9.53035 & 17.339 & 71.3070 & 195.7457 & -1.14302 & -4.3594\end{bmatrix}\times10^{-3} \tag{m}$$

of which the inversion is

$$[T]^{-1} = \begin{bmatrix} 1.07614 & 16.61685 & 69.8634 & 1.27286 & 0.00793 & -1.9918 \\ 14.73174 & 16.7602 & 54.56908 & 1.52734 & 0.00355 & -6.55997 \\ -1.22469 & -3.03723 & -77.7363 & 0.30312 & 0.00032 & 1.73728 \\ -0.97807 & 2.85477 & 17.6392 & 0.09893 & 0.000536 & 5.13639 \\ 0.1837122 & -0.041259 & 3.1763 & 0.026169 & 0.99998 & -0.512612 \\ -2.0551 & 182.6382 & -106.87 & -0.415132 & -0.20113 & -0.67247 \end{bmatrix} \quad \text{(n)}$$

Thus, $[T]^{-1}[D][\mathrm{T}] = [\Lambda]$ is obtained that can prove the correctness of Equation h. For Equation 8.54

$$[\exp([\Lambda])\,\Delta t] = \begin{bmatrix} 0.9608004 & -0.0326188 & 0 & 0 & 0 & 0 \\ 0.0326188 & 0.9608004 & 0 & 0 & 0 & 0 \\ 0 & 0 & 0.9842866 & -0.0842732 & 0 & 0 \\ 0 & 0 & 0.0842732 & 0.9842866 & 0 & 0 \\ 0 & 0 & 0 & 0 & 0.527769 & -1.14056 \\ 0 & 0 & 0 & 0 & 1.14056 & 0.0527769 \end{bmatrix} \quad \text{(o)}$$

For Equation o, sample calculations are illustrated for $i = 1$ and $\Delta t = 0.00625$ as shown in Equations p and q:

$$\exp(\mu_i \Delta t)\cos(\nu_i \Delta t) = \exp[(0.00625 \times (-6.306))]\cos[(0.00625 \times (-5.49986))]$$
$$= 0.961354\,(0.9994242) = 0.9608004;\ i = 1 \quad \text{(p)}$$
$$\exp(\mu_i \Delta t)\sin(\nu \Delta t) = \exp[(0.00625 \times (-6.306))]\sin[(0.00625 \times (-5.42986))]$$
$$= 0.961354\left(-3.39301 \times 10^{-2}\right) = -3.26188 \times 10^{-2}; i = 1 \quad \text{(q)}$$

Similar to Example 8.7.1, the response analysis is calculated as follows:

At $t = 0$ $(n = 0)$

$$\{E(0)\} = \{C\}\ddot{x}_0^{\mathrm{g}}(0) + \{\check{R}_0(0-1) = \{0\} \quad \text{(r)}$$
$$\{\Gamma\,(0)\} = [T]^{-1}\{E(0)\} = \{0\} \quad \text{(s)}$$

$$\{\Pi\,(0)\} = [\exp([\Lambda]\,\Delta t)]\;\;[\{\Pi(-1) + 0.00625\,\{\Gamma(0)\,\}] = \{0\} \tag{t}$$

$$\{\tilde{R}(0)\} = \left[\tilde{K}_{00}\right]\left[\left\{x_0^{\mathrm{tg}}\,(0)\right\}\right] + \frac{\Delta t}{2}\left(\left\{x_0^{\mathrm{tg}}\,(0)\right\} + \Delta t \sum_{m=1}^{160}\left[\dot{F}_{00}^{\mathrm{g}}\,(m)\;\{\,R_0\,(1-m)\,\}\right]\right) = \{0\} \tag{u}$$

At $t = 0.00625$ $(n = 1)$

$$\{E(1)\} = \begin{bmatrix}0 & 0 & 0 & -1 & -1 & 0\end{bmatrix}^{\mathrm{T}} 0.0268941 + \{\check{R}(0)\} = \begin{bmatrix}0 & 0 & 0 & -0.0268941 & -0.0268941 & 0\end{bmatrix}^{\mathrm{T}} \tag{v}$$

$$\{\Gamma\,(1)\} = [T]^{-1}\,\{E(1)\} = [-34.4459 \quad -41.1722 \quad 8.1436 \quad 2.6275 \quad -27.5960 \quad 16.5739]^{\mathrm{T}} \times 10^{-3} \tag{w}$$

$$\{\Phi(2)\} = \{\Pi(0)\} + \frac{0.00625}{2}\{\Gamma\,(1)\} = \begin{bmatrix}-0.1076 & -0.1287 & 0.0254 & 0.0082 & -0.0862 & 0.0518\end{bmatrix}^{\mathrm{T}} \times 10^{-3} \tag{x}$$

$$\{Z(1)\} = [T]\,\{\Phi(1)\} = \begin{bmatrix}0 & 0 & 0 & -0.0000840 & -0.0000840 & 0\end{bmatrix}^{T} \tag{y}$$

from which the floor displacement is zero. For Equation 8.31

$$\left\{\dot{Z}(1)\right\} = [D]\,\{Z(1)\} + \{E(1)\} = \begin{bmatrix}-0.0000840 & -0.0000840 & 0 & -0.0243604 & -0.0394539 & 0.0001451\end{bmatrix}^{\mathrm{T}} \tag{z}$$

The horizontal force R_x and moment R_θ are

$$\{R_0(1)\} = \left[\tilde{K}_\infty\right]\left\{X_0^{\mathrm{tg}}(1)\right\} - \{R_0(1)\} = \{0\}$$

The control is obtained using Equation 8.38 as

$$\left\{\vec{U}(1)\right\} = \left[G^{\mathrm{SSI}}\right]\{Z^{\mathrm{tg}}(1)\} = \left[G^{\mathrm{SSI}}\right]\begin{bmatrix}0 & 0 & 0 & -0.0000840 & -0.0000840 & 0\end{bmatrix}^{\mathrm{T}} = 0.001367474 \tag{aa}$$

where $\left[G^{\mathrm{SSI}}\right]$ is given in Equation d.

At $t = 0.0125$ $(n = 2)$

$$\{\Pi(1)\} = [\exp([\Lambda]\ \Delta t)]\ [\{\Pi(0)\} + 0.0625\ \{\Gamma(1)\}$$
$$= \left[-0.1985\ \ -0.2543\ \ \ 0.0487\ \ \ 0.0205\ \ -0.2092\ \ -0.1420\right]^{\mathrm{T}} \times 10^{-3} \quad \text{(bb)}$$

$$\{\Phi(2)\} = \{\Pi(1)\} + \frac{0.00625}{2}\{\Gamma\,(2)\}$$
$$= \left[-0.4139\ \ -0.5116\ \ 0.0996\ \ \ 0.0368\ \ \ -0.4087\ \ -0.0336\right]^{\mathrm{T}} \times 10^{-3} \quad \text{(cc)}$$

where

$$\{\Gamma\,(2)\} = [T]^{-1}\{E(2)\}$$
$$= \left[-68.957\ \ -82.3622\ \ 16.2811\ \ 5.2402\ \ -63.8611\ \ 34.8931\right]^{\mathrm{T}} \times 10^{-3}$$

$$\{Z(2)\} = [T]\,\{\Phi(2)\}$$
$$= \left[-0.0009\ \ -0.0013\ \ 0\ \ -0.3024\ \ -0.3998\ \ 0.0020\right]^{\mathrm{T}} \times 10^{-3} \quad \text{(dd)}$$

$$\left\{\dot{Z}(2)\right\} = [D]\,\{Z(2)\} + \{E(2)\}$$
$$= \left[-0.3024\ \ -0.3998\ \ 0.0020\ \ -43.2689\ \ -71.3274\ \ 0.6090\right]^{\mathrm{T}} \times 10^{-3} \quad \text{(ee)}$$

where

$$\{E(2)\} = \left[0\ \ \ 0\ \ \ 0\ \ \ -53.7882\ \ \ -62.4590\ \ \ -.0020\right]^{\mathrm{T}} \times 10^{-3}$$

The horizontal force R_x and moment R_0 are

$$\{R_0(2)\} = \left[\tilde{K}_{00}\right]\begin{bmatrix}-0.0000013\\ 0\end{bmatrix} - \begin{bmatrix}-0.0009363\\ 0.0004109\end{bmatrix} = \begin{bmatrix}-3.7368 \times 10^{-3}\\ 1.80226 \times 10^{-3}\end{bmatrix} \quad \text{(ff)}$$

The control force is

$$\{U(2)\} = \left[G^{\mathrm{SSI}}\right]\{Z^{\mathrm{tg}}(2)\} = -0.005717 \quad \text{(gg)}$$

The response calculations of subsequent time intervals are similar to those depicted above.

8.8 Computer Solutions for Building Structures with and without Control

A one-bay, ten-story shear-building structure is used to demonstrate the influence of structure–soil interaction with and without control. The structure has an active tendon system attached to its foundation and second floor (node no. 1) and is supported by a 6.0 × 6.0 m rigid square foundation having its 3.0-m depth embedded into ground. Structural properties are each floor mass (m_i) =10 ton; each floor mass moment of inertia ($I_i - m_i h_{ai}$) = 20.83 ton-m^2; foundation mass (m_0) = 28.75 ton; foundation mass moment of inertia (I_0) = 172.5 ton-m^2; floor translational stiffness (k_i) = 1244 MN/m; proportional damping ratios $\beta_1 = 0.02$ and $\beta_2 = 0.10$ for the first mode and the second mode; and floor height (h_i) 3.00 m for every floor. Half-plane properties are shear modulus of elasticity ($\wp$) = 7.2 MN/m^2; soil density (ρ) = 2.0 gram/cm^3; Poisson's ratio (υ) = 0.33; and hysteretic damping ratio (ζ) = 0.04. The shear wave velocity (C_S) is 60 m/s. The first 20-s 1940 El Centro earthquake acceleration record, north–south component is selected as the horizontal acceleration at point 0 of the ground system's rigid interface. Since vertically incident shear wave is assumed, the rotational component of the ground system is omitted. As for a one-controller system, the control-weighting matrix [R] consists of only one element r. To obtain an optimal performance of the system, sl/r ratio is varied parametrically.

The fundamental system frequency is 2.65 Hz for the FIX-model (structural supprt is on rock) and 1.15 Hz for the SSI-model. The smaller frequency in the SSI-model is a result of its greater flexibility. In a system with control, its frequency and damping ratio are increased as sl/r ratio reaches an optimal point (the minimum point of performance index). For the FIX-model (see Figure 8.24), the fundamental

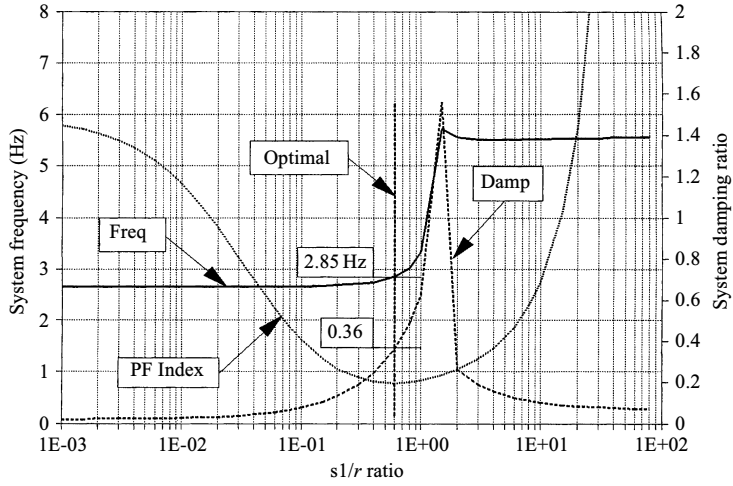

Figure 8.24 Fundamental frequency and damping ratio versus s1/r ratio, ten-story controlled structure, FIX-model.

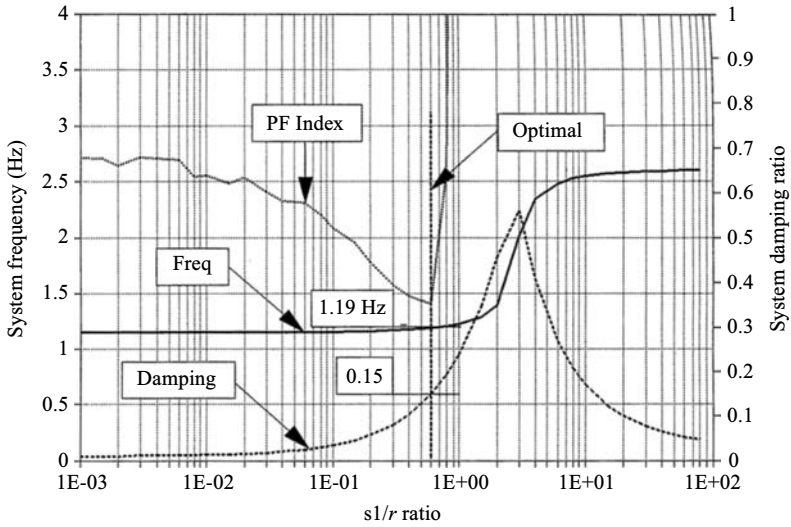

FIGURE 8.25 Fundamental frequency and damping ratio versus s1/r ratio, ten-story controlled structure, SSI-model.

system frequency and damping ratio are increased, at the optimal point (s1/r = 0.6), to 2.85 Hz and 0.36, respectively. For the SSI-model (Figure 8.25), at the optimal point (sl/r = 0.6), the fundamental system frequency and damping ratio are increased to 1.19 Hz and 0.15, respectively. This is because control force, which is related to the system's displacement and velocity vector by a gain matrix [G], helps to increase stiffness and damping of the system. Displacement control and velocity control are manipulated by s_D and s_V in the state-weighting matrix [S] and therefore in the gain matrix [G], which are chosen to be equal to an arbitrary real number sl.

In a system without control, the maximum of the top floor displacement relative to footing is equal to 0.053 m $\left(x_{10}^{tb}\right)$ for the FIX-model and 1.219 m $\left(x_{10}^{tg} - x_{0}^{tg}\right)$ for the SSI model. The larger displacement in the SSI-model is mainly due to foundation rotation θ_{10}^{tg} since the rigid rocking mode trends to dominate in a flexible high-rise structure. Figure 8.26 shows the comparison of the top floor displacement relative to footing $\left(x_{10}^{tb}\right)$ in the FIX-model and the top floor displacement relative to footing excluding rigid motion effect due to foundation $\left(x_{10}^{tg} - x_{0}^{tg} + h_{a10}\theta_{0}^{tg}\right)$ of the structure with control. The smaller displacement in the FIX-model implies that the system's control force is more effective in reducing the FIX-model's translational displacement than the SSI model's relative displacement excluding rotational effect. For the FIX-model with control (see Figure 8.27), an increase of sl/r ratio results in an increase of the maximum of control force and then a decrease of the maximum of the top floor displacement relative to footing $\left(x_{10}^{tb}\right)$.

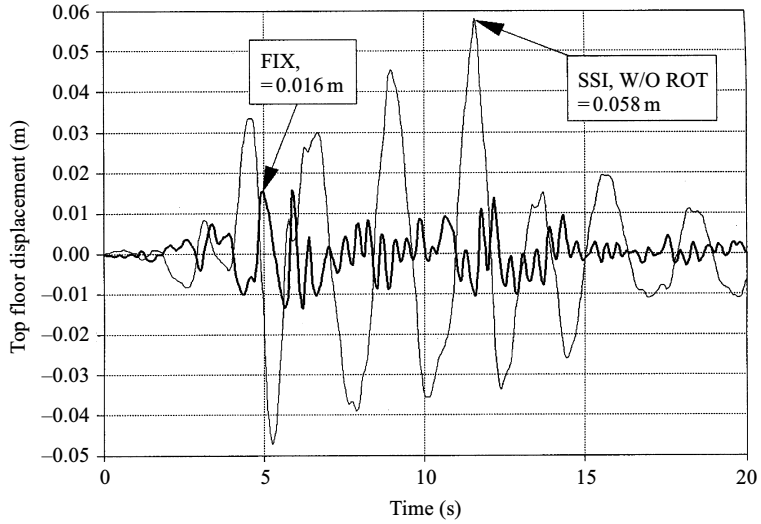

FIGURE 8.26 Top floor displacement relative to footing of FIX-model and SSI-model (excluding rotational effect), with control (s1/r = 0.6).

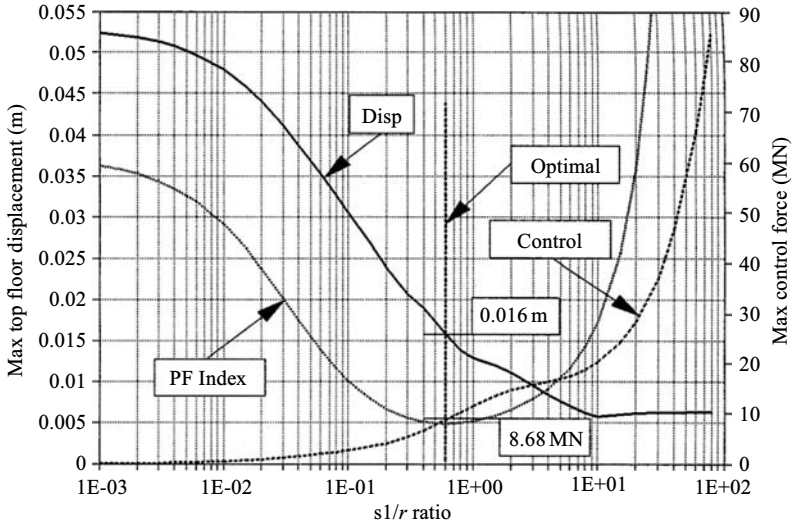

FIGURE 8.27 Maximum top floor displacement and horizontal control force versus s1/r ratio, FIX-model.

At the optimal point, the maximum displacement is reduced from 0.053 m (without control) to 0.016 m with the maximum control force of 8.68 MN.

For the SSI-model with control (see Figure 8.28), an increase of sl/r ratio also results in the same manner as the case of the FIX-model. But the change in the maximum of the top floor displacement relative to footing excluding rotational

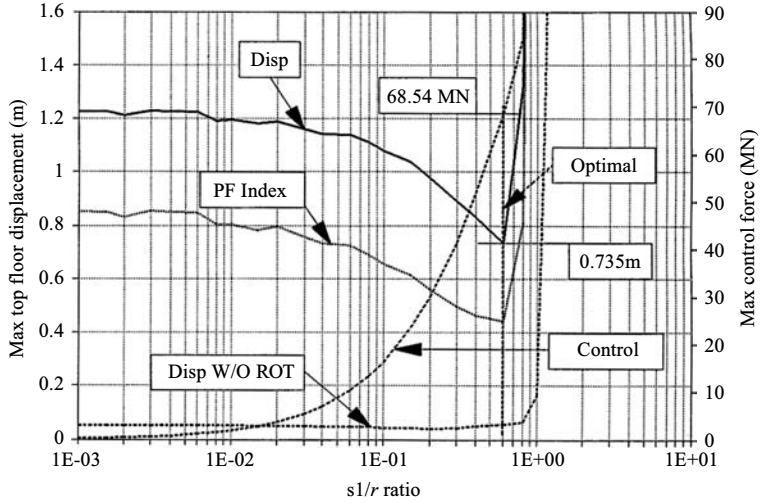

FIGURE 8.28 Maximum top floor displacement with and without rotational effect and horizontal control force versus s1/*r* ratio, SSI-model.

effect (DISP W/O ROT) as a function of sl/*r* ratio is very small. This indicates that the decrease of displacement relative to footing is mainly the result of the decrease of footing rotation. At the optimal point, the maximum displacement is reduced from 1.219 m (without control) to 0.735 m with the maximum control force of 68.54 MN. The footing rotation is reduced from 0.035 rad. (without control) to 0.022 rad. as shown in Figure 8.29. Therefore, the active tendon system, attached to the foundation and second floor of a structure embedded in a soft soil, can limit structural responses by means of reducing foundation rotation. This active system is not so effective in reducing relative floor translation. To limit structural responses even more, the second active system on the upper floor may be needed.

Since the foundation d.o.f. in an SSI-model distinguishes this model's behavior from a FIX-model's, the responses of these two models are different and thus require different control forces. The control force required in the SSI-model is greater than that in the FIX-model as a result of the former's larger response. Thus, an additional amount of control force is needed to limit the movement of foundation. Consequently the control force determined by a FIX-model's gain matrix may not be large enough to limit the foundation movement and thus the structural responses.

8.9 Summary and Concluding Remarks

A general mathematical model of a multiple-story seismic shear-building structure with active tendon control including SSI was presented. The derived formulations can be easily applied to controlled fixed-base model (FIX), and can also be employed for both SSI-model and FIX-model without control.

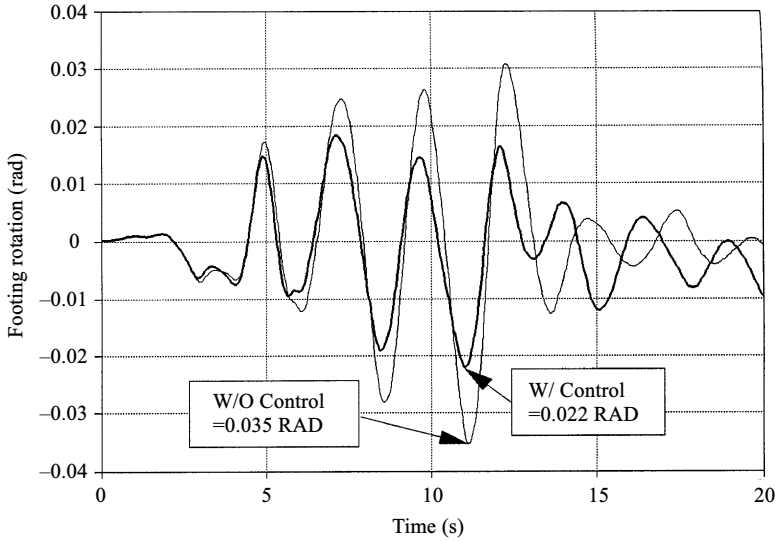

FIGURE 8.29 Footing rotation of system with control (s1/$r = 0.6$) and without control.

The SSI-model is established for the seismic structure having a rigid rectangular mat foundation embedded in an unbounded soil. The unbounded soil domain is modeled as unbounded horizontal layers stacked on a half-space (layered half-space). An isotropic viscoelastic property of soil may vary with depth but remain constant within the individual layers. The indirect boundary-element method is applied to unbounded part of soil (free-field system), while the finite element method with 4-node rectangular element is employed to bounded part (system's excavated part). In the indirect boundary-element method, an adaptive quadrature integration technique is used in a Green's influence function's transformation from the k wave-number domain to space domain. For the integration along a boundary (foundation-soil interface), Simpson's method is employed. The frequency-dependent time-derivative flexibility coefficient of ground system is determined and then, by using the discrete Fourier transformation (or fast Fourier transform) with causality condition, an impulse velocity coefficient is obtained. By virtue of the soil coefficient's time derivative, its static component is not required. In a discrete time fashion, an SSI force is computed through the convolution integral of the impulse velocity coefficient. This coefficient relates the difference of the ground system's and foundation's responses to the interaction force. Since vertically incident shear wave are assumed, the rotational component of the ground system's response is neglected.

In the integrated control systems, the concept of a GOAC is applied. The weighting matrix $[S]$ associated with the endpoint state vector is chosen to be either a row matrix or a symmetrical matrix. Since this weighting matrix is integrated into the gain matrix, the displacement control and velocity control are

manipulated by the weighting elements (S_D, γ_D and S_V, γ_V) corresponding to a system's displacement vector and velocity vector, respectively. In the SSI-model with control, foundation responses (translation and rocking) are included in the state vector and then dictate control force. Therefore, in a closed control, not only a response sensor on the floor but also an innovative sensor for foundation may be useful. The foundation sensor may detect the pressure (or stress or strain) at a foundation–soil interface and then convert to the foundation's response relative to the ground system.

References

1. Cheng, F.Y. and Suthiwong, S., *Active Control for Seismic-Resistant Structures on Embedded Foundation in Layered Half-Space*, NSF Report, National Technical Information Service, U.S. Department of Commerce, Springfield, VA, NTIS No. PB97-121354, 1996, p. 261.
2. Cheng, F.Y., *Matrix Analysis of Structural Dynamics–Application and Earthquake Engineering*, CRC Taylor & Francis Group, Boca Raton, FL; Marcel Dekker Inc., New York, 2001.
3. Cheng, F.Y. and Yeh, Y.T. (eds), *Research and Application for Multiple Hazards Mitigation*, Academia Sinica, Taiwan, Vols. I and II, 1998.
4. Cheng, F.Y., Response control based on structural optimization and its combination with active protection, theme paper, in *Proceedings of 9th World Conference on Earthquake Engineering*, Tokyo/Kyoto, Vol. VIII, Nissei Kogyo Co. Ltd., Tokyo, 1988, pp. 471–476.
5. Cheng, F.Y., Tian, P., and Suthiwong, S., Generalized optimal active control algorithm of seismic structures and related soil-structure formulation, in *Computational Mechanics in Structural Engineering-Recent Developments and Future Trends*, Cheng, F.Y. and Fu, Z.Z. (eds), Elsevier Applied Science, London, 1992, pp. 49–62.
6. Cheng, F.Y. and Fu, Z. (eds), *Computational Mechanics in Structural Engineering-Recent Developments and Future Trends*, Elsevier Applied Science, London, ISBN 1-85166-8675, 1992.
7. Cheng, F.Y. and Gu, Y.X. (eds), *Recent Advancement of Computational Mechanics In Structural Engineering*, Elsevier Science Ltd., Oxford, ISBN 0-08-043008-2, 1998.
8. Hayashi, Y. and Katukura, H., Effective time-domain soil–structure interaction analysis based on FFT algorithm with causality condition. *Earthquake Engineering and Structural Dynamics*, 19, 693–708, 1990.
9. Tuma, J.J. and Cheng, F.Y., *Dynamic Structural Analysis*, McGraw-Hill Publishing Company, New York, ISBN 0-07-065437-9, 1982.
10. Wolf, J.P. and Darbre, G.R., Dynamic-stiffness matrix of embedded and pile foundations by indirect boundary element method, *Trans. 7th. International Conference on Structural mechanic Reactor Technology*, Chicago, Paper K11/1, K(b), pp. 245–258, 1983.
11. Wolf, J.P., *Dynamic Soil–Structure Interaction*, Prentice-Hall, New Jersey, 1985.
12. Wolf, J.P. and Darbre, G.R., Dynamic-stiffness matrix of soil by the boundary-element method: embedded foundation, *Earthquake Engineering and Structural Dynamics*, 12, 401–406, 1984.

9 Hybrid Control of Structures on Shallow Foundation with Existing and Generated Earthquakes

9.1 Introduction

As discussed in Chapter 8, the assumption that a structure is fixed on the ground surface of geologic media may lead to some deviations in the analysis results, especially for structures on a soft base. In reality, a structure is mounted on the foundation that is in turn supported and surrounded by soil with various properties. The whole system is actually composed of three parts: structure, foundation and the soil base. The *soil–structure interaction* (SSI) evaluates the whole system under the input of free field ground motion, which describes the ground motion at the site without existence of a structure. Chapter 8 presents active controlled building structures constructed on embedded foundations with consideration of soil in horizontal layers and half space. This chapter introduces hybrid-controlled structures, equipped with hybrid damper-actuator-bracing control (HDABC), supported by shallow foundation.

Since future earthquake excitation at a given site must be different from the existing records and cannot be predicted deterministically, this chapter presents how to generate future ground motions based on the historical tectonic movements of the seismic plate with consideration of wave propagation and local site soil amplification. A group of motions is generated for a given earthquake magnitude, m_j, and time history analysis is then carried out for each motion in the group. The maximum values for a specific response (such as floor displacements, control forces, etc.) are collected, and then the nondeterministic Monte Carlo method is employed for the maximum response probability study.

9.1.1 Interaction Types

There are two kinds of interaction taking place with a vibrating structure on soil:

1. The inertial interaction is brought from the inertia of the structure due to its own vibration, and in turn causes displacement of the foundation,

which can be considered by the impedance function as describing the stiffness and damping characteristics between the foundation and the soil.

2. The *kinematic interaction* is the interaction between the soil and foundation, which causes the foundation motion to be different from the free field motion. It is called foundation input motion (FIM). The kinematic interaction is described by a frequency dependent transfer function that relates the free field motion and FIM [11,18].

The actual foundation motion is therefore composed of two parts as

$$\begin{aligned} X &= \text{FIM} + \text{Motion due to inertia interaction} \\ &= S_k(\omega)X_0 + X_1 \end{aligned} \tag{9.1}$$

where X_0 is the free field motion and $S_k(\omega)$ is the transfer function to consider the kinematic interaction. When the structure rests on a fixed base (infinitely stiff soil), the transfer function $S(\omega)$ is a unit scale number and X_1 is zero, so the motion of the foundation is the same as the ground motion of the free field.

9.1.2 Substructure Approach

Among the methods that include SSI in the system dynamic analysis, the direct method models soil, foundation, and structure together, and the finite element analysis is used to study the dynamic response. The *substructure approach* is composed of three distinct parts and they are independent of each other:

1. The first part is finding the FIM by considering the kinematic interaction effect.
2. The second part considers the inertial interaction, in which the impedance function is used.
3. The final part is the dynamic analysis for the structure supported on a compliant base represented by the impedance function, and subjected to a base excitation of FIM.

The kinematic interaction makes the FIM deviate from the free-field motion because of the existence of a stiff foundation on or in the soil media, which can be caused by *base-slab averaging*, embedment/deconvolution effects and wave scattering. Now, little is known about the effects of wave scattering on the base-slab motions, because the effect is very small compared with the more significant base-slab averaging and embedment effects [16].

In the inertial interaction consideration, *impedance function* is given as a general expression in the frequency domain as

$$F_c(\omega) = [K^I(\omega)]U_c(\omega) \tag{9.2}$$

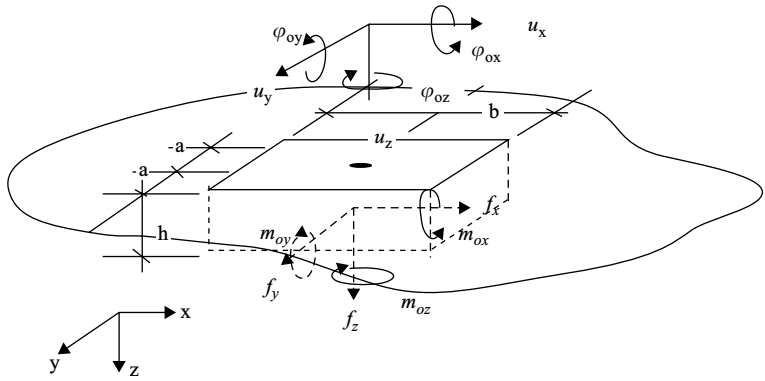

FIGURE 9.1 Foundation dynamic responses.

where, $F_c(\omega) = [f_x, f_y, f_z, m_x, m_y, m_z]^T$, is the reaction force-moment vector from the soil media to the foundation when the foundation has a movement of $U_c(\omega) = [u_x, u_y, u_z, \varphi_{ox}, \varphi_{oy}, \varphi_{oz}]^T$; and $[K^I(\omega)]$ is the impedance function matrix, which can be a 6×6 square matrix in a three-dimensional case as, shown in Figure 9.1. In general, there are eight different impedances in $[K^I(\omega)]$ as shown in Equation 9.3. Six of them correspond to the six possible modes of vibration of the rigid foundation, one vertical, K_{zz}, two horizontal, K_{xx} and K_{yy}; two rocking, K_{rx} and K_{ry}; and one torsional, K_{rz}. Moreover, the horizontal forces along its axes induce not only translational oscillations, but also the rotational, two more cross-coupling horizontal-rocking impedances: K_{xry} and K_{yrx}.

$$[K^I(\omega)] = \begin{bmatrix} K_{xx} & 0 & 0 & 0 & K_{xry} & 0 \\ 0 & K_{yy} & 0 & K_{yrx} & 0 & 0 \\ 0 & 0 & K_{zz} & 0 & 0 & 0 \\ 0 & K_{yrx} & 0 & K_{rx} & 0 & 0 \\ K_{xry} & 0 & 0 & 0 & K_{ry} & 0 \\ 0 & 0 & 0 & 0 & 0 & K_{rz} \end{bmatrix} \tag{9.3}$$

Each of the impedance in the matrix is composed of a real term and an imaginary term as shown below:

$$K_{prq}(\omega) = k_{prq}(\omega) + j\omega c_{prq}(\omega) \tag{9.4}$$

where $j = \sqrt{-1}$, and p, q can be x, y, z, or none to generally represent the impedance in Equation 9.2. On the basis of the Fourier transform theory, the real part in the impedance represents the stiffness, the imaginary the damping, and they are all frequency dependent. They can be physically expressed as spring/dashpot pairs with their stiffness and damping coefficient changing with excitation frequency.

The study of the dynamic response of the structure is limited to the in 2-dimension of the vertical plane, x-o-z, and the vertical seismic vibration is not

considered. Therefore, the impedance function of Equation 9.2 can be reduced as

$$\begin{Bmatrix} f_x \\ m_{oy} \end{Bmatrix} = \begin{bmatrix} K_{xx} & K_{xry} \\ K_{yrx} & K_{ry} \end{bmatrix} \begin{Bmatrix} u_x \\ \varphi_{oy} \end{Bmatrix} \tag{9.5a}$$

or

$$\begin{Bmatrix} F_c \\ M_c \end{Bmatrix} = \begin{bmatrix} k_{HH}(\omega) + j\omega c_{HH}(\omega) & k_{HM}(\omega) + j\omega c_{HM}(\omega) \\ k_{MH}(\omega) + j\omega c_{MH}(\omega) & k_{MM}(\omega) + j\omega c_{MM}(\omega) \end{bmatrix} \begin{Bmatrix} x_0 \\ \phi \end{Bmatrix} \tag{9.5b}$$

where x_0 and ϕ are the horizontal and rocking motions of the foundation, respectively; k_{HH} and c_{HH} replace the notations of k_{xx} and c_{xx} to represent the frequency dependent stiffness and damping in the horizontal direction; k_{MM} and c_{MM} replace the notation of k_{ry} and c_{ry} for the rocking; and k_{MH}, k_{HM} and c_{MH}, c_{HM} replace the notation of k_{yrx}, k_{xry} and c_{yrx}, c_{xry} for the coupling items. The coupling items are negligibly small in the case of surface and shallow foundation, but the effects may become appreciable for a larger depth of embedment, h, in Figure 9.1 [2].

9.2 Structural Formulation with HDABC

9.2.1 Hybrid Controlled Single-Story Structure without SSI

For a single-story building structure with the hybrid controller on the bracing known as HDABC system, the motion equations can be obtained based on the force balance of the free bodies, structure floor, and the brace (see Figure 9.2) as

The floor:

$$m_1\ddot{x}_1 + k_1x_1 + c_1\dot{x}_1 = f_a + f_p - m_1\ddot{x}_g \tag{9.6a}$$

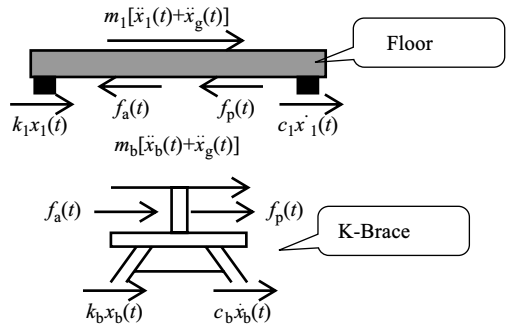

Figure 9.2 Free body diagrams for fixed base cases.

or

$$\ddot{x}_1 + \omega_1^2 x_1 + 2\rho_1\omega_1\dot{x}_1 = \frac{f_a}{m_1} + \left(\frac{f_p}{m_1}\right) - \ddot{x}_g \tag{9.6b}$$

The brace:

$$m_b\ddot{x}_b + k_b x_b + c_b\dot{x}_b = -f_a - f_p - m_b\ddot{x}_g \tag{9.7a}$$

or

$$\ddot{x}_b + \omega_b^2 x_b + 2\rho_b\omega_b\dot{x}_b = -\frac{f_a}{m_b} - \left(\frac{f_p}{m_b}\right) - \ddot{x}_g \tag{9.7b}$$

where x_1 and x_b are the displacements of the floor and brace, respectively, relative to the fixed base; m_1, k_1, and c_1 are the floor mass, column stiffness, and the damping, respectively; the subscript of 1 denotes that they are for the first floor and items of the brace are subscripted by lower case b. f_a,f_p, and $\ddot{x}_g$ are the active, passive forces, and the ground acceleration input, respectively. The motion equations of the controlled system can be assembled in a matrix form as

$$[M]\{\ddot{x}\} + [K]\{x\} + [C]\{\dot{x}\} = \{f_a\} + \{f_p\} - [M]\{I\}\ddot{x}_g \tag{9.8}$$

where

$$[M] = \begin{bmatrix} m_1 & 0 \\ 0 & m_b \end{bmatrix}; \quad [K] = \begin{bmatrix} k_1 & 0 \\ 0 & k_b \end{bmatrix}; \quad [C] = \begin{bmatrix} c_1 & 0 \\ 0 & c_b \end{bmatrix};$$

$$\{f_a\} = \begin{Bmatrix} f_a \\ -f_a \end{Bmatrix}; \quad \{f_p\} = \begin{Bmatrix} f_p \\ -f_p \end{Bmatrix}; \quad \{I\} = \begin{Bmatrix} 1 \\ 1 \end{Bmatrix}$$

The system modeled by the linear differential equations, can be represented in a state space form, which is composed of a series of first order differential equations. For the hybrid controlled single-story building structure, as in Equation 9.8, it can be written in four equations as

$$\frac{d}{dt}x_1 = \dot{x}_1 \tag{9.9a}$$

$$\frac{d}{dt}x_b = \dot{x}_b \tag{9.9b}$$

$$\frac{d}{dt}\dot{x}_1 = -\omega_1^2 x_1 - 2\rho_1\omega_1\dot{x}_1 + \frac{f_a}{m_1} + \left(\frac{f_p}{m_1}\right) - \ddot{x}_g \tag{9.9c}$$

$$\frac{d}{dt}\dot{x}_b = -\omega_b^2 x_b - 2\rho_b\omega_b\dot{x}_b - \left(\frac{f_a}{m_b}\right) - \left(\frac{f_p}{m_b}\right) - \ddot{x}_g \tag{9.9d}$$

Equations 9.9a through 9.9d can be organized in a matrix form as

$$\frac{\mathrm{d}}{\mathrm{d}t}\begin{Bmatrix} x_1 \\ x_\mathrm{b} \\ \dot{x}_1 \\ \dot{x}_\mathrm{b} \end{Bmatrix} = \begin{bmatrix} 0 & 0 & 1 & 0 \\ 0 & 0 & 0 & 1 \\ -\omega_1^2 & 0 & -2\rho_1\omega_1 & 0 \\ 0 & -\omega_\mathrm{b}^2 & 0 & -2\rho_\mathrm{b}\omega_b \end{bmatrix} \begin{Bmatrix} x_1 \\ x_\mathrm{b} \\ \dot{x}_1 \\ \dot{x}_\mathrm{b} \end{Bmatrix} + \begin{Bmatrix} 0 \\ 0 \\ 1/m_1 \\ -1/m_\mathrm{b} \end{Bmatrix} f_\mathrm{a} + \begin{Bmatrix} 0 \\ 0 \\ 1/m_1 \\ -1/m_\mathrm{b} \end{Bmatrix} f_\mathrm{p} + \begin{Bmatrix} 0 \\ 0 \\ -1 \\ -1 \end{Bmatrix} \ddot{x}_\mathrm{g} \tag{9.10}$$

that can be expressed, as in Equation 9.11, by defining the state vector of $z = [x_1\ x_\mathrm{b}\ \dot{x}_1\ \dot{x}_\mathrm{b}]^\mathrm{T}$.

$$\dot{z} = [A]z + \{B_\mathrm{a}\}f_\mathrm{a} + \{B_\mathrm{b}\}f_\mathrm{p} + \{B_\mathrm{r}\}\ddot{x}_\mathrm{g} \tag{9.11}$$

Equation 9.11 is the state space representation of the controlled single-story building equipped with HDABC system where $[A]$ is the plant matrix, $\{B\}$s are the input position vectors and the subscripts of a, p, r correspond to active, passive, and earthquake input, respectively.

9.2.2 Hybrid Controlled Single-Story Building with SSI

The soil influence of the inertia interaction is dominant for the shallow foundation [18,19], for which the reaction is expressed by a series of stiffness-damper units between the foundation and the soil with their values provided in the impedance function [1,16]. Figure 9.3 shows the SSI consideration for the hybrid controlled single story building resting on the soil. The impedance function is given in

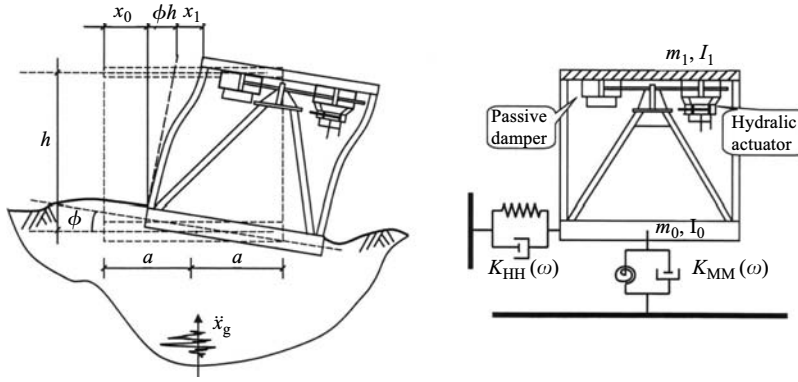

FIGURE 9.3 HDABC system on soil.

frequency domain, which is related to the reaction force from the soil to the foundation motions. In Equation 9.12, only the horizontal and rocking motions of the foundation are considered.

$$\begin{Bmatrix} F_c \\ M_c \end{Bmatrix} = \begin{bmatrix} k_{HH}(\omega) + j\omega c_{HH}(\omega) & k_{HM}(\omega) + j\omega c_{HM}(\omega) \\ k_{MH}(\omega) + j\omega c_{MH}(\omega) & k_{MM}(\omega) + j\omega c_{MM}(\omega) \end{bmatrix} \begin{Bmatrix} x_0 \\ \phi \end{Bmatrix} = \begin{bmatrix} K_{HH} & K_{HM} \\ K_{MH} & K_{MM} \end{bmatrix} \begin{Bmatrix} x_0 \\ \phi \end{Bmatrix} \tag{9.12}$$

where the upper case K represents the impedance, which includes both stiffness and damping. K_{MH} and K_{HM} are the couple items between the translational and the rocking motions, which are omitted in the study.

In consideration of the SSI, two more degrees of freedom are introduced when the translational and rocking motions of the foundation are included. Similar to the fixed base case, when the free body analysis is conducted, the force balances of the floor and the brace in the horizontal direction can be formulated as

$$m_1\left(\ddot{x}_0 + h_1(\ddot{\phi} + \ddot{\phi}_g) + \ddot{x}_1 + \ddot{x}_g\right) + c_1\dot{x}_1 + k_1x_1 = f_a + f_p \tag{9.13}$$

$$m_b(\ddot{x}_0 + h_b\left(\ddot{\phi} + \ddot{\phi}_g\right) + \ddot{x}_b + \ddot{x}_g) + c_b\dot{x}_b + k_bx_b = -f_a - f_p \tag{9.14}$$

For the foundation, the force balance in the horizontal direction gives

$$m_0(\ddot{x}_0 + \ddot{x}_g) + c_{HH}\dot{x}_0 + k_{HH}x_0 + F_{up} = 0 \tag{9.15}$$

where F_{up} is the reaction force from the superstructure to the foundation, k_{HH} and c_{HH} are frequency dependent stiffness and damping, in the impedance function. Their values at the fundamental frequencies of the soil structure system can be applied in the time domain analysis [16,20]. The reaction forces from the superstructure to the foundation is transferred at the column and brace footing, as shown in Figure 9.4, and can be given as

$$F_{up} = -c_1\dot{x}_1 - k_1x_1 - c_b\dot{x}_b - k_bx_b \tag{9.16}$$

that can be transformed as Equation 9.17 based on Equations 9.13 and 9.14

$$F_{up} = m_1\left(\ddot{x}_0 + h_1(\ddot{\phi} + \ddot{\phi}_g) + \ddot{x}_1 + \ddot{x}_g\right) + m_b\left(\ddot{x}_0 + h_b(\ddot{\phi} + \ddot{\phi}_g) + \ddot{x}_b + \ddot{x}_g\right). \tag{9.17}$$

Substituting Equations 9.16 and 9.17 into Equation 9.15 yields

$$m_0\ddot{x}_0 - c_1\dot{x}_1 - k_1x_1 - c_b\dot{x}_b - k_bx_b + c_{HH}\dot{x}_0 + k_{HH}x_0 = -m_0\ddot{x}_g \tag{9.18a}$$

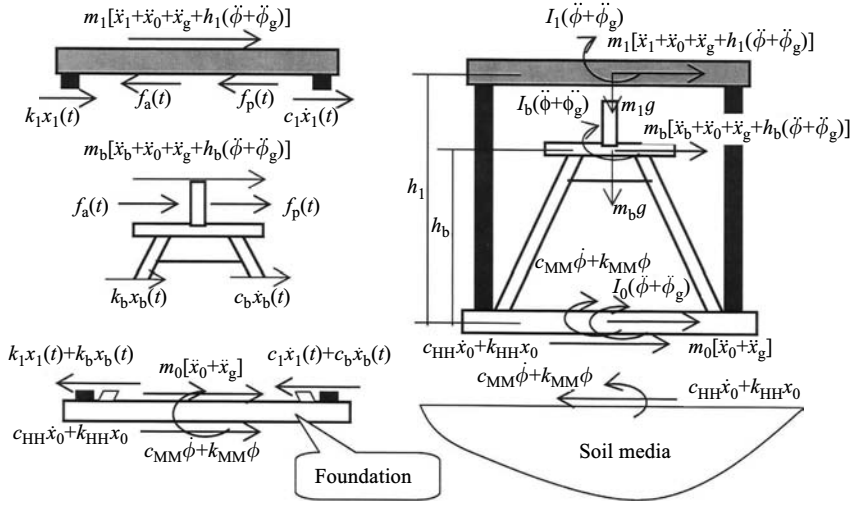

FIGURE 9.4 Free body diagrams for soil structure interaction case.

or

$$m\ddot{x}_0 + m_1\left(\ddot{x}_0 + h_1(\ddot{\phi}+\ddot{\phi}_g) + \ddot{x}_1\right) + m_b\left(\ddot{x}_0 + h_b(\ddot{\phi}+\ddot{\phi}_g) + \ddot{x}_b\right) + k_{HH}x_0 + c_{HH}\dot{x}_0 = -(m_1+m_b+m_0)\ddot{x}_g \tag{9.18b}$$

where $\ddot{\phi}_g$ is the ground rotational acceleration input. The moment balance of the whole system about the foundation's centroid gives the rotational motion equation as

$$I_T(\ddot{\phi}+\ddot{\phi}_g) + m_1h_1\left(\ddot{x}_0 + h_1(\ddot{\phi}+\ddot{\phi}_g) + \ddot{x}_1 + \ddot{x}_g\right) + m_bh_b(\ddot{x}_0 + h_b(\ddot{\phi}+\ddot{\phi}_g) + \ddot{x}_b + \ddot{x}_g) + c_{MM}\dot{\phi}_0 + k_{MM}\phi + m_1gx_1 + m_bgx_b = 0 \tag{9.19a}$$

where $I_T = I_1 + I_b + I_0$ and I_1, I_b and I_0 are mass moment of inertias of floor, brace, and foundation about their centroids, respectively; terms m_1gx_1 and m_bgx_b are moments due to the superstructure weight. It is P-Δ effect, which is omitted in this study but should be considered for tall buildings. Considering general building configurations and simplicity of formulation, we may let $h_b = h_1$, then Equation 9.19a can be expressed as Equation 9.19b based on Equations 9.13 and 9.14

$$I_T(\ddot{\phi}+\ddot{\phi}_g) - c_1h_1\dot{x}_1 - k_1h_1x_1 - c_bh_b\dot{x}_b - k_bh_bx_b + c_{MM}\dot{\phi}_0 + k_{MM}\phi = 0 \tag{9.19b}$$

Let $x_{t1} = x_1 + x_0 + \phi h_1$ and $x_{bt} = x_b + x_0 + \phi h_1$ express the displacements of floor and brace relative to the ground. Rearranging items in

Equations 9.13, 9.14, 9.18a, and 9.19b yields Equations 9.20a through d as

$$m_1\ddot{x}_{1t} + c_1(\dot{x}_{1t} - \dot{x}_0 - h_1\dot{\phi}) + k_1(x_{1t} - x_0 - h_1\phi) = f_a + f_p - m_1\ddot{x}_g - m_1h_1\ddot{\phi}_g \tag{9.20a}$$

$$m_b\ddot{x}_{bt} + c_b(\dot{x}_{bt} - \dot{x}_0 - h_1\dot{\phi}) + k_b(x_{bt} - x_0 - h_1\phi) = -f_a - f_p - m_b\ddot{x}_g - m_bh_1\ddot{\phi}_g \tag{9.20b}$$

$$\begin{aligned} &m_0\ddot{x}_0 - c_1(\dot{x}_{1t} - \dot{x}_0 - h_1\dot{\phi}) - c_b(\dot{x}_{bt} - \dot{x}_0 - h_1\dot{\phi}) - k_1(x_{1t} - x_0 - h_1\phi) \\ &- k_b(x_{bt} - x_0 - h_1\phi) + c_{HH}\dot{x}_0 + k_{HH}x_0 = -m_0\ddot{x}_g \end{aligned} \tag{9.20c}$$

$$\begin{aligned} &I_T\ddot{\phi} - c_1h_1(\dot{x}_{1t} - \dot{x}_0 - h_1\dot{\phi}) - c_bh_1(\dot{x}_{bt} - \dot{x}_0 - h_b\dot{\phi}) - k_1h_1(x_{1t} - x_0 - h_1\phi) \\ &- k_bh_1(x_{bt} - x_0 - h_1\phi) + c_{MM}\dot{\phi}_0 + k_{MM}\phi = -I_T\ddot{\phi}_g \end{aligned} \tag{9.20d}$$

Equations 9.20c and d can be transformed to Equations 9.21a and b by arranging coefficients for $[x_{1t}x_{bt}x_0\phi]$ and their derivatives as

$$\begin{aligned} &m_0\ddot{x}_0 - c_1\dot{x}_{1t} - c_b\dot{x}_{bt} + (c_1 + c_b + c_{HH})\dot{x}_0 + (c_1h_1 + c_bh_1)\dot{\phi} \\ &- k_1x_{1t} - k_bx_{bt} + (k_1 + k_b + k_{HH})x_0 + (k_1h_1 + k_bh_1)\phi = -m_0\ddot{x}_g \end{aligned} \tag{9.21a}$$

$$\begin{aligned} &I_T\ddot{\phi} - c_1h_1\dot{x}_{1t} - c_bh_1\dot{x}_{bt} + (c_1h_1 + c_bh_1)\dot{x}_0 + (c_1h_1^2 + c_bh_b^2 + c_{MM})\dot{\phi} \\ &- k_1h_1x_{1t} - k_bh_1x_{bt} + (k_1h_1 + k_bh_1)x_0 + (k_1h_1^2 + k_bh_1^2 + k_{MM})\phi = -I_T\ddot{\phi}_g \end{aligned} \tag{9.21b}$$

The motion equation of the one-story hybrid controlled system with SSI can then be given in the matrix form of Equation 9.22 by assembling Equations 9.20 a, b, 9.21a, and b as

$$\begin{bmatrix} m_1 & 0 & 0 & 0 \\ 0 & m_b & 0 & 0 \\ 0 & 0 & m_0 & 0 \\ 0 & 0 & 0 & I_T \end{bmatrix} \begin{Bmatrix} \ddot{x}_{1t} \\ \ddot{x}_{bt} \\ \ddot{x}_0 \\ \ddot{\phi} \end{Bmatrix} + \begin{bmatrix} c_1 & 0 & -c_1 & -c_1h_1 \\ 0 & c_b & -c_b & -c_bh_b \\ -c_1 & -c_b & c_1 + c_b + c_{HH} & c_1h_1 + c_bh_b \\ -c_1h_1 & -c_bh_1 & c_1h_1 + c_bh_1 & c_1h_1^2 + c_bh_b^2 + c_{MM} \end{bmatrix} \begin{Bmatrix} \dot{x}_{1t} \\ \dot{x}_{bt} \\ \dot{x}_0 \\ \dot{\phi} \end{Bmatrix} + \begin{bmatrix} k_1 & 0 & -k_1 & -k_1h_1 \\ 0 & k_b & -k_b & -k_bh_1 \\ -k_1 & -k_b & k_1 + k_b + k_{HH} & k_1h_1 + k_bh_1 \\ -k_1h_1 & -k_bh_1 & k_1h_1 + k_bh_1 & k_1h_1^2 + k_bh_1^2 + k_{MM} \end{bmatrix} \begin{Bmatrix} x_{1t} \\ x_{bt} \\ x_0 \\ \phi \end{Bmatrix}$$

$$= \begin{Bmatrix} 1 \\ -1 \\ 0 \\ 0 \end{Bmatrix} f_{\mathrm{a}} + \begin{Bmatrix} 1 \\ -1 \\ 0 \\ 0 \end{Bmatrix} f_{\mathrm{p}} + \begin{Bmatrix} -m_1 \\ -m_{\mathrm{b}} \\ -m_0 \\ 0 \end{Bmatrix} \ddot{x}_{\mathrm{g}} + \begin{Bmatrix} -m_1 h_1 \\ -m_{\mathrm{b}} h_1 \\ 0 \\ -I_{\mathrm{T}} \end{Bmatrix} \ddot{\phi}_{\mathrm{g}} \tag{9.22}$$

9.2.3 Hybrid Controlled Multiple-Story Building without SSI

For an n-story building with the hybrid control at each floor, the motion equations of the controlled system can be given in a general form as [5,7]

$$[M]\{\ddot{x}(t)\} + [C]\{\dot{x}(t)\} + [K]\{x(t)\} = [\delta_{\mathrm{a}}]\{f_{\mathrm{a}}(t)\} + [\delta_{\mathrm{p}}]\{f_{\mathrm{p}}(t)\} + [\delta_{\mathrm{r}}] \begin{Bmatrix} \ddot{x}_{\mathrm{g}}(t) \\ \ddot{\phi}_{\mathrm{g}}(t) \end{Bmatrix} \tag{9.23}$$

where $\{x(t)\}$ is a $2n \times 1$ vector of structural and bracing displacements; and $\{f_a(t)\}$, $\{f_p(t)\}$ are $n \times 1$ vectors of active and passive control forces, respectively; also

$$\{x(t)\} = [\, x_1(t) \quad x_2(t) \quad \ldots \quad x_n(t) \quad x_{\mathrm{b}1}(t) \quad x_{\mathrm{b}2}(t) \quad \ldots \quad x_{\mathrm{b}n}(t)]^{\mathrm{T}} \tag{9.24}$$

$$\{f_{\mathrm{a}}(t)\} = [f_{\mathrm{a}1}(t) \quad f_{\mathrm{a}2}(t) \quad \cdots \quad f_{\mathrm{a}n}(t)]^{\mathrm{T}} \tag{9.25}$$

$$\{f_{\mathrm{p}}(t)\} = [f_{\mathrm{p}1}(t) \quad f_{\mathrm{p}2}(t) \quad \cdots \quad f_{\mathrm{p}n}(t)]^{\mathrm{T}} \tag{9.26}$$

$[M], [C]$, and $[K]$ are $2n \times 2n$ matrixes of the structural mass, damping, and stiffness matrixes, respectively and they can be given as

$$[M] = \begin{bmatrix} [M_{\mathrm{s}}] & \\ & [M_{\mathrm{b}}] \end{bmatrix}; \quad [C] = \begin{bmatrix} [C_{\mathrm{s}}] + [C_{\mathrm{bsb}}] & [C_{\mathrm{sb}}] \\ [C_{\mathrm{bs}}] & [C_{\mathrm{b}}] \end{bmatrix};$$

$$[K] = \begin{bmatrix} [K_{\mathrm{s}}] + [K_{\mathrm{bsb}}] & [K_{\mathrm{sb}}] \\ [K_{\mathrm{bs}}] & [K_{\mathrm{b}}] \end{bmatrix} \tag{9.27}$$

with

$$[M] = \begin{bmatrix} m_1 & & & \\ & m_2 & & \\ & & \ddots & \\ & & & m_n \end{bmatrix}; \quad [M_{\mathrm{b}}] = \begin{bmatrix} m_{b1} & & & \\ & m_{\mathrm{b}2} & & \\ & & \ddots & \\ & & & m_{\mathrm{b}n} \end{bmatrix} \tag{9.28a,b}$$

$$[K_s] = \begin{bmatrix} k_1 + k_2 & -k_2 & & & \\ -k_2 & k_2 + k_3 & & & \\ & & \cdots & & \\ & & & k_{n-1} + k_n & -k_n \\ & & & -k_n & k_n \end{bmatrix};$$

$$[K_b] = \begin{bmatrix} k_{b1} & & & \\ & k_{b2} & & \\ & & \ddots & \\ & & & k_{bn} \end{bmatrix} \tag{9.29a,b}$$

$$[K_{sb}] = [K_{bs}]^T = [\Phi]^T[K_b]; \quad [K_{bsb}] = [\Phi]^T[K_b][\Phi] \tag{9.30a,b}$$

and

$$[\Phi] = \begin{bmatrix} 0 & & & \\ -1 & 0 & & \\ & \cdots & & \\ & -1 & 0 & \\ & & -1 & 0 \end{bmatrix}_{n \times n} \tag{9.31}$$

The damping matrixes are similarly given as

$$[C_s] = \begin{bmatrix} c_1 + c_2 & -c_2 & & & \\ -c_2 & c_2 + c_3 & & & \\ & & \cdots & & \\ & & & c_{n-1} + c_n & -c_n \\ & & & -c_n & c_n \end{bmatrix};$$

$$[C_b] = \begin{bmatrix} c_{b1} & & & \\ & c_{b2} & & \\ & & \ddots & \\ & & & c_{bn} \end{bmatrix} \tag{9.32a,b}$$

$$[C_{sb}] = [C_{bs}]^T = [\Phi]^T[C_b]; \quad [C_{bsb}] = [\Phi]^T[C_b][\Phi] \tag{9.33a,b}$$

$[\delta_a]$ and $[\delta_p]$ are $2n \times n$ controller location matrixes for actuators and dampers, respectively; $[\delta_r]$ is the location matrix for the inputs of horizontal and rotational ground motions. They can be given as

$$[\delta_a] = [\delta_p] = \begin{bmatrix} [\gamma_s] \\ [\gamma_b] \end{bmatrix}; \quad [\gamma_s] = -[\gamma_b] = n\text{th order identity matrix} \tag{9.34}$$

and

$$[\delta_{\mathrm{r}}] = -[M][\Gamma]; \quad \Gamma = \begin{bmatrix} 1 & \dots & 1 & 1 & \dots & 1 \\ h_1 & \dots & h_n & h_1 & \dots & h_n \end{bmatrix}^{\mathrm{T}} \tag{9.35}$$

If the brace stiffness is not considered in the controlled system, then matrices in Equation 9.23, Equations 9.24 through 9.27 should be modified as

$$\begin{cases} \{x(t)\} = [x_1(t) & x_2(t) & \dots & x_n(t)]^{\mathrm{T}} \\ \{f_{\mathrm{a}}(t)\} = [f_{\mathrm{a}1}(t) & f_{\mathrm{a}2}(t) & \cdots & f_{\mathrm{a}n}(t)]^{\mathrm{T}} \\ \{f_{\mathrm{p}}(t)\} = [f_{\mathrm{p}1}(t) & f_{\mathrm{p}2}(t) & \cdots & f_{\mathrm{p}n}(t)]^{\mathrm{T}} \end{cases} \tag{9.36}$$

$[M]$, $[C]$, and $[K]$ are $n \times n$ matrixes of the structural mass, damping, and stiffness matrixes, respectively and they can be given as

$$[M] = [M_{\mathrm{s}}]; \quad [C] = [C_{\mathrm{s}}]; \quad [K] = [K_{\mathrm{s}}] \tag{9.37}$$

If controllers are put at some specific floors, rather than at each floor, the bracing location matrix, $[\theta]$, is introduced, which is a $n \times m$ matrix if there are m braces. The elements of this matrix are all zero except that $\theta(i,j) = 1$ when the jth bracing is supported on the ith floor ($j = 1, \dots, m$). Then

$$\begin{cases} [C_{\mathrm{bs}}]^{\mathrm{T}}_{n\times m} = [C_{\mathrm{sb}}]_{n\times m} = [\Phi]^{\mathrm{T}}_{n\times n}[\theta]_{n\times m}[C_{\mathrm{b}}]_{m\times m} \\ [K_{\mathrm{bs}}]^{\mathrm{T}}_{n\times m} = [K_{\mathrm{sb}}]_{n\times m} = [\Phi]^{\mathrm{T}}_{n\times n}[\theta]_{n\times m}[K_b]_{m\times m} \end{cases} \tag{9.38a,b}$$

$$\begin{cases} [C_{\mathrm{bsb}}]_{n\times n} = [\Phi]^{\mathrm{T}}_{n\times n}[\theta]_{n\times m}[C_{\mathrm{b}}]_{m\times m}[\theta]^{\mathrm{T}}_{m\times n}[\Phi]_{n\times n} = [C_{\mathrm{sb}}]_{n\times m}[\theta]^{\mathrm{T}}_{m\times n}[\Phi]_{n\times n} \\ [K_{\mathrm{bsb}}]_{n\times n} = [\Phi]^{\mathrm{T}}_{n\times n}[\theta]_{n\times m}[K_{\mathrm{b}}]_{m\times m}[\theta]^{\mathrm{T}}_{m\times n}[\Phi]_{n\times n} = [K_{\mathrm{sb}}]_{n\times m}[\theta]^{\mathrm{T}}_{m\times n}[\Phi]_{n\times n} \end{cases} \tag{9.39a,b}$$

and the controller input matrixes in Equation 9.34 become

$$[\delta_{\mathrm{a}}]_{(n+m)\times m} = [\delta_{\mathrm{p}}]_{(n+m)\times m} = \begin{bmatrix} [\gamma_{\mathrm{s}}]_{n\times n}[\theta]_{n\times m} \\ [\theta]^{\mathrm{T}}_{m\times n}[\gamma_{\mathrm{b}}]_{n\times n}[\theta]_{n\times m} \end{bmatrix} \tag{9.40}$$

Then the motion equations for the n-story building with m hybrid controllers are established for the system resting on a fixed base.

9.2.4 Hybrid Controlled Multiple-Story Building with SSI

The controlled building is illustrated in Figure 9.5. The difference of forces on free bodies of floor or bracing is that two more items appear in the inertia forces when foundation motion is considered. They are $m_i\ddot{x}_0$ and $m_i h_i \ddot{\phi}$, where m_i and h_i are mass of the ith free body and its height. So the motion equation of the

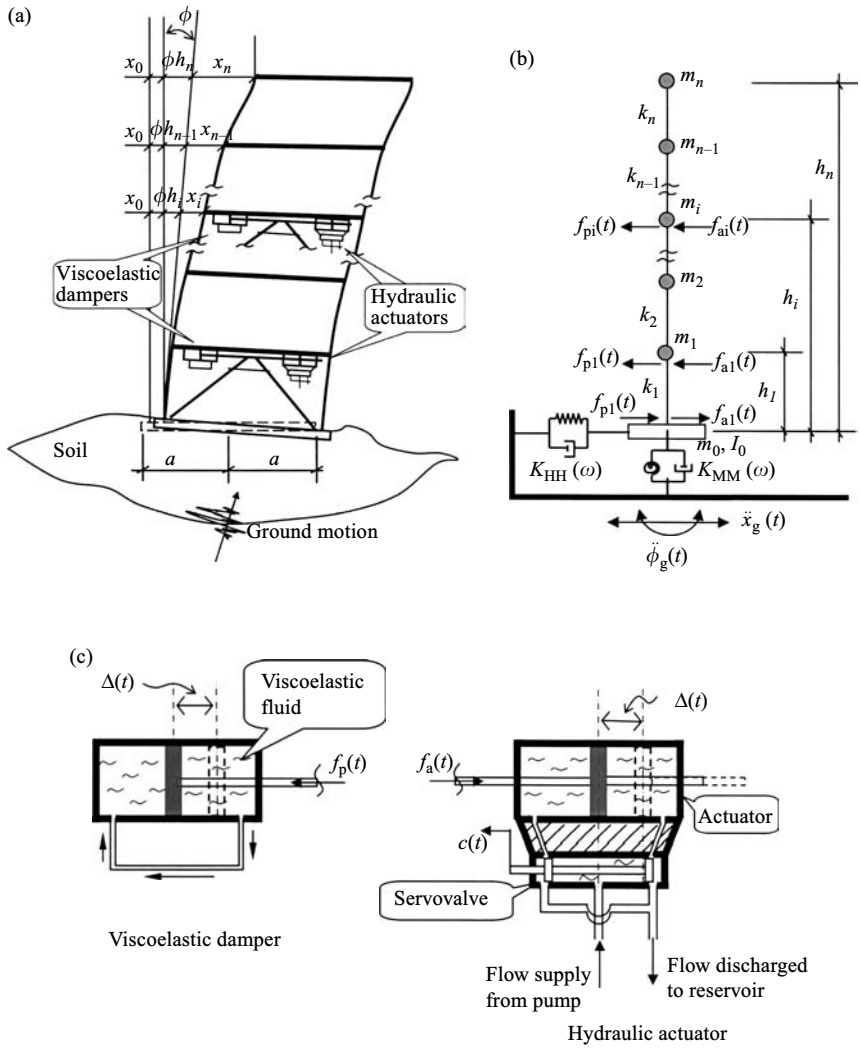

FIGURE 9.5 HDABC SSI structure system: (a) multiple-story structure, (b) mathematical model, and (c) viscoelastic damper and hydraulic actuator.

superstructure can be obtained for the SSI case by adding those inertia forces to that of the fixed base case as

$$[M]\{\ddot{x}(t)\} + [M][\Gamma]\begin{Bmatrix} \ddot{x}_0(t) \\ \ddot{\phi}(t) \end{Bmatrix} + [C]\{\dot{x}(t)\} + [K]\{x(t)\} = [\delta_a]\{f_a(t)\} + [\delta_p]\{f_p(t)\} + [\delta_r]\begin{Bmatrix} \ddot{x}_g(t) \\ \ddot{\phi}_g(t) \end{Bmatrix} \tag{9.41}$$

that can be rearranged as

$$[M]\{\ddot{x}(t)\} + [C]\{\dot{x}(t)\} + [K]\{x(t)\} = [\delta_a]\{f_a(t)\} + [\delta_p]\{f_p(t)\} + [\delta_r]\begin{Bmatrix} \ddot{x}_0(t) + \ddot{x}_g(t) \\ \ddot{\phi}_(t) + \ddot{\phi}_g(t) \end{Bmatrix} \tag{9.42}$$

The horizontal-force balance of the free-body foundation generates the lateral-motion equation for the foundation as

$$m_0(\ddot{x}_0 + \ddot{x}_g) + c_{HH}\dot{x}_0 + k_{HH}x_0 + F_{up} = 0 \tag{9.43}$$

where F_{up} is the force from the superstructure to the foundation transferred through column (and bracing if there is a control at the first floor).

$$F_{up} = -c_1\dot{x}_1 - k_1x_1 - c_b\dot{x}_b - k_bx_b = -[1 \quad 1\cdots 1]_{1\times(n+m)}\left([K]\{x\} + [C]\{\dot{x}\}\right) \tag{9.44}$$

that can be written in another form by substituting the motion equation of the superstructure of Equation 9.42 into Equation 9.44. It becomes

$$F_{up} = -[1 \;\; 1 \;\; \cdots \;\; 1]_{1\times(n+m)} \left(-[M]\{\ddot{x}(t)\} + [\delta_a]\{f_a(t)\} + [\delta_p]\{f_p(t)\} + [\delta_r]\begin{Bmatrix} \ddot{x}_0(t) + \ddot{x}_g(t) \\ \ddot{\phi}_(t) + \ddot{\phi}_g(t) \end{Bmatrix}\right) \tag{9.45}$$

Because the forces of active and passive are internally acting on the floors and braces, which are self balanced within the superstructure, there are

$$-[1 \;\; 1 \;\; \cdots \;\; 1]_{1\times(n+m)}\left([\delta_a]\{f_a(t)\} + [\delta_p]\{f_p(t)\}\right) = 0. \tag{9.46}$$

So, Equation 9.45 can be simplified as

$$F_{up} = -[1 \;\; 1 \;\; \cdots \;\; 1]_{(1\times(n+m)}\left(-[M]\{\ddot{x}(t)\} + [\delta_r]\begin{Bmatrix} \ddot{x}_0(t) + \ddot{x}_g(t) \\ \ddot{\phi}_(t) + \ddot{\phi}_g(t) \end{Bmatrix}\right) \tag{9.47a}$$

Noting that $[\delta_r] = -[M][\Gamma]$, Equation 9.47a can be written as Equation 9.47b as

$$F_{up} = [1 \;\; 1 \;\; \cdots \;\; 1]_{1\times(n+m)}[M]\left(\{\ddot{x}(t)\} + [\Gamma]\begin{Bmatrix} \ddot{x}_0(t) + \ddot{x}_g(t) \\ \ddot{\phi}_(t) + \ddot{\phi}_g(t) \end{Bmatrix}\right) \tag{9.47b}$$

Substituting Equation 9.47b into Equation 9.43, the motion equation of the foundation in the horizontal direction can be

$$m_0(\ddot{x}_0 + \ddot{x}_g) + [1 \;\; 1 \;\; \cdots \;\; 1]_{(1\times(n+m))}[M]\left(\{\ddot{x}(t)\} + [\Gamma]\begin{Bmatrix}\ddot{x}_0(t)+\ddot{x}_g(t)\\ \ddot{\phi}(t)+\ddot{\phi}_g(t)\end{Bmatrix}\right) + c_{HH}\dot{x}_0 + k_{HH}x_0 = 0 \tag{9.48}$$

where the first item in the equation is the inertia force at the foundation, the second item expresses the force transferred from the superstructure, and the last two items are the reaction force of the soil to the foundation in the lateral direction.

The motion equation of the foundation in rocking can be obtained by the moment balance of the whole system. Similar to the single story building, it can be obtained as

$$I_0(\ddot{\phi} + \ddot{\phi}_g) + [\,h_1 \;\; \cdots \;\; h_n \;\; h_1 \;\; \cdots \;\; h_n\,]_{1\times(n+m)}[M] \times \left(\{\ddot{x}(t)\} + [\Gamma]\begin{Bmatrix}\ddot{x}_0(t)+\ddot{x}_g(t)\\ \ddot{\phi}(t)+\ddot{\phi}_g(t)\end{Bmatrix}\right) + c_{MM}\dot{\phi}_0 + k_{MM}\phi = 0 \tag{9.49}$$

The first item in the equation is the inertia moment at the foundation. The centroidal moment of inertia of the superstructure can be neglected in the seismic response of simple building-foundation systems [4], so there is I_0, rather than I_T, in the item. The second item expresses the moments caused from the horizontal inertia forces at each mass of the superstructure. The last two items are the reaction moment of the soil to the foundation.

Equations 9.48 and 9.49 can be combined to give the motion equations for the foundation as

$$\begin{bmatrix} m_0 & 0\\ 0 & I_0\end{bmatrix}\begin{Bmatrix}\ddot{x}_0(t)+\ddot{x}_g(t)\\ \ddot{\phi}(t)+\ddot{\phi}_g(t)\end{Bmatrix} + [\Gamma]^T[M]\left(\{\ddot{x}(t)\} + [\Gamma]\begin{Bmatrix}\ddot{x}_0(t)+\ddot{x}_g(t)\\ \ddot{\phi}(t)+\ddot{\phi}_g(t)\end{Bmatrix}\right) = -\begin{bmatrix} c_{HH} & \\ & c_{MM}\end{bmatrix}\begin{Bmatrix}\dot{x}_0\\ \dot{\phi}\end{Bmatrix} - \begin{bmatrix} k_{HH} & \\ & k_{MM}\end{bmatrix}\begin{Bmatrix}x_0\\ \phi\end{Bmatrix} \tag{9.50a}$$

Substituting the motion of the superstructure into Equation 9.50a yields

$$\begin{bmatrix} m_0 & 0\\ 0 & I_0\end{bmatrix}\begin{Bmatrix}\ddot{x}_0(t)+\ddot{x}_g(t)\\ \ddot{\phi}(t)+\ddot{\phi}_g(t)\end{Bmatrix} + [\Gamma]^T(-[C]\{\dot{x}(t)\} - [K]\{x(t)\}[\delta_a]\{f_a(t)\} + [\delta_p]\{f_p(t)\}) = -\begin{bmatrix} c_{HH} & \\ & c_{MM}\end{bmatrix}\begin{Bmatrix}\dot{x}_0\\ \dot{\phi}\end{Bmatrix} - \begin{bmatrix} k_{HH} & \\ & k_{MM}\end{bmatrix}\begin{Bmatrix}x_0\\ \phi\end{Bmatrix} \tag{9.50b}$$

that can be expanded as

$$\begin{bmatrix} m_0 & 0 \\ 0 & I_0 \end{bmatrix} \begin{Bmatrix} \ddot{x}_0(t) + \ddot{x}_g(t) \\ \ddot{\phi}(t) + \ddot{\phi}_g(t) \end{Bmatrix} - [\Gamma]^T[C]\{\dot{x}(t)\} + \begin{bmatrix} c_{HH} & \\ & c_{MM} \end{bmatrix} \begin{Bmatrix} \dot{x}_0 \\ \dot{\phi} \end{Bmatrix}$$
$$- [\Gamma]^T[K]\{x(t)\} + \begin{bmatrix} k_{HH} & \\ & k_{MM} \end{bmatrix} \begin{Bmatrix} x_0 \\ \phi \end{Bmatrix} = -[\Gamma]^T[\delta_a]\{f_a(t)\} - [\Gamma]^T[\delta_p]\{f_p(t)\} \tag{9.51}$$

Similar to the single story case, the displacement of floor and brace relative to the ground are defined as

$$\{x_t(t)\} = \{x(t)\} + [\Gamma]\{X_f(t)\} = \{x(t)\} + [\Gamma] \begin{Bmatrix} x_0(t) \\ \phi(t) \end{Bmatrix} \tag{9.52}$$

where $\{X_f(t)\}$ defined in the above equation is the motion vector of the foundation, which includes the horizontal, transversal, and rocking motions.

Replacing $\{x(t)\}$ based on Equation 9.52, in the motion equation of the superstructure, Equation 9.42, it becomes

$$[M]\{\ddot{x}_t(t)\} - [M][\Gamma] \begin{Bmatrix} \ddot{x}_0(t) \\ \ddot{\phi}(t) \end{Bmatrix} + [C]\{\dot{x}_t(t)\} - [C][\Gamma] \begin{Bmatrix} \dot{x}_0(t) \\ \dot{\phi}(t) \end{Bmatrix}$$
$$+ [K]\{x_t(t)\} - [K][\Gamma] \begin{Bmatrix} x_0(t) \\ \phi(t) \end{Bmatrix}$$
$$= [\delta_a]\{f_a(t)\} + [\delta_p]\{f_p(t)\} + [\delta_r] \begin{Bmatrix} \ddot{x}_0(t) + \ddot{x}_g(t) \\ \ddot{\phi}(t) + \ddot{\phi}_g(t) \end{Bmatrix} \tag{9.53}$$

Noting that $[\delta_r] = -[M][\Gamma]$, Equation 9.53 can be reduced as

$$[M]\{\ddot{x}_t(t)\} + [C]\{\dot{x}_t(t)\} - [C][\Gamma] \begin{Bmatrix} \dot{x}_0(t) \\ \dot{\phi}(t) \end{Bmatrix} + [K]\{x_t(t)\} - [K][\Gamma] \begin{Bmatrix} x_0(t) \\ \phi(t) \end{Bmatrix}$$
$$= [\delta_a]\{f_a(t)\} + [\delta_p]\{f_p(t)\} + [\delta_r] \begin{Bmatrix} \ddot{x}_g(t) \\ \ddot{\phi}_g(t) \end{Bmatrix} \tag{9.54}$$

By replacing $\{x(t)\}$, based on Equation 9.52, in the motion equation of the foundation, Equation 9.51 becomes

$$\begin{bmatrix} m_0 & 0 \\ 0 & I_0 \end{bmatrix} \begin{Bmatrix} \ddot{x}_0(t) \\ \ddot{\phi}(t) \end{Bmatrix} - [\Gamma]^T[C]\{\dot{x}_t(t)\} + \left([\Gamma]^T[C][\Gamma] + \begin{bmatrix} c_{HH} & \\ & c_{MM} \end{bmatrix} \right) \begin{Bmatrix} \dot{x}_0 \\ \dot{\phi} \end{Bmatrix}$$
$$- [\Gamma]^T[K]\{x_t(t)\} + \left([\Gamma]^T[K][\Gamma] + \begin{bmatrix} k_{HH} & \\ & k_{MM} \end{bmatrix} \right) \begin{Bmatrix} x_0 \\ \phi \end{Bmatrix}$$
$$= -[\Gamma]^T[\delta_a]\{f_a(t)\} - [\Gamma]^T[\delta_p]\{f_p(t)\} - \begin{bmatrix} m_0 & 0 \\ 0 & I_0 \end{bmatrix} \begin{Bmatrix} \ddot{x}_g(t) \\ \ddot{\phi}_g(t) \end{Bmatrix} \tag{9.55}$$

The motion equation of the whole system can be obtained by assembling Equation 9.54 for superstructure, and Equation 9.55 for foundation, as

$$\begin{bmatrix} [M] & 0 \\ 0 & [M_{\mathrm{f}}] \end{bmatrix} \begin{Bmatrix} \ddot{x}_t(t) \\ \ddot{X}_{\mathrm{f}}(t) \end{Bmatrix} + \begin{bmatrix} [C] & -[C][\Gamma] \\ -[\Gamma]^{\mathrm{T}}[C] & [\Gamma]^{\mathrm{T}}[C][\Gamma] + [C_{\mathrm{s}}] \end{bmatrix} \begin{Bmatrix} \dot{x}_t(t) \\ \dot{X}_{\mathrm{f}}(t) \end{Bmatrix} + \begin{bmatrix} [K] & -[K][\Gamma] \\ -[\Gamma]^{\mathrm{T}}[K] & [\Gamma]^{\mathrm{T}}[K][\Gamma] + [K_s] \end{bmatrix} \begin{Bmatrix} x_t(t) \\ X_{\mathrm{f}}(t) \end{Bmatrix} = -\begin{bmatrix} -[\delta_{\mathrm{a}}] \\ [\Gamma]^{\mathrm{T}}[\delta_{\mathrm{a}}] \end{bmatrix} \{f_{\mathrm{a}}(t)\} - \begin{bmatrix} -[\delta_{\mathrm{p}}] \\ [\Gamma]^{\mathrm{T}}[\delta_{\mathrm{p}}] \end{bmatrix} \{f_{\mathrm{p}}(t)\} - \begin{bmatrix} [M] & 0 \\ 0 & [M_{\mathrm{f}}] \end{bmatrix} \begin{bmatrix} [\Gamma] \\ [I_2] \end{bmatrix} \begin{Bmatrix} \ddot{x}_{\mathrm{g}}(t) \\ \ddot{\phi}_{\mathrm{g}}(t) \end{Bmatrix} \tag{9.56}$$

where $[M_{\mathrm{f}}] = \begin{bmatrix} m_0 & 0 \\ 0 & I_0 \end{bmatrix}$; $[C_{\mathrm{s}}] = \begin{bmatrix} c_{\mathrm{HH}} & \\ & c_{\mathrm{MM}} \end{bmatrix}$; $[K_{\mathrm{s}}] = \begin{bmatrix} k_{\mathrm{HH}} & \\ & k_{\mathrm{MM}} \end{bmatrix}$; $[I_2]$ is an identity matrix with order of 2. By defining the mass, stiffness, and damping matrixes of the global SSI system as

$$[M_{\mathrm{SSI}}] = \begin{bmatrix} M & 0 \\ 0 & M_{\mathrm{f}} \end{bmatrix}; \quad [C_{\mathrm{SSI}}] = \begin{bmatrix} C & -C\Gamma \\ -\Gamma^{\mathrm{T}}C & \Gamma^{\mathrm{T}}C\Gamma + C_{\mathrm{s}} \end{bmatrix};$$
$$[K_{\mathrm{SSI}}] = \begin{bmatrix} K & -K\Gamma \\ -\Gamma^{\mathrm{T}}K & \Gamma^{\mathrm{T}}K\Gamma + K_{\mathrm{s}} \end{bmatrix} \tag{9.57a,b,c}$$

and defining the input location matrixes for the global system as

$$[\delta_{\mathrm{a}}^{\mathrm{s}}] = -\begin{bmatrix} -\delta_{\mathrm{a}} \\ \Gamma^{\mathrm{T}}\delta_{\mathrm{a}} \end{bmatrix}; \quad [\delta_{\mathrm{p}}^{\mathrm{s}}] = -\begin{bmatrix} -\delta_{\mathrm{p}} \\ \Gamma^{\mathrm{T}}\delta_{\mathrm{p}} \end{bmatrix}; \quad [\delta_{\mathrm{r}}^{\mathrm{s}}] = -[M_{\mathrm{SSI}}] \begin{bmatrix} \Gamma \\ I_2 \end{bmatrix} \tag{9.58a,b,c}$$

Equation 9.56 can be simply expressed as

$$[M_{\mathrm{SSI}}]\{\ddot{x}_t(t)\} + [C_{\mathrm{SSI}}]\{\dot{x}_t(t)\} + [K_{\mathrm{SSI}}]\{x_t(t)\} = [\delta_{\mathrm{a}}^{\mathrm{s}}]\{f_{\mathrm{a}}(t)\} + [\delta_{\mathrm{p}}^{\mathrm{s}}]\{f_{\mathrm{p}}(t)\} + [\delta_r^{\mathrm{s}}] \begin{Bmatrix} \ddot{x}_{\mathrm{g}}(t) \\ \ddot{\phi}_{\mathrm{g}}(t) \end{Bmatrix} \tag{9.59}$$

that is the motion equation of the SSI system in a form similar to the fixed base case, except with the coefficient matrixes replaced. By putting the superstructure property matrixes of the single story case

$$[M] = \begin{bmatrix} m_1 & \\ & m_{\mathrm{b}} \end{bmatrix}; \quad [K] = \begin{bmatrix} k_1 & \\ & k_{\mathrm{b}} \end{bmatrix}; \quad [C] = \begin{bmatrix} c_1 & \\ & c_{\mathrm{b}} \end{bmatrix}$$

and

$$[\delta_{\mathrm{a}}] = [\delta_{\mathrm{p}}] = \begin{bmatrix} 1 \\ -1 \end{bmatrix}; \quad [\Gamma] = \begin{bmatrix} 1 & h_1 \\ 1 & h_1 \end{bmatrix}$$

into Equation 9.59, the motion equation for the single story case can be obtained, which produces the same results as Equation 9.22.

9.3 State Space Formulation of HDABC Systems with and without SSI

9.3.1 Single-Story Structural System without SSI

As discussed in Chapter 4 the state space representation is composed of a series of first order differential equations for which equations of the structural system are given as Equations 9.9a through d. The equations of the control system can be written based on Equations 5.35b, 5.36, and 5.39a which become Equations 9.60, 9.61, and 9.62, respectively.

$$\frac{\mathrm{d}}{\mathrm{d}t} f_{\mathrm{a}}(t) = \alpha_1 \left(\dot{x}_1(t) - \dot{x}_{\mathrm{b}}(t)\right) + \alpha_2 c(t) \tag{9.60}$$

$$\frac{\mathrm{d}}{\mathrm{d}t} c(t) = -\frac{1}{\tau} c(t) + \frac{1}{\tau} u(t) \tag{9.61}$$

$$\frac{\mathrm{d}}{\mathrm{d}t} f_{\mathrm{p}}(t) = p_1 \left(\dot{x}_1(t) - \dot{x}_{\mathrm{b}}(t)\right) + p_2 f_{\mathrm{p}}(t) \tag{9.62}$$

where new notations of $p_1 = \frac{C_0}{\lambda_0}$, $p_2 = -\frac{1}{\lambda_0}$, $\alpha_1 = \frac{2\beta A^2}{V}$, and $\alpha_2 = \frac{\beta A K_{\mathrm{v}}}{V}\sqrt{2P_{\mathrm{s}}}$ are to simplify the expressions as introduced in Equation 5.35. By selecting the state vector of

$$z(t) = \left[\dot{x}_1(t), \dot{x}_{\mathrm{b}}(t), x_1(t), x_{\mathrm{b}}(t), f_{\mathrm{a}}(t), f_{\mathrm{p}}(t), c(t)\right]^{\mathrm{T}} \tag{9.63}$$

the state space representation for the whole hybrid controlled system can be given in Equation 9.64 using Equations 9.9a through d and Equations 9.60 through 9.62 as

$$\dot{z}(t) = [A_t] z(t) + \{B_{\mathrm{u}}\} u(t) + \{B_{\mathrm{r}}\} \ddot{x}_{\mathrm{g}}(t) \tag{9.64}$$

where $[A_t]$ is the plant matrix as

$$[A_t] = \left[\begin{array}{cccc:ccc} 0 & 0 & 1 & 0 & 0 & 0 & 0 \\ 0 & 0 & 0 & 1 & 0 & 0 & 0 \\ -\omega_1^2 & 0 & -2\rho_1\omega_1 & 0 & 1/m_1 & 1/m_1 & 0 \\ 0 & -\omega_{\mathrm{b}}^2 & 0 & -2\rho_{\mathrm{b}}\omega_{\mathrm{b}} & -1/m_{\mathrm{b}} & -1/m_{\mathrm{b}} & 0 \\ \hdashline 0 & 0 & \alpha_1 & -\alpha_1 & 0 & 0 & \alpha_2 \\ 0 & 0 & p_1 & -p_1 & 0 & p_2 & 0 \\ 0 & 0 & 0 & 0 & 0 & 0 & -1/\tau \end{array}\right]_{7\times 7} \tag{9.65}$$

and the input location vectors for the control command, $u(t)$, and the ground acceleration $\ddot{x}_g(t)$ have their forms as

$$\{B_u\}_{7\times 1} = \begin{bmatrix} 0 & 0 & 0 & 0 & 0 & 0 & -1/\tau \end{bmatrix}^T \tag{9.66}$$

$$\{B_r\}_{7\times 1} = \begin{bmatrix} 0 & 0 & -1 & -1 & 0 & 0 & 0 \end{bmatrix}^T \tag{9.67}$$

9.3.2 Single-Story Structural System with SSI

The state space representation for the hybrid-controlled system with soil considered can be obtained by using the motion equation of the SSI system of Equation 9.22. Four more items need to be added in the state vector for the foundation's motions as

$$z(t) = \left[\dot{x}_1(t), \dot{x}_b(t), \dot{x}_0(t), \dot{\phi}(t), x_1(t), x_b(t), x_0(t), \phi(t), f_a(t), f_p(t), c(t)\right]^T \tag{9.68}$$

and the state space representation for the SSI system is given as

$$\dot{z}(t) = [A_t^s]z(t) + \{B_u^s\}u(t) + [B_r^s]\begin{Bmatrix} \ddot{x}_g(t) \\ \ddot{\phi}_g(t) \end{Bmatrix} \tag{9.69}$$

where the plant matrix and the input location vectors are different from those for the fixed base case. They are marked with the superscript s to indicate that they are for the SSI case. The plant matrix is given in Equation 9.70 as

$[A_t^s]_{11\times 11} =$

$$\begin{bmatrix}
0 & 0 & 0 & 0 & 1 & 0 & 0 & 0 & 0 & 0 & 0 \\
0 & 0 & 0 & 0 & 0 & 1 & 0 & 0 & 0 & 0 & 0 \\
0 & 0 & 0 & 0 & 0 & 0 & 1 & 0 & 0 & 0 & 0 \\
0 & 0 & 0 & 0 & 0 & 0 & 0 & 1 & 0 & 0 & 0 \\
-\omega_1^2 & 0 & \omega_1^2 & \omega_1^2 h_1 & -2\rho_1\omega_1 & 0 & 2\rho_1\omega_1 & 2\rho_1\omega_1 h_1 & 1 & 1 & 0 \\
0 & -\omega_b^2 & \omega_b^2 & \omega_b^2 h_1 & 0 & -2\rho_b\omega_b & 2\rho_b\omega_b & 2\rho_b\omega_b h_1 & -1 & -1 & 0 \\
\frac{k_1}{m_0} & \frac{k_b}{m_0} & -\frac{(k_1+k_b+k_{HH})}{m_0} & -\frac{(k_1 h_1+k_b h_1)}{m_0} & \frac{c_1}{m_0} & \frac{c_b}{m_0} & -\frac{(c_1+c_b+c_{HH})}{m_0} & -\frac{(c_1 h_1+c_b h_1)}{m_0} & 0 & 0 & 0 \\
\frac{k_1 h_1}{I_T} & \frac{k_b h_1}{I_T} & -\frac{(k_1 h_1+k_b h_1)}{I_T} & -\frac{(k_1 h_1^2+k_b h_1^2+k_{MM})}{I_T} & \frac{c_1 h_1}{I_T} & \frac{c_b h_1}{I_T} & -\frac{(c_1 h_1+c_b h_1)}{I_T} & -\frac{(c_1 h_1^2+c_b h_1^2+c_{MM})}{I_T} & 0 & 0 & 0 \\
0 & 0 & 0 & 0 & \alpha_1 & -\alpha_1 & 0 & 0 & 0 & 0 & \alpha_2 \\
0 & 0 & 0 & 0 & p_1 & -p_1 & 0 & 0 & 0 & p_2 & 0 \\
0 & 0 & 0 & 0 & 0 & 0 & 0 & 0 & 0 & 0 & -\frac{1}{\tau}
\end{bmatrix} \tag{9.70}$$

The input location vectors for the control command and the ground acceleration in the SSI system are given as

$$\{B_u^s\}_{11\times 1} = [0\ 0\ 0\ 0\ 0\ 0\ 0\ 0\ 0\ 0\ -1/\tau]^T \tag{9.71}$$

and

$$[B_r^s]_{11\times 2} = \begin{bmatrix} 0 & 0 & 0 & 0 & -1 & -1 & -1 & 0 & 0 & 0 & 0 \\ 0 & 0 & 0 & 0 & -h_1 & -h_1 & 0 & -1 & 0 & 0 & 0 \end{bmatrix}^T \tag{9.72}$$

9.3.3 Multiple-Story Building System without SSI

The motion equation of the controlled structure system is given in Equation 9.23. The equations of m hybrid controllers can be assembled as

$$\{\dot{f}_{\mathrm{p}}(t)\} = [P_1]\{\dot{x}(t)\} + [P_2]\{f_{\mathrm{p}}(t)\} \tag{9.73}$$

$$\{\dot{f}_{\mathrm{a}}(t)\} = [F_x]\{\dot{x}(t)\} + [F_{\mathrm{c}}]\{c(t)\} \tag{9.74}$$

$$\{\dot{c}(t)\} = [C_{\mathrm{c}}]\{c(t)\} + [C_{\mathrm{u}}]\{u(t)\} \tag{9.75}$$

where $[P_1]$ is a $m \times (n+m)$ matrix with each row describing damper properties. Supposing the kth damper is put between the ith floor and the jth brace, there are only two nonzero elements at the kth row of $[P_1]$. They are

$$P_1(k,i) = -\frac{C_{0k}}{\lambda_{0k}}; \quad P_1(k,n+j) = \frac{C_{0k}}{\lambda_{0k}} \tag{9.76}$$

and $[P_2]$ is a $m \times m$ diagonal matrix with its elements

$$P_2(k,k) = \frac{-1}{\lambda_{0k}} \tag{9.77}$$

where C_{0k} and λ_{0k} are the damping coefficient and relaxation time corresponding to the kth damper, respectively [8]. When bracing stiffness is not involved, then $[P_1]$ is a $m \times n$ matrix. Supposing the kth damper is put at the ith floor, there are two nonzero elements at the kth row of $[P_1]$ and they are

$$P_1(k,i) = -\frac{C_{0k}}{\lambda_{0k}}; \quad P_1(k,i-1) = \frac{C_{0k}}{\lambda_{0k}}$$

where $P_1(k,i-1)$ is nonexistent for the case of $i = 1$.

$[F_x]$ is a $m \times (n+m)$ matrix with each row describing an actuator. Supposing the kth actuator is put between the ith floor and the jth brace, there are only two nonzero elements at the kth row of $[F_x]$. They are

$$F_x(k,i) = -\alpha_{1k} \quad \text{and} \quad F_x(k,n+j) = \alpha_{1k} \tag{9.78}$$

and $[F_{\mathrm{c}}]$ is a $m \times m$ diagonal matrix with its elements as

$$F_{\mathrm{c}}(k,k) = \alpha_{2k} \tag{9.79}$$

and $[C_{\mathrm{c}}]$ and $[C_{\mathrm{u}}]$ are $m \times m$ diagonal matrices with their elements as

$$C_{\mathrm{c}}(k,k) = \frac{-1}{\tau_k}; \quad C_{\mathrm{u}}(k,k) = \frac{1}{\tau_k} \tag{9.80}$$

where subscripts of k denote that the item corresponds to the kth controller. Select the state space vector as

$$\{z\} = \left[\{x\}_{n+m}^{\mathrm{T}} \ \{\dot{x}\}_{n+m}^{\mathrm{T}} \ \{f_{\mathrm{a}}\}_{m}^{\mathrm{T}} \ \{f_{\mathrm{p}}\}_{m}^{\mathrm{T}} \ \{c\}_{m}^{\mathrm{T}}\right]^{\mathrm{T}} \tag{9.81}$$

and combine the structure equations and controller equations; the state space representation of the hybrid-controlled multiple-story building on the fixed base can be given as

$$\dot{z}(t) = [A_t]z(t) + [B_{\mathrm{u}}]u(t) + [B_{\mathrm{r}}]\begin{Bmatrix} \ddot{x}_{\mathrm{g}}(t) \\ \ddot{\phi}_{\mathrm{g}}(t) \end{Bmatrix} \tag{9.82}$$

with the plant matrix as

$$[A_t]_{(2n+5m)\times(2n+5m)} = \begin{bmatrix} [zero]_{(n+m)\times(n+m)} & [I]_{(n+m)\times(n+m)} & & [zero]_{(n+m)\times 3m} & \\ -[M]^{-1}[K] & -[M]^{-1}[C] & -[M]^{-1}[\delta_{\mathrm{a}}] & -[M]^{-1}[\delta_{\mathrm{p}}] & [zero]_{(n+m)\times m} \\ [zero]_{m\times(n+m)} & [F_x] & [zero]_{m\times m} & [zero]_{m\times m} & [F_{\mathrm{c}}] \\ [zero]_{m\times(n+m)} & [P_1] & [zero]_{m\times m} & [P_2] & [zero]_{m\times m} \\ [zero]_{m\times(n+m)} & [zero]_{m\times(n+m)} & [zero]_{m\times m} & [zero]_{m\times m} & [C_{\mathrm{c}}] \end{bmatrix} \tag{9.83}$$

The input location vectors for the control command and the ground acceleration are given as

$$[B_{\mathrm{u}}]_{(2n+5m)\times m} = \begin{bmatrix} [zero]_{(2n+4m)\times m} \\ [C_{\mathrm{u}}] \end{bmatrix} \tag{9.84}$$

and

$$[B_{\mathrm{r}}]_{(2n+5m)\times 2} = \begin{bmatrix} [zero]_{(n+m)\times 2} \\ -[\Gamma] \\ [zero]_{3m\times 2} \end{bmatrix} \tag{9.85}$$

9.3.4 Multiple-Story Structural System with SSI

The state space representation for the SSI case can be obtained in the manner similar to Equation 9.81, which becomes

$$\{z\} = \left[\{x\}_{n+m}^{\mathrm{T}} \quad \begin{Bmatrix} x_0 \\ \phi \end{Bmatrix}^{\mathrm{T}} \quad \{\dot{x}\}_{n+m}^{\mathrm{T}} \quad \begin{Bmatrix} \dot{x}_0 \\ \dot{\phi} \end{Bmatrix}^{\mathrm{T}} \quad \{f_{\mathrm{a}}\}_{m}^{\mathrm{T}} \quad \{f_{\mathrm{p}}\}_{m}^{\mathrm{T}} \quad \{c\}_{m}^{\mathrm{T}}\right]^{\mathrm{T}} \tag{9.86}$$

The plant matrix has dimensions of $(2n + 5m + 4) \times (2n + 5m + 4)$ and is the same form as Equation 9.83, with the mass stiffness and damping matrix replaced

by $[M_{SSI}]$, $[K_{SSI}]$, and $[C_{SSI}]$ in Equations 9.57a, b, and c respectively. $[P_1]$ and $[F_x]$ need to be reset for the SSI system as

$$P_1(k,i) = \frac{-C_{0k}}{\lambda_{0k}}; \quad P_1(k,n+2+j) = \frac{C_{0k}}{\lambda_{0k}} \tag{9.87}$$

and

$$F_x(k,i) = -\alpha_{1k}; \quad F_x(k,n+2+j) = \alpha_{1k} \tag{9.88}$$

The input location vectors for the control command and the ground acceleration in the SSI system are given as

$$[B_u]_{(2n+5m+4)\times m} = \begin{bmatrix} [zero]_{(2n+4m+4)\times m} \\ [C_u] \end{bmatrix} \tag{9.89}$$

and

$$[B_r]_{(2n+5m+4)\times 2} = \begin{bmatrix} [zero]_{(n+2+m)\times 2} \\ -\begin{bmatrix} \Gamma \\ I_2 \end{bmatrix} \\ [zero]_{3m\times 2} \end{bmatrix} \tag{9.90}$$

9.4 Numerical Examples Using MATLAB®

In order to use MATLAB® [12] for response analysis of controlled structures, the mathematical formulations of state space and plant matrix presented in earlier sections should be modified in different expressions. As discussed in Appendix A, MATLAB® has a number of features for various engineering applications; this section presents seven numerical examples to illustrate the fundamental procedures relevant to the subject including this chapter.

For simplicity, six-story building shown in Figure 9.5 is used for all the examples. The building has a mass, 1.1×10^5 kg for each floor, the column stiffness of 3.51×10^8, 2.25×10^8, 1.70×10^8, 1.24×10^8, 0.88×10^8, 0.60×10^8 N/m for first story through sixth story, story-height of 3.75 m for each story and 2% damping ratio. Controllers are installed at the top two floors, which are the optimal control locations based on the optimal location index analysis.

For simplicity, ground rotational acceleration $\ddot{\phi}_g$, bracing stiffness K_b, and actuator effect, F_x (see Equation 9.74) are not considered. In this study presented herein for the given data, the mass, damping, and stiffness and matrices are calculated and listed in Equations 9.91, 9.92, and 9.93 according to Equations 9.28a,

9.29a, and 9.32a, respectively.

M =

$$\begin{bmatrix} 110000 & 0 & 0 & 0 & 0 & 0 \\ 0 & 110000 & 0 & 0 & 0 & 0 \\ 0 & 0 & 110000 & 0 & 0 & 0 \\ 0 & 0 & 0 & 110000 & 0 & 0 \\ 0 & 0 & 0 & 0 & 110000 & 0 \\ 0 & 0 & 0 & 0 & 0 & 110000 \end{bmatrix} \tag{9.91}$$

K =

$$\begin{bmatrix} 576451000 & -225167000 & 0 & 0 & 0 & 0 \\ -225167000 & 394835000 & -169668000 & 0 & 0 & 0 \\ 0 & -169668000 & 293908000 & -124240000 & 0 & 0 \\ 0 & 0 & -124240000 & 212111000 & -87871000 & 0 \\ 0 & 0 & 0 & -87871000 & 147403000 & -59532000 \\ 0 & 0 & 0 & 0 & -59532000 & 59532000 \end{bmatrix} \tag{9.92}$$

C =

$$\begin{bmatrix} 1.5306e+006 & -9.6761e+005 & 2.9474e+005 & -5.2481e+004 & 0 & 0 \\ -9.6761e+005 & 9.7222e+005 & -3.8823e+005 & 7.7709e+004 & -2.0481e+004 & 0 \\ 2.9474e+005 & -3.8823e+005 & 4.0703e+005 & -1.4155e+005 & 1.0378e+004 & -7.1862e+003 \\ -5.2481e+004 & 7.7709e+004 & -1.4155e+005 & 2.1505e+005 & -6.3351e+004 & -8.5838e+003 \\ 0 & -2.0481e+004 & 1.0378e+004 & -6.3351e+004 & 1.4791e+005 & -4.7664e+004 \\ 0 & 0 & -7.1862e+003 & -8.5838e+003 & -4.7664e+004 & 9.0230e+004 \end{bmatrix} \tag{9.93}$$

The ground acceleration input, $\ddot{x}_g(t) = [\text{time; acc}]$ with time interval of 0.01 s, for all the examples is given in Figure 9.6.

9.4.1 Fixed Support without Control

For MATLAB® application, the structural system's state space representation modified is expressed as

$$\{z\} = [\{x\}^T \{\dot{x}\}^T]^T \tag{9.94}$$

$$\{\dot{z}(t)\} = [A_s]\{z(t)\} + \{B_r\}\ddot{x}_g(t) \tag{9.95}$$

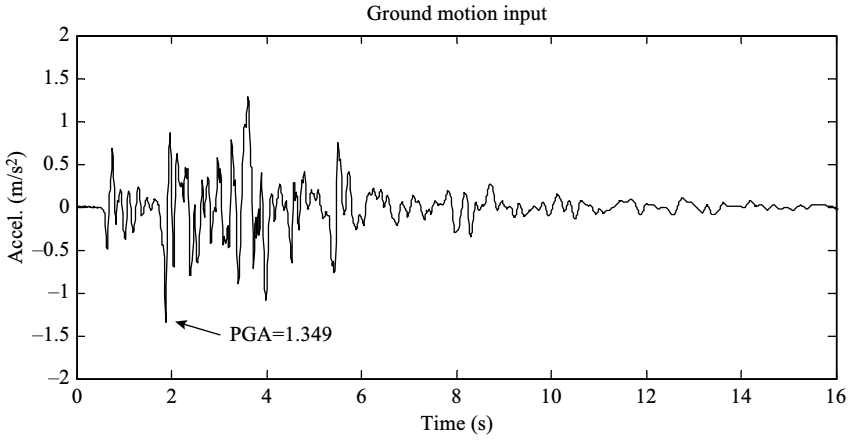

FIGURE 9.6 Typical ground motion with earthquake magnitude $m_j = 6.0$.

where $[A_s]$ is named as the system matrix in the following form:

$$[A_s] = \begin{bmatrix} [zero] & [I] \\ -[M_s]^{-1}[K_s] & -[M_s]^{-1}[C_s] \end{bmatrix} \tag{9.96}$$

In which the $[M]$, $[K]$, and $[C]$ are already obtained as shown above. Thus, the numerical value of the system matrix is

```
As =

Columns 1 through 4

                0                0                0                0
                0                0                0                0
                0                0                0                0
                0                0                0                0
                0                0                0                0
                0                0                0                0
 -5.2405e+003     2.0470e+003                0                0
  2.0470e+003    -3.5894e+003     1.5424e+003                0
                0     1.5424e+003    -2.6719e+003     1.1295e+003
                0                0     1.1295e+003    -1.9283e+003
                0                0                0     7.9883e+002
                0                0                0                0
```

Columns 5 through 8

0	0	1.0000e+000	0
0	0	0	1.0000e+000
0	0	0	0
0	0	0	0
0	0	0	0
0	0	0	0
0	0	−1.3914e+001	8.7965e+000
0	0	8.7965e+000	−8.8384e+000
0	0	−2.6795e+000	3.5294e+000
7.9883e+002	0	4.7710e−001	−7.0645e−001
−1.3400e+003	5.4120e+002	0	1.8619e−001
5.4120e+002	−5.4120e+002	0	0

Columns 9 through 12

0	0	0	0
0	0	0	0
1.0000e+000	0	0	0
0	1.0000e+000	0	0
0	0	1.0000e+000	0
0	0	0	1.0000e+000
−2.6795e+000	4.7710e−001	0	0
3.5294e+000	−7.0645e−001	1.8619e−001	0
−3.7003e+000	1.2868e+000	−9.4345e−002	6.5329e−002
1.2868e+000	−1.9550e+000	5.7592e−001	7.8034e−002
−9.4345e−002	5.7592e−001	−1.3447e+000	4.3331e−001
6.5329e−002	7.8034e−002	4.3331e−001	−8.2027e−001

(9.97)

The time history solution is calculated from the first-order differential equations shown in Equation 9.95 as

$$\{z(t)\} = \mathrm{e}^{A_\mathrm{s}(t-t_0)}\{z(t_0)\} + \int_0^t \mathrm{e}^{A_\mathrm{s}(t-\tau)}\{B_\mathrm{r}\}\ddot{x}_\mathrm{g}(\tau)\,\mathrm{d}\tau \tag{9.98}$$

where t_0 is the initial time and

$$\{B_\mathrm{r}\} = \begin{Bmatrix} \{0\} \\ [M]^{-1}\{\delta_\gamma\} \end{Bmatrix} \tag{9.99}$$

where $\{\delta_\chi\}$ is given by Equation 9.35 without bracing d.o.f. as well as the rotational input of $\ddot{\phi}_\mathrm{g}(\tau)$.

The solution can be given by using MATLAB® *lsim* command as

$$[y_1 e, t_1] = lsim(A_s, B_r, C, D, \text{acc}, \text{time}) \tag{9.100}$$

and the output of each state space representation can be given from

$$\{y(t)\} = [C]\{z(t)\} + [D]\ddot{x}_g(t) \tag{9.100a}$$

By choosing proper output matrix of $[C]$ and $[D]$, the structural responses, control forces, and ground motion input can be obtained from output.

For this sample, the top story displacement response is calculated using Equation 9.98 and is printed out according to Equation 9.100a by assigning $[C]$ and $[D]$ as follows:

$$[C] = [0\ \ 0\ \ 0\ \ 0\ \ 0\ \ 1\ \ 0\ \ 0\ \ 0\ \ 0\ \ 0\ \ 0]; [D] = [0] \tag{9.101}$$

For saving printing space, the displacement output response is listed for the first nine and the last six time intervals ($\Delta t = 0.01$ s) of the record's first second as

$$\begin{Bmatrix} & 0.0000000\text{e}+000 & -1.5180748\text{e}-008 & -9.2071484\text{e}-008 & -1.7511972\text{e}-007 \\ -2.0869892\text{e}-007 & -2.5346746\text{e}-007 & -3.6924003\text{e}-007 & -4.9691076\text{e}-007 & -5.7786466\text{e}-007 \\ \vdots & & & & \\ -5.8247944\text{e}-003 & -6.1688493\text{e}-003 & -6.3814962\text{e}-003 & -6.4567591\text{e}-003 & -6.3963595\text{e}-003 \\ -6.2098135\text{e}-003 & & & & \end{Bmatrix} \tag{9.102}$$

Similarly, the top floor velocity response can be output by assigning

$$[C] = [0\ \ 0\ \ 0\ \ 0\ \ 0\ \ 0\ \ 0\ \ 0\ \ 0\ \ 0\ \ 0\ \ 1]; [D] = [0] \tag{9.103}$$

and the results are listed first nine and the last six time intervals as

$$\begin{Bmatrix} & 0.0000000\text{e}+000 & -4.5532990\text{e}-006 & -9.4100365\text{e}-006 & -5.7882451\text{e}-006 \\ -2.4234283\text{e}-006 & -8.0223436\text{e}-006 & -1.3651329\text{e}-005 & -1.0405323\text{e}-005 & -7.3129074\text{e}-006 \\ \vdots & & & & \\ -4.0681896\text{e}-002 & -2.7972638\text{e}-002 & -1.4438435\text{e}-002 & -6.4355854\text{e}-004 & 1.2559711\text{e}-002 \\ 2.4496688\text{e}-002 & & & & \end{Bmatrix} \tag{9.104}$$

9.4.2 SSI without Control

The foundation for the building is square with dimensions of 12×12 m, mass of 2.2×10^5 kg, and with elastic soil conditions $V_s = 150$ m/s. Since the stiffness

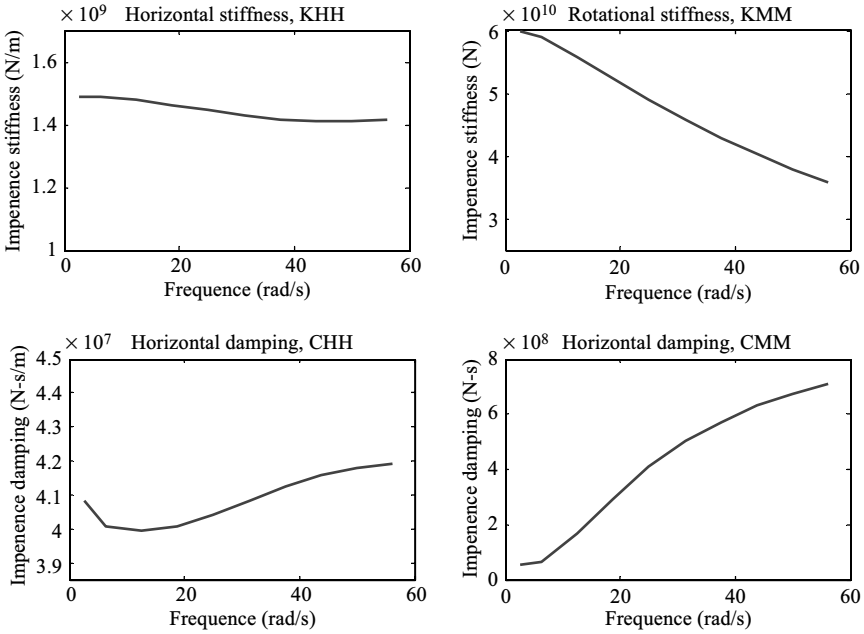

FIGURE 9.7 Impedance function curves.

and damping in Equation 9.5 are in the frequency domain, in order to apply them to online control, they must be expressed in the time domain. This can be done by using the structural system's fundamental frequency of 9.70 rad/s in the impedance function curves shown in Figure 9.7 [1]. The coefficients are then

$$k_{\mathrm{HH}} = 1.5/\mathrm{e9\,N/m}; \quad k_{\mathrm{MM}} = 5.6\mathrm{e10N}; \quad c_{\mathrm{HH}} = 4\mathrm{e7N\text{-}s/m}; \quad c_{\mathrm{MM}}{=}1.3\mathrm{e8N\text{-}s} \tag{9.105}$$

For MATLAB® application, let

$$\{X\} = [\{x_t\}^{\mathrm{T}}\{X_f\}^{\mathrm{T}}]^{\mathrm{T}} \tag{9.106}$$

$$\{x_t\} = \{x\} + [\Gamma]\{X_f\} \tag{9.107}$$

$$\{z\} = [\{X\}^{\mathrm{T}}\{\dot{X}\}^{\mathrm{T}}]^{\mathrm{T}} \tag{9.108}$$

$$\{\dot{z}(t)\} = [A_{\mathrm{SSI}}]\{z(t)\} + \{B_{\mathrm{r}}\}\ddot{x}_{\mathrm{g}}(t) \tag{9.109}$$

where $[A_{\mathrm{SSI}}]$ is the system matrix for the SSI system as

$$[A_{\mathrm{SSI}}] = \begin{bmatrix} [0] & [I] \\ -[M_{\mathrm{SSI}}]^{-1}[K_{\mathrm{SSI}}] & -[M_{\mathrm{SSI}}]^{-1}[C_{\mathrm{SSI}}] \end{bmatrix} \tag{9.110}$$

in which the submatrices are based on Equations 9.57a through c, and, [Γ] is modified from Equation 9.35b as

$$
\begin{array}{l}
\texttt{Gama} = \\
\quad \begin{array}{ll}
1.0000\text{e}+000 & 3.7500\text{e}+000 \\
1.0000\text{e}+000 & 7.5000\text{e}+000 \\
1.0000\text{e}+000 & 1.1250\text{e}+001 \\
1.0000\text{e}+000 & 1.5000\text{e}+001 \\
1.0000\text{e}+000 & 1.8750\text{e}+001 \\
1.0000\text{e}+000 & 2.2500\text{e}+001
\end{array}
\end{array}
\tag{9.111}
$$

Thus, the MATLAB® assembles the system matrix $[A_{SSI}]$ as

Columns 1 through 4

0	0	0	0
0	0	0	0
0	0	0	0
0	0	0	0
0	0	0	0
0	0	0	0
0	0	0	0
0	0	0	0
−5.2405e+003	2.0470e+003	0	0
2.0470e+003	−3.5894e+003	1.5424e+003	0
0	1.5424e+003	−2.6719e+003	1.1295e+003
0	0	1.1295e+003	−1.9283e+003
0	0	0	7.9883e+002
0	0	0	0
1.5967e+003	0	0	0
4.4786e+001	7.9960e+001	0	0

Columns 5 through 8

0	0	0	0
0	0	0	0
0	0	0	0
0	0	0	0
0	0	0	0
0	0	0	0
0	0	0	0
0	0	0	0
0	0	3.1935e+003	4.2994e+003
0	0	0	7.6761e+003
0	0	0	0
7.9883e+002	0	0	0
−1.3400e+003	5.4120e+002	0	0
5.4120e+002	−5.4120e+002	0	0
0	0	−8.4149e+003	−5.9878e+003
0	0	−1.2475e+002	−6.0707e+003

```
Columns 9 through 12

  1.0000e+000                   0                   0                   0
                0   1.0000e+000                   0                   0
                0                   0   1.0000e+000                   0
                0                   0                   0   1.0000e+000
                0                   0                   0                   0
                0                   0                   0                   0
                0                   0                   0                   0
                0                   0                   0                   0
 -1.3914e+001   8.7965e+000  -2.6795e+000   4.7710e-001
  8.7965e+000  -8.8384e+000   3.5294e+000  -7.0645e-001
 -2.6795e+000   3.5294e+000  -3.7003e+000   1.2868e+000
  4.7710e-001  -7.0645e-001   1.2868e+000  -1.9550e+000
                0   1.8619e-001  -9.4345e-002   5.7592e-001
                0                   0   6.5329e-002   7.8034e-002
  3.6602e+000  -1.4836e+000   7.9630e-001   1.2180e-001
  2.8366e-002   1.1180e-001   1.9755e-002   3.7668e-002

Columns 13 through 16

                0                   0                   0                   0
                0                   0                   0                   0
                0                   0                   0                   0
                0                   0                   0                   0
  1.0000e+000                   0                   0                   0
                0   1.0000e+000                   0                   0
                0                   0   1.0000e+000                   0
                0                   0                   0   1.0000e+000
                0                   0   7.3203e+000   2.7231e+000
  1.8619e-001                   0  -2.9672e+000   1.0733e+001
 -9.4345e-002   6.5329e-002   1.5926e+000   1.8964e+000
  5.7592e-001   7.8034e-002   2.4360e-001   3.6161e+000
 -1.3447e+000   4.3331e-001   2.4360e-001   1.8270e+001
  4.3331e-001  -8.2027e-001   2.4360e-001   1.8270e+000
  1.2180e-001   1.2180e-001  -1.8516e+002  -1.1311e+001
  1.9031e-002   1.9031e-002  -2.3565e-001  -1.3972e+001
```

(9.112)

Following Equations 9.98 and 9.101a, the top floor displacement response can be obtained by assigning:

$$[C] = [0\ 0\ 0\ 0\ 0\ 1\ 0\ 0,\ 0\ 0\ 0\ 0\ 0\ 0\ 0\ 0]; \quad [D] = [0] \tag{9.113}$$

The foundation translational response can be output by assigning

$$[C] = [0\ 0\ 0\ 0\ 0\ 0\ 1\ 0,0\ 0\ 0\ 0\ 0\ 0\ 0\ 0]; \quad [D] = [0] \tag{9.114}$$

Similarly, the foundation translational response can be output by assigning

$$[C] = [0\ 0\ 0\ 0\ 0\ 0\ 0\ 1,0\ 0\ 0\ 0\ 0\ 0\ 0\ 0]; \quad [D] = [0] \tag{9.115}$$

9.4.3 Fixed Support with Passive Control

For this case, the state space vector is

$$\{z\} = \left[\{x\}^{\mathrm{T}} \quad \{\dot{x}\}^{\mathrm{T}} \quad \{f_{\mathrm{p}}\}^{\mathrm{T}} \right]^{\mathrm{T}} \tag{9.116}$$

and state space representation is

$$\{\dot{z}(t)\} = [A_{\mathrm{p}}]\{z(t)\} + \{B_{\mathrm{r}}\}\ddot{x}_{\mathrm{g}}(t) \tag{9.117}$$

with the system matrix as

$$[A_{\mathrm{p}}] = \begin{bmatrix} [0] & [I] & [0] \\ -[M]^{-1}[K] & -[M]^{-1}[C] & -[M]^{-1}[\delta_{\mathrm{p}}] \\ [0] & [P_1] & [P_2] \end{bmatrix} \tag{9.118}$$

Two passive dampers are placed at the top two floors with its coefficients of $C_0 = 3.84 \times 10^6$ N-s/m and $\lambda_0 = 0.063$ s. The system matrix is obtained as

```
As =
Columns 1 through 4
                0                0                0                0
                0                0                0                0
                0                0                0                0
                0                0                0                0
                0                0                0                0
                0                0                0                0
 -5.2405e+003     2.0470e+003                0                0
  2.0470e+003    -3.5894e+003     1.5424e+003                0
                0     1.5424e+003    -2.6719e+003     1.1295e+003
                0                0     1.1295e+003    -1.9283e+003
                0                0                0     7.9883e+002
                0                0                0                0
Columns 5 through 8
                0                0     1.0000e+000                0
                0                0                0     1.0000e+000
                0                0                0                0
                0                0                0                0
                0                0                0                0
                0                0                0                0
                0                0    -1.3914e+001     8.7965e+000
                0                0     8.7965e+000    -8.8384e+000
                0                0    -2.6795e+000     3.5294e+000
     7.9883e+002                0     4.7710e-001    -7.0645e-001
    -1.3400e+003     5.4120e+002                0     1.8619e-001
     5.4120e+002    -5.4120e+002                0                0
```

```
Columns 9 through 12

         0         0         0         0
         0         0         0         0
 1.0000e+000       0         0         0
         0 1.0000e+000       0         0
         0         0 1.0000e+000       0
         0         0         0 1.0000e+000
-2.6795e+000 4.7710e-001       0         0
 3.5294e+000 -7.0645e-001 1.8619e-001       0
-3.7003e+000 1.2868e+000 -9.4345e-002 6.5329e-002
 1.2868e+000 -1.9550e+000 5.7592e-001 7.8034e-002
-9.4345e-002 5.7592e-001 -1.3447e+000 4.3331e-001
 6.5329e-002 7.8034e-002 4.3331e-001 -8.2027e-001
```
(9.119)

where $[\delta_p]$ is given in Equation 9.34a without inclusion of $[\delta_b]$. [M], [K], and $[C]$ are given in Equations 9.91 through 9.93. Since the bracing stiffness is not considered, Equation 9.76 should be modified as

$$P_1(k,i) = \frac{-C_{0k}}{\lambda_{0k}}; \quad P_1(k,i-1) = \frac{C_{0k}}{\lambda_{0k}}; \quad P_2(k,i) = \frac{-C_{0k}}{\lambda_{0k}} \tag{9.120}$$

In general, $[P_1]$ is a $m \times n$ matrix. Supposing the kth damper is put at the ith floor, there are two nonzero elements at the kth row of $[P_1]$ and $P_1(k, i-1)$ is nonexistent for the case of $i = 1$. Substituting Equation 9.119 in Equation 9.98 with integration yields the top story displacement response that can be obtained by assigning

$$[C] = [0\ 0\ 0\ 0\ 0\ 1,\ 0\ 0\ 0\ 0\ 0\ 0,\ 0\ 0]; \quad [D] = [0] \tag{9.121}$$

The floor displacement data is listed for the first and the last eight time intervals of the first second response as

```
0.0000000e+000 -1.5180748e-008 -9.2071490e-008 -1.7511974e-007 -2.0869836e-007
-2.5346223e-007 -3.6921609e-007 -4.9683639e-007 -5.7768380e-007 -6.7329550e-007
      ⋮
-3.6039016e-003 -4.0424234e-003 -4.3963286e-003 -4.6629900e-003 -4.8454755e-003
-4.9508065e-003 -4.9897082e-003 -4.9720251e-003 -4.9080436e-003 -4.8074307e-003
```
(9.122)

The passive control force at the top floor can be similarly obtained with $[C] = [0\ 0\ 0\ 0,\ 0\ 00\ 0\ 0\ 0\ 0\ 0,\ 1\ 0]; \quad [D] = [0]$. The passive control forces curve is given as

```
0.0000000e+000 -3.1103359e-006 -4.8395167e-005 2.0737333e-004 2.8595425e-003
1.1603871e-002 2.8603207e-002 5.3379192e-002 9.0042582e-002 1.6108784e-001
      ⋮
5.3728194e+004 5.6279889e+004 5.4810873e+004 4.9509233e+004 4.0924620e+004
2.9926228e+004 1.7645287e+004 5.3869639e+003 -5.5019444e+003 -1.3807857e+004
```
(9.123)

9.4.4 SSI with Passive Control

By choosing the state space vector of

$$\{z\} = \left[\{X\}^{\mathrm{T}} \;\; \{\dot{X}\}^{\mathrm{T}} \;\; \{f_{\mathrm{p}}\}^{\mathrm{T}}\right]^{\mathrm{T}} \tag{9.124}$$

the state space representation of the passive controlled multiple-story building on the fixed base can be given as

$$\{\dot{z}(t)\} = \left[A^{\mathrm{p}}_{\mathrm{SSI}}\right]\{z(t)\} + \{B_{\mathrm{r}}\}\ddot{x}_{\mathrm{g}}(t) \tag{9.125}$$

with the system matrix as

$$\left[A^{\mathrm{p}}_{\mathrm{SSI}}\right] = \begin{bmatrix} [0] & [I] & [0] \\ -[M_{\mathrm{SSI}}]^{-1}[K_{\mathrm{SSI}}] & -[M_{\mathrm{SSI}}]^{-1}[C_{\mathrm{SSI}}] & -[M_{\mathrm{SSI}}]^{-1} \\ [0] & [P_1] & [P_2] \end{bmatrix} \tag{9.126}$$

where $[M_{\mathrm{SSI}}]$, $[K_{\mathrm{SSI}}]$, and $[C_{\mathrm{SSI}}]$ are the same as used in Equation 9.110. $[P_1]$ should be modified from Equation 9.87 because no bracing stiffness is involved and the damper is on the top floor. Thus, $[P_1]$ and $[P_2]$ are the same as given in Equation 9.120.

The numerical values of Equation 9.126 are

```
Columns 1 through 5

                0                0                0                0                0
                0                0                0                0                0
                0                0                0                0                0
                0                0                0                0                0
                0                0                0                0                0
                0                0                0                0                0
                0                0                0                0                0
                0                0                0                0                0
  -5.2405e+003     2.0470e+003                0                0                0
   2.0470e+003    -3.5894e+003     1.5424e+003                0                0
                0     1.5424e+003    -2.6719e+003     1.1295e+003                0
                0                0     1.1295e+003    -1.9283e+003     7.9883e+002
                0                0                0     7.9883e+002    -1.3400e+003
                0                0                0                0     5.4120e+002
   1.5967e+003                0                0                0                0
   4.4786e+000     7.9960e+001                0                0                0
                0                0                0                0                0
                0                0                0                0                0
```

Columns 6 through 10

0	0	0	1.0000e+000	0
0	0	0	0	1.0000e+000
0	0	0	0	0
0	0	0	0	0
0	0	0	0	0
0	0	0	0	0
0	0	0	0	0
0	0	0	0	0
0	3.1935e+003	4.2994e+003	−1.3914e+001	
0	0	7.6761e+003	8.7965e+000	8.8384e+000
0	0	0	−2.6795e+000	3.5294e+000
0	0	0	4.7710e−001	−7.0645e−001
5.4120e+002	0	0	0	1.8619e−001
−5.4120e+002	0	0	0	0
0	−8.4149e+003	−5.9878e+003	3.6602e+000	−1.4836e+000
0	−1.2475e+002	−6.0707e+003	2.8366e−002	1.1180e−001
0	0	0	0	0
0	0	0	0	0

Columns 11 through 15

0	0	0	0	0
0	0	0	0	0
1.0000e+000	0	0	0	0
0	1.0000e+000	0	0	0
0	0	1.0000e+000	0	0
0	0	0	1.0000e+000	0
0	0	0	0	1.0000e+000
0	0	0	0	0
−2.6795e+000	4.7710e−001	0	0	7.3203e+000
3.5294e+000	−7.0645e−001	1.8619e−001	0	−2.9672e+000
−3.7003e+000	1.2868e+000	−9.4345e−002	6.5329e−002	1.5926e+000
1.2868e+000	−1.9550e+000	5.7592e−001	7.8034e−002	2.4360e−001
−9.4345e−002	5.7592e−001	−1.3447e+000	4.3331e−001	2.4360e−001
6.5329e−002	7.8034e−002	4.3331e−001	−8.2027e−001	2.4360e−001
7.9630e−001	1.2180e−001	1.2180e−001	1.2180e−001	−1.8516e+002
1.9755e−002	3.7668e−002	1.9031e−002	1.9031e−002	2.3565e−001
0	0	6.0921e+007	−6.0921e+007	0
0	6.0921e+007	−6.0921e+007	0	0

Columns 16 through 18

0	0	0
0	0	0
0	0	0
0	0	0
0	0	0
0	0	0
0	0	0
1.0000e+000	0	0
2.7231e+000	0	0
1.0733e+001	0	0
1.8964e+000	0	0
3.6161e+000	0	−9.0909e−006
1.8270e+000	−9.0909e−006	9.0909e−006
1.8270e+000	9.0909e−006	0
−1.1311e+001	0	0
1.3972e+001	0	0
0	−1.5873e+001	0
0	0	−1.5873e+001

(9.127)

The displacements and the control forces at the top floor can be output with Equations 9.128a and b, respectively.

$$[C] = [0\ 0\ 0\ 0\ 0\ 1\ 0\ 0,\ 0\ 0\ 0\ 0\ 0\ 0\ 0\ 0,\ 0\ 0]; \quad [D] = [0] \tag{9.128a}$$

$$[C] = [0\ 0\ 0\ 0\ 0\ 0\ 0\ 0,\ 0\ 0\ 0\ 0\ 0\ 0\ 0\ 0,\ 1\ 0]; \quad [D] = [0] \tag{9.128b}$$

9.4.5 Fixed Support with Active Control

There are several control algorithms in MATLAB® as introduced in Appendix A. This study is based on the optimal LQR technique. As there are two controllers placed on the top two floors, the weighting matrices have the unit value of element (6, 6) and other elements as zeros in $[Q]$; and $[R] = r[I_2]$ for two forces with $[I_2]$ as an identity matrix of order 2. From optimal LQR results, the value of r is set at as 8×10^{-15}. The feedback gain matrix is already discussed in Chapter 4 and is given as

$$[G] = -R^{-1}B_{\mathrm{a}}^{\mathrm{T}}P; \quad [B_{\mathrm{a}}] = \begin{bmatrix} [zero] \\ [M]^{-1}[\delta_{\mathrm{a}}] \end{bmatrix} \tag{9.129, 9.130}$$

in which $[\delta_{\mathrm{a}}]$ is given in Equation 9.34a without the bracing d.o.f. The numerical values of the feedback gain given can be found by MATLAB® *lqr* command, [G] = lqr($A_{\mathrm{s}}, B_{\mathrm{a}}, Q, R$) from which $[A_{\mathrm{s}}]$, $[B_{\mathrm{a}}]$, $[Q]$, $[R]$ are provided. The values of [G] are then obtained and are given in Equation 9.131 as

Columns 1 through 6

```
−2.1913e+004  −5.1223e+004  −5.1158e+004  1.1263e+005  6.6938e+005  1.0403e+006
−1.3381e+004  −5.8003e+003   7.9547e+004  2.7820e+005  4.4980e+005  2.4212e+005
```

Columns 7 through 12

```
6.4264e+003  1.6260e+004  3.1083e+004  6.5103e+004  1.5838e+005  3.4217e+005
8.3606e+003  2.5787e+004  6.1924e+004  1.3295e+005  2.4291e+005  3.3618e+005
```

(9.131)

The state vector is expressed in the following form:

$$\{\dot{z}(t)\} = [A_{\mathrm{a}}]\{z(t)\} + \{B_{\mathrm{r}}\}\ddot{x}_{\mathrm{g}}(t) \tag{9.132}$$

where the system matrix is

$$[A_{\mathrm{a}}] = [[A_{\mathrm{s}}] - [B_{\mathrm{a}}][G]] \tag{9.133}$$

The numerical values of the system matrix are

$A_a =$

Columns 1 through 4

0	0	0	0
0	0	0	0
0	0	0	0
0	0	0	0
0	0	0	0
0	0	0	0
−5.2405e + 003	2.0470e + 003	0	0
2.0470e + 003	−3.5894e + 003	1.5424e + 003	0
0	1.5424e + 003	−2.6719e + 003	1.1295e + 003
−1.2165e − 001	−5.2730e − 002	1.1302e + 003	−1.9258e + 003
−7.7560e − 002	−4.1293e − 001	−1.1882e + 000	7.9732e + 002
1.9921e − 001	4.6566e − 001	4.6507e − 001	−1.0239e + 000

Columns 5 through 8

0	0	1.0000e + 000	0
0	0	0	1.0000e + 000
0	0	0	0
0	0	0	0
0	0	0	0
0	0	0	0
0	0	−1.3914e + 001	8.7965e + 000
0	0	8.7965e + 000	−8.8384e + 000
0	0	−2.6795e + 000	3.5294e + 000
8.0292e + 002	2.2011e + 000	5.5311e − 001	−4.7203e − 001
−1.3380e + 003	5.4846e + 002	−1.7583e − 002	9.9581e − 002
5.3511e + 002	−5.5066e + 002	−5.8422e − 002	−1.4782e − 001

Columns 9 through 12

0	0	0	0
0	0	0	0
1.0000e + 000	0	0	0
0	1.0000e + 000	0	0
0	0	1.0000e + 000	0
0	0	0	1.0000e + 000
−2.6795e + 000	4.7710e − 001	0	0
3.5294e + 000	−7.0645e − 001	1.8619e − 001	0
−3.7003e + 000	1.2868e + 000	−9.4345e − 002	6.5329e − 002
1.8498e + 000	−7.4640e − 001	2.7842e + 000	3.1342e + 000
−3.7472e − 001	−4.0877e − 002	−2.1131e + 000	4.8771e − 001
−2.1725e − 001	−5.1381e − 001	−1.0065e + 000	−3.9309e + 000

(9.134)

The top story displacement response is calculated of which the output is obtained by assigning

$$[C] = [0\ \ 0\ \ 0\ \ 0\ \ 0\ \ 1, 0\ \ 0\ \ 0\ \ 0\ \ 0\ \ 0]; \quad [D] = [0] \tag{9.135}$$

The displacement response is listed for the first and the last eight time intervals of the first second as

$$\begin{array}{lllll}
0.0000000\text{e}+000 & -1.4967685\text{e}-008 & -8.9095564\text{e}-008 & -1.6466819\text{e}-007 & -1.8804065\text{e}-007 \\
-2.2183257\text{e}-007 & -3.2369861\text{e}-007 & -4.3255191\text{e}-007 & -4.9218214\text{e}-007 & -5.6659233\text{e}-007 \\
\vdots & & & & \\
-2.6145128\text{e}-003 & -3.2908604\text{e}-003 & -3.9284376\text{e}-003 & -4.5008196\text{e}-003 & -4.9847384\text{e}-003 \\
-5.3610395\text{e}-003 & -5.6170953\text{e}-003 & -5.7446741\text{e}-003 & -5.7432281\text{e}-003 & -5.6199689\text{e}-003
\end{array} \tag{9.136}$$

The active control force is calculated from

$$f_{\text{a}}(t) = [G]z(t) \tag{9.137a}$$

To output the active control force, the feedback matrix [G] is used as the [C] matrix in the following form:

$$[C] = [G(1,:)]; \quad [D] = [0] \tag{9.137b}$$

To output the control force at a specific floor, the corresponding row in feedback matrix is used. The active forces of the top floor corresponds to the first row in the matrix and are listed below.

$$\begin{array}{lllll}
0.0000000\text{e}+000 & 2.8186439\text{e}+000 & 5.8122516\text{e}+000 & 3.5403720\text{e}+000 & 1.4305953\text{e}+000 \\
4.8808915\text{e}+000 & 8.3434010\text{e}+000 & 6.2980511\text{e}+000 & 4.3498852\text{e}+000 & 8.0719603\text{e}+000 \\
\vdots & & & & \\
2.9577003\text{e}+004 & 2.9169098\text{e}+004 & 2.8323750\text{e}+004 & 2.6938674\text{e}+004 & 2.4984396\text{e}+004 \\
2.2456557\text{e}+004 & 1.9280117\text{e}+004 & 1.5383576\text{e}+004 & 1.0920631\text{e}+004 & 6.0261856\text{e}+003
\end{array} \tag{9.138}$$

9.4.6 Fixed Support with Hybrid Control

The hybrid control system is combing the passive and active controls. Its state space is the similar to that used for the passive system as

$$\{\dot{z}(t)\} = [A_{\text{hy}}]\{z(t)\} + \{B_{\text{r}}\}\ddot{x}_{\text{g}}(t) \tag{9.139}$$

in which

$$[A_{\text{hy}}] = \begin{bmatrix} [A_{\text{a}}] & & [0] \\ & & -[M]^{-1}[\delta_{\text{p}}] \\ [0] & [P_1] & [P_2] \end{bmatrix} \tag{9.140}$$

where $[A_{\text{a}}]$ is the system matrix of active control already given in Equation 9.134.

The output of each of the state space representation can be given as shown in Equation 9.100a. By choosing proper output matrix of [C] and [D], the structural states, and control forces can be obtained. The numerical values of $[A_{hy}]$ are

A_hy =

Columns 1 through 5

0	0	0	0	0
0	0	0	0	0
0	0	0	0	0
0	0	0	0	0
0	0	0	0	0
0	0	0	0	0
−5.2405e + 003	2.0470e + 003	0	0	0
2.2470e + 003	−3.5894e + 003	1.5424e + 003	0	0
0	1.5424e + 003	−2.6719e + 003	1.1295e + 003	0
−1.2165e − 001	−5.2730e − 002	1.1302e + 003	−1.9258e + 003	8.0292e + 002
−7.7560e − 002	−4.1293e − 001	−1.1882e + 000	7.9732e + 002	−1.3380e + 003
1.9921e − 001	4.6566e − 001	4.6507e − 001	−1.0239e + 000	5.3511e + 002
0	0	0	0	0
0	0	0	0	0

Columns 6 through 10

0	1.0000e + 000	0	0	0
0	0	1.0000e + 000	0	0
0	0	0	1.0000e + 000	0
0	0	0	0	1.0000e + 000
0	0	0	0	0
0	0	0	0	0
0	−1.3914e + 001	8.7965e + 000	−2.6795e + 000	4.7710e − 001
0	8.7965e + 000	−8.8384e + 000	3.5294e + 000	−7.0645e − 001
0	−2.6795e + 000	3.5294e + 000	−3.7003e + 000	1.2868e + 000
2.2011e + 000	5.5311e − 001	−4.7203e − 001	1.8498e + 000	−7.4640e − 001
5.4846e + 002	−1.7583e − 002	9.9581e − 002	−3.7472e − 001	−4.0877e − 002
−5.5066e + 002	−5.8422e − 002	−1.4782e − 001	−2.1725e − 001	−5.1381e − 001
0	0	0	0	0
0	0	0	0	6.0921e + 007

Columns 11 through 14

0	0	0	0
0	0	0	0
0	0	0	0
0	0	0	0
1.0000e + 000	0	0	0
0	1.0000e + 000	0	0
0	0	0	0
1.8619e − 001	0	0	0
−9.4345e − 002	6.5329e − 002	0	0
2.7842e + 000	3.1342e + 000	0	−9.0909e − 006
−2.1131e + 000	4.8771e − 001	−9.0909e − 006	9.0909e − 006
−1.0065e + 000	−3.9309e + 000	9.0909e − 006	0
6.0921e + 007	−6.0921e + 007	−1.5873e + 001	0
−6.0921e + 007	0	0	−1.5873e + 001

(9.141)

The top story displacement response can be an output with the same [C], [D] matrix as in passive control case. The sample results are listed for the first and the

last eight time intervals of the first second as

$$\begin{array}{ccccc}
0.0000000\text{e}+000 & -1.4967953\text{e}-008 & -8.9111786\text{e}-008 & -1.6482265\text{e}-007 & -1.8870857\text{e}-007 \\
-2.2371253\text{e}-007 & -3.2779114\text{e}-007 & -4.4013424\text{e}-007 & -5.0475103\text{e}-007 & -5.8566056\text{e}-007 \\
\vdots & & & & \\
-3.1523889\text{e}-003 & -3.5818958\text{e}-003 & -3.9348402\text{e}-003 & -4.2074518\text{e}-003 & -4.4012590\text{e}-003 \\
-4.5212843\text{e}-003 & -4.5758353\text{e}-003 & -4.5721830\text{e}-003 & -4.5182980\text{e}-003 & -4.4221408\text{e}-003
\end{array} \tag{9.142a}$$

To output the hybrid control force at the top floor, we use $[C] = [G(1,:), 1, 0]; [D] = [0]$. The force response is similar to

$$\begin{array}{ccccc}
0.0000000\text{e}+000 & -3.1103359\text{e}-006 & -4.8395167\text{e}-005 & 2.0737333\text{e}-004 & 2.8595425\text{e}-003 \\
1.1603871\text{e}-002 & 2.8603207\text{e}-002 & 5.3379192\text{e}-002 & 9.0042582\text{e}-002 & 1.6108784\text{e}-001 \\
\vdots & & & & \\
5.3728194\text{e}+004 & 5.6279889\text{e}+004 & 5.4810873\text{e}+004 & 4.9509233\text{e}+004 & 4.0924620\text{e}+004 \\
2.9926228\text{e}+004 & 1.7645287\text{e}+004 & 5.3869639\text{e}+003 & -5.5019444\text{e}+003 & -1.3807857\text{e}+004
\end{array} \tag{9.142b}$$

9.4.7 SSI with Hybrid Control

The state space representation is similar to that of Equation 9.139 and is expressed as

$$\{\dot{z}(t)\} = \left[A_{\text{SSI}}^{\text{hy}}\right]\{z(t)\} + \{B_{\text{r}}\}\ddot{x}_{\text{g}}(t) \tag{9.143}$$

in which

$$\left[A_{\text{SSI}}^{\text{hy}}\right] = \begin{bmatrix} \left[A_{\text{SSI}}^{\text{a}}\right] & & [0] \\ & & -[M_{\text{SSI}}]^{-1}[\delta_{\text{p}}] \\ [0] \quad [P_1] & & [P_2] \end{bmatrix} \tag{9.144}$$

where the system matrix $\left[A_{\text{SSI}}^{\text{hy}}\right]$ obtained from $\left[A_{\text{SSI}}^{\text{p}}\right]$, Equation 9.125, by replacing $[A_{\text{SSI}}]$, Equation 9.110, with $[A_{\text{SSI}}^{\text{a}}]$, system matrix of the active control with SSI, $[A_{\text{SSI}}^{\text{a}}]$, is given in Equation 9.148.

On the basis of the conclusion of Reference 11 that "The effects of ignoring the interaction between the structure and the soil in the calculation of the control gains are small and result in a slightly lower response of the structure and the foundation at the expense of a slightly larger control force," we let the feedback gain be the same as the fixed base case. However, the active control force is then determined with this gain matrix multiplying the response of superstructure, which is calculated including the effect of SSI as presented in Equations 9.146 through 9.148.

The active force is expressed as

$$f_{\mathrm{a}}(t) = [G]\,[x(t), \dot{x}(t)]^{\mathrm{T}} \tag{9.145}$$

or

$$f_{\mathrm{a}}(t) = [G_{\mathrm{SSI}}]\left[X(t), \dot{X}(t)\right]^{\mathrm{T}} = [G]\,[[I \;\; -\Gamma] \;\; [I \;\; -\Gamma]]\,[X(t), \dot{X}(t)]^{\mathrm{T}} \tag{9.146}$$

Then, the state space representation of the active controlled multiple-story building can be given as

$$\{\dot{z}(t)\} = \left[A^{\mathrm{a}}_{\mathrm{SSI}}\right]\{z(t)\} + \{B_{\mathrm{r}}\}\ddot{x}_{\mathrm{g}}(t) \tag{9.147}$$

where the system matrix is

$$\left[A^{\mathrm{a}}_{\mathrm{SSI}}\right] = [[A_{\mathrm{SSI}}] - [B_{\mathrm{a}}]\,[G_{\mathrm{SSI}}]] \tag{9.148}$$

The numerical values of $[G]$ are same as given in Equation 9.131; the numerical values of $[G_{\mathrm{SSI}}]$ are calculated according to Equation 9.146 and are given in Equation 9.149. Consequently, the numerical values of Equation 9.148 can be calculated and are not given here. However, the numerical values of system matrix based Equation 9.144 are listed in Equation 9.150.

```
G_feed_ssi =

Columns 1 through 5

  -2.1913e+004   -5.1223e+004   -5.1158e+004    1.1263e+005    6.6938e+005
  -1.3381e+004   -5.8003e+003    7.9547e+004    2.7850e+005    4.4980e+005

Columns 6 through 10

   1.0403e+006   -1.6980e+006   -3.6605e+007    6.4264e+003    1.6260e+004
   2.4212e+005   -1.0305e+006   -1.8856e+007    8.3606e+003    2.5787e+004

Columns 11 through 16

   3.1083e+004    6.5103e+004    1.5838e+005    3.4217e+005   -6.1942e+005   -1.2141e+007
   6.1924e+004    1.3295e+005    2.4291e+005    3.3618e+005   -8.0811e+005   -1.5034e+007
```
(9.149)

The top floor displacement can be an output with

$$[\mathrm{C}] = [0\;\;0\;\;0\;\;0\;\;0\;\;1\;\;0\;\;0, 0\;\;0\;\;0\;\;0\;\;0\;\;0\;\;0\;\;0, 0\;\;0]; \quad [D] = [0]$$

The comparison of the floor displacement responses is shown in Figure 9.8 to reveal the differences among cases of without control, and with passive control as

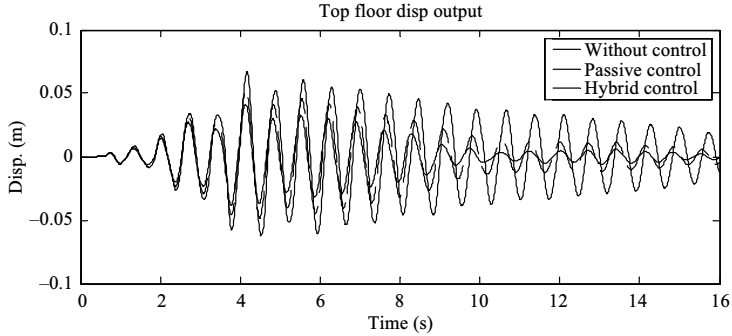

FIGURE 9.8 Comparison of top floor displacements for passive or hybrid control and without control.

well as hybrid control. The output of the hybrid control forces at the top floor can be obtained by [C] = [G_ssi(1, :), 1, 0]; [D] = [0].

```
Columns 1 through 5

                0                0                0                0                0
                0                0                0                0                0
                0                0                0                0                0
                0                0                0                0                0
                0                0                0                0                0
                0                0                0                0                0
                0                0                0                0                0
                0                0                0                0                0
  -5.2405e+003     2.0470e+003                0                0                0
   2.0470e+003    -3.5894e+003     1.5424e+003                0                0
                0     1.5424e+003    -2.6719e+003     1.1295e+003                0
  -1.2165e-001    -5.2730e-002     1.1302e+003    -1.9258e+003     8.0292e+002
  -7.7560e-002    -4.1263e-001    -1.1882e+000     7.9732e+002    -1.3380e+003
   1.9921e-001     4.6566e-001     4.6507e-001    -1.0239e+000     5.3511e+002
   1.5967e+003                0                0                0                0
   4.4773e+001     1.9688e+001     1.6142e+001     1.3054e+001     1.0461e+001
                0                0                0                0                0
                0                0                0                0                0

Columns 6 through 10

                0                0                0     1.0000e+000                0
                0                0                0                0     1.0000e+000
                0                0                0                0                0
                0                0                0                0                0
                0                0                0                0                0
                0                0                0                0                0
                0                0                0                0                0
                0                0                0                0                0
                0     3.1935e+003     4.2994e+003    -1.3904e+001     8.7965e+000
                0                0     1.8920e+003     8.7965e+000    -8.8384e+000
                0                0     1.5487e+003    -2.6795e+000     3.5294e+000
   2.2011e+000    -9.3680e+000     1.0684e+003     5.5311e-001    -4.7203e-001
   5.4846e+002    -6.0682e+000     8.0475e+002    -1.7583e-002     9.9581e-002
  -5.5066e+002     1.5436e+001     2.3623e+003    -5.8422e-002    -1.4782e-001
                0    -8.4149e+003    -5.9878e+003     3.6602e+000    -1.4836e+000
   2.1596e+001    -1.2571e+002    -6.6781e+003     1.0101e-001     2.2237e-002
                0                0                0                0                0
                0                0                0                0                0
```

Columns 11 through 15

0	0	0	0	0
0	0	0	0	0
1.0000e+000	0	0	0	0
0	1.0000e+000	0	0	0
0	0	1.0000e+000	0	0
0	0	0	1.0000e+000	0
0	0	0	0	1.0000e+000
0	0	0	0	0
−2.6795e+000	4.7710e−001	0	0	7.3203e+000
3.5294e+000	−7.0645e−001	1.8619e−001	0	−2.9672e+000
−3.7003e+000	1.2868e+000	−9.4345e−002	6.5329e−002	1.5926e+000
1.8498e+000	−7.4640e−001	2.7842e+000	3.1342e+000	−7.1029e+000
−3.7472e−001	−4.0877e−002	−2.1131e+000	4.8771e−001	1.9590e+000
−2.1725e−001	−5.1381e−001	−1.0065e+000	−3.9309e+001	5.8747e+000
7.9630e−001	1.2180e−001	1.2180e−001	1.2180e−001	−1.8516e+002
9.7640e−002	1.3079e−001	2.1010e−001	3.2866e−001	−8.9043e−001
0	0	6.0921e+007	−6.0921e+007	0
0	6.0921e+007	−6.0921e+007	0	0

Columns 16 through 18

0	0	0
0	0	0
0	0	0
0	0	0
0	0	0
0	0	0
0	0	0
1.0000e+000	0	0
9.1929e+000	0	0
7.0132e−001	0	0
6.2027e+000	0	0
−1.3087e+002	0	−9.0909e−006
3.2795e+001	−9.0909e−006	9.0909e−006
−1.1880e+002	9.0909e−006	0
−1.8408e+001	0	0
−2.7251e+001	−3.5511e−007	−3.5511e−007
2.2845e+008	−1.5873e+001	0
2.2845e+008	0	−1.5873e+001

(9.150)

9.5 Extreme Value Distribution

As introduced at the beginning of this chapter, any future earthquake excitation at a given site must be different from the existing records and cannot be predestined deterministically. A controlled structure is designed to be protected from earthquake during the structural lifetime. Since seismic structural response based on existing earthquake records cannot adequately reflect future response behavior, a methodology is introduced here for generating ground motions based on historical tectonic movements of the seismic plate with consideration of wave propagation and local site soil amplification. After a group of motions is generated for an earthquake magnitude, m_j, and time history structural analyses are then performed for each motion in the group. The maximum values of a specific structural response (such as floor displacements, control forces, etc.) are collected from the group, and the nondeterministic Monte Carlo method is finally employed for the maximum response probability study from which the result is used for designing a controlled structure.

9.5.1 Extreme Value and Description

Probability of the extreme value theory deals with the stochastic behavior of the maximum and the minimum of random variables; the maximum is focused on in this section. *Extreme value distributions* are usually considered in the mathematical model of (Gumbel-type distribution) [9,10] as

$$\Pr[X \leq x] = \exp\left[-\exp\frac{(a-x)}{b}\right] \tag{9.151}$$

where a and b are parameters describing the distribution.

9.5.2 Gumbel-Type Distribution

9.5.2.1 Distribution representations, mean value, and variance

The probability distribution function (PDF) is given in Equation 9.151. The probability density function (pdf) can be found by taking derivation of x on PDF as

$$p_{\mathrm{e}}(x) = \frac{1}{b}\exp\left(\frac{a-x}{b}\right)\exp\left[-\exp\left(\frac{a-x}{b}\right)\right] \tag{9.152}$$

The case with $a = 0$ and $b = 1$ is called the standard Gumbel distribution. The equation for the standard *Gumbel distribution* is reduced to

$$p_{\mathrm{es}}(x) = \exp(-x)\exp[-\exp(-x)] \tag{9.153}$$

On the basis of the Equation 9.151, x can be solved as the expression with respect to the probability P_{r},

$$x = a - b\ln[-\ln(P_{\mathrm{r}})] = G(P_{\mathrm{r}}) \tag{9.154}$$

or

$$G(P_{\mathrm{r}}) = a - b\ln\left[\ln\left(\frac{1}{P_{\mathrm{r}}}\right)\right] \tag{9.155}$$

and $G(P_{\mathrm{r}})$ is called percentage point function (PPF). The expected value (*mean value*) of x denoted as $\bar{x}$, and standard deviation of x, denoted as σ (σ^2 is the

variance of x), can be found based on their definitions of

$$\bar{x} = E[x] = \int_{-\infty}^{+\infty} x p_e(x)\, dx \tag{9.156}$$

$$\sigma^2 = E[(x-\bar{x})^2] = \int_{-\infty}^{+\infty} (x-\bar{x})^2 p_e(x)\, dx \tag{9.157}$$

Mean value $\bar{x}$

Substituting Equation 9.152 into Equation 9.156 yields the mean value as

$$\bar{x} = \int_{-\infty}^{+\infty} x p_e(x)\, dx = \frac{1}{b}\int_{-\infty}^{+\infty} x \exp\left(\frac{a-x}{b}\right) \exp\left[-\exp\left(\frac{a-x}{b}\right)\right] dx \tag{9.158}$$

Define a new variable of z as

$$z = \exp\left(\frac{a-x}{b}\right) \tag{9.159}$$

From which

$$x = a - b\ln z \tag{9.160}$$

$$dz = -\frac{1}{b}\exp\left(\frac{a-x}{b}\right) dx \tag{9.161}$$

Using Equations 9.159 through 9.161 in Equation 9.158, we then have

$$\bar{x} = \int_{0}^{+\infty} (a - b\ln z)\exp(-z)dz = Int(1) \tag{9.162}$$

which is denoted as $Int(1)$ for that the solution will be given later in this section.

Variance σ^2

Variance in Equation 9.157 may be expressed as

$$\sigma^2 = \int_{-\infty}^{+\infty} x^2 p_e(x)\, dx + 2\bar{x}\int_{-\infty}^{+\infty} x p_e(x)\, dx + \bar{x}^2 \int_{-\infty}^{+\infty} p_e(x)\, dx \tag{9.163}$$

that can be transformed into the integral with respect to z based on Equations 9.160 and 9.161 as

$$\sigma^2 = \int_0^{+\infty} (a - b\ln z)^2 \exp(-z)\,\mathrm{d}z + 2\bar{x}\int_0^{+\infty} (a - b\ln z)\exp(-z)\,\mathrm{d}z + \bar{x}^2 \int_0^{+\infty} \exp(-z)\,\mathrm{d}z \tag{9.164}$$

By using notations for each integral, the variation is given as

$$\sigma^2 = Int(2) + 2\bar{x}Int(1) + \bar{x}^2 Int(3) \tag{9.165a}$$

or

$$\sigma^2 = Int(2) + 2Int(1)^2 + Int(1)^2 Int(3) \tag{9.165b}$$

Then, the problem of finding mean value and variance becomes one of finding the integrals of $Int(1)$, $Int(2)$, and $Int(3)$. They can be calculated on the basis of the theorem of Euler–Mascheroni integral.

Euler–Mascheroni integral

The theorem of *Euler–Mascheroni integral* and the integral solution are given as [17,21]

$$I_n = (-1)^n \int_0^{+\infty} (\ln z)^n \exp(-z)\,\mathrm{d}z \tag{9.166}$$

$$I_0 = \int_0^{+\infty} \exp(-z)\,\mathrm{d}z = [-\exp(-z)\,\mathrm{d}z]_0^{+\infty} = 0 + 1 = 1 \tag{9.167a}$$

$$I_1 = -\int_0^{+\infty} \ln z \exp(-z)\,\mathrm{d}z = \gamma \tag{9.167b}$$

$$I_2 = \int_0^{+\infty} (\ln z)^2 \exp(-z)\,\mathrm{d}z = \gamma^2 + \frac{1}{6}\pi^2 \tag{9.167c}$$

$$I_3 = -\int_0^{+\infty} (\ln z)^3 \exp(-z)\,\mathrm{d}z = \gamma^3 + \frac{1}{2}\gamma\pi^2 + 2\zeta(3) \tag{9.167d}$$

and

$$I_4 = \int_0^{+\infty} (\ln z)^4 \exp(-z)\, \mathrm{d}z = \gamma^4 + \gamma^2\pi^2 - \frac{3}{20}\pi^4 + 8\gamma\zeta \tag{9.167e}$$

where γ is Euler–Mascheroni constant defined by the series as

$$\lim_{n\to\infty}\left(\sum_{k=1}^{n}\frac{1}{k} - \ln(n)\right) \tag{9.167f}$$

The Euler–Mascheroni constant numerically equals 0.57721566 …. and looks like an irrational number, but irrationality of γ is still an unsolved problem. ζ is Apéry's constant, which numerically equals 1.2020569…. and is an irrational number. Then $Int(1)$, $Int(2)$, and $Int(3)$ can be found as

$$Int(1) = aI_0 + bI_1 = a + b\gamma \tag{9.168a}$$

$$Int(2) = a^2I_0 + 2abI_1 + b^2I_2 = a^2 + 2ab\gamma + b^2\left(\gamma^2 + \frac{1}{6}\pi^2\right) \tag{9.168b}$$

and

$$Int(3) = I_0 = 1 \tag{9.168c}$$

The mean value and standard deviation of x can finally be obtained from Equations 9.162 and 9165 by substitution of Equations 9.168a through c as

$$\bar{x} = a + b\gamma \tag{9.169}$$

$$\sigma = \frac{b\pi}{\sqrt{6}}. \tag{9.170}$$

9.5.2.2 Distribution parameters estimation

From the results in Equations 9.169 and 9.170, the distribution parameters can be solved in terms of mean value and standard deviation as

$$a = \bar{x} - \frac{\sqrt{6}\gamma\sigma}{\pi} = u; \quad b = \frac{\sqrt{6}\sigma}{\pi} = \frac{1}{\alpha} \tag{9.171a,b}$$

in which a and b are replaced by u and $1/\alpha$. The replacement has physical meanings: u is actually the most probable value of x, because the PPF has its maximum

peak at $x = u$. This can be verified by seeking the derivative of ppf as

$$\frac{\mathrm{d}p_{\mathrm{e}}(x)}{\mathrm{d}x} = \frac{1}{b^2}\exp\left[-\exp\left(\frac{a-x}{b}\right)\right]\left[\exp\left(2\left(\frac{a-x}{b}\right)\right) - \exp\left(\frac{a-x}{b}\right)\right] \tag{9.172}$$

that equals zero for the value of $u = a$. α is inversely proportional to the standard deviation, which actually expresses the degree of dispersing. A smaller α corresponds to a loose distribution. With the distribution parameters adopting u and α, the PDF, pdf, and PPF can be obtained from Equations 9.151, 9.152, and 9.155 that are expressed in Equations 9.173 through 9.175, respectively, using η_{e} to denote the extreme value variable.

$$P_{\mathrm{e}}(\eta_{\mathrm{e}}) = \exp[-\exp(-\alpha(\eta_{\mathrm{e}} - u))] \tag{9.173}$$

$$p_{\mathrm{e}}(\eta_{\mathrm{e}}) = \alpha\exp(-\alpha(\eta_{\mathrm{e}} - u))\exp[-\exp(-\alpha(\eta_{\mathrm{e}} - u))] \tag{9.174}$$

and

$$G(P_{\mathrm{r}}) = u - \frac{1}{\alpha}\ln\left(\ln\frac{1}{P_r}\right) \tag{9.175}$$

With N_{s} samples observed for the random variable, which follows extreme value distribution, the sample based mean value and standard deviation can be statistically calculated as

$$\hat{\bar{\eta}}_{\mathrm{e}} = \frac{1}{N_{\mathrm{s}}}\sum_{i=1}^{N_{\mathrm{s}}}\eta_{\mathrm{e}}^{i} \tag{9.176}$$

$$\hat{\sigma}_{\eta_{\mathrm{e}}} = \sqrt{\frac{1}{N_{\mathrm{s}}}\sum_{i=1}^{N_{\mathrm{s}}}\left(\eta_{\mathrm{e}}^{i} - \overline{\eta}_{\mathrm{e}}\right)^2} \tag{9.177}$$

Then, the estimated distribution parameters can be obtained based on Equations 9.171a,b as

$$\tilde{\alpha} = \frac{\pi}{\sqrt{6}\hat{\sigma}}, \quad \tilde{u} = \hat{\bar{\eta}}_{\mathrm{e}} - \frac{\sqrt{6}\gamma\hat{\sigma}}{\pi} \tag{9.178a,b}$$

Note that the estimation is based on the sample set and the accuracy depends on the number of samples. When a large sample set can be provided, the mean and variation can be calculated reliably, but a Gumbel suggested correction may be applied when the sample set size is small.

9.6 Ground Motion Generation

9.6.1 Modeling Concept

The uncertainty of a future earthquake is presented herein, based on probability with groups of ground motions generated considering the *seismic plate tectonic movements*. While the seismic threat comes from a fault between two seismic plates, the vibrations are set up by the partial rupture and slipping of two contact surfaces and they spread out in all directions in the earth's crust from the hypocenter. An earthquake is the passage of these vibrations and it comes to a building as the vibration reaches it. The mathematical simulation model is demonstrated in Figure 9.6a, and the rupture is regarded as composed of many small ruptures in subfaults. The rupture plane is supposed to be rectangular and appears within the rectangular seismic source in an earthquake. The rupture begins at the hypocenter, one of the subfaults, and the vibration propagates from the hypocenter to the building site. At the same time, the rupture expands rapidly over the whole rupture plane. Elastic waves are generated at each subfault and they propagate to the building site simultaneously. At the base rock surface under the site, motions from all subfaults are integrated considering the time delays. The integrated motion is then transformed to site surface motions by considering the surface soil amplification [14,20,21].

In the traditional point source model, the causative faults can be considered as point sources. This assumption is appropriate when the distance between the rupture and the site is large, compared to the fault dimensions. When the distance becomes small, the finite-fault effects become significant and the point source model is weak. The finite-fault effect is primarily due to the limited speed of the rupture propagation within the rupture plane. Parts of the fault radiate energy earlier than other parts, and the delayed waves then interfere and cause directivity effect. Directivity effect causes earthquake ground motion in the direction of the rupture propagation to be more severe than in other directions. For this reason, the finite-source model has been under development in seismology for decades, in which the fault is discretized into finite elements and each element is treated as a small source. In this model, the radiation from all subsources is summed with proper time delays.

9.6.2 Ground Motion Generated at Bed Rock Surface

With the finite source model, Beresnev and Atkinson [3], developed the FINSIM program. In this model, the rupture is regarded to be composed of many small ruptures in subfaults, which are properly divided from the whole rupture plane with consideration of the earthquake magnitude. The rupture plane is supposed to be rectangular in appearance within the rectangular fault plane in an earthquake. The size of the rupture plane ($L \times W$) can be determined based on their empirical relations to tectonic motion types, such as intraplate, or interplate earthquakes, with motions of normal, reverse, or strike slip (see Figure 9.9).

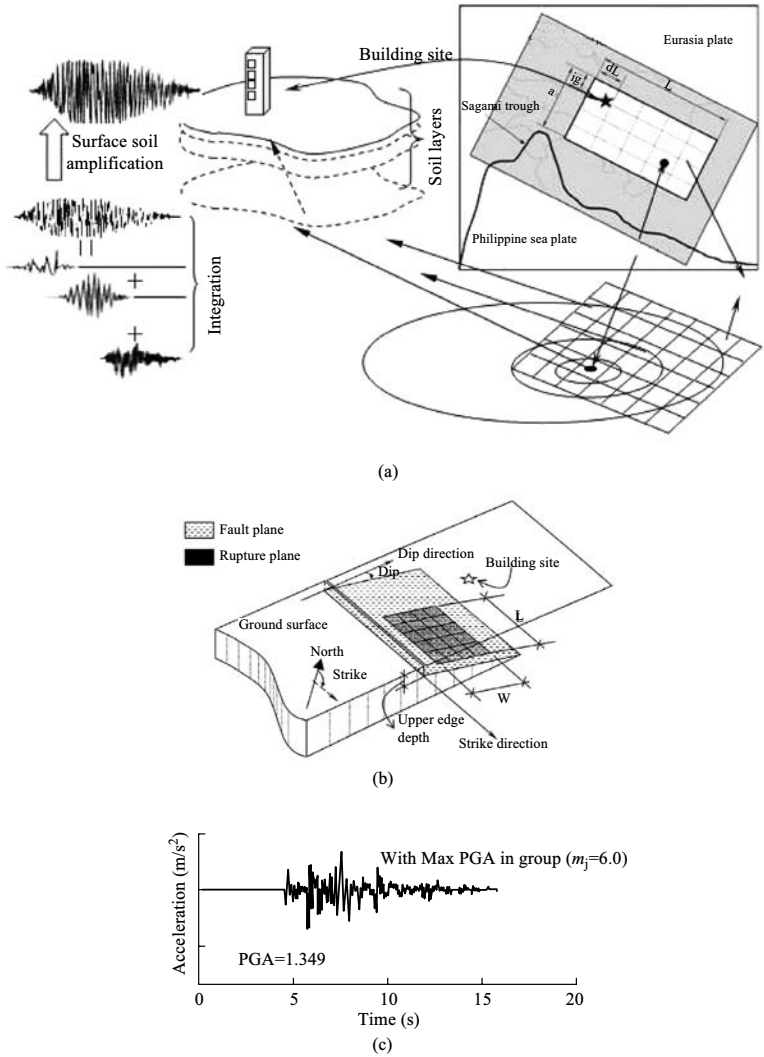

FIGURE 9.9 Generation of earthquakes with tectonic movements: (a) Earthquake generation procedure, (b) Fault and rupture planes, and (c) Sample ground motion $m_j = 6.0$.

The FINSIM program employs a standard summation procedure, with the rupture propagating rapidly from the hypocenter and triggering subsources as it passes them. In the program, the motion from each subfault is modeled by the point source stochastic Green's function used. First, a Gaussian white noise is modulated in time domain by use of a shaping window [15] as

$$w(t) = at^{\mathrm{b}} \exp(-ct)H(t) \tag{9.179}$$

where $H(t)$ is a unit step function and normalizing factor a, shape parameters b and c are given as

$$a = \left[\frac{(2c)^{2b+1}}{\Gamma(2b+1)}\right]^{1/2} \tag{9.180a}$$

$$b = \frac{-\varepsilon \ln \eta}{[1+\varepsilon(\ln \eta - 1)]} \tag{9.180b}$$

$$\mathrm{c} = \frac{b}{\varepsilon T_{\mathrm{w}}} \tag{9.180c}$$

where $T_{\mathrm{w}} = 2T_{\mathrm{d}}, \varepsilon = 0.2, \eta = 0.05$ and Γ is the gamma function. $T_{\mathrm{d}} = 2\pi/\omega_{\mathrm{c}}$ and ω_{c} is the corner frequency. The time history is then transformed into the frequency domain to be multiplied by the acceleration spectrum, $A(\omega)$, and finally transformed back into the time domain. The acceleration spectrum of the shear wave at the distance, R_{d}, from the rupture fault is given as

$$A(\omega) = C_n M_0 S(\omega) P(\omega) \exp\left(-\frac{\omega R_d}{2QV_{\mathrm{s}}}\right) R_{\mathrm{d}} \tag{9.181}$$

in which C_n is a constant with the expression of

$$C_n = \frac{R_{\theta\phi} \cdot FS \cdot RD}{4\pi\rho V_{\mathrm{s}}^3} \tag{9.182}$$

where $R_{\theta\phi}$ of the radiation pattern coefficient; $FS = 2$ of the amplification due to the free surface; and $RD = 1/\sqrt{2}$ of the reduction factor for partitioning the energy into two horizontal components; ρ and V_{s} are density and shear velocity, respectively; and Q is the propagation factor. M_0 is the seismic moment, which represents the physical strength of an earthquake. Its empirical formula related to the earthquake magnitude m_j [13] as

$$\log_{10} M_0 = 1.5 m_j + 16.1 \tag{9.183}$$

where M_0 is in dyne-cm (1 dyne $= 10^{-5}$ N). $P(\omega)$ is the high-cut filter, which is used to consider sharp decreases with increasing frequency at some cutoff frequency of ω_m observed in the acceleration spectra. $P(\omega)$ is given as

$$P(\omega) = \left[1 + \left(\frac{\omega}{\omega_m}\right)^{2\mathrm{s}}\right]^{-1/2} \tag{9.184}$$

where s controls the decay rate at the high frequencies for which the value of 4 is used. $S(\omega)$ is the source spectrum given as

$$S(\omega) = \frac{\omega^2}{1 + (\omega/\omega_c)^2} \tag{9.185}$$

in which ω_c is the corner frequency expressed as

$$\omega_c = 7.8 \times 10^5 V_s \left(\frac{\Delta\sigma}{M_0}\right)^{1/3} \tag{9.186}$$

where ω_c is in rad/s; V_s is in km/s; and $\Delta\sigma$ is in bars (1 bar $= 10^5$ Pa) that is a parameter controlling the strength of high-frequency radiation and it has been referred in literature by a variety of names such as effective stress, dynamic stress drop and so forth.

For the generation of ground motions at the bedrock under the building site, as in the aforementioned procedure, the following information needs to be provided:

(a) A target earthquake magnitude;
(b) Fault geometry: strike, dip, length, width of the fault plane, depth of the upper edge;
(c) Fault location (geographic coordinates of one of its corner);
(d) Building site location (geographic coordinates); and
(e) Seismic source parameters: density and shear-wave velocity of crystal bed rock; the rupture velocity, dynamic stress drop ($\Delta\sigma$) fault slip distribution, and model for shear wave Q.

9.6.3 Ground Motion Generated at Ground Surface

On the basis of the method in the previous section, the ground motion is generated at the bedrock surface beneath the building site. It is known that the cover soil has an amplification effect as the wave goes through. The cover soil is actually composed of many layers and cannot simply be taken as a homogenous elastic material. The motions at the ground surface can be transformed from the motions at the bedrock surface by SHACK'91 [9] with the soil layer profile provided.

9.6.4 One-Hundred Ground Motions Generated at $m_j = 6.0$

The building site is at geographic coordinates of 139.67°E, 35.69°N, where the seismic fault is the *Sagami trough* between the Philippine Sea plate and the Eurasia plate as shown in Figure 9.9b. There were more than 100 earthquakes (equal or larger than magnitude $m_j = 6.0$) recorded on the fault in last 400 years. The fault plane is rectangular with size of 222 × 167 km, of which the dip and strike are

TABLE 9.1
Site Soil Layer Profile

Layer label	Depth H (m)	Soil type	ρ (kg/m^3)	V_s (m/s)
1	2.35	Sandy gravel	2.10×10^3	220
2	3.45	Sand	1.75×10^3	210
3	1.45	Silty clay	1.96×10^3	180
4	4.55	Sandy gravel	2.10×10^3	260
5	1.90	Sand	1.80×10^3	230
6	10.0	Sand	1.89×10^3	230
7	4.00	Silty clay	1.61×10^3	190
8	3.00	Silt	1.70×10^3	280
9	8.60	Sand	1.90×10^3	380

15° and 290°, respectively. The upper edge depth is 2.6 km below ground level. The geographic coordinates of the southeast corner is 140.50°E, 34.5°N. The interplate earthquake is considered and the rupture plane size as $L = 10^{0.5m_j - 1.88}$ and $W = L/2$. dL and dW are assumed to be same, with d$L = 10^{0.4m_j - 2}$ [14, 20].

The geologic properties for the ground motion generation are: mass density, $\rho = 2.8 \times 10^3$ kg/m^3, and *shear wave velocity*, $V_s = 3700$ m/s, for the crystal bedrock; radiation pattern coefficient is $R_{\theta\phi} = 0.55$, constant $Q(\omega)$ model is $Q(\omega) = 1000$; and dynamic stress drop $\Delta\sigma = 50$ bars. One hundred ground motions are generated for magnitude of $m_j = 6.0$. After the motions at the base rock have been generated, the soil layer amplification is included in the calculation with soil layer profile given in Table 9.1. In one hundred ground motions, a typical record with the maximum peak acceleration (PGA = 1.349) in the group as shown in Figure 9.9c, which is also shown in Figure 9.6 used as the sample input in Section 9.5.

The PGA values of the hundred motions are collected in Table 9.2.

From Table 9.2, the mean value and standard deviation is calculated per Equations 9.176 and 9.177 and are listed as follows

m_j	Mean equation 9.176	Max data No. 27	Min data No. 61	σ_{PGA} equation 9.177
6.0	0.559	1.349	0.186	0.254

9.7 Case Studies Using Generated Earthquakes

9.7.1 Numerical Examples of Fixed Supported Buildings with and without Controls

Case study without controls

The studies are conducted on the responses of top floor displacement (denoted as D) of the six-story building given in Section 9.5. Following the procedure used in

TABLE 9.2
PGA Values (unit in $g = 8.9\ m/s^2$) of the Hundred Motions as

2.2163000e–002	3.9188000e–002	4.6966000e–002	1.9385000e–002	5.9694000e–002
5.7904000e–002	1.0324100e–001	6.7898000e–002	6.2166000e–002	9.6509000e–002
9.1479000e–002	4.3148000e–002	4.8812000e–002	4.9929000e–002	5.9816000e–002
2.2431000e–002	5.9440000e–002	4.7242000e–002	3.1733000e–002	4.7393000e–002
4.0315000e–002	3.7225000e–002	4.9633000e–002	2.0478000e–002	6.4554000e–002
1.0662900e–001	2.9209000e–002	2.3501000e–002	3.9990000e–002	4.2936000e–002
6.5342000e–002	1.3761300e–001	4.3262000e–002	3.3697000e–002	4.6564000e–002
2.4018000e–002	7.6674000e–002	5.8616000e–002	7.3019000e–002	4.9589000e–002
5.3130000e–002	2.3730000e–002	3.8002000e–002	9.3334000e–002	4.3250000e–002
6.2835000e–002	2.9571000e–002	6.5344000e–002	8.9327000e–002	4.5639000e–002
1.1625300e–001	6.6702000e–002	6.1335000e–002	3.1505000e–002	1.2153100e–001
5.8913000e–002	6.3420000e–002	7.0751000e–002	5.1899000e–002	4.6724000e–002
5.6053000e–002	3.9228000e–002	8.0302000e–002	6.8195000e–002	9.6827000e–002
3.5884000e–002	5.9477000e–002	2.4800000e–002	2.7936000e–002	2.6732000e–002
7.4444000e–002	3.5567000e–002	7.1005000e–002	2.8639000e–002	5.8373000e–002
3.8765000e–002	6.5798000e–002	8.0711000e–002	9.7065000e–002	6.5551000e–002
8.4825000e–002	1.3688200e–001	4.7734000e–002	4.7256000e–002	3.9393000e–002
4.1409000e–002	2.5946000e–002	4.9186000e–002	6.8966000e–002	9.3723000e–002
5.0828000e–002	4.4205000e–002	4.3358000e–002	2.6451000e–002	1.3366600e–001
4.5041000e–002	6.5195000e–002	6.6580000e–002	4.0916000e–002	7.3444000e–002

Section 9.5.1 for each of ground motions, we then obtain 100 maximum top floor displacements as listed in Table 9.3.

Per Equations 9.176 and 9.177, the mean value and the standard deviation are calculated using the MTLAB *mean*(), and *std*() command [12]. They are computed as 1.829 and 0.85 cm, respectively. With mean value and standard deviation calculated, the estimated distribution parameters, $\tilde{u}$ and $\tilde{\alpha}$ are calculated per Equation 9.178a,b. They are 1.44 cm and 150.2 m^{-1}. With those parameters, the distribution curves are drawn for pdf, PDF, and PPF curves of D are shown in Figures 9.10 through 9.12, respectively. In PPF, the response at the 80% probability is marked as 2.44 cm.

Case with active controlled

There are two controllers placed on the top two floors based on optimal placement evaluation. The weighting matrices have the unit value of element (6, 6) and other elements as zeros in $[Q]$; and $[R] = r[I_2]$ for two forces with $[I_2]$ as an identity matrix of order 2. Two active cases are studied with values of r as 2×10^{-14} and 0.4×10^{-14}, which are called cases of low active and high active, respectively. The low active and high active are selected to compare the controlled results by reducing 60 and 80% of the highest response among 100 case studies, respectively. For these

TABLE 9.3
Maximum Top Floor Displacements for Each of 100 Generated Earthquakes at $m_j = 6$

6.9952774e–003	1.1622844e–002	2.6024768e–002	1.2235273e–002	1.7738517e–002
1.5830980e–002	3.1307899e–002	3.4857899e–002	1.9169070e–002	2.8713341e–002
2.1309704e–002	1.4845813e–002	1.2208368e–002	1.4035297e–002	1.7671105e–002
1.1357112e–002	1.3203714e–002	1.1584301e–002	1.1961589e–002	1.3195988e–002
1.6308843e–002	7.8208370e–003	1.2468054e–002	5.7960097e–003	1.7908874e–002
1.6289151e–002	1.1723282e–002	1.1307750e–002	1.5316215e–002	1.6966958e–002
1.0714708e–002	4.5539123e–002	1.5978571e–002	1.5328523e–002	2.3575813e–002
1.5749865e–002	2.8710848e–002	1.4604420e–002	1.1830335e–002	2.4884417e–002
1.2136181e–002	8.1256962e–003	1.2883588e–002	2.1593194e–002	1.3859180e–002
3.1234868e–002	4.0481161e–003	1.9253519e–002	3.0467801e–002	2.2228775e–002
3.2251159e–002	2.3591399e–002	3.2476367e–002	9.1715923e–003	2.9875830e–002
1.3260341e–002	1.1208590e–002	9.9839325e–003	3.4843176e–002	1.0343875e–002
1.6897899e–002	1.2857184e–002	2.9215770e–002	1.2141709e–002	1.9365095e–002
1.7721922e–002	2.1671960e–002	8.0525160e–003	9.4938487e–003	1.2602486e–002
3.1138851e–002	2.1263212e–002	2.5863081e–002	9.0625395e–003	1.1208515e–002
1.8547359e–002	2.6170644e–002	2.1203813e–002	1.7366696e–002	4.5492611e–002
2.1395242e–002	3.0160590e–002	2.6403480e–002	9.2426569e–003	1.0468309e–002
1.2288499e–002	1.4169281e–002	1.5682268e–002	1.2073521e–002	3.7369668e–002
2.8119390e–002	1.6554266e–002	1.4915960e–002	5.1516929e–003	1.7761363e–002
2.4265040e–002	1.8051349e–002	1.6925718e–002	1.3940251e–002	2.9232536e–002

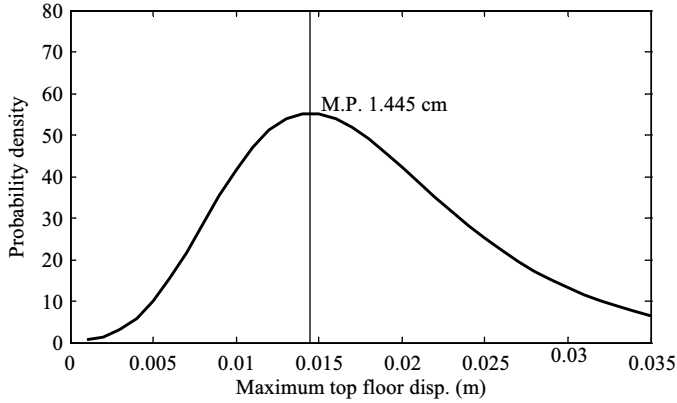

FIGURE 9.10 pdf curve for top floor displacement without control.

two cases the time history analyses are performed for each of the individual 100 ground motions, and from which the maximum top floor displacements are listed in Tables 9.4 and 9.5 corresponding to low active control and high active control, respectively.

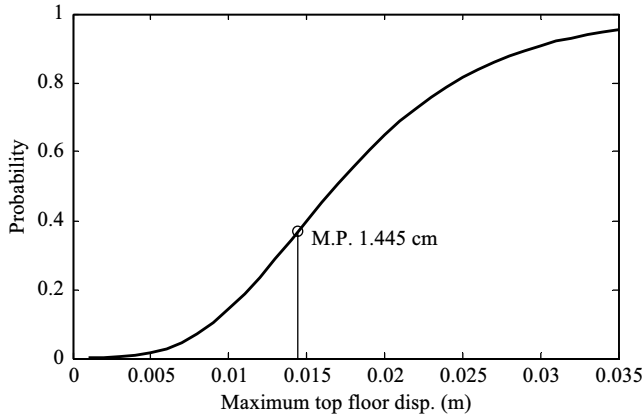

FIGURE 9.11 PDF curve for top floor displacement without control.

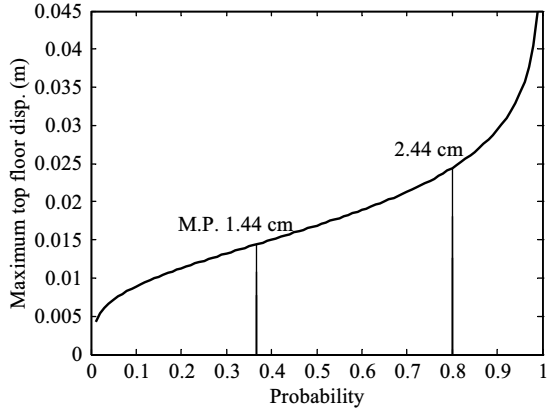

FIGURE 9.12 PPF curve for top floor displacement without control.

The mean values and standard deviations are statistically calculated for a sample set; and u, α are then estimated based on Equations 9.178a,b. The distribution curves are drawn for pdf, PDF, and PPF in Figures 9.13 through 9.15, respectively. For comparison presented in the figures, the curve associated without control case is included that is from Figure 9.12, Active Control 1 and Active Control 2 are corresponding to low-active and high active control, respectively. The studies are also conducted on the responses of active control forces. The data sets are collected for the maximum responded forces at the top floor as listed in Tables 9.6 and 9.7 for low active and high active control, respectively.

Using the identical procedures presented for displacement studies yields the PPF distribution curves of control forces shown in Figure 9.16.

TABLE 9.4
Maximum Top Floor Displacements for Low Active Control

5.1289596e–003	8.6198820e–003	1.7702796e–002	9.2654603e–003	1.2141910e–002
1.1869313e–002	2.4599024e–002	2.6030855e–002	1.4635382e–002	2.2363254e–002
1.5172050e–002	1.0673688e–002	9.4925131e–003	1.1687839e–002	1.4694775e–002
8.4121282e–003	9.7942984e–003	9.3960069e–003	8.6969681e–003	1.0436796e–002
1.2200463e–002	5.9494618e–003	8.9100243e–003	4.8452807e–003	1.3820017e–002
1.4193169e–002	8.8703914e–003	8.9664304e–003	1.1775394e–002	1.0902482e–002
8.6301431e– 003	3.1986830e–002	1.1505305e–002	1.0962026e–002	1.5981735e–002
1.1379719e– 002	2.2972540e–002	1.0120243e–002	1.0031615e–002	1.7325917e–002
9.8143322e– 003	6.0160409e–003	1.0864788e–002	1.5691410e–002	1.0843926e–002
2.3096616e– 002	3.3616753e–003	1.4109335e–002	2.1363170e–002	1.7489121e–002
2.5012299e– 002	1.8051135e–002	2.1342829e–002	6.2254047e–003	2.0856387e–002
1.0761401e– 002	8.3355557e–003	7.3951351e–003	2.3463821e–002	8.9012644e–003
1.1451321e– 002	1.0862512e–002	1.9950573e–002	9.3429136e–003	1.6711550e–002
1.2676602e– 002	1.6968271e–002	5.2621195e–003	6.9647782e–003	9.1067257e–003
2.6016315e– 002	1.4402639e–002	2.0361636e–002	6.6632501e–003	1.0175736e–002
1.3509288e– 002	1.8349737e–002	1.5761859e–002	1.4709276e–002	3.1042586e–002
1.8060334e– 002	2.2424997e–002	2.0046076e–002	7.7832177e–003	8.4955017e–003
9.5336808e– 003	9.6846822e–003	1.0781619e–002	9.1410755e–003	3.1129551e–002
1.8239482e– 002	1.2412410e–002	1.1067976e–002	4.4041374e–003	1.3620109e–002
1.5908318e– 002	1.2845564e–002	1.1281613e–002	1.0986243e–002	2.2589853e–002

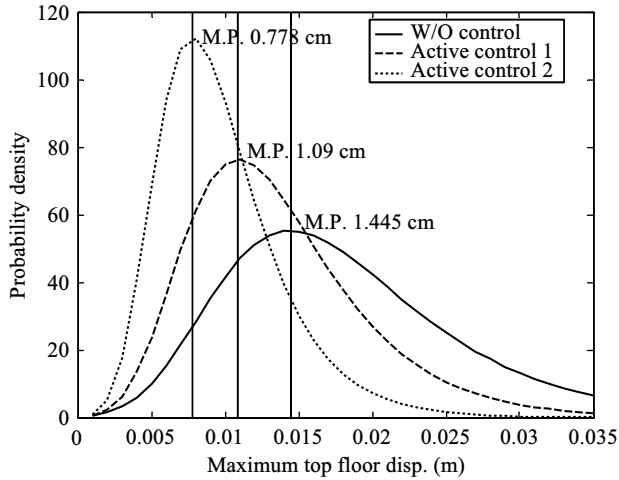

FIGURE 9.13 pdf curve for top floor displacement with control.

TABLE 9.5
Maximum Top Floor Displacements for High Active Control

3.4421495e–003	6.6145150e–003	1.0813343e–002	6.8037560e–003	7.8616926e–003
8.4946591e–003	1.7008717e–002	1.7494799e–002	1.0523090e–002	1.5212598e–002
1.0640084e–002	6.8412143e–003	6.9831965e–003	9.0466346e–003	1.0865165e–002
5.6264631e–003	6.6328650e–003	7.4368790e–003	5.7625780e–003	8.3537440e–003
8.0415593e–003	4.2592508e–003	7.1783311e–003	3.6773028e–003	9.3795445e–003
1.1165938e–002	5.8771102e–003	6.2706353e–003	8.6856583e–003	7.4265880e–003
7.9511752e–003	2.1575347e–002	7.3441841e–003	7.5709014e–003	1.1070878e–002
7.2598619e–003	1.6137825e–002	7.0070346e–003	7.7967679e–003	1.0994198e–002
7.1628939e–003	4.6181660e–003	8.6630404e–003	1.2617502e–002	7.7777395e–003
1.5653436e–002	3.0507572e–003	1.0177720e–002	1.4180157e–002	1.2352291e–002
1.8122740e–002	1.2802206e–002	1.3227205e–002	5.2033151e–003	1.3702283e–002
7.6638583e–003	5.9878746e–003	5.0780105e–003	1.4422666e–002	6.7752170e–003
8.1803109e–003	8.7077925e–003	1.2598076e–002	6.3238832e–003	1.3793370e–002
8.4746517e–003	1.2109435e–002	3.5781812e–003	5.2168290e–003	6.0621725e–003
2.0314397e–002	1.0412264e–002	1.5644797e–002	4.6126183e–003	8.5107336e–003
9.3293367e–003	1.2156429e–002	1.1336370e–002	1.1994391e–002	1.8885916e–002
1.4303663e–002	1.6169177e–002	1.4265549e–002	7.2744920e–003	5.8969954e–003
6.7710741e–003	6.1079400e–003	7.1455092e–003	6.5139137e–003	2.3089655e–002
1.0843503e–002	8.2793968e–003	7.0874034e–003	3.3987109e–003	1.0434634e–002
1.1170663e–002	9.6955214e–003	8.1089172e–003	7.7778808e–003	1.5805625e–002

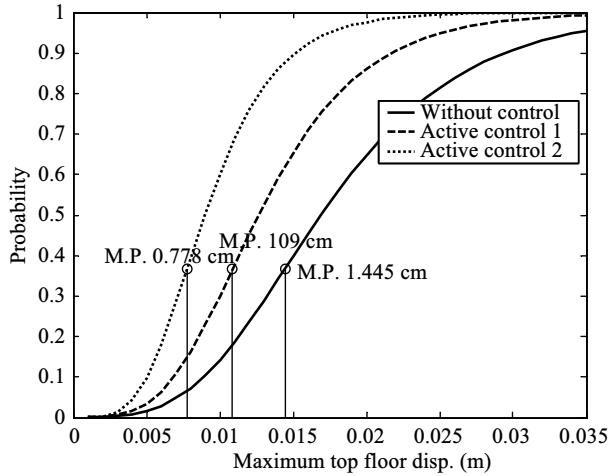

FIGURE 9.14 PDF curve for top floor displacement with control.

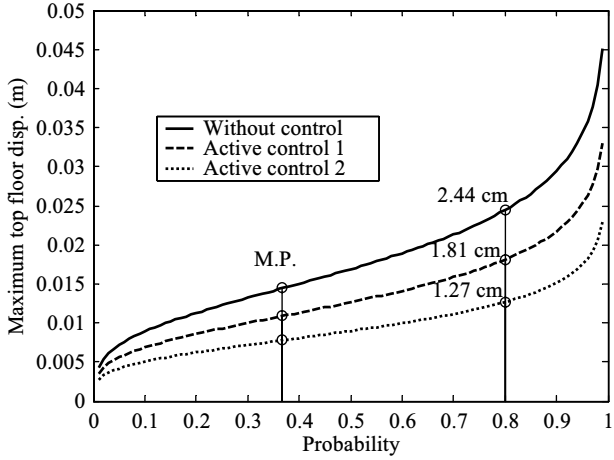

FIGURE 9.15 PPF curve for top floor displacement with control.

TABLE 9.6
Maximum Control Forces for Low Active Control

1.4415338e+004	2.3916624e+004	4.9741247e+004	2.4987756e+004	3.6381729e+004
3.7383476e+004	6.3690815e+004	7.5187519e+004	4.3532195e+004	6.9926075e+004
4.5725133e+004	3.0486744e+004	2.9862784e+004	3.4384217e+004	4.0938419e+004
2.4531282e+004	2.7277057e+004	2.5771325e+004	2.3567829e+004	3.1651222e+004
3.4914166e+004	1.5481403e+004	2.9946043e+004	1.4732457e+004	3.9898205e+004
4.5971948e+004	2.7351086e+004	2.5343439e+004	3.1839153e+004	2.8863500e+004
2.7141553e+004	9.6518571e+004	3.1232921e+004	3.0570845e+004	4.2176575e+004
3.1347748e+004	6.4277728e+004	2.9205492e+004	2.6284539e+004	4.4992865e+004
2.6367889e+004	1.9429745e+004	3.4534329e+004	4.8656912e+004	3.0355755e+004
6.4778920e+004	9.6388244e+003	4.0590185e+004	5.9885536e+004	5.0220330e+004
7.7583462e+004	5.3901934e+004	6.1497043e+004	1.6567862e+004	6.0928743e+004
3.0544679e+004	2.2768627e+004	2.0594427e+004	6.5768956e+004	2.4800970e+004
3.3245926e+004	3.3131549e+004	6.0938571e+004	2.8274639e+004	4.4536382e+004
3.4798945e+004	4.5390978e+004	1.5748191e+004	2.0352103e+004	2.5719021e+004
7.5773637e+004	4.2046762e+004	5.6783502e+004	1.9346155e+004	2.5391254e+004
3.8076525e+004	5.1618481e+004	5.1230357e+004	4.7663776e+004	8.2169113e+004
5.3965148e+004	6.7357604e+004	5.8248101e+004	2.4359342e+004	2.2496121e+004
2.7191886e+004	2.8319741e+004	3.0600480e+004	2.6205223e+004	8.7106940e+004
5.1685620e+004	3.4130906e+004	3.1423849e+004	1.1829736e+004	3.8369313e+004
4.6498354e+004	3.7667630e+004	3.5263074e+004	3.1168595e+004	6.8724676e+004

TABLE 9.7
Maximum Control Forces for High Active Control

2.9957653e+004	5.8261063e+004	8.5979878e+004	5.5091286e+004	6.7984181e+004
8.1036903e+004	1.3382486e+005	1.4464882e+005	9.8253811e+004	1.4614586e+005
9.3124677e+004	5.9090242e+004	5.8075603e+004	8.0353777e+004	9.0950887e+004
4.7412075e+004	5.6792034e+004	6.0933303e+004	4.7243884e+004	7.5730025e+004
6.8968307e+004	3.3768710e+004	7.0550381e+004	3.3113833e+004	7.9407438e+004
1.0531278e+005	5.5529568e+004	5.3493711e+004	7.3718842e+004	6.3281912e+004
6.9258223e+004	1.9714186e+005	6.0979338e+004	6.3807511e+004	8.8761181e+004
6.0456413e+004	1.3502908e+005	6.0705792e+004	5.9248470e+004	8.3858101e+004
6.2617290e+004	4.3433081e+004	7.6367405e+004	1.1614645e+005	6.8490966e+004
1.3174677e+005	2.4605608e+004	8.1650050e+004	1.1740060e+005	1.0071855e+005
1.6625235e+005	1.1419355e+005	1.1382887e+005	4.0654487e+004	1.1568031e+005
7.0458263e+004	4.9005641e+004	4.3439487e+004	1.1687743e+005	5.9318326e+004
7.4299961e+004	7.4548564e+004	1.1334501e+005	6.1581910e+004	1.0199015e+005
6.9275184e+004	9.3734588e+004	3.3154535e+004	4.2976162e+004	5.0816995e+004
1.6470820e+005	8.9184070e+004	1.2900974e+005	4.4920242e+004	6.0181750e+004
7.5167888e+004	1.0313171e+005	1.0841025e+005	1.2003993e+005	1.5198232e+005
1.2893578e+005	1.6008103e+005	1.2384542e+005	6.6338918e+004	4.9586132e+004
5.4787533e+004	5.2237350e+004	5.9957209e+004	5.8307076e+004	1.9484353e+005
8.8417109e+004	6.7327005e+004	6.0127475e+004	2.4757544e+004	8.8103164e+004
9.3549721e+004	7.7749493e+004	7.1600084e+004	6.5555498e+004	1.4165673e+005

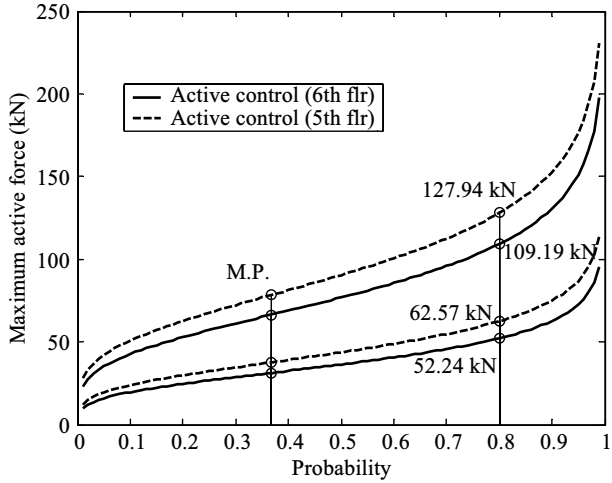

FIGURE 9.16 PPF curve for active control forces.

9.7.2 Numerical Examples of Buildings with SSI and Hybrid Control

The study is identical to the example illustrated in Section 9.4.7 and therefore no detail is necessary to be given here. For comparison purposes, this section also includes several other cases as (1) fixed support and SSI without control, (2) fixed support and SSI with passive control, and (3) fixed support with hybrid control (already presented, see Section 9.4).

Following the procedures illustrated in Section 9.6.4, we can calculate the mean values and standard deviation of these cases by using MATLAB®. The PPF responses of D/H (ratio of top floor displacement and building height) are given in Figure 9.17 from which the control effectiveness can be observed by comparing the D/H associated with the given cases.

9.8 Concluding Remarks

This chapter comprises of four major parts: The first part includes fundamental behavior of SSI behavior and its formulation for a shallow foundation (see Section 9.1). The second presents motion equations of the hybrid controlled systems of single- and multiple-story buildings with and without SSI for which the state space is formulated in accordance with the numerical algorithms developed in the previous chapters. This part is in Sections 9.2 and 9.3. The third part, presented in Section 9.4, is mainly developed for MATLAB® applications for that the state space formulation is modified from the conventional expressions given in the second part, in order to fit MATLAB's® analytical procedures as well as input and output formats. Seven numerical examples are provided to illustrate the necessary procedures for various cases. The last part outlines technical details of generating

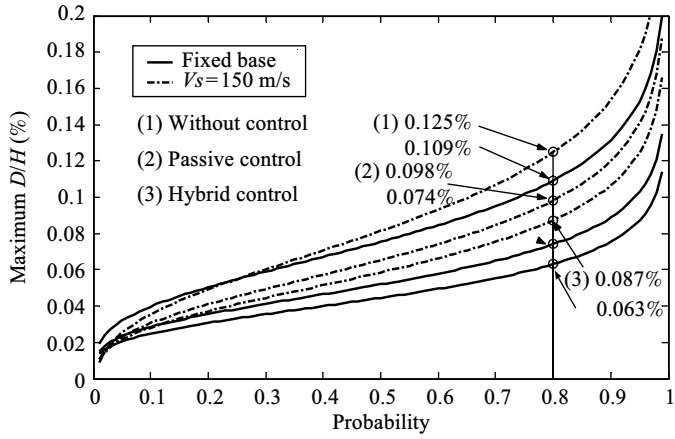

Figure 9.17 PPF curve for top-floor displacement with and without SSI for various control cases.

ground motions based on historical tectonic movements and geological data of a given seismic fault. Relevant mathematical formulations comprising of modeling of ground motion generation, extreme value distribution, and its representation of the mean value and variance are included. It is to aim that a controlled-structural system can be designed based on both the existing and future earthquakes. Extensive numerical examples are provided for a six-story building subjected to one hundred generated ground motions of seismic magnitude $m_j = 6.0$. The building is investigated for various controlled cases of passive, active, or hybrid controllers with and without SSI. The control effectiveness is thus assessed by comparing the maximum floor displacements and control forces of these cases using Monte Carlo technique. The comparison is expressed in PDF and PPF. The study of control effectiveness can be extended to include more generated earthquakes of $m_j = 7.0$ and 8.0 and earthquake recurrence during structure's life period in order to have a larger spectrum of response data from which the type and the number of controllers may be decided for optimal cost of a controlled structural system [14,21].

References

1. Apsel, R.J. and Luco, J.E., Impendence functions for embedded in a layered medium: an integral equation approach, *Earthquake Engineering and Structural Dynamics,* 15, 213–231, London, 1987.
2. Banerjee, P.K. and Butterfield, R., *Dynamic Behavior of Foundation and Buried Structures*, Elsevier Applied Science, 1987.
3. Beresnev, I.A. and Atkinson, G.M., FINSIM—a FORTRAN program for simulating stochastic acceleration time histories from finite faults, *Seismological Research Letter*, 69, 27–32, 1998.
4. Bielak, J., Dynamic response of non-linear building foundation systems, *Earthquake Engineering and Structural Dynamics*, 6, 17–30, 1978.
5. Cheng, F.Y., *Matrix Analysis of Structural Dynamics: Application to Earthquake Engineering,* Marcel Dekker, Inc., New York, NY; CRC Press/Taylor & Francis Group, Boca Raton, FL, 2001.
6. Chun, B.Y. and Cheng, F.Y., (eds.), Proceedings of U.S.–Korea Workshop on *Smart Structural Systems*, Techno-Press, Daejeon, Korea, 2002.
7. Chun, B.Y., Cheng, F.Y., and Choi, C.K. (eds.), *Smart Structural Systems*, Special Issue of the International Journal of Structural Engineering and Mechanics, Techno-Press, Daejeon, Korea, 2004.
8. Darby, R., *Viscoelastic Fluids: An Introduction to Their Properties and Behavior*, M. Dekker, New York, 1976.
9. Idriss, I.M. and Sun, J.I., *User's Manual for SHAKE91: A Computer Program for Conducting Equivalent Linear Seismic Response Analysis of Horizontally Layered Soil Deposits,* Center for Geotechnical Modeling, Department of Civil and Environmental Engineering, University of California, Davis, California, 1992.
10. Kotz, S. and Nadarajah, S., *Extreme Value Distributions: Theory and Applications*, Imperial College Press, River Edge, NJ, 2000.
11. Luco, J.E., A simple model for structural control including soil-structure interaction effects, *Earthquake Engineering and Structural Dynamics*, 27, 225–242, 1998.

12. MATLAB®: *The Language of Technical Computing*, The Math Works, Inc., 1994–2007.
13. Purcaru, G. and Berckhemer H., A magnitude scales for very large earthquakes, *Technophysics*, 49, 189–198, 1978.
14. Saragoni G.R. and Hart G.C., Simulation of artificial earthquakes, *Earthquake Engineering and Structural Dynamics*, 2, 249–167, 1974.
15. Stewart, J.P., Seed, R.B., and Fenves, G.L., *Empirical Evaluation of Inertial Soil-Structure Interaction Effects*, Berkley: Pacific Earthquake Engineering Research Center, Report No. PEER-98/07, 1998.
16. Takahashi, Y., Kiureghian, A.D., and Ang, A.H., Life-cycle cost analysis based on a renewal model of earthquake occurrences, *Earthquake Engineering and Structural Dynamics*, 33, 859–880, 2004.
17. Weisstein E.E., *Euler–Mascheroni Integrals*, from *MathWorld*—A Wolfram Web Resource. http://mathworld.wolfram.com/Euler-MascheroniIntegrals.html, 1999.
18. Wolf, J.P., *Soil-Structure Interaction Analysis in Time Domain*, Prentice-Hall, New York, 1987.
19. Zhang, X.Z., Cheng, F.Y., and Jiang, H.P., Hybrid actuator–damper–bracing control (HDABC) system with intelligent strategy and soil–structure interaction, *Engineering Structures*, 28, 2010–2022, 2006.
20. Zhang, X.Z., Cheng, F.Y., Lou, M.L., Jiang, H.P, and Takahashi, Y., Intelligent hybrid damper-actuator bracing control (HDABC) with deterministic and non-deterministic seismic input, soil–structure interaction, and tectonic movements, *Proceedings of 3rd International Conference on Earthquake Engineering*, Nanjing, China, 2004.
21. Zhang, X.Z., Intelligent hybrid damper-actuator bracing control (HDABC) with deterministic and non-deterministic seismic input, soil-structure interaction, and tectonic movements, Ph.D. Thesis, Civil, Architectural & Environmental Engineering Dept., Univ. of Missouri, Rolla, 2004.

Appendix A: MATLAB®

MATLAB® is a powerful software package that provides an interactive numerical computing environment and technical programming language for high-performance numerical analysis and data visualization [1,2]. Developed by the company *The MathWorks*, MATLAB® is available for Windows, UNIX, and Macintosh systems. The latest release for Windows, MATLAB® Version 2007a, includes MATLAB® 7.4, SIMULINK 6.6, as well as add-on extensions such as Control System Toolbox 8.0. MATLAB® is a very successful technical software. It is now commonly used as a teaching tool for linear algebra and numerical analysis. It is also very popular among scientists and engineers for problem solving in areas that involve mathematics.

MATLAB® provides an easy-to-use platform for matrix operation, 2D and 3D graphical representation of functions and data, algorithm implementation, numerical analysis, signal processing, creation of graphical user interfaces, and interfacing with programs written in other languages. As its name stands for "matrix laboratory," MATLAB® uses a matrix as its basic data element. With this setup, MATLAB® users can easily solve complex computational problems, without writing tedious programs in traditional programming languages such as FORTRAN or C++. MATLAB® also provides add-on toolboxes for a wide range of applications, including control system design, system identification, signal and image processing, communications, test and measurement, financial modeling and analysis, and computational biology. With its powerful features, especially its Control System Toolbox, MATLAB® has become a very popular tool for analysis and design of smart seismic structures. This appendix introduces some basics on how to apply the MATLAB® for such purposes. Detailed information of MATLAB® can be found from its manuals, its online help information, and related publications [1,2].

A.1 MATLAB® LANGUAGE

MATLAB® users can use it in two ways, the interactive shell or the script program. The interactive shell has the Command Window after MATLAB® starts. It allows users to directly enter calculation commands at the prompt, ». The script program is to physically store sequences of commands in a text file (called *M*-files) by intelligent built-in MATLAB® editor/debugger or any external text editor

or word processor. Such a program can be encapsulated into a function to extend the available commands. With this important extensibility feature, MATLAB® users can easily create their own MATLAB® functions to supplement those that are built into the package. In fact, the optional MATLAB® toolboxes are *M*-files written by the MATLAB® vendor, *The MathWorks*.

The MATLAB® language is called *M*-code or simply *M*. *M*-code can be simply entered and executed at the »prompt in the Command Window. The syntax of MATLAB® commands is *C*-like, especially these selective statements, loop structures, and I/O statements. Learning MATLAB® is much easier than learning C/C++ as the simple arithmetic-like syntax of MATLAB® programs are short and easy to read. In the MATLAB® Command Window, the user can just enter an expression or equation at the MATLAB® command prompt, ». For example, to perform simple arithmetic, you enter an expression or equation at the MATLAB® command prompt as follows:

» 3*8

After you hit the Enter key, MATLAB® calculates the expression and returns the result stored in the default variable *ans*

ans =

24

MATLAB® users can also create their own variables to store the input data and results with the assignment operator, =. For example, if the following command is entered

» *product* = 3*8

MATLAB® responds

product =

24

MATLAB® variables are assigned without declaring their data type, and the data type of a variable can change by its overriding assignment. A variable can be assigned by a constant, another variable, a function, or an expression. For example, the command

» *product='new'*

reassigns the variable *product* to string data *'new'*; and the command

» *product* = 3* sin(0.5)

updates the value of *product* to real data 1.4382 by an expression with built-in function sin().

Since it uses the matrix as its basic element, MATLAB® provides very convenient ways for creating matrices of various dimensions, such as $1 \times N$, $N \times 1$, $N \times M$, and $N \times M \times L$, and so forth, where N, M, and L can be any integer number. The $1 \times N$ or $N \times 1$ matrix in MATLAB® is actually a vector or referred as an array in common programming languages. Matrix variables are treated the same way as scalar variables in MATLAB® for the syntax for matrix operations and function

arguments. Matrices are defined by a list of data elements enclosed by square brackets []. The list uses blank space or comma to separate the elements of a row and a semicolon at the end of each row. For example, the following two commands define an array *Vector1* and a matrix *Matrix1*:

» *Vector1* = [1 2 3 4 5];

Vector1 =

1 2 3 4 5

» *Matrix1* = [11 12 13; 21 22 23; 31 32 33]

*Matrix*1 =

11 12 13

21 22 23

31 32 33

Elements and submatrices of a matrix are accessed using parenthesis () operator. For example,

» *Matrix1*(2,3)

ans = 23

» *Matrix1*(1:2,2:3)

ans =

12 13

22 23

MATLAB® also provides a simple way to define array or matrix elements by the syntax: init:increment:terminator. For instance,

» *array1* = 1:2:9

array1 =

1 3 5 7 9

The variable *array1* is assigned with a 5-element array consisting of the values 1, 3, 5, 7, and 9. The command means that the array starts at the initial value, 1, and adds elements with increment by 2 until it reaches but not exceeds the terminator, 9.

As noted, MATLAB® also has powerful and easy-to-use graphics tool. For example, the following program produces a graph of sine curve in the range of $(0, 2\pi)$ by two vectors x and y:

$x = 0 : pi/100 : 2*pi;$

$y = \sin(x);$

$plot(x, y)$

A.2 Common Functions Used for Analysis and Design of Smart Seismic Structures

This section introduces common MATLAB® functions that are useful for analysis and design of smart seismic structures. MATLAB® users can easily get their detailed information either by the help menu or by the *help* command in the Command Window. For instance, the command

» *help EIG*

would give detailed information of function *EIG*.

- *RANK*: matrix rank.
  » *RANK*(A) yields the number of linearly independent rows or columns of a matrix A.
- *EYE*(N): generates a square identity matrix of size N.
- *ZEROS*(M, N): generates a matrix with all elements zero.
- *ONES*(M, N): generates a matrix with all elements one.
- *EIG*: solves eigenvalues and eigenvectors of a matrix.
  » $E = EIG(X)$ is a vector containing the eigenvalues of a square matrix X.
  » $[V, D] = EIG(X)$ produces a diagonal matrix D of eigenvalues and a full matrix V whose columns are the corresponding eigenvectors so that $XV = VD$.
- *ACKER*: pole placement technique by Ackermann's formula.
  » $K = ACKER(A, B, P)$ calculates the feedback gain matrix K so that the single-input system $\dot{x} = Ax + Bu$ (u is a scalar variable) with a feedback law of $u = -Kx$ has closed-loop poles at the values specified in vector P, that is, $P = EIG(A - BK)$.
- *PLACE*: pole placement technique for single- or multi-input systems.
  » $K = PLACE(A, B, P)$ computes the feedback gain matrix K so that the closed-loop poles are those specified in vector P.
- *ARE*: solves algebraic Riccati equation.
  » $X = ARE(A, B, C)$ solves algebraic Riccati equation $A^{\mathrm{T}}X + XA - XBX + C = 0$ and returns the Riccati matrix X.
- *CARE*: solves continuous-time algebraic Riccati equations.
  » $[X, L, G, RR] = CARE\ (A, B, Q, R, S, E)$ solves the continuous-time algebraic Riccati equation $A^{\mathrm{T}}XE + E^{\mathrm{T}}XA - (E^{\mathrm{T}}XB + N)R(B^{\mathrm{T}}XE + N^{\mathrm{T}}) + Q = 0$ and returns Riccati matrix X. Q, R, S, and E are weighting matrices, and the last three are optional and set to default values ($R = I$, $S = 0$, and $E = I$) if omitted. L, G, and RR are optional outputs, which are vector of closed-loop poles, gain matrix, and the Frobenius norm of the relative residual matrix, respectively.
- *DARE*: solves discrete-time algebraic Riccati equations.
  » $[X, L, G, RR] = DARE\ (A, B, Q, R, S, E)$ solves the discrete-time algebraic Riccati equation and returns Riccati matrix X. Its arguments have the same meaning as the *CARE* function.

- *LQR*: linear-quadratic regulator design for continuous-time systems.
  » $[K, S, E] = LQR(A, B, Q, R, N)$ calculates the optimal gain matrix K for the system $\dot{x} = Ax + Bu$ such that the state-feedback law $u = -Kx$ minimizes the cost function $J = \int \left(x^{\mathrm{T}}Qx + u^{\mathrm{T}}Ru + 2x^{\mathrm{T}}Nu\right) \mathrm{d}t$. Q, R, and N are weighting matrices, and N is an optional argument and set to zero when omitted. This function also solves the Riccati matrix S in the Riccati equation $SA + A^{\mathrm{T}}S - (SB + N)R(B^{\mathrm{T}}S^{\mathrm{T}} + N^{\mathrm{T}}) + Q = 0$ and the closed-loop poles $E = EIG(A - BK)$.
- *RLOCUS*: plots Evans root locus.
  » *RLOCUS*(*SYS*) computes and plots the root locus of the SISO (single-input, single-output) system *SYS*. The root locus plot shows the loci of the closed-loop poles when the feedback gain K varies from 0 to ∞. *RLOCUS* automatically generates enough positive gain K values so that a smooth plot can be generated.
  » *RLOCUS*(*SYS*, K) uses a user-specified vector K of gain values.
- *LSIM*: simulates time–history response of a linear system to single or multiple inputs.
  » *LSIM*(*SYS*, U, T) plots the time–history response of the linear system *SYS* to the input signal described by U and T. The time vector T consists of time instants, and U is a matrix with as many columns as excitations and whose i-th row is the value of excitations at time instant $T(i)$. In smart structure applications, there is only one excitation—the earthquake ground motion. Thus, U will be a vector whose i-th element is the value of ground acceleration at time instant $T(i)$.

MATLAB® interactive command window allows users to directly enter function calls. Take the numerical calculations in Example 6.3.1 as an example here. The following syntax inputs the observability matrix $[M_{\mathrm{o}}]$ in the MATLAB® command window

$>>M_{\mathrm{o}} = [0, 1, 0, 0; 0, 0, 0, 1; 671.234, -671.234, 0.300, -0.474; -483.607, 415.886, 670.965, -670.965]$

and MATLAB® responds

M_{o}

```
        0    1.0000         0         0
        0         0         0    1.0000
  671.2340 -671.2340    0.3000   -0.4740
 -483.6070  415.8860  670.9650 -670.9650
```

The following syntax of MATLAB® function call determines that the rank of matrix $[M_{\mathrm{o}}]$ is 4

```
>> rank(Mo)
ans=
     4
```

Then, calling the function $eig(M_o)$ with the following syntax gives the eigenvalues of matrix $[M_o]$ (note that the command on the first line specifies the e-type data format for report):

```
>> format short e
>> eig(Mo)
  ans =
    -6.7211e+002
     2.2337e-001  +2.5913e+001i
     2.2337e-001  -2.5913e+001i
     9.9815e-001
```

In Chapters 4 and 5, closed-form solutions are derived for the response of smart seismic structures. With MATLAB® functions, this complicated process can be easily implemented by the following three steps.

Step 1. Build open-loop system model in state-variable representation, Equation 4.19. As noted in Section 4.1.3, this model is just a different format of the structural motion equations derived by structural dynamics. In detail, for a structure with n-d.o.f. and r active controls, the open-loop state equation is

$$\{\dot{Z}(t)\} = [A]\{Z(t)\} + [B_u]\{u(t)\} + \{B_r\}\ddot{x}_g(t) \tag{A.1}$$

where

$$\begin{aligned} \{Z(t)\} &= \begin{Bmatrix} \{x(t)\} \\ \{\dot{x}(t)\} \end{Bmatrix}, \quad \{\dot{Z}(t)\} = \begin{Bmatrix} \{\dot{x}(t)\} \\ \{\ddot{x}(t)\} \end{Bmatrix}_{2n\times 1} \\ [A] &= \begin{bmatrix} [0] & [I] \\ -[M]^{-1}[K] & -[M]^{-1}[C] \end{bmatrix}_{2n\times 2n} \\ [B_u] &= \begin{bmatrix} [0] \\ [M]^{-1}[\gamma] \end{bmatrix}_{2n\times r}, \quad \{B_r\} = \begin{Bmatrix} \{0\} \\ [M]^{-1}\{\delta\} \end{Bmatrix}_{2n\times 1} \end{aligned} \tag{A.2}$$

The structural motion equation is given by

$$[M]\{\ddot{x}(t)\} + [C]\{\dot{x}(t)\} + [K]\{x(t)\} = [\gamma]\{u(t)\} + \{\delta\}\ddot{x}_g(t) \tag{A.3}$$

The only difference is that Equation A.1 has $2n$ first-order equations while Equation A.3 has n second-order equations. Because Equations A.1 and A.3 are essentially the same, solving Equation A.1 would yield exactly the same results as Equation A.3. This step, building the open-loop model in MATLAB®, is to calculate the coefficient matrices $[A]$, $[B_u]$, and $\{B_r\}$. As shown in Equation A.2, this calculation can be easily done by entering structural dynamic properties (such as mass,

stiffness, and damping) into MATLAB® matrix/vector variables for the coefficient matrices.

Note that both structural response and control forces are unknown variables at this step. This means that Equation A.1 is not solvable as there are only $2n$ equations but $(2n + r)$ unknowns ($2n$ in state vector $\{Z(t)\}$ and r in the vector of active control force $\{u(t)\}$). Same thing for Equation A.3—there are only n equations but $(n + r)$ unknowns (n in vector $\{x(t)\}$ and r in the vector of active control force $\{u(t)\}$). Additional r equations are needed, which are the feedback control law determined in the next step.

Step 2. Determine feedback control law as per Section 4.1.4. This step is also called controller design. As shown in the following equation, the feedback law introduces r additional linear equations to the system provided that the gain matrix $[G]$ is determined.

$$\begin{aligned}\{u(t)\}_{r\times 1} &= -[G]\{Z(t)\} = -\left[[G_{\mathrm{d}}]_{r\times n}\,[G_{\mathrm{v}}]_{r\times n}\right]\begin{Bmatrix}\{x(t)\}_{n\times 1}\\ \{\dot{x}(t)\}_{n\times 1}\end{Bmatrix}\\ &= -\left([G_{\mathrm{d}}]_{r\times n}\{x(t)\}_{n\times 1} + [G_{\mathrm{v}}]_{r\times n}\{\dot{x}(t)\}_{n\times 1}\right)\end{aligned} \tag{A.4}$$

As discussed in Sections 4.2 and 4.3, gain matrix $[G]$ is determined by control algorithms. MATLAB® provides functions *ACKER* and *PLACE* for pole placement algorithm (see Section 4.2.2) and *ARE*, *CARE*, *DARE*, and *LQR* for Riccati optimal control algorithm (Section 4.2.1).

Step 3. Solve the closed-loop state equations, Equation 4.24 or Equation A.5a given below. MATLAB® has implemented a function *LSIM* for the complex solution procedure in Section 4.1.5. Substituting Equation A.4 into Equations A.1 and A.3 yields the closed-loop state equations and motion equations of the system, respectively, as

$$\{\dot{Z}(t)\} = [A_{\mathrm{c}}]\{Z(t)\} + \{B_{\mathrm{r}}\}\ddot{x}_{\mathrm{g}}(t) \tag{A.5a}$$

where

$$\begin{aligned}[A_{\mathrm{c}}] &= [A] - [B_{\mathrm{u}}][G]\\ &= \begin{bmatrix}[0] & [I]\\ -[M]^{-1}[K] & -[M]^{-1}[C]\end{bmatrix} - \begin{bmatrix}[0]\\ -[M]^{-1}[\gamma]\end{bmatrix}\begin{bmatrix}[G_{\mathrm{d}}] & [G_{\mathrm{v}}]\end{bmatrix}\\ &= \begin{bmatrix}[0] & [I]\\ -[M]^{-1}\left([K] + [\gamma][G_{\mathrm{d}}]\right) & -[M]^{-1}\left([C] + [\gamma][G_{\mathrm{v}}]\right)\end{bmatrix}\end{aligned} \tag{A.5b}$$

and

$$[M]\{\ddot{x}(t)\} + \left([C] + [\gamma][G_{\mathrm{v}}]\right)\{\dot{x}(t)\} + \left([K] + [\gamma][G_{\mathrm{d}}]\right)\{x(t)\} = \{\delta\}\ddot{x}_{\mathrm{g}}(t) \tag{A.6}$$

Now Equation A.5 is solvable as it has $2n$ first-order equations for $2n$ unknowns. It has the same results as solving the n second-order motion equations in Equation A.6. There are numerical methods (such as Runge-Kutta, Wilson-θ, and Newmark-β methods) in structural dynamics for directly solving the second-order equations in Equation A.6. They shall yield the same results as MATLAB® solution of Equation A.5, which uses a different numerical method for first-order equations. Once the state vector $\{Z(t)\}$ is determined, it can be substituted back to the feedback law (Equation A.4 to get the control forces $\{u(t)\}$. The state equation format is essential for the controller design (i.e., to determine the feedback gain matrix $[G]$) as all control algorithms are based on first-order equations.

The above steps use smart structures with active control and without considering dynamics of control devices as example. Smart structures with semiactive and hybrid control would have the same procedure. The only difference is that in Step 1, the state model shall also include dynamics of the control devices in addition to dynamics of the structure. The following section shows a MATLAB® example for a smart structure with HDABC system.

A.3 SAMPLE MATLAB® *.M* PROGRAM

A sample MATLAB® program is included below for reference. It generates closed-loop displacement response at each floor of the 6-story smart seismic structure with HDABC system. Figure 6.8 of this book is one of the plots. It is easy to read, and more information on any MATLAB® functions/statements in the program can be easily found by MATLAB® help. Statements starting with a % symbol are comments in the program.

```
%Matlab .m code for simulating the behavior of the 6-story shear building with
%       HDABC system at 1st floor under El-Centro N-S earthquake excitation.
%     It generates the displacement response plots, including Figure 6.18 of
%     the book of Smart Structures, Innovative Systems for Seismic Response
%     Control.
%
%       by Hongping Jiang, Ph.D., P.E.  August 1998 revised on 04/25/2007
%
%       Units: Mass -- tons; Force -- kN; Length -- meters.
%
%       Control Algorithms: LQG/LTR & Pole Placement
%
clear all; close all; format short e;
% Step 1 -- Input the system parameters
%Structure data
M1=109.78; M2=109.62; M3=109.24;
M4=108.86; M5=108.48; M6=107.03;             %Lumped mass (tons)
M=diag([M1,M2,M3,M4,M5,M6]);                 %Mass Matrix
K(1)=351284; K(2)=225167; K(3)=169665;
K(4)=124242; K(5)=87872;  K(6)=59532;        %Stiffness Coefficient(kN/m)
Sm = zeros(6,6);
for i=1:5
  Sm(i,i)=K(i)+K(i+1);
end
Sm(6,6)=K(6);
```

```
for i=1:5
  Sm(i,i+1)=-K(i+1);
end
for i=2:6
  Sm(i,i-1)=-K(i);
end                                          %Stiffness Matrix
W=[9.79 24.05 37.40 49.56 63.44 83.76];      %Natural Frequencies(rad/sec)
Zeta1=2/100.0;                               %Damping Ratio of first mode
alfa=Zeta1*W(1); beta=Zeta1/W(1);
for i=1:6
  for j=1:6
    Dm(i,j)=alfa*M(i,j)+beta*Sm(i,j);        %Damping Matrix
  end
end
K5=Sm(5,5); M5=M(5,5); C5=Dm(5,5);
K6=Sm(6,6); M6=M(6,6); C6=Dm(6,6);
%K-bracing parameters
Mb=2.0; Kb=2.0e5; Zetab=0.001;
Cb=2*Zetab*Mb*sqrt(Kb/Mb);
%Parameters of the hydraulic system
beta=100e3*0.454*9.81/(0.0254^2*1000);
Ps=3000*0.454*9.81/(0.0254^2*1000);
%Moog 760-102A Actuator parameters
Kv=3.85*(0.0254^3)*15/sqrt(1000*0.454*9.81/(0.0254^2*1000));
tau=1/(2*pi*35.63);
A=0.4; V=2.0; Mp=0.005; Zetap=0.002;       %Mp,Zetap are assumed
Kp=2*beta*Kv*A*sqrt(Ps/2)/V; Cp=2*Zetap*Mp*sqrt(Kp/Mp);
Mp=0; Cp=0;
%Parameters of Passive Damper
C0=20000*0.454*9.81/(1000*0.0254); lm=0.05;
% Step 2 -- Load the Excitation Data
Te=0.01; TT=10;         %el-centro: sampling rate: 100 Hz, total: 10 sec.
Ts=0.01;                %sampling time for controller
np=TT/Ts;               %total points
%t=0:Ts:(TT-Ts);
fid=fopen('elns1000.dat','r');
[xg,count]=fscanf(fid,'%f',inf);
xg=xg*9810;
xg(1001:1600)=0*xg(1:600);
tt=0:Ts:(16-Ts);
num=Te/Ts;
if(num>1)
 x0(num:num:np)=xg; clear xg;
 dx0=x0(num)/num; num1=num-1;
  for j=1:num1
    x0(j)=dx0*j;
  end
 nx1=count-1;
  for i=1:nx1
    i1=num*i; i2=num*(i+1);
    dx0=(x0(i2)-x0(i1))/num;
    for j=1:num1
      ij=i1+j; x0(ij)=x0(i1)+dx0*j;
    end
  end
 xg=x0; clear x0;
end
%Step 3 -- State variable representation
%coefficients of Actuator equation
```

```
A0=1+Mp/M1+Mp/Mb; A1=Mp*K5/M5*(Cb/Mb-C6/M6)/A0;
A2=(Mp*((K5+K6)/M5*(C6/M6-Cb/Mb)-Kb/Mb*(Cb/Mb+Cb/M5)+C6/M6*(Kb/M5+K6/M6))
+Cp*(Kb/Mb-K6/M6))/A0;
A3=(Mp*(K6*Cb/M5/Mb-K6*C6/M5/M6-K6*C6/M6^2)+Cp*K6/M6)/A0;
A4=(Mp*(Kb*Cb/M5/Mb+Kb*Cb/Mb^2-Kb*C6/M5/M6)-Cp*Kb/Mb)/A0;
A5=Mp*C5/M5*(Cb/Mb-C6/M6)/A0;
A6=(Mp*((C5+C6)/M5*(C6/M6-Cb/Mb)-Cb/Mb*(Cb/Mb+Cb/M5)+C6/M6*(Cb/M5+C6/M6)
+(Kb/Mb-K6/M6))+Cp*(Cb/Mb-C6/M6))/A0;
A7=(-2*beta*A^2/V+Cp*C6/M6+(Mp/M6+Mp/Mb)*C0/lm+Mp*K6/M6-Mp*C6^2/M6^2
-Mp*C6/M5*(C6/M6+Cb/Mb))/A0;
A8=(2*beta*A^2/V-Cp*Cb/Mb-(Mp/Mb+Mp/M6)*C0/lm-Mp*Kb/Mb+Mp*Cb^2/Mb^2
-Cb/M5*(C6/M6+Cb/Mb))/A0;
A9=(-Cp/Mb-Cp/M6+Mp*C6/M6^2-Mp*Cb/Mb^2)/A0;
A10=(-Cp/Mb-Cp/M6+(Mp/Mb+Mp/M6)/lm+Mp*C6/M6^2+Mp*Cb/Mb^2)/A0;
A11=2*beta*A*Kv*sqrt(Ps/2)/(V*A0);
%Aa,Bu,Br
MM=diag([diag(M);Mb]);
KK=[Sm [0;0;0;0;-Kb;0]; 0 0 0 0 -Kb 0 Kb];KK(5,5)=KK(5,5)+Kb;
DC=[Dm [0;0;0;0;-Cb;0]; 0 0 0 0 -Cb 0 Cb];DC(5,5)=DC(5,5)+Cb;
Aa(1:7,1:17)=[0*eye(7),eye(7),zeros(7,3)];
Aa(8:14,1:17)=[-inv(MM)*KK,-inv(MM)*DC,[zeros(5,3);1/M6,1/M6,0;-1/Mb,-1/Mb,0]];
Aa(15,1:17)=[zeros(1,3),A1,A2,A3,A4,zeros(1,3),A5,A6,A7,A8,A9,A10,A11];
Aa(16,1:17)=[zeros(1,7) zeros(1,5) -C0/lm C0/lm 0 -1/lm 0];
Aa(17,1:17)=[zeros(1,16) -1/tau];
Bu=-Aa(17,:)'; Br=[zeros(1,7) -1 -1 -1 -1 -1 -1 -1 A8 0 0]';
clear A A0 A1 A2 A3 A4 A5 A6 A7 A8 M1 M2 M3 Mb MM DC KK Kb;
% Step 4 -- Convert to digital system
[Ad,Bud]=c2d(Aa,Bu,Ts);
[Ad,Brd]=c2d(Aa,Br,Ts);
% Step 5 -- Observability
% Only one accelerometer is used at 6-th floor
Cdc=[Sm(6,1:6)/M(6,6) 0, Dm(6,1:6)/M(6,6) 0, 0 0 0;[zeros(1,14),1,0,0]];
Kob=rank(obsv(Ad,Cdc));
if Kob==size(Ad,1)
  disp('This system is observable. Program continues...');
else
  disp('This system is unobservable! Rank of observability matrix is:');
  Kob
  pause
end
% Step 6 -- Controller Design by LQG + Pole Placement algorithm
Q=eye(size(Aa)); R=1.0e-5*eye(size(Bu,2));
K=lqr(Aa,Bu,Q,R);
Po=eig(Aa-Bu*K); Pd=Po;
Pd(17)=Pd(17)*2.5;
Pd(15:16)=12.0*real(Po(15:16))+imag(Po(15:16))*sqrt(-1);
Pd(13:14)=7.0*real(Po(13:14))+imag(Po(13:14))*sqrt(-1);
Pd(11:12)=5.0*real(Po(11:12))+imag(Po(11:12))*sqrt(-1);
Pd(9:10)=2.0*real(Po(9:10))+imag(Po(9:10))*sqrt(-1);
disp('The expected closed poles are:'); Pd
KK=place(Aa,Bu,Pd); %clear Po;
disp('The poles of the designed closed loop system are:');
Ac=Aa-Bu*KK; Pc=eig(Ac)
% Step 7 -- Calculate the responses
Cc=[1 zeros(1,16)]; Dc=0;
[y1,x1]=lsim(Ac,Br,Cc,Dc,xg,tt);
% Step 8 -- Compare performances of the systems with/without observer
%   system without observer has been investigated previously
%
```

```
%  System with observer ...
%   1. Observer design
Qe=Q; Re=1e-5*eye(size(Cdc,1));
disp('The gain matrix of the observer is:');
L=lqr(Aa',Cdc',Qe,Re)'
disp('Check the poles of the observer (Designed by LQG algorithm)');
Poles_observer=eig(Aa-L*Cdc)
clear Q Qe R Re Poles_observer;
%
%   2. State variable representation
Aaug=[Aa -Bu*KK; L*Cdc Aa-Bu*KK-L*Cdc];
Baug=[Br;Br]; Caug=[Cc 0*Cc]; Daug=0;
%
%   3. Response
[y2,x2]=lsim(Aaug,Baug,Caug,Daug,xg,tt);
%
%   4. Comparison of responses
FigNum=1; figure; subplot(3,1,1); plot(tt,y1,tt,y2);
title('Figure 1  Displacement Responses to Scaled El-Centro N-S Earthquake');
ylabel('1st Floor (mm)'); %axis([0 6.0 -4.5 7.5]);
gtext('Full-State Feedback System');
gtext('Observer/Controller System');
subplot(3,1,2); plot(tt,x1(:,2),tt,x2(:,2));
ylabel('2nd Floor (mm)'); %axis([0 6.0 -5 5]);
subplot(3,1,3); plot(tt,x1(:,3),tt,x2(:,3));
%axis([0 6.0 -3 3]);
xlabel('Time(seconds)'); ylabel('3rd Floor (mm)');
FigNum=1; figure; subplot(3,1,1); plot(tt,x1(:,4),tt,x2(:,4));
title('Figure 2  Displacement Responses to Scaled El-Centro N-S Earthquake');
ylabel('4th Floor (mm)'); %axis([0 6.0 -4.5 7.5]);
subplot(3,1,2); plot(tt,x1(:,5),tt,x2(:,5));
ylabel('5th Floor (mm)');%axis([0 6.0 -5 5]);
subplot(3,1,3); plot(tt,x1(:,6),tt,x2(:,6));
%axis([0 6.0 -3 3]);
xlabel('Time(seconds)'); ylabel('6th Floor (mm)');
gtext('Full-State Feedback System');
gtext('Observer/Controller System');
```

REFERENCES

1. Moler, C., *The Origins of Matlab*. Video clips on the Internet at *The MathWorks* website http://www.mathworks.com/company/aboutus/founders/clevemoler.html, retrieved on April 15, 2007.
2. Moler, C., *Numerical Computing with MATLAB*, electronic edition on the Internet at *The MathWorks* website http://www.mathworks.com/moler, retrieved on April 15, 2007.

Appendix B: Green's Function

In the indirect boundary element method, a so-called fundamental solution is needed for an applied load acting on a continuous system. In order to determine the dynamic stiffness of the free-field system in Section 8.6.2, displacements $u_{\mathrm{pr}}(x,z)$ and $w_{\mathrm{pr}}(x,z)$, on the assumed line that subsequently forms the structure–soil interface, are needed for the applied distributed loads acting on the same line of a continuous soil system.

B.1 Displacements in k-Domain for Loads on Vertical Line

As shown in Figure B.1, the horizontal linearly distributed load $p(x,z)$, with nodal values of p_j and p_{j+1}, and the vertical linearly distributed load $r(x,z)$, with nodal vales of r_j and r_{j+1}, act on part of the vertical assumed line between node j and node $j+1$ in x- and z-directions, respectively. The procedure to determine the displacements is divided into two parts. In part I (superscript I) as shown in Figure B.2, an additional horizontal interface needs to be introduced through node j. The introduced layer j on which the distributed loads act is fixed at the interfaces. Corresponding reaction forces $P_j^{\mathrm{I}}(k)$, $P_{j+1}^{\mathrm{I}}(k)$, and $R_j^{\mathrm{I}}(k)$, $R_{j+1}^{\mathrm{I}}(k)$ in x- and z-directions are calculated to achieve this condition whereby local displacements $u_{\mathrm{pr}}^{\mathrm{I}}(k,z)$ and $w_{\mathrm{pr}}^{\mathrm{I}}(k,z)$, between the nodes, are determined. In part II (subscript II) as shown in Figure B.3, amplitudes of the reaction forces are then applied at the nodes of the total soil system with the opposite direction; displacements $u_{\mathrm{pr}}^{\mathrm{II}}(k,z)$ and $w_{\mathrm{pr}}^{\mathrm{II}}(k,z)$ along the vertical assumed line are calculated. To find global displacements $u_{\mathrm{pr}}(k,z)$ and $w_{\mathrm{pr}}(k,z)$, local displacements (part I) have to be superimposed on them (part II). Subscript pr indicates that displacements u and w in x- and z-directions are the result of both applied distributed loads p and r.

B.1.1 Fixed Layer (Part I)

For harmonic excitation with frequency ω, the dynamic equilibrium equations of loaded layer j (see Figure B.1) in Cartesian coordinates x and z can be written as

$$\sigma_{x,x}(x,z) + \tau_{xz,x}(x,z) = -\rho\omega^2 u(x,z) - p(x,z) \tag{B.1}$$

$$\tau_{zx,x}(x,z) + \sigma_{z,z}(x,z) = -\rho\omega^2 w(x,z) - r(x,z) \tag{B.2}$$

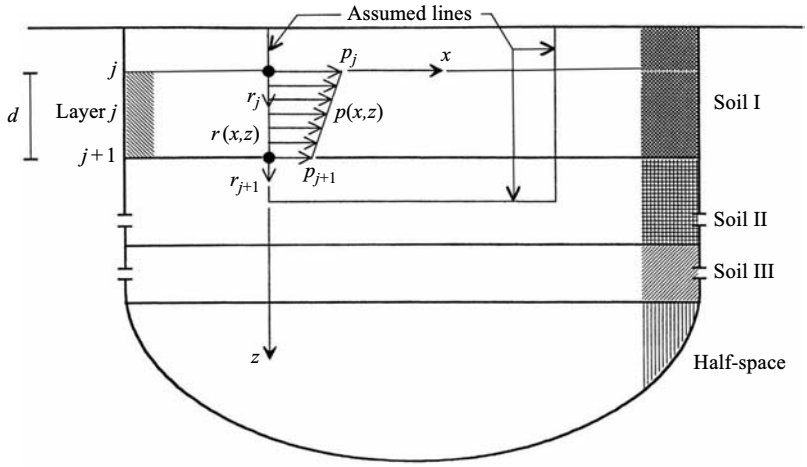

FIGURE B.1 Linearly distributed loads on vertical assumed line.

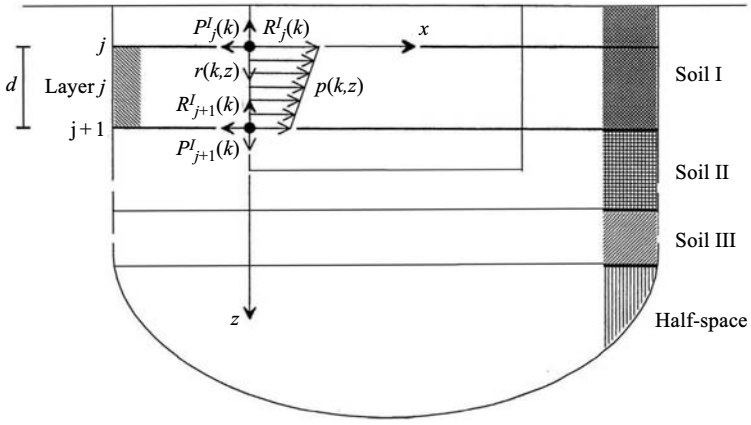

FIGURE B.2 Loaded layer with reaction forces (Part I).

Normal stress and shear stress are denoted as σ and τ, respectively. The first subscript denotes the direction of the stress component. The second one denotes the direction of the infinitesimal area's normal that the stress component acts on. A comma denotes a partial derivative with respect to the subscript following it. The letter ρ represents the mass density. Displacement amplitudes $u(x, z)$ and $w(x, z)$ are in x- and z-directions, respectively. Linearly distributed loads $p(x, z)$ and $r(x, z)$ can be expressed as

$$p(x,z) = \left[p_j + (p_{j+1} - p_j)\frac{z}{d}\right]\delta(x) \tag{B.3}$$

$$r(x,z) = \left[r_j + (r_{j+1} - r_j)\frac{z}{d}\right]\delta(x) \tag{B.4}$$

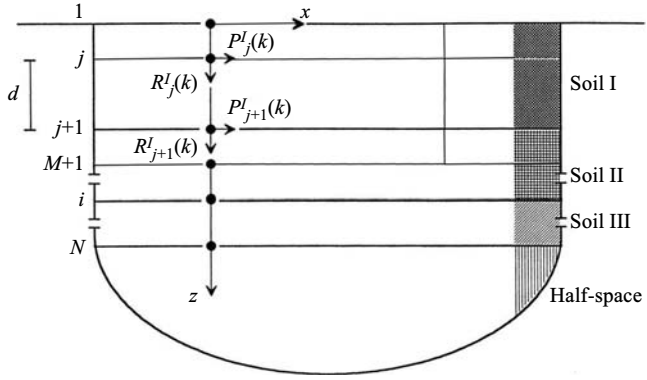

FIGURE B.3 Total soil system with external forces (Part II).

where the letter d represents the depth of the loaded layer j and δx represents the Dirac-delta function equal to 1 at $x = 0$, and 0 where $x \neq 0$. By using the stress–strain relationship (Hook's law) and strain–displacement relationship, the normal stress and shear stress amplitudes can be expressed as

$$\sigma_x(x,z) = \left[2\wp^* + \lambda^*\right] u_{,x}(x,z) + \lambda^* w_{,z}(x,z) \tag{B.5}$$

$$\sigma_z(x,z) = \left[2\wp^* + \lambda^*\right] w_{,z}(x,z) + \lambda^* u_{,x}(x,z) \tag{B.6}$$

$$\tau_{xz}(x,z) = \tau_{zx}(x,z) = \wp^* \left[u_{,z}(x,z) + w_{,z}(x,z)\right] \tag{B.7}$$

where the complex shear modulus $\wp^*$ and the complex lame constant λ^* (Equations 8.110, 8.117, and 8.113) can be expressed as the functions of Young's modulus of elasticity E, Poisson's ratio ν, and the ratio of the linear hysteretic damping ζ as follows:

$$\wp^* = \frac{(1 + 2\iota\zeta)}{2(1+\nu)}E \quad \text{and} \quad \lambda^* = \frac{\nu(1 + 2\iota\zeta)}{(1+\nu)(1-2\nu)}E \tag{B.8}$$

As discussed in Equations 8.166 through 8.169, the x–z plane displacement equations of layer can be derived and expressed as follows:

$$u(x,z) = u(k,z)\exp(-\iota kx) \tag{B.9}$$

$$w(x,z) = w(k,z)\exp(-\iota kx) \tag{B.10}$$

with

$$u(k,z) = l_x \left[A_{\mathrm{P}} \exp(\iota kfz) + B_{\mathrm{P}} \exp(-\iota kfz)\right] - m_x s \left[A_{\mathrm{SV}} \exp(\iota ksz) - B_{\mathrm{SV}} \exp(-\iota ksz)\right] \tag{B.11}$$

$$w(k,z) = -l_x f \left[A_{\mathrm{P}} \exp(\iota kfz) - B_{\mathrm{P}} \exp(-\iota kfz)\right] - m_x \left[A_{\mathrm{SV}} \exp(\iota ksz) + B_{\mathrm{SV}} \exp(-\iota ksz)\right] \tag{B.12}$$

where the notations are defined in Section 8.4.2.3 and $l_x/C_{\mathrm{P}} = m_x/C_{\mathrm{S}}$ needs to be enforced.

Substituting the stresses in Equations B.5 through B.7 and the displacements in Equations B.9 and B.10 into the dynamic-equilibrium Equations B.1 and B.2 results in

$$\left\{\wp^* u_{,zz}(k,z) - \iota k \left[\wp^* + \lambda^*\right] w_{,z}(k,z) - k^2 \left[2\wp^* + \lambda^*\right] u(k,z)\right\} \exp(-\iota kx) = -\rho\omega^2 u(k,z) \exp(-\iota kx) - p(x,z) \tag{B.13}$$

$$\left\{-k^2 \wp^* w(k,z) - \iota k \left[\wp^* + \lambda^*\right] u_{,z}(k,z) + \left[2\wp^* + \lambda^*\right] w_{,zz}(k,z)\right\} \exp(-\iota kx) = -\rho\omega^2 w(k,z) \exp(-\iota kx) - r(k,x) \tag{B.14}$$

Distributed loads $p(x,z)$ and $r(x,z)$, defined in Equations B.3 and B.4, are then expanded in the x-direction into Fourier integrals, with term $\exp(-\iota kx)$, as

$$p(k,z) = \frac{1}{2\pi} \int_{-\infty}^{\infty} p(x,z) \exp(\iota kx)\, \mathrm{d}x = \frac{1}{2\pi} \left[p_j + (p_{j+1} - p_j) \frac{z}{d}\right] \tag{B.15}$$

$$r(k,z) = \frac{1}{2\pi} \int_{-\infty}^{\infty} r(x,z) \exp(\iota kx)\, \mathrm{d}x = \frac{1}{2\pi} \left[r_j + (r_{j+1} - r_j) \frac{z}{d}\right] \tag{B.16}$$

Thus, using Equations B.13 through B.16 and omitting term $\exp(-\iota kx)$, the equilibrium equations of loaded layer, for harmonic motion in k-domain, can be written as

$$\wp^* u_{,zz}(k,z) - \iota k \left[\wp^* + \lambda^*\right] w_{,z}(k,z) - k^2 \left[2\wp^* + \lambda^*\right] u(k,z) = -\rho\omega^2 u(k,z) - \frac{1}{2\pi} \left[p_j + (p_{j+1} - p_j) \frac{z}{d}\right] \tag{B.17}$$

$$-k^2 \wp^* w(k,z) - \iota k \left[\wp^* + \lambda^*\right] u_{,z}(k,z) + \left[2\wp^* + \lambda^*\right] w_{,zz}(k,z) = -\rho\omega^2 w(k,z) - \frac{1}{2\pi} \left[r_j + (r_{j+1} - r_j) \frac{z}{d}\right] \tag{B.18}$$

By inspection, the particular solutions (superscripts P) of Equations B.17 and B.18 can be obtained and written in matrix form as

$$\begin{Bmatrix} u^{\mathrm{P}}(k,z) \\ w^{\mathrm{P}}(k,z) \end{Bmatrix} = \left[uwpr^{\mathrm{P}}(k,z) \right]_j \begin{Bmatrix} p_j \\ r_j \\ p_{j+1} \\ r_{j+1} \end{Bmatrix} \tag{B.19}$$

with

$$\left[uwpr^{\mathrm{P}}(k,z) \right]_j = \frac{1}{2\pi} \times \begin{bmatrix} -(1-z/d)\tilde{A}(k) & \tilde{B}(k) & -(z/d)\tilde{A}(k) & -\tilde{B}(k) \\ \tilde{B}(k) & -(1-z/d)\tilde{C}(k) & -\tilde{B}(k) & -(z/d)\tilde{C}(k) \end{bmatrix}. \tag{B.20}$$

where

$$\tilde{A}(k) = \frac{1}{k^2 \wp^* f^2 \tilde{D}}; \quad \tilde{B}(k) = \frac{\iota(1-1/\tilde{D})}{k^3 \wp^* \mathrm{d} f^2 s^2}; \quad \tilde{C}(k) = \frac{1}{k^2 \wp^* s^2}; \quad \tilde{D} = \frac{\mathrm{C}_{\mathrm{P}}^2}{\mathrm{C}_{\mathrm{S}}^2} \tag{B.21}$$

and the j subscription for vectors or matrices denotes that they are associated with distributed loads on and/or physical properties of layer j. At the top (node $j, z = 0$) and the bottom (node $j+1, z = d$) of loaded layer j, the particular parts of corresponding displacement can be obtained as

$$\begin{bmatrix} u_j^{\mathrm{P}}(k) & w_j^{\mathrm{P}}(k) & u_{j+1}^{\mathrm{P}}(k) & w_{j+1}^{\mathrm{P}}(k) \end{bmatrix}^{\mathrm{T}} = \left[uwpr_*^{\mathrm{P}}(k) \right]_j \begin{bmatrix} p_j & r_j & p_{j+1} & r_{j+1} \end{bmatrix}^{\mathrm{T}} \tag{B.22}$$

with

$$\left[uwpr_*^{\mathrm{P}}(k) \right]_j = \frac{1}{2\pi} \begin{bmatrix} -\tilde{A}(k) & \tilde{B}(k) & 0 & -\tilde{B}(k) \\ \tilde{B}(k) & -\tilde{C}(k) & -\tilde{B}(k) & 0 \\ 0 & \tilde{B}(k) & -\tilde{A}(k) & -\tilde{B}(k) \\ \tilde{B}(k) & 0 & -\tilde{B}(k) & -\tilde{C}(k) \end{bmatrix} \tag{B.23}$$

where the subscript * denotes that the given matrix yields nodal values. On the basis of Equations B.6, B.7, B.9, B.10, and B.19 on any z-planes (z = constant), the particular parts in k-domain of the normal stress in z-direction and of the shear

stress in x-direction can be obtained as

$$\begin{aligned}
\sigma_z^{\mathrm{P}}(k,z) &= \left[2\wp^* + \lambda^*\right] w_{,z}^{\mathrm{P}}(k,z) - \iota k \lambda^* u^{\mathrm{P}}(k,z) \\
&= \frac{\wp^*}{2\pi\, d}\Big[\iota k\tilde{A}(k)(\tilde{D}-2)(d-z) \quad -\iota k \mathrm{d}\tilde{B}(k)(\tilde{D}-2) + \tilde{C}(k)\tilde{D} \\
&\qquad \iota k\tilde{A}(k)(\tilde{D}-2)z \;\; \iota k \mathrm{d}\tilde{B}(k)(\tilde{D}-2) - \tilde{C}(k)\tilde{D}\Big] \begin{Bmatrix} p_j \\ r_j \\ p_{j+1} \\ r_{j+1} \end{Bmatrix}
\end{aligned} \tag{B.24}$$

$$\begin{aligned}
\tau_{xz}^{\mathrm{P}}(k,z) &= \wp^*\left[u_{,z}^{\mathrm{P}} - \iota k w^{\mathrm{P}}(k,z)\right] \\
&= \frac{\wp^*}{2\pi\, d}\left[\tilde{A}(k) - \iota k \mathrm{d}\tilde{B}(k) \;\; \iota\tilde{C}(k)(d-z) \;\; -\tilde{A}(k) + \iota k \mathrm{d}\tilde{B}(k) \;\; \iota k\tilde{C}(k)z\right] \begin{Bmatrix} p_j \\ r_j \\ p_{j+1} \\ r_{j+1} \end{Bmatrix}
\end{aligned} \tag{B.25}$$

The particular parts of reactions at the top and bottom of the loaded layer are defined as $P_j^{\mathrm{P}}(k) = -\tau_{xz}^{\mathrm{P}}(k,0), R_j^{\mathrm{P}}(k) = -\sigma_z^{\mathrm{P}}(k,0), P_{j+1}^{\mathrm{P}}(k) = \tau_{xz}^{\mathrm{P}}(k,d)$, and $R_{j+1}^{\mathrm{P}}(k) = \sigma_z^{\mathrm{P}}(k,d)$. By using Equations B.24 and B.25, they can be obtained in matrix form as

$$\begin{Bmatrix} P_j^{\mathrm{P}}(k) \\ R_j^{\mathrm{P}}(k) \\ P_{j+1}^{\mathrm{P}}(k) \\ R_{j+1}^{\mathrm{P}}(k) \end{Bmatrix} = \left[PRpr_*^{\mathrm{P}}(k)\right]_j \begin{Bmatrix} p_j \\ r_j \\ p_{j+1} \\ r_{j+1} \end{Bmatrix} \tag{B.26}$$

with

$$\left[PRpr_*^{\mathrm{P}}(k)\right]_j = \frac{\wp^*}{2\pi\,\mathrm{d}} \begin{bmatrix} \left[PRpr_{(1,1)}^{\mathrm{P}}\right] & \left[PRpr_{(1,2)}^{\mathrm{P}}\right] \\ \left[PRpr_{(2,1)}^{\mathrm{P}}\right] & \left[PRpr_{(2,2)}^{\mathrm{P}}\right] \end{bmatrix} \tag{B.27}$$

where

$$\left[PRpr_{(1,1)}^{\mathrm{P}}\right] = \begin{bmatrix} -\tilde{A}(k) + \iota k \mathrm{d}\tilde{B}(k) & -\iota k \mathrm{d}\tilde{C}(k) \\ -\iota k \mathrm{d}\tilde{A}(k)(\tilde{D}-2) & \iota k \mathrm{d}\tilde{B}(k)(\tilde{D}-2) - \tilde{C}(k)\tilde{D} \end{bmatrix} \tag{B.28}$$

$$\left[PRpr_{(1,2)}^{\mathrm{P}}\right] = \left[PRpr_{(2,1)}^{\mathrm{P}}\right] = \begin{bmatrix} \tilde{A}(k) - \iota k \mathrm{d}\tilde{B}(k) & 0 \\ 0 & -\iota k \mathrm{d}\tilde{B}(k)(\tilde{D}-2) + \tilde{C}(k)\tilde{D} \end{bmatrix} \tag{B.29}$$

$$\left[PRpr^{\mathrm{P}}_{(1,1)}\right] = \begin{bmatrix} -\tilde{A}(k) + \iota k \mathrm{d}\tilde{B}(k) & \iota k \mathrm{d}\tilde{C}(k) \\ \iota k \mathrm{d}\tilde{A}(k)(\tilde{D}-2) & \iota k \mathrm{d}\tilde{B}(k)(\tilde{D}-2) - \tilde{C}(k)\tilde{D} \end{bmatrix} \tag{B.30}$$

To complete the first part of the procedure, the homogeneous parts (superscript H) of the displacements and reactions will be determined and superimposed on the particular ones. Boundary conditions at node j and $j+1$ of the homogeneous equation of Equations B.11 and B.12 must be equal to negative values $u^{\mathrm{P}}_j(k), w^{\mathrm{P}}_j(k), u^{\mathrm{P}}_{j+1}(k)$, and $w^{\mathrm{P}}_{j+1}(k)$ in order to fix those two interfaces of the loaded layer. The homogenous equation of Equations B.11 and B.12 can be rewritten into matrix form in terms of the unknowns $A_{\mathrm{P}}, B_{\mathrm{P}}, A_{\mathrm{SV}}$, and B_{SV} as

$$\begin{Bmatrix} u(k,z) \\ w(k,z) \end{Bmatrix}_j = [uwAB(k,z)]_j \begin{Bmatrix} A_{\mathrm{P}} \\ B_{\mathrm{P}} \\ A_{\mathrm{SV}} \\ B_{\mathrm{SV}} \end{Bmatrix} \tag{B.31}$$

with

$$[uwAB(k,z)]_j = \begin{bmatrix} l_x \exp(\iota kfz) & l_x \exp(-\iota kfz) & -m_x s \exp(\iota ksz) & m_x s \exp(\iota ksz) \\ -l_x f \exp(\iota kfz) & l_x f \exp(-\iota kfz) & -m_x \exp(\iota ksz) & -m_x \exp(-\iota ksz) \end{bmatrix} \tag{B.32}$$

By using Equation B.31, the unknowns $A_{\mathrm{P}}, B_{\mathrm{P}}, A_{\mathrm{SV}}$, and B_{SV} can be expressed in terms of four boundary conditions at the top and bottom of the layer as

$$\begin{Bmatrix} A_{\mathrm{P}} \\ B_{\mathrm{P}} \\ A_{\mathrm{SV}} \\ B_{\mathrm{SV}} \end{Bmatrix}_j = [uwAB_*(k)]^{-1}_j \begin{Bmatrix} u_j(k) \\ w_j(k) \\ u_{j+1}(k) \\ w_{j+1}(k) \end{Bmatrix} \tag{B.33}$$

with

$$[uwAB_*(k)]_j = \begin{bmatrix} \left[uwAB_{(1,1)}\right] & \left[uwAB_{(1,2)}\right] \\ \left[uwAB_{(2,1)}\right] & \left[uwAB_{(2,2)}\right] \end{bmatrix} \tag{B.34}$$

where

$$\left[uwAB_{(1,1)}\right] = l_x \begin{bmatrix} 1 & 1 \\ -f & f \end{bmatrix} \tag{B.35}$$

$$\left[uwAB_{(1,2)}\right] = m_x \begin{bmatrix} -s & s \\ -1 & -1 \end{bmatrix} \tag{B.36}$$

$$\left[uwAB_{(2,1)}\right] = l_x \begin{bmatrix} \exp(\iota kfd) & \exp(-\iota kfd) \\ -f\exp(\iota kfd) & f\exp(-\iota kfd) \end{bmatrix} \tag{B.37}$$

$$\left[uwAB_{(2,2)}\right] = m_x \begin{bmatrix} -s\exp(\iota ksd) & s\exp(-\iota ksd) \\ -\exp(\iota ksd) & -\exp(-\iota ksd) \end{bmatrix} \tag{B.38}$$

Knowing the boundary conditions and then using Equations B.22, B.31, and B.33, the homogeneous parts of the displacements can be obtained as

$$\begin{Bmatrix} u^{\mathrm{H}}(k,z) \\ w^{\mathrm{H}}(k,z) \end{Bmatrix}_j = \left[uwpr^{\mathrm{H}}(k,z)\right]_j \begin{Bmatrix} p_j \\ r_j \\ p_{j+1} \\ r_{j+1} \end{Bmatrix} \tag{B.39}$$

with

$$\left[uwpr^{\mathrm{H}}(k,z)\right]_j = -\left[uwAB(k,z)\right]_j \left[uwAB_*(k)\right]_j^{-1} \left[uwpr_*^{\mathrm{P}}(k)\right]_j \tag{B.40}$$

Local displacements (part I) are the summation of the particular parts in Equation B.19 and the homogenous parts in Equation B.39, which can be expressed as

$$\begin{Bmatrix} u_{\mathrm{pr}}^{\mathrm{I}}(k,z) \\ w_{\mathrm{pr}}^{\mathrm{I}}(k,z) \end{Bmatrix}_j = \left[uwpr^{\mathrm{I}}(k,z)\right]_j \begin{Bmatrix} p_j \\ r_j \\ p_{j+1} \\ r_{j+1} \end{Bmatrix} \tag{B.41}$$

with

$$\begin{aligned} \left[uwpr^{\mathrm{I}}(k,z)\right]_j &= \left[uwpr^{\mathrm{P}}(k,z)\right]_j + \left[uwpr^{\mathrm{H}}(k,z)\right] \\ &= \left[uwpr^{\mathrm{P}}(k,z)\right]_j - \left[uwAB(k,z)\right]_j \left[uwAB_*(k)\right]_j^{-1} \left[uwpr_*^{\mathrm{P}}(k)\right]_j \end{aligned} \tag{B.42}$$

Homogenous parts of the reaction forces can be determined by using the dynamic stiffness of the horizontal layer in k-domain. As shown in Equation 8.190, external forces and nodal displacements of layer j are related to its stiffness matrix as

$$\begin{Bmatrix} P_j(k) \\ R_j(k) \\ P_{j+1}(k) \\ R_{j+1}(k) \end{Bmatrix} = \left[S_{\mathrm{P-SV}}^{\mathrm{L}}(k)\right]_j \begin{Bmatrix} u_j(k) \\ w_j(k) \\ u_{j+1}(k) \\ w_{j+1}(k) \end{Bmatrix} \tag{B.43}$$

By substituting negative values of the particular parts of the nodal displacements into Equation B.43, homogeneous parts of the reactions can be obtained as

$$\begin{Bmatrix} P_j^{\mathrm{H}}(k) \\ R_j^{\mathrm{H}}(k) \\ P_{j+1}^{\mathrm{H}}(k) \\ R_{j+1}^{\mathrm{H}}(k) \end{Bmatrix} = \left[PRpr_*^{\mathrm{H}}(k) \right]_j \begin{Bmatrix} p_j \\ r_j \\ p_{j+1} \\ r_{j+1} \end{Bmatrix} \tag{B.44}$$

with

$$\left[PRpr_*^{\mathrm{H}}(k) \right]_j = - \left[S_{\mathrm{P-SV}}^{\mathrm{L}}(k) \right]_j \left[uwpr_*^{\mathrm{P}}(k) \right]_j \tag{B.45}$$

For loaded layer j, the reaction forces (see Figure B.2) to counterbalance the linearly distributed loads and fix the interfaces can be obtained by combining Equations B.26 and B.44 as

$$\begin{Bmatrix} P_j^{\mathrm{I}}(k) \\ R_j^{\mathrm{I}}(k) \\ P_{j+1}^{\mathrm{I}}(k) \\ R_{j+1}^{\mathrm{I}}(k) \end{Bmatrix} = \left[PRpr_*^{\mathrm{I}}(k) \right]_j \begin{Bmatrix} p_j \\ r_j \\ p_{j+1} \\ r_{j+1} \end{Bmatrix} \tag{B.46}$$

with

$$\begin{aligned} \left[PRpr_*^{\mathrm{I}}(k) \right]_j &= \left[PRpr_*^{\mathrm{P}}(k) \right]_j + \left[PRpr_*^{\mathrm{H}}(k) \right]_j \\ &= \left[PRpr_*^{\mathrm{P}}(k) \right]_j - \left[S_{\mathrm{P-SV}}^{\mathrm{L}}(k) \right]_j \left[uwpr_*^{\mathrm{P}}(k) \right]_j \end{aligned} \tag{B.47}$$

B.1.2 Free Layer (Part II)

The dynamic stiffness matrix $\left[S_{\mathrm{P-SV}}^{\mathrm{T}}(k) \right]$ of the total soil system that consists of $N-1$ layers and a half-space (see Figure B.4) is first assembled by using the direct stiffness approach. In the assembling process, the stiffness matrices of two adjacent layers and half-space are overlapped on the matrix's elements corresponding to the same side. Superscript T stands for the total soil system. In Equations 8.190 and 8.215, the dynamic-stiffness matrices $\left[S_{\mathrm{P-SV}}^{\mathrm{L}}(k) \right]_i$ of any horizontal layer i, for $i = 1, 2, \ldots . N-1$, relate displacement amplitudes u and w at node i and node $i+1$ to load amplitudes P and R at the same nodes. The force–displacement relationship of the half-space can be obtained by dynamic stiffness matrices $\left[S_{\mathrm{P-SV}}^{\mathrm{R}}(k) \right]$ in

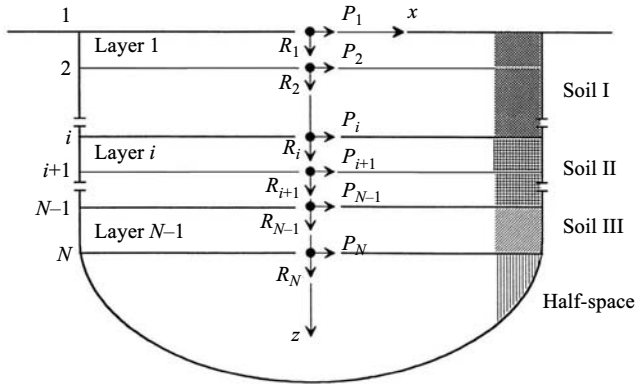

FIGURE B.4 Total soil system in k-domain.

Equations 8.228, 8.236, and 8.244. Both relationships can be expressed as follows:

$$\begin{Bmatrix} P_i(k) \\ R_i(k) \\ P_{i+1}(k) \\ R_{i+1}(k) \end{Bmatrix} = \left[S^{\mathrm{L}}_{\mathrm{P-SV}}(k)\right]_i \begin{Bmatrix} u_i(k) \\ w_i(k) \\ u_{i+1}(k) \\ w_{i+1}(k) \end{Bmatrix} \tag{B.48}$$

$$\begin{Bmatrix} P_0(k) \\ R_0(k) \end{Bmatrix} = \left[S^{\mathrm{L}}_{\mathrm{P-SV}}(k)\right]_i \begin{Bmatrix} u_0(k) \\ w_0(k) \end{Bmatrix} \tag{B.49}$$

As shown in Equations B.9 and B.10, the variation of displacement amplitudes $u(x,z)$ and $w(x,z)$ in the x-direction is determined by wave number k and is thus constant with depth for the layer. Boundary conditions at the interface of the two adjacent layers and half-space force the value of k to be constant for the total soil system. For a given frequency ω, phase velocity C has to be constant $\left(C = \omega/k\right)$ for all layers and half-space. After determining $\left[S^{\mathrm{L}}_{\mathrm{P-SV}}(k)\right]_i$ and $\left[S^{R}_{\mathrm{P-SV}}(k)\right]$ by taking this into consideration, the total dynamic-stiffness matrix in k-domain $\left[S^{\mathrm{T}}_{\mathrm{P-SV}}(k)\right]$ can be assembled and expressed as

$$\begin{aligned} &\begin{bmatrix} P_1(k) & R_1(k) & \cdots & P_i(k) & R_i(k) & \cdots & P_{\mathrm{N}}(k) & R_{\mathrm{N}}(k) \end{bmatrix}^{\mathrm{T}} \\ &= \left[S^{\mathrm{T}}_{\mathrm{P-SV}}(k)\right] \begin{bmatrix} u_1(k) & w_1(k) & \cdots & u_i(k) & w_i(k) & \cdots & u_{\mathrm{N}}(k) & w_{\mathrm{N}}(k) \end{bmatrix}^{\mathrm{T}} \end{aligned} \tag{B.50}$$

For the distributed loads acting on the vertical assumed line of any layer j between node j and node $j+1$, reactions at the corresponding nodes were determined in part I as shown in Equation B.46. Applying these forces in the opposite direction at the same nodes to the total soil system (see Figure B.3), nodal displacements at any node i and node $i+1$ can be calculated. Using Equations B.46

and B.50, they can be expressed as

$$\begin{Bmatrix} u_i^{\mathrm{II}}(k) \\ w_i^{\mathrm{II}}(k) \\ u_{i+1}^{\mathrm{II}}(k) \\ w_{i+1}^{\mathrm{II}}(k) \end{Bmatrix} = \left[uwpr_*^{\mathrm{II}}(k) \right]_j^i \begin{Bmatrix} p_j \\ r_j \\ p_{j+1} \\ r_{j+1} \end{Bmatrix} \tag{B.51}$$

with

$$\begin{aligned} \left[uwpr_*^{\mathrm{II}}(k) \right]_j^i &= -SUB_{ij} \left(\left[S_{\mathrm{P-SV}}^{\mathrm{T}}(k) \right]^{-1} \right) \left[PRpr_*^{\mathrm{I}}(k) \right]_j \\ &= -SUB_{ij} \left[S_{\mathrm{P-SV}}^{\mathrm{T}}(k) \right]^{-1} \left(\left[PRpr_*^{\mathrm{P}}(k) \right]_j - \left[S_{\mathrm{P-SV}}^{\mathrm{L}}(k) \right]_j \left[uwpr_*^{\mathrm{P}}(k) \right]_j \right) \end{aligned} \tag{B.52}$$

where $SUB_{ij} \left(\left[S_{\mathrm{P-SV}}^{\mathrm{T}}(k) \right]^{-1} \right)$ is the submatrix of dimension 4 by 4, comprising the coefficients in the matrix $\left[S_{\mathrm{P-SV}}^{\mathrm{T}}(k) \right]^{-1}$ from row $4i-3$th to row $4i$th and column $4j$–3th to column $4j$th and $\left[PRpr_*^{\mathrm{I}}(k) \right]_j$ is shown in Equation B.47. The i superscription for vectors or matrices indicates that they are associated with layer i's displacements.

Displacements $u_{\mathrm{pr}}^{\mathrm{II}}(k,z)$ and $w_{\mathrm{pr}}^{\mathrm{II}}(k,z)$ between node i and $i+1$ are determined by using nodal displacements in Equation B.51 as the boundary conditions of homogeneous equation of Equations B.11 and B.12. Using Equations B.31, B.33, and B.51, the displacement vector in part II can be obtained as

$$\begin{Bmatrix} u_{\mathrm{pr}}^{\mathrm{II}}(k) \\ w_{\mathrm{pr}}^{\mathrm{II}}(k) \end{Bmatrix}_j^i = \left[uw_{\mathrm{pr}}^{\mathrm{II}}(k,z) \right]_j^i \begin{Bmatrix} p_j \\ r_j \\ p_{j+1} \\ r_{j+1} \end{Bmatrix} \tag{B.53}$$

with

$$\begin{aligned} \left[uwpr^{\mathrm{II}}(k,z) \right]_j^i &= \left[uwAB(k,z) \right]_i \left[uwAB_*(k) \right]_i^{-1} \left[uwpr_*^{\mathrm{II}}(k) \right]_j^i \\ &= -\left[uwAB(k,z) \right]_i \left[uwAB_*(k) \right]_i^{-1} SUB_{ij} \left(\left[S_{\mathrm{P-SV}}^{\mathrm{T}}(k) \right]^{-1} \right) \\ &\quad \times \left(\left[PRpr_*^{\mathrm{P}}(k) \right]_j - \left[S_{\mathrm{P-SV}}^{\mathrm{L}}(k) \right]_j \left[uwpr_*^{\mathrm{P}}(k) \right]_j \right) \end{aligned} \tag{B.54}$$

B.1.3 Global Displacements

Along the vertical line in any layer i, for $i = 1, 2, \ldots, M$, where M = number of layers along the vertical assumed line, on which no distributed loads act

$(i \neq j)$; global displacements $u_{\mathrm{pr}}(k,z)$ and $w_{\mathrm{pr}}(k,z)$ are equal to the displacements determined in part II (Equation B.53) and can be written as

$$\begin{Bmatrix} u_{\mathrm{pr}}(k,z) \\ w_{\mathrm{pr}}(k,z) \end{Bmatrix}_j^{i,\,i\neq j} = \begin{Bmatrix} u_{\mathrm{pr}}^{\mathrm{II}}(k,z) \\ w_{\mathrm{pr}}^{\mathrm{II}}(k,z) \end{Bmatrix}_j^{i} = [uwpr(k,z)]_j^{i,\,i\neq j} \begin{Bmatrix} p_j \\ r_j \\ p_{j+1} \\ r_{j+1} \end{Bmatrix} \tag{B.55}$$

with

$$[uwpr(k,z)]_j^{i,\,i\neq j} = -\,[uwAB(k,z)]_i\;[uwAB_*(k)]_i^{-1}\,SUB_{ij}\left(\left[S_{\mathrm{P-SV}}^{\mathrm{T}}(k)\right]^{-1}\right) \times \left(\left[PRpr_*^{\mathrm{P}}(k)\right]_j - \left[S_{\mathrm{P-SV}}^{\mathrm{L}}(k)\right]_j \left[uwpr_*^{\mathrm{P}}(k)\right]_j\right) \tag{B.56}$$

Along the vertical line in any layer i on which the distributed loads act $(i = j)$, global displacements $u_{\mathrm{pr}}(k,z)$ and $w_{\mathrm{pr}}(k,z)$ are the combination of displacements contained in part I (Equation B.41) and part II (Equation B.53), and can be expressed as

$$\begin{Bmatrix} u_{\mathrm{pr}}(k,z) \\ w_{\mathrm{pr}}(k,z) \end{Bmatrix}_j^{i,i=j} = \begin{Bmatrix} u_{\mathrm{pr}}^{\mathrm{I}}(k,z) \\ w_{\mathrm{pr}}^{\mathrm{I}}(k,z) \end{Bmatrix}_j^{+} \begin{Bmatrix} u_{\mathrm{pr}}^{\mathrm{II}}(k,z) \\ w_{\mathrm{pr}}^{\mathrm{II}}(k,z) \end{Bmatrix}_j^{i} = [uwpr(k,z)]_j^{i,i=j} \begin{Bmatrix} p_j \\ r_j \\ p_{j+1} \\ r_{j+1} \end{Bmatrix} \tag{B.57}$$

with

$$\left[uwpr(k,z)\right]_j^{i,i=j} = \left[uwpr^{\mathrm{P}}(k,z)\right]_j - \left[uwAB(k,z)\right]_j \left[uwAB_*(k)\right]_j^{-1} \left[uwpr_*^{\mathrm{P}}(k)\right]_j - \left[uwAB(k,z)\right]_i \left[uwAB_*(k)\right]_i^{-1} SUB_{ij} \left(\left[S_{\mathrm{P-SV}}^{\mathrm{T}}(k)\right]^{-1}\right) \times \left(\left[PRpr_*^{\mathrm{P}}(k)\right]_j - \left[S_{\mathrm{P-SV}}^{\mathrm{L}}(k)\right]_j \left[uwpr_*^{\mathrm{P}}(k)\right]_j\right) \tag{B.58}$$

B.2 Displacements in *k*-Domain for Loads on Horizontal Line

As shown in Figure B.5, the horizontal linearly distributed load $p(x)$, with nodal values of p_l and p_{l+1} in x-direction, and the vertical linearly distributed load $r(x)$, with nodal values r_l and r_{l+1} in z-direction, act on part of the horizontal assumed

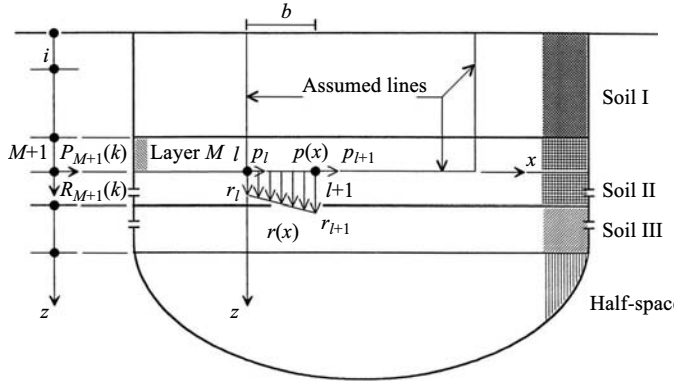

FIGURE B.5 Linearly distributed loads on horizontal assumed line.

line between node l and node $l + 1$, which lies underneath layer M. Since the distributed loads act on the horizontal interfaces, not between the interfaces, the first part of the procedure mentioned in the previous subsection is not required.

Linearly distributed loads $p(x)$ and $r(x)$ can be expressed in matrix form as

$$\begin{Bmatrix} p(x) \\ r(x) \end{Bmatrix} = \begin{bmatrix} (1-x/b) & 0 & x/b & 0 \\ 0 & (1-x/b) & 0 & x/b \end{bmatrix} \begin{Bmatrix} p_l \\ r_l \\ p_{l+1} \\ r_{l+1} \end{Bmatrix} \tag{B.59}$$

where the letter b is the length between node l and node $l+1$. Then the distributed loads are expanded in the x-direction into Fourier integrals, with term $\exp(-\iota kx)$

$$\begin{Bmatrix} P_{M+1}(k) \\ R_{M+1}(k) \end{Bmatrix} = \frac{1}{2\pi} \int_0^{\mathrm{b}} \begin{Bmatrix} p(x) \\ r(x) \end{Bmatrix} \exp(\iota kx)\,\mathrm{d}x = [PRpr_*(k)]_{M,l} \begin{Bmatrix} p_l \\ r_l \\ p_{l+1} \\ r_{l+1} \end{Bmatrix} \tag{B.60}$$

with

$$[PRpr_*(k)]_{M,l} = \frac{1}{2\pi} \begin{bmatrix} Pp_l & 0 & Pp_{l+1} & 0 \\ 0 & Rr_l & 0 & Rr_{l+1} \end{bmatrix} \tag{B.61}$$

where

$$Pp_l = Rr_l = \frac{\iota}{k}\Big[1 - \exp(\iota kb)\Big] - \frac{1}{k^2 b}\Big[\exp(\iota kb)(1 - \iota kb) - 1\Big] \tag{B.62}$$

$$Pp_{l+1} = Rr_{l+1} = \frac{1}{k^2 b}\Big[\exp(\iota kb)(1 - \iota kb) - 1\Big] \tag{B.63}$$

The M, l subscription for the vectors and matrices denotes that they are associated with distributed loads on the horizontal element between node l and $l+1$, which are on the horizontal interface underneath layer M.

These external loads are then applied to the total soil system at node $M+1$ corresponding to the horizontal assumed line (see Figure B.5). By using the total dynamic-stiffness matrix $\left[S^{\mathrm{T}}_{\mathrm{P-SV}}(k)\right]$ mentioned in Equation B.50 and the external loads in Equation B.60, nodal displacements at any node i and $i+1$ on vertical line can be obtained as

$$\begin{Bmatrix} u_i(k) \\ w_i(k) \\ u_{i+1}(k) \\ w_{i+1}(k) \end{Bmatrix}_{M,l} = [uwpr_*(k)]^i_{M,l} \begin{Bmatrix} p_l \\ r_l \\ p_{l+1} \\ r_{l+1} \end{Bmatrix} \tag{B.64}$$

with

$$\left[uwpr_*(k)\right]^i_{M,l} = \mathrm{sub}_{iM}\left(\left[S^{\mathrm{T}}_{\mathrm{P-SV}}(k)\right]^{-1}\right)\left[PRpr_*(k)\right]_{M,l} \tag{B.65}$$

where $\mathrm{sub}_{iM}\left(\left[S^{\mathrm{T}}_{\mathrm{P-SV}}(k)\right]^{-1}\right)$ is the submatrix of dimension 4 by 2. This dimension comprises elements in the matrix $\left[S^{\mathrm{T}}_{\mathrm{P-SV}}(k)\right]^{-1}$ from row $4i-3$th to row $4i$th and column $4M-1$th to column $4M$th. $[PRpr_*(k)]$ can be obtained from Equation B.61. The i superscription for vectors or matrices indicates that they are associated with layer i's displacements.

Analogous to part II of displacements for loads on the vertical assumed line in the previous subsection, displacements $u_{\mathrm{pr}}(k,z)$ and $w_{\mathrm{pr}}(k,z)$ between node i and node $i+1$ are calculated by using nodal displacements in Equation B.64 as boundary conditions of displacements in Equations B.11 and B.12. Using Equations B.31, B.33, and B.34, the displacement vector can be obtained as

$$\begin{Bmatrix} u_{\mathrm{pr}}(k,z) \\ w_{\mathrm{pr}}(k,z) \end{Bmatrix}^i_{M,l} = \left[uwpr(k,z)\right]^i_{M,l} \begin{Bmatrix} p_l \\ r_l \\ p_{l+1} \\ r_{l+1} \end{Bmatrix} \tag{B.66}$$

with

$$\begin{aligned} &\left[uwpr(k)\right]^i_{M,l} \\ &\quad = \left[uwAB(k,z)\right]_i \left[uwAB(k,z)\right]^{-1}_{\mathrm{i}} \left[uwpr_*(k)\right]^i_{M,l} \\ &\quad = \left[uwAB(k,z)\right]_i \left[uwAB_*(k,z)\right]^{-1}_{\mathrm{i}} \mathrm{sub}_{\mathrm{iM}}\left(\left[S^{\mathrm{T}}_{\mathrm{P-SV}}(k)\right]^{-1}\right) \left[PRpr_*(k)\right]_{M,l} \end{aligned} \tag{B.67}$$

B.3 Displacement for Vertical Incident Wave

B.3.1 Loads on Vertical Line

A procedure is analogous to Section B.1. For the vertically incident waves that correspond to a zero wave number k, displacement equations (see Equations 8.170 and 8.171) can be expressed as

$$u(x,z)^{k=0} = -A_{\mathrm{SV}} \exp\left(\frac{\iota\omega}{C_{\mathrm{S}}} z\right) + B_{\mathrm{SV}} \exp\left(-\frac{\iota\omega}{C_{\mathrm{S}}} z\right) \tag{B.68}$$

$$w(x,z)^{k=0} = -A_{\mathrm{P}} \exp\left(\frac{\iota\omega}{C_{\mathrm{P}}} z\right) + B_{\mathrm{P}} \exp\left(-\frac{\iota\omega}{C_{\mathrm{P}}} z\right) \tag{B.69}$$

Using stress formulation in Equations B.6 and B.7 and displacement formulation of Equations B.68 and B.69, the dynamic-equilibrium formulation of Equations B.1 and B.2 for loaded layer j can be reformulated as

$$\wp^* u_{,zz}(z) = -\rho\omega^2 u(z) - \frac{1}{2\pi}\left[p_j + \left(p_{j+1} - p_j\right)\frac{z}{d}\right] \tag{B.70}$$

$$\left[2\wp^* + \lambda^*\right] w_{,zz}(z) = -\rho\omega^2 w(z) - \frac{1}{2\pi}\left[r_j + \left(r_{j+1} - r_j\right)\frac{z}{d}\right] \tag{B.71}$$

Displacements in Equations B.70 and B.71 are uncoupled. By inspection, the particular solutions of these equations can be obtained in matrix form as

$$\begin{Bmatrix} u^{\mathrm{P}}(z) \\ w^{\mathrm{P}}(z) \end{Bmatrix}_j = \left[uwpr^{\mathrm{P}}(z)\right]_j^{k=0} \begin{Bmatrix} p_j \\ r_j \\ p_{j+1} \\ r_{j+1} \end{Bmatrix} \tag{B.72}$$

with

$$\left[uwpr^{\mathrm{P}}(z)\right]_j^{k=0} = \frac{-C_{\mathrm{S}}^2}{2\pi\omega^2\wp^*} \begin{bmatrix} 1 - z/d & 0 & z/d & 0 \\ 0 & 1 - z/d & 0 & z/d \end{bmatrix} \tag{B.73}$$

At the top (node $j, z = 0$) and bottom (node $j + 1, z = d$) of the loaded layer, the particular parts of corresponding displacement can be obtained as

$$\begin{Bmatrix} u_j^{\mathrm{P}} \\ w_j^{\mathrm{P}} \\ u_{j+1}^{\mathrm{P}} \\ w_{j+1}^{\mathrm{P}} \end{Bmatrix} = \left[uwpr_*^{\mathrm{P}}\right]_j^{k=0} \begin{Bmatrix} p_j \\ r_j \\ p_{j+1} \\ r_{j+1} \end{Bmatrix} \tag{B.74}$$

with

$$\left[uwpr_*^{\mathrm{P}}\right]_j^{k=0} = \frac{-C_{\mathrm{S}}^2}{2\pi\omega^2\wp^*}\begin{bmatrix}1 & 0 & 0 & 0\\ 0 & 1 & 0 & 0\\ 0 & 0 & 1 & 0\\ 0 & 0 & 0 & 1\end{bmatrix} \tag{B.75}$$

Based on Equations B.6, B.7, and B.72, on any z-planes (z = constant) the particular parts of the normal stress in z-direction and the shear stress on x-direction can be obtained as

$$\sigma_z^{\mathrm{P}}(z) = \left[2\wp^* + \lambda^*\right] w_{,z}^{\mathrm{P}}(z) = \frac{C_{\mathrm{P}}^2}{2\pi\omega^2 d}\left(r_j - r_{j+1}\right) \tag{B.76}$$

$$\tau_{xz}^{\mathrm{P}}(z) = \wp^* u_{,z}^{\mathrm{P}}(z) = \frac{C_{\mathrm{P}}^2}{2\pi\omega^2 d}\left(p_j - p_{j+1}\right) \tag{B.77}$$

By using Equations B.76 and B.77, the particular parts of reactions at the top and bottom of the loaded layer can be obtained in matrix form as

$$\begin{Bmatrix} P_j^{\mathrm{P}} \\ R_j^{\mathrm{P}} \\ P_{j+1}^{\mathrm{P}} \\ R_{j+1}^{\mathrm{P}} \end{Bmatrix} = \left[PRpr_*^{\mathrm{P}}\right]_j^{k=0} \begin{Bmatrix} p_j \\ r_j \\ p_{j+1} \\ r_{j+1} \end{Bmatrix} \tag{B.78}$$

with

$$\left[PRpr_*^{\mathrm{P}}\right]_j^{k=0} = \frac{1}{2\pi\omega^2 d}\begin{bmatrix} -C_{\mathrm{S}}^2 & 0 & C_{\mathrm{S}}^2 & 0 \\ 0 & -C_{\mathrm{P}}^2 & 0 & C_{\mathrm{P}}^2 \\ C_{\mathrm{S}}^2 & 0 & -C_{\mathrm{S}}^2 & 0 \\ 0 & C_{\mathrm{P}}^2 & 0 & -C_{\mathrm{P}}^2 \end{bmatrix} \tag{B.79}$$

Homogeneous equation of Equations B.68 and B.69 can be rewritten in matrix form in terms of the unknowns $A_{\mathrm{P}}, B_{\mathrm{P}}, A_{\mathrm{SV}}$, and B_{SV} as

$$\begin{Bmatrix} u(z) \\ w(z) \end{Bmatrix}_j = \left[uwAB(z)\right]_j^{k=0} \begin{Bmatrix} A_{\mathrm{P}} \\ B_{\mathrm{P}} \\ A_{\mathrm{SV}} \\ B_{\mathrm{SV}} \end{Bmatrix} \tag{B.80}$$

with

$$\left[uwAB(z)\right]_j^{k=0} = \begin{bmatrix} 0 & 0 & -\exp(\iota\omega z/C_S) & \exp(-\iota\omega z/C_S) \\ -\exp(\iota\omega z/C_P) & \exp(-\iota\omega z/C_P) & 0 & 0 \end{bmatrix} \tag{B.81}$$

By using Equation B.80, the unknowns A_P, B_P, A_{SV}, and B_{SV} can be expressed in terms of four boundary conditions at the top and bottom of the layer as

$$\begin{Bmatrix} A_P \\ B_P \\ A_{SV} \\ B_{SV} \end{Bmatrix}_j = \left[\left[uwAB(z)\right]_j^{k=0}\right]^{-1} \begin{Bmatrix} u_j \\ w_j \\ u_{j+1} \\ w_{j+1} \end{Bmatrix} \tag{B.82}$$

with

$$[uwAB_*]_j^{k=0} = \begin{bmatrix} 0 & 0 & -1 & 1 \\ -1 & 1 & 0 & 0 \\ 0 & 0 & -\exp(\iota\omega d/C_S) & \exp(-\iota\omega d/C_S) \\ -\exp(\iota\omega d/C_P) & \exp(-\iota\omega d/C_P) & 0 & 0 \end{bmatrix} \tag{B.83}$$

Knowing the boundary conditions that equal the negative values of $u_j^P(k)$, $w_j^P(k)$, $u_{j+1}^P(k)$, and $w_{j+1}^P(k)$ and then using Equations B.74, B.80, and B.82, the homogeneous parts of the displacements can be obtained as

$$\begin{Bmatrix} u^H(z) \\ w^H(z) \end{Bmatrix} = \left[uwpr^H(z)\right]_j^{k=0} \begin{Bmatrix} p_j \\ r_j \\ p_{j+1} \\ r_{j+1} \end{Bmatrix} \tag{B.84}$$

with

$$\begin{aligned} \left[uwpr^H(z)\right]_j^{k=0} &= -\left[uwAB(z)\right]_j^{k=0}\left[\left[uwAB_*\right]_j^{k=0}\right]^{-1}\left[uwpr_*^P\right]_j^{k=0} \\ &= \frac{C_S^2}{2\pi\omega^2\wp^*}\begin{bmatrix} uwpr_{(1,1)}^H & 0 & uwpr_{(1,3)}^H & 0 \\ 0 & uwpr_{(2,2)}^H & 0 & uwpr_{(2,4)}^H \end{bmatrix} \end{aligned} \tag{B.85}$$

where

$$uwpr^{\mathrm{H}}_{(1,1)} = \frac{\sin\left[\omega\left(d-z\right)/C_{\mathrm{S}}\right]}{\sin(\omega d/C_{\mathrm{S}})} \tag{B.86}$$

$$uwpr^{\mathrm{H}}_{(1,3)} = \frac{\sin(\omega z/C_{\mathrm{S}})}{\sin(\omega z/C_{\mathrm{S}})} \tag{B.87}$$

$$uwpr^{\mathrm{H}}_{(2,2)} = \frac{\sin\left[\omega\left(d-z\right)/C_{\mathrm{P}}\right]}{\sin(\omega d/C_{\mathrm{P}})} \tag{B.88}$$

$$uwpr^{\mathrm{H}}_{(2,4)} = \frac{\sin\left(\omega \mathrm{z}/C_{\mathrm{P}}\right)}{\sin\left(\omega \mathrm{d}/C_{\mathrm{P}}\right)} \tag{B.89}$$

Local displacements for $k = 0$ are the summation of the particular parts in Equation B.72 and the homogeneous parts in Equation B.85, which can be expressed as

$$\begin{Bmatrix} u^{\mathrm{I}}_{\mathrm{pr}}(z) \\ w^{\mathrm{I}}_{\mathrm{pr}}(z) \end{Bmatrix}_j = \left[uwpr^{\mathrm{I}}(z)\right]_j^{k=0} \begin{Bmatrix} p_j \\ r_j \\ p_{j+1} \\ r_{j+1} \end{Bmatrix} \tag{B.90}$$

with

$$\begin{aligned} \left[uwpr^{\mathrm{I}}(z)\right]_j^{k=0} &= \left[uwpr^{\mathrm{P}}(z)\right]_j^{k=0} + \left[uwpr^{\mathrm{H}}(z)\right]_j^{k=0} \\ &= \frac{C_{\mathrm{S}}^2}{2\pi\omega^2 \wp^*} \begin{bmatrix} uwpr^{\mathrm{I}}_{(1,1)} & 0 & uwpr^{\mathrm{I}}_{(1,3)} & 0 \\ 0 & uwpr^{\mathrm{I}}_{(2,2)} & 0 & uwpr^{\mathrm{I}}_{(2,4)} \end{bmatrix} \end{aligned} \tag{B.91}$$

where

$$uwpr^{\mathrm{I}}_{(1,1)} = \frac{\sin\left[\omega\left(d-z\right)/C_{\mathrm{S}}\right]}{\sin(\omega d/C_{\mathrm{S}})} + \frac{z}{d} - 1 \tag{B.92}$$

$$uwpr^{\mathrm{I}}_{(1,3)} = \frac{\sin(\omega z/C_{\mathrm{S}})}{\sin(\omega z/C_{\mathrm{S}})} - \frac{z}{d} \tag{B.93}$$

$$uwpr^{\mathrm{I}}_{(2,2)} = \frac{\sin\left[\omega\left(d-z\right)/C_{\mathrm{P}}\right]}{\sin(\omega d/C_{\mathrm{P}})} + \frac{z}{d} - 1 \tag{B.94}$$

$$uwpr^{\mathrm{I}}_{(2,4)} = \frac{\sin\left(\omega \mathrm{z}/C_{\mathrm{P}}\right)}{\sin\left(\omega \mathrm{d}/C_{\mathrm{P}}\right)} - \frac{z}{d} \tag{B.95}$$

As shown in Equation 8.215, external forces and nodal displacements of layer j, for $k = 0$, are related to its stiffness matrix as

$$\begin{Bmatrix} P_j \\ R_j \\ P_{j+1} \\ R_{j+1} \end{Bmatrix} = \left[S^{\mathrm{L}}_{\mathrm{P-SV}} \right]_j^{k=0} \begin{Bmatrix} u_j \\ w_j \\ u_{j+1} \\ w_{j+1} \end{Bmatrix} \tag{B.96}$$

By substituting negative values of the particular parts of nodal displacements (Equation B.74) into Equation B.96, the homogeneous parts of the reactions can be obtained as

$$\begin{Bmatrix} P^{\mathrm{H}}_j \\ R^{\mathrm{H}}_j \\ P^{\mathrm{H}}_{j+1} \\ R^{\mathrm{H}}_{j+1} \end{Bmatrix} = \left[PRpr^{\mathrm{H}}_* \right]_j^{k=0} \begin{Bmatrix} p_j \\ r_j \\ p_{j+1} \\ r_{j+1} \end{Bmatrix} \tag{B.97}$$

with

$$\begin{aligned} \left[PRpr^{\mathrm{H}}_* \right]_j^{k=0} &= - \left[S^{\mathrm{L}}_{\mathrm{P-SV}} \right]_j^{k=0} \left[uwpr^{\mathrm{P}}_* \right]_j^{k=0} \\ &= \frac{C_{\mathrm{S}}}{2\pi\omega} \begin{bmatrix} PRpr^{\mathrm{H}}_{(1,1)} & 0 & PRpr^{\mathrm{H}}_{(1,3)} & 0 \\ 0 & PRpr^{\mathrm{H}}_{(2,2)} & 0 & PRpr^{\mathrm{H}}_{(2,4)} \\ PRpr^{\mathrm{H}}_{(3,1)} & 0 & PRpr^{\mathrm{H}}_{(3,3)} & 0 \\ 0 & PRpr^{\mathrm{H}}_{(4,2)} & 0 & PRpr^{\mathrm{H}}_{(4,4)} \end{bmatrix} \end{aligned} \tag{B.98}$$

where

$$PRpr^{\mathrm{H}}_{(1,1)} = PRpr^{\mathrm{H}}_{(3,3)} = \cot\left(\frac{\omega d}{C_{\mathrm{S}}}\right) \tag{B.99}$$

$$PRpr^{\mathrm{H}}_{(1,3)} = PRpr^{\mathrm{H}}_{(3,1)} = \frac{-1}{\sin(\omega d / C_{\mathrm{S}})} \tag{B.100}$$

$$PRpr^{\mathrm{H}}_{(2,2)} = PRpr^{\mathrm{H}}_{(4,4)} = \left(\frac{C_{\mathrm{P}}}{C_{\mathrm{S}}}\right) \cot(\omega d / C_{\mathrm{P}}) \tag{B.101}$$

$$PRpr^{\mathrm{H}}_{(2,4)} = PRpr^{\mathrm{H}}_{(4,2)} = \left(\frac{C_{\mathrm{P}}}{C_{\mathrm{S}}}\right) \frac{-1}{\sin(\omega d / C_{\mathrm{P}})} \tag{B.102}$$

For loaded layer j, the reaction forces for $k = 0$ (see Figure B.2) to counterbalance linearly distributed loads and to fix the interfaces can be obtained by

combining Equations B.78 and B.97 as

$$\begin{Bmatrix} P_j^{\mathrm{I}} \\ R_j^{\mathrm{I}} \\ P_{j+1}^{\mathrm{I}} \\ R_{j+1}^{\mathrm{I}} \end{Bmatrix} = \left[PRpr_*^{\mathrm{I}} \right]_j^{k=0} \begin{Bmatrix} p_j \\ r_j \\ p_{j+1} \\ r_{j+1} \end{Bmatrix} \tag{B.103}$$

with

$$\begin{aligned} \left[PRpr_*^{\mathrm{I}} \right]_j^{k=0} &= \left[PRpr_*^{\mathrm{P}} \right]_j^{k=0} + \left[PRpr_*^{\mathrm{H}} \right]_j^{k=0} \\ &= \frac{C_{\mathrm{S}}}{2\pi\omega} \begin{bmatrix} PRpr_{(1,1)}^{\mathrm{I}} & 0 & PRpr_{(1,3)}^{\mathrm{I}} & 0 \\ 0 & PRpr_{(2,2)}^{\mathrm{I}} & 0 & PRpr_{(2,4)}^{\mathrm{I}} \\ PRpr_{(3,1)}^{\mathrm{I}} & 0 & PRpr_{(3,3)}^{\mathrm{I}} & 0 \\ 0 & PRpr_{(4,2)}^{\mathrm{I}} & 0 & PRpr_{(4,4)}^{\mathrm{I}} \end{bmatrix} \end{aligned} \tag{B.104}$$

where

$$PRpr_{(1,1)}^{\mathrm{I}} = PRpr_{(3,3)}^{\mathrm{I}} = \cot\left(\frac{\omega d}{C_{\mathrm{S}}}\right) - \frac{C_{\mathrm{S}}}{\omega d} \tag{B.105}$$

$$PRpr_{(1,3)}^{\mathrm{I}} = PRpr_{(3,1)}^{\mathrm{I}} = \frac{-1}{\sin(\omega d / C_{\mathrm{S}})} + \frac{C_{\mathrm{S}}}{\omega d} \tag{B.106}$$

$$PRpr_{(2,2)}^{\mathrm{I}} = PRpr_{(4,4)}^{\mathrm{I}} = \left(\frac{C_{\mathrm{P}}}{C_{\mathrm{S}}}\right) \cot(\omega d / C_{\mathrm{P}}) - \frac{C_{\mathrm{P}}^2}{C_{\mathrm{S}} \omega d} \tag{B.107}$$

$$PRpr_{(2,4)}^{\mathrm{I}} = PRpr_{(4,2)}^{\mathrm{I}} = \left(\frac{C_{\mathrm{P}}}{C_{\mathrm{S}}}\right) \frac{-1}{\sin(\omega d / C_{\mathrm{P}})} + \frac{C_{\mathrm{P}}^2}{C_{\mathrm{S}} \omega d} \tag{B.108}$$

Analogous to the derivation of Equations B.55, global displacements $u_{\mathrm{pr}}\,(k = 0, z)$ and $w_{\mathrm{pr}}\,(k = 0, z)$ along the vertical line in any layer i, on which no distributed loads act ($i \neq j$), can be expressed as

$$\begin{Bmatrix} u_{\mathrm{pr}}(k=0,z) \\ w_{\mathrm{pr}}(k=0,z) \end{Bmatrix}_j^{i,i\neq j} = \left[uwpr(k=0,z) \right]_j^{i,i\neq j} \begin{Bmatrix} p_j \\ r_j \\ p_{j+1} \\ r_{j+1} \end{Bmatrix} \tag{B.109}$$

with

$$\left[uwpr(k=0,z)\right]_j^{i,i\neq j} = -\left[uwAB(z)\right]_j^{k=0}\left[\left[uwAB_*\right]_j^{k=0}\right]^{-1} \times SUB_{ij}\left(\left[\left[S_{\mathrm{P-SV}}^{\mathrm{T}}\right]^{k=0}\right]^{-1}\right)\left[PRpr_*^{\mathrm{I}}\right]_j^{k=0} \quad \text{(B.110)}$$

where $\left[PRpr_*^{\mathrm{I}}\right]_j^{k=0}$ can be obtained from Equation B.104. Similar to the derivation of Equation B.57, global displacements $u_{\mathrm{pr}}(k=0,z)$ and $w_{\mathrm{pr}}(k=0,z)$ along the vertical line in any layer i, on which the distributed loads act ($i=j$), can be expressed as

$$\begin{Bmatrix} u_{\mathrm{pr}}(k=0,z) \\ w_{\mathrm{pr}}(k=0,z) \end{Bmatrix}_j^{i,i\neq j} = \left[uwpr(k=0,z)\right]_j^{i,i\neq j} \begin{Bmatrix} p_j \\ r_j \\ p_{j+1} \\ r_{j+1} \end{Bmatrix} \quad \text{(B.111)}$$

with

$$\left[uwpr(k=0,z)\right]_j^{i,i\neq j} = \left[uwpr^{\mathrm{I}}(z)\right]_j^{k=0} - \left[uwAB(z)\right]_i^{k=0}\left[\left[uwAB_*\right]_i^{k=0}\right]^{-1} \times SUB_{ij}\left(\left[\left[S_{\mathrm{P-SV}}^{\mathrm{T}}\right]^{k=0}\right]^{-1}\right)\left[PRpr_*^{\mathrm{I}}\right]_j^{k=0} \quad \text{(B.112)}$$

where $\left[uwpr^{\mathrm{I}}(z)\right]_j^{k=0}$ and $\left[PRpr_*^{\mathrm{I}}\right]_j^{k=0}$ can be obtained from Equations B.91 and B.104, respectively.

B.3.2 Loads on Horizontal Line

Analogous to Section B2, external loads $P(k=0)$ and $R(k=0)$ can be formulated as

$$\begin{Bmatrix} P_{M+1}^{(k=0)} \\ R_{M+1}^{(k=0)} \end{Bmatrix} = \frac{1}{2\pi}\int_0^{\mathrm{b}} \begin{Bmatrix} p(x) \\ r(x) \end{Bmatrix} \mathrm{d}x = \left[PRpr_*\right]_{M,l}^{k=0} \begin{Bmatrix} p_l \\ r_l \\ p_{l+1} \\ r_{l+1} \end{Bmatrix} \quad \text{(B.113)}$$

with

$$\left[PRpr_*\right]_{M,l}^{k=0} = \frac{b}{4\pi}\begin{bmatrix} 1 & 0 & 1 & 0 \\ 0 & 1 & 0 & 1 \end{bmatrix} \quad \text{(B.114)}$$

Similar to the derivation of Equation B.66, displacements $u_{\mathrm{pr}}(k=0,z)$ and $w_{\mathrm{pr}}(k=0,z)$ between node i and node $i+1$, for loads on the horizontal element l underneath layer M, can be expressed as

$$\begin{Bmatrix} u_{\mathrm{pr}}(k=0,z) \\ w_{\mathrm{pr}}(k=0,z) \end{Bmatrix}_{M,l}^{i} = \Big[uwpr(k=0,z)\Big]_{M,l}^{i} \begin{Bmatrix} p_l \\ r_l \\ p_{l+1} \\ r_{l+1} \end{Bmatrix} \tag{B.115}$$

with

$$\Big[uwpr(k=0,z)\Big]_{M,l}^{i} = \Big[uwAB(z)\Big]_{i}^{k=0} \left[\Big[uwAB_{*}\Big]_{i}^{k=0}\right]^{-1} \times \mathbf{SUB}_{iM} \left(\left[\Big[S_{\mathrm{P-SV}}^{\mathrm{T}}\Big]^{k=0}\right]^{-1}\right) \Big[PRpr_{*}\Big]_{M,l}^{k=0} \tag{B.116}$$

B.4 Green's Influence Functions in Space Domain

In the previous subsections, displacements were determined in k-domain. The inverse Fourier transform needs to be formulated in order to obtain Green's influence functions in the space domain. The z-axis is based on the local z-axis of layer i. The x'-axis is based on the local x-axis of layer for distributed loads on vertical interface, and of elements l for distributed loads on horizontal interface.

Green's influence function in any layer i on x'–z plane, for the linearly distributed loads on the vertical assumed line in any layer j, can be expressed as

$$\begin{Bmatrix} u_{\mathrm{pr}}(x',z) \\ w_{\mathrm{pr}}(x',z) \end{Bmatrix}_{j}^{i} = \big[\mathbf{UWPR}(x',z)\big]_{j}^{i} \begin{Bmatrix} p_j \\ r_j \\ p_{j+1} \\ r_{j+1} \end{Bmatrix} \tag{B.117}$$

with

$$\big[\mathbf{UWPR}(x',z)\big]_{j}^{i} = \int_{-\infty}^{\infty} \Big[uwpr(k,z)\Big]_{j}^{i} \exp(-\iota k x')\mathrm{d}k \tag{B.118}$$

where $[uwpr(k,z)]_j^i$ can be obtained from Equations B.56 or B.58 for nonzero wave numbers k and from Equation B.110 or B.112 for a zero wave number k. Bold letters in the matrix indicate that the corresponding matrix is in the space domain.

As for linearly distributed loads on the horizontal element with any node l and node $l+1$, which are on the horizontal interface underneath layer M, Green's

influence function in any layer i on x'–z plane can be expressed as

$$\begin{Bmatrix} u_{\mathrm{pr}}(x', z) \\ w_{\mathrm{pr}}(x', z) \end{Bmatrix}^{i}_{M,l} = \left[\mathbf{UWPR}(x', z)\right]^{i}_{M,l} \begin{Bmatrix} p_l \\ r_l \\ p_{l+1} \\ r_{l+1} \end{Bmatrix} \tag{B.119}$$

with

$$\left[uwpr(x', z)\right]^{i}_{M,l} = \int_{-\infty}^{\infty} \left[\mathbf{UWPR}(k, z)\right]^{i}_{M,l} \exp\left(-\iota kx'\right) \mathrm{d}k \tag{B.120}$$

where $[uwpr(k, z)]^{i}_{M,l}$ can be obtained from Equation B.67 for nonzero wave number k and from Equation B.116 for zero wave number k.

Appendix C: Element Stiffness and Mass Coefficients

C.1 Element Stiffness Coefficients

The local coordinate and node numbering system of a four-node rectangular element is shown in Figure C.1. The element has lengths b_e and d_e along x- and z-axes, respectively. For a plane elastic problem, the element has eight degrees of freedom, two degrees of freedom on each node.

Therefore, the displacement pattern can be represented by eight unknown coefficients of the polynomial as

$$u(x,z) = \alpha_1 + \alpha_2 x + \alpha_3 z + \alpha_4 xz \tag{C.1}$$

$$w(x,z) = \alpha_5 + \alpha_6 x + \alpha_7 z + \alpha_8 xz \tag{C.2}$$

Substituting the values of nodal coordinates in Equations C.1 and C.2 and then solving for $\{\alpha\}$, displacement shape functions can be expressed in terms of nodal displacements as

$$\begin{Bmatrix} u(x,z) \\ w(x,z) \end{Bmatrix} = \left[\overline{N}(x,z)\right] \begin{bmatrix} u_1 & w_1 & \dots & u_i & w_i & \dots & u_4 & w_4 \end{bmatrix}^{\mathrm{T}} \tag{C.3}$$

with

$$[N(x,z)] = \begin{bmatrix} \overline{N}_{(1,1)} & 0 & \overline{N}_{(1,3)} & 0 & \overline{N}_{(1,5)} & 0 & \overline{N}_{(1,7)} & 0 \\ 0 & \overline{N}_{(2,2)} & 0 & \overline{N}_{(2,4)} & 0 & \overline{N}_{(2,6)} & 0 & \overline{N}_{(2,8)} \end{bmatrix} \tag{C.4}$$

where

$$\overline{N}_{(1,1)} = \overline{N}_{(2,2)} = 1 - \frac{x}{b_e} - \frac{z}{d_e} + \frac{xz}{b_e d_e} \tag{C.5}$$

$$\overline{N}_{(1,3)} = \overline{N}_{(2,4)} = \frac{z}{d_e} - \frac{xz}{b_e d_e} \tag{C.6}$$

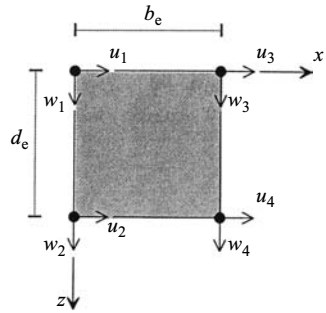

FIGURE C.1 Four-node rectangular element.

$$\overline{N}_{(1,5)} = \overline{N}_{(2,6)} = \frac{x}{b_e} - \frac{xz}{b_e d_e} \tag{C.7}$$

$$\overline{N}_{(1,7)} = \overline{N}_{(2,8)} = \frac{xz}{b_e d_e} \tag{C.8}$$

The strain–displacement relationship can be expressed as

$$\varepsilon_x = u_{,x}(x, z) \tag{C.9}$$

$$\varepsilon_y = w_{,z}(x, z) \tag{C.10}$$

$$\gamma_{xz} = \gamma_{zx} = u_{,z}(x, z) + w_{,x}(x, z) \tag{C.11}$$

where the normal strain and shear strain amplitudes are denoted by ε and γ, respectively. The first subscript denotes the direction of the strain component. The second denotes the direction of the infinitesimal area's normal where the strain component is. A comma denotes a partial derivative with respect to the subscript following it.

Using Equation C.3, the strains in Equations C.9 through C.11 can be expressed in terms of nodal displacements as

$$\begin{Bmatrix} \varepsilon_x(x,z) \\ \varepsilon_z(x,z) \\ \gamma_{xz}(x,z) \end{Bmatrix} = \left[\overline{B}(x, z)\right] \begin{bmatrix} u_1 & w_1 & \dots & u_i & w_i & \dots & u_4 & w_4 \end{bmatrix}^{\mathrm{T}} \tag{C.12}$$

with

$$\left[\overline{B}(x,z)\right] = \begin{bmatrix} \overline{B}_{(1,1)} & 0 & \overline{B}_{(1,3)} & 0 & \overline{B}_{(1,5)} & 0 & \overline{B}_{(1,7)} & 0 \\ 0 & \overline{B}_{(2,2)} & 0 & \overline{B}_{(2,4)} & 0 & \overline{B}_{(2,6)} & 0 & \overline{B}_{(2,8)} \\ \overline{B}_{(3,1)} & \overline{B}_{(3,2)} & \overline{B}_{(3,3)} & \overline{B}_{(3,4)} & \overline{B}_{(3,5)} & \overline{B}_{(3,6)} & \overline{B}_{(3,7)} & \overline{B}_{(3,8)} \end{bmatrix} \tag{C.13}$$

where

$$\overline{B}_{(1,1)} = \overline{B}_{(3,2)} = -\overline{B}_{(1,5)} = -\overline{B}_{(3,6)} = \frac{-1}{b_e} + \frac{z}{b_e d_e} \tag{C.14}$$

$$\overline{B}_{(1,3)} = \overline{B}_{(3,4)} = -\overline{B}_{(1,7)} = -\overline{B}_{(3,8)} = \frac{-z}{b_e d_e} \tag{C.15}$$

$$\overline{B}_{(2,2)} = \overline{B}_{(3,1)} = -\overline{B}_{(2,4)} = -\overline{B}_{(3,3)} = \frac{-1}{d_e} + \frac{x}{b_e d_e} \tag{C.16}$$

$$\overline{B}_{(2,6)} = \overline{B}_{(3,5)} = -\overline{B}_{(2,8)} = -\overline{B}_{(3,7)} = \frac{-x}{b_e d_e} \tag{C.17}$$

Normal stress and shear stress amplitudes can be obtained in terms of normal strain and shear strain amplitudes, ε and γ, in matrix form as

$$\begin{Bmatrix} \sigma_x \\ \sigma_z \\ \tau_{xz} \end{Bmatrix} = \left[\overline{D}\right] \begin{Bmatrix} \varepsilon_x \\ \varepsilon_z \\ \gamma_{xz} \end{Bmatrix} \tag{C.18}$$

with

$$\left[\overline{D}\right] = \begin{bmatrix} 2\wp + \lambda & \lambda & 0 \\ \lambda & 2\wp + \lambda & 0 \\ 0 & 0 & \wp \end{bmatrix} \tag{C.19}$$

where the shear modulus of elasticity

$$\wp = \frac{E}{2\,(1+\upsilon)} \tag{C.20}$$

the Lame constant

$$\lambda = \frac{\upsilon E}{(1+\upsilon)(1-2\upsilon)} \tag{C.21}$$

and the letter E represents Young's modulus of elasticity. The symbol ν represents Poisson's ratio.

By using Equations C.12 and C.18 and applying the principle of virtual work, nodal forces relate to the nodal displacements in terms of the symmetrical element stiffness matrix as

$$\begin{aligned} &\begin{bmatrix} P_1 & R_1 & \cdots & P_i & R_i & \cdots & P_4 & R_4 \end{bmatrix}^{\mathrm{T}} \\ &\quad = \left[\overline{\mathrm{K}}^{\mathrm{e}}\right]_j \begin{bmatrix} u_1 & w_1 & \ldots & u_i & w_i & \ldots & u_4 & w_4 \end{bmatrix}^{\mathrm{T}} \end{aligned} \tag{C.22}$$

with

$$\left[\overline{K}^{\,\mathrm{e}}\right]_j = \int_0^{d_\mathrm{e}} \int_0^{b_\mathrm{e}} \left[\overline{B}(x,z)\right]^T \left[\overline{D}\right]_j \left[\overline{B}(x,z)\right] \mathrm{d}x\mathrm{d}z$$

$$= \begin{bmatrix} \overline{K}^{\mathrm{e}}_{(1,1)} & \overline{K}^{\mathrm{e}}_{(1,2)} & \overline{K}^{\mathrm{e}}_{(1,3)} & \overline{K}^{\mathrm{e}}_{(1,4)} & \overline{K}^{\mathrm{e}}_{(1,5)} & \overline{K}^{\mathrm{e}}_{(1,6)} & \overline{K}^{\mathrm{e}}_{(1,7)} & \overline{K}^{\mathrm{e}}_{(1,8)} \\ & \overline{K}^{\mathrm{e}}_{(2,2)} & \overline{K}^{\mathrm{e}}_{(2,3)} & \overline{K}^{\mathrm{e}}_{(2,4)} & \overline{K}^{\mathrm{e}}_{(2,5)} & \overline{K}^{\mathrm{e}}_{(2,6)} & \overline{K}^{\mathrm{e}}_{(2,7)} & \overline{K}^{\mathrm{e}}_{(2,8)} \\ & & \overline{K}^{\mathrm{e}}_{(3,3)} & \overline{K}^{\mathrm{e}}_{(3,4)} & \overline{K}^{\mathrm{e}}_{(3,5)} & \overline{K}^{\mathrm{e}}_{(3,6)} & \overline{K}^{\mathrm{e}}_{(3,7)} & \overline{K}^{\mathrm{e}}_{(3,8)} \\ & & & \overline{K}^{e}_{(4,4)} & \overline{K}^{\mathrm{e}}_{(4,5)} & \overline{K}^{\mathrm{e}}_{(4,6)} & \overline{K}^{\mathrm{e}}_{(4,7)} & \overline{K}^{\mathrm{e}}_{(4,8)} \\ & & & & \overline{K}^{\mathrm{e}}_{(5,5)} & \overline{K}^{\mathrm{e}}_{(5,6)} & \overline{K}^{\mathrm{e}}_{(5,7)} & \overline{K}^{\mathrm{e}}_{(5,8)} \\ & \textit{symm} & & & & \overline{K}^{\mathrm{e}}_{(6,6)} & \overline{K}^{\mathrm{e}}_{(6,7)} & \overline{K}^{\mathrm{e}}_{(6,8)} \\ & & & & & & \overline{K}^{\mathrm{e}}_{(7,7)} & \overline{K}^{\mathrm{e}}_{(7,8)} \\ & & & & & & & \overline{K}^{\mathrm{e}}_{(8,8)} \end{bmatrix} \tag{C.23}$$

where

$$\overline{K}^{\mathrm{e}}_{(1,1)} = \overline{K}^{\mathrm{e}}_{(3,3)} = \overline{K}^{\mathrm{e}}_{(5,5)} = \overline{K}^{\mathrm{e}}_{(7,7)} = \frac{1}{3}\left[\left(2\wp_j + \lambda_j\right)\frac{d_\mathrm{e}}{b_\mathrm{e}} + \wp_j \frac{b_\mathrm{e}}{d_\mathrm{e}}\right] \tag{C.24}$$

$$\overline{K}^{\mathrm{e}}_{(2,2)} = \overline{K}^{\mathrm{e}}_{(4,4)} = \overline{K}^{\mathrm{e}}_{(6,6)} = \overline{K}^{\mathrm{e}}_{(8,8)} = \frac{1}{3}\left[\left(2\wp_j + \lambda_j\right)\frac{b_\mathrm{e}}{d_\mathrm{e}} + \wp_j \frac{d_\mathrm{e}}{b_\mathrm{e}}\right] \tag{C.25}$$

$$\overline{K}^{\mathrm{e}}_{(1,2)} = \overline{K}^{\mathrm{e}}_{(3,6)} = \overline{K}^{\mathrm{e}}_{(4,5)} = \overline{K}^{\mathrm{e}}_{(7,8)} = \frac{1}{4}\left(\wp_j + \lambda_j\right) \tag{C.26}$$

$$\overline{K}^{\mathrm{e}}_{(1,8)} = \overline{K}^{\mathrm{e}}_{(2,7)} = \overline{K}^{\mathrm{e}}_{(3,4)} = \overline{K}^{\mathrm{e}}_{(5,6)} = \frac{-1}{4}\left(\wp_j + \lambda_j\right) \tag{C.27}$$

$$\overline{K}^{\mathrm{e}}_{(1,6)} = \overline{K}^{\mathrm{e}}_{(2,3)} = \overline{K}^{\mathrm{e}}_{(4,7)} = \overline{K}^{\mathrm{e}}_{(5,8)} = \frac{1}{4}\left(\lambda_j - \wp_j\right) \tag{C.28}$$

$$\overline{K}^{\mathrm{e}}_{(1,4)} = \overline{K}^{\mathrm{e}}_{(2,5)} = \overline{K}^{\mathrm{e}}_{(3,8)} = \overline{K}^{\mathrm{e}}_{(6,7)} = \frac{-1}{4}\left(\lambda_j - \wp_j\right) \tag{C.29}$$

$$\overline{K}^{\mathrm{e}}_{(1,3)} = \overline{K}^{\mathrm{e}}_{(5,7)} = \frac{1}{6}\left[\left(2\wp_j + \lambda_j\right)\frac{d_\mathrm{e}}{b_\mathrm{e}} - 2\wp_j \frac{b_\mathrm{e}}{d_\mathrm{e}}\right] \tag{C.30}$$

$$\overline{K}^{\mathrm{e}}_{(2,6)} = \overline{K}^{\mathrm{e}}_{(4,8)} = \frac{1}{6}\left[\left(2\wp_j + \lambda_j\right)\frac{b_\mathrm{e}}{d_\mathrm{e}} - 2\wp_j \frac{d_\mathrm{e}}{b_\mathrm{e}}\right] \tag{C.31}$$

$$\overline{K}^{\mathrm{e}}_{(2,4)} = \overline{K}^{\mathrm{e}}_{(6,8)} = \frac{-1}{6}\left[2\left(2\wp_j + \lambda_j\right)\frac{b_\mathrm{e}}{d_\mathrm{e}} - \wp_j \frac{d_\mathrm{e}}{b_\mathrm{e}}\right] \tag{C.32}$$

$$\overline{K}^{\mathrm{e}}_{(1,5)} = \overline{K}^{\mathrm{e}}_{(3,7)} = \frac{-1}{6}\left[2\left(2\wp_j + \lambda_j\right)\frac{d_\mathrm{e}}{b_\mathrm{e}} - \wp_j \frac{b_\mathrm{e}}{d_\mathrm{e}}\right] \tag{C.33}$$

$$\overline{K}^{\mathrm{e}}_{(1,7)} = \overline{K}^{\mathrm{e}}_{(3,5)} = \frac{-1}{6}\left[2\left(2\wp_j + \lambda_j\right)\frac{d_\mathrm{e}}{b_\mathrm{e}} + \wp_j \frac{b_\mathrm{e}}{d_\mathrm{e}}\right] \tag{C.34}$$

$$\overline{K}^{\mathrm{e}}_{(2,8)} = \overline{K}^{\mathrm{e}}_{(4,6)} = \frac{-1}{6}\left[2\left(2\wp_j + \lambda_j\right)\frac{b_{\mathrm{e}}}{d_{\mathrm{e}}} + \wp_j\frac{d_{\mathrm{e}}}{b_{\mathrm{e}}}\right] \tag{C.35}$$

C.2 Element Mass Coefficients

Instead of using lumped mass at each node, consistent mass is considered. The mass of element j distributed to each degree of freedom can be defined as

$$\left[\overline{M}^{\mathrm{e}}\right]_j = \int_0^{d_{\mathrm{e}}}\int_0^{b_{\mathrm{e}}} \rho_j \left[\overline{N}(x,z)\right]^{\mathrm{T}}\left[\overline{N}(x,z)\right]\mathrm{d}x\mathrm{d}z \tag{C.36}$$

Inserting Equation C.4 into Equation C.36 results in the symmetrical element mass matrix as

$$\left[\overline{M}^{\mathrm{e}}\right]_j = \rho_j b_{\mathrm{e}} d_{\mathrm{e}} \begin{bmatrix} 1/9 & 0 & 1/8 & 0 & 1/8 & 0 & 1/36 & 0 \\ & 1/9 & 0 & 1/8 & 0 & 1/8 & 0 & 1/36 \\ & & 1/9 & 0 & 1/8 & 0 & 1/8 & 0 \\ & & & 1/9 & 0 & 1/8 & 0 & 1/8 \\ & & & & 1/9 & 0 & 1/8 & 0 \\ & \textit{symm} & & & & 1/9 & 0 & 1/8 \\ & & & & & & 1/9 & 0 \\ & & & & & & & 1/9 \end{bmatrix} \tag{C.37}$$

Notation

Roman Symbols

A	cross-section area of an actuator cylinder, or system plant matrix in discrete-time domain
A_{P}, A_{SV}	amplitudes of incident P- and SV-wave traveling in negative z-direction/ amplitudes of general P- and SV-wave
A_{SH}	amplitudes of general SH-wave
A_{b}	bearing's bonded area of rubber
A_{l}	lead-plug area of lead-plug bearing
A_{p}	cross-sectional areas of liquid mass damper's cylinder
A_{t}	cross-sectional areas of liquid mass damper's tube
a_{e}	external excitation to represent measurand, $\ddot{x}_{\mathrm{e}}(t)$
$\{a_i\}$	real part of plant matrix's ith eigenvector
$[A]$	plant matrix in open-loop, or matrix-related degrees of freedom of nodes along rigid interface to rigid-body degrees of freedom at point 0; characteristic matrix of controlled system
$[A_{\mathrm{a}}]$	system matrix with active control but without SSI for MATLAB® application
$[A_{\mathrm{c}}]$	system plant matrix in closed loop, or plant matrix without SSI for state space presentation
$[A_{\mathrm{hy}}]$	system matrix with hybrid control but without SSI for MATLAB® application
$[A_{\mathrm{p}}]$	system matrix with passive control but without SSI for MATLAB® application
$[A_{\mathrm{s}}]$	system matrix without control and SSI for MATLAB® application
$[A_{\mathrm{SSI}}]$	system matrix without control but with SSI for MATLAB® application
$[A^{\mathrm{a}}_{\mathrm{SSI}}]$	system matrix with active control and SSI for MATLAB® application
$[A^{\mathrm{hy}}_{\mathrm{SSI}}]$	system matrix with hybrid control and SSI for MATLAB® application
$[A^{\mathrm{p}}_{\mathrm{SSI}}]$	system matrix with passive control and SSI for MATLAB® application
$[A^{0}_{\mathrm{c}}]$	plant matrix with SSI for state space presentation
B	half-width of rectangular mat foundation
B_{D}	numerical coefficient for effective damping related to the design earthquake
B_{M}	numerical coefficient for effective damping related to the MCE
B_{R}	numerical coefficient for effective damping, β_{R}
B_{P}, B_{SV}	amplitudes of incident P- and SV-wave traveling in positive z-direction
B_{V+I}	numerical coefficient for effective damping, β_{V+I}
$B_{m\mathrm{D}}$	the mth mode numerical coefficient for effective damping, β_{mD}

$B_{m\mathrm{M}}$	the mth mode numerical coefficient for effective damping, $\beta_{m\mathrm{M}}$
b	the shortest dimension of the structure above the isolation system, or length of horizontal element on structure–soil interface
b_{e}	width of discretizing element in excavated part domain
$\{B_{\mathrm{i}}\}$	earthquake input vector
$\{b_i\}$	imaginary part of plant matrix's ith eigenvector
$\{B_{\mathrm{r}}\}$	coefficient vector for earthquake excitation
$[B]$	actuator location matrix, or matrices related to controller location
$[B_{\mathrm{a}}]$	input matrix for active force
$[B_{\mathrm{p}}]$	input matrix for passive force
$[B_{\mathrm{u}}]$	coefficient matrix for control force vector
$[\overline{B}]$	element strain nodal-displacement matrix in excavated part system
C	phase velocity of wave traveling in soil domain, or sensor output matrix in discrete-time domain
C_{P}	P-wave velocity, dilatational wave velocity
C_{S}	seismic response coefficient, or S-wave velocity, shear wave velocity
$C_{\mathrm{S}m}$	seismic response coefficient at the mth d.o.f., $m = 1, \ldots, n$
C_{SR}	the residual mode seismic response coefficient of a damped structure
C_{d}	diagonal matrix related to the damper installed at the ith story, or deflection amplification factor
$C_{m\mathrm{FD}}$, $C_{m\mathrm{FV}}$	coefficients determined by Equations 3.52, 3.52a, 3.52b, and 3.52c
C_{t}	coefficient to determine the building period with the fixed base, T_{a}, given in Table 3.2
C_{u}	coefficient as the upper bound to the calculated period
C_{x}, C_{y}, C_{z}	nondimensionalized damping coefficients in horizontal direction, rocking, and vertical direction, respectively
C_{xy}	nondimensionalized coupling damping coefficients of horizontal direction and rocking
C_0	damper's damping coefficient, or relaxation modulus of Maxwell model
c_{a}	damping coefficient of accelerometer system
c_{b}	damping coefficient of the isolation system, or damping coefficient of bracing
$c_{\mathrm{b}i}$	damping coefficient of the ith brace
c_{d}	damping coefficient of fluid viscous damping device
$c_{\mathrm{d}i,j}$	damping coefficient of the jth damper at the ith story level
c_i, c_{m}	damping at the ith, or the mth d.o.f. of a structure, $i, m = 1, \ldots, n$
c_{p}	damping coefficient actuator cylinder's piston and its rods
$c_{\mathrm{p}k}$	damping coefficient of the kth spring damper
c_{s}	structural damping coefficient
c_0	damping coefficient
c_1	translational damping coefficient of single-story shear building structure

$c(t)$	servovalve–piston displacement
$c(\omega)$	frequency-dependent damping coefficient
$\{C\}$	vector associated with wave amplitude; vectors related to structure-base's acceleration
$[C]$, $[C^*]$	damping matrix
$[C_\mathrm{b}]$	damping matrix of braces
$[C_\mathrm{s}]$	damping matrix of structural elements
$[C_1]$, $[C_2]$	location matrix of accelerometers and sensors, respectively
D	dead load, or depth of foundation embedment
D_D	the design displacement at the isolation system's center of the rigidity
D_M	the maximum displacement at the isolation system's center of the rigidity
D_RD	the design displacement of the residual mode at the roof
D_RM	the maximum displacement of the residual mode at the roof
D_TD	the total design displacement
D_TM	the total maximum displacement
D_Y	displacement corresponding to effective yield point of SFRS at roof of structure
D_g	floor displacement relative to ground system
D_i	absolute displacement at the ith floor
D_m	horizontal component of damping force, P_m, at the mth d.o.f., $m = 1, \ldots, n$
$D_{m\mathrm{D}}$	the mth mode design displacement at roof of a structure, $m = 1, \ldots, n$
$D_{m\mathrm{M}}$	the mth mode maximum displacement at roof of a structure, $m = 1, \ldots, n$
D_s	floor relative displacement excluding rigid motion effect due to foundation rotation
D_y	yield displacement of bearing
d	the longest dimension of the structure above the isolation system, or depth of soil layer
d_e	depth of discretizing element in excavated part of domain
d_i	depth of soil layer i
$\dot{D}$	velocity of friction pendulum bearing's movement
$[D]$	matrix of horizontal component of damping force, or plant matrix
$[\overline{D}]$	element stress–strain matrix in excavated part system, or volumetric strain
E	Young's modulus of elasticity
E_D	bearing's energy dissipated per cycle of the design displacement
E_M	bearing's energy dissipated per cycle of the maximum displacement
E_R, E_i	Young's modulus of elasticity of layer i and of half-space
e	eccentricity between the center of the mass above the isolation interface and the isolation system's center of the rigidity combined with an accidental eccentricity
E^*	control energy
$\{E\}$	external disturbance vectors
F_a	site coefficient specified in Table 2.1

F_i	design lateral force at story level i
$F_{i,\mathrm{R}}$	the residual mode design lateral force at story level i
$F_{i,m}$	design lateral force of the mth mode at story level i
F_{v}	site coefficient specified in Table 2.2
F_{x}	vertical distribution of the minimum lateral force, V_{s}
F_{y}	yield force of bearing
f_{L}	coefficient related to postyield stiffness of lead-plug bearing
$f_{\mathrm{a}i}$	active control force generated by the ith actuator and the ith damper
f_{b}	servovalve bandwidth
f_{c}	friction force related to the fluid yield stress
f_i	the lateral force applied at level i
$f_{\max}$	friction coefficient at fast velocity under movement of friction pendulum bearing
$f_{\min}$	friction coefficient at slow velocity under movement of friction pendulum bearing
$f_{\mathrm{p}i}$	passive control force generated by the ith actuator and the ith damper
f_{yl}	lead yield stress of lead-plug bearing
$\dot{F}^{\mathrm{g}}_{\mathrm{xx}}, \dot{F}^{\mathrm{g}}_{x\theta}, \dot{F}^{\mathrm{g}}_{\theta\mathrm{x}}, \dot{F}^{\mathrm{g}}_{\theta\theta}, \dot{F}^{\mathrm{g}}_{\mathrm{zz}}$	ground system's time-derivative displacement coefficients corresponding to the first subscript's degree of freedom due to a unit force excitation corresponding to the second subscript's degree of freedom
$F( )$	augmented functional of functional f
$F_{\mathrm{c}}(t)$	control force
$\{F_{\mathrm{D}}(t)\}$	damping force vectors
$\{F_{\mathrm{K}}(t)\}$	restoring force vectors
$\{F\}_m$	the mth mode vertical distribution of the design lateral force, $m = 1, \ldots, n$
f_0	offset force
$f( )$	quadratic energy function
$f(t)$	system's state-variable representation
$f(x)$	objective function as given in Equation 7.108
$f_{\mathrm{a}}(t)$	active control force
$f_{\mathrm{p}}(t)$	passive control force, or force applied on spring
$f_{\mathrm{sa}}(t)$	force generated by linear viscous damper
$[F]$	soil-flexibility matrix (strain–stress relationship)
$[F^{\mathrm{g}}_{00}]$	dynamic-flexibility matrix of ground system with rigid interface
$[\dot{F}^{\mathrm{g}}_{00}]$	ground system's time-derivative dynamic-flexibility matrix
G	tangent shear modulus of bearing, or shear modulus of elastic materials
G_0	the spectral intensity of the ground acceleration

g	acceleration of gravity
GF	stain-gage factor
$G(\ )$	augmented function of function g
$G(s)$	transfer function
$G(\omega)$	spectral density
$g(\ )$	quadratic function related to state vector at t_n
$g(x)$	control objective as given in Equation 7.108
$[G]$, $[G^{SSI}]$	feedback gain matrix
$[G_C]$	Lyapunov matrix
$[G_d]$, $[G_v]$	gain matrices for displacements and velocities
H	depth of homogeneous layer on rock
$H_{\delta\gamma}$	the transfer function from reference input as shown in Equation 7.3
h_{ai}	accumulated height from rotational point 0 to the centroid of mass m
h_i	the height of the structure above the base at story level i
h_n	the height of the structure above its base
h_{si}	the story height at any level i
h_0	depth of rectangular mat foundation
$H_{CP}(\omega)$	Clough and Penzien low-band frequency filter
$H_{KT}(\omega)$	Kanai and Tajimi filter
I	the occupancy importance factor
I_i	the ith floor mass moment of inertia with respect to point 0
I_0	foundation mass moment of inertia with respect to point 0
$[I]$	identity matrix
J	performance index
J_E	control energy index
J_R	response index
J_n	performance index of the nth time interval
J_1	average dissipated energy defined by the first objective function
J_2	weighted sum of damping ratios for dominant modes defined by the second objective function
J_3	H_2 cost of interstory drift defined by the third objective function
J_4	Maximum of peak interstory drift defined by the fourth objective function
J_5	maximum root-mean-square interstory drift defined by the fifth objective function
j	imaginary number $= \sqrt{-1}$
$J_p(t)$	time-dependent performance index
K_v	servovalve pressure-loss coefficient
K_x, K_y, K_z	nondimensionalized spring coefficients in horizontal direction, rocking, and vertical direction, respectively
K_{xy}	nondimensionalized coupling spring coefficients of horizontal direction and rocking
k	linear spring with stiffness constant, or spring coefficient of a force sensor in Equation 6.4, or wave number

k_{a}	stiffness of accelerometer system
k_{Dmax}	maximum effective stiffness of the isolation system at the design displacement
k_{Dmin}	minimum effective stiffness of the isolation system at the design displacement
k_{Mmax}	maximum effective stiffness of the isolation system at the maximum displacement
k_{Mmin}	minimum effective stiffness of the isolation system at the maximum displacement
k_{b}	lateral stiffness of the isolation system, or stiffness of bracing
$k_{\mathrm{b}i}$	stiffness of the ith brace
k_{com}	compressive stiffness of bearing
k_{e}	bearing elastic stiffness
k_{eff}	effective stiffness of bearing
k_i, k_m	stiffness at the ith, or the mth d.o.f. of a structure, $i, m = 1, \ldots, n$
k_i, k_1	translational spring-stiffness coefficient of multistory shear structure at the ith floor and of single-story shear structure, respectively
k_{p}	postyield stiffness of bearing
k_{pk}	spring coefficient of spring damper
k_{s}	linear lateral stiffness of a damped structure
k_{ten}	tensile stiffness of bearing
k_{torsion}	torsional stiffness of the isolation system
$k(\omega)$	frequency-dependent stiffness
$[K]$, $[K^*]$	stiffness matrix
$[K_{\mathrm{b}}]$	stiffness matrix of braces
$[K_{\mathrm{s}}]$	stiffness matrix of structural elements
$[K^{\mathrm{e}}]$	stiffness matrix of system's excavated part
$[K^I(w)]$	impedance function matrix
$[\tilde{K}_{00}]$	symmetric spring-stiffness matrix corresponding to foundation degrees of freedom using in state weighting matrix [Q]
L	live load, or half-number of elements on horizontal part of structure–soil interface, or observer model matrix
L_{e}	half-number of even portions along width of system's excavated part
L_{t}	tube length of liquid mass damper
l	time-instant number where impulse velocity functions approach zero
l_x, l_y, l_z	propagating directional cosine to x-, y-, z-axes of incident P-wave
l^+, l^-	positive or negative testing displacement
$[L]$	gain matrix, or interpolation matrix of distributed forces
M_0	seismic moment
m	mass of a SDOF structure, or number of K-braces
m_{a}	mass of accelerometer system
m_{b}	mass of bracing
$m_{\mathrm{b}i}$	stiffness of the ith brace
$m_{\mathrm{e}k}$	effective liquid mass due to liquid motion in the tube of the kth damper
m_i, m_m	mass at the ith, or the mth d.o.f. of a structure, $i, m = 1, \ldots, n$

m_{p}	mass coefficient of actuator cylinder's piston and its rods
m_0	mass of rectangular mat foundation
$M_{\mathrm{base}}^{\mathrm{SSI}}$	base moment for SSI model
$m_1(t)$	fluid mass of the left actuator chamber
$[M], [M^*]$	mass matrix
$[M_{\mathrm{b}}]$	mass matrix of braces
$[M_{\mathrm{c}}]$	controllability matrix
$[M^{\mathrm{e}}]$	mass matrix of the system's excavated part
$[M_{\mathrm{f}}]$	foundation mass matrix
$[M_{\mathrm{o}}]$	observability matrix in Equation 6.15
$[M_{\mathrm{s}}]$	mass matrix of structural elements
N	order of state equations, or order of plant matrix $[A_{\mathrm{c}}]$
NCR	number of controllers
NS	number of sampling steps in discrete Fourier transform
NT	number of time intervals
$\overline{N}$	blow count
n	number of structure stories
nl	minimum of n and l
$[N]$	rigid-body kinematics matrix of rigid interface
P	gravity load, or damping force in axial direction of a damping device, or spring force in tension/compression of a force sensor
P_{R}	discharge pressure of hydraulic actuator
P_{S}	supply pressure of hydraulic actuator
P_{c}	axial force applied at the friction pendulum bearing
P_{g}	gravity load on friction pendulum bearing
P_i	horizontal force at node i
$P_{i,j}$	damping force of the jth damper at the ith story level
P_m	damping force in axial direction of a damping device at the mth d.o.f.
$P_{\max}, P_{\min}$	modified maximum and minimum properties of a bearing, respectively
P_{n}	nominal properties of a bearing
p	horizontal linearly distributed load
p_i	the ith system poles, or horizontal load intensity at node i
p_j^{H}	homogeneous part of horizontal reaction force at node j
p_j^{I}	part I horizontal reaction force at node j
p_j^{P}	particular part of horizontal reaction force at node j
P-	primary
P^+, P^-	positive or negative testing force at displacement of l^+ and l^- for each cycle
$P_1(t), P_2(t)$	hydraulic pressure
$[P]$	damping force matrix or Riccati matrix
Q	characteristic strength of bearing, or structural force of a damped structure
Q_{DSD}	the mth mode design force of displacement-dependent damping devices

Q_{E}	the seismic force determined from the MCE
Q_m	structural force of a damped structure at the mth d.o.f., $m = 1, \ldots, n$
$Q_{m\mathrm{DVS}}$	the mth mode design force of velocity-dependent damping devices
$Q_{m\mathrm{SFRS}}$	the mth mode design force from the seismic force-resisting system
q	number of significant modes in Equation 7.2
q_{H}	hysteretic loop adjustment factor
$q(t)$	displacement in modal space
$\{q(t)\}$	vector of modal coordinates
$Q_1(t)$, $Q_2(t)$	hydraulic flow rate
$[Q]$	structural force matrix, or weighting matrix in performance indices, or state weighting matrix
R	response modification coefficient, or radius of curvature of the sliding surface, or the resistance of the undeformed gauge given in Equation 6.3
R_{I}	a numerical coefficient related to the type of the seismic force-resisting system above the isolation system
R_i	vertical force at node i
R_x, R_z	horizontal and vertical interaction force at point 0 between structure system and ground system
R_1, R_2	resistors in the amplifiers
r	number of actuators as given in Equation 7.20, or vertical linearly distributed load
r_i	vertical load intensity at node i
R_j^{H}	homogeneous part of vertical reaction force at node j
R_j^{I}	part I vertical reaction force at node j
R_j^{P}	particular part of vertical reaction force at node j
R_θ	interaction moment around y-axis at point 0 between structure system and ground system
$r(k)$	sampled value of seismic excitation, $\ddot{x}_{\mathrm{g}}(t)$, at the kth sampling time
$\{R_0\}$	vector consisting of horizontal interaction force and interaction moment
$\{\tilde{R}_0\}$	dynamic-equivalent-force vector
$[R]$	weighting matrix in performance indices, or control weighting matrix
S_{A}	pseudoacceleration
S_{D}	spectral displacement
S_{D1}	the design spectrum acceleration parameter at 1s
S_{DS}	the design spectrum acceleration parameter at a short period
S_{MS}	MCE spectral response acceleration at a short period
S_{M1}	MCE spectral response acceleration at 1s
S_{S}	MCE spectral response acceleration parameter at a short period
S_{V}	pseudovelocity
S_{a}	design spectral response acceleration
$S_{\mathrm{a}m}$	pseudoacceleration at the mth d.o.f., $m = 1, \ldots, n$

S_1 MCE spectral response acceleration parameter at period of 1s
S- secondary horizontal
SH- secondary vertical
SV- horizontal base shear for SSI-model
s number of dampers
s_1, s_2 numbers of accelerometers and state sensors, respectively
$\bar{s}_u$ undrained shear strength
$S_{qi}(\omega)$ power spectrum density of the modal displacement response $q_i(t)$
$[S]$ weighting matrix in performance indices
$[S^e]$ dynamic-stiffness matrix of system's excavated part corresponding to all nodal points
$[S_{00}]$ dynamic-stiffness matrix of system with rigid interface
T building's fundamental period
T_D effective period of the isolated structure at the design displacement
T_L long-period transition period
T_M effective period of the isolated structure at the maximum displacement
T_R period of the residual mode for a damped structure
T_S period defined as the ratio of S_{D1}/S_{DS}
T_a building period with the fixed base
T_m period of structure at the mth d.o.f., $m = 1, \ldots, n$
T_0 period equal to $0.2S_{D1}/S_{DS}$
T_{1D} effective period of the damped structure's fundamental mode at the design displacement
T_{1M} effective period of the damped structure's fundamental mode at the maximum displacement
t time variable, or total rubber thickness of bearing
t_i time instant
t_f final time instant
t_0 initial time instant
T^* possible time
$[T]$ eigenvalues of plant matrix [A], or transformation matrix
u simplified notation of an isolation system's movement, or horizontal displacement/prescribed horizontal displacement/displacement in x-direction
u_i nodal horizontal displacement at node i
$u_{i,max}$ saturation limit of the ith control force specified in Equation 7.20
u_j horizontal component of the active tendon force generated by the jth actuator
u_m displacement or movement of a seismically isolated structure at story m
u_x displacement of fluid viscous damper in x direction
$\vec{u}_i$ horizontal control force corresponding to the ith controller
$u(k)$ sampled values of $\{u(t)\}$ at the kth sampling time
$u(t)$ movement of an isolation system, or active control command
$\{u(t)\}$ control command vector
$\{\bar{u}(t)\}$ control force

$\{\vec{U}\}$ horizontal force vector
V actuator/damper chamber volume, or minimum lateral force determined from the structure with the fixed base, or sensor output voltage
V_{D} design base shear of a damped structure
V_{R} the residual mode base shear of a damped structure
V_{b} minimum lateral force to design the isolation system, the structural elements below the isolation system, and the foundation
V_i minimum lateral force to fully activate the isolation system or the wind-restraint system
$V_{i,j}$ velocity of the jth damper at the ith story level
V_m design base shear at the mth d.o.f., $m = 1, \ldots, n$
V_{s} minimum shear force to design the structural elements above the isolation system
v displacement in y-direction
v_{s} shear wave velocity of soil
$V_{\mathrm{i}}(t)$ voltage of input signals
$V_{\mathrm{o}}(t)$ voltage of output signals
$V_{\mathrm{l}}(t)$ fluid volume in the left actuator chamber
W effective seismic weight of the structure above the isolation interface
$W_{\mathrm{D}m}$ the total work done by all damping devices at the mth mode
$W_{\mathrm{S}m}$ maximum strain energy of all damping devices at the mth mode
$W_{mi,j}$ the work done by the jth damper at the ith story in one complete cycle of dynamic response at the mth mode
$\overline{W}_m$ effective seismic weight of the mth mode, $m = 1, \ldots, n$
$\overline{W}_{\mathrm{R}}$ effective residual mode seismic weight of a damped structure
w vertical displacement/prescribed vertical displacement/displacement in z-direction
w_i, w_j portion of W that is located at story level i and j, respectively
X percent of total structure height at the actuator location
x simplified notation of relative displacement of a SDOF structure, or coefficient to determine the building period with the fixed base, T_{a}, or controllability index in Equation 7.9, or design variable for optimization problem
$x_{\mathrm{b}j}$ displacement of the ith floor and the jth K-brace
x_{a} displacement of accelerometer system
x_i the ith floor relative displacement
x_0^{e} horizontal displacement at point 0 of rigid interface of system's excavated part
x_0^{g} horizontal displacement at point 0 of rigid interface of ground system
x_0^{f} horizontal displacement at point 0 of rigid interface of free-field system
x_0^{t} horizontal displacement at point 0 of rigid interface of total system
x_i^{t} horizontal ith floor displacement of total system
x_i^{tb} horizontal ith floor displacement of total system that is relative to structure-base's displacement
x_i^{tg} horizontal ith floor displacement of total system that is relative to horizontal displacement of ground system with rigid interface

$_{,x}$, $_{,xx}$	partial derivative with respect to successive variable(s)
x'_m	the mth component of the generalized response vector
$\dot{x}_{\mathrm{a}}$	velocity of accelerometer system
$\ddot{x}_{\mathrm{a}}$	acceleration of accelerometer system
$\ddot{x}^{\mathrm{b}}$	horizontal acceleration of structure-base
$x(t)$	relative displacement of a SDOF structure
$x_{\mathrm{g}}(t)$	earthquake ground motion
$x_i(t), x_m(t)$	relative displacement at the ith, or the mth d.o.f. of a structure, $i, m = 1, \ldots, n$
$\dot{x}(t)$	velocity of SDOF structure
$\dot{x}_i(t), \dot{x}_m(t)$	velocity at the ith, or the mth d.o.f. of a structure, $i, m = 1, \ldots, n$
$\ddot{x}(t)$	acceleration of SDOF structure
$\ddot{x}_{\mathrm{a}}(t)$	directly sensed value by the accelerometer
$\ddot{x}_{\mathrm{g}}(t)$	earthquake ground acceleration
$\ddot{x}_i(t), \ddot{x}_m(t)$	acceleration at the ith, or the mth d.o.f. of a structure, $i, m = 1, \ldots, n$
$\{X_{\mathrm{S}}^t\}$	floor displacement vector of total dynamic system
$\{X_{\mathrm{S}}^{\mathrm{tb}}\}$	floor displacement vector of total dynamic system that is relative to that of structure-base
$\{X_{\mathrm{S}}^{\mathrm{tg}}\}$	floor displacement vector of total dynamic system that is relative to that of ground system
$\{X_0^{\mathrm{tg}}\}$	foundation displacement vector of total dynamic system that is relative to that of ground system
$\{x'\}$	generalized response vector
$Y_j(t)$	the jth mode maximum response spectrum value
$\{y(t)\}$	sensor output
z_i	vertical displacement corresponding to node i
z_0^{e}	vertical displacement at point 0 of rigid interface of excavated part
z_0^{g}	vertical displacement at point 0 of rigid interface of ground system
z_0^{f}	vertical displacement at point 0 of rigid interface of free-field system
z_0^{t}	vertical displacement at point 0 of rigid interface of total system
$z(k)$	system state vector in digital domain
$\{Z\}$	state vector
$\{Z(t)\}$	system state vector in analog domain
$\{1\}$	$1 \times n$ unit vector

Greek Symbols

α	Rayleigh damping coefficient in $[C] = \alpha[M] + \beta[K]$, or velocity exponent of fluid viscous damping device
$\alpha_{i,j}$	velocity exponent of the jth damper at the ith story level
$\{\alpha\}$	polynomial coefficients vector
β	fluid bulk modulus, or Rayleigh damping coefficient in $[C] = \alpha[M] + \beta[K]$, or damping ratio
β_{D}	effective damping of the isolation system at the design displacement

β_{HD}, β_{HM}	effective damping due to postyield hysteretic performance of the SFRS combined with structural elements of the damping system under the design earthquake or the MCE
β_I	effects of the structural damping of damped structure
β_{M}	effective damping of the isolation system at the maximum displacement
β_{R}	total effective damping of the residual mode
β_{V}	effective damping of damping devices
$\beta_{\mathrm{V}+I}$	effective damping equal to $\beta_I + \beta_{\mathrm{V1}}$
β_{VR}	effective damping of the residual mode
$\beta_{\mathrm{V}m}$	the mth mode viscous damping
β_{b}	damping ratio of a SDOF seismically isolated structure
β_{eff}	effective damping of bearing or effective modal damping
β_m	damping ratio at the mth mode of a seismically isolated structure, $m = 1, \ldots, n$
$\beta_{m\mathrm{D}}$	total effective damping of the mth mode at the design displacement
$\beta_{m\mathrm{M}}$	total effective damping of the mth mode at the maximum displacement
χ	bearing's system property adjustment factor
$\dot{\chi}^{\mathrm{g}}_{xx}$, $\dot{\chi}^{\mathrm{g}}_{x\theta}$, $\dot{\chi}^{\mathrm{g}}_{\theta x}$, $\dot{\chi}^{\mathrm{g}}_{\theta\theta}$, $\dot{\chi}^{\mathrm{g}}_{zz}$	ground system's impulse velocity coefficients corresponding to the first subscript's degree of freedom due to a unit force excitation corresponding to the second subscript's degree of freedom
$[\chi^{\mathrm{g}}_{00}]$	impulse velocity matrix of ground system
$[\tilde{\chi}_{00}]$	pseudostatic-stiffness matrix of ground system
Δ	the nth order vector for interstory drifts for an n-story building
$\Delta_{i,\mathrm{D}}$	the total story drift between story i and $i-1$
$\Delta_{i,m\mathrm{D}}$	the story drift between story i and $i-1$ of the mth mode
Δt	time increment
$\Delta\omega$	frequency increment
δ	displacement converted by the spring of a force sensor in Equation 6.4, or Dirac-delta function
δ_i	the story drift at level i
$\delta_{i,\mathrm{RD}}$	design displacement of story i at the residual mode
$\delta_{i,m\mathrm{D}}$, $\delta_{i-1,m\mathrm{D}}$	displacement or deflection at story i and $i-1$ of the mth mode
$\Delta(t)$	actuator/damper piston displacement
$\Delta_{\mathrm{a}}(t)$, $\Delta_{\mathrm{a}k}(t)$	displacement of an actuator piston
$\Delta_{\mathrm{p}}(t)$, $\Delta_{\mathrm{p}k}(t)$	piston displacement of viscous fluid damper
$\Delta_1(t)$	the force-caused displacement of a spring
$\nabla_{i,\mathrm{D}}$	the total design velocity of story i
$\nabla_{i,m\mathrm{D}}$	design velocity of story i at the mth d.o.f., $m = 1, \ldots, n$

$\nabla_{i,\mathrm{RD}}$	design velocity of story i at the residual mode
$\delta(t)$	interstory drift in the third objective function
$\{\delta\}$	coefficient vector for earthquake excitation
$[\delta_{\mathrm{a}}]$	active controller-location matrix
$[\delta_{\mathrm{p}}]$	passive controller-location matrix
$[\delta_{\mathrm{r}}]$	input location matrix for horizontal and rotational ground acceleration
$\varepsilon_x, \varepsilon_y, \varepsilon_z$	normal strain in x-, y-, z-directions, respectively
$\phi_{i,\mathrm{R}}$	the residual mode shape of the structure at story i
$\phi_{i,m}, \phi_{n,m}$	the mth mode shape of the structure at story i, or at the roof level
$\ddot{\phi}_{\mathrm{g}}$	ground rotational acceleration
$\{\Phi\}$	solution vector of transformed state equation
$\{\Phi\}_m$	the mth mode shape of the structure, $m = 1, \ldots, n$
$[\Phi]$	modal matrix, or eigenvectors of plant matrix [A]
Γ_{R}	the residual mode participation factor
Γ_m	the mth modal participation factor, $m = 1, \ldots, n$
γ	shear strain of viscoelastic material
$\gamma_{xy}, \gamma_{xz}, \gamma_{yz}$	shear strains in direction of first subscript on infinitesimal area, normal in direction of second subscript
$\gamma_{yx}, \dot{\gamma}_{yx}$	components of strain tensor and rate of strain, respectively
$\{\gamma_i\}$	vector of sensitive effect to active control force
$[\gamma]$	$n \times r$ location matrix of control forces
$[\gamma_{\mathrm{a}}], [\gamma_{\mathrm{p}}]$	location matrices for actuators and dampers, respectively
$[\gamma_{\mathrm{s}}]$	controller-location matrix for superstructure
$[\gamma_0]$	controller-location matrix for foundation
$[\bar{\gamma}]$	controller-location matrix
η	ratio of the postyield stiffness to the elastic stiffness, or fluid viscosity
η_1, η_2	proportional damping ratios of two translational modes
ι	imaginary number $= \sqrt{-1}$
$\wp$	shear modulus of elasticity
φ	angle of damper's inclination to horizontal direction
$\varphi_{i,j}$	angle of the jth damper's inclination to horizontal direction at ith story level
φ_m	damper inclination to horizontal direction at the mth d.o.f., $m = 1, \ldots, n$
$\wp^*$	complex shear modulus of elasticity
$[\varphi]$	modal shapes of structure
κ	ratio of bearing's elastic stiffness to its postyield stiffness
λ	gamma function
$\lambda_{i,j}$	gamma function of the jth damper at the ith story level
$\lambda_{\max}, \lambda_{\min}$	adjusted modification factors to maximum or minimum bearing properties
$\lambda_{\max,i}, \lambda_{\min,i}$	maximum or minimum modification factors to bearing properties

λ_0	damper relaxation time, or material viscosity of Maxwell model, or mean square value of the ground acceleration
λ^*	complex Lame's constant
$\{\lambda_g\}, \{\lambda_f\}$	multiplier vectors for quadratic function g and functional f, respectively
$[\Lambda]$	diagonal matrix equal to $[T]^{-1}[A_c][T]$, or matrix consisting of plant matrix's eigenvalues
μ	viscosity of linear viscous material, or factor determined by required probability of structural safety as given in Equation 7.44
μ_i	real part of the ith eigenvalue
μ_D	effective ductility demand of a damped structure under the design earthquake
μ_M	effective ductility demand of a damped structure under the MCE
μ_b	breakaway friction coefficient of the friction pendulum system
μ_i, μ_j	the real part of the ith or jth eigenvalue of matrix $[A]$
μ_{max}	maximum value of the effective ductility demand
μ_s	sliding coefficient related to sliding velocity of friction pendulum bearing
ν	command signal
ν_i, ν_j	the imaginary part of the ith or jth eigenvalue of matrix $[A]$
ν_{max}	voltage associated with the saturation of magnetic field in the MR damper
ν_x	fluid velocity of fluid viscous damper
$\bar{\nu}_s$	average shear wave velocity
$\Pi(t)$	state transition matrix
$[\Theta]$	transformation matrix of $[\Phi]$ as given in Equation 7.59
$[\theta_a]$	matrix of actuator locations in a structure
$[\theta_b]$	matrix of brace locations in a structure
$[\theta_p]$	matrix of damper locations in a structure
ρ	fluid mass density, or mass density
ρ_i, ρ_R	soil mass density of layer i and of half-space
$\rho(X)$	controllability index
$\rho_1(t)$	mass density of the fluid
$\sum \lvert F_D^+ \rvert_{max}$	sum of the maximum absolute lateral force at a positive design displacement, D_D
$\sum \lvert F_D^+ \rvert_{min}$	sum of the minimum absolute lateral force at a positive design displacement, D_D
$\sum \lvert F_D^- \rvert_{max}$	sum of the maximum absolute lateral force at a negative design displacement, D_D
$\sum \lvert F_D^- \rvert_{min}$	sum of the minimum absolute lateral force at a negative design displacement, D_D
$\sum \lvert F_M^+ \rvert_{max}$	sum of the maximum absolute lateral force at a positive maximum displacement, D_M
$\sum \lvert F_M^+ \rvert_{min}$	sum of the minimum absolute lateral force at a positive maximum displacement, D_M

$\sum \left\lvert F_{\mathrm{M}}^{-} \right\rvert_{\max}$	sum of the maximum absolute lateral force at a negative maximum displacement, D_{M}.
$\sum \left\lvert F_{\mathrm{M}}^{-} \right\rvert_{\min}$	sum of the minimum absolute lateral force at a negative maximum displacement, D_{M}
$\sigma_x, \sigma_y, \sigma_z$	normal stresses in x-, y-, z-directions
$\sigma_{\delta i}$	root-mean-square value for interstory drift at the ith story
τ	shear stress of viscoelastic material, or parameter related to the servovalve bandwidth, f_{b}, or time variable
τ_u	yield stress induced by the electric field
$\tau_{xy}, \tau_{xz}, \tau_{yz}$	shear stresses in direction of first subscript on infinitesimal area, normal in direction of second subscript
τ_{yx}	shear stress of elastic materials
$\upsilon, \upsilon_i, \upsilon_{\mathrm{R}}$	Poisson's ratio, Poisson's ratio of soil layer i and of half-space
Ω_{T}	truncated frequency
Ω_{o}	overstrength factor
ω	harmonic excitation frequency
ω_{b}	angular frequency of a SDOF seismically isolated structure
ω_{f}	forcing frequency
ω_{g}	prevailing circular frequency defined in Equation 7.29
ω_i	the ith mode natural frequency of an uncontrolled structure, or harmonic excitation frequency corresponding to the ith mode
ω_m	angular frequency at the mth d.o.f., $m = 1, \ldots, n$
ω_{n}	natural frequency of an uncontrolled SDOF structure, or filter's natural frequency in Equation 6.7
$\overline{\omega}_{\mathrm{b}}$	damped frequency of a SDOF seismically isolated structure
$\overline{\omega}_i$	the ith mode damped natural frequency
$\hat{\omega}_i$	the ith mode natural frequency of structure with control
$\{\Omega\}$	rotational-strain vector
ξ	characteristic sliding velocity of friction pendulum bearing given in Equation 2.34
ψ_i	scalar weighting factor in Equation 7.2
$\psi_{\mathrm{p}}, \psi_{\mathrm{S}}$	angles of incident P- and S-wave measured from positive x-axis
$\{\psi(t)\}$	modal state vector
$\{\psi_i(t), \bar{\psi}_i(t)\}$	the ith pair of conjugate complex modal coordinates as shown in Equation 7.52
ζ	the filter's damping ratio in Equation 6.7, or hysteretic damping ratio
ζ_{i}	damping ratio of the ith mode, or the ith mode damping ratio of an uncontrolled structure, or hysteretic damping ratio of soil layer i, of half-space
ζ_{g}	damping ratio defined in Equation 7.29
ζ_{n}	damping ratio of an uncontrolled SDOF structure
$\zeta_j, \zeta_{\mathrm{R}}$	discretizing soil element j
$\hat{\zeta}_i$	the ith mode damping ratio of structure with control

Abbreviations

AASHTO	American Association of State Highway and Transportation Officials
AMD	active mass damper
ASCE	American Society of Civil Engineers
CQC	complete quadratic combination
d.o.f.	degree of freedom
FEM	finite element method
FEMA	Federal Emergency Management Agency
FIM	foundation input motion
FIX	fixed base
ft	feet
GOAC	generalized optimal active control
HDABC	hybrid damper actuator bracing control
HMD	hybrid mass damper
IBC	International Building Code
ICBO	International Conference of Building Officials
in	inch
IOAC	instantaneous optimal active control
k	1000 lbs
kg	kilogram
kN	1000 Newtons
ksi	1000 lb/in^2
lb	pound
IBEM	indirect boundary element method
LVDT	linear variable differential transformer
MCE	maximum considered earthquake
MDOF	multiple-degree-of-freedom
NEHRP	National Earthquake Hazard Reduction Program
pdf	probability density function
PDF	probability distribution function
PGA	peak ground acceleration
PPF	percentage point function
rad	radium
RMS	root-mean-square
ROAC	Riccati optimal active control
SEAOC	Structural Engineers Association of California
SDOF	single-degree-of-freedom
sec, s	second
SFRS	seismic force-resisting system
SRSS	square root of the sum of the squares
SSI	soil–structure interaction, or structure–soil interaction
TLD	tuned liquid damper
TMD	turned mass damper
UBC	Uniform Building Code

Index

C

D

E

F

G

H

I

K

L

M

N

O

P

Q

R

S

T

U

V

W

X

CIVIL ENGINEERING

SMART STRUCTURES

Innovative Systems for Seismic Response Control

Designing more resilient structures against the potentially catastrophic effects of earthquakes and fierce winds is one of the more major challenges inherent in contemporary structural engineering. An innovative concept, smart structural systems have proven to be extremely effective in absorbing damaging energy and/or counteracting potentially devastating force, thus limiting structural collapse and subsequent injury. As this technology rapidly evolves, there is an ever-increasing need for an authoritative reference that will allow those in the field to stay abreast of the very latest advances.

Smart Structures: Innovative Systems for Seismic Response organizes current research and technology to provide current researchers and practicing engineers, as well as advanced students with the means to learn about and apply the very latest smart structure innovations. Key features include–

- Complete mathematical formulations and numerical procedures for topics presented
- New technologies
- Design guidelines and examples based on current official codes
- Consideration of smart structures on a variety of foundations
- Discussion of the use of smart structures with passive or semi-active devices
- Extensive references

Designed for self-teaching, the text emphasizes essential information on structural formulations, mechanism of control systems, and numerical algorithms. It also provides step-by-step numerical examples to illustrate mathematical formulations and interpret physical representations, enabling readers to understand the forumulae vis-à-vis their applications. Each chapter comprehensively explores a specific topic, from smart structure systems currently in vogue, to case studies utilizing simulated earthquake data.

With contributions from an ASIE award winning author, this seminal volume is the authoritative resource for those looking to design and build the safest structures that technology will allow.

8532

ISBN 0-8493-8532-6

90008

9 780849 385322

CRC Press
Taylor & Francis Group
an **informa** business
www.taylorandfrancisgroup.com

6000 Broken Sound Parkway, NW
Suite 300, Boca Raton, FL 33487
270 Madison Avenue
New York, NY 10016
2 Park Square, Milton Park
Abingdon, Oxon OX14 4RN, UK

www.crcpress.com